BRNO UNIVERSITY OF TECHNOLOGY
VYSOKÉ UČENÍ TECHNICKÉ V BRNĚ

FACULTY OF CHEMISTRY
FAKULTA CHEMICKÁ

INSTITUTE OF PHYSICAL AND APPLIED CHEMISTRY
ÚSTAV FYZIKÁLNÍ A SPOTŘEBNÍ CHEMIE

BIOPHYSICAL CHEMISTRY – PHYSICAL CHEMISTRY IN SERVICE OF THE LIFE SCIENCES

HABILITATION THESIS

AUTHOR: Petr Sedláček, Ph.D.

Brno, 2022

Abstract

The habilitation thesis presents the author's personal view of biophysical chemistry as a modern, distinctive chemical discipline. In the introductory part of the thesis, the author presents his own perspective on the current state of the field, in the context of historical moments, which in his opinion have contributed to the formation of biophysical chemistry as an independent scientific discipline. Furthermore, the author presents a subjective view of the main challenges that this discipline currently faces, as well as the opportunities in which the author sees the main merit of biophysical chemistry in the near future. The second part of the work then summarizes the author's own contribution to the development of the state of knowledge in the field. This part is thematically divided into three sections, which gradually summarize the author's scientific contribution in the field of physical chemistry of biopolymers, the application of physical chemistry in the field of microbiology and biotechnology, and in research and development of hydrogel materials. Emphasis is placed on acquainting the reader with the unifying elements that these three seemingly different research topics combine in the author's scientific work - a general physico-chemical view, focused on the connection between thermodynamic state, supramolecular architecture and resulting system properties, and unique methodology, based on unconventional biophysical applications of standard physicochemical and spectroscopic methods.

Abstrakt

Habilitační práce prezentuje osobní pohled autora na biofyzikální chemii coby moderní svébytnou chemickou disciplínu. V úvodní části práce autor předkládá vlastní perspektivu současného stavu oboru, a to v kontextu historických okamžiků, které se dle jeho názoru klíčovou měrou přispěly k formování biofyzikální chemie jako samostatné vědní disciplíny. Dále autor prezentuje subjektivní pohled na hlavní výzvy, kterým tato disciplína v současnosti čelí, a také příležitostí, v nichž autor spatřuje hlavní přínos biofyzikální chemie v blízké budoucnosti. Druhá část práce poté sumarizuje vlastní příspěvek autora k rozvoji stavu poznání oboru. Tato část je tematicky rozdělena do tří oddílů, které postupně sumarizují autorův vědecký přínos v oblasti fyzikální chemie biopolymerů, aplikace fyzikální chemie v oblasti mikrobiologie a biotechnologie, a při výzkumu a vývoji hydrogelových materiálů. Důraz je kladen na seznámení čtenáře se sjednocujícími prvky, který tyto tři zdánlivě odlišná výzkumná témata v autorově vědecké práci spojují – na obecný fyzikálně-chemický náhled, zaměřený na spojitost mezi termodynamickým stavem, supramolekulární architekturou a výslednými užitnými vlastnostmi systému, a na unikátní metodologii, založenou na nekonvenčních biofyzikálních aplikacích standardních fyzikálně-chemických a spektroskopických metod.

Table of contents

Part I:
Current state of Biophysical chemistry: Looking further from the shoulders of giants

"If I have seen further it is by standing on the shoulders of Giants."
(*Isaac Newton*)

Chapter 1:
Biophysical chemistry: When physical chemists think "bio"

„Chemistry works with an enormous number of substances,
but cares only for some few of their properties; it is an extensive science.
Physics on the other hand works with rather few substances, such as mercury, water,
alcohol, glass, air, but analyses the experimental results very thoroughly; it is an intensive
science. Physical chemistry is the child of these two sciences; it has inherited the extensive
character from chemistry. Upon this depends its all-embracing feature, which has
attracted so great admiration. But on the other hand, it has its profound quantitative
character from the science of physics."
(Svante Arrhenius)

„If physics and biology one day meet, and one of the two is swallowed up,
that one will be biology."
(J. B. S. Haldane)

1.1 Introduction: Is there a need for bio- in physical chemistry?

At first glance, one can get an impression that contemporary science has been captured in an era of prefixes. Grant applications and manuscripts of scientific papers hardly gain the attention and respect of referees without being hyphenated already in their title with *nano-*, *bio-*, *inter-*, *multi-*, *trans-* or another one from the long list of the most frequent prefixes. Some of them represent a natural result of the progress in science. For instance, in terms of new approaches to the research, *multi-* (disciplinarity) and *inter-* (nationality) have become necessary conditions for success. Multidisciplinarity proved to be an effective mechanism to solve scientific problems too complex to be viewed from the perspective of a single scientific discipline. Moreover, just as the research projects benefit from the synergy of the variety of disciplines, so do individuals. Some level of interdisciplinarity or personal expertise beyond a single discipline becomes the highly appreciated pre-requisite for a career in industry, which becomes reflected also in modern trends of university education. Similarly, internationality has become a characteristic attribute of the modern research environment. The time when top-class research was a license of a few separate countries is long gone. Now, high-quality research is practiced all over the world and international collaborations are becoming more and more frequent. Their establishment provides not only the benefit of bringing together complementary strengths and instrumental facilities of the participating institutions but also a considerable educational growth and broadening of cultural horizons to all researchers involved in them.

Aside from that, some of these prefixes become so trendy that their use is managed by design rather than by an evolution of knowledge alone. *Nano-* can be used as a good example. On the one hand, an explosion of revolutionary advances in the ways of analyzing, manipulating and engineering materials at the nanoscale in the last decades has resulted in the natural and undoubtedly beneficial boom of nanosciences. On the other hand, the result of the google search for the entry "nano" (for a simplification, limited to the products of everyday use) may lead to a legitimate concern that the human world is in fact more "nano" than the world of viruses and colloids.

This thesis will operate with another popular prefix, i.e. –*bio*. In general, this prefix implies relating to life or living organisms. In particular, however, the real meaning of this prefix is highly dependent

on the field where it is used. For example, in the cultivation of crops and production of foodstuff, the use of bio- (e.g. in bio-farming), is strictly understood and legislatively clearly defined to methods and products complying with the standards of organic farming. In this context, the bio- prefix is rightly considered a synonym for higher quality. In contrast, in many fields of everyday products, the use of the same prefix is much less comprehensible and its interpretation may be misleading. Customers are rarely familiar with the difference between *bio-based* and *bio-degradable* products which together are commonly categorized under the broad umbrella of biomaterials, although not all bio-based materials are biodegradable (and *vice versa*). The term bio-based refers to the type of raw material used to manufacture a product, and it does not relate to the materials produced. In a fact, this means that one can take some biomass, subject it to "hard" chemical processing, mix it with other fully synthetic components, and – *voilà* – gets a bio-product. It is not necessarily more environmentally friendly, nor better working, but it is *bio*. Evidently, the use of this comprehensible prefix can sometimes be surprisingly confusing.

As a matter of fact, even in science, one can find a bar of gold that does not tarnish. Physical chemistry is indisputably such a piece of gold. It explains the behavior, namely interaction and transformation, of matter with the use of principles and theories that are conservative and not subject to fashion trends. Still, this thesis is focused on Bio-physical chemistry. The reader may be in doubt whether the prefix is used only as a purposive decoration enhancing the attractiveness of the old known discipline for students and for funding agencies. On the following pages, I will try to convince you that this is not the case, and that, in a fact, the prefix bio- defines an independent, rapidly evolving yet already long tradition bearing scientific discipline.

1.2   Biophysical chemistry as a scientific discipline

So what is biophysical chemistry and what is it good for? The traditional classification of scientific disciplines determines Biology, Chemistry and Physics as fundamental pillars of human knowledge. As Merriam-Webster defines them, biology is the study of life, more specifically "a branch of knowledge that deals with living organisms and vital processes"; chemistry consists of "a science that deals with the composition, structure and properties of substances and with the transformations that they undergo"; and physics means "a science that deals with matter and energy and their interactions." Primary schools and even most secondary schools (e.g. grammar schools) usually teach these three disciplines as separate classes which imply in many people the false notion that the three disciplines have only little in common. College students of life sciences soon find out that it is reasonable to integrate individual pairs of these disciplines, giving rise to Physical chemistry, Biochemistry and Biophysics (see Fig. 1). In the Physical chemistry course, they learn how to apply physical methods and theories to the study of chemical systems and how to explain the physical behavior and properties of the systems based on their chemical composition and transformations. Biochemistry, in short, deals with how life depends on chemical processes. It studies molecular components of living organisms and explains how they participate in a series of chemical processes called metabolic pathways. Last but not least, Biophysics blurs the line between biology and physics by studying how the laws of matter and energy work in living systems, involving the fundamental concepts of physics (such as mechanics, heat, electricity, light, and sound) in understanding biological processes and in experimental analyses of biological systems.

The main purpose of this thesis is to illustrate on the research interests of its author that it is equally reasonable to integrate all three basic disciplines. This integration is provided in Biophysical chemistry. The truest description of a living organism, regardless of its degree of biological and structural complexity, is obtained when biological, physical and chemical elements are taken into account altogether. For example, it was not possible to fully understand the biological principle of heredity without the determination of the chemical structure of DNA molecules and the physical constraints that rule its intermolecular binding. Similarly, only the combined knowledge of the specific chemical structure of photosynthetic pigments and the molecules involved in the electron transport chain with

the physical laws of electron excitation and transfer provides insight into the mechanism of an essentially biological process of how plants harvest energy from the sunlight. And, finally, the examples are not necessarily limited to living systems. This can be nicely illustrated by the concept of humification which explains how the remains of the dead plants and animals via processes of biological and chemical transformation give rise to the specific molecular structure of humic substances, which in turn predetermines their physical and chemical properties (e.g. sorption ability and reactivity) and biological activity in the environment.
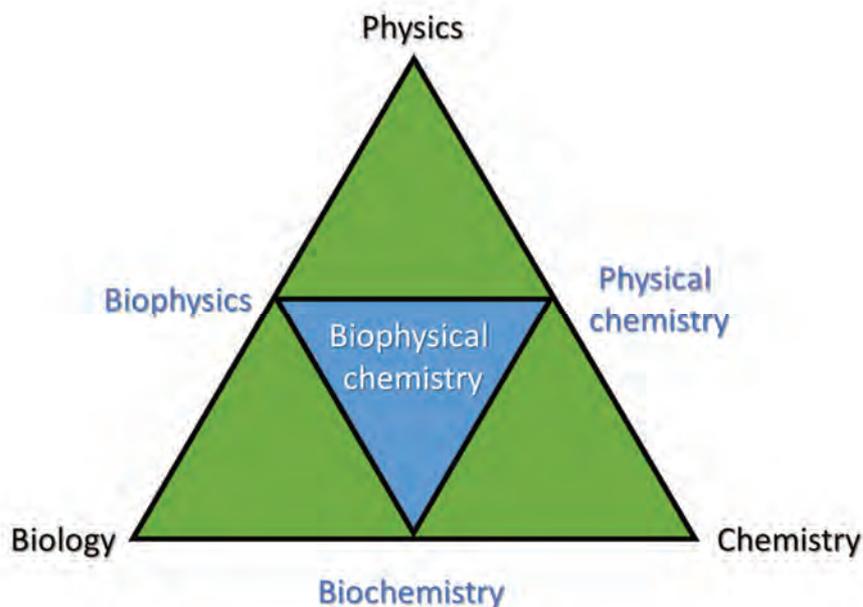
Fig. 1   Biophysical chemistry standing in the intersection of scientific disciplines (inspired by [1])

From a similar point of view, the vast majority of the analytical methods used in biology are built on physico-chemical principles. This holds well for spectroscopic techniques where the physical laws rule the way how different levels of chemical structure contribute to the interaction of a material with an electromagnetic field. But it equally applies also for a chromatography, based on non-covalent interactions between (bio)molecules and a stationary phase, or for electrophoresis, which makes the use of the movement of charged particles in an electric field.

So, Biophysical chemistry* is a field where biology, physics and chemistry meet. It is a broad discipline with a very wide scope delimited by the range of biological systems that are subject to its interest. Probably most studies are aimed at the molecular level, where the structure-function relationship is investigated for the main (groups of) biomolecules, and thermodynamic and kinetic description is being sought for the chemical reactions, physical transformations (e.g. conformation changes), or transport phenomena (e.g. molecular transport across biological membranes) that participate in diverse biological processes. Nevertheless, the field also includes physiological, anatomical, and even environmental approaches to the physical chemistry of living systems.

---

*It should be noted that in English-speaking countries, this discipline of Biophysical chemistry is often mixed up with Biophysics and in many textbooks the shorter title is used for the discipline even if the chemical context is taken into account or if such a sovereign topic of physical chemistry as thermodynamics is dealt like in the case of bioenergetics. To make the terminology even more confusing, one can often meet also such terms as Physical biochemistry, or Biochemical physics, usually indicating which of the basic discipline the author is more inclined to. In this text I will keep the term "biophysical chemistry" to stress out its perception as an application of physical chemistry in biology.

For instance, sensory biophysical chemistry is the branch of physiological biophysical chemistry that describes among others how a vision is formed – starting with a relatively small photochemical change in the respective light-sensitive biomolecule that transduces the light signal, followed by the cascade of trans-membrane transport processes that mediate the transmission of the visual signal into the brain. Environmental biophysical chemistry, on the other hand, focuses on the physico-chemical aspects of the relationship between organisms and their environment. In particular, the flow of energy and matter in an ecosystem is described and modeled.

Fig. 2 illustrates how the wide range of the relative size of its subjects is covered by Biophysical chemistry. Shifting the relative scale of the subjects into the world of objects more accessible to our imagination, we can see that the discipline applies the same principles of physical chemistry to subjects that differ in their size approximately as single organisms and the entire planets. From this extraordinary wide scope, I will narrow the focus of the following text mainly to the phenomena that occur at the molecular and (sub-)cellular levels.
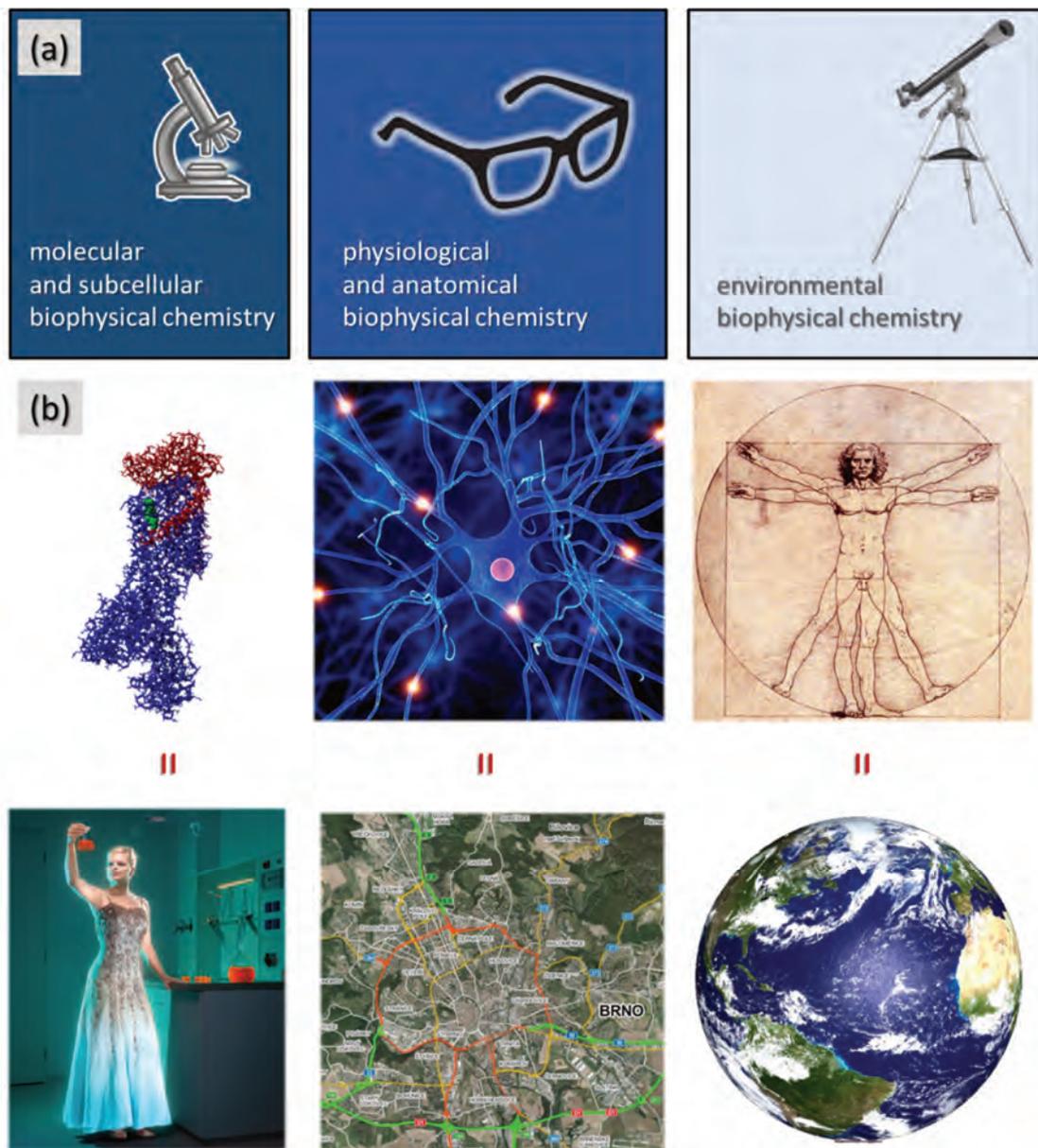
Fig. 2   *a*) *Classification of disciplines of biophysical chemistry based on the relative size of the subject of their focus. b*) *Relative range of the scope of disciplines of biophysical chemistry.* (*inspired by* [2])

1.3   Who is a biophysical chemist?

For now, let me close this introductory chapter by defining who, in my view, is a biophysical chemist (see the graphical projection of the idea in Fig. 3). It is a scientist whose subjects of research interest are biological systems. He/she focuses on the chemical components and chemical processes that form these systems and applies physical laws to understand how the systems behave. Inevitably, he/she needs to use math to express the problems and find the solutions[†]. In short, it is a person who every day asks the essential question: "What is life?", or, more specifically, "What is the physical chemistry of life?". He/she takes inspiration from many great personalities who had been asking the same questions before (Chapter 2). He/she realizes the urgent challenges of life science that should be dealt (Chapter 3) and understand that on the quest to reach these noble goals, he/she can contribute by a series of tiny steps provided by solving the partial topics of his/her interest (Chapter 4 to 7).
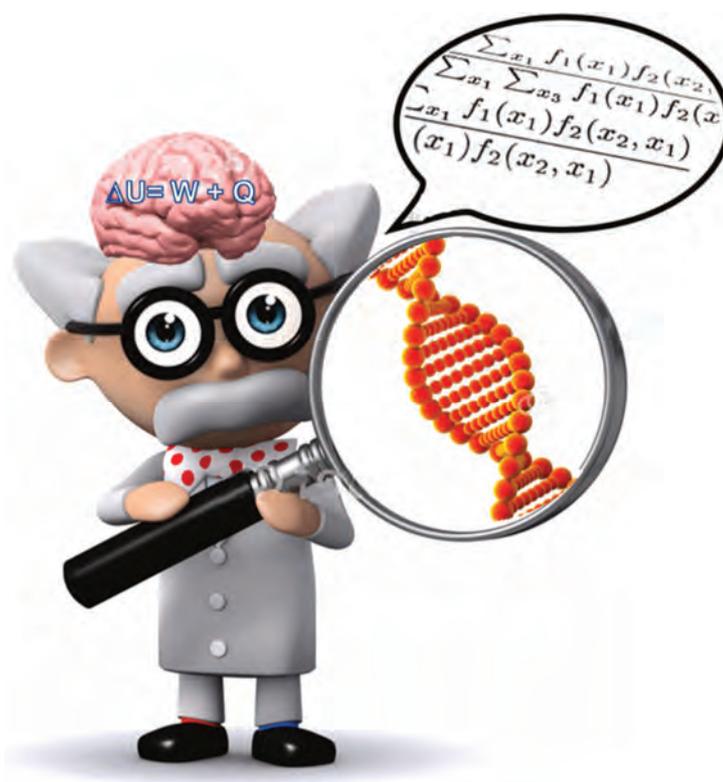
Fig. 3   The author's view of who is a biophysical chemist

References

[1]   Sjöström, J. *Chemistry international*, 2006, 28, 9–13.
[2]   Goldfarb, D. *Biophysics DeMYSTiFied*. McGraw-Hill Professional: 2010.

[†] Although the essential role of mathematics in physical and biophysical chemistry is acknowledged and appreciated (including the historical perspective provided in section 2.1.2), I will stay off the mathematical background of the discussed phenomena in this text. In the topics where the mathematical framework is the most relevant (e.g. the diffusion experiments in hydrogels discussed in section 5.1 and chapter 7), an inquisitive reader is reliant on my original published works referenced in the text.

Chapter 2:
Historical perspective: erasing borders in science

"The history of science is rich in example of the fruitfulness of bringing two sets of techniques, two sets of ideas, developed in separate contexts for the pursuit of new truth, into touch with one another."
(*J. Robert Oppenheimer*)

2.1 A brief history of biophysical chemistry: meet the giants!

How old is the Biophysical chemistry? Of course, as a separate field of science, it is far younger than the three disciplines that it integrates. On the other hand, it should not be ranked alongside the numerous "modern" life-science disciplines arisen in the 20th century such as genetic engineering or computational biology. In a fact, the long history of science (a brief topical timeline is shown in Fig. 4) is full of examples of how an integration of physical and chemical perspectives pushed the level of understanding of biological systems. Let me stress out a few of them that in my opinion contributed significantly to the emergence of Biophysical chemistry as an independent discipline.

2.1.1 Diffusion: as matter and time flow

With respect to my personal research focus, I consider it natural to start with the history of the science of diffusion. As it is well recognized today, diffusion is the process that originates from the random motion of molecules and results in the net flow of a substance from a region of higher to a region of lower concentration. It is the crucial physicochemical phenomenon that follows the same physical laws when it governs the flow of the matter in technological reactors as well as through the biological membranes in an organism. As one could expect, the history of discovering the phenomenon is paved with contributions from famous names from the history of chemistry (e.g. Thomas Graham and his fundamental finding that gases of different nature do not arrange themselves according to their density but rather spontaneously diffuse through each other) [3] and physics (e.g. Albert Einstein who once and for all ended the controversy around the kinetic theory of gases and statistical mechanics and provided the theoretical basis for empirical evidence for the existence of atoms by providing the stochastic model of the motion of particles suspended in liquids) [4]. Nevertheless, it may be surprising that some of the most crucial findings in this area were contributed by the leading scientists of apparently unrelated disciplines. The two names I would like to highlight will come in chronological order.

Robert Brown (1773 – 1858) was a famous Scottish biologist who had unsuccessfully sought a degree in medicine before he turned his interest to botany where he later gained a great reputation, especially but not only for the discovery that the plant cells contain a nucleus. In 1827, when he was studying the fertilization process in plants using a very primitive single-lens microscope, he observed a *zigzag* motion of tiny objects that had been released from the pollen grains. As a biologist by the nature, he first considered that he had been observing the movement of microscopic living organisms responsible for passing on the life between the parental plant and its descendants. Nevertheless, he had soon started to doubt the living nature of the particles as their motion evidently did not tend to stop. He subsequently proved these doubts valid as he repeated the observation also for finely grounded inorganic particles (grains of sand, silica or clay) suspended in water. This finding led Brown to the pioneering conclusion that the dead pieces of matter spontaneously move in liquid. [5]
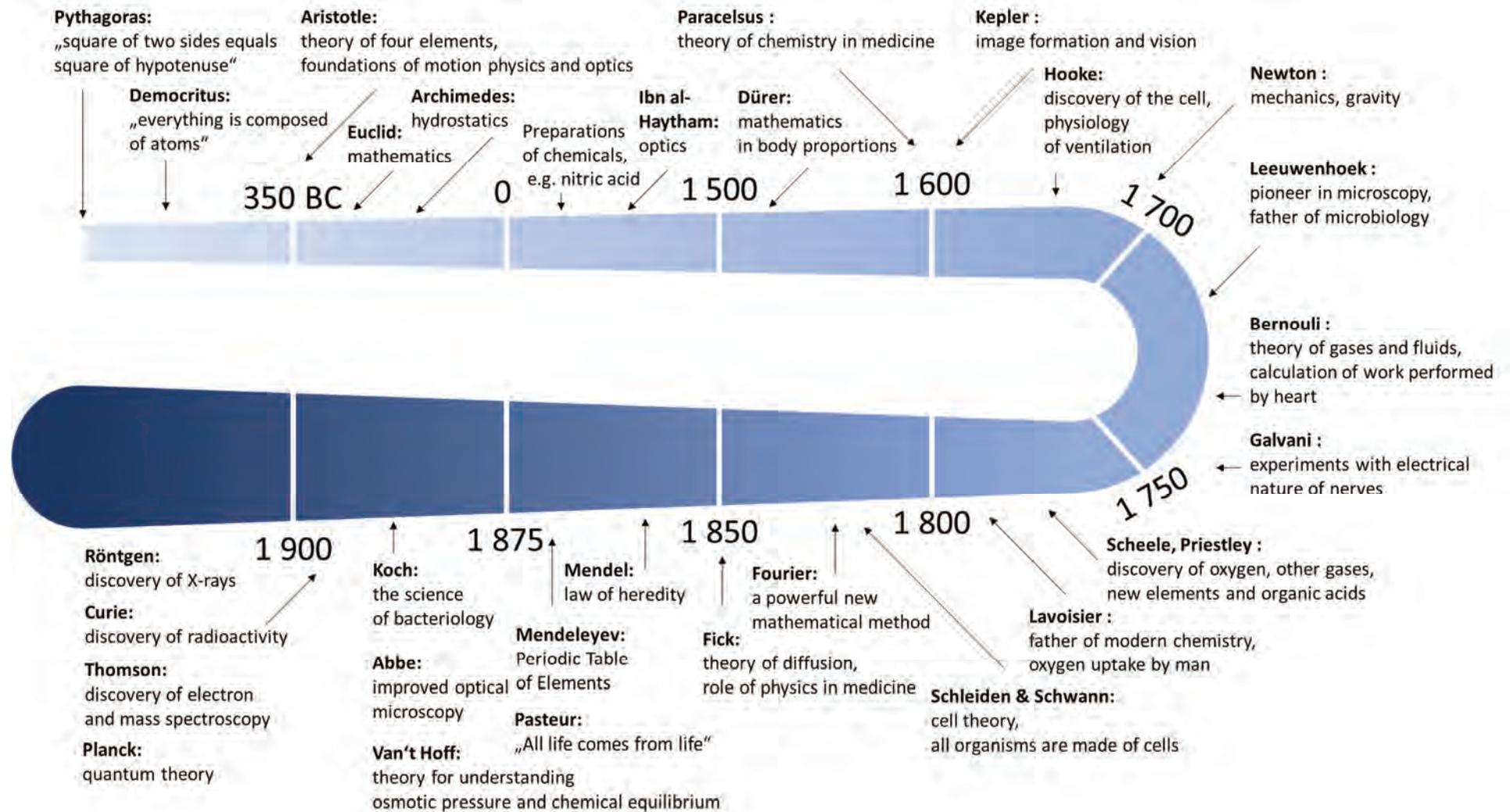
Fig. 4   A timeline of the brief history of science with special respect to moments that formed the disciplines of biophysics and biophysical chemistry (adopted with modifications from [2], complemented from [6])
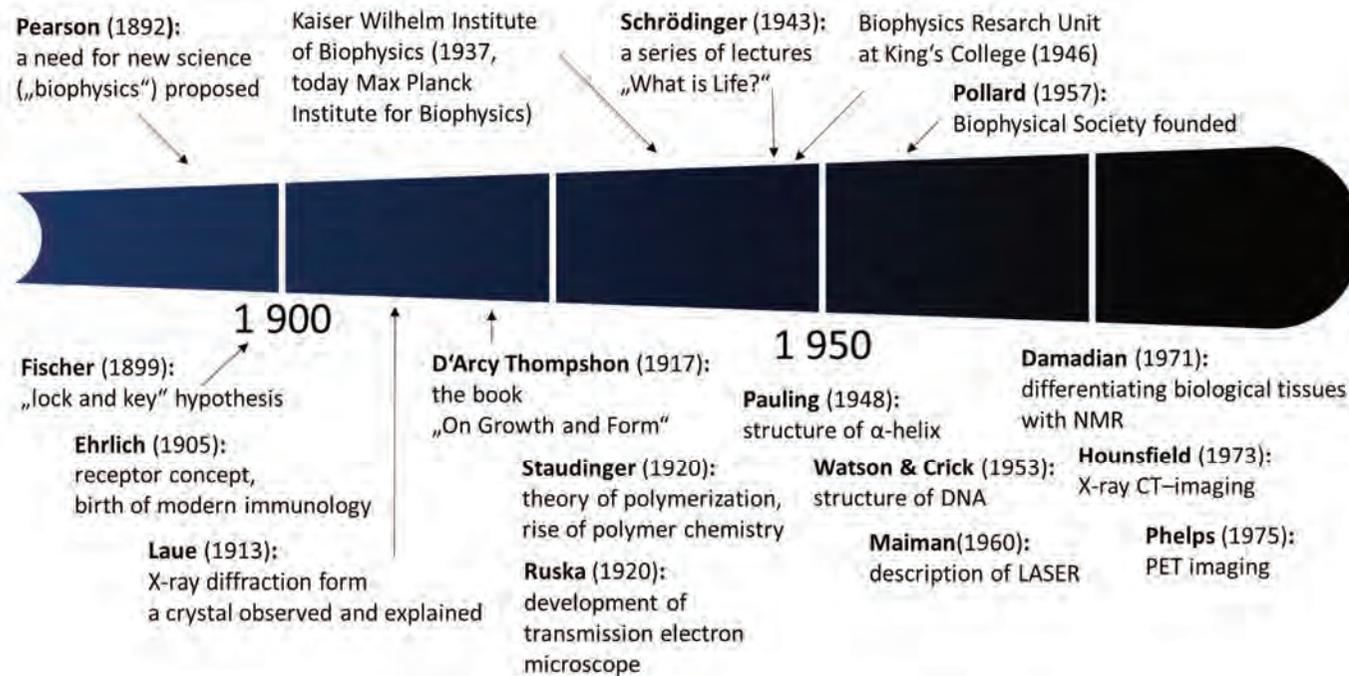
Fig. 4 A timeline of the brief history of science with special respect to moments that formed the disciplines of biophysics and biophysical chemistry (cont.)

The spontaneity of the motion (named Brownian according to its describer) remained controversial not only for the rest of Brown's life but also for almost 50 more years until Albert Einstein (as mentioned above) provided a mathematical explanation of Brownian motion as a visible manifestation of thermal motion of particles and Jean Perrin experimentally proved the validity of Einstein's theoretical framework [4, 5]. The cross-disciplinary contribution of Robert Brown to the science of diffusion hence confirms the words of his contemporary, British poet Mary Howitt, who proposed that: "*He is happiest who hath power to gather wisdom from a flower*".
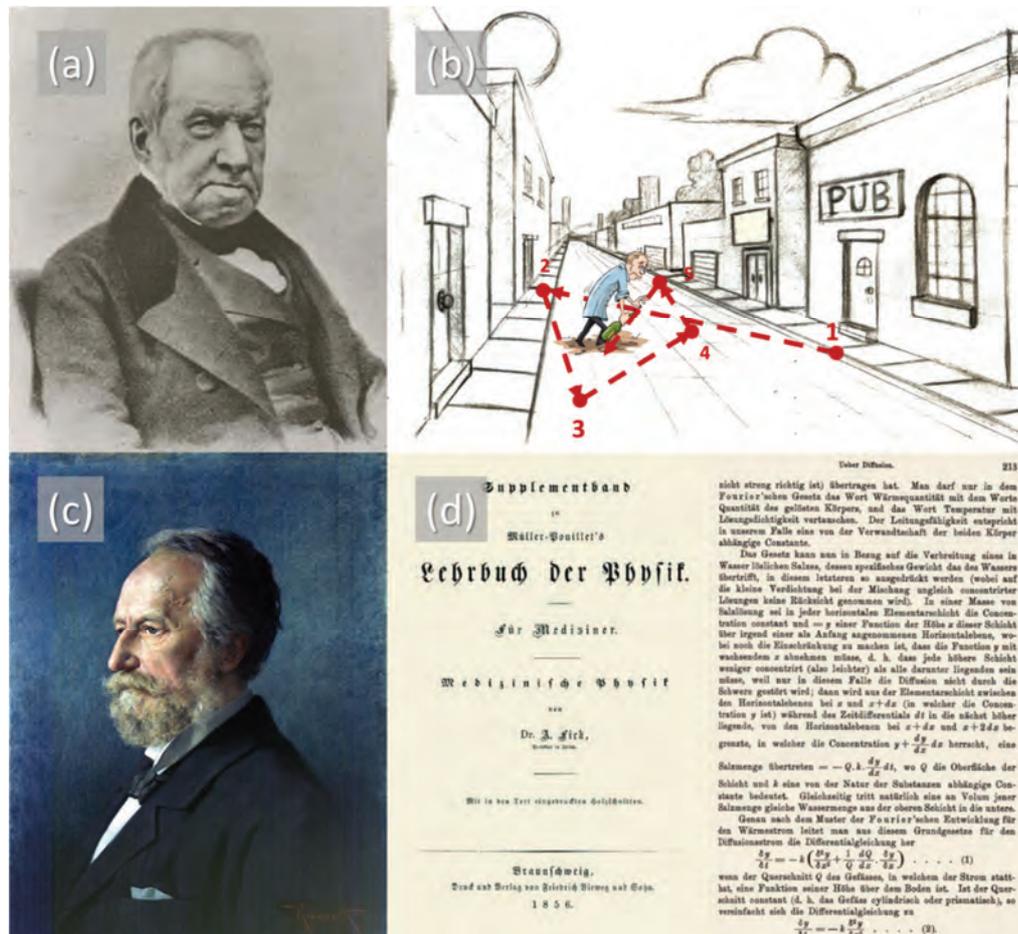
Fig. 5   Giants of the history of biophysical chemistry I: Fathers of the diffusion phenomenon. (a) Robert Brown (1773 – 1858) and (b) the Brownian motion and his common depiction as "a drunkard's walk". (c) Adolf Eugene Fick (1829 – 1901) and (d) his masterpiece Die Medizinische Physik.

After the story of one unsuccessful student of medicine, we will now turn our attention to a graduated medical doctor whose name is indivisibly linked to the phenomenology of diffusion for every undergraduate student of physical chemistry. Adolf Eugene Fick (1829 – 1901) [3, 7] was a German physiologist who was born in 1829 in Kassel as the youngest of nine children. As a student, he excelled in mathematics and physics, the subjects that he had also studied for a short time before he switched to Medical school at the University of Marburg where two of his older brothers worked as professors at the time. During his medical education, he met Carl Ludwig, later referred to as "perhaps the greatest teacher of physiology who ever lived", whose great contribution to physiology and anatomy was published under the names of his students. This meeting essentially influenced Fick's professional career as well as personal life as Ludwig soon became his mentor, research cooperator and life-long personal friend. Fick's fondness for mathematics and physics always ruled his research interests. He had received the doctorate for his work on visual errors due to astigmatisms which he later summarized in a thematic textbook "*The anatomy of Sense Organs*". He also played an irreplaceable

role in the history of cardiology – today, all the hemodynamic studies and cardiac output calculations are based on the principle devised by Fick. Last but not least, Fick also contributed significantly to understanding the physiology of muscle contraction and mechanics of muscular movement. Nevertheless, it was none of these great physiological or anatomical discoveries but rather his phenomenological approach to the theory of diffusion that brought him immortal fame and which also caused his name not to be missing in any physics textbook.

In 1855, at the age of 26, Fick formulated the fundamental mathematical apparatus describing stationary and transient diffusion, today referred as Fick's laws. He developed this concept not from his own experiments (actually, experimental proof of Fick's concept was provided 25 years later), but mathematically by analogy with Fourier's theory of heat transfer applied to Thomas Graham's observations on gasses (therefore the First Fick Law is alternatively called Graham-Fick law of diffusion). Analogically to a heat flow resulting from a temperature gradient, Fick proposed that the intensity of diffusion flow (i.e. the flow rate) of chemical species between two adjacent regions is proportional to the concentration difference between the regions. This concentration difference acts as the driving force for the spontaneous movement of the particles from the region of higher concentration toward the region of lower concentration, similar to the temperature difference that is forcing the heat flow from warmer to a colder body. Fick explained this concept thoroughly one year later in his opus magnum *Die Medizinische Physik* ("Medical Physics", [8]), where he also provided physical analyses of other physiological problems such as the mixing of air in the lungs, work of the heart, hydrodynamics of blood circulation and many others. This book is often considered the first real biophysics text and Fick's ideas presented there significantly impacted aside from human physiology also many other fields of life sciences (e.g. plant sciences), environmental science (e.g. volcanology or climatology), and civil engineering [9].

In general, there are two ways how to teach diffusion in an undergraduate physical chemistry course. The first and more common approach is constructed on a phenomenological approach based on Fick's laws. The other one considers the atomistic nature of the system, describes diffusion as the result of a random motion of particles and utilizes mathematical analysis of this movement introduced by Einstein. As expected, both approaches lead to the same physico-chemical laws governing the diffusion process. But what is worth emphasizing once more, the history of both physico-chemical concepts begins with a groundbreaking experimental or theoretical work of life-scientists – physiologist Adolf Fick and botanist Robert Brown, respectively. This brings us to the leitmotiv of this text once again.

2.1.2 Are biologists scared of mathematics?

My personal experience with cooperation with biologists makes me inclined to positively answer the question raised in the title of this section. To be more illustrative, I have been told repeatedly by one of my colleagues that the number of readers who have completed the reading of an article in a biological journal decrease exponentially with the number of equations presented in the text. Nevertheless, there are convincing historical shreds of evidence that mathematics and biology may live in a strong symbiosis. In this context, it is worth reminding another famous Scotsman, D'Arcy Wentworth Thompson (1860 – 1948) [10], the man who has never studied mathematics and often expressed disbelief in his mathematical skills, but who, however, authored the first mathematical biology book [11].

Like van't Hoff laid the foundations of mathematical chemistry, Thompson is considered a father of biomathematics. Following da Vinci's and Bacon's view of mathematics as *porta et clavis scientiarum* (the gate and the key to the sciences), he believed that biological phenomena can be reduced to a mathematical problem. In his masterpiece work *On Growth and Form* (1917) [12], Thompson focused primarily on morphogenesis – the process of structural forms of plant and animal bodies. He highlighted how the structures in living organisms echo those that can be found in the inorganic world and hence deduced that mathematical principles are superseding natural selection in shaping living

patterns. Interestingly, even if Thomson's education trajectory had copied those of Charles Darwin almost precisely (both switched to zoology after incomplete medicine study), Thompson became one of the main opponents of the contemporary Darwinism as he saw the role of natural selection as rather secondary and supplementary to physical principles in governing the origin of new species. He demonstrated the subordination of the biological phenomena to the physical and mathematical constraints on many other examples, including growth, flight and locomotion trajectories, geometrical compartmentation and microstructural shaping of organism. Thompson's legacy on how to see the role of physics in the biology of living organisms is best expressed by himself in the introduction section of On Growth and Form: "Of how it is that the soul informs the body, physical science teaches me nothing; and that living matter influences and are influenced by the mind is a mystery without a clue. Consciousness is not explained to my comprehension by all the nerve-paths and neurons of the physiologist; nor do I ask of physics how goodness shines in one man's face, and evil betrays itself in another. But of the construction and growth and working of the body, as of all else that is of the earth earthy, physical science is, in my humble opinion, our only teacher and guide." [12]

Fig. 6   *Giants of the history of biophysical chemistry II: Father of biological mathematics. (*a*) D'Arcy Wentworth Thompson (*1860 – 1948*) and (*b*) the drawing he used for the description of the geometry of the shell of nautilus by logarithmic spiral.* [10]

Going back to the question asked in the title of this section, I will use the words of Thompson's contemporary, British statistician Karl Pearson (1857 – 1936), who more than a century ago expressed his belief that: "…day must come when the biologist will — without being a mathematician — not hesitate to use mathematical analysis when he requires it."[13] Actually, they are some biologists who already do so and who see the future of biology and mathematics as closely intertwined, as nicely discussed in Joel Cohen's essay "Mathematics is biology's next microscope, only better; biology is mathematics' next physics, only better" [14].

2.1.3   Asking the right questions

There are a few questions that probably everyone asked himself/herself at least once in the lifetime. One of those may be "What is life?". Actually, it is probably this particular question that stood as a starting shot at the beginning of the history of biophysics and/or biophysical chemistry as a separate discipline. On 5 February 1943, the Nobel prize laureate, physicist Erwin Schrödinger, started a course of three public lectures at Trinity College in Dublin that were bearing in their title exactly the question raised above [15]. Calling himself a "naive physicist", Schrödinger ponders on the apparent discrepancy between the second law of thermodynamics – the general tendency of all order in the universe to break down continuously – and the high degree of order maintained by all living organisms without any distinction. He asked himself what was so special about the living systems that made them

so odd in the view of the known laws of physics. And he immediately suggests the answer: life is distinguished by a "code-script" that directs the "entire pattern of the individual's future development and of its functioning in the mature state". In Schrödinger's view, the code-script is formed by the non-repetitive molecular structure of at the time yet unidentified hereditary molecule (called by himself the "aperiodic crystal"), where, unlike the common (i.e. periodic) crystals, the position of each atom matters. Schrödinger further suggests that organisms feed on "negative entropy" to follow the guideline coded in the genetic information, hence sustaining their structural organization while paying the thermodynamic dues via increasing the disorder of the environment. The lectures aroused a great response (they attracted an audience of about 400) and resulted in the publication of a book of the same name one year later [16].
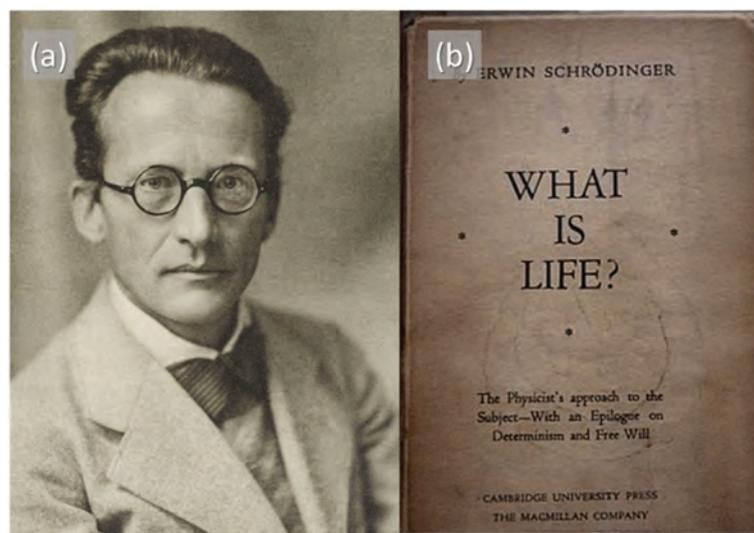
Fig. 7   *Giants of the history of biophysical chemistry III:* (*a*) *Erwin Schrödinger* (*1887 – 1961*) *and* (*b*) *his book What is life?*

Although some of Schrödinger's contemporaries were critical of his views (for instance, Linus Pauling considered negative entropy a "negative contribution to biology", while Max Perutz contributed that "what was true in the book was not original, and most of what was original was known not to be true even when the book was written) [17], there can be no doubt about the influence of the book on the subsequent history of biology and the science in general. Figuratively speaking, Schrödinger has built the bridge between physics and biology; he encouraged numerous physicists (including key figures such as Maurice Wilkins or Francis Crick) to turn to biology and became the source of inspiration for what was to come soon and what is sometimes referred to as "the race for DNA".

2.1.4   What is hidden in the grooves: The race for DNA

The 1950s were a really exciting time for the life sciences, especially for the field of structural biology. In spring 1951, world-leading structural chemist, Linus Pauling, together with his co-worker from Caltech, Robert Corey, published a series of seven papers providing a detailed overview of the key structural motifs found in the protein molecules, with the structures of alpha-helix and beta-sheet standing at the pivotal positions (the papers are nicely reviewed in [18]). Pauling, who was enjoying the spotlights when repeating over and over the famous story of how he had discovered the alpha helix with a sheet of paper drawn with a polypeptide chain while resting in the bed after catching a cold [19], was at the time the head of chemistry department at Caltech, author of hundreds of scientific papers and world-recognized genius in solving complex molecular structures. It is hence not surprising that Pauling was by himself and by the vast majority of the scientific community considered the only possible future discoverer of the still unknown structure of genetic material – the master molecule of life.
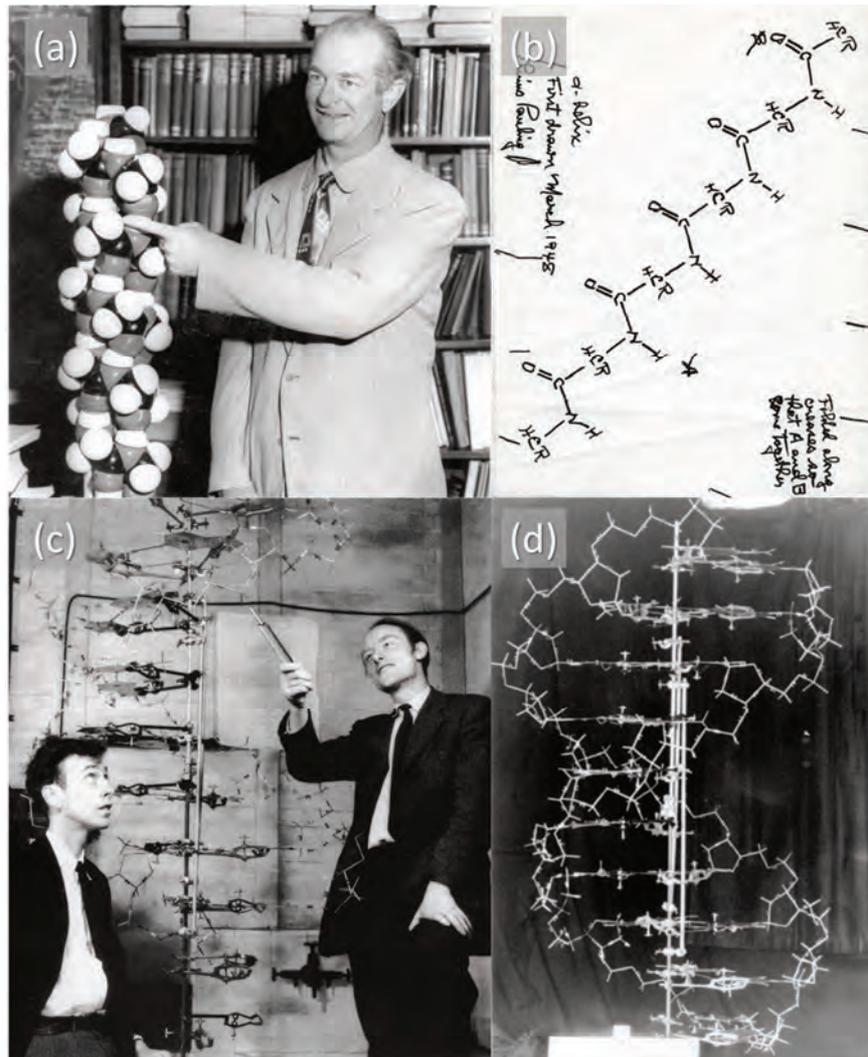
Fig. 8   Giants of the history of biophysical chemistry IV: Main protagonists of the race for DNA.
(a) Linus Pauling (1901 – 1994) showing his space-filling model of alpha helix. (b) the
sheet of paper used by Pauling when discovering structure of alpha helix in 1948. (c)
*James Dewey Watson (left, * 1928) and Francis Harry Compton Crick (1916 – 2004) and*
(d) their original DNA demonstration model designed in 1953.

At the time. it was long clear that the genes were located in chromosomes – two-component supramolecular systems made of proteins and nucleic acids. However, proteins, with their well-known structural and functional complexity, were generally favored over structurally boring nucleic acids as the candidate component responsible for carrying the hereditary material. Although some works evidenced against protein-based genes (such as the experiment of Oswald Avery, who found in 1944 that DNA, apparently by itself, could transfer genetic information between *Pneumococcus* bacteria) [20] these arguments were long overlooked. Pauling, with his lifelong passion for proteins, was no exception. Nevertheless, there were some who did not ignore the faint but convincing voices in favor of the role of DNA in heredity and who were working hard on understanding its structure. Among them, one quite unconventional Anglo-American duo stood above all.

In the same year that Linus Pauling was celebrating his triumph with the series of papers published on protein structure, his compatriot – a biochemist James Watson - took on his postdoctoral fellowship at the Cavendish laboratory in Cambridge, where he was assigned to share an office with a graduate physicist named Francis Crick. Watson, tired of his previous work on DNA biochemistry and still fascinated by the X-ray photos of DNA he had recently been shown by Maurice Wilkins, and Crick, a

too-old graduate with too-slow scientific progress who nevertheless knew crystallography inside and out, immediately agreed on the common research target – discovering the structure of DNA – and also on the way how to hit the target. For this purpose, the couple decided to "imitate Linus Pauling and beat him at his own game" [21].

Sooner in his career, Pauling had spent almost two decades describing chemical bonds in terms of quantum chemistry, which resulted in publishing not only numerous journal papers but also his masterpiece book "*The Nature of the Chemical Bond*" [22]. With this manual of molecular interactions in the hands and with Wilkins's X-ray crystallographic data in mind, Watson and Crick started to solve the puzzle of DNA structure. Consequently, only a few months later, when the Hershey-Chase's "Waring blender experiment" [23] finally proved the role of DNA as the master molecule in genes and started the worldwide hunt for discovering the DNA structure, the Cavendish laboratory couple had already passed their first unsuccessful attempts and held the lead over the rest of the world, including Linus Pauling. While Pauling was repeating the missteps taken by Watson and Crick before without losing his belief that only himself is capable of solving the puzzle, the two young men with the great new X-ray pictures from Rosalind Franklin [24, 25] in their hands and the finally recognized role of hydrogen bonds in the base paring in their minds were refining their ingenious structural model. In April 1953, Watson and Crick submitted the manuscript introducing the structure to Nature and Pauling, during his personal visit to Cambridge, had to gracefully admit that the race for DNA has its – unexpected but well-deserved – couple of winners.

The discovery of DNA structure is considered a major milestone in the history of biophysical chemistry and/or biophysics [26]. It has provided an explicit manifestation of the close interlink between thermodynamics of the molecular binding, supramolecular architecture, and biological functioning of the key molecular component of living organisms. It brought physical chemistry to the spotlights of the life scences by demonstrating how essential the correct application of general physicochemical principles is for revealing the molecular mechanism of general biological phenomenon (heredity). Because of the unprecedented attention that not only the discovery itself but also the path to it, gained in the scientific community worldwide, it became a tangible example of the synergy between biology and physics that motivated further symbiosis of the two disciplines.

Interestingly, to find an inconspicuous spark that ignited the fire of this influential moment, we have to go some years back - according to the words of James Watson: "To have success in science, you need some luck. Without it, I would never have become interested in genetics. I was 17, almost 3 years into college, and after a summer in the North Woods, I came back to the University of Chicago and spotted the tiny book What is Life by the theoretical physicist Erwin Schrodinger. In that little gem, Schrodinger said the essence of life was the gene. Up until then, I was interested in birds. But then I thought, well if the gene is the essence of life, I want to know more about it. And that was fateful because, otherwise, I would have spent my life studying birds and no one would have heard of me." [27].

2.2 Where are we now?

Naturally, the text in the previous chapter provides the author's subjective selection rather than a complete list of the historical moments and the great figures that formed the history of biophysics and biophysical chemistry. Many others deserve to be included – how could for example biological thermodynamics be established without pivotal calorimetric studies of heat generation of mammals conducted by Laplace and Lavoisier as early as about 1780 [28]? How would an understanding of cellular processes be progressed without laying the foundations of non-equilibrium thermodynamics [29]? And how the Schrödinger's naive idea of the "code-script" could grow into the present view of regulation of biological systems without the rise of Claude Shannon's information theory [30] and Norbert Wiener's cybernetics [31]?

Anyway, all these great moments gave rise to biophysics and biophysical chemistry as a mature scientific discipline with a strong institutional background. In 1957, the Biophysical Society [32] was founded in order to lead the development and dissemination of knowledge in the field of biophysics. For this purpose, the Society organizes annual meetings, publishes the official journal (*Biophysical Journal*) and covers many other activities such as community outreach, and career placement. Currently, the Society has over 7,500 members working in academia, industry, and government agencies worldwide. Also, the education in biophysics and biophysical chemistry currently stands on solid foundations as colleges and universities offer graduate and undergraduate degrees in the field worldwide. Last but not least, several specialized research institutes focused on biophysical chemistry and biophysics have been founded in the second half of 20th century. Probably the most famous among them, the Max Planck Institute of Biophysics, was created in 1971 by merging the Max Planck Institutes for Physical Chemistry and for Spectroscopy in Göttingen. The institute, currently employing about 850 people, has to date been honored by affiliating four Nobel prize laureates [33].

To sum up, since its modern history began with the epochal Schrödinger lecture, biophysical chemistry has been fully established at the heart of life sciences. During that time, almost fifty Nobel prizes in Chemistry, Physics and Physiology or Medicine were awarded to works either entirely or partly focused on biophysical topics (the list of these Nobel prizes is shown elsewhere [34]). Nevertheless, the dawn of the new century has brought new trends, needs and opportunities in science. Some of them, to which a specific contribution of biophysical chemistry can be expected, are discussed in the following chapter.

References

[3]   Philibert, J. *Diffusion Fundamentals*, 2005, 2, 1–10.

[4]   Mehrer, H. et al. *Diffusion Fundamentals*, 2009, 11, 1–32.

[5]   Brush, S. G. *Archive for History of Exact Sciences*, 1968, 5, 1–36.

[6]   Gedeon, A. *Science and technology in medicine: an illustrated account based on ninety-nine landmark publications from five centuries*. Springer: 2006.

[7]   Vandam, L. D. et al. *Anesthesiology*, 1998, 88, 514–518.

[8]   Fick, A. *Die medizinische Physik*. Braunschweig/ Friedrich Vieweg und Sohn: 1858.

[9]   de la Barrera, E. *Nature Structural & Molecular Biology*, 2005, 12, 280.

[10]   Dobell, C. *Obituary Notices of Fellows of the Royal Society*, 1949, 6, 599–617.

[11]   Ball, P. *Nature*, 2013, 494, 32–33.

[12]   Thompson, D. W. *On Growth and Form*. Cambridge University Press: 1917.

[13]   Sutherland, J. *Nature*, 1901, 63, 275–276.

[14]   Cohen, J. E. *PLoS Biology*, 2004, 2, e439.

[15]   Yoxen, E. J. *History of Science*, 1979, 17, 17–52.

[16]   Schrödinger, E. *What Is Life? The Physical Aspect of the Living Cell*. Cambridge University Press: 1944.

[17]   Ball, P. *Nature*, 2018, 560, 548–550.

[18]   Eisenberg, D. *Proceedings of the National Academy of Sciences*, 2003, 100, 11207–11210.

[19]   "The DNA Story." Video clip: Pauling Discovers the Alpha-Helix. (2:40). http://scarc.library.oregonstate.edu/coll/pauling/dna/video/1973v.3-alpha.html (accessed Mar. 27, 2022).

[20]   Russell, N. *The British Journal for the History of Science*, 1988, 21, 393–400.

[21]   Watson, J. D. *The Double Helix: A Personal Account of the Discovery of the Structure of DNA*. Atheneum Press: 1968.

[22] Pauling, L. *The nature of the chemical bond: and the structure of molecules and crystals; an introduction to modern structural chemistry*. Cornell University Press: 1940.

[23] Hernandez, V. The Hershey-Chase Experiments (1952), by Alfred Hershey and Martha Chase. 2019. http://embryo.asu.edu/handle/10776/13109 (accessed Apr. 11, 2022).

[24] Klug, A. *Nature,* 1968, 219, 808–810.

[25] Grove, J. W. *Queen's Quarterly*, 2003, 110, 77+.

[26] Cartwright, J. H. E. et al. *Philosophical Transactions of the Royal Society A: Mathematical, Physical and Engineering Sciences*, 2016, 374, 20150071.

[27] Watson, J. D. *Science*, 1993, 261, 1812–1813.

[28] Guerlac, H. *Historical Studies in the Physical Sciences*, 1976, 7, 193–276.

[29] Lebon, G. et al. *The European Physical Journal H*, 2015, 40, 205–240.

[30] Nahin, P. J. *The Logician and the Engineer: how George Boole and Claude Shannon created the information age*. Princeton University Press: 2017.

[31] Wiener, N. *Cybernetics or Control and Communication in the Animal and the Machine*. MIT press: 2019.

[32] Biophysical Society . https://www.biophysics.org/ (accessed Mar. 27, 2022).

[33] Max Planck Institute of Biophysics. https://www.biophys.mpg.de/en (accessed Apr. 11, 2022).

[34] The Nobel Prize and Biophysics. https://www.biophysics.org/nobels-in-biophysics (accessed Mar. 27, 2022).

Chapter 3:
Future prospects: systems, not particulars

"Nothing in life is to be feared, it is only to be understood.
Now is the time to understand more, so that we may fear less."
(*Marie Curie*)

"Make things as simple as possible…
…but not simpler!"
(*Albert Einstein*)

In more or less regular intervals, scientific heavyweights and celebrities express their opinion and suggestions on what the future of their scientific discipline will be like. Some of these efforts sometimes end infamously (such as professor Hudlicky's Angewandte Essay Affair [35]), the others become successful in directing and fueling further progress in the scientific field. Some of such strong inspiring opinions on the future trends for the large field of chemistry were formed repeatedly by Ronald Breslow, most famously in his visionary 2003 National Research Council report "Beyond The Molecular Frontier" [36], and also in the 2016 essay "Back to the future of chemistry" [37]. Among the main challenges for contemporary and near-future chemistry, Breslow emphasizes the "Systems, not substances" approach, which means focusing the scientific interest on complex interacting chemical systems rather than on individual substances. Following the legacy of Watson and Crick, Breslow points out that although the structure of DNA as the key molecule of life was described more than 50 years ago, we are still far from a complete understanding of how life works or how it can be imitated synthetically. In the author's words: "Life is a process in which many substances interact in organized systems, and chemistry is in its infancy in understanding these systems." A bacterial cell is proposed as an illustrative example - although bacteria are considered among the simplest living organism, we still know little about how to mimic the functions found in their cells in synthetically created systems. It is also stressed out by the author that in order to accept and face this challenge, chemists must broaden their training, they need to have a strong foundation also in modern biology and physics. In short, modern chemistry must continue to be creative and useful science without stagnating in form of the narrow science. Biophysical chemistry may in this perspective become a great platform where to concentrate endeavors to face this demanding mission.

The understanding of complex functional systems invented by nature is the first and necessary step in imitating their functional complexity when developing new materials. This has particularly been true for the research and utilization of biopolymers. Biopolymers are the main structural and functional components of living organisms. With their molecular backbones composed of repeating units of bio-monomers (mostly saccharides, nucleotides, and amino acids), sometimes accompanied by various side chains, they provide an unlimited pool of chemical and physicochemical functionalities that predefine their natural roles as well as potential applications. Regarding their utilization by humans, aside from the traditional uses as food or in form of clothing or furniture, they found an irreplaceable position mainly in the field of medical applications [38]. Furthermore, in the last few decades, environmental concerns over the use of polymers from fossil fuels brought the renaissance of biopolymers-based material chemistry introducing biopolymers into a wide range of applications covering routine use materials such as packaging as well as special biopolymer components of high-value materials (e.g. sensors or actuators) [39]. There are several ways how to promote the competitiveness of the particular biopolymer in the desired application. Firstly, understanding the interconnection between the structure of the substance at various levels (molecular and supra-molecular), its fundamental physicochemical properties and the way how these are exploited in playing their natural role in an organism allows the reasonable prediction of its application performance. Furthermore, as far as the high production costs of biopolymers still represent the main

economical factor limiting their further expansion in the production of plastics at the expense of synthetic polymers, the search for new source organisms or cheaper biotechnologies for their production represent an additional central point of upcoming biopolymer research [40, 41]. Finally, another challenge in this field is represented by supplementing the traditional biotechnological processes with tools of genetic engineering to produce biopolymers with tailored structures and properties. These and other challenges of biopolymer research are discussed in further detail in several works [42, 43].

Another research field, where the areas of interest of chemistry, physics, and biology have long been intertwined, is the research and development of soft matter [44]. Soft matter research covers a wide range of condensed materials with deformation behavior and physico-chemical properties determined by their specific supramolecular architecture provided by the ordering of their molecular components on the mesoscopic level. Various self-organized biological materials fall into this category, including biological membranes, cytosol, nucleosol or extracellular matrix. Among the synthetic soft matter representatives, colloids, liquid crystals, and gels are perhaps the most common ones. For all these materials, mechanical, transport and various other aspects of their behavior cannot be understood or predicted directly from the properties of their constituents without taking into account how they are interacted and organized on the large scale. The close interconnection between soft matter physics and biology has been well known since the close analogies between liquid crystals and biological membranes were recognized and it resonates soundly also in recently published future perspectives on soft matter research [45–48].

One specific type of soft matter which attracts particular interest both in modeling real biological environments and in the field of biomedical applications are hydrogels. These were the first biomaterials designed intentionally for use in the human body. In biomedical uses, hydrogels benefit mainly from the outstanding biocompatibility that results from a combination of high water content and physicochemical similarity to the native extracellular matrix [49]. Their unique mechanical and transport properties make them material of choice mainly for controlled release systems, or in the field of tissue engineering. Aside from their biocompatibility and comparable deformation and transport performance with native biological matrices, some hydrogels provide an additional analogy with the biological soft matter – they both behave as active matter. These are non-equilibrium systems that are able to transform energy sources to generate flow patterns and mechanical stresses, large-scale collective motion, active force generation or non-equilibrium phase transitions. Numerous synthetic routes were proposed to prepare hydrogels that provides a dynamic response to changes in environmental condition. These materials, collectively called *stimuli responsive gels* comprise systems that can react to a wide range of physical stimuli, including light, temperature pressure, electric or magnetic fields, mechanical stress or other impulses that affect molecular interactions in the structure. Other materials from this family are sensitive to chemical stimuli such as pH, ionic strength or specific chemical agents. Chemically responsive gels have already been used to mimic chemical communication that underpins a plethora of biological functions [50]. Basically, all the dynamic responses in these materials are based on a change in the interactions between polymer chains and solvents and between polymer chains at the molecular level. Therefore, there is still a need for new ways how to manipulate the internal architecture of gels in order to tailor their properties and dynamics, not only for creating novel biomaterials, but also to find appropriate experimental models on which behavior of complex and hardly explorable living systems could be better understood [51, 52].

Another of the never-ending challenges of contemporary life sciences is to search for still new solutions on how to produce more and more food from the shrinking *per capita arable* land and how to keep the environment safe at the same time. From this point of view, agriculture can be considered among the most topical and burning branches of applied life sciences. Although the concept of sustainable agriculture [53, 54] was proposed already in 1980s and the agricultural practice has changed significantly since then, the need for the adoption of agricultural strategies and technologies that improve productivity further without harming the environment remains as urgent as at that time.

To improve the quality of the soil, prevent erosion and at the same time maintain the high yields of the crops new modern agricultural technologies need to be developed. Among the most common strategies currently considered, improvement of the content and quality of soil organic matter, rationalized management with water in the soil, and biological management of soil microbiota can be emphasized.

The stable fraction of soil organic matter called humus is, to put it very simply, what by its content of only a few percent of weight makes the great difference between "dead" sandy dust and fertile arable soil. In a sense, it is like air – ubiquitous, renewable and essential for life as we know it. Humic substances have been continuously used as a proxy for soil humus research since they were first isolated by means of alkaline extraction from peat in the late 17th century. Nevertheless, in the last two decades, humic substances face a kind of identity crisis [55]. One part of the humus research community struggles in the endless fight between the traditional (macromolecular) and emerging (supramolecular) view on the structure of humics. The other part, that finds humics a promising feedstock for variable agricultural or industrial application, does not care so much about what type of bonds holds the structure of this material together but rather calls for a unified classification scheme, based on consensual quality criteria and objective standardization protocols, that would help in selecting the most suitable source material for the desired functions. Aside from these and independently of each other, microbiologists and botanists involved are focusing on understanding biological activity, organic chemists on chemical reactivity, and physical chemists on the sorption ability of humics. And to make the view on humics even more complicated and fragmented, a debate has risen recently whether humic substances exist naturally at all or they just represent a molecular construct artificially brought by the process of alkaline extraction [56]. Several attempts have been made in this difficult period to objectively evaluate the state of art of humus research and to provide a rigorous assessment the main challenges of the field [55, 57]. Although most targets defined there remain unmet, the importance and the usefulness of research and development in this field is still perceived as can be clearly illustrated by the fact that artificial humic matter from biomass has been selected for the 2021 Top Ten Emerging Technologies in Chemistry [58]. Anyway, the unique combination of complex chemical structure, multiple chemical reactivity and physico-chemical interactivity and diverse biological activity makes humus an especially attractive subject of interest in biophysical chemistry.

Soil organic matter represents only one of the key players ensuring the proper functioning of the soil ecosystem. Other crucial protagonists are certainly soil water and soil microbiota. In reasonable management of these two factors, the beneficial role of hydrogel materials has recently been recognized. Unique ability to retain high volumes of water in their structure together with the release of the solutes from the absorbed solution in a controllable manner make hydrogels promising candidates for novel agricultural preparations – some of these are already in the use such as slow-release fertilizer hydrogels or gels super absorbant hydrogels. Furthermore, hydrogel carriers also represent the state-of-the-art form of bioinnoculants - biological agents, most often based on plant growth-promoting (rhizo)bacteria (PGPR), that are applied in the soil to enhance or restore its fertility [59]. In this application, the gel matrix assures mainly physical protection of the cells against various environmental stress factors. Evidently, agriculture represents a surprisingly promising field for modern applications of soft matter and hydrogels in particular. However, as far as the agro-industrial technologies have the principal requirement of low cost, the task is to find the appropriate technologically feasible, and economically competitive techniques for the preparation of hydrogel formulations for this market segment and to adjust their physicochemical (e.g. mechanical or transport) properties according to their intended function remains the same challenging.

Previous paragraphs show only a few selected examples illustrating the great diversity of the challenges that the life sciences currently face. The focus of these examples may seem so wide that it cannot be covered in a single study curriculum or scientific career. Nevertheless, the "systems, not particulars" concept endorsed by Breslow provides a remarkable platform on which all these life

science topics can be approached with a similar physico-chemical description apparatus and common instrumental methodology. In a sense, this approach pushes chemistry back to its historical roots – under the wide wings of philosophy. It may seem that chemists, who are rightly proud of founding their claims on experimental evidences, look down at philosophers, who conducts no experiments at all. Nevertheless, it is indeed the philosophical way of thinking (incidently, the relevance of the philosophy as an independent scientific field of chemistry has recently been debated [60, 61]) that brings a chemist out of the world of naïve realism, relieves him/her of the narrowmided insisting on the particularity of the employed experimental model, and arms him/her with the ability of generalizing the knowledge, of depicting the phenomena of interest in the broadest terms. In this particular perspective, a hidden resemblance between cell cytoplasm and synthetic hydrogels, from the viewpoint of their mechanical and transport properties, becomes surprisingly obvious, and the essential role of "molecular sociology" in complex supramolecular systems seems astonishingly universal, regardless of whether it is applied on the architecture of biopolymer inclusions in bacterial cells, or on the structure of soil humus. It will be the task of the following chapters to show how focusing on this unifying concept shaped the scientific curriculum of the author of this thesis.

References

[35]   Sydnes, L. K. *Chemistry International*, 2021, 43, 42–44.

[36]   National Research Council. *Beyond the Molecular Frontier*. National Academies Press: 2003.

[37]   Breslow, R. *Chemical & Engineering News*, 2016, 94, 28–29.

[38]   Ruso, J. M. et al. *Biopolymers for Medical Applications*. CRC Press: 2017.

[39]   Shamsuddin, M. I. *Advances in Bioscience and Bioengineering*, 2017, 5, 63.

[40]   di Bartolo, A. et al. *Polymers*, 2021, 13, 1229.

[41]   Rosenboom, J. G. et al. *Nature Reviews Materials*, 2022, 7, 117–137.

[42]   Chassenieux, C. et al. Biopolymers: State of the Art, New Challenges, and Opportunities. *In Handbook of Biopolymer-Based Materials*; Wiley, 2013; pp. 1–6.

[43]   Queiroz, A. U. B. et al. *Polymer Reviews*, 2009, 49, 65–78.

[44]   Nagel, S. R. *Reviews of Modern Physics*, 2017, 89, 025002.

[45]   van der Gucht, J. *Frontiers in Physics*, 2018, 6.

[46]   Renaud, J. P. et al. *Nature Reviews Drug Discovery*, 2016, 15, 679–698.

[47]   Dickinson, E. *Advances in Colloid and Interface Science,* 2011, 165, 7–13.

[48]   Sackmann, E. *Soft Matter*, 2013, 9, 5512.

[49]   Rowley, J. A. et al. *Biomaterials*, 1999, 20, 45–53.

[50]   Active Matter - BonLab. https://www.bonlab.info/nonequil (accessed Mar. 27, 2022).

[51]   Hoare, T. R. et al. *Polymer*, 2008, 49, 1993–2007.

[52]   Zhang, Y. S. et al. *Science*, 2017, 356, eaaf3627.

[53]   Lichtfouse, E. et al. *Agronomy for Sustainable Development*, 2009, 29, 1–6.

[54]   Wezel, A. et al. *Agronomy for Sustainable Development*, 2014, 34, 1–20.

[55]   Schnitzer, M. et al. Quo Vadis Soil Organic Matter Research? A Biological Link to the Chemistry of Humification. *In Advances in* Agronomy, 2011; pp. 143–217.

[56]   Lehmann, J. et al. *Nature*, 2015, 528, 60–68.

[57]   CONCLUSIONS the 14th Meeting of IHSS Meeting of IHSS." http://www.mgumus.chem.msu.ru/ihss-14/docs/IHSS-14-draft-conclusions-Sep-18.pdf (accessed Mar. 27, 2022).

[58]   IUPAC Announces The 2021 Top Ten Emerging Technologies in Chemistry. https://iupac.org/iupac-announces-the-2021-top-ten-emerging-technologies-in-chemistry/ (accessed Mar. 27, 2022).

[59]   Nehra, V. et al. *Journal of Applied and Natural Science*, 2015, 7, 540–556.

[60]   Scerri, E. R. et al. *Synthese*, 1997, 111, 213–232.

[61]   Schummer, J. *Endeavour*, 2003, 27, 37–41.

Part II:
Personal contribution of the author to the discipline

"The practice of science happens at the border between the known and the unknown.
Standing on the shoulders of giants, we peer into the darkness with eyes opened not in
fear but in wonder."
(*Brian Cox*)

Chapter 4:
Standing astride a borderline: diverse systems, similar questions

„This is an era of specialists, each of whom sees his own problem and is unaware of or intolerant of the larger frame into which it fits."
(*Rachel Carson*)

"Principles don't have borders."
(*Alisha Rai*)

Naturally, this habilitation thesis aims not only at introducing the author's personal view on the history, current state, and near-future of biophysical chemistry as a scientific discipline (provided in the previous three chapters) but mainly at summarizing the author's scientific contribution to the field. This will be conceived primarily as a commentary on the published scientific studies contributed by the author[iii]. Before I will focus on particular experimental studies and findings brought by these, I will first introduce a brief overview of my scientific evolution. Furthermore, as far as the particular subjects of these studies are as diverse as those discussed in the previous chapter, I will also try to explain the unifying conceptual and methodological framework that I have been using when approaching these topics.
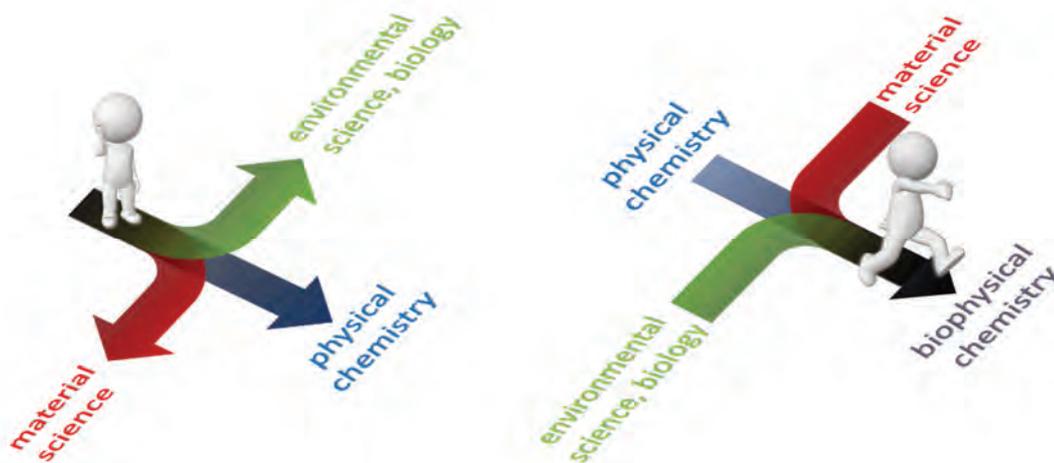
Fig. 9   *On a crossroad? No, all roads join in the biophysical science.*

Chronologically taken, as a graduated physical chemist, I had started my scientific career on the topic of humus chemistry. Studying the interactions of humics in hydrogel matrices to simulate their effect on the transport phenomena in natural humus-containing systems, soon brought me to a more detailed focus on the research and development of hydrogels. Later on, the apparent similarity of the gel matrix and intracellular space caused that I was invited to utilize the methodology developed for the hydrogels in the analyses of microbial cells. Hence, my personal experience confirms that – as was generally introduced in chapter 1 - in the field of biophysical chemistry, miscellaneous scientific roads may join (Fig. 9). At my crossroad, the three connected routes are environmental science and biology, material science, and, last but not least, physical chemistry. The former two represent the main subjects of my research interest – on the one hand, natural substances (natural organic matter and

---

[iii] For an easier orientation of a reader in the text, publications of the author of this thesis will be referenced as footnotes throughout the text, while external references will be listed at the end of a corresponding chapter.

biopolymers) and soft-matter materials (gels) made from these, on the other microbial cells as perhaps the simplest possible but still remarkably complex living systems. The last one stands for the research attitude used in investigating all these systems.

The unifying physico-chemical concept I have been using in these studies (Fig. 10) is based on efforts to understand how the molecular thermodynamics (mainly the interactivity of molecular principal components) of the particular system –regardless of its degree of complexity – rules its structural (e.g. supramolecular architecture) and material (deformation, transport) behavior and how this relationship manifests itself in the environmental, ecological or biological functioning of the system. Also, the methodology used in these studies was largely the same regardless of the specific system studied. The methodology combines methods of structural analysis (various spectroscopic techniques), morphological tests involving techniques of advanced microscopy, and both routinely used (e.g. thermal analysis or rheometry) and originally developed (e.g. diffusion-based) techniques providing further material and physicochemical characterization of the studied system. In some cases, these analyses were further supplemented by specific biological assays (e.g. viability tests). Aside from providing a complex overview of different aspects of system performance, the methodology was also designed in order to combine the macro-and micro-scale view on the system properties. The benefits of this multi-scale complex analytical approach for the particular examples of bacterial cells and hydrogels are discussed in detail in section 6.1. and 7.1., respectively.
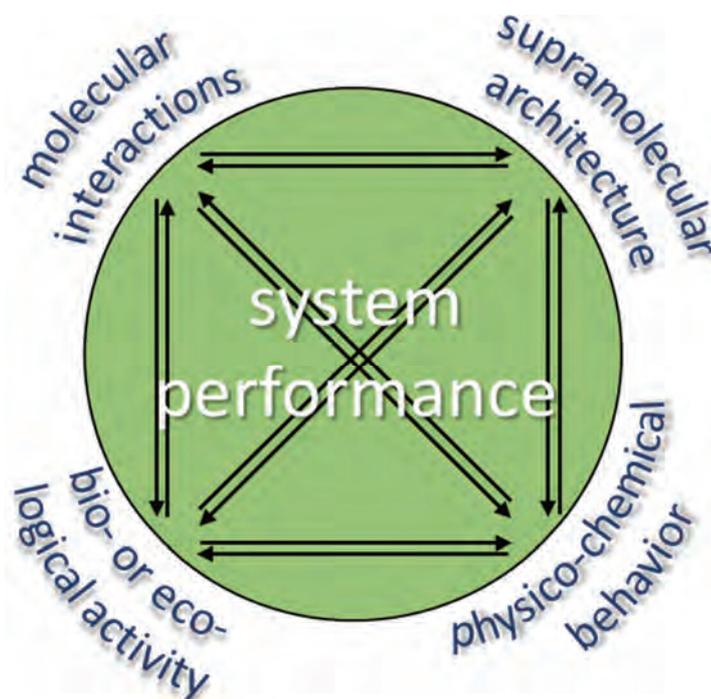
Fig. 10   *Unifying concept in the biophysical studies of the author*

In all the contributed topics, I have also tried to combine a quest for understanding how the natural systems work with an application of this fundamental knowledge in applied research and development of new functional bio-based materials, in the famous legacy of Louis Pasteurs' work (Fig. 11). Hence the studies on the structure of humic substances and on the barrier and controlled release role they play in natural ecosystems were accompanied by the analyses of bioabsorption of these substances from artificial biostimulants and the development of original humics-based soil amendments. In a similar way, fundamental research projects focused on the evolutionary and ecological role of polyhydroxyalkanoates went hand in hand with applying the revealed knowledge on how these materials affect the stress robustness of microbial cells in defining novel trends in their biotechnological production and also in the development of their application forms with tunable material properties.
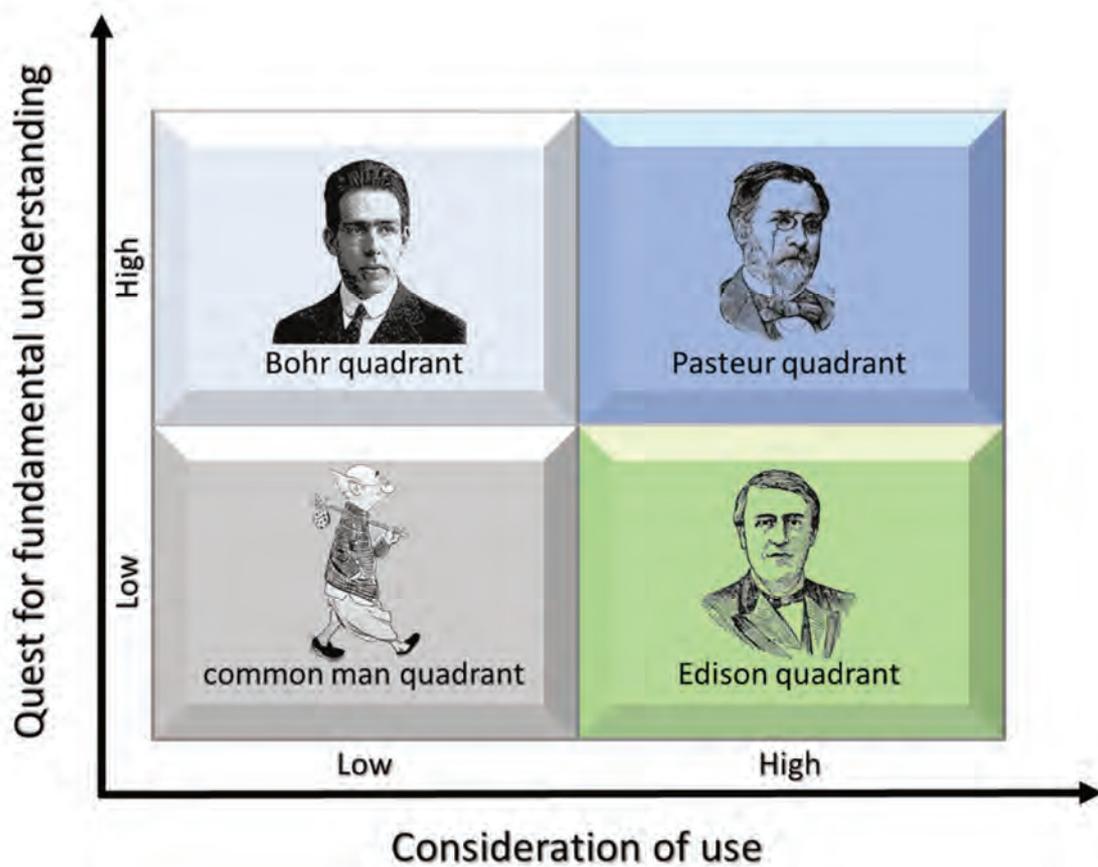
Fig. 11   Pasteur's quadrants. Classification of scientific research based on seeking the fundamental understanding of scientific problems and/or having an immediate use for society.

If I was asked to characterize my scientific career so far in a single slogan, I would probably use "standing astride". For the whole time, I have been standing astride borderlines between apparently diverse scientific topics, between fundamental and applied research projects and sometimes also with each leg embedded in a different research team. Probably, this may seem to someone like a lack of a firm thematic anchoring or even like scientific volatility. Nevertheless, as every colloidal chemist can confirm, it is exactly the boundary separating different phases where the most exciting phenomena take place. It will be the main goal of the following chapters to prove that this "standing astride" position may be in a fact surprisingly beneficial in science.

Chapter 5:
Molecular interactions in biopolymers and natural organic matter: from structural principles to macro-scale effects

„He who loves practice without theory is like a seafarer who boards ship without wheel or compass and knows not wither he travels."
(Leonardo da Vinci)

At first glance, biopolymers and humus, respectively, may be considered just two different stages of the life cycle of carbonaceous organic substances, differing fundamentally in their structure as well as their environmental fate. Nevertheless, in a more careful view, a surprising similarity between these two families of natural compounds becomes evident. In a fact, it can even be said that biopolymers mean the same for living organisms as humics do for the non-living part of nature. Based on their wide supply of chemical functionalities, they both play a variety of structural, nutritional and functional roles where they are irreplaceable by other components of their natural environs. In all these functions, the performance of both types of compounds lies primarily in the way they interact with other polymers and low-molecular components of the system.

Another common feature of humic substances and biopolymers is that they both represent a promising feedstock for a wide range of applications. As a nature-derived, renewable and bio-degradable substances with plentiful chemical functionality they find potential uses in agriculture, industry, and medicine. Regarding their commercial uses, they also both face the same problems – due to the very diffuse nature of their sources and isolation methods, the quality of these compounds may differ widely. Therefore, extensive inventory studies are needed for particular biopolymers as well as for humic substances. Similarly, a systematic investigation of the causal relations between their chemical structure and their application-relevant performance is necessary for the definition of reasonable quality criteria and standardization protocols of how to test whether these criteria are met by a particular material.

In our research studies, we have focused on humic acids (HAs) as the key constituent of NOM regarding its interactivity in condensed natural environments, and to polyhydroxyalkanoates (PHAs) as the family of microbial polyesters with a complex biological role and great potential in replacing petroleum-based polymers in the production of plastics. In the case of humic acids, we paid attention mainly to how their ability to bind specific low-molecular compounds affects their mobility in natural humics-containing environments (details in sections 5.1.1. and 5.1.2.). Furthermore, we have also tried to contribute to the current debate on the supramolecular architecture of humics via introducing a simple method of their polarity-based fractionation (section 5.1.3). Finally, we have utilized our experience gained in these fundamental research studies in developing simple experimental techniques for the assessment of the bioabsorption of humic substances (section 5.1.4) and also in the design of novel humic-based soft matter materials for agricultural and health-care applications (section 5.1.5).

Similarly, in our studies on PHAs, we have first focused on understanding the mechanisms that maintain these polymers in microbial cells in a biological active but thermodynamically unfavorable amorphous state (section 5.2.1). Later on, we have utilized our knowledge of the relationship between primary chemical structure and phase behavior of PHAs in the development of PHAs' films with tailorable material properties intended for use in modern packaging and biomaterial applications (section 5.2.2).

5.1 Humic substances: native transport systems & promising artificial carriers

Natural organic matter provides a remarkably complex pool of organic compounds. Among its various constituents, the stable organic fraction called *humus* (the latin expression for "earth, soil", originating probably from *humi, "on the ground"*) attracts special attention mainly as the major cause of fertility of soils. This vital ecological merit of humus arises from the finely tuned interplay between various chemical, physical and biological mechanisms of action. On the one hand, humus represents a storehouse for essential soil nutrients and minerals, on the other, it supports soil structure and improves physical parameters such as porosity, thus improving soil aeration as well as water absorbency and drainage. Moreover, humus supports the biological activity of soils, not only indirectly by serving as an energy source for soil microorganisms, but their decomposition products can also selectively inhibit or stimulate the growth of soil microbiota or, in some cases (e.g. via the production of auxins) it directly chemically promotes growth of higher plants.
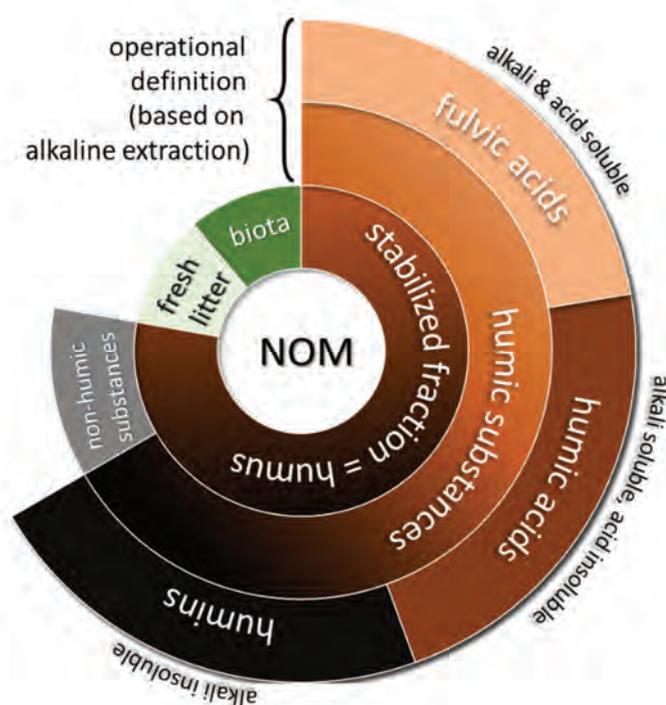
Fig. 12   Operational definition and classification of humic substances. Adopted with modifications from [62]

The rise of humus chemistry is intimately linked to the isolation and investigation of humic substances (HS). These are the organic matter extraction products defined and classified operationally according to their solubility at various pHs (see Fig. 12). The alkaline extraction procedure was applied for the first time by Achard on peat more than three centuries ago [63]. In the ongoing decades, the development of the concept of humic substances was based on great contributions of such scientific authorities as de Saussure, Liebig, or Berzelius, who isolated HS from a Swedish spring and widened the view on humus from a specific organic component of soils to a universal constituent of non-living nature. All these pivotal works (for a more detailed review on the history of humus chemistry, see e.g. [64]) laid the foundation for the traditional view of humic substances as specific natural compounds synthesized via physical, chemical and microbiological transformation (collectively embraced by a process called humification) of plant, animal, and microbial residues (see Fig. 14a).

Since the early years of HS research, most of the essential biological functions of humus have been attributed to the specific chemical structure of humic substances. For instance, a complex structural skeleton with a great diversity of functional groups leads to a surprising affinity of HS to interact with almost any compound, regardless of its hydrophilic or hydrophobic nature. It is just this affinity that has been believed to stand behind crucial environmental impacts of humus such as speciation and immobilization of both nutrients and pollutants in the environment, hence regulating their biological uptake. Similarly, the recalcitrant nature and environmental stability of HS is attributed to the combination of high aromaticity of the core of its structure and the ability to bind to the mineral components of soil via the peripheral polar groups. [65, 66]

It is this remarkably universal binding ability that is also the key to a number of industrial applications in which the beneficial use of humic substances has been suggested. Comprising about 25 % of the total organic carbon on the earth [67], HS are supposed to be the largest reservoir of carbonaceous compounds – more abundant than biomass or crude petroleum. Hence, aside from the traditional applications of HS in agriculture and environmental technologies [68], and leaving aside applications utilizing the biological activity of HS (which will be discussed in sections 5.1.4 and 5.1.5), HS have been proposed as antioxidant additives to plastics, viscosity- and hardening- modulating agent in concrete technology, efficient emulsifier, and, of course, a versatile feedstock for chemical syntheses (for more details on industrial applications of HS, see e.g. [69, 70]). In all these fields, the unique amphiphilic structure with a specific balance between polar and aromatic structural motifs makes the position of HS so exclusive.
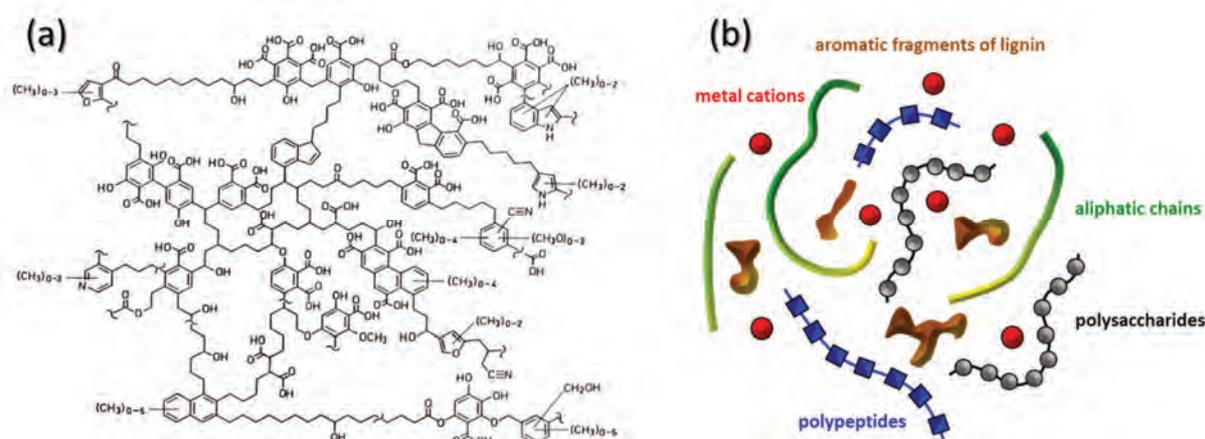
Fig. 13   Two concepts of the structure of humic acids. (*a*) *Macromolecular structural model proposed by Schulten and Schnitzer [71].* (*b*) *Schematic representation of the supramolecular concept proposed by Simpson [72].*

On the other hand, it is also the structure of HS that has brought the most controversy in recent years. Firstly, the original concept of HS as macromolecules, produced by polymerization of low-molecular (mainly phenolic) compounds as a result of microbial activity, was challenged by several authors [72–77] who have suggested a "new view" of humic substances as micelle-like supramolecular aggregates of molecular constituents much lower in molecular mass than originally expected (Fig. 13). In these supramolecular structures, polyvalent cations, hydrogen bonding and hydrophobic effects are considered the main mechanism to aggregate HS and increase their apparent molecular mass as supported by results of size exclusion chromatography with selective destruction of these linkages [75, 76]. And even more recently, while the macromolecular-supramolecular debate inside the HS' community continued, the very existence of HS was questioned by two authors standing outside this community. Lehmann and Kleber criticized the "traditional view" (humic substances concept) and proposed an "emergent view" of soil organic matter with the absence of HS. In their view (see Fig. 14b), the residence time of organic soil constituents is an environmental property and has no support in or need for a specific chemical structure. Without any strong experimental arguments supporting
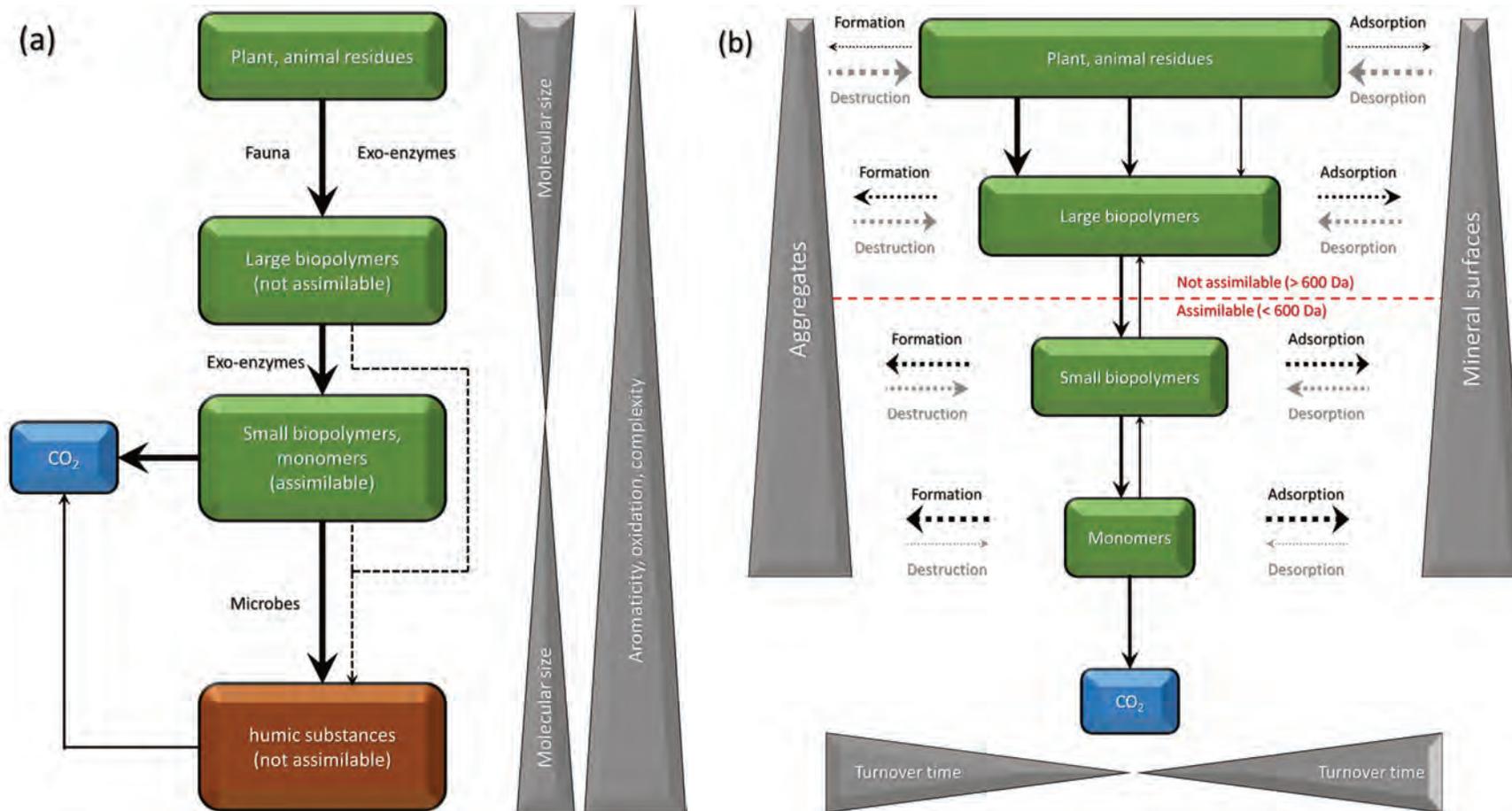
Fig. 14   Two competing theories explaining (non-)existence of humic substances and transformation of soil organic matter. (a) The classical theory of humification. (b) The Soil continuum model proposed by Lehman and Kleber [56].

this, they suggest that humic substances represent just an experimental artifact - the artificial result of the traditional extraction procedure – and consider HS an invalid proxy for SOM research [62]. Although the wave of criticism from the HS community did not take long and the collection of arguments against Lehmanns' and Klebers' attack on HS were soon provided [78, 79], damage on the reliability of HS research and its perception by the general scientific public has remained.

Evidently, although the history of HS research lasts more than three centuries, many fundamental questions about these fascinating compounds remain unanswered. Much experimental work is still needed before a comprehensive general concept of the structure-performance relationship for natural HS may be proposed and used as a guide in designing meaningful applications of HS and selecting suitable materials for them. In the following subchapters, the author's contribution to this challenging quest is summarized.

5.1.1 Development of novel methodology for interaction studies based on diffusion processes

One of the most inspiring scientific events that I attended during my Ph.D. study was IHSS-14, the 14th International Meeting of IHSS (International Humic Substances Society), which took place aboard a ship sailing from Moscow to St. Petersburg in September 2008. In addition to the non-traditional venue, this meeting was exceptional also in a rare effort of its scientific committee to conclude the scientific program with a tangible formulation of the state-of-the-art of HS research and definition of the main gaps in knowledge on HS. A summary of these concluding remarks is still available on the website of the conference [57]. In general, the authors called for a knowledge transfer between fundamental (mainly environmental) research of the role that humic substances play in nature, and the industrial segments where the potential of HS as a promising feedstock is under consideration. To achieve this goal, nine specific research priorities for HS were identified. Among them, a systematic reactivity and interactivity mapping of HS was urged in order to reveal how the exact chemical structure and particular chemical functionalities of HS contribute to their inherent environmental performance and also to their value for individual application fields.

While the methodology for the chemical reactivity studies on HS is quite straightforward – numerous options for modification or substitution of the chemical skeleton of HS can be found in classical textbooks on organic synthesis – a method to study physical interactivity (non-covalent binding) of HS in a reasonable and standardizable manner is more difficult to find. On the one hand, such a method should provide a meaningful demonstration of the way how is the physical binding on HS manifested in environmental humics-containing systems, i.e. it should reasonably simulate the form and physico-chemical conditions at which the binding occurs in nature. On the other hand, the method should be quantitative and robust enough to allow comparative studies involving humic substances of a different type, source or degree of chemical modification, or even to include relevant non-humic materials as a reference (e.g. other environmental components).

In the case of humic substances, the first and the foremost trouble lies in the selection of the appropriate colloidal form of analyzed HS. Traditionally, experimental studies on the binding of low-molecular solutes on HS had been realized either in solution with both components dissolved or via sorption experiments with solid HS dispersed in a solution of the sorbate. Nevertheless, these experimental setups suffer several drawbacks regarding the above-mentioned specific requirements. Some of these are rather specific regarding the experimental design – for example, available analytics for the determination of unbound solute in the solution of both components is limited to the methods that are not interfered by dissolved HS (e.g. by their spectral or hydrodynamic behavior). Similarly, the results of the sorption experiments are influenced by numerous physical parameters of the solid HS (e.g. particle size or porosity) or experimental setup (e.g. stirring rate) that are difficult to maintain which reduces experimental reproducibility. Moreover, some limitations of these experimental designs are more general. For instance, neither the fully dissolved nor the solid particulate forms simulate properly the form that HS naturally adopts in soils or sediments. Furthermore, it also brings information mainly on the equilibrium partition of the solute between a bound and unbound form with

a limited idea of how this influences the dynamics of the solute distribution in the natural HS-containing systems [80].

At the time of the IHSS-14 conference, we were already working on the development of an alternative methodology based on diffusion experiments in hydrogels made from HS (humic acids in particular). Diffusion, as a process that results from a dynamic behavior on the level of individual molecules but its manifestations can be easily observed on the macro-scale level, represents a smart solution for the sought experimental design. As far as it is directly influenced by all chemical and physical interactions that the molecules of the diffusing compound undergo, it allows investigation of the molecular binding in a quantitative way, and, at the same time, an effect of this binding on the macro-scale system dynamics is directly demonstrated. Another advantage of the diffusion-based methods lies in a broad variety of setups that can be used according to the specific requirements regarding the volume of the analyzed sample, the concentration of the tested solute, time duration of the experiment, etc. (various diffusion setups used in our study on HS are illustrated in Fig. 15). For all these experimental designs, corresponding mathematical solutions of Fickian diffusion equations are available [81]. This allows determining the effective diffusion coefficient as a primary experimental outcome by which the interactions in the studied system may be quantitatively and reproducibly characterized.

Hydrogel media provide numerous benefits as far as the experimental analysis of diffusion is concerned. Firstly, the diffusion rate in a gel is comparable with the one in a solution with the same solvent, whereas liquid-specific experimental obstacles (such as density- or temperature-based convective mixing of the sample) are suppressed. Moreover, gel form allows preparation of the sample in defined shape and/or dimensions which is necessary for a correct application of the selected diffusion model and accurate determination of quantitative diffusion parameters. In the specific case of humics, hydrogel also reasonably imitates highly humid natural habitats of HS (soils, sediments), where they occur in the partially swelled form.

Initially, we adopted the diffusion-in-gel method in an investigation of heavy metal transport in humus-containing systems [1 - III]. Copper was used as a model metal mainly because of its outstanding affinity towards humic substances [82] and also because of its easy spectroscopic quantification. As an experimental gel matrix, we used humic acid hydrogels that were prepared by controlled coagulation of humic acids by acidification of their alkaline solution. In general, the experimental procedure was as follows: the gel phase (obtained by centrifugation and removal of supernatant) was filled into a suitable container (usually a plastic or glass tube with well-defined internal dimensions) and brought into contact with a source of the diffusing solute (cupric ions). At the given time(s), we then determined the concentration of the solute at different positions of the gel sample by the manual slicing of the gel and gel-liquid extraction of the solute. The main steps of the experimental procedure are illustrated in Fig. 16. Naturally, the published experimental studies were preceded by an extensive optimization of the methodology regarding the geometry of the diffusion apparatus, time duration of the experiment, selection of appropriate extractants, etc.

In our first published work, we designed and tested three different experimental setups corresponding to those presented in Fig. 15. In the paper, we have also summarized a simple Fickian mathematical model that explains how the solute binding in the gel affects the value of its diffusion coefficient that represents the primary experimental outcome. We have found a very good agreement between obtained experimental data and the proposed mathematical model. Determined values of Cu^{2+} diffusivity in the humic gels varied between 35% to 55% of the value that corresponds to its diffusion in water. This decrease in diffusivity demonstrates the combined effect of porosity of the gel

---

[1] Sedláček, P. and Klučáková, M. Diffusion experiments as a new approach to the evaluation of copper transport in humics-containing systems. *Collection of Czechoslovak Chemical Communications.* 2009, 74, 1323–1340. Attached as Appendix 1.
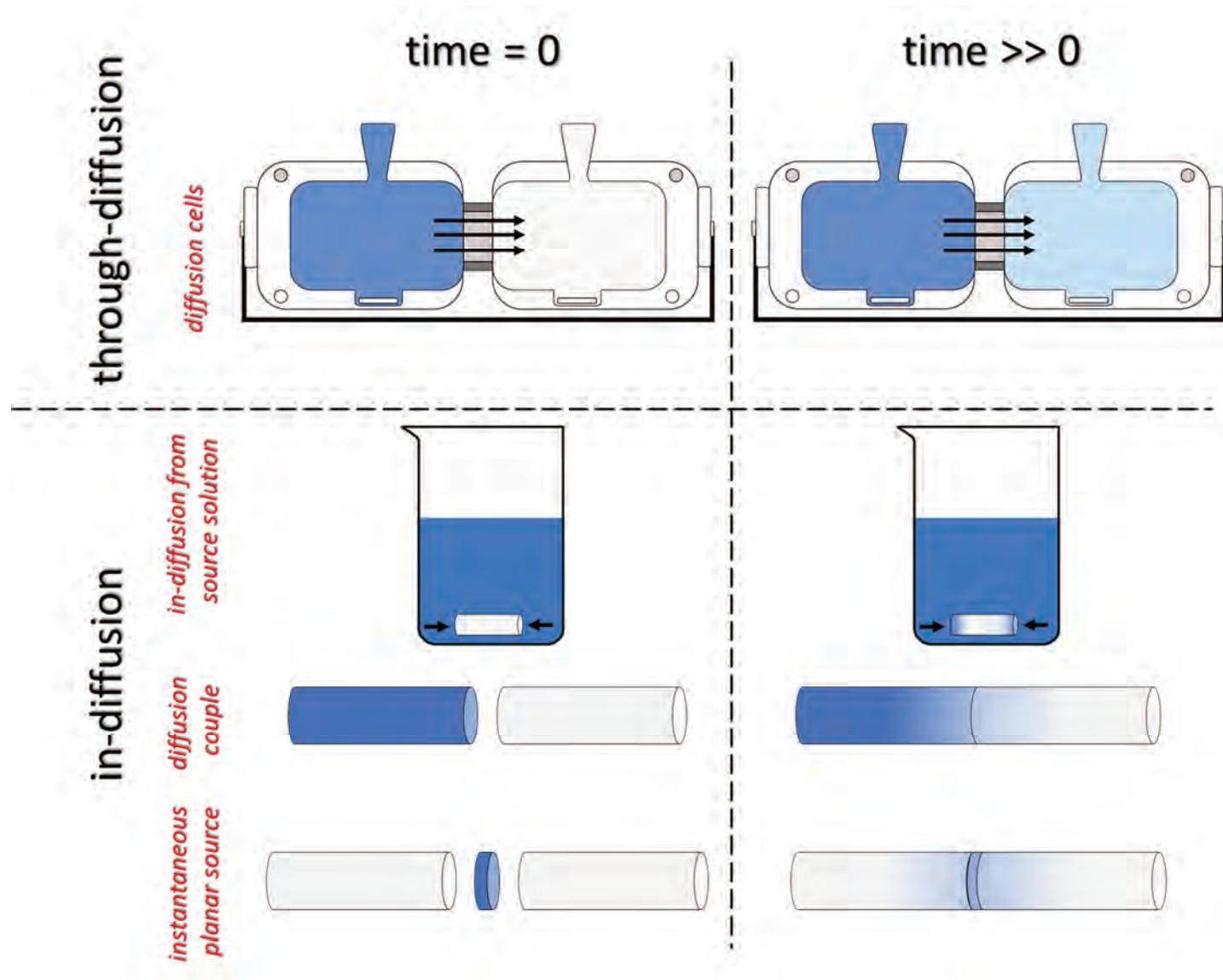
Fig. 15   Various setups used in the developed diffusion methodology

matrix and binding of copper ions to the contained humic acids and hence represents a quantitative parameter that illustrates how the binding of the solute on a molecular scale is manifested on the macroscopically visible slowdown of the diffusion process. This study hence confirmed that the diffusion-in-gel method represents a valuable option for reactivity and permeability mapping studies on both natural and artificial matrices containing humic substances. All tested methods proved themselves experimentally feasible and allowed easy and relatively quick determination of the diffusion coefficient as a parameter that characterizes and quantifies dynamic effects of HA-solute binding. The same conclusions have been reached also in a parallel study, in which the diffusion from the source solution with time-variable concentration[II]. In this work, we have also determined (effective) partition coefficient as an additional parameter that characterizes the macroscopic manifestation of HA-solute binding on the preferential absorption of the solute by the gel at the solution-gel interface.
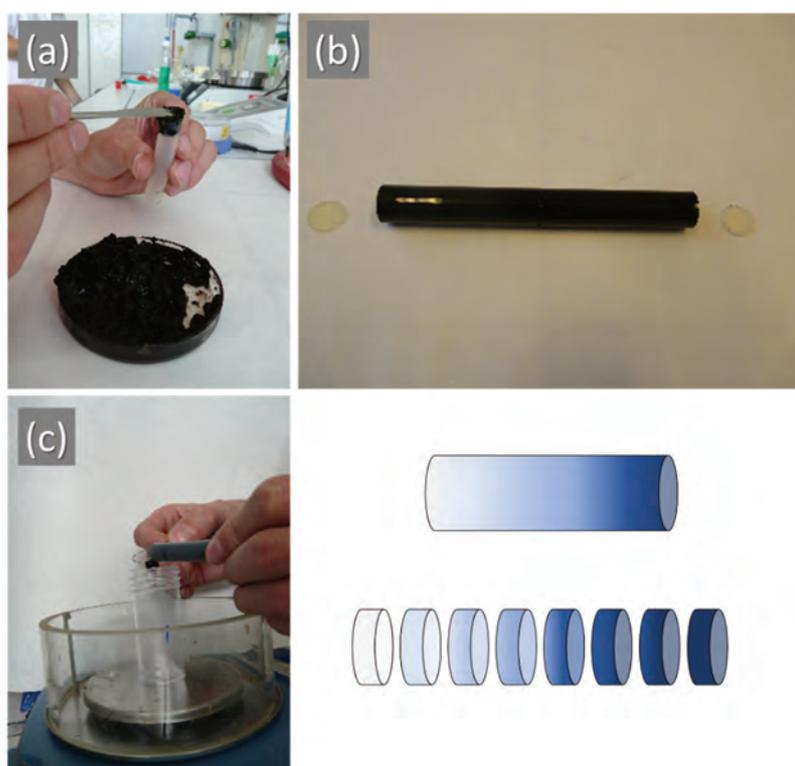
Fig. 16   The main experimental steps in diffusion studies on the humic acid gels. (a) Filling the gel into the tube carrier. (b) Diffusion experiment (in diffusion couple on the picture). (c) Slicing the gel in order to determine the concentration profile of the diffusing solute.

The basic methodology developed and successfully utilized in these initial works was supplemented with fractionation of the diffused copper ions according to the strength of its binding in the humic gel in the subsequent study[III]. For this purpose, extraction agents with increasing affinity to copper were used (water, 1 M $MgCl_2$ and 1M HCl, respectively). The results of this study showed that the distribution of diffusing copper ions among the determined fractions (freely moving, weakly, and strongly bound) stayed constant after passing a certain time. This indicates the existence of a binding equilibrium which is created and maintained as the diffusion of the ions proceeds. Hereby, an original diffusion-in-gel

---

[II]   Sedláček, P. and Klučáková, M. Simple diffusion method applied in evaluation of metal transport in model humic matrices. *Geoderma.* 2009, 153, 11–17. Attached as Appendix 2.

[III]   Kalina, M., Klučáková, M., and Sedláček, P. Utilization of fractional extraction for characterization of the interactions between humic acids and metals. *Geoderma.* 2013, 207–208, 92–98. Attached as Appendix 3.

technique was further enhanced in revealing the close interconnection between the strength of a solute binding and its mobility in the reactive matrix.

The above-mentioned works represented an important first step in the involvement of diffusion assays in an investigation of solute binding on HS and how it is reflected in the dynamics (e.g. barrier behavior) of the HS-containing systems. Nevertheless, we were well aware that this simple method suffered also some severe limitations. Above all, the procedure for the humic hydrogel preparations did not allow control of the relative content of HS in the gel. The low internal pH of the gel, induced by the acid-induced coagulation, also suppresses the dissociation of weakly acidic groups of HS and reduces the electrostatic binding of cationic solutes. Moreover, the aggregation behavior of HS is influenced by their molecular structure and it is, therefore, uncertain how the solute diffusion process would be affected by inevitable changes in the internal (physical) structure of the gel brought by the use of different HS (e.g. HS from different sources or with various chemical modifications). Therefore, we launched parallel research aiming at the development of an alternative methodology where these drawbacks would be overcome.

This research effort resulted in the design of novel method, that was first introduced in two subsequent papers published in the journal "Reactive and Functional Polymers"[IV,V] (the experimental framework is schematically shown in Fig. 17). The main innovation lies in the use of a carrier gel matrix, without any specific binding affinity towards the diffusing solute, in which the solute-binding humic component is physically trapped. Agarose was used as the inert gel-forming polymer and lignitic humic acids (HA) were penetrated in the physically crosslinked agarose matrix during the cooling of the agarose-HA solution. By this procedure, both the agarose and HA content in the gel can easily be manipulated. Furthermore, because the whole volume of the solution gelatinizes, gel samples of variable shapes and sizes can be prepared directly during the gelation in the suitable container without a need for filling of gel into a holder *ex post*. Aside from the lack of solute-binding structural functionality, agarose was chosen also because the process of its thermoreversible gelation is well understood and the textural properties of the resulting gels are described in details [83].

In the first from the paper series[IV], agarose (reference) and agarose-HA gels were subjected to through-diffusion of Methylene blue (MB) organic dye. This solute was chosen as a representative of amphiphilic organic cations (a detailed discussion of the environmental relevance of this class of compound will be provided in the next section). Although in the published studies we have continued to pay attention just to this type of solutes, during the optimization steps we confirmed experimentally that the methodology is universal with respect to the solute of interest. We have first focused on the steady-state through-diffusion arrangement implemented by the use of diffusion cells apparatus (see Fig. 15 and Fig. 17e,f). From the analysis of experimental data using a simple mathematical model (re-summarized in the paper) both the structural (effective porosity, tortuosity factor) and interaction parameters (apparent reaction equilibrium constants) that affect the diffusion of the solute were calculated. Similar to the diffusion of copper in the humic gels, the binding of MB to humic acids was demonstrated to have a significant influence on the diffusion process – with the content of HA in the gel, the time needed by MB to penetrate the gel from the donor to the acceptor solution increased, and the rate of MB's increase in concentration in the acceptor solution decreased at the same time. In this study, the outstanding potential of the diffusion-cells setup in the dynamic reactivity-mapping studies was confirmed. The great advantage of this method is that it is well applicable for the study of

---

[IV] Sedláček, P., Smilek, J., and Klučáková, M. How the interactions with humic acids affect the mobility of ionic dyes in hydrogels – Results from diffusion cells. *Reactive and Functional Polymers.* 2013, 73, 1500–1509. Attached as Appendix 4.

[V] Sedláček, P., Smilek, J., and Klučáková, M. How the interactions with humic acids affect the mobility of ionic dyes in hydrogels – 2. Non-stationary diffusion experiments. *Reactive and Functional Polymers.* 2014, 75, 41–50. Attached as Appendix 5.

the effects of various physico-chemical conditions such as temperature (as presented in the paper) or others such as pH or ionic strength (confirmed in other non-published experiments).
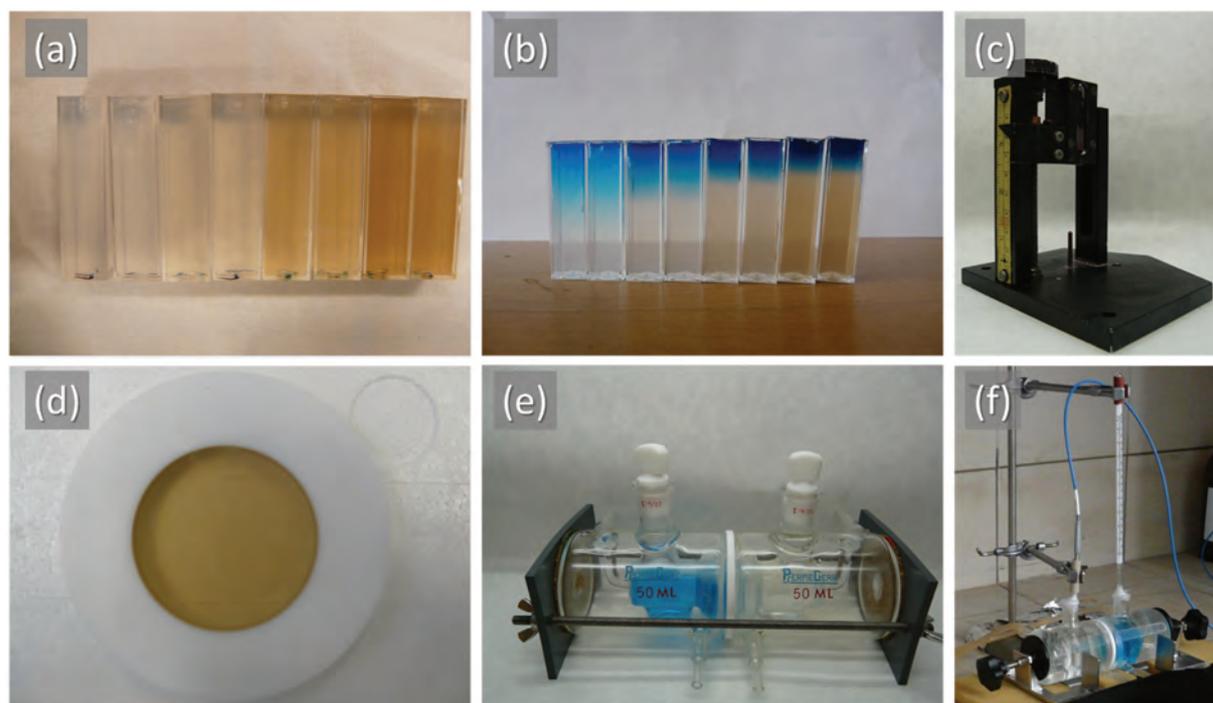
Fig. 17   Developed methodology for solute binding studies based on diffusion studies in agarose gels. Equipment for non –stationary (a – c) and steady-state (d – f) diffusion experiments. (a) Cuvettes with various concentrations of humic acids immobilized in agarose hydrogel, (b) the same cuvettes after 48 hours of contact with a solution of methylene blue. (c) Original accessory for measurement of UV-VIS spectra at different positions from the solution-gel interface. (d) Gel-holding insert for the diffusion cell apparatus. (e) Side-by-side diffusion cell setup with (f) online monitoring of solute concentration in the acceptor compartment by fiber optic spectrophotometry.

The steady-state diffusion experiments were complemented by a non-stationary in-diffusion study presented in the succeeding paper[V]. In this study, another representative of cationic dyes (Rhodamine 6G, R6G) was used in parallel to MB to provide a more general view of the interactions between HA and organic cations. Diffusion proceeded from the source solution of the respective dye into the plastic cuvette filled with the gel (agarose or agarose-HA with different HA content, see Fig. 17a). As can be seen in Fig. 17b, the effects of the solute binding to HA can be seen even visually. On the one hand, the solute is concentrated in the gel by the presence of HA (note that the intensity of the gel coloring near the boundary increases with the content of HA in Fig. 17b). On the other hand, mobility of the solute is (once again) significantly reduced by the presence of HA as demonstrated by decreasing depth of the solute penetration. The power of the technique to embrace both these effects simultaneously is very important, because, in a fact, it is exactly the balance of these two opposing effects (tendency to "suck" the solute out of the surroundings vs. slowing down its movement in the system) that forms the actual barrier performance of a reactive system. In order to quantify these visually observed effects, we have constructed a simple accessory that allowed vertical movement of the gel cuvette with the gel sample in a spectrophotometer (Fig. 17c) and we, hereby, determined the distribution (i.e. the concentration profile) of the diffusing dye in the gel at different experimental times. We have also described how the temperature, pH and ionic strength influence the diffusion of the solutes. Same as in the previous paper, we calculated apparent equilibrium constants and partition coefficients as the quantitative parameters describing the HA affinity towards the solutes under corresponding experimental conditions.

In general, all the above-summarized studies confirmed that diffusion-in-gel methodology represents an innovative and valuable experimental tool for the investigation of interactivity and barrier properties not only for HA, but of diverse functional polymers of a biological, environmental or industrial concern. The combination of steady-state and non-stationary diffusion experiments provides a reasonably complex overview of the transport properties of a studied system. While the experiments in diffusion cells focus on the steady-state stage of the diffusion process and illustrate primarily the barrier properties of a material after its penetration by the solute, the transient stage of the process is described by the non-stationary experiments more elaborately, enabling further insight into particular effects which define the rate of the solute transport. In both diffusion setups, the influence of various physico-chemical conditions can be studied. Last but not least, the effects of the specific interaction between the solute and the reactive medium are so pronounced that they can be followed with simple and cheap laboratory equipment (or even visually), which makes this methodology attractive also for educative purposes. As will be discussed in the following chapters, the diffusion-in-gel methodology developed in this study was successfully applied also in the characterization of interactions of low molecular solutes with other reactive polymers (see chapter 7.1) and in a modified form also in the study on transcuticular penetration of humate-based biostimulants (chapter 5.1.4). Furthermore, it also inspired us in the development of the concept of semi-interpenetrated polymer network gels as novel promising soft-matter materials with tailorable mechanical and transport performance (chapter 7.2).

Nevertheless, the usability of all the above-discussed techniques is limited to the systems, where the reactive component (HA) is capable of being transformed into the gel form. But what if this is not the case? For instance, what if the required concentration of the component is so high or the molecular weight is so low that it can be neither gelled nor interpenetrated into a supporting gel? Fulvic acids can be given as a simple example of these hard-to-gelatinize compounds. We, therefore, searched for an alternative diffusion-based experimental technique also for these systems and found the solution in dialysis experiments[VI] (see Fig. 18). These experiments can be easily performed in the diffusion cells apparatus used also for the through-diffusion assays. In the dialysis binding study, diffusion cells, initially filled with solutions of HS and low-molecular solute, respectively, are separated by a dialysis membrane that is permeable only for the later solute. During the experiment, the decrease of the concentration of the permeant solute in its source compartment is monitored in time until the equilibrium is reached. Hereby, both the kinetics of the solute diffusion and its equilibrium distribution between bound and unbound forms can be investigated. This method hence complements well the diffusion-in-gel techniques in the robust methodology that we have developed and optimized for the solute-binding studies on HS.

5.1.2 On the role of carboxylic groups in the binding of amphiphilic substances by humics

In the preliminary binding studies, summarized in the previous section, the newly developed diffusion methodology was used in experiments that aimed primarily at verifying that the solute-HS interaction occurs and that it is effectively demonstrated in the solute diffusion in the system. To provide a more detailed understanding of the mechanism of these interactions, a follow-up study was designed to focus more on the structural aspects of the solute binding.

As already emphasized, HS possess a complex amphipathic (supra)molecular structure that provides the universal binding ability. The irreplaceable role of polar structural moieties (mainly carboxyls and alcoholic/phenolic hydroxyls) in binding the hydrophilic solutes and surfaces [84] has been widely reported. Similarly, sorption capacity for non-polar compounds such as polycyclic aromatic hydrocarbons has usually been attributed to the content of hydrophobic moieties including aromatic rings [85] and aliphatic carbon groups [86]. We decided to focus our research on the role of HA's carboxylic groups in binding hydrophilic and amphiphilic solutes. For this purpose, we

---

[VI] Rybárik, J., Sedláček, P., and Klučáková, M. Transport of Organic Dyes in Systems Containing Humic Acids. *Inżynieria Mineralna.* 2019, 21.
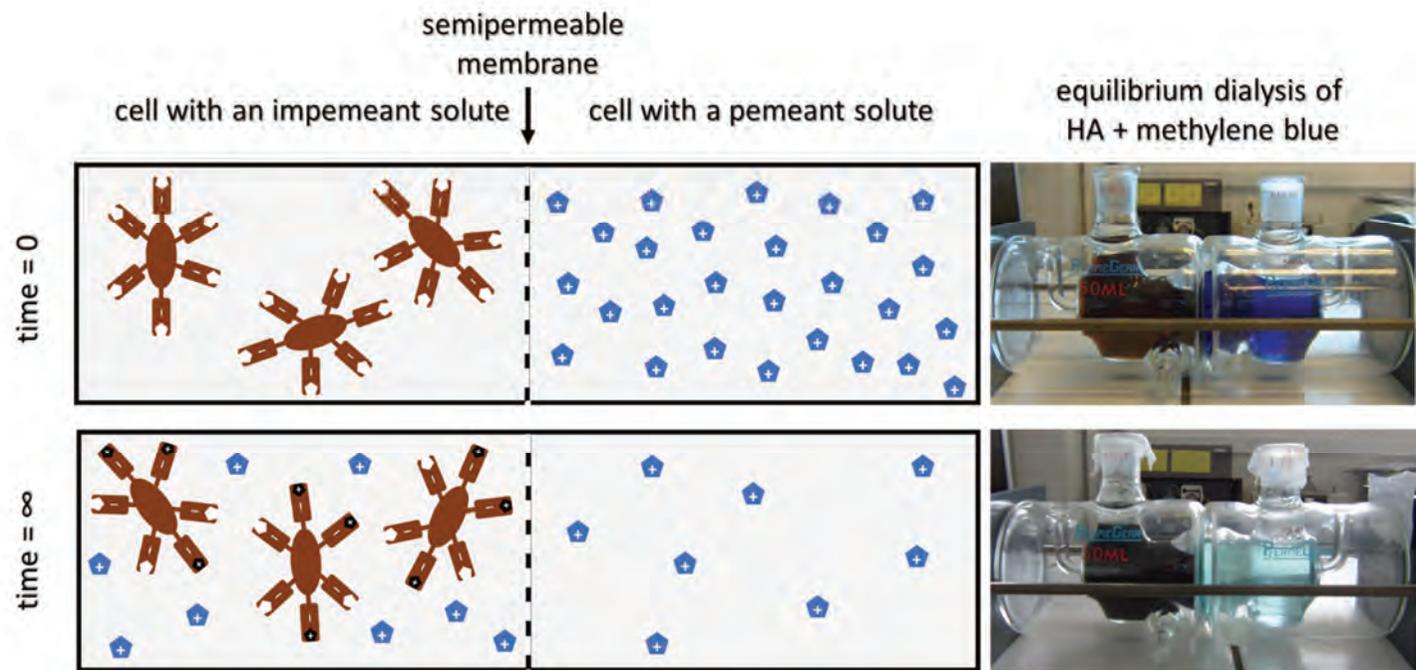
Fig. 18   Schematic diagram of the solute binding study based on equilibrium dialysis (*left*). At the start of the experiment, the impermeant binding solute is separated from the permeant solute by an appropriate semi-permeable membrane. The concentration of the permeant solute is monitored until the equilibrium is reached. Images of the experimental apparatus at the start of the experiment (*top*) and at the equilibrium (*bottom*) are also shown (*right*).

were looking for the way how the content of –COOH binding sites in the structure of studied HS may be controlled. Based on our copperation with research group of Prof. Laurent Grasset from University of Poitiers, we have implemented the method of selective methylation of HA's carboxyls in order to block these binding sites; among the published methylation procedures, we have chosen exposure of HA to TMS-diazomethane in methanol [87]. The reaction mechanism of this methylation procedure is shown in Fig. 19. High effectivity of this substitution procedure was repeatedly confirmed spectroscopically (^{13}C NMR, FTIR) as well as by means of potentiometric titration.

At first, we implemented the use of methylated lignitic HA into the original methodology developed for the study of copper-binding in coagulated HA hydrogels[VII]. Using the technique of instantaneous planar source, we monitored the diffusion of copper ions in hydrogels prepared from mixtures with different relative content of original and methylated HA. As expected, the relative content of methylated humic acids affected the rate of the transport of copper in the gel. Nevertheless, from the more detailed evaluation of the diffusion data, we have found that this effect originates from the structural changes in the gels rather than from the affected solute binding. This confirmed the expected drawbacks of the coagulated humic gels – the internal structure of these gels can be severely altered when the chemical structure of the HS is changed. Therefore, further experiments were performed with HA (original and the methylated ones) interpenetrated in the supporting agarose gels.
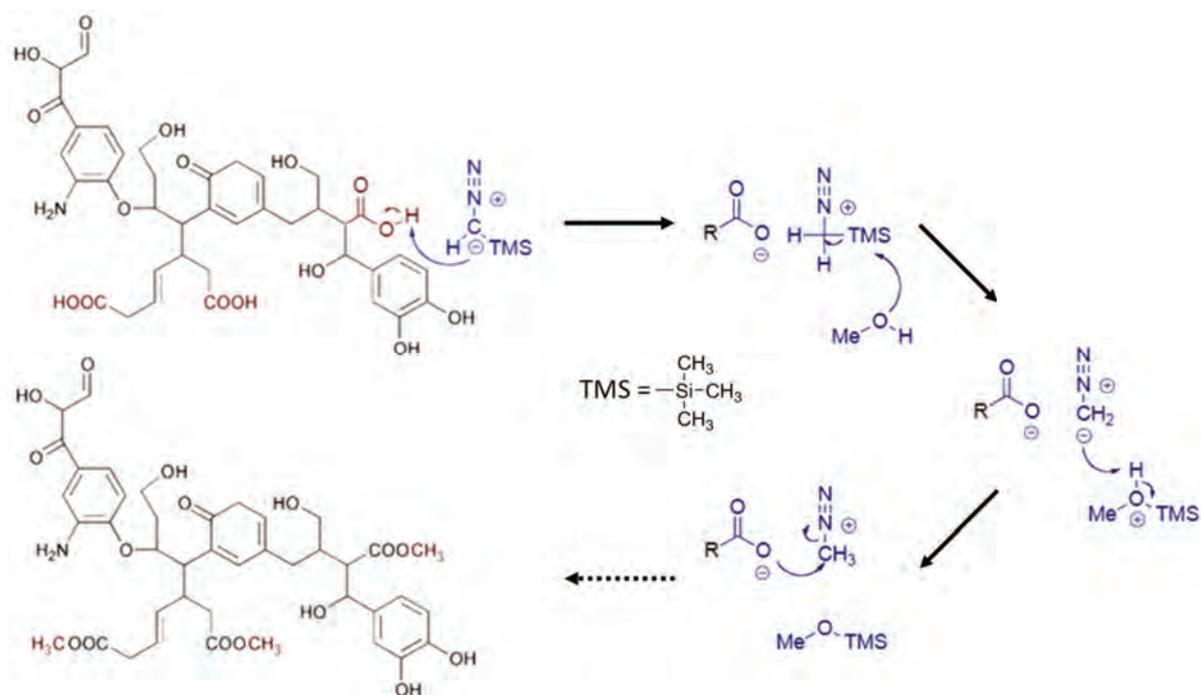
Fig. 19   Reaction mechanism of HA methylation by trimethylsilyldiazomethane in methanol used in our study on –COOH involvement in solute binding on humic substances.

In these experiments, we have also turned our attention from metal ion solutes to cationic organic dyes. The first reason for this switch comes from the experimental constraints – the higher absorption coefficient of the organic dye allows for analyzing diffusion and binding of the solute at lower concentrations as compared to the inorganic ions. Nevertheless, the main motivation for the involvement of this type of organic solutes lies in their environmental relevance – the combination of aromatic and/or aliphatic structural backbone with a positively charged polar group(s) is common for

---

[VII]   Klučáková, M., Kalina, M., Sedláček, P., and Grasset, L. Reactivity and transport mapping of Cu(II) ions in humic hydrogels. *Journal of Soils and Sediments.* 2014, 14, 368–376. Attached as Appendix 6.

numerous compounds of considerable ecological importance like pesticides, growth retardants, and industrial waste materials (e.g. surfactants, disinfectants or industrial dyes).

We have published the results of a comprehensive study on the role of –COOH groups in the binding of charged organic solutes (Methylene blue and Rhodamine 6G) on lignite HA in the journal "Chemosphere"[VIII]. In this study, we analyzed HA entrapped in agarose gels via steady-state through-diffusion experiments, transient in-diffusion study and also an equilibrium partitioning assay. In this complex transport-mapping study, we have revealed surprisingly similar effects of original (HA) and methylated (mHA) humic acids on the partitioning and rate of transport of both tested solutes in the humics-interpenetrated agarose gels. Because the methylated carboxyls in mHA are unable to dissociate, this has indicated the simple electrostatic attraction between the positive charge on the solute and the negative charge brought by the HA's carboxyls contributes to the binding of the charged organic solutes less than expected. We proposed in the paper that the interactions between aromatic moieties in the molecular structure of the solute and humic substances play a crucial role. Moreover, we have complemented this diffusion study also with conventional batch-sorption experiments in the suspension of HA. On the significant discrepancy that we found between the sorption and diffusion results, we have experimentally demonstrated the previously proposed benefits of our methodology – we have shown how methylation of HA changes the textural properties of solid HA and hence also their sorption performance. Unlike the suspension, in the form of gel-immobilized hydrated chains, HA's binding performance is driven primarily by the molecular structure and the structural aspects of the interactions are hence monitored much more reasonably.

In the follow-up study, we have subjected original and methylated lignite HA also to the dialysis experiments introduced in the previous section[VI]. From the collection of the data obtained by the diffusion and dialysis experiments, it can be clearly illustrated that a wide range of solute-to-HA concentration settings can be covered by different setups in the proposed methodology. In Fig. 20, values of apparent binding constants of the solute (MB) are provided for interactions with HA (original lignitic and methylated lignitic, respectively) as calculated from the diffusion and dialysis data. In a fact, this constant represents the effective equilibrium constant of the supposed transition between free and bound solute

$$\mathrm{MB_{free}} \xrightarrow{K_{app}} \mathrm{MB_{bound}}$$

$$K_{app} = \frac{[\mathrm{MB_{bound}}]}{[\mathrm{MB_{free}}]},$$
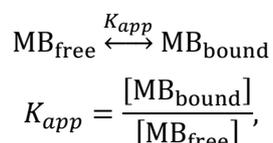
where $[\mathrm{MB_{bound}}]$ and $[\mathrm{MB_{free}}]$ represent the equilibrium activity (that equals dimensionless concentration for the diluted systems) of the bound and free solute, respectively. We have discussed in detail in our published works[I, III-V, VII] how the value of the apparent binding constant can be calculated from the experimentally determined diffusion coefficients. In the dialysis study, the constant is determined directly from the distribution of a solute between the two chambers (equilibrium constraint of the same activity of the free form of the solute is assumed).

It can be seen in Fig. 20 that the particular value of the binding constant varies in the orders of magnitude not only with the change in solute-to-HA concentration but also when the constraints of the transport phenomenon or the colloidal form of HA are altered. Once again, this illustrates that the manifestations of the binding of the solute on its transport in a system are strongly conditions-specific. On the other hand, it also shows that the proposed methodology is outstandingly robust – selection of an appropriate experimental technique enables investigation of the binding under particular required circumstances (transient, steady-state or equilibrium). Last but not least, a comparison of K_{app} values of original HA and the methylated ones show that the contribution of –COOH groups to the solute binding depends strongly on the solute-to-HA concentration and the mode of transport. It can be seen

---

[VIII]   Smilek, J., Sedláček, P., Kalina, M., and Klučáková, M. On the role of humic acids' carboxyl groups in the binding of charged organic compounds. *Chemosphere.* 2015, 138, 503–510. Attached as Appendix 7.

that under some circumstances, the binding of MB on methylated HA is apparently stronger as compared to the original HA. This further indicates an essential role of other than carboxylic structural motifs in the binding of positively charged organic compounds.
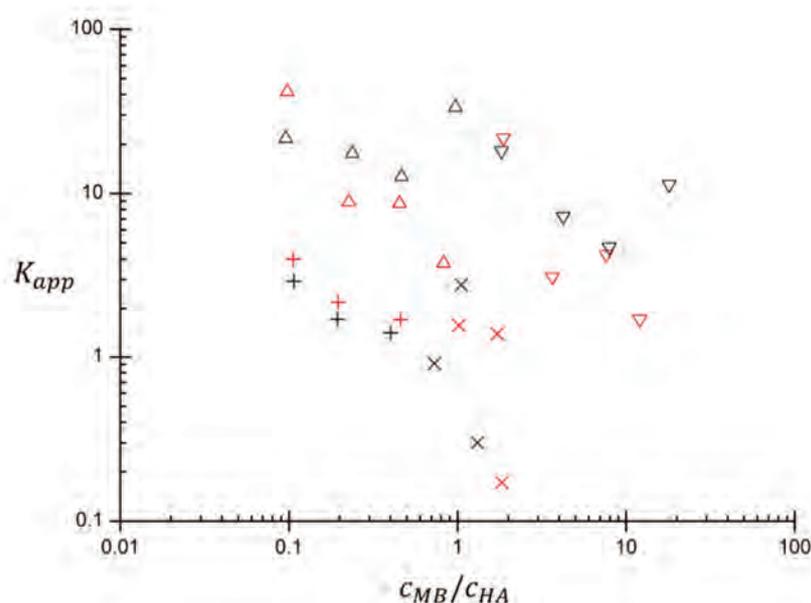

*Fig. 20   Equilibrium of HA-charged organic solute binding is strongly concentration-dependent. The figure shows values of the apparent binding constant of MB binding on lignite humic acids original (*black*) and selectively modified by methylation of carboxylic groups (*red*) plotted against the ratio of total concentrations of MB and HA in the sample (*in the agarose-HA gel in diffusion experiments, in the HA containing receptor cell in dialysis experiments*). K_{app} values were calculated from data obtained in steady-state through-diffusion experiments (×), transient in-diffusion experiments (+), dialysis experiments with 0.1 g/L HA receptor solution (Δ) and dialysis experiments with 0.05 g/L HA receptor solution (∇). For the diffusion experiments, c_{MB}/c_{HA} represents the sample-averaged value calculated as the ratio of total contents of the two components in the gel sample.*

It should be emphasized that this phenomenon seems to be general for the binding of various charged organic compounds on diverse humic acids. Aside from the lignitic HA, we have confirmed the similar binding behavior of original and methylated humic acids also for IHSS reference humic material[IX]. Furthermore, most recently, we have also found similar binding behavior for cationic surfactants (Septonex in particular) – similarly to the aromatic organic cations, also these aliphatic charged structures are significantly bound to humic acids and this binding is only slightly suppressed when the HA's carboxyl groups are masked with selective methylation (data not published yet). Hence, I can summarize a great deal of experimental work that we have devoted to understanding the binding of charge organic compounds to humic substances as follows: unlike the binding of strictly hydrophilic (e.g. metal ions or polar mineral surfaces) or hydrophobic (e.g. polyaromatic hydrocarbons) materials that can be easily attributed to distinct binding regions in the supramolecular conformation of humics (hydrophobic core in the latter case, polar surface in the former one), in the binding of amphiphilic solutes both HA's regions participate on the solute binding with the relative contributions depending on the particular binding conditions (the correspondingly updated general concept of HA binding is provided in Fig. 21).

[IX] Smilek, J., Sedlacek, P., Lastuvkova, M., Kalina, M., and Klucakova, M. Transport of Organic Compounds Through Porous Systems Containing Humic Acids. *Bulletin of Environmental Contamination and Toxicology.* 2017, 98, 373–377.
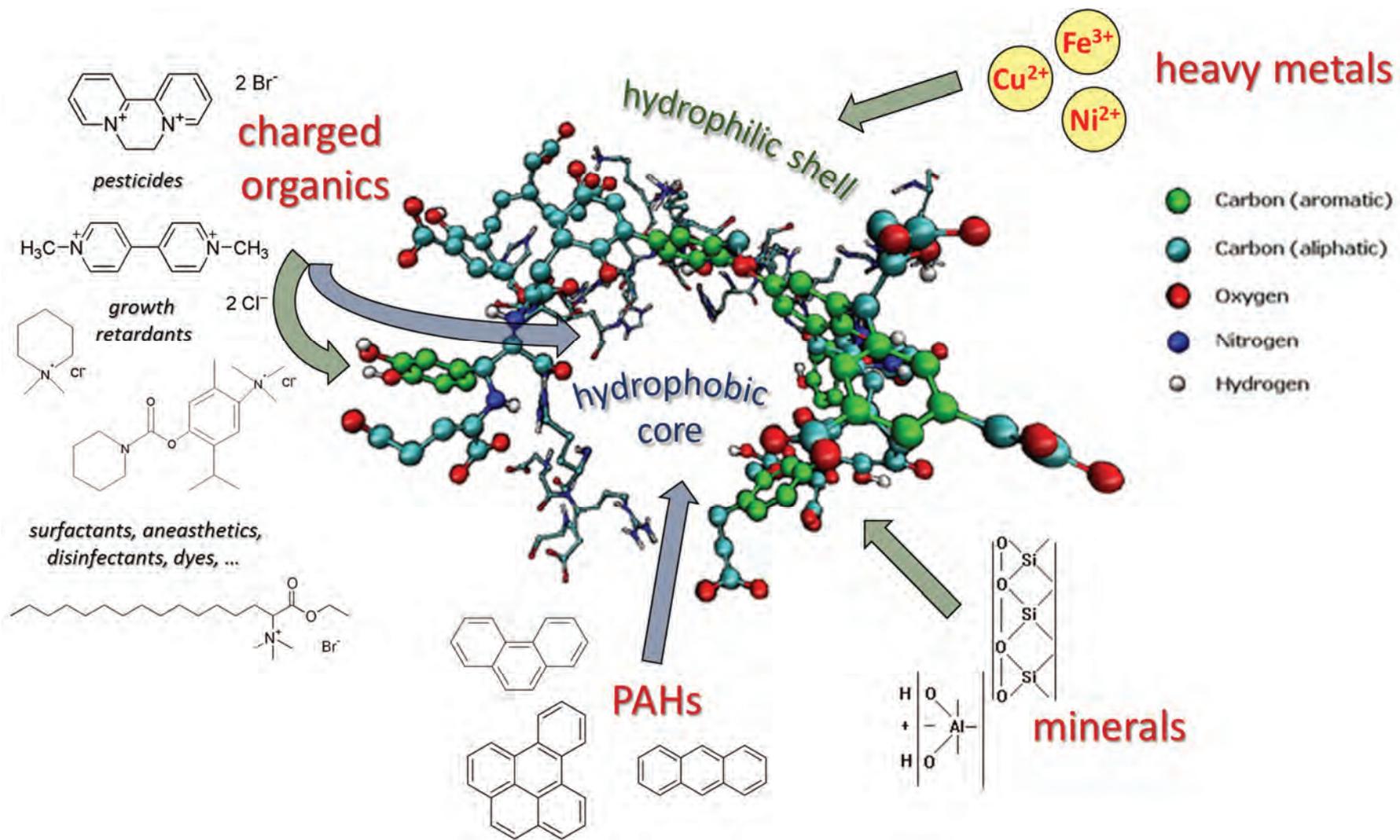
Fig. 21   Supramolecular architecture of humic acids providing different binding preferences according to the sorbate molecular structure. The concept of binding charged organic compounds was updated based on our experimental study.

Last but not least, we have also performed a preliminary study focused on identifying the particular non-polar functionalities that mediate this HA-organic ion binding. Using methods of thermal analysis (isothermal titration calorimetry) we revealed that the binding enthalpy of the interaction is negligible. This excludes from further consideration strong non-covalent interactions such as ion-ion and hydrogen bonding. Furthermore, in results of absorption and fluorescence UV-VIS spectroscopywe have revealed characteristic signatures of charge-transfer interactions. Static quenching of the solute fluorescence was found for interactions of MB and R6G both with HA (both methylated and the original ones). Differential absorption spectra manifested charge transfer with the characteristic red-shift and hypochromic effect (see Fig. 22a,b). For the non-fluorescent solute (Septonex), we turned our attention to the autofluorescence of humic acids and found the signs of charge-transfer interactions in the HA's excitation-emission matrices (note the blue shift in fluorescence peaks in Fig. 23). Therefore, we conclude this interaction-mapping study (not published yet) in that the aromatic functionalities play a crucial role in the binding of organic ions on humic acids probably via cation-π, and π -π stacking.
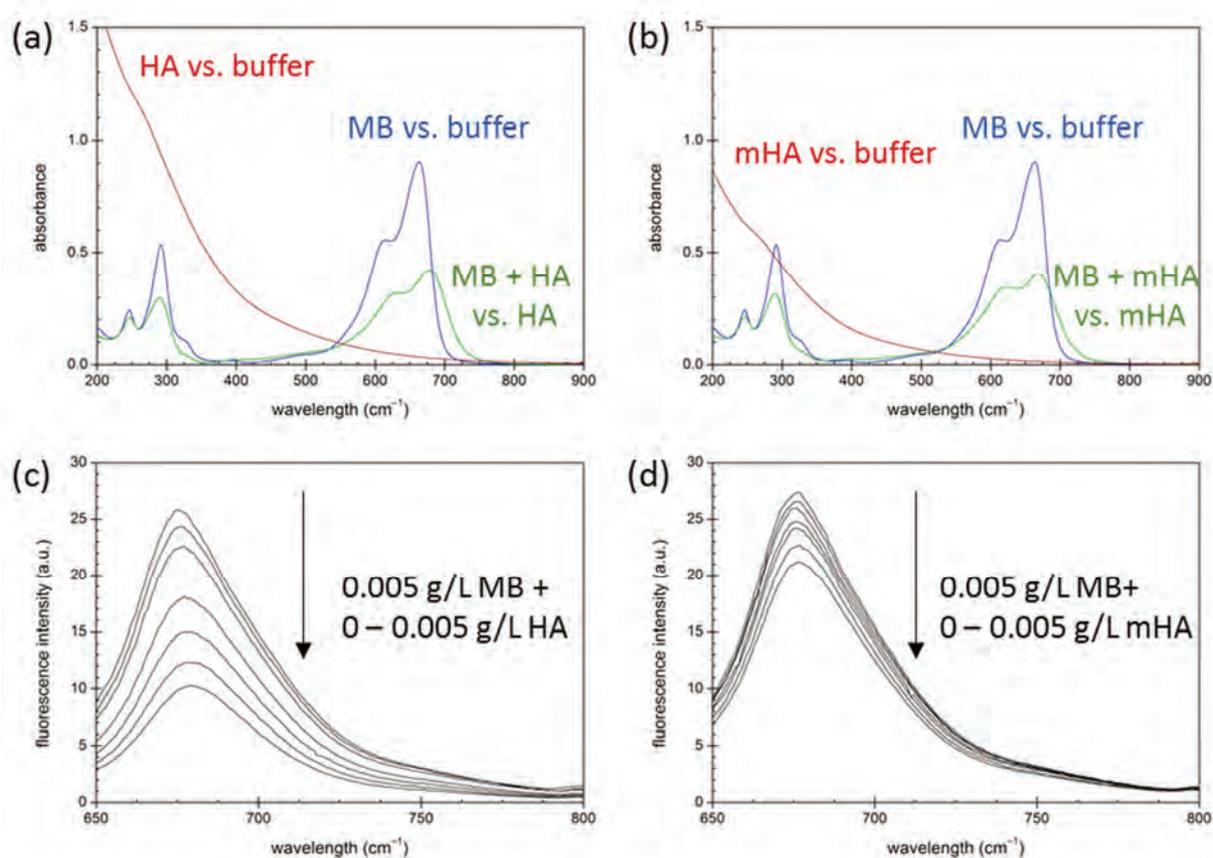
Fig. 22   Spectral manifestations of interaction between Methylene Blue and Leonardite standard IHSS humic acids (a, c) and methylated Leonardite standard IHSS humic acids (b, d). Results of differential UV-VIS absorption spectroscopy (a, b) and steady-state fluorescence spectroscopy (c, d). For differential absorption UV-VIS spectroscopy, data for 20 mg/L HA and mHA and 5 mg/L MB are shown; green spectra represent spectra recorded for mixture solution of (m)HA and MB measured against corresponding (m)HA solution.
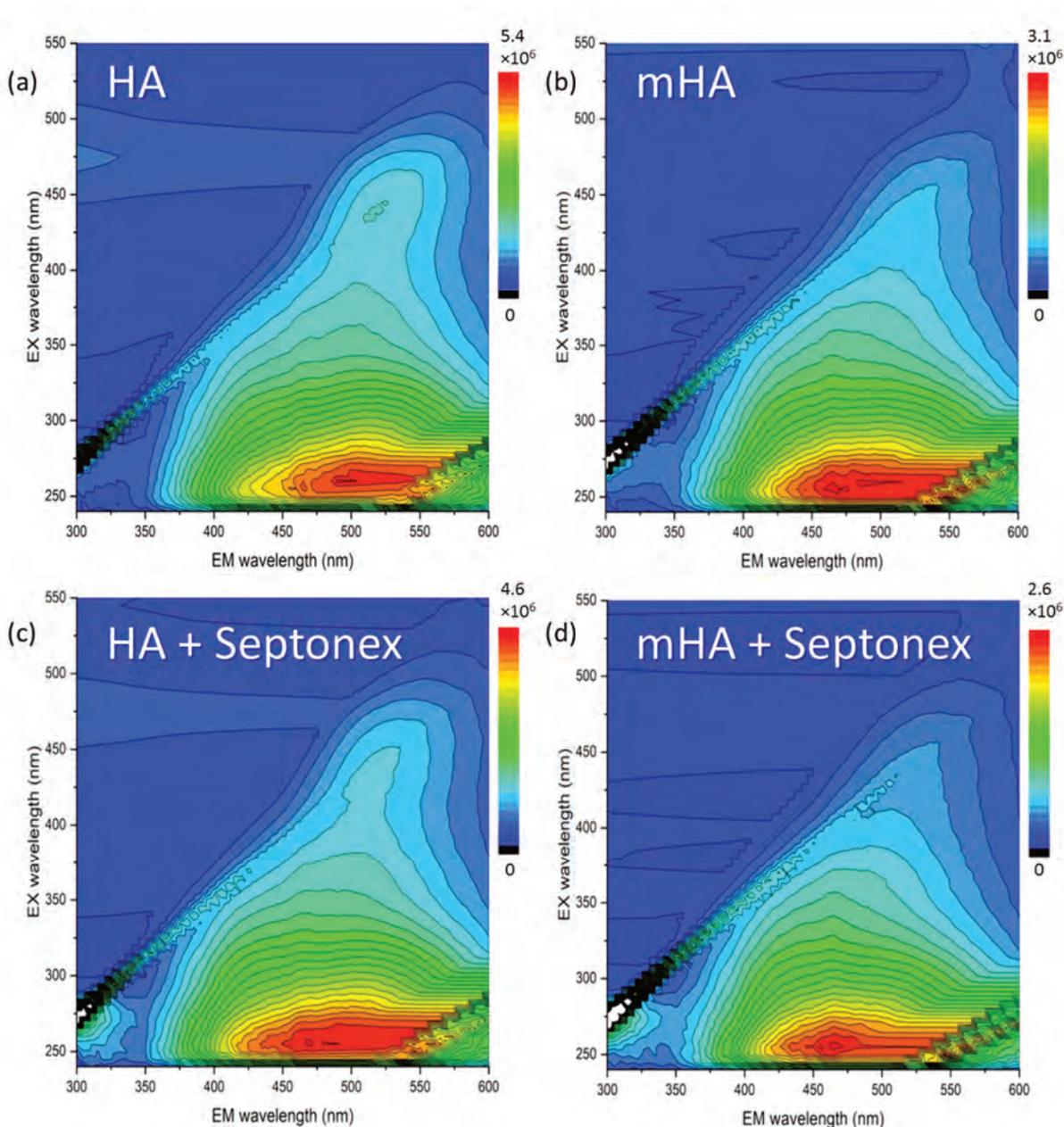
Fig. 23 Results of steady-state fluorescence study on the interactions between Septonex (0.001 g/L) and 0.01 g/L Leonardite standard IHSS humic acids (a, c) and methylated Leonardite standard IHSS humic acids (b, d). It can be seen that the interaction is manifested in the spectra by blue shift in fluorescence maxima both for original and methylated HA.

5.1.3   Polarity-based fractionation: an easy tool for revealing the molecular architecture

In the previous two parts of this chapter, I have shown how we had started with an initial physico-chemical assessment of the question of how binding of a solute on the reactive component of an environment affects the solute's molecular transport there and came to the development of a simple, widely accessible experimental methodology that allows a reasonable investigation of this phenomenon both in a qualitative and quantitative way. We have placed a great emphasis, particularly on the simplicity and instrumental modesty of the approach because we believe that it is necessary for its wide dissemination and verifying its usefulness by as many research teams as possible. Similarly, we approached another of the current hot-topics in humic research – experimental analysis of the supramolecular architecture of HS.

We have been inspired by recent trends in structural analyses on HS. In 2011, a novel stepwise fractionation procedure was proposed by the Italian research team of prof. Piccolo for separation of individual molecular components according to the strength of their binding in the structure of the HS [88]. The authors conceived the experimental approach on the supramolecular conception of humic substances that they had continuously supported [75, 76], and called it "Humeomics". The sequential extraction procedure is designed in order to release constituents of humic supramolecular aggregate bound by weak intermolecular forces and ester or ether linkages. During each fractionation step (there are four in total), aqueous and organic fractions are obtained which are characterized for their structure by advanced analytical techniques (GC-MS, HPSEC-ESI-MS, NMR). The authors proposed that their stepwise fractionation increases significantly the analytical identification of molecular components of HS and that the Humeomics approach is a reasonable experimental path for mapping humic molecular composition and for assessing humus origin and formation.

In our work, we focused on an alternative way of reducing the structural complexity of humics. We have proposed an original sequential fractionation approach using organic solvents of increasing polarity on peat HA (see Fig. 24) and subjected the obtained organic fractions to a complex physicochemical characterization utilizing rather basic and widely accessible methods of structural and compositional analysis (elemental analysis and various spectroscopic methods – UV-VIS, FTIR, fluorescence spectroscopy, and NMR)[X]. Although the use of solvents with varying polarity had been used before in some studies on the extraction of the humics from their natural sources [89–91] and solubility of isolated HS in various organic solvents had been assessed as well [89], to our best knowledge, none systematic polarity-based fractionation of isolated HS had been performed before. We hence suggested this approach as a logical and easy to implement an alternative to more experimentally elaborate and instrumentally demanding designs such as Humeomics.
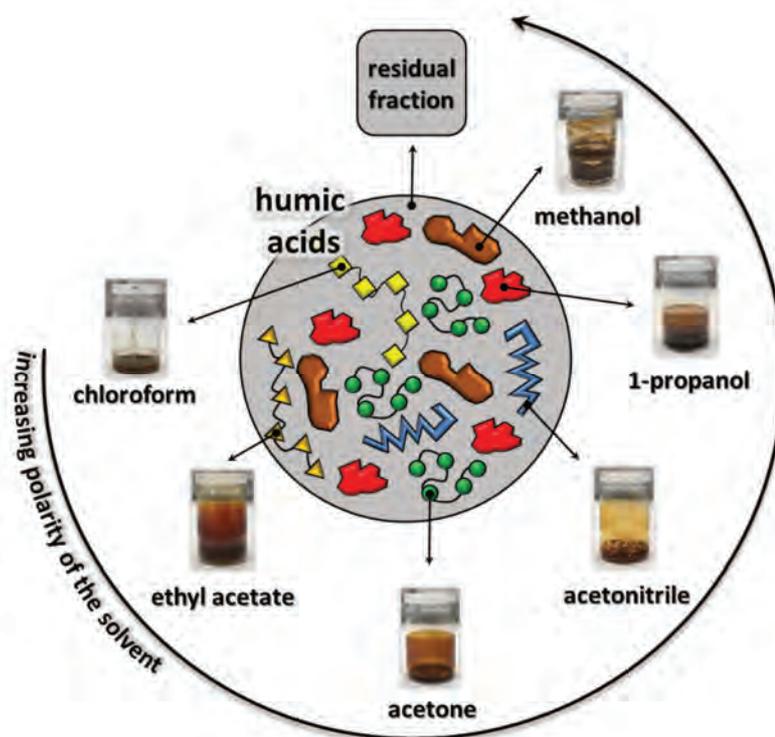

Fig. 24   Schematic diagram of original polarity-based extraction method developed for fractionation of humic acids

---

[X] Enev, V., Sedláček, P., Kubíková, L., Sovová, Š., Doskočil, L., Klučáková, M., and Pekař, M. Polarity-Based Sequential Extraction as a Simple Tool to Reveal the Structural Complexity of Humic Acids. *Agronomy.* 2021, 11, 587. Attached as Appendix 8.

Experimental results that we published in the study[X] support the current view that not only the natural organic matter but also the isolated HS still represent a complex mixture of separable molecular constituents with specific structural and physicochemical properties. For the peat HA analyzed in our study, we confirmed that the individual fractions, isolated by the proposed polarity-resolved fractionation technique, are mutually different concerning their origin, molecular weight, aromaticity, and the content and composition of heteroatomic functional groups. As expected, fractions extracted with most apolar solvents (trichloromethane and ethyl acetate in our sequence), showing the structural features characteristic of lipidic compounds (such as low aromaticity, low oxygen and nitrogen content, high CH_2 to CH_3 ratio), while the other fractions are in general more aromatic and richer in polar (mainly oxygen-containing) groups. Fraction extracted with acetonitrile stood out from the others with low aromaticity and high content of protein-like structural motifs, while the last two (alcohol extracted) fractions were rich in carbohydrate and plant pigment residues.

The pilot experimental study that we published has hence provided a clear confirmation that the proposed polarity-based fractionation procedure represents a simple but useful approach to a structural analysis of complex heterogeneous organic matrices such as humic substances. Systematic utilization of this methodology in the comparative study involving HS differing in type (HA, FA, humin) and origin (terrestrial, aquatic) could contribute to refining the current notion of the supramolecular structure of humic substances. In the paper, we also proposed further improvements of the approach. For instance, it would be extremely interesting to complement the complexity-reducing analytical step (i.e. the fractionation) with the reversed "synthetic" perspective where the compositional and structural parameters of the obtained fractions would be synthesized and then reassembled structural characteristics (e.g. the synthesized spectra) were compared with those of the parental humic material. This could provide a more complex view on - not only what constituents form, but also how they are bound together in - the humic suprastructure. And as I emphasized in chapter 4 (see Fig. 10), it is just the understanding of specific roles of molecular interactions in the structure and performance of natural systems where I see the irreplaceable contribution of physical chemistry in life sciences.

5.1.4   Transport of humic substances through skin and plant cuticle

As I have already stressed in the introduction to humic substances, it is not only the intrinsic environmental and ecological role that they play in their natural habitats but also their outstanding application potential, that makes these substances so attractive scientifically. Among the wide range of proposed application fields (a few of them are highlighted in the introduction part of section 5.1), utilization of biological effects of humic substances in the production of plant growth stimulants, veterinary medicine and also human health-care is currently gaining ground. Figuratively speaking, the scientific attention is slowly but surely shifting from the effect of HS on environmental health to the effect on the health of individuals (plants, animals and humans). We have been attracted by this fascinating branch of HS research as well. Leaving the biological effects themselves aside for experts in the field, we have focused on another aspect common for all kinds (i.e. plant, animal or human) of health care applications of HS –the ability of HS to penetrate into an organism through its surface.

Initially, we focused our attention on the penetration of liquid HS through plant cuticles. This was motivated by the growing interest – not just scientific, but also commercial – in the utilization of liquid HS in the production of plant biostimulants (mainly for foliar application). Numerous works reported on the biostimulant effects of humates, namely on the effect on plant growth [92, 93] and nutrient uptake [94], hormone-like [95, 96] and enzyme-promoting effects [97, 98], as well as some effects enhancing photosynthesis and seed-germination [99, 100]. On the other hand, a debate has arisen about the real efficiencyand economical feasibility of the application of humates in agriculture. It was stressed by some authors that the actual data on the benefits of the use of humates is rather ambiguous or inconsistent [101–103] and that a comprehensive physico-chemical characterization and a careful assessment of the mechanism of their foliar action are still needed [103]. Considering the absorption of humate by the plant organism as a critical step preceding the biological action, and taking

into account our previous experience with diffusion-in-gel techniques, we, therefore, focused on the development of experimental methodology for assessment of the rate of trans-cuticular transport of humates into plants.
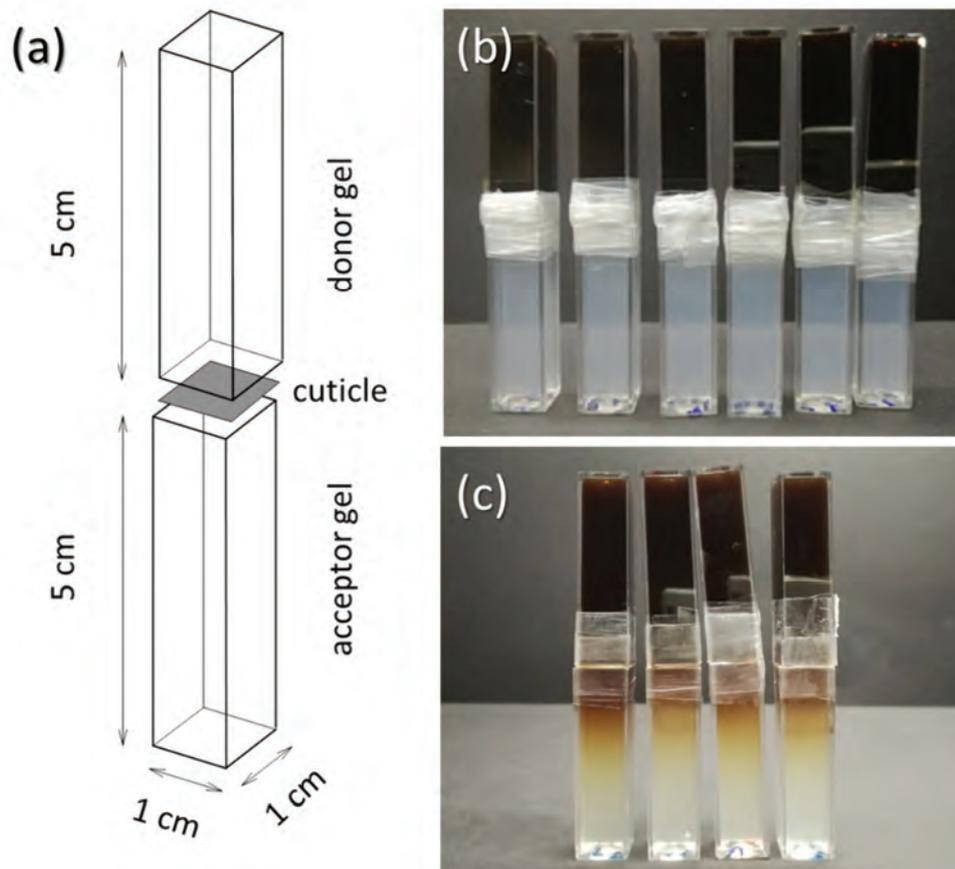
Fig. 25   Experimental study of the transport of humate-based biostimulants through plant cuticles. (*a*) *Schematic diagram of the experimental setup – diffusion couple of donor (i.e. humate containing) and acceptor agarose gels separated by isolated plant leaf cuticle.* (*b*) *Diffusion couples at the start of the experiment.* (*c*) *Diffusion couples after 7 days of the experiment (chemically isolated abaxial cuticle).*

We have designed a simple diffusion-mapping technique for the in-vitro investigation and quantitative description of the penetration of humates through the plant cuticle. The method is based on spectrophotometric monitoring of the humate diffusion through an isolated plant cuticle that is placed between two agarose hydrogels forming the common diffusion couple arrangement. We published results of the pilot study[XI] on the usability of the technique where we had used artificial lignohumate and the cuticles obtained from the leaves of *Prunus laurocerasus* plant via chemical and enzymatic isolation procedure, respectively. The schematic representation of the method together with an illustration of the time evolvement of the diffusion experiment is shown in Fig. 25. In the study, we have demonstrated how the rate of lignohumate penetration differs for the cuticles isolated in a chemical and enzymatic way. Furthermore, we have also confirmed that barrier properties of the stomatous and astomatous sides of a leaf differ significantly. Aside from the particular results on the transport of used lignohumate through the tested cuticles, we have provided a general discussion of the pros and cons of the proposed technique in the paper. In general, the proposed diffusion technique represents an easy and cheap tool for an in-vitro experimental assessment of the transcuticular penetration ability of humates from liquid agrochemical preparations. It has no ambition to simulate

---

[XI] Smilkova, M., Smilek, J., Kalina, M., Klucakova, M., Pekar, M., and Sedlacek, P. A simple technique for assessing the cuticular diffusion of humic acid biostimulants. *Plant Methods.* 2019, 15, 83. Attached as Appendix 9.

the real conditions during the foliar feeding process. Rather, it aims to answer general research questions concerning the penetration of humic-based substances into leaves, such as how the permeability of cuticles for humates varies among either various plant species or diverse humic materials.

At the next step, we turned our attention to the penetration of liquid humates through the skin. The motivation was straightforward and conceptually similar to that of the previous plants-involving study. There is a growing number of reports dealing with actual and/or potential applications of humic substances in medicine, pharmaceutics and cosmetics. Some of them are traditional and unsurprising, such as the balneotherapeutic use of peat, whose origin dates back to the ancient times of Babylonia and the Roman Empire, where the healing effects of mud baths were already recognized. Nevertheless, there are numerous specific properties of HS, beneficial for human health and wellness, that were described and explained quite recently. Comprehensive reviews on this topic are provided elsewhere [104, 105], it is hence sufficient to recall the antiviral, antibacterial, and anti-inflammatory effects (commonly attributed to the high binding affinity of HS towards cationic domains), anti- and des-mutagenic activity, binding of misfolded prions hence eliminating their infectivity, engagement of HS' quinones in the evolvement of ROS for wound healing and cancer therapy. In cosmetics, the ability of HS to absorb light in the visible and near-UV range is used in sunscreen, anti-aging, and skincare products, where the antiviral and antioxidant properties of HS provide additional benefits. Apart from functioning as active pharmaceutical or cosmetic ingredients, HS also offer numerous indirect effects that have been engaged in these application fields. Above all, the specific amphiphilic nature of HS provides them a solubilizing activity, thus enhancing the water solubility of hydrophobic drugs. Evidently, the potential of HS for use as an active or auxiliary ingredient for pharmaceutical and cosmetic products is steeply growing. Because the topical administration route belongs to the most often way how the active agents from the HS-containing products enter the body, it is of great importance to establish a standard methodology for the assessment of percutaneous absorption of HS. Once again, we have utilized our experience with the development of diverse laboratory techniques for diffusion-mapping studies to address this topic.

We have conducted a preliminary screening on the transdermal penetration of HS (not published yet), utilizing the same commercial lignohumate as in the previous study on plant cuticle permeation for the model humic substance. As a substitute for human skin, we have used porcine ear skin, because it is widely reported that it represents a suitable model regarding human skin histology [106] and mechanical properties [107]. Skin samples were carefully cut off from fresh porcine ear with a scalpel used either immediately or after being stored at −20°C until utilized. Before using a skin sample in the penetration experiment, its surface quality and physical intactness were always checked by a light microscope. Contrarily to the highly brittle and rupture-sensitive plant cuticles, the superior mechanical properties of the porcine skin did not require any special mechanical support during the diffusion experiment. Therefore, the penetration experiments were performed using a standard vertical Franz diffusion cell, where the skin was mounted between the donor and receptor compartments with the epidermal side up (schematics of the experiment are shown in Fig. 26). As the source of lignohumate for the penetration experiments, we used hydrogels prepared by stirring of a defined amount of the solid humate powder, commercial thickener (we tested various carbomers, and also xanthan as a representative of polysaccharide thickeners) and water until a homogeneous gel material was obtained (Fig. 26a,b). Aqueous buffer (isotonic NaCl solution) was used as the receptor environment. To evaluate the barrier properties of the porcine skin towards the lignohumate, the skin-penetration experiment was always supplemented with a reference diffusion experiment where the lignohumate transport from the same source gel was monitored in the same apparatus through a reference porous membrane (nitrocellulose filter membrane Pragopore 8, 0.23 μm pore size).
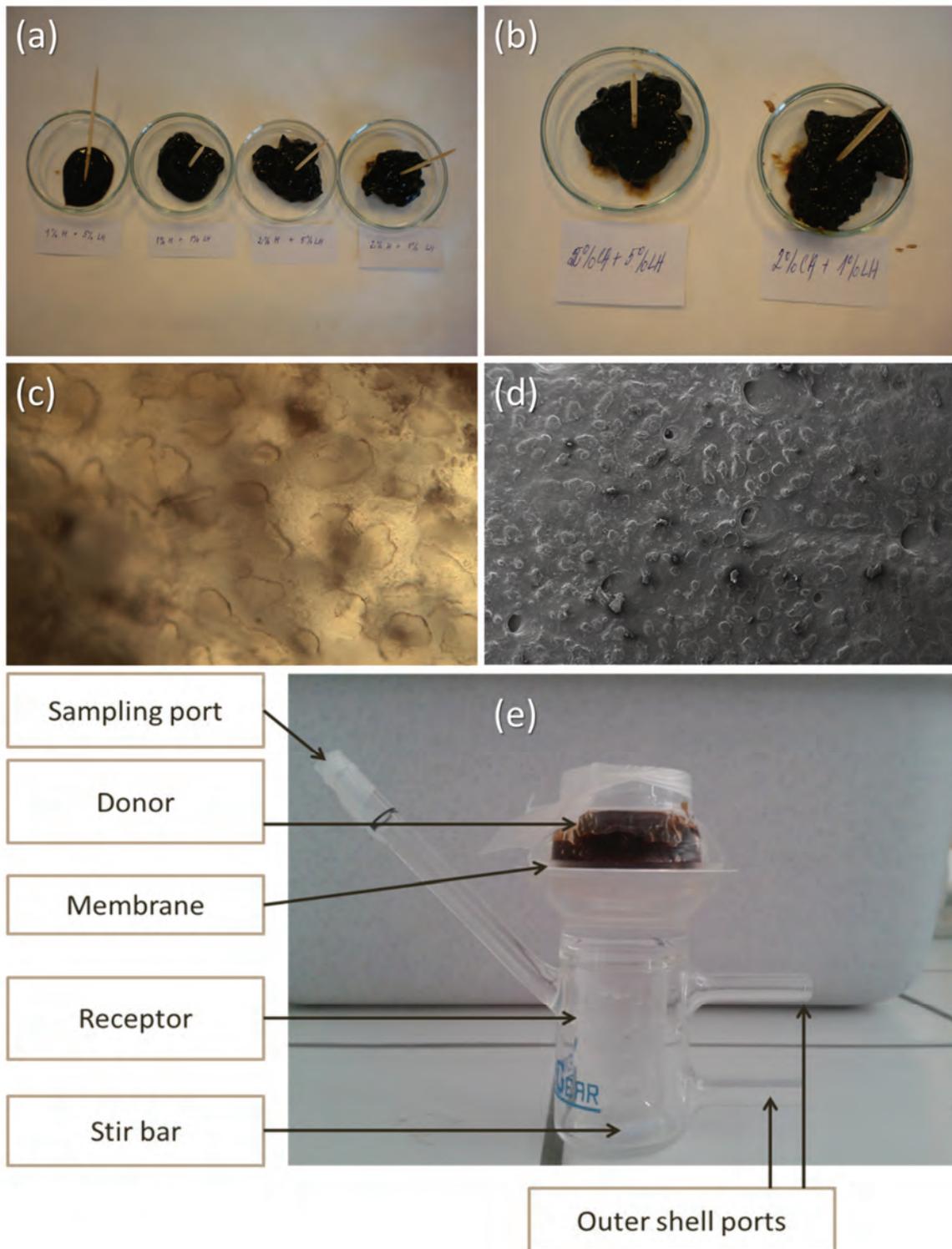
Fig. 26 Experimental study on transdermal penetration of lignohumate and/or active pharmaceutical ingredients from hydrogel material. Various tested compositions of the hydrogels with carbomer thickener (Synthalen M (a), and Polygel CA (b)) as the gelling component. Micrographs of the pig ear skin membrane from optical (c) and electron (d) microscopy. (e) Marked picture of the experimental setup based on the commercial Franz diffusion cell apparatus (SES-Analytical Systems, GmbH, Germany, receptor cell: 20 ml, donor surface 490 mm²).

In this preliminary study, we have found that the rate of lignohumate penetration through the model skin is surprisingly high. As can be seen in Fig. 27, the rate of lignohumate transport was only moderately suppressed by the skin as compared to the porous reference membrane. Similar results were obtained regardless of the particular gel composition. The high percutaneous absorption of lignohumate – similarly to its ability to penetrate the waxy plant cuticles – represents another important manifestation of the complex amphiphilic nature of HS. Considering the combination of this outstanding ability to penetrate the body surfaces with the universal binding capacity towards diverse substances, this finding strongly supports further research and development of pharmaceutical and cosmetic preparations for topical administration of HS as not only active but also an auxiliary ingredient, influencing the rate of dermal absorption of other active agents.
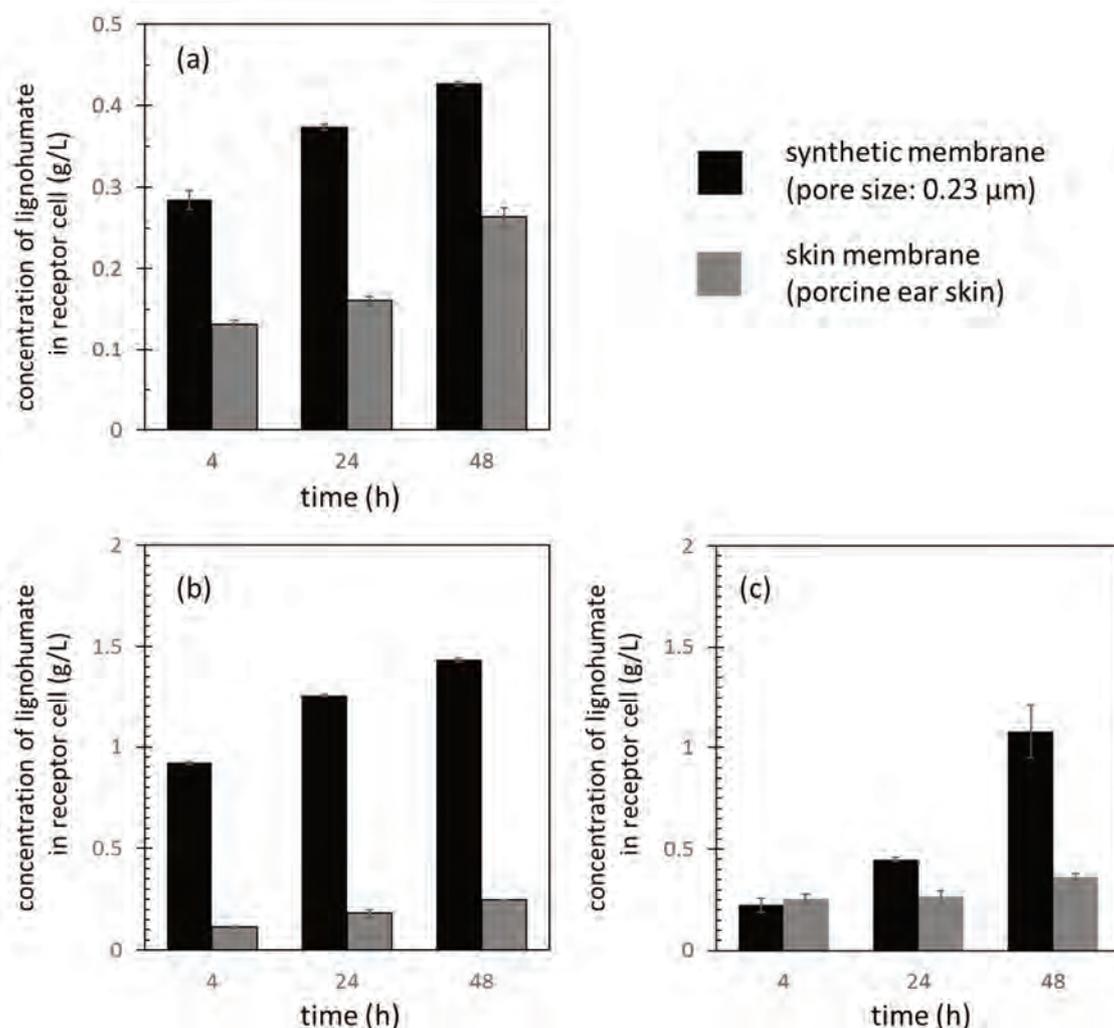
Fig. 27   Example of results of the skin-penetration study on lignohumate, performed in the experimental setup shown in Fig. 26. (a) Penetration of lignohumate from hydrogel containing 2 wt. % of carbomer thickener (Polygel CB) and 1 wt. % lignohumate thorough model skin and reference porous membrane, respectively. (b) Results of the same experiment for hydrogel with 4 wt. % of carbomer thickener (Polygel CB) and 5 wt. % lignohumate. (c) Results for hydrogel containing 5 wt. % of polysaccharide thickener (Xanthan) and 5 wt. % lignohumate.

5.1.5   From understanding the natural function to the development of novel application forms

As I repeatedly pointed out when introducing the concept of biophysical research that I have been involved in, I have always put a special effort into implementing the fundamental knowledge gained from the basic phenomenological investigations into an applied research attitude to the topic. In course of the study on interactions of humic substances, we have practically experienced how the binding ability of HS comes to the fore when the humics are incorporated in a hydrogel medium. This could be employed not only in a reasonable simulation of the binding performance of natural HS but also in designing and developing new application forms of HS. Taking into account the high apparent molecular weight of HS and the proven ability to coagulate HS from solution by non-covalent crosslinking, their universal binding capability and complex inherent biological activity and also the demonstrated ability of some humic fractions to penetrate the surface of the plant and human body, development of hydrogels with incorporated HS seem exceptionally promising for the application fields ranging from agriculture to human medicine. Humic component of the gels could provide numerous functions according to the specific requirements of the application [105]. In soil amendment preparations, HS are primarily intended as an active ingredient that aims at improving the quality and content of soil humus, whereby the gel form can help to assure a controlled release of the humic component to increase the effectivity of its fixation in soil and prevent unwanted losses e.g. by rainwater washout. The proven ability of lower-molecular-weight HS to penetrate plant cuticles also rationalizes the idea that the humic substances released from the gel carrier into the soil could also provide direct bio-stimulating effects on plants [108]. Moreover, their widely described binding ability towards diverse solutes also determines HS as the potent colloidal carriers, that can control the soil concentration level and mediate the bioabsorption of various compounds, ranging from in-/organic nutrients [109], through growth enhancers and retardants, to pesticides [80, 110]. Similarly, also in the applications focused on the care of human health and wellness, the combination of the gel form and a humic ingredient as either active (providing direct medicinal or other biological effects) or auxiliary (utilized in order to solubilize and/or improve the absorption of other bioactive compounds) ingredient [111, 112] seems increasingly attractive. Furthermore, either in agricultural or topical health-care applications, the gel form provides also one additional significant benefit – it manages the water content at the place and prevents its drying out. Naturally, this capability is of similar importance for agriculture (e.g. prevention of rainwater run-off and keeping the soil moist) as for medical or cosmetic applications (e.g. wound healing, skin hydration etc.). We have therefore paid attention to both types of potential applications of HS prepared and characterized some original hydrogel compositions with HS incorporated in them.

Regarding the design of humics-containing gels intended for use as soil amendments, we have followed two basic preparation routines. The first path that we followed in the development of HS-containing hydrogels for agricultural uses led us to superabsorbent hydrogels, where the humic component is chemically trapped in the poly(acrylic acid) polymer network. These materials, designed in order to provide a combined controlled release of HS and mineral nutrients together with extremely high water-holding capacity, will be discussed in detail in section 7.3.1. The second way of the applied research was focused on the electrostatic cross-linking of humic acids with the use of oppositely charged biopolymer chitosan (see Fig. 28). The main findings of the pilot study dealing with this original gelation approach, based on the combination of two abundant and renewable natural materials, were described in detail in a book chapter[XII]. The formed polyelectrolyte complexes (the concept will be further discussed in 7.3.2) provided hydrogels, whose properties - such as dry matter content, swelling behavior, mechanical properties of both swelled and dried material, but also sorption performance – can be significantly influenced by the preparation procedure (concentration of the gelling component, pH and ionic strength in the HA and chitosan solutions, addition of low-molecular electrostatic crosslinker, temperature, etc.). To sum up, for both HS-gelation strategies that we followed, we have

---

[XII] Klučáková, M.; Sedláček, P.; and Ondruch, P. Preparation and characterization of new application forms of humic acids. *In Recent Research Developments in Materials Science*; Research Signpost: Kerala, 2009; pp. 59–80.

demonstrated that the particular material properties of the gels - including the possibility of managing them through the preparation process - are extraordinary promising, and I believe that our contribution in this field may open the door to new, unconventional trends in the design of HS-based formulations for the use in agricultural and environmental technology.
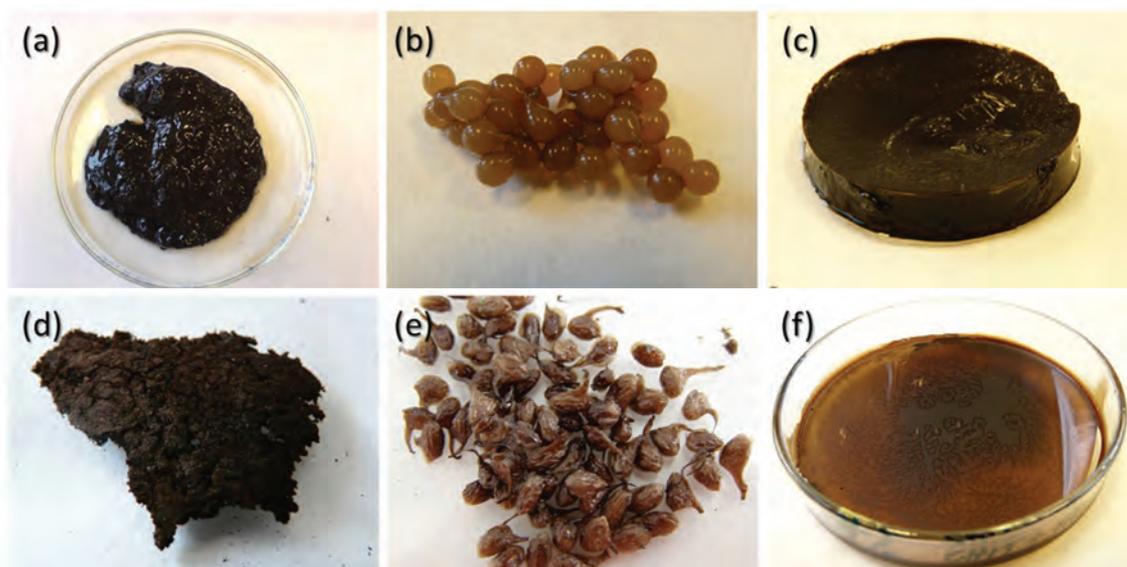

Fig. 28   Swelled (a-c) and the corresponding dried (d-f) forms of HA-chitosan hydrogels. (a,d) Macrogel prepared by fusion of chitosan and HA solutions. (b,e) Hydrogel beads prepared by adding a viscous chitosan solution dropwise into HA solution. (c, f) Whole-volume gelation via alkalization of chitosan/HA mixture by ammonia vapors. Drying of the gel (c) results in film (f) with a high swelling ability.

As we have already partially discussed in the previous section, apart from the design, preparation and characterization of the HS-containing gels intended for agricultural use, we have also dealt with the potential utilization of HS in gels for cosmetic and pharmaceutical applications. We have demonstrated how the ability of HS to enter the body through the skin can elucidate the biological effects of topical applications of HS *per se*. Nevertheless, we also considered whether and how the presence of HS affects the transdermal absorption of other active pharmaceutical ingredients (APIs). We have therefore complemented the already discussed skin-penetration experiments in Franz cells with a screening study where an API was contained in the hydrogel with or without HS (lignohumate in particular). Again, we tested various hydrogel compositions (several carbomers and xanthan were used as thickeners) and we compared penetration of the API (diclofenac, ketoprofen and salicylic acid were used as model analgesics) through the synthetic porous membrane and the model skin (porcine ear skin). Surprisingly, we have revealed reproducible enhancement of the skin-penetration rate for all tested APIs when the lignohumate was present. Our results (not published yet) hence strongly supports the idea that the solubilizing ability, caused by their complex amphiphilic molecular structure, provides HS with a great potential for use in topical preparations as a skin absorption enhancer. We have also found out that our finding is consistent with several studies provided recently by Mirza [113–115] who demonstrated how complexation with HS enhances a pharmacokinetic profile of several drugs in oral delivery.

Altogether, both the new insights into the structural aspects and binding behavior of HS, uncovered during our extensive fundamental research on these compounds, and the preliminary suggestions on their possible application merits, resulting from the applied research studies, led us to the strong conviction that humic substances represent a clear example of how fascinating materials, multi-faceted in their natural roles, and at the same time beneficial and inspiring in their artificial use, nature has created and offers us to explore.
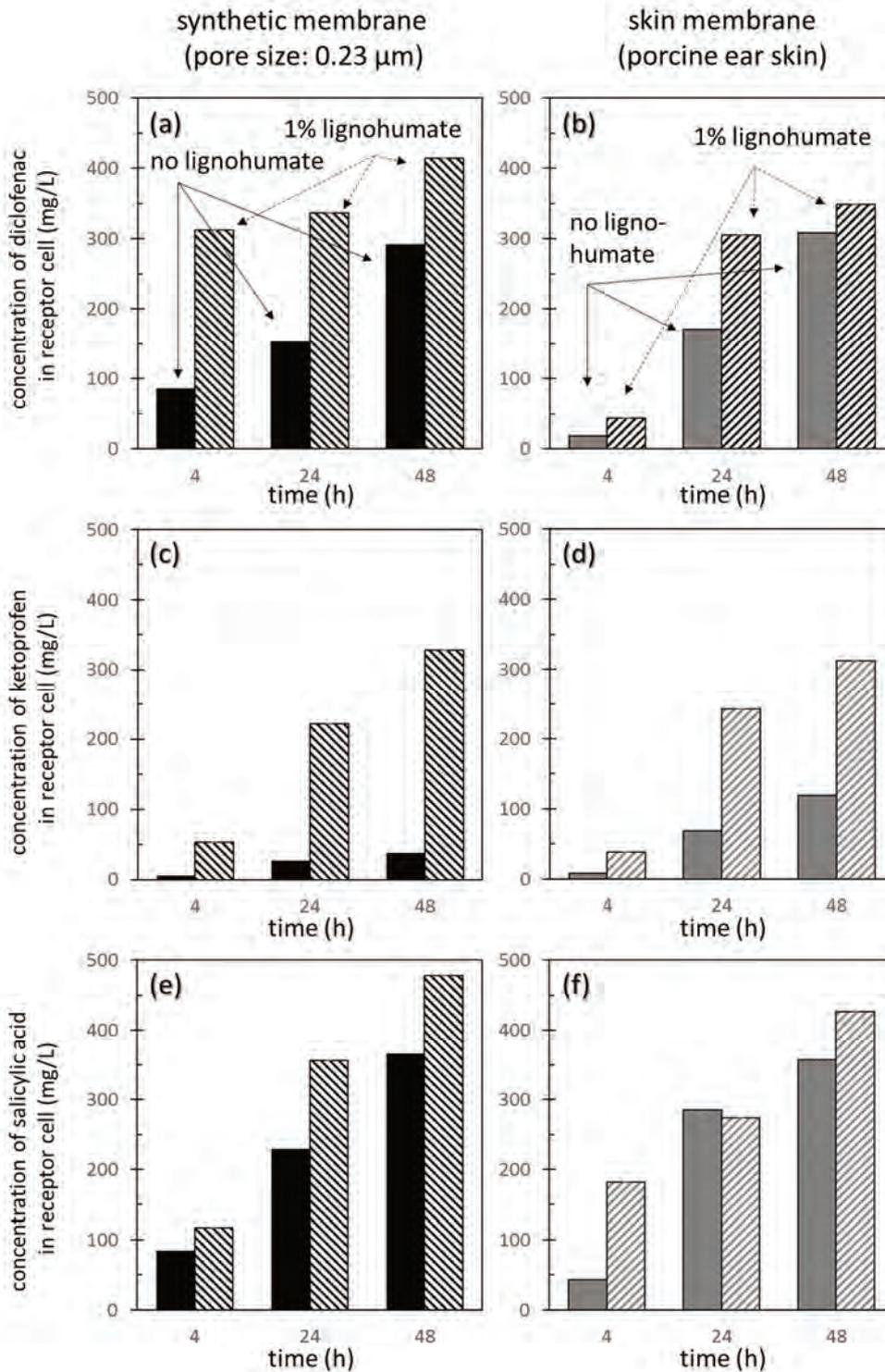
Fig. 29   Results on the effect of lignohumate on penetration of model analgesic APIs from 5 wt.% xanthan hydrogels through skin., Experiments were performed in the experimental setup shown in Fig. 26. Data show penetration of diclofenac (a,b), ketoprofen (c,d) and salicylic acid (e,f) through synthetic Pragopor 8 membrane (a,c,e) and model skin - porcine ear skin (b,d,f). Source compartment was filled with 2 g of the 5 wt.% xanthan hydrogel containing 1 wt. % API and either 0 wt.% (filled) or 1 wt.% (striped) lignohumate.

5.2   Microbial polyesters: what makes their structure in cells so special?

Obviously, HS represent just one of many examples of fascinating natural materials that have long been and still are attracting the attention of scientists worldwide. The number of choices for a curious material scientist is increased vastly when shifting his/her attention from the non-living to the living nature. Let me highlight one special example from the large family of biopolymers. Polyhydroxyalkanoates (PHA, chemical structure is shown in Fig. 30) has continuously been attracting a great and still growing deal of scientific interest since they were discovered by Lemoigne in 1926. PHA are microbial polyesters accumulated by numerous prokaryotes in form of intracellular granules (see Fig. 31), primarily as a carbon and energy storage material. Poly(3-hydroxybutyrate), or PHB, the homopolymer of 3-hydroxybutyric acid, is the most widespread natural representative of these polymers, however, it was reported that there are more than 150 hydroxyalkanoic acids that can be introduced into the polymer chain by various microbes [116], PHA in a fact offer a great variety of structural functionalities and hence cover a wide range of material properties. According to the particular monomers contained, PHA are referred to as short-chain-length (scl-PHA) when they are composed of hydroxyacids with 3 − 5 carbon atoms, whereas medium-chain-length PHA (mcl-PHA) contain monomers with 6 − 14 carbon atoms.
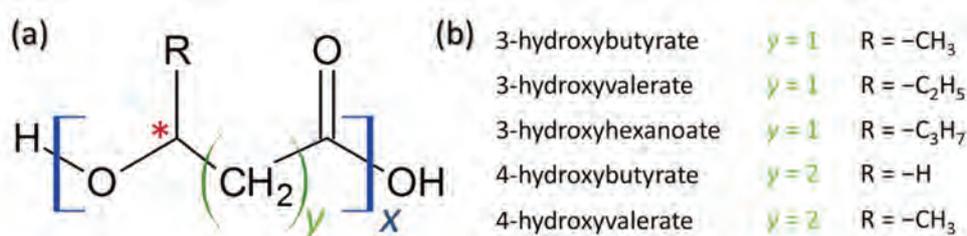
Fig. 30   (*a*) *Schematic representation of the molecular structure of PHA.* (*b*) *The most common PHA monomers. The main chiral center of the structure is marked with an asterisk.*

Although the purpose for PHA accumulation had long been seen just in the energy metabolism, recent research findings (including the results of our research projects introduced in Chapter 6 of this thesis) revealed the biological (or even the evolutionary) role of PHA is in fact much more complex. The specific role of PHA in protection against and adaptation to diverse stress factors will be discussed thoroughly later. Apart from that, it has also been described that PHA contributes to the establishment of symbiosis between prokaryotes and plants [117, 118] or insects [119], and participates in other survival strategies such as endospore formation in Bacilli and related species [120].

Analogically to HS, PHA as well play not only an irreplaceable natural role but they are also considered to be auspicious materials for artificial uses. Being produced from renewable resources by approaches of microbial biotechnology, and offering highly esteemed application- and lifecycle-related features such as biocompatibility, biodegradability and compostability, PHA represent highly promising "green" candidates for replacement of petrochemical polymers on the way toward sustainable production of plastics. As mentioned in Chapter 3, the involvement of biopolymers in the production of bioplastics represents one of the most topical R&D issues. Current global production of bioplastics (2.11 million tons in 2020, [121]) is expected to increase by more than 35% by 2025, still representing less than 1% of the total annual production of plastics (368 million tons in 2020 according to Bioplastics market data, 2020). Among the bioplastics currently on the market, PHA yet represent a minor contributor (1.7% of the total amount of bioplastics produced in 2020); nevertheless, the market share is foreseen to increase significantly to 11.5% by 2025.

One reason for this expected growth certainly lies in the aforementioned versatility of composition that can be provided by various members of PHA family. However, there are two constraints that need to be overcome to open the door for a broader expansion of PHA on market. First, a complex understanding of how the application performance of PHA products can be tailored by chemical

structure (i.e. monomer composition and polymerization degree) and physical conformation (i.e. degree of crystallinity) is needed. Second, technologically feasible and economically competitive processes for the biosynthesis of PHA with adjustable composition and molecular weight must be developed.
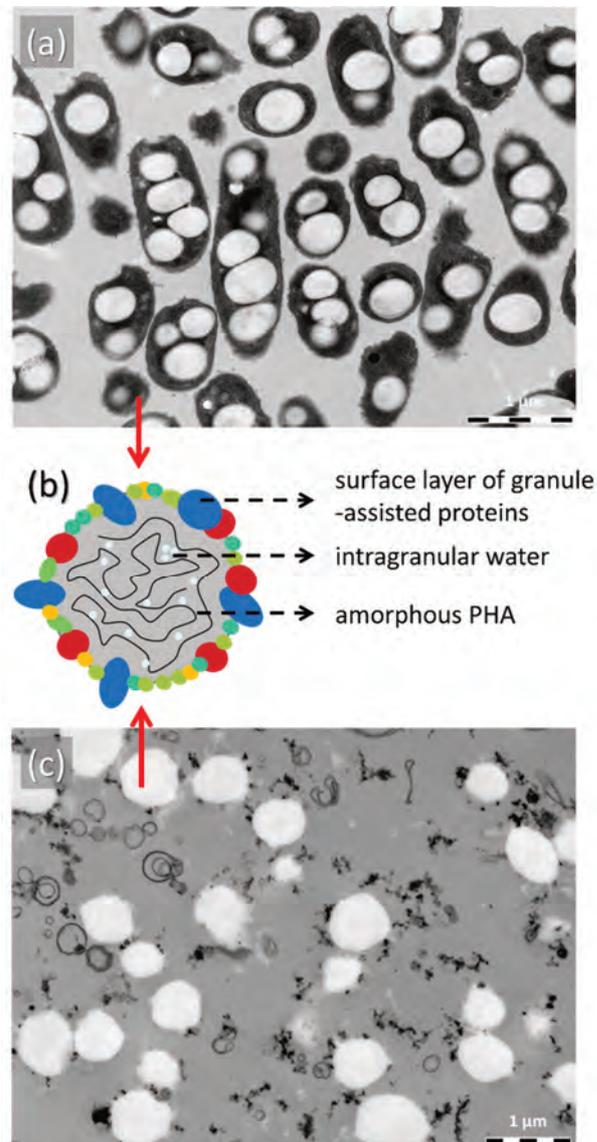
Fig. 31   Morphology of PHA granules in PHA-producing bacteria. (a) PHA granules in the cells of the mesophilic PHA producer Cupriavidus necator H16. (b) Schematic representation of fundamental structural features of PHA granules. (c) Isolated PHA granules.

In this section, I will introduce our research studies focused on the material aspects of PHA. First, I will describe *in vivo* investigation in that we focused on the native structure of PHA in bacterial cells (5.2.1). Then, I will describe the biotechnological process, developed by us, that allows the preparation of PHA materials with structure and application properties that can easily be manipulated by the cultivation conditions (5.2.2).

5.2.1   Polyhydroxyalkanoates *in vivo*: staying unfavorable

At first glance, it could seem that structural biologists must find PHA molecules absolutely boring. Their primary chemical structure does not compare to the complexity of other fascinating biopolymers such as proteins or nucleic acid. Nevertheless, a closer look at structural aspects of PHA can bring an

unexpected attractiveness for biologists and also at least one surprising similarity with the above-mentioned biopolymer family stars: the fact that we can distinguish a native and denatured (i.e. the biologically active and inactivated, respectively) form of the compound and that transformation between the two forms can be induced easily (at least in one direction).

There are in fact two especially fascinating structural aspects of the intracellular PHA. First, the way how the hydrophobic polymer is made compatible with the aqueous cell cytoplasm and compartmentalized there in a form capable of metabolic utilization. Second, the fundamental difference between basic material (mainly mechanical) properties of PHA inside and after isolation from the bacterial cells. It is well known that isolated PHB, the most common member of PHA family, constitutes a brittle material with an elongation to break as low as a few percent. This deformation behavior is attributed to the high crystallinity of the polymer. Nevertheless, it is well evidenced that inside the bacterial cells, the same polymer shows astonishing flexibility. It was repeatedly demonstrated by visualization of PHA accumulating bacteria with scanning electron cryomicroscopy (cryoSEM) that the cells, fixed and fractured at temperatures below -100 °C, show a specific plastic deformation of PHA granules, manifested by characteristic needle-type deformation artifacts where the granule stretches by more than 100% its original size (see Fig. 32b,d). Although the first reports on this unusual deformation behavior of cellular PHA date back to the 1960s, little attention was paid to the obvious discrepancy with the highly crystalline nature of the isolated polymer back then.
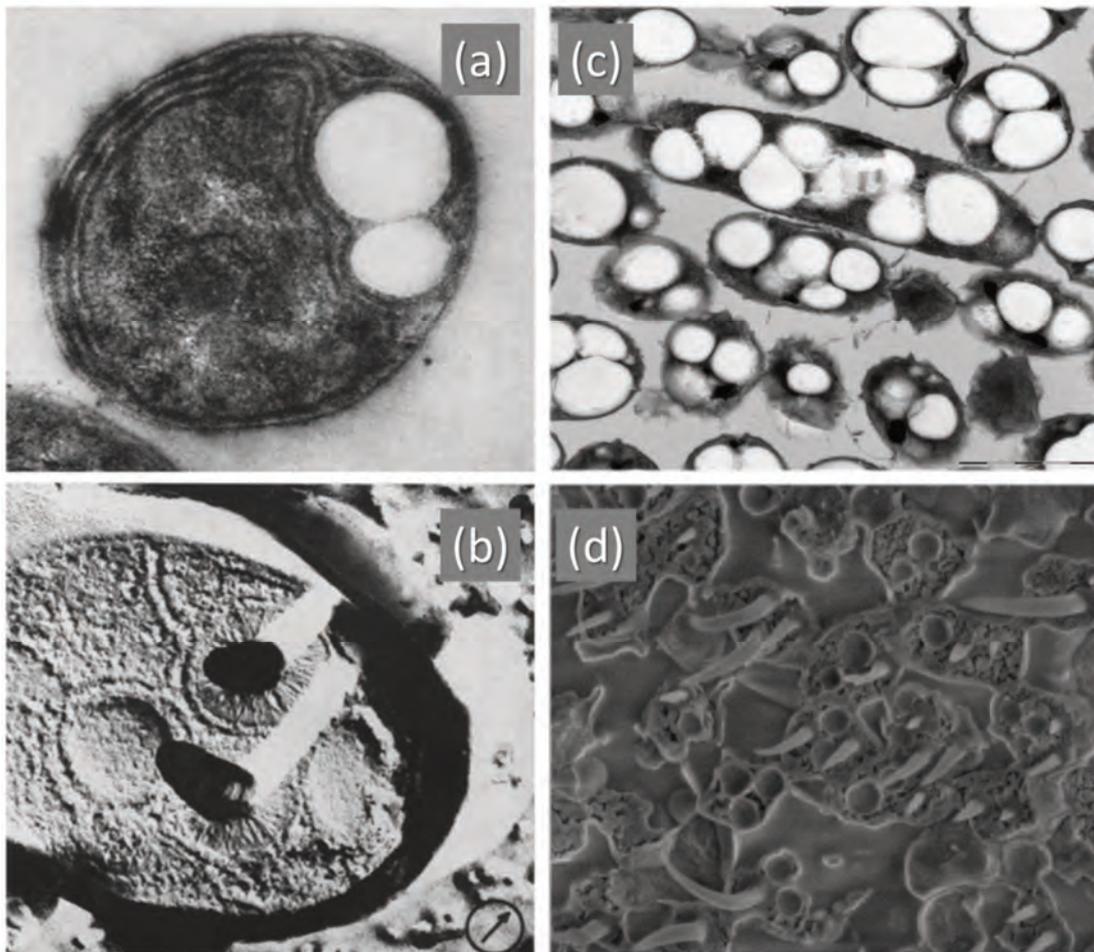
*Fig. 32 Characteristic plastic deformation of PHA granules during cryoSEM imaging of PHA accumulating cells. (a, b) First report on the needle-type deformation published for Nitrobacter cells by Van Gool [122] in 1969. (c, d) Similar deformation behavior of C. necator H16 revealed in our study[XXIV]. (Results of cryoSEM (b, d) and TEM (a, c) visualization of the cells are compared for clarity.)*

We have provided an in-depth review the history of structural studies on the structure and supramolecular architecture of PHA granules *in vivo* in our review article[XIII] where we have also summarized our original contribution to the topic. We have described how the view on the mechanism of PHA solubilization in the cell shifted from the original idea of the polymer granule core covered by a layer of phospholipids [123] to the currently accepted notion of the surface layer of so-called PHA granule-associated proteins (PGAPs), that include PHA synthase, PHA depolymerase, functionally multifaceted surface proteins so-called phasins, and regulatory proteins [124]. We have also described how this supramolecular protein-polyester composite is involved in the metabolism of PHA. Nevertheless, in our research, we have paid our attention mainly to the second interesting attribute of the native PHA – their strictly amorphous nature.

Speaking in exaggeration, the discovery of the inherent amorphousness of intracellular PHA was brought about more by scientific ignorance than by intent. It was in the 1980s, when the research group of Sanders measured ^{13}C NMR spectra of intact PHA-containing cells. The authors later conceded that they had ignored the conventional wisdom prejudging NMR to fail in analyzing cellular PHA, and therefore succeeded to record spectra of PHA in the resolution unattainable for a crystalline polymer. Later, they supported their NMR results with X-ray diffractometry and proved the absence of a substantial quantity of crystalline PHA in the cells. Since then, the biological importance of the amorphous structure of intracellular PHA has continuously been debated as well as a mechanism by which this thermodynamically unfavorable state of the polymer is maintained. The mechanism was expected to be simple, universally available and undemanding for any specific chemical or biological mediator because it was soon revealed that the transfer of genes related to PHA synthase enabled the formation of apparently fully biologically functional PHA granules not only in PHA non-accumulating bacteria [125], but also in green plants [126].

Two main plasticizing effects has been proposed (see Fig. 33). The first one calls for the presence of an anonymous substance that acts as a plasticizer in the granule – it restricts the PHA chains from the molecular reorientation necessary for the crystallites to be formed. It is well known that despite its hydrophobic nature, PHA granules contain a significant amount of water inside (up to 10 wt. % according to Lauzier [127]).

Therefore, since the very beginning of these considerations, speculations on the role of water in this effect have been arising repeatedly (as reviewed in[XIII]), however, without any experimental evidence. The alternative mechanism for PHA plasticization was proposed by those who had evidenced the need for it – by the group of Sanders. Their explanation follows the laws of chemical kinetics and suggests that the crystallization of native PHA is restricted by the extremely low volume of the polymer granule where the rate of nucleation converges to zero [124, 128]. The authors also supported their theory with an experimental study on the rate of crystallization of artificially synthesized amorphous PHA of the submicron size. Nevertheless, even this explanation was not fully consistent with all experimental observations (e.g. with the crystalline-shell/amorphous-core PHA granules described by Lauzier [127]).

When reviewing the literature sources on this topic, our attention was caught by frequent reports on how various chemical and physical treatments "denature" PHA – i.e. alter the structure of PHA into the form not utilizable by the cells (again, the summary of these works is provided in our paper[XIII]). At the time, we had already been fully engaged in the topic of the involvement of PHA in stress survival and robustness of bacteria (discussed in detail in 6.2). Therefore, we were inspired to design a

---

[XIII] Obruca, S., Sedlacek, P., Slaninova, E., Fritz, I., Daffert, C., Meixner, K., Sedrlova, Z., and Koller, M. Novel unexpected functions of PHA granules. *Applied Microbiology and Biotechnology.* 2020, 104, 4795–4810. Attached as Appendix 10.

systematic study relating stress exposure of PHA-containing cells, structural and morphological changes induced on PHA granules by the stress, and the impacts of these changes on the survival and cultivability of the cells.
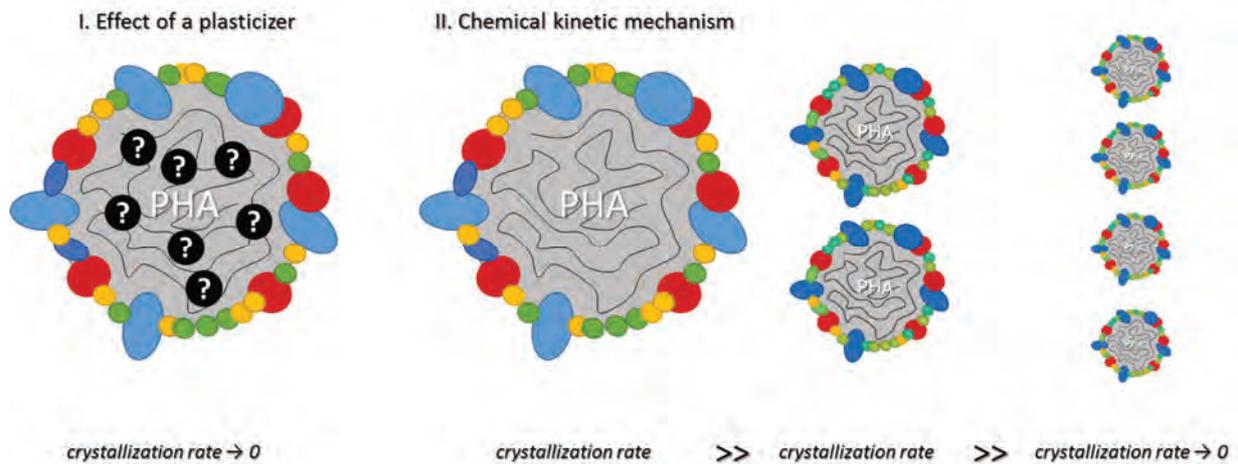

Fig. 33   Two formerly proposed theories on the mechanism of PHA plasticization in vivo – I. effect of a molecular plasticizer, and II. chemico-kinetic model based on limited volume of the granules.

In our study[XIV], we exposed bacterial cultures of a PHA producer (*C. necator* H16) with high content of accumulated PHA in the cells (above 70% of cell dry weight) to various stress conditions (elevated temperature, freezing/thawing cycles, high salinity, acidic pH). With TEM, we determined changes caused in the cellular morphology and ultrastructure, and with time-resolved ATR (*attenuated total reflection*) FTIR spectroscopy, we monitored changes in PHA crystallinity in the cultures as they were freely dried on the ATR crystal (the methodology for assessing crystallinity of PHA by vibration spectroscopy will be further discussed in 6.1.1). We have confirmed by the combination of these two assays that only those stress factors that caused the aggregation of intracellular granules induced also the crystallization of PHA. With respect to the significant spectral signs of protein denaturation in these samples, we inferred that the aggregation process was initiated by stress-induced structural changes in the granule-associated proteins inactivating their surfactant role on the granule-cytoplasm interface. The fatal impact of granule aggregation on cell physiology was also confirmed in our study by the cell cultivation test. This finding that granule aggregation is a necessary condition for PHA crystallization could in itself be considered strong evidence for the correctness of the chemical kinetic explanation of the amorphousness of intracellular PHA proposed by Lauzier. Nevertheless, we have also revealed that in the otherwise intact cells with the stress-induced aggregation of PHA granules, the crystallization never followed the stress exposure immediately. Instead, it always occurred with a significant time delay after the cell culture got dried. Obviously, the increased volume of coalesced granules was not by itself able to initiate the crystallization process. The importance of the cell drying hence brought the plasticizing role of water back to the scene.

Based on these experimental results, we proposed an updated view on the way of PHA plasticization *in vivo* that assumes concurrency and synergism of both previously considered mechanisms (see the schematics of our idea on the mechanism of stress-induced PHA crystallization *in vivo* in Fig. 34). We consider the metastable amorphous state of PHA as a result of the well-tuned interplay of kinetic effects resulting from the sub-micron volume of the granules and the plasticizing effect of intragranular water. Anyway, the physical state of cellular PHA is another obvious example

---

[XIV] Sedlacek, P., Slaninova, E., Enev, V., Koller, M., Nebesarova, J., Marova, I., Hrubanova, K., Krzyzanek, V., Samek, O., and Obruca, S. What keeps polyhydroxyalkanoates in bacterial cells amorphous? A derivation from stress exposure experiments. *Applied Microbiology and Biotechnology.* 2019, 103, 1905–1917. Attached as Appendix 11.

of a topic where physical chemistry and biology shake their hands. The long-known inability of intracellular depolymerases to cleave crystalline PHA has led to the current use of the terms "native" and "denatured" PHA as synonyms for amorphous and crystalline PHA, respectively [129]. Furthermore, I will discuss in the next chapter (section 6.1.3) that recent studies (including ours) have shown that the biological consequences of the unique physical state of native PHA are not limited to the metabolism of this compound and are in fact much more complex. To conclude, this particular research topic can hence be used as another example of the general message repeatedly emphasized in this thesis – the fact that the (molecular) interactions build up the specific supramolecular architecture of the system, which in turn rules its material properties and – in this case – also the biological performance. Designing and performing the experimental studies in order to uncover this relationship for diverse ecological and biological systems is where I see the exclusive and irreplaceable role of biophysical chemistry.
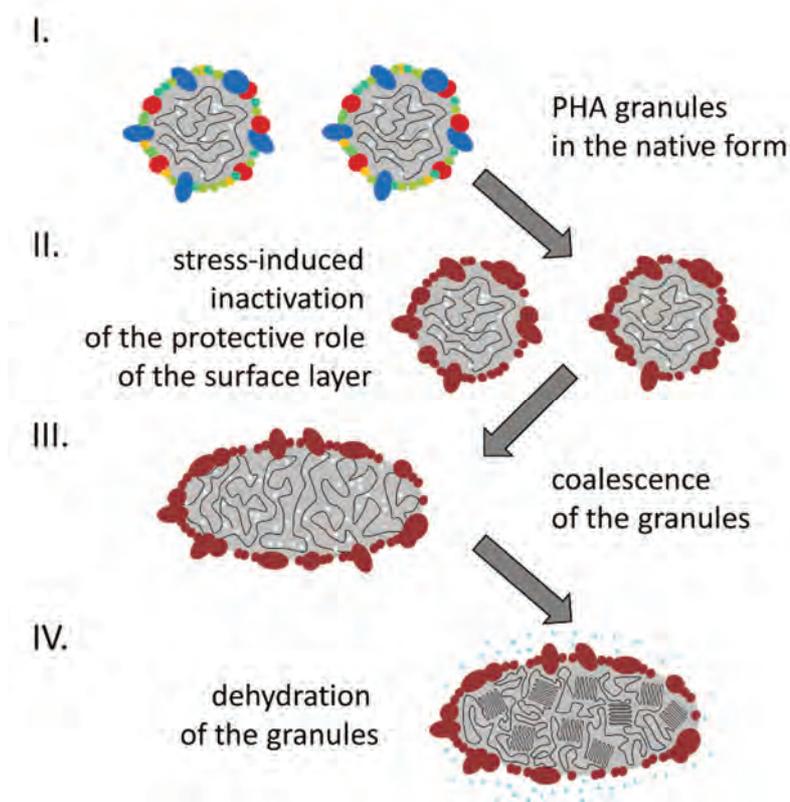
Fig. 34   Stress-induced crystallization of PHA in the cells as explained by the synergy of chemical-kinetic and water-mediated effects proposed as the updated view on PHA plasticization in vivo[XIII,XIV].

5.2.2   Development of nature-inspired bioplastics with tailorable properties

Similar to our research interests in humic substances, also in the case of PHA we have put an effort into utilizing the fundamental knowledge gained on the native behavior of the material also in its applied research. The application potential of PHA is outstanding. Over the past years, the range of end uses that PHA has been proposed or tested for, as well as the list of PHA producing and/or researching companies has steadily grown. Certainly, the most often proposed use of PHA-based plastics is in the packaging industry. With its biodegradability and good gas barrier properties, PHA seems a great candidate for the production of materials with a short lifespan, such as food utensils and daily consumables. Other low-cost uses of PHA are intended in agriculture (e.g. production of biodegradable mulch films or growth bags) and in the production of single-use disposable items such as bottles, cups, shopping bags or cosmetic containers. On the other hand, specific biological (e.g. biocompatibility) and chemical properties (e.g. chiral purity, easy chemical modification) make PHA beneficial also for various high-end applications, including biomedical uses in tissue engineering (e.g.

PHA-based medical implants) and in drug delivery, and, last but not least, involvement of PHA as the chemical precursor in the synthesis of various fine chemicals. More details on the current state of PHA applications are provided elsewhere [130].

In the current commercial uses of - as well as in the applied research on - PHA, PHB still represents the main subject of interest. Nevertheless, the already discussed inherent crystallinity and the associated brittleness and rigidity of PHB represent a severe limitation of the material, especially in the film-forming segment, e.g. in the packaging industry. Therefore, special attention has recently been paid to alternative PHA materials – mainly copolymeric and mcl-PHA, and also the PHA-containing polymer blends or resins [131–133]. Furthermore, regardless of the relative growth of the segment of PHA bioplastics in recent years, incomparably high current production costs compared to other (bio)plastics still represent the severe limitation hindering the further expansion of PHA in the market. Therefore, strong efforts are currently targeted also on searching for novel trends in the biotechnological production of PHA that would increase the economic feasibility and competitiveness of PHA uses.

In our applied research interest in PHA materials, we have been trying to aim at both above-mentioned targets. We have developed and published several biotechnological processes for microbial production of PHA copolymers or terpolymers[XV,XVI,XVII]. The cost-effectiveness and competitiveness of the technological process were improved by the involvement of thermophilic producers[XVI,XVII] with respect to the recently proposed concept of Next-Generation Industrial Biotechnologies (will be discussed further in 6.2.3). In general, the crystallinity of the polyester should be substantially decreased by the incorporation of monomers with additional carbon atoms either in the main chain or in the side groups. We have therefore aimed at embedding 3-hydroxyvalerate and 4-hydroxybutyrate monomer units in the 3HB polyester chain. Naturally, my role and competence in these studies lays in the complex physicochemical characterization of the obtained materials with a special focus on their crystallinity. To evaluate the crystallinity of the produced polymers both qualitatively and quantitatively, we have supplemented traditional techniques (DSC, XRD) with ATR FTIR spectroscopy. The main advantage of this technique is that it provides fast analysis and also spatial resolution – for instance, it allows evaluation of the spatial homogeneity of the crystallinity in polymer films.

We have confirmed that changing the monomer composition of PHA by varying cultivation conditions enables manipulation with the crystallinity of the material in a wide range. Fig. 35 shows how the relative content of 3HV in P(3HB-co-HV) polymers biosynthesized by *Schlegelella thermodepolymerans* influences crystallinity markers obtained by DSC and FTIR analysis[XVI]. Evidently, with the single bacterial producer cultivated under different conditions, it is possible to obtain copolymers with crystallinity ranging from about 60 % (P(3HB)) to apparently zero (P(3HB-co-33% 3HV)).

In the subsequent study[XVII] (the schematic representation of the strategy used in the study is shown in Fig. 36), we evaluated our own thermophilic isolate (the unique protocol of "osmoselection" that we developed and used for its isolation will be described in 6.2.3) as a candidate producer of PHA copolymers. This bacterium, isolated from the urban composting plant located in Brno, was

---

[XV] Kucera, D., Novackova, I. , Pernicova, I. , Sedlacek P. , and Obruca, S. Biotechnological Production of Poly(3-Hydroxybutyrate-co-4-Hydroxybutyrate-co-3-Hydroxyvalerate) Terpolymer by Cupriavidus sp. DSM 19379. *Bioengineering.* 2019, 6, 74.

[XVI] Kourilova, X., Pernicova, I., Sedlar, K., Musilova, J., Sedlacek, P., Kalina, M., Koller, M., and Obruca, S. Production of polyhydroxyalkanoates (PHA) by a thermophilic strain of Schlegelella thermodepolymerans from xylose rich substrates. *Bioresource Technology.* 2020, 315, 123885.

[XVII] Pernicova, I., Novackova, I., Sedlacek, P., Kourilova, X., Kalina, M., Kovalcik, A., Koller, M., Nebesarova, J., Krzyzanek, V., Hrubanova, K., Masilko, J., Slaninova, E., and Obruca, S. Introducing the Newly Isolated Bacterium Aneurinibacillus sp. H1 as an Auspicious Thermophilic Producer of Various Polyhydroxyalkanoates (PHA) Copolymers–1. Isolation and Characterization of the Bacterium. *Polymers.* 2020, 12, 1235. Attached as Appendix 12.

taxonomically classified as a member of the genus *Aneurinibacillus*, designated as *Aneurinibacillus* sp. H1 and deposited in the Czech Collection of Microorganisms.
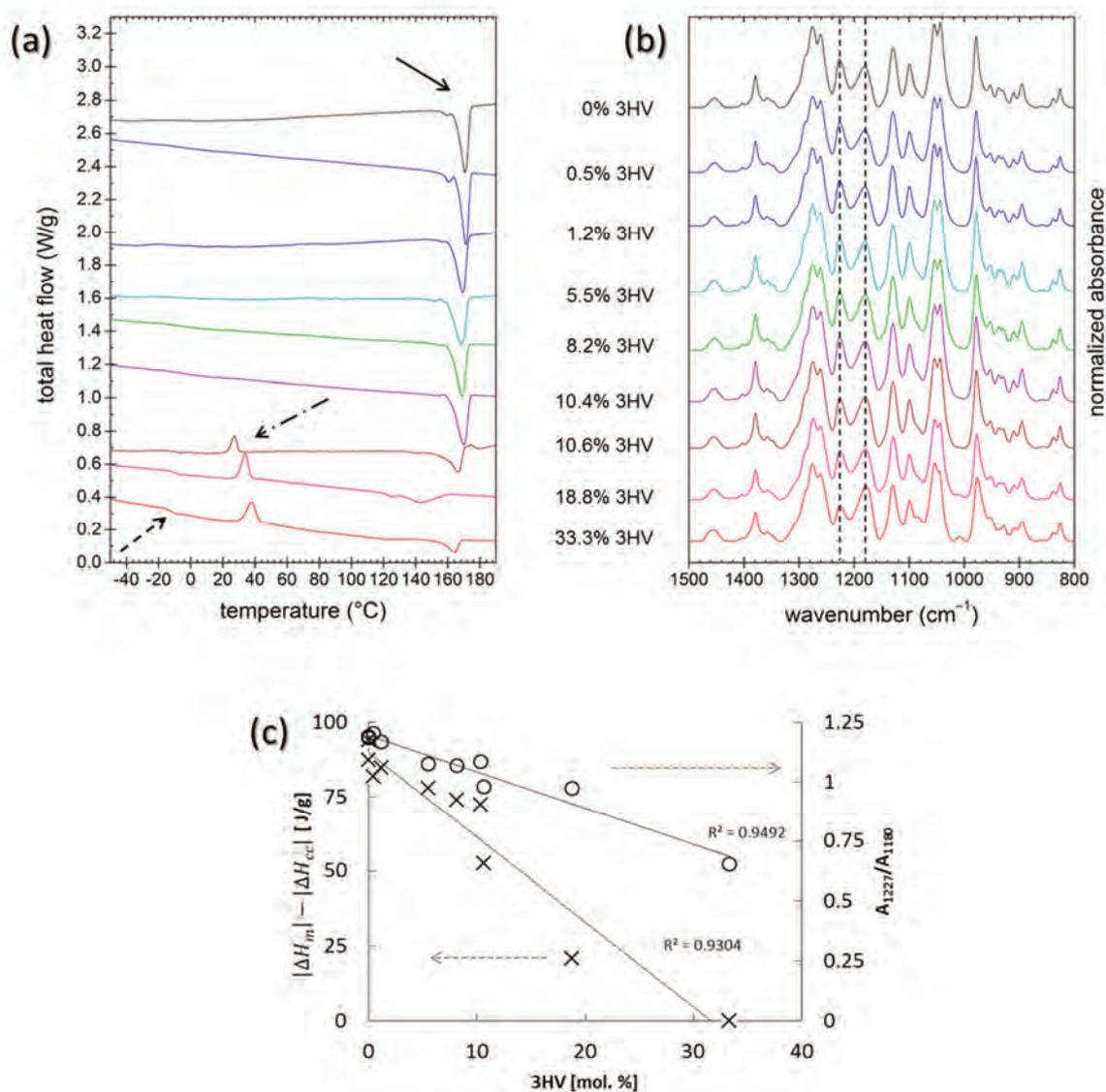
Fig. 35   Results of DSC (a) and ATR-FTIR (b) analysis of P(3HB-co-3HV) copolymers with the relative content of 3HV ranging from 0 to 33.3 % produced by Schlegelella thermodepolymerans under various cultivation conditions[XVI]. (a) In DSC heating thermograms, endothermic melting (solid arrow), glass transition (dashed arrow) and exothermic cold crystallization (dash-dotted arrow) of the polymers can be monitored. (b) ATR FTIR spectrum in the spectral range of 1500 cm–1 to 800 cm–1 shows the main structural differences among individual P(3HB-co-3HV) copolymers including crystallinity sensitive bands at 1180 cm–1 and 1227 cm–1 (dashed lines). (c) Decrease of crystallinity of P(3HB-co-3HV) copolymers with relative content of 3HV monomer illustrated by crystallinity markers determined by DSC ($|\Delta H_m| - |\Delta H_{cc}|$) and FTIR (A_{1227}/A_{1180}), respectively.

In the pilot assessment of its biotechnological potential, we have revealed its extraordinary ability to synthesize PHA copolymersand terpolymers containing high molar fractions of 3HV and 4HB subunits when valerate and/or 1,4-butanediol are used as 3HV and 4HB precursors, respectively. The study was followed by a thorough material analysis of the produced polymers in form of the solvent

(chloroform) casted films[XVIII]. Results of infrared spectroscopy, X-ray diffractometry, and differential scanning calorimetry clearly demonstrated that in 3HB prevailing polymers, the 4HB monomer acted as a structure-breaking component of P(3HB) crystalline lattice and, similarly, when the 4HB monomer predominated the polymer composition, residual 3HB units reduced the overall P(4HB) crystal lattice content. Polymers with a comparable content of 3HB and 4HB in the polymer chain showed the lowest crystallinity and the amorphous character predominated. When 3HV was also incorporated into the chain, the effects of the 4HB presence were strengthened. We hence proved that the developed technology for the biosynthesis of P(3HB-co-4HB) allows controlling crystallinity of material both qualitatively (regarding the type of predominating crystalline lattice) and quantitatively (overall degree of crystallinity). In this study, we also demonstrated that the monomeric composition and corresponding crystallinity of the material affect also its thermochemical stability (determined by thermogravimetry) and also the rate of enzymatic degradation. In the two studies, we hence evidenced that the isolated bacterium *Aneurinibacillus* sp. H1 is an outstandingly auspicious candidate for the next-generation biotechnological production of PHA. It combines the economic benefits of thermophile-based production with the capability to "tune" the chemical composition and physical structure of the produced polymer according to the required material performance.
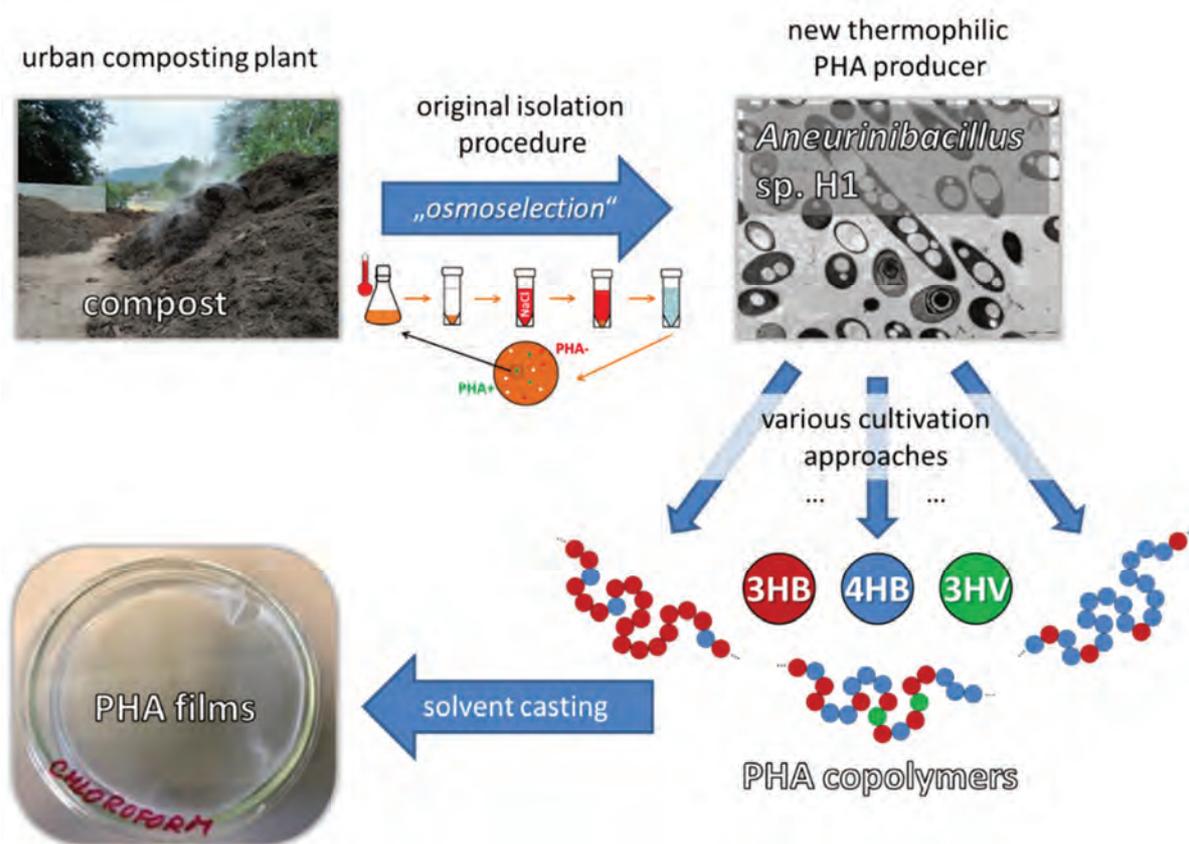
Fig. 36   Schematic diagram of recently developed strategy for the production of copolymer PHA-based bioplastic films

Most recently, we have launched a follow-up in-depth study on the application-relevant properties of the produced PHA copolymers produced by *Aneurinibacillus* sp. H1 . With respect to the potential

[XVIII] Sedlacek, P., Pernicova, I., Novackova, I., Kourilova, X., Kalina, M., Kovalcik, A., Koller, M., Nebesarova, J., Krzyzanek, V., Hrubanova, K., Masilko, J., Slaninova, E., Trudicova, M., and Obruca, S. Introducing the Newly Isolated Bacterium Aneurinibacillus sp. H1 as an Auspicious Thermophilic Producer of Various Polyhydroxyalkanoates (PHA) Copolymers–2. Material Study on the Produced Copolymers. *Polymers.* 2020, 12, 1298. Attached as Appendix 13.

use of the materials in the production of active and/or intelligent packaging, we have been focusing mainly on the deformation behavior (stress-strain response) of the films, their surface properties (wettability), transport properties (i.e. release kinetics of hydrophilic and hydrophobic solutes from the polymer films) and barrier performance (gas permeability of the films). Considering also potential biomedical uses of the polymers, we have assayed also the biodegradation of the films in model body fluids. Although the study is still in progress, the preliminary results confirm that all these properties, expectedly dependent on the crystallinity of the material, can be tailored via adjustment of the monomer composition of PHA copolymers by controlling the conditions of the biotechnological process (some examples of the preliminary results on the barrier and transport properties are shown in Fig. 37 and 38, first results on the biodegradation have already been submitted for publication).

To conclude, the degree of the molecular order in the architecture of PHA systems is not only of great biological importance in the natural intracellular PHA granules but also of extraordinary significance in the development of reasonable PHA materials for artificial uses. As nature has found ways of how dealing with PHA crystallinity in the living cells, we also need to find our options on how to manipulate this essential, performance-ruling property of PHA utilized technologically. In our work, we have experienced how beneficial the synergy between bio(techno)logy and material (or physical) chemistry might be in taking this challenge.
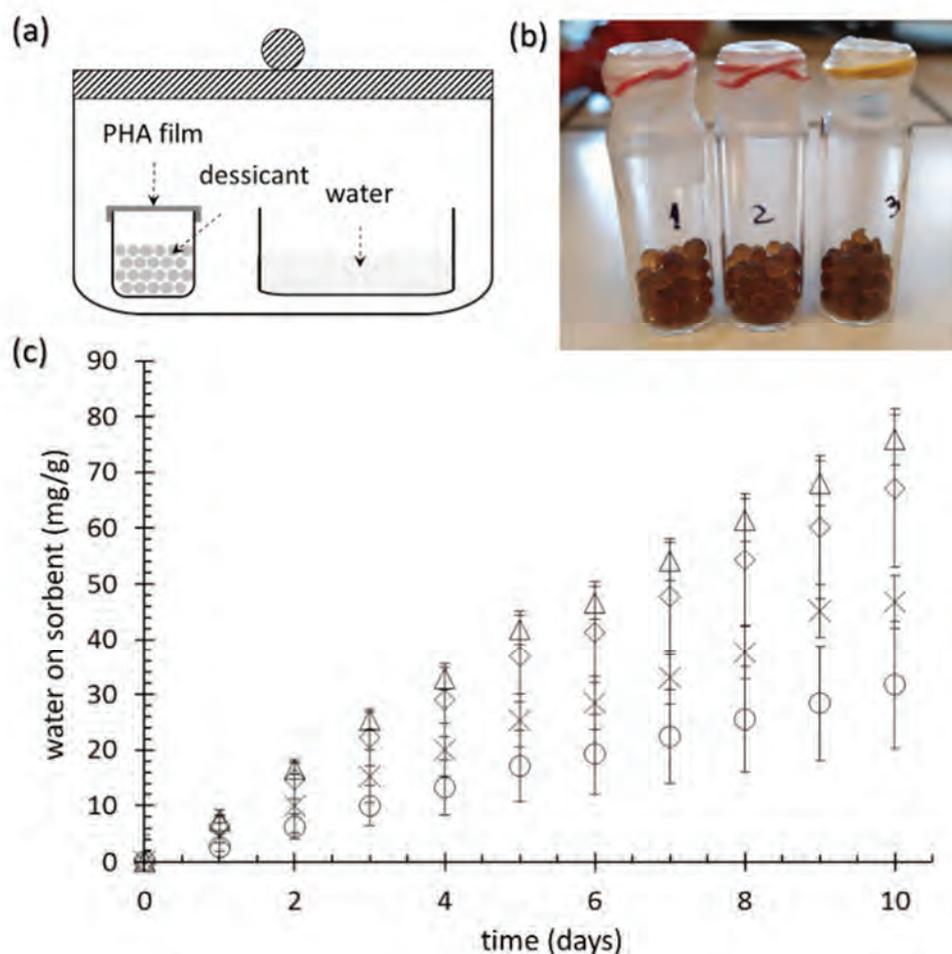
Fig. 37   Example of results from a preliminary study on barrier properties of PHA polymers with different monomer compositions. (a) Schematics of the experimental setup for determination of water vapor permeability of the PHA polymer films. (b) Picture of the sorbent (desiccant) container with the PHA film fixed on the orifice. (c) Amount of water absorbed by the desiccant as a function of time for P(3HB-co-4HB) copolymers containing different relative contents of 4HB: 0% (○), 39% (◇), 54% (×), and 94% (△).
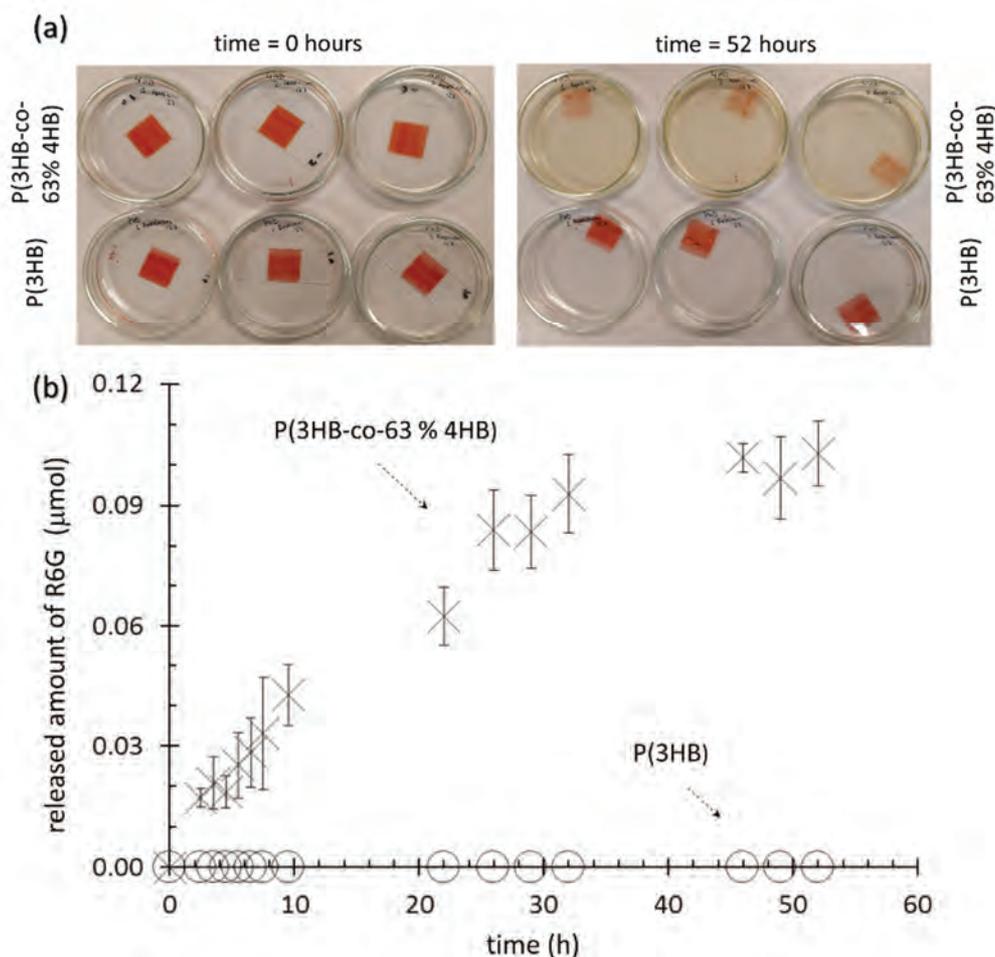
Fig. 38   Example of results from a preliminary study on transport properties of PHA polymers with different monomer composition – release of Rhodamine 6G incorporated into the film during solvent-casting (concentration of R6G in the polymer solution 1g/L). (a) Picture of the samples at the start and the end of the release experiment. (b) Kinetics of RG6 release during the first ten hours of the experiment.

References

[62]   Kleber, M. et al. *Journal of Environmental Quality*, 2019, 48, 207–216.

[63]   Achard, F. K. *Chemische untersuchung des torf*. Crell's Annalen: 1786.

[64]   Feller, C. *Advances in Geoecology*. 1997, 29, 15–46.

[65]   Gerke, J. *Agronomy*. 2018, 8, 76.

[66]   García, A. C. et al. *Scientific Reports,* 2016, 6, 20798.

[67]   Weber, J. et al. *Journal of Soils and Sediments*, 2018, 18, 2665–2667.

[68]   Mosa, A. et al. *Egyptian Journal of Soil Science*, 2020, 30, 211–229.

[69]   Rupiasih, N. N. et al. *Asian Journal of Water, Environment and Pollution*, 2008, 5, 39–47.

[70]   Peña-Méndez, E. M. et al. *Journal of Applied Biomedicine*, 2005, 3, 13–24.

[71]   Schulten, H. R. et al. *Naturwissenschaften*, 1993, 80, 29–30.

[72]   Simpson, A. J. et al. *Naturwissenschaften*, 2002, 89, 84–88.

[73]   Sutton, R. et al. *Environmental Science & Technology*, 2005, 39, 9009–9015.

[74]   Wershaw, R. L. *Soil Science*, 1999, 164, 803–813.

[75]   Piccolo, A. *Soil Science*, 2001, 166, 810–832.

[76]   Piccolo, A. *Advances in Agronomy*, 2002, 75, 57–134.

[77]   von Wandruszka, R. *Soil Science*, 1998, 163, 921–930.

[78]   Olk, D. C. et al. *Journal of Environmental Quality* 2019, 48(2), 217–232.

[79]   Olk, D. C. et al. *Journal of Environmental Quality* 2019, 48(6), 1633–1643.

[80]   Chianese, S. et al. *Molecules*, 2020, 25, 918.

[81]   Crank, J. *The mathematics of diffusion*. Oxford University Press, U.S.A.: 1979.

[82]   Stevenson, F. J. *Humus chemistry: genesis, composition, reactions*. John Wiley and Sons Ltd.: 1994.

[83]   Xiong, J.-Y. et al. *The Journal of Physical Chemistry B*, 2005, 109, 5638–5643.

[84]   Liu, A. et al. *Langmuir*, 2000, 16, 3902–3909.

[85]   de Paolis, F. et al. *Chemosphere*, 1997, 34, 1693–1704.

[86]   Ran, Y. et al. *Environmental Science & Technology*, 2007, 41, 3952–3958.

[87]   Kühnel, E. et al. *Angewandte Chemie International Edition*, 2007, 46, 7075–7078.

[88]   Nebbioso, A. et al. *Biomacromolecules*, 2011, 12, 1187–1199.

[89]   Hayes, M. H. B. *Soil Science Society of America Journal*, 2006, 70, 986–994.

[90]   Senesi, N. et al. *Journal of Soil Science*, 1983, 34, 801–813.

[91]   Piccolo, A. *Soil Science*, 1988, 146, 418–426.

[92]   Canellas, L. P. et al. *Chemical and Biological Technologies in Agriculture*, 2014, 1, 3.

[93]   Nardi, S. et al. *Scientia Agricola*, 2016, 73, 18–23.

[94]   Tejada, M. et al. *Biological Agriculture & Horticulture*, 2003, 21, 277–291.

[95]   Pizzeghello, D. et al. *New Phytologist*, 2001, 151, 647–657.

[96]   Zandonadi, D. B. et al. *Planta*, 2007, 225, 1583–1595.

[97]   Jackson, T. A. Effects of clay minerals, oxyhydroxides, and humic matter on microbial communities of soil, sediment, and water. *In Environmental Impact of Soil Component Interactions: Metals, Inorganics and Microbial Activity*; CRC Press, 1995; pp. 165–200.

[98]   Parandian, F. et al. *International Research Journal of Applied and Basic Sciences*, 2012, 3, 924–929.

[99]   P. Dorer, S. et al. *The International Turfgrass Society Research Journal*, 1997, 8, 437–443.

[100] Liu, C. et al. *HortScience*, 1998, 33, 1023–1025.

[101] Olk, D. C. et al. *Journal of Soils and Sediments*, 2018, 18, 2881–2891.

[102] Rose, M. T. et al. *Advances in Agronomy*, 2014, 124, 37–89.

[103] Lyons, G. et al. *Agronomy*, 2016, 6, 50.

[104] Klöcking, R. et al. Medical aspects and applications of humic substances. *In Biopolymers for Medical and Pharmaceutical Applications*; Wiley-VCH Verlag GmbH, 2005; pp. 3–16.

[105] de Melo, B. A. G. et al. *Materials Science and Engineering: C*, 2016, 62, 967–974.

[106] Jacobi, U. et al. *Skin Research and Technology*, 2007, 13, 19–24.

[107] Ranamukhaarachchi, S. A. et al. *Scientific Reports*, 2016, 6, 32074.

[108] Canellas, L. P. et al. *Scientia Horticulturae*, 2015, 196, 15–27.

[109] Gerke, J. *Journal of Plant Nutrition and Soil Science*, 2021, 184, 329–338.

[110] Farenhorst, A. *Soil Science Society of America Journal*, 2006, 70, 1005–1012.

[111] Veryho, N. et al. *Acta Balneologica*, 2016, 58, 45–49.

[112] Tian, X. et al. Property of mud and its application in cosmetic and medical fields: A review. *Environmental Geochemistry and Health*, 2022.

[113] Mirza, M. A. et al. *Results in Pharma Sciences*, 2011, 1, 16–26.

[114] Mirza, M. A. et al. *Science of Advanced Materials*, 2011, 3, 223–232.

[115] Mirza, M. A. et al. *Drug Development and Industrial Pharmacy*, 2011, 37, 310–319.

[116] Steinbüchel, A. *FEMS Microbiology Letters*, 1995, 128, 219–228.

[117] Silveira Alves, L. P. et al. *Applied and Environmental Microbiology*, 2019, 85, e02586-18.

[118] Sun, Y.-W. et al. *Applied and Environmental Microbiology*, 2019, 85, e00717-19.

[119] Kim, J. K. et al. *Proceedings of the National Academy of Sciences*, 2013, 110, e2381-9.

[120] Sadykov, M. R. et al. *Molecular Microbiology*, 2017, 104, 793–803.

[121] Bioplastics market development update 2020. https://docs.european-bioplastics.org/conference/Report_Bioplastics_Market_Data_2020_short_version.pdf (accessed Mar. 28, 2022).

[122] Gool, A. P. et al. *Archiv für Mikrobiologie*, 1969, 69, 281–293.

[123] Pötter, M. et al. Biogenesis and Structure of Polyhydroxyalkanoate Granules. *In Inclusions in Prokaryotes*; Springer-Verlag, 2006; pp. 109–136.

[124] de Koning, G. J. M. et al. *Polymer*, 1992, 33, 3292–3294.

[125] Schubert, P. et al. *Journal of Bacteriology*, 1988, 170, 5837–5847.

[126] Poirier, Y. et al. *Science*, 1992, 256, 520–523.

[127] Lauzier, C. et al. *FEMS Microbiology Letters*, 1992, 103, 299–310.

[128] Bonthrone, K. M. et al. *FEMS Microbiology Letters*, 1992, 103, 269–277.

[129] Gebauer, B. et al. *Applied and Environmental Microbiology*, 2006, 72, 6094–6100.

[130] Polyhydroxyalkanoate (PHA) Market Global Forecast to 2025. https://www.marketsandmarkets.com/Market-Reports/pha-market-395.html (accessed Mar. 28, 2022).

[131] Israni, N. et al. Polyhydroxyalkanoates in Packaging. *In Biotechnological Applications of Polyhydroxyalkanoates*; Springer Singapore, 2019; pp. 363–388.

[132] Vandewijngaarden, J. et al. *Journal of Polymers and the Environment*, 2016, 24, 104–118.

[133] Zhang, M. et al. *Advances in Polymer Technology*, 2011, 30, 67–79.

Chapter 6:
"Physical microbiology": physicochemical support for biotechnology and microbiology

"Gentlemen, it is the microbes who have the last word"
(*Louis Pasteur*)

In the next chapter, we will unzoom our focus from individual chemical components (such as the biocompounds discussed previously) to whole organisms – although perhaps the simplest ones. My personal scientific interest in microbes began in 2015 when I was invited to join a research project dealing with PHA-producing bacteria. Before I had considered bacteria as something that no physical chemist would intentionally keep company with and if someone accidentally met it, after all, he or she would care only about getting himself/herself prescribed antibiotics. Very soon, I realized how silly my original idea of bacteria was.

Bacteria are the oldest known and the most widespread inhabitants of the planet Earth. We can find some of the approximately five million trillion trillion (no, the second trillion is not there by mistake!) of them literally everywhere – from deep thermal vents to clouds in the atmosphere, to the inside of our body (in there, the number of bacterial cells outnumbers the human body cells by tens of percent). Lined up end to end, they would stretch some 10 billion light-years — literally from here to the edge of the visible universe. Among these huge numbers, the vast majority of them is harmless or even helpful for humans. And, furthermore, these "simple" organisms are outstandingly attractive for scientists. Not just because most of them are yet to be identified, but also the old acquaintances are still full of surprise, as we have experienced in our research. And, as I will try to illustrate in this chapter, also in the study of these living organisms, physical chemistry can do a great job. Not only by expanding the methodology for cell analysis by techniques and analytical approaches conventionally utilized in totally different research areas (section 6.1), but also by providing original concepts and perceptions in understanding and explaining interesting biological phenomena (sections 6.2 and 6.3).

During the last 7 years, on the research topics dealing with bacteria, we have built an original interdisciplinary scientific approach involving microbiology, biotechnology, and physical and material chemistry. To emphasize the equal partnership of all participants, we internally call it "physical microbiology". This chapter aims at summarizing how this original approach has contributed to the state-of-the-art in understanding the ecological and evolutionary role of microbial polyhydroxyalkanoates.

6.1 Being stuffed with plastics: polyhydroxyalkanoates in bacteria

Nowadays, when plastic pollution becomes one of the most pressing environmental issues, we may easily have the plastics up to our necks. But what if this is not just figuratively speaking? How would it feel to have our bodies stuffed with plastic? Terrible vision, isn't it? Surprisingly, we know organisms that experience exactly this feeling and, moreover, it seems that in fact, they enjoy it very much.

Again, we are of course talking about bacteria. More specifically, about some of the polyhydroxyalkanoates (PHA) accumulating bacteria. These organisms literally stuff their cells with PHA in form of cellular inclusions called carbonosomes or PHA granules (I have discussed them already in section 5.2.1). In Fig. 39, one of the most potent producers of PHA, *Cupriavidus necator* H16 is shown (for comparison, together with PHA non-accumulating mutant strain *C. necator* PHB–4) to illustrate how crowded the intracellular space of PHA producers can be. It has been known for a long time that the ability to produce and accumulate PHA is widespread in the microbial world. It is possessed by various Gram-negative and Gram-positive bacteria, autotrophic as well as heterotrophic, aerobes and anaerobes, and also by some archae strains. Interestingly, PHA synthesis is also surprisingly frequent

among the extremophilic organisms that colonized some of the most adverse niches of our planet. Since the accumulation of PHA is so popular within the bacteria genus, it is very likely that they provide their producers with a significant ecological advantage.
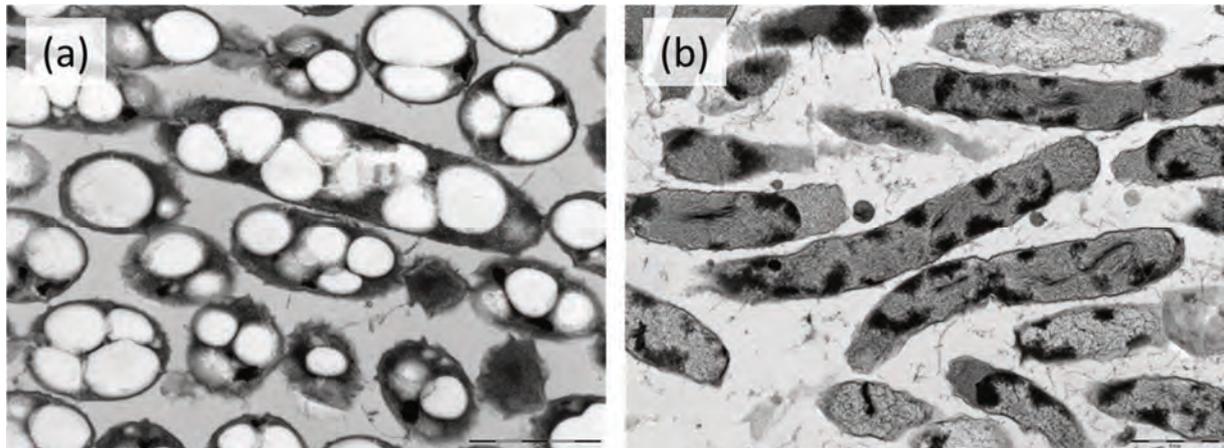

Fig. 39   Cells of (a) PHA accumulating Cupriavidus necator H16 and (b) PHA non-accumulating C. necator PHB–4 observed by TEM.

Originally, it was assumed that the role of PHA is solely in the storage of energy and carbon for the situations when their other sources are depleted. Nevertheless, at the time when I entered the topic of PHA, more and more suggestions began to appear that the ecological role of these polymers is in fact much more complex. At that time, great attention was paid to the biotechnological production of PHA at Faculty of Chemistry, BUT, and the involved researchers came up with various reports on how exposition of bacterial culture to controlled stress dose might be beneficial in terms of providing enhanced accumulation of PHA in bacterial producers [134–136]. Moreover, several other authors had reported that some PHA accumulating strains revealed higher stress resistance against various environmental stress factors than mutants unable of PHAs production or degradation [137–142]. Among them, Kadouri proposed that a detailed understanding of the role of PHA in stress resistance and adaptation represented a great challenge to the microbial ecology [142]. Altogether, this motivated the establishment of a new interdisciplinary research group at Faculty of Chemistry, BUT, that decided to accept this challenge and perform a complex study on how the PHA presence affects the biochemical and biophysical state of bacterial cells and what are the particular mechanisms of PHA involvement in stress robustness of bacteria.

I have joined this research group to provide methodological and descriptive approaches of physical chemistry, that I had been using by that time mainly in soft matter analysis. In the following text, I will summarize how these attitudes, rather unconventional concerning the study of living organisms, were found beneficial in providing original information on the effects of PHA on the chemical and physical structure of the cells (section 6.1.1), their morphology (6.1.2) as well as biophysical (6.1.3) and physiological state (6.1.3), and how this knowledge was transformed into understanding the interconnection between PHA and stress resistance and adaptation of microbial cells (sections 6.2 and 6.3).

6.1.1   Qualitative and quantitative determination of PHA in the cells

Naturally, either the fundamental research or the biotechnological production of PHA brings a constant need for analytical tools for PHA determination in the cell biomass. Routinely, this is provided by chromatographic analysis (gas or liquid) of the polymer after its isolation and necessary chemical transformation. These analytical methods are robust and precise, nevertheless, their main drawback lies in the time-demanding step of the sample treatment before the analysis. Altogether, it usually takes several hours to obtain the result which might be very limiting, mainly when just a rapid confirmation of the presence or a semi-quantitative screening of PHA content is needed for control of

71

the experiment or the biotechnological process. We have therefore put a lot of effort into finding an alternative method for rapid screening of PHA content in the bacterial culture.

Among various tested methods, we identified several promising candidates for a fast screening of PHA content in the biomass. For instance, we have confirmed experimentally that in a thermogram obtained from TGA analysis of *C. necator H16*, PHB content can be determined indirectly from the relative weight loss of the sample in the range from 200 °C to 400 °C, which shows a good correlation with percent content of PHA in cell dry weight determined by GC (Fig. 40). Nevertheless, vibrational spectroscopy methods proved to be the most powerful tool regarding not only the quantitative determination of PHA but also concerning direct mapping of the structure of PHA in the cells. Among the main advantages of the techniques of vibrational spectroscopy (infrared and Raman spectroscopy) belong the fast determination of molecular spectra of the sample with no special sample treatment required (timeline of the analysis is schematically shown in Fig. 41), and also high spectral sensitivity and specificity (i.e. low spectral interference of other biomass components).
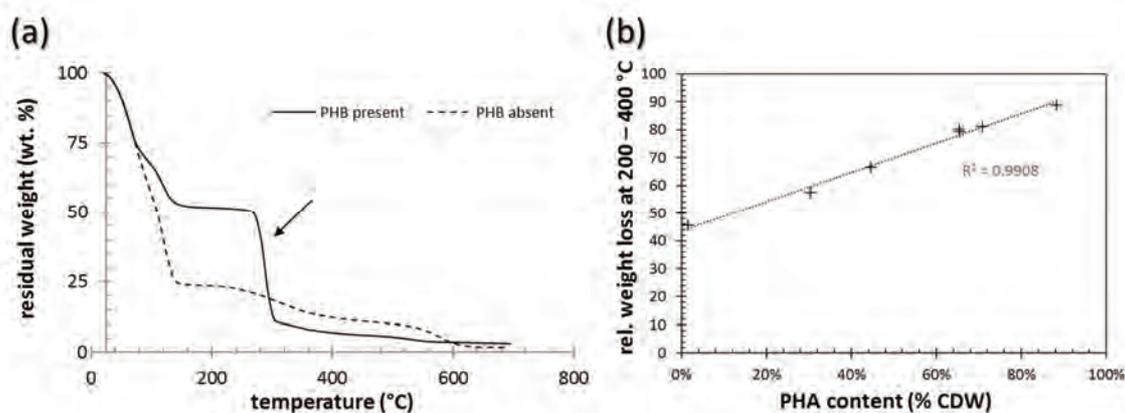
Fig. 40   Thermogravimetry of PHA producing cells (heating rate: 10°C/min, atmosphere: air). (a) Thermogram showing the temperature range at which PHA degradation is manifested (marked with arrow). (b) Correlation between relative weight loss in the range from 200 to 400 °C and the weight content of PHA.
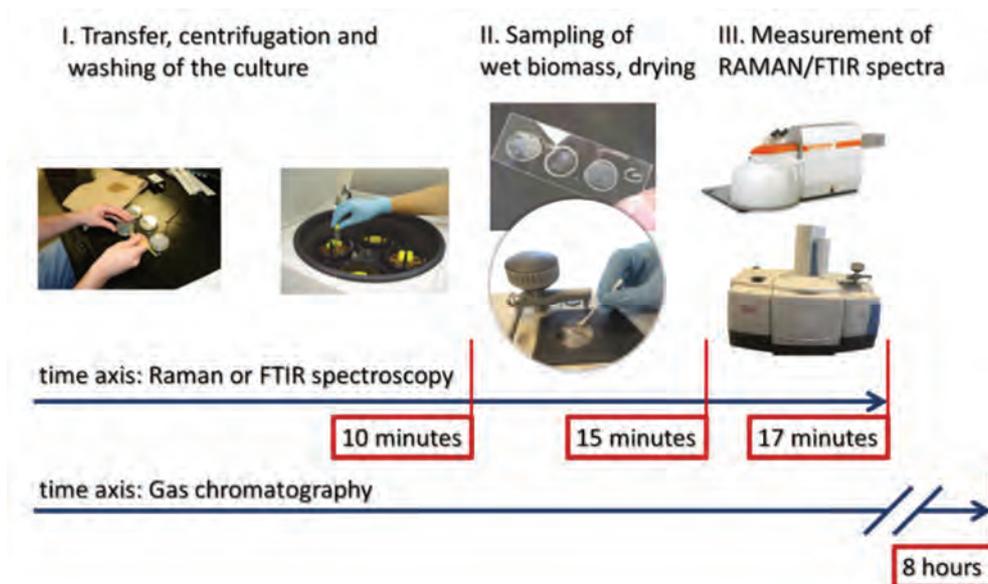
Fig. 41   Timeline showing a reduced time demands on the determination of PHA content in biomass by means of vibrational spectroscopy (Raman or FTIR) as compared to commonly used GC analysis (adopted with modifications from our published study[XIX]).

An example of Fourier-transform infrared (FTIR) spectra of biomass containing PHA obtained by the method of Attenuated Total Reflection (ATR) is shown in Fig. 42a. It can be seen that a presence of PHA in the culture can easily been identified from the spectra (mainly by the presence of stretching C=O vibration in the polyester group at about 1720 cm^{-1}) as we have been using for sorting of PHA positive/negative cultures (will be discussed in 6.2.3). We have also found that among the various characteristic vibration bands, good correlations with the PHA content can be found for individual PHA-producing strains. In Fig. 42b it can be seen that signal of the most intensive FTIR absorption band at 1720 cm^{-1} does not provide a linear correlation with PHA content in the most potent PHA producers (such as *C. necator* H16) and other bands (e.g. C–O–C stretching at 1180 cm^{-1}) are more suitable for quantitative PHA determination. On the other hand, the band at 1720 cm^{-1} was found to be much more useful for quantitative PHA determination in cyanobacteria or other PHA producers where the accumulated PHA content is much lower (lower than ca 20% of CDW).
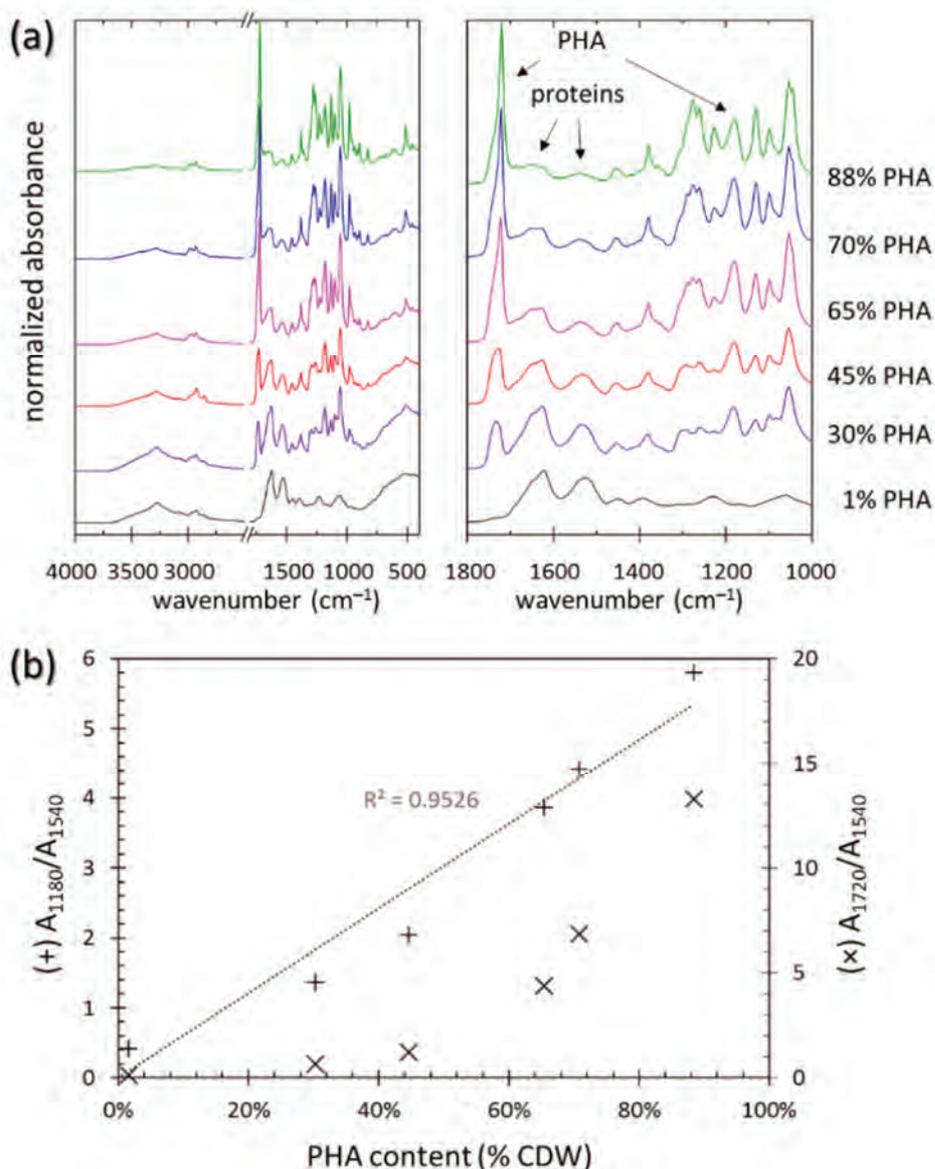
Fig. 42   Semi-quantitative analysis of PHA in biomass by ATR-FTIR spectroscopy. (a) ATR spectra of dry biomass of C. necator H16 with different amounts of accumulated PHA (determined by GC-FID). (b) Correlation of selected FTIR markers of PHA (absorbances at 1720 and 1180 cm^{-1}, respectively, normalized on amide II band at 1540 cm^{-1}) with PHA content in biomass.

We have performed a comprehensive study on the usability in the determination of PHA in bacterial biomass also for Raman spectroscopy[XIX]. Unlike FTIR, in the Raman spectra we have found linear correlation between the signal of the stretching C=O band (at about 1730 cm^{-1}, normalized to signal of protein or DNA) and PHA in the wide range of accumulated amounts (from 10 to about 90 % of CDW). Hence, we demonstrated that both techniques provide clear benefits over commonly used techniques of PHA identification, such as gas chromatography, in the speed and noninvasiveness of the quantification process.
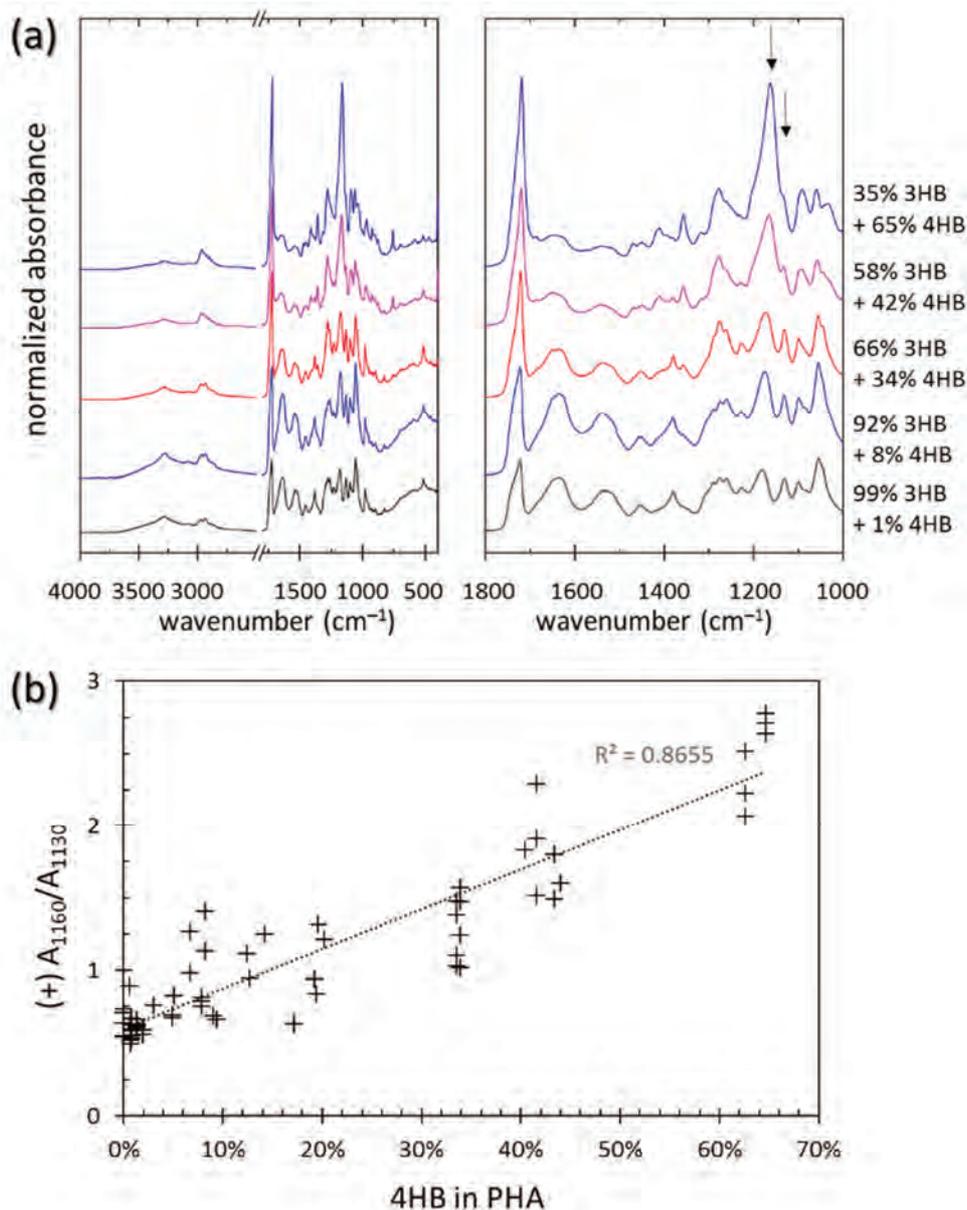
Fig. 43   ATR-FTIR analysis of PHA monomer composition in biomass. (*a*) *ATR FTIR spectra of Aneurinibacillus sp. H1 biomass with accumulated P(3HB-co-4HB) copolymers with various monomer compositions.* (*b*) *Correlation of selected FTIR marker of 4HB/3HB content* (*ratio of absorbances at 1160 and 1130 cm^{-1}*) *with relative content of 4HB in the copolymer* (*determined for various cultivations including data provided in Fig. 43a*)*.

[XIX] Samek, O., Obruča, S., Šiler, M., Sedláček, P., Benešová, P., Kučera, D., Márova, I., Ježek, J., Bernatová, S., and Zemánek, P. Quantitative Raman Spectroscopy Analysis of Polyhydroxyalkanoates Produced by Cupriavidus necator H16. *Sensors.* 2016, 16, 1808.

FTIR analysis was found useful also in qualitative analyses concerning the monomer composition of the produced PHA polymers. Aside from the obvious effects of the monomer composition on the FTIR spectra of isolated polymers (discussed in detail in the papers dealing with the biotechnological production of the copolymer PHA[XVI,XVIII], see also Fig 35), we have also experienced that the manipulation with the monomer composition of PHA by the biotechnological process can be monitored by FTIR also directly in microbial biomass without the need for polymer isolation (Fig. 43). Last but not least, aside from the quantification and monomer composition analysis, vibration spectroscopy techniques allow also monitoring of the structural changes that PHA undergoes in the cells. We have already discussed in 5.2.1 that the crystallization of PHA can be monitored by FTIR as we demonstrated in our study focused on the stress-induced crystallization of PHA in *C. necator* cells[XIV]. We have described similar spectral signatures of the changes in the degree of the molecular order of PHA also in Raman spectra[XX] of stress-exposed cells. As it is illustrated in Fig. 44, the crystallization of intracellular PHA can be induced also in dry biomass, for instance by pressure applied (see Fig. 44a,b) or by radiant heat (see Fig. 44c,d). We have confirmed that, in all these cases, both Raman and FTIR spectroscopy allow easy and "real-time" monitoring of the changes in PHA crystallinity. The results of these techniques were also proved to be in good agreement with other methods of crystallinity analysis, such as X-ray diffractometry (see Fig. 44d).

Obviously, we have gathered a wide collection of experimental shreds of evidence that the vibration spectroscopy techniques represent a powerful and versatile analytical tool that can be beneficially used in the research studies and technological processes involving PHA-producing bacteria. Of course, interpretation of the vibrational spectra need not be limited to PHA. We have shown in our PHA-crystallization study[XIV] that the structural changes overcome by cell proteins can be monitored in the culture at the same time. Similarly, we have experienced that the techniques can be used for simultaneous monitoring of other metabolites that accompany the accumulation of PHA, such as polyphosphates, or glycogen that is often co-accumulated by PHA producing cyanobacteria.

Speaking of PHA accumulation by cyanobacteria, another example can be offered of how an unconventional spectroscopic approach with little instrumental and cost demands can simplify the way of monitoring compositional changes in culture during a cultivation process. It is well known that during nitrogen starvation which induces PHA accumulation, the cells gradually change from a vegetative to a dormant state [143]. The most obvious feature of this is the change in color of the cell culture from blue-green to brownish-yellow which is caused by the degradation of photosynthetic pigments (see Fig. 45a). The most often used way how to monitor the changes in pigment composition is by extracting the pigments from the biomass by ethanol. This procedure is time-consuming and destructive for the cell sample. Direct spectrophotometric monitoring of the pigment composition in the cell culture is disabled by significant light scattering (see Fig. 45b,d). To overcome this, we have introduced the method of diffuse transmittance spectrophotometry. This method allows the determination of UV-VIS spectra even in highly turbid samples such as cell cultures. As can be seen in Fig. 45, this method provides spectral evidence of the alteration in pigment composition with a nice resolution directly in the liquid cell culture. Recently, we have published an experimental study where the agreement between the conventional pigment extraction technique and the diffuse transmittance spectroscopy was demonstrated[XXI]. Additional ways of how the technique can contribute to the analysis of bacterial cultures will be discussed in 6.1.3. Clearly, the technique provides another

---

[XX] Obruca, S., Sedlacek, P., Mravec, F., Krzyzanek, V., Nebesarova, J., Samek, O., Kucera, D., Benesova, P., Hrubanova, K., Milerova, M., and Marova, I. The presence of PHB granules in cytoplasm protects non-halophilic bacterial cells against the harmful impact of hypertonic environments. *New Biotechnology.* 2017, 39, 68–80. Attached as Appendix 14.

[XXI] Meixner, K., Daffert, C., Dalnodar, D., Mrázová, K., Hrubanová, K., Krzyzanek, V., Nebesářová, J., Samek, O., Šedrlová, Z., Slaninova, E., Sedláček, P., Obruča, S., and Fritz, I. Glycogen, poly(3-hydroxybutyrate) and pigment accumulation in three Synechocystis strains when exposed to a stepwise increasing salt stress. *Journal of Applied Phycology.* 2022**.**

Fig. 44 Monitoring of PHA crystallization in biomass by various methods of structural analysis. PHA crystallization was induced by exposing the dry biomass of C. necator H16 to mechanic pressure (a, b) and radiant heat (c, d). Spectral markers of crystallization as observed in FTIR 2D and 1D spectra, respectively (a, b), Raman spectra (c) and X-ray diffraction spectrum (d).

illustration of a successful transfer of methodology and knowledge in the fields of physical chemistry and biology.
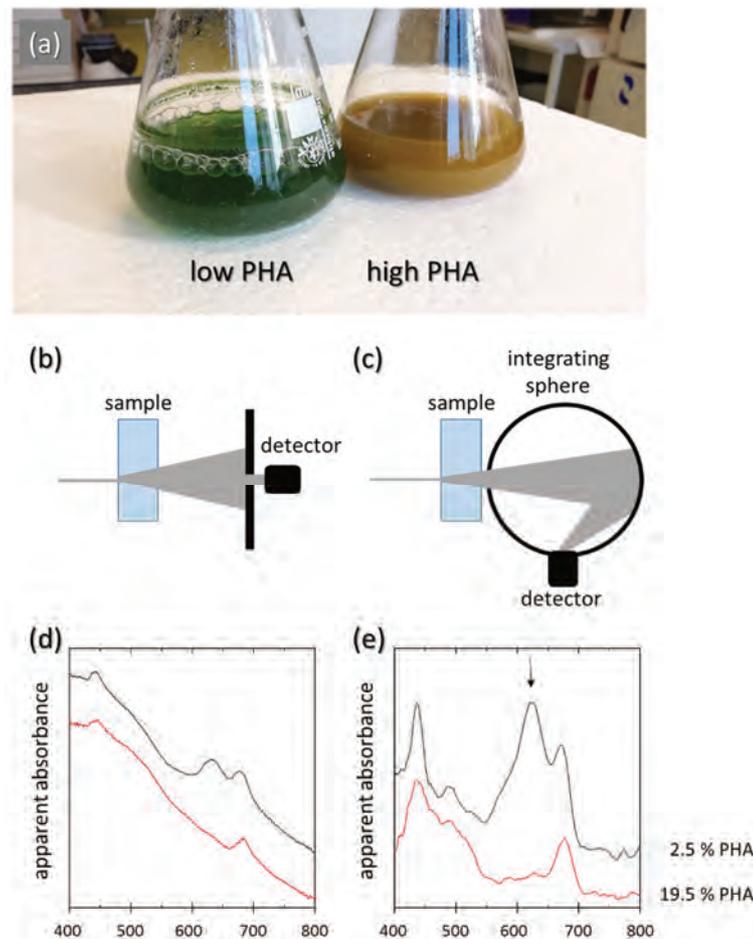
Fig. 45   Monitoring the changes in pigment compositions in the cultures of PHA-accumulating cyanobacteria Synechocystis CCALA192. (a) Nitrogen limitation that induces PHB accumulation in the cells is accompanied by the color change from blue-green to brownish-yellow. Schematic representation of conventional spectrophotometric analysis (b) that provides spectra significantly affected by light scattering (d). Schematic representation of Diffuse transmittance spectrophotometry where the scattered light is collected with an integrating sphere and the spectra information on the pigment composition changes with a good resolution (e). In the spectra, the degradation of phycocyanin is depicted by the disappearance of characteristic absorption at 630 nm (marked with an arrow).

6.1.2   Morphology and ultrastructure of PHA containing cells

On the other hand, there are also methods, that have already been shared effectively between life and material sciences for a long time. For example, methods that visualize morphology, topography and ultrastructure of a sample represent an essential part of the experimental equipment no matter whether the subject of the study subject is an artificial material or a living cell.

In our studies dealing with the ecological and evolutionary role of microbial PHA, we have involved these techniques as well. Transmission electron microscopy – providing cell images such as those shown in Fig. 39 - has continuously been involved to illustrate the physiological state of the studied cultures under specific conditions by showing how the cells in the culture are sized, shaped, what are their ultrastructures, and whether any signs of the cell damage (e.g. loss of cell membrane integrity) are visible. Similarly, we tested and employed diverse microscopy techniques focused on monitoring

the surface of the cells and complementing hence ultrastructural information from TEM with that concerning the cell topography (the techniques are summarized in Fig. 46). Also in our work, the major goal of using these techniques was in providing qualitative findings regarding the cell culture under investigation. Nevertheless, beyond the frontiers of these common uses, we have also suggested and successfully utilized several approaches how to extract important quantitative data from microscopy images.

We already emphasized in the previous section that, considering PHA is the cellular component of our primary concern, the amount of PHA in the cells has always represented an experimental parameter essential for a reasonable interpretation of the culture behavior under the particular environmental conditions. In addition to expressing PHA content in the cells only in terms of the relative share of cell dry weight, as usual, we considered also how the amount is distributed in the cell ultrastructure and how it participates in the total cell volume. This is essential for understanding the general consequences of the presence of PHA granules in the cells, as far as any changes in cell morphology affecting the ratio of cell surface and cell effective volume influence the metabolic activity of the cells – it affects fluxes of metabolites, exchange of nutrients etc. [144].
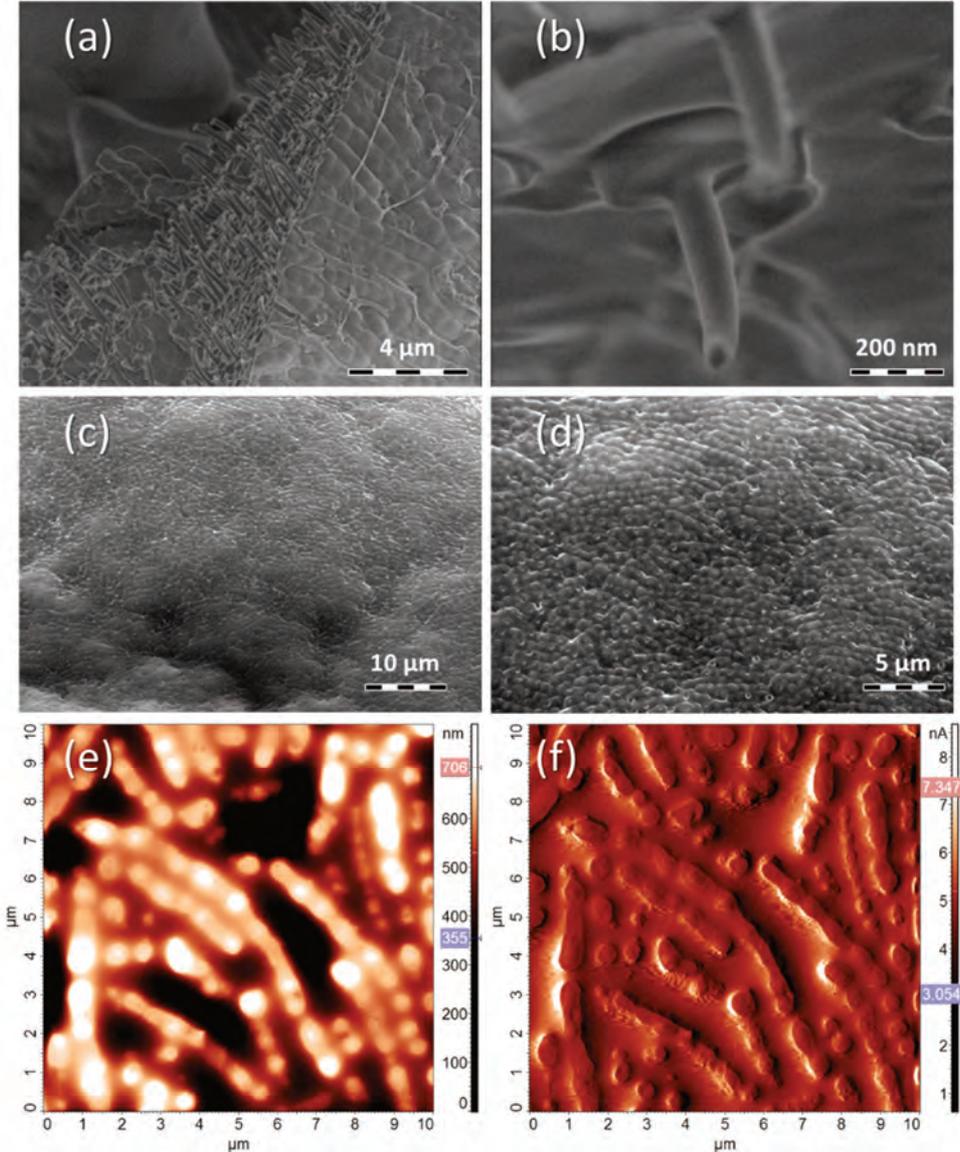
Fig. 46   Topography of PHA accumulating cells visualized by various methods of advanced microscopy: cryoSEM (a, b), Environmental SEM (c, d), AFM (e. f).

Fig. 47a shows typical TEM image of the culture with randomly oriented cells of *C. necator* H16 with a high content of accumulated PHA (in particular, 78 % of cell dry weight as determined by GC). Obviously, the shape and structure of the visualized cells are affected by their orientation with respect to the direction of slicing (see Fig. 47b). On the one hand, this can sometimes complicate qualitative interpretation of the displayed structural features, because only the cells cut in the middle provide an accurate projection of the internal structure. Nevertheless, it is known from stereology that in systems with random morphology, the volume fraction and the area fraction in a random section through the system are approximately equal [145]. Therefore, we have been continuously using TEM images such as the one shown in Fig. 47a to determine the volume fraction of PHA granules in the imaged cells.
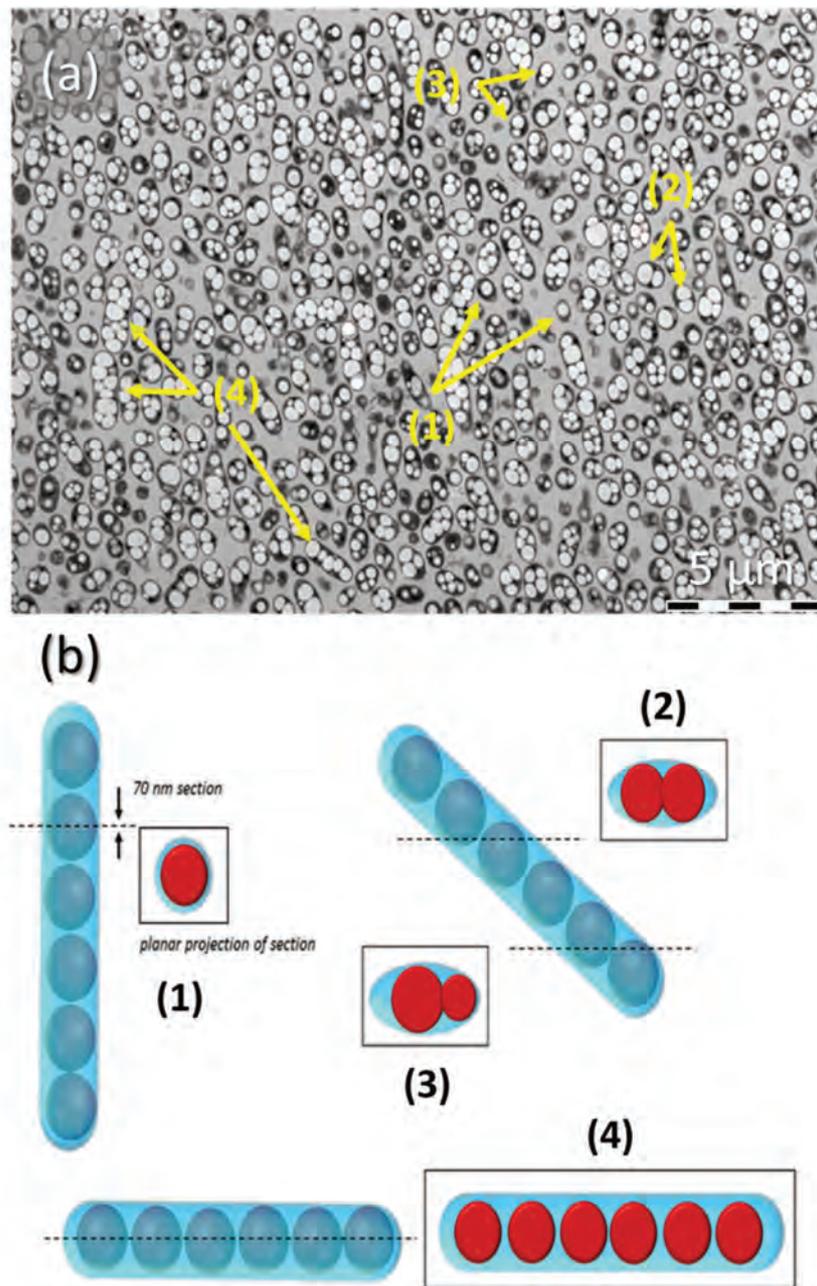
Fig. 47   TEM visualization of the ultrastructure of PHA accumulating cells. (a) Example of TEM micrograph used for the quantitative image analyses. (b) The effect of the preparation of thin-slices for TEM on observed morphologies and diameters of PHA accumulating cells and granules. The corresponding cell section is marked in Fig. 47a. The figure was adopted from our publication[XXII].

The method of TEM image analysis that we developed for this purpose was described in our paper which focuses primarily on morphological analysis of PHA accumulating bacteria by confocal fluorescence microscopy (will be shortly discussed later)[XXII]. In this study, TEM analysis was used as a reference method to confirm the results determined by the fluorescence technique. The TEM image analysis procedure is illustrated in Fig. 48. We used a set of different TEM micrographs (10 in total), including also various magnification levels, to obtain a statistically reliable result. The crucial step of the analysis is the selection of appropriate threshold levels to provide independent visualization of PHA granules and remaining intracellular space, respectively. To find the thresholds, we performed the fractal analysis of the images using the software HarFA, developed at the Faculty of chemistry, BUT. To visualize the cell cytosol, threshold level 1 (see Fig. 48a) was selected as the value, for which the fractal characteristics showed minimal change in the course of the range analysis. On the other hand, for the depiction of the PHA granules, the threshold level 2 (Fig. 48b) showed a local minimum on the function, corresponding to the interface between black and white fractal structures. Area fraction of the cell cytosol and PHA granules, respectively, were calculated from the relative fraction of black/white pixels at the corresponding threshold level.
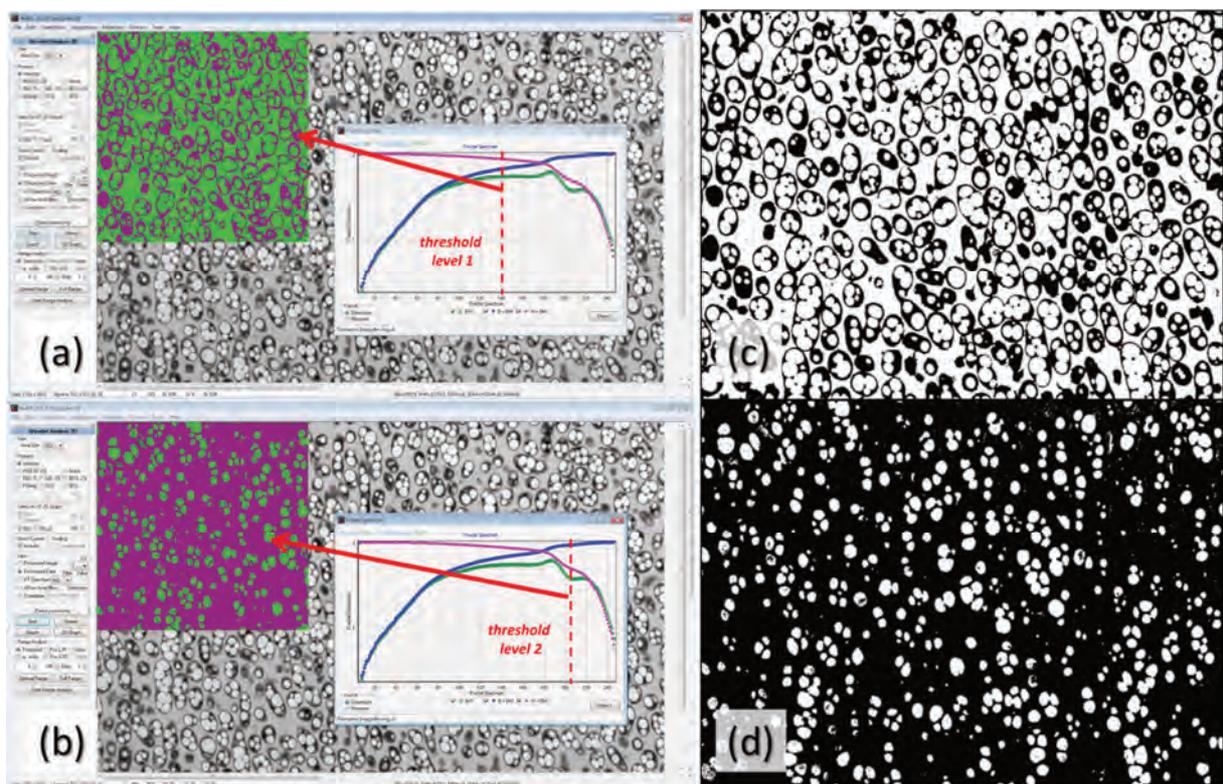
Fig. 48   Use of image analysis (software tool HarFA developed at Brno University of Technology) in the determination of the volume fraction of PHA granules in the cells of C. necator H16 from TEM micrographs (illustrated on the TEM image shown in Fig. 47a). The rule of stereology is used that states for random morphology systems with the volume fraction and the area fraction in a random section through the system are approximately equal. Fractal analysis was applied to find appropriate threshold levels which provided a separate depiction of the cell cytosol (a, c) and of the PHB granules (b, d), respectively. Respective area fractions of PHA granules in the cells were determined by simple B/W pixel counting in the resulting images (c, d).

[XXII] Mravec, F., Obruca, S., Krzyzanek, V., Sedlacek, P., Hrubanova, K., Samek, O., Kucera, D., Benesova, P., and Nebesarova, J. Accumulation of PHA granules in Cupriavidus necator as seen by confocal fluorescence microscopy. *FEMS Microbiology Letters.* 2016, 363, fnw094.

Results of the analysis presented in paper[XXII] showed that the content of PHA corresponding to 78% of the cell dry weight is equivalent to 35 ± 3% of the cell volume occupied by the PHA granules. Evidently, this value provides a much more reliable projection of the extent to which the available space in the cell is limited by the presence of PHA granules. The results were also in good agreement with the fluorescence microscopy technique, where the volume fractions of the granules were determined on the single-cell level.

Since the pilot use of the TEM image analysis[XXII], we have utilized similar analytical approaches in various studies where changes in cell ultrastructure related to PHA were monitored. For example, in the study dealing with stress-induced crystallization of PHA in *C. necator* H16 cultures[XIV], we monitored coagulation of the granules by employing automatic identification and analysis of granules in TEM images with ImageJ software. Fig. 49 shows an example of the data obtained. It can be seen that the granule coagulation can be quantitatively expressed in the increased average value and the shifted distribution of sizes of the detected granules. Similarly, the circularity of the detected aggregates is significantly lowered compared to the intact granules. To sum up, both above-mentioned examples show that supplementing the conventional TEM imaging of the cell cultures with an appropriate image analysis approach can significantly enhance the contribution of the technique beyond the pure qualitative visualization and structural observation of the investigated biological objects. In the specific case of PHA accumulating bacteria, this combination also provides valuable information on how the intracellular space is affected by presence of PHA granules and how are the PHA-related ultrastructural features of the cells affected by the environmental conditions.

Considering the 2D projection artifacts mentioned above, to extract reliable quantitative morphological information from TEM analysis, it is necessary to image a statistically significant number of cells at once. This can sometimes be a difficult task, mainly under conditions where the cell growth is restricted and the cell density in the sample is low. Furthermore, it is difficult to address the variability in the morphological and ultrastructural features among the individual cells with this technique. Therefore, we have paid attention also to finding an analytical technique that would enable basic morphological characterization of the PHA producing cells also at a single-cell level.

The design of the method was described in the already mentioned morphological[XXII] study on *C. necator* H16 strain, its principle is schematically described in Fig. 50. The main aim was to find a method allowing monitoring changes in the size of the cells and PHA granules content and structure simultaneously. For this purpose, cell cultures were stained with DiD fluorescent probe (selective affinity for amphiphilic cell envelope) and Nile Red (staining of intracellular PHA granules). Signals from both probes were recorded simultaneously and separated based on their spectral and fluorescence lifetime properties. In combination with a confocal microscopy setup, this provided resolution of the analysis on the level of individual cells. Growths of the PHA-accumulating *C. necator* H16 strain and the PHA non-accumulating mutant *C. necator* PHB-4 were monitored in parallel. This study resulted in a very interesting finding that, during the growth and PHA biosynthesis, the volume fraction of PHA in a cell does not exceed 40% regardless of still increasing the weight content of PHA in CDM. During the gradual accumulation of PHA, cells appear to increase their lengths and regulate their diameters to assure that this maximal level of the volumetric fraction of PHA will not be exceeded. It indicates that the "overcrowding" of the intracellular space, with its multifaceted effect on cell metabolism, morphology, and also biophysical state (which will be discussed in the following section) of the cells, in the case of this PHA production champion reaches a kind of a physiological limit.
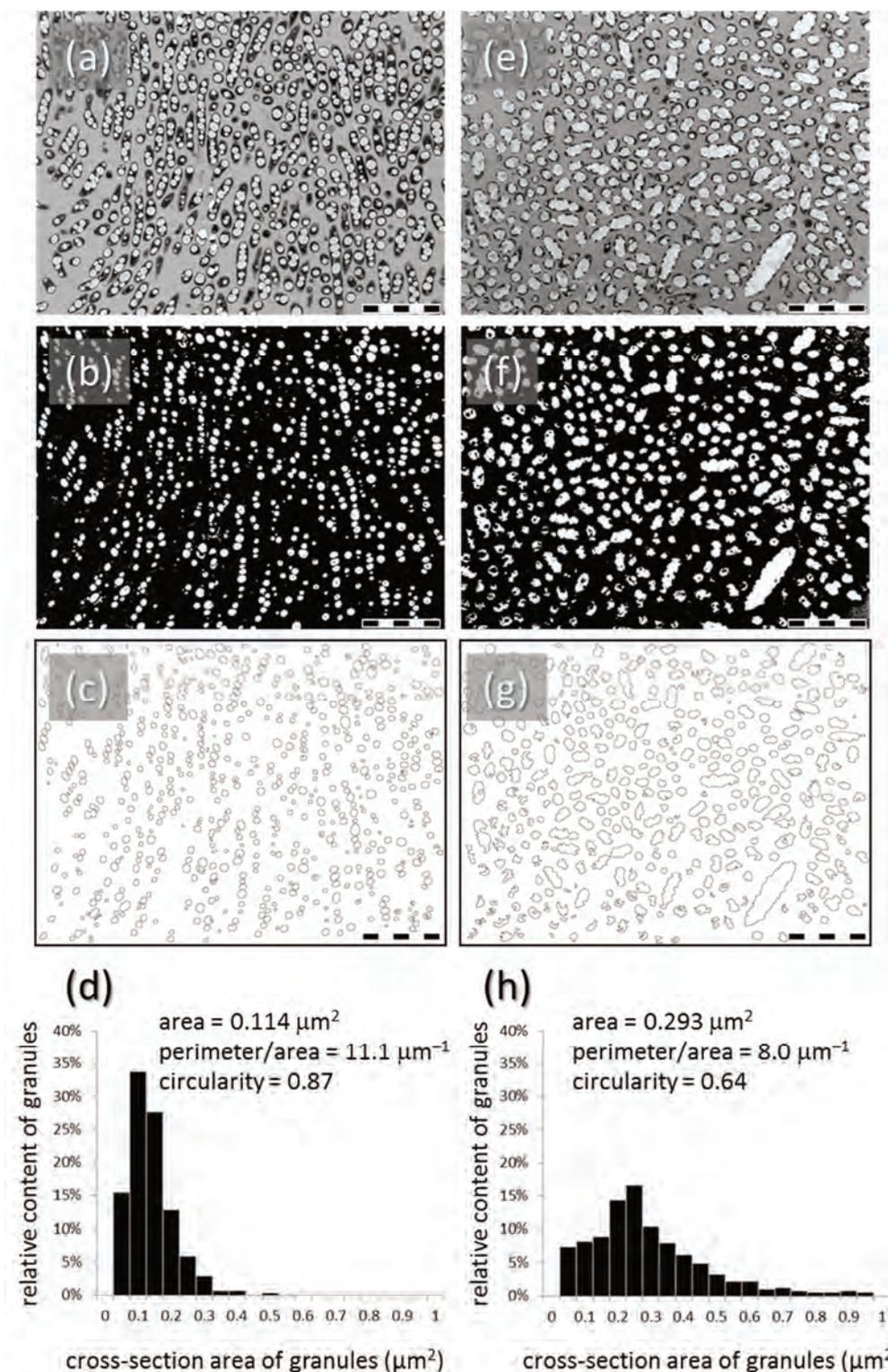
Fig. 49   Detection and analysis of PHA granules in TEM micrographs (scale bar = 5 μm) of C. necator H16 strain incubated at 25°C (a – d) and 80°C (e – h), respectively, using Particle analysis tool in ImageJ software. Original TEM image (a, e), corresponding binary image (b, f) and the final image of the detected granules (c,g) are shown. For every detected granule, a collection of basic size and shape parameters (e.g. area, perimeter, circularity or solidity) is obtained from the Particle analysis tool. The distribution of cross-section area among the detected granules are shown (d, h). Average values of selected parameters provided by the image analysis are inserted. Data from the published study[XIV].
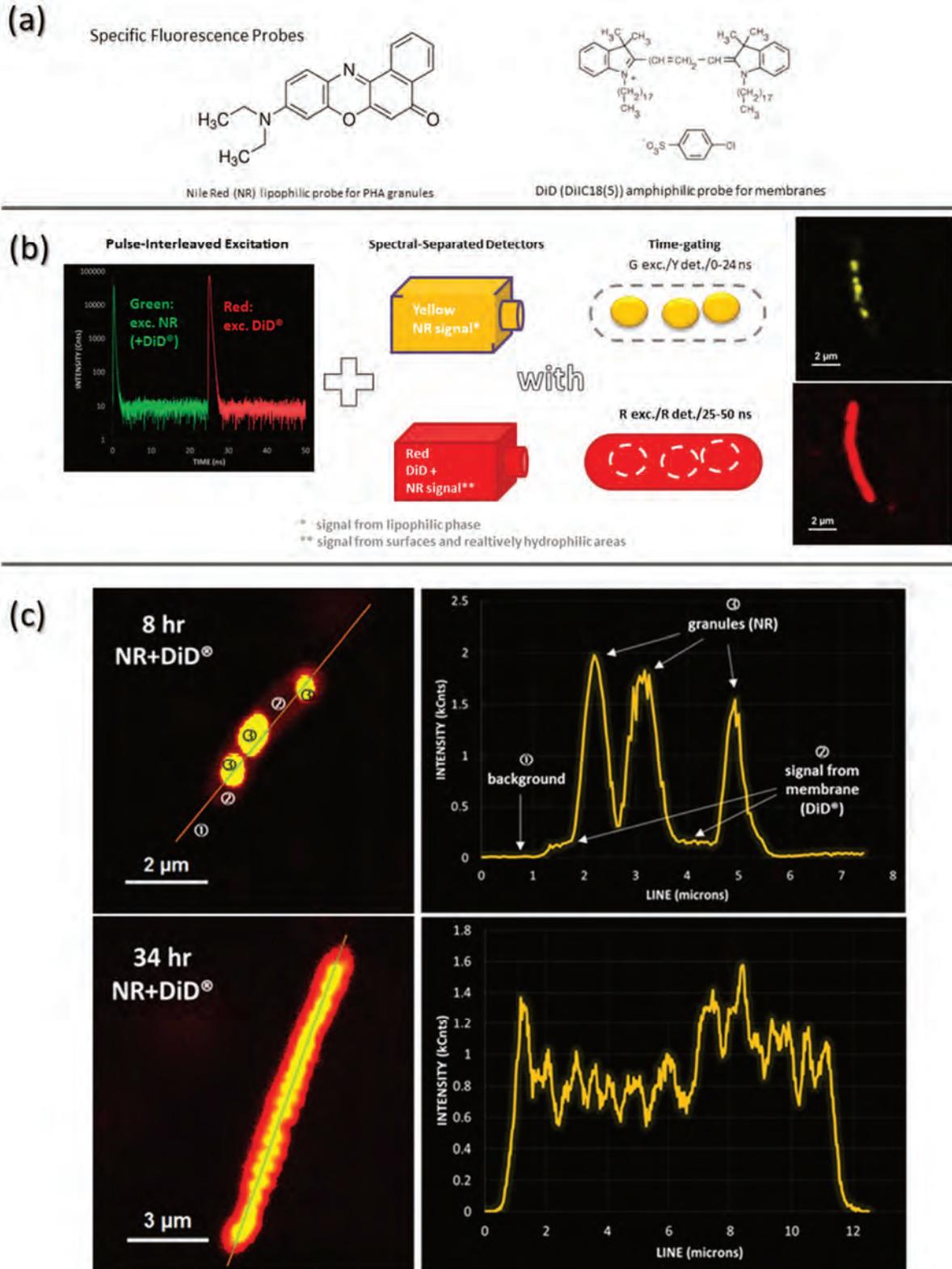
Fig. 50 Use of confocal fluorescence microscopy in the morphological characterization of PHA-containing cells at a single-cell level. The technique is based on dual staining of the cells with fluorescent dyes providing specific affinity for cell membranes (DiD) and PHA granules (NR), respectively. (a) Chemical formulas of individual fluorescent probes, (b) principle of separation of fluorescence signals from both probes (c) and the basic principle of data analysis. Adopted from the published study[XXII].

6.1.3 Biophysical consequences of PHA in cells

A comprehensive understanding of the physiological state of a cell always involves putting together numerous pieces of a puzzle, that are brought from different angles of analytical perspective. Aside from metabolic, morphological or chemical analyses, the determination of various physicochemical parameters of the cellular space (such as pH, redox potential, viscosity and many others) has long been recognized as especially contributive. Therefore, a number of biophysical techniques providing these parameters have already become a standard part of an analytical toolbox for biologists. Definitely, fluorescence spectroscopy represents a great example. With a plethora of fluorescent probes with specific affinity to individual cell components or sensitivity to particular physicochemical conditions, and in combination with advanced microscopy or microfluidics instrumentation, fluorescence methods become an outstandingly powerful approach covering a wide range of applications, from a routine cell viability testing to study of dynamic cellular processes and events. Not surprisingly, we have involved a battery of techniques of fluorescence spectroscopy also in our research on PHA-producing bacteria. In particular, intracellular pH, microviscosity, and the presence of reactive oxygen species were analyzed during the stress-exposure experiments by means of fluorescence techniques. Nevertheless, because this methodology was covered by another part of our team, I will deal with this method rather marginally in this text (e.g. in the next section, where I will briefly introduce how I contributed to the optimization of viability testing of PHA producers based on the combination of fluorescent staining and image analysis). Instead, I am going to focus more on the methods whose previous application in (micro)biology was rather scarce.

First of all, let's get straight to another of the basic spectroscopic methods. In section 6.1.1, I have discussed how the light scattering caused by cells limits spectral information on the cell culture that is accessible by the conventional spectrophotometric analysis, and how this can be overcome by the use of integrating sphere in the diffuse transmittance measurement. Furthermore, we have demonstrated how powerful the combination of these two spectroscopy approaches – light scattering measurement and diffuse transmittance spectrophotometry – can be in understanding how the accumulation of PHA granules affects the radiation exposition behavior of bacterial cells. In the study where we focused on the evaluation of the protection role of PHA granules against the harm brought by UV radiation to bacterial cells[XXIII], we investigated PHA accumulating (*C. necator* H16) and non-accumulating (*C. necator* PHB^{-4}) cultures by the combination of standard spectrophotometric (direct transmittance), nephelometric (measurement of scattered light intensity at 90°) and diffuse transmittance analyzes. The illustrative results of this analysis are shown in Fig. 51.

Evidently, PHA accumulating cells shown much more intensive light scattering in Vis region (see Fig. 51a,b). Taking into account the similar size and shape of both strains, it is obvious that the extra scattering (the most clearly represented by the increased slope of the dependence shown in Fig. 51b) is provided by the cell ultrastructure – i.e. by the PHA granules. Not surprisingly, no significant light absorption was found neither for PHA positive nor negative culture in the VIS region confirming that no pigments or other cell components photoactive in this spectral region are present (Fig. 51c). On the other hand, specific absorption in UV region (absorption band at about 254 nm can be attributed to light absorption by nucleic acids, DNA in particular) was found to be significantly reduced (by around one-third) in the PHA accumulating culture. In the paper, we attributed this reduced absorption of harmful UV radiation to the protective shielding effect of PHA granules resulting from their great light-scattering ability (note that PHA granules are not randomly distributed in bacterial cells, but they are attached to DNA via specific proteins). These assumptions were also supported by the results of nephelometric analysis where the relative efficiency of light scattering by the PHA producer as compared to the mutant strain increases significantly in the UV-region (Fig. 51e). We have also experimentally proved the biological consequences brought by this protective effect on the survival of

---

[XXIII] Slaninova, E., Sedlacek, P., Mravec, F., Mullerova, L., Samek, O., Koller, M., Hesko, O., Kucera, D., Marova, I., and Obruca, S. Light scattering on PHA granules protects bacterial cells against the harmful effects of UV radiation. *Applied Microbiology and Biotechnology.* 2018, 102, 1923–1931. Attached as Appendix 15.

the cells exposed to UV radiation in the study (will be summarized in 6.2.1). In this study, we have demonstrated that utilization of unusual, yet simple and widely available, spectroscopic approaches may be surprisingly beneficial in understanding even such complex biological phenomena as the resistance of bacterial cells against UV irradiation.
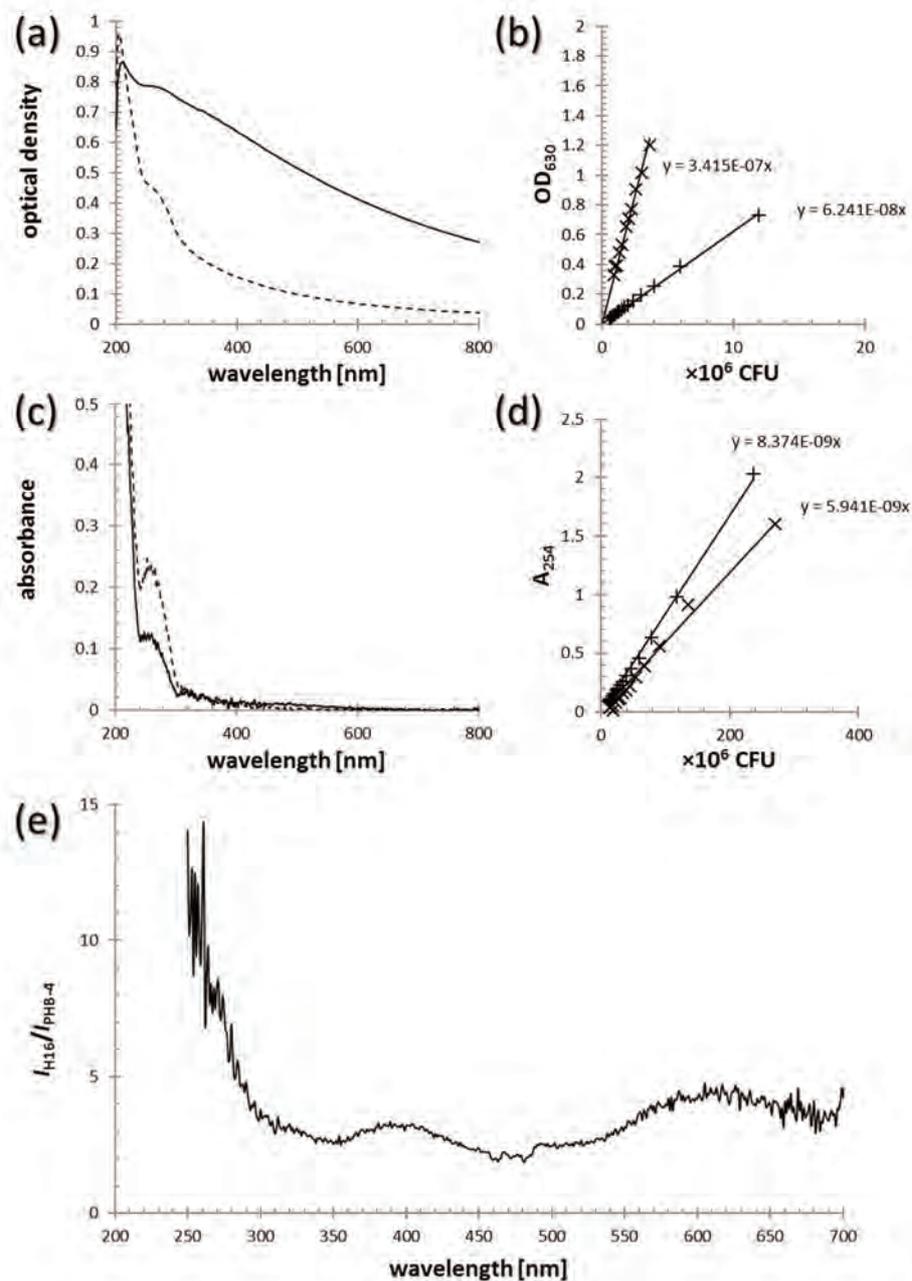
Fig. 51 Spectral characteristics of PHA accumulating (C. necator H16) and non-accumulating (C. necator PHB–4) cultures. (a,c) Spectra of C. necator H16 (solid) and C. necator PHB–4 (dashed) with the same cell density (1×10^6 CFU) obtained by direct transmittance measurement (a), and by diffuse transmittance measurement (c), respectively. (b) Optical density at 630 nm, determined by direct transmittance measurement as a marker of total light scattering, as a function of cell density of C. necator H16 (×) and PHB^{-4} (+), respectively. (d) Absorbance at 254 nm, determined by diffuse transmittance measurement as a marker of specific UV absorption by DNA, as a function of cell density of C. necator H16 (×) and PHB^{-4} (+), respectively. (e) Ratio of the normalized intensities of scattered light for C. necator H16 and PHB^{-4} at 90° as determined by nephelometry. Data were taken from publication[XXIII].

Now, I will move from spectroscopy to a completely different field of physicochemical instrumentation and analytics –thermal analysis. In general, the utilization of thermoanalytical (mainly calorimetry) in biophysical sciences is nothing new. It has long been used in analyzing various aspects of thermodynamics of biomolecules – binding equilibrium is commonly studied by isothermal calorimetry, denaturing and other phase transitions of biopolymers by scanning microcalorimetry etc. Nevertheless, we have experienced in our work that, although their contributions to the analysis of living systems have been rather underappreciated so far, thermoanalytical methods represent a surprisingly powerful tool also in the biophysical characterization of cellular systems. Aside from the experiments, I am going to summarize here, I will later provide additional evidence of this also when I discuss a microcalorimetry technique that we used in monitoring bacteria growth (sections 6.1.4 and 6.2.2).

We have utilized various methods of thermal analysis primarily to reveal how a behavior of cellular water is influenced by the presence of PHA. Differential scanning calorimetry was applied to analyze the freezing/thawing behavior of water in bacterial cultures with the presence and absence of accumulated PHA, respectively. In Fig. 52, DSC thermograms, taken from our publication[XXIV] are shown that illustrate how the presence of PHA in the culture shifts the onset of ice melting into higher temperatures. This was a reproducible calorimetric feature confirmed for different cultures as well as by different calorimetric approaches (compare e.g. results of TMDSC dynamic analysis and quasi-isothermal TMDSC analysis shown in Fig.52a and 52b, respectively). The particular magnitude of the melting point shift depended on the experimental conditions, mainly on the heating rate. From this perspective, the quasi-isothermal TMDSC technique (for more details on the method, see e.g. [146]), where the underlying heating rate is zero, was found to be an especially powerful experimental approach.

In the calorimetric analyses of the cell cultures, we utilized the benefits of the temperature-modulated DSC technique. In general, the main advantage of temperature modulated over standard DSC analysis is that it allows separation of the heat-flow signals related to simultaneously running reversible and non-reversible processes, respectively. The deconvolution of the total heat-flow signal (such as the one shown in Fig. 52a) into the corresponding reversible and non-reversible components (Fig. 52c, d) can for instance provide experimental evidence that, because of supercooling of water in the samples, freezing of water is an almost completely non-reversible process regardless of the cell culture type. On the other hand, one reproducible difference in the water-melting process between the PHB-containing and non-containing cultures was revealed: the non-reversible component of the melting signal in the absence of PHB was always significantly more pronounced. As in the case of melting point elevation, also this interesting water-melting feature can be added to numerous experimental indications suggesting that the activity of intracellular water is significantly affected by the presence of PHA granules. We proposed in the paper[XXIV] , which discussed the results of this calorimetric study with respect to the newly revealed cryoprotective effect of PHA, that a possible explanation of both findings can be found in an alteration of the adhesive forces between water and cellular components in the presence and absence of PHA. We hypothesized that the "dilution" of the strongly hydrophilic species in the intracellular space by the less hydrophilic surfaces of PHB granules could partially lower the strength of the hydration of the remaining solutes, shifting the melting onset to higher temperatures. Similarly, a stronger non-reversible component of the melting signal in the absence of PHB supports the assumption that the released water is more strongly attracted to the cellular components in these cultures than in PHB-containing bacteria.

[XXIV] Obruca, S., Sedlacek, P., Krzyzanek, V., Mravec, F., Hrubanova, K., Samek, O., Kucera, D., Benesova, P., and Marova, I. Accumulation of Poly(3-hydroxybutyrate) Helps Bacterial Cells to Survive Freezing. *PLOS ONE.* 2016, 11, e0157778. Attached as Appendix 16.
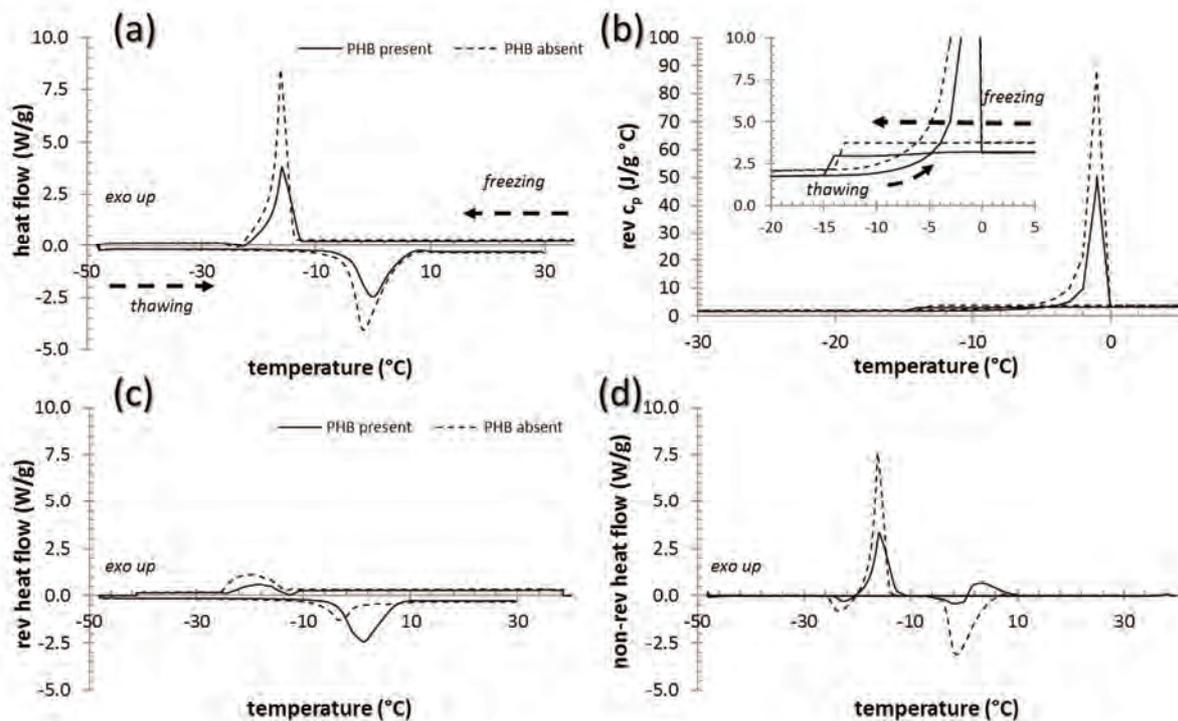
Fig. 52   Freezing and thawing behavior of water in C. necator cultures studied by Differential scanning calorimetry. (a, c, d) Thermograms of temperature-modulated DSC analysis (underlying heat/cool rate 5°C/min, temperature modulation of ± 1°C every 60 s) of C. necator H16 cultures with (solid) and without (dashed) accumulated PHB: overall heat flow signal (a) and the respective reversible (b) and non-reversible (c) component of the signal. (b) Quasi-isothermal temperature-modulated DSC thermogram of the same cultures. In this analysis, samples were cooled down from 5°C to -30°C and heated back up in 1°C increment with an isotherm of 10 min at each increment. Temperature modulation of ±1°C every 60 s was applied.

In the same study, we have also introduced thermogravimetry as an additional tool how to evaluate differences in the activity of intracellular water between the PHA accumulating and non-accumulating cultures. We have found that the total amount of water in the sample did not differ for the respective cultures, however, the drying rate profiles varied significantly. In good agreement with the DSC results, also the results of thermogravimetry show the PHA accumulating cultures apparently contain higher amounts of water that can be more freely released from the cell. This original experimental finding has later been found essential when explaining the increased robustness of the PHB accumulating cells against stress conditions, that give rise to cell desiccation, such as exposure to high salinity or subzero temperatures (will be discussed in 6.2).

The above-mentioned study[XXIV] was also the first time when we utilized thermogravimetry as a method of determination of the intracellular water content. We have optimized the technique originally proposed by Uribelarrea [147] in which the intracellular and extracellular water are distinguished by the specific change in the drying rate during an isothermal drying procedure. The technique is schematically introduced in Fig. 53 (the change in the drying rate is depicted with arrow). Over time, we have successfully applied the method in several studies where the changes in either intracellular water content or in cell membrane integrity, affecting the drying profile of the cells, took place (more detail in 6.2). An example of the results obtained by the technique is shown in Fig. 54, where can be seen the expectedly higher specific content of intracellular water for PHA non-accumulating culture (compare the critical points marked with arrows that correspond to solid curves in Figs. 54b and 54d, respectively) as well as obvious cell desiccation caused by a hyperosmotic environment (compare the solid and dashed curves and their critical points for the respective cultures in Figs. 54b and 54d).

87
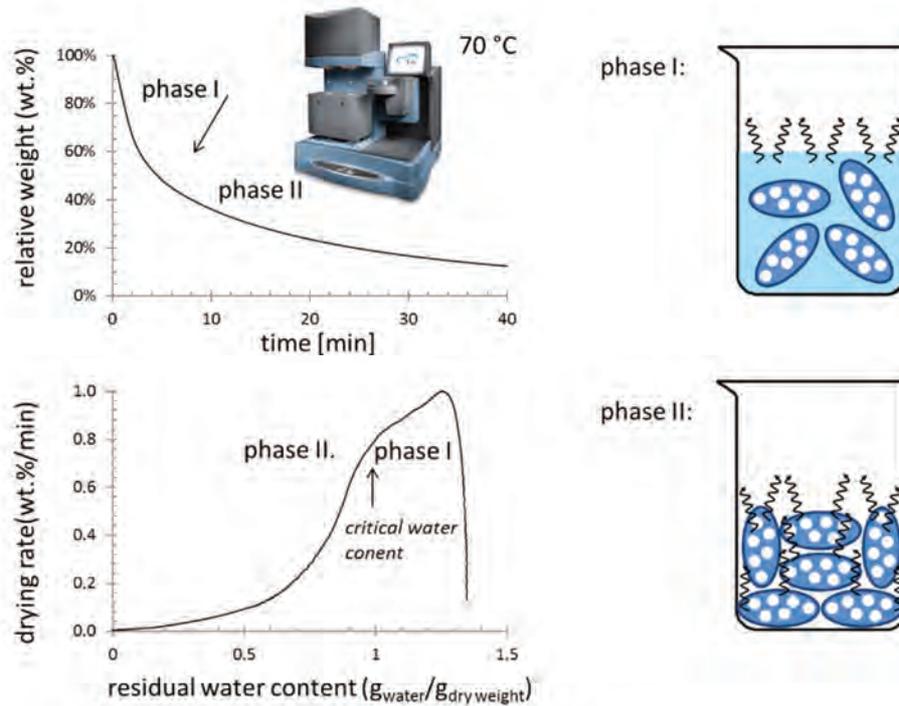
Fig. 53 Schematic representation of the determination of intracellular water content by isothermal thermogravimetry. Effective intracellular water content is determined from the critical point in the drying profile where the steep change in the drying rate appears (marked with an arrow).
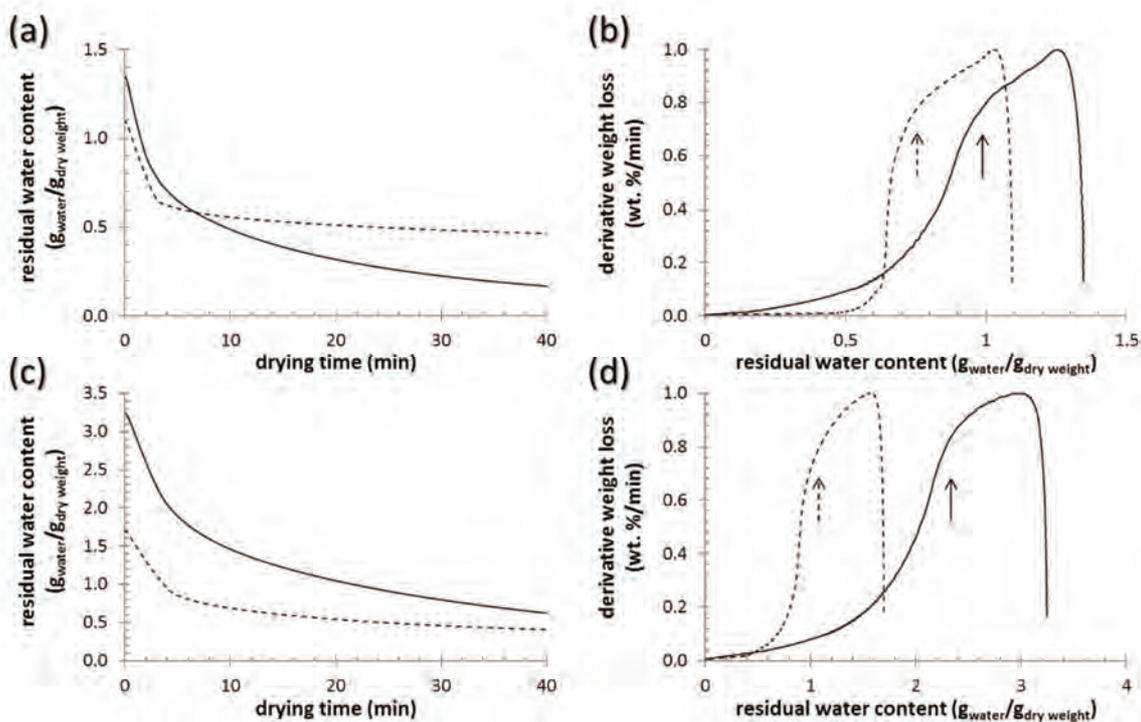
Fig. 54 Results of isothermal thermogravimetry determination of intracellular water content. Raw thermograms (a, c) and drying rate profiles (b, d) of PHA containing cultures of C. necator H16 (a, b) and non-accumulating mutant C. necator PHB[-4] in control isotonic buffer (solid line) and in 200 g/L NaCl (dashed line).

Furthermore, aside from the spectroscopic and thermoanalytical methods, our long-term research on PHA producing bacteria also convinced us that the biophysical characterization of bacterial cells represents an interesting field of application also for various methods designed and developed for use in the analysis of soft matter and colloidal systems. For example, we used oscillatory rheometry to monitor how the presence of PHA granules in the cells affects the behavior of the culture under mechanical stress. We have found that accumulation of PHB in the culture increases elastic modulus up to about 10 fold. Furthermore, we have experienced that, using the temperature sweep analysis, oscillatory rheometry can complement the above-mentioned DSC experiments by monitoring the cell culture during its freezing and thawing regarding specific changes in its viscoelasticity. Furthermore, we have successfully involved also several methods of colloidal analysis in the biophysical analyses of bacterial cultures. For example, by the sedimentation analysis of *C. necator* H16 cultures containing different amounts of accumulated PHA, we have demonstrated how the presence of PHA influences the density of the cells[xxv]. The dispersion analyzer LumiSizer, used in the study, measures the intensity of transmitted light as a function of time and position over the entire sample length simultaneously for up to 12 samples. This analysis revealed that the higher amount of PHA cells accumulate, the higher tendency to sedimentation they exhibited. This is of considerable importance not only from the technological point of view (higher PHA accumulation speeds up the centrifugation as a crucial step of polymer isolation during its biotechnological production), but also from the ecological perspective (concerning the importance of cell sedimentation e.g. in the formation of biofilms).

Another method, routinely used in the analysis of colloids and dispersions, is represented by dynamic light scattering. The main purpose of its use lies in the determination of particle size distribution in a system via monitoring fluctuations of the intensity of the light scattered by dispersed particles. In combination with electrophoretic light scattering analysis, it provides also the average Zeta potential – effective surface potential - of the dispersed particles. We have involved this technique in the analytical toolbox for bacterial cell analysis for two main reasons. The first one is the determination of the effective isoelectric point (pH at which cell surface bears zero effective charges). This is a robust physicochemical parameter that has long been used also in the microbiology for the description of the electrochemical properties of the cell surface and the resulting electrophoretic behavior of the cells [148]. In Fig. 55d, it can be seen that for *C. necator* H16 (and also for PHB^{-4} mutant strain), the IEP is around 4.2 (regardless of the PHA content in the cells). Maximum of the effective cell size at IEP (also shown in Fig. 55d) illustrates another expected phenomenon - aggregation of the cells that is enhanced as their surface potential diminishes.

The other purpose of the use of light scattering techniques in the characterization of bacterial cultures consisted in providing advanced characterization options wherever the most basic scattering parameter – the optical density - is commonly measured as an indicator of cell number in the culture. Hereby, the conventional growth curves (expressed as the time dependence of optical density) can be supplemented with information on the time progress in average cell size or surface potential. Similarly, we have proposed an interesting combination of light scattering techniques and a standard BATH (*Bacterial Adherence to Hydrocarbons*) assay. This technique represents a simple and popular way how to assess cell-surface hydrophobicity [149, 150]. It consists of vortexing a turbid, aqueous suspension of cells in a presence of a test immiscible non-polar (hydrocarbon) liquid. After the mixing, the two phases are let to separate. During the experiment, the adherent cells (i.e. the ones with an affinity to hydrophobic surfaces) become bound to hydrocarbon droplets and are transferred to the upper "creamy" phase. The percentage of adherent cells is estimated by the decrease in optical density of the lower aqueous phase after the phase separation, as compared to the value of the original bacterial suspension.

[xxv] Obruca, S., Doskocil, L., Krzyzanek, V., Hrubanova, K., Sedlacek, P., Mravec, F., Samek, O., Kucera, D., Benesova, P., and Marova, I. Polyhydroxyalkanoates in Bacterial Cells - More Than just Storage Materials. *Materials Science Forum.* 2016, 851, 20–25.
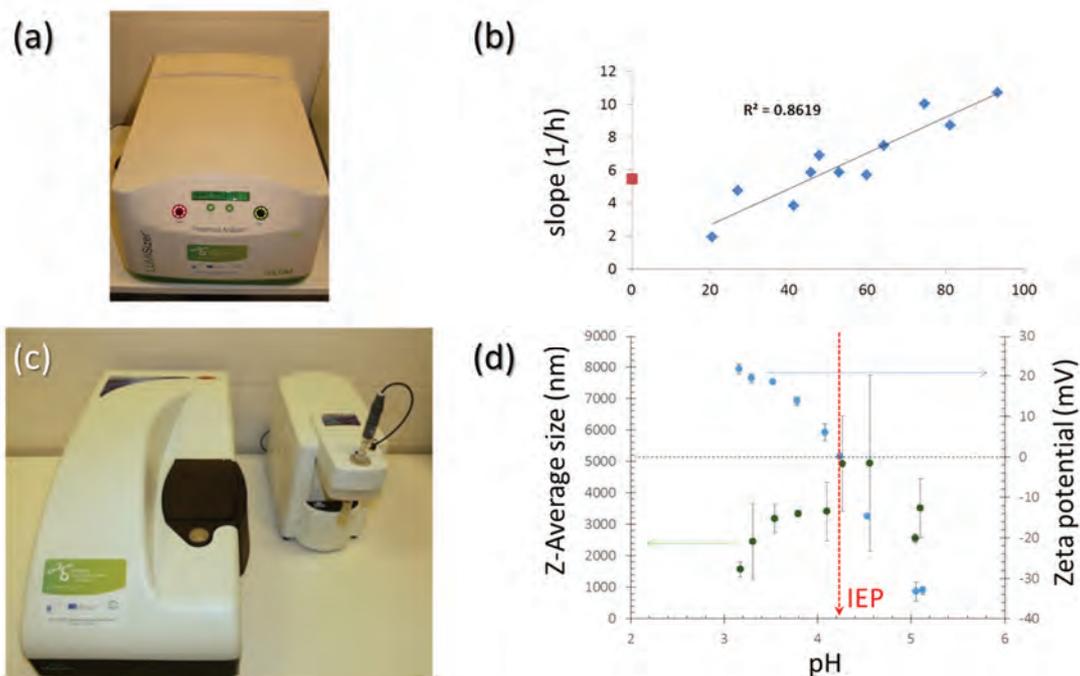
Fig. 55 Examples of involvement of methods of colloidal analysis in the characterization of bacterial cell cultures. (a, b) Sedimentation analysis. (a) Analytical centrifuge LumiSizer was used to monitor sedimentation stability of bacterial cultures of C. necator H16 with various amounts of accumulated PHA (25°C, 1500 RPM). (b) Results of the sedimentation analysis expressed as an index of instability. The culture of the mutant strain (C. necator PHB⁻⁴) is shown red. (c,d) Electrophoretic light scattering technique complemented with acid basic titration used to determine effective isoelectric point of the cell culture of C. necator H16. (c) ZetaSizer Nano ZS with titrator was used for the analysis. (d) Results of the analysis show average cell size and effective surface potential as a function of pH.

This technique provides information of wide relevance in ecology (biofilm formation properties of a bacterial strain depends on its adherence to diverse surfaces), medical sciences (correlation have been made between BATH and adherence of bacteria to epithelial cell, teeth etc.), and biotechnology (a modified BATH procedure allows separation of bacterial cells according to their hydrophobicity, and can be used for instance in isolating the most hydrophobic strains from the mixed cultures). When the advanced light scattering characterization of the aqueous cell suspension before and after the BATH assay is added, more detail on the preferably adhered cells can be obtained. As it is shown in Fig. 56c, average cell size decreased following the BATH assay, while their negative surface potential increased at the same time. This indicates that the larger cells in the culture (in the case of *C. necator* H16 usually those with a higher PHA content) are also the more hydrophobic ones with lower negative surface potential. Nevertheless, the hydrophobicity of the cells seemed to be connected to their physiological state (e.g. nutrient limitation) rather than directly to the content of PHA, because similar results were obtained also for PHA non-producing mutant *C. necator* PHB⁻⁴ cultivated under the same conditions.

As I tried to demonstrate in this section, in the field of microbiology analysis, there is plenty of room for the use of instrumentation and experimental approaches brought by physical chemistry. Only a few examples have been offered, nevertheless, even this small extension of the methodology implemented in our research has resulted in a significant broadening of the knowledge gained from it, regarding both the general effects of PHA presence in the cells and the specific consequences of these effects when the stress robustness of bacteria is concerned.
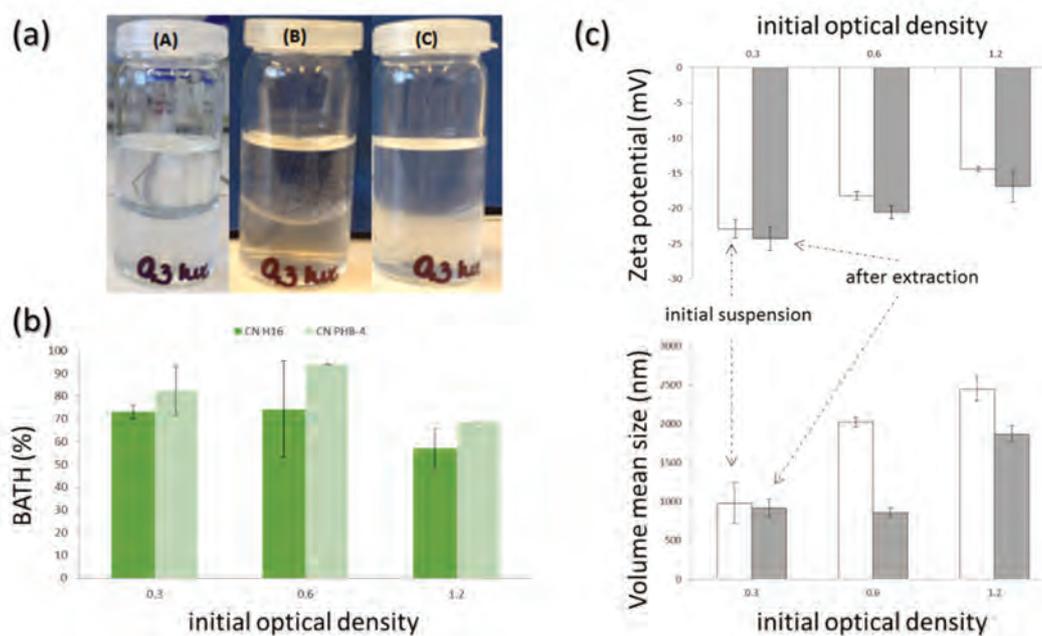
Fig. 56   Original combination of BATH assessment of hydrophobicity of bacterial cells with DLS and ELS characterization of the aqueous cell culture after partial extraction of cells to a non-polar liquid. (a) Illustration of the BATH experiment: an immiscible mixture of cell culture and non-polar liquid aliquots before (A) vortexing, immediately after that (B), and after phase separation (C). (b) Results of the BATH experiment expressed the relative decrease in optical density of the aqueous cell culture caused by the adherence of cells to the non-polar liquid. (c) Results of ELS (top) and DLS (bottom) characterization of the cell culture of C. necator H16 before (white) and after (grey) the BATH experiment.

6.1.4   Physico-chemical approaches to evaluate cell viability and metabolic activity

As far as our main interest in the study of PHA producing bacteria was aimed at their behavior under adverse conditions, there was also one additional analytical focus especially crucial for us. We needed a methodology for a quantitative determination of cell survival and for a qualitative understanding of what are the particular mechanisms of cell damage induced by exposure to specific stressors. In other words, we needed a suitable viability test(s). As simple as it may seem, in fact, it is a quite demanding methodological requirement, because the viability of a cell is not a clearly measurable property. The universally accepted operational definition of cell viability is its ability to form a colony on an appropriate agar medium [151]. Therefore, the traditional viability tests are based on cultivations experiments which are time-demanding and provide little information about the specific physiological state in which the original inoculated cells were.

Again, it has been recognized a long time ago that spectroscopic techniques may be exceptionally helpful for this purpose. A vast number of different spectroscopic viability assays have been proposed [152]. In general, such a test involves staining of the cell culture with a dye, that provides a specific binding affinity to a cell component or undergoes a specific molecular transformation, that causes a change in spectral properties of the culture with respect to the physiological state of the cells. Various physiological conditions may be assayed, such as redox potential, ATP content, the activity of a specific enzyme, but also membrane integrity, DNA denaturation, and many others. Changes in the overall spectral properties of the culture may be measured via standard spectroscopy, but there are also some instrumental improvements that allow zooming the viability tests and the spectral information collection to the single-cell level. Confocal fluorescence microscopy (discussed in the previous section) represents a good example of such instrumentation. Using this method, spectral information can be obtained independently for the individual cells, and, furthermore, other methodical improvements are available, such as imaging the cellular space not only according to spectral variation but also regarding

the different fluorescence lifetimes. The main limitation of this method lies (aside from its limited availability and high purchase price) in the high time demands and low analytical capacity.

However, the state of the art in spectroscopy-based viability testing is represented by flow cytometry. In this technique (the principle is schematically illustrated in Fig. 57a), cells from the analyzed suspension are entrained into the narrow laminar stream of a liquid, where they are hit by a laser beam. The intensity of the light scattered and emitted, respectively, by individual cells is monitored. In this way, multiple physical characteristics of a statistically significant number of cells at a single-cell level can be determined in a short time. This method proved to be extremely useful also in our research dealing with PHA producing bacteria, where the use of appropriate fluorescent labels provided, for instance, sorting the cells according to their viability and PHA presence/absence at the same time (see Fig. 57b-e). On the other hand, the method lacks the direct possibility of a deeper investigation of selected cells, provided by microscopy techniques. Therefore, we searched for a method providing a reasonable compromise between the pros and cons of both above mentioned sophisticated and instrumentally demanding approaches. A method allowing rapid statistical analysis of a significant number of cells together with the possibility of a detailed examination of the individual cells selected at will. And, if possible, a method accessible enough so it could be suggested for routine use in the bacterial cell analysis. Inspired by our previous experience with the analysis of electron microscopy images (section 6.1.2), we have been looking for a solution in ordinary epifluorescence microscopy complemented with advanced tools of image analysis.

Pilot testing of this methodology was performed with *C. necator* strains (both PHA producing *C. necator* H16 and the non-accumulating *C. necator* PHB^{-4} were used), whereby the tested cell cultures were prepared as defined mixtures of intact as-cultivated cells, and the cells previously exposed to a defined lethal condition (ethanol addition, acidic pH etc.). Various common live/dead fluorescence probes were tested, such as Acridine Orange (that shows different fluorescence when bound to native and denatured DNA, respectively), or a combination of Propidium Iodide (membrane integrity probe) and SYTO9 (universal cell-staining dye). A few examples of the results obtained in this study are shown in Fig. 58. Obviously, a significant advantage of the microscopy technique is the direct visual control of the physiological state of a statistically relevant number of cells. Nevertheless, this qualitative information can easily be complemented with quantitative description when the image analysis is included. Some of the simple image analysis approaches have been used quite commonly, such as integration of total fluorescence signal and/or determination of a total number of cells at individual channels (e.g. red and green). Beyond this, we have experienced what additional information can be provided by deeper processing of the images. For example, Fig. 58f-h shows color profiles detected for the selected cells. This way, further morphological nuances, such as changes of the fluorescence intensity with the presence of the granules in the cells, can be evaluated. Furthermore, this single-cell analysis may provide also interesting hints regarding the physiology of the labeled cells, e.g. in the case of Acridine Orange staining, the localization of green and red fluorescence indicates the distribution of native and denatured, respectively, DNA in the cells.

Furthermore, statistical processing of the fluorescence images may be extended beyond the basic cell counting. For instance, Fig. 59 shows results of size distribution determination for the particles (cells, but also fluorescent cell fragments or aggregates) automatically detected in the red and green channels of micrograph Fig. 59a for *C. necator* H16, and for a corresponding fluorescence image recorded for *C. necator* PHB^{-4} (not shown). Evidently, the particle size distributions for the PHA accumulating and non-accumulating strains differ significantly, in particular, *C. necator* H16 culture shows higher relative content of cells of a greater size. Even more, interestingly, we have found that the ratio of total particle areas detected on the green and red channels, respectively, is significantly higher for sp. PHB^{-4} indicates that the denaturing effect of the acidic pH on DNA may be strain-specific. Last but not least, data shown in Fig. 59 also revealed an interesting feature, represented by the fact that the green fluorescence is preferentially contributed by smaller particles. This indicates that the larger cells are in a physiological state that makes them more prone to a damaging impact of acidic pH.
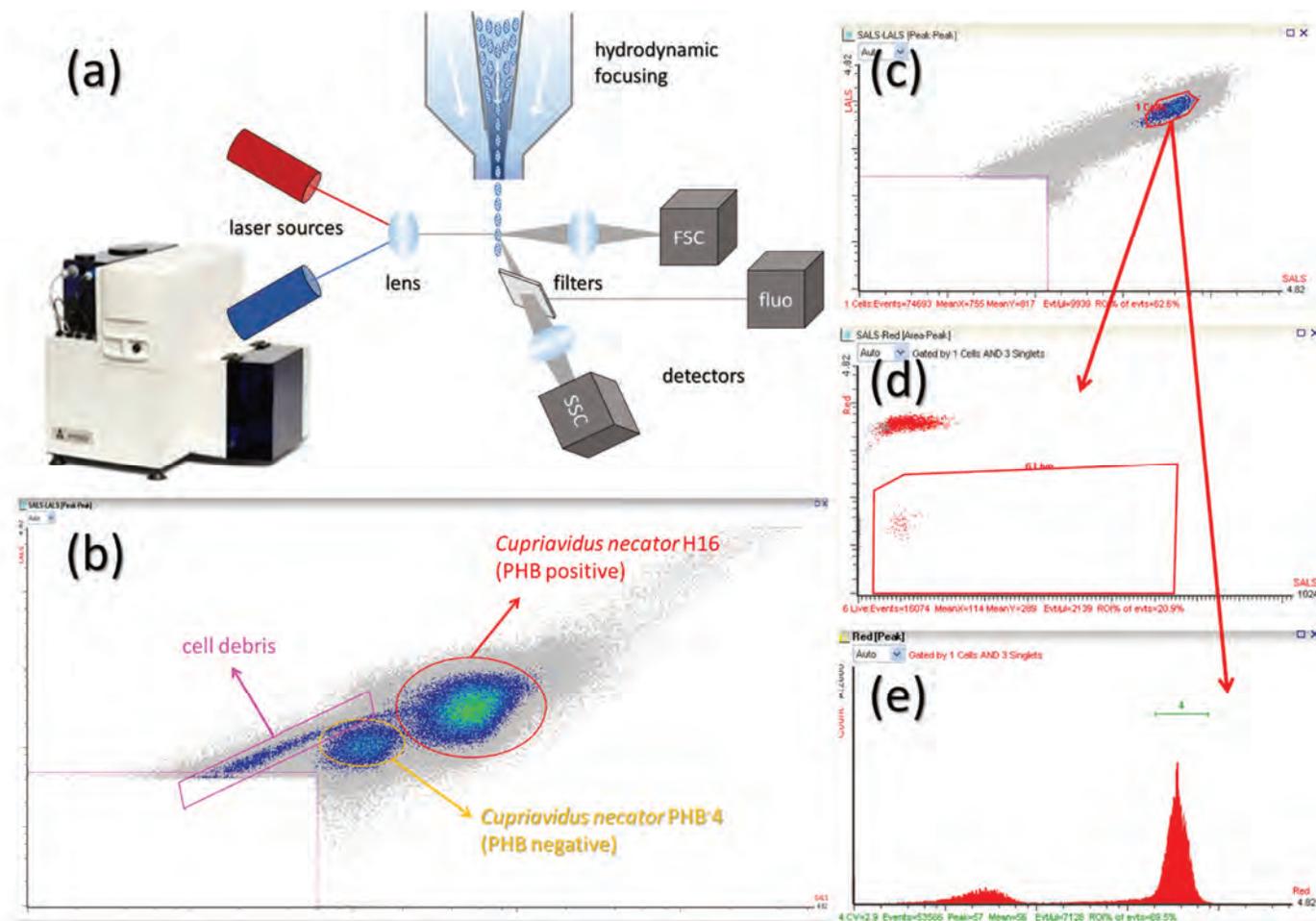
Fig. 57   Flow cytometry (FC) as an instrumentalized way of using spectroscopy for simultaneous viability and (ultra)structural analysis of bacteria at the single-cell level. (a) Schematic diagram of the method. (b) Distinguishing the sub-populations of C.necator H16 with and without accumulated PHA in the FC scattergram. (c-e) Viability analysis of the C.necator H16 cells stained with propidium iodide. Distribution of the single population of C. necator cells in the scattergram (c) into two sub-populations (live-dead) based on their different fluorescence intensity (d, e).
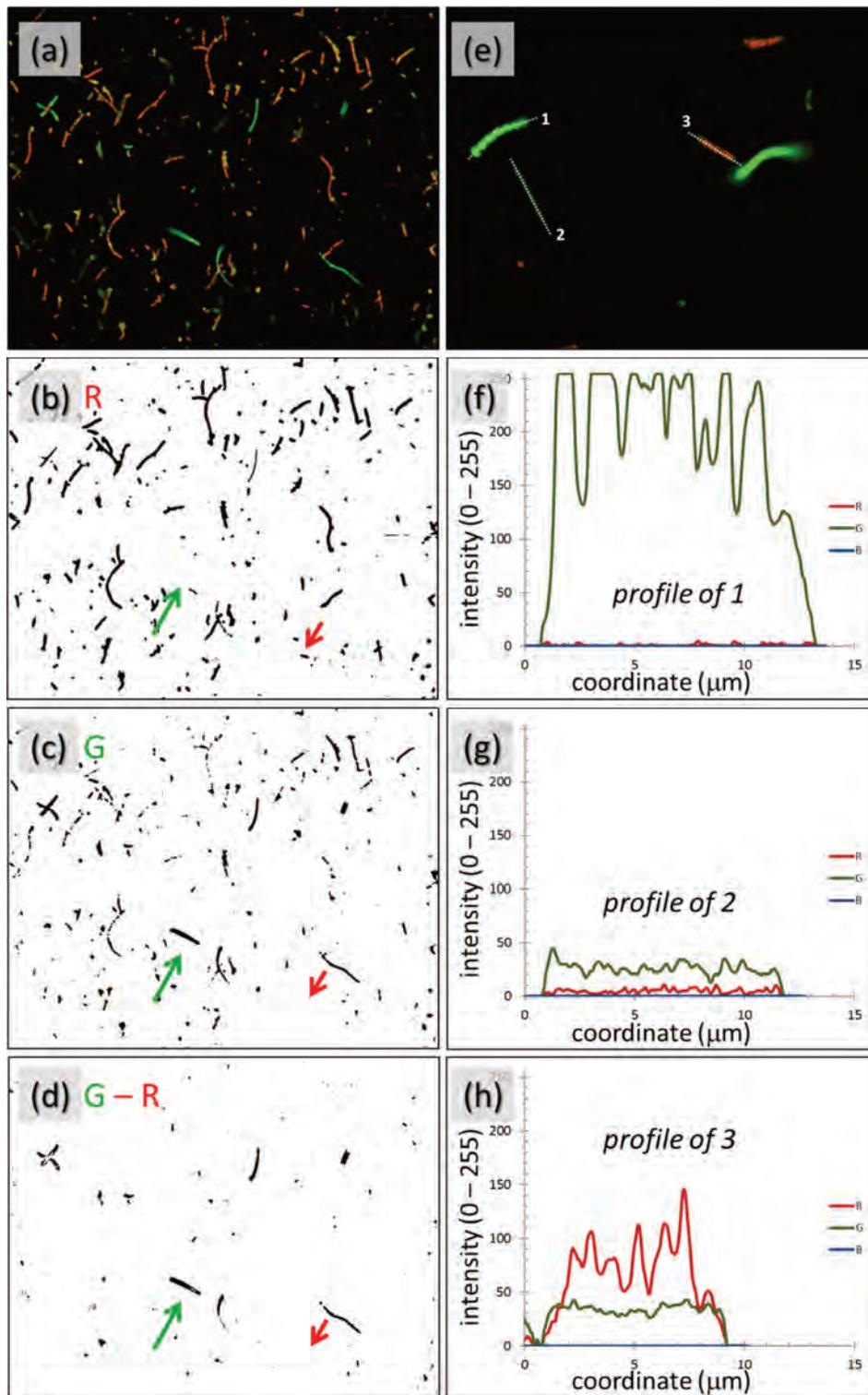
Fig. 58   Utilization of image analysis in evaluation of cell viability with epi-fluorescence microscopy. (a-d) Original and processed images (40× magnified) of a mixed sample of fresh C. necator H16 culture with the culture pre-exposed to pH = 1. The mixed sample was stained with Acridine orange. Viable (green) and dead (orange) cells can be distinguished by decomposing the original image (a) into red (b) and green color components and, more precisely, from the subtraction of the two-component images (d). (e-h) The same mixed sample was stained with the combination of propidium iodide and SYTO9. Original image with magnification 100× and with indicated intersection lines (e) and the corresponding color profiles of the analyzed intersections (f − h) illustrating the color difference between alive (profile 1) and dead cells (profile 3), respectively.
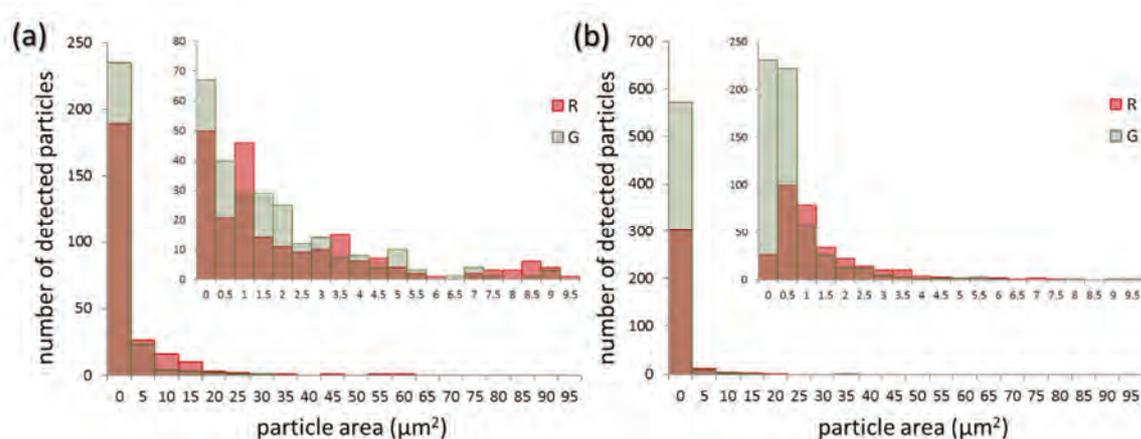
Fig. 59   Use of ImageJ Particle analyzer tool to evaluate size distribution of particles detected at the green and red channel, respectively, of the fluorescence images recorded during the study introduced in Fig. 58. (a) Results for the mixed culture of fresh and acid-exposed cells of C. necator H16 (results of analysis of images shown in Fig. 58b and 58c). (b) Results for the mixed culture of fresh and acid-exposed cells of C. necator PHB^{-4} (analyzed images not shown).

The last method I am going to introduce here as another example of where the fields of physical chemistry and biology overlap is the monitoring the cell growth by microcalorimetry. This technique measures the energy in form of heat produced by metabolic reactions. As far as different organisms produce different levels of energy during their growth, they generate a unique heat signature that can be recorded by microcalorimetry. The main advantage of the technique lies in its sensitivity which is several orders of magnitude higher than the classical optical assay. Furthermore, the changes in metabolic activity of the cells can be monitored also under growth conditions where the number and size of the cells (and hence the corresponding optical signal) do not significantly change (e.g. in the stationary phase). On the other hand, the main weakness of the technique may be found in the specific instrumental limitations – during the measurement, cell culture is usually stored in the calorimeter in dark without stirring or any other kind of aeration.
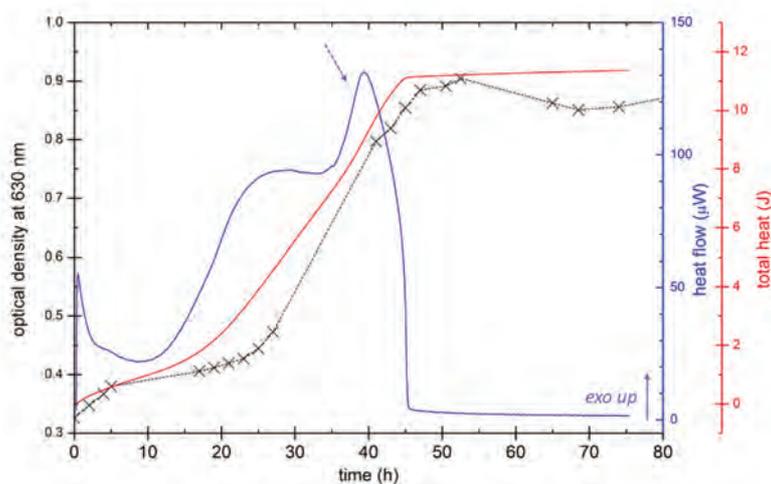
Fig. 60   Monitoring the growth of C. necator H16 culture at 25°C by classical photometric assay (×) and via microcalorimetry (blue and red curves). Results from the microcalorimetric assay are provided as instantaneous heat flow between the sample cell and the heat sink (blue) and as integral heat released from the sample (red). Calorimetry and optical density measurements correspond to two independent cultivations.

95

Fig. 60 shows the growth curves that we have determined for *C. necator* H16 strain (cultivated in the standard mineral medium at 25°C) by optical assay for the cultivation in flasks and by the determination of the heat signature for cultivation in a microcalorimeter. Obviously, the growth curves show similar fundamental qualitative features, such as the lag phase before the growth and metabolic activity start to increase. In a fact, there are also evident discrepancies between the two assays, caused by the specific conditions of the cultivation in the calorimeter. It is evident that the termination of metabolic activity is shifted to lower times in the calorimetric assay, probably as the result of oxygen limitation in the non-agitated sample. This is evident from the fact that the maximal metabolic activity (marked with an arrow in the figure) is normally found in the initial stage of the stationary growth phase where the mathematical product of the number of cells and the metabolic activity per cell reaches its peak. Nevertheless, as far as the method allows parallel cultivation of up to six different cultures at the same time, rather than comparing the assay with the cultivations outside the calorimeter, its main strength is in the comparison of heat signatures from various cultivations under comparable conditions (one example will be provided in 6.2.2).

To conclude this rather methodological section, I have tried to illustrate here (on the particular example of the research of PHA producing bacteria) that physical chemistry can complement the other specializations and methodical approaches in the analysis of biological systems with the distinct, irreplaceable, and particularly contributive perspective. Only when put together, the individual pieces of the puzzle, provided by all these contributors, can create a complete picture of the understanding of how living organisms work (Fig. 61). An example of a particular biological phenomenon, approached in such a complex interdisciplinary way, will be given in the next chapter where our contribution to understanding the broader ecological and evolutionary context of the ability of bacteria to accumulate PHA will be discussed.

Fig. 61   Physical chemistry as an indispensable piece of the complex puzzle of understanding the living systems

6.2   Feeling stronger: role of PHA in bacterial stress-response

Although bacteria are among the most abundant organisms in nature, nature is not always very kind to them. Without a moment of rest, bacteria are challenged by the environment, being exposed to rapidly fluctuating physical conditions such as temperature, pH or salinity, and intensity of light, or to chemical restraints like limited availability of nutrients. To cope with the inhospitality of their natural habitats, bacteria developed numerous strategies which help them to face various stress conditions. It was likely just their astonishing variability in stress-response scenarios that made bacteria so successful in the process of natural selection in various highly competitive environments. [153, 154]

As it was already mentioned, PHA, since their discovery almost a century ago, were long considered simply carbon storage materials. Hence, their stress-coping role was seen just in providing energy during periods of starvation and their involvement in other protective mechanisms were overlooked, until the first study indicating their more complex biological role was published by Tal and Okon [155]. The authors reported that bacterial cells of *Azospirilum brasilense* accumulating PHA up to about 40% of CDM were significantly more resistant to UV irradiation, desiccation and osmotic pressure than cells containing a very low amount of PHA (about 5% of CDM). Suggestions of this pioneer study was further supported mainly by the work of Kadouri [142, 156–158] and Zhao [140] who were the first that compared the stress resistance of wild-type PHA producers with their mutants incapable of PHA biosynthesis or hydrolysis. Since that time, few other reports appeared indicating that PHA supports cell survival under various stress conditions, including extreme temperatures, freezing, osmotic and oxidative pressure, or exposure of the cell to UV irradiation, ethanol, or heavy metals. Furthermore, it was discovered that some bacteria are even capable of PHA biosynthesis from toxic substances such as methanol or styrene [159–161]. Hence, the idea of PHA as an "ordinary" single-purpose storage molecule began to slowly shift to the notion caricatured in Fig. 62 - PHA as the crucial cellular component contributing significantly to the actual cell fitness and robustness.
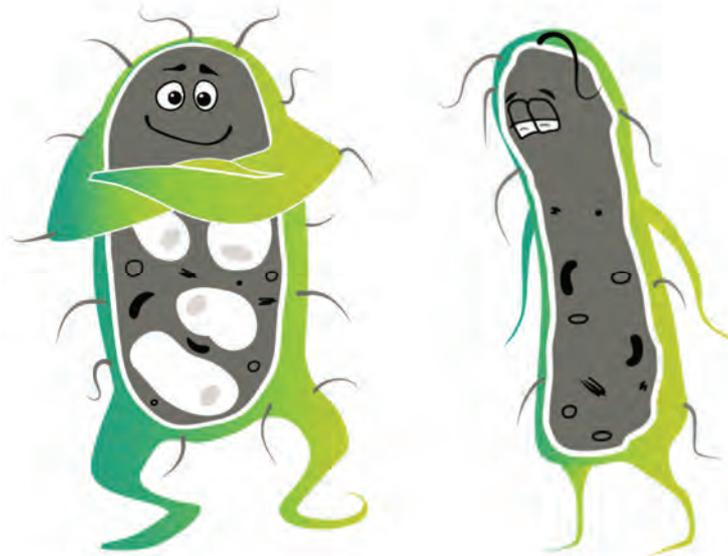
Fig. 62   Modern idea of PHA as a cellular component which is essential in its contribution to the overall cell robustness.

We have followed up on these first works with an extensive research study, where we exposed the famous representative of PHA accumulating bacteria, *C. necator* H16, to various adverse conditions, and compared not only its overall stress-survival but also various specific aspects of its stress-response behavior, to those of the PHA non-accumulating culture (most often the PHA synthase deletion mutant *C. necator* PHB^{-4}). The main outcomes of several years of this research are summarized in 6.2.1. This

research also brought us to consider not only the involvement of PHA in surviving exposure to acute doses of the stressor but also its role in adaptation to mild stress doses, taking into account both the evolutionary and technological relevance of this topic (section 6.2.2). Finally, most recently we have turned the main focus of our research to PHA accumulation by extremophiles, the fascinating organisms that are currently in the spotlight of numerous scientific disciplines, such as eco-biology, evolutionary biology, next-generation biotechnology, but also astrobiology (6.2.3).

6.2.1   Stress survival of PHA accumulating bacteria

As introduced above, the general experimental strategy, that we utilized in this research, was based on the parallel exposure of PHA accumulating and non-accumulating cultures of *C. necator* to an environmentally relevant stress factor followed by complex characterization of the intact and stressed cell cultures, respectively, with a wide spectrum of analytical methods.

First, we paid attention to the resistance of the *C. necator* cultures against low temperature and freezing[XXIV]. As far as approximately 80% of our planet's biosphere is permanently cold with average temperatures below 5°C and even in the remaining regions the temperature fluctuates wildly, low or cryo temperatures represent one of the most common types of adverse conditions that bacteria have to cope with. The mechanism of cell damage for this case is well-described and depends on whether or not the temperature decreases below the water freezing point. Above, the bacterial cells are usually capable of active defense against, usually involving synthesis and action of cold shock proteins or other specific cold-fighting metabolites. On the other hand, when the temperature reaches the value at which water starts freezing, most prokaryotes lose the ability to respond actively, which usually leads to the death of cells. As the extracellular ice crystals grow, osmotic pressure in the medium increases since the excluded solutes concentrate in a decreasing volume of water. This effect leads to "freeze dehydration", and has harmful consequences for challenged cells similar to that of cell exposure to an environment with high salinity. Other lethal effects are caused by the formation of intracellular ice crystals that bring damage to membranes and organelles and cause also the formation of intracellular gas bubbles. Last but not least, cells can also be damaged by reactive oxygen species formed in cells during freezing, and by the mechanical injury induced by the decreasing volume of the bacteria-inhabited channels of unfrozen liquid surrounded by growing ice crystals [162].

In our study[XXIV], we compared the viability of *C. necator* H16 (with PHA content of 76 % CDW) and the mutant strain C. necator PHB^{-4} (PHA content 0.4 % CDW) after a single freeze-thaw cycle, whereby various freezing temperatures were applied (-5, -10, -15 and -20°C). We have confirmed that the bacterial strain capable of PHA accumulation revealed a significantly higher ability to endure freezing than its PHA non-producing mutant strain. The difference between the viabilities of the respective bacterial strains increased with decreasing freezing temperature, the protective effect of PHA was hence the most obvious at -20°C where 84.1% of C. necator H16 cells retained viability, while only 34.5% of *C. necator* PHB^{-4} cells were identified as viable (by Propidium Iodide staining and flow cytometry detection). We have also evidenced that the protective effect is not connected with direct metabolic utilization of PHA (polymer content in the cells did not change during the experiment).

A lot of effort was put into the paper to the detailed discussion of the mechanism of this cryoprotection provided by PHA. Taking together the specific effect of PHA on the activity of intracellular water (already described in 6.1.3), specific viscoelastic properties of PHA granules (also discussed in 5.2.3) and the higher cellular content of cryoprotective 3-hydroxybutyrate molecule in PHA producing bacteria (yet to be discussed in 6.3), we have proposed a concept of the simultaneous interplay of all these contributions in the complex protective effect of PHA. Specific physico-chemical properties of PHA-containing cells seem of crucial importance in this fine-tuned mechanism. The flexible scaffold of PHA granules with the liquid-like properties provides physical protection for cells against the formation of ice crystals and shearing stress associated with the freezing of extracellular water. Furthermore, the affected activity of intracellular water (determined by calorimetric and thermogravimetric assays) influences the rate of cell dehydration during freezing. It is well known that

a compromise between a too high degree of cell dehydration (causing the harm effect of "freeze-drying") and a total suppression of it (supporting the formation of intracellular ice) is optimal in order to minimize the resulting cell mortality. It is therefore very likely that the effect of PHA presence on the rate of transmembrane transport of water may represent an important contribution to the overall cryoprotective strategy of PHA-producing bacteria.

Next, we turned our attention to the resistance of PHA-producing bacteria against UV irradiation. Again, UV light belongs among the most frequent environmental stress factors. It brings various harmful impacts on living organisms, for instance, UV light absorption induces oxidative pressure by stimulating the production of reactive oxygen species (ROS). Furthermore, it causes damage to the molecular structure of essential biomolecules, mainly nucleic acids, but also lipids or proteins [163]. The ubiquitous nature of sunlight exposure makes the resistance against its UV components one of the most critical factors of natural selection. Moreover, it can be expected that the evolutionary significance of UV radiation and the ability to face this stressor may even increase because it has been estimated that by the end of the twenty-first century, the intensity of UV radiation at the Earth's surface would increase by approximately 5–10% in temperate latitudes and by about 20% in high latitudes [164]. Consequently, microbes have developed various strategies how to cope with the negative effects of solar radiation. Some of them rely on active defense against oxidative stress or on the molecular DNA repair mechanism. The others utilize special UV light-absorbing metabolites, e.g. pigments, melanin, ectoines, or special amino acids [165]. Furthermore, several reports dealing with the stress robustness of PHA producing bacteria indicated that also the presence of PHA granules in microbial cells provides protection against UV radiation [150, 157, 158, 166]; however, none of these studies focused on revealing the particular UV-protective mechanism of the granules.

Therefore, in our study[XXIII] we exposed *C. necator* H16 and PHB[-4] cultures to UVA radiation and measured cell viability at different time intervals. We confirmed that PHA accumulating strain showed significantly higher survival than the non-accumulating one. We complemented this study with a comprehensive investigation of light absorption and scattering properties of the cultures, results of which have already been discussed in 6.1.3. We have shown that, as expected, PHA granules do not considerably absorb UV radiation but they are effective light scatterers. Apart from that, we revealed a significantly lower absorption of UV light by DNA molecules, and, moreover, a considerably reduced level of ROS in the PHA-accumulating cells. It is well known that PHA granules are not randomly distributed in bacterial cells, but they are specifically attached to DNA, the most UV-sensitive molecule which enhances their shielding effect [167]. Furthermore, as will be discussed further in 6.3, the most common monomer unit of PHA – 3-hydroxybutyric acid, which is continuously produced in PHA accumulating cells, provides chaperon effects – it protects the structure of biomolecules. Hence, we have suggested in the paper that the UV-protective effect of PHA granules is in fact, similarly to the cryoprotective one, contributed by several physical ("shielding" of the DNA molecules from the UV absorption by the effective light scattering) and chemical (reducing ROS content, synthesis of chemical chaperon 3-hydroxybutyrate in cyclic PHA metabolism) factors.

Another environmental stress factor that, naturally must not be missed in our study, is osmotic stress. Changes in external osmolarity are experienced by prokaryotes on a daily basis. Soil bacteria, for instance, are exposed to quick fluctuations in external salinity depending upon the weather. When bacterial cells are exposed to hypertonic conditions caused by a high extracellular concentration of solutes, water goes out of the cells causing quick dehydration of the cytoplasm. Moreover, as the volume of cytoplasm decreases, the cytoplasm membrane shrinks and separates from the outer layers of the cell envelope in the process known as plasmolysis. Conversely, when bacterial cells are exposed to hypotonic conditions, water influx tends to increase the cell volume and put significant mechanical forces on the membrane. Because the cytoplasm membrane is weak in tensile properties and cannot cope with significant volume changes (it was reported that is not capable of shrinking more than 2–5% [168]), both processes often result in a loss in integrity or even collapse of the cytoplasmic membrane (in the case of osmotic down down-shock referred to as hypotonic lysis).

Also in the case of osmotic fluctuations, bacterial cells developed sophisticated protective mechanisms to cope with their negative effects. For instance, special membrane-associated channels are used for detecting variations in osmolality of the cell surrounding. When an increased osmolality is detected, synthesis of osmolytes (also called compatible solutes) is induced in the cell. These small solutes (among which belong for example trehalose, ectoines, glutamate or glycine betaine) balances water activity between the cell and its surrounding, reduce the osmotic pressure, and, therefore, protect bacterial cells from the harmful effect of the osmotic up-shock. Usually, these molecules also often serve as chemical chaperones, protecting various sensitive cellular components from denaturation and loss of biological activity. Furthermore, mechanosensitive channels are able to respond to cell exposure to a hypotonic environment by pumping water (and solutes) out of the cell [169].

Again, protective effects of PHA were reported before also for osmotically challenged bacterial cells [140, 157, 166]. We supplemented these works with a study[XX] where we confirmed that the PHA-accumulating wild-type strain (*C. necator* H16) survived osmotic up-shock much better than the PHA non-accumulating mutant (*C. necator* PHB^{-4}). Besides, we proved that the protective mechanism is not connected to the direct metabolic utilization of PHA, since we found that the osmotic up-shock did not induce any intracellular PHA degradation. Our multidisciplinary perspective, involving morphological and biophysical analyses of the intact and stress-exposed cultures, led us to the understanding that the PHA granules provide a scaffold-like effect to the cells and prevent them against massive plasmolysis which was manifested in PHA non-accumulating cells. An interesting contribution to this understanding was provided by thermogravimetric assay for the determination of intracellular water (using the method described in 6.1.3). As expected, the critical water content (that is considered equivalent to the content of water in the cells) decreased for osmotically challenged cells compared to the intact ones, however, we discovered that for PHA accumulating cells, this osmotically induced decrease in intracellular water content was significantly less pronounced compared to the cells unable of PHA accumulation. Another important observation was provided by cell morphology imaging by TEM (and complemented with cryoSEM). When the plasmolysis occurred in the very close vicinity of PHA granules, it was possible to observe that PHA partially stabilized membranes by "plugging" small gaps. Therefore, it is likely that the osmoprotective effect of PHA granules is at least partially enabled by the unique mechanical properties of amorphous intracellular PHA granules. Fluorescence microscopy further revealed that in the PHA non-accumulating cells, the value of pH is significantly more lowered as a result of osmotic up-shock. Similarly, also the viscosity of cytoplasm is more affected by the osmotic challenge for the non-accumulating mutant, which is another evidence of the loss of integrity of the cell membrane. On top of that, Raman spectroscopy evidenced that PHA in the cells hyperosmotically challenged PHA producing strain undergo partial crystallization which is in good agreement with our study on stress-induced crystallization of PHA *in vivo*[XIV].

We later conducted a follow-up study[XXVI] focused on the fate of the same bacterial cultures exposed to subsequent osmotic up- and down-shock. Once again, the PHA accumulating wild-type strain *Cupriavidus necator* H16 survived this challenging sequence much better than the PHA negative mutant. It was evidenced both by the morphological and thermogravimetry assay that the PHA non-accumulating cells underwent massive hypertonic lysis, while the PHA-accumulating culture was capable of maintaining the cell integrity when suddenly transferred from hypertonic solution to distilled water. Isothermal TGA analysis proved to be a powerful technique for the detection of membrane integrity loss which was also confirmed by TEM analysis. To untie the down-shock behavior from the specific effects of previous hyperosmotic challenges, we included in this study also an investigation of the hypoosmotic challenge of PHA-accumulating halophilic bacterium *Halomonas halophila* which is adapted to high salinity and, therefore, did not experience any osmotic up-shock

---

[XXVI] Sedlacek, P., Slaninova, E., Koller, M., Nebesarova, J., Marova, I., Krzyzanek, V., and Obruca, S. PHA granules help bacterial cells to preserve cell integrity when exposed to sudden osmotic imbalances. *New Biotechnology.* 2019, 49, 129–136. Attached as Appendix 17.

during the experiment. Also in this microorganism, exposure of the cells to hypotonic conditions (distilled water in particular) resulted in massive lysis of PHA-poor cells and considerable capability of keeping the cell integrity and viability in PHA-rich cells.

Beyond the scope of the above-mentioned studies, by the way of our research, we have met several additional manifestations of the increased cell robustness of PHA accumulating bacterial cells. For example, when we tested the usability of an analytical centrifuge in the analysis of PHA producing cultures (discussed in 6.1.3), we have found that boiled cultures of cells rich in PHA were much less prone to cell lysis than those with low PHA content[XXV]. We have summarized the state of the art in understanding PHAs' role in stress-robustness in one review article[XXVII] and one book chapter[XXVIII]. Anyway, all the published reports and our original findings on the involvement of PHA in the stress-resistance of bacteria have led us to the conclusion that bacteria use PHA like we use a Swiss army knife (Fig. 63). Like a better tool can be found for each of its purposes, there are mechanisms more sophisticated and powerful, that some bacteria can use when coping with an individual stressor. Nevertheless, like in the Swiss knife, the main advantage stands in the versatility of the PHA effects. For both tools, a wide range of benefits is obtained for a reasonable price.
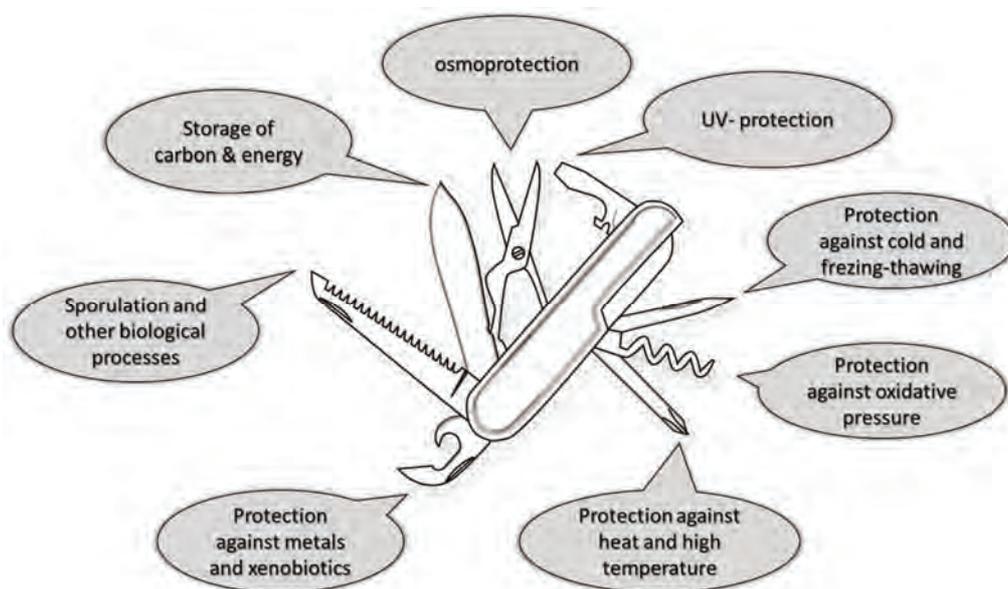
Fig. 63   Bacterial PHA granules are like a Swiss army knife: they offer versatile performance for a reasonable price

6.2.2   The role of PHA in stress adaptation

Understanding the improved survival of PHA accumulating cells when exposed to acute stress doses does not provide a complete overview of the role of PHA in responding to stress conditions. Equally, important information is brought by investigating how the PHA participates in the behavior of bacterial cells exposed to moderate or low doses of stress, those that do not directly threaten the life of the cells but can induce crucial changes in cell physiology. Mechanisms of cell response to this exposure play an essential role in what is understood by stress adaptation – preparation of the organism for

---

[XXVII] Obruca, S., Sedlacek, P., Koller, M., Kucera, D., and Pernicova, I. Involvement of polyhydroxyalkanoates in stress resistance of microbial cells: Biotechnological consequences and applications. *Biotechnology Advances.* 2018, 36, 856–870. Appendix 18.

[XXVIII] Obruca, S.; Sedlacek, P.; Pernicova, I.; Kovalcik, A.; Novackova, I.; Slaninova, E.; and Marova, I. Interconnection between PHA and Stress Robustness of Bacteria. *In The Handbook of Polyhydroxyalkanoates*; CRC Press, 2020; pp. 107–132.

future stress encounters. As the adaptation occurs, the stress previously experienced feels less stressful in future sessions.

As was already emphasized, there are numerous reports supporting the empirical experience that the controlled introduction of various stress conditions (e.g. osmotic pressure, heavy metals, H_2O_2 or ethanol) supports PHA accumulation in bacteria [135]. This finding is not only of fundamental ecological importance but also of great biotechnological significance. Stress-assisted biotechnology has been identified as an underexplored auspicious strategy to improve PHA production processes, as we summarized partly in the review focused on the general role of PHA in stress response[XXVII], and in more detail also in the later, technologically focused review[XXIX].

The enhancement of PHA productivity by moderate stress doses were previously reported mainly for "good" PHA producers, such as *C. necator* H16. Nevertheless, we have recently conducted also a study employing cyanobacteria. Apart from the specific ecological and evolutionary position of these prokaryotes, another motivation of this study was in that the accumulation of PHA in these organisms is much lower and the physiological role of PHA may be different. However, also this study supported the general conclusion that PHA accumulation is supported by controlled stress, in particular to salt exposure[XXI] and UV-B irradiation[XXX]. PHA accumulation can hence be considered one of the immediate mechanisms contributing to the stress adaptation process in prokaryotes.

The simple idea of the phenomenon of adaptation can be illustrated by the old saying "No pain, no gain". Wherever an organism is exposed to adverse conditions, its fate is governed by the actual dose of the stressor in the way described already by Paracelsus [170]. It is fascinating how similar the basic features of dose-response performance seem to be, regardless of the level of complexity of the organism, or of the particular stress factor that the organism faces. For instance, such biologically independent phenomena as the toxicity effect of an antibiotic on bacterial cells on the one side and the performance of a human under physiological or mental arousal on the other, show conceptually similar dose-response relationships. This universality of the dose-response forms the foundation of the general concept of stress biology called hormesis [171]. Taking together all the knowledge gained on the interconnection between mild stress exposure and PHA accumulation, we have suggested in our recent paper[XXIX] the original opinion that accumulation of PHA in bacterial cells represents in fact an additional, not yet recognized, example of the hormetic stress response (Fig. 64). This concept emphasizes once again the unique evolutionary role of PHA in the world of prokaryotes.

As far as the evolutionary perspective on PHA accumulation is concerned, there is one additional point that has attracted our experimental attention. It has been suggested [172] that the cell robustness of microbial strains and their resistance to various stress factors (including physical stressors as well as molecular inhibitors) could be enhanced by the application of tools of evolutionary engineering. A general principle of evolutionary engineering (sometimes also referred to as "directed evolution") is demonstrated in Fig. 65. It follows nature's 'engineering' principle by variation and selection. In the adaptive laboratory evolution level of evolutionary engineering, serial batch cultivations are performed to evolve microbial cells. In a certain interval (usually based on the cell growth), the culture cells are transferred to a fresh medium with the same or an increased dose of the selection factor (the stressor) for another round of propagation [172]. A combination of evolutionary engineering together with an in-depth analysis of evolved strains represents an extremely efficient tool for understanding various adaptation and evolutionary strategies of microorganisms at the morphological, biophysical or molecular level.

[XXIX] Obruca, S., Sedlacek, P., and Koller, M. The underexplored role of diverse stress factors in microbial biopolymer synthesis. *Bioresource Technology.* 2021, 326, 124767. Attached as Appendix 19.

[XXX] Daffert, C., Grammelhofer, D., Meixner, K., Obruca, S., Sedlacek, P., Samek, O., Slaninova, E., Sedrlova, Z., Mrazova, K., Hrubanova, K., Krzyzanek, V., Nebesarova, J., and Fritz, I. Effect of UV-B irradiation on the formation of polyhydroxybutyrate in Synechocystis. *Submitted for publication.*
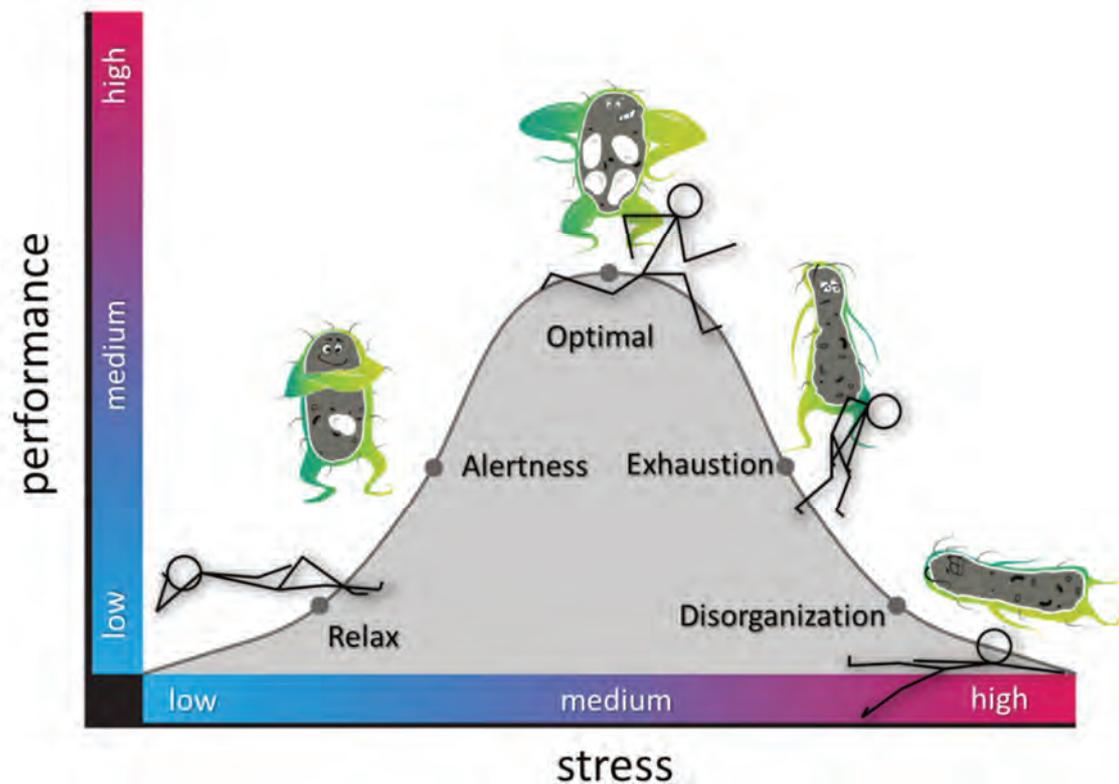
Fig. 64   Common features in hormetic stress dose responses: i. Yerkes-Dodson curve is used by psychologists to describe the relationship between pressure and performance for humans. ii. Dose-response performance of PHA producing bacteria under stress.

In our study, we have performed long term evolutionary experiments with *Halomonas halophila* and *C. necator* using various stress factors such as high and low temperature, the high and low osmotic pressure of cultivation media, presence of heavy metals (Cu^{2+}), organic pollutants (p-nitrophenol), organic acids (acetic acid and levulinic acid), phenolics and also furfurals. Typically, the laboratory evolution lasted for $30 - 75$ passages, then the evolved bacterial cultures were in-depth characterized and compared with the wild-type strain to find phenotype changes induced by the directed evolution. We have confirmed that the adaptation of the bacteria to stress conditions has never been accompanied by suppression of the PHA synthetic pathway resulting in a decrease in PHA accumulation or PHA content in bacterial cells. Oppositely, in several cases (e.g. adaptation of *C. necator* to levulinic acid or Cu^{2+} ions) we observed a considerable increase in PHA production and activities of PHA synthetic enzymes. These results further confirmed the leitmotif of our PHA research as they confirmed the essential role of PHA metabolism not only for survival but also for the adaptation of prokaryotes to stress conditions.

As part of the in-depth characterization of the phenotype changes in the evolved (adapted) bacterial strains, we relied not only on biochemical analyses (through the determination of specific activities of selected enzymes) and the evaluation of the biotechnological potential of the strains. We utilized also the physico-chemical and spectroscopic methodology, introduced in section 6.1. For example, in the study where we investigated the adaptation of *Cupriavidus necator* to levulinic acid for enhanced
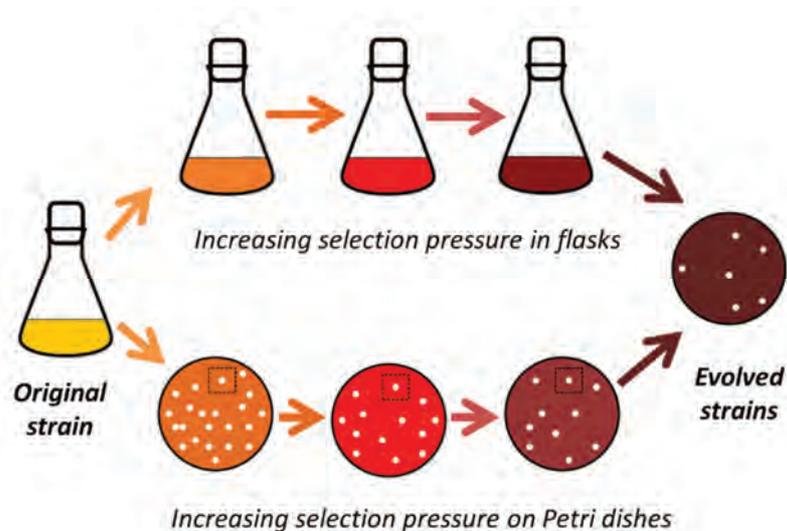
Fig. 65   Utilizing the concept of evolutionary engineering in research and development of bacterial strains adapted to diverse physical and chemical stress factors.

production of P(3HB-co-3HV) copolyesters[XXXI], we performed a detailed material analysis of the PHA polymers produced by the wild-type strain and various adapted strains. In this study, the already discussed (in 5.2.2) connection between monomer composition of PHA (3HV content in this case), their crystallinity, and other important polymer processing parameters such as melting temperature have been confirmed again. Same as for the metabolic characterization, we processed and evaluated the obtained data by the correlation analysis and multivariate characterization based on Principal Component Analysis (PCA). As far as different mutual projections of individual strains were found in PCA diagrams derived from metabolic and material assays, respectively, we concluded that no obvious link between general metabolic strategies of the strains and the shifts in the quality of the produced polymer might be identified. Furthermore, as part of the investigation of the adaptation of *C. necator* to levulinic acid (LA), we have offered another demonstration of the benefits of monitoring the growth of bacteria by microcalorimetry. As can be seen in Fig. 66a and b, it can be seen how the presence of levulinic acid in the cultivation medium inhibits the growth of the wild-type strain. Obviously, the experiment provides better sensitivity compared to the traditional growth curve determination by spectrophotometry. Because the metabolic signature of the growth process is a more reasonable sign of cell viability than an optical density, the method is especially contributive when a suitable range of the inhibitor concentrations for the adaptation studies is explored. Moreover, it can be seen that the microcalorimetric assay provided clear evidence of the successful adaptation – obviously, the growth of the LA-adapted strains is significantly less restricted by the presence of levulinic acid as compared to the wild-type strain (see Fig. 66c).

Similarly, also the *C. necator* strains resulting from the long-term laboratory adaptation to the high salinity (20 g/L NaCl) and the heavy metal exposure (50 mg/L Cu^{2+}) were analyzed for the phenotype changes brought by the evolutionary engineering process[XXXII]. Again, the adaptation was induced by repetitive passaging of the cells into the medium with the stressor (78 passages were performed in the copper-adaptation experiment, 68 in the evolutionary engineering of the salinity-adapted strain).

[XXXI] Novackova, I., Kucera, D., Porizka, J., Pernicova, I., Sedlacek, P., Koller, M., Kovalcik, A., and Obruca, S. Adaptation of Cupriavidus necator to levulinic acid for enhanced production of P(3HB-co-3HV) copolyesters. *Biochemical Engineering Journal.* 2019, 151, 107350.

[XXXII] Novackova, I., Hrabalova, V., Slaninova, E., Sedlacek, P., Samek, O., Koller, M., Krzyzanek, V., Hrubanova, K., Mrazova, K., Nebesarova, J., and Obruca, S. The role of polyhydroxyalkanoates in adaptation of Cupriavidus necator to osmotic pressure and high concentration of copper ions. *International Journal of Biological Macromolecules.* 2022, 206, 977–989.
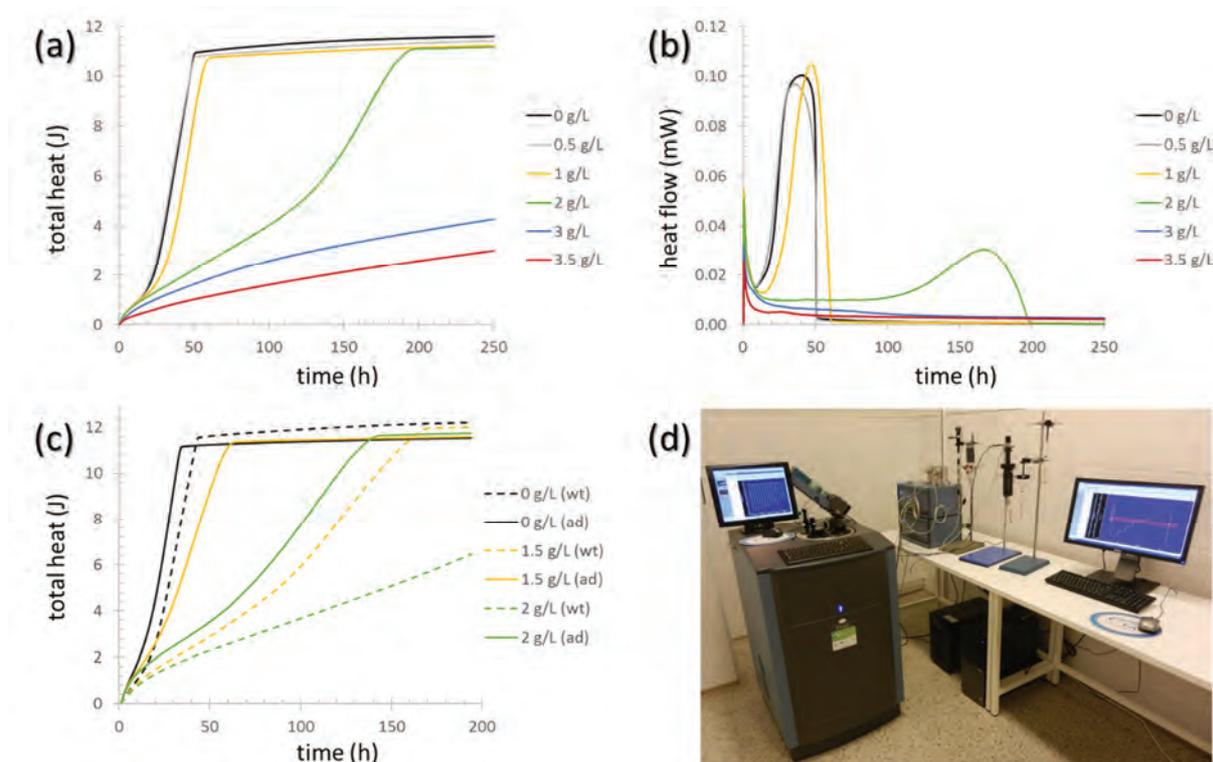
Fig. 66   Microcalorimetry applied in the study on adaptation of bacteria to molecular inhibitors. The harmful effect of levulinic acid (LA) on the growth of C. necator H16 cells as confirmed by monitoring the total produced metabolic heat (a) and the instantaneous heat flow (b) overtime for different concentrations of LA in the medium. (c) Comparison of the growth thermograms of the wild-type culture (dashed) and culture pre-adopted to low doses of LA (solid). (d) TAM III multi-channel microcalorimeter that was used in the study.

The optimal dose of the stressor was selected to induce a 50 % reduction in growth of the original wild-type strain. Again the strains evolved from this experiment were compared to the original one in their growth characteristics, enzyme activities, and also from the viewpoint of cell morphology. In general, the results confirmed the involvement of PHA metabolism in adaptation to both tested stressors. Apart from the biochemical assays, we searched for the possible changes in the chemical structure of the wild type and evolved strains using molecular spectroscopy (ATR FTIR and Raman). As can be found in Fig. 67, where the results of this spectroscopy assays for the salinity-adaptation experiment are provided in terms of full-spectrum PCA (in the range $1800 - 800$ cm^{-1}), the evolved culture adapted to high osmolality shows independent clustering outside the region that corresponds to the wild-type culture both in FTIR and Raman PCA diagram. Apparently, this culture shows distinctive structural features as compared to the original strain. Nevertheless, from a closer look into the loading of principal components that provides this separation, it can be seen that the variance between the cultures is contributed almost exclusively by the spectral signature of the PHA content, with no specific alteration in content or molecular structure of other cellular components resulting from the adaptation process was revealed by the spectroscopic assay. Moreover, we have also revealed that, in the NaCl-evolved culture, PHA show a significantly lower tendency for crystallization during biomass drying. I have already emphasized the connection between the crystallization of PHA in the cells and their stress-robustness (5.2.1). Therefore, this particular result represents further confirmation of the increased stress robustness of the NaCl-evolved culture. Furthermore, the merit of the involvement of vibrational spectroscopy in microbial cell analysis was demonstrated in this study once again.
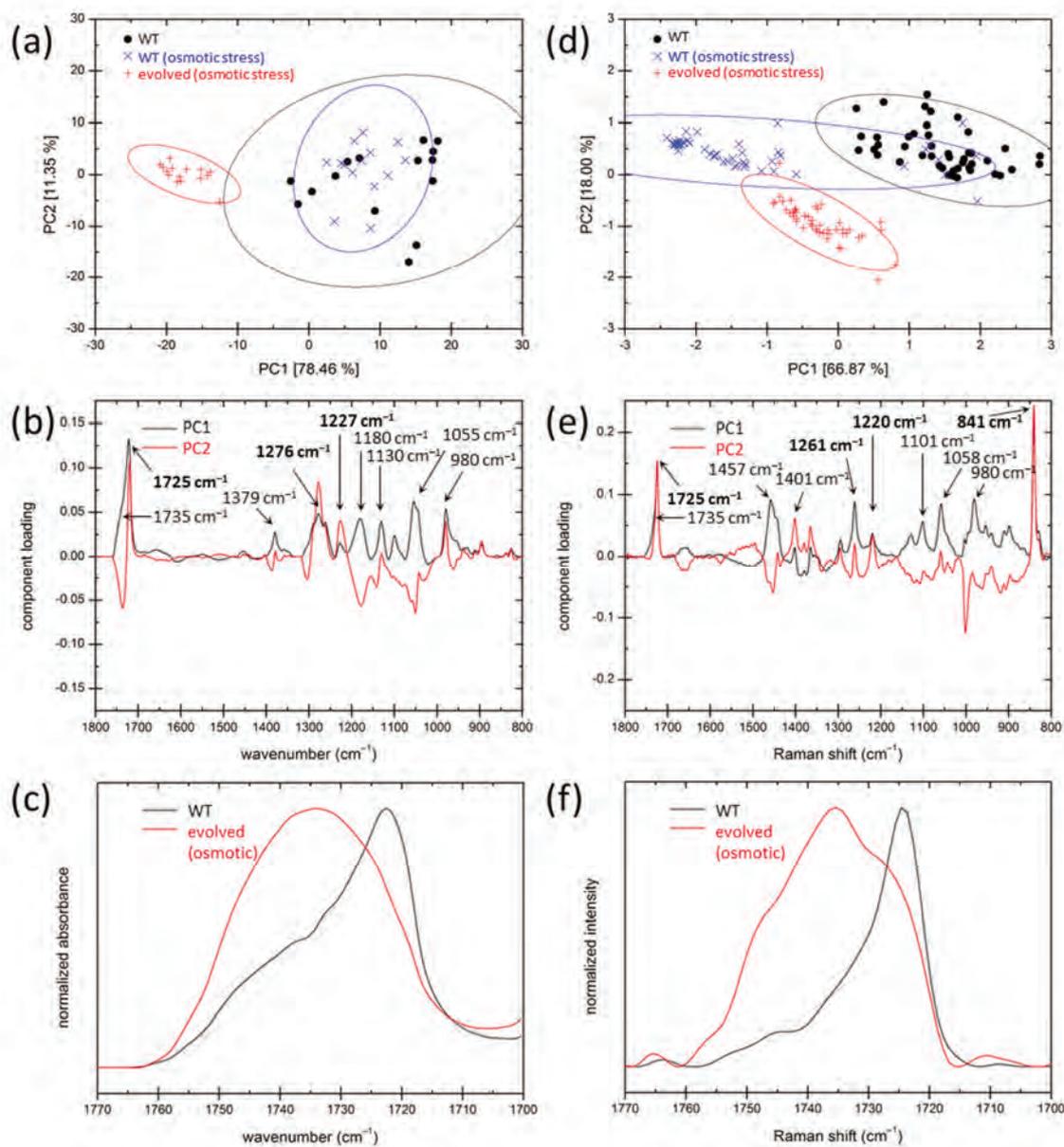
Fig. 67   Results of the ATR-FTIR (a-c) and Raman (d-e) spectroscopy analysis of the original (WT) and the salinity-adapted strain provided by evolutionary engineering of C. necator in media with 20 g/L NaCl. (a, c) Results of Principal Component Analyses of the sets of spectra of bacterial cultures: wild type, wild type exposed to 20 g/L NaCl, and adapted strain exposed to 20 g/L NaCl. The PCA was performed with all measured spectra. The value in the square bracket represents the relative variance that is composed in the respective principal component. Ellipses represent the 95% interval of confidence. (b, e) Spectral loadings of the Principal components used in the PCA diagrams are shown. (c, f) Comparison of C=O stretching bands showing the reduced crystallinity of PHA in the dried biomass of the salinity-adapted strain compared to the wild type.

Other evolutionary engineering experiments have been also performed which are still awaiting publication. For example, we confirmed that following the concept of evolutionary engineering, the adaptation to a salinity below the optimum level for a halophilic bacterium (*H. Halophila*) can enhance the resistance of the organism to hypotonic shock, as was evidenced not only by the results of viability assays but also by TGA evidence of cell integrity (using method discussed in 6.1.3). Altogether, we have confirmed in our studies that the concept of evolutionary engineering represents an exceptionally

promising experimental tool not only in the development of bacterial strains with enhanced performance but also in the general understanding of the adaptation process (and how the specific contributors – such as PHA – participates in it). Furthermore, the merit of the involvement of various methods of biophysical analysis in the directed evolution concept was demonstrated.

6.2.3   Accumulation of PHA in extremophiles

In the almost 4 billion of years of history of life on our planet, life has managed to penetrate all, even the least imaginable environmental niches. Obviously, evolution has developed plenty of mechanisms how to push the boundaries of life and some of them have certainly remained hidden from our knowledge. And not surprisingly, it is just prokaryotic organisms such as bacteria or archaea, who have been witnessing the history of evolution since its very beginning, and who therefore represent the most suitable study subjects in our quest for understanding of how life at the extremes has evolved.

Extremophiles are microorganisms capable of surviving and prospering in conditions, which are considered lethal for "ordinary" organisms. Some of them can live and prosper even in the harshest possible habitats, from extremely hot hydrothermal vents to deep-cold Antarctic soils, from the Dead sea ultra-salty water to acidic mine drainages. Extremophile microbes hence display impressive examples of how terrestrial life has been constrained, providing crucial implications not only for considering the origin of life on our planet but also for the search for extraterrestrial life. Furthermore, as we humans have been employing microbes for centuries to improve our lives, research of these extreme-thriving microorganisms also opens up new horizons in various fields of science and technology. For instance, traditional biotechnologies utilizing mesophilic microorganisms usually suffer from numerous weaknesses, mainly from a high risk of contamination that imposes demanding sterility requirements, but also from heavy consumption of water and energy used in the temperature maintenance of the biotechnological process, and from the non-effective operation in the batch mode. Contrarily, most of these shortcomings are easily overcome by the employment of extremophiles in the process. Therefore, the concept of "Next Generation Industrial Biotechnologies" (NGIBs) has evolved that relies on extremophiles as naturally robust microorganisms which are capable of surviving and prospering under conditions that reduce the risk of contamination as well as some operating costs of the technology [173, 174].

Numerous reports on the production of PHA by extremophiles (mainly halophiles) can be found in literature, as we summarized in our review articles[XXVII,XXXIII]. Not surprisingly, the topic of PHA accumulation by extremophilic bacteria attracted our attention not only because of its technological relevance but as an additional perspective to be included in the overview on the ecological role and evolutionary significance of these fascinating polymers. First of all, we focused our attention on halophilic PHA producers. We proposed *H. Halophila* as an auspicious candidate strain for the biotechnological synthesis of PHA in the study[XXXIV], where we, among other things, demonstrated that material properties (molecular weight as well as various thermoanalytical parameters) of the polyhydroxybutyrate accumulated by this strain can be tailored by the salinity of the used cultivation medium. As already discussed in sections 6.2.2 and 6.2.3. we have also included this bacterium in our stress-survival and stress-adaptation studies (mainly with respect to its behavior under hypotonic conditions).

Nevertheless, mainly from the technological point of view, employing halophiles for PHA production still bring some considerable obstacles, mainly related to the high concentration of salt in

---

[XXXIII] Obruča, S., Dvořák, P., Sedláček, P., Koller, M., Sedlář, K., Pernicová, I., and Šafránek, D. Polyhydroxyalkanoates synthesis by halophiles and thermophiles: towards sustainable production of microbial bioplastics. *Biotechnology Advances.* 2022, 107906. Appendix 20.

[XXXIV] Kucera, D., Pernicová, I., Kovalcik, A., Koller, M., Mullerova, L., Sedlacek, P., Mravec, F., Nebesarova, J., Kalina, M., Marova, I., Krzyzanek, V., and Obruca, S. Characterization of the promising poly(3-hydroxybutyrate) producing halophilic bacterium Halomonas halophila. *Bioresource Technology.* 2018, 256, 552–556.

the cultivation media. Apart from the direct additional production costs connected with NaCl demands, also the problems with the treatment of the salty wastewaters from the process, and the corrosive effects of NaCl on the reactor should be emphasized. From this point of view, the use of thermophilic bacteria is more technologically feasible. It might seem at first glance that the cultivation of thermophiles at elevated temperatures must necessarily bring additional energy costs to the process. Nevertheless, all fermentation processes are in fact "self-heating" processes, as far as the heat is generated by the microbial metabolism as well as by the mechanical stirring. Consequently, thermophilic fermentations are actually less energy demanding because great energy savings are caused by the reduced requirements for cooling of the bioreactor. We have therefore searched for suitable thermophilic producers that could be suggested as the candidate strains for PHA biosynthesis, and are also involved in our study dealing with general ecological and evolutionary aspects of PHA metabolism.

Two independent research directions were followed. First, we focused on the isolation of thermophilic PHA producers from mixed microbial consortia. In this effort, we utilized our previous knowledge on the enhancement of the stress robustness of bacterial cells brought by the presence of PHA. This original experimental approach that we developed for enrichment of the consortium in PHA producing strains (referred to as "osmoselection") is based on the exposure of the original mixed microbial consortia to osmotic challenge consisting of hypertonic (100 g/L NaCl) and subsequent hypotonic (distilled water) shock. The cells robust enough to survive this challenge provide growing colonies when plated on agar. As far as the standard way of distinguishing PHA producing colonies by Nile red staining [175] turned out to be unusable in the case of thermophilic strains (false positive staining of PHA non-producers was observed), we developed an alternative procedure based on ATR-FTIR screening. This identification procedure is rapid (2 – 3 minutes are needed before the biomass sample transferred from the agar plate to the ATR crystal surface dehydrates), requires an only a small amount of the biomass, and provides not only direct structural evidence of PHA presence but also a semi-quantitative estimate of the level of its intracellular content (the use of FTIR for identification and quantitative analysis has already been discussed in 6.1.1). We have introduced this original combination of enrichment (osmoselection) and identification (ATR FTIR) procedures in the published study[XXXV], where we proved its usability in the isolation of thermophilic and thermotolerant PHA-producing bacteria from activated sludge. Since then, the method provided us with several interesting thermophilic PHA producing strains, and, among them, the isolate taxonomically classified as *Aneurinibacillus* sp. H1 was identified to be the most promising one[XVII, XVIII]. We have already discussed the technological potential of this strain in the production of PHA copolymers with auspicious material properties (5.2.2).

Apart from the isolation and characterization of original PHA-producing thermophilic isolates, we have recently turned our attention to one thermophile that has already been known for quite a long time. *Schlegelella thermodepolymerans* DSM 15344 is a moderately thermophilic bacterium, that was isolated from activated sludge in 2003, when its ability to degrade various polyesters was also described [176]. Nevertheless, apart from this plastics degrading ability, only a little attention was paid to this bacterium, until we have reported that *S. thermodepolymerans* is also capable of the production of high amounts of polyhydroxyalkanoates[XVI]. In this study, we have also proved the capability of the bacterium to incorporate quite high contents of 3-hydroxyvalerate into the PHA structure, which alters the material properties of the produced polymers significantly as already discussed in 5.2.1. This, together with several other newly recognized aspects of its metabolism (e.g. preferential utilization of xylose) and genetic information (e.g. genetic disposition for transformation and degradation of aromatic compounds) make *S. thermodepolymerans* an exceptionally promising candidate for

---

[XXXV] Pernicova, I. Novackova, I., Sedlacek, P., Kourilova, X., Koller, M., and Obruca, S. Application of osmotic challenge for enrichment of microbial consortia in polyhydroxyalkanoates producing thermophilic and thermotolerant bacteria and their subsequent isolation. *International Journal of Biological Macromolecules.* 2020, 144, 698–704.

implementation in NGIBs. Most recently, we have started a research project dealing with the biochemical, biophysical, and stress-response importance of PHA for this bacterium, where we hope to extend our understanding of the role of PHA in bacteria also to the unique world of thermophiles.
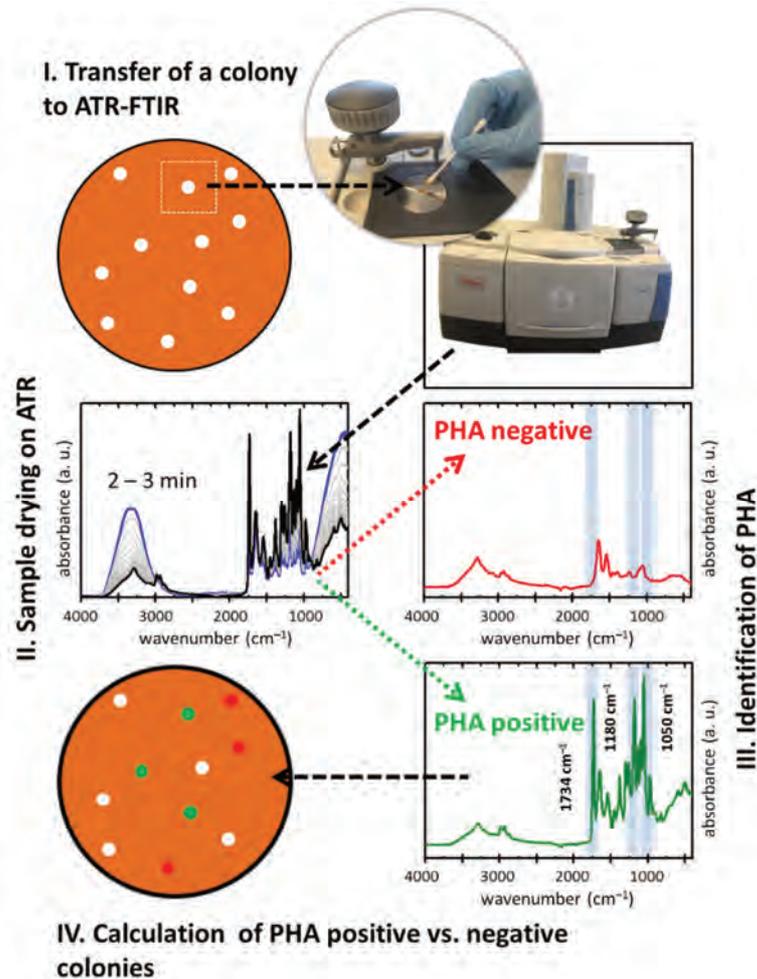
Fig. 68   General experimental procedure for identification of PHA positive and PHA negative colonies by ATR-FTIR as utilized in isolation of thermophilic PHA producers from mixed microbial consortia.

6.3   Another brick in the wall: monomer comes to the scene

Physical work is widely accepted as a great stress and anger relief. Nevertheless, imagine how relaxed and un-irritated would you feel, if you, for instance, were building a wall and, at the same time, someone next to you was demolishing the wall back to the bricks with a hammer? You may be asking why would he do that? Well, maybe just because he needed the bricks for another purpose.

Actually, nature provides numerous examples of how functional this apparently nonsense combination of constructive and destructive processes can be. One of those can be found also in the metabolism of polyhydroxyalkanoates in PHA-producing bacteria. It is well known that the PHA metabolism has a cyclic nature. It means that at a given moment, although the rate of PHA synthesis or hydrolysis prevails according to the current physiological state, both metabolic pathways are still active in the cell. The PHA metabolism is therefore referred to as the so-called "PHA cycle" [142]. Consequently, PHA-producing cells always contain a substantial amount of PHA monomers. So why do these cells aside from the energy investment into building the wall (PHA synthesis) maintain also the energy input into the wall demolishing (monomer production)? For what do they need a constant supply of the loose bricks?

At the time when we came to the topic of PHAs´ role in cell robustness, there was to our best knowledge single report indicating that 3-hydroxybutyrate (3HB) *per se* could provide a protective effect to the bacterial cells (or, more specifically, to the cellular proteins) [177]. Aside from the study focusing on the protective role of polymer PHA and its intracellular granules, we hence performed the experiments where we confirmed the interesting chaperonic effects of the monomer unit (details in 6.3.1), and also the follow-up physico-chemical study where the light was shed on some of these effects from the viewpoint of the phase behavior of 3HB in aqueous solutions.
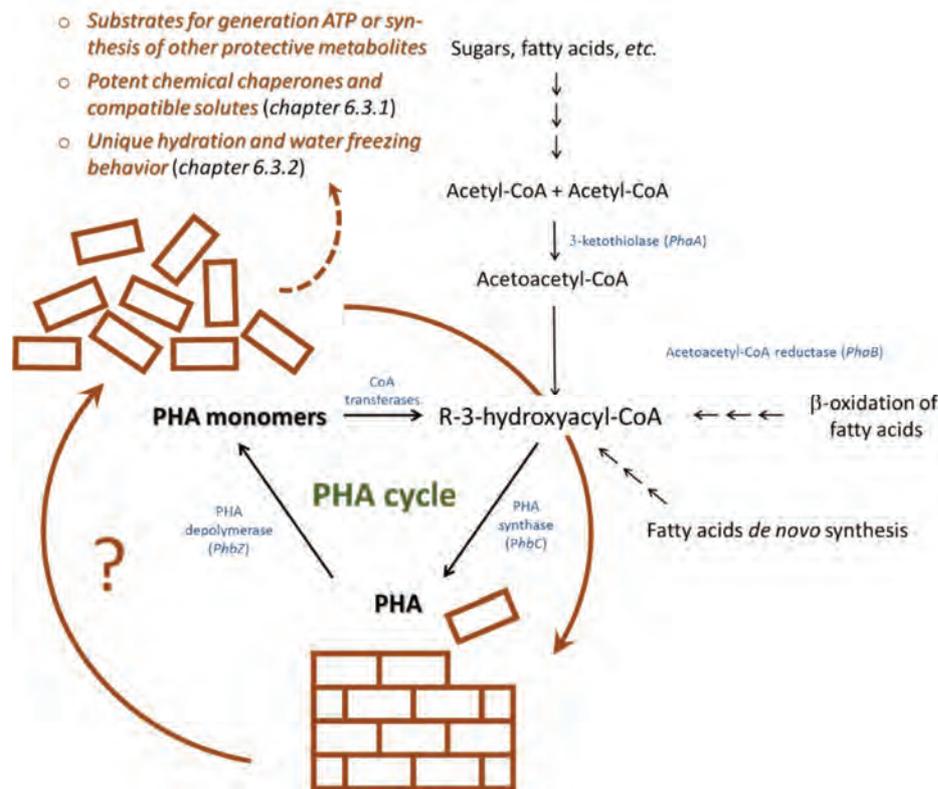
Fig. 69   What is the reason for breaking the wall? Apparent energetic nonsense of the PHA cycle is clarified by the protective effects provided by monomer molecules.

6.3.1   Protective effects of 3-hydroxybutyrate

In order to evaluate the protective effects of the monomer unit most frequently contained in the polymer structure of PHA, i.e. 3- hydroxybutyric acid (or 3-hydroxybutyrate as its dissociated form), we first investigated[XXXVI] its capability of protecting model enzymes (lipase, lysozyme) from heat-induced or chemical (oxidative) denaturation. For this purpose, we used not only standard biochemical assays (enzyme activity measurement), but in parallel also physicochemical methods, namely DLS (monitoring the increase in the hydrodynamic volume of the proteins during the denaturation) and DSC (investigating the denaturation by its heat signature). Surprisingly for us at the moment, we have revealed that when compared at the same molar concentration, 3HB showed a greater protective effect than the well-known chemical chaperones, such as trehalose or hydroxyectoine. Furthermore, in the study[XXIV] dealing with the role of PHA in the survival of microbes under freezing, we, to our best knowledge for the first time, manifested the structure-stabilizing effect of 3HB on an enzyme also during cyclic freezing/thawing. With the increasing addition of 3HB, the residual activity of the analyzed enzyme (lipase) increased significantly during the repetitive (up to 7 consecutive cycles)

[XXXVI] Obruca, S., Sedlacek, P., Mravec, F., Samek, O., and Marova, I. Evaluation of 3-hydroxybutyrate as an enzyme-protective agent against heating and oxidative damage and its potential role in stress response of poly(3-hydroxybutyrate) accumulating cells. *Applied Microbiology and Biotechnology.* 2016, 100, 1365–1376. Attached as Appendix 21.

freezing and thawing. This protective effect was, again, comparable to that of trehalose, a well-recognized cryoprotectant.

Apart from the chaperonic effect for the biomolecules, we further revealed in the study[XXIV] that 3HB provides the cryoprotective effect also to whole microbial cells. When added extracellularly, it served as a very potent cryoprotectant both for yeast cells (*Saccharomyces cerevisiae*) and bacteria (*C. necator sp.* H16 and PHB^{-4}). Moreover, we have proved experimentally[XXXVI] that the PHA-producing strain *Cupriavidus necator* H16 reveals a 16.5-fold higher intracellular concentration than the PHA non-producing mutant *C. necator* PHB−4. Taking together all the obvious protective effects of 3HB and its evidently higher content in the PHA accumulating cells, it can be deduced that constant degradation of PHA into the monomer units represents an additional piece in the puzzle of the complex mechanism of the contribution of PHA to the stress resistance of bacteria.

6.3.2   On the hydration of 3-hydroxybutyrate

The chaperonic, and mainly the newly recognized cryoprotective, effect of 3HB attracted our attention not only from the purely biological point of view. The mechanism of the universal bioprotective performance of compounds like trehalose – often referred to as compatible solutes or chemical chaperones – is not clearly understood, nevertheless, it is believed that they are able to stabilize labile biopolymers (e.g. proteins) by affecting their hydration in the cell [178]. Furthermore, I have already emphasized in 6.2.1 that in the particular case of cell freezing, the cell survival is affected by the activity of intracellular water, as it influences the rate of the cell freeze-dehydration as well as the tendency to formation of intracellular ice crystals.

Bearing this essential role of water in mind, we decided to perform a comprehensive study[XXXVII] on the thermodynamics of the aqueous solutions of sodium salt of 3HB (Na3HB) as an inevitable first step to a better understanding of stabilizing effects provided by 3HB. Two distinct experimental strategies were used for this purpose: first, hydration of 3HB was studied using a combination of three different methods of sorption analysis (vapor sorption TGA, water activity analyzer and sorption calorimetry), second, phase transitions in aqueous solutions of Na3HB were studied via DSC under equilibrium and non-equilibrium conditions, respectively.

Our experiments proved an outstandingly hydrophilic nature of 3HB which is at least comparable to, but in some perspectives (solubility, water activity decrease in solution) even better than some well recognized compatible solutes such as trehalose. This represents a crucial finding not only with respect to understanding the natural protective role of 3HB in PHA-accumulating organisms but also from the view of its potential application in the technological fields in which stabilization of biological molecules is required (e.g. cryopreservation of biological samples, food preservation, cosmetics, etc.). Apart from this, the study also revealed that sodium salt of 3HB can form, depending on the conditions (temperature, relative humidity), at least two different crystalline forms – anhydrous crystal and crystalline dihydrates.

The study also confirmed the high cryoprotective potential of 3HB in many aspects of the equilibrium (the corresponding phase diagram is shown in Fig. 70b) and non-equilibrium (Fig. 70c) phase behavior of the Na3HB/water mixtures. For instance, the effect of 3HB presence on the water freezing curve in the equilibrium phase diagram and the position of the eutectic point that represent the least achievable water freezing temperature (-28.1°C for Na3HB content of 40.5 wt.%) is, again, comparable to the effects found for compatible solutes and routinely used cryoprotectants such as trehalose, glycerol or sucrose. Similarly, the cryoprotective effects of 3HB can also be illustrated by its non-equilibrium behavior in aqueous systems. Water freezing was reduced partially (below Na3HB content of 40-50 wt.%) or completely (above this Na3HB content). Furthermore, in the region where

---

[XXXVII] Slaninova, E., Obruca, S., Kocherbitov, V., and Sedlacek, P. On the bioprotective effects of sodium 3-hydroxybutyrate: thermodynamic study of binary Na3HB-water systems. *Submitted for publication.* Attached as Appendix 22.

the water freezes a significant freezing temperature depression was found again. Last but not least, from the total enthalpies of the ice melting endotherms (determined by DSC) we determined the amount of nonfrozen water to be approximately 1.35 g water per g of Na3HB (or 0.57 g water per g of water/Na3HB mixture). Once again, this illustrates the outstanding position of Na3HB among the recognized compatible solutes. For instance, published values of non-freezing water for sugars range from 0.21 g water per g of fructose, through 0.26 g water per g sucrose, to 0.31 g water per g trehalose [179].
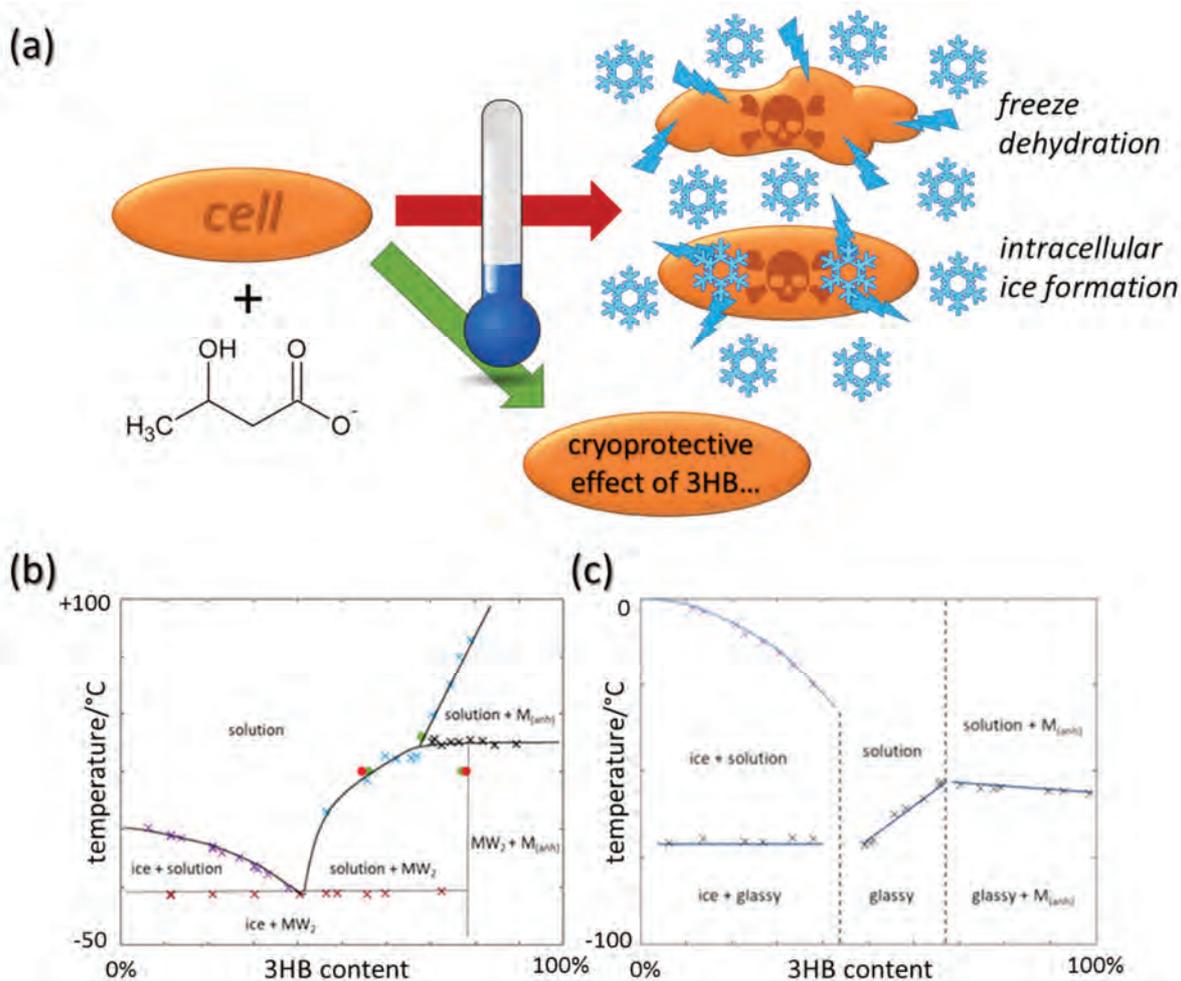
Fig. 70   Cryoprotective role of 3HB as understood from the phase behavior of 3HB-water mixtures. (a) Schematic representation of the two main mechanisms of the lethal effect of freezing to cells. (b) The phase diagram in the equilibrium of 3HB-water complex using DSC (×); sorption calorimetry (●) and DVS (●). All lines are drawn as a guide for the eye to follow the respective phase boundaries. (c) The phase diagram in non-equilibrium of Na3HB-water complex using DSC data from second scans represented by stars (×). All lines are drawn as a guide for the eye to follow the respective phase boundaries.

The above-mentioned study hence represents another illustration of a valuable input of the physicochemical way of thinking to shed light on biological phenomena. The particular results on the hydrophilicity of 3HB and phase behavior of 3HB/water systems allow us to fully appreciate the contribution of the monomer to the overall protective function of PHA (the complete idea of the protective effect is illustrated in Fig. 71). It can also explain why the capability of PHA synthesis is so widespread among psychrophilic bacteria. Last but not least, this study might also open a gate for the application of Na3HB for instance in the food industry or biotechnology as a potent cryoprotectant or lyoprotectant.

Fig. 71   The updated idea on the protective role of PHA in bacterial cell concluding our studies: biophysical mechanisms that contribute to the complex protective effect of PHA in the bacterial cells

References

[134] Obruca, S. et al. *Folia Microbiologica*, 2010, 55, 17–22.

[135] Obruca, S. et al. *World Journal of Microbiology and Biotechnology*, 2010, 26, 1261–1267.

[136] Obruca, S. et al. *World Journal of Microbiology and Biotechnology*, 2013, 29, 2417–2428.

[137] Ayub, N. D. et al. *Current Microbiology*, 2004, 49, 170–174.

[138] Ayub, N. D. et al. *Plasmid*, 2007, 58, 240–248.

[139] Ayub, N. D. et al. *Extremophiles*, 2009, 13, 59–66.

[140] Zhao, Y. H. et al. *FEMS Microbiology Letters*, 2007, 276, 34–41.

[141] Ruiz, J. A. et al. *Applied and Environmental Microbiology*, 2001, 67, 225–230.

[142] Kadouri, D. et al. *Critical Reviews in Microbiology*, 2005, 31, 55–67.

[143] Allen, M. M. et al. *Archiv für Mikrobiologie*, 1969, 69, 114–120.

[144] Young, K. D. *Current Opinion in Microbiology*, 2007, 10, 596–600.

[145] Slouf, M. et al. *Polymer Testing*, 2015, 42, 8–16.

[146] Otun, S. O. et al. *Pharmaceutical Research*, 2015, 32, 1316–1324.

[147] Uribelarrea, J. L. et al. *Biotechnology Letters*, 1985, 7, 75–80.

[148] Harden, V. P. et al. *Journal of Bacteriology*, 1953, 65, 198–202.

[149] Rosenberg, M. *FEMS Microbiology Letters*, 1984, 22, 289–295.

[150] Rosenberg, M. *FEMS Microbiology Letters*, 2006, 262, 129–134.

[151] Barer, M. R. Bacterial growth, physiology and death.*In Medical Microbiology*; Elsevier, 2012; pp. 39–53.

[152] Braissant, O. et al. *Frontiers in Microbiology*, 2020, 11, 547458.

[153] Foster, P. L. *Mutation Research/Fundamental and Molecular Mechanisms of Mutagenesis*, 2005, 569, 3–11.

[154] MacLean, R. C. et al. *Nature Reviews Genetics*, 2013, 14, 221–227.

[155] Tal, S. et al. *Canadian Journal of Microbiology*, 1985, 31, 608–613.

[156] Kadouri, D. et al. *Applied and Environmental Microbiology*, 2002, 68, 2943–2949.

[157] Kadouri, D. et al. *Applied and Environmental Microbiology*, 2003, 69, 3244–3250.

[158] Kadouri, D. et al. *Archives of Microbiology*, 2003, 180, 309–318.

[159] Khosravi-Darani, K. et al. *Applied Microbiology and Biotechnology*, 2013, 97, 1407–1424.

[160] Mokhtari-Hosseini, Z. B. et al. *Bioresource Technology*, 2009, 100, 2436–2443.

[161] Goff, M. et al. *Journal of Biotechnology*, 2007, 132, 283–286.

[162] Mazur, P. *American Journal of Physiology-Cell Physiology*, 1984, 247, C125–C142.

[163] Gabani, P. et al. *Applied Microbiology and Biotechnology*, 2013, 97, 993–1004.

[164] Pérez, V. et al. *Frontiers in Microbiology*, 2017, 8, 1173.

[165] Koller, M. et al. *Algal Research*, 2014, 6, 52–63.

[166] Wang, Q. et al. *Microbial Cell Factories*, 2009, 8, 47.

[167] Wahl, A. et al. *BMC Microbiology*, 2012, 12, 262.

[168] Mahler, N. et al. *Biochemical Engineering Journal*, 2018, 130, 39–46.

[169] Bialecka-Fornal, M. et al. *Journal of Bacteriology*, 2015, 197, 231–237.

[170] Gantenbein, U. L. Poison and Its Dose. *In Toxicology in the Middle Ages and Renaissance*; Elsevier, 2017; pp. 1–10.

[171] Calabrese, E. *Microbial Cell*, 2014, 1, 145–149.

[172] Zhu, Z. et al. *Applied Microbiology and Biotechnology*, 2018, 102, 4615–4627.

[173] Chen, G.-Q. et al. *Current Opinion in Biotechnology*, 2018, 50, 94–100.

[174] Yu, L. et al. *Biotechnology Journal*, 2019, 14, 1800437.

[175] Spiekermann, P. et al. *Archives of Microbiology*, 1999, 171, 73–80.

[176] Elbanna, K. et al. *International Journal of Systematic and Evolutionary Microbiology*, 2003, 53, 1165–1168.

[177] Soto, G. et al. *Extremophiles*, 2012, 16, 455–462.

[178] da Costa, M. S. et al. An overview of the role and diversity of compatible solutes in Bacteria and Archaea. *In Advances in Biochemical Engineering/Biotechnology*; 1998; pp. 117–153.

[179] Xu, M. et al. *Journal of Pharmaceutical Sciences*, 2017, 106, 83–91.

Chapter 7:
Hydrogels: experimental model of biological systems, soft-matter material for future applications

"What do we mean by soft matter? Americans prefer to call it 'complex fluids.' This is a rather ugly name, which tends to discourage the young students."
(*Pierre-Gilles de Gennes*)

"Just because you are soft doesn't mean you are not a force."
(*Victoria Erickson*)

When something is soft, it is not necessarily weak as well. Soft-matter, as already introduced in chapter 3, is in fact a family of exceptionally powerful materials. Among them, hydrogels represent yet special category. Hydrogels are three-dimensional networks of polymer chains (or associated colloidal particles in the case of particulate gels) that are able to retain a large amount of water in their swollen state. Since the term "hydrogel" first appeared in the scientific literature, these materials have continuously attracted substantial attention in research and development (see Fig. 72 and historical review [180]). Currently available hydrogels are materials of versatile composition, preparation, and properties [181]. They are utilized in numerous applications like biomedical, environmental, or in the fields of personal care and bioseparations [182]. In general, the essence of their technical functionality is rooted in their structure, i.e. network architecture, mesh or pore size, pore distribution etc., and in their binding ability based on a combination of chemical and physical structural features.
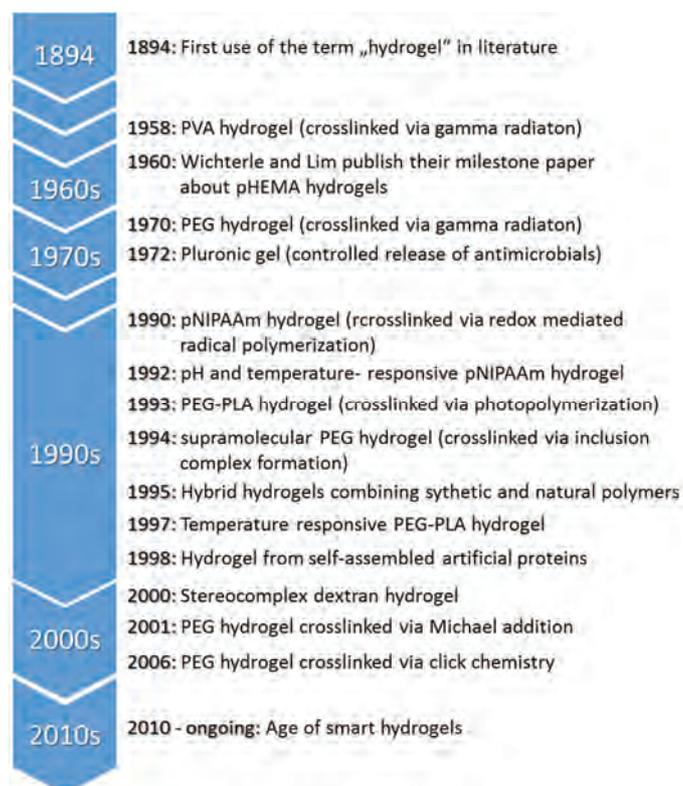

Fig. 72   *The most important event in the history of hydrogel research. Adopted from [180]. References to the original works can be found ibid.*

Hydrogels are especially attractive also from the "bio" perspective [183]. Actually, they have been found in nature since life appeared on Earth. Bacterial biofilms, formed by hydrated extracellular matrix (ECM) components, represent probably the evolutionary oldest example of a natural hydrogel-like structure [184]. Numerous bacterial strains are capable of secreting gel-forming components such as alginate (e.g. *Azotobacter* sp., which will be further discussed in 7.3.3), hyaluronate, or microbial cellulose as a part of their defense and survival strategies. Nevertheless, many other examples can be found also in the higher organisms. In general, plants represent a good example [185] as they possess a remarkable ability to support very large volumes of water without losing tissue cohesion. However, similar water-swollen structural motifs are can be found also in the animal world. For example, the body of jellyfish is about 95 % water [186]. The prevalence of hydrogel-like structures in nature clarifies why, since the beginning of the research and development of artificial hydrogels, the use of these materials was intended primarily for bio-applications. From the traditional uses of natural gel-forming compounds, such as gelatine and agar, to the "smart" hydrogels developed for modern biomedical uses, the main motivations for the application of hydrogels in bioanalytical and biomaterial areas were always based on the unique combination of biological (biocompatibility, ECM- and tissue-mimicking structure), mechanical (viscoelasticity and adhesion) and transport (barrier and release) properties that these materials offer. In a fact, all these specific material attributes result from the combination of a chemically or physically crosslinked polymer network, penetrating the whole volume of the gel, and a large amount of water, entrapped in it. Regarding, for instance, the deformation performance of the gels, their softness and liquid-like deformation attributes (such as viscous flow under high shear rates) results from the amount of aqueous solution contained in their structure, while the rigidity and elastic behavior, prevailing under normal deformation rates, are provided by the network formed in their structure by the dispersed component [187, 188].

Another practical consequence of the specific ambivalent structure of hydrogels can be found in their transport properties. This topic was already opened in 5.1.1 where we discussed the major benefits that the hydrogel medium provides for experimental monitoring of diffusion processes. Kinetics of the molecular movements in gels is fast (the rate of diffusion of a solute in a hydrogel medium is of the same order of magnitude as in the liquid solution, only partially reduced by the specific effects of the dispersed network). The specific effects of the dispersed component on solute diffusion may be illustrated in considering hydrogel as a specific type of porous diffusion medium. In such a medium, the rate of diffusion of a solute is influenced by two inevitable effects: a reduced cross-sectional area, available for the diffusive flux compared to the macroscopic cross-sectional area (assuming that the compound cannot penetrate the dispersed particles), and a more tortuous transport of the compound into the pores of medium. Furthermore, the diffusing compound may also interact with or even bind to the dispersed particles (e.g. with the polymer network in the hydrogel). The appropriate mathematical model for the description of diffusion in porous media, including all the above-mentioned effects, can be found for instance in [189]. Aside from maintaining the rate of diffusion processes in hydrogel near to those of the corresponding liquid medium, all the disturbing effects typical for liquids, such as thermal or mechanical convections, are significantly reduced in the gels as a result of their high apparent viscosity. Altogether, this makes hydrogel media so useful and widespread wherever the diffusion-related phenomena are studied.

Some of the simple, yet popular demonstrations of the special transport properties of gels are presented in Figure 73. Chemical gardens, a phenomenon discovered more than three centuries ago [190], represent not only a popular chemical experiment for middle-school chemistry lessons but nowadays there is also a growing interest in them in disciplines as varied as chemistry, physics, nonlinear dynamics, and materials science [191,192]. Liesegang rings, periodical bands or ring patterns formed by inorganic precipitation in a polymer gel medium, have attracted the attention of chemists, geologists and biologists, in experiments in order to understand natural patterning. Although numerous qualitative and mathematically formulated models have been suggested, we still lack a complete explanation of both phenomena [193].
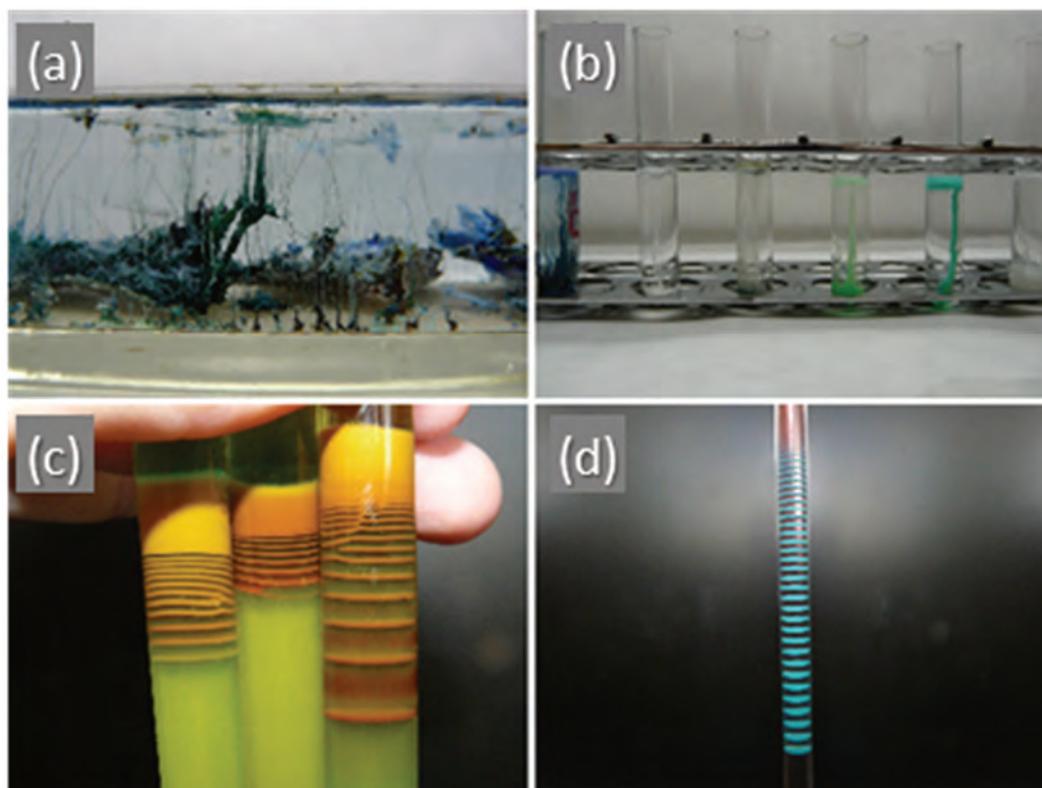
Fig. 73   Common practical demonstrations of diffusion-related phenomena in hydrogels: chemical gardens (a, b), Liesegang rings (c, d). The procedures used for preparation of the shown phenomena are provided in our paper[XXXVIII].

I have already discussed in 5.1 why and how the hydrogel forms of humic substances were used as a model of natural humus-containing environments. Similarly, gels are often used to simulate diffusion processes in soft tissues. In particular, hydrogel prepared from agarose (linear polysaccharide of red algae, made up of the repeating monomeric unit of agarobiose) was proposed as a suitable reference medium for such experiments [194, 195]. Agarose gels (Fig. 74) provides also additional benefits such as an easy preparation procedure (the solution, warmed up to a temperature above 60 °C, is gelled in the whole volume by cooling to ambient temperature). Furthermore, the mechanical and textural properties of agarose hydrogels as well as the gelation mechanism are well understood [83, 196, 197]. Therefore, a great deal of our work focused on hydrogels were associated with this particular gel system.

Like in the previous chapter, also in this part I will first (in section 7.1) describe a unique methodology, that we have developed for the complex and multi-scale analysis of hydrogels in order to provide a comprehensive understanding of composition–structure–performance relationships valid for these materials. Then, I will continue by introducing a novel concept that we proposed for the development of novel semi-interpenetrating polymer network gels with engineered material (mainly mechanical and transport) properties (section 7.2). Finally, I will briefly discuss also other specific hydrogel forms that we developed and investigated considering their use in various application fields (section 7.3). In this last section, I will also introduce one special case of hydrogel materials, in which all three, apparently separate directions of my previous research interests (natural organic matter and the care for improving soil quality, "physical" microbiology and biotechnology, and research and development of hydrogels), have recently joined back in a single research topic (section 7.3.3)

[XXXVIII] Sedlacek, P., Smilek, J., Lastuvkova, M., Kalina, M., and Klucakova, M. Hydrogels: invaluable experimental tool for demonstrating diffusion phenomena in physical chemistry laboratory courses. *Journal of Materials Education.* 2017, 39, 59–90.
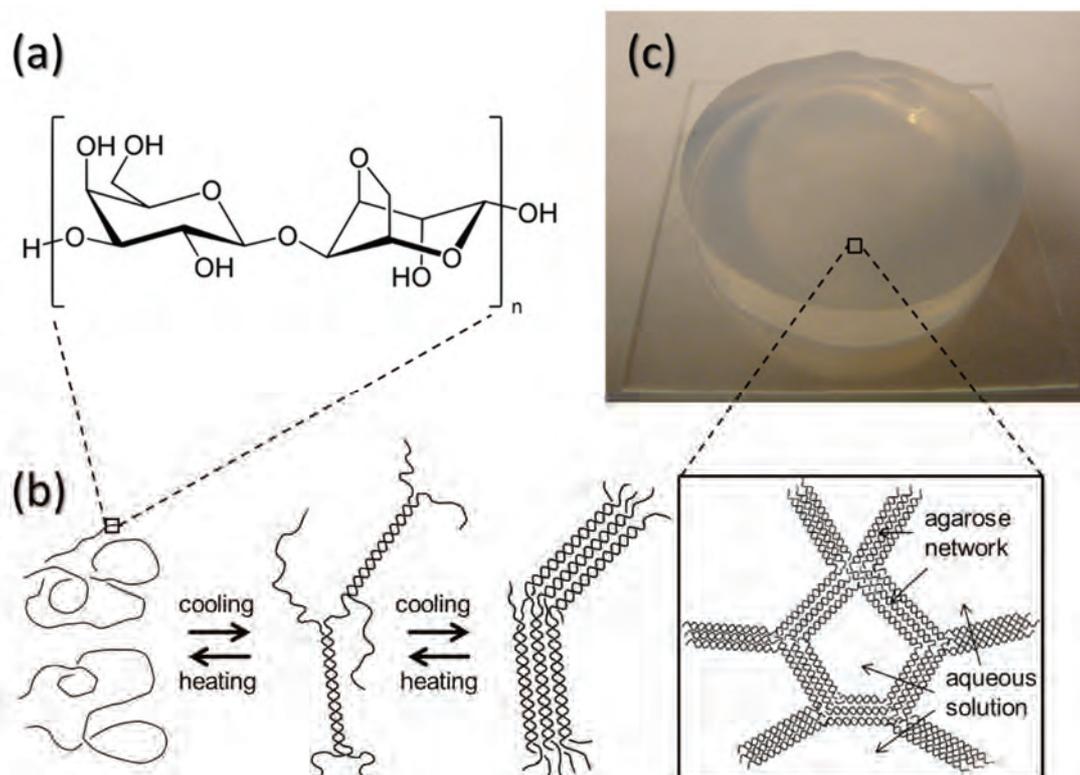
Fig. 74   Agarose hydrogel as a multi-purpose medium for experimental diffusion studies. Molecular structure of agarose (a) and the schematic illustration of the macromolecular aggregation processes (b) which take place during the thermoreversible agarose gelatinization leading to the final agarose hydrogel (c).

7.1   From electron beams and single photons to the naked eyes: multiscale investigation of hydrogels

As was stressed already, there is a close interconnection between the internal structure of the hydrogels (both chemical and morphological) and their main application-relevant properties, such as mechanical or transport performance. We have put a great effort to gain insight into this causal relationship, whose comprehension is crucial not only for understanding the specific material properties of commonly used existing hydrogels but also for the engineering of novel gel materials "tailor-made" for required properties. For this purpose, we have gradually - in the course of our hydrogel-related research - developed a unique methodology, that combines methods of macroscopic and microscopic analyses focusing on the three crucial aspects of the studied hydrogels: their morphological and ultrastructural architecture, barrier and release properties, and viscoelasticity (Fig. 75).

The wide range of different laboratory setups that can be used for the investigation of diffusion processes in gels (and for the determination of quantitative parameters that characterizes the rate of this process, e.g. diffusion coefficients) has been already discussed in the chapter where I demonstrated their use in our study on interactions of humic substances (5.1.1). Our experience with the benefits of diffusion-in-gel methodology was also utilized in the plant cuticle penetration research study (5.1.4). For a systematic use on agarose-based and other semi IPN gels that will be discussed in the next section, we suggested two diffusion techniques that be especially convenient, it is the method of horizontal (side-by-side) diffusion cells and non-stationary in-diffusion in cuvettes. The usefulness of both techniques was proved in our publications on humic substances[IV, V, VIII]. The experimental setup of both techniques are illustrated in Fig. 17 (s. 5.1.1), for the non-stationary in-diffusion (from source solution) further in Fig. 76.

laboratory diffusion techniques
(diffusion cells and/or
non-stationary diffusion tests)
&
molecule tracking studies
(e.g. FCS)

transport

structure

indirect structural analyses
(porometry, scattering methods)
&
direct visualization
(electron microscopy
+ image analysis)

hydrogels

flow

rheometry (e.g. oscillatory)
&
microrheometry (particle tracking by FCS, DLS)
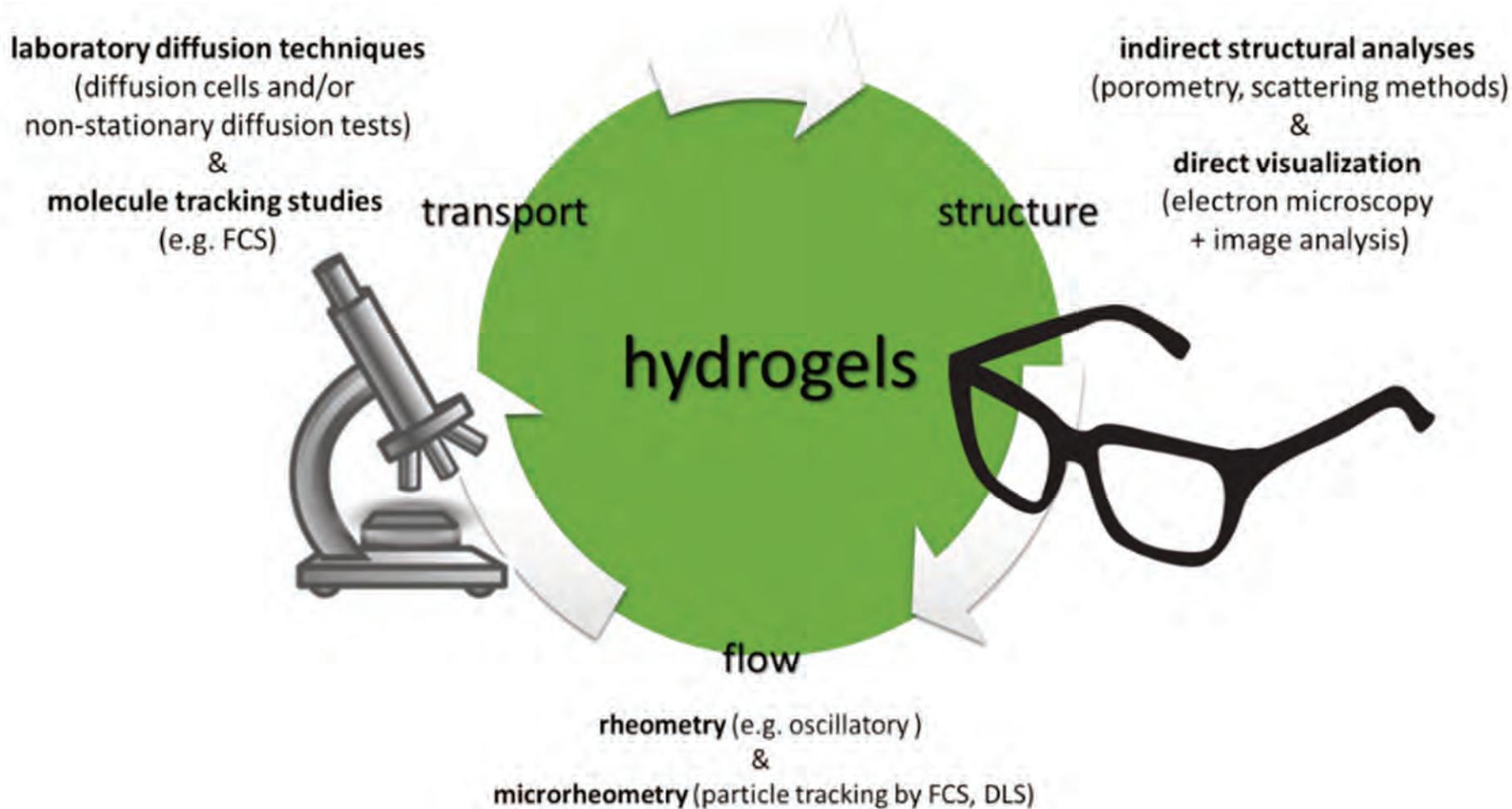
Fig. 75   Schematic representation of the developed methodology for multiscale experimental study on the relationships between internal structure, mechanical (flow) properties, and transport or barrier properties of hydrogels under investigation.
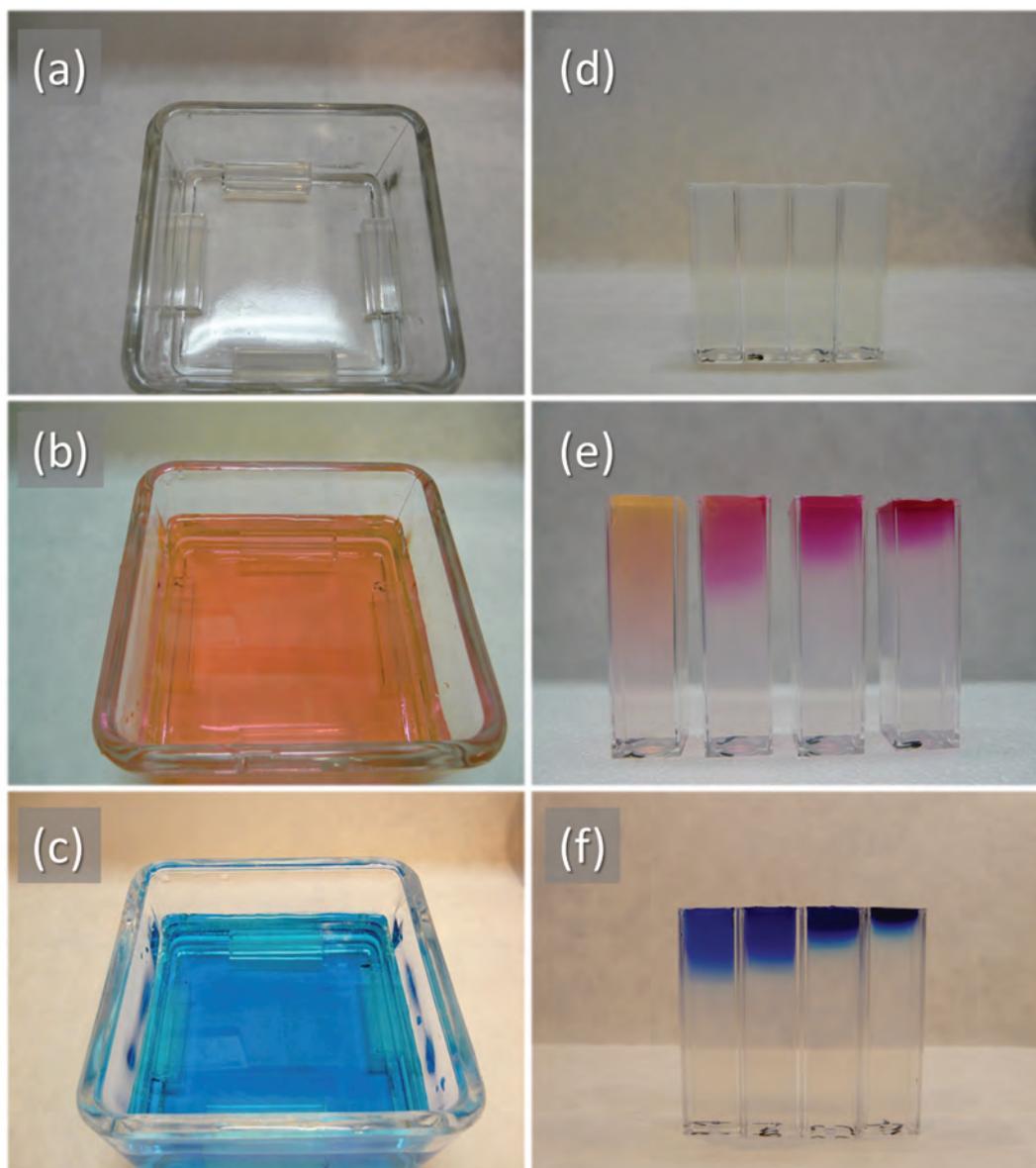
Fig. 76   Non-stationary (macro)diffusion experiments in agarose (and agarose-based semi-IPN gels). (a-c) Experimental setup. Hydrogel-filled cuvettes are put in the vessel (a) and immersed with source solution of the diffusion probe ((b)Rhodamine 6G, (c) Methylene blue). (d-f) Cuvettes with hydrogels before (d) and after 72 hours of diffusion of R6G (e) and MB (f). Concentration of solute-binding component (poly(styrenesulfonate), PSS) in the gels shown in (d-f) increases from 0 to 0.01 wt.% from left to right.

During the implementation of the diffusion methodology into our research of hydrogels, it kept fascinating me how illustrative and visually perceptible the experiments are. During the experiment, the macroscopic manifestation of the effects of morphological (e.g. crosslinking density), and chemical or physico-chemical (binding affinity for the diffusing solute) features of the microscopic structure on the diffusion uptake, barrier, and release properties of the gels can easily be visually monitored. Taking together with the wide range of parameters describing these effects quantitatively, that can be obtained by the appropriate mathematical analysis of the experimental results (described in detail in our publications already referenced in 5.1, and further introduced in 7.2), and also with the

undemanding experimental setup (only instrumentation widely available in a common university/commercial lab is used), we proposed this methodology not only as an innovative experimental tool for the soft matter research, but we have also suggested implementing this methodology also into practical chemical education[XXXVIII].

The uniqueness of our approach towards the material analysis of gels does not lie only in its complexity, aiming at covering all aspects of the composition–structure–performance relationships, but also in its multiscale nature. It means that our ambition was to monitor the mechanical, transport and structural properties of the analyzed hydrogels not only on the macroscopic (i.e. the sample-averaged) scale but also in the relevant microcosms of the gel architecture. Therefore, we were aiming at complementing the macroscopic diffusion methods, presented above, by monitoring the self-diffusion of the solute in the gels on the molecular scale. This can be provided by several methods, whereby tracer techniques and NMR are among the most often used [198]. In our experimental toolbox, we involved Fluorescence Correlation Spectroscopy (FCS) for the purpose. The technique allows the determination of the self-diffusion coefficient of a homogeneously distributed molecular fluorophore in the gel via analysis of the fluctuations in the intensity of fluorescence that the thermal motion of the molecules induces. This "zooming in" to the molecular level of the diffusion process brings several benefits. The analysis proceeds in a concentration-homogeneous sample (concentration gradient of the solute is not needed), which can eliminate some concentration-dependent artifacts (e.g. molecular aggregation or other self-interactions of the solute). Furthermore, when the influence of molecular interactions on the diffusivity of the solute is concerned, it can be derived not only from the value of the self-diffusion coefficient but also from the additional parameters that can be obtained by the analysis (e.g. from the fluorescence lifetime in the case of time-resolved FCS). This was successfully utilized for instance in our study on the diffusivity of fluorescent dyes in semi-IPN agarose gels (will be discussed in 7.2).

As far as the mechanical behavior of the hydrogels is concerned, it is usually analyzed by standard rheological assays, most often by oscillatory rheometry. We have utilized this conventional approach, represented most often by strain-sweep and frequency-sweep tests, also in our analytical concept, primarily for determining the relative contributions of solid-like and liquid-like deformational performance of the gels and quantifying their overall rigidity on the sample-averaged (i.e. macroscopic) scale. From the obtained results, it is possible to discuss the strength of interactions involved in the gel network formation, cross-linking density and other information crucial for describing the internal gel structure. Beyond this, we again focused also on the viscoelasticity of the micro-environment of the gel pores. For this purpose, we tested several techniques of passive microrheology [199], the method based on monitoring the thermal motion of an appropriate probe (inert microparticles with well-defined size and shape) in the studied environment and determining the viscoelastic parameters of this environment based on how it affects particles' displacement behavior. Among the tested techniques, passive microrheology assays based on DLS and FCS seemed the most promising. These techniques interpret time-fluctuations of light-scattering and fluorescence intensities, respectively, in terms of the thermal motion of the light scattering/emitting units. The example of qualitative outcomes of both microrheology assays in form of mean square displacement (MSD) curves are shown in Fig. 77. The information resulting from the microrheological analysis was found to complement the macrorheological study reasonably, as far as it provides a detailed investigation of the liquid gel pore environment, compared to the macroscopic deformation analysis, where the elasticity of the solid gel network plays the principal role and the solid-like mechanical behavior of the gel predominates.
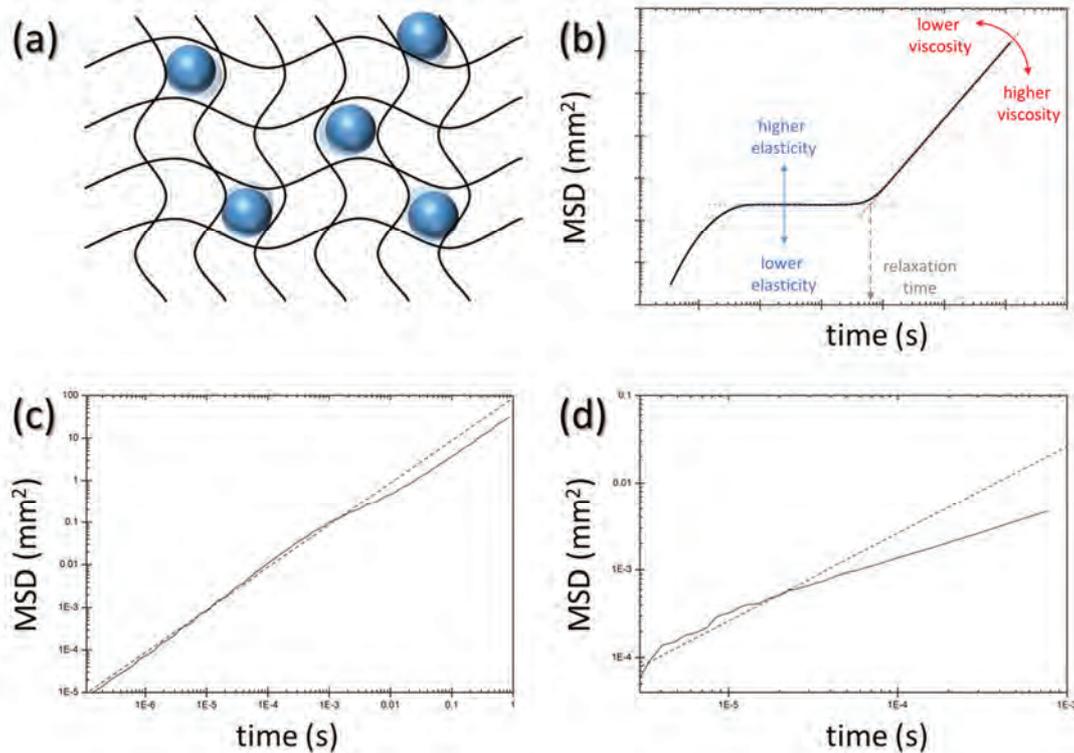
Fig. 77   Microrheology assays used for viscoelasticity mapping in the hydrogel pores. (a) Schematic representation of passive microrheology – the thermal movement of microparticles incorporated in the gel structure is analyzed via monitoring fluctuations of intensity of emitted or scattered light. (b) Mean square displacement (MSD) curve as a primary output of the passive microrheology assays. Demonstrations of viscoelasticity of the environment on the shape of MSD curve. (c) Results of FCS microrheology: MSD curve of 30 nm microparticles in 1 wt. % agarose gels (solid) as compared to calculated MSD for the same particles in water (dashed). (d) Results of DLS microrheology: MSD curve of 100 nm microparticles in 0.5 wt. % agarose gels (solid) as compared to calculated MSD for the same particles in water (dashed).

Obviously, to interpret the mechanical, transport, or any other application-relevant aspect of the hydrogel behavior, it is absolutely essential to be capable of analyzing and describing the internal morphology and ultrastructure of the studied systems. Therefore, a great deal of our attention was paid to the selection and optimization of methods of structural analysis of the gels. With respect to our multiscale concept of hydrogel investigation, also in this case we aimed at combining some simple and widely available experimental tools for the indirect sample-averaged structural analysis, and advanced methods capable of direct ultrastructural imaging of the hydrogel architecture. As was successfully demonstrated in our study on semi-IPN gels (see the following section), turbidity measurements provided by ordinary spectrophotometry and oscillatory rheometry were found appropriate for determining the average mesh sizes of the gel network (see Fig. 78). In the turbidimetry assay, the average structural parameters are calculated from the shape of the light-scattering spectrum. In particular, the wavelength exponent (determined as a slope of the log-log plot of turbidity vs. wavelength) is known to be dependent on the mesh size of the scattering element (for a detail description on the technique, see e.g. [200]). Similarly, from the basic viscoelastic parameters of the gels (elastic and viscous moduli), determined by oscillatory rheometry, the average density of crosslinks and average mesh size of the gel can be calculated elastic by a simple fitting procedure based on a generalized Maxwell model [201] using the procedure described by Pescolido et al. [202]. These methods were successfully applied in our study on agarose-based semi-IPN gels (data shown in Fig. 78).
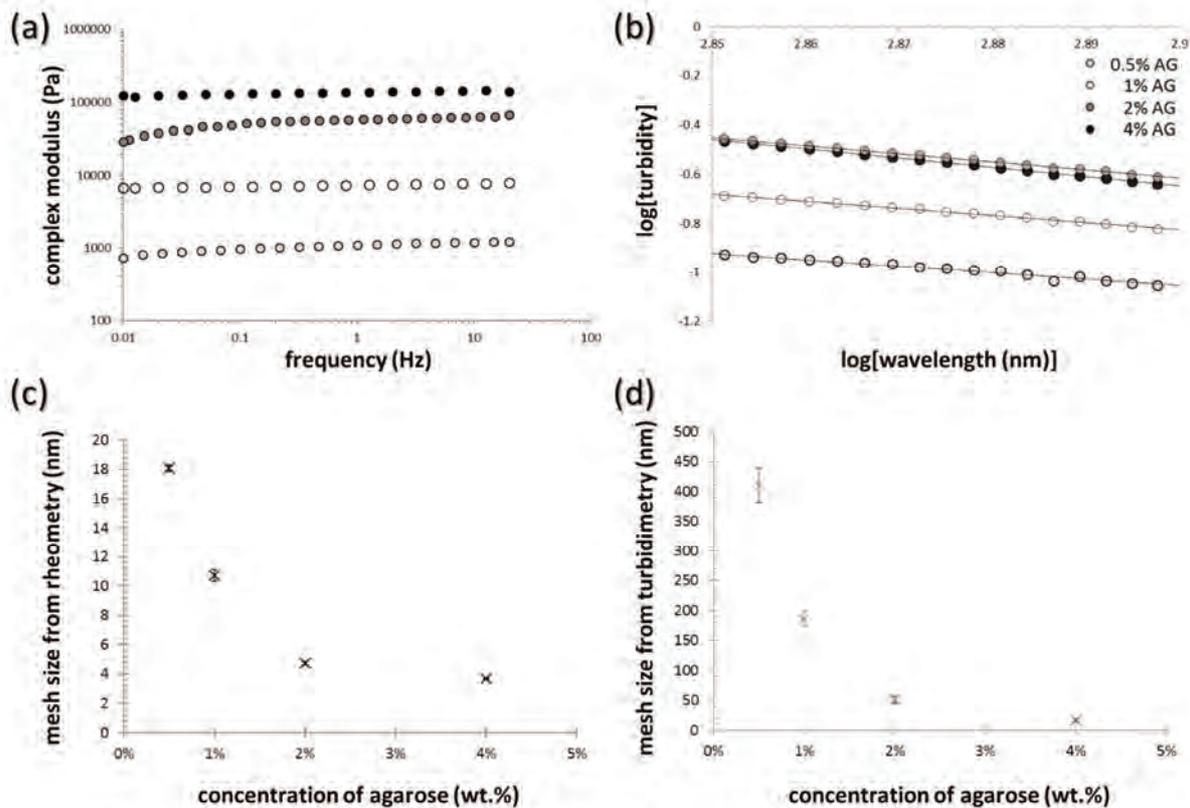
Fig. 78   Indirect determination of pore size of the agarose hydrogels from oscillatory rheometry (a,c) and turbidimetry (b,d). Original data was obtained by the technique (a, b), and calculated mesh sizes were calculated from these data (c,d) as a function of agarose concentration in the gel. Data published in[XL].

Surprisingly for us, finding an appropriate method for imaging the internal structure of the gel in a native, non-altered form, proved to be a much more challenging task than originally expected. The basic setup of scanning electron microscopy (mainly the high vacuum maintained during the sample analysis) makes this technique inapplicable for the gels in their original, water-swollen form. In cooperation with the group from the Institute of Scientific Instruments, Czech Academy of Sciences, we hence launched a research project focused on the optimization of SEM technique in order to obtain more relevant visualization of the gel ultrastructure. The first approach used for this purpose was based on freeze-drying of the gels followed by a standard SEM imaging of the dried sample. It is well described that the free-drying of the gels leads to a collapse of the original structure and is not applicable in the analysis of the native structure of the original hydrogels [203]. Freeze-drying is useful in preventing structural collapse, nevertheless, even in this drying technique, both involved experimental steps (freezing and solid water sublimation) may affect the structure of the resulting material significantly. In Fig.79a, it can be seen how the slow freezing of the agarose gels in a standard laboratory refrigerator destroys the inherent microporous structure of the hydrogel as a result of ice crystal growth. This is a common experimental artifact that limits the hydrogel structure analysis in the freeze-dried form. Nevertheless, we have tested various techniques of gel freezing and experienced that a kind of shock freezing (provided for instance by immersion of the sample in liquid nitrogen) helps to maintain the microporous structure of the gel after freeze-drying to a large extent, enabling much more reliable visualization of its internal structure in the dried by standard SEM imaging (Fig. 79b).
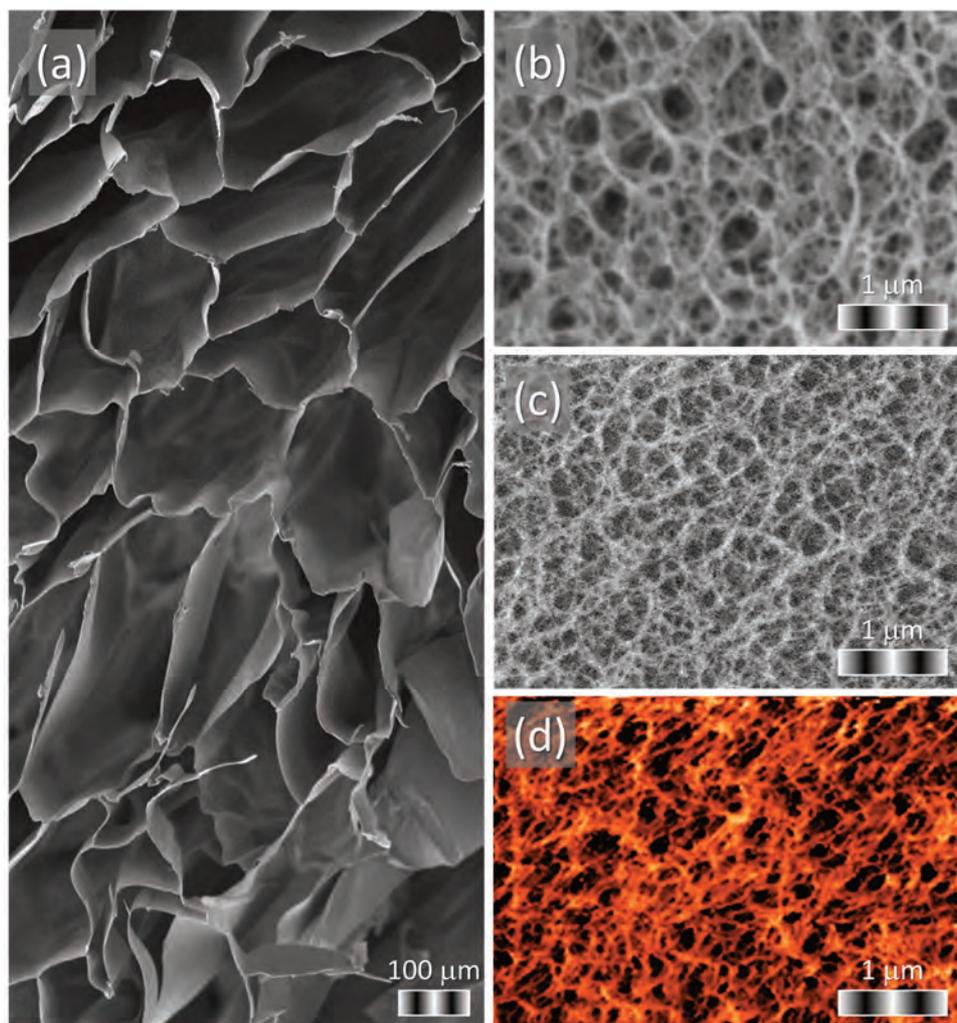
Fig. 79   Micrographs of the internal structure of agarose hydrogels (*agarose content 2 wt.%*) *obtained from various imaging techniques. (a) SEM image* (*ZEISS EVO LS 10*) *of the agarose gel freeze-dried* (*VirTis BenchTop K*) *after freezing in a standard laboratory refrigerator. (b) SEM image of the same gel freeze-dried after shock freezing provided by immersing the sample in liquid nitrogen. (c) cryo-SEM image* (*SEM Magellan 400L*) *of the same gel plunge-frozen and freeze-fractured before the analysis* (*EM ACE600 preparation chamber*)*. (d) AFM image* (*toolbox for gel-structure analysis. The great advantage of this technique is that it allows structural*) *of the same gel submerged in water.*

Cryogenic SEM (cryo-SEM) was tested as another way how to monitor the internal morphology of the gels. We have performed a detailed methodological study that involved testing two different techniques of gel freezing (plunge-freezing, high-pressure freezing) and assessing and interpreting the experimental artifacts found in the structure[XXXIX]. As can be seen in Fig. 79c, using the optimized experimental protocols, cryo-SEM imaging enables lucid visualization of the internal gel microstructure lacking the structural artifacts typical for the electron microscopy analyses performed on the dried gel samples. As will be shown right away, we have demonstrated that this technique enables qualitative monitoring of the morphology differences among the various gels (e.g. agarose- based gels) as well as determinations of the various parameters that can illustrate these structural differences quantitatively. Most recently, we have included atomic force microscopy (AFM) in our toolbox for gel-structure analysis.

[XXXIX] Adamkova, K., Trudicova, M., Hrubanova, K., Sedlacek, P., and Krzyzanek, V. *An appropriate method for assessing hydrogel pore sizes by cryo-SEM*, 2019. Paper presented at the NANOCON 2018 – Conference Proceedings, 415-420.
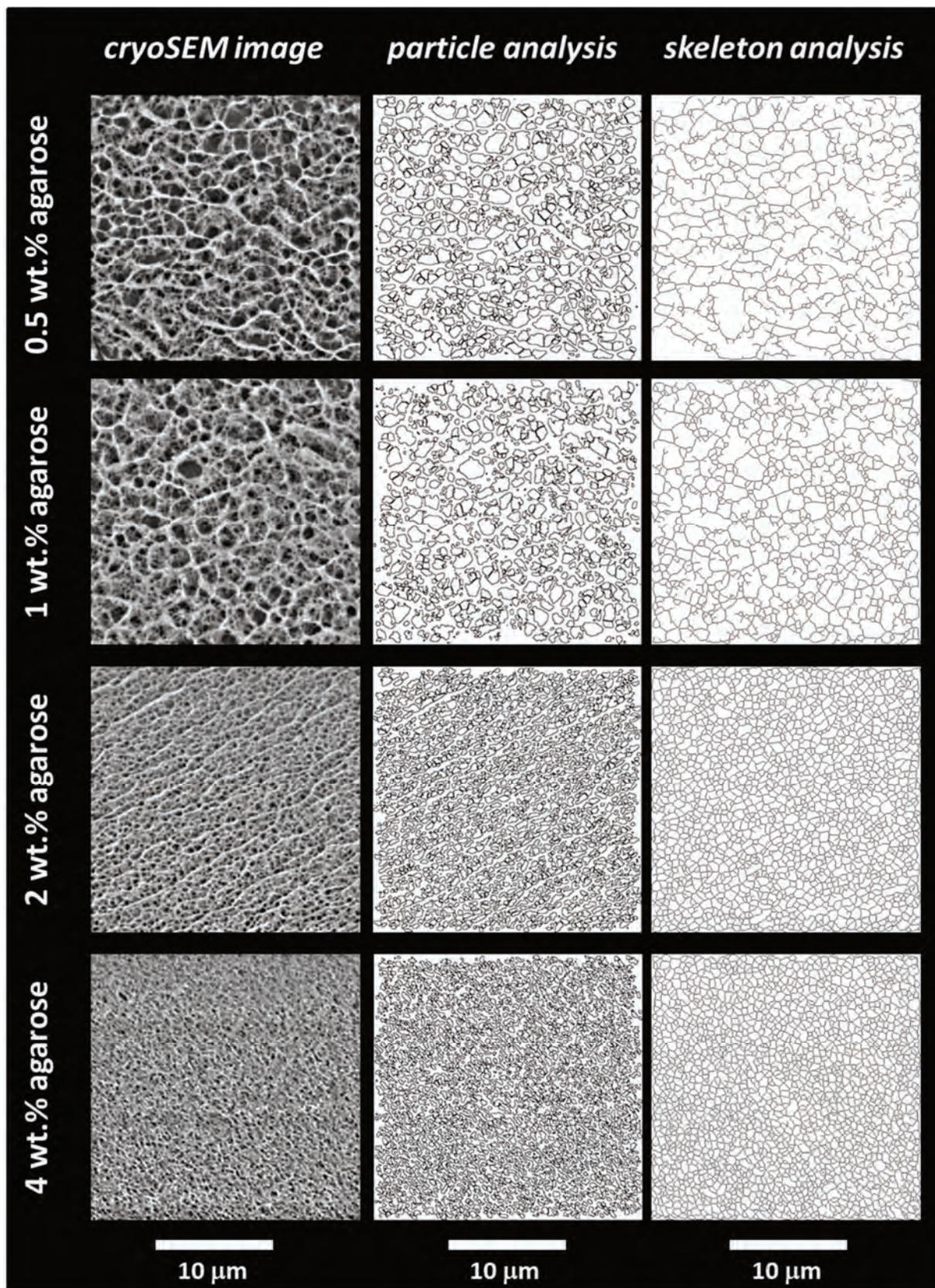
Fig. 80   Determination of pore size of the agarose hydrogels via analysis of cryoSEM images using two image processing tools implemented in ImageJ (Skeleton analysis and Particle analysis).

The great advantage of this technique is that it allows structural analysis of the swollen sample at ambient temperature and even under submersion with water (to prevent drying of the gel surface during the analysis). As can be seen in Fig. 79d, the preliminary results show good qualitative agreement between gel structure imaging by AFM and cryo-SEM. Further optimization of the AFM technique for various types of hydrogel samples is currently in progress.

As already mentioned, the micrographs obtained from the morphological assays of the studied gels provide not only the qualitative illustration of the internal gel structure but allow one also to determine some quantitative parameters that can be used for instance in comparing/correlating them with indirect structural (such as those determined by turbidimetry or rheology) or other material (material, transport) characteristics. For instance, Fig. 80 shows two ways of processing and analyzing the cryo-SEM images of agarose gels in the ImageJ software toolbox. First, Particle analysis tool (an automatic particle segmentation algorithm implemented in ImageJ) can be used to identify individual pores of the gel network (see the pore outlines in the second column in Fig. 80). As a numerical result of this analysis, every pore which is detected in the structure is described by its area and perimeter, the distribution of pore areas and perimeters is hence obtained and processed into statistical parameters, e.g. average or mean values. Another image processing technique, applicable in the morphological analysis of porous materials, is represented by Skeleton analysis. In this technique, the network structure displayed in the analyzed image is skeletonized, i.e. replaced by the line skeleton using a topology maintaining medial axis thinning algorithm (skeletonized representations of the analyzed images are shown in the third column in Figure 80). Using the Skeleton analysis tool, branches and junctions of such a skeleton are then classified, counted, and measured. As an example of a quantitative parameter, useful in the description of the porosity of the analyzed structure, average branch length is provided among the results of the Skeleton analysis.

A comparison of the quantitative results of the two image analysis approaches is shown in Fig. 81. For both methods, the average value of a linear parameter that represents the pore size is provided as a function of the concentration of agarose in the gel. In the case of Particle analysis, the average size of the pore was calculated from the average pore area (using the simplifying assumption of the circular cross-section of the pores); from the Skeleton analysis, the average branch length was used for the same purpose. It can be seen that the results of both methods are in good agreement and their trend with the agarose content in the gel corresponds well with those determined by the indirect structural assays (Fig. 78).

In this section, I have introduced the original methodological approach that we have involved in our fundamental research studies dealing with hydrogels. In the following one, I will demonstrate the specific benefits of this approach in the particular example of our investigation of semi-interpenetrated polymer network gels.
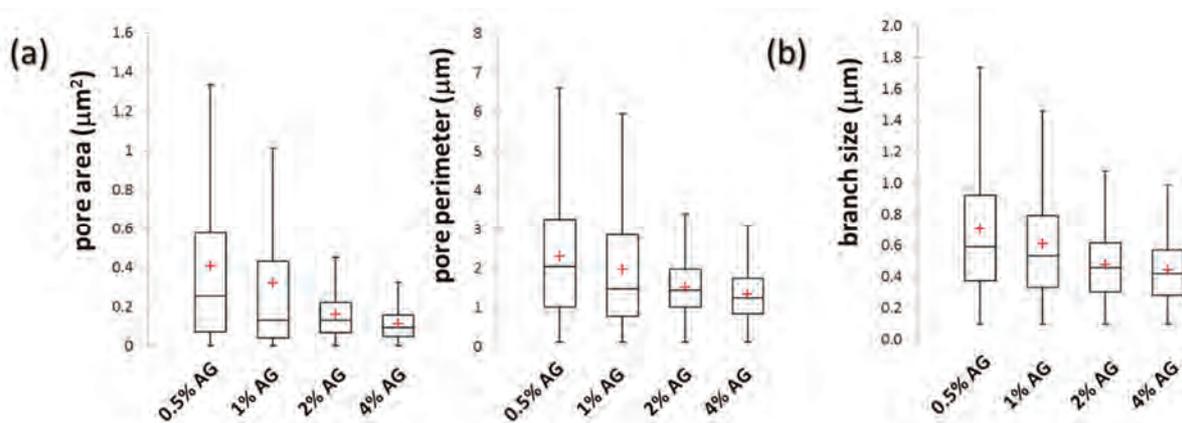
Fig. 81   Results of structural analysis of agarose gels provided by processing cryoSEM images using Particle analysis (a) and Skeleton analysis (b) in ImageJ.

7.2 Semi-Interpenetrating Polymer Networks: Controlling structure and interactions independently

In the introduction to chapter 7, I have discussed many beneficial properties that make hydrogel matrix so attractive for modern "bio" applications. Nevertheless, concerning the utilization of hydrogels in the specific field of controlled release systems, there are still some limitations and risks to be considered regarding the use of hydrogels. In this section, I will for now skip the limited ability of hydrogels to solubilize hydrophobic active solutes (which will be addressed in 7.3.2). Nevertheless, even when concerning hydrogels as carriers of hydrophilic substances (that are in general well compatible with the water-swollen hydrogel environment), there are some specific issues and demands of this application field that needs to be considered. Primarily, finding an appropriate balance between mechanical and solute-binding performance is crucial for providing the required release kinetics of a gel carrier. For example, the mechanical properties of the gel carrier must be capable of withstanding deformations associated with its application and delivery in the organism to prevent premature disintegration of the gel carrier and instantaneous release of the active substance. As far as the absorption and release of the active solute are concerned, the number of specific problems of the gel matrix increases further. Drug loading capacity, as a complex product of multiple influences (drug solubility in water, its partition between gel and solution, or its effect on the stability of the gel network junctions) is usually limited even in the case of hydrophilic active substances. Furthermore, the high water content and highly porous nature predetermine hydrogels for a rather rapid drug release on a time scale of hours to days, making them barely competing for the long-term release profiles of other delivery systems such as microspheres.

Until now, a range of strategies has been proposed to improve the partition of the active substance in the gel and to retard its release from the hydrogel carrier. These strategies usually aim at supporting the binding (either chemical or physical) between the drug and the polymer network. We have recently put forward an alternative strategy, which aims to address both critical issues of the hydrogel drug carriers – i.e. its mechanical and transport properties - independently of each other. The concept found its inspiration in our previous works on the solute-binding properties of humic substances, where we immobilized the dissolved humics in the supporting agarose gels (section 5.1.1). We have realized in this study, how specifically the relative contents of the inert gel-forming component (agarose) and the reactive substance (humic acids), contribute to the various aspects of the gel behavior.
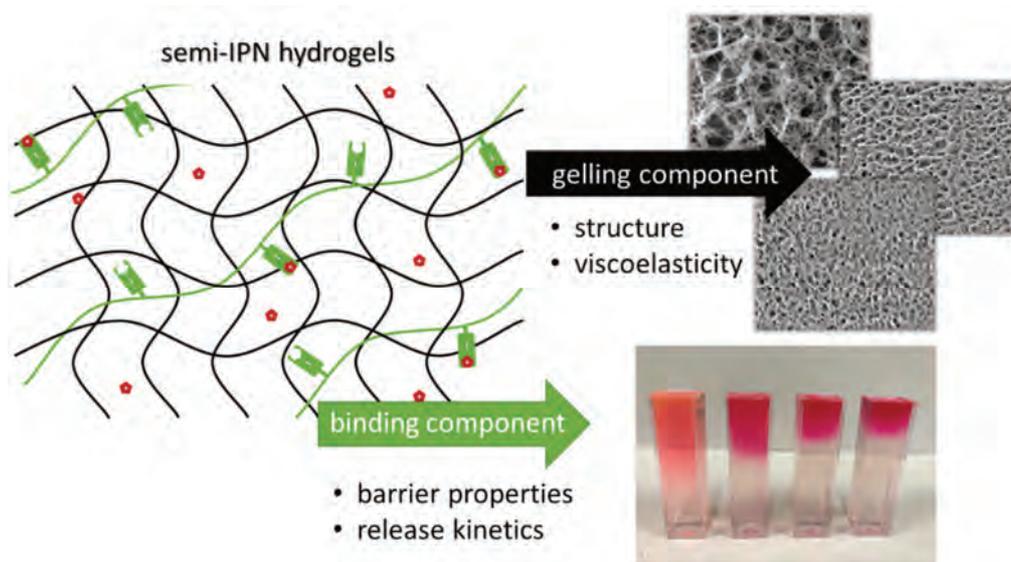
Fig. 82   Proposed strategy of tailoring performance and properties of semi-IPN hydrogels. An inert gel-forming polymer network is interpenetrated by a linear polymer component with the properly selected binding functionality. Mechanical and transport performance of the material is adjusted independently via manipulating the relative content of the two structural components.

The concept that we have proposed (it is represented schematically in Fig. 82) is based on semi-interpenetrating polymer networks (semi-IPNs) which, together with the interpenetrating polymer networks (IPNs) represent a novel and especially promising class of polymer blends. IPNs are defined by the International Union of Pure and Applied Chemistry (IUPAC) as "A polymer comprising two or more networks which are at least partially interlaced on a molecular scale but not covalently bonded to each other and cannot be separated unless chemical bonds are broken." [204]. Semi-IPNs differ from IPNs in the fact that the chains of the second polymer are dispersed in the network formed by the first polymer without forming a separate network. We have suggested that semi-IPN hydrogels may be easily designed to provide independent control and adjustment of gel ultrastructure and all the associated properties (e.g. viscoelasticity) on the one side, and the binding ability and consequent barrier/release performance on the other. For this purpose, the semi-IPN hydrogels comprise in its dual network a "structure–ruling" gel-forming component which is interpenetrated by a "binding" polymer chains. The gel-forming component is physico-chemically inert – i.e. possesses a negligible binding affinity to the active substance. Its main task is to ensure a reproducible and controllable gelation process, providing gel architecture with adjustable parameters such as cross-linking density and average pore size, without interfering significantly with the kinetics of absorption and/or release of the active substance. On the other hand, the "binding" component, because of its significantly lower relative content, does not affect the internal morphology of the gel, but significantly improves its binding properties. Such a system hence offers an independent dual-tuning of mechanical and transport performance via manipulating the relative content of the two structural components.

We have performed a systematic case study of the proposed strategy on agarose-based semi-IPN gels. We have tested the incorporation of various interpenetrating components (poly-(styrenesulfonate) (PSS), alginate (ALG), hyaluronic acid, chitosan, quaternized dextran, etc.) in the supporting agarose matrix, and investigated the transport properties of diverse model solutes (cationic or anionic organic molecules) in the resulting semi-IPN hydrogels. To analyze all aspects of the material behavior of the gels, we applied the original multiscale analytical approach introduced in the previous section. The most important results were summarized in the comprehensive publication[XL]. The conclusions of this study strongly supported the validity of the proposed concept. In particular, it was found that the viscoelastic behavior of the gels (represented e.g. by the value of complex modulus) can be adjusted in a wide range by the gelling component (agarose) with the negligible effect of the interpenetrating component (results shown for PSS and ALG). On the other hand, the content of PSS as low as 0.01 wt.% of the gel (it means about 100× lower compared to agarose) resulted in a more than the 10-fold decrease of diffusivity in model-charged organic solute (Rhodamine 6G).

The pilot study summarized in the publication[XL], confirmed the great application potential of the proposed concept in the development of controlled-release hydrogel systems. Furthermore, it also demonstrated that the original analytical approach designed by us and applied in this study can be used as a valuable methodological framework providing complex insights into the composition–structure–performance relationships in hydrogel materials. Another indisputable advantage of the proposed concept is that it imposes no special requirements on the gelation procedure – various common gelling polymers can apparently be used as a gel-forming component. To make sure of this, we have recently performed some follow-up studies, where we confirmed the applicability of the concept on the poly(vinylalcohol) (PVA) gels (see Fig. 83), and most recently also on the poly(hydroxyethyl methacrylate) (PHEMA) gels[XLI].

[XL] Trudicova, M., Smilek, J., Kalina, M., Smilkova, M., Adamkova, K., Hrubanova, K., Krzyzanek, V., and Sedlacek, P. Multiscale Experimental Evaluation of Agarose-Based Semi-Interpenetrating Polymer Network Hydrogels as Materials with Tunable Rheological and Transport Performance. *Polymers.* 2020, 12, 2561. Attached as Appendix 23.

[XLI] Trudicova, M., Papezikova, H., Sedlacek, P., and Pekar, M. *Tailoring the internal microstructure of the hydrogels based on poly-HEMA targeted for drug delivery systems*, 2021. Paper presented at the NANOCON 2021 – Conference Proceedings, 280-285.
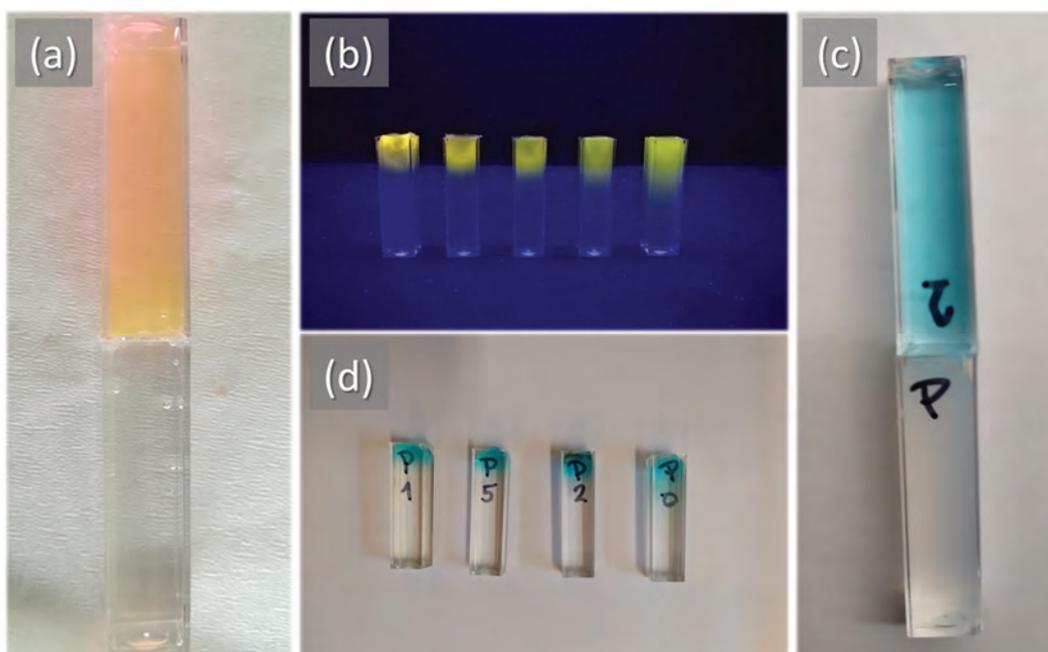
Fig. 83 PVA-based semi-IPN hydrogels with tailored structure and binding properties. Interpenetration of PSS into chemically (with borax, (a, b)) and physically (by cyclic freezing-thawing, (c,d)) cross-linked PVA gels alters the rate of diffusion of Rhodamine 6G (a, b) and Methylene blue (c,d) as determined by the diffusion-couple experiment (a,c). In (b) and (d), the relative weight content of PSS in the PVA gels decrease from left to right as follows: 0.1 wt.% (only in (b)), 0,01 wt.%, 0,005 wt.%, 0,002 wt.% and 0 wt.%.

7.3   Hydrogels: Multipurpose materials with versatile applications

As emphasized repeatedly throughout this text, in all my research interests I have always tried to combine the quest for fundamental knowledge with the rational transfer of the gained knowledge as close to real applications as possible. This is doubly true for the hydrogels, that intertwine throughout my scientific career, across actually all the research projects I have been involved in. In the previous section, I have demonstrated how we utilized the experience gained during the development of the diffusion-in-gel methodology for the reactivity mapping studies on natural compounds in the design of novel hydrogel materials for drug delivery. In this chapter, I will follow with a brief introduction of other types of hydrogel materials, that we designed and investigated according to the specific requirements of various applications.

7.3.1   Novel multi-purpose hydrosorbents for agricultural uses

In 5.1.5, I have already described some types of hydrogel forms of humic acids (HA) that we have proposed for use in agriculture and health-care. I have intentionally left apart from one specific type of gels that we have paid special attention to – HA-containing superabsorbent composite hydrogels. These are novel multifunctional materials that we have suggested for agricultural and environmental applications. These hydrogels are based on conventional superabsorbent polymers (SAPs) – polyelectrolyte networks formed of chemically cross-linked polyacrylate or poly(acrylate-*co*-acrylamide) – that are, because of their exceptional water absorption and retention capacity, currently utilized in sanitary and hygiene supplies, but increasingly also in agriculture, where they are used primarily to enhance water retention capacity of low-quality soils. We have adapted the conventional polymerization procedure to incorporate into the structure of these SAPs also the humic component (commercial lignohumate) and inorganic nutrient component (NPK inorganic fertilizer). The final materials hence provide not only the great water swelling capacity (see Fig. 84), but also
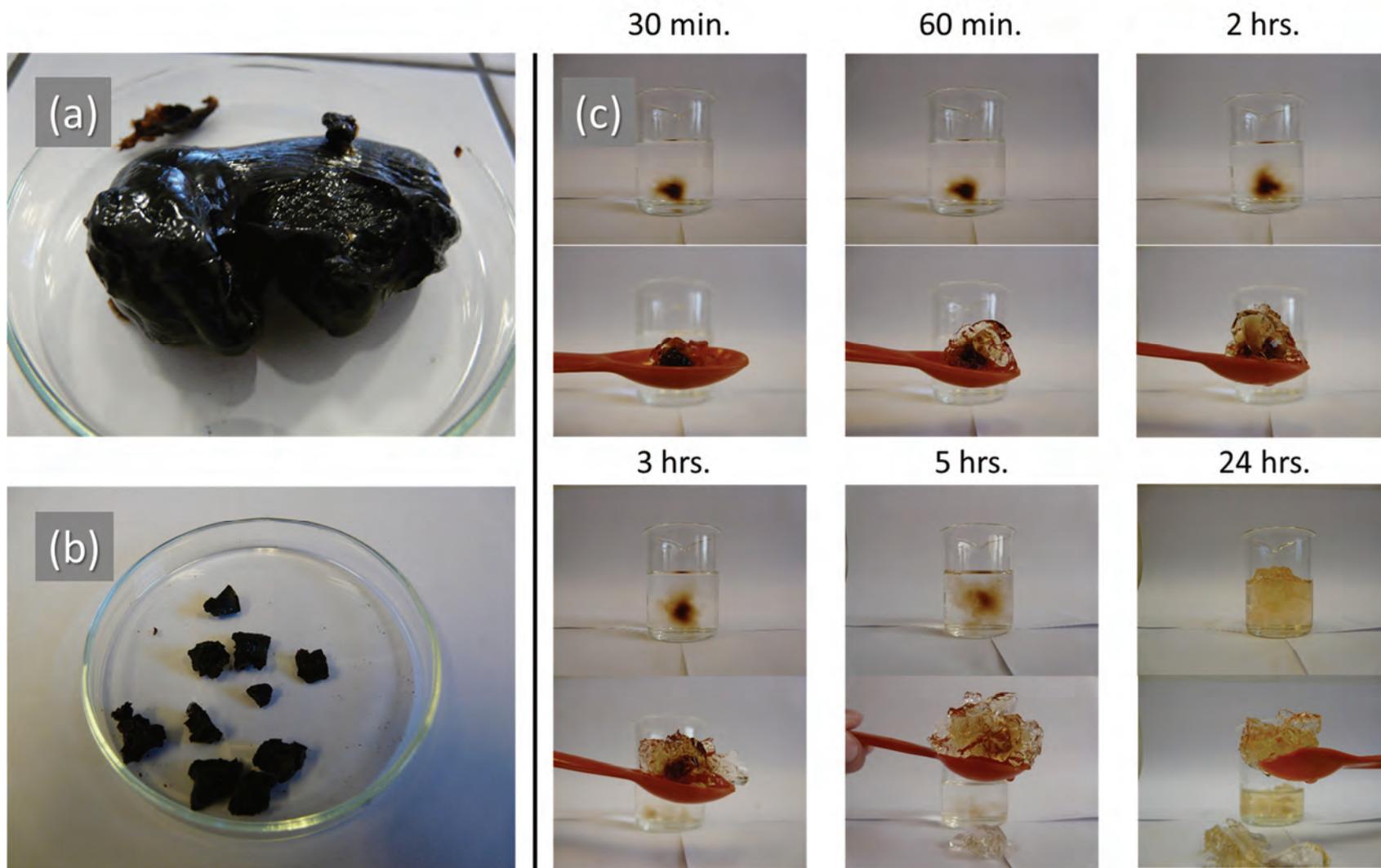
Fig. 84   Superabsorbent polymer (SAP) material based on polyacrylate chains grafted on humic substances. Polymerized SAP as-prepared (a) and in the dried form (b). Monitoring the swelling of the SAP in deionized water (c).

the capability of controlled release of the plant growth-promoting humic component as well as the inorganic nutrients.

We have tested various combinations of SAP composition (with/without acrylamide), and contents of Lignohumate and NPK, respectively. Potassium peroxydisulfate was used as the initiator and N,N–methylenebisacrylamide as the crossing agent during the SAP preparation. We have performed a comprehensive study on how the composition of the material affects its structure in the dry form, swelling behavior in various aqueous environments, and mechanical properties in the swollen form (i.e. viscoelasticity of the formed hydrogel). Furthermore, to support their suggested application as novel controlled-release fertilizers, we have tested also the release of the active components as well as the biological activity of the gels (influence of the addition of SAPs on corn growth was studied in pot experiments). Among others, we have confirmed experimentally that the swelling of the SAPs was fast (completed always in 24 hours) and the final water absorbency of all samples was in the range 100 – 300 g/g, whereby the presence of Lignohumate had a positive effect on the swelling, contrarily to NPK that reduced the water absorbency. As expected the swelling ratio of the gel was conversely proportional to the strength and rigidity of the swollen gels. Similarly, the swelling also influenced the release of nutrients from superabsorbents. The release of mineral nutrients was ruled primarily by their contents in different samples. Although the presence of Lignohumate had a negligible influence on the release of P and N, it increased the amount of released K. On the other hand, the release of the humic component was partially suppressed by the higher content of NPK. We have also evidence that the application of composite SAPs supported water retention of soils and the growth of corn. Better water management and a gradual supply of nutrients enhanced both height of plants and the length of roots. The most important results of this study were published[XLII].

Obviously, the developed composite hydrogel materials represent the state-of-the-art controlled release systems for modern sustainable agriculture. It combines multiple functions – water management in soils, the release of the bio-stimulating humic component as well as inorganic nutrient elements, whose kinetics can be tailored by the composition of the material. We suggest the use of these materials mainly in problematic areas with dry soils and low levels of organic matter and nutrient elements.

7.3.2   Hydrogels based on electrostatically cross-linked polyelectrolytes

In our research group focused on the investigation of biocolloids, a great deal of work has been concentrated on (bio)polyelectrolytes. I have already discussed how we utilized the binding potential of polyions in our concept of hybrid semi-IPN gels. Obviously, the tendency to undergo electrostatic attraction with oppositely charged compounds can be employed also within the development of strategies for gelation of these polymers. Consequently, the polyelectrolyte complexes (PECs) – i.e. the associates formed by electrostatic interaction between oppositely charged macromolecules – became a hot topic in the production of modern soft-matter preparation for various applications [205–207]. As far as the strength and density of linkages between the constituent polymers are ruled by the dissociation of their functional groups, the formation, and properties of PECs can be easily manipulated by parameters such as pH or ionic strength. This variability in quality and quantity of cross-linking is especially attractive in the development of hydrogels with adjustable application-relevant properties.

I have already described in 5.1.5 the PEC hydrogels based on the combination of humic acids and chitosan that we investigated regarding their potential agricultural and/or environmental uses. Apart from that, I participated also in another project that was focused on the different types of PEC-based hydrogels intended for use in drug-delivery systems. The original idea of these materials was first published by Venerová and Pekař [208] and is based on a combination of polyelectrolyte and

oppositely charged surfactant in micellar form (see Fig. 85b). Main benefit of this gelation strategy lies in the involvement of hydrophobic nanodomains in the inherently hydrophilic structure of hydrogels. This breaks one of the greatest barriers regarding the use of hydrogels in drug delivery – it expands the range of active compounds that can be solubilized in the gel structure from strictly polar and water-soluble also to non-polar and hydrophobic ones. The project hence focused on the preparation of hydrogels from various combinations of polyelectrolytes (cationized DEAE dextran, anionic hyaluronan), surfactants (anionic sodium dodecyl sulfate (SDS) and sodium tetradecyl sulfate (STS), cationic Septonex and Cetyltrimethylammonium bromide (CTAB)) and comprehensive characterization of the gel materials including their composition, morphology, rheology, and of course their solubilization and release performance. I have joined this project mainly to provide methodological support for the investigation of the type and extent the hydration that occurs in the structure of these gels.
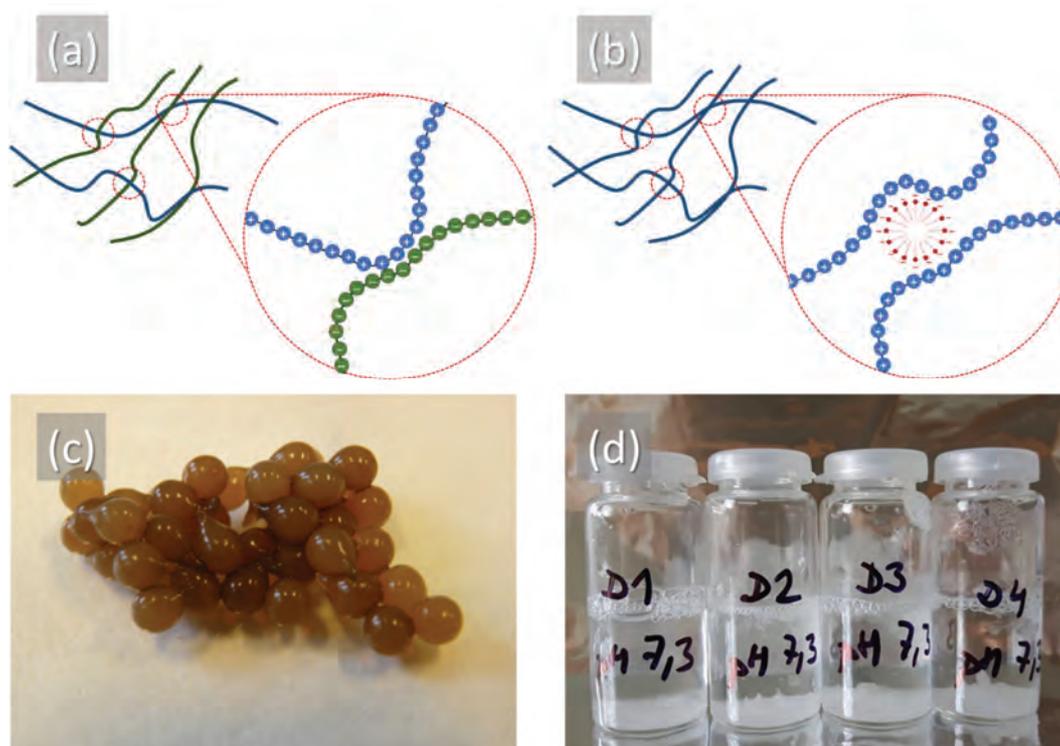
Fig. 85   Schematic   representation   of   the   electrostatically   cross-linked   hydrogels   under investigation: a) *Polyelectrolyte complexes. b*) *Surfactant-polyelectrolyte hydrogels. Examples of the developed hydrogels: c*) *Humic acids complexed with chitosan. d*) *DEAE-SDS hydrogels.*

For this purpose, we have designed and optimized a method based on the combination of ATR-FTIR spectroscopy and thermogravimetry. This combination proved valuable both for the qualitative (FTIR) and quantitative (TGA) description of the drying process. Using the time-resolved FTIR spectroscopy, details on the structural changes, underwent by water in the gel structure during the drying process, can be derived particularly from the broadband located around 3350 cm^{-1} that corresponds to the O–H stretching of water molecules. Based on the time dependence of the absorbance signal in this spectral region, we have observed that drying of the polyelectrolyte-surfactant gels is not a continuous process but it rather proceeds in several distinct steps. For a deeper structural analysis of the nature of these drying steps, we performed deconvolution of the broad stretching band and identified several subpopulations of water molecules that correspond to water with different types and strengths of hydrogen bonding. The quantitative analysis provided by (isothermal) TGA utilized the experience we gained when using this method for the determination of different forms of water in samples of bacterial cells (6.1.3). Changes in drying rate were hence monitored as the function of residual water content to determine the contents of water with different strengths of binding in the gel structure. We

have published the results of the study where we applied this methodology on four different hydrogels prepared from cationized dextran and two anionic surfactants[XLIII]. We have revealed significant differences between the dehydration processes among the analyzed gels, in particular, water molecules in the hydrogels containing a higher concentration of surfactants demonstrated a more ordered hydrogen network. We have hence demonstrated in this study that the proposed experimental approach represents another valuable contribution to the methodology that we have developed for the complex analysis of hydrogels (7.1).

Recently, I have followed the concept of polyelectrolyte-surfactant hydrogels with a preliminary study focused on the possibility of replacing synthetic tensides with biosurfactants. These are the compounds of microbial origin that are biosynthesized mainly to provide the capability of emulsifying hydrophobic molecules and increase their availability for microbial utilization. In the concept of PEC hydrogels, the main advantage of their employment would be found in improving the ecotoxicology of the material, and in the enhancement of its biocompatibility and biodegradability. Preliminary results of this pilot study support the hypothesis that the electrostatic gelation of polyelectrolytes may be provided also by the biosurfactants. In Fig. 86, the example of hydrogel materials prepared via gelation of chitosan by addition of rhamnolipids. It can be seen that the primary requirement on the gels – i.e. the combined solubilizing capacity for polar and non-polar active ingredients – was successfully fulfilled. This pilot study hence opened the door for further research and development in the area of polyelectrolyte-surfactant hydrogels. I have found this topic especially attractive not only because it, once again, interlinked two areas of my scientific interest, i.e. hydrogel research and microbial biotechnology. Apart from that, I believe that the incorporation of surfactants of natural origin could significantly enhance the relevance of this type of PEC hydrogel materials regarding their use in drug delivery and other fields of cosmetics and healthcare applications.
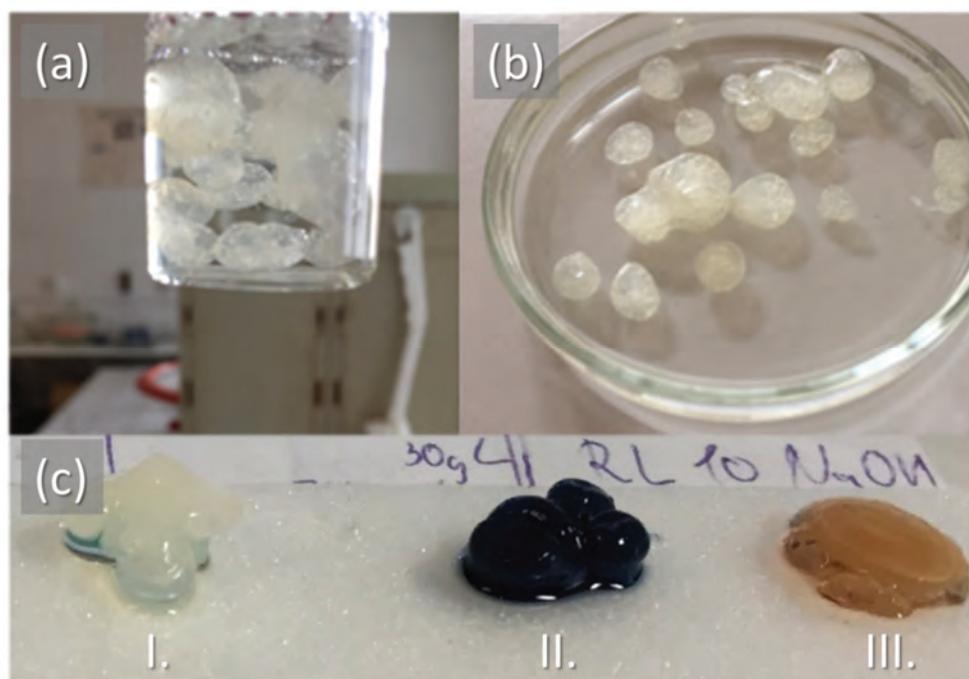
Fig. 86   Hydrogels prepared via cross-linking of chitosan by rhamnolipids. (a,b) Hydrogel beads are prepared by dropwise addition of acidic chitosan into the aqueous solution of rhamnolipids. (c) The ability of the chitosan-rhamnolipid gels (I.) to solubilize hydrophobic compounds as demonstrated for non-polar dyes Sudan black (II.) and Sudan red (III.).

[XLIII] Enev, V., Sedláček, P., Jarábková, S., Velcer, T., and Pekař, M. ATR-FTIR spectroscopy and thermogravimetry characterization of water in polyelectrolyte-surfactant hydrogels. *Colloids and Surfaces A: Physicochemical and Engineering Aspects.* 2019, 575, 1–9. Attached as Appendix 25.

7.3.3   Encapsulation of microbes in hydrogels

As it is quite obvious from the previous text, the wide range of topics to which I found the concept of biophysical chemistry useful and contributive, took me to various, apparently distinct, areas of research interest. Nevertheless, recently I found one special topic where the distinct routes of my previous scientific career began to reconnect. It is the topic of the research and development of bio-inoculants – the carriers of microbial cells intended for agricultural and environmental uses.

As emphasized already in Chapter 3, improving the quality of arable soils represents nowadays one of the most urgent needs among all research fields covered by life-sciences. In this text, I have already paid great attention to the quality of soils regarding their chemistry – i.e. from the point of view concerning the quality and content of humus there. Nevertheless, the same emphasis should be put also on soil biology, or more specifically, microbiology. Currently, the development of biological agents based on plant growth-promoting (rhizo)bacteria (PGPR) for the restoration of soil fertility represents a hot topic in modern agricultural technologies. In general, PGPR affects plants or crops directly (biofertilization, rhizoremediation, stimulation of root growth, and plant stress control) or indirectly by reducing the impact of diseases. The mechanisms of plant growth-promoting effects of PGBR are summarized in Fig. 87 and described in detail elsewhere [209–211].

Generally, the primary role of the formulation of an inoculant is to form a stable micro-environment that provides the microbial strain(s) with physical and/or chemical protection over a prolonged period, in order to avoid a rapid decrease of the cells' viability during storage and after being introduced into the soil [212]. The bioinoculant formulation design is hence aimed at providing a reliable source of living cells available to interact with plants and soil microbiome. Especially the liquid formulations often fail in this requirement because of their short shelf-life (2-3 months) and insufficient protection of the microbial cells after introduction to the soils. A longer shelf-life is provided by solid bio-inoculants. Nevertheless, the state-of-the-art formulations in the bioinoculants' production with respect to the effectiveness of cell entrapment and protection and the reproducibility of the preparation process are represented by the formulations based on the hydrogel carriers. Encapsulation of PGPR cells in hydrogels formed from cross-linked polysaccharides such as alginate and carrageenan has been proposed a long time ago as a technique to ensure the controlled release of plant beneficial microorganisms into the soil [213]. In general, the gel matrix assures mainly physical protection of the cells against various environmental stress factors, nevertheless, there are also strong shreds of evidence that polysaccharides play an important specific role in the mechanisms of abiotic stress protection of microorganisms [214]. However, as far as the agro-industrial technologies have the principal requirement of low cost, the task to find the appropriate technologically feasible and economically competitive PGPR encapsulation technique is still challenging [215].

Currently, the vast majority of hydrogel inoculant formulations use alginate as the gel-forming polymer. Alginate represents the family of linear polyanionic polysaccharides made up of L-glucuronic acid (G) and D-mannuronic acid (M). Alginate possesses numerous properties that make it the candidate-of-choice for the production of various gel carriers and controlled release systems: it is non-toxic, biocompatible, non-immunogenic, biodegradable, mucoadhesive, readily available, and has a relatively low cost. Ionic gelation is the most common method used to obtain alginate-based gels. In this process, alginate is cross-linked in aqueous solutions via chelating the Ca^{2+} (or other multivalent cation) by pendant carboxylic acid moieties of G units, generating 3D hydrogel networks that allow entrapment of other components dispersed in the aqueous solution (such as cells, dissolved bioactive compounds etc.). Currently, alginate is usually extracted from brown seaweeds, however, since only a few of the many species of brown algae are suitable and are limited in abundance and location for commercial alginate production, there is at present interest in the bacterial production of alginate-like polymers. Bacterial producers also provide alginate of defined monomer composition to gain determined properties instead of alginate isolated from seaweed, which in general suffers from heterogeneity in composition and quality [216].
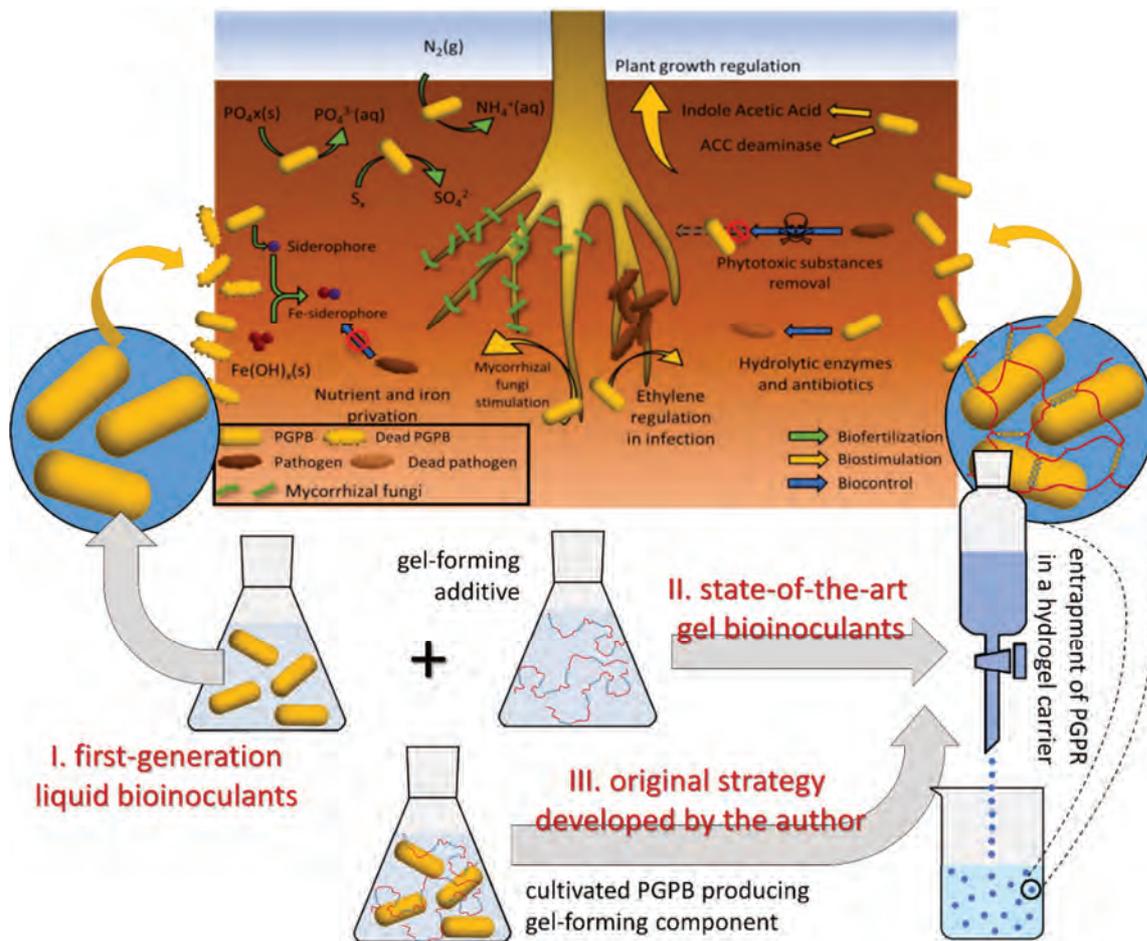
Fig. 87   Schematic representation of the recent trends in the development of bioinoculants (from the 1st gen. liquid formulations to the state-of-the-art hydrogel carriers) together with the original strategy proposed and tested in the project (overview of the positive effects of PGPB on plants was adopted from Ferreira et al. [209].

We have recently proposed a novel strategy for the preparation of PGPR-based biofertilizers. It is based on the entrapment of the bacterial cells in the hydrogel formed from alginate, which is produced directly by the PGPR bacteria (the concept is schematically described in Fig. 87). For this purpose, we have employed PGPR which belongs to the genus *Azotobacter*. The members of this genus are gram-negative nitrogen-fixing non-pathogenic bacteria. Probably the best-studied representative, *Azotobacter vinelandii*, is known to produce numerous low-molecular compounds providing stimulating effects on plants, such as indolacetic acid, gibberellins and cytokinins. Even more, interestingly, *A. vinelandii* has been recognized as an efficient producer both of extracellular alginate and intracellular PHA. It was exactly this combination of alginate and PHA production capability that attracted our attention. While the alginate biosynthesis induced a possibility to overcome one of the crucial technological and economic demands of the conventional gel inoculant production – i.e. the necessity to add an external gel-forming component, PHA accumulation carried a promise of enhanced stress robustness of the bacterial cells (as discussed thoroughly in 6.2), and, consequently, improved survival of the cells when applied in form of a bio-inoculant to a soil. Surprisingly, the combination of plant-growth-promoting effects and high production yields of alginate provided by the single bacterium has not attracted yet any attention in the design of bio-inoculants although it offers a significant simplification and streamlining of the process of their preparation. The fact that the gel-forming biopolymer is produced by plant-growth-promoting bacteria themselves is a crucial distinguishing sign and the most innovative feature of the proposed strategy that gives a great potential to simplify the preparation procedure and reduce the costs of the intended PGPR application.

136
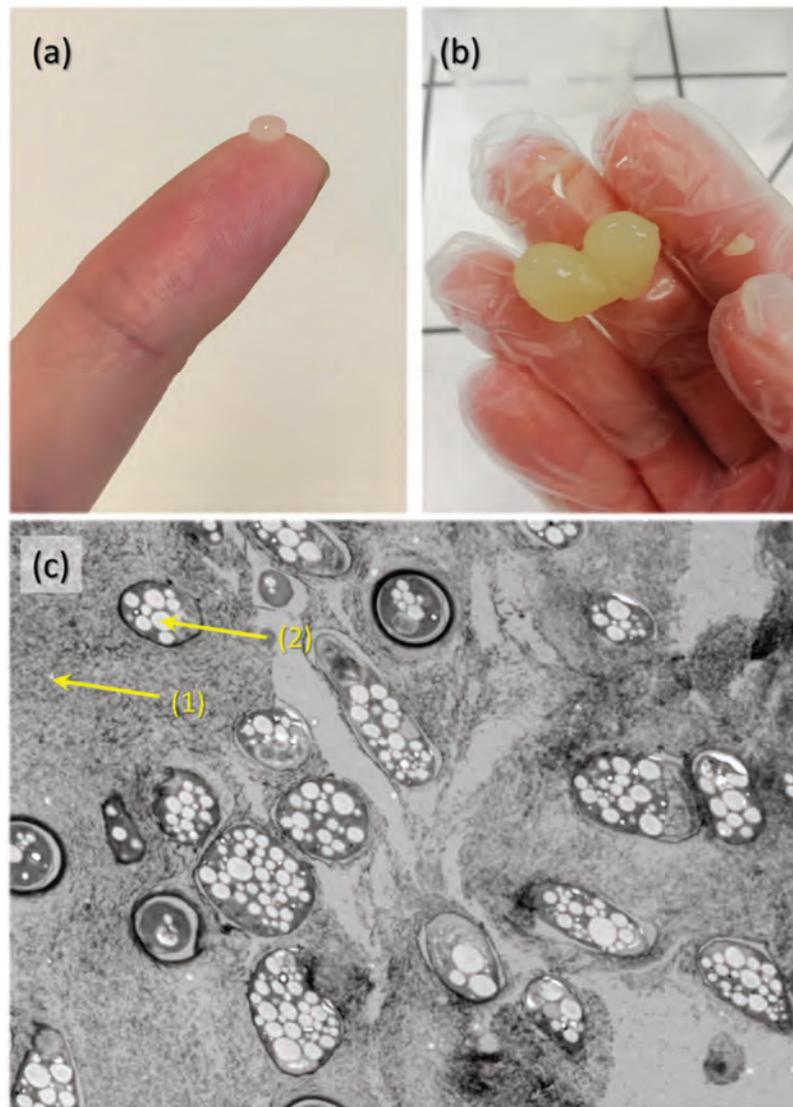
Fig. 88   PGPR containing hydrogel bio-inoculants prepared by the original self-entrapment strategy. (a) Hydrogel bead prepared by dropping PGPR culture into Ca^{2+} solution. (b) Hydrogel prepared by in-situ ionotropic gelation induced by the evolvement of Ca^{2+} ions from insoluble form ($CaCO_3$) directly in the cultivation medium. (c) TEM image of the hydrogel showing the alginate matrix (1) and the entrapped cells with high content of PHA granules (2).

In the preliminary experiments, we have already proved the validity of the proposed strategy. As can be seen in Fig. 88, we are now capable of preparing PGPR cultures, that can be easily transferred to hydrogel form simply by the addition of calcium ions. We have also successfully induced in-situ ionotropic gelation in the cultivation medium via spontaneous evolvement of the calcium ions from an originally insoluble form. Currently, we are performing an in-depth optimization study on all the essential steps involved in the proposed technological process. The optimization of the cultivation properties has already provided a functional balance between the yield and quality of alginate and accumulated PHA content. Now we are focusing on optimization of the subsequent steps of the bio-inoculant production process – gelation and drying as well as a pilot evaluation of the biological activity of prepared bio-inoculants. Hereby, we wish to collect essential fundamental knowledge on the causal relationship between preparation procedure, structure and crucial properties of the hydrogel-entrapped bio-inoculants based on this original strategy. Furthermore, based on our experience with the bio-stimulating effects of humic substances, we also intend to incorporate these compounds as an additional component of the developed hydrogel bio-inoculant preparations.

References

[180] Buwalda, S. J. et al. *Journal of Controlled Release*, 2014, 190, 254–273.

[181] Ullah, F. et al. *Materials Science and Engineering: C*, 2015, 57, 414–433.

[182] Caló, E. et al. *European Polymer Journal*, 2015, 65, 252–267.

[183] Hoffman, A. S. *Advanced Drug Delivery Reviews*, 2012, 64, 18–23.

[184] Ido, N. et al. *Soft Matter*, 2020, 16, 6180–6190.

[185] Ajdary, R. et al. *Advanced Materials*, 2021, 33, 2001085.

[186] Zhu, J. et al. *Journal of the Mechanical Behavior of Biomedical Materials*, 2012, 6, 63–73.

[187] Bashir, S. et al. *Polymers*, 2020, 12, 2702.

[188] Shibayama, M. *Soft Matter*, 2012, 8, 8030.

[189] Shackelford, C. D. et al. *Engineering Geology*, 2013, 152, 133–147.

[190] Glauber, J. R. *Furni novi philosophici*. Amsterdam, J. Janssonius: 1658.

[191] Cartwright, J. H. E. et al. *Journal of Colloid and Interface Science*, 2002, 256, 351–359.

[192] Glaab, F. et al. *Angewandte Chemie International Edition*, 2012, 51, 4317–4321.

[193] Kopinsky, J. et al. *AIChE Journal*, 1988, 34, 2005–2010.

[194] Nicholson, C. et al. *Biophysical Journal*, 1993, 65, 2277–2290.

[195] Nicholson, C. et al. *The Journal of Physiology*, 1981, 321, 225–257.

[196] Barrangou, L. M. et al. *Food Hydrocolloids*, 2006, 20, 184–195.

[197] Barrangou, L. M. et al. *Food Hydrocolloids*, 2006, 20, 196–203.

[198] Suárez-Iglesias, O. et al. *Journal of Chemical & Engineering Data*, 2015, 60, 2757–2817.

[199] Mansel, B. W. et al. A Practical Review of Microrheological Techniques. *In Rheology – New Concepts, Applications and Methods*; InTech, 2013, pp. 1–21.

[200] Aymard, P. et al. *Biopolymers*, 2001, 59, 131–144.

[201] Lapasin, R. et al. *Rheology of Industrial Polysaccharides:Theory and Applications*. Springer: 1995.

[202] Pescosolido, L. et al. *Soft Matter*, 2012, 8, 7708.

[203] Adams, D. *Gels*, 2018, 4, 32.

[204] Jenkins, A. D. et al. *Pure and Applied Chemistry*, 1996, 68, 2287–2311.

[205] Lankalapalli, S. et al. *Indian Journal of Pharmaceutical Sciences*, 2009, 71, 481.

[206] Buriuli, M. et al. Polyelectrolyte Complexes (PECs) for Biomedical Applications. *In Advances in Biomaterials for Biomedical Applications*; Springer Singapore, 2017; pp. 45–93.

[207] Meka, V. S. et al. *Drug Discovery Today*, 2017, 22, 1697–1706.

[208] Venerová, T. et al. *Carbohydrate Polymers*, 2017, 170, 176–181.

[209] Ferreira, C. M. H. et al. *Science of The Total Environment*, 2019, 682, 779–799.

[210] Chaudhary, T. et al. *3 Biotech*, 2020, 10, 199.

[211] Tallapragada, P. et al. Application of bioinoculants for sustainable agriculture. *In Probiotics and Plant Health*; Springer Singapore, 2017; pp. 473–495.

[212] Mishra, J. et al. Bioformulations for Plant Growth Promotion and Combating Phytopathogens: A Sustainable Approach. *In Bioformulations: For Sustainable Agriculture*; 2016; pp. 3–33.

[213] Vassilev, N. et al. *Frontiers in Plant Science*, 2020, 11, 270.

[214] Vassilev, N. et al. *Applied Microbiology and Biotechnology*, 2012, 95, 851–859.

[215] Arora, N. K. et al. Plant Growth Promoting Rhizobacteria: Constraints in Bioformulation, Commercialization, and Future Strategies. Springer, Berlin, Heidelberg, 2010; pp. 97–116.

[216] Hay, I. D. et al. *Microbial Biotechnology*, 2013, 6, 637–650.

Afterword

The main aim of this habilitation thesis was to introduce biophysical chemistry as the modern interdisciplinary scientific discipline that can offer fresh, unconventional conceptual perspectives on – but also powerful methodological apparatus for – answering miscellaneous research questions from the field of life sciences. Apart from the brief summarization of some historical moments that, in my opinion, helped to form the current state of the discipline, and besides emphasizing some crucial challenges that it nowadays faces, I tried to illustrate how a wide range of research interests can be covered under the wings of this discipline in a single scientific curriculum. I leave it up to the reader to assess how well the goal has been achieved by this text.

A friend of mine told me that, when working on his habilitation, he was feeling like writing memoirs. I was experiencing a kind of similar feeling when writing this thesis. Nevertheless, together with all the memories, even a stronger feeling came to my mind - gratitude. Gratitude to all who have helped me throughout my previous scientific career. My scientific supervisors, bosses, colleagues, and – last but not least – students. They all played an irreplaceable role in providing me with their experiences, knowledge, open-mindedness, inspiration, diligence, and enthusiasm. And, of course, my family, who showed boundless tolerance when scarifying the time spend with me for letting me do what I love. In spite of my name on the cover, this thesis is a collective work of all of these people.

List of the self-cited references

[I]   Sedláček, P. and Klučáková, M. Diffusion experiments as a new approach to the evaluation of copper transport in humics-containing systems. *Collection of Czechoslovak Chemical Communications.* 2009, 74, 1323–1340. Attached as Appendix 1.

[II]   Sedláček, P. and Klučáková, M. Simple diffusion method applied in evaluation of metal transport in model humic matrices. *Geoderma.* 2009, 153, 11–17. Attached as Appendix 2.

[III]   Kalina, M., Klučáková, M., and Sedláček, P. Utilization of fractional extraction for characterization of the interactions between humic acids and metals. *Geoderma.* 2013, 207-208, 92–98. Attached as Appendix 3.

[IV]   Sedláček, P., Smilek, J., and Klučáková, M. How the interactions with humic acids affect the mobility of ionic dyes in hydrogels – Results from diffusion cells. *Reactive and Functional Polymers.* 2013, 73, 1500–1509. Attached as Appendix 4.

[V]   Sedláček, P., Smilek, J., and Klučáková, M. How the interactions with humic acids affect the mobility of ionic dyes in hydrogels – 2. Non-stationary diffusion experiments. *Reactive and Functional Polymers.* 2014, 75, 41–50. Attached as Appendix 5.

[VI]   Rybárik, J., Sedláček, P., and Klučáková, M. Transport of Organic Dyes in Systems Containing Humic Acids. *Inżynieria Mineralna.* 2019, 21.

[VII]   Klučáková, M., Kalina, M., Sedláček, P., and Grasset, L. Reactivity and transport mapping of Cu(II) ions in humic hydrogels. *Journal of Soils and Sediments.* 2014, 14, 368–376. Attached as Appendix 6.

[VIII] Smilek, J., Sedláček, P., Kalina, M., and Klučáková, M. On the role of humic acids' carboxyl groups in the binding of charged organic compounds. *Chemosphere.* 2015, 138, 503–510. Attached as Appendix 7.

[IX]   Smilek, J., Sedlacek, P., Lastuvkova, M., Kalina, M., and Klucakova, M. Transport of Organic Compounds Through Porous Systems Containing Humic Acids. *Bulletin of Environmental Contamination and Toxicology.* 2017, 98, 373–377.

[X]   Enev, V., Sedláček, P., Kubíková, L., Sovová, Š., Doskočil, L., Klučáková, M., and Pekař, M. Polarity-Based Sequential Extraction as a Simple Tool to Reveal the Structural Complexity of Humic Acids. *Agronomy.* 2021, 11, 587. Attached as Appendix 8.

[XI]   Smilkova, M., Smilek, J., Kalina, M., Klucakova, M., Pekar, M., and Sedlacek, P. A simple technique for assessing the cuticular diffusion of humic acid biostimulants. *Plant Methods.* 2019, 15, 83. Attached as Appendix 9.

[XII]   Klučáková, M.; Sedláček, P.; and Ondruch, P. Preparation and characterization of new application forms of humic acids. *In Recent Research Developments in Materials Science*; Research Signpost: Kerala, 2009; pp. 59–80.

[XIII] Obruca, S., Sedlacek, P., Slaninova, E., Fritz, I., Daffert, C., Meixner, K., Sedrlova, Z., and Koller, M. Novel unexpected functions of PHA granules. *Applied Microbiology and Biotechnology.* 2020, 104, 4795–4810. Attached as Appendix 10.

[XIV]   Sedlacek, P., Slaninova, E., Enev, V., Koller, M., Nebesarova, J., Marova, I., Hrubanova, K., Krzyzanek, V., Samek, O., and Obruca, S. What keeps polyhydroxyalkanoates in bacterial cells amorphous? A derivation from stress exposure experiments. *Applied Microbiology and Biotechnology.* 2019, 103, 1905–1917. Attached as Appendix 11.

[XV]   Kucera, D., Novackova, I. , Pernicova, I. , Sedlacek P. , and Obruca, S. Biotechnological Production of Poly(3-Hydroxybutyrate-co-4-Hydroxybutyrate-co-3-Hydroxyvalerate) Terpolymer by Cupriavidus sp. DSM 19379. *Bioengineering.* 2019, 6, 74.

[XVI]   Kourilova, X., Pernicova, I., Sedlar, K., Musilova, J., Sedlacek, P., Kalina, M., Koller, M., and Obruca, S. Production of polyhydroxyalkanoates (PHA) by a thermophilic strain of Schlegelella thermodepolymerans from xylose rich substrates. *Bioresource Technology.* 2020, 315, 123885.

[XVII] Pernicova, I., Novackova, I., Sedlacek, P., Kourilova, X., Kalina, M., Kovalcik, A., Koller, M., Nebesarova, J., Krzyzanek, V., Hrubanova, K., Masilko, J., Slaninova, E., and Obruca, S. Introducing the Newly Isolated Bacterium Aneurinibacillus sp. H1 as an Auspicious Thermophilic Producer of Various Polyhydroxyalkanoates (PHA) Copolymers–1. Isolation and Characterization of the Bacterium. *Polymers.* 2020, 12, 1235. Attached as Appendix 12.

[XVIII] Sedlacek, P., Pernicova, I., Novackova, I., Kourilova, X., Kalina, M., Kovalcik, A., Koller, M., Nebesarova, J., Krzyzanek, V., Hrubanova, K., Masilko, J., Slaninova, E., Trudicova, M., and Obruca, S. Introducing the Newly Isolated Bacterium Aneurinibacillus sp. H1 as an Auspicious Thermophilic Producer of Various Polyhydroxyalkanoates (PHA) Copolymers–2. Material Study on the Produced Copolymers. *Polymers.* 2020, 12, 1298. Attached as Appendix 13.

[XIX] Samek, O., Obruča, S., Šiler, M., Sedláček, P., Benešová, P., Kučera, D., Márova, I., Ježek, J., Bernatová, S., and Zemánek, P. Quantitative Raman Spectroscopy Analysis of Polyhydroxyalkanoates Produced by Cupriavidus necator H16. *Sensors.* 2016, 16, 1808.

[XX] Obruca, S., Sedlacek, P., Mravec, F., Krzyzanek, V., Nebesarova, J., Samek, O., Kucera, D., Benesova, P., Hrubanova, K., Milerova, M., and Marova, I. The presence of PHB granules in cytoplasm protects non-halophilic bacterial cells against the harmful impact of hypertonic environments. *New Biotechnology.* 2017, 39, 68–80. Attached as Appendix 14.

[XXI] Meixner, K., Daffert, C., Dalnodar, D., Mrázová, K., Hrubanová, K., Krzyzanek, V., Nebesarova, J., Samek, O., Šedrlová, Z., Slaninova, E., Sedláček, P., Obruča, S., and Fritz, I. Glycogen, poly(3-hydroxybutyrate) and pigment accumulation in three Synechocystis strains when exposed to a stepwise increasing salt stress. *Journal of Applied Phycology.* 2022**.**

[XXII] Mravec, F., Obruca, S., Krzyzanek, V., Sedlacek, P., Hrubanova, K., Samek, O., Kucera, D., Benesova, P., and Nebesarova, J. Accumulation of PHA granules in Cupriavidus necator as seen by confocal fluorescence microscopy. *FEMS Microbiology Letters.* 2016, 363, fnw094.

[XXIII] Slaninova, E., Sedlacek, P., Mravec, F., Mullerova, L., Samek, O., Koller, M., Hesko, O., Kucera, D., Marova, I., and Obruca, S. Light scattering on PHA granules protects bacterial cells against the harmful effects of UV radiation. *Applied Microbiology and Biotechnology.* 2018, 102, 1923–1931. Attached as Appendix 15.

[XXIV] Obruca, S., Sedlacek, P., Krzyzanek, V., Mravec, F., Hrubanova, K., Samek, O., Kucera, D., Benesova, P., and Marova, I. Accumulation of Poly(3-hydroxybutyrate) Helps Bacterial Cells to Survive Freezing. *PLOS ONE.* 2016, 11, e0157778. Attached as Appendix 16.

[XXV] Obruca, S., Doskocil, L., Krzyzanek, V., Hrubanova, K., Sedlacek, P., Mravec, F., Samek, O., Kucera, D., Benesova, P., and Marova, I. Polyhydroxyalkanoates in Bacterial Cells - More Than just Storage Materials. *Materials Science Forum.* 2016, 851, 20–25.

[XXVI] Sedlacek, P., Slaninova, E., Koller, M., Nebesarova, J., Marova, I., Krzyzanek, V., and Obruca, S. PHA granules help bacterial cells to preserve cell integrity when exposed to sudden osmotic imbalances. *New Biotechnology.* 2019, 49, 129–136. Attached as Appendix 17.

[XXVII] Obruca, S., Sedlacek, P., Koller, M., Kucera, D., and Pernicova, I. Involvement of polyhydroxyalkanoates in stress resistance of microbial cells: Biotechnological consequences and applications. *Biotechnology Advances.* 2018, 36, 856–870. Appendix 18.

[XXVIII] Obruca, S.; Sedlacek, P.; Pernicova, I.; Kovalcik, A.; Novackova, I.; Slaninova, E.; and Marova, I. Interconnection between PHA and Stress Robustness of Bacteria. *In The Handbook of Polyhydroxyalkanoates*; CRC Press, 2020; pp. 107–132.

[XXIX] Obruca, S., Sedlacek, P., and Koller, M. The underexplored role of diverse stress factors in microbial biopolymer synthesis. *Bioresource Technology.* 2021, 326, 124767. Attached as Appendix 19.

[XXX] Daffert, C., Grammelhofer, D., Meixner, K., Obruca, S., Sedlacek, P., Samek, O., Slaninova, E., Sedrlova, Z., Mrazova, K., Hrubanova, K., Krzyzanek, V., Nebesarova, J., and Fritz, I. Effect of UV-B irradiation on the formation of polyhydroxybutyrate in Synechocystis. *Submitted for publication*.

[XXXI] Novackova, I., Kucera, D., Porizka, J., Pernicova, I., Sedlacek, P., Koller, M., Kovalcik, A., and Obruca, S. Adaptation of Cupriavidus necator to levulinic acid for enhanced production of P(3HB-co-3HV) copolyesters. *Biochemical Engineering Journal.* 2019, 151, 107350.

[XXXII] Novackova, I., Hrabalova, V., Slaninova, E., Sedlacek, P., Samek, O., Koller, M., Krzyzanek, V., Hrubanova, K., Mrazova, K., Nebesarova, J., and Obruca, S. The role of polyhydroxyalkanoates in adaptation of Cupriavidus necator to osmotic pressure and high concentration of copper ions. *International Journal of Biological Macromolecules.* 2022, 206, 977–989.

[XXXIII] Obruča, S., Dvořák, P., Sedláček, P., Koller, M., Sedlář, K., Pernicová, I., and Šafránek, D. Polyhydroxyalkanoates synthesis by halophiles and thermophiles: towards sustainable production of microbial bioplastics. *Biotechnology Advances.* 2022, 107906. Appendix 20.

[XXXIV] Kucera, D., Pernicová, I., Kovalcik, A., Koller, M., Mullerova, L., Sedlacek, P., Mravec, F., Nebesarova, J., Kalina, M., Marova, I., Krzyzanek, V., and Obruca, S. Characterization of the promising poly(3-hydroxybutyrate) producing halophilic bacterium Halomonas halophila. *Bioresource Technology.* 2018, 256, 552–556.

[XXXV] Pernicova, I. Novackova, I., Sedlacek, P., Kourilova, X., Koller, M., and Obruca, S. Application of osmotic challenge for enrichment of microbial consortia in polyhydroxyalkanoates producing thermophilic and thermotolerant bacteria and their subsequent isolation. *International Journal of Biological Macromolecules.* 2020, 144, 698–704.

[XXXVI] Obruca, S., Sedlacek, P., Mravec, F., Samek, O., and Marova, I. Evaluation of 3-hydroxybutyrate as an enzyme-protective agent against heating and oxidative damage and its potential role in stress response of poly(3-hydroxybutyrate) accumulating cells. *Applied Microbiology and Biotechnology.* 2016, 100, 1365–1376. Appendix 21.

[XXXVII] Slaninova, E., Obruca, S., Kocherbitov, V., and Sedlacek, P. On the bioprotective effects of sodium 3-hydroxybutyrate: thermodynamic study of binary Na3HB-water systems. *Submitted for publication.* Attached as Appendix 22.

[XXXVIII] Sedlacek, P., Smilek, J., Lastuvkova, M., Kalina, M., and Klucakova, M. Hydrogels: invaluable experimental tool for demonstrating diffusion phenomena in physical chemistry laboratory courses. *Journal of Materials Education.* 2017, 39, 59–90.

[XXXIX] Adamkova, K., Trudicova, M., Hrubanova, K., Sedlacek, P., and Krzyzanek, V. *An appropriate method for assessing hydrogel pore sizes by cryo-SEM*, 2019. Paper presented at the NANOCON 2018 – Conference Proceedings, 415-420.

[XL] Trudicova, M., Smilek, J., Kalina, M., Smilkova, M., Adamkova, K., Hrubanova, K., Krzyzanek, V., and Sedlacek, P. Multiscale Experimental Evaluation of Agarose-Based Semi-Interpenetrating Polymer Network Hydrogels as Materials with Tunable Rheological and Transport Performance. *Polymers.* 2020, 12, 2561. Attached as Appendix 23.

[XLI] Trudicova, M., Papezikova, H., Sedlacek, P., and Pekar, M. *Tailoring the internal microstructure of the hydrogels based on poly-HEMA targeted for drug delivery systems*, 2021. Paper presented at the NANOCON 2021 – Conference Proceedings, 280-285.

[XLII] Kratochvilova, R., Sedlacek, P., Porizka, J., and Klucakova, M. Composite materials for controlled release of mineral nutrients and humic substances for agricultural application. *Soil Use and Management.* 2021, 37, 460–467. Attached as Appendix 24.

[XLIII] Enev, V., Sedláček, P., Jarábková, S., Velcer, T., and Pekař, M. ATR-FTIR spectroscopy and thermogravimetry characterization of water in polyelectrolyte-surfactant hydrogels. *Colloids and Surfaces A: Physicochemical and Engineering Aspects.* 2019, 575, 1–9. Attached as Appendix 25.

List of the Appendices

Appendix 1:

Sedláček, P. and Klučáková, M. Diffusion experiments as a new approach to the evaluation of copper transport in humics-containing systems. *Collection of Czechoslovak Chemical Communications.* 2009, 74, 1323–1340.

Appendix 2:

Sedláček, P. and Klučáková, M. Simple diffusion method applied in evaluation of metal transport in model humic matrices. *Geoderma.* 2009, 153, 11–17.

Appendix 3:

Kalina, M., Klučáková, M., and Sedláček, P. Utilization of fractional extraction for characterization of the interactions between humic acids and metals. *Geoderma.* 2013, 207–208, 92–98.

Appendix 4:

Sedláček, P., Smilek, J., and Klučáková, M. How the interactions with humic acids affect the mobility of ionic dyes in hydrogels – Results from diffusion cells. *Reactive and Functional Polymers.* 2013, 73, 1500–1509.

Appendix 5:

Sedláček, P., Smilek, J., and Klučáková, M. How the interactions with humic acids affect the mobility of ionic dyes in hydrogels – 2. Non-stationary diffusion experiments. *Reactive and Functional Polymers.* 2014, 75, 41–50.

Appendix 6:

Klučáková, M., Kalina, M., Sedláček, P., and Grasset, L. Reactivity and transport mapping of Cu(II) ions in humic hydrogels. *Journal of Soils and Sediments.* 2014, 14, 368–376.

Appendix 7:

Smilek, J., Sedláček, P., Kalina, M., and Klučáková, M. On the role of humic acids' carboxyl groups in the binding of charged organic compounds. *Chemosphere.* 2015, 138, 503–510.

Appendix 8:

Enev, V., Sedláček, P., Kubíková, L., Sovová, Š., Doskočil, L., Klučáková, M., and Pekař, M. Polarity-Based Sequential Extraction as a Simple Tool to Reveal the Structural Complexity of Humic Acids. *Agronomy.* 2021, 11, 587.

Appendix 9:

Smilkova, M., Smilek, J., Kalina, M., Klucakova, M., Pekar, M., and Sedlacek, P. A simple technique for assessing the cuticular diffusion of humic acid biostimulants. *Plant Methods.* 2019, 15, 83.

Appendix 10:

Obruca, S., Sedlacek, P., Slaninova, E., Fritz, I., Daffert, C., Meixner, K., Sedrlova, Z., and Koller, M. Novel unexpected functions of PHA granules. *Applied Microbiology and Biotechnology.* 2020, 104, 4795–4810.

Appendix 11:

Sedlacek, P., Slaninova, E., Enev, V., Koller, M., Nebesarova, J., Marova, I., Hrubanova, K., Krzyzanek, V., Samek, O. and Obruca, S. (2019). What keeps polyhydroxyalkanoates in bacterial cells amorphous? A derivation from stress exposure experiments. *Applied microbiology and biotechnology*, 103(4), 1905-1917.

Appendix 12:

Pernicova, I., Novackova, I., Sedlacek, P., Kourilova, X., Kalina, M., Kovalcik, A., Koller, M., Nebesarova, J., Krzyzanek, V., Hrubanova, K., Masilko, J., Slaninova, E., and Obruca, S. Introducing the Newly Isolated Bacterium Aneurinibacillus sp. H1 as an Auspicious Thermophilic Producer of Various Polyhydroxyalkanoates (PHA) Copolymers–1. Isolation and Characterization of the Bacterium. *Polymers.* 2020, 12, 1235.

Appendix 13:

Sedlacek, P., Pernicova, I., Novackova, I., Kourilova, X., Kalina, M., Kovalcik, A., Koller, M., Nebesarova, J., Krzyzanek, V., Hrubanova, K., Masilko, J., Slaninova, E., Trudicova, M., and Obruca, S. Introducing the Newly Isolated Bacterium Aneurinibacillus sp. H1 as an Auspicious Thermophilic Producer of Various Polyhydroxyalkanoates (PHA) Copolymers–2. Material Study on the Produced Copolymers. *Polymers.* 2020, 12, 1298.

Appendix 14:

Obruca, S., Sedlacek, P., Mravec, F., Krzyzanek, V., Nebesarova, J., Samek, O., Kucera, D., Benesova, P., Hrubanova, K., Milerova, M., and Marova, I. The presence of PHB granules in cytoplasm protects non-halophilic bacterial cells against the harmful impact of hypertonic environments. *New Biotechnology.* 2017, 39, 68–80.

Appendix 15:

Slaninova, E., Sedlacek, P., Mravec, F., Mullerova, L., Samek, O., Koller, M., Hesko, O., Kucera, D., Marova, I., and Obruca, S. Light scattering on PHA granules protects bacterial cells against the harmful effects of UV radiation. *Applied Microbiology and Biotechnology.* 2018, 102, 1923–1931.

Appendix 16:

Obruca, S., Sedlacek, P., Krzyzanek, V., Mravec, F., Hrubanova, K., Samek, O., Kucera, D., Benesova, P., and Marova, I. Accumulation of Poly(3-hydroxybutyrate) Helps Bacterial Cells to Survive Freezing. *PLOS ONE.* 2016, 11, e0157778.

Appendix 17:

Sedlacek, P., Slaninova, E., Koller, M., Nebesarova, J., Marova, I., Krzyzanek, V., and Obruca, S. PHA granules help bacterial cells to preserve cell integrity when exposed to sudden osmotic imbalances. *New Biotechnology.* 2019, 49, 129–136..

Appendix 18:

Obruca, S., Sedlacek, P., Koller, M., Kucera, D., and Pernicova, I. Involvement of polyhydroxyalkanoates in stress resistance of microbial cells: Biotechnological consequences and applications. *Biotechnology Advances.* 2018, 36, 856–870.

Appendix 19:

Obruca, S., Sedlacek, P., and Koller, M. The underexplored role of diverse stress factors in microbial biopolymer synthesis. *Bioresource Technology.* 2021, 326, 124767.

Appendix 20:

Obruča, S., Dvořák, P., Sedláček, P., Koller, M., Sedlář, K., Pernicová, I., and Šafránek, D. Polyhydroxyalkanoates synthesis by halophiles and thermophiles: towards sustainable production of microbial bioplastics. *Biotechnology Advances.* 2022, 107906.

Appendix 21:

Obruca, S., Sedlacek, P., Mravec, F., Samek, O., and Marova, I. Evaluation of 3-hydroxybutyrate as an enzyme-protective agent against heating and oxidative damage and its potential role in stress response of poly(3-hydroxybutyrate) accumulating cells. *Applied Microbiology and Biotechnology.* 2016, 100, 1365–1376.

Appendix 22:

S Slaninova, E., Obruca, S., Kocherbitov, V., and Sedlacek, P. On the bioprotective effects of sodium 3-hydroxybutyrate: thermodynamic study of binary Na3HB-water systems. *Submitted for publication*.

Appendix 23:

Trudicova, M., Smilek, J., Kalina, M., Smilkova, M., Adamkova, K., Hrubanova, K., ... & Sedlacek, P. (2020). Multiscale experimental evaluation of agarose-based semi-interpenetrating polymer network hydrogels as materials with tunable rheological and transport performance. *Polymers.* 2020, 12(11), 2561.

Appendix 24:

Kratochvilova, R., Sedlacek, P., Porizka, J., and Klucakova, M. Composite materials for controlled release of mineral nutrients and humic substances for agricultural application. *Soil Use and Management.* 2021, 37, 460–467.

Appendix 25:

Enev, V., Sedláček, P., Jarábková, S., Velcer, T., and Pekař, M. ATR-FTIR spectroscopy and thermogravimetry characterization of water in polyelectrolyte-surfactant hydrogels. *Colloids and Surfaces A: Physicochemical and Engineering Aspects.* 2019, 575, 1–9.

Appendix 1

Sedláček, P. and Klučáková, M. Diffusion experiments as a new approach to the evaluation of copper transport in humics-containing systems. *Collection of Czechoslovak Chemical Communications* **2009**, 74, 1323–1340.

DIFFUSION EXPERIMENTS AS A NEW APPROACH TO THE EVALUATION OF COPPER TRANSPORT IN HUMICS-CONTAINING SYSTEMS

Petr SEDLÁČEK[1],* and Martina KLUČÁKOVÁ[2]

*Institute of Physical and Applied Chemistry, Faculty of Chemistry,
Brno University of Technology, Purkyňova 118, 612 00 Brno, Czech Republic;
e-mail: [1] sedlacek-p@fch.vutbr.cz, [2] klucakova@fch.vutbr.cz*

Diffusion measurements seem to provide a valuable approach to mapping studies on heavy metal transport in systems containing humic substances. The paper deals with the diffusion of cupric ions in a humic hydrogel. The diffusion coefficients of Cu^{2+} in this medium were determined using in-diffusion from the constant source, diffusion couple and instantaneous planar source. The applicability of the experimental arrangements and mathematical description of metal ion transport are discussed in terms of the influence of complexation of Cu^{2+} with humic acids. All determined diffusion coefficients of Cu^{2+} in humic gel were lower but of the same order of magnitude compared with that obtained in water.
Keywords: Diffusion; Heavy metals; Humic acids; Immobilization; Hydrogels; Copper transport.

Because of their complex nature, humic substances face an identification dilemma. A part of scientific community (mainly environmental scientists) recognizes humic acids (HA) as a component of natural organic matter (NOM) that plays a key role in such issues as global warming, carbon cycle in the nature or self-detoxification of soils and sediments, while the others consider this material one of the greatest sources of organic carbon for industry. Industrial applications of humic substances are encouraged by rich alternative natural sources – peat, young coal etc. – from which they can be obtained by simple and cheap methods of extraction and purification[1]. Humics are also chemically reactive. They contain a wide range of functionalities that could change when structural modifications are made to acquire desired properties[2].

Due to a diffuse nature and diverse functionalities of humic substances, fundamental knowledge regarding their chemistry and properties is still

missing. These substances are not well understood with regard to exact structure; it is hence necessary to develop an appropriate methodology in order to compare applicable properties of humic substances from different sources and to confront them with other materials (e.g. synthetic polymers and biopolymers). Therefore, systematic reactivity and biological activity mapping studies are needed.

Humic acids provide the outstanding ability to sorb common groups of pollutants such as metallic cations. Many works focused on sorption of different toxic chemicals on solid humic acid and/or humic sols[3–9] have been published. But it is also well known that the sorption ability depends strongly on the mobility and the transport of adsorbed ions (or molecules) into humic particles. Involvement of diffusion transport of a sorbate in a specific form of humic material is therefore necessary for modeling sorption on HA in their natural environments. It is necessary to study and understand both complex behavior of this natural system and the role of its constituents. Published studies of diffusion in humic systems are relatively scarce. Wang et al.[10] investigated the effect of HA on Eu^{3+} diffusion in compacted bentonite. They found that HA hinder the Eu^{3+} diffusion and migration because of a formation of Eu–HA complexes which precipitate at the surface of compacted bentonite. Consequently, only a small part of Eu exists as a free ion in the humics-containing system. Wold and Eriksen[11] carried out similar experiments with diffusion of Eu^{3+}, Co^{2+} and humic colloids through compacted bentonite. Humic colloids diffused through the bentonite regardless its compaction. The apparent diffusivities of both metals increased significantly in the presence of humic colloids. Chang et al.[12] investigated the sorption kinetics of volatile organic compounds in dry, pressed humic acid disks by tracking the weight change of the sorbent with a microbalance. Kinetics of sorption and desorption are successfully described by a diffusion model.

Masaro et al.[13] present a detailed overview of diffusion in polymer solutions, gels and solids. Various theoretical descriptions of the diffusion processes are proposed. The theoretical models are based on different physical concepts such as obstruction effects, free volume effects and hydrodynamic interactions. References therein illustrate an applicability of these models in treatment of diffusion data for various systems.

Our previous results confirmed that kinetics of metal–humic interactions are generally dependent on the colloidal state of HA[14,15]. In natural state, HA are usually found in wet environments (water sediments, peat etc.) in swollen form, hence recent contributions focus on the study of HA in the hydrogel form[15,16]. Besides good simulation of natural humic environment,

the gel form of HA provides some additional benefits. The most valuable one is preparation of HA with defined size and shape, which is necessary for the evaluation of transport parameters by means of a mathematical model. Besides, the gel form of HA can be considered as a system which allows fixation of humic material while enabling interactions in its bulk. Consequently, not only these physicochemical interactions but also transport within the humic matrix can be studied. Humic hydrogels can also be prepared in a simple and cheap way using a method of controlled coagulation[9].

The diffusion studies on humics could be utilized in easy characterization of the material. Parameters such as effective diffusion coefficients of common pollutants in hydrogel forms of humic acids can be used in discussing the quality of humic substances of different origin in comparison with other synthetic or natural materials regarding desired applications. Determination of diffusion coefficient of various substances in polymer gels is taken as a topic for numerous works[17–29]. Seki and Suzuki[17] prepared composite adsorbents containing humic acids entrapped in an alginate gel and carried out a kinetic study of lead adsorption on this gel. The shrinking core model was used to determine apparent lead diffusion coefficients in the gels. Scally et al.[18] derived diffusion coefficients of metal ions and metal–ligand complexes in polyacrylamide hydrogels at different ionic strengths using a diffusion cell. Effects of humic and fulvic acids as ligands were also studied.

Although the accurate measurement of diffusion coefficients usually needs expensive and sophisticated equipment, e.g. nuclear methods such as NMR, Rutherford backscattering spectrometry (RBS) or elastic recoil detection analysis (ERDA), simple laboratory techniques exist for determination with standard error below 10%[19]. In general, measurement in diffusion cells is the method used most frequently in gel[20–25]. Besides, several other simple methods for determination of diffusivity in solids and gels have been developed, such as a method of instantaneous planar source[26,27] which differs from others by the fact that diffusion coefficient is calculated from a linearized concentration profile in the gel sample instead of using a time dependence of total diffusion flux. García-Guttieréz[29] provides in-depth summary of methods for the determination of diffusion coefficients in solids. Pros and cons of each method are discussed on the example of diffusion of both neutral (tritium) and ionic (Cl^-, I^-, SO_4^{2-}, Na^+, Ca^{2+}, …) substances in compacted bentonite.

The cupric ion is well known for its high affinity to humic substances[1,9] and the ability to form one of the strongest bonds with them. Due to the

above and also because of easy quantification of Cu^{2+} content (e.g. by means of UV-Vis spectroscopy), cupric ions have been chosen as a model of heavy metal sorbate. The diffusivity of cupric ions in the humic gel is determined by their reduced mobility in a porous gel phase and by their interactions with HA. Mathematically, these effects are described by the following equation derived from conservation of mass

$$\frac{\partial c_1}{\partial t} = D_{eff}^0 \frac{\partial^2 c_1}{\partial x^2} - \dot{r} \qquad (1)$$

where c_1 is the concentration of Cu^{2+} in time t and distance x in a humic gel. D_{eff}^0 is the value of the diffusion coefficient that embraces the influence of the porous phase. This coefficient is usually defined by the relation[19]

$$D_{eff}^0 = \phi \frac{D}{\tau} \qquad (2)$$

where D is the diffusivity in dispersion medium (water in the case of hydrogel), ϕ represents the porosity of the porous medium and τ stands for its tortuosity. Tortuosity is related to longer diffusion pathway in three-dimensional network as compared with diffusion in an aqueous solution. For highly porous media, its value lies between 2 and 6, usually it is close to 3 as the substance diffuses in 3 directions instead of 1 and the pathway is consequently approximately three times longer. The second term of Eq. (1) represents the rate of chemical reaction between Cu^{2+} and HA and it is defined as

$$\frac{\partial c_2}{\partial t} = \dot{r} \,. \qquad (3)$$

This balance describes distribution of the fixed Cu^{2+} ions in time and space.

If fast immobilization with the presence of local equilibrium between mobile and immobilized Cu^{2+} is presumed, Eq. (1) is written now as

$$\frac{\partial c_1}{\partial t} = D_{eff}^0 \frac{\partial^2 c_1}{\partial x^2} - K\frac{\partial c_1}{\partial t} \qquad (4)$$

and, consequently,

$$\frac{\partial c_1}{\partial t} = \frac{D_{eff}^0}{1+K} \frac{\partial^2 c_1}{\partial x^2} = D_{eff} \frac{\partial c_1}{\partial x^2} \qquad (5)$$

where K is the proportionality constant between mobile (c_1) and immobilized (c_2) Cu^{2+} ions defined as

$$c_2 = Kc_1. \tag{6}$$

Equation (5) defines a new effective diffusion coefficient

$$D_{eff} = \frac{D_{eff}^0}{1 + K}. \tag{7}$$

In this case, "the effective value" means the value in which effects of both chemical reaction and porous character of the gel are involved. From the analytical solution of Eq. (5), mathematical expressions for the concentration profiles of diffusing ions in the gel can be designed for corresponding experimental conditions (for more details, see ref.[14]). The aforementioned simplification is often used wherever an interaction between a diffusing substance and a medium can be assumed fast enough in comparison with the diffusion itself. In practice, this condition is usually fulfilled if the macroscopic diffusion characteristics obey rules for the Fick's diffusion (i.e. cumulative diffusion flux is directly proportional to square root of time).

EXPERIMENTAL

Isolation of Humic Acids

HA were extracted from South-Moravian lignite by alkaline extraction. Lignite was stirred with the extractant (0.5 M NaOH and 0.1 M $Na_4P_2O_7$) in the 20 g per 1 dm^3 ratio for 12 h. The formed suspension was kept standing overnight and the next day the solution was separated from the solid phase and acidified with 20% hydrochloric acid to pH below 1. The solid residue was put into another 1 dm^3 of the extractant and after 1-h stirring the extract was separated and acidified in the same way. The acid extracts were kept in refrigerator overnight. Precipitated HA were separated by centrifugation (4 000 rpm), washed by deionized water several times and centrifuged again (until Cl^- ions were removed) and dried at 50 °C. Before humic gel preparation, HA were washed by deionized water, centrifuged and dried once more.

Characterization of HA

Obtained HA were characterized by elemental analysis (CHNSO Microanalyser Flash 1112, Carlo Erba) and UV-Vis (Hitachi U 3300). For UV-Vis spectroscopic characterization, dry HA (7 mg) were diluted with 0.1 M NaOH and absorbance at wavelengths 200–900 nm was measured.

Preparation of Humic Gel

For the preparation of the humic gel, solid HA were dissolved in 0.5 M NaOH. The hydrogel was then obtained by precipitation of sodium humate after acidification with HCl to pH below 1. The formed mixture was kept overnight and the next day the mixture was centrifuged, the supernatant was discarded and the gel (labeled as 'gel A') was repeatedly washed with deionized water and centrifuged. About 86% of total weight of the resulting hydrogel is represented by water content.

Diffusion Experiments

The paper compares three simple experimental methods for determination of D_{eff}. In all of them, non-stationary (transient) diffusion of Cu^{2+} is assumed. Each of the following experiments was done in triplicate; the individual diffusion flux was calculated as the arithmetic mean of the three corresponding values with determination of the standard error.

In-diffusion from constant source. The first diffusion experiment was focused on the diffusion from constant source of Cu^{2+}. This method is often used in determining diffusion coefficients in various solid samples[29–31]. The humic gel (gel A) was packed into cylinders (1 cm internal diameter and 5 cm length). These cylindrical samples were put separately into 50 ml of saturated $CuCl_2$ solution with ca. 2 g of crystalline $CuCl_2$ added before. As the rate of dissolution of the crystalline salt is assumed to be higher in comparison with the rate of diffusion, we can suppose that the concentration of Cu^{2+} in solution is maintained at a constant value during diffusion experiments. In given times, gel samples were sliced and the slices were extracted separately with 0.025 M NH_4EDTA solution. Previous extraction experiments had confirmed the 100% effectiveness of the leaching of Cu^{2+} ions from humic gel to 1 M HCl up to the 1 mol l^{-1} content in the gel. Acid extraction is advantageous because dissolved humic acids do not interfere with the UV-Vis signal of Cu^{2+} in extracts. Nevertheless, higher Cu^{2+} concentrations require the use of NH_4EDTA as the leaching agent. The Cu^{2+} content in each extract was quantified by UV-Vis spectrophotometry (Hitachi U3300). Consequently, the concentration profile was determined by assessing the concentration of Cu^{2+} determined from a slice from a corresponding position in the gel cylinder. Simultaneously, the cumulative diffusion flux was calculated from the sum of the Cu^{2+} contents over the whole cylinder.

Diffusion pair. Diffusion pair (also called Half-plugs method) is often used for determination of diffusivity in solids[29,32,33]. The measurement is carried out by connecting two samples (usually tubes filled with a studied material) which differ only in concentration of diffusing matter. This approach was implemented as follows. The humic gel with incorporated Cu^{2+} ions (gel B) was prepared by diffusing the ions into the humic gel described in the previous chapter (gel A). The gel A was gently pressed into a silicone tube (inner diameter 1 cm and length 3 cm) and placed into 1 M $CuCl_2$ solution (30 ml). Cu^{2+} ions were diffusing into the gel for 8 days, until a constant concentration in the tube was achieved. The diffusion pair was then realized by connecting two silicone tubes, one filled with the humic gel containing Cu^{2+} ions (gel B) and the other filled with the humic gel without metal ions (gel A, tube length 5 cm). In a given time, the samples were disconnected and the concentration of diffusing substance was found in different positions. For this purpose, gel-slicing was used again, determining the concentration of Cu^{2+} ions in a separate slice after extraction with 1 M HCl by UV-Vis spectrophotometry. Satisfactory effectiveness of this extraction in the particular region of Cu^{2+} concentrations in the gel was confirmed again. From the

dependence of cumulative diffusion flux (total mass of substance transported through the interface of the diffusion pair) on time or from the shape of concentration profile of the diffusing substance in the sample, diffusion coefficient is then calculated.

Instantaneous planar source. For an instantaneous planar source of the diffusing matter, an infinitesimally small width of the initial concentration pulse is presumed[26–29]. This can be considered, e.g., when a filter paper tagged with a highly soluble substance is located at the end of a tube filled with the studied hydrogel. In the particular experiment, a circular slice of filter paper (1 cm in diameter) was immersed into 1 M $CuCl_2$ solution for 1 min. The humic gel (gel A) was packed into a plastic tube (1 cm inner diameter and 5 cm length) with the immersed filter paper placed at one end. At given times, gel samples were sliced and both paper and gel slices were extracted separately with 1 M HCl. Concentrations of Cu^{2+} ions in separate slices were determined using UV-Vis spectrophotometry.

RESULTS AND DISCUSSION

Characterization of HA

Results of the HA elementary analysis illustrate the major content of H (42.12 mole %) and C (41.16 mole %); high content of O (15.64 mole %) and the minor amount of N and S (0.91 and 0.17 mole %, respectively). All values are normalized on dry ash-free HA. These results are in accordance with previous elementary analysis published for lignitic humic acids[1,7]. From the UV-Vis spectrum of sodium humate, standard optical characteristics were calculated. They are very useful for the determination of the chemical structure of HA[1]. The absorption ratio A_{280}/A_{465}, which corresponds to the ratio between resistant lignin structures and HA with the low degree of humification[34], was 3.75. A_{465}/A_{665} ratio ($E4/6$) indicates the humification index and decreases with increasing molecular weight or degree of dispersion. Low $E4/6$ (3.35) hence indicates high molecular weight of the applied HA. Kumada[35] connected the value of $\Delta \log K$ ($\Delta \log K = \log A_{400} - \log A_{600}$) with the degree of humification of HA. According to this value, the author distinguishes three basic types of the material: A-type ($\Delta \log K$ up to 0.6), B-type (0.6–0.8) and R_p-type (0.8–1.1); the lower the $\Delta \log K$ value the higher humification degree. The used HA belong to A-type ($\Delta \log K$ = 0.57) which indicates high degree of humification. Particular FT-IR, UV-Vis, elemental, ^{1}H and solid-state ^{13}C NMR characterization of used HA can be found in more details in Peuravuori et al.[36].

Diffusion Experiments

Schematic representations of all methods described in the following section are shown in Fig. 1. Corresponding initial conditions are also implied.

In-Diffusion from Constant Source

Prior to the start of the experiment, homogeneous distribution of concentration of a diffusing substance is required. In our experiment, the diffusing species of interest are Cu^{2+} ions and the homogeneous concentration in the gel in time $t = 0$ s is zero. When the phase boundary (a circular surface at the end of the gel cylinder) is kept at a constant concentration ($x = 0$ m: $c_1 = c_{x=0}$ for $t > 0$ s), Eq. (5) can be easily processed by Laplace transformation. The time development of the concentration profile of diffusing substance in the gel can be calculated from the following equation[19,29,37]

$$c_1 = c_{x=0} \text{ erfc} \frac{x}{\sqrt{4D_{eff}t}} . \tag{8}$$

A diffusion flux J can be expressed by Eq. (9)

$$J = -D_{eff}\left(\frac{\partial c_1}{\partial x}\right)_{x=0} . \tag{9}$$

The derivative of the concentration profile incorporated in Eq. (9) gives the expression for the total amount of substance transported through the solution/gel interface (cumulative diffusion flux). From this flux, D_{eff} can be calculated

Fig. 1
Schematic representation of the used diffusion methods

$$m = 2\,c_{x=0}\,\sqrt{\frac{D_{\text{eff}}\,t}{\pi}}\;. \tag{10}$$

In nonstationary diffusion of ions through two circular planes at both ends of the gel cylinder, concentration profiles of Cu^{2+} in the gel show a typical symmetrical shape with a minimum in the middle of the gel sample, as was verified experimentally (concentration profiles are not listed here). For constant concentration of Cu^{2+} at solution/gel interface, the total diffusion flux dependence on the square root of time is assumed to be linear. As can be seen in Fig. 2, the agreement between this theory and experimental results is good. From the slope of the linear regression of this dependence, the value of diffusion coefficient of cupric ion in the humic gel was calculated using Eq. (10). Values of $c_{x=0}$ are determined by extrapolation of concentration profiles. The resulting value of diffusion coefficient together with all the values determined by the following methods and the value published for diffusion in water are shown in Table I.

Diffusion Pair

An example of the experimental concentration profile obtained for gel B in the diffusion pair with gel A is given in Fig. 3. It shows that concentrations at both sides of the A–B interface are equal or, in other words, no concentration jump is observed. The reason is clear; both gels are of the same material origin. First step of their preparation is the same; they differ just in
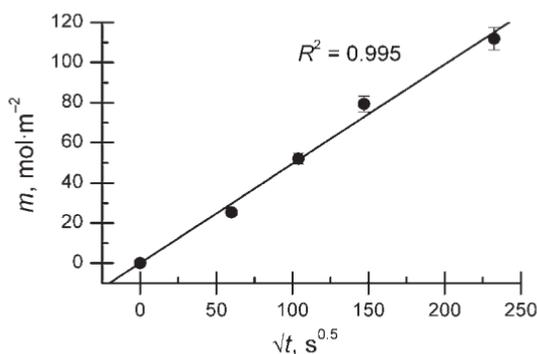
FIG. 2
Dependence of the total diffusion flux on the square root of time (in-diffusion from constant source)

the presence of Cu^{2+} in one of them when starting the experiment. These ions enter the final complete gel structure and can be consequently trapped only by functional groups of HA, not involved in the formation of primary gel structure. The nature, structure and properties of gel B are in this respect similar to those of the gel A.

A mathematical description of the diffusion in this diffusion pair is simple. When the diffusion starts, gel B has a constant concentration of Cu^{2+} ions along the whole tube length ($x < 0$ m: $c_1 = c_0$ for $t = 0$ s), whereas their concentration in the gel A is zero ($x > 0$ m: $c_1 = 0$ mol m^{-3} for $t = 0$ s). These initial conditions were verified experimentally. The solution of second Fick's law is the same as in the previous case and leads to the concentration profile of Cu^{2+} in diffusion pair in the following form[19,29,37]

TABLE I
Diffusion coefficients D_{eff} determined by different diffusion methods (with a 95% confidence interval)

Method	D_{eff}, m^2 s^{-1}
In diffusion method	$(7.9 \pm 0.6) \times 10^{-10}$
Half-plugs method	$(7.1 \pm 0.2) \times 10^{-10}$
Instantaneous planar source (slopes)	$(4.8 \pm 0.4) \times 10^{-10}$
Instantaneous planar source (intersection points)	$(5.0 \pm 1.4) \times 10^{-10}$
Diffusion in water[a]	14.3×10^{-10}

[a] Cited from Lide et al.[38]
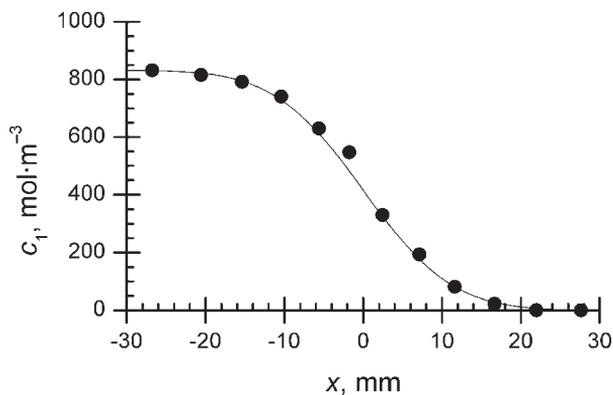
FIG. 3
Comparison of calculated (line) and measured concentration profile in diffusion pair after 16 h

$$c_1 = \frac{1}{2}\, c_0 \,\mathrm{erfc}\, \frac{x}{\sqrt{4D_{\mathrm{eff}}t}}\, . \tag{11}$$

From Eq. (*11*), it can be seen that concentration of diffused component on the interface is time-independent and equal to $c_0/2$.

The total diffusion flux m which goes through the interface between gel B and the gel A ($x = 0$) in time t can be calculated as

$$m = c_0 \sqrt{\frac{D_{\mathrm{eff}}t}{\pi}}\, . \tag{12}$$

A comparison of Eqs (*9*) and (*10*) with Eqs (*11*) and (*12*) indicates that, in fact, diffusion in diffusion pair corresponds to that from constant source; the outer part of the pair serves as a source which ensures constant concentration of diffusing substance (equal to $c_0/2$) at the interface with the "in" part.

Again, the dependence of experimentally determined m on $\sqrt{t}$ is strongly linear (Fig. 4). Therefore, Eq. (*12*) can be used for calculation of diffusion coefficient. The value of D_{eff} obtained for the Cu^{2+} diffusion from gel B into gel A is slightly lower than the value determined by diffusion from constant source (Table I) but the confidence interval is markedly more narrow.

To test the validity of calculated D_{eff}, Eq. (*11*) was used in order to calculate theoretical concentration profiles for different times. As it can be seen in Fig. 3, there is a good agreement between experimentally measured profile and the calculated one.
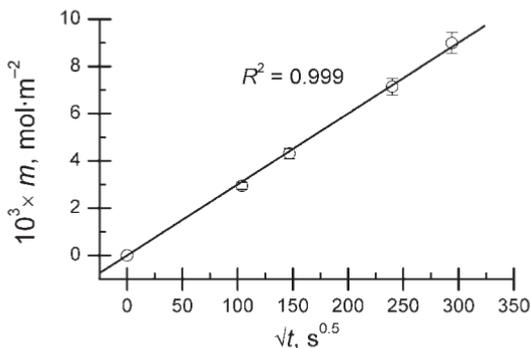
FIG. 4
Dependence of the total diffusion flux on the square root of time (diffusion pair)

Instantaneous Planar Source

The method of instantaneous planar source differs from the other methods mainly because that diffusion coefficient is primarily determined from the shape of measured concentration profiles of diffusing matter instead from the dependence of the total diffusion flux on time.

Instantaneous planar source involves an initial concentration pulse of infinitesimally small width. For this presumption and for the zero initial concentration of Cu^{2+} in the gel, the solution of the second Fick's law gives the following relationship for concentration profile[19,29,37]

$$c_1 = \frac{n_{Cu}}{S\sqrt{\pi D_{eff} t}} \exp\left(-\frac{x^2}{4 D_{eff} t}\right) \tag{13}$$

where n_{Cu} stands for total Cu^{2+} content in sample, x is the distance from the intercept between the gel and the paper filter and S is the cross-section area.

Linearization of this equation provides Eq. (*14*)

$$\ln c_1 = \ln \frac{n_{Cu}}{S\sqrt{\pi D_{eff} t}} - \frac{x^2}{4 D_{eff} t} \tag{14}$$

where it can be seen that while the linear regression of $\ln c_1 = f(x^2)$ is found in the form $\ln c_1 = B - Ax^2$, the effective diffusion coefficient influences both slope A and intersection point B

$$A = \frac{1}{4 D_{eff} t}, \qquad B = \ln \frac{n_{Cu}}{S\sqrt{\pi D_{eff} t}} . \tag{15}$$

For a better readability, the linear regressions for all three times are listed starting from 0 in Fig. 5. As mentioned before, the effective diffusivity can be derived from both A and B. In Fig. 6, the value of D_{eff} is shown as a slope of time-dependence of $1/(4A)$. For the calculation of D_{eff} from intersection point B, the following substitution can be used

$$Y = \frac{1}{\pi}\left(\frac{n_{Cu}}{S}\right)^2 \exp(2B) . \tag{16}$$

If compared with Eq. (*15*), it can be easily found, that $Y = D_{eff} t$. D_{eff} can be therefore calculated as the slope of time-dependence of Y (see Fig. 6).

Using the calculated diffusivity, the theoretical concentration profiles can be found. Figure 5 shows the agreement between measured and theoretical profiles, calculated using the value of D_{eff} derived from slopes of the linearized profiles.
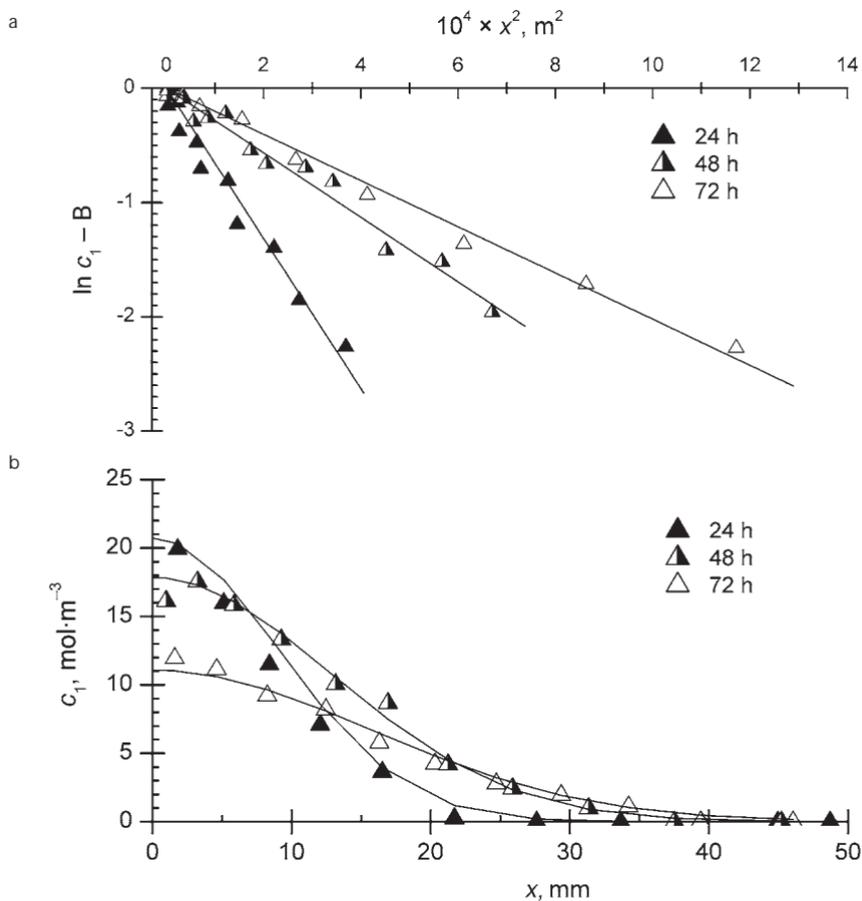
F IG. 5
Linearized concentration profiles of Cu^{2+} in humic gel (a) and a comparison of measured profiles (b) with those calculated (b, lines) using subsequently determined diffusion coefficient

Calculated Diffusion Coefficients

All calculated values of the diffusivities are listed in Table I. It can be seen that all values are of the same order of magnitude as that published for diffusion of Cu^{2+} in water[38]. This finding is common for diffusion in hydrogels. These values are also in good agreement with published diffusivities of Cu^{2+} in various hydrogels. Already in 1930's, diffusion coefficient of Cu^{2+} was measured in silica gel (ca. 4×10^{-10} m^2 s^{-1})[39] and in 2% agar gel (2.9×10^{-10} m^2 s^{-1})[40]. Much more recently, Garmo et al.[41] determined diffusion
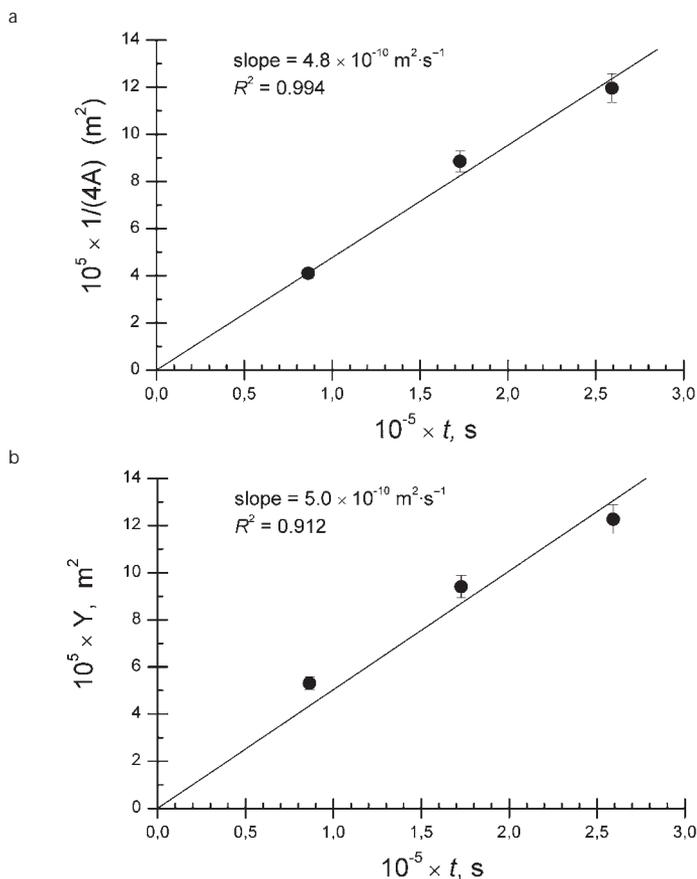
FIG. 6
Time dependence of the substituted slopes (a) and intersection points (b) of linearized concentration profiles

coefficients of 55 elements in DGT (diffusive gradients in thin films) equipment which consisted of diffusive agarose polyacrylamide gel and iminodiacetate chelating resin. Effective coefficient of Cu^{2+} in this complex medium was in the range 5.5–6.6×10^{-10} m^2 s^{-1} for pH 4.7–5.9. Scally et al.[18] studied transport of Cu^{2+} in the gels used for DGT method as well. They obtained values 6.30–6.45×10^{-10} m^2 s^{-1} for agarose cross-linked polyacrylamide and 4.18–4.81×10^{-10} m^2 s^{-1} for restricted polyacrylamide gel. The solid contents of both gels were very close to those of humic gel (~15%). The range of diffusivity corresponds to various $NaNO_3$ amounts added to source solutions of Cu^{2+}.

Table I shows a good agreement between D_{eff} values determined by the methods of in-diffusion and diffusion pair. The relative difference between the highest and the lowest mean values is slightly above 10%. These values correspond to about 50% of diffusivity of Cu^{2+} in water. As expected, Cu^{2+} ion movement in the gel matrix is slower than in water regardless of a high content of the aqueous phase in the gel. The reaction of Cu^{2+} with the active sites of HA in combination with a tortuous pathway decelerates the transport of Cu^{2+} through the phase interface. In other words, the driving force for the diffusion may be the same but the resistance to ion movement is higher when diffusing in the gel.

Both values of D_{eff} determined experimentally with an instantaneous planar source are noticeably lower. This can be caused by a dependence of a diffusion coefficient on concentration of diffusing substance as is often published[19]. In the former experiments, considerably higher amounts of diffusing substance were used and the concentration of Cu^{2+} in humic gel was always at least one order higher there and therefore an influence of the chemical reaction on the transport can be more pronounced. Because the value of D_{eff} is governed by the shapes of concentration profiles, the standard error of D_{eff}, characterized by the 95% confidence interval, is higher here. Nevertheless, this method possesses many advantages including low demands on supply of diffusing matter.

CONCLUSIONS

For the various applications of humic acids utilizing the natural sorption ability, it is necessary to combine classical sorption experiments with modeling of the sorbate transport in humic material which simulates the natural forms of HA. For this reason, basic diffusion experiments were performed. They were focused on the Cu^{2+} transport in the humic gel and the main goal was to test the applicability of theoretical mathematical apparatus and

simple laboratory methods to the study of the pollutant transport in materials that model natural humic environments.

In general, these diffusion measurements seem to provide a valuable method for reactivity and permeability mapping studies on materials containing humic substances. All methods proved themselves suitable for easy and quick description of transport phenomena. All experimental data fit theoretical calculations well. Specific parameters of each method (e.g. concentration of diffusing substance) must be taken into account when choosing an appropriate method for defined conditions. Consequently, either in-diffusion from a constant source or a diffusion pair can be utilized wherever the amount of the diffusing substance is not a limiting factor. In opposite cases, instantaneous planar source represents the method of choice.

As compared to diffusion of Cu^{2+} in water, the experimentally determined values of diffusion coefficient of Cu^{2+} in the humic gel were lower but of the same order of magnitude. This finding agrees with an increase in resistance to transport, which is well known for the reactive gels. The investigation of the diffusion behavior of typical pollutants in the gel forms of humic acids (from various sources or methods of extraction and purification) can serve as an important tool for the evaluation and standardization of their usability in a large range of applications.

SYMBOLS

c_0	initial concentration of diffusing substance in source gel (diffusion pair), mol m^{-3}
c_1	concentration of a diffusing substance, mol m^{-3}
c_2	concentration of an immobilized diffusing substance, mol m^{-3}
$c_{x=0}$	constant concentration at the phase interface (constant source), mol m^{-3}
D	diffusion coefficient in dispersion medium (water for hydrogels), m^2 s^{-1}
D_{eff}^0	effective value of diffusion coefficient excluding any reaction effect, m^2 s^{-1}
D_{eff}	effective value of diffusion coefficient including a reaction effect, m^2 s^{-1}
erfc	complimentary error function
J	intensity of diffusion flux, mol m^{-2} s^{-1}
K	proportionality constant between mobile and immobilized form of diffusing substance (dimensionless)
m	cumulative diffusion flux, mol m^{-2}
n_{Cu}	total amount of Cu applied in experiment (instantaneous source), mol
S	cross-section area, m^2
t	time, s
x	distance, dimension, m
ϕ	porosity of a porous medium (dimensionless)
τ	tortuosity of a porous medium (dimensionless)

REFERENCES

1. Stevenson F. J.: *Humus Chemistry: Genesis, Composition, Reactions*, 2nd ed. Wiley–Interscience, New York 1982.
2. Almendros G.: *Commun. Soil Sci. Plant Anal.* **1994**, *17*, 2711.
3. Klučáková M., Pelikán P., Lapčík L., Lapčíková B., Kučerík J., Kaláb M.: *J. Polym. Mater.* **2000**, *17*, 337.
4. Kerndorff H., Schnitzer M.: *Geochim. Cosmochim. Acta* **1980**, *44*, 1701.
5. Tipping E., Hurley M. A.: *Geochim. Cosmochim. Acta* **1992**, *56*, 3627.
6. Klučáková M., Kaláb M., Pekař M., Lapčík L.: *J. Polym. Mater.* **2002**, *19*, 287.
7. Klučáková M., Pekař M.: *Colloids Surf., A* **2006**, *286*, 126.
8. Klučáková M., Pekař M.: *J. Polym. Mater.* **2003**, *20*, 145.
9. Martyniuk H., Wieckovska A.: *Fuel Process. Technol.* **2003**, *84*, 23.
10. Wang X., Chen Y., Wu Y.: *Appl. Radiat. Isot.* **2004**, *60*, 963.
11. Wold S., Eriksen T.: *Phys. Chem. Earth* **2007**, *32*, 477.
12. Chang M. L., Wu S. C., Chen C. Y.: *Environ. Sci. Technol.* **1997**, *31*, 2307.
13. Masaro L., Zhu X. X.: *Prog. Polym. Sci.* **1999**, *24*, 731.
14. Klučáková M., Pekař M. in: *Humic Substances: Molecular Details and Applications in Land and Water Conservation* (E. A. Ghabbour and G. Davies, Eds), p. 167. Taylor & Francis, New York 2005.
15. Klučáková M., Pekař M.: *J. Polym. Mater.* **2003**, *20*, 155.
16. Klučáková M., Pekař M. in: *Humic Substances: Nature's Most Versatile Materials* (E. A. Ghabbour and G. Davies, Eds), p. 263. Taylor & Francis, New York 2004.
17. Seki H., Suzuki A.: *J. Colloid Interface Sci.* **1999**, *211*, 375.
18. Scally S., Davison W., Hao Zhang: *Anal. Chim. Acta* **2006**, *558*, 222.
19. Cussler E. L.: *Diffusion: Mass Transfer in Fluid Systems*. Cambridge University Press, Cambridge 1984.
20. Lakatos I., Lakatos-Szabó J.: *Colloids Surf., A* **1998**, *141*, 425.
21. Lakatos I., Lakatos-Szabó J.: *Colloids Surf., A* **2004**, *246*, 9.
22. Potter K., McFarland E. W.: *Solid State Nucl. Magn. Reson.* **1996**, *6*, 323.
23. Matsukawa S.: *Prog. Polym. Sci.* **1999**, *24*, 995.
24. Tamagawa H., Popovic S., Taya M.: *Polymer* **2000**, *41*, 7201.
25. Falk B., Garramone S., Shivkumar S.: *Mater. Lett.* **2004**, *58*, 3261.
26. Climent M. A., de Vera G., Lopez J. F., Viqueira E., Andrade C.: *Cem. Concr. Res.* **2002**, *32*, 1113.
27. de Vera G., Climent M. A., Viqueira E., Antón C., Andrade C.: *Cem. Concr. Res.* **2007**, *37*, 714.
28. Schantz E. J., Lauffer M. A.: *Biochemistry* **1962**, *1*, 658.
29. García-Gutiérrez M., Cormenzana J. L., Missana T., Mingarro M., Molinero J.: *J. Iberian Geol.* **2006**, *32*, 37.
30. Cave L., Al T., Yan Xiang, Vilks P.: *J. Contam. Hydrol.* **2009**, *103*, 1.
31. Suzuki K., Fukano T., Kataoka Y.: *J. Electrochem. Soc.* **1991**, *138*, 2201.
32. Balcone-Boissard H., Baker D. R., Villemant B., Boudon G.: *Chem. Geol.* **2009**, *263*, 89.

33. Paul A., Kodentsov A. A., van Loo F. J. J.: *J. Alloys Compd.* **2005**, *403*, 147.
34. Chen Y., Senesi N., Schnitzer M.: *Soil Sci. Soc. Am. J.* **1977**, *41*, 352.
35. Kumada K.: *Food Fertilizat. Technol. Centre* **1975**, *22*, 10.
36. Peuravuori J., Žbánková P., Pihlaja K.: *Fuel Process. Technol.* **2006**, *87*, 829.
37. Crank J.: *The Mathematics of Diffusion*. Clarendon Press, Oxford 1956.
38. Lide D. R.: *Handbook of Chemistry and Physics*, 76th ed. CRC Press, New York 1995.
39. Eversole W. G., Doughty E. W.: *J. Phys. Chem.* **1936**, *40*, 55.
40. Ricketts V. L., Culbertson J. L.: *J. Am. Chem. Soc.* **1931**, *53*, 4002.
41. Garmo A., **Røyset** O., Steinnes E., Flaten T. P.: *Anal. Chem.* **2003**, *75*, 3573.

Appendix 2

Sedláček, P. and Klučáková, M. Simple diffusion method applied in evaluation of metal transport in model humic matrices. *Geoderma* **2009**, 153, 11–17.

Contents lists available at ScienceDirect

Geoderma

journal homepage: www.elsevier.com/locate/geoderma
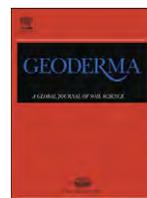
Simple diffusion method applied in evaluation of metal transport in model humic matrices

Petr Sedláček *, Martina Klučáková

Institute of Physical and Applied Chemistry, Faculty of Chemistry, Brno University of Technology, Purkyňova 118, 612 00 Brno, Czech Republic

ABSTRACT

Humic acids play an important role in soil and natural water chemistry. Many works dealing with sorption of different toxic chemicals on both solid humic acids and humic sols have been published. This paper focuses on the transport and immobilization of Cu^{2+} in a humic gel. Use of humic acids in a gel form brings several advantages: it enables preparation of samples with defined size and shape and gives a true picture of natural form of humic acids in soils and sediments. Due to its high affinity for humic acids and a good stability of formed complexes copper was used as a model metal. The two following concepts of nonstationary diffusion were adopted: diffusion from constant source and diffusion from time-variable source of a diffusing matter. In the latter case, effects of time and of the initial concentration of Cu^{2+} ions source were determined. Usability of an applied experimental arrangement and mathematical description of metal ions transport and immobilization are discussed.

© 2009 Elsevier B.V. All rights reserved.

1. Introduction

The ability of soils and sediments to reduce the mobility of chemical pollutants or even to immobilize them represents their important natural feature. It affects biological uptake and bioaccumulation of toxic chemicals in plants as well as the pollution of the underground water supplies. Most of agricultural soils have gradually lost much of this ability which must be supported artificially now because the use of heavy machinery and synthetic fertilizers had replaced considerate soil utilization and natural fertilization.

As the most beneficial fraction of soil organic matter, responsible for mentioned natural detoxification of soils, humic acids (HAs) provide outstanding sorption ability towards common groups of pollutants. Humic substances can be gained from their rich alternative natural sources – peat, young coal etc. – from which they can be obtained by simple and cheap methods of extraction and purification (Stevenson, 1982). They are chemically reactive, and they possess a wide range of functionalities that could change when structural modifications are made to acquire desired properties. This makes HAs very promising for production of soil remediation agents.

Due to a diffuse nature and diverse functionality of humic substances, fundamental knowledge regarding their chemistry and properties is still missing. Because these substances are not well understood with regards to exact structure, it is necessary to develop an appropriate methodology in order to compare properties of humic substances from different sources and to confront them with other materials (e.g. synthetic polymers and biopolymers). Therefore, systematic reactivity and biological activity mapping studies are needed.

Many works focused on sorption of different chemicals on solid humic acid and/or humic sols have been published (Kerndorff and Schnitzer, 1980; Tipping and Hurley, 1992; Klučáková et al., 2000, 2002; Klučáková and Pekař, 2003a,b, 2004, 2005, 2006). It is well known that sorption ability depends on size of humic particles strongly. One important reason is the transport of adsorbed ions (or molecules) into humic particles in order to bind with active centre. Involvement of diffusion transport of a sorbate in a specific form of humic material is therefore necessary for modeling of sorption on HAs in their natural environments.

In general, transport processes including diffusion play important role in soils and it is necessary to study and understand both complex behavior of this natural system and the role of its constituents. Diffusion studies on humics could be utilized in easy characterization of this reactive component of soils. Because parameters such as effective diffusion coefficients of common pollutants in various forms of different HAs are always markedly affected by an interaction between diffusing matter and a humic matrix, they can be used in discussing the quality of humic substances from different origin. Regarding desired applications, these quantitative parameters can also provide an easy comparison with other synthetic or natural materials and they possess the great potential in computer simulation of transport phenomena in natural environments.

Nevertheless, studies of diffusion in humic systems are relatively scarce. Wang et al. (2004) investigated the effect of HAs on Eu^{3+} diffusion in compacted bentonite. They found that HAs hinder the Eu^{3+} diffusion

---

* Corresponding author. Tel.: +420 541149488; fax: +420 541149398.
E-mail address: sedlacek-p@fch.vutbr.cz (P. Sedláček).

and migration because of formation of Eu–humic complexes which precipitate at the surface of compacted bentonite. Consequently, only a small part of Eu exists as a free ion. Wold and Eriksen (2007) carried out similar experiments with diffusion of Eu^{3+}, Co^{2+}, and humic colloids through compacted bentonite. Humic colloids diffused through the bentonite regardless its compaction. The apparent diffusivities of both metals increased significantly in the presence of humic colloids. Seki and Suzuki (1999) prepared composite adsorbents containing humic acids entrapped in an alginate gel and carried out a kinetic study of lead adsorption to this gel. The shrinking core model was used to determine apparent lead diffusion coefficients in the gels.

HAs are usually found in highly humid environments (water sediments, peat etc.) in swollen form, hence recent contributions focus on the study of HAs in a form of the hydrogel. Our previous results confirmed that kinetics of metal–humic interactions is generally dependent on the colloidal state of HAs (Klučáková and Pekař, 2005). The gel models a transport in highly wet substrates where molecular diffusion plays the major role in mass transport. It can stand for real substrates like highly wet sediments, mud etc. Further, coal is known to swell in aqueous media; applications of low-rank, humic-rich coal as soil conditioner and as a plant nutrition support are well known. Controlled release of nutrients from coal-derived amendment would be diffusion-controlled rather than dissolution-controlled and knowledge on diffusion in humic gels can be also important for the design of such systems. Even if the true state of humic materials in soils and sediments is far from mineral-free form of used HAs, the system is acceptable in terms of description of the transport affected by complex interaction with humic constitu-ents; simple interactions with the mineral content are well-observed and described by basic adsorption kinetics (a detailed review is given in McBride, 1991).

Besides good simulation of natural humic environments, the gel form of HAs provides some additional benefits. The most valuable one is the possibility of preparation of samples with defined size and shape, which is necessary for mathematical description of the observed processes. The gel form of HAs can be considered a system allowing fixation of humic material while enabling interactions in its whole volume. Consequently, not only physicochemical interactions but also transport within humic matrix can be studied. Humic hydrogel can be prepared in a simple and cheap way using a method of guided coagulation (Martyniuk and Wieckovska, 2003). Therefore, humic hydrogel is proposed as a suitable colloid form of humic acids for diffusion experiments.

Cupric ion is well known for both its high affinity for humic substances (Stevenson,1982) and ability to form one of the strongest bonds with them. Due to the above and also because of easy quantification of Cu^{2+} content by means of UV–VIS spectroscopy, cupric ions have been chosen as a model heavy metal sorbate. Previous work (Klučáková and Pekař, 2004) demonstrated effective-ness of simple "tubing" method in diffusion studies of humic gels and determination of diffusion coefficients. The main goal of the recent work was to propose a suitable methodology for the study of cupric ions transport in a multiphase system containing humics, to estimate a correctness of applied mathematical model and to determine crucial diffusion parameters (i.e. diffusion coefficient, concentration ratio at the interface) for their subsequent application in modeling pollutant transport in nature and in artificial humic materials.

2. Experimental

2.1. Isolation of HAs

HAs were extracted from South-Moravia lignite by means of the alkaline extraction. The procedure represents our own modification of a published method (Piccolo et al., 1999) and has previously been utilized in other experimental work (e.g. in Klučáková and Pekař,

2008). Lignite was stirred with extractant (0.5 mol/L NaOH + 0.1 mol/L $Na_4P_2O_7$) in the 20 g per 1 dm^3 ratio for 12 h. The formed suspension was kept overnight and next day the solution was separated from the solid phase and acidified by 20% hydrochloric acid to pH below 1. The solid residue was put into another 1 dm^3 of extractant and after 1 h of stirring the extract was separated and acidified in the same way. The acid extracts were kept in the refrigerator overnight. Precipitated HAs were separated by means of centrifugation (4000 min^{-1}), washed in deionized water several times and centrifuged until Cl^- ions removal and dried at 50 °C. Before humic gel preparation, HAs were washed in water, centrifuged and dried once more. Obtained HAs were characterized by means of elemental analysis (CHNSO Microanalyser Flash 1112 Carlo Erba), FT-IR spectrometry (Nicolet Impact 400; measurement in KBr pellet) and UV–VIS (Hitachi U 3300). For UV–VIS spectroscopic characterization dry HAs (7 mg) were diluted by 0.1 mol/L NaOH and absorbance at wavelengths from 200 nm to 900 nm was measured.

2.2. Preparation of humic gel

For the preparation of humic gel, solid HAs were dissolved in 0.5 mol/L NaOH. The hydrogel was then acquired via the precipitation of sodium humate after acidification by HCl to pH below 1. The formed suspension was kept overnight and next day the mixture was centrifuged, the supernatant was discarded and the gel was repeatedly washed by deionized water and centrifuged.

2.3. Diffusion experiments

The diffusion study was divided into two experiments. The first one was focused on the diffusion from constant source of Cu^{2+}. Humic gel was packed into a plastic tube as a 5 cm long cylinder. Each cylindrical sample was then put separately into 50 mL of saturated $CuCl_2$ solution with one spoon of crystalline $CuCl_2$ added before. Different times of diffusion were chosen and each test was triplicated. After passing the chosen time, corresponding gel samples were sliced and each slice was extracted in 0.025 M NH_4–EDTA separately (100% effectiveness of the leaching of Cu^{2+} from humic gel to this agent had previously been experimentally confirmed). Cu^{2+} content in each extract was quantified by UV–VIS spectrophoto-metry, and the concentration profile of the gel cylinder and the cumulative diffusion flux across two solution–gel interfaces were determined.

In all remaining experiments, diffusion of cupric ions from time-variable sources was studied. The diffusion was implemented in the apparatus shown in Fig. 1. Again, humic gel was packed into a plastic tube and two side containers were filled with 2 mL of $CuCl_2$ solution
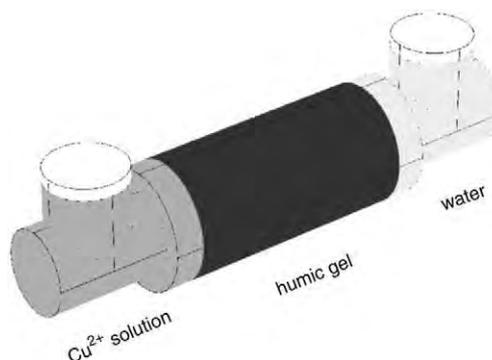

Fig. 1. Scheme of an apparatus for the study of a nonstationary diffusion.

and 2 mL of deionized water, respectively. Changing the initial concentration of $CuCl_2$ solution placed in the apparatus container monitored dependence of the cumulative diffusion flux on initial concentration of Cu^{2+} in solution. Initial values of Cu^{2+} concentration were 0.1 mol/L, 0.3 mol/L and 0.6 mol/L. Effect of time duration of diffusion experiment was tested then. The following times were chosen: 1 and 6 h, 1 day, 3 days and 5 days. Copper concentrations in the gel were analyzed as described previously for the constant source experiments.

3. Calculation

Diffusivity of cupric ions in the humic gel is determined by reduced mobility of ions in the gel phase (related to longer diffusion pathway in three-dimensional network as compared with diffusion in an aqueous solution) and by the complexation of ions by functional groups of humic acids (mainly carboxylic and phenolic –OH groups and aromatic rings). This paper deals with the transport of Cu^{2+} from aqueous solutions into humic gel samples. Mathematically, the concept of unsteady diffusion with chemical reaction in a semi-infinite media is adopted in two variations: diffusion from constant source and diffusion from time-variable source. For cylindrical gel sample, nonstationary diffusion of ions is assumed only through circular planes at both ends of gel cylinder. Mathematical description of transport phenomena arises from the solution of the Fick's equation

$$\frac{\partial c_g}{\partial t} = D_g \frac{\partial^2 c_g}{\partial x^2}, \tag{1}$$

where c_g is the concentration of Cu^{2+} at time t and distance x in a humic gel, and D_g is the effective value of Cu^{2+} diffusion coefficient in the humic gel. In this case, "effective value" means the value in which two effects are involved: chemical reaction between Cu^{2+} and HAs and porous character of the gel. From the analytical solution of Eq. (1), mathematical expressions for the concentration profiles of diffusing ions in the gel can be designed for corresponding conditions (for more details see Crank, 1956). *Initial condition*: before the experiment, homogeneous distribution of concentration of the diffusing substance is supposed. In this case, the concentration of metal ions in the gel in time $t=0$ is zero. *Boundary condition*: two concepts can be adopted according to the arrangement of a diffusion experiment. When the boundary of phase is kept at a constant concentration ($x=0$: $c_g=c_s$ for $t>0$), Eq. (1) can be processed by Laplace transformation and the time development of the concentration profile of diffusing substance in the gel can be calculated from Eq. (2).

$$c_g = c_s erfc \frac{x}{\sqrt{4D_g t}} \tag{2}$$

The condition mentioned above can be provided e.g. by diffusion of a salt from its saturated solution in which an addition of the crystalline form ensures constant concentration of the solution during the experiment.

Because the intensity of diffusion flux J can be expressed by the equation

$$J = -D_g \left(\frac{dc_s}{dx} \right)_{x=0} \tag{3}$$

the derivative of Eq. (2) incorporated into Eq. (3) gives the expression for the total amount of substance transported through the solution/gel interface (cumulative diffusion flux m)

$$m = 2c_s \sqrt{\frac{D_g t}{\pi}} \tag{4}$$

If concentration of the solution changes, (caused by the diffusion process), the concentration profile of diffusing substance in the gel can be expressed by equation

$$c_g = \frac{\varepsilon c_0}{(1 + \varepsilon \sqrt{D_g / D})} erfc \frac{x}{\sqrt{4D_g t}} \tag{5}$$

where ε is ratio of concentration of Cu^{2+} in the gel and in the solution in final equilibrium (at the hypothetical "end of diffusion"), c_0 is the initial concentration in the solution and D is the diffusion coefficient of Cu^{2+} in solution. The dependence of cumulative diffusion flux on time can be derived in a similar way like in the previous case (see Eq. (6))

$$m = \frac{2\varepsilon c_0}{1 + \varepsilon \sqrt{D_g / D}} \sqrt{\frac{D_g t}{\pi}} \tag{6}$$

4. Results and discussion

4.1. Characterization of used HAs and the humic gel

Results of the HAs elementary analysis illustrate the major content of H (42.12 at.%) and C (41.16 at.%); high content of O (15.64 at.%) and the minor amount of N and S (0.91 and 0.17 at.%, respectively). All values are normalized on dry ash-free HAs.

From the UV–VIS spectrum of sodium humate, standard optical characteristics were calculated. They are very useful for the determination of chemical structure of HAs (Stevenson, 1982). Absorption ratio A(280 nm)/A(465 nm) (calculated to 3.745) corresponds to the proportion between resistant lignin structures and "young" HAs (HAs with the low degree of humification).

A(465 nm)/A(665 nm) ratio (E4/6) represents so-called humification index. In case of HAs this index decreases with increasing molecular weight or degree of dispersion (Chen et al., 1977). Hence, low E4/6 (3.350) indicates high molecular weight of the applied humic acids. Kumada (1975) connected the value of $\Delta \log K$ ($\Delta \log K = \log A_{400} - \log A_{600}$) with the degree of humification of HAs. According to this value, the author distinguishes three basic types of the material: A-type ($\Delta \log K$ up to 0.6), B type (the value from 0.6 to 0.8) and R_p type (from 0.8 to 1.1); the higher the $\Delta \log K$ value represents the higher humification degree. The used HAs belong to A-type ($\Delta \log K = 0.565$) which indicates high degree of humification. Particular FT-IR, UV–VIS, elemental, ^{1}H and solid-state ^{13}C NMR characterization of used HAs can be found in more details in Peuravuori et al. (2006, 2007).

Resulting humic gel was characterized, too. About 86% of its total weight is represented by water content. As expected, results of oscillatory rheometry (not listed here) confirmed strongly viscoelastic behavior with the storage moduli (G') about one order higher than the lost moduli (G''). The concentration of dry ash-free HAs in the gel is about 107 g/L. Determination of acidity of the humic acids in various colloid forms including the gel was determined by the methods of conductometric and potentiometric titrations, the results are listed elsewhere (Klučáková and Kotková, 2007). The total and carboxylic acidities were 13.26 mmol/g and 6.63 mmol/g, respectively (as calculated per weight of the dry and ash-free humic acids). Total acidity is close to that of the corresponding sodium humate and slightly higher in comparison with related suspension.

4.2. Determination of the diffusion characteristics

For the determination of diffusion coefficient of Cu^{2+} in humic gel, values of total diffusion flux from saturated solution with constant concentration were examined. In Fig. 2, Cu^{2+} concentration profiles corresponding to different times of diffusion in humic gel samples can
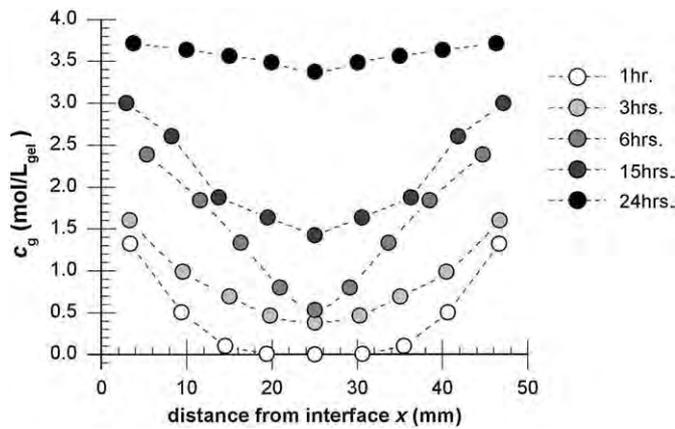
Fig. 2. Concentration profiles of Cu^{2+} in gel samples (constant source).
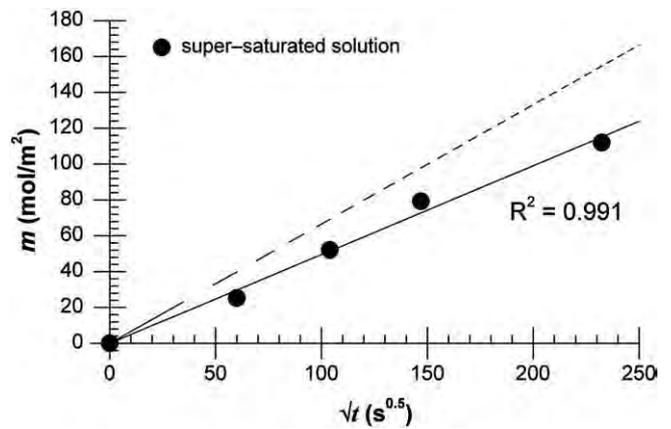
Fig. 3. Dependence of the total diffusion flux on the square root of time (constant source) as compared with the flux calculated for diffusion in water (dashed line).

be seen. In case of nonstationary diffusion of ions only through two circular planes at both ends of gel cylinder and for constant concentration of Cu^{2+} at solution/gel interface, the total diffusion flux dependence on the square root of time is supposed to be linear (see Eq. (4)). As can be seen in Fig. 3, agreement between this theory and experimental results is satisfactory. The figure also shows the difference from a solution calculated for diffusion in water. From the slope of the linear regression of experimentally determined dependence, the value of diffusion coefficient of cupric ion in humic gel was calculated (using Eq. (4)). Values of c_s were determined via the extrapolation of concentration profiles. The effective value of diffusion coefficient was calculated to 7.92×10^{-10} m^2 s^{-1}; diffusivity of Cu^{2+} in water is 1.43×10^{-9} m^2 s^{-1} (Lide, 1995). This value is in good agreement with published diffusivities of Cu^{2+} in various reactive hydrogels. Garmo et al. (2003) determined diffusion coefficients of 55 elements in DGT (Diffusive Gradients in Thin films) equipment which consisted of diffusive agarose polyacrylamide gel and iminodiacetate chelating resin. Effective coefficient of Cu^{2+} in this complex medium was in the range $5.5–6.6 \times 10^{-10}$ m^2 s^{-1} for pH 4.7–5.9. Scally et al. (2006) studied transport of Cu^{2+} in the gels used for DGT method as well. The solid weight content of the gel was close to that of humic gel (15%). They obtained values $6.30–6.45 \times 10^{-10}$ m^2 s^{-1} for agarose cross-linked polyacrylamide and $4.18–4.81 \times 10^{-10}$ m^2 s^{-1} for restricted polyacrylamide gel. The ranges correspond to various NaNO$_3$ amounts added to source solutions of Cu^{2+}.

As can be seen, diffusivity of Cu^{2+} in humic gel corresponds to about 55% of diffusivity in water. The decrease in diffusivity as compared with the aqueous solution allows a complex view on the manifold interaction between the ions and the humic matrix. All types of the interaction participate in this decrease, no matter if we suppose a complexation with acidic groups of humic acids, hydrophobic interaction or any other effects. In Klučáková and Pekař (2004), widespread approach is applied in explaining the value of the effective diffusion coefficient. The authors assume this value to be closely linked with the diffusivity in an inert medium D (medium with the same material characteristics but with zero effect of the interactions):

$$D_g = \frac{D}{1 + K},$$
(7)

where K represents the equilibrium constant of the interaction, when the direct proportionality between immobilized and mobile forms of the diffusing matter is presumed. In the first approximation, D can be substituted by diffusivity in an aqueous solution, because of the high water content in the gel. Using Eq. (7), we can consequently estimate a distribution of diffusing ions between mobile and immobilized fraction. The decrease in diffusivity to about 50% corresponds to $K = 1$, which indicates that about half the actual concentration of the

ions in the gel is immobilized in the form of a HAs-complex. This distribution was independently confirmed by extraction experiments using leaching agents of the different strength (unpublished results).

The next experiment was focused on Cu^{2+} diffusion into humic gel from solutions with time-variable Cu^{2+} concentration. Effects of time and initial concentration of Cu^{2+} in solution were tested. Experimental concentration profiles can be seen in Fig. 4. In analogous diffusion experiments, constant ratio of concentration of diffusing matter in the gel and in the solution at the interface is usually assumed. As is apparent from relation Eq. (6), the total diffusion flux through the interface should increase with initial Cu^{2+} concentration in the solution and with the square root of time linearly.

Diffusion fluxes were calculated as sums of concentration of cupric ions detected in the gel slices and were verified by spectroscopically measured decrease of the solution concentration (in average, 98% agreement was found). In no experiment, any Cu^{2+} break-through was observed from UV–VIS spectra of initially pure water behind the gel sample. Fig. 5 shows dependences of the diffusion flux on the initial solution concentration for 5 tested times. It can be seen, that linearity of all dependences is apparent and that the slope of linear regression increases with time duration of experiments.

Time dependence of total diffusion flux is much more complicated. In the region of very short times, total flux rises linearly with the square root of time in agreement with Eq. (6). The slope of this line (see solid lines in Fig. 6) increases with increasing initial concentration of cupric ions in the solution linearly. After 6 h initially linear
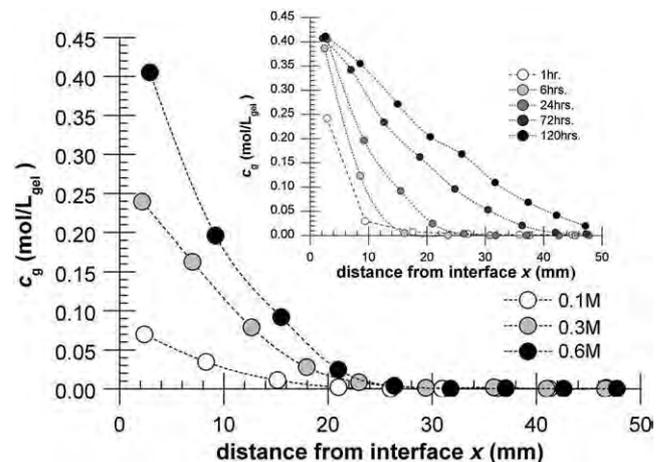
Fig. 4. Concentration profiles of Cu^{2+} in gel samples (time-variable source) for different initial concentrations of solution (larger figure; example for time duration 24 h) and for various times (smaller figure; example for initial concentration of solution 0.6 mol/L).
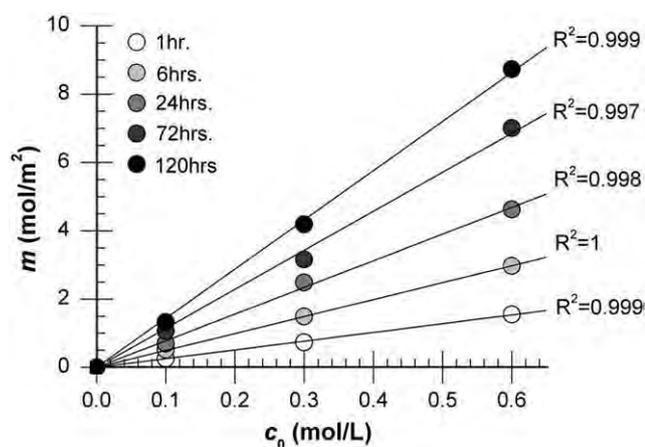
Fig. 5. Total diffusion flux as a function of the initial ion concentration in the solution (time-variable source).

Fig. 7. Time-shifting of theoretical constant ε.

dependence of diffusion flux deflects to lower values. The divergence rises with the square root of time proportionally so the following course of the diffusion flux is approximately linear, again. Discussed deflection of the time-dependence of the diffusion flux indicates some changes of solution–gel system occurring later. These changes make the velocity of diffusion slower than corresponds to the simple mathematical model.

Explanation of this behavior is not easy. Nevertheless, the most probable reason for this disagreement between theoretical relation and experimental data lies in preconditions linked with chemical reaction between HAs and Cu^{2+} ions. Diffusion of metal ions in humic gel combined with a complexation reaction provides a model described by partial differential equations based on Fick's laws, which cannot be solved analytically. We used simple equations, which consider so-called effective diffusion coefficient. Its value embraces diffusion transport combined with a chemical reaction on condition that the concentration of immobilized cupric ions is directly proportional to the concentration of free (movable) ions in humic gel. Main advantage of this model is its simplicity and relatively wide utilization. However, in case of diffusion in humic gel, real situation is much more complex. The complexity influences a partition of diffusing matter at the solution/gel interface which is described by the ratio of the ion concentration in the gel and in the solution — the partition coefficient ε. Its permanency is presumed while deriving Eqs. (6) and (5). If other possible influences (such as non-permanency of diffusion coefficient) are neglected and ε is calculated from experimental diffusion flux values following Eq. (6), with changing initial concentration of ions in the solution ε really stays constant, but there is a dependence of ε on the diffusion time which can be seen in Fig. 7. There are several possible explanations of this unexpected dependence,
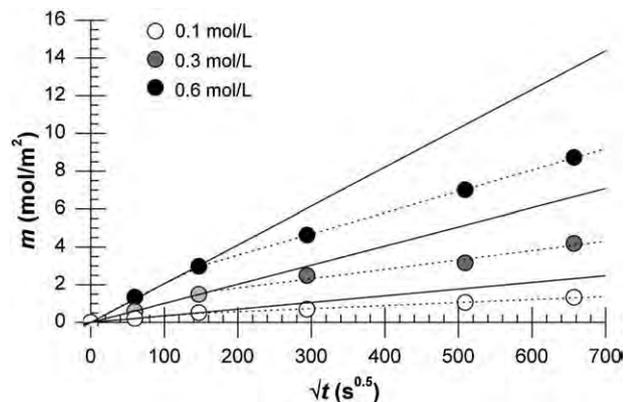
Fig. 6. Total diffusion flux as a function of the square root of time (time-variable source).
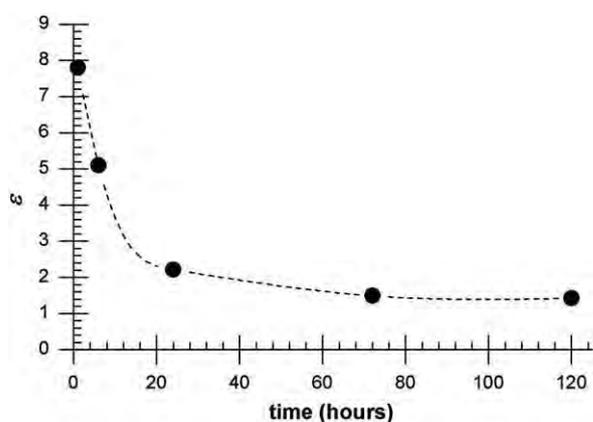
but until an experimental verification none of them can be accepted for a certainty. First possible reason of a shift of ε could be time-dependent Donnan potential between solution and negatively charged gel. Donnan potential enhances the concentration of metal cations at gel surface (Scally et al., 2006). This enhancement steepens the gradient within the gel and increases diffusion flux. As the reaction between acidic groups of HAs gel and transported Cu^{2+} neutralizes negative charge of the gel, Donnan potential decreases and so does the diffusion flux. The fall of Donnan potential is proportional to the diffusion flux of Cu^{2+} and therefore the deflection of time-dependence of the flux is most pronounced for the highest initial concentration of Cu^{2+} in the solution. For better understanding of this phenomenon, measurement for different ionic strengths should be repeated; at higher ionic strengths Donnan potential is negligible, with no effect on diffusion.

It is also necessary to keep in mind that although, in a first approximation, we assume diffusion of Cu^{2+} solely, in fact counterions (Cl^-) are transported into the gel, too. The shift of gel pH related to the accumulation of Cl^- certainly affects dissociation of acidic groups of HAs and their reaction with Cu^{2+}.

Other effects of the dependence of the diffusion flux on time are caused by the geometry of used experimental arrangement. We applied mathematical model of semi-infinite medium. Although no cupric ions were detected for $x \rightarrow 5$ cm (length of tube), obtained results could be influenced by interaction of humic gel with deionized water from a side container. This interaction can affect water content in humic gel. Consequently, diffusivity of Cu^{2+} in the gel could become time-dependent. Furthermore, the source solution does not have the character of a semi-infinite medium; its volume is quite low comparing to the volume of gel phase. Besides, while deriving whole mathematical apparatus the diffusion coefficient was supposed to be independent on Cu^{2+} concentration. Possible dependence of D_{eff} on the concentration of cupric ions in solution should be experimentally examined so as to be able to discuss its participation on the above-mentioned abnormalities.

The knowledge of the ε allows the calculation of theoretical concentration profiles of the Cu^{2+} in the humic gel for individual experiment conditions (initial concentration and time duration). Examples in Fig. 8 show good agreement between calculated and measured concentration profiles. This agreement supports ideas presented in the previous paragraphs. Fig. 8 also illustrates the difference between diffusion in the hydrogel and in aqueous solution.

4.3. FT-IR analysis

The FT-IR spectra of dried hydrogels illustrate the way Cu^{2+} ions are bound in humic gel. The measurements were performed in KBr pellet in a spectral domain 400–4000 cm^{-1}. The result for humic acids used in the gel preparation shows typical transmission spectrum of highly
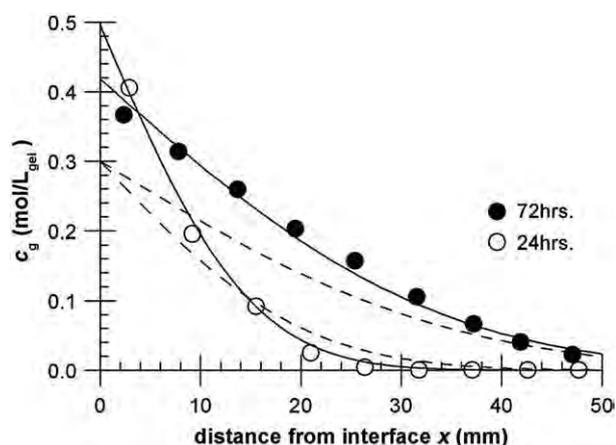
Fig. 8. Comparison of the experimental (points) concentration profiles (c_0=0.6 mol/L) with those calculated for determined diffusion characteristics (solid line) and for diffusion in water (dashed lines).

Fig. 9. Transmittance FT-IR spectra of used HAs (A), humic gel (B) and humic gel with diffused Cu^{2+} ions (C).

humified organic matter. It is well known that oven drying of HAs can cause irreversible changes of surface areas, including cross-linking and perhaps even decarboxylation. Nevertheless, there is no evident difference between IR spectra of used HAs and spectra of dried humic gel. Therefore, important chemical or structural changes of HAs taking place during these procedures were not confirmed.

Consequently, several differences which can be found in the IR spectrum of dried humic gel with diffused Cu^{2+} can be caused by interactions between HAs and Cu^{2+}. Wide absorption band at about 3400 cm^{-1} represents moisture; HAs form hydrocomplexes with cupric ions. This band makes detail interpretation of the spectrum in the range from 3500 cm^{-1} to 3000 cm^{-1} impossible (therefore, this spectral domain is not shown). Important changes occur below 2000 cm^{-1} as can be seen in Fig. 9. Complexation of Cu^{2+} affects absorption bands of the carboxylic groups markedly. In the area of 1700 cm^{-1}, where the absorption of carboxylic –OH takes place, strong decrease of the absorption peak can be seen in comparison with spectra of HAs and the raw gel. Moreover, absorption band with its maximum at about 1610 cm^{-1} corresponding to dissociated –COO^- is shifted to lower wavelengths (1604 cm^{-1}). Intensity of a small wide band resulting from vibration of phenolic –OH groups (around 1370 cm^{-1}) decreases after the diffusion of Cu^{2+}. Similar observations concerning Hg^{2+}–humate complexes are listed and explained in details in literature (Terkhi et al., 2008) and some more focused on Cu^{2+}, Pb^{2+} and Ca^{2+} complexes are also referenced to (Piccolo and Stevenson, 1982). These results verify published participation of carboxylic and phenolic groups of HAs on the complexation of metal ions. This complexation releases H^+ ions that increase the acidity of side water solutions. This fact was experimentally confirmed; pH of deionized water in the side container decreased with increasing time and with increasing initial concentration of Cu^{2+} solution (i.e. with increasing flux of Cu^{2+} into the gel).

5. Conclusions

Humic acids (HAs) represent a valuable material for various applications utilizing their outstanding sorption ability. Mainly for agricultural use, it is necessary to combine classical sorption experiments with a modeling of the sorbate transport in humic material which simulates natural form of HAs. The article deals with the study of cupric ions diffusion in the humic hydrogel. The experimental part is focused on the determination of diffusion coefficient of Cu^{2+} in humic gel (calculated value corresponds well with the one determined by another method in previous work (Klučáková and Pekař, 2005) and on effects of the main experimental parameters (initial concentration of Cu^{2+} in solution and diffusion time) on the total diffusion flux across the solution–gel interface. The
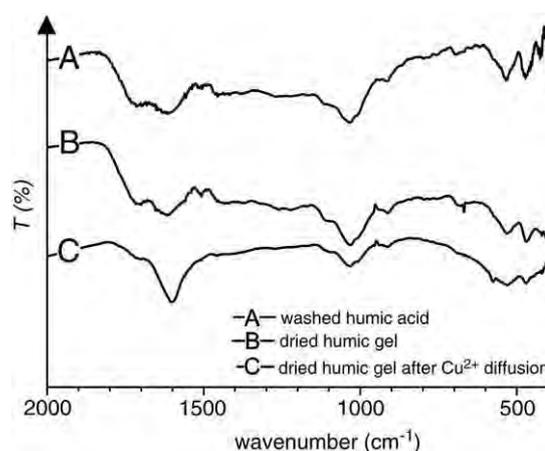
knowledge of determined diffusion characteristics (i.e. diffusion coefficient and partition of Cu^{2+} at the interface) is essential for subsequent experiments which will focus on an effect of other physicochemical parameters (e.g. solution pH, ionic strength).

It was found that theoretically constant partition of Cu^{2+} at the solution/gel interface is time-dependent. The shift of ε is more pronounced for higher diffusion flux of Cu^{2+} and causes an incurvation of theoretically linear dependence of the diffusion flux on the square root of time. The explanation of this phenomenon will be taken as the scope for a future experimental work.

The main aim of the work was to check the applicability of used devices and means (designed apparatus and mathematical model) in diffusion experiments. In general, diffusion measurements seem to provide valuable method for reactivity mapping studies on humic substances. Parameters such as effective diffusion coefficients of common pollutants in hydrogel forms of humic acids can be used in order to discuss the quality of humic substances from different origin in comparison with other synthetic or natural materials regarding desired application (e.g. in agriculture). Although the presented apparatus is very simple and could be improved for following experiments (higher solution volumes should be used), experimental data are valuable and they also fit theoretical calculations well. Consequently, it can be concluded that this method proved to be a very useful natural-like model for the wide spectrum of diffusion experiments using hydrogel forms of humic substances.

References

Chen, Y., Senesi, N., Schnitzer, M., 1977. Information provided on humic substances by E4/E6 ratios. Soil Sci. Soc. Am. J. 41, 352–358.
Crank, J., 1956. The Mathematics of Diffusion. Clarendon Press, Oxford.
Garmo, A., Røyset, O., Steinnes, E., Flaten, T.P., 2003. Performance study of diffusive gradients in thin films for 55 elements. Anal. Chem 75, 3573–3580.
Kerndorff, H., Schnitzer, M., 1980. Sorption of metals on humic acid. Geochim. Cosmochim. Acta 44, 1701–1708.
Klučáková, M., Kotková, L., 2007. Acid–base properties of humic acids in various dispersion forms. 11th Conference on Environment and Mineral Processing. Part II. Ostrava, 31.5.–3.6.2007, pp. 91–95. 978-80-248-1278-6.
Klučáková, M., Pekař, M., 2003a. Study of structure and properties of humic and fulvic acids. III. Study of complexation of Cu^{2+} ions with humic acid in sols. J. Polym. Mater. 20, 145–154.
Klučáková, M., Pekař, M., 2003b. Study of structure and properties of humic and fulvic acids. IV. Study of interactions of Cu^{2+} ions with humic gels and final comparison. J. Polym. Mater. 20, 155–162.

Klučáková, M., Pekař, M., 2004. Study of diffusion of metal cations in humic gels. In: Ghabbour, E.A., Davies, G. (Eds.), Humic Substances: Nature's Most Versatile Materials. InTaylor & Francis, New York, pp. 263–274.

Klučáková, M., Pekař, M., 2005. Physical and chemical kinetics in humic dispersions. In: Ghabbour, E.A., Davies, G. (Eds.), Humic Substances: Molecular Details and Applications in Land and Water Conservation. InTaylor & Francis, New York, pp. 167–188.

Klučáková, M., Pekař, M., 2006. New model for equilibrium sorption of metal ions on solid humic acids. Colloids Surf., A Physicochem. Eng. Asp. 286 (1–3), 26–133.

Klučáková, M., Pekař, M., 2008. Behaviour of partially soluble humic acids in aqueous suspension. Colloids Surf., A Physicochem. Eng. Asp. 318 (1), 106–110.

Klučáková, M., et al., 2000. Structure and properties of humic and fulvic acids. I. Properties and reactivity of humic and fulvic acids. J. Polym. Mater. 17, 337–356.

Klučáková, M., et al., 2002. Study of structure and properties of humic and fulvic acids. II: Study of adsorption of Cu^{2+} ions to humic acids extracted from lignite. J. Polym. Mater 19, 287–294.

Kumada, K., 1975. The chemistry of soil organic matter. Food Fertil. Technol. Centre 22, 10–36.

Lide, D.R., 1995. Handbook of Chemistry and Physics, 76th Edn. CRC Press, New York.

Martyniuk, H., Wieckovska, 2003. Adsorption of metal ions on humic acids extracted from brown coals. J. Fuel Process. Technol. 84, 23–36.

McBride, M.B., 1991. Processes of heavy and transition metal sorption by soil minerals. NATO ASI Series, Series E: Applied Sciences, 190 (Interact. Soil Colloid–Soil Solution Interface), pp. 149–175.

Peuravuori, J., Zbankova, P., Pihlaja, K., 2006. Aspects of structural features in lignite and lignite humic acids. Fuel Process. Technol. 87 (9), 829–839.

Peuravuori, J., Simpson, A.J., Lam, B., Zbankova, P., Pihlaja, K., 2007. Structural features of lignite humic acid in light of NMR and thermal degradation experiments. J. Mol. Struct. 826 (2–3), 131–142.

Piccolo, A., et al., 1999. Effects of mineral and monocarboxylic acids on the molecular association of dissolved humic substances. Eur. J. Soil Sci. 50 (4), 687–694.

Piccolo, A., Stevenson, F.J., 1982. Infrared spectra of Cu^{2+} Pb^{2+} and Ca^{2+} complexes of soil humic substances. Geoderma 27, 195–208.

Scally, S., Davison, W., Zhang, Hao, 2006. Diffusion coefficients of metals and metal complexes in hydrogels used in diffusive gradients in thin films. Anal. Chim. Acta 558, 222–229.

Seki, H., Suzuki, A., 1999. Kinetic study of lead adsorption to composite biopolymer adsorbent. J. Colloid Interface Sci. 211, 375–379.

Stevenson, F.J., 1982. Humus Chemistry: Genesis, Composition, Reactions, 2nd ed. Wiley-Interscience Publ., New York.

Terkhi, M.C., et al., 2008. Fourier transform infrared study of mercury interaction with carboxyl groups in humic acids. J. Photochem. Photobiol. Chem. 198, 205–214 (2008).

Tipping, E., Hurley, M.A., 1992. A unifying model of cation binding by humic substances. Geochim. Cosmochim. Acta 56, 3627–3641.

Wang, X., Chen, Y., Wu, Y., 2004. Diffusion of Eu(III) in compacted bentonite — effect of pH, solution concentration and humic acid. Appl. Radiat. Isotopes 60, 963–969.

Wold, S., Eriksen, T., 2007. Diffusion of humic colloids in compacted bentonite. Phys. Chem. Earth 32, 477–484.

Appendix 3

Kalina, M., Klučáková, M., and Sedláček, P. Utilization of fractional extraction for characterization of the interactions between humic acids and metals. *Geoderma* **2013**, 207–208, 92–98.

CrossMark
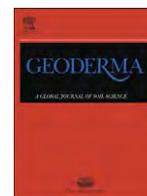
Utilization of fractional extraction for characterization of the interactions between humic acids and metals

Michal Kalina *, Martina Klučáková, Petr Sedláček

Brno University of Technology, Faculty of Chemistry, Centre for Materials Research CZ.1.05/2.1.00/01.0012, Purkyňova 464/118, 612 00 Brno, Czech Republic

ARTICLE INFO

ABSTRACT

Diffusion experiments in humic hydrogels provide valuable findings on reactivity of humic matrices. This article concentrates on the study of interactions between humic acids and copper(II) ions in diffusion experiments. The diffusion experiments were supplemented with selective extraction of the diffused copper(II) ions. For this purpose, the leaching agents with increasing affinity towards copper(II) ions were used. The presented results showed that several different forms of the diffused ions exist in the humic gel, which is given by the strength of bonds towards humic acids. Distribution of copper into these forms becomes constant after some initial period, which indicates local equilibration of interactions between the ions and the humic content of the gel during the transport process. The proposed experimental method seems promising in order to shed new light on the effects of humic acids reactivity on mobility of important compounds in nature.

© 2013 Elsevier B.V. All rights reserved.

1. Introduction

Humic substances are currently assumed to be the most widely distributed organic material on the earth's surface. They are formed through the biological activity of microorganisms and through the biochemical changes of organic residues. According to their solubility, humic substances are classified into three main fractions: fulvic acids are soluble in aqueous media, humic acids (HA) are insoluble under acidic conditions and humins stay insoluble throughout the whole range of pH-values. Humic materials are present in soils, waters, sediments and coals (Stevenson, 1982). Humic acids, as the major fraction of humic substances, were even extracted from a living plant (Ghabbour et al., 1994). The main sources of HA are peat and coal, from which they can be extracted by well-known chemical methods (Stevenson, 1982). HA represent material of outstanding biological and environmental impact. The main function of HA in soils and sediments is to impact the porosity and to act as a sorbent and reservoir of water and different kinds of chemicals (Jansen et al., 1996). Many potential applications of HA in agriculture, industry, environmental engineering and medicine are listed in Schnitzer and Khan (1972) and Peña-Méndez et al. (2005). For many decades, HA have been substantially investigated in light of their remarkable affinity towards heavy metals and they have frequently been proposed for utilization in decontamination of areas loaded with toxic metals (Tipping and Hurley, 1992).

Heavy metals naturally exist in different chemical forms and can be bound to various matrices with different bond strength. Determination

of different metal binding modes can give us the information on their mobility, (bio)availability or toxicity. This can be essential for description of their effects on nature, especially on the living organisms. Diversity in metal-binding ability of a soil can be assigned to its complex nature; different soil constituents have a different ability to reduce mobility or even to immobilize metal ions. Among these constituents, organic matter and especially humic substances play the key role. In Kyziol et al. (2006), sorption of chromium on different fractions of natural organic matter was studied. The results indicate that most Cr(III) ions were immobilized in a stable complex, only a small fraction was bound by ion exchange mainly to aliphatic carboxylic acids.

The widely used method for determination of the mobility of metals in soils is leaching by chemical extractants (Main et al., 2000). Using the method of sequential extraction, the whole amount of metals, originally sorbed on organic matter, is divided into different fractions by sequential addition of various extractant agents. The leached amount of the metal is then given by the strength of the extraction agent (and thus the strength of metal-soil interaction). The first studies proposing sequential extraction for this purpose were designed by Tessier et al. (1979). Tessier et al. (1979) distinguished five different groups of metal ions according to their bond strengths towards soil: exchangeable, bound to soils carbonates, bound to iron and manganese oxides, bound to organic matter and the residual fraction. Zeien and Bruemer (1991) came with an even more selective technique for sequential extraction of metals from soil samples. Following their procedure, the metal content is fractionated into seven fractions. Other works (Slavek et al., 1982; Rauret, 1998; Groenflaten and Steinnes, 2005) submit modifications of Tessier's extraction technique. These studies indicate chelating agents (EDTA, DTPA and their salts) and acid solutions (e.g. HCl, HNO_3, HAc) to be the most efficient substances for

---

* Corresponding author. Tel.: +420 541 149 488.
  E-mail address: xckalina@fch.vutbr.cz (M. Kalina).

total extraction of the whole metal content. Further, the extraction yields decrease in following order: buffered salt solutions (e.g. NH_4OAc, NaOAc), salt solutions (e.g. $MgCl_2$, $CaCl_2$, $NaNO_3$, $BaCl_2$, $AlCl_3$, NH_4NO_3) and water. Copper is often used as a model heavy metal mainly because of its renowned affinity to humic acids (Stevenson, 1982). In Siqueria et al. (1989), the total extractability of copper(II) ions, previously sorbed on humic acids was verified, when 0.5 M HCl or 1 M HNO_3 was applied. To summarize, most of numerous extraction procedures proposed so far utilize ionic salt solutions (e.g. $MgCl_2$ or NH_4NO_3) as extraction agents for ion-exchangeable fractions of metals. The strong acids or chelating agents are utilized in order to leach the organic-bound fraction of metal ions.

Humic acids can be found as solids, colloidal solutions and also as swollen hydrogels in the nature. Simple laboratory procedures were proposed for preparation of model humic hydrogels (Martyniuk and Wieckovska, 2003; Sedláček and Klučáková, 2009a, 2009b). A hydrogel form of humic acids enables not only modeling the material's natural occurrence, but also brings some experimental benefits. It simplifies the manipulation with humic samples and allows their preparation in precise size and shape. As far as interactions between HA and other compounds are concerned, the gel form can be considered a system allowing fixation of humic matrix in aqueous medium while retaining its binding ability in the whole volume. Consequently, not only physico-chemical interactions of the studied compound with the humic content but also its simultaneous transport within the volume of the humic matrix are observed experimentally and the exact effect of the interactions on the transport are monitored. In such experiments, disturbance coming from mechanical and thermal convection of a liquid is markedly suppressed in the gel matrix compared to the above phenomena in liquid state. All the above mentioned advantages represent an outstanding support for the idea of studying transport (i.e. diffusion) processes in humic hydrogels. Such diffusion processes are (under appropriate experimental conditions) easily observed; moreover, the mathematical apparatus used for data evaluation is well explained (Crank, 1956) and provides some standard parameters – diffusion coefficients – that involve all interactions in the system.

1.1. Diffusion experiments

In previous works (Klučáková and Pekař, 2004; Sedláček and Klučáková, 2009a, 2009b), diffusion experiments in humic hydrogels were proposed and confirmed as suitable tools for the innovative study of reactivity of HA. The main object of this paper is to supplement the classical diffusion experiment in humic hydrogels with a subsequent selective extraction of individual ion fractions from humic matrices.

First part of the experimental procedure presented in the paper deals with the transport of copper(II) ions from aqueous solutions into humic gel samples. Numerous undemanding methods of choice for the study of diffusion in solid and semi-solid samples can be proposed; for example, the article by García-Gutiérrez et al. (2006) gives in-depth summary of such methods. Pros and cons of individual methods are exemplified by diffusion of both neutral (tritium) and ionic (Cl^-, I^-, SO_4^{2-}, Na^+, Ca^{2+}...) substances in compacted bentonite.

In experiments presented in this paper, diffusion proceeded from an aqueous solution of a copper(II) salt into cylindrical gel samples through both circular ends of the gel cylinder. Mathematically, the concept of unsteady diffusion with chemical reaction in a semi-infinite media was adopted concerning diffusion from time-variable source. Mathematical description of such non-stationary transport phenomena arises from the solution of Fick's law in the following form

$$\frac{\partial c_g}{\partial t} = D^0 \frac{\partial^2 c_g}{\partial x^2} + \dot{r}, \tag{1}$$

where c_g is the concentration of copper(II) ions at time t and distance x in a humic gel, D^0 is the value of diffusion coefficient of the ions in a gel matrix without assuming any chemical interaction between the diffusing compound and the environment (in other words, D^0 represents diffusion coefficient of ions in a hypothetical hydrogel with the same structural properties – e.g. porosity – as the real one, but without any ability to bind diffusing compound) and $\dot{r}$ represents the rate of chemical reaction between the ions and the humic matter in the gel.

If the Fickian character of the transport is preserved in the system, Eq. (1) can be simplified as follows:

$$\frac{\partial c_g}{\partial t} = D_g \frac{\partial^2 c_g}{\partial x^2}. \tag{2}$$

In this case, D_g stands for an "effective" value of diffusivity, a value in which the effect of chemical reaction between copper(II) ions and HA is already involved.

From the analytical solution of Eq. (2), mathematical expressions for the concentration profiles in the gel and for the total amount of diffusing ions can be derived considering the conditions of the particular experimental design (for more details see Ref. Crank (1956) and Cussler (1984)). In particular experiments, the time variation of concentration of the solution is caused by the diffusion process, and the concentration profile of diffusing substance in the gel can be expressed by equation

$$c_g = \frac{\varepsilon \, c_0}{(1 + \varepsilon \, \sqrt{D_g/D}} \, erfc \frac{x}{\sqrt{4 \, D_g \, t}} \tag{3}$$

where ε is the ratio of concentration of copper(II) ions in the gel and in the solution at the interface between both media, c_0 is the initial concentration in the solution and D is the diffusion coefficient of copper(II) ions in aqueous solution. The dependence of cumulative diffusion flux (total amount of the transported ions) on time can be obtained in a similar way in the following form

$$m = \frac{2\varepsilon c_0}{1 + \varepsilon \sqrt{D_g/D}} \sqrt{\frac{D_g t}{\pi}}. \tag{4}$$

The second term of the general Eq. (1) represents the rate of chemical reaction between copper(II) ions and HA and its exact mathematical formulation arises from the particular kinetic model of the interaction. For the first approximation, we can consider fast immobilization with the existence of local equilibrium between mobile and immobilized copper(II) ions. It is described by equilibrium constant K, which represents mathematically the proportionality constant between immobilized and mobile copper(II) ions. The higher is K, the more pronounced is the immobilization of copper(II) ions. Eq. (1) then turns to the following form

$$\frac{\partial c_g}{\partial t} = D^0 \frac{\partial^2 c_g}{\partial x^2} - K \frac{\partial c_g}{\partial t} \tag{5}$$

and consequently

$$\frac{\partial c_g}{\partial t} = \frac{D^0}{1 + K} \frac{\partial^2 c_g}{\partial x^2} = D_g \frac{\partial^2 c_g}{\partial x^2}, \tag{6}$$

$$D_g = \frac{D^0}{1 + K}. \tag{7}$$

Eq. (7) then defines mathematically, how the simple immobilization of the ions affects the value of their effective diffusion coefficient.

2. Materials and methods

2.1. Materials

Humic acids, studied in this work, were isolated by alkaline extraction from South-Moravian lignite (Klučáková and Pekař, 2004, 2005; Sedláček and Klučáková, 2009a). More details on chemical structure of both the original lignite matrix and isolated HA can be found in previously published papers (Barančíková et al., 2003; Klučáková and Pekař, 2005; Peuravuori et al., 2006, 2007). Barančíková et al. (2003) compared the lignite humic acids used in this work with samples extracted from various soil types on the basis of UV–vis and ^{13}C NMR spectroscopy. The results showed that the lignite humic acids have the lowest content of aliphatic C and the highest content of aromatic C in comparison with other (soil) samples. Klučáková and Pekař (2005) described acid–base properties and dissociation behavior of the lignite humic acids. They developed the model of partial solubility of humic acids in aqueous solutions and determined their pK_a values. Peuravuori et al. (2006, 2007) studied structural features of lignite and lignite humic acids by means of FT-IR, ^{13}C NMR, ^{1}H NMR and thermal degradation experiments. The structural differences between original lignite and extracted humic acids were relatively minor. The results verified that certain aliphatic compounds have their special tasks in the complicated structural network of the lignite humic acids in spite of their relatively high aromaticity. Authors referred to surprisingly large content of different carboxylic acids as their free-acid forms. The structural interpretations performed by special ^{1}H NMR pulse techniques verified the complexity of aliphatic moieties, the presence of hydroaromatic carbons, residual lignin derivatives, the abundance of aliphatic and aromatic carboxylic acids and the ability of aliphatics to form intermolecular bridges between aromatic building blocks. Elemental composition of the studied humic sample is listed in Table 1.

Humic hydrogel was prepared by dissolving HA in 0.5 M NaOH and acidifying the solution with HCl to value of pH close to 1. After 24 hours, the gel phase was separated from the solution by repeated centrifugation followed by washing with deionized water. The content of dry matter all prepared humic hydrogels ranged between $14.8 \pm 1.6\%$ (wt.).

All diffusion and extraction solutions were prepared using distilled millipore water (milli-Q).

2.2. Methods

Diffusion experiments were carried out with HA in the form of hydrogel. The gel was packed into the cylindrical glass tubes (length 3 cm, diameter 1 cm). These tubes were sunk into the source solution of 0.05 M CuCl$_2$. The copper(II) ions diffused into the humic gels through both circular planes at both ends of the tubes (Fig. 1).

In certain times (1, 3, 5, 7, 9, 11, 14 and 20 days), humic gel was sliced and the diffused copper(II) ions were extracted by selected leaching solution from each slice separately. All gel slices from the same tube were leached with the same extraction solution. The used leaching agents were water, 1 M MgCl$_2$ and 1 M HCl. The solutions were chosen on the basis of results published by Rauret (1998) and Tessier et al. (1979).

Copper content in all prepared extracts were determined by the means of an electrochemical analyzer EcaFlow 150 GLP. Obtained data were used for computing the concentration profiles of copper(II) ions in the tubes and diffusion fluxes (total amounts diffused in the gel at given times).

Table 1
Elementary analysis of studied humic acids (normalized on dry ash free sample).

	C	H	O	N	S
Atomic %	41.1	44.4	13.5	0.8	0.2
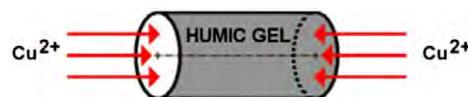
Fig. 1. Scheme of the diffusion of copper(II) ions into the hydrogels.

The source solutions of CuCl$_2$ were analyzed by an UV–vis spectrometer (Hitachi U 3900H) before and after the diffusion experiments. Diffusion fluxes were calculated from obtained decrease of concentration of copper(II) ions (caused by the diffusion process) in these solutions. These values were compared to the diffusion fluxes calculated for different fractions of diffusing copper(II) ions as the sum of copper(II) ions extracted for individual slices of the gel sample.

All the experiments were carried at laboratory temperature (25 ± 1 °C) in triplicate. The results are expressed as the mean values.

3. Results and discussion

The main goal of this work was the description of the interactions between humic acids and copper(II) ions in simple diffusion experiments. Fig. 2 shows the concentration profiles of copper(II) ions extracted with three different leaching solutions after 24 hours. The concentration profiles have the same symmetrical shape with the minimum in the middle. As can be seen, the individual extractants are able to leach different amount of copper(II) ions, which corresponds with their different affinity to the metal. Water is a weak leaching agent, which can extract only mobile fractions of copper(II) ions. In order to obtain the ion-exchangeable fraction of copper(II) ions 1 M MgCl$_2$ solution was used. But this agent is able to extract the ion-exchangeable fraction as well as the mobile fraction, therefore the real concentration profile of the exchangeable copper(II) ions is given by the difference between the data obtained for 1 M MgCl$_2$ solution and those acquired for water. Similarly, the difference between copper(II) ions extractable by 1 M HCl and by 1 M MgCl$_2$ solution is the fraction of strongly bound metal ions (Tessier et al., 1979 and Rauret, 1998). The concentration of copper(II) ions in the humic gel c_g at a given time t and distance x thus can be divided into three parts

$$c_g = c_{g,1} + c_{g,2} + c_{g,3}, \tag{8}$$

where $c_{g,1}$ is the concentration of the mobile fraction, $c_{g,2}$ is the concentration of the ion-exchangeable fraction and $c_{g,3}$ is the
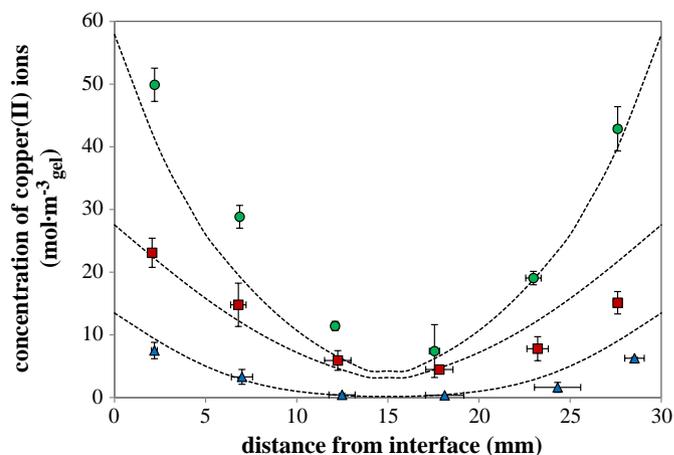
Fig. 2. Concentration profiles of diffused copper (II) ions extractable by water (△), 1 M MgCl$_2$ (□), 1 M HCl (○) after one day. Data fitted by theoretical Eq. (3) (dashed lines).

concentration of the strongly bound fraction of copper(II) ions. Using water as the leaching agent, $c_{g,1}$ can be measured directly. On the other hand, the measurements carried out using other leaching solutions give results corresponding with sums of concentrations: $c_{g,1} + c_{g,2}$ (1 M MgCl$_2$) and $c_{g,1} + c_{g,2} + c_{g,3}$ (1 M HCl). An accurate determination of $c_{g,2}$ or $c_{g,3}$ at a concrete distance x is not possible because we are not able to measure concentrations at the same distance x for all used extractants. As we can see in Fig. 3, the distance x can change not only with the extraction agent but also with time. Time development of concentration profiles in Fig. 3 shows also that the minimum in the middle disappears gradually and the concentration of copper(II) throughout the gel is constant after several days. On the basis of this fact, we determined ε values for the individual leaching solutions as the ratios of average concentration of copper(II) ions in the humic gel after twenty days (when the concentration is constant and it does not depends on the distance x in the gel for all used leaching solutions) and concentration of copper(II) ions in the solution surrounding the humic gel in tubes. The calculated values of ε for the individual leaching solutions are listed in Table 2. For 1 M HCl as an extractant, the ratio of concentration of copper(II) ions in the gel and in the solution at the interface between both media is higher than 1. It corresponds with the character of chemical reaction between humic acid and copper(II) ions in the diffusion process. The strongly bound metal ions are not able to diffuse in the gel and they are "invisible" for this process, because their chemical character differs from that of the diffusing copper(II) fraction. Similar situation can be observed in the case of MgCl$_2$, where ε value is close to 1. Although we cannot subtract a profile from another one, we can determine ε values for individual copper(II) fractions because

measured concentrations are not dependent on distance x after twenty days. Therefore we can calculate ε value for an ion-exchangeable fraction as

$$\varepsilon = \frac{c_{g,1} + c_{g,2}}{c} - \frac{c_{g,1}}{c}, \tag{9}$$

where the first fraction on the right side can be determined using 1 M MgCl$_2$ and the second one by water as an extractant (c is the concentration of copper(II) ions in solution surrounding humic gel); ε value for a strongly bound fraction can be determined analogously as the difference between data obtained using 1 M HCl and 1 M MgCl$_2$

$$\varepsilon = \frac{c_{g,1} + c_{g,2} + c_{g,3}}{c} - \frac{c_{g,1} + c_{g,2}}{c}. \tag{10}$$

The ε values computed for the individual fraction of copper(II) ions, presented in Table 3, were utilized for the determination of diffusion coefficients D_g. Our experiment was designed as the diffusion of copper(II) ions from the solution with time-variable concentration (Crank, 1956; Cussler, 1984; Sedláček and Klučáková, 2009a). It means that the concentration of copper(II) solution decreases gradually during diffusion of the metal ions into humic gel. If we assume that the value of D in the solution is equal to the published value for copper(II) ions in water $D = 1.43 \times 10^{-9}$ m^2 s^{-1} (Lide, 1995), we can compute the effective value of diffusivity D_g by means of Eq. (4). The dependence of total diffusion flux on the square root of time for the individual extractants and also for the individual copper(II) fractions is shown in Fig. 4. In an ideal case the constructed dependences should be linear for all three used extractants and all three fractions of extracted ions.
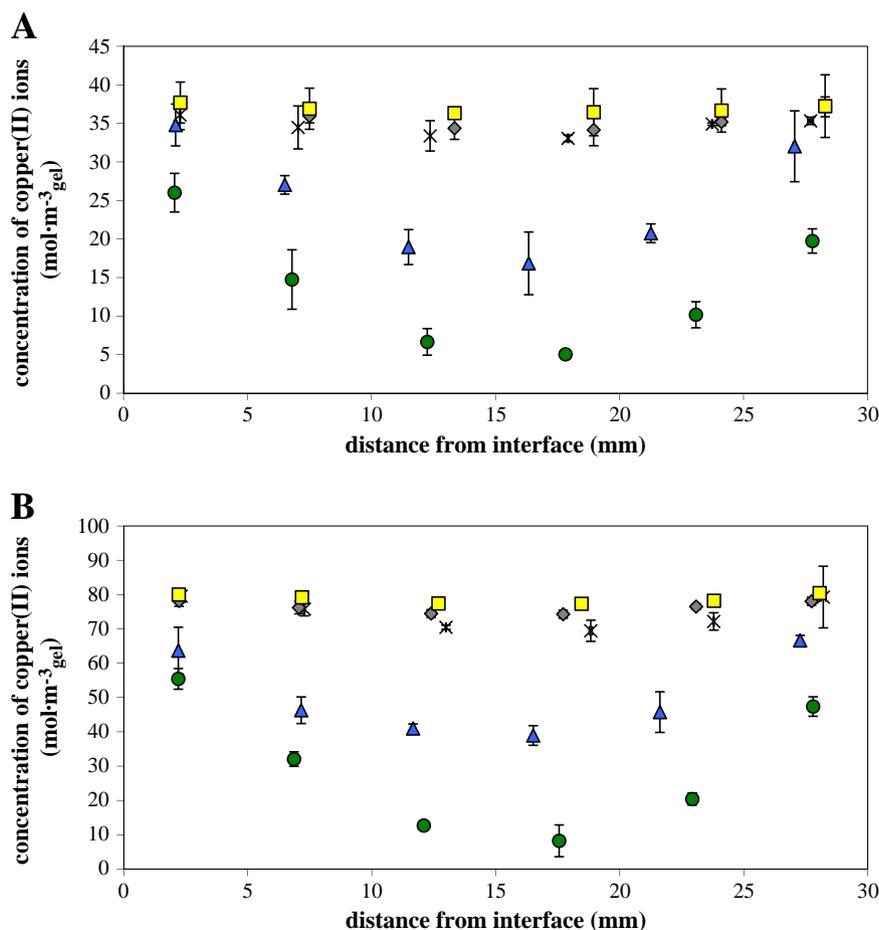
Fig. 3. Time development of concentration profiles of diffused copper (II) ions extractable by 1 M MgCl$_2$ (A) and 1 M HCl (B). The profiles after 1 (○), 3 (△), 7 (×), 11 (◇) and 20 (□) days are shown.

Table 2
The computed values of effective diffusivity in humic gel D_g, ratio of concentration of copper(II) ions in the gel and in the solution ε and apparent equilibrium constant K for the individual extractants.

Extractant	D_g (m^2 s^{-1})[a]	ε	K
Water	$2.11 \times 10^{-10} \pm 1.90 \times 10^{-12}$	$3.17 \times 10^{-1} \pm 1.67 \times 10^{-2}$	0
MgCl$_2$	$5.37 \times 10^{-10} \pm 2.10 \times 10^{-12}$	$8.69 \times 10^{-1} \pm 7.25 \times 10^{-2}$	$1.55 \times 10^0 \pm 1.03 \times 10^{-1}$
HCl	$1.40 \times 10^{-9} \pm 1.98 \times 10^{-12}$	$1.89 \times 10^0 \pm 8.04 \times 10^{-2}$	$5.65 \times 10^0 \pm 4.04 \times 10^{-2}$

[a] D^0 for water used as an extractant.

Table 3
The calculated values of effective diffusivity in humic gel D_g, ratio of concentration of copper(II) ions in the gel and in the solution (ε) and apparent equilibrium constant K for the individual copper(II) fractions.

Fraction	D_g (m^2 s^{-1})[a]	ε	K
Mobile	$2.11 \times 10^{-10} \pm 1.90 \times 10^{-12}$	$3.17 \times 10^{-1} \pm 1.67 \times 10^{-2}$	0
Ion-exchangeable	$5.03 \times 10^{-10} \pm 3.31 \times 10^{-12}$	$5.52 \times 10^{-1} \pm 4.44 \times 10^{-2}$	$1.39 \times 10^0 \pm 7.36 \times 10^{-2}$
Strongly bound	$3.75 \times 10^{-10} \pm 2.42 \times 10^{-12}$	$1.02 \times 10^0 \pm 7.64 \times 10^{-2}$	$7.81 \times 10^{-1} \pm 2.70 \times 10^{-2}$

[a] D^0 for the mobile fraction.

It is apparent, that for shorter duration of diffusion experiments all three curves provide linear dependence of diffusion flux on the square root of time as had been assumed according to the mathematical apparatus. All three dependences start to deviate from linear trend with increasing duration of diffusion experiments — the diffusion fluxes start to slow their increase with square root of time. Since the duration of diffusion experiment about 9 days, the fluxes stay constant.

The total fluxes for the individual copper(II) fractions in humic gel are calculated as the differences between measured diffusion fluxes of the individual extractants. The diffusion flux of the ion-exchangeable fraction is a difference between 1 M MgCl$_2$ and water. Analogously, the strongly bound fraction is a difference between 1 M HCl and 1 M MgCl$_2$. The diffusion fluxes could be subtracted because they do not depend on distance x, they were always measured for the whole
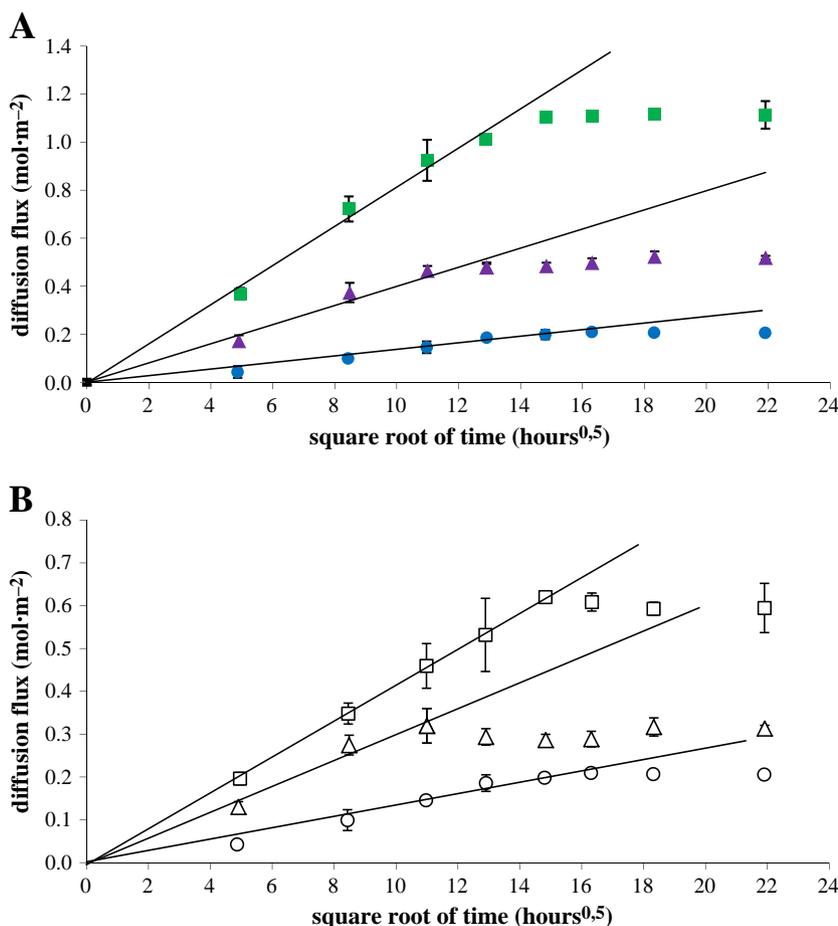
Fig. 4. The dependence of diffusion flux on square root of time (Eq. 4) for total diffusion fluxes determined using the individual extractants (A): water (●), 1 M MgCl$_2$ (▲), 1 M HCl (■); and for diffusion fluxes computed for the individual copper(II) fractions (B): mobile (○), ion-exchangeable (△), strongly bound (□). Linear parts of the dependences are fitted with lines.
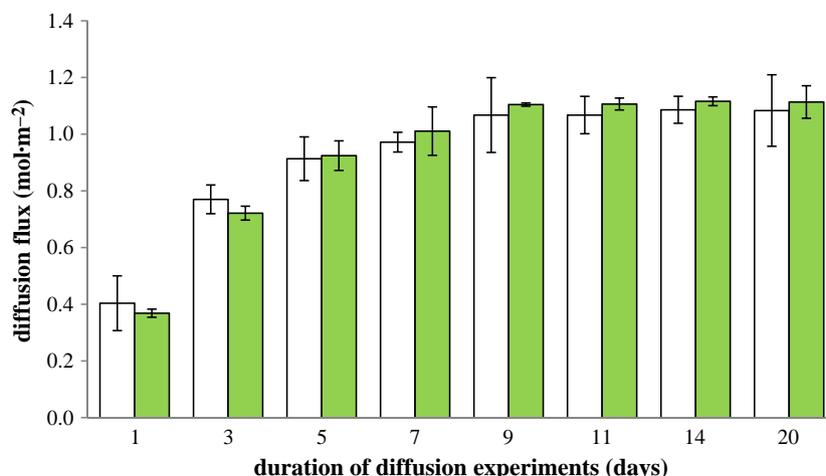
Fig. 5. The comparison of diffusion fluxes determined using 1 M HCl as extractant (empty columns) and results determined from the decrease of concentration of CuCl₂ solution during diffusion (full columns).

sample of humic gel in a given glass tube. The values of D_g were computed from the slopes of lines in Fig. 4. While the values in Table 2 are average ones valid for all fractions extractable by a given leaching solution, the values listed in Table 3 were computed for individual copper(II) fractions. In order to verify the determined D_g values we computed concentration profiles for the individual extractants and compared them with the experimental data. Selected data fitted by Eq. (3) are shown in Fig. 2. Good agreement between experiment and theory is apparent. In this case, D_g stands for an "effective" value of diffusivity, a value in which the effect of chemical reaction between immobilized and diffusing copper(II) ions is included. If we assumed that the diffusivity determined for the mobile fraction using water as extractant is D^0 and the value is influenced only by space arrangement of humic acid in the gel but not by the chemical reaction, we can compute also the apparent equilibrium constant K by means of Eq. (7). The value of K is then equal to 0 for the mobile fraction. The determined values are designated as "apparent" ones because the chemical reaction between copper(II) ions and humic acids in gel can be more complex than the simple transformation of "free" metal ions into immobilized ones, for example H^+ ions can split off in reaction of metal ions with COOH functional groups. It is interesting that K value is higher for ion-exchangeable copper(II) ions in comparison with the strongly bound ones (see Table 3). The above might be caused by affinity of acidic functional groups to copper(II) ions which is higher that affinity of other binding sites to

copper(II) ions (for example aromatic structures) (Klučáková and Pekař, 2006).

The solution of 1 M HCl was proved as the extraction agent able to leach all copper(II) ions in humic gel. This was concluded by comparison of experimental data and results acquired from the decrease of concentration of copper(II) ions in a particular solution surrounding humic gel (see Fig. 5). Although HCl solution was used as 100% effective leaching solution also in previous works (Klučáková and Pekař, 2004 and Klučáková and Pekař, 2009), the verification of its efficiency is very important. It was observed, that the efficiency decreases, if the content of copper(II) ions is very high and then the stronger extractant (e.g. EDTA) has to be used (Sedláček and Klučáková, 2009a, 2009b).

Simultaneously, our results showed that the dependence of diffusion fluxes on square root of time for extraction with water corresponds to the changes of diffusion flux for mobile fractions of ions during the experiments. It is obvious that, the distribution of copper(II) ions between the fractions stays constant after passing certain time (see Fig. 6). This indicates equilibrium between the fractions, which is created and then maintained during the experiments.

4. Conclusions

The aim of this work was to explore the interactions between humic acids and copper(II) ions in diffusion. The research method
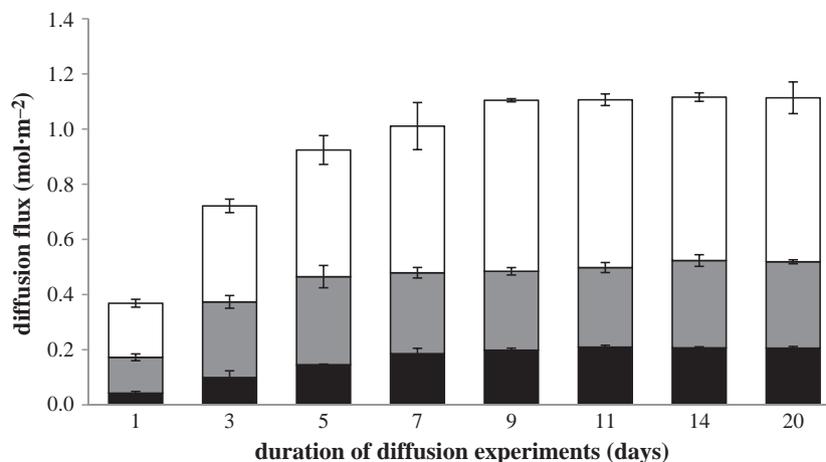
Fig. 6. The time dependence of diffusion fluxes of the individual copper(II) fractions: mobile (black), ion-exchangeable (gray), strongly bound (white).

combined the diffusion experiments with selective extraction of diffused ions. The common view on diffusion experiments as a method for studying the mobility of metals in chosen matrices was extended with the study of bond strength. The results showed that the interactions between copper(II) ions and humic acids can be classified into some main fractions, which corresponds to used extractants. In our case, water, 1 M MgCl$_2$ and 1 M HCl were chosen as leaching solutions. The distribution of copper(II) ions stayed constant after passing certain time. This indicates existence of an equilibrium which was created and maintained during the experiments. The obtained results showed that the used combination of methods is suitable for the study of mobility of metals and interactions between the metals and humic matrices that are considered as the main reactive parts of soils in nature.

Acknowledgements

References

Barančíková, G., Klučáková, M., Madaras, M., Makovníková, J., Pekař., M., 2003. Chemical structure of humic acids isolated from various soil types and lignite. Humic Substances Environment 3 (1/2), 3–8.

Crank, J., 1956. The Mathematics of Diffusion. Clarendon Press, Oxford.

Cussler, E.L., 1984. Diffusion: Mass Transfer in Fluid Systems. Cambridge University Press, Cambridge.

García-Gutiérrez, M., Cormenzana, J.L., col, 2006. Overview of laboratory methods employed for obtaining diffusion coefficients in FEBEX compacted bentonite. Journal of Iberian Geology 32, 37–53.

Ghabbour, E.A., Khairy, A.H., col, 1994. Isolation of humic acid from the brown alga *Pilayella littoralis*. Journal of Applied Psychology 6, 459–468.

Groenflaten, L.K., Steinnes, E., 2005. Comparison of four different extraction methods to assess plant availability of some metals in organic forest soil. Communications in Soil Science and Plant Analysis 36, 2699–2718.

Jansen, S.A., Malaty, M., Nwabara, S., Johnson, E., Ghabbour, E., Davies, G., 1996. Structural modeling in humic acids. Mater Science and Engineering C4, 175–179.

Klučáková, M., Pekař, M., 2004. Study of Diffusion of Metal Cations in Humic Gels. In: Davies, G. (Ed.), Ghabbour, E.A. Taylor& Francis, New York, pp. 263–274.

Klučáková, M., Pekař, M., 2005. Solubility and dissociation of lignitic humic acids in water suspensions. Colloids and Surfaces, A: Physiochem. Eng. Aspects 252 (2–3), 157–164.

Klučáková, M., Pekař, M., 2006. New model for equilibrium sorption of metal ions on solid humic acids. Colloids and Surfaces, A: Physiochem. Eng. Aspects 286 (1–3), 126–133.

Klučáková, M., Pekař, M., 2009. Transport of copper(II) ions in humic gel — new results from diffusion couple. Colloids and Surfaces, A: Physicochem. Eng. Aspects. 349 (1–3), 96–101.

Kyziol, J., Twardowska, I., Schmitt–Kopplin, Ph., 2006. The role of humic substances in chromium sorption onto natural organic matter (peat). Chemosphere 63, 1974–1982.

Lide, D.R., 1995. Handbook of Chemistry and Physics, 76th edn. CRC Press, New York.

Main, I., Arambarri, I., Garcia, R., Millán, E., 2000. Evaluation of heavy metal availability in polluted soils by two sequential extraction procedures using factor analysis. Environmental Pollution 110, 3–9.

Martyniuk, H., Wieckovska, J., 2003. Adsorption of metal ions on humic acids extracted from brown coals. Fuel Processing Technology 84, 23–36.

Peña-Méndez, E.M., Havel, J., Patočka, J., 2005. Humic substances — compounds of still unknown structure: applications in agriculture, industry, environment, and biomedicine. Journal of Applied Biomedicine 3, 13–24.

Peuravuori, J., Zbankova, P., Pihlaja, K., 2006. Aspects of structural features in lignite and lignitehumic acids. Fuel Processing Technology 87 (9), 829–839.

Peuravuori, J., Simpson, A.J., Lam, B., Zbankova, P., Pihlaja, K., 2007. Structural features of lignitehumic acid in light of NMR and thermal degradation experiments. Journal of Molecular Structure 826 (2–3), 131–142.

Rauret, G., 1998. Extraction procedures for the determination of heavy metals in contaminated soil and sediment. Talanta 46, 449–455.

Schnitzer, M., Khan, S.U., 1972. Humic substances in environment. New York.

Sedláček, P., Klučáková, M., 2009. Simple diffusion method applied in evaluation of metal transport in model humic matrices. Geoderma 153 (1–2), 11–17.

Sedláček, P., Klučáková, M., 2009. Diffusion experiments as a new approach to the evaluation of copper transport in humics-containing systems. Collect Czech Chem C. 74 (9), 1323–1340.

Siqueria, R.N.B., et al., 1989. Extracao selectiva de cadmio, chumbo, cobre e zinco pre-adsrvidos po acidos humicos. Quimica nova. 12, 9–13.

Slavek, J., Wold, J., Pickering, W.F., 1982. Selective extraction of metal ions associated with humic acids. Talanta 29, 743–749.

Stevenson, F.J., 1982. Humus Chemistry: Genesis, Composition, Reactions, second ed. Willey, New York.

Tessier, A., et al., 1979. Sequential Extraction Procedure for the Speciation of Particulate Trace Metals. Analytical Chemistry 51, 844–851.

Tipping, E., Hurley, M.A., 1992. A unifying model of cation binding by humic substances. Geochimica et Cosmochimica Acta 56, 3627–3641.

Zeien, H., Bruemer, G.W., 1991. Chemische extraktionen zur bestimmung von schwermetallbindungsformen in böden. Berichte aus der Oekologischen Forschung 6, 62–91.

Appendix 4

Sedláček, P., Smilek, J., and Klučáková, M. How the interactions with humic acids affect the mobility of ionic dyes in hydrogels – Results from diffusion cells. *Reactive and Functional Polymers* **2013**, 73, 1500–1509.
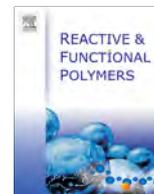
How the interactions with humic acids affect the mobility of ionic dyes in hydrogels – Results from diffusion cells

Petr Sedláček *, Jiří Smilek, Martina Klučáková

Brno University of Technology, Faculty of Chemistry, Materials Research Centre CZ.1.05/2.1.00/01.0012, Purkyňova 118, 612 00 Brno, Czech Republic

ABSTRACT

The complexation of charged compounds by humic acids represents the process of exceptional environmental importance. Nevertheless, traditional methods utilized in the complexation studies do not address the way, how these interactions affect the transport of ions in humic-rich environments. To overcome this dilemma, the diffusion cells technique is proposed as an innovative reactivity mapping technique. Using this method, the diffusion of methylene blue was studied in aqueous solutions and in agarose gels with and without the addition of humic acids. Experimental results clearly illustrate the immobilizing effects of humic acids on the transport of methylene blue in gels. The partitioning of methylene blue at the solution-gel interface and the specific interactions between methylene blue and humic acids is discussed on the basis of experimental data. Effective structural parameters of hydrogels (effective porosity, tortuosity factor) were calculated, as well as some standard diffusion and interaction parameters (diffusion and partition coefficients and apparent equilibrium constants).

© 2013 Elsevier Ltd. All rights reserved.

1. Introduction

Humic acids (HA) represent the crucial component of many non-living parts of nature, such as soils, waters and sediments, where they – in diverse colloidal forms – play numerous irreplaceable environmental roles. In soils and sediments, precipitated humic acids impact the porosity and act as sorbents and reservoirs of water and different kinds of chemicals [1], while, in water aquifers, dissolved HA serve as important colloidal carriers of solutes [2,3]. HA also represent a promising raw material. Many potential applications of HA in agriculture, industry, environmental engineering and even in medicine are proposed [4–6]. Exact structure of humic acids is still unknown – controversy lasts on whether HA are of macromolecular or supramolecular (i.e. aggregate) nature [7] – anyway, high content of diverse functional groups (e.g. carboxyls, phenols, aromatic rings) gives to these compounds an outstanding ability to bind solutes of various chemical nature.

It is generally accepted, that the mobility of ionic compounds in soils and waters is affected by their interaction with negatively charged dissolved or precipitated humic acids (HA) [4,8,9]. Ion–HA interactions are thus essentially of an electrostatic origin, but due to diverse degree of structural complexity of HA, it is not possible to explain or predict the destiny of ions in humic matrices

universally. For the experimental study of ion–HA interaction, the inspiration can be drawn from the studies on ion binding by standard polyelectrolytes (e.g. charged biopolymers like chitosan, hyaluronan or others). Many works were published on theoretical modeling of interaction between low-molecular ions and such compounds on the molecular scale [10–12], nevertheless, to our best knowledge, there is no standard experimental methodology utilized routinely in the observation and quantification of ion-polyelectrolyte matrices and their influence on the rate of transport in these systems. The most widespread experimental approaches are still based on simple adsorption experiments [13–16], nevertheless, the batch sorption approach brings several serious drawbacks as far as humic substances are utilized. For example, the size of colloidal humic particles is of a great importance; the homogenous distribution of particle sizes in such colloidal forms as sols or suspensions is always questionable and the interactions/sorption in such systems can be limited just to the surface of the particle. The actual experimental conditions – e.g. the rate of agitation of the mixture – play a crucial role as well.

Simple experimental techniques for the study on solutediffusion in hydrogels prepared from humic acids put forward an interesting experimental alternative, as was discussed in details in our previous works [17–20]. Such diffusion processes are easily realizable; the mathematical apparatus for the data evaluation is well explained [21] and provides some reasonable parameters – e.g. apparent diffusion coefficients – the values of which involve the interactions in the system. A comprehensive handlist of several simple laboratory methods is presented in [22,23] for the

---

* Corresponding author. Tel.: +420 54114 9486; fax: +420 54114 9398.
  E-mail addresses: sedlacek-p@fch.vutbr.cz (P. Sedláček), xcsmilek@fch.vutbr.cz (J. Smilek), klucakova@fch.vutbr.cz (M. Klučáková).
  URL: http://www.materials-research.cz/en (P. Sedláček).

Nomenclature

α	rock capacity factor (–)	K_{app}	apparent equilibrium constant (–)
β	cell constant (m^{-2})	L	sample thickness (m)
ε_{eff}	effective porosity (–)	L_e	actual distance traveled by diffusant (m)
Φ	partition coefficient (–)	n	total solute mass absorbed in gel (mol)
Φ_{app}	apparent partition coefficient (–)	r	Stokes–Einstein radius of solute (m)
η	dynamic viscosity (Pa s)	R	ideal gas constant ($J\ mol^{-1}\ K^{-1}$)
A	pre-exponential factor for diffusion coefficient ($m^2\ s^{-1}$)	t	time (s) (for better comprehensibility, the time unit is changed from seconds (s) to hours (h) in the figures and tables)
c	molar concentration (subscript D refers to the donor solution, subscript A to the acceptor solution and subscript "gel" represents the concentration inside hydrogel) ($mol\ m^{-3}$)	t_L	time lag (s) (for better comprehensibility, the time unit is changed from seconds (s) to hours (h) in the figures and tables)
D_0	free solution diffusion coefficient ($m^2\ s^{-1}$)	t	temperature (°C)
D_e	effective diffusion coefficient ($m^2\ s^{-1}$)	T	absolute temperature (K)
D_a	apparent diffusion coefficient ($m^2\ s^{-1}$)	T_m	tortuosity factor (–)
E_A	activation energy of diffusion ($J\ mol^{-1}$)	w	weight concentration (wt.%)
f	oscillation frequency (Hz)	x	direction of diffusion (m)
$|G^*|$	complex modulus magnitude (Pa)		
J_d	steady-state diffusion flux ($mol\ m^{-2}\ s^{-1}$)		
k	Boltzmann constant ($J\ K^{-1}$)		

experimental arrangement of the diffusion experiment. For the routine determination of diffusion coefficients in semi-solid samples (like hydrogels), the method of the diffusion cells (alternatively called the diaphragm, Stokes or Franz cells) represents the method of choice [24–27].

The main objective of this work was to test the applicability of the method of diffusion cells to study the interactions between humic acids (HA) and the model organic dye – methylene blue. In our previous works, several laboratory techniques were used in order to study the diffusion of ions in gel prepared from controlled coagulation of alkaline humic acids solutions simply by the decrease of their pH [17–20]. This humic gel reasonably modeled natural environments with homogenously distributed, partially dissolved, partially highly swelled solid humic substances. On the other hand, this hydrogel form was not suitable for the in-depth studies on the interactions between the humic content of gel and a diffusing solute, because such elementary properties of gels as the inner pH or relative content of HA were difficult to control. The preparation of interpenetrating polymer network (IPN) gels [28] from humic acids in a supporting gel-forming polymer is proposed to overcome these difficulties. Agarose (linear polysaccharide of red algae, made up of the repeating monomeric unit of agarobiose) was used as a supporting polymer in the experiments presented in this paper. The network of agarose chains is interpenetrated by molecules of HA at higher temperatures where both compounds are dissolved (>60 °C) and the mixture is then easily gelled by cooling to normal temperature (~20 °C). The mechanical and textural properties of agarose hydrogels as well as the gelation mechanism are well understood [29–31]. In the IPN hydrogels used in the presented paper, HA are immobilized and their reactive groups are homogenously distributed in the supporting agarose matrix.

The diffusion in agarose gels has already been subjected to a vast concern. Golmohamadi et al. [32] studied the self- and mutual- diffusion of Cd^{2+} and organic cations in agarose hydrogel by means of fluorescence correlation spectroscopy and the diffusion cell method, respectively. The gel's Donnan potential was measured and used for the explanation of discrepancy between the results of the mutual and self-diffusion measurements and of the pronounced enhancement of cation concentrations in hydrogel. For agarose hydrogels, the diffusion cells were utilized in determining the diffusion coefficient of e.g. humic acids [33], proteins

[34] or ethanol [35]. Other authors subjected agarose gels to other techniques for determining the diffusion coefficients such as the refractive index measurement [36], electronic speckle pattern interferometry [37], fluorescence correlation spectroscopy [38] or fluorescence recovery after photobleaching [39].

Methylene blue (MB) is well-known cationic organic dye, commonly used for dying cotton, wood and silk. As can be generalized for all organic dyes, its transport in nature is the matter of concern from both toxicological and aesthetical point of view. Many works focused on the sorption of methylene blue and other cationic dyes on humics and humic-rich materials in last decades. Guy et al. in their study on organocation speciation in natural waters [40] determined the sorption isotherms for MB on humic acids at different solution pH values and KNO_3 concentrations. The variation of pH was not found to play an important role during the sorption process. In the desorption studies it was found, that more than 50 wt.% of MB remains bound to HA at pH = 1 on contrary to other sorbates (paraquat, Cu^{2+}). Sheng et al. introduced a new photometric method which evaluates the adsorption capability of humic acids for another cationic dye – toluidine blue – from the difference between visible spectra of dye and dye-HA complex [41]. Contrary to previous authors, they found the pH and ionic strength to strongly influence the dye sorption on humics. Zhou et al. [42] presented a considerable enhancement of both the adsorption rate and the capacity of Fe_3O_4 nanoparticles for the MB sorption by coating these particles with humic acids. Moreover, the MB desorption ability and the reused performance of Fe_3O_4/HA nanoparticles were also excellent. Janoš [43] proposed iron humate as a cost-effective sorbent of basic dyes. Experimental data on sorption of several dyes including MB were evaluated by the multisite Langmuir isotherm model and gave the sorption capacities ranging from 0.01 to 0.09 mmol/g for individual dyes (0.03 mmol/g for MB). The leachability of dye from the loaded sorbent was found to be very low, especially in water. The sorption of methylene blue was only slightly affected by pH and the presence of inorganic salts, the presence of anionic surfactant (sodium dodecyl sulfate), however, dramatically enhanced the sorption of MB. In other works [44,45], the author studied the sorption of cationic and anionic dyes on oxihumolite – kind of oxidatively altered young brown coal that originated on the surface of lignite deposits by post-sedimentary oxidation. This material is composed of up to

70 wt.% by humic substances. The authors identified the interparticle diffusion processes as the main mechanism controlling the rate of the dye sorption. Fernandes et al. analyzed the removal of MB from aqueous solutions by peat, another humic-rich material [46]. The kinetics studies and the determination of adsorption isotherms were performed at different initial concentrations of MB and at three different temperatures. Fast equilibration of the sorption process was found – after 4.5 h, the equilibrium was reached at all studied temperatures. All the above mentioned examples clearly illustrate that the interactions between humic acids and organic dyes are a topic of an outstanding concern. The comprehensive reviews can be found summarizing the relative studies on the application of peat, coal and other diverse biomaterials as low-cost sorbents for removal of organic dyes [47,48] or MB in particular [49].

2. Theory

The method of diffusion cell (or *through-diffusion method*) represents one easy way to study the diffusion experimentally. In the presented work, the diffusion cell apparatus (see Fig. 1) was applied in order to study the diffusion of charged compound (methylene blue) in aqueous solution and in polyelectrolyte hydrogels, respectively.

In order to determine the diffusion coefficient of a solute in water (or other solvent), one compartment of the diffusion cell is filled with a solution of known concentration of the solute and the other with the solvent. The compartments are separated with a porous diaphragm – a glass frit, special membrane or even a piece of filter paper. The solute concentration in the compartments then changes with time according to equation (see e.g. [23]).

$$\ln \frac{(c_D - c_A)_t}{(c_D - c_A)_0} = -\beta D_0 t \qquad (1)$$

where D_0 is the diffusion coefficient of a solute in the solvent (commonly called *free solution diffusion coefficient*), $(c_D - c_A)_0$ and $(c_D - c_A)_t$ represent the difference between molar concentrations of diffusing matter in donor and acceptor compartments at time 0 and t, respectively. Coefficient β is the geometrical parameter (called 'cell constant') which specifies the apparatus and the membrane. In order to determine an unknown diffusion coefficient of studied solute in water, the diffusion cell apparatus is at first calibrated with an aqueous solution of a solute with well-known diffusivity. For this

purpose, KCl is commonly used (the method of calibrating the cell with KCl is described in details in [50]).

From the value of free solution diffusion coefficient D_0, the *Stokes–Einstein radius r* of the diffusing solute can be calculated as follows

$$D_0 = \frac{kT}{6\pi\eta r} \qquad (2)$$

where k is the Boltzmann constant, T is the temperature and η is the viscosity of the solvent. Besides, from the dependence of D_0 on the temperature, the *activation energy of diffusion E_A* can be calculated according to the general Arrhenius equation

$$D_0 = A \exp\left(-\frac{E_A}{RT}\right) \qquad (3)$$

The diffusion cell apparatus can simply be utilized also in the experimental studies on solute diffusion in porous materials. In these experiments, the diffusion cell compartments are separated by the studied porous specimen and the solute concentration in the acceptor compartment is measured as a function of time. Fig. 2 shows typical breakthrough curve obtained experimentally. As can be seen, the breakthrough curve shows two distinct parts, in the first part, which corresponds to the transient stage of the diffusion process, the solute penetrates from the donor compartment through the porous specimen – i.e. through a hydrogel in this work. Therefore, the concentration of the diffusant in the acceptor compartment is initially equal to zero and then (after its penetration through the hydrogel) slowly increases. At this stage, the transport of solute is driven by the time-dependent concentration gradient across the hydrogel, which comes from the unequal initial concentrations of the solute in both compartments of the diffusion cell apparatus. In the diffusion cell experiments, the transient stage of the process is characterized by the time lag t_L representing the x-axis intercept of the steady state portion of data, see Fig. 2).

Soon after the penetration of solute through the hydrogel, its concentration in the acceptor cell starts increasing linearly as the second – steady-state – stage of the diffusion process comes into act. At this period, the concentration difference between the opposite boundaries of the hydrogel specimen remains constant and a linear concentration profile of the solute across the gel is established. Due to the constant concentration difference, also the value of *diffusive flux J_d*, (i.e. the rate of change in the mass of solute per unit cross-sectional area perpendicular to the direction of transport; in mol m^{-2} s^{-1}) is time-independent during the stationary diffusion stage.
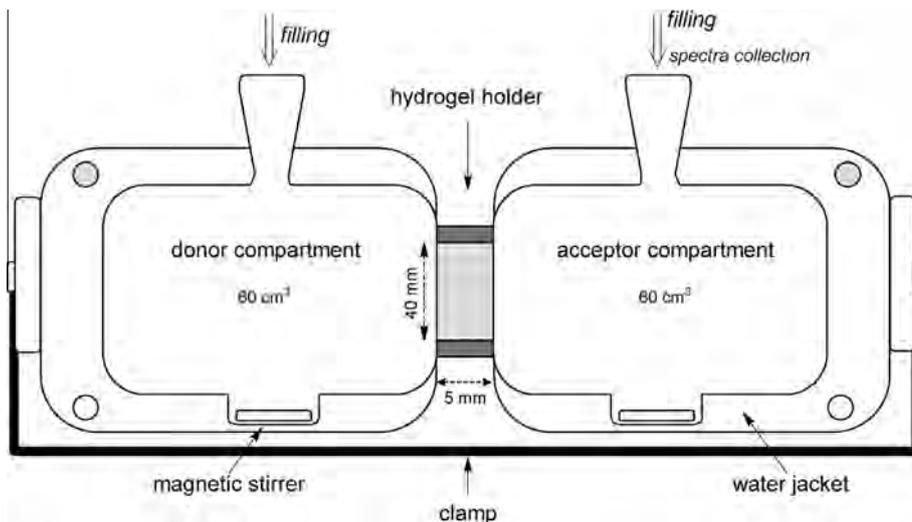
Fig. 1. Schematic representation of applied diffusion cell apparatus (drawing not to scale).
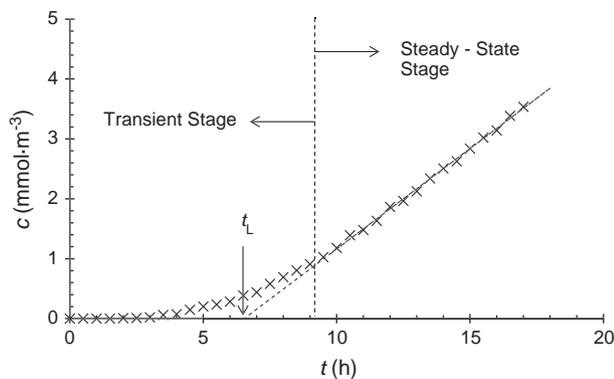
Fig. 2. Concentration of the solute in acceptor compartment as function of time (1 wt.% agarose hydrogel, 25 °C).

For the processing data from the diffusion cell experiments with porous materials, the theoretical model summarized by Shackelford and Moore (see [51]) was applied in this work. This theory is based on the assumption that the porous character of medium essentially affects the diffusion of a solute in two general ways. First, reduced cross-sectional area is available for the diffusive mass flux of the solute relative to the macroscopic cross-sectional area (because we assume that solute simply cannot penetrate into solid phase). Second, the existence of impenetrable solid phase results in more tortuous transport (solute pathway meanders through the medium). As a result, modified Fick's first law gives the formula for the steady-state diffusive flux of the solute through the porous specimen (the flux which stays constant during the second stage of the diffusion cell experiment):

$$J_d = \frac{\varepsilon_{eff}}{T_m} D_0 \frac{\Delta c_{gel}}{L} = D_e \frac{\Delta c_{gel}}{L} \qquad (4)$$

D_0 is the free solution diffusion coefficient, Δc_{gel} is the constant difference of molar concentration of the solute across the hydrogel specimen of thickness L, ε_{eff} is the *effective porosity* of the medium and T_m is the *tortuosity factor*, defined as follows

$$T_m = \left(\frac{L_e}{L}\right)^2 \qquad (5)$$

where L_e is the actual distance, traveled by a molecule of solute when overcoming a macroscopic distance L. Both structural effects are summarized in the value of *effective diffusion coefficient D_e*.

The concentration difference between the opposite boundaries of gel is not necessarily equal to the concentration difference between the solutions in donor and acceptor compartments, because hydrogel in a fact represents different phase than aqueous solution and a phase-equilibrium is established at the solution – gel interface. When the partitioning of the solute takes place between the two phases, a discontinuity in the concentration of solute at the interface occurs (see e.g. [52]), described by the following condition of phase equilibrium:

$$\frac{c_{gel}}{c} = \Phi \qquad (6)$$

where the *partition coefficient* Φ describes the distribution of solute between solution (molar concentration c) and hydrogel (molar concentration c_{gel}) at both boundaries of the specimen. The steady-state diffusion flux can be then expressed in the terms of constant difference between solute concentrations in the donor and acceptor solutions ($\Delta c = c_D - c_A$)

$$J_d = \Phi D_e \frac{\Delta c}{L} \qquad (7)$$

The transient stage of the through-diffusion process follows different rules than the steady-state stage. While in the steady-state stage the hydrogel is partially saturated by the diffusant and its distribution in the hydrogel does not change, the transient diffusion is affected by specific interactions between the solute and solid phase. The interactions proceed gradually with the movement of the diffusion front through the hydrogel and only after its breakthrough into the acceptor compartment the chemical equilibrium can be established in the whole hydrogel volume. Modified Fick's second law for the diffusion in porous media can be written as follows

$$\frac{\partial c}{\partial t} = \frac{D_e}{\alpha} \frac{\partial^2 c}{\partial x^2} = D_a \frac{\partial^2 c}{\partial x^2} \qquad (8)$$

This equation introduces the *apparent diffusion coefficient D_a* and the *rock capacity factor α*, which represents the ability of hydrogel to interact with the diffusant and to immobilize it in the internal hydrogel structure [51]. If the linear, reversible and instantaneous sorption of the solute on the solid content is assumed, the rock capacity factor can be expressed in the terms of *apparent equilibrium constant* of the sorption

$$\alpha = \varepsilon_{eff}(1 + K_{app}) \qquad (9)$$

where the apparent equilibrium constant K_{app} represents a sorbed-to-free solute mass ratio. In the through-diffusion experiments, the transient stage of the diffusion process is characterized by the time lag t_L, which is inversely proportional to the apparent diffusion coefficient according to (for the exact derivation, see [53])

$$t_L = \frac{L^2}{6D_a} \qquad (10)$$

Eqs. (9) and (10) are based on the following assumptions (for details, see Ref. [51]): if the solute cannot penetrate into the solid phase and diffuses only in the hydrogel pores filled by a solution, the time lag is not dependent on the pore cross-sectional area but only on the shape and real length of diffusion pathway in the internal pore structure of the hydrogel and the migration can be accompanied by specific interactions between the solute and the solid phase. In this case, the diffusant (small in comparison with pore size) behaves like the particle inside the 'tube' of complicated shape (with potentially reactive walls) and the duration of its migration through the tube is not affected by the tube diameter (the porosity inside the tube is equal to 1) but only by its effective length expressed by the tortuosity factor T_m and the chemical affinity of diffusant with solid phase around the tube represented by the apparent equilibrium constant K_{app}. Because the Fick's first law (Eq. (4)) is valid for the steady-state diffusive flux of the solute through the whole hydrogel specimen, the value of its effective porosity ε_{eff} as the portion available for the diffusion has to be used for the definition of the hydrogel rock capacity factor α (see [51]).

From the presented mathematical model, it can be seen, how the information about the chemical interactions between the solute and solid content of the porous medium can be extracted from through-diffusion data: at first, the values of apparent and effective diffusion coefficients are determined from the transient and steady-state stages of the breakthrough curve and, from their ratio, K_{app} is calculated if the effective porosity of the medium is known.

3. Materials and methods

3.1. Chemicals

Agarose (routine use class, <10 wt.% moisture content) and methylene blue hydrate (C.I. Basic Blue 9, dye content, ⩾95 wt.%) were purchased from Sigma–Aldrich and used without further

purification. Humic acids were isolated by alkaline extraction from South-Moravian lignite [17,19,54]. The total acidity and the content of carboxylic groups in HA were determined by means of potentiometric and conductometric titration on Schott TitroLine Alpha utilizing the methods of Riggle and von Wandruszka [55] and the standard Ca-acetate method [56], respectively. More details on the chemical structure of both the original lignite matrix and isolated HA (elemental and spectroscopic analysis), can be found in previously published papers [54,57].

3.2. Preparation of hydrogels

All hydrogels, utilized in subsequent diffusion experiments, were prepared via the thermoreversible gelation of aqueous solution of agarose. Agarose hydrogels (without addition of HA) were prepared from the aqueous solution of agarose (1, 2 and 4 wt.%), while agarose/HA gels from the aqueous solution of both agarose (1 wt.%) and HA (0.002, 0.005 and 0.010 wt.%).

A simple gelation procedure was applied: accurately weighted amount of agarose powder was dissolved in deionized water (preparation of agarose gels) or in aqueous solution of HA of the corresponding concentration (preparation of agarose/HA gels), respectively. The mixture was slowly heated when stirring continuously to 80 °C, maintained at the temperature until the occurence of the transparent solution. The solution was subsequently degassed in ultrasonic bath for 1 min. (at 80 °C) and slowly poured between two glass slides placed on the opposite sides of plastic ring mold (the mold and the slides were pre-heated to 80 °C to prevent rapid cooling of the mixture at the contact with the mold). Upon the cooling to room temperature, the mixture gradually solidified into the cylindrical hydrogel plate sample (40 mm in diameter and 5 mm thick). The removal of the glass slides after the solidification resulted in obtaining the hydrogel sample, fixed in the plastic mold, with two smooth circular surfaces in contact with surrounding environment.

To verify that HA would not be released from the agarose/HA samples during the diffusion experiments, UV–VIS spectra were taken at different times of leaching of the hydrogels in deionized water. It was determined that less than 5% of the original content of HA is released during 5 days of the leaching experiment.

3.3. Rheometric characterization of hydrogels

To compare the viscoelastic properties of all prepared hydrogels, 1 mm thick samples of gel were introduced into AR-G2 rheometer (TA Instruments Ltd.) equipped with a Peltier plate for the temperature control using a plate-plate geometry (titanium, 40 mm diameter) and the Rheology Advantage Instrument Control AR software. Silicon oil was used to prevent drying of gels and gels were left to relax for 5 min. The rheometric parameters (the storage and the loss moduli) were then measured at 25 °C, at the strain of 0.05% and for the frequency range of 0.01–1 Hz.

3.4. Diffusion experiments

The diffusion studies presented in this paper were divided into three separate experimental sections. In the first one, the diffusion of the model low-molecular dye – methylene blue – was studied in aqueous solution by the method of diffusion cell using well-defined inert membrane as a diffusion barrier. In the following steps, the diffusion cell experiments with methylene blue were repeated with the application of non-reactive (agarose) and reactive (agarose/HA) hydrogels, respectively, as the diffusion barriers.

3.5. Diffusion cell apparatus

The water-jacketed side-by-side diffusion cell apparatus by Permegear Inc. was utilized in the experimental work. The schematic diagram of the apparatus is shown in Fig. 1. The cell volumes were 60 cm³ and the diameter of the circular orifice was 40 mm. A circulating water bath was used in order to perform the experiments at specific temperatures. The continuous stirring of solutions in the donor and acceptor compartments at constant rate (250 RPM) was arranged by magnetic stirrer.

3.6. Determination of diffusivity in aqueous solutions

Before the determination of diffusivity of methylene blue in aqueous solution, the apparatus was calibrated with a 100 mol m^{-3} KCl solution; the diffusion proceeded from the KCl solution (donor compartment) to deionized water (acceptor compartment) at 25 °C through the Spi-pore™ polycarbonate membrane with 2 μm pore size. This membrane is suitable for the diffusion experiments, because it contains uniform cylindrical pores preferentially etched into the membrane, allowing an even distribution of a diffusing compound in one plane across the entire exposed membrane surface. The conductivity in the cells was measured in order to observe the changes in KCl concentration.

In the next step, the diffusion coefficients of methylene blue in aqueous solutions were determined at 25, 40 and 50 °C, respectively. In these experiments, 10 g m^{-3} solution of MB was used as a donor solution and the VIS absorption spectra were collected automatically in the acceptor solution (initially deionized water) by the fiber spectrometer USB 2000+ (Ocean Optics, Inc.) equipped with the optical fiber dip probe. No samples were taken from the cells and the total volumes of the solutions hence stayed constant during the diffusion experiment. The Spi-pore™ membrane was applied in these experiments, again.

3.7. Through-diffusion experiments with hydrogels

The diffusion experiments with the hydrogel samples (both agarose and agarose/HA) were performed in the similar way, only the membrane was replaced by the 5 mm thick hydrogel sample fixed in the plastic mold, tightened in the apparatus by the silicon seal. 10 g m^{-3} MB solution was used as a source of diffusing MB and the VIS absorption spectra of the acceptor solution were continuously collected, again. After the termination of the diffusion experiment, the absorbance was measured in both cells. For every experiment, the values of the steady-state diffusion flux and the time lag were derived from linear regression of the line part of the break-through curve. Besides, the total mass of methylene blue absorbed in the hydrogel specimen was determined from the mass balance in the diffusion cell compartments at the initial and the final state.

The reproducibility of the method of diffusivity determination in hydrogels was tested by repeated (5×) experimental determination of the steady-state diffusion flux and the time lag of MB using 1 wt.% agarose hydrogel (without addition of HA). The standard relative deviation of the diffusive coefficient was about 5%.

5. Results and discussion

Presented diffusion experiments were designed in order to describe separately the three major effects which act together giving an overall influence on the transport of ionic solutes in reactive hydrogels. These effects are: (i) partitioning of the solute at the solution/gel boundary, (ii) lower permeability caused by porous character of the hydrogels, and finally (iii) specific physico-

chemical interactions between the solute and reactive content of the solid hydrogel network (e.g. sorption). For this purpose, the diffusion of the model dye – methylene blue – was studied separately in water, in hydrogels which can be regarded as non-reactive (agarose hydrogels) and in hydrogels with small addition of a highly reactive humic component (agarose/HA hydrogels). The differences in determined diffusion characteristics of these environments can be used for the evaluation of relative significance of the individual above-mentioned effects.

5.1. Diffusivity of methylene blue in aqueous solutions

In Fig. 3, the time dependence of the solute concentration in acceptor compartment (i.e. the breakthrough curve) is shown both for KCl (reference solute) and MB. The values of the free solution diffusion coefficient D_0 of MB, calculated using Eq. (1) were $(8.44 \pm 0.09) \times 10^{-10}$ m^2 s^{-1} (25 °C), $(1.29 \pm 0.01) \times 10^{-9}$ m^2 s^{-1} (40 °C) and $(1.64 \pm 0.01) \times 10^{-9}$ m^2 s^{-1} (50 °C). The standard error values were determined from the error of linear regression in the single experiment. The values of diffusivity agree with the values determined by Leaist [58] and by Hori [59] by means of conductometry and the modified diaphragm cell method, respectively. The diffusivity in water can be utilized in calculating apparent Stokes radius of MB using the fundamental Stokes–Einstein equation (Eq. (2)). The calculated value $(0.27 \pm 0.02$ nm) is consistent with the molecular dimensions of MB ($0.5 \times 0.1 \times 0.3$ nm) as well as with the experimental value which Hogan determined by means of triplet anisotropy decay (0.36 nm, [60]).

As can be seen in Fig. 4, the increase of diffusivity with the temperature fits the linearized Arrhenius relation (Eq. (3)) which allows the determination of activation energy of the diffusion. Calculated value of the energy (21.4 kJ mol^{-1}) is in good agreement again with the published value (19.5 kJ mol^{-1} calculated by Hori [59]). Hori interprets the value as the energy required to form a hole for a diffusion "jump" to take place in the diffusion medium (water).

5.2. Diffusivity of methylene blue in the agarose hydrogels

For the purposes of this work, agarose hydrogels were used as a model porous medium, in which no or little specific chemical interactions between the diffusing solute and the solid content are expected. This presumption is difficult to verify directly, nevertheless, it is supported by the very few published works on the sorption of similar solutes on agarose (to our knowledge, only the authors of [61] have dealt with the topic) and by the results of diffusion experiments discussed in [32]. As will be explained later in this section, our experimental data indicate the correctness of this presumption as well.
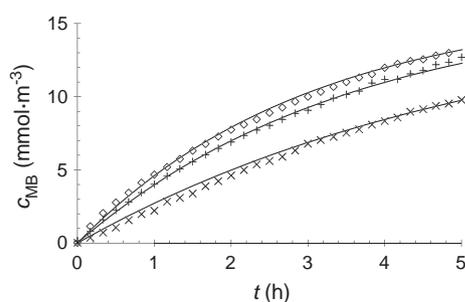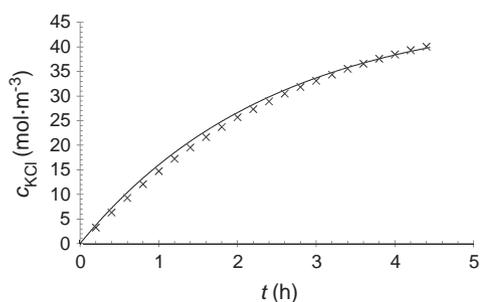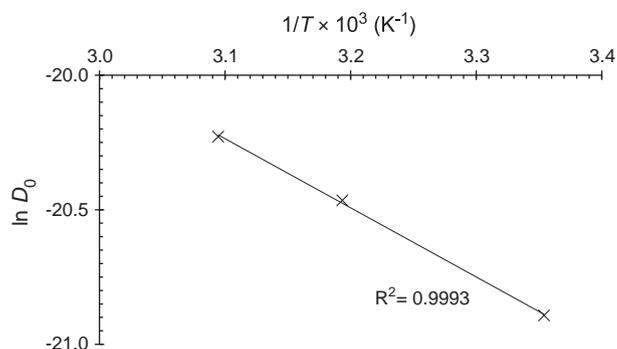
Fig. 4. Arrhenius plot for the estimation of activation energy of diffusion (diffusion of methylene blue in aqueous solution).

As evident from Table. 1, the value of the steady-state diffusion flux (calculated from the slope of linearly increasing branch of a breakthrough curve) gradually falls with the dry solid content of the hydrogel, while the time lag seems to be independent of the dry solid content of the gel for all three studied temperatures. Besides, hydrogels with higher dry solid content show evident increase in total absorbed dye. The amount of dye in hydrogels related to the mass unit of dry agarose decreases with increasing solid content, which is caused by structural changes of hydrogels with the higher agarose content. Deeper processing of the data according to the model described in chapter 2 (Theory) is necessary for the explanation of these experimental results in the following text.

First of all, the steady-state diffusion flux is proportional to the stationary concentration difference between the diffusion cell compartments Δc (Eq. (7)), which is essentially different from the initial concentration difference between the donor and the acceptor compartments, because an appreciable amount of the solute had been transported from the donor cell into the hydrogel before the start of the steady-state stage of the experiment. The exact value of the Δc can be determined by continuous measurement of solute concentration in both solutions. When the solute concentration is measured only in acceptor compartments (like in presented experiments), Δc can be determined even at the end of the experiment if the experiment is terminated still at the steady-state stage of the diffusion process. The exact value of Δc differed for hydrogels with different dry content of agarose.

The value of steady-state diffusion flux also depends on the solute partitioning between the solution and gel. The partition coefficient Φ was calculated directly from the mass of the solute absorbed in the gel, determined experimentally at the end of experiment. In a fact, this coefficient equals to the ratio of mean solute concentration in the gel and arithmetic average of the solute concentrations in donor and acceptor solutions at the end of


Fig. 3. Breakthrough curves of KCl (left) and MB (right) for diffusion through SPI-Pore membrane. Line represents the theoretical model, scatter plot show the experimental data at 25 °C (×), 40 °C (+) and 50 °C (◇).

Table 1
Experimental results for the diffusion of methylene blue through hydrogels with different agarose weight content.

$w_{agarose}$ (wt.%)	t (°C)	$J_d \times 10^9$ (mol m^{-2} s^{-1})	t_L (h)	$n \times 10^7$ (mol)	$D_e \times 10^{10}$ (m^2 s^{-1})	$D_a \times 10^{10}$ (m^2 s^{-1})
1	25	4.39	6.5	4.9	1.42	1.80
	40	6.02	2.6	2.9	3.28	4.48
	50	8.02	1.7	3.3	3.87	6.66
2	25	3.83	6.3	9.5	0.64	1.84
	40	6.15	2.8	6.1	1.59	4.21
	50	7.29	1.9	5.8	1.96	6.07
4	25	1.73	7.8	13.3	0.20	1.48
	40	3.84	2.6	10.7	0.56	4.40
	50	6.08	1.5	8.7	1.10	7.63

Table 2
Experimental results for the diffusion of methylene blue through 1 wt.% agarose hydrogels with different weight content of HA.

w_{HA} (wt.%)	t (°C)	$J_d \times 10^9$ (mol m^{-2} s^{-1})	t_L (h)	$n \times 10^7$ (mol)	$D_e \times 10^{10}$ (m^2 s^{-1})	$D_a \times 10^{10}$ (m^2 s^{-1})
0	25	4.39	6.5	4.9	1.42	1.80
	40	6.02	2.6	2.9	3.28	4.48
	50	8.02	1.7	3.3	3.87	6.66
0.002	25	4.11	7.5	6.6	1.39	1.55
	40	5.64	3.6	5.7	3.68	3.22
	50	6.50	2.2	5.7	3.70	5.31
0.005	25	2.76	11.2	7.6	1.11	1.03
	40	5.40	4.7	8.0	4.22	2.44
	50	6.87	3.7	8.6	4.94	3.11
0.010	25	1.73	20.2	10.5	0.76	0.57
	40	2.88	8.3	9.6	2.62	1.40
	50	6.95	4.8	10.5	6.03	2.42

experiment. As it can be seen from Fig. 5, strong partitioning of MB in agarose was observed. This is not an unexpected finding, the partitioning of solutes in agarose hydrogels was thoroughly discussed in literature [52,32]. Golmohamadi et al. in [32] attribute high partitioning of Cd^{2+} and rhodamine cations in agarose hydrogels to non-specific Donnan effects linked with the hydrogel charge rather than to any direct effects on the diffusion of charged probes.

An alternative explanation of the increasing total absorbed mass of MB in hydrogels with higher dry agarose content could be based on consideration of some specific chemical interactions between agarose and MB despite the initial presumption. Nevertheless, this kind of interactions should significantly affect the transient stage of the diffusion, resulting in increased time lag (see Eqs. (8) and (10)), which would also be probably dependent on the total amount of binding sites – i.e. on the dry agarose content. Evidently, this is not the case for agarose hydrogels (compare with the time lags of agarose/HA gels in Table. 2), from which we can deduce that the presumption of no specific interactions between MB and agarose was used reasonably.

On the other hand, the total amount of absorbed MB related to the dry mass in the hydrogels decreases with the agarose content, which points to the decrease of its partitioning ability. It is probably caused by the denser network of more concentrated hydrogels and corresponding changes in the conformation of agarose chains and porous structure. As the agarose content increases, the number of polymer–polymer interactions between helices increases, which results in more compact structure [30,31]. Some authors [62,63] investigated that the mechanism of gel formation depends on the agarose concentration and the gelation proceeds from the homogenous solutions only if the agarose content is higher than 2 wt.%. The change of mechanism influenced significantly the gel structure
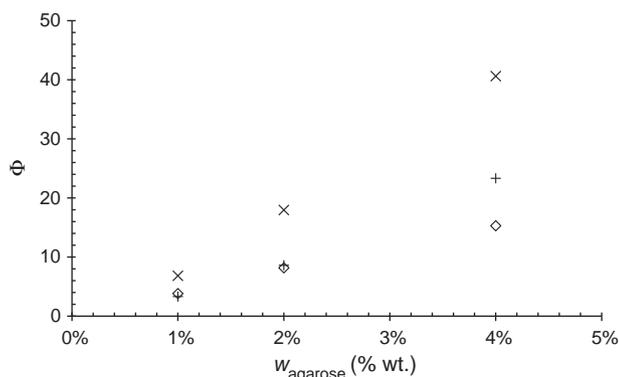
Fig. 5. Partition coefficient for the methylene blue partitioning at the boundary of agarose hydrogels at 25 °C (×), 40 °C (+) and 50 °C (◇).

and its final properties, which could be one of reasons of the lower partitioning ability related to the gel dry mass.

Similarly, the agarose content affected the effective (and slightly also the apparent) diffusion coefficients. Their values were calculated from the experimental data using Eqs. (7) and (10), (see Table. 1). As expected, the effective diffusion coefficient of MB in agarose gels decreases with the dry agarose content (see Table. 1) In [64], the linear decrease in relative diffusion coefficient (D_e/D_0) with the dry solid content of the gel is shown for the diffusion of small cations (Na^+ and Cs^+) in agar hydrogels. Our results with MB showed that the decrease is not linear and it is steeper for low agarose content. As the network gets denser, the diffusivity of MB in the hydrogel decreases slowly as a result of structural and conformational changes.

From the comparison of D_e and D_a, the crucial structural parameters of ε_{eff} and T_m can be calculated (see Eqs. 4, 8, and 9; note that for the no-reaction presumption the $K_{app} = 0$ in Eq. (9)). The calculated values are shown in Fig. 6. As it was mentioned above, the network of agarose chains becomes more densely packed with increasing weight content of agarose in the gels, which strongly affects the mechanical and textural properties of the hydrogels (e.g. viscoelastic characteristics, pore size). These effects are described in detail [30,31] and were experimentally confirmed for used hydrogel samples by measuring their viscoelastic properties (see Fig. 7). The complex modulus increases with the agarose content of hydrogel in whole measuring range, which indicates more densely cross-linked network of hydrogels with higher concentration of agarose giving a decrease in the pore size. We can see that the complex modulus is frequency independent for the agarose content 1 wt.% and the dependence was observed only for more concentrated hydrogels. The obtained results correspond both with our diffusion data and with the rheological behavior described in other works [30,62]. In order to estimate the actual pore sizes, a simplespectrophotometric method published by Aymard et al. [65] was utilized in calculating the effective pore size as a function of agarose concentration in the gel. Calculated pore sizes of all utilized hydrogels (0.36 μm, 0.16 μm and 0.09 μm for 1 wt.%, 2 wt.% and 4 wt.% of agarose hydrogels, respectively) exceed significantly the Stokes hydrodynamic radius of MB.

The total porosities of gels can be estimated from the weight concentration assuming ideal mixing of agarose and water, dry agarose density can be found in literature [66]. For the utilized agarose hydrogels, these estimated values are very close to unity (0.976–0.994 for gels with decreasing dry agarose content). It is evident, that the experimentally determined values of ε_{eff} are significantly lower. According to the applied model, the effective porosity differs from the total porosity of the medium, because
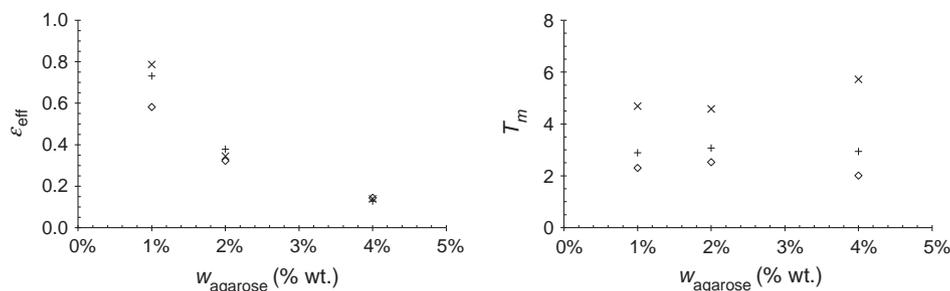
Fig. 6. Calculated effective porosities and tortuosity factors of agarose hydrogels at 25 °C (×), 40 °C (+) and 50 °C (◇).

not all the pores of medium are equally available for a mass transport (e.g. some pores can form "dead ends") [51]. The value of ε_{eff} decreases with increasing dry agarose content of the hydrogels as expected in connection with above described results. The changes in the density of hydrogel network together with the increase of its rigidity, the changes in water dynamics and the hydration of agarose chains are probably the reasons of the observed discrepancy between the effective porosity ε_{eff} and the weight content of water in the used hydrogels [67]. Nevertheless, mainly for more concentrated agarose hydrogels, the actual difference between estimated total and calculated effective porosity is so great that it deserves a detailed verification in future experiments.

The calculated values of tortuosity factor T_m indicate significant meandering of actual solute pathway. At 25 °C, the actual distance traveled by the solute molecules when penetrating the hydrogel specimen is about twice longer than the gel thickness (see Eq. (5)). This is quite surprising finding, because the tortuosity effects are not commonly considered in the case of agarose hydrogels. Diluted agar and agarose gels (about 0.5 wt.%) are used even as reference medium with a unit tortuosity in determining transport properties of some tissues [68,69]. The published values of tortuosity factors of highly porous hydrogels are predominantly close to unity [70]. Also the model, proposed by Tao and Nicholson [71], which considers a simple relationship between tortuosity and porosity of a medium, gives the estimation of T_m insignificantly shifted from unity. Experimental results also show the decrease of T_m with the temperature, which indicates that the diffusion pathway is straightened at higher temperatures.

5.3. Diffusivity of methylene blue in the agarose/humic acids hydrogels

As can be seen from experimental data shown in Table. 2 and Fig. 8, a small addition of humic acids as a reactive component into the agarose hydrogels resulted in a significant change in the barrier

properties of the gels. Like in the case of dry agarose content, increasing content of humic acids in the gel led to a considerable increase in absorbed amount of MB in the gel and to the decrease in steady-state diffusion flux. Nevertheless, note that similar effect on these two parameters is caused by 1000× lower addition of HA compared to agarose. Furthemore, unlike agarose, the total content of humic acids significantly affected also the value of time lag, which indicates extensive physico-chemical interactions between diffusing MB and humic acids contained in the gel.

For the subsequent data analysis, a following presumption is applied: neither the structural properties of the agarose hydrogels nor the partitioning at the solution/hydrogel boundary is affected by added HA. The presumption takes into account very small total content of HA in the gel. The invariance of the structural parameters was supported by the rheological characterization of the hydrogels – no significant difference in rheometrical parameters was found for 1 wt.% agarose gels with and without HA (see smaller graph in Fig. 7). The assumption of similar partitioning of solute at the boundary between the solution and agarose gel with and without HA was required to calculate the value of D_e from the steady-state diffusion flux, because the partition coefficient Φ cannot be derived directly from the absorbed amount of the solute (the absorbed amount represents the sum of free and bound solute, while the partitioning takes only the concentration of free solute into account). Anyway, the experimental verification of this assumption should be taken as a scope of the future work.

From the values of steady-state diffusion flux and time lag, the effective and apparent diffusion coefficients for the diffusion of methylene blue in the humic-containing hydrogels were calculated in the same manner as above. The effective diffusion coefficient characterizes the steady-state stage of the diffusion process which should not be affected by any specific interactions between the solute and the reactive sites of the medium (the reaction equilibrium in the gel is already established at the beginning of this stage).
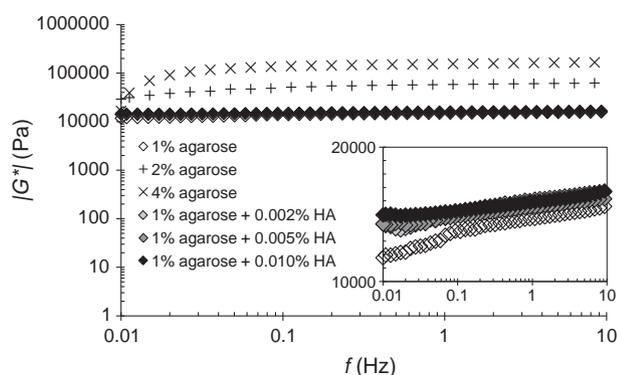
Fig. 7. Rheometric analysis of all utilized hydrogels (smaller graph shows detail on gels with various HA content).
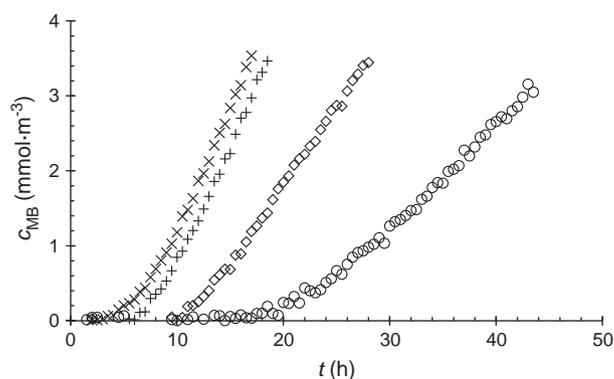
Fig. 8. Breakthrough curves of MB for the diffusion at 25 °C through 1 wt.% agarose hydrogels with 0 wt.% (×), 0.002 wt.% (+), 0.005 wt.% (◇) and 0.010 wt.% (○) of HA.

Therefore, for a given temperature, the effective diffusion coefficient is expected to be independent of a small addition of reactive component into the hydrogel. Nevertheless, small differences were found between D_e of the agarose/HA hydrogels and the respective agarose gel (see Table. 2). As was already discussed, the value of D_e was calculated according to Eq. (7) using the value of Φ determined for respective agarose gel without HA. This discrepancy thus indicates that the presumption of negligible effect of HA on the partitioning of MB at the boundary is not actually met perfectly. Unlike the effective diffusivity, the apparent diffusion coefficient characterizes the transient stage of the diffusion process and, therefore, its value involves the effect of specific interactions between the solute and the medium. It can be seen that the interactions between MB and HA in the hydrogels significantly suppress the mobility of methylene blue, resulting in increased time lag and decreased D_a (see Fig. 8 and Table. 2).

For a deeper insight into the interactions of MB with HA during the diffusion process, let us consider, that these interactions can be modeled by instantaneous (i.e. very fast in comparison with the diffusion) reversible sorption, summarized by the reaction scheme $MB_{free} \leftrightarrow MB_{bound}$. This sorption mechanism (resulting in a linear sorption isotherm) is applicable in the systems, where a high excess of reactive sites on the sorbent is assumed. This presumption is suitable for the systems with binding sites distributed homogenously in the whole volume (like in reactive hydrogels), unlike e.g. the sorption experiments in suspensions, where the sorption is restricted to the surface of solid sorbent particles. Nevertheless, in presented experiments, the presumption is questionable because of small addition of reactive component (HA) to the gel. The apparent equilibrium constant K_{app} of the reversible sorption can be calculated from the value of D_a (see Eq. (9)) using the value of ε_{eff} determined for respective agarose gel without HA. It can be seen in Fig. 9 that the value of K_{app} significantly increases with higher content of HA in gel. Higher temperature has a positive effect on the sorption as characterized by an increase of K_{app} with temperature. This indicates the endothermic nature of the interactions, which agrees with the results of MB sorption on humic-rich peat, published by Fernandes et al. [46,72]. This temperature effect can be attributed to the changes in conformation of HA causing higher availability of their binding sites for MB sorption at higher temperatures. In general, strong interaction between HA and cationic solutes is commonly attributed to a high content of acid functional groups. As the results of potentiometric and conductometric titration show, the total acidity of the utilized HA is 5.28 mmol g^{-1} and the content of carboxylic groups is 2.12 mmol g^{-1}. The high content of carboxylic and phenolic groups were also confirmed by the results of detailed elemental and spectroscopic analysis (for detailed results, see [17,57]).
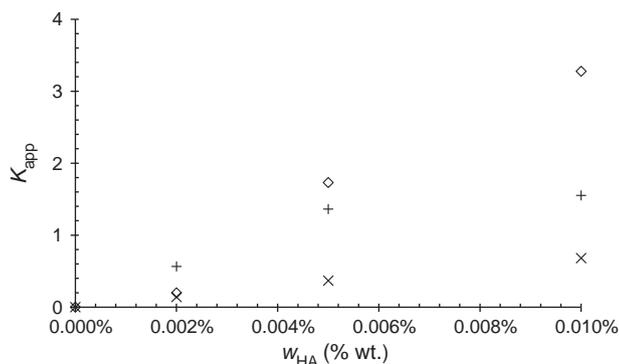
The value of K_{app}, which corresponds to the defined sorption model, can be estimated also from the total absorbed amount of MB in the gels. As was already discussed, the total amount of MB in the gel represents the sum of free and bound fractions. If we introduce the parameter Φ_{app} as a ratio of mean total concentration of MB in the gel and the arithmetic average of concentrations in both compartments of the diffusion cell at the end of a diffusion experiment, then for the ratio of this parameter and corresponding partition coefficient (determined by the experiments with agarose gel without HA), the following equation can be derived:

$$\frac{\Phi_{app}}{\Phi} = \frac{c(free) + c(bound)}{c(free)} = 1 + K_{app} \qquad (11)$$

It was found, that the values of K_{app}, calculated using Eq. (11) were always higher than those calculated from D_a (usually two to three times). This discrepancy is another sign that even the small addition of humic acids affects the partitioning of MB at solution/gel boundary and that using the partition coefficients determined for pure agarose gels for the description of transport in agarose/HA gels is not completely correct.

6. Conclusions

Experimental results, presented in the paper, clearly illustrate the effect of interactions between humic acids and methylene blue on the transport of this ionic dye in model aqueous environments provided by agarose hydrogels. It can be seen, that the binding of methylene blue by humic acids strongly decelerates its transport, which is characterized by higher time needed to penetrate the samples with higher concentration of humic acids. These findings are of the crucial importance in the case of humic substances, whose barrier behavior in natural environments, so important for playing their irreplaceable environmental role, cannot be reliably predicted just from the results of traditional batch sorption experiments.

The diffusion techniques, successfully applied in these experiments, hence represent an interesting alternative approach for the traditional reactivity mapping studies in the systems containing humic substances and similar reactive compounds. The method is not equipment-demanding and can be applied with minor modifications for various semi-solid or solid samples. Numerous structural (effective porosity, tortuosity factor) and interaction parameters (apparent reaction equilibrium constants) are calculated easily, as was illustrated for the studied systems. The method is also well applicable for the study on the effects of adjustable conditions such as temperature (as presented in this paper) or others (e.g. pH or ionic strength).

The pilot experiments, introduced in the paper, represent the first step towards a broader utilization of the diffusion techniques in the studies on reactivity and barrier ability of humic acids. The potential applicability of the presented method is great – without any significant modification of the experimental procedure, the technique can be utilized in order to compare the barrier properties of the humic acids toward various solutes. As well, the diffusion experiments can be used to assess the solute-immobilization effects of diverse humic substances (e.g. humic acids of the different origin or specifically chemically modified humic substances) or the similar compounds.

Nevertheless, some questions remain unanswered. As was discussed, the diffusion of methylene blue through agarose gel did not always provide the expected results (as is represented by obviously too high value of the calculated tortuosity). It seems likely that, contrary to the initial expectations, methylene blue interacts to some degree with the applied agarose. To suppress this effect, utilization of either a different agarose (with the carefully

**Fig. 9.** Apparent equilibrium constant for the sorption of methylene blue in agarose/HA gels at 25 °C (×), 40 °C (+) and 50 °C (◇).

characterized key properties like the charge structure) or diffusing compound should be considered in the future study. Besides, it was also illustrated that the experiments in diffusion cells do not provide complete info about the partitioning of a studied solute at the boundary between the solution and the reactive medium. The non-stationary diffusion experiments are hence recommended as the next step of the method development – these experiments are based on the direct determination of solute concentration at different distances in the diffusion medium which gives easy distinguishing of the diffusion and the partitioning effects.

Acknowledgements

References

[1] S.A. Jansen, M. Malaty, S. Nwabara, E. Johnson, E. Ghabbour, G. Davies, Mater. Sci. Eng. C – Biol. Sci. 4 (1996) 175–179.
[2] S.N. Bolan, C.D. Adriano, A. Kunhikrishnan, T. James, R. McDowell, N. Senesi, Adv. Agron. 110 (2011) 1–75.
[3] J.F. McCarthy, J.M. Zachara, Environ. Sci. Technol. 23 (1989) 496–502.
[4] M. Schnitzer, S.U. Khan, Humic Substances in the Environment, Marcel Dekker, Inc., New York, 1972.
[5] E.M. Peña-Méndez, J. Havel, J. Patočka, J. Appl. Biomed. 3 (2004) 13–24.
[6] R. Klocking, B. Helbig, Biopolymers 1 (2001) 379–392.
[7] R. Sutton, G. Sposito, Environ. Sci. Technol. 39 (2005) 9009–9015.
[8] E. Tipping, Cation Binding by Humic Substances, Cambridge University Press, Cambridge, 2002.
[9] W. Kördel, M. Dassenakis, J. Lintelmann, S. Padberg, Pure Appl. Chem. 69 (1997) 1571–1600.
[10] M. Borkovec, G.J.M. Koper, C. Piguet, Curr. Opin. Colloid. Interface 11 (2006) 280–289.
[11] N.B. Ferapontov, L.R. Parbuzina, V.I. Gorshkov, N.L. Strusovskaya, A.N. Gagarin, React. Funct. Polym. 45 (2000) 145–153.
[12] A.V. Dobrynin, M. Rubinstein, Prog. Polym. Sci. 30 (2005) 1049–1118.
[13] M. Klučáková, M. Pekař, J. Polym. Mater. 20 (2003) 145–154.
[14] M. Klučáková, Environ. Chem. Lett. 8 (2010) 145–148.
[15] C. Mizuno, S.H. Bao, T. Hinoue, et al., Anal. Sci. 21 (2005) 281–286.
[16] W.S. Wan Ngah, L.C. Teong, M.A.K.M. Hanafiah, Carbohydr. Polym. 83 (2011) 1446–1456.
[17] P. Sedláček, M. Klučáková, Geoderma 153 (2009) 11–17.
[18] P. Sedláček, M. Klučáková, Collect. Czech. Chem. Commun. 74 (2009) 1323–1340.
[19] M. Klučáková, M. Pekař, Study of diffusion of metal cations in humic gels, in: E.A. Davies (Ed.), Humic Substances: Nature's Most Versatile Materials, Taylor & Francis, New York, 2004, pp. 263–273.
[20] M. Klučáková, M. Pekař, J. Polym. Mater. 20 (2003) 155–162.
[21] J. Crank, The Mathematics of Diffusion, Clarendon Press, Oxford, 1956.
[22] M. García-Gutiérrez et al., J. Iber. Geol. 32 (2006) 37–54.
[23] E.L. Cussler, Diffusion Mass: Transfer in Fluid Systems, Cambridge University Press, Cambridge, 1984.
[24] B. Falk, S. Garramone, S. Shivkumar, Mater. Lett. 58 (2004) 3261–3265.
[25] R. Ibrahim, G.B. Kasting, Int. J. Pharm. 435 (2012) 33–37.
[26] R.B. Mustapha, C. Lafforgue, N. Fenina, J.P. Marty, Indian J. Pharmacol. 43 (2011) 157–162.
[27] M.A. Pellett, A.C. Watkinson, J. Hadgraft, K.R. Brain, Int. J. Pharm. 154 (1997) 205–215.
[28] M. Schulz, H.L. Frisch, J. Chem. Phys. 107 (1997) 2673–2683.
[29] J.Y. Xiong, J. Narayanan, et al., J. Phys. Chem. – US 109 (2005) 5638–5643.
[30] L.M. Barrangou, C.R. Daubert, et al., Food Hydrocolloids 20 (2006) 184–195.
[31] L.M. Barrangou, C.R. Daubert, et al., Food Hydrocolloids 20 (2006) 196–203.
[32] M. Golmohamadi, T.A. Davis, et al., J. Phys. Chem. A 116 (2012) 6505–6510.
[33] J.R. Lead, K. Starchev, et al., Environ. Sci. Technol. 37 (2003) 482–487.
[34] J. Gutenwik, B. Nilson, et al., Biochem. Eng. J. 19 (2004) 1–7.
[35] B.A. Westrin, A. Axelsson, Biotechnol. Tech. 5 (1991) 303–306.
[36] S.M. Liang, J. Xu, et al., J. Controlled Release 115 (2006) 189–196.
[37] S.X. Tan, H.J. Dai, et al., J. Biomed. Opt. 14 (2009) 050503.
[38] J. Labille, N. Fatin-Rouge, et al., Langmuir 23 (2007) 2083–2090.
[39] A. Pluen, P.A. Netti, et al., Biophys. J. 77 (1999) 542–552.
[40] R.D. Guy, D.R. Narine, S. DeSilva, Chemistry 58 (1980) 547–554.
[41] Guo-Ping Sheng, Meng-Lin Zhang, Yu. Han-Qing, J. Colloid Interface Sci. 331 (2009) 15–20.
[42] C. Zhou, Z. Wu, W. Zhang, M. Xia, et al., Funct. Mater. Lett. 4 (2011) 373–376.
[43] P. Janoš, Environ. Sci. Technol. 37 (2003) 5792–5798.
[44] P. Janoš, P. Šedivý, M. Rýznarová, S. Grötschelová, Chemosphere 59 (2005) 881–886.
[45] P. Janoš, P. Michálek, L. Turek, Dyes Pigm. 74 (2007) 363–370.
[46] A.N. Fernandes, C.A.P. Almeida, C.T.B. Menezes, N.A. Debacher, M.M.D. Sierra, J. Hazard. Mater. 144 (2007) 412–419.
[47] G. Crini, Bioresour. Technol. 97 (2006) 1061–1085.
[48] V.K. Gupta, J. Environ. Manage. 90 (2009) 2313–2342.
[49] M. Rafatullah, O. Sulaiman, R. Hashim, A. Ahmad, J. Hazard. Mater. 177 (2010) 70–80.
[50] R.H. Stokes, J. Am. Chem. Soc. 73 (1951) 3527–3528.
[51] C.D. Shackelford, S.D. Moore, Eng. Geol. 152 (2013) 133–147.
[52] N. Fatin-Rouge, A. Milon, J. Buffle, R.R. Goulte, A. Tessier, Phys. Chem. B 107 (2003) 12126–12137.
[53] H.L. Frisch, J. Phys. Chem. 61 (1957) 93–95.
[54] M. Klučáková, M. Pekař, Colloids Surf., A 252 (2005) 157–164.
[55] J. Riggle, R. von Wandruszka, Talanta 57 (2002) 519–526.
[56] F.J. Stevenson, Humus Chemistry: Genesis, Composition, Reactions, second ed., Wiley-Interscience Publ., New York, 1982.
[57] J. Peuravuori, P. Žbánková, K. Pihlaja, Fuel Process. Technol. 87 (2006) 829–839.
[58] G.D. Leaist, Can. J. Chem. 66 (1988) 2452–2456.
[59] T. Hori, N. Kamon, et al., J. Soc. Dyers Colour. 103 (1987) 265–270.
[60] M. Hogan, J. Wang, R.H. Austin, C.L. Monitto, S. Hershkowitz, Proc. Natl. Acad. Sci. USA 79 (1982) 3518–3522.
[61] S. Babak, F. Ashoori, Chem. Cent. J. 6 (2012) 14–27.
[62] E. Fernández, D. López, C. Mijangos, M. Duskova-Smrckova, M. Ilavsky, K. Dusek, J. Polym. Sci. Polmer. Phys. 46 (2008) 322–328.
[63] P.L. San Biagio, D. Bulonel, A. Emanuele, M.B. Palma-Vittorelli, M.U. Palma, Food Hydrocolloid 10 (1996) 91–97.
[64] C. Nicholson, Rep. Prog. Phys. 64 (2001) 815–884.
[65] P. Aymard, D.R. Martin, et al., Biopolymers 59 (2001) 131–144.
[66] T.C. Laurent, Biochim. Biophys. Acta 136 (1967) 199–205.
[67] A. Deriu, F. Cavatorta, D. Cabrini, C.J. Carlile, H.D. Middendorf, Europhys. Lett. 24 (1993) 351–357.
[68] C. Nicholson, L. Tao, Biophys. J. 65 (1993) 2277–2290.
[69] C. Nicholson, J.M. Phillips, J. Physiol. 321 (1981) 225–257.
[70] P. Lesný, J. De Croos, M. Prádný, J. Vacík, J. Michálek, S. Woerly, E. Syková, J. Chem. Neuroanat. 23 (2002) 243–247.
[71] L. Tao, C. Nicholson, J. Theor. Biol. 229 (2004) 59–68.
[72] A.N. Fernandes, C.A. Policiano Almeida, N.A. Debacher, M.M. de Souza Sierra, J. Mol. Struct. 982 (2010) 62–65.

Appendix 5

Sedláček, P., Smilek, J., and Klučáková, M. How the interactions with humic acids affect the mobility of ionic dyes in hydrogels – 2. Non-stationary diffusion experiments. *Reactive and Functional Polymers* **2014**, 75, 41–50.
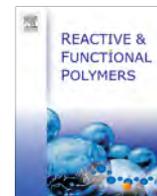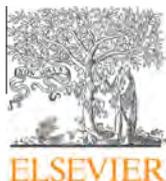
How the interactions with humic acids affect the mobility of ionic dyes in hydrogels – 2. Non-stationary diffusion experiments

Petr Sedláček *, Jiří Smilek, Martina Klučáková

Brno University of Technology, Faculty of Chemistry, Materials Research Centre CZ.1.05/2.1.00/01.0012, Purkyňova 118, 612 00 Brno, Czech Republic[1]

ABSTRACT

Non-stationary diffusion of two cationic dyes (Methylene Blue and Rhodamine 6G) was studied in hydrogels with different content of agarose and humic acids (HA). A simple spectrophotometrical method was utilized in the *in situ* measurement of dye concentration in the gel samples at different distances from the boundary. The effect of temperature, pH and ionic strength was investigated. The results confirmed the considerable partitioning of both dyes in agarose gels as well as the strong immobilization of dyes caused by their sorption on HA. The apparent diffusion coefficients of both dyes decreased with increasing solid content in gels. In the case of agarose gels without the addition of HA, this decrease was attributed to increased tortuosity of diffusion caused by denser agarose network. The apparent equilibrium constant of the sorption of dyes on HA in agarose/HA gels was calculated from their apparent diffusion coefficients. The value of the equilibrium constant increased with the content of HA in gel and, surprisingly, also with decreasing pH inside gel.

© 2013 Elsevier Ltd. All rights reserved.

1. Introduction

Humic substances form the key organic component of soils, sediments and young coals. From the chemical point of view, they represent complex heterogeneous mixtures of polydispersed materials with the complicated structural skeleton and can be divided operatively into three main fractions: humic acids (HA), fulvic acids and humin. Humic and fulvic acids are extracted from soil and other solid phase sources using a strong base. HA are insoluble at low pH, and they are precipitated by adding strong acid. Humin cannot be extracted with either a strong base or a strong acid [1]. Although they are well known to stand behind the crucial environmental phenomena (*e.g.* the carbon sequestration or self-detoxification of soils), even after more than two centuries of substantial research, the basic chemical nature, biosynthetic pathways, and the reactivity of humic substances and soil organic matter are still poorly understood [2].

The key feature of natural behavior and of function of humics lies in their outstanding ability to bind compounds of diverse chemical nature. This process is of an exceptional biological, environmental and even industrial importance. In soils, sediments and in water aquifers, binding on solid or dissolved humic substances determines the local concentrations and the fluxes of bound compounds, which crucially affects the dynamics of essentially all other components of the systems. Hereby, the presence of humic substances controls the ecotoxicity of harmful pollutants and the bioavailability of essential nutrients in soils at the same time.

Therefore, a considerable experimental effort has been directed towards describing the interactions of humic substances with the diverse model pollutants – *e.g.* heavy metals [3], radionuclides [4], pesticides [5] or pharmaceuticals [6] – and as well with some typical nutrients [7]. Moreover, the development of some humics – based sorbents and artificial barriers for various environmental and industrial applications has become a subject of vast concern [8,9].

Practically all the above referenced reviews summarize the studies which focus on the common batch sorption experiments, aiming at the detailed description of the sorption equilibrium and the sorption kinetics in the solute–humics systems. The experimental procedures are always similar and the individual studies usually differ just in the preferred combination of solute and humics and often also in the level of complexity of the mathematical model used for the interpretation of sorption data (compare various models reviewed in [10]).

On the other hand, in our recent works, simple diffusion studies were put forward as the reasonable experimental alternative which better describes the actual effects of the humics–solute interactions on the transport of a solute in humics-containing matrices [11–16]. In these papers, a hydrogel form of humic acids is utilized both as a reasonable model of native humic environments and also because a semi-solid hydrogel sample provides

---

better feasibility of the diffusion experiments. In the most recent work [16], the diffusions of Methylene Blue (as a model cationic organic dye) in aqueous solutions and in agarose gels with and without the addition of humic acids were studied by the method of diffusion cells. The method is based on the measurement of time needed by the solute to penetrate through the studied porous specimen and, after the penetration, of the steady-state flux of the solute. The results of these experiments clearly showed the barrier effect of humic acids on the transport of Methylene Blue in gels. The experimental results were processed using the comprehensive theoretical model, summarized by Shackelford and Moore [17] for the description of the diffusion of solutes in the porous media, in order to calculate some diffusion and interaction parameters of the studied systems. Nevertheless, apart from the obvious illustration of reactivity and barrier properties of humic acids, the experiments in the diffusion cells proved the insufficiency for an adequate separation of the two independent effects, acting simultaneously in the systems: (i) of the partitioning (*i.e.* unequal distribution caused by a phase-equilibrium) of free solute at the solution–gel boundary and (ii) of the immobilization of solute in gel caused by some specific solute – HA interactions (for details, see [16]).

To address the two effects independently, the non-stationary diffusion studies could provide an improved experimental tool (a comprehensive handlist of the non-stationary diffusion models with the basic experimental layout can be found *e.g.* in [18]). In the non-stationary experiments, the actual concentration of diffusing solute is measured in the studied material at different times and different distances from the solute source. The diffusion coefficients of solute are then calculated either from the time change of the solute concentration profile in the sample or from the solute total diffusion flux. Diverse sophisticated analytical techniques were applied previously in the measurement of solute concentration profiles in gels, *e.g.* fluorescence microscopy [19], nuclear magnetic resonance techniques [20] or ultrasonic acoustics [21]. Some of the uncomplicated non-stationary diffusion techniques were also utilized in our preliminary study on the transport of cupric ions in the model humic matrices [11–15].

The experiments presented here improve the previous studies of humic matrices by introducing a direct, non-destructive, spectrophotometric method of determination of the solute concentration profiles in the supporting hydrogels loaded with different amounts of humic acids. It utilizes the characteristic visible light absorption of the solutes (charged organic dyes) in order to measure their concentration when diffusing in the appropriately selected hydrogel materials which allow the transmission of light. This method features the advantage of great availability – UV–VIS spectroscopy represents the routine laboratory method with low equipment demands. Moreover, it can be used for a wide range of model hydrogels and solutes. Direct *in situ* imaging of the concentration profile of solutes in hydrogels was already used as a powerful tool in the diffusion studies; Dunmire et al. [22] developed and evaluated automated UV spectrophotometric method for analyzing molecular transport of several test molecules into gels with a relevance to the design of controlled drug-delivery systems, similar techniques for UV or visible imaging of a solute diffusion in optical transparent hydrogels were utilized also in other pharmaceutical [23–25] or food engineering studies [26,27]. The experiments presented in this paper focus on the diffusion of two solutes – Methylene Blue and Rhodamine 6G – in agarose hydrogels loaded with different amounts of lignite-derived humic acids. Both selected solutes represent positively charged organic dyes with well-known affinity to bind on the humic substances [28,29]. Methylene Blue was included, *inter alia*, to provide a basis for the comparison with results of our previously published diffusion-cell experiments, Rhodamine 6G was added because its diffusion in hydrogels have been extensively studied by several authors

[30–32]. Experimentally determined concentration profiles of solutes were subjected to the least-square regression with a suitable mathematical model in order to calculate the diffusion and partition coefficients of solutes. Moreover, the influence of pH and ionic strength on the diffusion process was analyzed as well.

2. Materials and methods

2.1. Chemicals

Agarose (routine use class, <10 wt.% moisture content), Methylene Blue hydrate (C.I. Basic Blue 9, dye content, $\geqslant$95 wt.%) and Rhodamine 6G (C.I. Basic Red 1, dye content, $\geqslant$95 wt.%) were purchased from Sigma–Aldrich and used without further purification. Humic acids were isolated by alkaline extraction from South-Moravian lignite [11,33]. The details on the chemical structure of both the original lignite matrix and isolated HA (total and carboxylic acidity, elemental and spectroscopic analysis), can be found in previously published papers [16,33,34].

Phosphate buffer saline (PBS), used for the adjustment of pH of the dye solution and of inner pH of hydrogels (Section 5.3), was prepared by the dissolution of accurate amount of $Na_2HPO_4 \cdot 2H_2O$ and $NaH_2PO_4 \cdot 2H_2O$ (p.a., Sigma–Aldrich) in deionized water. Three different pH values (3, 7 and 11) and two buffer ionic strengths (10 mM and 200 mM) were used.

2.2. Preparation of hydrogels

All hydrogels, utilized in subsequent diffusion experiments, were prepared via the same method of thermoreversible gelation of aqueous solution of agarose as in previous work [16]. Agarose hydrogels (without the addition of HA, dry agarose content in gel: 0.5 wt.%, 1 wt.%, 2 wt.% and 4 wt.%) gelatinized from the solution of agarose in water (Section 5.1) or in the respective buffer solution (Section 5.3), while agarose/HA gels did from the solution of both agarose (1 wt.%) and HA (0.002 wt.%, 0.005 wt.% and 0.010 wt.%) in water (Section 5.2) or in the buffer solution (Section 5.3).

A simple gelation procedure was applied: accurately weighted amount of agarose powder was dissolved in deionized water or in the buffer solution (preparation of agarose gels) or in the solution of HA of the corresponding concentration (preparation of agarose/HA gels), respectively. The mixture was slowly heated when stirring continuously to 80 °C and maintained at the temperature until the occurrence of transparent solution. The solution was degassed in ultrasonic bath for 1 min. (at 80 °C) and slowly poured into the PMMA spectrophotometric cuvette (inner dimensions: $10 \times 10 \times 45$ mm). The cuvette orifice was immediately covered with pre-heated plate of glass to prevent drying and shrinking of gel. Flat surface of the boundary of resulting hydrogels was provided by wiping an excess solution away. Gentle cooling of cuvettes at the laboratory temperature led to the gradual gelation of the mixture.

2.3. Diffusion experiments

The non-stationary diffusion experiments with hydrogels were performed as follows: Pre-prepared hydrogel samples in the PMMA cuvettes were immersed in horizontal positions in 0.01 g dm^{-3} aqueous solution of the respective dye (Methylene Blue or Rhodamine 6G, four cuvettes in one container filled with 250 cm^3 of the dye solution). The dye solution was stirred continuously by the magnetic stirrer and the dye was left to diffuse from the solution into the gel samples through the square orifices of the cuvettes. Each experiment was duplicated. In selected time

intervals, the cuvettes were taken out of the solution and the UV–VIS spectra were measured at various distances from the orifice on Varian Cary 50 UV–VIS spectrophotometer equipped with the special accessory providing controlled fine vertical movement of the cuvette in the spectrophotometer.

From the collected UV–VIS spectra, the concentration of the dye was determined at different positions in gels. For this purpose the UV–VIS spectra were calibrated for hydrogels with known concentration of the dye, homogenously distributed in the whole volume of gel. These hydrogels samples were prepared using exactly the same preparation procedure as for the samples for the diffusion experiments; only the precise amount of the dye was added to the solution before gelatinization. In this way, the reference samples, covering at least three different concentrations of the dye, were prepared for all tested hydrogel compositions.

When testing the influence of pH and ionic strength (Section 5.3), the non-stationary diffusion experiments were repeated using buffered dye solutions and buffered gels (1 wt.% agarose gels). PBSs were used as a standard tool for the pH adjustment (see Section 2.2). Agarose hydrogels (1 wt.% of agarose) with 0 wt.% HA and 0.01 wt.% HA were utilized in these experiments. The desired values of the inner pH of the resulting hydrogels were experimentally verified using the spearhead pH electrode designed for measurements in semi-solid samples (Metrohm, Inc.). Difference between the pH values of the buffer solution and the resulting hydrogel never exceeds 0.1. The preparation of the reference samples for all buffered hydrogels and the collection of UV–VIS spectra were performed in the way described above.

3. Nomenclature

ε_{eff}	effective porosity (–)
Φ	partition coefficient (–)
c	concentration of the solute (g dm^{-3})[a]
D	diffusion coefficient (m^2 s^{-1})
D_0	free solution diffusion coefficient (m^2 s^{-1})
D_a	apparent diffusion coefficient (m^2 s^{-1})
erfc	complementary error function
K_{app}	apparent equilibrium constant (–)
t	time (s)
T_m	tortuosity factor (–)
w	weight concentration (wt.%)
x	direction coordinate (m)

[a] Particular concentration variants are distinguished by the corresponding subscripts and explained in the text.

4. Theory

When a solute diffuses in a medium, the rate of its molecular transport is governed by the solute's concentration gradient. For the simplest case of one-dimensional fickian diffusion (along the x-axis), neglecting other effects such as the concentration flux induced by the temperature gradient or the concentration changes caused by the interaction between the solute and the medium, the governing equation for the transient diffusion can be expressed by the renowned Fick's second law

$$\frac{\partial c}{\partial t} = D \frac{\partial^2 c}{\partial x^2} \tag{1}$$

if the diffusion coefficient of the solute in the medium D is time and concentration independent. When the diffusion proceeds in a por-

ous medium, the transport of the solute is complicated by two major effects: (i) reduced cross-sectional area is available for the diffusive mass flux of the solute relative to the macroscopic cross-sectional area (because we assume that solute simply cannot penetrate into solid phase), and (ii) the existence of impenetrable solid phase results in more tortuous transport (solute pathway meanders through the medium). As a result, modified Fick's equations describe the transport of the solute through the porous specimen. The exact mathematical model for the description of such diffusion processes is discussed in details by Shackelford and Moore [17] and summarized briefly in our previous paper [16].

Furthermore, when the solute interacts specifically with the solid content of the porous medium, the Fick's equation (1) must be supplemented by a reaction rate component which depends on the actual interaction mechanism. Simple reversible immobilization of the solute on the solid content of the porous medium is commonly presumed as a first approximation. The interaction mechanism can be expressed as

$$S_{\text{free}} \xleftrightarrow{K_{\text{app}}} S_{\text{sorbed}} \tag{2}$$

where S_{free} and S_{sorb} represent the free and the sorbed solute, respectively, and the *apparent equilibrium constant* K_{app} represents a sorbed-to-free solute mass ratio at the equilibrium:

$$K_{\text{app}} = \left[\frac{c_{\text{sorbed}}}{c_{\text{free}}} \right]_{\text{eq}} \tag{3}$$

For the porous systems where the interactions between the solid content and the solute follow the above proposed mechanism, the *apparent diffusion coefficient* of the solute is defined in the following way:

$$D_a = \frac{D_0}{T_m(1 + K_{\text{app}})} \tag{4}$$

where T_m is the *tortuosity factor* (for the used definition of the tortuosity factor, see [16]) and the Second Fick's law for the transport of free solute can then be simply rearranged:

$$\frac{\partial c_{\text{free}}}{\partial t} = D_a \frac{\partial^2 c_{\text{free}}}{\partial x^2} \tag{5}$$

The analytic solution of the last equation according to the corresponding experimental arrangement gives the relation which describes the time-spatial dependence of the free solute concentration in the medium. One commonly used experimental arrangement represents the 'constant source in-diffusion technique'. In this case, the free solute concentration at the boundary of the diffusion medium is kept constant during the experiment. Eq. (5) can be easily processed by the Laplace transformation and the time development of the concentration profile of diffusing solute in the porous medium is given by the following equation:

$$c_{\text{free}} = c_{\text{free},x=0} \cdot \text{erfc} \frac{x}{\sqrt{4D_a t}} \tag{6}$$

where $c_{\text{free}, x=0}$ is the time-independent concentration of the free solute at the boundary from the side of porous medium. Because the concentration profile of the bound (sorbed) fraction of the solute can easily be derived from Eqs. (3) and (6), the total concentration of the solute in gel follows the equation:

$$c_{\text{tot}} = c_{\text{free}} + c_{\text{sorbed}} = c_{\text{free},x=0}(1 + K_{\text{app}}) \cdot \text{erfc} \frac{x}{\sqrt{4D_a t}} \tag{7}$$

The solute partitioning (non-equal distribution) often takes place at the boundary between two phases (*e.g.* the solute solution and the porous medium which the solute diffuses into) which results in a discontinuity in the concentration of free solute at the

interface (see *e.g.* [31]). The partition coefficient Φ then describes the distribution of the free solute between the solution and the porous medium at the boundary:

$$\Phi = \frac{c_{\text{free},x=0}|_{\text{porous}}}{c_{\text{free},x=0}|_{\text{solution}}} \tag{8}$$

and Eq. (7) transforms as follows:

$$c_{\text{tot}} = c_{\text{tot},x=0}|_{\text{porous}} \cdot \text{erfc}\frac{x}{\sqrt{4D_a t}}$$

$$= \Phi \cdot c_{\text{free},x=0}|_{\text{solution}} \cdot (1 + K_{\text{app}}) \cdot \text{erfc}\frac{x}{\sqrt{4D_a t}} \tag{9}$$

where the boundary concentration of the free solute from the solution side $c_{\text{free},x=0}|_{\text{solution}}$ equals the bulk concentration of the solution when the solution is stirred sufficiently.

Consequently, the determination of the total concentration of solute across the porous medium at various times and the processing of data using Eq. (9) result in the determination of the two crucial parameters which describe the partition and the interaction effects independently – *i.e.* the partition coefficient Φ and the apparent equilibrium constant K_{app}.

5. Results and discussion

The diffusion experiments, presented in this paper, follow the previous work, which investigated the barrier effects of humic acids on the transport of Methylene Blue by means of the diffusion cells method [16]. Main disadvantage of those experiments was the inability to directly distinguish the relative impacts of the solute partitioning and the solute binding on the solid content, which proceed in gel simultaneously. The non-stationary experiments overcome this trouble in a simple and highly illustrative way. Because the utilized agarose matrix is transparent, the effects of small additions of a reactive component on the transport of a colored compound can be estimated even visually and the quantitative assessment by means of spectrophotometry poses no problems.

5.1. Diffusion in agarose hydrogels

To provide a comprehensive comparison with the previously published stationary diffusion experiments, the transient diffusion of the dyes in hydrogels with different dry contents of agarose was investigated before turning our attention to hydrogel with the addition of HA.

Fig. 1 shows the concentration profiles of Methylene Blue in gels at 30 °C. The profiles indicate that the penetration of Methylene Blue into gel is only slightly decelerated by increased agarose weight content. This finding is not surprising because the small overall content of agarose is not anticipated to restrict the solute motion considerably. It also corresponds well to the results of diffusion cells experiments. More interesting finding concerns the total concentration of dye at the boundary of gel. The results indicate that gels with higher content of agarose show higher concentration of dye near the boundary. This partitioning effect of agarose in hydrogels is well known and was discussed elaborately [31–35]. The agarobiose backbone of agarose usually contains ionic impurities like sulfonates, ester sulfates, pyruvates and carboxylic groups [36] and the resulting Donnan potential of the agarose network is commonly addressed in the explanation of the enhancement of cation concentrations in hydrogel. Similar concentration profiles as those shown for Methylene Blue in Fig. 1 were determined also when the diffusion of Rhodamine 6G was investigated.

In order to evaluate the above discussed effects quantitatively, the experimental data were processed using the in-diffusion model, presented in Section 4. Measured concentration profiles were
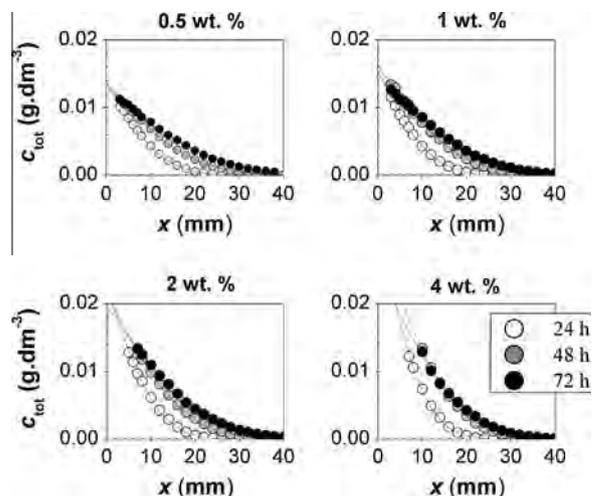
Fig. 1. Experimental (points) and theoretical (lines) concentration profiles of Methylene Blue in agarose gels at 30 °C (the corresponding weight content of agarose is shown above each graph).

fitted by Eq. (9) via the least square method using the Solver add-in in Microsoft Excel. The regression characterized by the solid lines in Fig. 1 resulted in two parameters, *i.e.* the total concentration of the dye at the boundary $c_{\text{tot},x=0}$ and the apparent diffusion coefficient D_a. The standard errors of the diffusion parameters for individual gels were calculated from minimally six determined values (duplicated experiments at three diffusion times).

As can be seen in Fig. 2, the decrease in the diffusivity with increasing agarose content in hydrogel was found for both dyes. This confirms the trend revealed in our previous work by the diffusion cells method [16], although the actual values of D_a are about two times higher here. To explain this difference, it is worth mentioning that in the diffusion cells method, D_a is calculated indirectly from the time needed by solute to penetrate through the hydrogel specimen of known thickness. This time is estimated by the extrapolation of linear part of the break-through curves of the solute although the concentration of the solute in compartment behind hydrogel gradually increases even before (see Fig. 2 in Ref. [16]). By contrast, the non-stationary diffusion method is better suited for the description of the transient stage of the diffusion process, because the time-development of the concentration profiles can be observed repeatedly over the long period of time which significantly reduces the experimental error.

For deeper insight into the meaning of D_a, it is illustrative to compare its value with the diffusion coefficient which describes the transport of the solute in the respective solution (*i.e.* with the free solution diffusion coefficient D_0). The values of free solution diffusion coefficient D_0 of both dyes were determined by the diffusion cells method (the exact experimental procedure is described in [16]) at all studied temperatures. The determined values of D_0 are shown in Tables 1 and 2, together with the free diffusion coefficients of the dyes in the buffer solutions (will be discussed later). Determined free solution diffusivity of Methylene Blue agrees with published values [37,38]. On the other hand, literature values of D_0 for Rhodamine 6G vary by nearly an order of magnitude (for the summary of the values determined by different methods, see [39]). The poorly characterized values of diffusion coefficient of Rhodamine dyes in water are usually attributed to concentration effects caused by molecular aggregation [40]. The diffusion cells experiment provided the value of D_0 at high end of the interval of literature values.

It was found that the diffusivity of both dyes in agarose hydrogels were close to their diffusion coefficients in water (see the half-filled points in Fig. 2). This is the well-expected result for hydrogels
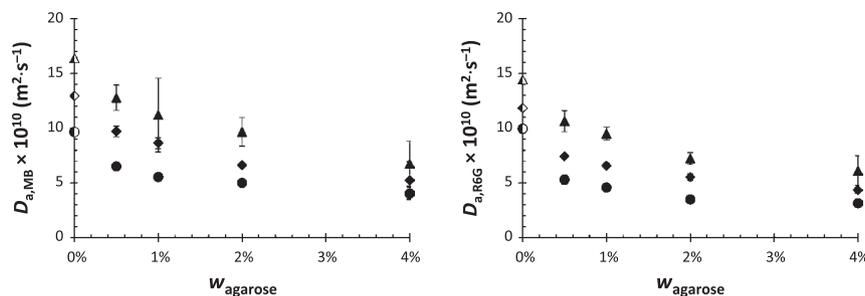
Fig. 2. Apparent diffusion coefficients of Methylene Blue (left) and Rhodamine 6G (right) in hydrogels with different weight content of agarose at 30 °C (○), 40 °C (◇) and 50 °C (△). Half – filled points represent the free solution diffusion coefficients.

Table 1
Free solution diffusion coefficients D_0 of Methylene Blue in all tested solutions (determined by the diffusion cells method; standard error calculated from the triplicated experiment).

	t (°C)	pH	$D_0 \times 10^{10}$ (m² s⁻¹)
Water	30	–	9.66 ± 0.08
	40		12.95 ± 0.01
	50		16.41 ± 0.07
10 mM PBS	30	3	8.74 ± 0.05
		7	7.34 ± 0.23
		11	9.20 ± 0.62
200 mM PBS	30	3	8.88 ± 0.02
		7	8.50 ± 0.09
		11	11.24 ± 0.06

Table 2
Free solution diffusion coefficients D_0 of Rhodamine 6G in all tested solutions (determined by the diffusion cells method; standard error calculated from the triplicated experiment).

	t (°C)	pH	$D_0 \times 10^{10}$ (m² s⁻¹)
Water	30	–	9.94 ± 0.02
	40		11.84 ± 0.05
	50		14.44 ± 0.05
10 mM PBS	30	3	7.45 ± 0.05
		7	6.07 ± 0.01
		11	6.25 ± 0.04
200 mM PBS	30	3	6.98 ± 0.01
		7	7.12 ± 0.03
		11	6.90 ± 0.03

with no specific interactions between diffusing solute and solid content of gel, where the transport of solute is restricted only by more tortuous diffusion pathway caused by the solid content of gel.

Higher standard errors of D_a values of both dyes at 50 °C are evident in Fig. 2; this could imply some structural changes of gel induced by elevated temperature which could bring confusion into the diffusion results. The temperature-controlled phase transition behavior of agarose gels is well known and described in the literature [41]. Nevertheless, it is reasonable to expect that any important structural and textural differences should be associated with the considerable changes in mechanical properties of gels and negligible changes of the viscoelastic characteristics at higher temperatures were revealed by the results of rheometric analysis of gels (see Supporting Info).

Because no specific interactions between the diffusing dyes and the solid content of agarose gels are expected, the decrease in the diffusivity of dyes in agarose gels can be attributed fully to the tortuosity effect and the determined boundary concentration of dye in gel clearly characterizes the partitioning effect described by Eq. (8).

Substituting $K_{app} = 0$ in Eqs. (4) and (8), the values of tortuosity factor T_m and of partition coefficient Φ can be calculated from the determined values of D_a and $c_{tot,x = 0}$, respectively. As can be seen in Fig. 3, the partition coefficient of studied dyes increases with the content of agarose in gel and for Methylene Blue also with the temperature. It complies with the similar tendency, determined previously by the diffusion cells method [16]. Nevertheless, the actual values of Φ are, again, significantly lower (in average about three times lower) than those derived from the steady-state experiments in the diffusion cells. The explanation of the difference is very much the same as in the case of D_a. In the diffusion cells experiment, the partitioning coefficient is estimated from the loss of dye from the solution assuming the linear concentration profile of dye in the gel sample. Unfortunately, this assumption cannot be verified experimentally, which burdens the results of increased uncertainty.

At 30 °C, the values of Φ in 1 wt.% agarose hydrogel are close to unity for Methylene Blue which means that the dye is almost equally distributed between the source solution and hydrogel in equilibrium. Rhodamine concentrates slightly more in agarose gel, as indicated by the value of $\Phi = 2.4$. In more concentrated agarose hydrogels, the value of Φ for both dyes in most cases does not exceed 10. The values of Φ obtained in this work are in better agreement with the published results than those determined previously in [16]. Fatin-Rouge et al. [31] focused on partitioning of different solutes including Rhodamine 6G in gels with the agarose content of about 1 wt.%. They determined the partition coefficients of Rhodamine in the range from 1 to 4, depending on the pH. Also the values of Φ determined in another work for various inorganic and organic low-molecular ions in agarose hydrogel usually fall within the range from 1 to 10 [30]. In general, higher standard errors of Φ were found for the higher temperature, again. Furthermore, the standard errors of the values of Φ determined for Methylene Blue at 40 °C and 50 °C in the 4 wt.% agarose gel were so high (relative error higher than 50 %) that these values were excluded from Fig. 3. To understand this deviation, note that in the concentration profiles shown in Fig. 1, the points representing the concentration values near the boundary are missing for gels with higher weight content of agarose; this is caused by increased turbidity of hydrogels with higher solid content, which in combination with increased concentration of the dye made the values of absorbance close to the interface too high to be assessed properly. Fewer experimental points are therefore subjected to the non-linear regression and the resulting parameters are less precise.

Also the values of tortuosity factor T_m differ from those calculated from the diffusion cells experiments (they are about two times lower here). As can be seen in Fig. 4, the tortuosity factors for both dyes in all agarose gels are not distant from unity which indicates almost straight movement of the solute in gels (consider that T_m represents the square of actual distance traveled by the solute relative to the macroscopic distance). This fact matches the
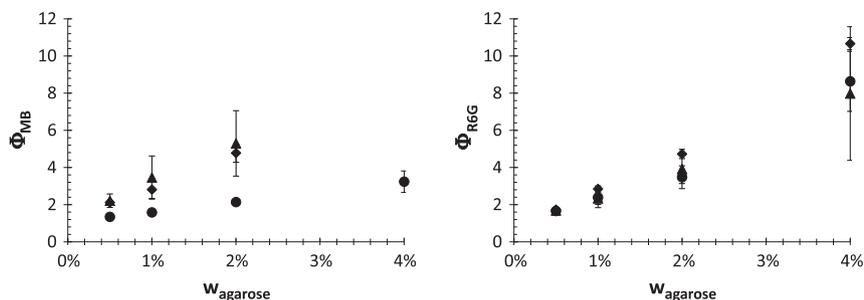
Fig. 3. Partition coefficients of Methylene Blue (left) and Rhodamine 6G (right) in hydrogels with different weight content of agarose at 30 °C (○), 40 °C (◇) and 50 °C (△).
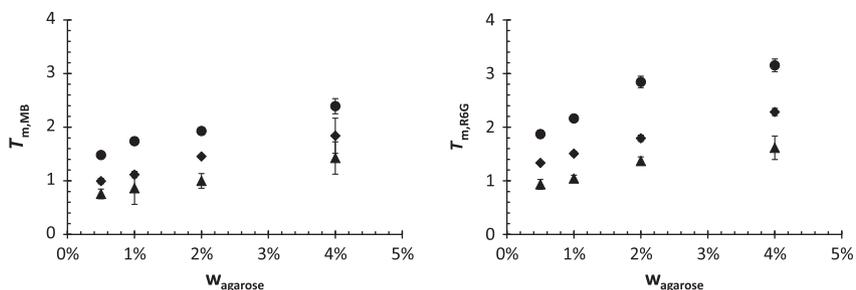
Fig. 4. Tortuosity factors for the diffusion of Methylene Blue (left) and Rhodamine 6G (right) in hydrogels with different weight content of agarose at 30 °C (○), 40 °C (◇) and 50 °C (△).

published results again, because little tortuosity effects are commonly considered in the case of agarose hydrogels [42]. Dilute agar and agarose gels (about 0.5 wt.%) are even used as reference medium with a unit tortuosity in determining the transport properties of some tissues [43,44]. The value of T_m decreases with increasing temperature, indicating that the solid network of gel obstructs less the transport of the solute at higher temperatures.

Looking back to Figs. 2–4, it can also be concluded that both cationic dyes – Methylene Blue and Rhodamine 6G – do not differ essentially in their partitioning and diffusive behavior in agarose hydrogels. It indicates that both effects are driven primarily by the total charge of the solute and slight differences in its other structural parameters (*e.g.* molecular weight and shape) play no crucial role.

5.2. Diffusion in agarose/HA hydrogels

The central intent of the presented work was to shed a new light on the effects of interactions between humic acids and ionic dyes on the transport of the dyes in humics-containing systems. The main set of experiments therefore focused on the comprehensive investigation of diffusive transport of the dyes in agarose hydrogels (1 wt.% of agarose) with various small additions of humic acids, homogeneously spread in the hydrogel matrix. Under all tested experimental conditions, the addition of humic acids into the gel matrix resulted in a strong change in transport properties of the studied dyes, as is clearly shown in Fig. 5.

As is evident from the concentration profiles shown in Fig. 6, a small content of humic acids, more than two orders of magnitude lower in comparison with agarose, leads to the obvious slowdown of the dye penetration in gel as well as to the significant increase in total concentration of dye near the boundary. This is in perfect agreement with the strong enhancement of the barrier properties of gels, found for Methylene Blue in the previous diffusion cells experiments [16].

The observed slowdown of the diffusion process was quantitatively expressed by the shift in apparent diffusivity, calculated

Fig. 5. Picture of the gel samples after 24 h of diffusion of Methylene Blue at 30 °C (four duplicates from left to right: 0 wt.%, 0.002 wt.%, 0.005 wt.% and 0.010 wt.% HA in 1 wt.% agarose gel).

from the least-square fitting of the concentration profiles by Eq. (9). The values of D_a for both cationic dyes decrease considerably with the content of humic acids in gels. As can be seen in Eq. (4), two possible effects can be addressed in searching for the explanation of this interesting behavior. Strong increase in the tortuosity factor could result in the important drop in apparent diffusivity. Nevertheless, the total added amount of humic acids is so small that no significant effect on the structural and mechanical properties of gel should be expected, as was also experimentally proved by the measurement of viscoelastic properties of gels in the previous work [16]. Therefore, it is more reasonable to attribute the observed decrease of D_a entirely to the effect of specific interactions between the diffusing dyes and the humic content of gel.

As far as no changes in tortuosity are expected as a result of small HA addition to agarose hydrogel, the apparent equilibrium constant K_{app} of the reversible sorption can be calculated from the corresponding value of D_a (see Eq. (4)). As can be seen in Fig. 7, the value of K_{app} for most of the studied systems is higher
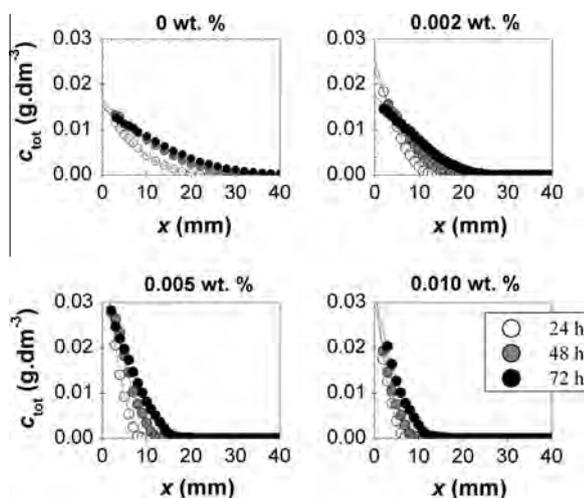
Fig. 6. Experimental (points) and theoretical (lines) concentration profiles of Methylene Blue in 1 wt.% agarose gels with the addition of humic acids at 30 °C (the corresponding weight content of HA is shown above each graph).

than one, which means that the sorption equilibrium, described by the reaction mechanism proposed in Eq. (3), is shifted to the side of products. The immobilization of both solutes is strong enough to affect the overall transport crucially. An interesting difference between both dyes can be seen in Fig. 7. The results of the diffusion experiments indicate that while the sorption of Methylene Blue is strongly suppressed by increasing temperature, no distinct temperature effect was observed on the sorption of Rhodamine 6G. The temperature dependence observed for Methylene Blue is in contradiction with the results of diffusion cells experiments, where the values of K_{app}, calculated indirectly from the breakthrough times, indicated the opposite – the increase of K_{app} with the temperature. This discrepancy in the determination of the *exo*- versus *endo*-thermic character of the HA-MB interactions deserves further investigation in the follow-up experiments, possibly by means of a specialized method for the determination of the heat of reaction (*e.g.* by isothermal calorimetry).

Fig. 8 illustrates the effect of HA on the partitioning of the dyes. It can be seen, that the addition of HA rather suppresses the partitioning of the free solute as compared with respective agarose gel without HA (except for the diffusion of Methylene Blue in hydrogels with 0.002 wt.% HA, where the higher value of Φ was determined at 40 °C and 50 °C). This implies that the effect of specific solute binding on HA over dominates the attraction of the free solute by Donnan potential of gel. While the fall in Φ with the weight content of HA is gradual for Methylene Blue, in the case of Rhodamine 6G, all tested additions of HA led to almost the same reduction in Φ. The differences between both dyes in their temperature-dependent partitioning resemble the above-mentioned depen-

dences of K_{app}. The increase in temperature from 30 °C to 40 °C resulted in noticeable increase in the partition coefficient of Methylene Blue in agarose/HA gels. Interestingly, this trend was not kept when the temperature was further increased from 40 °C to 50 °C. For the partitioning of Rhodamine 6G, the influence of the temperature was not so important.

As was already mentioned, the non-stationary diffusion experiments allow more reasonable investigation of the partitioning phenomena than the steady-state experiments in diffusion cells. Nevertheless, when the partitioning of solute which interacts specifically with the solid content of gel is described using the diffusion model introduced in Section 4, one should bear in mind several issues which may complicate the assessment of accurate values of Φ. Maybe the most critical problem is the experimental differentiation of free and bound form of the solute. Various analytical techniques can specifically quantify the concentration of the respective fraction. In the presented experiments, we assume that the introduced spectrophotometric technique provides the total concentration – *i.e.* the sum of both forms – at different positions of gel. Of course, the visible spectrum of free and bound dye will differ. We tried to overcome this complication by evaluating the spectra using simple calibration technique based on the measurement of the visible spectra of reference samples with known total concentration of the dye, added to the agarose mixture prior to its gelation. This approach is based on the expectation that the distribution of the solute between free and bound forms is the same regardless of whether the solute is incorporated in gel during the preparation or is transported to the already gelatinized sample. The experimental verification of this expectation is problematic, but the utilization of a fractional extraction method like those applied in the study of metal transport in hydrogels made from coagulated humic acids [14] may offer an interesting experimental option for the follow-up work. Anyway, it was found that the absorbance of either Methylene Blue or Rhodamine 6G at the characteristic wavelengths, after the subtraction of the background spectrum of respective hydrogel (the gel free of the dyes), is directly proportional to the total amount of the dye added to the gelling mixture. This zero-intercept linear trend was confirmed for all tested hydrogels, only the slope of the line differed with altered content of agarose and HA in gel and with the different inner pH and ionic strength (results of the later will be discussed in Section 5.3). It is worth mentioning that the linear character of this dependence reduces the experimental problems like inappropriate calibration just to the determination of the nominal value of the solute concentration (and hence the partitioning coefficient Φ), but the shape of the concentration profile (and consequently the calculated D_a) is not affected.

Another crucial point of the method is represented by the selection of an appropriate diffusion model. The model used in this work presumes constant concentration of the solute at the solution/gel interface. To verify the correctness of the presumption, the decrease in total amount of the dye in the source solution
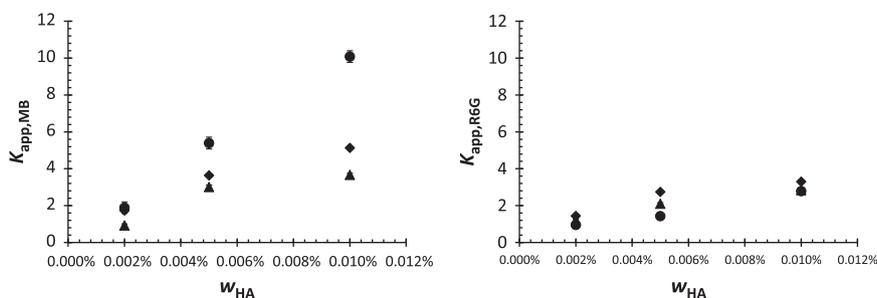
Fig. 7. Apparent equilibrium constants for the diffusion of Methylene Blue (left) and Rhodamine 6G (right) in 1 wt.% agarose hydrogels with different weight content of HA at 30 °C (○), 40 °C (◇) and 50 °C (△).
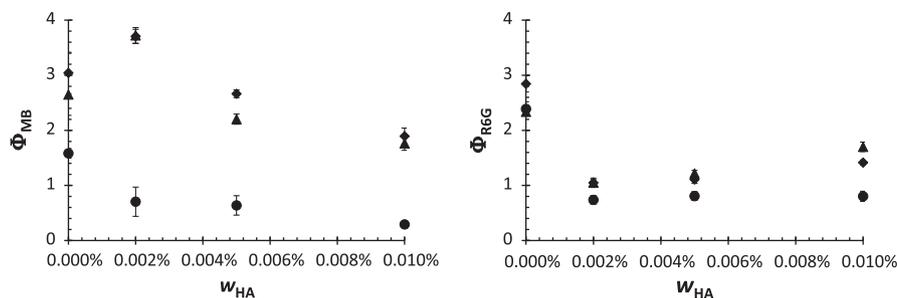
Fig. 8. Partition coefficients for the diffusion of Methylene Blue (left) and Rhodamine 6G (right) in 1 wt.% agarose hydrogels with different weight content of HA at 30 °C ($\bigcirc$), 40 °C ($\diamond$) and 50 °C ($\triangle$).
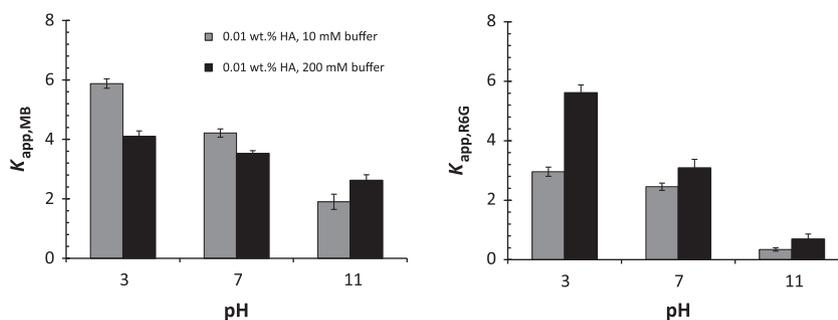
Fig. 9. Apparent equilibrium constants for the diffusion of Methylene Blue (left) and Rhodamine 6G (right) in 1 wt.% agarose hydrogels with 0.01 wt.% of HA at various pH values and ionic strengths at 30 °C.

was determined after the diffusion experiments. It was found that in none of the experiments (including those discussed in Section 5.3) the decrease was higher than 5 rel.%, which together with continuous agitation of the solution guarantees the constant concentration of the dye at the solution side of the boundary during the whole diffusion experiment. Anyway, as was indicated by some determined concentration profiles in gels (see Figs. 1 and 6) the boundary concentration of the solute in some gels seems to vary somewhat with the time. Two possible explanations of the time-dependent solute concentration at the boundary can be proposed. First, the enhanced uptake of the solute from solution, caused by its partitioning at the interface, may lead to the local decrease in the solution concentration near the boundary even when the solution is continuously stirred. Second, partitioning of the solute can vary in time in contradiction with the model. This can happen *e.g.* as a result of changing Donnan potential of the gel as the charged functional groups in the gel are gradually blocked by the specific interactions with the solute. Nevertheless, any quest to include the time-variability of the boundary concentration in the model would result in severely complex mathematical apparatus, inconvenient for the straightforward data evaluation.

A final question concerns the selected sorption mechanism, included in the model and characterized by Eqs. (2) and (3). This sorption mechanism (resulting in a linear sorption isotherm) represents a common approximation, routinely applied in diffusion studies in reactive porous media [17]. It is best applicable in the systems, where a high excess of reactive sites on the sorbent is assumed. This presumption is suitable for the systems with binding sites distributed homogenously in the whole volume (like in reactive hydrogels), unlike *e.g.* the sorption experiments in suspensions, where the sorption is restricted to the surface of solid sorbent particles. However, in the presented experiments, the presumption of the sufficient excess of reactive sites is questionable because of a very small content of the reactive component (HA) in gel. It should also be noted that any discrepancy between the model and the actual interaction mechanism will affect also the determined partition coefficient, because the value of K_{app} is in-

volved in the calculation of Φ from the experimentally determined value of $c_{tot,\ x\ =\ 0}$ (see Eq. (9)). More complex sorption isotherms can be taken into account when compiling the diffusion model. Nevertheless, their involvement inevitably results in the concentration-dependent value of apparent diffusion coefficient of the sorbing solute [45], which will significantly complicate any subsequent data processing. From this perspective, the linear sorption mechanism, utilized in this study, represents a reasonable approximation for the first insight into the specific HA-solute interactions.

5.3. Influence of pH and ionic strength

If the interactions between cationic solutes and humic acids (rich in diverse negatively charged functional groups) were considered as the electrostatic attraction at the first approximation, we should expect important changes in the diffusion of the solutes with different experimental conditions such as pH or ionic strength. Therefore, the non-stationary diffusion experiments were repeated using the dye solutions and hydrogel samples with carefully adjusted values of pH and ionic strength. 1 wt.% agarose hydrogel with no addition of HA and with the highest tested addition (0.01 wt.% HA), respectively, were used in this section.

In order to allow the subsequent processing of the data by the diffusion model presented in Section 4, it was necessary to obtain the values of free solution diffusion coefficients of both dyes in the buffer solutions. In Tables 1 and 2, the values of D_0, determined by the means of the diffusion cells experiments, are shown. It can be seen, that the diffusivities of both dyes in the buffer solutions are slightly suppressed in comparison with their diffusive transport in water. This is not an unexpected finding – the decrease of Methylene Blue diffusivity in ternary mixtures with water and NaCl was thoroughly explained [37]. Methylene Blue and Rhodamine 6G are planar molecules which can bear positive charge. For such solutes, the molecular aggregation to dimers, trimers or larger aggregates will significantly affect the solute's diffusivity in a solution. The aggregation of Methylene Blue was confirmed spectrophotometrically during the diffusion experiment (dimers of Methylene Blue
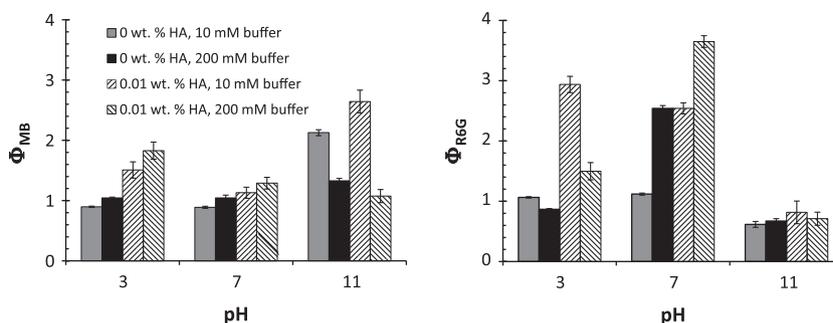
Fig. 10. Partition coefficients for the diffusion of Methylene Blue (left) and Rhodamine 6G (right) in 1 wt.% agarose hydrogels with 0.01 wt.% of HA at various pH values and ionic strengths at 30 °C.

absorb strongly at 605 nm while monomers at 665 nm [46]). When the repulsive electrostatic forces between the like charges of the solute's molecules are shielded by higher ionic strength, the aggregation is supported and the apparent size of the diffusing aggregate increases. The self-aggregation of Methylene Blue, Rhodamine 6G and also some other dyes was thoroughly studied mainly by Mukerjee in late 1960s (see *e.g.* [47,48]) or by others more recently [40,49]. Surprisingly, at pH = 7 and at high ionic strength, Methylene Blue shows even higher diffusivity than in water. This finding is difficult to explain merely on the basis of diffusion cells data and deserves a detailed investigation in the future work.

The main aim of this experimental part was to assess the influence of pH and ionic strength on the specific interactions between diffusing dyes and humic acids. The sorption of cationic dyes – and of the Methylene Blue in particular – on humics and humic-rich materials was subjected to the vast concern in last decades, as was reviewed in our last paper [16]. The effects of pH and low molecular electrolytes were investigated thoroughly. Although the increase in pH usually enhances the sorption of Methylene Blue on the surface of other acidic environmental sorbents like clay [50] or silt [51], the sorption of MB on some humate-based sorbents was found to be only slightly pH-dependent [28,29]. The results of the non-stationary diffusion experiments, presented here, showed even more surprising finding – the immobilizing power of humic acids for both tested cationic dyes decreased with increasing pH, as is characterized by decreasing value of K_{app} in Fig. 9.

This result indicates that the dominating interactions in the systems are not necessarily those of the electrostatic origin. Apart from the usually emphasized dissociable groups (carboxylic and phenolic), humic acids possess plenty of other structural units (*e.g.* aromatic rings, aliphatic alcohols) which offer the suitable binding sites for complex organic molecules like the used dyes. For example, the sorption of polycyclic aromatic hydrocarbons to aromatic residues in the structure of humic acids by a hydrophobic stacking is well known [52] and was found to be crucial for the biodegradation of these harmful species (*e.g.* [53]). Such interactions themselves are less sensitive to a shift in pH or ionic strength than the electrostatic ones; nevertheless, some pH-dependent changes in the conformation of humic acids might play an important role for example by affecting the spatial availability of the hydrophobic sites to the diffusing solute.

Furthermore, the aggregation of the dyes should be taken into account yet again. The dimerization of Methylene Blue at the pH = 11 was confirmed from significant change in UV–VIS spectra of the dye in gel. In Fig. 9, it can be seen that only at this pH, the increase in the buffer strength resulted in the enhancement of sorption of MB in gel. Higher ionic strength of the solution is known to enhance the dimerization of MB [54]. Therefore, the results in Fig. 9 indicate that, at the pH = 11, aggregated MB is bound to humic acids preferentially and the increase in aggregation

(caused *e.g.* by higher ionic strength) may support this binding. In the case of Rhodamine 6G, the enhancement in the K_{app} by increased ionic strength was found at all pH values. The aggregation of this dye seems to play even more important role, as can be deduced also from the comparison of the results shown in Figs. 7 and 9. It can be seen that while the value of K_{app} for Methylene Blue is significantly lower in buffered hydrogels as compared to unbuffered ones (at 30 °C, the value of K_{app} in 0.01 wt.% HA hydrogels without the adjustment of pH was as high as 10), for Rhodamine 6G at the pH = 3 and 7, comparable values of K_{app} were determined in unbuffered gel (K_{app} = 2.8) and in that with the use of 10 mM buffers (3.0 and 2.5 at the pH = 3 and 7, respectively) and even higher values K_{app} were obtained with 200 mM buffers. Only at the pH = 11, the sorption of Rhodamine 6G on humic acids was suppressed, as indicated by the values of K_{app} lower than 1.

As can be seen in Fig. 10, the effect of pH and ionic strength on the partition coefficient Φ is even more complex and hardly explainable. Again, Methylene Blue behaves extraordinarily at the pH = 11. While at other pH values, both the ionic strength and the HA content elevate the partitioning of the free solute, the effect of ionic strength at the pH = 11 is opposite. The explanation of this finding may be found in the aggregation behavior of the dye once again. The same holds also for Rhodamine 6G. Both, the sorption of Rhodamine 6G in gel, as well as the partitioning of its free fraction are suppressed at the pH = 11. The partitioning behavior of Rhodamine at the pH = 3 and 7 is so incomprehensible that it should be further addressed in a future work.

The above discussed variation in the diffusion and partitioning characteristics of gels at different pH and ionic strength cannot be attributed to the changes in the structural and textural properties, because all tested gels show very similar viscoelastic properties (see Supporting Info).

6. Conclusions

The results of the non-stationary diffusion experiments, presented in the paper, clearly confirmed the crucial influence of the presence of humic acids in a system on the molecular transport of cationic solutes. Outstanding sorption ability of humic acids results in the strong decrease in mobility of the solutes, more pronounced for the systems with higher content of humic acids. As was indicated by the experiments, performed at various pH values and ionic strengths, the interaction between the humic content and the oppositely charged organic dyes are more complex than expected and should not be considered as just simple electrostatic attraction. Apart from the immobilizing effects of humic acids, one famous feature of agarose hydrogels – the considerable partitioning of low-molecular cations in gels – was confirmed once again.

The diffusion technique, introduced in the presented experiments, represent the next step in the development of a thorough diffusion methodology, applicable universally in the study on reac-

tivity and barrier ability of reactive and functional polymers of a biological, environmental or industrial concern. The non-stationary diffusion experiments complement the previously used method of diffusion cells reasonably. While the experiments in diffusion cells focus on the steady-state stage of the diffusion process and illustrate primarily the barrier properties of a material after its penetration by the solute, the transient stage of the process is described by the non-stationary experiments more elaborately, enabling the further insight into particular effects which define the rate of the solute transport. Some of these essential effects, like partitioning or specific interactions of the solute on diffusion movement, are observable in so illustrative way that the method should be appreciated also for educative purposes.

Nevertheless, in the evaluation of the results from either the steady-state or non-stationary diffusion experiments, the selection of a suitable mathematical model and careful compliance with the corresponding experimental conditions represent the necessary requirement in order to obtain the data of the sufficient quality. As is discussed above, an extensive experimental work should follow to prove the validity of some assumptions applied in the utilized model – mainly the time-independent partitioning of the dyes at the solution/gel boundary and the simplified linear mechanism of the sorption process.

Acknowledgements

Appendix A. Supplementary material

Supplementary data associated with this article can be found, in the online version, at http://dx.doi.org/10.1016/j.reactfunctpolym.2013.12.002.

References

[1] IHSS What are Humic Substances? Official website of International Humic Substances Society. <http://www.humicsubstances.org> (2007) Accessed: August 2013.
[2] M. Schnitzer, C.M. Monreal, Adv. Agron. 113 (2011) 139–213.
[3] H.B. Bradl, J. Colloid. Interf. Sci. 277 (2004) 1–18.
[4] X.L. Tan, M. Fang, et al., Molecules 15 (2010) 8431–8468.
[5] B. Gevao, K.T. Semple, et al., Environ. Pollut. 108 (2000) 3–14.
[6] J. Tolls, Environ. Sci. Technol. 35 (2001) 3397–3406.
[7] C.N. Guppy, N.W. Menzies, et al., Aust. J. Soil Res. 43 (2005) 189–202.
[8] M. Havelcova, J. Mizera, et al., Chem. Listy 105 (2011) 913–917.
[9] M.M. Scherer, S. Richter, et al., Crit. Rev. Env. Sci. Technol. 30 (2000) 363–411.
[10] H.M. Selim, H. Zhang, J. Environ. Qual. 42 (2013) 640–653.
[11] P. Sedláček, M. Klučáková, Geoderma 153 (2009) 11–17.
[12] P. Sedláček, M. Klučáková, Collect. Czech. Chem. Commun. 74 (2009) 1323–1340.
[13] M. Klučáková, M. Pekař, Colloids Surfaces A 349 (2009) 1–3.
[14] M. Kalina, M. Klučáková, P. Sedláček, Geoderma 207–208 (2013) 92–98.
[15] M. Klučáková, M. Kalina, P. Sedláček, L. Grasset, J. Soil. Sediment (2013) in press (Available online: 26 June 2013), http://dx.doi.org/10.1007/s11368-013-0730-2.
[16] P. Sedláček, J. Smilek, M. Klučáková, React. Funct. Polym. 73 (2013) 1500–1509. http://dx.doi.org/10.1016/j.reactfunctpolym.2013.07.008.
[17] C.D. Shackelford, S.D. Moore, Eng. Geol. 152 (2013) 133–147.
[18] M. García-Gutiérrez et al., J. Iber. Geol. 32 (2006) 37–54.
[19] B.T. Henry, J. Adler, et al., J. Pharm. Pharmacol. 44 (1992) 543–549.
[20] S.J. Gibbs, E.N. Lightfoot, et al., J. Phys. Chem. 96 (1992) 7458–7462.
[21] A.W. Wang, B.J. Costello, et al., Anal. Chem. 65 (1993) 1639–1642.
[22] E.N. Dunmire, A.M. Plenys, et al., J. Control. Release 57 (1999) 127–140.
[23] J. Ostergaard, E. Meng-Lund, et al., Pharm. Res. 27 (2010) 2614–2623.
[24] F.B. Ye, A. Yaghmur, et al., Eur. J. Pharm. Sci. 43 (2011) 236–243.
[25] F.B. Ye, S.W. Larsen, et al., Eur. J. Pharm. Sci. 46 (2012) 72–78.
[26] K. Samprovalaki, P.T. Robbins, et al., J. Food Eng. 110 (2012) 441–447.
[27] K. Samprovalaki, P.T. Robbins, et al., J. Food Eng. 111 (2012) 537–545.
[28] R.D. Guy, D.R. Narine, S. DeSilva, Chemistry 58 (1980) 547–554.
[29] P. Janoš, Environ. Sci. Technol. 37 (2003) 5792–5798.
[30] M. Golmohamadi, T.A. Davis, et al., J. Phys. Chem. A 116 (2012) 6505–6510.
[31] N. Fatin-Rouge, A. Milon, J. Buffle, R.R. Goulte, A. Tessier, Phys. Chem. B 107 (2003) 12126–12137.
[32] M. Golmohamadi, K.J. Wilkinson, Carbohyd. Polym. 94 (2013) 82–87.
[33] M. Klučáková, M. Pekař, Colloids Surface A 252 (2005) 157–164.
[34] J. Peuravuori, P. Žbánková, K. Pihlaja, Fuel Process. Technol. 87 (2006) 829–839.
[35] E.M. Johnson, D.A. Berk, et al., Biophys. J. 68 (1995) 1561–1568.
[36] S. Dumitriu, Polysaccharides: Structural Diversity and Functional Versatility, second edition., CRC Press, 2004.
[37] G.D. Leaist, Can. J. Chem. 66 (1988) 2452–2456.
[38] T. Hori, N. Kamon, et al., J. Soc. Dyers Colour. 103 (1987) 265–270.
[39] P.O. Gendron, F. Avaltroni, et al., J. Fluoresc. 18 (2008) 1093–1101.
[40] S. Dare-Doyen, D. Doizi, et al., J. Phys. Chem. B 107 (2003) 13803–13812.
[41] M.F. Lai, C.Y. Lii, Int. J. Biol. Macromol. 21 (1997) 123–130.
[42] A.N. Fernandes, C.A. Policiano, J. Mol. Struct. 982 (2010) 62–65.
[43] P. Lesný, J. De Croos, M. Prádný, J. Vacík, J. Michálek, S. Woerly, E. Syková, J. Chem. Neuroanat. 23 (2002) 243–247.
[44] L. Tao, C. Nicholson, J. Theor. Biol. 229 (2004) 59–68.
[45] N.F.E.I. Nestle, R. Kimmich, J. Phys. Chem. 100 (1996) 12569–12573.
[46] K. Bergmann, C.T. Okonski, J. Phys. Chem. 67 (1963) 2169–2177.
[47] A.K. Ghosh, P. Mukerjee, J. Am. Chem. Soc. 92 (1970) 6408–6412.
[48] A.K. Ghosh, P. Mukerjee, J. Am. Chem. Soc. 92 (1970) 6413–6415.
[49] R. Sariri, M.S. Zakerhamidi, et al., J. Mol. Liq. 115 (2004) 55–61.
[50] C.H. Weng, Y.F. Pan, J. Hazard. Mater. 144 (2007) 355–362.
[51] Y. Zaker, M.A. Hossain, T.S.A. Islam, Int. Res. J. Environ. Sci. 2 (2013) 1–7.
[52] B. Marschner, J. Plant Nutr. Soil Sci. 162 (1999) 1–14.
[53] K.E.C. Smith, M. Thullner, et al., Environ. Sci. Technol. 43 (2009) 7205–7211.
[54] J.B. Ghasemi, M. Miladi, J. Chin. Chem. Soc. – Taip. 56 (2009) 459–468.

Appendix 6

Klučáková, M., Kalina, M., Sedláček, P., and Grasset, L. Reactivity and transport mapping of Cu(II) ions in humic hydrogels. *Journal of Soils and Sediments* **2014**, 14, 368–376.

IHSS 16: FUNCTIONS OF NATURAL ORGANIC MATTER IN CHANGING ENVIRONMENT

Reactivity and transport mapping of Cu(II) ions in humic hydrogels

**Martina Klučáková · Michal Kalina · Petr Sedláček ·
Laurent Grasset**

Abstract

Purpose Reactivity and transport properties of metal ions are important both for evaluating and understanding role of humic substances in natural systems and human-driven applications as solving their structural questions. This paper focuses on metal ions diffusion and immobilization in humic hydrogels with various contents of reactive functional groups of humic substances in order to study an effect of their selective blocking on the mobility and immobilization of Cu(II) ions.

Materials and methods Cu(II) ions were chosen as an example of reactive metal for the diffusion experiments. The environment for the diffusion experiment was prepared from the hydrogel form of humic acids. Humic acids were modified by the methylation with trimethylsilyl-diazomethan. Various ratios between untreated and methylated humic acids were used in order to regulate the content of carboxylic groups in humic hydrogels. The hydrogels were pressed gently in glass tubes and used for diffusion experiments (method of instantaneous planar source). After the diffusions the hydrogel from the tubes was sliced and Cu(II) ions were extracted separately from the slices of hydrogels by the 1 M HCl. The concentration of Cu(II) ions in extractants was determined by means of ultraviolet/visible spectrometry.

Results and discussion Previous works showed that transport of metal ions in humic gels is strongly influenced by reactivity of humic acids, therefore changes in the content of carboxylic groups result in changes of diffusivity. The diffusion coefficients of Cu(II) ions, determined in this work, showed the significant dependence on reaction ability of humic hydrogels. Lower amounts of the carboxylic groups caused the decrease of the diffusion rate. The reason could be that the interactions of Cu(II) ions with HA in gel cause their immobilization. The immobilized metal ions are strongly bonded with HA and are not able to diffuse. It results in the increase of the concentration gradient of movable Cu(II) ions, which is the driving force of their transport.

Conclusions The used mathematical description is discussed in terms of the influence of reaction of Cu(II) ions with humic acids and their structural arrangement in hydrogels with various content of reactive functional groups. In general, diffusion experiments seem to provide valuable method for reactivity mapping studies on humic substances.

Abbreviations

DLS	Dynamic light scattering
FTIR	Fourier transform infrared spectroscopy
HA	Humic acids
MHA	Methylated humic acids
UV/VIS	Ultraviolet/visible

M. Klučáková · M. Kalina (✉) · P. Sedláček
Faculty of Chemistry, Materials Research Centre,
Brno University of Technology, Purkyňova 118,
612 00, Brno, Czech Republic
e-mail: xckalina@fch.vutbr.cz

L. Grasset
CNRS, Laboratoire de Synthèse et de Réactivité des Substances
Naturelles-UMR 6514, Université de Poitiers,, 4 rue M. Brunet,
86022, Poitiers Cedex, France

1 Introduction

Humus, or more specifically humic substances, is like air in a sense—it is ubiquitous, renewable, and essential for life to exist on planet Earth. Nevertheless, even after more than two

centuries of substantial research, the basic chemical nature, biosynthetic pathways, and reactivity of humic substances and soil organic matter are still poorly understood (Schnitzer and Monreal 2011). Humic substances represent complex heterogeneous mixtures of polydispersed materials and can be divided into three main fractions: humic acids (HA), fulvic acids and humin. The humic and fulvic acids are extracted from soil and other solid phase sources using a strong base. HA are insoluble at low pH, and they are precipitated by adding strong acid. Humin cannot be extracted with either a strong base or a strong acid (IHSS 2007).

The less is known about the exact structure and origin of humic substances, the more their environmental importance becomes clear (Schnitzer and Khan 1972; Tan 2003). Soon after the first isolation of humic acids (Achard 1786), their surprising affinity to interact with almost any compound, regardless of its hydrophilic or hydrophobic nature, became the main factor motivating research on different aspects of behavior of this fascinating natural material. It is just this affinity which is now well-known to stand behind crucial environmental impacts of humic substances such as speciation and immobilization of both nutrients and pollutants in the environment. Complex structural skeleton with the great diversity of functional groups makes an exact understanding of mechanisms of such interactions almost impossible; nevertheless, numerous attempts have been made focusing on interaction with different types of compounds—e.g., heavy metals (Bradl 2004; Kerndorff and Schnitzer 1980; Klucakova and Pekar 2006), radionuclides (Tan et al. 2010) or polycyclic aromatic hydrocarbons (Marschner 1999)—and utilizing different chemical and physicochemical techniques as spectroscopic techniques, titrations, chromatography pyrolysis, anodic stripping voltammetry, etc. (Swift 1996). Copper (Cu) is widely utilized in complexation studies on humic acids, not only for its health and environmental issues. Cu causes stomach and intestinal distress, liver and kidney damage, and anemia, its environmental occurrence is therefore subject to strict regulations (e.g., US drinking water regulation from 1992). Besides, Cu is well-known for both its high affinity for humic substances and ability to form one of the strongest bonds with them (Stevenson 1994). Due to the above and also because of easy quantification of Cu(II) content (e.g., by means of ultraviolet/visible (UV/VIS) spectroscopy), cupric ions are utilized also in this work.

Carboxylic groups are generally considered the main humic functional components involved in complexation of metal ions, other groups are usually either neglected (Lieser et al. 1991) or only weakly acidic groups such as phenolic, enolic or alcoholic are taken into account (Stevenson 1994). Detailed information on exact structural motifs, in which the Cu(II) are bonded, can be achieved by modern spectroscopic methods such as X-ray absorption near-edge structure spectroscopy or extended X-ray absorption fine-structure spectroscopy. These

methods were applied, e.g., by Frenkel et al. (2000) and Karlsson et al. (2008), results of their studies illustrate significant role of nitrogen-containing groups of HA in complexation of Cu(II), mainly at low Cu(II)/HA ratios. Cu(II) forms five-membered rings with possible combinations of amine, carboxyl, and carbonyl functional groups. As can be seen, experimental facilities for differentiation of relative involvement of particular functional groups on the sorption process exist; nevertheless, availability of sophisticated methods, like the two mentioned above, is still poor especially in the soil research.

One promising tool to decrease the level of complexity of the sorption processes can be provided by selective structural derivatization of utilized humic acids. O-alkylation of acidic groups has long been recognized as a valuable aid in structural mapping of humic acids. Methylation was utilized for direct determination of the OH groups' content in coal- and peat-derived humic acids (Kuran et al. 2008). The O-alkylation also improves solubility of humic acids in organic solvents, which supports chromatographic fractionation and characterization by nuclear magnetic resonance. Alkylated humics give simpler (though still complex) spectral data with improved resolution providing deeper structural insight. Last but not the least, alkylated OH groups do not form hydrogen bonds which is well utilized in determination of molecular mass distribution (Bartle et al. 1987; Ricca et al. 2000). Numerous papers have therefore been published on characterization of alkylated humic acids by means of nuclear magnetic resonance (Bartle et al. 1987; Ogner 1979; Ricca et al. 2000; Sachs et al. 2002), Fourier transform infrared spectroscopy (FTIR) (Andjelkovic et al. 2006; Ricca et al. 2000; Schmeide et al. 2003; Wagner and Stevenson 1965), size exclusion chromatography (Bartle et al. 1987; Ricca et al. 2000), potentiometry (Andjelkovic et al. 2006), X-ray absorption (Schmeide et al. 2003), and others. To illustrate another interesting purposes for O-alkylation of humics, protection of acidic groups during controlled oxidation (Deserra and Schnitzer 1972; Ogner 1973), enhancement of extraction of hydrophobic constituents from HA (Khan and Schnitzer 1972) or exploration and modeling of involvement of particular chemical groups at initial stages of low rank coal liquefaction (Clemow et al. 1999) can be mentioned.

So far, much fewer reports have been presented on utilization of alkylation in order to study sorption processes on humics. In a previous work, methylation followed by controlled hydrolysis of methyl ester groups in humic acids was applied to selectively block phenolic groups before complexation of uranium(VI) ion (Schmeide et al. 2003). Results of this experiment confirmed that predominantly monodentate HA carboxylate groups are responsible for binding uranyl ions and that an effect of phenolic OH is insignificant under the applied experimental conditions (pH=2). Other authors compared the Cu(II) binding properties of native peat HA,

methyl-esterified HA and base hydrolyzed HA (Gardea-Torresdey et al. 1996). A limited decrease in metal-binding capacity after esterification and a subsequent regain of the capacity after hydrolysis demonstrated the unique role of carboxylic groups in complexation of heavy metals accompanied by partial involvement of other HA groups. Infrared analysis was utilized to confirm the esterification and hydrolysis and to exclude any degradation of used HA.

Numerous reaction pathways have been proposed in order to alkylate acidic OH groups of HAs. Generally, the reactions can be divided into two categories. The first is represented by harsh alkylation by thermochemolysis (alternatively called thermally assisted hydrolysis), e.g., with tetramethylammonium hydroxide (Grasset et al. 2002; Deport et al. 2006), which involves cleavage of ester, amide and ether bonds, followed by methylation of the resulting polar groups (alcoholic and carboxylic OH). The reaction takes place in gas phase at high temperatures, hence severe chemical changes occur and the resulting structure of derivatized material is poorly reproducible. The second category of *O*-alkylation of humics includes reactions under mild conditions which minimize chemical destruction of the backbone of humic acids. Several alkylation agents have been tested for this purpose, such as dimethylsulfate (Kuran et al. 2008; Morita 1966), alkyl halides (Clemow et al. 1999; Ogner 1979; Piccolo et al. 2006; Ricca et al. 2000), trimethoxymethane (Gardea-Torresdey et al. 1996) or the most frequently diazomethane (Bartle et al. 1987; Deserra and Schnitzer 1972; Khan and Schnitzer 1972; Ogner 1973; Sachs et al. 2002; Schmeide et al. 2003; Wagner and Stevenson 1965). Very good review of applications, mechanisms, and limitations of simple alkylating agents for carboxylic, phenolic, and other oxygen-containing groups is presented in the work (Lamoureux and Aguero 2009). Trimethysilyldiazomethane (TMS-DM) is proposed as a convenient alternative for diazomethane whose explosive and toxic nature is a cause for concern. The use of TMS-DM as a methylation agent is clean, safe, time-saving, and cost-effective (Park et al. 2001; van 't Erve et al. 2010) and the mechanism of the methylation is well understood (Kuhnel et al. 2007; Meek et al. 1968).

In our recent papers (Klucakova and Pekar 2009; Sedlacek and Klucakova 2009a, b), simple diffusion experiments were introduced as an innovative tool to study interactions of humic substances with metal ions. This approach overcomes the main drawbacks of standard batch sorption experiments in a suspension of humics—it suppresses undesirable side effects of experimental setup (e.g., particle size of humic acids, rate of agitation) and it allows the direct observation of an effect of the interactions on actual mobility of the compound under investigation. As a suitable medium for such experiments, hydrogel forms of humic acids were proposed. These hydrogels can be prepared easily as described elsewhere (Klucakova and Pekar

2009; Martyniuk and Wieckovska 2003; Sedlacek and Klucakova 2009a, b), and they provide homogenous distribution of reactive sites of the humics throughout the sample. Besides, semi-solid hydrogel media provide other experimental advantages: diffusion transport proceeds almost as fast as in a solution but any undesirable mechanical and thermal mixing of the system is suppressed markedly, a hydrogel sample can be shaped and sized as needed, which is necessary for correct interpretation of diffusion results, and the mathematical apparatus used for data evaluation is well explained (Crank 1956; Cussler 1984) and provides some standard parameters—e.g., diffusion coefficients—that quantitatively describe influences of the interactions on transport in the system. The presented article focuses on diffusion of Cu(II) ions in humic gels with different contents of untreated and methylated humic acids in order to discuss an effect of selective blocking of the reactive groups of HA on the mobility of Cu(II) in the system.

1.1 Theoretical background for diffusion experiments

Mathematical apparatus utilized in description of any nonstationary diffusion process comes from an appropriate analytical solution of general Fick's equation, which characterize time-spatial distribution of the diffusing matter. For the simplest case of one-dimensional diffusion, the Fick's equation can be written in following form:

$$\frac{\partial c}{\partial t} = D \frac{\partial^2 c}{\partial x^2} \tag{1}$$

where c represents the concentration of the diffusing compound in the time t and the position x (the coordinate parallel to the direction of diffusion movement). Diffusion coefficient D is the main parameter characterizing rate of the diffusion process. While solving this partial differential equation, appropriate initial and boundary conditions must be applied according to the particular experimental settings (Crank 1956; Cussler 1984).

In Eq. (1), strictly one-dimensional diffusion in an "inert" medium is considered ("inert" means that the medium does not chemically interact with the diffusing particles). When studying diffusion in such complex media as reactive hydrogels (such as in this work), where the movement of the diffusing particles gets tortuous because of the porous character of the gel and some interactions between the diffusing matter and the gel network can be assumed, mathematical apparatus becomes much more complicated. Theoretically, all the reaction rate components must be added to the right side of Eq. (1) and an analytical solution of the equation becomes hardly accessible. Nevertheless, a simplification is often applied: it presumes that all the mentioned interactions between diffusing compound and the surrounding medium do

not destroy the fickian character of the diffusion process, but the value of diffusion coefficient is altered. Mathematically, this presumption is expressed by the modified form of Eq. (1):

$$\frac{\partial c}{\partial t} = D_{eff} \frac{\partial^2 c}{\partial x^2} \qquad (2)$$

where D_{eff} is the so called "effective diffusion coefficient" (or "effective diffusivity") in which all the mentioned effects (tortuous movement of the diffusing matter, chemical interactions in the system) are involved.

For experimental settings presented in this paper, mathematical concept of unsteady diffusion from instantaneous planar source of the diffusing matter can be adopted. This concept represents a solution of the Fick's equation for the case of diffusion from initial concentration pulse of infinitesimally small width. For this presumption and for the zero initial concentration of diffusing matter in surrounding media, following mathematical solution can be found:

$$c = \frac{n}{S\sqrt{\pi D_{eff} t}} \exp\left(-\frac{x^2}{4 D_{eff} t}\right) \qquad (3)$$

where n stands for the total mass of diffusing compound applied in the form of a narrow pulse and S is the cross–section area available for the transport of the compound. For calculation of effective diffusivity directly from the experimental concentration profiles (concentrations of the diffusing compound at different positions), the linearization of Eq. (3) is usually applied in the form

$$\ln c = \ln \frac{n}{S\sqrt{\pi D_{eff} t}} - \frac{x^2}{4 D_{eff} t} \qquad (4)$$

The effective diffusion coefficient D_{eff} can then be determined from the slope of linear regression of $\ln c = f(x^2)$ (Crank 1956; Cussler 1984; Sedlacek and Klucakova 2009a).

2 Materials and methods

2.1 Humic acids

The humic acids (HA), used in this work, were isolated by alkaline extraction from South-Moravian lignite (Klucakova and Pekar 2004, 2005a; Sedlacek and Klucakova 2009b). The methylated humic acids (MHA) were prepared from HA by following procedure: 1 g of nonmodified humic acids was mixed with 4 cm³ of CHCl₃ and 2 cm³ of methanol. After that 4 cm³ of 2 M solution of trimethylsilyl-diazomethan in hexane (TMS-DM) were added. Mixture was continuously stirred for 2 h on vortex. Subsequently, additional 0.75 cm³ of (TMS-DM) was added. Obtained methylated humic acids were dried 2 h under nitrogen atmosphere and then overnight at 50 °C in oven.

Both samples, HA and MHA were characterized by the means of elemental analysis, carboxylic acidity, FTIR spectrometry and dynamic light scattering (DLS). The elemental analysis was carried out using the CHNSO Microanalyser Flash 1112 Carlo Erba. The content of carboxylic functional groups was determined by standard acetate method (Schnitzer and Khan 1972; Stevenson 1994). For determination of total acidity HAs were suspended in water in ratio 1 g/50 cm³ and stirred 24 h to achieve the equilibrium. The equilibrated dispersion was titrated by 1 M NaOH standard solution. The methods of conductometric and potentiometric titrations were used for monitoring the course of neutralization (Klucakova and Pekar 2005a). The inflexion points of potentiometric titration curves were determined on the basis of their derivative forms and the total acidity was calculated using the added volume of NaOH in this point. In the case of conductometry, the acidity was determined from the intersection of two linear sections of the titration curve by solving their linear equations. The final value of total acidity is the average of conductometry and potentiometry (both triplicated). The FTIR spectra of solid humic powders in KBr pellets were measured by spectrometer Nicolet Impact 400. Particle sizes of MHA and HA samples were determined in their alkaline solutions (0.5 M NaOH) with humic concentration 0.8 g dm⁻³ by means of Zetasizer Nano ZS with backscattering detection.

More details on chemical structure of both the original lignite matrix and the isolated HA can be found in previously published works (Klucakova and Pekar 2005a; Peuravuori et al. 2006).

2.2 Humic hydrogels

Humic hydrogels were prepared from the mixtures containing HA and MHA in various weight ratios MHA/HA (0–0.6). The mixtures of humic powders were dissolved in 0.5 M NaOH and then acidified with concentrated HCl solution up to pH-value close to 1. The precipitated humic hydrogel was separated from the solution by repeated centrifugation and washing with deionized water. The content of dry matter in the prepared hydrogels was 14.9±0.5 wt.%.

2.3 Diffusion experiments

The hydrogels were pressed gently in glass tubes (length, 3 cm and diameter, 1 cm). A circular slice of filtering paper (diameter, 1 cm) was sunk into the solution of the 1 M solution of CuCl₂ for 1 min and then added to one side of the tube filled by hydrogel. The tube was packed with parafilm and aluminium foil to prevent hydrogel drying. The duration of diffusion experiments was 5, 24, and 48 h, respectively. Then the glass tube was removed and the hydrogel was sliced (thickness of slices was 3–4 mm) and both

Table 1 Elemental composition and carboxylic and total acidity of humic acids (HA) and methylated humic acids (MHA) samples (normalized on dry ash-free samples)

Sample	C (at.%)	H (at.%)	N (at.%)	S (at.%)	O (at.%)	COOH (mmol/g)	Total acidity (mmol/g)
HA	39.97	40.74	0.81	0.26	18.22	4.24	4.45
MHA	37.72	46.84	0.83	0.09	14.52	0	0

paper and hydrogel slices were extracted separately in the 1 M HCl solution. The concentration of Cu(II) ions in extractants was determined by means of UV/VIS spectroscopy spectrometry (Hitachi U3900H). Simultaneous diffusion experiments for the determination of equilibrium constant K in Eqs. (5) and (6) were carried out. In this case humic gels were not sliced but only extracted by two various leaching agents (up to the achievement of constant concentrations in extractants). The 1 M MgCl$_2$ solution was used as an extraction agent for mobile and ion-exchangeable fraction of Cu(II) ions which are not firmly immobilized in the HA structure. The strongly bonded fraction of Cu(II) ions is the difference between the amount obtained from HCl and MgCl$_2$ extractions. The HCl and MgCl$_2$ solutions were chosen on the basis of results published in previous works (Rauret 1998; Tessier et al. 1979).

All the experiments were carried out at laboratory temperature (25±1 °C) in triplicate.

3 Results and discussion

The humic samples used in this work were characterized by several methods. Their elemental composition corresponds to structural changes of carboxylic functional groups and the replacement of H$^+$ ion in COOH by methyl CH$_3$ group. The methylation resulted in the increase of the elemental C/O ratio from 2.19 to 2.59 accompanied by the decrease of the elemental C/H ratio from 0.98 to 0.80. It corresponds to the replacement of H$^+$ ions by CH$_3$ in carboxylic groups and the results of acidity titrations, which confirmed that the content of acidic functional groups in the methylated sample is equal to zero (see Table 1). The FT-IR spectra of HA and MHA confirmed changes in humic structure after methylation (Fig. 1). In the spectrum of MHA, intensity of absorption bands attributed to CH$_3$ group are markedly increased, as can be seen in regions 2,700–3,000 cm^{-1} (stretching vibration of C–H bond in CH$_3$ group) and 1,400–1,500 cm^{-1} (C–H deformation of CH$_3$ group). Additionally, characteristic absorption bands of OH and COOH groups of HA are strongly affected. Intensity of the broad peak around 3,500 cm^{-1} is somewhat decreased by the methylation. The shallow broad band centered at around 2,580 cm^{-1} is completely absent in MHA. Absorption band originally found at 1,720 cm^{-1}, corresponding to C=O stretching, is shifted to higher wave numbers after methylation (1,735 cm^{-1}) and the absorption is increased. Absorption at 1,260 cm^{-1} is enhanced as well. These findings agree with extensively published effect of methylation on humic acids (Schmeide et al. 2003; Andjelkovic et al. 2006; Gardea-Torresdey et al. 1996) and can be attributed to formation of methyl ether and ester groups via derivatization of original HA by TMS-DM.

The hydrogels for the diffusion experiments were prepared either from HA sample or from a mixture of HA and MHA. Various ratios between HA and MHA were used in order to

Fig. 1 The FT-IR spectra of HA and MHA samples
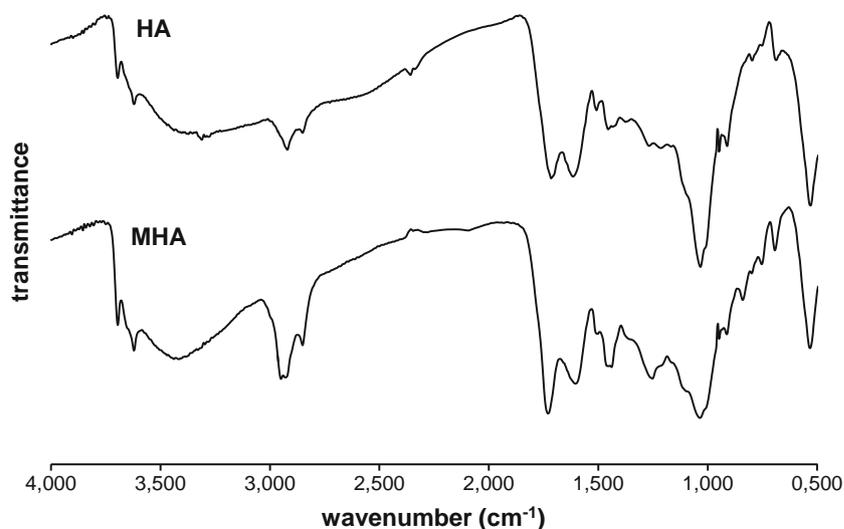
Table 2 The ratio between methylated humic acids (MHA) and humic acids (HA) in prepared humic hydrogels, the corresponding values of effective diffusion coefficient D_{eff}, and the structure parameter μ

Hydrogel No.	MHA/HA (g/g)	D_{eff} (m²/s)	μ
1	0	5.30×10^{-10}	0.79
2	0.14	4.94×10^{-10}	0.74
3	0.25	4.53×10^{-10}	0.68
4	0.33	4.31×10^{-10}	0.64
5	0.60	3.88×10^{-10}	0.58

regulate the content of carboxylic groups in humic hydrogels (Table 2). Our previous studies (Klucakova and Pekar 2004, 2005b, 2009; Sedlacek and Klucakova 2009a, b) showed that transport of metal ions in humic gels is strongly influenced by reactivity of humic acids, therefore changes in the content of carboxylic groups result in changes of obtained values of effective diffusion coefficient. In this work, the values of D_{eff} were determined by means of the method of an instantaneous planar source. It means that the small amount of metal ions is placed on the one side of hydrogel and then the time development of concentration profile is monitored. Linearized concentration profiles are then background for computing the D_{eff} values (Eq. 4). The experimental concentration profiles for three various duration of diffusion experiment are shown in Fig. 2. As we can see the concentration of metal ions decreases rapidly with the distance from the source of metal ions. It is clear that the metal ions do not diffuse to the end of hydrogel which corresponds to the used mathematical concept. Experimental data in Fig. 2 are fitted by the profiles computed using Eq. 3. The profiles computed from the simple one-dimensional diffusion equation using the obtained values of D_{eff} are in good accord with measured ones, which is another verification of the experimental procedure. The computed values of D_{eff} depend on the content of MHA in the

humic gel (see Table 2). Lower amounts of the carboxylic groups caused the decrease of the diffusion rate and the D_{eff} value. The reason could be that the interactions of Cu(II) ions with HA in gel cause their immobilization. The immobilized metal ions are strongly bonded with HA and are not able to diffuse. It results in the increase of the concentration gradient of movable Cu(II) ions, which is the driving force of their transport.

In general, the transport in gel medium is influenced by its porous structure. In case of humic gels, the transport is influenced by two factors. The first one is the reactivity of humic acids in the gel and corresponding interactions proceeding in diffusion experiments. The other is the internal structure of used hydrogel including the content and spatial arrangement of fluid-filled pores. Both factors result in the value of the effective diffusion coefficient D_{eff}, which can by expressed as

$$D_{eff} = D \frac{\varphi}{\tau(K+1)} = D \frac{\mu}{K+1} \qquad (5)$$

where D is the diffusion coefficient for aquo Cu^{2+} ions in water. The parameter φ is the ratio of the effective diffusive cross section, which is available for transport of Cu(II) ions, to the bulk cross section. The available cross section is smaller than in case of a homogenous material because the diffusion takes place only through the fluid-filled pores and voids of humic hydrogels. Because the pores are not straight, the diffusion effectively takes place over a longer distance than it would in a homogenous material. The tortuosity τ is a value characterizing the longer distance traversed in the pores. The parameter μ represents the influences of the structure of humic hydrogel and its local geometry in the diffusion (Dullien 1992). D can be substituted by diffusivity in an aqueous solution, because of the high water content in the gel. K in Eq. (5) represents the influence of HA interactions with Cu(II)

Fig. 2 The concentration profiles determined for hydrogel No. 3 after 5 (*circles*), 24 (*triangles*), and 48 h (*squares*). The lines are profiles computed using Eq. (3)
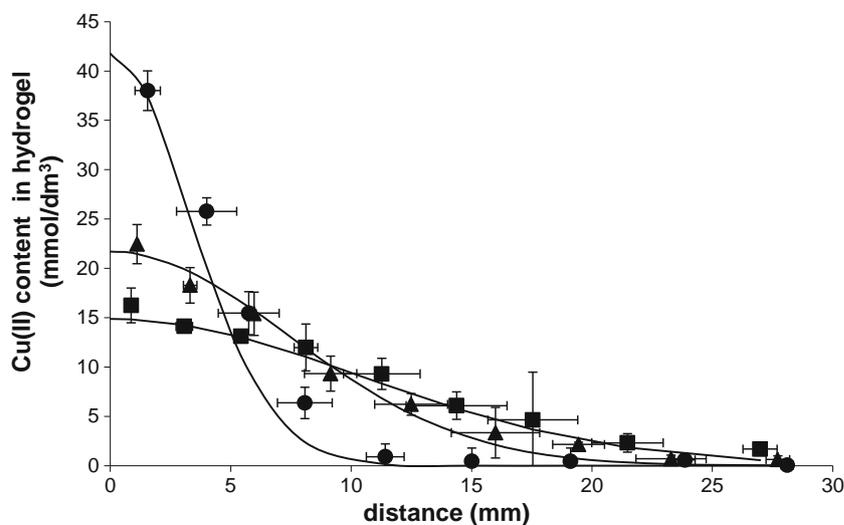
Fig. 3 The dependence of scattered light intensity on particle size determined for HA and MHA samples by DLS
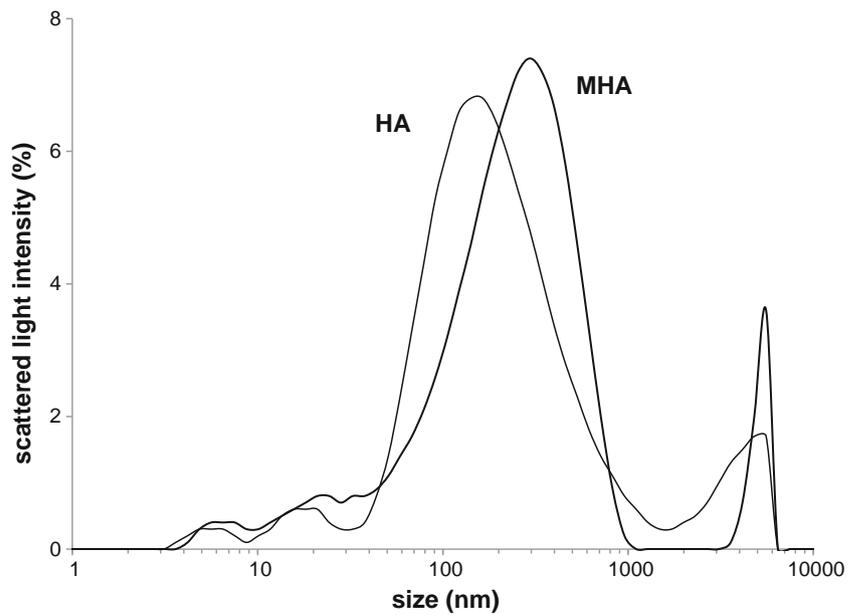
ions. It is the ratio between immobilized and free Cu(II) ions in humic hydrogel:

$$K = \frac{c_{im}}{c_{free}} \qquad (6)$$

and it can be considered as an equilibrium constant of local interactions between HA and Cu(II) ions in hydrogel (Crank 1956; Dullien 1992; Klucakova and Pekar 2004).

In spite of the fact that both the reaction and the diffusion are kinetic processes, the immobilization of Cu(II) ions proceeds very rapidly compared with the diffusion process and the local equilibrium can be assumed to exist between the free and immobilized metal ions. In this work, the ratio between

the strongly bond fraction of Cu(II) in humic gel and the amount of Cu(II) ions extractable by the 1 M MgCl$_2$ solution was used as the estimate of apparent equilibrium constant K. Its value is 1.14±0.03, which corresponds to well-known high affinity of Cu(II) ions to humic acids. The K in Eqs. (5) and (6) is not a true thermodynamic constant, because the immobilization of Cu(II) by humic acids can be connected with splitting off hydrogen ions, and therefore the value is valid only under circumstances used in this work. Its constant value determined in this work, which does not depend on time, confirmed, that the rate of immobilization is much faster than the diffusion and its kinetics can be neglected. Although the reactivity of HA decreases with increasing content of MHA in humic gel, the value of K is practically the same for all used

Fig. 4 The dependencies of the ration D_{eff}/D (*circles*) and the structure parameter μ (*triangles*) on the MHA content in dry matter of gel
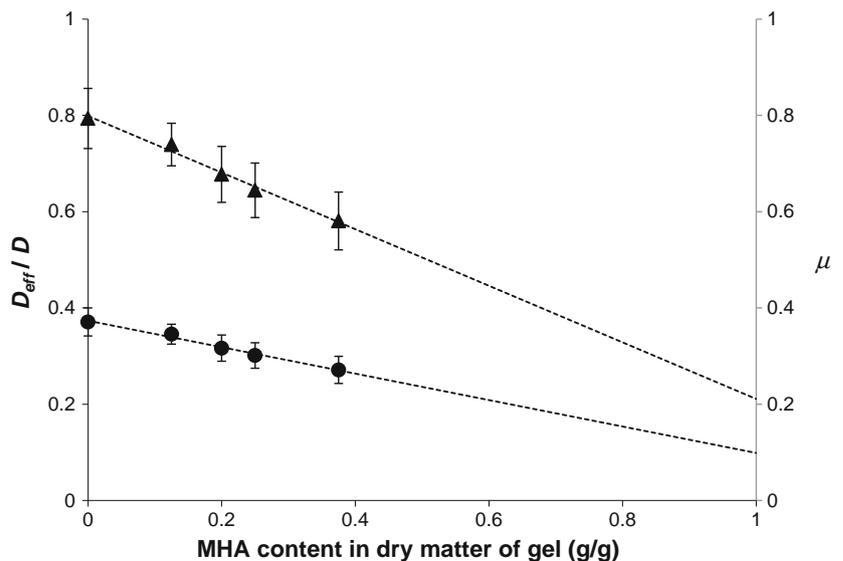
gels. The reason is that its value expresses a "quality" of reaction. If we assume, that Cu(II) ions are immobilized mainly by acidic functional groups, the character of reaction does not change with changing MHA/HA ratio in gel. On the other hand, the structural parameter μ is dependent on the content of MHA similarly as the D_{eff} value. DLS confirmed differences in size and distribution of the humic particles for HA and MHA samples (Fig. 3). The increase of molecular size measured by DLS is probably caused by more factors. The hydrodynamic radius of humic particles is influence not only by the replacement of H^+ ions with larger CH_3 group but also the change of charge on the polyelectrolyte chains. The charge distribution in methylated sample can cause conformational changes resulting in the change of molecular size. Other reason could be the hydrophobic intermolecular associations, which influences the molecular size of methylated humic acids more strongly in comparison with unmethylated ones, but the problem of the internal structure of the gel is more complex. The μ value decreases with increasing content of MHA. Since the content of dry matter is practically the same for all used gels, its effective diffusive cross section should be similar and the decrease could be influenced mainly by tortuosity. It is related to the complexity of pores and the necessity to move through more complex structure of the gel. Therefore the parameter μ is an effective value including all these influences similarly as the effective diffusion coefficient. If we assume that the dependence between the structural parameter μ and the content of MHA is linear in whole concentration range, we can estimated its apparent value for unreactive hydrogel. The extrapolated value of μ for gel without carboxylic groups (100 % MHA in dry matter) is 0.21 and the corresponding ratio of D_{eff} and D is 0.10 (Fig. 4). It means that the diffusion flux would achieve 10 % in comparison with the diffusion of Cu(II) ions in water. The decrease of the diffusion flux is caused both by the decrease of the diffusion driving force and by the change of pore structure in gel represented by the structure parameter μ.

4 Conclusions

Structural complexity of humic acids is manifested in nonsimple kinetic behavior of their interactions with Cu(II) ions, knowledge of which is important for various applications of these materials. The main goal was to test the applicability of theoretical mathematical apparatus to the study of the metal transport in humic gel and to investigate the influence of HA reactivity and internal gel structure on this process. In general, diffusion experiments seem to provide valuable method for reactivity mapping studies on humic substances. In spite of its simplicity, the method may be successfully employed for the intended purpose. Parameters such as effective diffusion coefficients, structural

parameters, and equilibrium constants can be used in order to discuss the quality of humic substances from different origin and with various contents of reactive functional groups.

References

Achard FK (1786) Chemische Untersuchung des Torfs. Chem Ann die Freunde der Naturlehere von L Crell 2:391–403

Andjelkovic T, Perovic J, Purenovic M, Blagojevic S, Nikolic R, Andjelkovic D, Bojic A (2006) Spectroscopic and potentiometric studies on derivatized natural humic acid. Anal Sci 22:1553–1558

Bartle KD, Pomfret A, Pappin AJ, Mills DG, Evliya H (1987) Analysis of methylated humic acids from fossil-fuels by size exclusion chromatography and NMR. Org Geochem 11:139–149

Bradl HB (2004) Adsorption of heavy metal ions on soils and soils constituents. J Colloid Interface Sci 277:1–18

Clemow LM, Favas G, Jackson WR, Marshall M, Patti AF, Redlich PJ (1999) Humic acids and methylated humic acids as models for reactions of brown coal with CO/H_2O and with H_2. Fuel 78:567–572

Crank J (1956) The mathematics of diffusion. Clarendon Press, Oxford

Cussler EL (1984) Diffusion: mass transfer in fluid systems. Cambridge University Press, Cambridge

Deport C, Lemee L, Ambles A (2006) Comparison between humic substances from soil and peats using TMAH and TEAAc thermochemolysis. Org Geochem 37:649–664

Deserra MO, Schnitzer M (1972) Extraction of humic acid by alkali and chelating resin. Can J Soil Sci 52:365–374

Dullien FAL (1992) Porous media. Fluid transport and pore structure, 2nd edn. Academic, San Diego

Frenkel AI, Korshin GV, Ankudinov AL (2000) XANES study of Cu^{2+}-binding sites in aquatic humic substances. Environ Sci Technol 34:2138–2142

Gardea-Torresdey JL, Tang L, Salvador JM (1996) Copper adsorption by esterified and unesterified fractions of Sphagnum peat moss and its different humic substances. J Hazard Mater 48:191–206

Grasset L, Guignard C, Ambles A (2002) Free and esterified aliphatic carboxylic acids in humin and humic acids from a peat sample as revealed by pyrolysis with tetramethylammonium hydroxide or tetraethylammonium acetate. Org Geochem 33:181–188

IHSS (2007) What are Humic Substances? Official website of International Humic Substances Society. http://www.humicsubstances.org. Accessed 31 January 2013

Karlsson T, Elgh-Dalgren K, Skyllberg U (2008) Modeling copper(II) complexation in a peat soil based on spectroscopic structural information. Soil Sci Soc Am J 72:1286–1291

Kerndorff H, Schnitzer M (1980) Sorption of metals on humic acid. Geochim Cosmochim Acta 44:1701–1708

Khan SU, Schnitzer M (1972) Retention of hydrophobic organic compounds by humic acid. Geochim Cosmochim Acta 36:745–754

Klucakova M, Pekar M (2004) Study of diffusion of metal cations in humic gels. In: Ghabbour EA, Davies G (eds) Humic substances: nature`s most versatile materials. Taylor & Francis, New York, pp 263–273

Klucakova M, Pekar M (2005a) Solubility and dissociation of lignitic humic acids in water suspensions. Colloid Surf A 252:157–164

Klucakova M, Pekar M (2005b) Physical and chemical kinetics in humic dispersions. In: Ghabbour EA, Davies G (eds) Humic

substances: molecular details and applications in land and water conservation. Taylor & Francis, New York, pp 167–188

Klucakova M, Pekar M (2006) New model for equilibrium sorption of metal ions on solid humic acids. Colloid Surf A 286:126–133

Klucakova M, Pekar M (2009) Transport of copper(II) ions in humic gel—new results from diffusion couple. Colloid Surf A 349:96–101

Kuhnel E, Laffan DDP, Lloyd-Jones GC, del Campo TM, Shepperson IR, Slaughter JR (2007) Mechanism of methyl esterification of carboxylic acids by trimethylsilyldiazomethane. Angew Chem Int Ed 46:7075–7078

Kuran P, Janos P, Madronova L, Novak J, Kozler J (2008) Determination of OH groups in humic acids using methylation with dimethylsulfate. Talanta 76:960–963

Lamoureux G, Aguero C (2009) A comparison of several modern alkylating agents. ARKIVOC 1:251–264

Lieser KH, Hill R, Muhlenweg U, Singh RN, Tu S-D, Steinkopff T (1991) Actinides in the environment. J Radioanal Nucl Chem 147:117–131

Marschner B (1999) Sorption of polycyclic aromatic hydrocarbons (PAH) and polychlorinated biphenyls (PCB) in soil. J Plant Nutr Soil Sci 162:1–14

Martyniuk H, Wieckovska J (2003) Adsorption of metal ions on humic acids extracted from brown coals. Fuel Process Technol 84:23–36

Meek JS, Fowler JS, Monroe PA, Clark TJ (1968) Reaction of hindered phenols with diazomethane. J Org Chem 33:223–226

Morita H (1966) Facile methylation of humic acids from organic soils. Can J Chem 44:1593–1594

Ogner G (1973) Permanganate oxidation of methylated and unmethylated fulvic acid, humic acid, and humin isolated from raw humus. Acta Chem Scand 27:1601–1612

Ogner G (1979) [C-13] nuclear magnetic resonance spectrum of a methylated humic acid. Soil Biol Biochem 11:105–108

Park Y, Albright KJ, Cai ZY, Pariza MW (2001) Comparison of methylation procedures for conjugated linoleic acid and artifact formation by commercial (trimethylsilyl)diazomethane. J Agric Food Chem 49:1158–1164

Peuravuori J, Žbánková P, Pihlaja K (2006) Aspects of structural features in lignite and lignite humic acids. Fuel Process Technol 87:829–839

Piccolo A, Conte P, Patti AF (2006) O-alkylation of a lignite humic acid by phase-transfer catalysis. Anal Bioanal Chem 384:994–1001

Rauret G (1998) Extraction procedures for the determination of heavy metals in contaminated soil and sediment. Talanta 46:449–455

Ricca G, Severini F, Silvestro GD, Yuan CM, Adani F (2000) Derivatization and structural studies by spectroscopic methods of humic acids from Leonardite. Geoderma 98:115–125

Sachs S, Bubner M, Schmeide K, Choppin GR, Heise KH, Bernhard G (2002) Carbon-13 NMR spectroscopic studies on chemically modified and unmodified synthetic and natural humic acids. Talanta 57:999–1009

Schmeide K, Sachs S, Bubner M, Reich T, Heise KH, Bernhard G (2003) Interaction of uranium(VI) with various modified and unmodified natural and synthetic humic substances studied by EXAFS and FTIR spectroscopy. Inorg Chim Acta 351:133–140

Schnitzer M, Khan SU (1972) Humic substances in the environment. Marcel Dekker, New York

Schnitzer M, Monreal CM (2011) Quo vadis soil organic matter research?: a biological link to the chemistry of humification. Adv Agron 113:139–213

Sedlacek P, Klucakova M (2009a) Diffusion experiments as a new approach to the evaluation of copper transport in humics-containing systems. Collect Czechoslov Chem Commun 74:1323–1340

Sedlacek P, Klucakova M (2009b) Simple diffusion method applied in evaluation of metal transport in model humic matrices. Geoderma 153:286–292

Stevenson FJ (1994) Humus chemistry, genesis, composition, reactions. Wiley, New York

Swift RS (1996) Organic matter characterization. In: Bigham JM (ed) Methods of soil analysis. Part 3: chemical methods. American Society of Agronomy, Soil Science Society of America, Madison, pp 1011–1070

Tan KH (2003) Humic matter in soil and the environment. Principles and controversies. Marcel Dekker, New York

Tan X, Fang M, Wang X (2010) Sorption speciation of lanthanides/actinides on minerals by TRLFS, EXAFS and DFT studies: a review. Molecules 15:8431–8468

Tessier A, Campbell PGC, Bisson M (1979) Sequential extraction procedure for the speciation of particulate trace metals. Anal Chem 51:844–851

van 't Erve TJ, Rautiainen RH, Robertson LW, Luthe G (2010) Trimethylsilyldiazomethane: a safe non-explosive, cost effective and less-toxic reagent for phenol derivatization in GC applications. Environ Int 36:835–842

Wagner GH, Stevenson FJ (1965) Structural arrangement of functional groups in humic acid as revealed by infrared analyses. Soil Sci Soc Am J 29:43–48

Appendix 7

Smilek, J., Sedláček, P., Kalina, M., and Klučáková, M. On the role of humic acids' carboxyl groups in the binding of charged organic compounds. *Chemosphere* **2015**, 138, 503–510.

Contents lists available at ScienceDirect

Chemosphere

On the role of humic acids' carboxyl groups in the binding of charged organic compounds

Jiří Smilek [*,1], Petr Sedláček [1], Michal Kalina, Martina Klučáková

Brno University of Technology, Faculty of Chemistry, Materials Research Centre CZ.1.05/2.1.00/01.0012, Purkyňova 464/118, 612 00 Brno, Czech Republic

HIGHLIGHTS

- HAs–organic dyes interactions were studied by diffusion and sorption experiments.
- The interactions strongly affect mobility of the dyes in humics-containing systems.
- The interactions are not constrained by the presence of –COOH in structure of HAs.

ARTICLE INFO

ABSTRACT

Interactions of humic acids (HAs) with two cationic dyes (methylene blue and rhodamine 6G) were studied using a unique combination of diffusion and partitioning studies in HAs, containing hydrogels and batch sorption experiments. In order to investigate the involvement of carboxyl groups of HAs in these interactions, all experiments were performed for both, the original lignite HAs and HAs with selectively methylated carboxyls. The results of the diffusion experiments confirm that the interactions between the solute and humic substances have a strong impact on the rate of diffusion process. Surprisingly, the effect is almost equally approved for original and methylated HAs. On the other hand, the results of batch sorption experiments show strong improvement of the sorption capacity (methylated HAs), which is explained by changed morphology of alkylated HAs. The comparison of the results of diffusion and adsorption experiments shows that the diffusion experiments simulate the transport of solutes in natural humics containing environment more reasonably.

© 2015 Elsevier Ltd. All rights reserved.

1. Introduction

Humic acids (HAs) represent the key constituent of natural organic matter in the sense of the pollutant binding. In the present view, which have replaced the traditional macromolecular concept of HAs, these substances are postulated as large self-assemblies of relatively small and heterogeneous molecules, stabilized mainly by weak dispersive forces, e.g. van der Waals, π–π and CH-π (Piccolo, 2002; Sutton and Sposito, 2005). Resulting complex supramolecular structure with great diversity of functional groups results in universal binding ability of humic acids. The irreplaceable role of polar structural moieties (mainly carboxyls and alcoholic/phenolic hydroxyls) in binding the hydrophilic solutes (Liu and Gonzalez, 2000) and surfaces (Guan et al., 2006) has been widely reported. On the other hand, the sorption capacity for non-polar compounds such as polycyclic aromatic hydrocarbons has been for correlated

mainly with the content of hydrophobic moieties i.e. with the aromaticity of humic matter (De Paolis and Kukkonen, 1997) or with the content of aliphatic carbon groups (Ran et al., 2007).

Recently, a great deal of attention has been focused also on description of the molecular mechanism of HAs' interactions with low-molecular compounds of amphiphillic (combined hydrophilic and hydrophobic) nature e.g. with charged aromatic solutes. This represents a crucial aspect of the environmental role of humic substances because such combined molecular structure is common for numerous compounds of considerable ecological importance like pesticides, growth retardants, and industrial waste materials (e.g. surfactants, disinfectants or dyes). Senesi et al. (1995) applied a combination of spectroscopic methods to investigate the adsorption mechanism of N-rich atrazine and bipyridylium herbicides with humic acids. The results demonstrated the interactions of diverse origin (ionic, charge-transfer and hydrogen bonds) between the herbicide and suitable complementary groups of HAs. Iglesias et al. (2009) investigated the effect of pH and ionic strength on the binding of basic (paraquat) and acidic (MCPA) pesticides by soil fulvic and humic acids. They applied a simple

---

electrostatic model in the description of these interactions providing hereby an excellent reproduction of the experimental isotherms. Similarly, binding affinities of charged organic dyes (Janos, 2003), ionizable pharmaceuticals (Maszkowska et al., 2014) or polar aromatic compounds (Liu et al., 2008; Shi et al., 2010) for either whole soils or isolated HAs has been determined experimentally.

Generally, the works mentioned above are confined to describing the sorption kinetics and the equilibrium in the systems where a solute binds to HAs in the form of suspension of solid particles. This approach, although widely accepted, provides only limited information on the effect of studied interactions on the mobility of solutes in real environments. More reasonable experimental approach was proposed in the works of Goss, who designed and optimized a HPLC system for comprehensive sorption studies on soils and its constituents (see e.g. Droge and Goss, 2013). In our recent works (Sedlacek and Klucakova, 2009a,b; Klucakova and Pekar, 2009), we have introduced the laboratory diffusion experiments as an alternative methodology, which provides direct experimental tracking of a manifestation of intermolecular interactions in altered mobility of the solutes in model humic matrices. Humic-based hydrogels were proposed as a diffusion medium which reasonably corresponds to the natural form of humic substances and facilitates the design of the diffusion experiments at the same time. The interactions between diffusing solute and humic acids, contained in hydrogels, result in changed partitioning of the solute between the solution and gel and also in a shift in diffusivity of the solute. Additionally, in our most recent experiments, we have also implemented selective esterification of HAs carboxyl groups in order to discuss their involvement in the solute (Cu^{2+} ions in particular) binding (Klucakova et al., 2014).

The work presented here combines both original approaches in the study on interactions between lignite-derived humic acids and two representatives of amphiphilic compounds, charged organic dyes methylene blue (CI 52015) and rhodamine 6G (CI 45160). The previously declared benefits of the diffusion-tracking methodology are verified via the comparison of diffusion and batch-sorption experiments. Two complementary types of diffusion experiments were performed in order to cover the transport dynamics in the systems as comprehensively as possible: the through-diffusion experiments in the diffusion cells and the in-diffusion experiments. Furthermore, an involvement of carboxylic groups of humics in studied interactions is discussed on the basis of comparison of the behavior of raw humic acids with those with carboxyl groups masked by means of selective methylation with TMS-diazomethane.

2. Materials and methods

2.1. Chemicals

Agarose (routine use class, <10 wt.% moisture content), methylene blue hydrate (MB, CI basic blue 9, dye content, ⩾95 wt.%) and rhodamine 6G (R6G, CI Basic red 1, dye content, ⩾95 wt.%) were purchased from Sigma–Aldrich and used without further purification.

Humic acids were isolated by alkaline extraction from South-Moravian lignite (Klucakova and Pekar, 2005). The details on the chemical structure of both, the original lignite matrix and isolated lignite humic acids (LHAs) can be found in previously published papers (Peuravuori et al., 2006). Methylated humic acids (MHAs) were prepared from LHAs using trimethylsilyldiazomethan as a methylation agent and the alkylation procedure described in (Klucakova et al., 2014). In the same work, complete and selective esterification of carboxylic groups was evidenced

by means of acid-base titrations and chemical and structural analyses.

2.2. Preparation of hydrogels

All hydrogels, utilized in subsequent diffusion experiments, were prepared via the method of thermoreversible gelation of aqueous solution of agarose described in our previous works (Sedlacek et al., 2013, 2014). Blank agarose hydrogel (without the addition of HAs) gelatinized from the 1 wt.% solution of agarose in water, while agarose/HAs gels did from the solution of both agarose (1 wt.%) and HAs (LHAs or MHAs, dry concentration of HAs: 0.002 wt.%, 0.005 wt.% and 0.010 wt.%). For the diffusion cells experiments, the cylindrical gel samples (40 mm in diameter, 5 mm in thickness) were fixed in the supporting plastic ring. The samples for non-stationary diffusion were prepared directly in PMMA spectrophotometric cuvettes (inner dimensions: $10 \times 10 \times 45$ mm) and for equilibrium partitioning experiments in small glass tubes (inner diameter 10 mm, thickness 10 mm).

2.3. Diffusion experiments

The diffusion studies presented in this paper were divided into three separate experimental sections, steady-state through-diffusion experiments in the diffusion cells, non-stationary in-diffusion experiments and equilibrium partitioning experiments.

In the first section, the diffusion of MB and R6G through the agarose or agarose/HAs gels was studied in the water-jacketed side-by-side diffusion cell.

This through-diffusion technique gives the basic information on both of the two dissimilar steps of the diffusion process which take place when a solute diffuses through a studied medium, i.e. the transient stage (before the solute breaks through the medium) and the steady-state stage (after the breaking-through). In general, any interactions between diffusing solute and penetrated medium have an impact on both stages of the transport process. While the former stage is influenced directly because binding of the solute will indispensably decrease the rate of its passing through the medium, an indirect effect on the later stage is caused by changed concentration gradient along the gel. The gradient is changed by both, already bound amount of the solute and also all changes in its solution–gel partitioning. The fundamental experimental data, which characterize respective stages of the diffusion process, are the break-through time (alternatively called the lag time) and the steady-state diffusion flux of the solute through the sample. They are determined from fitting o the linear part of the break-through curves (see Fig. 1), where the break-through time (t_{BT}) is calculated from the x-axis intercept and the steady-state diffusion flux (J_d) from the slope of the regression. The diffusion cells were purchased from Permegear Inc. The schematic diagram of the diffusion apparatus including the most important dimensions was published in (Sedlacek et al., 2013) and is provided in Supplementary Materials (Fig. S1). A circulating water bath was used in order to maintain the experiments at 25 °C. Continuous stirring of solutions in the donor and acceptor compartments at constant rate (250 RPM) was arranged by magnetic stirrer. Aqueous solution of dye (MB or R6G, concentration: 10 g m^{-3}) was used as a source of diffusing solute and the VIS absorption spectra of the acceptor solution were continuously collected. All experiments were performed in duplicates.

The non-stationary in-diffusion experiments with hydrogels were performed as follows: the hydrogel samples in the cuvettes were immersed in horizontal positions in 10 g m^{-3} aqueous solution of respective dye (MB or R6G). Four cuvettes were placed simultaneously in a single container filled with 250 cm^3 of the dye solution, one cuvette for each weight content of HAs in gel
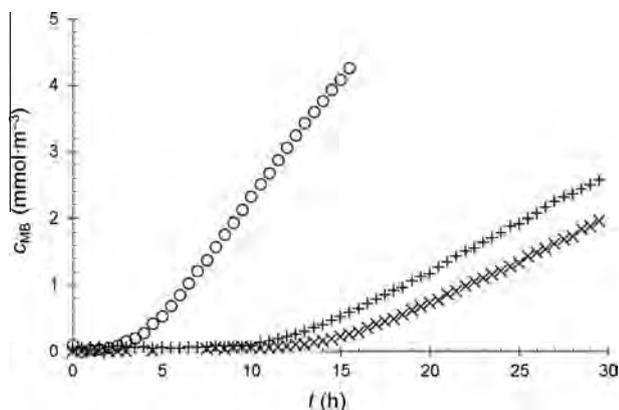
Fig. 1. Break-through curves from the diffusion cell experiments. The curves show the concentration of MB in acceptor cell as a function of time for the diffusion through 1 wt.% agarose gel with 0 wt.% HAs (○), 0.01 wt.% MHAs (+) and 0.01 wt.% LHAs (×).

(0 wt.%, 0.002 wt.%, 0.005 wt.% and 0.010 wt.%, respectively). The dye solution was stirred continuously by the magnetic stirrer (250 RPM). Subsequently the dye was left to diffuse from the solution to the gel samples through the square opening of a cuvette. Each experiment was duplicated. In selected time intervals, the cuvettes were taken out of the solution and the UV–VIS spectra were measured at various distances from the opening of the cuvette on Varian Cary 50 UV–VIS spectrophotometer equipped with the special accessory providing controlled fine vertical movement of the cuvette in the spectrophotometer. From collected spectra, the concentration of dye was determined at different positions in gels.

The concentration can be quantified via fitting the experimental profiles by an appropriate theoretical model. According to this model, total solute concentration c_{solute} at the distance x in gel follows the equation:

$$c_{solute} = c_{b,solute} \cdot \mathrm{erfc}\left(x / \sqrt{4D_{solute}t} \right) \tag{1}$$

where $c_{b,solute}$ is the solute concentration at the gel/solution boundary (from the side of hydrogel if there is a step change in the concentration at the boundary) and D_{solute} is the apparent diffusion coefficient of the solute in gel (for detailed definition and explanation of different forms of diffusion coefficients, see e.g. (Shackelford and Moore, 2013). The exact way, in which the D_{solute} implicates the effects of specific interactions between the solute and the solid content of gel, is discussed in (Sedlacek et al., 2014).

Finally, the equilibrium partitioning experiments were performed as follows: each of the cylindrical gel samples (10 mm in diameter, 10 mm in length), filled in supporting glass tubes, were placed separately in 10 cm^3 of the dye solution (10 g m^{-3}). The gel samples were kept in the solutions for 7 days in order to reach the equilibrium amount of absorbed dye. Then the samples were taken out, placed in 10 cm^3 of water for another 7 days. Finally, the samples were taken out and they were placed in 10 cm^3 of 1 M HCl for the final 7 days. UV–VIS spectra of the initial and equilibrium dye solutions as well as the water and HCl extracts were measured and the amount of dye absorbed in gel, and further released to water and extracted by HCl were calculated from the mass balance of dye.

2.4. Adsorption study

Simple batch adsorption experiment was also involved in this study. 50 mg of solid HAs (MHAs or LHAs) were put in 50 cm^3 of

the respective dye solution (MB or R6G, concentration range 25–150 g m^{-3}) in closed vessel and the samples were continuously rotated end-over-end 40 RPM for 72 h. Adsorbed amount of dye was calculated from UV–VIS spectra of the initial and final solutions. For all spectrophotometric analyses, the absorbances at 665 nm and 525 nm were evaluated for MB and R6G, respectively.

3. Results and discussion

3.1. Diffusion experiments

The results of all diffusion experiments are summarized in Tables 1 and 2. In general, these results confirmed that positively charged dyes interact strongly with humic acids. From the results of through-diffusion experiments, it is evident that the value of the break-through time increased with the content of HAs in gel which manifests how the binding to the humic content of gel decelerates the penetration of dye through the gel sample. While the penetration of MB through the sample of 1 wt.% agarose gel took about 4 h, more than 14 h were needed for the same gel containing 0.01 wt.% LHAs., the break-through time decreased only partially (to about 11 h in average) when the same amount of esterified humic acids (MHAs) was incorporated in the agarose gel. The diffusion of R6G shows practically the same dependency on the content of LHAs and MHAs, respectively. This finding is contradictory to the assumption that the interactions between HAs and positively charged organic dyes are primarily caused by the electrostatic attraction of carboxyl groups with oppositely charged ionic groups. Instead, it points to the fact that the actual involvement of other structural moieties of the HAs molecule in these interactions is much more important than generally accepted. On the other hand, this conclusion is in agreement i.a. with the recent work of Maszkowska et al. (2014) who performed thermodynamic calculations for sorption of model pharmaceutical compounds onto soil. The results of this work indicate that even for organic cations, other forces (weaker than ion-exchange) may affect the sorption process to a great extent. Furthemore, from the comparison of more than 1000 natural organic matter (NOM)/air partitioning coefficients covering polar and nonpolar organic compounds measured in 10 different humic and fulvic acids, Niederer concluded that in their sorption characteristics, diverse NOM samples differ in the number of available sorption sites per mass rather than in the chemical characteristics of these sites. Therefore, even NOM samples with much different content of polar binding sites may show similar sorption affinities toward polar solutes (Niederer et al., 2007).

Similar deduction can be derived from the dependence of the steady-state diffusion flux on the concentration of LHAs and MHAs, respectively. Here, the attractive interactions between the solute and the HAs content of penetrated sample are represented by decreasing steady-state diffusion flux in the case of hydrogels with HAs in comparison with blank agarose gels. Because our previous work (Sedlacek et al., 2013) confirmed that no significant changes in the hydrogel structure emerge from the addition of HAs, we can assume that the differences in the diffusion fluxes are primarily caused by changed solute concentration gradient between the pair of diffusion cells separated by hydrogel sample.

There are two possible explanations of the shift in the concentration gradient. Above all, the bound amount of solute inside the gel sample decreases its actual concentration in the donor diffusion cell at the moment of breaking-through into the acceptor cell. Apart from this, the partitioning of free solute between gel and solution is sensitive to any changes in physico-chemical properties of gel, mainly in its Donnan potential. Adding a polyelectrolyte component (such as HAs) to the gel matrix will definitely

Table 1
Results of the diffusion and partitioning experiments for the diffusion of methylene blue in 1 wt.% agarose hydrogels with different weight content of HAs.[a]

w_{HAs} (wt.%)	HAs	Steady-state diffusion		Transient diffusion		Partitioning experiment
		$J_{d,MB} \times 10^9$ (mol m^{-2} s^{-1})	$t_{BT,MB}$ (h)	$D_{MB,HAs}/D_{MB,0}$	$c_{b,MB,HAs}/c_{b,MB,0}$	$c_{\infty,MB,HAs}/c_{\infty,MB,0}$
0%	–	4.54 ± 0.30	4.03 ± 0.11	–	–	–
0.002%	LHAs	3.45 ± 0.23	5.92 ± 0.32	0.33 ± 0.04	3.21 ± 0.44	0.82 ± 0.26
	MHAs	3.61 ± 0.30	5.87 ± 0.05	0.36 ± 0.03	2.96 ± 0.47	0.89 ± 0.23
0.005%	LHAs	1.76 ± 0.32	9.02 ± 1.16	0.16 ± 0.01	4.66 ± 0.70	1.05 ± 0.26
	MHAs	2.38 ± 0.31	8.20 ± 0.74	0.26 ± 0.02	3.97 ± 0.86	0.96 ± 0.26
0.010%	LHAs	1.54 ± 0.18	14.54 ± 0.71	0.09 ± 0.02	4.45 ± 1.23	1.44 ± 0.27
	MHAs	1.78 ± 0.18	11.29 ± 1.80	0.23 ± 0.02	3.44 ± 1.08	1.20 ± 0.24

[a] $J_{d,MB}$: steady-state diffusion flux (diffusion of MB through hydrogels with various content of HAs). $t_{BT,MB}$: break-through time (diffusion of MB through hydrogels with various content of HAs). D_{MB}: apparent diffusion coefficient of MB in the corresponding gel (agarose hydrogels with and without HAs are referenced using respective subscripts "HAs" and "0"). $c_{b,MB}$: concentration of MB at the gel/solution boundary (agarose hydrogels with and without HAs are referenced using respective subscripts "HAs" and "0"). $c_{\infty,MB}$: equilibrium concentration of MB in gel (agarose hydrogels with and without HAs are referenced using respective subscripts "HAs" and "0").

Table 2
Results of the diffusion and partitioning experiments for the diffusion of Rhodamine R6G in 1 wt.% agarose hydrogels with different weight content of HAs[a].

w_{HAs} (wt.%)	HAs	Steady-state diffusion		Transient diffusion		Partitioning experiment
		$J_{d,R6G} \times 10^9$ (mol m^{-2} s^{-1})	$t_{BT,R6G}$ (h)	$D_{R6G,HAs}/D_{R6G,0}$	$c_{b,R6G,HAs}/c_{b,R6G,0}$	$c_{\infty,R6G,HAs}/c_{\infty,R6G,0}$
0%	–	2.67 ± 0.04	4.84 ± 0.20	–	–	–
0.002%	LHAs	1.29 ± 0.10	6.69 ± 0.20	0.36 ± 0.02	1.78 ± 0.23	0.91 ± 0.23
	MHAs	1.60 ± 0.20	5.51 ± 0.13	0.47 ± 0.01	1.69 ± 0.27	0.81 ± 0.22
0.005%	LHAs	1.25 ± 0.07	8.30 ± 0.03	0.28 ± 0.01	2.82 ± 0.41	1.07 ± 0.24
	MHAs	1.29 ± 0.31	7.71 ± 0.18	0.40 ± 0.03	2.41 ± 0.36	1.00 ± 0.22
0.010%	LHAs	1.05 ± 0.01	13.93 ± 0.10	0.21 ± 0.01	4.05 ± 0.48	1.28 ± 0.33
	MHAs	1.33 ± 0.16	9.54 ± 0.46	0.37 ± 0.05	3.24 ± 0.57	1.10 ± 0.27

[a] $J_{d,R6G}$: steady-state diffusion flux (diffusion of R6G through hydrogels with various content of HAs). $t_{BT,R6G}$: break-through time (diffusion of R6G through hydrogels with various content of HAs). D_{R6G}: apparent diffusion coefficient of R6G in the corresponding gel (agarose hydrogels with and without HAs are referenced using respective subscripts "HAs" and "0"). $c_{b,R6G}$: concentration of R6G at the gel/solution boundary (agarose hydrogels with and without HAs are referenced using respective subscripts "HAs" and "0"): $c_{\infty,R6G}$: equilibrium concentration of R6G in gel (agarose hydrogels with and without HAs are referenced using respective subscripts "HAs" and "0").

affect these properties of gel. Unfortunately, the method of diffusion cell is not suitable for a reasonable experimental tracking of these effects.

The interactions directly affect the transient step of the solute diffusion. In order to investigate this phase of the transport process more deeply, the non-stationary in-diffusion experiments were carried out. The changes in concentration of the diffusing solute inside the gel sample are continuously monitored during these experiments. The main advantage, as compared to the diffusion cells experiment, is better ability to directly distinguish the relative impacts of the solute partitioning and the solute binding to the solid content, which proceed in gel simultaneously.

The prime experimental outcome is represented by the concentration profile of the diffusing solute in gel such as those presented in Fig. 2. This figure clearly shows how the content of humic acids (LHAs) in gel affects the mobility of charged organic solute (MB). Two effects are illustrated by the changes in shape of the concentration profile. Although the diffusion proceeds from the same source solution, total concentration of the solute in gel near its boundary gets significantly higher at the presence of LHAs. In our previous work, we have demonstrated that this increase in overall solute concentration involved partly the fraction of solute bound to LHAs, partly the increased partition coefficient of free solute (Sedlacek et al., 2014). The other effect is manifested in obvious slowdown of solute penetration in gel. It is evident from Fig. 2, that the fall of the solute concentration with the distance from the gel boundary is much steeper in gels where HAs were added.

A simplified idea, sufficient for the purposes of the discussion of current experimental results, is that the more intensive attractive interactions between the solute and the interior of gel, the lower the value of the diffusion coefficient.

The results of regression of experimental concentration profiles are shown in Tables 1 and 2. Unlike the standard diffusion cells
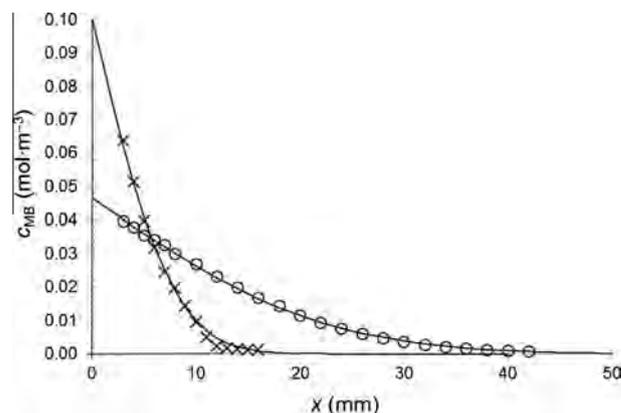
Fig. 2. Concentration profiles of methylene blue in 1 wt.% agarose gels with 0 wt.% LHAs (○) and 0.01 wt.% LHAs (×) after 72 h of the in-diffusion experiment.

apparatus, the experimental arrangement for in-diffusion experiment is more susceptible for inevitable artifacts, such as random change in the solution temperature, and uneven stirring of the source solutions. Nevertheless, the undesirable effect of these experimental artifacts is minimized when the particular results of the transient diffusion experiments (diffusion coefficients, boundary concentrations) are given in the normalized form i.e. divided by the same parameter determined for the blank agarose hydrogels. The reason is that the solute diffuses into the blank (i.e. HAs-free) and HAs-containing gels simultaneously from the single source solution and under the identical experimental conditions.

The relative diffusion coefficients shown in Table 1 indicate that even the smallest addition of HAs resulted in more than 50% reduction in the diffusivity of solute (both MB and R6G) as compared to

blank agarose hydrogel ($D_{solute,HAs}/D_{solute,0} < 0.5$). This decrease can undoubtedly be attributed to the binding of the solute to HAs, contained in gel. Interestingly, similar effect is shown also for esterified humic acids. Actually, some differences in the effects of LHAs and MHAs can be seen; the decrease of the solute diffusivity in hydrogels with the addition of LHAs is higher to some extent than in MHAs-containing hydrogels. This finding is in contrast to our previously published experiments (Klucakova et al., 2014), where we studied the diffusion of Cu^{2+} in physically cross-linked humic hydrogels with different ratios of LHAs/MHAs content. There, we evidenced the decrease in apparent diffusivity of Cu^{2+} ions in gels with higher relative content of MHAs. Nevertheless, the effect was explained by specific influence of LHAs/MHAs ratio on the structure of gel. Similar structural effect is unlikely for the agarose/HAs hydrogels where the gel structure is practically independent on the HAs content in the studied range, as was evidenced by means of rheometry and SEM (not published).

Nevertheless, the effect of esterification of carboxylic groups is, once again, less pronounced than expected. As was already indicated by the results of through-diffusion experiments, it seems that the majority of attractive interactions is not influenced by the transformation of HAs' carboxyls into the non-dissociable form. Therefore, the common notion of cation binding to HAs preferentially by means of Coulomb attraction or proton-exchange interaction on dissociated or protonized carboxyl groups is not fully acceptable in the case of complex organic cations. This represents a significant original finding on the reactivity of HAs, which can be of the principal importance in explaining and predicting the fate of organic pollutants in nature. The involvement of structural moieties other than carboxyl groups in the binding of charged organic compounds has already been proposed e.g. by Zanini et al. (2006) who have confirmed strong and rather non-electrostatic binding of oxazine dye to humic acids. Nevertheless, the results of our experiments show that the participation of this kind of interactions is much more important than expected so far. Moreover, our results also directly demonstrate how the changed interaction influences the solute mobility in humics-containing systems.

LHAs and MHAs behave in surprisingly similar way also regarding the above mentioned increase in the boundary concentration of the solute in the gel. Although a slightly lower concentration shift was determined for esterified humic acids, the overall partitioning effect is almost equal. These results can easily be translated into the terms of thermodynamics. Similar partitioning of the solute in LHAs and MHAs containing gels indicates that the chemical potential of humic acids is not substantially changed by blocking the carboxyl groups. These groups must hence contribute to the overall chemical potential of HAs much less than previously assumed.

3.2. Solute partitioning experiments

The above discussed diffusion studies, give in addition to the fundamental information on the solute mobility also a basic survey of the partitioning phenomena, i.e. of distribution of the solute between the solution and hydrogel at the interface of these two phases. More specifically, they characterize the dynamic partitioning, i.e. the partitioning under the out-of-equilibrium circumstances. To obtain a complete view on the partitioning in the studied systems, the equilibrium absorption of the solute was investigated as well. In these experiments, the diffusion proceeded from the solution through both circular surfaces of small cylindrical hydrogel sample.

The results of these experiments are shown in Tables 1 and 2. It can be seen, that unlike the boundary concentration in the course of dynamic experiments, the equilibrium concentration of the solute in gel is not affected considerably by the presence of either LHAs or MHAs. The minor effect of HAs on the total solute concentration in gel at equilibrium is not as inconsistent with the results of dynamic diffusion experiments as it might seem at the first sight. For the in-diffusion experiments, the solute concentration at the boundary was expected to be time-independent in applied diffusion model. Nevertheless, it was found that in fact, it gradually decreased with time. Similar decrease of boundary concentration was also found and discussed in our previous work (Sedlacek et al., 2014). One reasonable explanation of the variable partitioning of solute between solution and gel could work on the presumption of the time-dependent free-to-bound solute concentration ratio in gel. To verify this hypothesis, we subjected the gel samples, with the equilibrium concentration of absorbed solute, to the sequential extraction by water and hydrochloric acid. These two leaching agents were chosen on the basis of our previous experience with fractional extraction of solutes according to the strength of binding to HAs (Kalina et al., 2013). We assume that water-extractable amount represents the fraction of freely mobile form, while the residual amount of solute (i.e. non-extractable even by HCl) is the most strongly bound to the solid content of hydrogel.

Fig. 3 illustrates the equilibrium fractionation of absorbed solute in all studied gels according to the strength of binding in gel. The data reveal two interesting facts. First, the major portion of equilibrium content of the solute is represented by the most strongly bound fraction, which is surprisingly dominant also in the case of blank agarose hydrogel. This finding indicates the binding of solute to the agarose backbone which is relatively strong but at the same time the reaction rate is so low that its influence grows and becomes significant mainly at later (near equilibrium) stages of the diffusion process. These interactions probably also stand behind the well-known partitioning effects of dilute agarose hydrogels, discussed e.g. in Golmohamadi et al. (2012). Another interesting finding of the sequential extraction experiments is that the presence of HAs influences mainly the relative content of mobile (I) and less strongly bound (II) fractions. The water-extractable amount of solute decreases as a consequence of its binding to HAs while the amount of HCl-extractable form increases correspondingly. Similar distribution of absorbed solute was found also for hydrogels with the presence of esterified MHAs. The above mentioned general findings from the partitioning experiments are common to both tested solutes (MB and R6G). Some particular differences between the partitioning of the solutes can be found in Fig. 3, however, these are not significant concerning the data uncertainty (see error bars in Fig. 3).

In general, these results show that the interactions with HAs are preserved also at the equilibrium. Nevertheless, their relative effect is markedly suppressed by an emergent binding of the solute to agarose chains (note that agarose is in a substantial excess over HAs in hydrogel).

3.3. Adsorption of the solutes on solid HAs

In our recent works, we have proposed the diffusion experiments as more reasonable alternative to traditional sorption experiments. Therefore, another objective of present work was to search for a potential correlation between the immobilizing effects of HAs on tested solutes, as evidenced by the diffusion study, and their sorption performance, revealed by simple batch sorption study. It should be noted, that the performed experiments did not aim at exhaustive description of the adsorption of studied solutes on HAs which other authors have already dealt with (Crini, 2006). Therefore, just a basic experiment was performed where a solute (MB or R6G) was adsorbed on solid HAs particles from aqueous solutions with various initial concentrations.
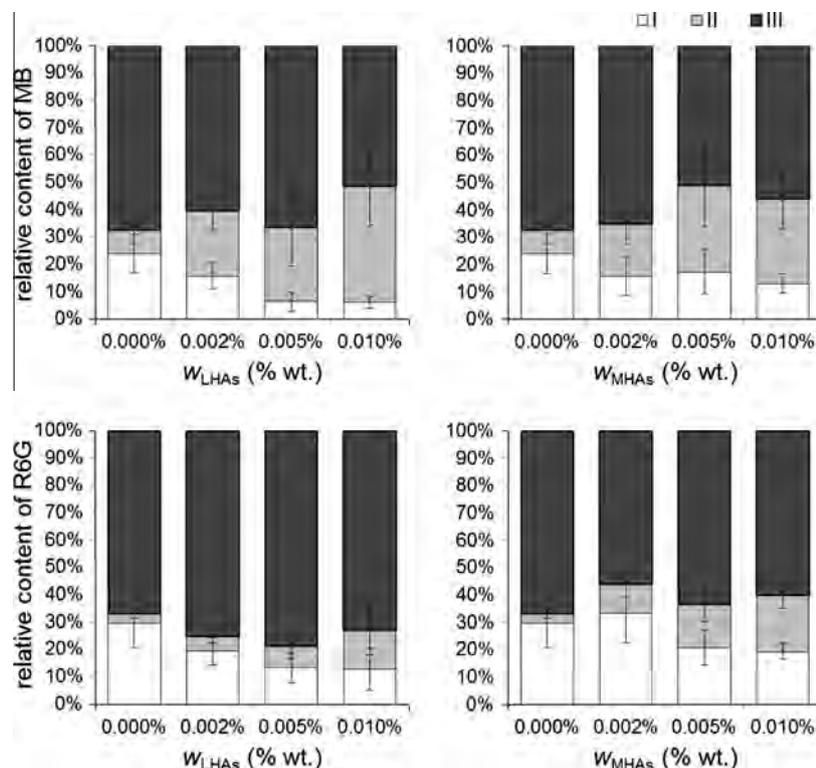
Fig. 3. Distribution of the equilibrium content of the solute in hydrogels into three fractions according to the binding strength: water extractable (I), HCl-extractable (II) and residual (III).

The sorption experiment provided highly surprising results regarding the sorption performance of LHAs and MHAs, respectively. MHAs showed obviously higher ability to decolorize the solutions of either MB or R6G. The difference became more evident as the initial concentration of the solution increased. Dissimilar sorption behavior of LHAs and MHAs is clearly illustrated by the specific amounts of adsorbed solutes, shown in Fig. 4. For instance, while the mass of MB, absorbed on MHAs, increases almost linearly with the initial concentration of MB in the solution, the amount adsorbed on LHAs does not change significantly over a wide range of concentrations. This indicates that the sorption capacity of LHAs gets exhausted in more concentrated solutions where MHAs adsorb significantly higher amounts of the solute. Analogous enhancement of sorption capacity of humic acids as a result of esterification of carboxylic groups was already described by Andelkovic et al. (2010) for the adsorption of cadmium. When comparing results obtained for the two solutes involved in the study (MB and R6G), it is evident that both LHAs and MHAs show higher affinity for MB than for R6G. Furthermore, the non-linearity of the dependence of MHAs-bound amount of R6G on the initial concentration indicates that the corresponding binding sites in MHAs become depleted for the more concentrated solutions of R6G. These particular differences in adsorption behavior of MB and R6G probably result from dissimilarities in the molecular weight and the level of hydrophilicity of the two solutes (Li and Yalkowsky, 1994).

In general, the results of the sorption experiment are in strong disagreement with the formerly discussed effects of LHAs and MHAs on the mobility of the same solutes in the hydrogel form, where the raw and esterified HAs showed only minor differences and slightly higher solute-immobilizing power was provided by LHAs. When discussing this discrepancy, it is necessary to take into account the fundamental distinctions between both experimental approaches. Above all, the crucial point is represented by the

different colloidal form of humic acids in the sorption and diffusion experiments. While the interpenetration of dissolved HAs in the agarose network provides a homogenous matrix where the HAs molecules are homogeneously distributed and fully accessible to the diffusing solute, the dispersion of solid HAs in the solute solution represents a heterogeneous system where the HAs, solute interactions are limited just to the surface of HAs particles and any changes in the textural and morphological properties of a sorbent will significantly affect the process.

Therefore, we turned our attention to the surface characteristics of solid MHAs and LHAs particles in order to explain their unexpected differences in their adsorption behavior. The crucial experimental finding was obtained from the determination of the surface of particles in the aqueous dispersion. As determined by the gas-adsorption technique (Nova 2200, Quantachrome), MHAs have more than twice the specific surface area of LHAs (241 m^2 g^{-1} vs 109 m^2 g^{-1}, while the distribution of particle sizes, determined by the light scattering method, was practically the same (see Fig. S2 in the Supplementary Materials). As revealed by scanning electron microscopy, the dissimilar surface area is caused by the different texture of LHAs and MHAs particles. The microphotographies of solid HAs particles at various magnifications (see Fig. S3 in Supplementary Materials) show greater microporosity of MHAs particles, whereas the surface of LHAs is obviously less rugged. The origin of this difference is not yet clear. It is highly probable, that the esterification of carboxylic groups will affect the association of the HAs molecules. Nevertheless, no important changes in the molecular size or shape of LHAs and MHAs were evidenced by the light scattering methods in the previous work (Klucakova et al., 2014). Apart from the interactions among HAs molecules themselves, the esterification will definitely influence also the way how these molecules interact with surrounding water, as the carboxylic groups are the most hydrophilic moieties in the structure of HAs. It is also well evidenced, that the
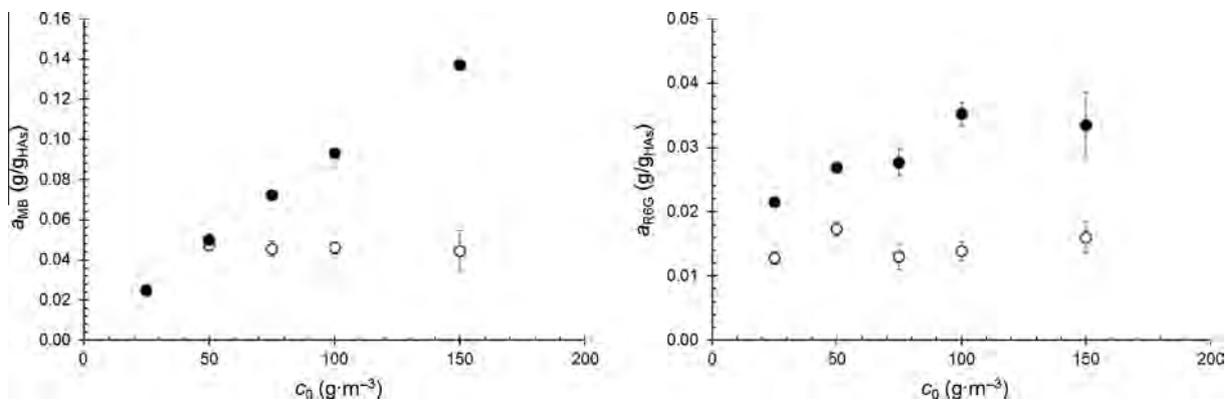
Fig. 4. Specific amount of MB (left) and R6G (right) adsorbed on solid LHAs (○) and MHAs (●) from aqueous solutions with different initial concentrations.

hydration level can strongly affect both the supramolecular structure (Schaumann and Bertmer, 2008) and the sorption performance of NOM (Graber et al., 2007). Perhaps, the surface of LHAs particles may be 'smoothed' by the presence of water molecules, strongly bound on the hydrophilic carboxyl or carboxylate groups. More strongly hydrated surface can consequently be less accessible for the binding of solutes by non-specific interactions (e.g. hydrophobic or van der Waals). Anyway, the hypothesis that enhanced sorption performance of methylated HAs is a consequence of changed hydration requires further experimental confirmation.

To summarize, the comparison of the results of diffusion and adsorption experiments clearly shows that the diffusion experiments model the transport of solutes in natural humics-containing environment much more reasonably. The interactions between flowing solute and humic substances have strong impact on the rate of diffusion process. Surprisingly, it was evidenced that these interactions do not involve carboxyl groups to such extent as commonly expected. It seems that, rather than a simple electrostatic attraction between oppositely charged compounds, the interactions between aromatic moieties in the molecular structure of the solute and humic substances play a major role. Nevertheless, a detailed study on these interactions is still needed. For this purpose, some advanced structural e.g. FTIR (Guan et al., 2006), or X-ray techniques (Manceau and Matynia, 2010) and thermal analysis techniques like ITC (Tan et al., 2009) represent the methods of choice as they have already been successfully utilized in revealing the exact mechanism of interactions between HAs and various compounds.

Acknowledgements

Appendix A. Supplementary material

Supplementary data associated with this article can be found, in the online version, at http://dx.doi.org/10.1016/j.chemosphere.2015.06.093.

References

Andelkovic, T., Nikolic, R., Bojic, A., Andelkovic, D., Nikolic, G., 2010. Binding of cadmium to soil humic acid as a function of carboxyl group content. Maced. J. Chem. Chem. Eng. 29, 215–224.

Crini, G., 2006. Non-conventional low-cost adsorbents for dye removal: a review. Bioresour. Technol. 97, 1061–1085.

De Paolis, F., Kukkonen, J., 1997. Binding of organic pollutants to humic and fulvic acids: influence of pH and the structure of humic material. Chemosphere 34, 1693–1704.

Droge, S.T.J., Goss, K.U., 2013. Development and evaluation of a new sorption model for organic cations in soil: contributions from organic matter and clay minerals. Environ. Sci. Technol. 47, 14233–14241.

Golmohamadi, M., Davis, T.A., Wilkinson, K.J., 2012. Diffusion and partitioning of cations in an agarose hydrogel. J. Phys. Chem. A 116, 6505–6510.

Graber, E.R., Tsechansky, L., Borisover, M., 2007. Hydration-assisted sorption of a probe organic compound at different peat hydration levels: the link solvation model. Environ. Sci. Technol. 41, 547–554.

Guan, X.H., Chen, G.H., Shang, C., 2006. Combining kinetic investigation with surface spectroscopic examination to study the role of aromatic carboxyl groups in NOM adsorption by aluminum hydroxide. J. Colloid. Interf. Sci. 301, 419–427.

Iglesias, A., Lopez, R., Gondar, D., Antelo, J., Fiol, S., Arce, F., 2009. Effect of pH and ionic strength on the binding of paraquat and MCPA by soil fulvic and humic acids. Chemosphere 76, 107–113.

Janos, P., 2003. Sorption of basic dyes onto iron humate. Environ. Sci. Technol. 37, 5792–5798.

Kalina, M., Klucakova, M., Sedlacek, P., 2013. Utilization of fractional extraction for characterization of the interactions between humic acids and metals. Geoderma 207–208, 92–98.

Klucakova, M., Pekar, M., 2005. Solubility and dissociation of lignitic humic acids in water suspension. Colloid. Surface. A 252, 157–164.

Klucakova, M., Pekar, M., 2009. Transport of copper(II) ions in humic gels – new results from diffusion couple. Colloid. Surface. A 349, 96–101.

Klucakova, M., Kalina, M., Sedlacek, P., Grasset, L., 2014. Reactivity and transport mapping of Cu(II) ions in humic hydrogels. J. Soil. Sediment. 14, 368–376.

Li, A., Yalkowsky, S.H., 1994. Solubility of organic solutes in ethanol–water mixtures. J. Pharm. Sci. 83, 1735–1740.

Liu, A., Gonzalez, R.D., 2000. Modeling adsorption of copper(II), cadmium(II) and lead(II) on purified humic acid. Langmuir 16, 3902–3909.

Liu, P., Zhu, D., Zhang, H., Shi, X., Sun, H., Dang, F., 2008. Sorption of polar and nonpolar aromatic compounds to four surface soils of eastern China. Environ. Pollut. 156, 1053–1060.

Manceau, A., Matynia, A., 2010. The nature of Cu bonding to natural organic matter. Geochim. Cosmochimica. Acta 74, 2556–2580.

Maszkowska, J., Wagil, M., Mioduszewska, K., Kumirska, J., Stepnowski, P., Bialk-Bielinska, A., 2014. Thermodynamic studies for adsorption of ionizable pharmaceuticals onto soil. Chemosphere 111, 568–574.

Niederer, C., Schwarzenbach, R.P., Goss, K.U., 2007. Elucidating differences in the sorption properties of 10 humic and fulvic acids for polar and nonpolar organic chemicals. Environ. Sci. Technol. 41, 6711–6717.

Peuravuori, J., Zbankova, P., Pihlaja, K., 2006. Aspects of structural features in lignite and lignite humic acids. Fuel Process. Technol. 87, 829–839.

Piccolo, A., 2002. The supramolecular structure of humic substances. A novel understanding of humus chemistry and implications in soil science. Adv. Agron. 75, 57–134.

Ran, Y., Sun, K., Yang, Y., Xing, B., Zeng, E., 2007. Strong sorption of phenanthrene by condensed organic matter in soils and sediments. Environ. Sci. Technol. 41, 3952–3958.

Schaumann, G.E., Bertmer, M., 2008. Do water molecules bridge soil organic matter molecule segments? Eur. J. Soil. Sci. 59, 423–429.

Sedlacek, P., Klucakova, M., 2009a. Diffusion experiments as a new approach to the evaluation of copper transport in humics-containing systems. Collect. Czech. Chem. C. 74, 1323–1340.

Sedlacek, P., Klucakova, M., 2009b. Simple diffusion method applied in evaluation of metal transport in model humic matrices. Geoderma 153, 11–17.

Sedlacek, P., Smilek, J., Klucakova, M., 2013. How the interactions with humic acids affect the mobility of ionic dyes in hydrogels – results from diffusion cells. React. Funct. Polym. 73, 1500–1509.

Sedlacek, P., Smilek, J., Klucakova, M., 2014. How the interactions with humic acids affect the mobility of ionic dyes in hydrogels – 2. Non-stationary diffusion experiments. React. Funct. Polym. 75, 41–50.

Senesi, N., Dorazio, V., Miano, T.M., 1995. Adsorption mechanisms of s-triazine and bipyridylium herbicides on humic acids from hop field soils. Geoderma 66, 273–283.

Shackelford, C.D., Moore, S.M., 2013. Fickian diffusion of radionuclides for engineered containment barriers: diffusion coefficients, porosities, and complicating issues. Eng. Geol. 152, 133–147.

Shi, X., Ji, L.L., Zhu, D., 2010. Investigating roles of organic and inorganic soil components in sorption of polar and nonpolar aromatic compounds. Environ. Pollut. 158, 319–324.

Sutton, R., Sposito, G., 2005. Molecular structure in soil humic substances: the new view. Environ. Sci. Technol. 39, 9009–9015.

Tan, W.F., Koopal, L.K., Norde, W., 2009. Interaction between humic acid and lysozyme, studied by dynamic light scattering and isothermal titration calorimetry. Environ. Sci. Technol. 43, 591–596.

Zanini, G.P., Avena, M.J., Fiol, S., Arce, F., 2006. Effects of pH and electrolyte concentration on the binding between a humic acid and an oxazine dye. Chemosphere 63, 430–443.

Appendix 8

Enev, V., Sedláček, P., Kubíková, L., Sovová, Š., Doskočil, L., Klučáková, M., and Pekař, M. Polarity-Based Sequential Extraction as a Simple Tool to Reveal the Structural Complexity of Humic Acids. *Agronomy* **2021**, 11, 587.

Polarity-Based Sequential Extraction as a Simple Tool to Reveal the Structural Complexity of Humic Acids

Vojtěch Enev [1],*,[†], Petr Sedláček [1],[†], Leona Kubíková [1], Šárka Sovová [1], Leoš Doskočil [2], Martina Klučáková [1] and Miloslav Pekař [1]

[1] Institute of Physical and Applied Chemistry, Faculty of Chemistry, Brno University of Technology, Purkynova 118, 612 00 Brno, Czech Republic; sedlacek-p@fch.vut.cz (P.S.); kubikova@fch.vut.cz (L.K.); xcsovova@fch.vut.cz (Š.S.); klucakova@fch.vut.cz (M.K.); pekar@fch.vut.cz (M.P.)

[2] Materials Research Centre, Faculty of Chemistry, Brno University of Technology, Purkynova 118, 612 00 Brno, Czech Republic; doskocil@fch.vut.cz

* Correspondence: enev@fch.vut.cz; Tel.: +420-541-149-483

† These authors contributed equally to this work.

Abstract: A sequential chemical extraction with a defined series of eluotropic organic solvents with an increasing polarity (trichloromethane < ethyl acetate < acetone < acetonitrile < *n*-propanol < methanol) was performed on peat-bog humic acid. Six organic fractions were obtained and subjected to a physicochemical characterization utilizing methods of structural and compositional analysis. Advanced spectroscopic techniques such as Attenuated Total Reflectance (ATR-FTIR), total luminescence, and liquid-state ^{13}C NMR spectrometry were combined with elemental analysis of the organic fractions. In total, the procedure extracted about 57% (wt.) of the initial material; the individual fractions amounted from 1.1% to 19.7%. As expected, the apolar solvents preferentially released lipid-like components, while polar solvents provided organic fractions rich in oxygen-containing polar groups with structural parameters closer to the original humic material. The fraction extracted with acetonitrile shows distinct structural features with its lower aromaticity and high content of protein-like structural motifs. The last two—alcohol extracted—fractions show the higher content of carbohydrate residues and their specific (V-type) fluorescence suggests the presence of plant pigment residues. The extraction procedure is suggested for further studies as a simple but effective way to decrease the structural complexity of a humic material enabling its detail and more conclusive compositional characterization.

1. Introduction

Natural organic matter (by which only the non-living part should be understood here) is an extremely complex pool of organic substances. Traditionally, its non-aqueous part was and is studied after extraction by an alkaline agent from solid natural matrix-like soil, peat, or coal. The alkaline extraction is criticized by some for its potential change in the structure and composition of isolated matter [1] but this view is refuted by others [2] and this debate remains still open [3]. Although there are attempts, increasing in number, to study the natural organic matter directly in its natural environment, i.e., without extraction [4], isolation of organics from natural matrix remains an important part of natural organic matter research, which is motivated mainly by efforts to reduce the inevitable structural complexity of the natural organic matter before subjecting it to the intended analyzes.

Besides alkaline extractants, various alternatives have been proposed and tested which were believed to be gentler or more specific to a certain class of organic matter constituents [5]. Hayes [5] overviewed solvent systems used for the isolation of organic

components from soils. He states that, in contrast to the traditional mixture of aqueous base and pyrophosphate, organic solvents are much less used, usually because of problems with recovering solutes. As the important parameters of organic solvents, Hayes presents the relative permittivity, the dipole moment, and the ability to make and break hydrogen bonds. Parameters like the boiling point, density, or viscosity are said to be of minor importance for the isolation but may be relevant in the recovery of the extracted solutes. A useful concept for predicting solubility is the solubility parameter concept developed mainly by Hildebrand et al. [6] and Hansen [7].

The aforementioned review [5] reports mainly on experience with the dissolution of classically isolated humic acids (HAs) in various organic solvents. Nevertheless, there is also a long history of work focused on the extraction or fractionation of organic matter directly from its raw natural sources. Senesi et al. [8] were the first researchers to use sequential extraction using organic solvents of increasing polarity to separate directly from soil organic matter fractions and characterize them chemically and spectroscopically. Independently on the source soil, chemical and structural properties of the extracted organic fractions varied according to the progression of the solvent series, with some similarities between the two successive extracts. Later on, Piccolo [9] extracted humic substances from three soils with several dipolar aprotic solvents (dimethylsulfoxide, dimethylformamide, acetone) applied in mixtures with dilute HCl. These mixtures were selected based on a preceding study that found their highest extracting capacity among various organic solvents. It is believed that the high dipole moment of the selected solvents permits disruption of the intermolecular hydrogen bonding in a natural matrix and to separate humic substances by the formation of strong hydrogen bonds with the solvent. The presence of HCl should help to break the polyvalent salt bridges with the soil mineral constituents and to keep humic substances in the protonated form which supports their solubilization by hydrogen bonding. The used solvent mixtures revealed lower extracting efficiency in comparison to the traditional alkaline extractants, but their extracts were of higher purity. The extracts were less contaminated with silicate compounds, contained a higher amount of organic carbon and oxygen-containing functional groups, and were richer in aliphatic components [10].

Aside from the extraction studies using organic solvents, numerous efforts were made also with fractionation procedures based on the traditional alkaline extraction process. Li et al. [11] used the traditional alkaline extraction but in a repetitive way and obtained eight humic fractions from the peat sample. The authors observed large variations in molecular, chemical, and functional properties among these fractions. For example, the O/C atomic decreased from the first to the last fraction as well as the contents of oxygen-containing and aromatic functional groups. On contrary, the contents of aliphatic groups increased in the same direction. The authors suggested the existence of two major subunits in the extracted HAs. An aliphatic subunit is derived biogeochemically from lipid-rich plant cell constituents and an aromatic subunit originating from lignin or plant tissue materials. The aliphatic subunit is less soluble in alkaline solution whereas the aromatic subunit is easily extracted due to its very good solubility in bases. The aliphatic subunit should have a major impact on the binding of less or nonpolar pollutants because of its relatively hydrophobic character. Each of the isolated fractions is then a specific mixture of these two subunits. Furthermore, Olk [12] reported on basic fractionation of soil organic matter into an unbound (mobile) fraction and a fraction bound to polyvalent cations. The fractionation was performed during the standard alkali extraction by a specific ordering of the extraction and acid-wash steps. The unbound fraction was found to cycle faster under land use than the cation-bound fraction. Shirshova et al. [13] isolated five fractions of humic substances from soil using three protocols. The protocols differed in the soil pre-treatment with the benzene-methanol mixture and in the use of sulfonate or carboxylate resins as an additional soil-pretreatment agent or as extractants. Resin-extracted materials were richer in carboxylic and phenolic groups and exhibited a higher fluorescence emission maximum.

Recently, an elaborate sequential extraction technique based also on organic liquids was designed and called the humeomics approach [14]. Humeomics is based on the supramolecular conception of humic substances [15] and designed as a sequential extraction procedure that releases constituents of humic supramolecular aggregate bound by weak intermolecular forces and ester or ether linkages. During each fractionation step, aqueous and organic fractions are obtained which are characterized for their structure by advanced analytical techniques. The humeomics extraction was applied to humic substances previously isolated from soil by the standard alkaline extraction [14] as well as directly on soil [16]. The authors report that the humeomics approach extracted about 2.35% higher yields of extracted soil organic carbon than the traditional alkaline extraction.

In this work, we applied an original sequential fractionation approach using organic solvents of increasing polarity on peat HA and subjected the obtained organic fractions to a complex physicochemical characterization utilizing methods of structural and compositional analysis. Peat HA was selected as a representative of the commonly studied isolates from natural organic matter. Fractionation according to the polarity of its constituents is put forward as a logical, easy to implement but yet still underestimated tool for reducing the structural complexity of an organic matter from various sources and of various origins.

2. Materials and Methods

2.1. Origin and Isolation of Humic Acids

The sample of peat used in this study was obtained from the peat-bog Branná (48°57′10.953″ N; 14°48′20.587″ E) located in the Trebon basin, South Bohemia, Czech Republic. The transitional peat was classified to the FAO soil classification system as a Eutric Histosol which corresponds to the Czech classification equivalent of an Organozem. The peat soil was characterized by dark brown to black color, advanced decomposition of original plant materials (i.e., sapric type of peatland), and bulk density of the homogenized sample was determined to be approximately 0.47 g mL^{-1}. A representative sample was collected from the surface layer 0–30 cm. The peat was used after drying at 105 °C for 24 h then let to equilibrate with ambient laboratory atmosphere at about 25 °C which resulted in the final equilibrium moisture content of about 8.2% by weight. The ash content was determined using a Q50 TG analyzer (TA Instruments, New Castel, DE, USA). The residual weight at 1000 °C (i.e., ash content) was determined of 54.1% by weight.

The detailed information on the isolation procedure of humic acid (SBPHA) from the peat sample is described in the Supplementary Materials (see Page S1).

2.2. Sequential Chemical Extraction

The as-extracted peat HA was subjected to the sequential chemical fractionation using organic solvents of increasing polarities [17] in the following order: trichloromethane (TCM), ethyl acetate (EAC), acetone (ACE), acetonitrile (ACN), 1-propanol (PRO), and methanol (MET). The physicochemical properties of used organic solvents are shown in the Supplementary Materials (see Table S1).

Briefly, HA was homogenized and 3500 mg was then inserted in a thimble, and Soxhlet sequential extracted for 48–120 h. The organic fractions extracted from the peat HA were concentrated using a rotary evaporator, and the yellow to dark brown extracts were dried in a vacuum desiccator using anhydrous sodium sulfate as a drying medium. The solid organic fractions will be referred to in the following text using the abbreviations of solvents and a number indicating the order of the extraction step (i.e., from TCM1 to MET6).

2.3. Organic Fractions Analysis

2.3.1. Elemental Composition

Thermogravimetry of the extracted organic fractions was performed using a Q5000 TG analyzer (TA Instruments, New Castel, DE, USA). Approximately 5 mg of sample was weighed into a platinum pan. During the analysis, the residual sample weight was recorded continuously (with ±0.1% mass accuracy) as the sample was heated at a heating

rate of 10 °C min^{-1} from ambient temperature to 1000 °C under air atmosphere. Moisture content was determined from the relative weight loss at 105 °C, while the residual weight at 1000 °C, was assigned to the ash content.

The relative content of organic elements in the solid organic fractions was determined using an EA 3000 CHNS/O analyzer (Euro Vector, Pavia, Italy). Approximately 0.5–1.0 mg of the sample was weighed in a tin capsule, the capsule was packed and combusted at 980 °C in the analyzer using oxygen as the combustion gas and helium as the carrier gas. Calibration of the determination of relative contents of carbon (C), hydrogen (H), nitrogen (N), and sulfur (S) from the obtained gas chromatograms were provided using sulfanilamide as a reference standard sample. The relative oxygen content was calculated from the residual combustible mass, and the data obtained were corrected for moisture and ash content. The analysis was triplicated for each extracted fraction. The sulfur content was under the limit of detection (0.5 wt.%) in all tested samples (SBPHA and organic fractions).

2.3.2. UV/Vis Spectrometry

The UV/Vis absorption spectra of alkaline aqueous solutions of the individual organic fractions at a concentration of 10 mg L^{-1} were recorded on Hitachi U-3900H double beam UV/Vis spectrometer (Hitachi, Tokyo, Japan) in the spectral range between 200 and 800 nm. Standard phosphate buffer (0.1 M NaH$_2$PO$_4$, Na$_2$HPO$_4$) was used as a solvent of the fractions as well as a blank solution.

2.3.3. ATR-FTIR Spectrometry

The Attenuated Total Reflectance (ATR-FTIR) technique was used for a deeper structural characterization of organic fractions. Fourier transform infrared (FTIR) spectra of the fractions were recorded on Nicolet *i*S50 spectrometer (Thermo Fisher Scientific, Waltham, MA, USA) using the Attenuated Total Reflectance (ATR) measuring technique (single-reflection built-in diamond ATR crystal). All measurements were taken at 25 °C in the spectral range 4000–400 cm^{-1} at 4 cm^{-1} resolutions as an average of 256 scans. A background spectrum was collected from the clean dry surface of the ATR crystal in an ambient atmosphere. Raw absorption infrared spectra with no artificial processing (such as baseline or ATR corrections, atmospheric suppression) are presented and evaluated.

2.3.4. Fluorescence Spectrometry

For fluorescence analysis, organic fractions were dissolved at a concentration of 10 mg L^{-1} of organic carbon in standard phosphate buffer (pH = 7). All spectra were obtained by FluoroLog fluorescence spectrometer (Horiba Scientific, New Jersey, USA) with a scan speed of 600 nm min^{-1}, using excitation and emission slit bandwidths of 5 nm. Excitation emission matrix (EEM) spectra were obtained by scanning the emission and excitation wavelengths over the range 300–600 nm and 240–550 nm, respectively, with the wavelength increment of 5 nm. The temperature of the sample cell was kept at 20 °C during the measurement. The background EEM spectrum of ultra-pure water (Milli-Q) was recorded and subtracted from the EEM spectra of the analyzed samples to eliminate the spectral signs of 1st- and 2nd- order Raman scattering. Primary and secondary inner filter effects were corrected according to the method proposed by Lakowicz [18]. For this purpose, absorbance spectra of the analyzed samples were recorded on Hitachi U-3900H UV/Vis spectrometer.

2.3.5. Liquid-state ^{13}C NMR Spectroscopy

^{13}C NMR spectra of the fractions were obtained using a liquid-state NMR technique using a Bruker Avance 500 DRX NMR spectrometer (Bruker, Karlsruhe, Germany) with the working frequency of 125.77 MHz. Organic fractions were dissolved at a concentration of 20 mg mL^{-1} of organic carbon in 0.5 M NaOD. All liquid-state spectra were obtained with the following settings of ^{13}C NMR spectrometer: temperature 25 °C, number of scans 25 000, excitation pulse 10.5 μs, acquisition time 0.52 s, spectral width 31 250 Hz pulse repetition

delay 2.0 s and NMR-cell diameter 5 mm. The aromaticity f_a of the organic fraction was calculated from the ^{13}C NMR spectra as a ratio of the areas of two chemical-shift regions $I_{(106–165\ ppm)}/I_{(0–165\ ppm)}$ [19] by integrating their relevant intensities.

2.3.6. Statistical Analysis

The relationships between the spectroscopic properties and other physicochemical indicators of organic fractions and peat HA were examined by principal component analysis (PCA). The main goal of statistical data processing was to find similarities and dissimilarities between the organic fractions and the original unfractionated peat HA. Origin 2019b (OriginLab, Northampton, MA, USA) was used to process data for PCA and create a bi-plot graph i.e., two-dimensional projection.

3. Results and Discussion

3.1. Yields, Ash Contents, and Elemental Analysis

The extraction yields, elemental composition, ash content, and atomic ratios (H/C, O/C, and C/N) of individual organic fractions, sequentially extracted from peat HA, are presented in Table 1, together with the relevant properties of the unfractionated HA.

Table 1. Extraction yields, ash contents, elemental compositions, and atomic ratios of organic fractions extracted from peat humic acid (HA). Relevant parameters of compositional analysis for original HA (SBPHA) are included for comparison.

	Yield	Ash	C	H	N	O	H/C	O/C	N/C
	(wt.%) [1]	(wt.%) [1]			(at.%) [2]				
SBPHA	-	0.7	35.00 ± 0.24	49.84 ± 0.16	1.12 ± 0.09	14.03	1.42	0.40	0.032
TCM1	3.76	0.07 ± 0.02	30.83 ± 0.11	67.10 ± 0.32	0.15 ± 0.02	1.92	2.18	0.06	0.005
EAC2	1.10	1.81 ± 0.09	33.30 ± 0.16	65.65 ± 0.28	0.63 ± 0.05	0.42	1.97	0.01	0.019
ACE3	13.00	0.34 ± 0.04	43.78 ± 0.20	34.62 ± 0.13	0.82 ± 0.05	20.77	0.79	0.47	0.019
ACN4	7.83	4.10 ± 0.08	30.52 ± 0.34	49.87 ± 0.19	3.30 ± 0.10	16.31	1.63	0.53	0.108
PRO5	19.74	0.83 ± 0.17	37.22 ± 0.21	44.23 ± 0.36	0.94 ± 0.07	17.61	1.19	0.47	0.025
MET6	11.91	2.99 ± 0.12	34.62 ± 0.37	46.18 ± 0.22	1.43 ± 0.12	17.77	1.33	0.51	0.041

[1] weight content calculated on a moisture-free basis. [2] atomic percentages calculated on a moisture-free and ash-free basis. Values of ash content and elemental compositions are means ± SD (n = 3).

The extraction yield of organic fractions ranged from 1.1% to 19.7% (relative to the initial weight of the unfractionated HA) varying with the polarity of the organic agent used. The highest extraction yields (13.0% and 19.7%, respectively) were obtained for organic fractions extracted with acetone (ACE3) and 1-propanol (PRO5). In contrast, the lowest yield of organic compounds (1.1%) was obtained in the case of the organic fraction EAC2 extracted using ethyl acetate, which may be caused by the similar values of polarity indices of the first two applied solvents (TCM and EAC). The enhanced release of organic constituents from HA to more polar extractants is not surprising with respect to HAs' high relative content of polar structural constituents rich in the oxygen-containing functional groups (such as carboxylic, phenolic, and carbonyl groups). It should be noted that the applied extraction procedure most likely releases only free organic compounds and/or weakly bound molecules from the complex organic matrix as indicated by the significant amount of an insoluble residuum in Soxhlet thimble after completion of the last extraction step. The content of residual, not-extracted organic compounds in peat HA was 43% (relative to the initial weight of unfractionated HA).

The organic elemental compositions of all obtained fractions are summarized in Table 1 in the form of an atomic percentage (calculated from the determined weight content based on dry-ash free organic content). Generally, the carbon content increased unevenly with increasing the polarity of the organic agent, while the hydrogen content decreased. The highest atomic content of carbon (43.78%) was found for organic fraction extracted using acetone (ACE3). Nitrogen represents a minor component of all obtained fractions and its content ranged from 0.15% to 3.30%, deviating on both sides from the nitrogen content of

the original HA (1.12%). As expected, non-polar organic fractions (i.e., TCM1 and EAC2) were relatively poor in oxygen. In general, the elemental composition of these two fractions was similar to that of lipid compounds extracted from various lignite and peat materials in other studies [20,21].

Atomic ratios are often used as basic markers of the main structural character of the analyzed material. For instance, H/C atomic ratio is considered an indicator of aliphaticity. For the isolated peat HA fractions, the value of the H/C ratio varied within a range from 0.79 to 2.18. The highest values of this parameter were obtained for the first two fractions (TCM1 and EAC2), which could be attributed to their prevailing aliphatic character and content of compounds with long carbon chains such as fatty acids and their esters. In contrast, the lower values of the H/C atomic ratio determined for the other samples indicate the presence of organic compounds with a higher degree of aromaticity.

As another fundamental compositional marker, O/C atomic ratio reflects the amount of oxygen-containing functional groups (e.g., carboxylic, phenolic, and carbonyl) in an organic matter. For our organic fractions, the determined values of the O/C ratio covered a broader range (0.06 to 0.53) than those reported in the literature [13]. In general, higher values of the O/C atomic ratio in humic substances indicate a high relative content of oxygenated compounds such as aromatic carboxylic acids, phenols, and/or polar substituted carboxylic compounds (e.g., amides). For the samples extracted using acetonitrile and methanol (ACN4 and MET6), a combination of the highest determined O/C ratios with relatively high H/C can be attributed to a presence of oxygen bonded alkyl groups, such as alkyl ethers and esters originated from lignin and/or polysaccharides residues. The O/C values of the most polar fractions are also in good agreement with the O/C ratio of the unfractionated HA material (0.40).

Finally, N/C atomic ratio reflects the amount of nitrogen in organic fractions and is commonly used as a proxy for the maturity of the organic material. Increasing N/C is usually attributed to a decrease in C rates in the decomposition process and higher values of the ratio are hence related to higher humified materials and vice-versa [22]. The N/C ratio values vary significantly among the analyzed HA fractions, ranging from 0.005 to 0.108, while the original HA show an N/C ratio of 0.032. While the lowest content of nitrogenous constituents was found for the fraction isolated with the most apolar solvent (TCM1), the highest content of nitrogen was detected in the fractions ACN4 and MET6. As far as these fractions were relatively rich also in oxygen, the nitrogen is likely introduced in these fractions mainly in form of amide groups of the protein-like compounds. This result is in good agreement with the FTIR spectrum (ACN4) listed in Figure 1. The van Krevelen diagram of atomic H/C ratio versus atomic O/C ratio for the original HA and organic fractions is provided in Figure S3 (Supplementary Materials).
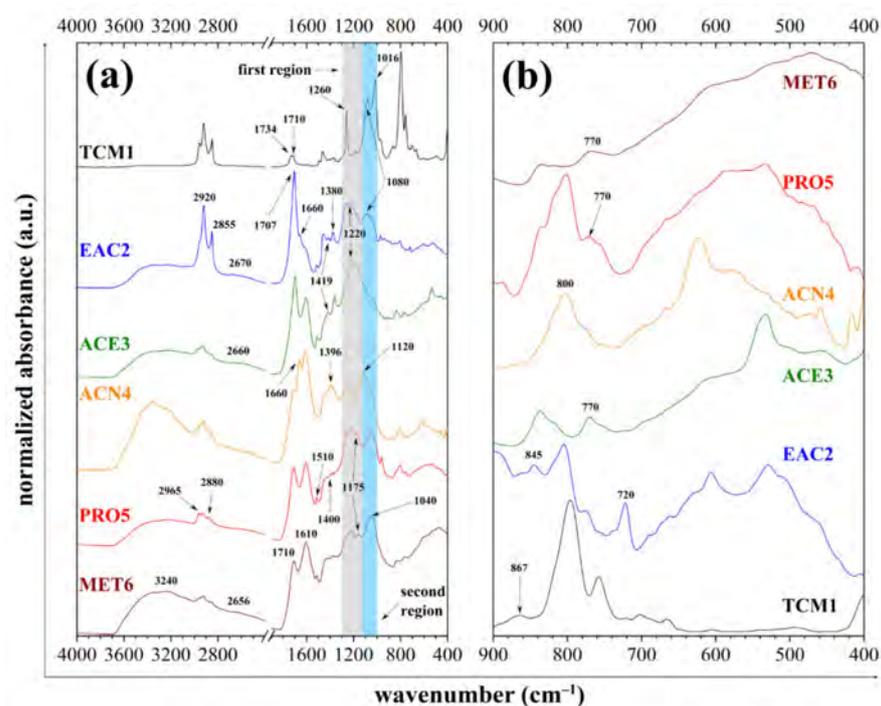
Figure 1. Attenuated Total Reflectance (ATR-FTIR) spectra of organic fractions extracted from peat HA, (**a**) spectral range of 4000–400 cm^{-1} and (**b**) spectral range of 900–400 cm^{-1} for the visualization of less intense absorption bands.

3.2. UV/Vis Spectrometry

No distinctive spectral features were observed in the measured UV/Vis spectra of all tested samples. In other words, the curves of UV/Vis spectra were characterized without visible local maxima and/or shoulders whereas their absorbance quasi-exponentially increases with decreasing wavelength (not shown). The UV-spectral behavior of organic fractions in this study was rather different from the behavior reported for organic extracts isolated from commercial humic substances where absorption peaks and/or shoulders in the 200–350 nm wavelengths range were reported [23].

All organic fractions obtained and analyzed in this study absorb significantly in the ultraviolet region. Significant absorption in this part of the electromagnetic radiation indicates that the vast majority of the types of chromophores include aromatic rings with various degrees and types of substitution [24]. In the context of basic molecular structure, these are compounds such as monosubstituted and polysubstituted phenolic substances derived from lignin residues, tannins, hydroxyl- or polyhydroxy- coumarins, etc. and various monoaromatic and/or polyaromatic acids [25]. Although UV/Vis spectra of humic substances, because of their characteristic featureless nature, might be considered of limited usefulness for a detailed interpretation of the molecular structure, the number of scientific studies have already illustrated that advanced analysis of these spectra, such as determination and interpretation of specific absorption parameters, may contribute significantly to understanding chemical structure and properties of complex organic compounds (e.g., humic substances, dissolved organic matter) and that they may suitably complement the information obtained using other analytical techniques such as potentiometric titration, light scattering methods, NMR, etc. [5,26,27]. Therefore, selected absorption ratios (E_2/E_4 and E_{ET}/E_{Bz}) and SUVA$_{254}$ parameters were used to characterize organic fractions obtained in this study.

Well known and traditionally used E_4/E_6 ratio (the ratio of absorbance at 465 nm to that 665 nm), which is also referred to as color coefficient $Q_{4/6}$ [28], reflects the degree of aromaticity and the average molecular weight of humic substances of different origins [29–31]. Unfortunately, the absorption in the 550–700 nm wavelength region of

the fractions studied was too low to allow calculation of the E_4/E_6 ratio, thus the E_2/E_4 ratio (the ratio of absorbance at 265 nm to that 465 nm) was used in analyzing the fractions, as it is consistent with the E_4/E_6 [32]. As can be seen in Table 2, the E_2/E_4 ratio values ranged from 7.18 to 12.00 and followed a downward trend with increasing polarity of the organic solvent. Furthermore, E_2/E_4 ratios likely indicate that high-molecular fractions (i.e., humic-like compounds) were extracted only with the most polar solvents (from ACN4 to MET6). Concerning the lowest E_2/E_4 ratio determined for the unfractionated HA (5.53), it could be deduced that all the organic solvents preferentially extract less aromatic organic constituents with a lower molecular weight. Nevertheless, as far as the value of E_2/E_4 ratio is increased also by the specific absorption of –C=O groups [33], it cannot be used as a reasonable marker of aromaticity and molecular weight among organic materials with widely differing content of oxygen-containing groups.

Table 2. Parameters calculated from UV/Vis and FTIR spectra.

	UV/Vis Ratios		UV Parameter	FTIR Intensity Ratios	
	E_{ET}/E_{Bz}	E_2/E_4	$SUVA_{254}$ [1]	I_{Ar}/I_{COOH} [2]	I_{CH2}/I_{CH3} [3]
SBPHA	0.74 ± 0.06	5.53 ± 0.12	5.68	1.26	1.06
TCM1	0.51 ± 0.02	11.87 ± 0.15	0.24	0.22	1.81
EAC2	0.70 ± 0.02	12.00 ± 0.06	0.66	0.34	1.87
ACE3	0.74 ± 0.01	9.77 ± 0.11	5.89	0.80	1.11
ACN4	0.66 ± 0.00	9.53 ± 0.10	2.03	1.44	1.11
PRO5	0.74 ± 0.04	7.64 ± 0.14	6.40	1.06	0.98
MET6	0.83 ± 0.02	7.18 ± 0.22	5.79	1.21	1.04

Values of UV/Vis ratios are means $\pm$ SD ($n = 3$). [1] calculated as absorbance at 254 nm divided by the concentration of total dissolved organic carbon in the solution (in mg L^{-1}). [2] FTIR ratio calculated as the ratio of intensity at 1610 cm^{-1} to an intensity at 1710 cm^{-1}. [3] FTIR ratio calculated as the ratio of intensity at 2920 cm^{-1} to an intensity at 2965 cm^{-1}.

Therefore, we calculated also the $SUVA_{254}$ parameter (the ratio of absorbance at 254 nm to total organic carbon) which was found to positively correlate with the aromaticity and molecular weight of humic substances without the interference of the carbonyl content [32]. In our study, the values of the $SUVA_{254}$ ranged from 0.24 to 6.40 (see Table 2) and followed an upward trend with increasing polarity of the organic solvent, except for the fraction ACN4. These results agree with E_2/E_4 in that significantly lower aromaticity is indicated for the organic fractions which were isolated in the first two steps of the extraction procedure. On the other hand, the organic fractions extracted with the acetone and alcohol solvents (ACE3, PRO5, and MET6) show $SUVA_{254}$ values close to that of the SBPHA (5.68) indicated a similar degree of aromaticity and molecular weight as the source HA. Interestingly, a significantly lower $SUVA_{254}$ value of ACN4 fraction indicates lower aromaticity of this fraction, not revealed by E_2/E_4. In this perspective, $SUVA_{254}$ seems to be a more suitable proxy for the determination of aromaticity of the obtained organic fractions.

The E_{ET}/E_{Bz} ratio (the ratio of absorbance at 253 nm to that 220 nm) is higher for compounds in which the aromatic structural units are predominantly substituted with oxygen-containing functional groups (e.g., hydroxyl, carbonyl, ester, and especially carboxyl groups), whereas lower values are associated with aliphatic substituents [24,34]. For the studied organic fractions, the E_{ET}/E_{Bz} ratio values ranged from 0.51 to 0.83 (see Table 2). Fractions isolated between the second and the fifth extraction step show E_{ET}/E_{Bz} values close to that of the unfractionated HA (0.74) indicating a similar type of substituents on the aromatic structures as distributed in the original peat HA. On the other hand, the organic fractions extracted with the least polar (TCM1) and the most polar (MET6) solvent, show E_{ET}/E_{Bz} values indicating considerably higher content of aliphatic (TCM1) and oxygen-containing (MET6) substituents, respectively, as compared to the original HA.

The optical parameters used in this work or numerous others proposed in the literature [32–35] do not represent the only way of extracting structural information from UV/Vis

spectra of humic substances and their constituents. For instance, second-order derivative UV/Vis spectra provide enhanced spectral resolution [36] and may hence be useful in the evaluation of weak and broad absorption bands such as the perylenequinone-type bands appearing in Vis spectra of humic acids as a result of fungal activity contributing to the humification process [37].

3.3. ATR-FTIR Spectrometry

The ATR-FTIR technique was chosen as it requires no mechanical pressing treatment of the sample which is necessary for the KBr transmission technique and, therefore, less opportunity is given for experimental artifacts such as pressure-induced deprotonation and/or decarboxylation of acidic functional groups [38]. The ATR-FTIR spectra of organic fractions are presented in Figure 1a,b. Interpretation of their absorption bands has been carried out according to the literature data [8,39,40].

The spectra of all fractions show several common features but also relevant differences. The first set of spectral attributes includes bands assigned to O-containing functional groups: (a) The broad absorption band centered at about 3240 cm^{-1} corresponds to O–H stretching of various functional groups (including the carboxylic), which are connected with an intermolecular hydrogen-bond. This band is well pronounced in FTIR spectra of all extracts except for the one extracted with the least polar solvent (TCM1) where the absorption is markedly suppressed. (b) A sharp band with variable intensity located at around 1710 cm^{-1} is attributed to symmetric C=O stretching in carboxylic groups. This band is common for all extracted fractions, whereby in the spectrum of TCM1 it is accompanied also by the band at 1734 cm^{-1} assigned carbonyl stretching in esters. The presence of the protonated carboxylic groups is often manifested also by a broad shoulder centered at about 2660 cm^{-1} resulting from the O–H stretching vibrations of the hydrogen-bonded dimers of COOH [41]. This weak band/shoulder is recognizable in fractions EAC2, ACE3, PRO5, and MET6, while it is reduced in the TCM1 and ACN4 fractions, where the formation of hydrogen-bonded dimers of carboxylic acids is reduced by their partial conversion to esters and carboxylates (see part (d) of this paragraph), respectively. (c) A characteristic band at 1660 cm^{-1} can be assigned to stretching C=O groups in secondary amides (amide I) of the protein-like structures. This band is apparent only in the spectra of EAC2 and ACN4 samples. The assignment of this absorption band to amide groups is supported by the presence of accompanying amide II bands (1570–1540 cm^{-1}) in deconvoluted spectra in the overlapping region 1750–1500 cm^{-1} (see Figure S4 in Supplementary Materials) (d) The deformation vibrations of carboxylate groups occur in the spectra as a weak band and/or shoulder at around 1395 ± 5 cm^{-1} [42]. This absorption band is well-identified only in the spectra of ACN4 and, considering the high relative ash content of this sample, it probably represents the presence of metal chelates in this fraction. (e) A weak band or shoulder at 1420 cm^{-1} can be ascribed to C–O–H in-plane bending in carboxylic groups. This band is easily recognized in the less polar fractions (TCM1, EAC2, and ACE3) while it is overlapped with other oxygen-containing functional groups in the more polar ones (ACN4, PRO5, and MET6). (f) Further differences among the isolated fractions concerning O-containing groups can be deduced from the deeper evaluation of fingerprint regions 1300–1125 cm^{-1} and 1120–1050 cm^{-1}. The first region (marked grey in Figure 1a) is characterized by a sharp and intensive C–O stretching band at 1260 cm^{-1} (aryl ethers) and relatively intensive bands and/or shoulders at 1220 cm^{-1} (C–O stretching and O–H bending of carboxylic groups, C–O stretching in phenoxy structures and ethers) and 1175 cm^{-1} (C–O stretching of phenols and ethers). Unlike other samples, ACN4 did not contain the vibration at 1220 cm^{-1}, as a result of the lower content of protonated carboxyls. The latter fingerprint zone (marked blue in Figure 1a) is characterized by two bands at 1120 cm^{-1} and 1080 cm^{-1} corresponding to the C–O–C vibration in alkyl ethers, and to the C–O stretching of secondary alcohols. The first of these bands was found only in the ACN4 sample. The band at 1040 cm^{-1} is the most intensive in the spectra of organic fractions extracted by alcohols (PRO5, MET6) due to the higher extracted amount of polysaccharide-like substances. The prominent band

at 1016 cm^{-1} which can be attributed to asymmetric C–C–O stretching in alkyl ethers [43] is visible only in the spectrum of TCM1 and is accompanied by symmetric stretching absorption at 867 cm^{-1}.

The second set of spectral features that are in common for all the fractions refer to their content of aliphatic molecular moieties. (a) The relative content of aliphatic chains is evaluated primarily in the 3000–2800 cm^{-1} spectral range. The presence of aliphatic groups is revealed by the bands at 2920 cm^{-1} and 2855 cm^{-1} which are attributed to asymmetric and symmetric C–H stretching in methylene groups, respectively. These bands are the most dominant in TCM1 and EAC2 but are also relatively intense in ACN4 samples. Additional bands at 2965 cm^{-1} and 2880 cm^{-1} were ascribed to asymmetric and symmetric C–H stretching in methyl groups. These bands are well recognizable mainly in the spectrum of the PRO5 sample, occurring as a weak band and/or shoulder in the rest of the samples. (b) The deformation vibrations of the –CH$_2$– and –CH$_3$ groups at 1465 cm^{-1} and 1380 cm^{-1}, respectively, only occur in the TCM1 and EAC2 spectra. (c) The presence of long carbon chains with more than four atoms (e.g., in fatty acids) was revealed by the band at 720 cm^{-1} which is ascribed to C–H in-plane bending of methylene groups. This band was found only for TCM1 and EAC2 samples, which supports the expectations that the least polar solvents would be the most efficient in the extraction of long-chain lipidic structures from the complex matrix of HA.

The third set of spectral absorptions that can be attributed to aromatic structures comprises: (a) the relatively intense symmetric ring stretching band occurring at 1610 cm^{-1}, which was observed only as a very weak shoulder in the spectrum of TCM1 sample, indicating low aromaticity of this fraction; (b) Another characteristic aromatic band is located at 1511 cm^{-1}, due to the aromatic C=C stretching of lignin residues. While this band is again apparently absent in the spectrum of TCM1, its relative intensity is comparable for all other fractions; (c) Out-of-plane C–H deformation bands were found in the 870–750 cm^{-1} region. The position of these peaks is used as a specific marker of the type of substitution of the aromatics, as far as it can distinguish aromatic structures with isolated hydrogens with aromatic carbon (870 cm^{-1}), two and/or three adjacent hydrogens per ring (845 cm^{-1} and 800 cm^{-1}), and four adjacent hydrogens (770 cm^{-1} and 750 cm^{-1}) [41,44]. Spectral bands that can be assigned to two and more adjacent aromatic hydrogens are apparent in the spectra of all fractions except for TCM1 (see Figure 1b), di-substituted aromatic rings being prevailing in fractions ACE3 and MET6 while tri- and/or tetra-substituted aromatic rings in EAC2, PRO5, and MET6. It should be noted that significant absorption in the spectral region of 800 cm^{-1} to 750 cm^{-1} can be found also for TCM1 fraction. Nevertheless, the above discussed spectral evidence of low content of aromatics in the sample indicates that this vibration should be assigned to some other structural motifs (out-of-plane C–H bending in lactones, C–Cl stretching in residual solvent).

Aside from the qualitative information on the structure of the extracted fractions, results of FTIR spectroscopy can also be used for semiquantitative analysis of the content of the main structural groups. The degree of carboxylic content in humic substances is usually represented by the I_{Ar}/I_{COOH} ratio (the ratio of the intensity at 1610 cm^{-1} to the intensity at 1710 cm^{-1}) [44]. The value of this ratio (Table 2) is the lowest for the organic fraction extracted by chloroform (TCM1). Nevertheless, the usability of this value for evaluating the carboxylic content quantitatively is questionable for fractions with significantly reduced aromaticity like it can be seen for TCM1 (note very weak absorption band at 1610 cm^{-1} for this fraction) and also for ACN4, where a significant portion of carboxyl groups occurs in the form of carboxylates. Among the other fractions which all show significant absorption bands both at 1710 cm^{-1} and 1610 cm^{-1}, the I_{Ar}/I_{COOH} ratio shows that the relative content of COOH groups (normalized on the content of aromatics) decreases in the following order of samples: EAC2 > ACE3 > PRO5 > MET6. Similarly, aliphatic structural moieties can be evaluated in a semiquantitative way by the I_{CH2}/I_{CH3} ratio (the ratio of the intensity at 2920 cm^{-1} to the intensity at 2965 cm^{-1}), which is used to estimate the length and degree of branching of aliphatic chains. The intensity ratio (Table 2) shows that longer (which

agrees with the presence of 720 cm^{-1} band) and less branched aliphatic chains are obtained in TCM1 and EAC2 samples compared with the other organic fractions.

3.4. Fluorescence Spectrometry

The EEM spectra and contour maps of the studied fractions are shown in Figure 2 (Rayleigh scattering peaks appear in the form of diagonal lines). In general, the shorter emission wavelengths and greater fluorescence intensity measured in EEM spectra belong to the fluorescence of simple aromatic structures and lower molecular weight organic components, while a shift of the fluorescence maximum to higher wavelengths indicates the presence of condensed aromatic structural units and electron-withdrawing substituents [45]. The emission maximum of organic compounds ranging from 340 to about 430 nm could be associated with three- and/or four-ring aromatic structures, four or more aromatic rings per structural unit of a fluorophore result in the light emission at longer wavelengths (i.e., from 400–500 nm). Furthermore, several authors observed in the EEM spectra of terrestrial HAs unique fluorescence domains located at even longer excitation and emission wavelengths in the visible spectral region [46–48], which are interpreted as fluorophores derived from phytochlorin (chlorophyll degradation by-product). Contemporary classification of the types of fluorophore domains in humic substances [49,50] is summarized in Table S2 (Supplementary Materials).
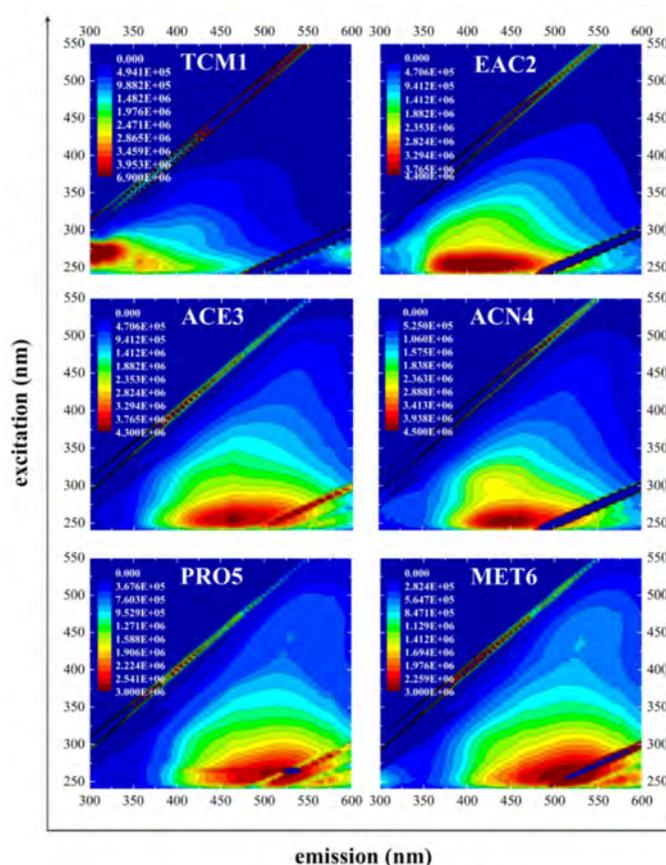
Figure 2. Excitation–emission matrix (EEM) spectra of organic fractions extracted from peat HA.

Organic fractions, isolated and analyzed in this study, contain fluorophores typical for fluorescence of caustobioliths (e.g., lignite, leonardite, and peat) and soil humic substances [51–53]. The excitation-emission wavelength pairs (EEWP) of the main peaks in the EEM spectra, their fluorescence intensity values, and assignments to the specific fluorophore classes are provided in Table 3. It can be seen that, except for the TCM1 fraction, excitation-emission characteristics of the primary fluorescence maxima of all other fractions

(250–265/415–505 nm) corresponds to the "A"—domain fluorophores typical for fulvic acids and dissolved organic matter (DOM). It means that isolated fluorophores excited in the UVC region are the main contributors to the fluorescence of all these fractions (from EAC2 to MET6). On the other hand, the fluorescence maximum of the fraction isolated with the least polar solvent (TCM1) lie within the "B" region which is most often assigned to the fluorescence of tyrosine in protein-like structures contained in the organic matter [54,55]. However, because no significant content of protein residues was revealed in the TCM1 fraction by the elemental and FTIR analyses, it is more likely that the blue shift of the emission maximum is caused rather by lower molecular weight and electron detaining ester substituents [56].

Table 3. Positions of excitation-emission wavelength pairs for fluorescence domains and values of fluorescence intensities for organic fractions and original peat HA.

| | Fluorescence Peak Region | | | | | | | | | |
| | A | | C | | V | | B | | H | |
	Ex/Em (nm)	I_F (CPS) [1]	Ex/Em (nm)	I_F (CPS) [1]	Ex/Em (nm)	I_F (CPS) [1]	Ex/Em (nm)	I_F (CPS) [1]	Ex/Em (nm)	I_F (CPS) [1]
SBPHA	255/495	1.77								
TCM1							270/305	6.86	255/355	3.23
EAC2 [2]	250/415	4.36					270/305	0.99		
ACE3	255/465	4.22								
ACN4	255/445	4.49	300/435	2.74			270/315	0.98		
PRO5	265/500	2.76			445/530	0.80				
MET6	260/505	2.57			435/525	0.72			250/300	0.99

[1] $I_F \times 10^6$ CPS (counts per second) of fluorescence peaks. [2] The C domain (humic-like) was observed in the EEM spectrum of the EAC2 sample as less pronounce shoulder.

Furthermore, from a detailed evaluation of the EEM spectra, secondary fluorescence maxima representing other types of fluorophores contained in the structure of isolated fractions can also be revealed (see the spectral cut-outs presented in Figure S5 in Supplementary Materials). As can be seen in Table 3, B-type fluorophores were determined in the EEM spectra of EAC2 and ACN4 fractions. One of the possible assignments of this fluorescence peak is represented by tyrosine-like fluorophores, which is also to some extent supported by results of elemental analysis (higher relative content of N) and FTIR (presence of characteristic amide I band) indicating a presence of protein residues. Tyrosine-like fluorophores were also recently found in DOM fractions isolated from the tropical peatlands [57]. Nevertheless, direct identification of these particular structural moieties in these fractions is beyond the resolving power of the methods used in this study and should be resolved in future work.

For the first (TCM1) and the last (MET6) extracted fractions, an additional fluorescence maximum was found with the EEWP in the range 250–255/300–355 nm. This emission is often assigned to the soluble microbial by-product-like compounds [58,59]. Doskočil et al. [21] in their work, focused on EEM spectra of lipids isolated from various coal basins, has introduced the term "peak H" attributed to fluorescence band if its maximum is situated in the UVA region with an excitation wavelength at about 250 nm. No structural model of fluorophore H has yet been proposed. Nevertheless, this signal can in general be attributed to simple aromatic structures (without condensed rings) with electron-donating substituents, such as the alkyl or methoxyl groups identified in TCM1 and MET6, respectively, by the other techniques.

Humic-like fluorophores referred to as the C-domain fluorophores (300–380/400–500 nm) are also typical for humic substances and DOM originating from peats, soils, and natural waters [60]. Fluorescence in this spectral domain reveals as a well-distinguished peak for ACN4, while it forms a less pronounced shoulder on the primary fluorescence peak in the spectrum of EAC2. Cao and Jiang observed this type of fluorescence in EEM spectra

of low molecular weight fractions of humic acids from bulk Leonardite HA [61]. Some authors [52,62] have suggested that the humic-like fluorophore can be attributed to the presence of phenolic acid derivatives and other substituted phenolic units originating from lignin, hydroxycoumarin-like, and/or quinone-like structures which originated from degraded terrestrial biomaterials such as plant tissue. Furthermore, McKnight et al. [63] reported in a study on spectrofluorometric characterization of DOM that the C may be interpreted such as domains from the autochthonous microbial process. We hence conclude that the C-domain fluorescence in the analyzed organic fractions is probably related to autonomous low-molecular fluorophores formed by aromatic systems highly substituted with reactive functional groups, especially –COOH substituents.

In the EEM spectra of the two fractions extracted with alcohols (PRO5 and MET6), fluorescence maxima having excitation wavelengths greater than 400 nm were also found. Fluorescence peaks in this spectral region are referred to as V and/or α [53,62] and usually occur in lignite, peat, and humus-rich soils. In general, for the fluorescence maxima with an emission wavelength greater than 470 nm it is suggested that the fluorescence originates from a transition of electronic charge from one region of a molecular species to another and/or from one molecular species to another rather than from independent fluorophores [64]. For PRO5 and MET6 fraction, the fluorescence peaks located in the V region thus probably reflect a presence of high-molecular fluorophores (e.g., linearly condensed networks of aromatic rings) substituted with electron-withdrawing functional groups. This is in good agreement with the results of UV/Vis (see the high values of $SUVA_{254}$ and E_{ET}/E_{BZ} and their discussion in Section 3.2) and with the high content of carboxylic groups confirmed by FTIR and NMR. The V-region fluorescence was not apparent in the EEM matrix of original HA used in this study (see Figure S2), nevertheless, as it was previously observed for another HAs isolated from a similar natural source [65], it may be suggested that the structural moieties responsible for fluorescence of peat HAs in the V region are preferentially extracted into the polar alcoholic fractions.

3.5. Liquid-State ^{13}C NMR Spectrometry

As the last part of the spectrometric study, the ^{13}C NMR spectra of the isolated organic fractions (see Figure S6 in the Supplementary Materials) were measured in the liquid state. EAC2 and ACN4 fractions were not analyzed by this technique because of their too low extraction yields. Relative distribution of individual carbon types typical for the natural organic matter was obtained from the integration of the raw spectra in the corresponding regions of resonance: alkyl carbon (0–45 ppm), carbohydrates and/or peptides (45–106 ppm); aromatic carbon (106–145 ppm), phenolic carbon (145–165 ppm), carboxylic carbon (165–190 ppm) and carbonyl carbon (190–220 ppm) [19,66]. The results of the integration are provided in Table 4.

Table 4. Average distribution of individual carbon types and calculated aromaticity index (f_a) for the studied organic fractions from the liquid-state ^{13}C NMR spectra.

Organic Fractions	Average Distribution of Individual Carbon Types (%)						(f_a) [1]
	0–45 ppm	45–106 ppm	106–145 ppm	145–165 ppm	165–190 ppm	190–220 ppm	
TCM1	78	8	8	2	3	1	0.10
ACE3	23	19	36	11	9	2	0.53
PRO5	24	22	33	9	10	2	0.48
MET6	16	30	31	8	13	2	0.46

[1] Aromaticity index calculated as the ratio of the intensity at 106–165 ppm to the intensity at 0–165 ppm.

As expected, the relative content of alkyl carbon, manifested in the spectra as methyl groups (20–22 ppm) and/or methylene groups (27, 31, and 40 ppm), varies within a broad range among the analyzed fractions, being the highest (78%) for the fraction extracted by the least polar solvent (TCM1). The opposite was found for the relative content of hydrophilic components such as polysaccharide residues and protein-like compounds (relative area

in 45–106 ppm) which was lowest for the TCM1 fraction while the highest for the most polar solvent used (MET6). Detailed analysis of the region of *O*-alkyl and peptide carbon resonances reveals the presence of quaternary carbons, methine groups (lignin, cellulose, and/or hemicellulose residues), and α-carbons (amino acids and/or polysaccharides). A common feature for all analyzed fractions is the signal at 56 ppm which may be attributed to methoxyl or amide groups [11]. Bearing in mind quite low overall N content, it can be expected that the signal most likely originates from the methoxyl groups in lignin and suberin residues. Another signal at about 63 ppm, preferentially ascribed to oxygen bonded methylene groups, was found only in the spectra of the alcoholic extract (PRO5 and MET6).

The region of chemical shifts between 106 and 165 ppm reflects the content and structural composition of aromatic components. The relative integrated area in this region is, again, the lowest (10%) for the least polar fraction TMC1 while its value is comparable (39–47%) for other analyzed fractions. The aromaticity index f_a (i.e., the ratio of the integrated areas in 106–165 ppm and 0–165 ppm, respectively) is usually used as a more accurate quantitative parameter expressing sample aromaticity. As can be seen in Table 4, also this parameter confirms comparable aromaticity of all but the first extracted fraction. From the qualitative point of view, spectra of all these fractions with higher aromaticity (ACE3, PRO5, and MET6) include signals typical for lignin residues [67]: (a) A sharp and intensive signal at 115 ppm corresponds to coniferyl alcohol and the intensive signal at about 130 ppm to 4-hydroxycinnamyl alcohol. (b) The presence of sinapyl and coniferyl units is further revealed by the signals at 145 and 148 ppm, which are attributed to Ar–O–R and Ar–O–CH$_3$ structural moieties [68]. (c) Phenolic groups are manifested by a distinctive signal at 150 ppm [69].

The presence of carboxylic groups in the structure of the fraction is manifested in the ^{13}C NMR spectra by two bands in the range of chemical shifts 172–175 ppm. The relative signal of carbon in carboxylic groups increased gradually with increasing polarity of the extraction agent (in the range of 3–13%). Finally, the relative integrated area in the range of chemical shifts characteristic for carbonyl carbon (190–220 ppm) was comparably low for all the analyzed fractions.

3.6. Statistical Analysis

The specific structural and compositional parameters provided by the individual physicochemical and spectroscopic assays were further subjected to statistical analysis using the principal component analysis (PCA) method. The dimension of the 13 input variables was reduced by PCA into two principal components with eigenvalues higher than one. These two principal components composed 88.0% of the variability of the original data set, of which 61.1% falls on the first (PC1) and 26.9% on the second principal component (PC2), respectively. Visual representation of the results of PCA is provided in form of a two-dimensional factor plane of principal components PC1 and PC2 in Figure 3.

It is observed from the bi-plot that O/C atomic ratio had the highest positive loading on PC1 while the opposite trend was observed for relative hydrogen content and ICH$_2$/ICH$_3$ ratio. In the left-side quadrants of the loading bi-plot, there are projected parameters that indicate the presence of aliphatic structures with long carbon chains poor in O- and/or N-containing functional groups. On the other hand, on the right side of the loading bi-plot can be found projections of parameters that reflect the presence of heteroatom elements as well as the aromaticity of the sample.

The PCA bi-plot in Figure 3 shows that the PC1 component provides the clear separation of the non-polar organic fractions (samples TCM1 and EAC2, designed as Group I in Figure 3) from the other organic fractions and also from the original peat HA (samples ACE3 to MET6, and SBPHA, designed as Group II). Evidently, the group I fractions can be characterized by structural markers of aliphatic substances, whereas group II gathers structural and compositional parameters of the typical building-blocks for the humic substances.
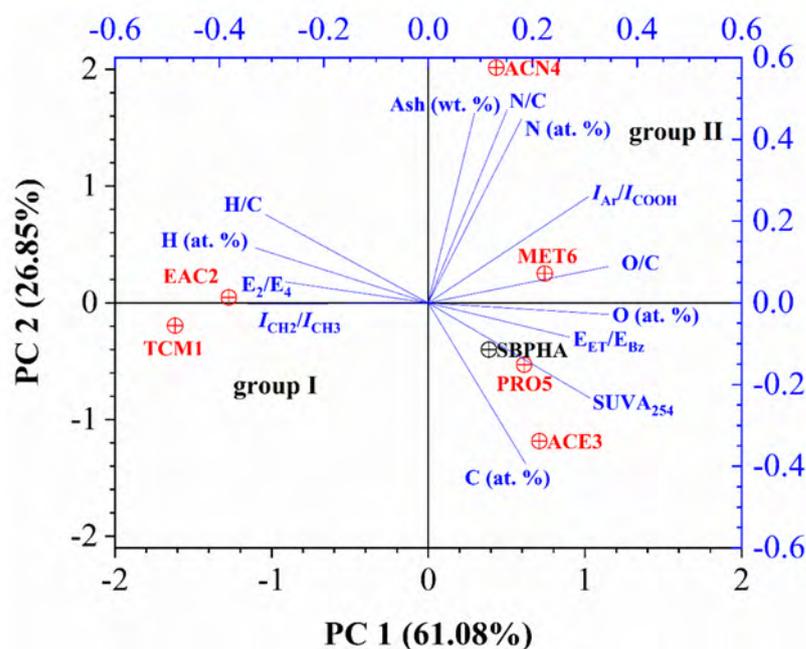
Figure 3. Projection of characterized organic fractions and original peat HA using PCA.

The second principal component (PC2) provides further separation of the polar organic fractions mainly according to their elemental composition. It can be seen that polar organic fractions PRO5 and MET6 are projected near to zero value of PC2 forming a cluster with the original humic material (SBPHA). On the other hand, the fraction extracted with acetonitrile (ACN4) is separated from the others due to its higher ash (wt. %) and nitrogen (at. %) content. This is in good agreement with the conclusion that this fraction is distinctive with its high content of polypeptide-like structures such as tyrosine-like structures and/or microbial activity by-products.

4. Conclusions

The results of our work support the current view that humic acids still represent a complex mixture of separable fractions with specific structural and physicochemical properties. For the analyzed peat-bog humic acid, it was confirmed that the individual fractions, isolated by the proposed polarity-resolved fractionation technique, are mutually different concerning their origin, molecular weight, aromaticity, and the content and composition of heteroatomic functional groups. In particular, the fractions extracted with the most apolar solvents (trichloromethane and ethyl acetate), as expected, show the structural features characteristic for basically lipidic compounds (low aromaticity, low oxygen, and nitrogen content, high CH_2/CH_3 ratio), while the other fractions are in general more aromatic and richer in polar (mainly oxygen-containing) groups. Interestingly, among these more polar fractions, the fraction extracted with acetonitrile stands at a unique position with its surprisingly lower aromaticity and higher content of protein-like structural motifs. Furthermore, the last two-alcohol extracted-fractions (PRO5 and MET6) also show some mutual structural features, mainly the higher content of carbohydrate residues (as confirmed by FTIR and NMR) and content of specific (V-type) fluorophores which are often associated with plant pigments residues in humic acids.

The experimental study presented in this paper hence represents a pilot demonstration of a simple but useful approach to a structural analysis of complex heterogeneous organic matrices such as humic substances. Nevertheless, a systematic follow-up study is still needed to evaluate the general usability and overall benefit of this experimental approach. In this pilot study, we used only one HA sample, which represents the single type of organic material that originated from a particular soil system with specific humification conditions. Therefore, to be able to critically evaluate experimental limitations of the approach and

to obtain structural information that could be generalized to a wider range of humics, it is essential to focus the follow-up work on a comparative study performed with humic substances differing in their types (fulvic and humic acids, humins) and origins (terrestrial soil, aquatic).

Moreover, also the methodology proposed here is still open to further modifications and improvements. Above all, solid residues remaining after the last extraction step should also be subjected to detail structural and compositional analysis to provide a conclusive description of the structural impacts of the extraction process. Furthermore, one of the general aims of the study was to contribute to refining the current notion of the supramolecular structure of humic substances. In this work, we focused on how this could be managed by reducing the level of the structural complexity of humic substances followed by a separate analysis of individual groups of molecular constituents. Nevertheless, for a more complex understanding of how these constituents are bound in the HA matrix, this analytic step should be supplemented with the "synthetic" perspective where the compositional and structural parameters of the obtained fractions were synthesized with respect to their relative contents and these reassembled characteristics were compared with those of the parental humic material.

Supplementary Materials: The following are available online at https://www.mdpi.com/2073-439 5/11/3/587/s1, Figure S1: ATR-FTIR and DRIFT spectrum of SBPHA, Figure S2: EEM spectrum of HA isolated from South Bohemian peat (SBPHA), Figure S3: Van Krevelen diagram of organic fractions and original SBPHA, Figure S4: Deconvolution of the overlapping region of ATR-FTIR spectra at 1800–1500 cm^{-1}, Figure S5: EEM spectral cut-outs showing secondary fluorescence maxima, Figure S6: Liquid-state ^{13}C NMR spectra of the studied organic fractions extracted from peat HA, Table S1: List of fundamental physicochemical properties of organic solvents used for extraction of organic fractions, Table S2: Summary of fluorescence domains characteristic of humic substances and/or dissolved organic matter.

Author Contributions: Investigation, methodology, writing—original draft, conceptualization, V.E. and P.S.; investigation, formal analysis, L.K., Š.S., L.D., and M.K.; writing—review and editing, supervision, M.P. All authors have read and agreed to the published version of the manuscript.

Institutional Review Board Statement: Not applicable.

Informed Consent Statement: Not applicable.

Data Availability Statement: All discussed and analyzed data is contained within the article or Supplementary Materials.

Conflicts of Interest: The authors declare that they have no known competing financial interests or personal relationships that could have appeared to influence the work reported in this paper.

References

1. Kleber, M.; Lehmann, J. Humic substances extracted by alkali are invalid proxies for the dynamics and functions of organic matter in terrestrial and aquatic ecosystems. *J. Environ. Qual.* **2019**, *48*, 207–216. [CrossRef] [PubMed]
2. Olk, D.C.; Bloom, P.R.; Perdue, E.M.; McKnight, D.M.; Chen, Y.; Farenhorst, A.; Senesi, N.; Chin, Y.P.; Schmitt-Kopplin, P.; Hertkorn, N.; et al. Environmental and agricultural relevance of humic fractions extracted by alkali from soils and natural waters. *J. Environ. Qual.* **2019**, *48*, 217–232. [CrossRef] [PubMed]
3. Myneni, S.C.B. Chemistry of Natural Organic Matter—The Next Step: Commentary on a humic substances debate. *J. Environ. Qual.* **2019**, *48*, 233–235. [CrossRef] [PubMed]
4. Hu, Y.; Zheng, Q.; Noll, L.; Zhang, S.; Wanek, W. Direct measurement of the in situ decomposition of microbial-derived soil organic matter. *Soil Biol. Biochem.* **2020**, *141*, 107660. [CrossRef]
5. Hayes, M.H.B. Solvent systems for the isolation of organic components from soils. *Soil Sci. Soc. Am. J.* **2006**, *70*, 986–994. [CrossRef]

6. Hildebrand, J.H.; Scott, R.L. *Regular Solutions*, 1st ed.; Prentice-Hall, Inc.: Englewood Cliffe, NJ, USA, 1962; p. 180.
7. Hansen, C.M. *Hansen Solubility Parameters: A User's Handbook*, 2nd ed.; CRC Press: Boca Raton, FL, USA, 2007; p. 544.
8. Senesi, N.; Testini, C.; Polemio, M. Chemical and spectroscopic characterization of soil organic matter fractions isolated by sequential extraction procedure. *J. Soil Sci.* **1983**, *34*, 801–813. [CrossRef]
9. Piccolo, A. Characteristic of soil humic extracts obtained by some organic and inorganic solvents and purified by HCl-HF treatment. *Soil Sci.* **1988**, *146*, 418–426. [CrossRef]
10. Fujitake, N.; Kusumato, A.; Tsukamato, M.; Kawahigashi, M.; Suzuki, T.; Otsuka, H. Properties of soil humic substances in fractions obtained by sequential extraction with pyrophosphate solutions at different pHs. I. Yield and particle size distribution. *Soil Sci. Plant Nutr.* **1998**, *44*, 253–260. [CrossRef]
11. Li, L.; Huang, W.; Peng, P.; Sheng, G.; Fu, J. Chemical and molecular heterogeneity of humic acids repetitively extracted from a peat. *Soil Sci. Soc. Am. J.* **2003**, *67*, 740–746. [CrossRef]
12. Olk, D.C. A Chemical fractionation for structure-function relations of soil organic matter in nutrient cycling. *Soil Sci. Soc. Am. J.* **2006**, *70*, 1013–1022. [CrossRef]
13. Shirshova, L.T.; Ghabbour, E.A.; Davies, G. Spectroscopic characterization of humic acid fractions isolated from soil using different extraction procedures. *Geoderma* **2006**, *133*, 204–216. [CrossRef]
14. Nebbioso, A.; Piccolo, A. Basis of a humeomics science: Chemical fractionation and molecular characterization of humic biosuprastructures. *Biomacromolecules* **2011**, *12*, 1187–1199. [CrossRef]
15. Vinci, G.; Mazzei, P.; Drosos, M.; Zaccone, C.; Piccolo, A. Molecular characterization of ombrotrophic peats by humeomics. *Chem. Biol. Technol. Agric.* **2020**, *7*, 18. [CrossRef]
16. Drosos, M.; Nebbioso, A.; Mazzei, P.; Vinci, G.; Spaccini, R.; Piccolo, A. A molecular zoom into soil Humeome by a direct sequential chemical fractionation of soil. *Sci. Total Environ.* **2017**, *586*, 807–816. [CrossRef]
17. Reichardt, C.; Welton, T. *Solvents and Solvent Effects in Organic Chemistry*, 4th ed.; WILEY-VCH: Weinheim, Germany, 2010; p. 718.
18. Lakowicz, J.R. *Principles of Fluorescence Spectroscopy*, 3rd ed.; Springer: Baltimore, MD, USA, 2006; p. 954.
19. Novák, F.; Šestauberová, M.; Hrabal, R. Structural features of lignohumic acids. *J. Mol. Struct.* **2015**, *1093*, 179–185. [CrossRef]
20. Thomas, J.D.R. Chemistry of peat bitumen: Fractionation and infra-red studies. *J. Appl. Chem.* **2007**, *12*, 289–294. [CrossRef]
21. Doskočil, L.; Enev, V.; Pekař, M.; Wasserbauer, J. The spectrometric characterization of lipids extracted from lignite samples from various coal basins. *Org. Geochem.* **2016**, *95*, 34–40. [CrossRef]
22. Martins, T.; Saab, S.D.C.; Milori, D.M.B.P.; Brinatti, A.M.; Rosa, J.A.; Cassaro, F.A.M.; Pires, L.F. Soil organic matter humification under different tillage managements evaluated by Laser Induced Fluorescence (LIF) and C/N ratio. *Soil Tillage Res.* **2011**, *111*, 231–235. [CrossRef]
23. Ma, X.; Green, S.A. Fractionation and spectroscopic properties of fulvic acid and its extract. *Chemosphere* **2008**, *72*, 1425–1434. [CrossRef] [PubMed]
24. Korshin, G.V.; Li, C.-W.; Benjamin, M.M. Monitoring the properties of natural organic matter through UV spectroscopy: A consistent theory. *Water Res.* **1997**, *31*, 1787–1795. [CrossRef]
25. del Vecchio, R.; Blough, N.V. On the origin of the optical properties of humic substances. *Environ. Sci. Technol.* **2004**, *38*, 3885–3891. [CrossRef] [PubMed]
26. Baigorri, R.; Fuentes, M.; González-Gaitano, G.; García-Mina, J.M. Analysis of molecular aggregation in humic substances in solution. *Colloids Surf. A Physicochem. Eng. Asp.* **2007**, *302*, 301–306. [CrossRef]
27. Song, J.; Jin, X.; Wang, X.C.; Jin, P. Preferential binding properties of carboxyl and hydroxyl groups with aluminium salts for humic acid removal. *Chemosphere* **2019**, *234*, 478–487. [CrossRef]
28. Boguta, P.; Sokołowska, Z. Zinc binding to fulvic acids: Assessing the impact of pH, metal concentrations and chemical properties of fulvic acids on the mechanism and stability of formed soluble complexes. *Molecules* **2020**, *25*, 1297. [CrossRef]
29. Chen, Y.; Senesi, N.; Schnitzer, M. Information provided on humic substances by E4/E6 ratios. *Soil Sci. Soc. Am. J.* **1977**, *41*, 352–358. [CrossRef]
30. Li, P.; Hur, J. Utilization of UV-Vis spectroscopy and related data analyses for dissolved organic matter (DOM) studies: A review. *Crit. Rev. Environ. Sci. Technol.* **2017**, *47*, 131–154. [CrossRef]
31. Zykova, M.V.; Schepetkin, I.A.; Belousov, M.V.; Krivoshchekov, S.V.; Logvinova, L.A.; Bratishko, K.A.; Yusubov, M.S.; Romanenko, S.V.; Quinn, M.T. Physicochemical characterization and antioxidant activity of humic acids isolated from peat of various origins. *Molecules* **2018**, *23*, 753. [CrossRef]
32. Rodríguez, F.J.; Schlenger, P.; García-Valverde, M. Monitoring changes in the structure and properties of humic substances following ozonation using UV-Vis, FTIR and 1H NMR techniques. *Sci. Total Environ.* **2016**, *541*, 623–637. [CrossRef]
33. Chen, J.; Gu, B.; LeBooeuf, E.; Pan, H.; Dai, S. Spectroscopic characterization of the structural and functional properties of natural organic matter fractions. *Chemosphere* **2002**, *48*, 59–68. [CrossRef]
34. Maeng, S.K.; Timmes, T.C.; Kim, H.-C. Characterization of EfOM fraction responsible for short-term fouling in ultrafiltration. *Sep. Sci. Technol.* **2015**, *50*, 2697–2707. [CrossRef]
35. Tinoco, P.; Almendros, G.; González-Vila, F.J.; Sanz, J.; González-Pérez, J.A. Revisiting molecular characteristics responsive for the aromaticity of soil humic acids. *J. Soils Sediments* **2015**, *15*, 781–791. [CrossRef]
36. Yakimenko, O.; Khundzhua, D.; Izosimov, A.; Yuzhakov, V.; Patsaeva, S. Source indicator of commercial humic products: UV-Vis and fluorescence proxies. *J. Soils Sediments* **2018**, *18*, 1279–1291. [CrossRef]

37. Kumada, K.; Sato, O. Characteristics of the green fraction of P type humic acid. *J. Soil Sci. Plant Nutr.* **1980**, *26*, 309–316. [CrossRef]

38. Davis, W.M.; Erickson, C.L.; Johnston, C.T.; Delfino, J.J.; Porter, J.E. Quantitative fourier transform infrared spectroscopic investigation humic substance functional group composition. *Chemosphere* **1999**, *38*, 2913–2928. [CrossRef]

39. Senesi, N.; Sipos, S. Molecular weight distribution, analytical and spectroscopic characterization of humic fractions sequentially isolated by organic solvents from a brown coal humic acid. *Org. Geochem.* **1985**, *8*, 157–162. [CrossRef]

40. Stuart, B.H. *Infrared Spectroscopy: Fundamentals and Applications*, 1st ed.; John Wiley & Sons: Hoboken, NJ, USA, 2004; p. 244.

41. Baes, A.U.; Bloom, P.R. Diffuse reflectance and transmission fourier transform infrared (DRIFT) spectroscopy of humic and fulvic acids. *Soil Sci. Soc. Am. J.* **1989**, *53*, 695–700. [CrossRef]

42. Terkhi, M.C.; Taleb, F.; Gossart, P.; Semmoud, A.; Addou, A. Fourier transform infrared study of mercury interaction with carboxyl groups in humic acids. *J. Photochem. Photobiol. A* **2008**, *198*, 205–214. [CrossRef]

43. Tatzber, M.; Stemmer, M.; Spiegel, H.; Katzlberger, C.; Haberhauer, G.; Mentler, A.; Gerzabek, M.H. FTIR-spectroscopic characterization of humic acids and humin fractions obtained by advanced NaOH, $Na_4P_2O_7$, and Na_2CO_3 extraction procedures. *J. Plant Nutr. Soil Sci.* **2007**, *170*, 522–529. [CrossRef]

44. Hanc, A.; Enev, V.; Hrebeckova, T.; Klucakova, M.; Pekar, M. Characterization of humic acids in a continuous-feeding vermicomposting system with horse manure. *Waste Manag.* **2019**, *99*. [CrossRef] [PubMed]

45. Senesi, N.; Miano, T.M.; Provenzano, M.R.; Brunetti, G. Characterization, differentiation, and classification of humic substances by fluorescence spectroscopy. *Soil Sci.* **1991**, *152*, 259–271. [CrossRef]

46. Enev, V.; Pospíšilová, Ľ.; Klučáková, M.; Liptaj, T.; Doskočil, L. Spectral characterization of selected humic substances. *Soil Water Res.* **2014**, *9*, 9–17. [CrossRef]

47. Stylianou, S.K.; Katsoyiannis, I.A.; Ernst, M.; Zouboulis, A.I. Impact of O_3 or O_3/H_2O_2 treatment via a membrane contacting system on the composition and characteristics of the natural organic matter of surface waters. *Environ. Sci. Pollut. Res.* **2018**, *25*, 12246–12255. [CrossRef] [PubMed]

48. Gao, J.-F.; Dou, S.; Wang, Z.-G. Structural analysis of humic acid in soil at different corn straw returning modes through fluorescence spectroscopy and infrared spectroscopy. *Int. J. Anal. Chem.* **2019**, *2019*. [CrossRef]

49. Sierra, M.M.D.; Giovanela, M.; Parlanti, E.; Soriano-Sierra, E.J. Fluorescence fingerprint of fulvic and humic acids from varied origins as viewed by single-scan and excitation/emission matrix techniques. *Chemosphere* **2005**, *58*, 715–733. [CrossRef] [PubMed]

50. Liu, S.; Benedetti, M.F.; Han, W.; Korshin, G.V. Comparison of the properties of standard soil and aquatic fulvic and humic acids based on the data of differential absorbance and fluorescence spectroscopy. *Chemosphere* **2020**, *261*, 128189. [CrossRef]

51. Alberts, J.J.; Takács, M. Total luminescence spectra of IHSS standard and reference fulvic acids, humic acids and natural organic matter: Comparison of aquatic and terrestrial source terms. *Org. Geochem.* **2004**, *35*, 243–256. [CrossRef]

52. Rodríguez, F.J.; Schlenger, P.; García-Valverde, M. A comprehensive structural evaluation of humic substances using several fluorescence techniques before and after ozonation. Part I: Structural characterization of humic substances. *Sci. Total Environ.* **2014**, *476–477*, 718–730. [CrossRef]

53. Doskočil, L.; Burdíková-Szewieczková, J.; Enev, V.; Kalina, L.; Wasserbauer, J. Spectral characterization and comparison of humic acids isolated from some European lignites. *Fuel* **2018**, *213*, 123–132. [CrossRef]

54. Fellman, J.B.; Hood, E.; Spencer, R.G.M. Fluorescence spectroscopy opens new windows into dissolved organic matter dynamics in freshwater ecosystems: A review. *Limnol. Oceanogr.* **2010**, *55*, 2452–2462. [CrossRef]

55. Yang, L.; Hur, J.; Zhuang, W. Occurrence and behaviors of fluorescence EEM-PARAFAC components in drinking water and wastewater treatment systems and their applications: A review. *Environ. Sci. Pollut. Res.* **2015**, *22*, 6500–6510. [CrossRef]

56. Yu, M.-D.; Xi, B.-D.; Zhu, Z.-Q.; Zhang, L.; Yang, C.; Geng, C.-M.; He, X.-S. Fate and removal of aromatic organic matter upon a combined leachate treatment process. *Chem. Eng. J.* **2020**, *401*, 126157. [CrossRef]

57. Zhou, Y.; Martin, P.; Müller, M. Composition and cycling of dissolved organic matter from tropical peatlands of coastal Sarawak, Borneo, revealed by fluorescence spectroscopy and parallel factor analysis. *Biogeosciences* **2019**, *16*, 2733–2749. [CrossRef]

58. Chen, W.; Westerhoff, P.; Leenheer, J.A.; Booksh, K. Fluorescence excitation-emission matrix regional integration to quantify spectra for dissolved organic matter. *Environ. Sci. Technol.* **2003**, *37*, 5701–5710. [CrossRef]

59. Sun, J.; Guo, L.; Li, Q.; Zhao, Y.; Gao, M.; She, Z.; Jin, C. Three-dimensional fluorescence excitation-emission matrix (EEM) spectroscopy with regional integration analysis for assessing waste sludge hydrolysis at different pretreated temperatures. *Environ. Sci. Pollut. Res.* **2016**, *23*, 24061–24067. [CrossRef] [PubMed]

60. Birdwell, J.E.; Engel, A.S. Characterization of dissolved organic matter in cave and spring waters using UV-Vis absorbance and fluorescence spectroscopy. *Org. Geochem.* **2010**, *41*, 270–280. [CrossRef]

61. Cao, J.; Jiang, J. Reducing capacities in continuously released low molecular weight fractions from bulk humic acids. *J. Environ. Manag.* **2019**, *244*, 172–179. [CrossRef]

62. Coble, P.G.; Lead, J.; Baker, A.; Reynolds, D.M.; Spencer, R.G.M. *Aquatic Organic Matter Fluorescence*, 1st ed.; Cambridge University Press: New York, NY, USA, 2014; p. 418.

63. McKnight, D.M.; Boyer, E.W.; Westerhoff, P.K.; Doran, P.T.; Kulbe, T.; Andersen, D.T. Spectrofluorometric characterization of dissolved organic matter for indication of precursor organic material and aromaticity. *Limnol. Oceanogr.* **2001**, *46*, 38–48. [CrossRef]

64. Boyle, E.S.; Guerriero, N.; Thiallet, A.; del Vecchio, R.; Blough, N.V. Optical properties of humic substances and CDOM: Relation to structure. *Environ. Sci. Technol.* **2009**, *43*, 2262–2268. [CrossRef] [PubMed]

65. Boguta, P.; D'Orazio, V.; Sokołowska, Z.; Senesi, N. Effects of selected chemical and physicochemical properties of humic acids from peat soils on their interaction mechanisms with copper ions at various pHs. *J. Geochem. Explor.* **2016**, *168*, 119–126. [CrossRef]

66. Conte, P.; Piccolo, A.; van Lagen, B.; Buurman, P.; de Jager, P.A. Quantitative differences in evaluating soil humic substances by liquid- and solid-state ^{13}C-NMR spectroscopy. *Geoderma* **1997**, *80*, 339–352. [CrossRef]

67. Khatami, S.; Deng, Y.; Tien, M.; Hatcher, P.G. Formation of water-soluble organic matter through fungal degradation of lignin. *Org. Geochem.* **2019**, *135*, 64–70. [CrossRef]

68. Hatcher, P.G.; Waggoner, D.; Chen, H. Evidence for the existence of humic acids in peat soils based on solid-state ^{13}C NMR. *J. Environ. Qual.* **2019**, *48*, 1571–1577. [CrossRef]

69. Schnitzer, M. Soil organic matter—The next 75 years. *Soil Sci.* **1991**, *151*, 41–58. [CrossRef]

Appendix 9

Smilkova, M., Smilek, J., Kalina, M., Klucakova, M., Pekar, M., and Sedlacek, P. A simple technique for assessing the cuticular diffusion of humic acid biostimulants. *Plant Methods* **2019**, 15, 83.

Plant Methods

METHODOLOGY

A simple technique for assessing the cuticular diffusion of humic acid biostimulants

Marcela Smilkova[1], Jiri Smilek[2], Michal Kalina[2], Martina Klucakova[1], Miloslav Pekar[1] and Petr Sedlacek[1*]

Abstract

Background: Experimental determination of the extent and rate of transport of liquid humates supplied to plants is critical in testing physiological effects of such biostimulants which are often supplied as foliar sprays. Therefore, an original experimental method for the qualitative investigation and quantitative description of the penetration of humates through plant cuticles is proposed, tested, and evaluated.

Results: The proposed method involves the isolation of model plant leaf cuticles and the subsequent in vitro evaluation of cuticular humate transport. The employed novel methodology is based on a simple diffusion couple arrangement involving continuous spectrophotometric determination of the amount of penetrated humate in a hydrogel diffusion medium. *Prunus laurocerasus* leaf cuticles were isolated by chemical and enzymatic treatment and the rate of cuticular penetration of a commercial humate (lignohumate) was estimated over time in quantitative and qualitative terms. Different rates of lignohumate transport were determined for abaxial and adaxial leaf cuticles also in relation to the different cuticular extraction methods tested.

Conclusions: The proposed methodology represents a simple and cheap experimental tool for the study on the trans-cuticular penetration of humic-based biostimulants.

Keywords: Diffusion, Hydrogel, *Prunus laurocerasus*, Liquid fertilization, Humic substances, Plant cuticle

Background

Foliar application of fertilizers and biostimulants has become a popular method in the field of agronomy and the plant nutrition since its first use in the early twentieth century. Nowadays, foliar uptake of nutrients widely complements standard root fertilizer treatments [1, 2]. Most aerial plant organs (leaves, stem, etc.) are long-known to be able to take up nutrients from sprays [3, 4]. Transcuticular penetration into leaf tissues and sorption on the leaf surface plays a key role in the foliar application of nutrients [5–7], surfactants [8, 9] and different types of pesticides [10–15].

Bidirectional transport of diverse substances in and out of plants is controlled primarily by the plant cuticle [16], a membrane which covers the aerial plant parts and forms the natural interface between plant organs and a surrounding environment [17]. From a chemical point of view, it can be considered as a heterogeneous composite material which is formed by lipophilic components such as waxes, water insoluble polymers cutin and/or cutan and phenolic compounds like flavonoids, mixed together with hydrophilic polar compounds such as polysaccharides [18].

The cuticle plays its biological role principally as a barrier to control the movement of gases, water and solutes and to impart pathogen resistance [17, 19–21]. Furthermore, it protects a plant against abiotic factors such as rain, frost and ultraviolet light [21, 22], and also against adverse biotic impacts of insects, pests, mycosis, etc. [20, 23]. Naturally, as the correct functioning

*Correspondence: sedlacek-p@fch.vut.cz
[1] Institute of Physical and Applied Chemistry, Brno University of Technology, Faculty of Chemistry, Purkynova 464/118, 612 00 Brno, Czech Republic
Full list of author information is available at the end of the article

Smilkova *et al. Plant Methods*   (2019) 15:83

Page 2 of 11

of plant cuticles is crucial for the well-balanced uptake of nutrients, minerals, adjuvants, or for plant growth preparation, cuticle-penetration experiments as well as laboratory studies of the structural physico-chemical properties of cuticles are an essential part of plant-nutrition research.

For more than 50 years, scientists have continuously been focusing their experiments on the penetration of active compounds through plant cuticles, or on their adsorption on the cuticle surface [3, 24]. For the purpose of the experimental determination of the extent and rate of foliar absorption of a nutrient, several techniques directly involving intact leaves were tested, e.g. dipping, brushing, sticking, spraying, or the droplet method [3]. However, attention has gradually been paid also to experiments performed with cuticles in an isolated form. The first successful attempts at cuticle isolation were made by Orgell, who developed a method based on the treatment of leaves by pectinase [25]. A chemical alternative to this enzymatic method is isolating cuticles with zinc chloride as introduced by Holloway and Baker [26] and further utilized by Solel and Edgington [10, 27, 28]. Various experimental settings have been used for cuticular permeability trials, such as a sole transpiration chamber [29], a side-by-side transport chamber, in which the cuticle is located between two compartments filled with donor and receptor solution [24], or a tube-in-tube setup, where the cuticle is affixed on the opening of small tube filled with deionized water and submerged in the larger tube with a donor solution [30].

Either in experiments performed with intact plant organs or with those utilizing isolated plant cuticles, another crucial step in the development of a particular methodology for studying foliar absorption is the use of an analytical method for the quantification of the cuticle-permeating compound. Foliar uptake of inorganic compounds has been often studied by means of radioactive isotope methods, where different radioactive isotopes of elements are used e.g. ^{14}C [30, 31], ^{32}P [32–35], ^{42}K or ^{45}Ca [36], or ^{86}Rb, ^{45}Ca, ^{36}Cl and ^{35}S [37]. Radionuclide assays have also been utilized successfully in foliar absorption studies of organic compounds such as urea [30] and atrazine [11]. Among other methods for studying the foliar uptake of organic molecules, HPLC was used to determine the quantity of the organic dye Congo Red and fungicides on the leaf surface [38]. Another experimental approach is based on tracking the penetrating compounds indirectly by observing their effects. This approach was used, for example, by Solel and Edgington [10] or, more recently, by Zelena and Veverka [13], who studied the rate of the transcuticular movement of fungicides by measuring the propagation of inhibitory zones in agar gel fed with a fungus sensitive to the tested

fungicide. The fungicide was always applied on top of the cuticle, placed in the center of the agar-filled Petri dish.

Humic substances are complex organic mixtures that fulfil a range of important functions in ecosystems and that are essential for their proper functioning. They represent an essential fraction of the natural organic matter of soils, peats, and young coals. In a dissolved form, they can also be found in aquatic systems such as rivers and lakes. A growing understanding of the positive effects of the presence of humic substances in their natural habitats has motivated the preparation of commercial products based on isolated natural or artificially synthesized humic substances. Positive impacts of the utilization of humic-based soil amendments on the chemical [39, 40], physical [41, 42], and microbial [43] fitness of soils have been thoroughly documented. Apart from the application of humic-based materials into soil, the foliar application of soluble humates has gradually become a popular way of application as well. This was initiated by numerous reports on the biostimulant effects of humates, namely on the effect on plant growth [44, 45] and nutrient uptake [46], hormone-like [47, 48] and enzyme-promoting effects [49, 50], as well as some effects enhancing photosynthesis and seed-germination [51, 52]. In particular, in greenhouse experiments using cuttings and young olive plants, Fernandez-Escobar found foliar-applied humic substances extracted from leonardite to have an effect on olive growth [53]; the tested leonardite extracts stimulated shoot growth and promoted the accumulation of elements in leaves. Maibodi et al. suggested that foliar application of humic substances might be of benefit with respect to enhancing nutrient uptake, root development, and drought resistance in ryegrass [54]. In addition, Bettoni [55] showed that a combination of foliar and immersion methods represented the most effective way of applying humic substances originating from leonardite, as far as the tested onion bulb yield and quality was concerned.

However, there is raising debate concerning the generally accepted beneficial effects of commercial humates in agriculture. Olk et al. [56] and Rose et al. [57] reviewed information on the benefits of using humic preparations in agriculture and stressed still ambiguous results. Similarly, Lyons and Genc [58] has pointed out that there is a surprising lack of evidence regarding the effectiveness of the on-farm application of humates, the findings concerning their beneficial effects being inconsistent. Among other recommendations, these authors call for a comprehensive physico-chemical characterization of humates and for a careful assessment of the mechanism of their foliar action. Thereby, the experimental determination of the rate of absorption and transport of humate solutions applied to plants also as foliar sprays

Smilkova *et al. Plant Methods*   (2019) 15:83

Page 3 of 11

is critical as preliminary step for assessing their biological effects. Recently, some attempts have been made in describing the root pathway of the humate absorption. For instance, Kulikova studied the uptake of leonardite humic substances by plant root and its transport and spatial distribution among the plant tissues using microautoradiography [59]. Nevertheless, as yet, no experimental procedure has been proposed for a systematic assay of the transcuticular uptake of humates. The aim of this paper is hence to introduce an original in vitro technique as a simple experimental option for this task. The proposed method enables the investigation and quantitative description of the penetration of humates through the plant cuticle via spectrophotometric monitoring of the diffusion of humates through an isolated plant cuticle fixed between a donor and an acceptor agarose hydrogels forming the common diffusion couple arrangement. The basic design of the method follows on from our previous work [60, 61]. The usability of the technique was tested on artificial lignohumate as a model commercial product and on cuticles obtained by enzymatic and chemical means of isolation.

Materials and methods

Isolation and characterization of cuticles

Leaf cuticles were isolated by two different methods (chemical and enzymatic) as described previously [10, 25]. In both cases, plant cuticles were isolated from *Prunus laurocerasus* (see "Results" and "Discussion"). Firstly, undamaged, young, fully-expanded leaves were immersed in distilled water. For the every plant leaf, the leaf blade (the lamina) was carefully cut off by scalpel from the other leaf parts (veins, petiole). In the case of enzymatic isolation, the lamina was then immersed into the isolation solution consisting of citric buffer (0.1 M and pH 3.5), supplemented with 2.5 wt% of pectinase from *Aspergillus niger* (>1 units/mg, Sigma-Aldrich), 2.5 wt% of cellulase from *Trichoderma logibrachiatum* (>1 units/mg, Sigma-Aldrich) and 0.25 wt% of sodium azide (p.a., Sigma-Aldrich). After 6 weeks, the leaf tissue, including isolated cuticles, was placed in distilled water and degraded mesophyll was gently removed by brushing. The chemical isolation procedure differed only in the composition of the isolation solution, i.e. 60 wt% zinc chloride (≥ 97%, Sigma-Aldrich) dissolved in concentrated hydrochloric acid (35%, Penta), and the shorter time duration of the chemical treatment (3 days).

Plant cuticles isolated by both the above mentioned methods were characterized by optical microscopy (Olympus IX71, objective Olympus PLN, magnification 20×, numerical aperture 0.40), by which differences in abaxial (stomatous) and adaxial (astomatous) cuticles were compared and the average radius of stomata was

determined (for the optical microscope images of the cuticles, see Fig. 1). Optical microscopy was also used in order to eliminate physically damaged cuticles. The morphology of isolated plant cuticles, especially average cuticle thickness and roughness, was determined by mechanical profilometer (DEKTA kXT, Bruker). VISION 64 was used as the control software and the pressure value of the stylus was set at 3 mg.

Preparation of hydrogels

All hydrogels used in this work were prepared via the thermoreversible gelation of agarose (< 10% moisture content, Sigma-Aldrich). These hydrogels acted as supporting matrix in which diffusion experiments on the active compound were performed. Lignohumate A was kindly provided by the Amagro (Prague, Czech Republic) and used as model active compound. It represents a commercial mixture of potassium humates and fulvates prepared by hydrolytic-oxidative conversion of technical lignosulfonates under strictly controlled conditions [62, 63]. The method of preparation of hydrogels is described in detail in our previous studies [60, 64]. Donor hydrogels containing 1 wt% agarose with the addition of 1 wt% potassium lignohumate (Lignohumate A) dissolved in distillated water and acceptor hydrogels consisting of only 1 wt% agarose were prepared in PMMA cuvettes (dimensions 10 × 10 × 45 mm). The thermoreversible gelation of agarose took place at ambient temperature and 100% relative humidity for at least 45 min. After the gelation process was completed, excess gel mass above the cuvette edge was cut off by scalpel for all prepared hydrogels. This provided a flat gel surface that allows even contact with the cuticle and with the second hydrogel in the diffusion couple arrangement (see below). This arrangement was obtained in the way that every single isolated plant cuticle was carefully placed between the donor and acceptor hydrogels and the contact area of both cuvettes was isolated from surroundings by parafilm to prevent unfavorable drying.

Diffusion experiments

Both abaxial and adaxial cuticles isolated by the two different isolation methods (chemical and enzymatic) were subjected to diffusion experiments. As can be seen in Fig. 2, the diffusion couple was formed by two agarose hydrogels—a hydrogel with an homogenously dispersed humate inside (i.e. the donor hydrogel) and a hydrogel with no initial content of the humate (i.e. the acceptor hydrogel)—and the isolated cuticle separating the two gels. As the humate can move freely inside the agarose matrix, it penetrates the cuticle and flows across the concentration gradient from the donor to the acceptor gel. These diffusion experiments were performed with 10 repetitions for abaxial and adaxial cuticles, respectively.

Smilkova *et al. Plant Methods* (2019) 15:83

Page 4 of 11
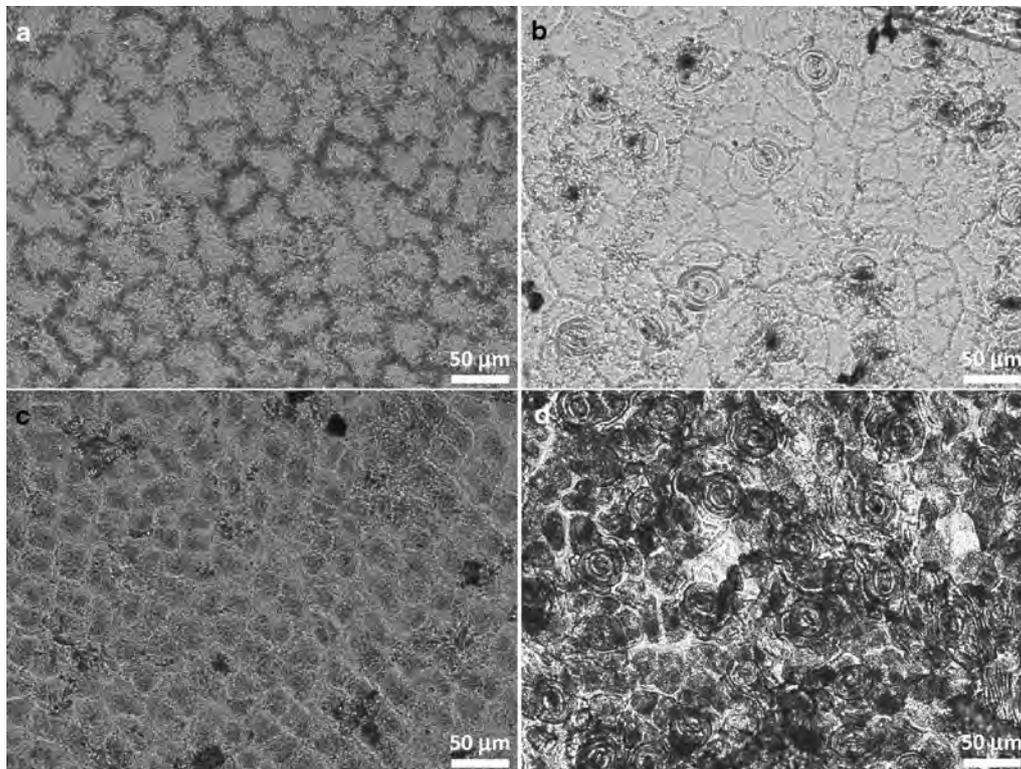
Fig. 1 Optical micrographs of the isolated cuticles. Adaxial (**a**, **c**) and abaxial (**b**, **d**) cuticles isolated by chemical (**a**, **b**) and enzymatical (**c**, **d**) methods, respectively
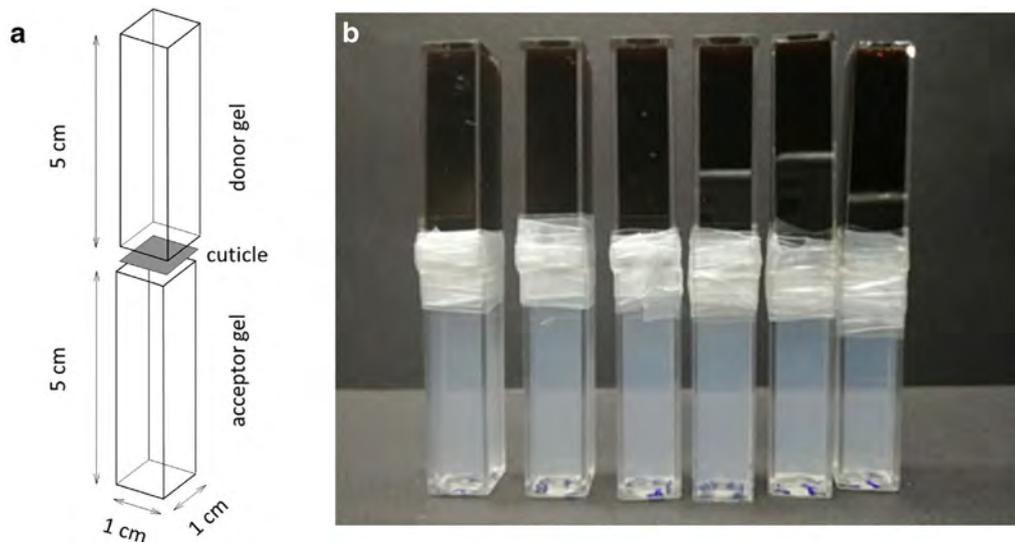
Fig. 2 Schematic drawing of the diffusion couple arrangement (individual parts are shifted for clarity) (**a**). Picture of the diffusion couple at the beginning of the experiment (**b**)

During the diffusion experiments, all the diffusion couples were placed in a closed container above water level (to maintain constant humidity of the surroundings). Experimental conditions—in particular, relative humidity (100%) and temperature (25 °C)—were held constant during the whole experimental period.

Smilkova *et al. Plant Methods*   (2019) 15:83

Page 5 of 11

The transport of lignohumate through the plant cuticle into the acceptor hydrogel was measured by a UV–VIS spectrophotometry (Varian Cary 50). At selected time intervals, the cuvettes were taken out and UV–VIS spectra of lignohumate in acceptor hydrogels were collected at distances from the hydrogel-cuticle interface ranging from 3 to 40 mm (with 1 or 2 mm increment in distance depending on the actual rate of the color change). The measurement of UV–VIS absorbance at different distances from the interface was performed by means of a special in-house made accessory providing controlled fine vertical movement of the cuvette in the spectrophotometer (see [65] for more detail and picture of the used cuvette holder).

Results

Isolation and characterization of cuticles

Two methods of cuticle isolation were tested. The main advantage of the enzymatic method is the use of less harmful isolation agents. The procedure is, therefore, more user-friendly and suitable for routine laboratory use. Furthermore, the presence of any structural artifacts arising from chemical damage to the cuticle is less likely than in the case of more drastic chemical treatment in hydrochloric acid. On the other hand, the enzymatic method is significantly more time-consuming in comparison with chemical isolation. In our study, however, both techniques resulted in the isolation of cuticles which were strong and easy to manipulate. Optical microscopy was used in order to exclude mechanically damaged cuticles, to distinguish between abaxial and adaxial cuticles, and to sort them for use in subsequent diffusion experiments.

Furthermore, microscopical observation of the cuticles also revealed some interesting differences in the efficiency of the two isolation methods. Apparently, chemical treatment of the leaves led to the more efficient removal of cell debris as compared to the enzymatic procedure (see the black spots on the micrographs shown in Fig. 1). This finding corresponds well with general differences in cuticle thickness for the two isolation methods as revealed by profilometry, i.e., it was found that the thickness was always greater for enzymatically isolated cuticles (see Table 1). Anyway, both types of cuticles (i.e. chemically and enzymatically isolated ones) were included in the next step of the testing of the proposed methodology, i.e. in the diffusion couple experiments with agarose hydrogels.

Diffusion of lignohumate through the cuticles

The main experimental core of the proposed diffusion methodology is based on our previous studies [60, 61, 65, 66]. Generally, as far as the experimental study of molecular diffusion is concerned, hydrogels represent a highly

Table 1 Basic morphological characteristics of the isolated cuticles

	Avg. cuticle thickness (µm)	Avg. dimensions of stomata (µm)
Chemically isolated		
Abaxial	4.4 ± 1.2	14×7
Adaxial	5.5 ± 0.3	–
Enzymatically isolated		
Abaxial	6.7 ± 2.0	12×5
Adaxial	9.2 ± 0.9	–

beneficial material form. In the gel phase, the diffusion flow of a solute is not disturbed by thermal or mechanical convection such as in liquid solution. Furthermore, a hydrogel sample of precisely defined shape and dimensions can be prepared, which enables correct description of the diffusion flow by quantitative parameters such as diffusion coefficients. In the current experiments, a simple diffusion couple arrangement was used [24, 67].

In order to evaluate this technique, the diffusion of lignohumate—a model artificial humate—was studied using the above-described experimental arrangement. The composition, structure, and physico-chemical properties of lignohumate are discussed in detail elsewhere [63, 68], as well as its biological effects [69, 70]. For our purposes, the main practical benefits of using lignohumate as a model humic biostimulant are its very high water solubility, low molecular size, and reproducible means of preparation, the latter resulting in a stable and standardized structure with standardized properties.

In Fig. 3, the movement of the dark-brown-colored lignohumate through the cuticle and its subsequent diffusion into the optically transparent agarose gel can be observed visually. It is evident how the local concentration of lignohumate and its depth of penetration increases with time and that the adaxial and abaxial cuticles show large differences in their barrier properties. As expected, the rate of diffusion is higher in the case of abaxial cuticles. The explanation is straightforward; isolation of stomateous cuticles results in membranes with freely permeably holes of several microns in size (guard cells which protect stomata against penetration are lost during the isolation). The penetration of lignohumate through these membranes is therefore controlled by the size and density of the holes and by the rate of free diffusion of lignohumate in solution rather than by the barrier properties of the neighbouring lipophilic cuticle area.

In addition, visual evaluation of the concentration of lignohumate in acceptor gels indicates a higher diffusion rate in the case of chemically isolated abaxial cuticles as compared to enzymatically isolated ones. For the adaxial cuticles, the differences were less pronounced. This can
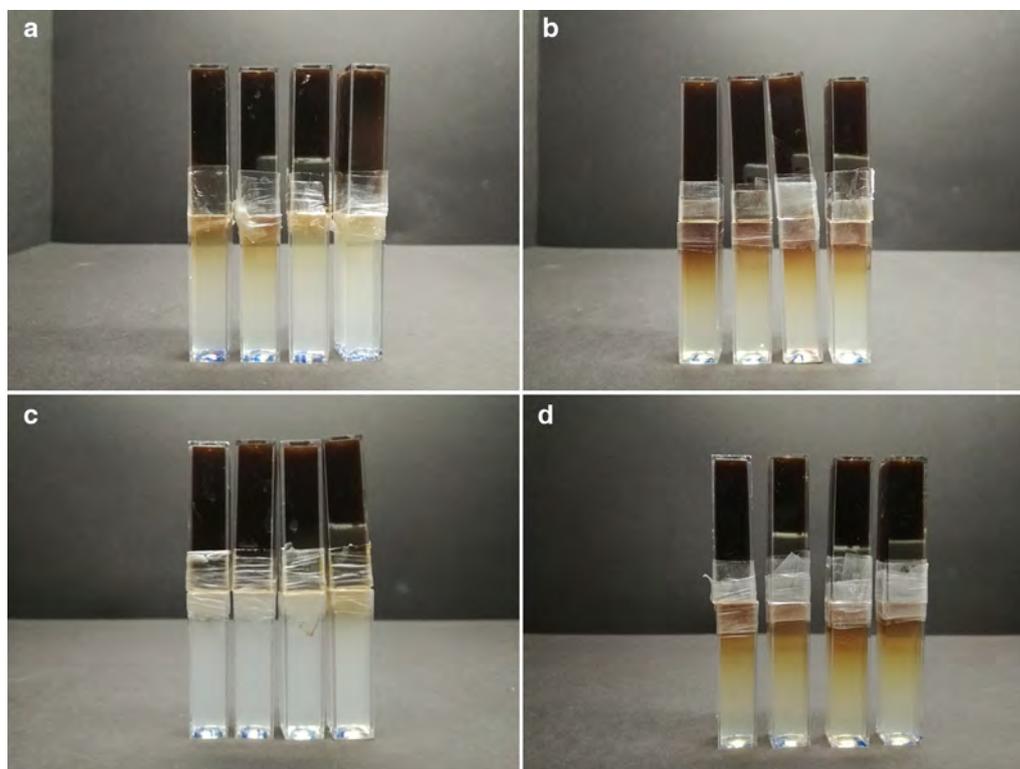
Fig. 3 Diffusion couples after 7 days of experiment. Comparison of diffusion progress for adaxial (**a**, **c**) and abaxial (**b**, **d**) cuticles and for chemical (**a**, **b**) and enzymatical (**c**, **d**) methods of cuticle isolation

be explained by the already mentioned outcomes of the structural analysis of the cuticles. Enzymatically isolated cuticles are thicker and mainly exhibit higher levels of contamination by debris from the leaf. It is likely that in the case of enzymatically isolated cuticles stomata are partially blocked by leaf debris and, consequently, contribute less effectively to the transport of lignohumate.

Quantitative description of the transcuticular transfer of lignohumate

Figure 4 shows example of the set of UV–VIS spectra collected at various positions in acceptor hydrogel that illustrates uneven distribution of lignohumate in the gel. It should be noted that each recorded spectrum (shown as the apparent absorbance vs. wavelength) is actually formed by the combination of two separate contributions—the turbidity of the hydrogel caused by light scattering on the solid agarose matrix and light absorption by the dissolved humate in the aqueous phase of the gel. While the former contribution was homogenous and constant for all the measured gels (i.e. it changed neither with time nor with location in the gel), the latter depended on the actual concentration of the humate at a particular time and at a particular point in the gel. In
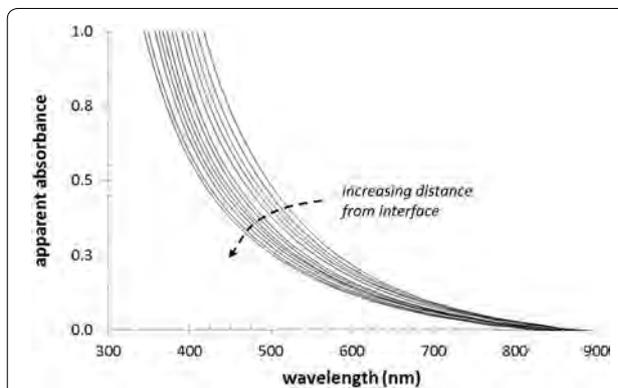
Fig. 4 UV–VIS spectra measured at different positions in the acceptor gel (adaxial chemically isolated cuticle, after 96 h). Spectra were taken in 2 mm increments of distance from the cuticle

order to calculate the concentration of lignohumate from the respective UV–VIS spectrum, we also measured the spectra of reference samples of agarose gels in which the exact concentration of homogenously distributed lignohumate was achieved by dispersion of a known amount of lignohumate in the agarose solution before its gelation. It is also evident from Fig. 4 that lignohumate provides a

continuous absorption spectrum covering a wide range of wavelengths instead of any separate absorption peak. This is a spectroscopic feature typical of humic substances and is the result of their complex structural nature. Therefore, we used a multiple calibration approach in which the concentration of the lignohumate was determined as an average of the values calculated for three different wavelengths (600, 700 and 800 nm). In this way, the concentration profiles of lignohumate in the particular acceptor gels were determined (see Fig. 5).

As can be seen from Fig. 5, the concentration profiles confirmed all above mentioned visual observations. The concentration of lignohumate at a given distance in the acceptor gel was significantly higher when the lignohumate penetrated through an abaxial cuticle. While enzymatically isolated abaxial cuticles had lower penetration rates than chemically isolated ones, no such significant difference was found for adaxial cuticles. The concentration profiles were also subjected to further mathematical processing in order to calculate the total amounts of lignohumate accumulated in the acceptor gels. For this purpose, we fitted the experimentally derived concentration profiles using the following relation

Fig. 5 Concentration profiles of lignohumate in the acceptor gel of the diffusion couple **a** after 96 h of diffusion through abaxial, and **b** after 168 h of diffusion through adaxial cuticles

$$c = \mathrm{A} \cdot \mathrm{erfc}\left(\frac{x}{\mathrm{B}}\right) \tag{1}$$

where c is the concentration of lignohumate in $\mathrm{mg_{LH}/g_{gel}}$ at distance x from the gel-cuticle interface, and A and B are the fitting parameters. The complementary error function erfc is a non-elementary function of sigmoid shape that generally occurs in non-stationary diffusion equations [71]. The fitting of experimental data was performed by non-linear least square regression using the Solver tool in Excel (Microsoft). With the known fitting parameters A and B at given time t, the total diffusion flux of lignohumate across unit area n (in $\mathrm{g_{LH}/m^2}$) can easily be determined from the integration of Eq. (1) in the range $x = 0$ to $x = \infty$, which leads to the relation

$$n(t) = \rho_{\mathrm{gel}} \cdot \frac{\mathrm{A} \cdot \mathrm{B}}{\sqrt{\pi}} \tag{2}$$

where the density of the gel (ρ_{gel}) was substituted by the density of pure water for simplicity because of the very low dry matter content of the gels (approximately 1 wt%).

For the non-stationary Fickian diffusion of a solute in a composite medium, the total diffusion flux n increases linearly with the square root of time. As can be seen in Fig. 6, the linearity of this dependency was confirmed for the diffusion of lignohumate through all forms of the tested cuticles (for the comparison, the results of lignohumate diffusion in absence of any cuticle is shown in Fig. 6a as well). In the case of abaxial cuticles, the linear regression of the function $n = f(\sqrt{t})$ crosses the origin of coordinates. In other words, lignohumate penetrates abaxial cuticles instantaneously. This confirms that the stomata on the abaxial side of the leaf, after the removal of the guard cells during the isolation process, represent freely penetrable parts of the cuticle. In contrast, the x-axis intercept of the function $n = f(\sqrt{t})$ for adaxial cuticles is shifted to significantly higher times. From the intercept, the time needed for lignohumate to penetrate the cuticle (usually called the lag time) was calculated. For both types of adaxial cuticle, quite high lag times were determined. This confirms that in the case of adaxial cuticles molecular transport takes place over a much more tortuous pathway. It is also further evidence that neither of the isolation procedures led to significant mechanical damage to the cuticles in the form of cracks or ruptures.

It was found that while lignohumate needed about 60 h to penetrate enzymatically isolated adaxial cuticles, this lag time increased to about 80 h in the case of chemically isolated ones. Interestingly, after the penetration of the cuticle was complete, the trend was reversed—the amount of lignohumate transported into the acceptor gel increased more rapidly in the case of chemically isolated

Smilkova *et al. Plant Methods* (2019) 15:83

Page 8 of 11

Fig. 6 Confirmation of the Fickian type of diffusion process. Dependence of total diffusion flux on the square root of time for abaxial (**a**) and adaxial (**b**) cuticles
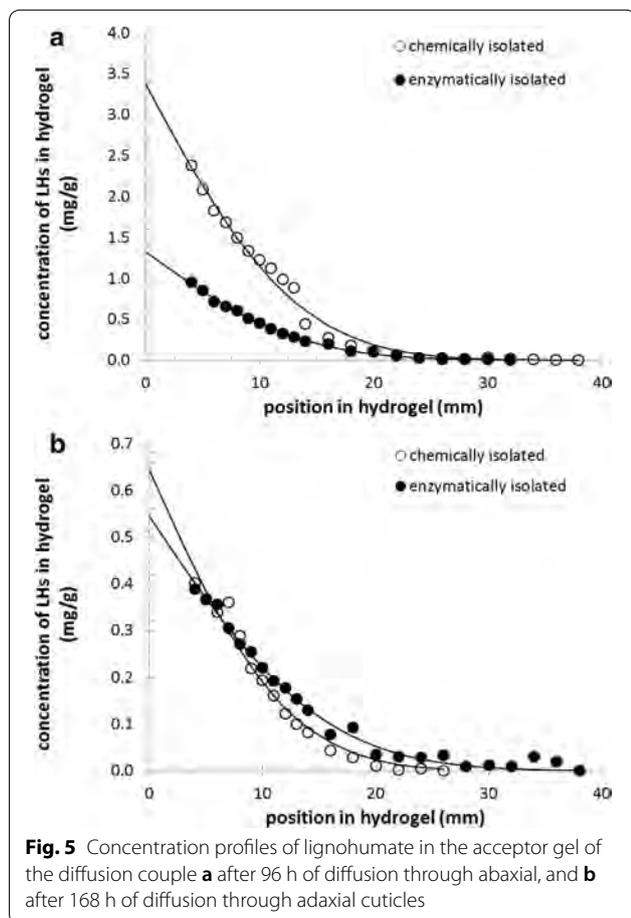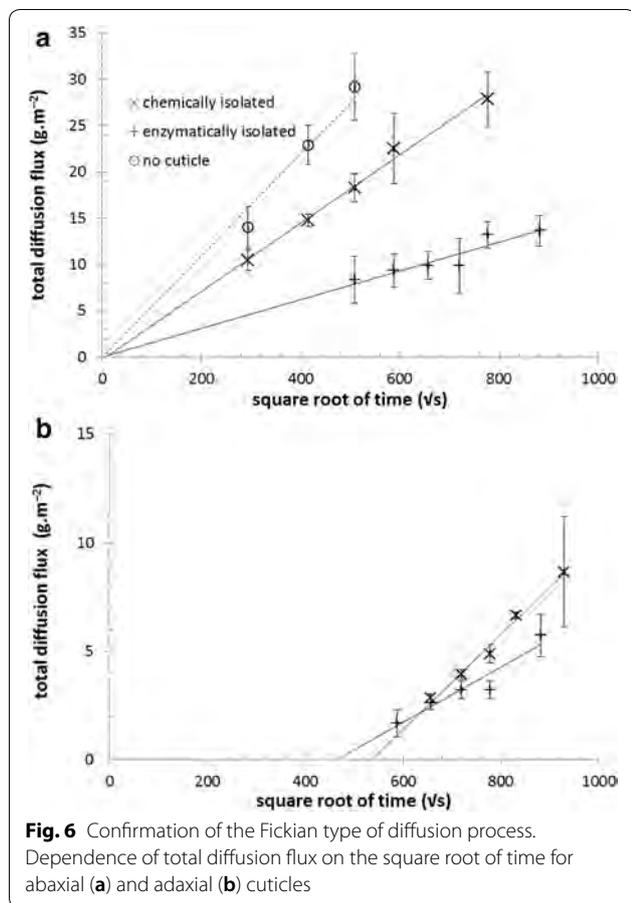
cuticles compared to enzymatically isolated ones. It is not possible to propose a reasonable explanation for this phenomenon just from the basic structural analysis of cuticles performed in this work, a comprehensive chemical assay of the isolated cuticles would be necessary for a detail discussion of these results (see "Discussion" section).

Discussion

The urgent need for an assembly of methods for a systematic study of foliar action of humates was claimed recently [58]. To contribute to this complex task, we hereby propose a simple experimental method for a quantitative description of permeability of plant cuticles for liquid humates. The main aim of the present work was to devise and to verify the usability of the proposed methodology.

We are well aware that the proposed experimental approach suffers several general limitations. First of all, the method is based on isolated plant cuticles. Taking into account that isolation of large-sized cuticular membranes is only successful with few species and that the resulting isolates may differ significantly in their structure

and chemical composition [72], even the choice of suitable plant becomes a non-trivial issue. In the current work, we proposed and tested *Prunus laurocerasus* as a source plant. The selected plant may not have any direct agricultural relevance as far as the foliar application of humates is concerned. Rather, its choice was based on specific experimental demands with respect to the universality and reproducibility of the developed methodology. The main requirements were as follows: there had to be adequate availability of the plant (both seasonal and regional); the method of cuticle separation had to be simple and reproducible; and the isolated cuticles had to exhibit suitable mechanical properties. From this viewpoint, *Prunus Laurocerasus* was chosen as a suitable candidate. Nevertheless, a proposal of an alternative plant with a specific relevance in current agricultural use of humic-based foliar formulations is highly welcome.

Another issue, which must be considered, is represented by possible artifacts brought by the process of cuticle isolation. Results of optical microscopy and profilometry confirmed higher efficiency of chemical removal of cell debris as compared to the enzymatic treatment. It can be expected that the presence of residual cell debris on the cuticle surface will negatively influence the accuracy of any experiments mapping barrier properties. From this point of view, the results of the structural characterization of the obtained cuticles support the choice of chemical method of isolation. On the other hand, it is likely that more adverse conditions employed during the chemical isolation treatment will result in more severe alteration of chemical composition of the isolated cuticles. It was suggested by several researchers [4, 73], that the isolation can induce changes in chemical structure of the cuticular membrane which may lead to the results of permeability studies different from those performed with intact leaves. Also our results (different permeability of chemically and enzymatically isolated) are consistent with this suggestion. As far as the importance of polysaccharides in the chemical structure of cuticle has been recently highlighted [74–76], it is likely that the observed differences in the barrier properties of the two types of cuticular isolates may be caused by hydrolysis of the cuticular polysaccharides during the acid treatment. Furthermore, potential influence of the isolation methods on the wax compositions of cuticles cannot be discarded. Therefore, a comprehensive chemical assay of the isolated cuticles is still needed before a definite choice of the most appropriate isolation procedure. Alternatively, a compromise between the two methods could be achieved by supplying the more user-friendly enzymatic method of isolation with a subsequent step of cuticle purification (e.g. treatment with chloroform or another organic solvent [19, 77].

Moreover, it was clearly demonstrated that the relevant information on the in situ barrier performance of the

Smilkova *et al. Plant Methods*   (2019) 15:83

Page 9 of 11

cuticle is given only when the astomatous cuticular membranes are used. In the case of stomatous membranes, no information is obtained about the stomatal penetration pathway, because the guard cells, which control opening and closing of the stomata in the intact plant, are lost during the isolation process. As far as several authors have stressed the general importance of this entry route [78, 79], stomatal absorption of humic substances remains to be an important issue for the future experimental concern. Nevertheless, since the liquid foliar formulations are usually primarily supplied to astomatous adaxial sides of leaves, we consider the model of transcuticular diffusion using this type of isolated membrane reasonable.

It is worth highlighting that the experimental arrangement of the diffusion experiment (diffusion couple with almost constant concentration of the solute in the donor compartment) has no ambition to simulate the real conditions during the foliar feeding process, where the solute concentration is changing dramatically in time by the evaporation, washing out by rain etc. Its application is aimed to answer the specific research questions concerning penetration of humic-based substances into leaves, such as the characterization and comparison of permeability of cuticles of different species to the single tested humate or the barrier properties of a specific cuticle against humic-based solutes of different size or solubility. It provides information on an upper limit of the rate of diffusional transport through cuticle. As was illustrated on the presented data, the barrier properties can be easily quantified. In this work, we used just the temporal development of the total diffusion flux for the quantification purposes. Nevertheless, if some additional experimental parameters were provided (e.g. the equilibrium amount of solute absorbed by the receptor compartment), it would be possible to calculate also further quantitative transport parameters, such as permeances or diffusion coefficients. The mathematical apparatus for these calculations are well described [71, 80]. On the basis of these parameters, barrier performance of cuticles against humic substances and other solutes (nutrients etc.) can be directly compared. Moreover, this applies also to comparison of the barrier properties of different types of membranes; permeability of a specific humate through a cuticle can hence be compared to the values obtained for different synthetic membranes etc.

Conclusions

The results of the performed diffusion experiments revealed usability of described methodology for the study on the transcuticular transport of humic-based biostimulants. The proposed methodology represents a simple and cheap experimental tool. Nevertheless, the penetration experiments provide only one part of the overall perspective on all processes which take place in a collective manner when the humate penetrates the cuticle from the liquid product into the leaf. One crucial separate process which deserves more detailed description is the adsorption of the humate on the cuticle surface. The assessment of such parameters as the total adsorption capacity and sorption isotherm, or an explanation of the sorption mechanism and kinetics would lead to a better understanding the specific effects and modes of operation of humate-based biostimulants after their application on plants.

Author details
[1] Institute of Physical and Applied Chemistry, Brno University of Technology, Faculty of Chemistry, Purkynova 464/118, 612 00 Brno, Czech Republic. [2] Materials Research Centre, Brno University of Technology, Faculty of Chemistry, Purkynova 464/118, 612 00 Brno, Czech Republic.

References
1. Neshev N, Manolov I. Content and uptake of nutrients with plant biomass of potatoes depending on potassium fertilization. Agric Agric Sci Procedia. 2015. https://doi.org/10.1016/j.aaspro.2015.08.039.
2. Peigne J, Vian JF, Payet V, Saby NPA. Soil fertility after 10 years of conservation tillage in organic farming. Soil Tillage Res. 2018. https://doi.org/10.1016/j.still.2017.09.008.

3. Okuda A, Kawasaki T, Yamada Y. Foliar absorption of nutrients. Soil Sci Plant Nutr. 1960. https://doi.org/10.1080/00380768.1960.10430928.

4. Fernandez V, Eichert T. Uptake of hydrophilic solutes through plant leaves: current state of knowledge and perspectives of foliar fertilization. Crit Rev Plant Sci. 2009. https://doi.org/10.1080/07352680902743069.

5. Fageria NK, Barbosa Filho MP, Moreira A, Guimaraes CM. Foliar fertilization of crop plants. J Plant Nutr. 2009. https://doi.org/10.1080/0190416090 2872826.

6. Mandic V, Simic A, Krnjaja Z, Bijelic Z, Tomic A, Stanojkovic D, Ruzic Music D. Effect of foliar fertilization on soybean grain yield. Biotechnol Anim Husb. 2015. https://doi.org/10.2298/BAH1501133M.

7. Li M, Wang S, Tian X, Li S, Chen Y, Jia Z, Liu K, Zhai A. Zinc and iron concentrations in grain milling fractions through combined foliar applications of Zn and macronutrients. Field Crop Res. 2016. https://doi.org/10.1016/j.fcr.2015.12.018.

8. Chamel A, Gambonnet B. Sorption and diffusion of an ethoxylated stearic alcohol and an ethoxylated stearic amine into and through isolated plant cuticles. Chemosphere. 1997. https://doi.org/10.1016/S0045 -6535(97)00033-7.

9. Liu H, Shao B, Long X, Yao Y, Meng Q. Foliar penetration enhanced by biosurfactant rhamnolipid. Colloid Surf B. 2016. https://doi.org/10.1016/j.colsurfb.2016.05.058.

10. Solel Z, Edgington LV. Transcuticular movement of fungicides. Phytopathology. 1972. https://doi.org/10.1094/Phyto-63-505.

11. Chamel A, Vitton N. Sorption and diffusion of C14-atrazine through isolated plant cuticles. Chemosphere. 1996. https://doi.org/10.1016/0045-6535(96)00241-X.

12. Wang CJ, Liu ZQ. Foliar uptake of pesticides—present status and future challenge. Pestic Biochem Phys. 2007. https://doi.org/10.1016/j.pestbp.2006.04.004.

13. Zelena V, Veverka K. Effect of surfactants and liquid fertilizers on transcuticular penetration of fungicides. Plant Prot Sci. 2007. https://doi.org/10.17221/2236-PPS.

14. Khayet M, Fernandez V. Estimation of the solubility parameters of model plant surfaces and agrochemicals: a valuable tool for understanding plant surface interactions. Theor Biol Med Model. 2012. https://doi.org/10.1186/1742-4682-9-45.

15. Khorram MS, Zhang Q, Lin D, Zheng Y, Fang H, Yu Y. Biochar: a review of its impact on pesticide behavior in soil environments and its potential applications. J Environ Sci. 2016. https://doi.org/10.1016/j.jes.2015.12.027.

16. Martin JT, Juniper BE. The cuticles of plants. New York: St. Martin's Press; 1970.

17. Riederer M, Schreiber L. Protecting against water loss: analysis of the barrier properties of plant cuticles. J Exp Bot. 2001. https://doi.org/10.1093/jexbot/52.363.2023.

18. Barel D. Foliar application of phosphorus compounds. Doctoral thesis, Iowa State University, USA; 1975. p. 1–345.

19. Villena JF, Dominguez E, Heredia A. Monitoring biopolymers present in plant cuticles by FT-IR. J Plant Physiol. 1999. https://doi.org/10.1016/S0176-1617(00)80083-8.

20. Pollard M, Beisson F, Li Y, Ohlrogge JB. Building lipid barriers: biosynthesis of cutin and suberin. Trends Plant Sci. 2008. https://doi.org/10.1016/j.tplants.2008.03.003.

21. Yeats TH, Rose JK. The formation and function of plant cuticles. Plant Physiol. 2013. https://doi.org/10.1104/pp.113.222737.

22. Riederer M, Müller C. Biology of the plant cuticle. Annual plant reviews. Oxford: Blackwell; 2006. https://doi.org/10.1002/9780470988718.

23. Gutschick VP. Biotic and abiotic consequences of differences in leaf structure. New Phytol. 1999. https://doi.org/10.1046/j.1469-8137.1999.00423.x.

24. Zeisler-Diehl V, Migdal B, Schreiber L. Quantitative characterization of cuticular barrier properties: methods, requirements, and problems. J Exp Bot. 2017. https://doi.org/10.1093/jxb/erx282.

25. Orgell WH. The isolation of plant cuticle with pectic enzymes. Plant Physiol. 1955;30:78–80.

26. Holloway PJ, Baker EA. Isolation of plant cuticles with zinc chloride-hydrochloric acid solution (short communication). Plant Physiol. 1968. https://doi.org/10.1104/pp.43.11.1878.

27. Solel Z. The systematic fungicidal effect of benzimidazole derivatives and thiophanate against Cercospora leaf spot of sugar beet. Phytopathology. 1970. https://doi.org/10.1094/Phyto-60-1186.

28. Edgington LV, Buchenauer H, Grossmann F. Bioassay and transcuticular movement of systematic fungicides. Pestic Sci. 1973. https://doi.org/10.1002/ps.2780040517.

29. Schonherr J, Lendzian K. A simple and inexpensive method of measuring water permeability of isolated plant cuticular membranes. Z Pflanzenphysiol. 1981. https://doi.org/10.1016/S0044-328X(81)80203-6.

30. Yamada Y, Wittwer SH, Bukovac MJ. Penetration of organic compounds through isolated cuticular membranes with special reference to C14 urea. Plant Physiol. 1964. https://doi.org/10.1104/pp.40.1.170.

31. Darlington WA, Cirulis N. Permeability of apricot leaf cuticle. Plant Physiol. 1963. https://doi.org/10.1104/pp.38.4.462.

32. Wittwer SH, Lundahl WS. Autoradiography as an acid in determining the grass absorption and utilization of foliar applied nutrients. Plant Physiol. 1951;26:792–7.

33. Eggert R, Kardos LT, Smith RD. The relative absorption of phosphorus by apple trees from foliar sprays and from soil applications of fertilizer using radioactive tracers. Proc Am Soc Hortic Sci. 1952;60:75–86.

34. Tukey HB, Ticknor RL, Hinsvark ON, Wittwer SH. Absorption of nutrients by stems and branches of woody plants. Science. 1952. https://doi.org/10.1126/science.116.3007.167.

35. Bargel H, Koch K, Cerman Z, Neinhuis Ch. Structure-function relationships of the plant cuticle and cuticular waxes—a smart material? Funct Plant Biol. 2006. https://doi.org/10.1071/FP06139.

36. Bukovac MH, Wittwer SH. Absorption and mobility of foliar applied nutrients. Plant Physiol. 1957. https://doi.org/10.1104/pp.32.5.428.

37. Yamada Y, Wittwer SH, Bukovac MJ. Penetration of ions through isolated cuticles. Plant Physiol. 1963. https://doi.org/10.1104/pp.39.1.28.

38. Yu JH, Lim HK, Choi GJ, Cho KY, Kim JH. A new method for assessing foliar uptake of fungicides using Congo Red as a tracer. Pest Manag Sci. 2001. https://doi.org/10.1002/ps.327.

39. Pinton R, Cesco S, Santi S, Varanini Z. Soil humic substances stimulate proton release by intact oat seedling roots. J Plant Nutr. 1997. https://doi.org/10.1080/01904169709365301.

40. Chen Y, Clapp CE, Magen H, Cline VW. Stimulation of plant growth by humic substances: effects on iron availability. In: Ghabbour EA, Davies G, editors. Understanding humic substances: advanced methods, properties and applications. Cambridge: Royal Society of Chemistry; 1999.

41. Russo RO, Berlyn GP. The use of organic biostimulants to help low input sustainable agriculture. J Sustain Agric. 1990. https://doi.org/10.1300/J064v01n02_04.

42. Tan KH. Humic matter in soil and the environment. 2nd ed. New York: Marcel Dekker; 2003.

43. Nardi S, Condheri G, Dell'Agnola G. Biological activity of humus. In: Piccolo A, editor. Humic substances in terrestrial ecosystems. Amsterdam: Elsevier; 1996. p. 361–406.

44. Canellas LP, Olivares FL. Physiological responses to humic substances as plant growth promoter. Chem Biol Technol Agric. 2014. https://doi.org/10.1186/2196-5641-1-3.

45. Nardi S, Pizzeghello D, Schiavon M, Ertani A. Plant biostimulants: physiological responses induced by protein hydrolyzed-based products and humic substances in plant metabolism. Sci Agric. 2016. https://doi.org/10.1590/0103-9016-2015-0006.

46. Tejada M, Gonzalez JL. Influence of foliar fertilization with amino acids and humic acids on productivity and quality of asparagus. Biol Agric Hortic. 2003. https://doi.org/10.1080/01448765.2003.9755270.

47. Pizzeghello D, Nicolini G, Nardi S. Hormone-like activity of humic substances in *Fagus sylvaticae* forests. New Phytol. 2001. https://doi.org/10.1046/j.0028-646x.2001.00223.x.

48. Basiolio ZD, Pasqualoto CL, Facanha AR. Indolacetic and humic acids induce lateral root development through a concerted plasmalemma and tonoplast H^+ pumps activation. Planta. 2007. https://doi.org/10.1007/s00425-006-0454-2.

49. Jackson TA. Effects of clay minerals, oxyhydroxides, and humic matter on microbial communities of soil, sediment, and water. In: Huang PH, et al., editors. Environmental impact of soil component interactions: metals, inorganics and microbial activity. Berlin Heidelberg: CRC Press, Springer; 1995. p. 165–200.

50. Parandian F, Samavat S. Effects of fulvic and humic acid on anthocyanin, soluble sugar, α-amylase enzyme and some micronutrient elements in Lilium. Int Res J Appl Basic Sci. 2012;3:924–9.

Smilkova *et al. Plant Methods*   (2019) 15:83

Page 11 of 11

51. Dorer SP, Peacock CH. The effect of humate and organic fertilizer on establishment and nutrient of creeping bent putting greens. Int Turfgrass Soc. 1997;78:437–43.
52. Liu C, Cooper RJ, Bowman DC. Humic acid application affects photosynthesis, root development, and nutrient content of creeping bentgrass. HortScience. 1998;33:1023–5.
53. Fernandez-Escobar R, Benlloch M. Response of olive trees to foliar application of humic substances extracted from leonardite. Sci Hortic. 1996. https://doi.org/10.1016/S0304-4238(96)00914-4.
54. Maibodi NDH, Kafi M, Nikbakht A, Rejali F. Effect of foliar applications of humic acid on growth, visual quality, nutrients content and root parameters of perennial ryegrass (*Lolium perenne* L.). J Plant Nutr. 2014. https://doi.org/10.1080/01904167.2014.939759.
55. Bettoni MM, Mogor AF, Pauletti V, Goicoechea N, Aranjuelo I, Germendia I. Nutritional quality and yield of onion as affected by different application methods and doses of humic substances. J Food Compos Anal. 2016. https://doi.org/10.1016/j.jfca.2016.06.008.
56. Olk DC, Dinnes DL, Rene Scoresby J, Callaway CR, Darlington JW. Humic products in agriculture: potential benefits and research challenges–a review. J Soils Sediments. 2018. https://doi.org/10.1007/s11368-018-1916-4.
57. Rose MT, Patti AF, Little KR, Brown AL, Roy Jackson W, Cavagnaro TR. A meta-analysis and review of plant-growth response to humic substances: practical implications for agriculture. Adv Agron. 2014. https://doi.org/10.1016/B978-0-12-800138-7.00002-4.
58. Lyons G, Genc Y. Commercial humates in agriculture: real substance or smoke and mirrors? Agronomy. 2016. https://doi.org/10.3390/agronomy6040050.
59. Kulikova NA, Abroskin DP, Badun G, Chernysheva MG, Korobkov VI, Beer AS, Tsvetkova EA, Senik SV, Klein OI, Perminova IV. Label distribution in tissues of wheat seedlings cultivated with tritium-labeled leonardite humic acid. Sci Rep. 2016. https://doi.org/10.1038/srep28869.
60. Sedlacek P, Smilek J, Klucakova M. How the interactions with humic acids affect the mobility of ionic dyes in hydrogels—2. Non-stationary diffusion experiments. React Funct Polym. 2014. https://doi.org/10.1016/j.reactfunctpolym.2013.12.002.
61. Smilek J, Sedlacek P, Klucakova M. On the role of humic acids' carboxyl groups in the binding of charged organic compounds. Chemosphere. 2015. https://doi.org/10.1016/j.chemosphere.2015.06.093.
62. Gladkov OA. U.S. Patent 7198805B2, Method for producing humic acid salts, Sankt-Peterburg (RU), chemical abstract (57). 2007.
63. Novak F, Sestauberova M, Hrabal R. Structural features of lignohumic acids. J Mol Struct. 2015. https://doi.org/10.1016/j.molstruc.2015.03.054.
64. Sedlacek P, Smilek J, Klucakova M. How the interactions with humic acids affect the mobility of ionic dyes in hydrogels—results from diffusion cells. React Funct Polym. 2013. https://doi.org/10.1016/j.reactfunctpolym.2013.07.008.
65. Sedlacek P, Smilek J, Kalina M, Lastuvkova M, Klucakova M. Hydrogels: invaluable experimental tool for demonstrating diffusion phenomena in physical chemistry laboratory courses. J Mater Educ. 2017;39:59–90.
66. Smilek J, Sedlacek P, Lastuvkova M, Kalina M, Klucakova M. Transport of organic compounds through porous systems containing humic acids. Bull Environ Contam Toxicol. 2017. https://doi.org/10.1007/s00128-016-1926-0.
67. Cussler EL. Diffusion: mass transfer in fluid systems. 2nd ed. London: Cambridge University Press; 1997.
68. Enev V, Pospisilova L, Klucakova M, Liptaj T, Doskocil L. Spectral characterization of selected humic substances. Soil Water Res. 2014. https://doi.org/10.17221/39/2013-SWR.
69. Prochazka P, Stranc P, Pzderu K, Strnc J, Jedlickova M. The possibilities of increasing the production abilities of soya vegetation by seed treatment with biologically active compounds. Plant Soil Environ. 2015. https://doi.org/10.17221/225/2015-PSE.
70. Prochazka P, Stranc P, Pazderu K, Stranc J. The influence of pre-sowing seed treatment by biologically active compounds on soybean seed quality and yield. Plant Soil Environ. 2016. https://doi.org/10.17221/570/2016-PSE.
71. Crank J. The mathematics of diffusion. 2nd ed. Oxford: Clarendon Press; 1956.
72. Guzman P, Fernandez V, Khayet M, Garcia ML, Fernandez A, Gil L. Ultrastructure of plant lead cuticles in relation to sample preparation as observed transmission electron microscopy. Sci World J. 2014. https://doi.org/10.1155/2014/963921.
73. Tyree MT, Scherbatskoy D, Tabor CA. Leaf cuticles behave as asymmetric membranes: evidence from the measurement of diffusion potentials. Plant Physiol. 1990. https://doi.org/10.1104/pp.92.1.103.
74. Guzman P, Fernandez V, Garcia ML, Khayet M, Fernandez A, Gil L. Localization of polysaccharides in isolated and intact cuticles of eucalypt, poplar and pear leaves by enzyme-gold labelling. Plant Physiol Biochem. 2014. https://doi.org/10.1016/j.plaphy.2013.12.023.
75. Guzman P, Fernandez V, Garcia J, Cabral V, Hayali N, Khayet M, Gil L. Chemical and structural analysis of *Eucalyptus globulus* and *E. camaldulensis* leaf cuticles: a lipidized cell wall region. Front Plant Sci. 2014. https://doi.org/10.3389/fpls.2014.00481.
76. Fernandez V, Guzman-Delgado P, Graca J, Santos S, Gil L. Cuticles structure in relation to chemical composition: re-assessing the prevailing model. Front Plant Sci. 2016. https://doi.org/10.3389/fpls.2016.00427.
77. Riederer M, Schönherr J. Accumulation and transport of (2,4-dichlorophenoxy)acetic acid in plant cuticles. 1. Sorption in the cuticular membrane and its components. Ecotoxicol Environ Saf. 1984. https://doi.org/10.1016/0147-6513(85)90022-3.
78. Eichert T, Burkhardt J. Quantification of stomatal uptake of ionic solutes using a new model system. J Exp Bot. 2001. https://doi.org/10.1093/jexbot/52.357.771.
79. Burkhardt J, Basi S, Pariyar S, Hunsche M. Stomatal penetration by aqueous solutions—an update involving leaf surface particles. New Phytol. 2012. https://doi.org/10.1111/j.1469-8137.2012.04307.x.
80. Schreiber L, Schonherr J. Water and solute permeability of plant cuticles. 1st ed. Berlin: Springer; 2009.

Publisher's Note

Appendix 10

Obruca, S., Sedlacek, P., Slaninova, E., Fritz, I., Daffert, C., Meixner, K., Sedrlova, Z., and Koller, M. Novel unexpected functions of PHA granules. *Applied Microbiology and Biotechnology* **2020**, 104, 4795–4810.

MINI-REVIEW

Novel unexpected functions of PHA granules

Stanislav Obruca[1] · Petr Sedlacek[1] · Eva Slaninova[1] · Ines Fritz[2] · Christina Daffert[2] · Katharina Meixner[2] ·
Zuzana Sedrlova[1] · Martin Koller[3,4]

Abstract

Polyhydroxyalkanoates (PHA), polyesters accumulated by numerous prokaryotes in the form of intracellular granules, have been for decades considered being predominantly storage molecules. However, numerous recent discoveries revealed and emphasized their complex biological role for microbial cells. Most of all, it was repeatedly reported and confirmed that the presence of PHA granules in prokaryotic cells enhances stress resistance and robustness of microbes against various environmental stress factors such as high or low temperature, freezing, oxidative, and osmotic pressure. It seems that protective mechanisms of PHA granules are associated with their extraordinary architecture and biophysical properties as well as with the complex and deeply interconnected nature of PHA metabolism. Therefore, this review aims at describing novel and unexpected properties of PHA granules with respect to their contribution to stress tolerance of various prokaryotes including common mesophilic heterotrophic bacteria, but also extremophiles or photo-autotrophic cyanobacteria.

Key points
• *PHA granules present in bacterial cells reveal unique properties and functions.*
• *PHA enhances stress robustness of bacterial cells.*

Introduction

Polyhydroxyalkanoates (PHA) are microbial polyesters accumulated by numerous prokaryotes in the form of intracellular granules. For decades, PHA were considered being predominantly storage materials which are accumulated in excess of

---

Stanislav Obruca and Petr Sedlacek contributed equally.

✉ Stanislav Obruca
   Stana.O@seznam.cz

1   Faculty of Chemistry, Brno University of Technology, Purkynova 118, 612 00 Brno, Czech Republic

2   University for Natural Resources and Life Sciences, IFA-Tulln, Konrad Lorenz Str. 20, 3430 Tulln, Austria

3   Institute of Chemistry, NAWI Graz, University of Graz, Heinrichstrasse 28/VI, 8010 Graz, Austria

4   ARENA Arbeitsgemeinschaft für Ressourcenschonende & Nachhaltige Technologien, Inffeldgasse 21b, 8010 Graz, Austria

external carbon source and degraded to fuel metabolism of bacterial cells when external carbon source is exhausted (Sudesh et al. 2000a). Nevertheless, in course of time, numerous evidences suggesting more complex biological role of PHA appeared. It was observed that PHA are involved in maintenance of anoxic photosynthesis and sulfur cycle in microbial mats dependent on photosynthetic carbon fixation (Rothermic et al. 2000; Urmeneta et al. 1995), triggering sporulation in Bacilli (Slepecky and Law 1961), supporting the prolongation of nitrogen fixation by diazotrophs in the dark (Bergersen et al. 1991), or maintaining energy production and NADH oxidation to NAD$^+$ by nitrogen fixing bacteria (Encarnación et al. 2002). Further, experiments with promoting bacteria plant growth, which can be employed as agricultural inoculants such as *Azospirillum brasilense*, substantiated the importance of PHA for stress robustness of bacteria. The first work systematically studying the influence of PHA content in bacterial cells with respect to survival rate under stress conditions was published in 1985 by Tal and Okon; these authors observed that PHA-rich cells of *Azospirillum*

brasilense were much less prone to the harmful effects of UV radiation, desiccation, and osmotic challenge than PHA-poor cells (Tal and Okon 1985). These preliminary observations were lately confirmed by numerous studies resorting to deletion mutants of *Azospirillum brasilense* in which the *phaC* gene was deleted, thus resulting in hampered PHA biosynthesis (Kadouri et al. 2002; Kadouri et al. 2003a), or by deletion of the *phaZ* gene, which disabled the bacterium to utilize stored PHA (Kadouri et al. 2003b). In all these cases, deletion mutants revealed substantially higher sensitivity to various stress conditions than wild-type strain. Very similar phenomena were also observed in other bacteria such as *Aeromonas hydrophila* (Zhao et al. 2007), *Pseudomonas oleovorans* (Ruiz et al. 2001), *Pseudomonas extremaustralis* (Tribelli et al. 2019), *Pseudomonas aeruginosa* (Pham 2004), or *Escherichia coli* (Wang et al. 2009). This confirms the fact that PHA are very complex metabolites and, apart from their primary storage function, they provide bacterial cells also with very important "secondary benefits" such as enhancement of robustness and survival rate when exposed to various environmentally relevant stress conditions. Table 1 summarizes microorganisms and stress factors in which protective function of PHA was described. Protective function of PHA granules is most likely the consequence of both PHA metabolism and its interconnection with other metabolic routes; however, it seems that unique biophysical properties of PHA intracellular granules are equally important. This review summarizes the recent understanding of protective mechanisms of PHA granules.

PHA metabolism and its impact on stress robustness of bacteria

In principle, there are three main metabolic pathways of PHA biosynthesis. So-called short chain length PHA (*scl*-PHA), comprising 4–5 carbon atoms per monomer subunit, such as poly(3-hydroxybutyrate) (P(3HB)), the homopolymer of 3-hydroxybutyrate (3HB), are synthesized via a metabolic pathway consisting of three enzymatically catalyzed reactions. At first, two acetyl-CoA molecules are condensed by the action of 3-ketothiolase (PhaA) resulting in formation of acetoacetyl-CoA, which is subsequently stereospecifically reduced by acetoacetyl-CoA reductase (PhaB) to *R*-3-hydroxybutyryl-CoA; this step regenerates the oxidized form of redox equivalents and therefore is often referred to as "pseudo fermentation." Finally, PHA synthase (PhaC) catalyzes incorporation of *R*-3-hydrobuytyryl-CoA into the long linear polyester chain of P(3HB) (Kessler and Witholt 2001). When PHA consisting of medium-chain-length monomers (*mcl*-PHA; 6–14 carbon atoms per monomer units) are synthesized, desired substrates for particular PHA synthase, namely diverse *R*-3-hydroxyacyl-CoA molecules, can be obtained either from β-

oxidation of fatty acids or from de novo fatty acids synthesis (Kim et al. 2007).

Mobilization of PHA granules is catabolized by a cocktail of intracellular PHA depolymerases (PhaZ), which are able to hydrolyze amorphous native PHA granules yielding PHA monomers as final products (Jendrossek 2007). The battery of PHA depolymerases and related enzymes is well described for *Cupriavius necator*; it consists of seven PHA depolymerases (PhaZ1–PhaZ7) and two oligomer hydrolases (PhaY1 and PhaY2), which further cleavage products of PhaZ to provide PHA monomers (Peplinski et al. 2010).

It should be pointed out that biosynthesis and degradation of PHA are interconnected processes which are occurring in the cells simultaneously. Therefore, even during PHA biosynthesis favoring conditions (excess of carbon substrate, etc.), PHA depolymerases are active to a certain extent. Hence, PHA metabolism is sometimes termed "PHA cycle" in order to stress out its cyclic character (Kadouri et al. 2005). Proper function of the PHA cycle is essential for bacterial cells since it ensures balanced flow of carbon to the transient demand for metabolic intermediates to balance the storage and use of carbon and energy; moreover, the PHA cycle also influences the number and size of PHA granules in bacterial cells (Prieto et al. 2016).

Bacterial cells possessing a functional PHA cycle feature a high intracellular pool of PHA monomers. For instance, it was demonstrated that P(3HB) accumulating cells of *Cupriavidus necator* have 16.5 higher intracellular concentration of 3HB than its PHA non-accumulating mutants (Obruca et al. 2016a). It should be noted that it was repeatedly demonstrated that 3HB constitutes a very potent chemical chaperone, which is capable of protecting biomolecules from denaturation under stress conditions. Soto et al. (2012) observed that 3HB was used as compatible solute by the halotolerant bacterium *Pseudomonas* sp. CT13 to cope with high salinity of cultivation media. Moreover, 3HB accumulation was also associated with the prevention of protein aggregation under combined salt, and thermal stresses in vivo and in vitro studies demonstrated that physiologically relevant concentrations of 3HB protected citrate synthase as a model enzyme from denaturation by high temperature. Moreover, Obruca et al. (2016a) studied the protective function of 3HB against heat and oxidative degradation of lysozyme and lipase as model enzymes and observed that chaperoning efficiency of 3HB is more than comparable to that of well-known chemical chaperones such as trehalose or hydroxyectoine. These observations might explain why bacterial strain capable of PHA synthesis but unable of PHA degradation to monomers revealed higher sensitivity to numerous stress factors (Kadouri et al. 2003b; Ruiz et al. 2001; Wang et al. 2009) which again underlies the importance of a functional PHA cycle for stress robustness of bacteria.

Table 1 Summary of stressors and microorganisms in which protective function of PHA was described

Stressor	Microorganism	Reference
Low temperature and freezing	*Aeromonas hydrophila*	Zhao et al. 2007
	Pseudomonas extremaustralis	Tribelli and López 2011
	Sphingopyxis chilensis	Pavez et al. 2009
	Cupriavidus necator	Obruca et al. 2016b
		Nowroth et al. 2016
Heat shock	*Aeromonas hydrophila*	Zhao et al. 2007
	Azospirillum brasilense	Kadouri et al. 2003a
		Kadouri et al. 2003b
	Bacillus thuringiensis	Wu et al. 2011
	Pseudomonas aeruginosa	Pham 2004
	Escherichia coli	Wang et al. 2009
Osmotic shock	*Aeromonas hydrophila*	Zhao et al. 2007
	Azospirillum brasilense	Kadouri et al. 2003a
		Kadouri et al. 2003b
	Escherichia coli	Wang et al. 2009
	Cupriavidus necator	Obruca et al. 2017
		Sedlacek et al. 2019b
	Halomonas halophila	Sedlacek et al. 2019b
	Rhizobium spp.	Breedveld et al. 1993
Oxidative pressure	*Aeromonas hydrophila*	Zhao et al. 2007
	Azospirillum brasilense	Kadouri et al. 2003a
		Kadouri et al. 2003b
	Pseudomonas extremaustralis	Ayub et al. 2009
	Herbaspirillum seropedicae	Batista et al. 2018
	Delftia acidovorans	Goh et al. 2014
UV protection	*Aeromonas hydrophila*	Zhao et al. 2007
	Azospirillum brasilense	Kadouri et al. 2003a
		Kadouri et al. 2003b
		Tal and Okon 1985
	Cupriavidus necator	Slaninova et al. 2018
	Escherichia coli	Wang et al. 2009
	Pseudomonas extremaustralis	Tribelli et al. 2019
Heavy metals	*Cupriavidus taiwanensis*	Chien et al. 2014
	Azospirillum brasilense	Kamnev et al. 2005

In addition, Ruiz et al. (2001) demonstrated that intensive degradation of stored PHA is associated not only with expected increase in intracellular levels of ATP, but it also enhances intracellular concentration of guanosine tetraphoshate (ppGpp) in *Pseudomonas oleovorans*. It is known that ppGpp serves as cell alarmone causing upregulation of many genes involved in stress response, including *rpoS* gene encoding for alternative sigma factor of RNA polymerase. RPoS proteins further control the expression of numerous genes involved in stress response of bacteria. This might be

additional very important factors supporting stress robustness of bacteria possessing functional PHA cycle.

Furthermore, Koskimäki et al. 2016 investigated PHA metabolism of the pine endophyte *Methylobacterium extorquens* and observed that the strain is during mobilization of PHA capable of producing methyl-esterified dimers and trimers of 3HB which revealed very strong antioxidant properties. Authors compared their antioxidant capacity to well-known cellular antioxidants and reported that they reveal 3-fold higher hydroxyl radical–scavenging activity than glutathione

and 11-fold greater activity than ascorbic acid (vitamin C). The authors suggested that the PHA reserves are mobilized for the synthesis of methyl-esterified 3HB oligomers in bacterial cells to eliminate hydroxyl radical stress introduced by infected plants.

The fact that PHA can be hydrolyzed under stress conditions to serve as substrate for synthesis of metabolites providing desirable shielding effect was also demonstrated by Breedveld et al. (1993), who observed that exposition of *Rhizobium leguminosarum* and *Rhizobium meliloti* to hypertonic pressure resulted in hydrolysis of PHA storage which fueled biosynthesis of trehalose as a compatible solute compensating increase in osmotic pressure.

Hence, numerous protective mechanisms and functions of PHA are related to their unique metabolism called PHA cycle. Table 2 summarizes studies in which direct protective function of PHA monomers or oligomers was suggested; the most important features of PHA metabolism and its impacts on stress resistance and robustness of bacteria are demonstrated in Fig. 1.

Structure of PHA granules and granule-associated proteins

In addition to their metabolism, numerous protective functions of PHA can be attributed to the structural and biophysical features related to a specific way how the PHA chains are stored inside the cell. Bioaccumulated PHA chains are stored in the form of granules, often designated as carbonosomes (Jendrossek 2009). The size and properties of PHA granules are already described in detail. Intracellular PHA granules are typically 0.2–0.5 μm in diameter (Sudesh et al. 2000a). These PHA inclusions consist of hydrophobic polyester core surrounded by an amphiphilic layer that provides solubilization of the water-insoluble polymer in the aqueous cytoplasmic environment. Although it had been originally accepted that phospholipids form the main structural and solubilizing component of this layer (Pötter and Steinbüchel 2006), it was later revealed that the lipids detected in the isolated granules in fact represent an artifact of the isolation procedure; actually,

the granules are covered by so-called PHA granule-associated proteins (PGAPs), which include PHA synthase (PhaC), PHA depolymerase (PhaZ), surface proteins so-called phasins (PhaP), and regulatory proteins (PhaR) (De Koning and Lemstra 1992) (see Fig. 2).

Localization of PHA granules in the cell's interior is closely connected with mechanisms of PHA granules formation. Up to now, four model mechanisms of the granule formation were proposed: (i) the micelle model, (ii) the budding model, (iii) the scaffold model, and (iv) the cell pole model (Jendrossek and Pfeiffer 2014; Rehm and Steinbüchel 1999). Originally, the micelle model had assumed that localization of PHA synthesis in the cell is conditioned only by a sufficiently high concentration of the substrate (3-hydroxybutyryl-CoA) and that the nascent water-insoluble chains of PHA consequently form micelle-like aggregates localized more or less randomly throughout the cell. Nevertheless, follow-up studies revealed that PHA granules are often localized in close vicinity of cytoplasmic membrane, which gave the rise of budding theory (Stubbe and Tian 2003) according to which PHA synthases, attached to the cytoplasmic membrane, liberate the growing PHA chains into the bilayer of the membrane forming an integral PHA blob which is subsequently detached from the membrane after it reaches a specific size. However, the budding model was later challenged by the results of a study performed by Jendrossek et al. (2007), which revealed that formation of intracellular PHA granules at the early stages of their synthesis in *Caryophanon latum* was localized close to membrane but without any attachment to it. Furthermore, numerous studies have confirmed that the PHA granule formation can be initiated at positions distant from cytoplasmic membrane. Consequently, the scaffold model proposed utilization of mediation elements at the center of the cells as nucleation sites for granules initiation, which was observed by transmission electron microscopy (TEM) in *Cupriavidus necator* H16 (Tian et al. 2005). This mechanism was further supported by studies on *Comamonas* sp. EB172 (Mumtaz et al. 2011). Additionally, the cell pole model describes an initiation of formation of PHA granules at the cell poles.

Table 2 Summary of direct protective function of PHA monomers and oligomers

Microorganism	PHA-related metabolite	Protective function	Reference
Pseudomonas sp. CT13	3HB monomer	3HB serves as compatible solute and prevent protein aggregation under stress conditions.	Soto et al. 2012
Cupriavidus necator	3HB monomer	3HB reveals chaperoning activity and protects enzyme from denaturation by heating and oxidation	Obruca et al. 2016a
Cupriavidus necator	3HB monomer	3HB is very potent cryo-protectant	Obruca et al. 2016b
Photobacterium profundum	3HB monomer and oligomers	Monomer and oligomers serve as osmolyte protecting cells from hydrodynamic pressure	Martin et al. 2002
Methylobacterium extorquens	Methyl-esters of 3HB and 3HB oligomers	Protection against oxidative pressure caused by hydroxyl radicals	Koskimäki et al. 2016

Fig. 1 PHA metabolism and
PHA cycle
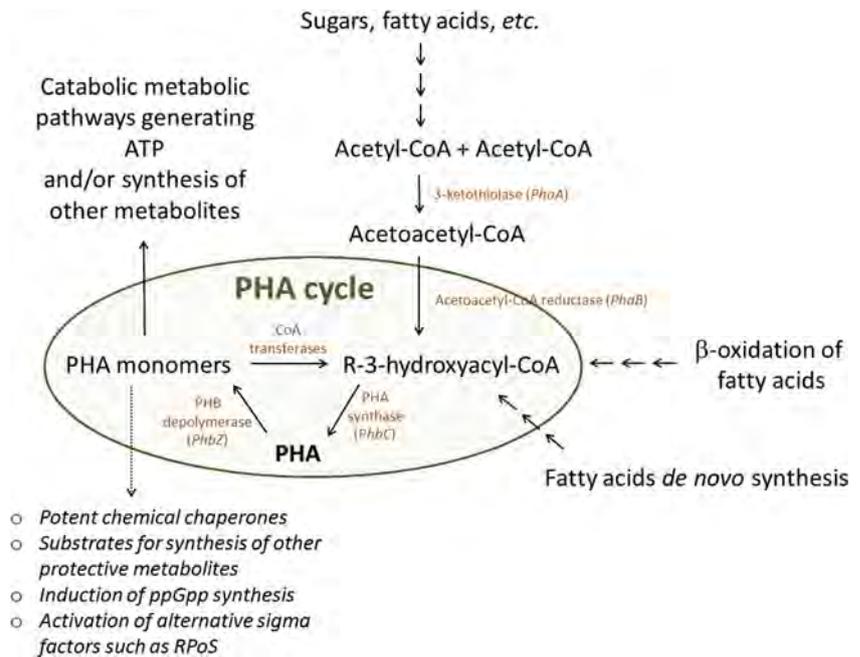
This mechanism is supported by several fluorescence microscopy studies on various microorganism such as *Rhodospirillum rubrum*, *Cupriavidus necator* H16, *Escherichia coli* (Jendrossek 2005), or by structural assays of *Dinoroseobacter* sp. JL 1447 obtained by TEM and AFM microscopy (Xiao et al. 2015).

As already emphasized, the surface layer of PHA granules is formed by granule-associated proteins. Among these, stereo-selective PHA synthases (PhaC) play the key role in PHA anabolism. Based on their structure, number of subunits, and substrate specificity, PHA synthases are classified into 4 types (Rehm 2003). Similarly, also intracellular PHA depolymerases (PhaZ), essential for PHA mobilization, form the integral part of the proteinaceous surface layer of the granules (Stuart et al. 1996) as well as the group of low-molecular-weight proteins with no catalytic activity generally called phasins (PhaP) (Sudesh et al. 2000a; Wieczorek et al. 1995; Zhao et al. 2016). Although phasins are not directly involved in PHA formation, it was experimentally confirmed that these proteins are expressed in the cells under PHA-accumulating conditions (York et al. 2001a) and that they play a fundamental role in PHA accumulation via regulating the ratio of surface area to volume of P(3HB) granules (Wieczorek et al. 1995) and also via a conformation change of PHA synthase as a result of its specific interactions with PhaP (York et al. 2001b). The last described granule-associated protein is PhaM, which is the physiological activator of PHA production. The mechanism of PhaC activation by PhaM was described in detail for *Cupriavidus necator* H16, where it reduces the lag phase of PhaC via inducing its transition from an inactive monomeric form into the active dimeric form (Pfeiffer and Jendrossek 2014). Mezzina et al. (2017) further

revealed that phasins may serve as chaperones during exposition to organic solvents providing higher resistance for PhaP overexpressing in PHA not producing *E. coli* in comparison with the wild-type strain. Likewise, cells with overproduction of PhaP are able to grow much better at high temperature where expression of the main regulator sigma factor RpoH is reduced (Mezzina et al. 2017). Production of phasins and biosynthesis of PHA granules is also efficiently regulated by transcriptional regulators PhaR, which inhibit transcription of PhaP under PHA biosynthesis unfavorable conditions (Kessler and Witholt 2001; York et al. 2002).

Unique structure and properties of PHA in granules

As it is obvious from the previous text focused on the protein shell of the intracellular PHA inclusions, a native PHA granule represents a fascinating supramolecular assembly, well-designed to provide multiple functionalities including compatibilization of the hydrophobic polymer inside the aqueous cytoplasmic environment and its deposition in a form capable of further metabolic utilization. Furthermore, it should also be emphasized that in the core of the granule interesting and not fully elucidated structural features can be found. Primarily, it has been repeatedly reported that inside the granule the polymer occurs in a physical state far different from the thermodynamically favorable one. Isolated *scl*-PHA (such as P(3HB) as the most common representative) are highly crystalline brittle polymers and it was initially believed that this intrinsic tendency to crystallize spontaneously is retained also in vivo (Ellar et al. 1968). Nevertheless, this view was soon challenged by the pioneer structural studies involving intact cells of PHA-producing bacteria. Already in the 1960s, freeze-
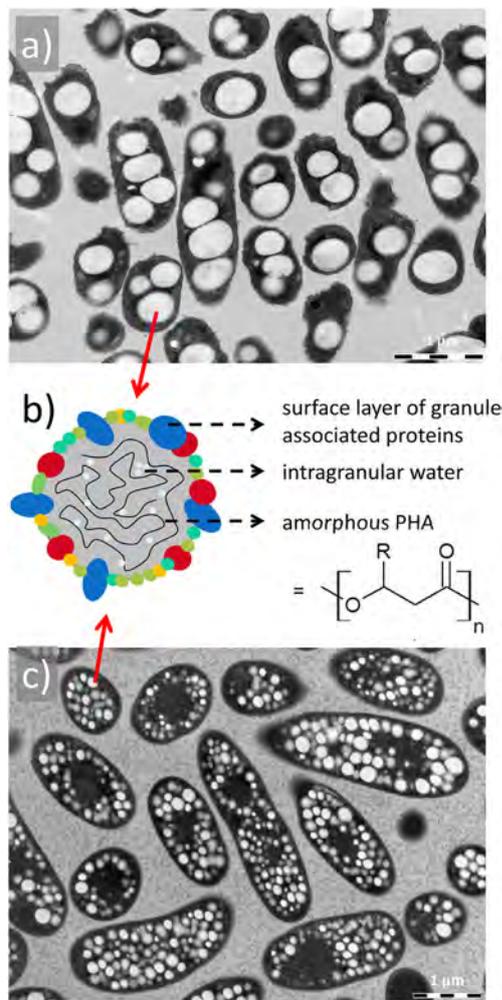
Fig. 2 Morphology of PHA granules in PHA-producing bacteria. **a** PHA granules in the cells of the mesophilic PHA producer *Cupriavidus necator* H16. **b** Schematic representation of fundamental structural features of PHA granules. **c** PHA granules in the cells of the halophilic PHA producer *Halomonas hydrothermalis*

fracture cryo-scanning electron microscopy (cryo-SEM), as the newly developed technique for imaging biological specimens, was utilized to investigate an ultrastructure of PHA-accumulating bacterial cells (van Gool et al. 1969; Remsen 1966). In these works, surprising imaging artifacts related to intracellular PHA granules were first described. In spite of the fact that the sample fracturing is performed at very low temperatures (below − 100 °C), PHA granules exhibited plastic deformation with the polymer elongation substantially higher than 100% (compare with the elongation at break of isolated P(3HB) at about 5% (Doi et al. 1995) leading to formation of characteristic needle-type deformation artifacts (for the more recent example of these deformation, see Fig. 3), which were later repeatedly confirmed by cryo-SEM imaging of a variety of PHA-containing species (Fuller et al. 1992). Nevertheless, the main concern of these cryo-SEM investigations was focused rather on the detailed description of how fracturing

conditions affect the physical features of these deformations (Sudesh et al. 2000b) than on the remarkable discrepancy of the general deformation behavior of intracellular PHA with its contemporary notion of a brittle crystalline material consisting of non-mobile polymer chains.

The idea of the crystalline state of PHA in native granules was finally disproved by the works of Sanders's research group in the late 1980s (Barnard and Sanders 1988). The authors used ^{13}C NMR to analyze intact cells of several PHA-producing bacteria and noticed a surprising resolution of the PHA signal in the spectra, which would be unattainable if the material was crystalline. The authors later conceded that their experiments were successful mainly because they ignored the conventional wisdom which was prejudging NMR to fail in analyzing cellular PHA (Bonthrone et al. 1992). Instead of that, they proved that the polymer in the cell actually behaves like an elastomer with the mobility of chain segments on the timescale of 10^{-7} s (Barnard and Sanders 1989). Furthermore, the authors supported their conclusion also by X-ray diffraction analysis of PHA-producing bacteria, which demonstrated an absence of a significant amount of crystalline polymer in the cells (Amor et al. 1991).

These results immediately raised the question how the crystallization of PHA is prevented in the cell granules. The soon revealed fact that a transfer of genes related to PHA synthase enables formation of apparently fully functional PHA granules in *E. coli* (Schubert et al. 1988) or even in green plants (Poirier et al. 1992) supported the suggestion that the mechanism of the PHA plasticization in vivo must be simple and universal. Since the beginning of this debate, the potential plasticizing role of water was considered. The presence of residual water inside the PHA granules was confirmed experimentally already in the original works of Sanders' group (Barnard and Sanders 1989). Furthermore, Lauzier et al. showed that the content of water in the native granules is at about 5–10% by mass (Lauzier et al. 1992a). At that time, the plasticizing effect of water had already been described for polymers such as nylon (Smith 1976) or poly(vinyl acetate) (Bair et al. 1981). Hence, Barnard and Sanders proposed that hydrogen bonding or dipole-dipole interactions between individual water molecules or localized pockets of water and the ester groups at PHA are responsible for inhibiting chain-chain proximity necessary for the crystallization to occur (Barnard and Sanders 1989). The idea was further elaborated by Lauzier who hypothesized that hydrogen-bonded water stabilizes newly biosynthesized PHA in extended conformation incapable of crystallization in the granule interior (Lauzier et al. 1992a; Lauzier et al. 1992b). Nevertheless, to our best knowledge, no report on stabilization of PHA in amorphous form solely on the basis of its water binding has been published. Furthermore, a simple experimental study on PHA plasticization by di-n-butylphtalate demonstrated that the effect of low-molecular plasticizing agent on crystallization

Fig. 3 Cryo-SEM images of *C. necator* H16 cells suspension quickly frozen and freeze-fractured at − 140 °C. **a** Overall image of fractured tubular sample. Details on **b** intact cell surfaces, **c** freeze-fracture area with characteristic needle-type plastic deformation of PHA granules and on **d** single deformed PHA granule. Reprinted with permission from Sedlacek et al. (2019a)
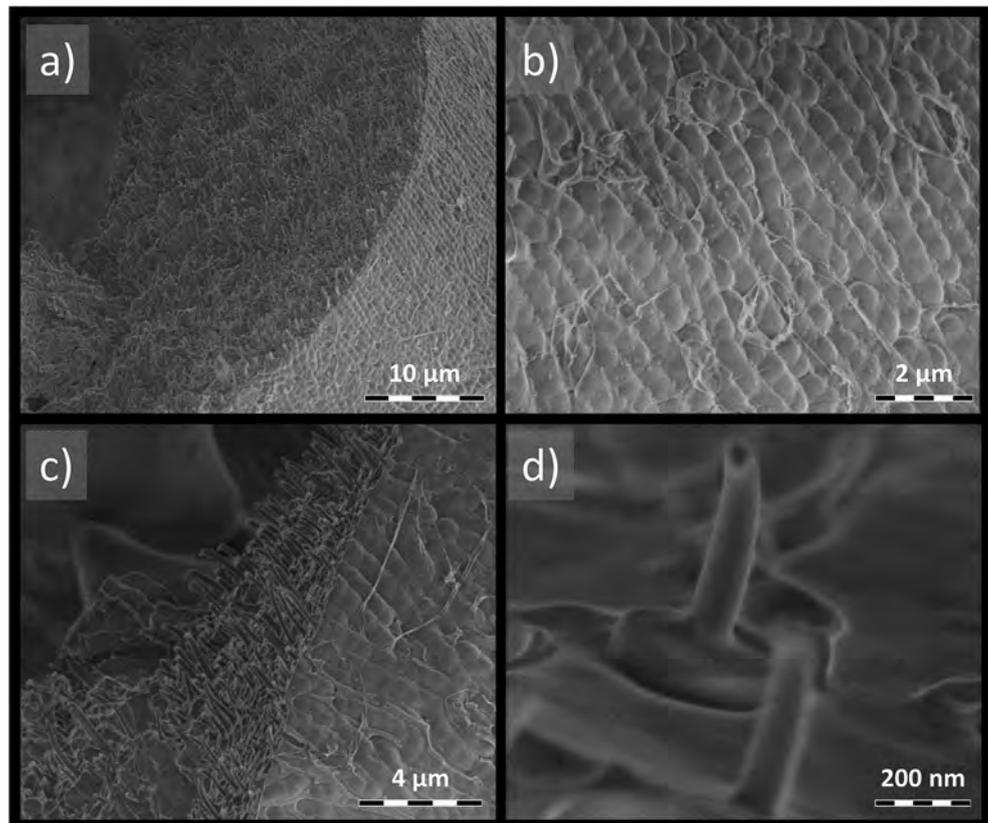
temperature is limited and that plasticization by water or by other cellular material can partially contribute to PHA mobility in vivo, but that also other mechanisms need to come into play to explain the prevention of PHA crystallization (Ceccorulli et al. 1992).

Alternative mechanism of protection of native form of PHA against crystallization was consequently proposed by Sanders' group (Bonthrone et al. 1992) and also by de Koning and Lemstra (1992). In this case, the mobility of PHA in vivo is explained solely on the basis of crystallization kinetics. According to this explanation, crystallization of native PHA, biosynthesized in the amorphous form, is restricted by the low (sub-micron) volume of the polymer granule where the frequency of nucleation as the rate determining step of the crystallization process is extremely low. Horowitz et al. showed that for the polymer crystallizing at the timescale of few minutes in the bulk melt, the crystallization half-life in the 0.25 μm granule will increase to more than 1000 years in the absence of heterogeneous nucleation (Horowitz et al. 1993). This straightforward physicochemical explanation was further experimentally supported by crystallization studies performed with artificial PHA granules (Horowitz and Sanders 1994; Horowitz and Sanders 1995). Nevertheless, the kinetic explanation is not fully consistent with some aspects of PHA crystallization in vivo such as with the observation of crystalline-shell/amorphous-core PHA granules described by Lauzier and

colleagues (Lauzier et al. 1992a) or acknowledgement of the cell dehydration as the necessary crystallization-inducing condition reported by Sedlacek et al. (2019a).

Already since the early studies on amorphous state of PHA in vivo, it has been repeatedly confirmed that the native structure of PHA in the granules can be altered as a result of certain physical or chemical treatment. Merrick and colleagues described the morphological changes (Merrick et al. 1965) and the consequent loss of biological activity of PHA (Merrick and Doudoroff 1964) as a result of various treatments including freezing and thawing, prolonged storage at 4 °C, centrifugation, or extraction with hypochlorite. Barnard and Sanders (1989) later linked this biological inactivation to crystallization of PHA and described similar changes in granules isolated from *Methylobacterium* AM1 after their exposure to low temperature (4 °C or freezing) and to aqueous solutions of acetone. Harrison et al. (1992) attributed a similar effect also to centrifugal force and to selected enzymatic treatments. Two decades later, Porter and Jian in their in situ study on the PHA crystallization kinetics used strongly acidic slurry in order to induce nucleation of PHA in the cells (Porter and Jian 2011a; Porter and Jian 2011b). Following these observations, Sedlacek et al. performed the systematic investigation of the effect of exposure of PHA-producing cells (*C. necator* H16) to various physical stressors (elevated temperature, high osmolarilty, freezing/thawing cycles, acidic pH value) on the

PHA crystallization in vivo (Sedlacek et al. 2019a). Using ATR-FTIR spectroscopy for the monitoring of the free dehydration of the cells at ambient conditions, the authors experimentally confirmed that dehydration was followed by crystallization of intracellular PHA only when the cells were previously stressed; nevertheless, not all the tested stress factors induced this in vivo crystallization. In accordance with the concept of suppressed crystallization rate in limited volume, the crystallization occurred only in those cells where the exposition to the stressor resulted in significant coalescence of the granules as revealed by TEM analysis. On the other hand, a time lag was observed between the dehydration step and subsequent PHA crystallization, which supports the idea of additional plasticizing effect of water. Finally, spectroscopic evidence was provided by the authors that the stress factors active in changes in morphology and crystallinity of the granules were the same ones that caused the most pronounced denaturation of intracellular proteins. These results thus provided an updated idea of stabilization of metastable amorphous form of PHA in the cells by a well-tuned interplay of kinetic effects resulting from sub-micron volume of the granules and the plasticizing effect of residual intra-granular water. In accordance with the current view on the surface structure of the granules (Bresan et al. 2016), the authors propose that
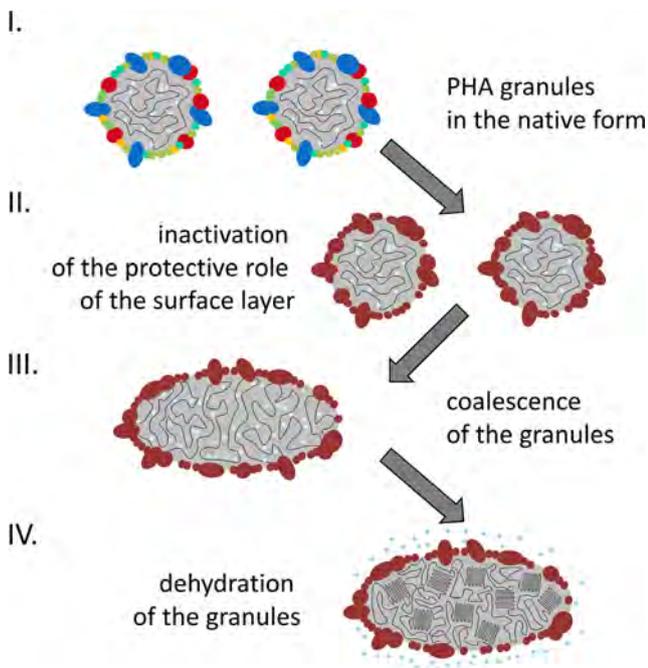
Fig. 4 Updated view of the mechanism protecting amorphous form of PHA in vivo (according to Sedlacek et al. (2019a). Crystallization of PHA in the cells occurs in the system where the exposure of the cells to a physical or chemical stressor induces inactivation of the protective function of granule-assisted proteins in the surface layer of PHA granules (step II), after the coalescence of the granules increases the effective volume of PHA (step III) if the cells are dried and the residual water is excluded from the granule with the subsequent loss of its plasticizing effect (step IV)

granule-associated proteins play an essential role in keeping both stabilization factors working (see Fig. 4). This conception is supported by several works reporting a strong influence of phasins on stabilization effect of PhaP against coalescence of separated PHA granules (Pötter et al. 2002; Wieczorek et al. 1995).

Biological and biophysical consequences of the presence of PHA granules in bacterial cells

Aside from the mechanical and physicochemical consequences of the elastomeric nature of PHA, numerous reports have stressed also the biological importance of the physical state of PHA in vivo. First of all, it was described long time ago that PHA depolymerases, which catalyze mobilization of PHA in the cells, are specific only to amorphous PHA with no ability to cleave crystalline PHA (Ellar et al. 1968; Merrick et al. 1999). This well-known fact restricts the capability to fill the primary role of a storage material exclusively to amorphous polymer and gives the reason for terms "native" and "denatured" PHA commonly used currently as synonyms for amorphous and crystalline PHA, respectively (Gebauer and Jendrossek 2006).

Nevertheless, recent studies show that the biological impact of the unique physical state of native PHA is in fact more general than previously considered. It was proposed by Obruca et al. that the flexibility of the PHA chains in its native intra-granular state may help bacterial cells to endure shearing deformations associated with growth of extracellular ice crystals during freezing (Obruca et al. 2016b) as well as during cell dehydration caused by a hyperosmotic environment (Obruca et al. 2017). Furthermore, the results of a detailed morphological study performed by the same research group also indicated that the liquid-like behavior supports and partially repairs the integrity of cytoplasmic membranes of bacterial cells exposed to suddenly induced hypertonic (Obruca et al. 2017) and hypotonic (Sedlacek et al. 2019b) conditions. The biological relevance of the native PHA state was also emphasized by the results of cell viability tests involved by Sedlacek et al. in their stress-induced crystallization study (Sedlacek et al. 2019a). In this study, the lowest number of cultivable cells was reported for bacterial cultures exposed to stressors, which strongly induced PHA granules aggregation, such as high temperature or strongly acidic conditions. The authors proposed that aggregation and crystallization of the granules may impede division of the bacterial cells. It can hence be seen from the previous text that even the morphology and physicochemical state of the PHA chains in the granules must be considered as an important piece of the puzzle representing the complete view on the biological role of PHA.

Aside from the role of the physical state of the polymer, the above referenced studies also described how the general changes in cell morphology and biophysics, caused by the

presence of PHA granules therein, are involved in protection of the cells against various types of adverse conditions. For instance, it was demonstrated that PHA protects non-halophilic bacteria against precarious osmotic up-shock; PHA-rich *C. necator* cells were expediently resistant to hypertonic challenge and revealed less plasmolysis when exposed to hypertonic media; in contrast, massive plasmolysis destroyed the cytoplasmic membrane and resulted in leakage of the cytoplasm of PHA-negative mutants of the same species. When present, PHA granules mechanistically serve as "internal scaffolds," which prevent bacteria from such detrimental plasmolysis (Obruca et al. 2017). In addition to osmotic up-shock, it was shown that PHA granules protect also against osmotic down-shock in hypotonic media, as described both for the halophilic bacterium *Halomonas halophila* and for the non-halophile *C. necator*. For both strains, capability to keep cell integrity when suddenly exposed to osmotic down-shock was substantially enhanced when PHA granules were stored in cells. The protective function of PHA granules in *C. necator* during osmotic up-shock was probably associated with less cytoplasm membrane damage caused by plasmolysis, which in turn harnished these cells with a survival advantage during a subsequent osmotic up-shock. In contrast, PHA-free cells suffered from massive hypotonic lysis when osmotic up- and subsequent down-shock were suddenly induced.

Furthermore, mechanistic description of the cryo-protective effect of P(3HB) in survival ability of bacteria under freezing conditions was accomplished by Obruca et al. by cryo-SEM, which allows studying the impact of PHA granules on the cells' mechanical properties, on solutes' mobility in the cytoplasm, and the cellular response to sudden temperature changes such as drying, freezing, or thawing. During freezing-and-thawing cycles, 3HB, the monomer from which the homopolyester P(3HB) is built up, acts as a strong cryo-protectant for enzymes, yeasts, and the PHA producer *C. necator*. For PHA-positive cultures, the survival rates after freezing were significantly higher than for PHA-negative mutants. High levels of 3HB in *C. necator* cells, which simultaneously produce and degrade P(3HB), were proposed by the authors to predominantly (but not exclusively!) cause this protective effect. Nevertheless, the reported results actually indicate that some biophysical mechanisms of the protection are involved as well. Cryo-SEM observations also showed that PHA granules maintain their expedient flexibility even at extremely low temperature, suggesting that these inclusions also prevent massive cellular damage resulting from the adverse effect of intracellular ice crystals; these effects encompass generation of gas bubbles, physical membrane damage, or even detriments of organelles. The presence of PHA granules covered with a surface layer of hydrated proteins probably changes the adhesion forces between water molecules and cellular components, resulting in a higher rate of water transport through membranes. This causes a faster discharge of water from cells harboring PHA granules during drying or freezing, which keeps intracellular formation of ice crystals to a minimum (Obruca et al. 2016a).

Last but not least, it was experimentally confirmed that the presence of PHA granules helps to protect cells against UV radiation. In a study by Slaninova et al. (2018), it was described that PHA granules efficiently scatter UV radiation, which provides a substantial UV-protective effect for bacterial cells and, moreover, decreases the intracellular level of reactive oxygen species in UV-challenged cells. In this study, *Cupriavidus necator* H16 producing PHA granules has much higher resistance to UV exposition than its non-accumulating mutant *Cupriavidus necator* PHB^{-4}. The protective properties of the PHA granules are enhanced by the fact that granules specifically bind to DNA, which in turn provides shield-like protection of DNA as the most UV-sensitive molecule. Similar findings were recently reported by Tribelli et al. for the psychrophilic bacterium *Pseudomonas extremaustralis* (Tribelli et al. 2019).

PHA in phototrophic prokaryotes

In several aspects, cyanobacteria are an extremely important group of organisms: in paleo-biology, as they were the first massive oxygen producers (Stanley 1999); in ecology, as they are responsible for 20–30% of the global photosynthetic synthesis of organic carbon (McArthur 2006; Stal 2012); in terms of evolutionary adaptation, as they have multiple photosynthetically active pigments while able to fix nitrogen (Mitsui et al. 1986) and can withstand drought, UV radiation, and extreme temperatures (Bhaya et al. 2000); and in biotechnology, as they can be grown strictly photo-autotrophically while producing different lipids, amino acids, fatty acids, some vitamins, and bioactive components (including, but not only toxins) for feed, food, and pharmaceutical applications (Masojidek and Prasil 2010; Meixner 2018).

Similar to heterotrophic bacteria, numerous cyanobacterial strains accumulate PHA, preferably the homopolyester P(3HB), in their cells in the form of granules (Ansari and Fatma 2016; Asada et al. 1999). As mentioned before, the primarily role of P(3HB) is the storage of carbon and energy (Sudesh et al. 2001). Similar to other prokaryotes, cyanobacterial P(3HB) synthesis is stimulated by unfavorable environmental conditions, such as nitrogen or phosphorous starvation, but requiring a surplus of energy and a carbon source (Panda et al. 2005). With emphasis on cyanobacteria-specific characteristics to morphology and to their extraordinary metabolic flexibility (photosynthesis, nitrogen fixation), the role of P(3HB) is expected to be highly complex. In contrast to most PHA-producing heterotrophs, cyanobacteria accumulate glycogen, lipids, and proteins besides P(3HB) in amounts and in relations to each other which substantially depend on the species and on the cultivation conditions

(Koch et al. 2019). At heterotrophic growth, for example, the P(3HB) content in cyanobacteria can reach similar values as in other bacteria, while at photo-autotrophic growth typically 10–15 but rarely ever more than 25% P(3HB) in the biomass is reached (Troschl et al. 2017).

While the cyanobacterial P(3HB) synthesis pathway does not differ from other heterotrophic bacteria, the involved enzymes and their respective genes are different in number, types, and location in the genome (Taroncher-Oldenburg et al. 2000) (see Fig. 5). Considering the sheer number of cyanobacteria species that can produce P(3HB) (Ansari and Fatma 2016), the knowledge about P(3HB) synthesis kinetics for each of them is far less profound than it is, for example, for *C. necator* (Haas et al. 2017; Yamane 1993).

While cyanobacteria genera such as *Synechocystis*, *Synechococcus*, and *Gloeothece* are spherical and single cellular, others such as *Anabaena*, *Calothrix*, *Chlorogloeopsis*, or *Nostoc* grow in irregular or filamentous aggregates, making the first group the preferred targets for deeper investigations, simply by allowing to take a representative sample from a bigger culture volume for analysis. Example images provided in Fig. 6 may give an impression about why it is almost impossible to accurately monitor the growth and development of aggregate forming cyanobacteria. From our own observations in *Synechocystis* sp. cultures (unpublished data), we experienced a wide variety of physiological stages of cells simultaneously present in each culture, e.g., containing no, a single or multiple P(3HB) granules. While growth and P(3HB) synthesis can be measured from a culture over time, the development of individual cells remains widely unclear.

It is expected that intracellular P(3HB) has more roles for cyanobacteria than just carbon and energy storage (Obruca et al. 2017; Pavez et al. 2009), but this is currently not proven. With respect to physiological differences, such as the lower P(3HB) content and its relation to glycogen and with respect to morphological differences, such as the required space for thylakoids, the total effect of P(3HB) may be weaker in cyanobacteria than it is in high accumulating heterotrophic bacteria. An example of the cellular distribution of P(3HB) granules in 8 weeks long cultivated *Synechocystis* culture
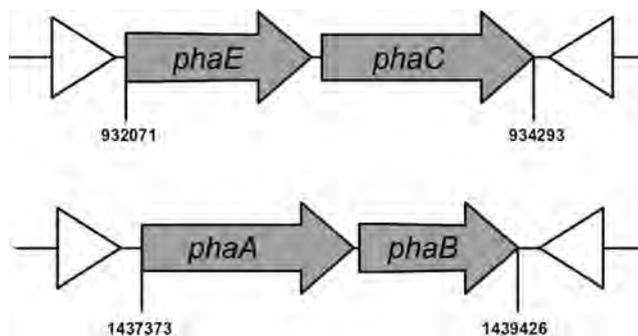
Fig. 5 Location of the four P(3HB) synthesis genes in *Synechocystis* PCC6803, reproduced from Silvestrini et al. (2016)

(not exceeding 20% P(3HB) in the biomass) is shown in Fig. 7. The granules are unevenly located in a small part of the cells, suggesting the occupation of a certain cell volume by other components.

Exploitation of cyanobacterial P(3HB) production is currently not done on industrial scale, not only for lack of knowledge about biochemical details, but for reasons of comparably slower growth and lower P(3HB) content per cell mass, resulting in an unacceptable high product price (Panuschka et al. 2019). Research activities, therefore, focus on either increased cellular P(3HB) synthesis and accumulation rates (Khetkorn et al. 2016), on increased overall biomass growth by optimization of media and reactor designs (Pulz 2001), or on utilization of production residues and waste streams as inexpensive nutrient resources (Meixner et al. 2016). Finally, a holistic approach is needed, taking ecological, economical, technical, and ethical aspects into account to best possible support a sustainable living (Koller et al. 2017). Undoubtedly, within those aspects, a better understanding of the evolution of prokaryotic PHA synthesis and of its ecological role in cyanobacteria is the key.

The importance of PHA granules for extremophiles

The specific role of PHA in survival and adaptation of microorganisms to adverse conditions is further illustrated by the well-known fact that a plethora of microbes adapted to life in various extreme environments like hot springs, bio-trickling filters, glaciers, salterns, or chemically polluted habitats have shown potential for PHA biosynthesis. A growing number of studies accomplished during the last couple of years suggest a unique evolutionary role of PHA biosynthesis in that adaptation to extreme environments (Koller et al. 2018).

Among different types of extremophiles, many representatives of extremely halophiles are readily studied PHA producers. Generally, PHA accumulation seems to be a widespread feature among different prokaryotic strains thriving in highly saline environments, including both extremely halophilic eubacteria and haloarchaea. This suggests that PHA accumulation plays a vital role in osmotic adaptation of microorganisms. Sedlacek et al. (2019b), studying the halophilic strain *H. halophila*, reported that hypo-osmotically burdened PHA-rich cells better maintained cell integrity compared to PHA-poor cells. Under hypertonic conditions, this moderately halophile *H. halophila* accumulates high quantities of organic osmolytes to compensate osmotic imbalance. When suddenly exposed to osmotic down-shock, halophiles are much more sensitive to a hypo-osmotic damage and hypotonic lysis than non-halophiles. Since hydrophobic PHA granules represent a substantial portion of the intracellular volume, the total amount of osmolytes per cell will be significantly lower in PHA-rich cells, which facilitates the quick adaptation from hyper- to hypotonic conditions. These findings substantiated
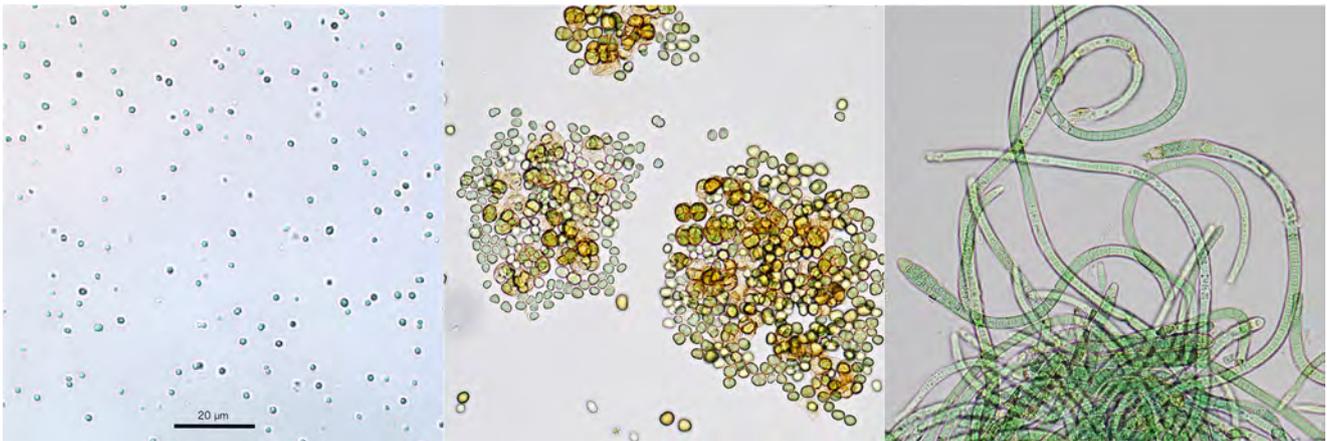
Fig. 6 Morphology of three selected cyanobacteria genera which are able to accumulate P(3HB) while growing under non-sterile conditions in bench-scale photobioreactors. All photos are in the same scale, from left to right: *Synechocystis*, *Chlorogloeopsis*, *Calothrix*

previous reports for the extremely halophilic archaeon *Haloquadratum walsbyi*, cells of which immediately lyse in distilled water and require a minimum of about 140 g/L salts for growth. This flat square-shaped haloarchaeon was grown aerobically under illumination on a medium containing about 200 g/L NaCl; detailed studies of cellular morphology via atomic force microscopy showed strong corrugation of the cellular surface due to the presence of tightly packed PHA granules. Already in this study, it was supposed that the primary function of these PHA granules was to reduce the cytosol volume to minimize the energy demand of cells for osmotic homeostasis; hence, they display an essential function for the cells to manage high salinity (Saponetti et al. 2011).

As an example for cryophilic (psychrophilic) PHA-producing strains, *Pseudomonas* sp. 14-3, isolated from samples taken in the Antarctic region, was investigated by Ayub et al. It was shown that the *phaRBAC* genes of this strain, responsible for PHA biosynthesis, are located on the same isolated gene region where also those genes presumably contributing to its high adaptability to low temperature are placed. To study the impact of PHA biosynthesis on the strain's adaptability to low temperature, its wild-type and PHA-negative mutant (deletion of the PHA synthase encoding gene) were compared. The PHA-negative mutant strain was more prone to freezing than the PHA-accumulating wild-type organisms; the mutant did not grow at all at 10 °C. It was suggested that the presence of PHA granules was essential for the strain to adequately respond to the oxidative stress caused by the low temperature. Importantly, for the mutant, sudden cold shock resulted in prompt decrease of the intracellular NADPH content and NADH/NAD$^+$ ratio, while sudden cold shock of the PHA-positive wild-type initiated sudden PHA degradation, but no tremendous loss of reduction equivalents due to regeneration of reducing power by PHA degradation. As a consequence, lipid peroxidation at low temperature was 25 times higher in the mutant strain than in the wild type. Hence, oxidative stress related to low temperature is relieved by degrading PHA due to generation of the needed reduction potential (Ayub et al. 2009). The importance of PHA for bacteria inhabiting cold environments was also confirmed by numerous studies dealing with composition of microflora occurring in niches constantly exposed to low and
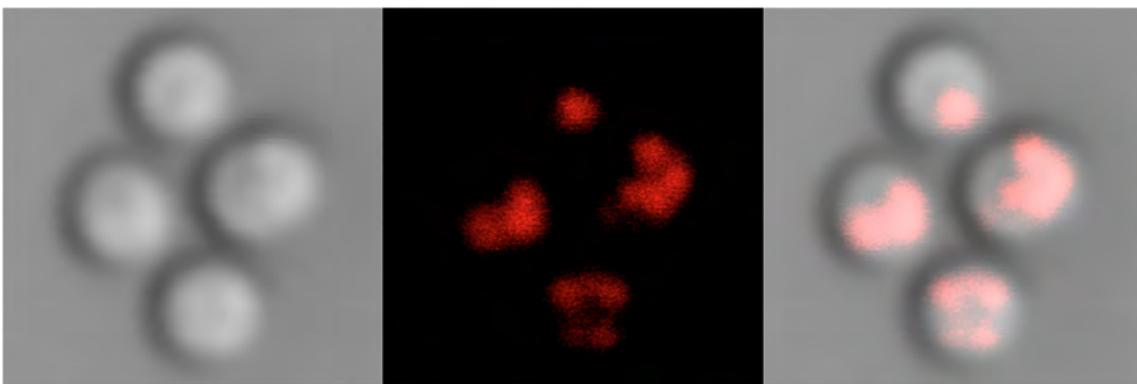
Fig. 7 Microscopy images of *Synechocystis* in bright field mode (left), in fluorescence mode after Nile Red staining (middle) and an overlay of both (right). × 1000 magnification, cell size is ca. 3.5–4 μm

even sub-zero temperatures. Numerous PHA producers were detected in Antarctic soil (Goh and Tan 2012), subarctic sea ice in Greenland (Kaartokallio et al. 2013), Antarctic freshwater (Ciesielski et al. 2014), the Baltic Sea (Pärnänen et al. 2015), or Pangi-Chamba trans-Himalayan region (Kumar et al. 2018).

At the first sight, biotechnological implementation of thermophilic production strains seems to be impractical because of technological issues associated with high temperature cultivations, e.g., reduced oxygen solubility at elevated temperatures and high energy required to maintain high cultivation temperature. Surprisingly, when thermophiles are used in bioreactor cultivations, these processes often are of considerable energy efficiency, mainly due to reduced energy-demanding cooling requirements. Additionally, cultivations of thermophiles are considered "self-heating systems" because heat energy is generated by their metabolism; this phenomenon is especially observed for large-scale cultivations with high cell density. Further, also the bioreactor stirring system produces heat energy, which additionally contributes to the heat energy supply to the cultivation. Combination of all these effects reduces both heating and cooling costs. As a further advantage, also energy-demanding sterility precautions (sterilization of equipment and media components) can be reduced to a minimum when working with thermophilic organisms (Ibrahim et al. 2010); this benefit is analogous to the reduced energy costs for sterilization when using extremely halophiles like, e.g., *Haloferax mediterranei* (Hermann-Krauss et al. 2013). Among the potential thermophilic producers for biotechnological production of PHA, *Chelatococcus daeguensis* TAD1 can be considered an auspicious candidate for PHA production from abundantly available inexpensive raw materials on an industrial scale. Improved productivity of this thermophilic strain, isolated from bio-layers of a bio-trickling NO$_x$ removal filter, as compared to its mesophilic relative *Chelatococcus* sp. strain MW10 was reported (Ibrahim and Steinbüchel 2010; Xu et al. 2014). However, as compared to halophiles or psychrophiles, PHA biosynthesis was not reported for many thermophiles, which indicates either that PHA biosynthesis is not very common among thermophiles or that thermophilic PHA biosynthesis is underinvestigated. To isolate novel promising thermophilic PHA producers, Pernicova et al. (2020) developed a novel isolation approach. Since conventional colony-Nile Red staining provided false positive signals in thermophiles, a mixed consortium was enriched by PHA-producing thermophiles by application of osmotic challenge relying on the osmoprotective function of PHA granules. PHA-positive colonies were subsequently identified by fast and reliable ATR-FTIR analysis. In this work, several potentially promising thermophilic PHA producers belonging to genus *Bacillus*, *Aneurinibacillus*, and *Chelatococcus* were gained.

Conclusions

As was shown in this review, the biological role of PHA is very complex and universal among diverse genera of prokaryotes, as can be illustrated by the fact that PHA production is common for such fundamentally different groups of microorganisms as heterotrophs and autotrophs on the one hand, or mesophiles and extremophiles on the other hand. Aside from the generally accepted storage function, recent experimental studies have decidedly elucidated that accumulation of PHA in the cells provides microorganisms with higher stress survival and robustness. Mechanisms involved in the PHA protective role combine various factors including unique cyclic character of PHA metabolism and its interconnection with other crucial metabolic pathways, multiple biological functions of PHA granules associated proteins and remarkable morphological and biophysical properties of native PHA granules. The understanding of the particular contributions of the individual mechanisms in the PHA stress-shielding is of the great interest not only from the fundamental scientific point of view, but it has also very promising potential in improving sustainability and comprehensibility of various biotechnological processes including, but not limited to, PHA production.

Compliance with ethical standards

Conflict of interest The authors declare that they have no conflict of interest.

Ethical approval This article does not contain any studies with human participants or animals performed by any of the authors.

References

Amor SR, Rayment T, Sanders JKM (1991) Poly (hydroxybutyrate) *in vivo*: NMR and x-ray characterization of the elastomeric state. Macromolecules 24(16):4583–4588. https://doi.org/10.1021/ma00016a017

Ansari S, Fatma T (2016) Cyanobacterial polyhydroxybutyrate (PHB): screening, optimization and characterization. PLoS One 11(6):1–20. https://doi.org/10.1371/journal.pone.0158168

Asada Y, Miyake M, Miyake J, Kurane R, Tokiwa Y (1999) Photosynthetic accumulation of poly-(hydroxybutyrate) by cyanobacteria—the metabolism and potential for CO$_2$ recycling. Int J Biol Macromol 25:37–42. https://doi.org/10.1016/S0141-8130(99)00013-6

Ayub ND, Tribelli PM, López NI (2009) Polyhydroxyalkanoates are essential for maintenance of redox state in the Antarctic bacterium *Pseudomonas sp.* 14-3 during low temperature adaptation. Extremophiles 13(1):59–66. https://doi.org/10.1007/s00792-008-0197-z

Bair HE, Johnson GE, Anderson EW, Matsuoka S (1981) Non equilibrium annealing behavior of poly (vinyl acetate). Polym Eng Sci 21(14):930–935. https://doi.org/10.1002/pen.760211410

Barnard GN, Sanders JKM (1988) Observation of mobile poly (β-hydroxybutyrate) in the storage granules of *Methylobacterium* AM1 by in vivo 13C-NMR spectroscopy. FEBS Lett 231(1):16–18. https://doi.org/10.1016/0014-5793(88)80693-8

Barnard GN, Sanders JKM (1989) The poly-beta-hydroxybutyrate granule in vivo. A new insight based on NMR spectroscopy of whole cells. J Biol Chem 264(6):3286–3291

Batista MB, Teixeira CS, Sfeir MZT, Alves LPS, Valdameri G, Pedrosa FO, Sassaki GL, Steffens MBR, de Souza EM, Dixon R, Müller-Santos M (2018) PHB biosynthesis counteracts redox stress in *Herbaspirillum seropedicae*. Front Microbiol 9:472. https://doi.org/10.3389/fmicb.2018.00472

Bergersen FJ, Peoples MB, Turner GL (1991) A role for poly-(beta)-hydroxybutyrate in bacteroids of soybean root nodules. Proc R Soc London B 245:59–64. https://doi.org/10.1098/rspb.1991.0088

Bhaya D, Schwarz R, Grossman AR (2000) Molecular responses to environmental stress. In: Whitton BA, Potts MK (eds) The ecology of Cyanobacteria: their diversity in time and space. Academic Publishers, New York. https://doi.org/10.1007/0-306-46855-7

Bonthrone KM, Clauss J, Horowitz DM, Hunter BK, Sanders JKM (1992) The biological and physical chemistry of polyhydroxyalkanoates as seen by NMR spectroscopy. FEMS Microbiol Rev 9(2–4):269–277. https://doi.org/10.1016/0378-1097(92)90320-N

Breedveld MW, Dijkema C, Zevenhuizen LPTM, Zehnder AJB (1993) Response of intracellular carbohydrates to a NaCl shock in *Rhizobium leguminosarum* biovar trifolii TA-1 and *Rhizobium meliloti* SU-47. J Gen Microbiol 139:3157–3163. https://doi.org/10.1099/00221287-139-12-3157

Bresan S, Sznajder A, Hauf W, Forchhammer K, Pfeiffer D, Jendrossek D (2016) Polyhydroxyalkanoate (PHA) granules have no phospholipids. Sci Rep 6:26612. https://doi.org/10.1038/srep26612

Ceccorulli G, Pizzoli M, Scandola M (1992) Plasticization of bacterial poly (3-hydroxybutyrate). Macromolecules 25(12):3304–3306. https://doi.org/10.1021/ma00038a045

Chien C-C, Wang L-J, Lin W-R (2014) Polyhydroxybutyrate accumulation by a cadmium-resistant strain of *Cupriavidus taiwanensis*. J Taiwan Instit Chem Eng 45:1164–1169. https://doi.org/10.1016/j.jtice.2014.02.004

Ciesielski S, Górniak D, Możejko J, Świątecki A, Grzesiak J, Zdanowski M (2014) The diversity of bacteria isolated from Antarctic freshwater reservoirs possessing the ability to produce Polyhydroxyalkanoates. Curr Microbiol 69:594–603. https://doi.org/10.1007/s00284-014-0629-1

De Koning GJM, Lemstra PJ (1992) The amorphous state of bacterial poly [(R)-3-hydroxyalkanoate] in vivo. Polymer 33(15):3292–3294. https://doi.org/10.1016/0032-3861(92)90249-V

Doi Y, Shiro K, Hideki A (1995) Microbial synthesis and characterization of poly (3-hydroxybutyrate-co-3-hydroxyhexanoate). Macromolecules 28(14):4822–4828. https://doi.org/10.1021/ma00118a007

Ellar D, Lundgren DG, Okamura K, Marchessault RH (1968) Morphology of poly-β-hydroxybutyrate granules. J Mol Biol 35(3):489–502. https://doi.org/10.1016/S0022-2836(68)80009-9

Encarnación S, del Carmen VM, Dunn MF, Dávalos A, Mendoza G, Mora Y, Mora J (2002) AniA regulates reserve polymer accumulation and global protein expression in *Rhizobium etli*. J Bacteriol 184:2287–2295. https://doi.org/10.1128/jb.184.8.2287-2295.2002

Fuller CR, O'Donnell JP, Saulnier J, Redlinger TE, Foster J, Lenz RW (1992) The supramolecular architecture of the polyhydroxyalkanoate inclusions in *Pseudomonas oleovorans*. FEMS Microbiol Rev 9(2–4):279–288. https://doi.org/10.1016/0378-1097(92)90321-E

Gebauer B, Jendrossek D (2006) Assay of poly (3-hydroxybutyrate) depolymerase activity and product determination. Appl Environ Microbiol 72(9):6094–6100. https://doi.org/10.1128/AEM.01184-06

Goh YS, Tan IKP (2012) Polyhydroxyalkanoate production by antarctic soil bacteria isolated from Casey Station and Signy Island. Microbiol Res 167:211–219. https://doi.org/10.1016/j.micres.2011.08.002

Goh L-K, Purama RK, Sudesh K (2014) Enhancement of stress tolerance in the polyhydroxyalkanoate producers without mobilization of the accumulated granules. Appl Biochem Biotechnol 172:1585–1598. https://doi.org/10.1007/s12010-013-0634-z

Haas C, El-Najjar T, Virgolini N, Smerilli M, Neureiter M (2017) High cell-density production of poly(3-hydroxybutyrate) in a membrane bioreactor. New Biotechnol 37:117–122. https://doi.org/10.1016/j.nbt.2016.06.1461

Harrison STL, Chase HA, Amor SR, Bonthrone KM, Sanders JKM (1992) Plasticization of poly (hydroxybutyrate) in vivo. Int J Biol Macromol 14(1):50–56. https://doi.org/10.1016/S0141-8130(05)80020-0

Hermann-Krauss C, Koller M, Muhr A, Fasl H, Stelzer F, Braunegg G (2013, 2013) Archaeal production of polyhydroxyalkanoate (PHA) co-and terpolyesters from biodiesel industry-derived by-products. Archaea. https://doi.org/10.1155/2013/129268

Horowitz DM, Sanders JKM (1994) Amorphous, biomimetic granules of polyhydroxybutyrate: preparation, characterization, and biological implications. J Am Chem Soc 116(7):2695–2702. https://doi.org/10.1021/ja00086a001

Horowitz DM, Sanders JKM (1995) Biomimetic, amorphous granules of polyhydroxyalkanoates: composition, mobility, and stabilization in vitro by proteins. Can J Microbiol 41(13):115–123. https://doi.org/10.1139/m95-177

Horowitz DM, Clauss J, Hunter BK, Sanders JKM (1993) Amorphous polymer granules. Nature 363:23–23. https://doi.org/10.1038/363023a0

Ibrahim MH, Steinbüchel A (2010) High-cell-density cyclic fed-batch fermentation of a poly (3-hydroxybutyrate)-accumulating thermophile, *Chelatococcus sp.* strain MW10. Appl Environ Microbiol 76(23):7890–7895. https://doi.org/10.1128/AEM.01488-10

Ibrahim MHA, Willems A, Steinbüchel A (2010) Isolation and characterization of new poly(3HB)-accumulating star-shaped cell-aggregates-forming thermophilic bacteria. J Appl Microbiol 109(5):1579–1590. https://doi.org/10.1111/j.1365-2672.2010.04786.x

Jendrossek D (2005) Fluorescence microscopical investigation of poly (3-hydroxybutyrate) granule formation in bacteria. Biomacromolecules 6(2):598–603. https://doi.org/10.1021/bm049441r

Jendrossek D (2007) Peculiarities of PHA granules preparation and PHA depolymerase activity determination. Appl Microbiol Biotechnol 74(6):1186–1196. https://doi.org/10.1007/s00253-007-0860-9

Jendrossek D (2009) Polyhydroxyalkanoate granules are complex subcellular organelles (carbonosomes). J Bacteriol 191(10):3195–3202. https://doi.org/10.1128/JB.01723-08

Jendrossek D, Pfeiffer D (2014) New insights in the formation of polyhydroxyalkanoate granules (carbonosomes) and novel functions of poly (3-hydroxybutyrate). Environ Microbiol 16(8):2357–2373. https://doi.org/10.1111/1462-2920.12356

Jendrossek D, Selchow O, Hoppert M (2007) Poly (3-hydroxybutyrate) granules at the early stages of formation are localized close to the cytoplasmic membrane in *Caryophanon latum*. Appl Environ Microbiol 73(2):586–593. https://doi.org/10.1128/AEM.01839-06

Kaartokallio H, Søgaard DH, Norman L, Rysgaard S, Tison JL, Delille B, Thomas DN (2013) Short-term variability in bacterial abundance, cell properties, and incorporation of leucine and thymidine in subarctic sea ice. Aquat Microb Ecol 71:57–73. https://doi.org/10.3354/ame01667

Kadouri D, Burdman S, Jurkevitch E, Okon Y (2002) Identification and isolation of genes involved in poly(β-hydroxybutyrate) biosynthesis in *Azospirillum brasilense* and characterization of a phbC mutant. Appl Environ Microbiol 68:2943–2949. https://doi.org/10.1128/AEM.68.6.2943-2949.2002

Kadouri D, Jurkevitch E, Okon Y (2003a) Involvement of the reserve material poly-beta-hydroxybutyrate in *Azospirillum brasilense* stress endurance and root colonization. Appl Environ Microbiol 69:3244–3250. https://doi.org/10.1128/AEM.69.6.3244-3250.2003

Kadouri D, Jurkevitch E, Okon Y (2003b) Poly beta-hydroxybutyrate depolymerase (PhaZ) in *Azospirillum brasilense* and characterization of a phaZ mutant. Arch Microbiol 180:309–318. https://doi.org/10.1007/s00203-003-0590-z

Kadouri D, Jurkevitch E, Okon Y, Castro-Sowinski (2005) Ecological and agricultural significance of bacterial polyhydroxyalkanoates. Crit Rev Microbiol 31(2):55–67. https://doi.org/10.1080/10408410590899228

Kamnev AA, Tugarova AV, Antonyuk LP, Tarantilis PA, Polissiou, Gardiner PHE (2005) Effects of heavy metals on plant-associated rhizobacteria: Comparison of endophytic and non-endophytic strains of Azospirillum brasilense. J Trace Elem Med Biol 19:91–95. https://doi.org/10.1016/j.jtemb.2005.03.002

Kessler B, Witholt B (2001) Factors involved in the regulatory network of polyhydroxyalkanoate metabolism. J Biotechnol 86(2):97–104. https://doi.org/10.1016/S0168-1656(00)00404-1Get

Khetkorn W, Incharoensakdi A, Lindblad P (2016) Enhancement of poly-3-hydroxybutyrate production in *Synechocystis sp.* PCC 6803 by overexpression of its native biosynthetic genes. Bioresour Technol 214:761–768. https://doi.org/10.1016/j.biortech.2016.05.014

Kim DY, Hyung WK, Moon GC, Young HR (2007) Biosynthesis, modification, and biodegradation of bacterial medium-chain-length polyhydroxyalkanoates. J Microbiol 45(2):87–97

Koch M, Doello S, Gutekunst K, Forchhammer K (2019) PHB is produced from glycogen turn-over during nitrogen starvation in *Synechocystis sp.* PCC 6803. Int J Mol Sci 20(8):1942. https://doi.org/10.3390/ijms20081942

Koller M, Marsalek L, de Sousa Dias MM, Braunegg G (2017) Producing microbial polyhydroxyalkanoate (PHA) biopolyester in a sustainable manner. New Biotechnol 37:24–38. https://doi.org/10.1016/j.nbt.2016.05.001

Koller M, Obruca S, Pernicova I, Braunegg G (2018) Physiological, kinetic, and process engineering aspects of polyhydroxyalkanoate biosynthesis by extremophiles. In: Williams H, Kelly P (eds) Polyhydroxyalkanoates: Biosynthesis, Chemical Structures and Applications. Nova Science Publishers Inc., pp 1–70

Koskimäki JJ, Kajula M, Hokkanen J, Ihantola EL, Kim JH, Hautajärvi H, Hankala E, Soukas M, Pohjanen J, Podolich O, Kozyrovska N, Turpeinen A, Pääkkönen M, Mattila S, Campbell BC, Pirttilä AM (2016) Methyl-esterified 3-hydroxybutyrate oligomers protect bacteria from hydroxyl radicals. Nat Chem Biol 12(5):332–338. https://doi.org/10.1038/nchembio.2043

Kumar V, Thakur VA, Kumar S, Singh D (2018) Bioplastic reservoir of diverse bacterial communities revealed along altitude gradient of Pangi-Chamba trans-Himalayan region. FEMS Microbiol Lett 365:14, art. no. fny144. https://doi.org/10.1093/femsle/fny144

Lauzier C, Revol J-F, Marchessault RH (1992a) Topotactic crystallization of isolated poly (β-hydroxybutyrate) granules from *Alcaligenes eutrophus*. FEMS Microbiol Rev 9(2–4):299–310. https://doi.org/10.1016/0378-1097

Lauzier C, Marchessault RH, Smith P, Chanzy H (1992b) Structural study of isolated poly (β-hydroxybutyrate) granules. Polymer 33(4):823–827. https://doi.org/10.1016/0032-3861(92)90343-U

Martin DD, Bartlett DH, Roberts MF (2002) Solute accumulation in the deep-sea bacterium *Photobacterium profundum*. Extremophiles 6:507–514. https://doi.org/10.1007/s00792-002-0288-1

Masojidek J, Prasil O (2010) The development of microalgal biotechnology in the Czech Republic. J Ind Microbiol Biotechnol 37(12):1307–1317. https://doi.org/10.1007/s10295-010-0802-x

McArthur JV (2006) Microbial ecology: an evolutionary approach. Elsevier Acad Press, Amsterdam. https://doi.org/10.1093/plankt/fbl013

Meixner K (2018) Integrating cyanobacterial poly(3-hydroxybutyrate) production into biorefinery concepts. Disertation, University of Natural Resources and Life Sciences, Vienna

Meixner K, Fritz I, Daffert C, Markl K, Fuchs W, Drosg B (2016) Processing recommendations for using low-solids digestate as nutrient solution for poly-ß-hydroxybutyrate production with *Synechocystis salina*. J Biotechnol 240:61–67. https://doi.org/10.1016/j.jbiotec.2016.10.023

Merrick JM, Doudoroff M (1964) Depolymerization of poly-β-hydroxybutyrate by an intracellular enzyme system. J Bacteriol 88(1):60–71

Merrick JM, Lundgren DG, Pfister RM (1965) Morphological changes in poly-β-hydroxybutyrate granules associated with decreased susceptibility to enzymatic hydrolysis. J Bacteriol 89(1):234–239

Merrick JM, Steger R, Dombroski D (1999) Hydrolysis of native poly (hydroxybutyrate) granules (PHB), crystalline PHB, and artificial amorphous PHB granules by intracellular and extracellular depolymerases. Int J Biol Macromol 25(1–3):129–134. https://doi.org/10.1016/s0141-8130(99)00026-4

Mezzina MP, Álvarez DS, Egoburo DE, Peña RD, Nikel PI, Pettinari MJ (2017) A new player in the biorefineries field: phasin PhaP enhances tolerance to solvents and boosts ethanol and 1, 3-propanediol synthesis in *Escherichia coli*. Appl Environ Microbiol 83(14):e00662–e00617. https://doi.org/10.1128/AEM.00662-17

Mitsui A, Kumazawa S, Takahashi A, Ikemoto HH, Cao S, Arai T (1986) Strategy by which nitrogen-fixing unicellular cyanobacteria grow photoautotrophically. Nature 323:720–722. https://doi.org/10.1038/323720a0

Mumtaz T, Suraini AA, Rahman NAA, Yee PL, Wasoh H, Shirai Y, Hassan MA (2011) Visualization of core-shell PHBV granules of wild type *Comamonas sp.* EB172 in vivo under transmission electron microscope. Int J Polym Anal Charact 16(4):228–238. https://doi.org/10.1080/1023666X.2011.569990

Nowroth V, Marquart L, Jendrossek D (2016) Low temperature-induced viable but not culturable state of *Ralstonia eutropha* and its relationship to accumulated polyhydroxybutyrate. FEMS Microbiol Lett 363:fnw249. https://doi.org/10.1093/femsle/fnw249

Obruca S, Sedlacek P, Mravec F, Samek O, Marova I (2016a) Evaluation of 3-hydroxybutyrate as an enzyme-protective agent against heating and oxidative damage and its potential role in stress response of poly(3-hydroxybutyrate) accumulating cells. Appl Microbiol Biotechnol 100(3):1365–1376. https://doi.org/10.1007/s00253-015-7162-4

Obruca S, Sedlacek P, Krzyzanek V, Mravec F, Hrubanova K, Samek O, Kucera D, Benesova P, Marova I (2016b) Accumulation of poly (3-hydroxybutyrate) helps bacterial cells to survive freezing. PLoS One 11(6):e0157778. https://doi.org/10.1371/journal.pone.0157778

Obruca S, Sedlacek P, Mravec F, Krzyzanek V, Nebesarova J, Samek O, Kucera D, Benesova P, Hrubakova K, Milerova M, Marova I (2017) The presence of PHB granules in cytoplasm protects non-halophilic bacterial cells against the harmful impact of hypertonic environments. New Biotechnol 39:68–80. https://doi.org/10.1016/j.nbt.2017.07.008

Panda B, Sharma L, Mallick N (2005) Poly-β-hydroxybutyrate accumulation in *Nostoc muscorum* and *Spirulina platensis* under phosphate limitation. J Plant Physiol 162(12):1376–1379. https://doi.org/10.1016/j.jplph.2005.05.002

Panuschka S, Drosg B, Ellersdorfer M, Meixner K, Fritz I (2019) Photoautotrophic production of poly-hydroxybutyrate – first detailed cost estimations. Algal Res 41:101558. https://doi.org/10.1016/j.algal.2019.101558

Pärnänen K, Karkman A, Virta M, Eronen-Rasimus E, Kaartokallio H (2015) Discovery of bacterial polyhydroxyalkanoate synthase (PhaC)-encoding genes from seasonal Baltic Sea ice and cold estuarine waters. Extremophiles 19:197–206. https://doi.org/10.1007/s00792-014-0699-9

Pavez P, Castillo JL, González C, Martínez M (2009) Poly-β-hydroxyalkanoate exert a protective effect against carbon starvation and frozen conditions in *Sphingopyxis chilensis*. Curr Microbiol 59:636–640. https://doi.org/10.1007/s00284-009-9485-9

Peplinski K, Ehrenreich A, Doring C, Bomeke M, Reinecke F, Hutmacher C, Steinbuchel A (2010) Genome-wide transcriptome analyses of the "Knallgas" bacterium *Ralstonia eutropha* H16 with regard to polyhydroxyalkanoate metabolism. Microbiol 156(7):2136–2152. https://doi.org/10.1099/mic.0.038380-0

Pernicova I, Novackova I, Sedlacek P, Kourilova X, Koller M, Obruca S (2020) Application of osmotic challenge for enrichment of microbial consortia in polyhydroxyalkanoates producing thermophilic and thermotolerant bacteria and their subsequent isolation. Int J Biol Macromol 144:698–704. https://doi.org/10.1016/j.ijbiomac.2019.12.128

Pfeiffer D, Jendrossek D (2014) PhaM is the physiological activator of poly (3-hydroxybutyrate)(PHB) synthase (PhaC1) in *Ralstonia eutropha*. Appl Environ Microbiol 80(2):555–563. https://doi.org/10.1128/AEM.02935-13

Pham TH (2004) The role of polyhydroxyalkanoate biosynthesis by *Pseudomonas aeruginosa* in rhamnolipid and alginate production as well as stress tolerance and biofilm formation. Microbiology 150:3405–3413. https://doi.org/10.1099/mic.0.27357-0

Poirier Y, Dennis DE, Klomparens K, Somerville C (1992) Polyhydroxybutyrate, a biodegradable thermoplastic, produced in transgenic plants. Science 256(5056):520–523. https://doi.org/10.1126/science.256.5056.520

Porter M, Jian Y (2011a) Crystallization kinetics of poly (3-hydroxybutyrate) granules in different environmental conditions. J Biomat Nanobiotechnol 2(03):301. https://doi.org/10.4236/jbnb.2011.23037

Porter M, Jian Y (2011b) Monitoring the *in situ* crystallization of native biopolyester granules in *Ralstonia eutropha* via infrared spectroscopy. J Microbiol Methods 87(1):49–55. https://doi.org/10.1016/j.mimet.2011.07.009

Pötter M, Steinbüchel A (2006) Biogenesis and structure of polyhydroxyalkanoate granules. In: Shively JM (ed) Inclusions in prokaryotes. Microbiology Monographs vol 1. Springer, Berlin. https://doi.org/10.1007/3-540-33774-1_5

Pötter M, Madkour MH, Mayer F, Steinbüchel A (2002) Regulation of phasin expression and polyhydroxyalkanoate (PHA) granule formation in *Ralstonia eutropha* H16. Microbiology 148(8):2413–2426. https://doi.org/10.1099/00221287-148-8-2413

Prieto A, Escapa IF, Martínez V, Dinjaski N, Herencias C, de la Peña F, Tarazona N, Revelles O (2016) A holistic view of polyhydroxyalkanoate metabolism in *Pseudomonas putida*. Environ Microbiol 18(2):341–357. https://doi.org/10.1111/1462-2920.12760

Pulz O (2001) Photobioreactors: production systems for phototrophic microorganisms. Appl Microbiol Biotechnol 57(3):287–293. https://doi.org/10.1007/s002530100702

Rehm BH (2003) Polyester synthases: natural catalysts for plastics. Biochem J 376(1):15–33. https://doi.org/10.1042/bj20031254

Rehm BH, Steinbüchel A (1999) Biochemical and genetic analysis of PHA synthases and other proteins required for PHA synthesis. Int J Biol Macromol 25(1–3):3–19. https://doi.org/10.1016/s0141-8130(99)00010-0

Remsen CC (1966) The fine structure of frozen-etched *Bacillus cereus* spores. Arch Mikrobiol 54(3):266–275. https://doi.org/10.1007/BF00408999

Rothermic MM, Guerrero R, Lenz RW, Goodwin S (2000) Characterization, seasonal occurrence, and diel fluctuation of poly(hydroxyalkanoate) in photosynthetic microbial mats. Appl Environ Microbiol 66:4279–4291. https://doi.org/10.1128/AEM.66.10.4279-4291.2000

Ruiz JA, Lopez NI, Fernandez RO, Mendez BS (2001) Polyhydroxyalkanoate degradation is associated with nucleotide accumulation and enhances stress resistance and survival of *Pseudomonas oleovorans* in natural water microcosms. Appl Environ Microbiol 67:225–230. https://doi.org/10.1128/AEM.67.1.225-230.2001

Saponetti MS, Bobba F, Salerno G, Scarfato A, Corcelli A, Cucoclo A (2011) Morphological and structural aspects of the extremely halophilic archaeon *Haloquadratum walsbyi*. PLoS One 6(4):e18653. https://doi.org/10.1371/journal.pone.0018653

Schubert P, Steinbüchel A, Schlegel HG (1988) Cloning of the *Alcaligenes eutrophus* genes for synthesis of poly-beta-hydroxybutyric acid (PHB) and synthesis of PHB in *Escherichia coli*. J Bacteriol 170(12):5837–5847. https://doi.org/10.1128/jb.170.12.5837-5847.1988

Sedlacek P, Slaninova E, Enev V, Koller M, Nebesarova J, Marova I, Hrubanova K, Krzyzanek V, Samek O, Obruca S (2019a) What keeps polyhydroxyalkanoates in bacterial cells amorphous? A derivation from stress exposure experiments. Appl Microbiol Biotechnol 103(4):1905–1917. https://doi.org/10.1007/s00253-018-09584-z

Sedlacek P, Slaninova E, Koller M, Nebesarova J, Marova I, Krzyzanek V, Obruca S (2019b) PHA granules help bacterial cells to preserve cell integrity when exposed to sudden osmotic imbalances. New Biotechnol 49:129–136. https://doi.org/10.1016/j.nbt.2018.10.005

Silvestrini L, Drosg B, Fritz I (2016) Identification of four polyhydroxyalkanoate structural genes in *Synechocystis cf. salina* PCC6909: *in silico* evidences. J Proteomics Bioinform 9(2):28–37. https://doi.org/10.4172/jpb.1000386

Slaninova E, Sedlacek P, Mravec F, Mullerova L, Samek O, Koller M, Hesko O, Kucera D, Marova I, Obruca S (2018) Light scattering on PHA granules protects bacterial cells against the harmful effects of UV radiation. Appl Microbiol Biotechnol 102(4):1923–1931. https://doi.org/10.1007/s00253-018-8760-8

Slepecky RA, Law JH (1961) Synthesis and degradation of poly-β-hydroxybutyric acid in connection with sporulation of *Bacillus megaterium*. J Bacteriol 82:37–42. https://doi.org/10.1128/JB.82.1.37-42.1961

Smith EG (1976) Pulsed NMR studies of molecular motion in wet nylon-6, 6 fibres. Polymer 17(9):761–767. https://doi.org/10.1016/0032-3861(76)90030-6

Soto G, Setten L, Lisi C, Maurelis C, Mozzicafreddo M, Cuccioloni M, Angeletti M, Ayub ND (2012) Hydroxybutyrate prevents protein aggregation in the halotolerant bacterium *Pseudomonas* sp. CT13 under abiotic stress. Extremophiles 16:455–462. https://doi.org/10.1007/s00792-012-0445-0

Stal LJ (2012) Cyanobacterial mats and stromatolites. In: Whitton BA (ed) Ecology of cyanobacteria II. Springer, Dordrecht, pp 65–125

Stanley SM (1999) Earth system history. Freeman, New York

Stuart ES, Foster LJR, Lenz RW, Fuller RC (1996) Intracellular depolymerase functionality and location in *Pseudomonas olevorans* inclusions containing polyhydroxyoctanoate. Int J Biol Macromol 19:171–176. https://doi.org/10.1016/0141-8130(96)01124-5

Stubbe JA, Tian J (2003) Polyhydroxyalkanoate (PHA) homeostasis: the role of the PHA synthase. Nat Prod Rep 20(5):445–457. https://doi.org/10.1039/B209687K

Sudesh K, Abe H, Doi Y (2000a) Synthesis, structure and properties of polyhydroxyalkanoates: biological polyesters. Prog Polym Sci (Oxford) 25(10):1503–1555. https://doi.org/10.1016/S0079-6700(00)00035-6

Sudesh K, Fukui T, Iwata T, Doi Y (2000b) Factors affecting the freeze-fracture morphology of *in vivo* polyhydroxyalkanoate granules. Can J Microbiol 46(4):304–311. https://doi.org/10.1139/w99-150

Sudesh K, Taguchi K, Doi Y (2001) Can cyanobacteria be a potential PHA producer? RIKEN Review 42:75–76

Tal S, Okon Y (1985) Production of the reserve material poly-β-hydroxybutyrate and its function in *Azospirillum brasilense* Cd. Can J Microbiol 31:608–613. https://doi.org/10.1139/m85-115

Taroncher-Oldenburg G, Nishina K, Stephanopoulos G (2000) Identification and analysis of the polyhydroxyalkanoate-specific ß-ketothiolase and acetoacetyl coenzymeA reductase genes in the cyanobacterium *Synechocystis* sp. strain PCC6803. Appl Environ Microbiol 66(10):4440–4448. https://doi.org/10.1128/aem.66.10.4440-4448.2000

Tian J, Sinskey AJ, Stubbe J (2005) Kinetic studies of polyhydroxybutyrate granule formation in *Wautersia eutropha* H16 by transmission electron microscopy. J Bacteriol 187(11):3814–3824. https://doi.org/10.1128/JB.187.11.3814-3824.2005

Tribelli PM, López NI (2011) Poly(3-hydroxybutyrate) influences biofilm formation and motility in the novel Antarctic species *Pseudomonas extremaustralis* under cold conditions. Extremophiles 15:541–547. https://doi.org/10.1007/s00792-011-0384-1

Tribelli PM, Pezzoni M, Brito MG, Montesinos NV, Costa CS, Lopez NI (2019) Response to lethal UVA radiation in the Antarctic bacterium *Pseudomonas extremaustralis*: polyhydroxybutyrate and cold adaptation as protective factors. Extremophiles 24:1–11. https://doi.org/10.1007/s00792-019-01152-1

Troschl C, Meixner K, Drosg B (2017) Cyanobacterial PHA production-review of recent advances and a summary of three years' working experience running a pilot plant. Bioengineering (Basel) 4(2):26. https://doi.org/10.3390/bioengineering4020026

Urmeneta J, Mas-Castella J, Guerrero R (1995) Biodegradation of poly-(beta)-hydroxyalkanoates in a lake sediment sample increases bacterial sulfate reduction. Appl Environ Microb 61:2046–2048. https://doi.org/10.1128/AEM.61.5.2046-2048.1995

van Gool AP, Lambert R, Laudelout H (1969) The fine structure of frozen etched Nitrobacter cells. Arch Microbiol 69(4):281–293. https://doi.org/10.1007/BF00408570

Wang Q, Yu H, Xia Y, Kang Z, Qi Q (2009) Complete PHB mobilization in *Escherichia coli* enhances the stress tolerance: a potential biotechnological application. Microb Cell Factories 8:47. https://doi.org/10.1186/1475-2859-8-47

Wieczorek R, Pries A, Steinbüchel A, Mayer F (1995) Analysis of a 24-kilodalton protein associated with the polyhydroxyalkanoic acid granules in *Alcaligenes eutrophus*. J Bacteriol 177(9):2425–2435

Wu D, He J, Gong Y, Chen D, Zhu X, Qiu N, Sun M, Li M, Yu Z (2011) Proteomic analysis reveals the strategies of *Bacillus thuringiensis* YBT-1520 for survival under long-term heat stress. Proteomics 11:2580–2591. https://doi.org/10.1002/pmic.201000392

Xiao N, Jiao N, Liu Y (2015) *In vivo* and *in vitro* observations of polyhydroxybutyrate granules formed by *Dinoroseobacter sp*. JL 1447. Int J Biol Macromol 74:467–475. https://doi.org/10.1016/j.ijbiomac.2014.11.045

Xu F, Huang S, Liu Y, Zhang Y, Chen S (2014) Comparative study on the production of poly(3-hydroxybutyrate) by thermophilic *Chelatococcus daeguensis* TAD1: a good candidate for large-scale production. Appl Microbiol Biotechnol 98(9):3965–3974. https://doi.org/10.1007/s00253-014-5524-y

Yamane T (1993) Yield of poly-D-(-)-3-hydroxybutyrate from various carbon sources: a theoretical study. Biotechnol Bioeng 41:165–170. https://doi.org/10.1002/bit.260410122

York GM, Junker BH, Stubbe JA, Sinskey AJ (2001a) Accumulation of the PhaP phasin of *Ralstonia eutropha* is dependent on production of polyhydroxybutyrate in cells. J Bacteriol 183(14):4217–4226. https://doi.org/10.1128/JB.183.14.4217-4226.2001

York GM, Stubbe J, Sinskey AJ (2001b) New insight into the role of the PhaP phasin of *Ralstonia eutropha* in promoting synthesis of polyhydroxybutyrate. J Bacteriol 183(7):2394–2397. https://doi.org/10.1128/JB.183.7.2394-2397.2001

York GM, Stubbe J, Sinskey AJ (2002) The *Ralstonia eutropha* PhaR protein couples synthesis of the PhaP phasin to the presence of polyhydroxybutyrate in cells and promotes polyhydroxybutyrate production. J Bacteriol 184(1):59–66

Zhao YH, Li HM, Qin LF, Wang HH, Chen G-Q (2007) Disruption of the polyhydroxyalkanoate synthase gene in *Aeromonas hydrophila* reduces its survival ability under stress conditions. FEMS Microbiol Lett 276:34–41. https://doi.org/10.1111/j.1574-6968.2007.00904.x

Zhao H, Wei H, Liu X, Yao Z, Xu M, Wei D, Wang J, Wang X, Chen G-Q (2016) Structural insights on PHA binding protein PhaP from *Aeromonas hydrophila*. Sci Rep 6:39424. https://doi.org/10.1038/srep39424

Appendix 11

Sedlacek, P., Slaninova, E., Enev, V., Koller, M., Nebesarova, J., Marova, I., Hrubanova, K., Krzyzanek, V., Samek, O. and Obruca, S. (2019). What keeps polyhydroxyalkanoates in bacterial cells amorphous? A derivation from stress exposure experiments. Applied microbiology and biotechnology, 103(4), 1905-1917.

APPLIED MICROBIAL AND CELL PHYSIOLOGY

CrossMark

What keeps polyhydroxyalkanoates in bacterial cells amorphous? A derivation from stress exposure experiments

Petr Sedlacek[1] · Eva Slaninova[1] · Vojtech Enev[1] · Martin Koller[2,3] · Jana Nebesarova[4,5] · Ivana Marova[1] · Kamila Hrubanova[6] · Vladislav Krzyzanek[6] · Ota Samek[6] · Stanislav Obruca[1]

Abstract

Polyhydroxyalkanoates (PHA) are storage polymers accumulated by numerous prokaryotes in form of intracellular granules. Native PHA granules are formed by amorphous polymer which reveals considerably higher elasticity and flexibility as compared to crystalline pure PHA polymers. The fact that bacteria store PHA in amorphous state has great biological consequences. It is not clear which mechanisms protect amorphous polymer in native granules from transition into thermodynamically favorable crystalline state. Here, we demonstrate that exposition of bacterial cells to particular stressors induces granules aggregation, which is the first but not sufficient condition for PHA crystallization. Crystallization of the polymer occurs only when the stressed bacterial cells are subsequently dried. The fact that both granules aggregation and cell drying must occur to induce crystallization of PHA indicates that both previously suggested hypotheses about mechanisms of stabilization of amorphous state of native PHA are valid and, in fact, both effects participate synergistically. It seems that the amorphous state of the polymer is stabilized kinetically by the low rate of crystallization in limited volume in small PHA granules and, moreover, water present in PHA granules seems to function as plasticizer protecting the polymer from crystallization, as confirmed experimentally for the first time by the present work.

Keywords Polyhydroxyalkanoates crystallization · Intracellular granules · Stress conditions

✉ Stanislav Obruca
obruca@fch.vut.cz

[1] Faculty of Chemistry, Brno University of Technology, Purkynova 118, 612 00 Brno, Czech Republic

[2] Institute of Chemistry, NAWI Graz, University of Graz, Heinrichstrasse 28/III, 8010 Graz, Austria

[3] ARENA Arbeitsgemeinschaft für Ressourcenschonende & Nachhaltige Technologien, Inffeldgasse 21b, 8010 Graz, Austria

[4] Biology Centre, The Czech Academy of Sciences, v.v.i., Branisovska 31, 370 05 Ceske Budejovice, Czech Republic

[5] Faculty of Science, University of South Bohemia, Branisovska 31, 370 05 Ceske Budejovice, Czech Republic

[6] Institute of Scientific Instruments, The Czech Academy of Sciences, v.v.i., Kralovopolska 147, 612 64 Brno, Czech Republic

Introduction

Polyhydroxyalkanoates (PHA) are polyesters produced and accumulated by numerous microbial strains in the form of granular cell inclusions. Although it is generally accepted that PHA serve primarily as a carbon and energy storage materials, it was reported repeatedly that presence of intracellular PHA provides a variety of additional beneficial functions when a microorganism faces adverse conditions; in this context, numerous experimental reports have demonstrated that the capability for PHA biosynthesis and degradation also substantially enhances the survival of bacteria when exposed to various physical stress conditions including high temperature (Wang et al. 2009; Zhao et al. 2007), freezing and thawing cycles (Obruca et al. 2016a; Pavez et al. 2009), low temperatures (Nowroth et al. 2016), osmotic up-shock (Obruca et al. 2017), oxidative pressure (Kadouri et al. 2003; Obruca et al. 2016b; Koskimäki et al. 2016), or exposure to UV irradiation (Slaninova et al. 2018). The unexpected universality of the protective effects of PHA, either from the viewpoint of a wide range of different applied stress factors or from the perspective of a vast variety of microbial genera for which the protective effect of PHA against these

stressors was confirmed, led to the currently recognized opinion that the presence of PHA granules has numerous biological and biophysical consequences, which, in a synergistic way, enhance the overall fitness and robustness of PHA-containing cells. Even more interestingly, it was demonstrated by several authors that some of these protective effects are not associated with mobilization of PHA, but simply with the presence of PHA granules in the cells per se (Obruca et al. 2018).

From the material point of view, PHA chains are of highly hydrophobic nature. Therefore, the granular PHA inclusions need to be separated from the surrounding aqueous cytoplasm by the action of cellular constituents with a surfactant-like behavior. For a long time, this role had been attributed to phospholipids, which were considered being arranged in a monolayer on the surface of the granules (Beeby et al. 2012). Nevertheless, it was revealed more recently that the granular surface is free of phospholipids and consists only of proteins, among which the surfactant function is provided mainly by a special family of granule-associated structural proteins generally called phasins (Bresan et al. 2016).

The specific molecular structure of PHA also results in a high degree of crystallinity of the pure polymer at ambient conditions. However, the intracellularly stored PHA reveal totally different material properties. The intracellular polymer is amorphous, and therefore, the polymer chains retain some mobility and flexibility. The amorphous state of the polymer is not only of crucial metabolic importance since crystalline PHA are not catabolized by intracellular PHA depolymerases (Jendrossek 2007); beyond that, our recent work indicates that amorphous polymer, which is resembling super-cooled liquids in its mechanical properties, is also directly employed in some protective effects of PHA granules against various stressors. For instance, it is likely that amorphous PHA granules protect bacteria from damage by extracellular ice during freezing (Obruca et al. 2016a); moreover, we have observed that amorphous polymer might stabilize cytoplasmic membranes stressed by osmotically induced plasmolysis (Obruca et al. 2017). Furthermore, we observed that exposition of PHA-positive microbial cells to some particular stressors induces crystallization of the intracellular polymer. Therefore, we decided to utilize a combination of spectroscopic, morphological, and biophysical analyses to investigate stress-induced crystallization of intracellular granules. Surprisingly, apart from stress response-related aspects of PHA crystallization, our results also shed light on mechanisms keeping native intracellular granules in thermodynamically non-stable amorphous state.

Materials and methods

Materials and microorganisms

The PHA-producing bacterial strain *Cupriavidus necator* H16 (CCM 3726) was purchased from the Czech Collection of

Microorganisms, Brno, Czech Republic; the PHA negative mutant *Cupriavidus necator* PHB^{-4} (DMS-541) was obtained from the Leibnitz Institute DSMZ-German Collection of Microorganism and Cell Cultures, Braunschweig, Germany. Cultivation was performed in nitrogen-limited Mineral Salt (MS) medium, which supports PHA accumulation. The particular composition of MS medium was as follows: 1 g $(NH_4)_2SO_4$, 1 g KH_2PO_4, 11.1 g $Na_2HPO_4 \cdot 12H_2O$, 0.2 g $MgSO_4 \cdot 7H_2O$, 20 g fructose, 1 mL of microelement solution, and 1 L of distilled water. The composition of microelement solution was as follows: 9.7 g $FeCl_3$, 7.8 g $CaCl_2$, 0.156 g $CuSO_4 \cdot 5H_2O$, 0.119 g $CoCl_2$, and 0.118 g $NiCl_2$ in 1 L of 0.1 M HCl. Erlenmeyer flasks (total volume 250 mL) containing 100 mL of MS medium were inoculated with 5 mL of an overnight culture of *C. necator* H16 grown in complex Nutrient Broth medium (10 g peptone, 10 g beef extract, 5 g NaCl per 1 L of distilled water). The cultivations were performed for 72 h at 30 °C under constant shaking (180 rpm) in a rotary incubator. After 72 h, the cultivation was finished, and biomass was harvested by centrifugation (5000×g, 5 min, the same condition were kept for all following centrifugation steps), washed with phosphate buffered saline (PBS; pH 7.4, 50 mM), and centrifuged again. The biomass concentration was measured gravimetrically and the PHA content of cell biomass was analyzed by GC-FID as reported previously (Obruca et al. 2013). The average content of PHA in the biomass after 72 h of cultivation was 74% of cell dry mass (CDM).

Exposure of the bacteria to various stress factors

The fresh cell cultures were exposed to various adverse environmental conditions as follows:

i. Effect of elevated temperature: Centrifuged washed cells were re-dispersed in phosphate buffer (pH 7.4, 50 mM) in microcentrifuge tubes (total volume of 2 mL, the same tubes were used also for all following experiments). The individual microcentrifuge tubes were then incubated in a water bath conditioned at 25 °C (control), 50 °C, and 80 °C, respectively. After 90 min, the tubes were removed from the bath and allowed to cool down to ambient temperature. Prior to further analyses, cells were centrifuged again. For each tested temperature, three separate samples were prepared in this way.

ii. Effect of high osmolarity: Centrifuged washed cells were re-dispersed in NaCl solution (200 g/L) in microcentrifuge tubes. After exposure to hyperosmotic conditions (2 h at 25 °C), the cells were separated by centrifugation, washed with phosphate buffer (pH 7.4, 50 mM), and centrifuged again. Again, the sample was prepared in triplicate.

iii. Effect of freezing/thawing: Centrifuged washed cells were re-dispersed in phosphate buffer (same as above) in microcentrifuge tubes. The cell dispersion was then frozen by incubation at −30 °C for 2 h and subsequently thawed at 25 °C. Individual samples were prepared (in triplicates) for

one, two, three, and four repeated freezing/thawing cycles (at − 30 °C) and also for five cycles with freezing temperature of the final cycle changed to − 70 °C.

iv. Effect of pH value: Centrifuged washed cells were re-dispersed in a solution with pH value adjusted to 1, 2, 3, and 4, respectively. For the pH adjustment, standard hydrochloric acid–potassium chloride buffer solutions (0.1 M, pH = 1 and 2) and acetate buffer solutions (0.1 M pH = 3 and 4) were used. Samples for individual pH values were prepared in triplicate. After exposure to acidic conditions (2 h at 25 °C), the cells were separated by centrifugation.

For all prepared samples (control sample and the samples exposed to different environmental challenges), the number of viable cells (CFU per mL) was determined by standard dilution plating assay on Petri dishes with complex medium agar, where the colonies were counted after 48 h of incubation in thermostat at 30 °C (three replicates per setup).

Infrared spectroscopy-assisted analysis of the cell drying

The infrared spectra of the cell dispersions were recorded with a Nicolet iS50 FTIR spectrometer (Thermo Scientific). All measurements were taken at ambient temperature (in air-conditioned room) on the built-in single-reflection diamond attenuated total reflectance (ATR) crystal. For time-resolved measurement, a small drop (approximately 5 μL) of the centrifuged cell dispersion was placed directly on the surface of the ATR crystal and the data collection using Omnic Series data collection software was started. While the water was freely evaporating from the cell dispersion, the FTIR spectra were collected in regular time intervals. The individual absorption spectrum was collected every 10 s as an average of 8 scans with resolution 1 cm^{-1} over the duration of the data collection (at least 150 min). For the time monitoring of water content and crystallinity of PHA, raw absorption spectra were evaluated without any correction. For investigation of structural changes in cell proteins, the envelope Amide I absorption band was further evaluated by deconvolution into individual overlapping component bands attributed to particular structural motifs. Positions of the overlapping bands were determined by second derivative methods. The deconvolution of the sharp band assigned to C=O and C–N stretching in Amide I region (1700–1600 cm^{-1}) was made by fitting the experimental envelope band by the summation of seven calculated Gaussian components using non-linear fitting tools of the Origin 8.1 software.

Transmission electron microscopy of the bacterial cells

Samples of the control and challenged bacterial cultures were visualized using the Transmission Electron Microscope (TEM) JEOL 1010. Individual samples (approximately 0.2 μL) in a special carrier were frozen in a high-pressure freezer (Leica EM Pact II) and transferred under liquid nitrogen into a freeze substitution unit (Leica EM AFS) with 2% osmium tetroxide in water-free acetone used as a substitution solution. The substitution protocol was as follows: first, samples were kept at − 90 °C for 96 h. Then, the samples were slowly warmed up to − 20 °C at a heating rate 5 °C per hour. At this elevated temperature, the samples were kept for 24 h, before the temperature was further increased to 4 °C with a heating rate 3 °C per hour. The samples were kept for 18 h at 4 °C before being finally warmed to room temperature. Subsequently, the samples were washed three times in anhydrous acetone (exposure time 15 min) and then infiltrated and embedded with Polybed resin (SPI). Three different acetone-to-resin mixtures (volume ratios 2:1, 1:1, and 1:2) were used sequentially; each setup was embedded for 1 h and then dried overnight in pure embedding media in desiccator evacuated by connection to the water pump. Polymerization was initiated by heating to 62 °C and proceeded for 48 h. Ultrathin sections were cut using an Ultracut UCT ultramicrotome (Leica) with a diamond knife (Diatome, cutting angle of 45°). Sections were transferred onto 300 Mesh copper grids and stained with uranyl acetate and lead citrate solutions.

Results

FTIR analysis of sample dehydration

Figure 1a shows the temporal development of FTIR spectra of the centrifuged dispersion of the control sample, i.e., of the intact (non-stressed) C. necator H16 cells. In the spectra, drying of the sample is connected with decreasing intensity of the characteristic vibration bands of water molecules, in particular in the spectral regions centered at around 3300 cm^{-1} (stretching modes, depicted as 1 in Fig. 1), 1640 cm^{-1} (bending modes, marked with arrow ibid), and at the spectral edge below 1000 cm^{-1} (rocking band, marked with arrow ibid.). In Fig. 1b, it can be seen that the dehydration of the sample can be clearly monitored and the completion of the dehydration is easily identified in time-resolved 2D ATR-FTIR spectrum. Therefore, any structural changes in the cell which are observable in the spectrum (such as the crystallization of PHA) can be chronologically related to the dehydration process (whether it precedes, accompanies or follows on the dehydration).

FTIR analysis of stress-induced PHA crystallization

The same method of ATR-FTIR analysis was applied also for the cell cultures exposed to various stress factors. In all cases, the main aim of the experiment was to evaluate the effect of the stress factor on the susceptibility of originally amorphous intracellular PHA to crystallize in situ. For the evaluation
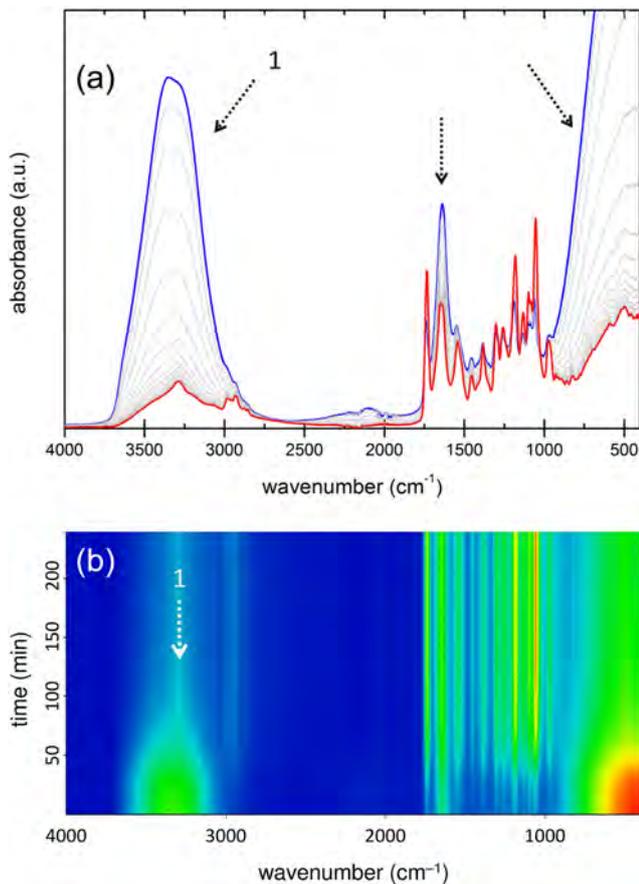
Fig. 1 Results of the ATR-FTIR analysis of the free drying of control *C. necator* H16 sample. (**a**) Time development of the ATR-FTIR spectra collected from the start of the experiment ($t = 0$, blue curve) in 10 min intervals ($t = 10$ to 150 min, grey spectra) till the last shown spectra collected at $t = 160$ min (red curve). Characteristic vibration bands for water are marked with arrows. (**b**) 2D time-resolved ATR-FTIR spectrum clearly illustrated the time needed for the completion of the dehydration of the sample (approx. 65 min)

purposes, several characteristic vibration bands were selected according to the previously published reports on phase transition of PHA (Porter and Yu 2011a; Hu et al. 2007) involving also one vibration band representing the content of water in the sample and also the Amide I band, which enables observing the structural changes in proteins. The selected bands are summarized in Table 1.

Crystallization of PHA imprints mainly in the spectral region which is shown in detail in Fig. 2. In this figure, a comparison of time-resolved FTIR spectra collected after dehydration of the sample is shown for the control culture (non-stressed *C. necator* culture, Fig. 2a) and for the cell suspension incubated at 80 °C for 90 min prior to ATR-FTIR measurement (Fig. 2b). While for the control sample the characteristic bands of PHA in the region 1000–1800 cm^{-1} do not show any significant changes in the course of the experiment (only the further dehydration of the sample is visible), changes in spectra of the heated sample can decidedly be attributed to the

partial crystallization of PHA. First of all, the originally symmetrical vibration band characteristic for carbonyl stretching in polyesters deforms with a significant red shift in its maximum (see the peaks marked 2 and 3 in Fig. 2 and Table 1). Furthermore, new vibration peaks appear at about 1278 and 1227 cm^{-1} as a result of crystallization (marked 6 and 7 ibid.). Finally, intensity of C–O–C stretching band at 1180 cm^{-1} (marked 8 in Fig. 2 and Table 1) drops as the content of amorphous PHA decreases. Among the vibration bands related to PHA, symmetric deformation of methyl groups is not affected by the crystallization process; therefore, the peak centered at 1382 cm^{-1} (marked 5 ibid.) was used as an internal reference to scale the spectra before the further analysis.

The results of the FTIR-assisted drying of stressed *C. necator* H16 cultures are summarized in Fig. 3. In this figure, the scaled absorbance values (relative to the absorbance at frequency of the reference peak) versus time are shown for all the above discussed characteristic vibration frequencies of PHA and also for the frequency 3300 cm^{-1} (water in sample). In Fig. 3a, it is shown that for the control sample the relative absorbance at all the PHA–related characteristic frequencies remains almost constant after the sample is completely dehydrated (depicted as stage II. in the figure). On the contrary, the results of drying of samples incubated at 50 °C and 80 °C (see Fig. 3b, c) show completely different time courses. It can be clearly seen that for both the samples, after the dehydration step (stage I.), PHA in the sample remains amorphous for a certain time period (stage II.) and, after this time lag, the crystallization occurs (stage III.). Moreover, it can be seen that the impact of crystallization on the spectra is more pronounced when a higher incubation temperature is used and that among the selected vibration bands, those at frequencies 1719 and 1227 cm^{-1} seem to be the most sensitive, while those at 1734 and 1180 cm^{-1} are least sensitive to the crystallization process.

The same evaluation method was utilized also for other types of stresses exerted on the *C. necator* H16 culture. In Fig. 3d, it can be seen that freezing of the sample exposed to − 30 °C followed by thawing and heated to the ambient temperature did not show any observable signs of PHA crystallization. Moreover, similar results were obtained also when the culture was subjected to the freezing and thawing repeatedly (up to 4 repetitions) and when the freezing temperature was lowered from − 30 to − 70 °C (data not shown). According to these results, neither repeated freezing nor thawing provides any negative effects on the intracellular state of PHA.

On the contrary, osmotically up-shocked *C. necator* H16 cells (the culture exposed to 200 g/L NaCl, see Fig. 3e) show significant spectral signs of PHA crystallization. Interestingly, contrary to the samples exposed to elevated temperature, the osmotically induced crystallization process begins immediately after the sample dehydration without any observable lag period. Again, PHA crystallization manifests mainly via

Table 1 Characteristic vibration frequencies selected for further analysis

Peak no.	Wavenumber	Assignment	Purpose
1	3300 cm^{-1}	Water (O–H stretching)	Monitoring of the sample dehydration
2	1734 cm^{-1}	Amorphous PHA (C=O stretching)	Detection of the PHA crystallization
3	1719 cm^{-1}	Crystalline PHA (C=O stretching)	Detection of the PHA crystallization
4	1700–1600 cm^{-1}	Amide I (amide C=O stretching)	Protein denaturation study
5	1382 cm^{-1}	CH$_3$ symmetric deformation	Reference peak (spectra scaling)
6	1278 cm^{-1}	Crystalline PHA (–CH$_2$ wagging in C–C–O backbone)	Detection of the PHA crystallization
7	1227 cm^{-1}	Crystalline PHA (asymmetric C–C–O stretching in helical chains)	Detection of the PHA crystallization
8	1180 cm^{-1}	Amorphous PHA (asymmetric C–O–C stretching)	Detection of the PHA crystallization

increase in the newly emerging peaks at 1278 and 1227 cm^{-1} and by the red shift of the carbonyl vibration peak to about 1719 cm^{-1}.

The last tested stress factor applied on the *C. necator* H16 culture was the acidic pH value induced by acetate buffer (pH = 3 and 4) or by hydrochloric acid (pH = 1 and 2), respectively. In general, no effect on the state of intracellular PHA was found for acetate buffer induced pH = 3 and 4. In Fig. 3f, results of the time-resolved FTIR show obvious crystallization at pH = 1. In this case, the time lag typical for the crystallization induced by the elevated temperature is seen again. For pH = 2, similar trends with just less intensive signs of crystallization were obtained (data not shown).

To properly understand the results of the time-resolved FTIR experiments (results provided in Figs. 1, 2, and 3), it is important to realize that at the beginning of the experiment, when the cells are still suspended in the residual water, the infrared signal is predominated by the water (as can be clearly seen in Fig. 1). Then, in the early stage of the experiment, two processes take place simultaneously: (i.) PHA-containing cells
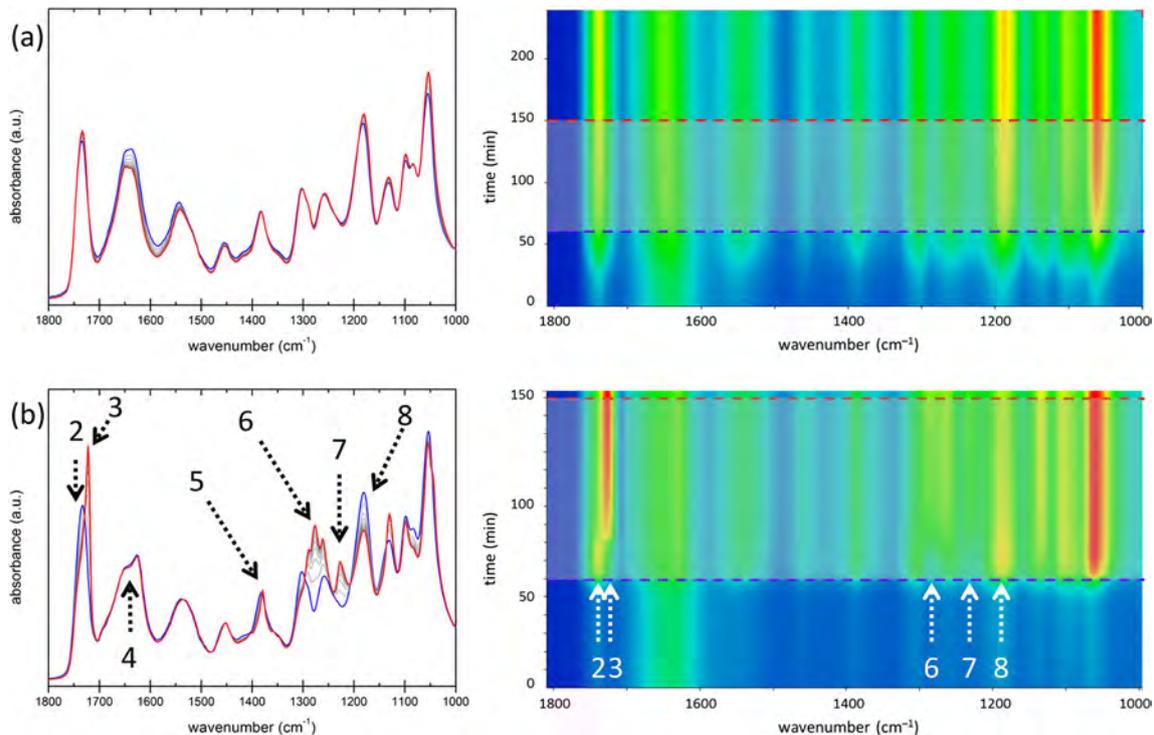
Fig. 2 In situ detection (time-resolved ATR-FTIR spectroscopy) of changes in PHA crystallinity in the cells after dehydration of the sample. Detail on spectral region with characteristic PHA vibration bands (1800–1000 cm^{-1}). Blue curve represents spectra collected at $t = 60$ (blue dashed line in the 2D spectrum), red curves stands for $t = 150$ min (red dashed line in the 2D spectrum), gray curves show time development of spectra between 60 and 150 min in 10-min intervals. (**a**) Drying of the control (non-stressed) culture of *C. necator* H16. No significant changes in characteristic vibration bands of PHA are observed. (**b**) Drying of the *C. necator* H16 culture previously incubated at 80 °C for 90 min. Main changes in spectra related to PHA crystallization are marked with arrows

Fig. 3 Time development of absorbances at frequencies relevant to the sample dehydration (3300 cm^{-1}) and crystallization of PHA (1734 cm^{-1}, 1719 cm^{-1}, 1278 cm^{-1}, 1227 cm^{-1}, and 1180 cm^{-1}), respectively. All the monitored absorbances were scaled using absorbance of the reference peak at 1382 cm^{-1}. Comparison of the results for the *C. necator* H16 control culture (**a**) and cultures incubated at 50 °C (**b**), 80 °C (**c**), − 30 °C (**d**), 200 g/L NaCl (**e**), and pH = 1 (**f**), respectively. In the results, sample dehydration stage (I.), presence of dehydrated cells with amophous PHA (II.) and the crystallization stage (III.) can be clearly distinguished. Dashed curves belong to the secondary axis
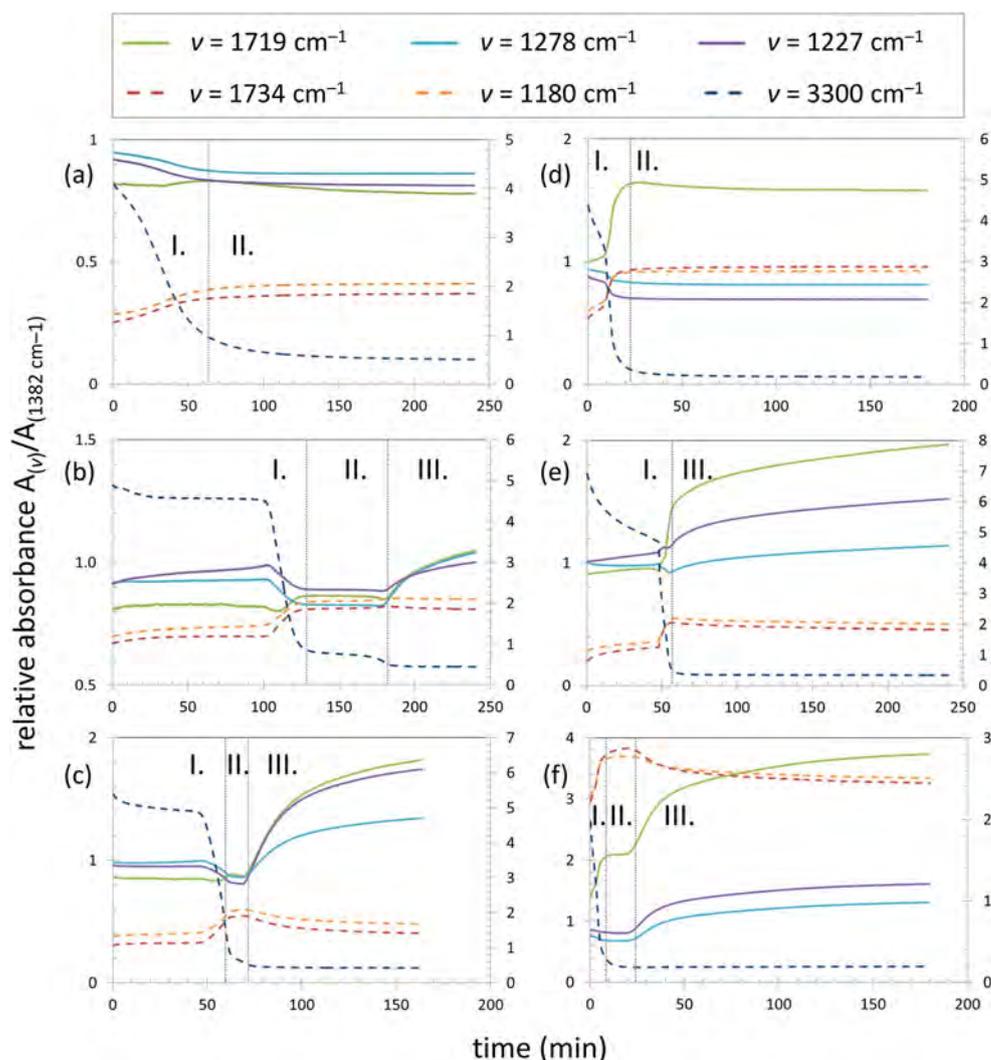
settle down onto the ATR crystal and (ii.) the residual free water in the sample evaporates. Both processes, proceeding with different rates, imprint in the collected infrared spectra. As the more biomass gradually settle on the ATR crystal, intensities of the corresponding infrared bands increase. On the other hand, as the free water evaporates from the surface of ATR crystal, the background absorption of water (with the highest absorption intensity centered at around 3300 cm^{-1}, 1600 cm^{-1} and below 1000 cm^{-1}) decreases. Therefore, in the early stage of the measurement when the free water is still present in the sample, the infrared signal of the biomass is influenced by this changing background absorption of water. Furthermore, different absorption bands of the biomass are affected to the different extent because of the dissimilar overlapping with the water absorption signal. It is also evident from Fig. 3 that the time dependence of the changes in the PHA-related bands follows the changes in absorption of water at 3300 cm^{-1}. To summarize, changing intensity of the scaled (relative to absorbance at 1382 cm^{-1}) absorption bands of

PHA in the drying period does not stand for changes in the PHA crystallinity. Rather, they represent inevitable spectral artifacts related to the sample drying.

Apart from PHA-accumulating strain *C. necator* H16, we have performed the same set of experiments also with its PHA negative mutant *C. necator* PHB^{-4}; the results are demonstrated in Supplementary Materials as Fig. S1 – Fig. S6.

In addition, time-resolved ATR experiment with the isolated granules was also performed and the results are shown in Supplementary Materials (see the results shown in Fig. S7 – Fig. S9). It is evident that the spectral changes assigned to the crystallization of PHA in the cells are present as well when the isolated granules are used. But unlike in the intact PHA-containing cells, in the case of the isolated granules, polyester crystallizes already during (not after) the drying step. This confirms that the isolation procedure may significantly influence the mechanisms of stabilization of the polymer against crystallization and therefore, it is not possible to compare stability of the granule in in vivo and ex vivo state.

Protein denaturation assay by deconvolution of Amide I band

It is well documented in published reports (Arrondo et al. 1993; Byler and Susi 1986) that the Amide I vibration band centered at about 1650 cm^{-1} is sensitive to changes in secondary and tertiary structure of proteins. Therefore, the Amide I band was further analyzed in order to reveal any observable effects of applied stress factors on the structure of bacterial proteins. For this purpose, deconvolution of the spectra of individual dehydrated samples was performed in the wavenumber range 1700–1600 cm^{-1}. First of all, frequencies of individual overlapping components were determined via Fourier self-deconvolution method. Subsequently, the spectrum was fitted by the cummulative function consisting of the respective Gaussian component peaks. Figure 4 shows three examples of the decovolution results: non-stressed control sample (Fig. 4a) and samples exposed to elevated temperature (80 °C, Fig. 4b) and high osmolarity (200 g/L NaCl, Fig. 4c), respectively.

From the rough comparison, the differences in the overall shape as well as in the composition of the Amide I band are obvious. In the next step, basic motifs of protein secondary structure were assigned to particular fitting components according to the table shown in Fig. 4d (Goormaghtigh et al. 1990; Susi and Byler 1986). In this way, the representative changes in the secondary structures of cellular proteins induced by particular stress conditions were revealed. Results of this protein structure assay are shown in Fig. 5. The provided data represent results of deconvolution of the last collected spectra from the particular drying experiments presented in Fig. 3. It can be seen that, related to the control sample, all the stress-exposed cultures show decrease in overall proportional representation of ordered structures (α-helices and β-sheets), whereas the content of partially (turns and bands) or totally disordered structures increases. In particular, for the sample incubated at 80 °C, the content of unordered protein chains emerged most significantly at the expense of destroying mainly the α-helical polypeptide motifs. On the other hand, for osmotically and acidically challenged samples, the decrease in ordered motifs was balanced by structures more equally distributed between turns and bands and the unordered ones. Finally, for the repeatedly frozen and thawn samples (only the result for 4th cycle of freezing/thawing is shown), the representation of ordered and disordered structures were similar as with the control sample.

peak position	assigned structure
1689 – 1680 cm^{-1}	turns and bands
1679 – 1670 cm^{-1}	β-sheet
1669 – 1660 cm^{-1}	turns and bands
1659 – 1650 cm^{-1}	α-helix
1649 – 1640 cm^{-1}	unordered
1639 – 1620 cm^{-1}	β-sheet
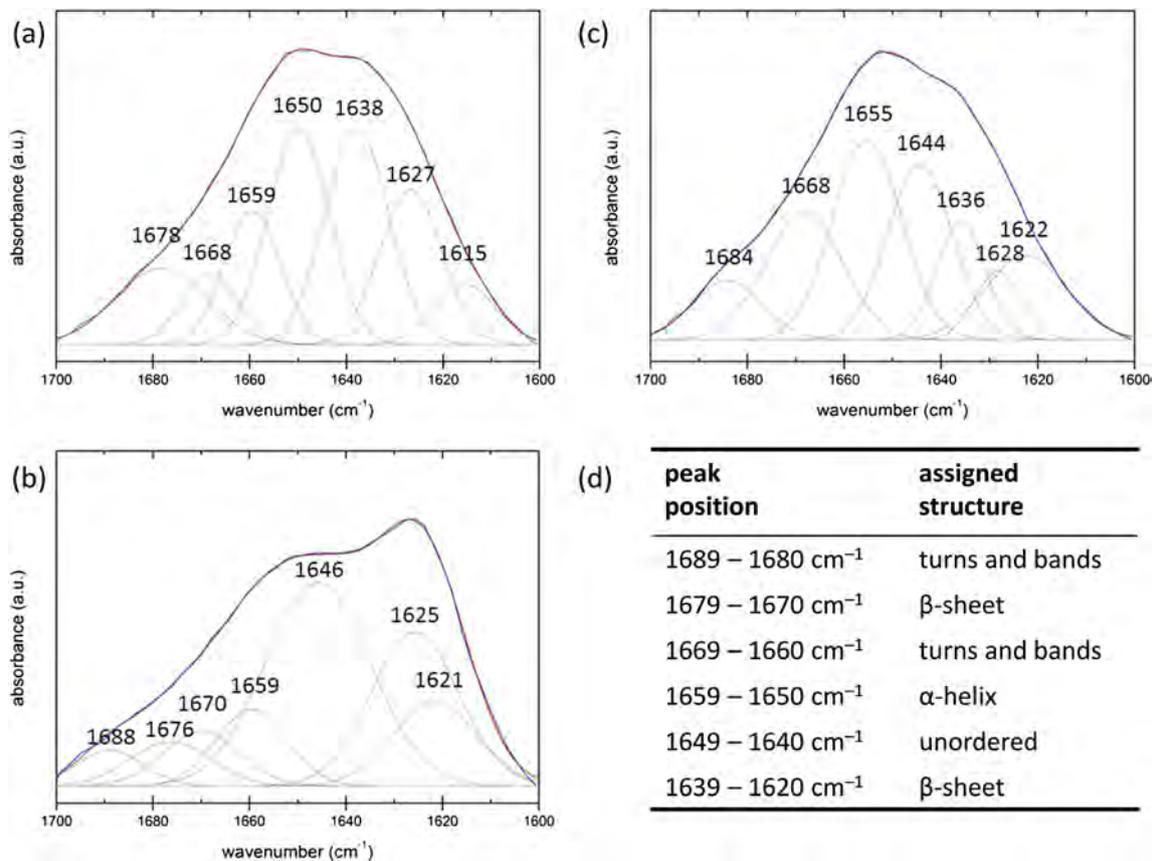
Fig. 4 Example of deconvolution of Amide I band in *C. necator* H16 (blue: measured spectrum, grey: deconvolution components, red: cummulative fitting spectrum) for (**a**) control sample, (**b**) sample incubated in 200 g/L NaCl solution, and (**c**) sample incubated at 80 °C. Assignment of individual components to various protein secondary structures is described in table (**d**)
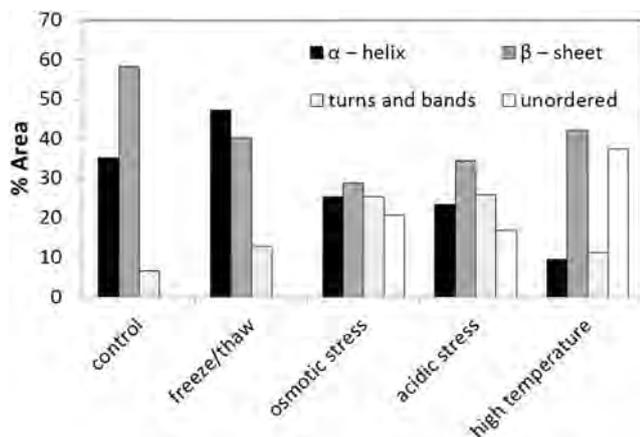
Fig. 5 Proportional representation (in % of peak area) of various secondary structures in *C. necator* H16 proteins according to deconvolution of Amide I band. (freeze/thaw: culture exposed to 4 cycles of freezing and thawing; osmotic stress: culture incubated in 200 g/L NaCl solution; acidic stress: culture incubated at pH = 1; high temperature: culture incubated at 80 °C)

Viability of cells after the stress exposure

Cell viability was assayed by comparing the numbers of cultivable cells (CFU/mL) in samples prior to (control sample) and after the exposure to the applied stress factors. Results are shown in Fig. 6. It is evident that among the selected stress factors, elevated temperature (80 °C) and strongly acidic conditions (pH = 1) show the most fatal effect on cell viability (CFU drops by more than five orders of magnitude). Only the results for extreme values of these two stress factors are shown; nevertheless, it was confirmed that the adverse effect decreased with decreasing the stress dose (the lower temperature, i.e., 50 °C and the less acidic pH, i.e., 2–4, was applied, the higher cell survival was detected; data not shown). On the
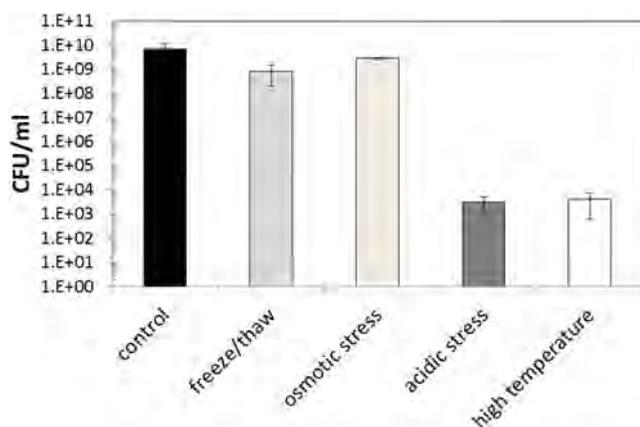
Fig. 6 Survival (plating viability test) of non-stressed *C. necator* H16 cells (control) and of the cells exposed to different stress factors. (freeze/thaw: culture exposed to 4 cycles of freezing and thawing; osmotic stress: culture incubated in 200 g/L NaCl solution; acidic stress: culture incubated at pH = 1; high temperature: culture incubated at 80 °C). Errors bars represent standard deviation of the 5 parallel samples

other hand, the cell survival was significantly higher for samples exposed to repeated freezing and thawing and also to high osmolarity (results of viability assay for the osmotically up-shocked *C. necator* H16 are in good agreement with our previously published data (Obruca et al. 2017)).

Cell morphology assay using TEM

As was reported in our previous works (Obruca et al. 2017), stress challenge of *C. necator* cells is often accompanied by significant changes in cell morphology. In order to reveal morphological changes induced by particular involved stress factors, TEM analysis of the control sample and the challenged cells was involved in the study (results are shown in Fig. 7). The assay confirmed some of the morphological consequences of the stress experiments, which were already described. For example, osmotic challenge resulted in wrinkling of the outer layer of the cell envelope and plasmolysis as was reported previously (Obruca et al. 2017). Similar changes in cell surface were found also for frozen cells and for those subjected to acidic pH values (plasmolysis is depicted as 2 in Fig. 7). Furthermore, hyperosmotically challenged cells also show extraordinary granules-associated behavior, where the liquid-like state of PHA results in the leakage of PHA into the cytoplasm (depicted as 3 in Fig. 7). It was hypothesized that this phenomenon could play an important role in protecting the cells from the harmful impacts of hypertonic environment (Obruca et al. 2017).

Nevertheless, the most important outcome of the morphological assay is represented by the finding that all the stress factors except for freezing (see Fig. 7d) of the sample resulted in more or less pronounced coagulation of initially separated PHA granules (depicted as 1 in Fig. 7). This seems to be a general stress-induced phenomenon. Furthermore, as can be seen from comparison of cultures exposed to elevated temperature (50 °C and 80 °C), it is likely that the extent of the coagulation is affected by the dose of the stress factor. Whereas the cells exposed to 50 °C preserve some of the granules separated, in case of exposure to 80 °C, the granules in the cells form nearly single aggregates occupying almost the entire cell volume. Data dealing with image analysis of the TEM results and distribution of the granule sizes in non-stressed and challenged bacterial cells are provided in Supplementary Materials as Fig. S10 and Fig. S11. It is noticeable that the extent to which the coagulation of the granules was observed is striking in accordance with the signs of crystallization of PHA as well as with the imprints of protein structural changes in FTIR spectra. For example, in the case of (repeated) freezing and thawing of the cells, little effect on protein structure and cell morphology was found (with no granule coagulation). At the same time, FTIR measurement revealed no signs of the PHA crystallization after the sample dehydration.

Fig. 7 Results of TEM analysis of *C. necator* H16 control culture (**a**) and cultures incubated at 50 °C (**b**), 80 °C (**c**), − 30 °C (**d**), 200 g/L NaCl (**e**), and pH = 1 (**f**), respectively (scale bar = 1 μm). In the micrographs, coagulation of PHA granules (depicted as 1), cell plasmolysis (depicted as 2) and special PHA structures related to granule leakage into cytoplasm reported in (Obruca et al. 2017) (depicted as 3) are marked with arrows
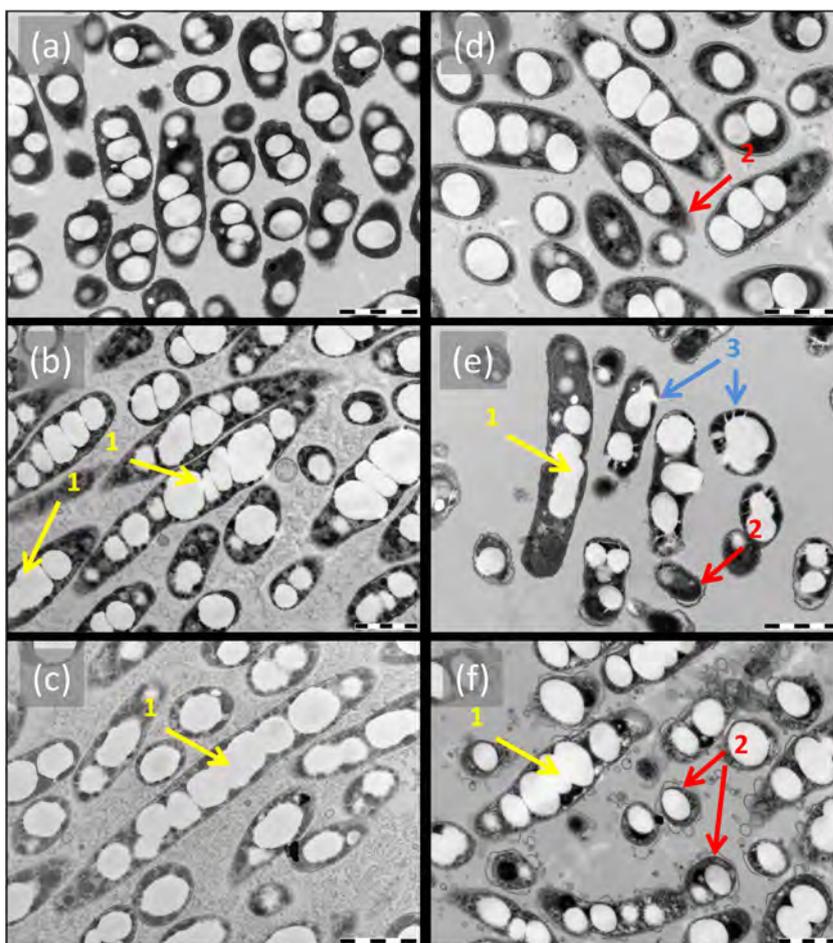
Discussion

The surprising fact that native intracellular PHA granules are formed in a thermodynamically unfavorable amorphous form of the polymer was discovered in 1986 by NMR study on the methanol utilizing *Methylobacterium* AM1 (Bonthrone et al. 1992). It should be noted that amorphous PHA reveals completely different mechanical properties as compared to its crystalline form. For instance, when poly(3-hydroxybutyrate) (PHB) is extracted from bacterial cells, it quickly crystalizes, which substantially reduces its flexibility. Extracted and purified PHB possesses an elongation to break of about 4% (Sudesh et al. 2000). On the contrary, native amorphous intracellular granules reveal behavior of supercooled liquids, which can be best demonstrated by Cryo-SEM pictures of freeze-fractured PHB rich bacterial cells (Fig. 8). Despite the fact that the bacterial cells were frozen and fractured at very low temperature (− 140 °C), the PHA granules retained high flexibility and formed so called needle-like plastic deformations demonstrating elongation to break of more than 100%.

Unique material properties of native amorphous PHA granules are not only of scientific interest but have also great biological impact. At first, intracellular polymer synthesis is catalyzed by PHA synthase (PhaC) which accepts two substrates into its enzyme pocket: the monomer (3-hydroxyacyl-CoA) and the growing polymeric chain (Wittenborn et al. 2016, Kim et al. 2017a). The substrates demonstrate binding affinity to PHA synthase via its N-terminal region (Kim et al. 2017b). It is very likely that amorphous state of the polymer chain is required for its binding into active site of the PHA synthase. Furthermore, since PHA serves primarily as a storage polymer, bacterial cells possess a sophisticated system of enzymes, so called PHA depolymerases (also designated as PhaZ proteins) catalyzing mobilization of the storage polymer predominantly when external carbon source is depleted. Intracellular PHA depolymerases are specific only to the amorphous form of the polymer and are not capable to cleave crystalline PHA (Jendrossek 2007; Uchino et al. 2008; York et al. 2003). Hence, it can be expected that crystallization of PHA granules prevents their utilization when bacterial cells are starving and, therefore, depreciates their storage function. Moreover, the final products of PHA mobilization were recently identified as very potent chemical chaperons protecting enzymes and other biomolecules from high temperature of oxidative pressure (Obruca et al. 2016b; Soto et al. 2012).

Fig. 8 Cryo-SEM images of *C. necator* H16 cells suspension quickly frozen and freeze-fractured at − 140 °C. (**a**) Overall image of fractured tubular sample. Details on (**b**) intact cell surfaces, (**c**) freeze-fracture area with characteristic needle-type plastic deformation of PHA granules and on (**d**) single deformed PHA granule. Method used for cryo-SEM analysis is described in our previous work (Obruca et al. 2016a).
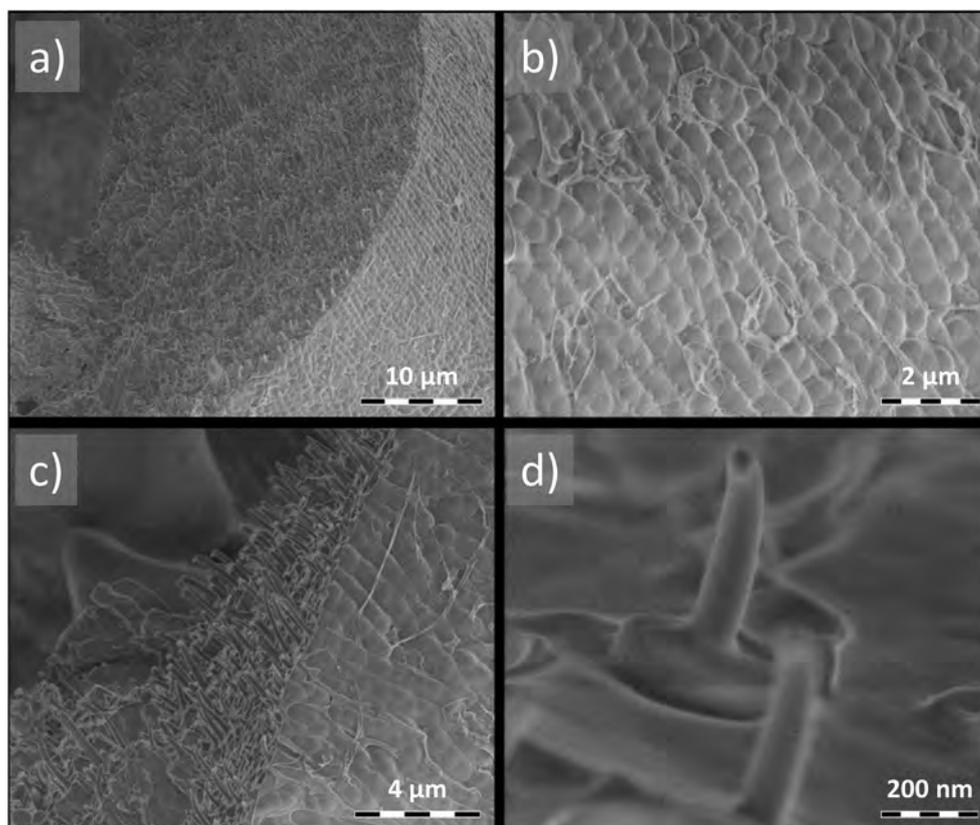
Hence, impairment of PHA mobilization can have complex biological consequences. In addition, there are also reports that liquid-like properties of native amorphous PHA granules are directly involved in their protective function against various stressors. For instance, it was recently hypothesized that amorphous PHA granules protect bacterial cells from damage by ice crystals during freezing (Obruca et al. 2016a), or that liquid-like amorphous PHA granules stabilize cytoplasmic membranes of bacterial cells exposed to suddenly induced hypertonic (Obruca et al. 2017) and hypotonic (Sedlacek et al. 2018) conditions.

Although the origin and importance of the amorphous character of native PHA granules has been debated extensively in the literature, the exact mechanism by which the polymer is protected from spontaneous crystallization in vivo is not yet completely understood. Two main explanations were proposed: (i) an involvement of intragranular plasticizers such as water or other low-molecular solutes (Ceccorulli et al. 1992; Choi and Park 2004) and (ii) a chemical-kinetic mechanism based on a low rate of crystallization in limited volume of sub-micron sized PHA granules (Bonthrone et al. 1992; De Koning and Lemstra 1992). Nevertheless, none of the two methods provides a consistent agreement with all available experimental reports.

It is already well evidenced that Fourier transform infrared (FTIR) spectroscopy represents an advantageous analytical tool for an investigation of PHA crystallinity. Porter and Yu correlated the values of polymer crystallinity determined by standard DSC technique with those determined by attenuated total reflectance FTIR spectroscopy (Porter and Yu 2011a) and then successfully adopted this spectroscopic technique in the in situ investigation of crystallization kinetics of PHA in *C. necator* H16 (formerly known as *Ralstonia eutropha*) cells biologically inactivated by storing at highly acidic conditions (0.2 M sulfuric acid) (Porter and Yu 2011a, b). For all the samples treated in this way, significant spectral manifestations of the crystallization were recorded during the sample drying. The authors also showed that the crystallization kinetics was altered when the primary acidic slurry was further treated by heating or pH adjustment. However, as these authors monitored the PHA crystallization only in the cells with the physiological and probably also the morphological state strongly affected by the applied acidic conditions, it led us to the question how the type and extent of the initial stress, adopted on the cells, influence an initialization and course of the crystallization process.

Our FTIR study indicated that *C. necator* H16 cells do not show any PHA crystallization when the non-stressed culture is dehydrated under ambient conditions. In other words, to induce the crystallization process, the cell culture must be first subjected to adverse conditions. On the other hand, not all of the tested stress factors resulted in the crystallization of PHA.

Combination of the crystallization assay with morphological study revealed that only the stress factors that had led to the coalescence of PHA granules induced crystallization of the polymer. Furthermore, for these stress factors, higher stress doses (e.g., higher temperature, lower pH) always led to the more pronounced manifestation of both the coagulation of granules and the PHA crystallinity. This finding is in very good agreement with the crystallization model proposed by De Koning and Lemstra and Bonthrone (Bonthrone et al. 1992; De Koning and Lemstra 1992). According to this model, the exceptionally low bulk crystallization rate in the submicron-sized granules of a PHA carbonosome results from the low frequency of spontaneous nucleation in such a limited volume. Coagulation of the granules enlarges the volume of the single polymer phase and increases the probability of spontaneous nucleation. The probable explanation of the granule coagulation may also be derived from the results of FTIR assay discussed above. It can be seen that for all the stress factors, which caused coagulation of granules and crystallization of PHA, significant signs of denaturation of proteins can be observed. Of course, the protein denaturation assay shown here cannot distinguish the signal of granule-associated proteins from that of residual cell proteins (it was estimated that the 24 kDa granule-associated phasin represents one of the predominant proteins in *C. necator* and accounts for approx. 5% of the total cell protein fraction (Wieczorek et al. 1995)); nevertheless, the agreement between the extent of granule coagulation and the loss of overall ordered structure in the cell proteins does not seem to be coincidental. In the prospective of the currently acknowledged assumption of the surface of granules being formed by proteins with no phospholipid content, these results let us suppose that stress-induced structural changes in phasins suppress their ability to serve as a surfactant, which separates the individual hydrophobic surfaces of the granules in the hydrophilic cytoplasm, thus preventing their contact and association. The crucial role of native protein structure in preventing granules aggregation can be illustrated by comparison of the results obtained for frozen/thawed cells as compared to all the other tested stress factors. Repeating freezing and thawing did not result in detectable changes in protein structure (Fig. 5) nor in a noticeable aggregation of the granules (Fig. 7 and Fig. S11).

Nevertheless, another important finding of the FTIR assay is that the crystallization process has always followed after the sample dehydration (see Fig. 3). Except for the osmotically stressed cells, the time lag was usually observed between the dehydration and crystallization step. This indicates that the granule coagulation itself is not sufficient for the crystallization to proceed. This in turn supports the active role of intragranular water in plasticizing PHA. It has been experimentally confirmed that the native PHA granules have a residual water content up to 10% by mass (Mas et al. 1985), and the plasticizing effect of water on polymers, even those structurally similar such as poly(vinyl acetate) (Bair et al. 1981), is well known. Lauzier et al. (1992a, b) proposed a hypothesis that chains of newly biosynthesized PHA, located in the granule's interior, are stabilized in the extended β-conformation by hydrogen-bonded water, resulting in a mobile amorphous form of PHA incapable of crystallization. This hypothesis has not been experimentally confirmed yet because no artificial amorphous form of PHA stabilized only by complexation with water had been prepared so far. Nevertheless, our results indicate that the plasticizing role of water represents not the exclusive, but the necessary additional effect which, in combination with low volume of the native intracellular granules, stabilizes PHA in the mobile amorphous form.

The lag time between the loss of the majority of cytoplasmic water and the crystallization process could then represent the time needed by the intragranular water to leave the granule. This may also explain the unique behavior of osmotically challenged cells where no such lag time was observed. From the morphological analysis (see Fig. 7e), it was found that in the osmotically up-shocked cells, integrity of the granule surface is disturbed and, consequently, the PHA polymer "leaks" from the granules to the cytoplasm. It is likely that, in a similar way, the rate of passage of water from inside to outside the granule is increased under this condition.

Furthermore, it should be noted that the fact that exposure to some stress factors stimulates aggregation of PHA granules might affect reproduction of the bacterial cells. Since aggregates are usually situated in the central part of the cells, aggregation might complicate division of the bacterial cells. Actually, in our stress challenge experiment (Fig. 6), we observed the lowest number of cultivable cells in bacterial cultures exposed to stressors, which strongly induced PHA granules aggregation, such as high temperature or strongly acidic conditions.

To conclude, the fact that intracellular PHA polymer in native intracellular granules occurs in a metastable amorphous form is not only of specific interest from the prospective of material or polymer science, but it has also numerous important biological consequences. We have demonstrated that exposure of bacterial cells to some of the tested stressors induces granules aggregation and subsequent crystallization of the polymer when the bacterial cells are dried. Actually, the fact that both granules aggregation and cell drying must occur to induce crystallization of PHA indicates that both previously suggested hypotheses about mechanisms of stabilization of amorphous state of native PHA are valid and in fact both effects participate synergistically. The amorphous state of the polymer is stabilized kinetically by the low rate of crystallization in limited volume in small PHA granules; moreover, intragranular water seems to function as plasticizer protecting polymer from crystallization. Nevertheless, it is expectable that some other important contributors to this complex phenomenon are still to be revealed. For example, the importance of granule-associated proteins in maintaining the granule

integrity was evidenced by our results, nevertheless, detailed analysis of the specific structural changes during the stress exposure should be provided. Moreover, the significance of the content of monomer units of PHA in PHA-accumulating cells together with its important biological activity was discussed in our previous work (Obruca et al. 2016b). However, no information is yet available on the concentration of the monomer and/or oligomers in the granules nor on their effect on phase transition of the polymer form. Therefore, and taking into account its widely discussed biological importance, there remains a lot to be elucidated before finding a complete answer to the question raised in the title of this paper.

Compliance with ethical standards

Conflict of interest The authors declare that they have no conflict of interest.

Ethical approval This article does not contain any studies with human participants or animals performed by any of the authors.

References

Arrondo JLR, Muga A, Castresana J, Goni FM (1993) Quantitative studies of the structure of proteins in solution by Fourier-transform infrared-spectroscopy. Prog Biophys Mol Biol 59(1):23–56. https://doi.org/10.1016/0079-6107(93)90006-6

Bair HE, Johnson GE, Anderson EW, Matsuoka S (1981) Non equilibrium annealing behavior of poly(vinyl acetate): phase diagram, thermal and crystallization behavior. Polym Eng Sci 21:930–935. https://doi.org/10.1002/pen.760211410

Beeby M, Cho M, Stubbe JA, Jensen GJ (2012) Growth and localization of polyhydroxybutyrate granules in *Ralstonia eutropha*. J Bacteriol 194(5):1092–1099. https://doi.org/10.1128/JB.06125-11

Bonthrone KM, Clauss J, Horowitz DM, Hunter BK, Sanders JKM (1992) The biological and physical-chemistry of Polyhydroxyalkanoates as seen by NMR-spectroscopy. FEMS Microbiol Lett 103(2-4):269–277. https://doi.org/10.1111/j.1574-6968.1992.tb05848.x

Bresan S, Sznajder A, Hauf W, Forchhammer K, Pfeiffer D, Jendrossek D (2016) Polyhydroxyalkanoate (PHA) granules have no phospholipids. Sci Rep 6:26612. https://doi.org/10.1038/srep26612

Byler DM, Susi H (1986) Examination of the secondary structure of proteins by deconvolved Ftir spectra. Biopolymers 25(3):469–487. https://doi.org/10.1002/bip.360250307

Ceccorulli G, Pizzoli M, Scandola M (1992) Plasticization of bacterial poly(3-Hydroxybutyrate). Macromolecules 25:3304–3306. https://doi.org/10.1021/ma00038a045

Choi JS, Park WH (2004) Effect of biodegradable plasticizers on thermal and mechanical properties of poly(3-hydroxybutyrate). Polym Test 23:455–460. https://doi.org/10.1016/j.polymertesting.2003.09.005

De Koning GJM, Lemstra PJ (1992) The amorphous state of bacterial poly[(R)-3-hydroxyalkanoate] in vivo. Polymer 33:3292–3294. https://doi.org/10.1016/0032-3861(92)90249-V

Goormaghtigh E, Cabiaux V, Ruysschaert JM (1990) Secondary structure and dosage of soluble and membrane proteins by attenuated total reflection Fourier-transform infrared spectroscopy on hydrated films. Eur J Biochem 193(2):409–420. https://doi.org/10.1111/j.1432-1033.1990.tb19354.x

Hu Y, Zhang J, Sato H, Noda I, Ozaki Y (2007) Multiple melting behavior of poly(3-hydroxybutyrate-co-3-hydroxyhexanoate) investigated by differential scanning calorimetry and infrared spectroscopy. Polymer 48:4777–4785. https://doi.org/10.1016/j.polymer.2007.06.016

Jendrossek D (2007) Peculiarities of PHA granules preparation and PHA depolymerase activity determination. Appl Microbiol Biotechnol 74(6):1186–1196. https://doi.org/10.1007/s00253-007-0860-9

Kadouri D, Jurchevitch E, Okon Y (2003) Involvement of the reserve material poly-β-hydroxybutyrate in *Azospirillum brasilense* stress endurance and root colonization. Appl Environ Microbiol 69(6):3244–3250. https://doi.org/10.1128/AEM.69.6.3244-3250.2003

Kim J, Kim YJ, Choi SY, Lee SY, Kim KJ (2017a) Crystal structure of *Ralstonia eutropha* polyhydroxyalkanoate synthase C-terminal domain and reaction mechanisms. Biotechnol J 12(1):1600648. https://doi.org/10.1002/biot.201600648

Kim YJ, Choi SY, Kim J, Jin KS, Lee SY, Kim KJ (2017b) Structure and function of the N-terminal domain of *Ralstonia eutropha* polyhydroxyalkanoate synthase, and the proposed structure and mechanisms of the whole enzyme. Biotechnol J 12(1):1600649. https://doi.org/10.1002/biot.201600649

Koskimäki JJ, Kajula M, Hokkanen J, Ihantola EL, Kim JH, Hautajärvi H, Hankala E, Suokas M, Pohjanen J, Podolich O, Kozyrovska N, Turpeinen A, Pääkkönen M, Mattila S, Campbell BC, Pirttilä AM (2016) Methyl-esterified 3-hydroxybutyrate oligomers protect bacteria from hydroxyl radicals. Nat Chem Biol 12(5):332–338. https://doi.org/10.1038/nchembio.2043

Lauzier C, Marchessault RH, Smith P, Chanzy H (1992a) Structural study of isolated poly(β-hydroxybutyrate) granules. Polymer 33:823–827. https://doi.org/10.1016/0032-3861(92)90343-U

Lauzier C, Revol JF, Marchessault RH (1992b) Topotactic crystallization of isolated poly(beta-hydroxybutyrate) granules from *Alcaligenes eutrophus*. FEMS Microbiol Lett 103:299–310. https://doi.org/10.1111/j.1574-6968.1992.tb05851.x

Mas J, Pedros-Alio C, Guerrero R (1985) Mathematical-model for determining the effects of intracytoplasmic inclusions on volume and density of microorganisms. J Bacteriol 164:749–756

Nowroth V, Marquar L, Jendrossek D (2016) Low temperature-induced viable but not culturable state of *Ralstonia eutropha* and its relationship to accumulated polyhydroxybutyrate. FEMS Microbiol Lett 363(23):fnw249. https://doi.org/10.1093/femsle/fnw249

Obruca S, Snajdar O, Svoboda Z, Marova I (2013) Application of random mutagenesis to enhance the production of polyhydroxyalkanoates by *Cupriavidus necator* H16 on waste frying oil. World J Microbiol Biotechnol 29(12):2417–2428. https://doi.org/10.1007/s11274-013-1410-5

Obruca S, Sedlacek P, Krzyzanek V, Mravec F, Hrubanova K, Samek O, Kucera D, Benesova P, Marova I (2016a) Accumulation of Poly(3-hydroxybutyrate) helps bacterial cells to survive freezing. PLoS One 11:e0157778. https://doi.org/10.1371/journal.pone.0157778

Obruca S, Sedlacek P, Mravec F, Samek O, Marova I (2016b) Evaluation of 3-hydroxybutyrate as an enzyme-protective agent against heating

and oxidative damage and its potential role in stress response of poly(3-hydroxybutyrate) accumulating cells. Appl Microbiol Biotechnol 100:1365–1376. https://doi.org/10.1007/s00253-015-7162-4

Obruca S, Sedlacek P, Mravec F, Krzyzanek V, Nebesarova J, Samek O, Kucera D, Benesova P, Hrubanova K, Milerova M, Marova I (2017) The presence of PHB granules in cytoplasm protects non-halophilic bacterial cells against the harmful impact of hypertonic environments. New Biotechnol 39:68–80. https://doi.org/10.1016/j.nbt.2017.07.008

Obruca S, Sedlacek P, Koller M, Kucera D, Pernicova I (2018) Involvement of polyhydroxyalkanoates in stress resistance of microbial cells: biotechnological consequences and applications. Biotechnol Adv 36(3):856–870. https://doi.org/10.1016/j.biotechadv.2017.12.006

Pavez P, Castillo JL, Gonzalez C, Martinez M (2009) Poly-β-hydroxyalkanoate exert a protective effect against carbon starvation and frozen conditions in Sphingopyxis chilensis. Curr Microbiol 59:636–640. https://doi.org/10.1007/s00284-009-9485-9

Porter M, Yu J (2011a) Monitoring the in situ crystallization of native biopolyester granules in Ralstonia eutropha via infrared spectroscopy. J Microbiol Methods 87(1):49–55. https://doi.org/10.1016/j.mimet.2011.07.009

Porter M, Yu J (2011b) Crystallization kinetics of poly(3-hydroxybutyrate) granules in different environmental conditions. J Biomater Nanobiotechnol 2:301–310. https://doi.org/10.4236/jbnb.2011.23037

Sedlacek P, Slaninova E, Koller M, Nebesarova J, Marova I, Krzyzanek V, Obruca S (2018) PHA granules help bacterial cells to preserve cell integrity when exposed to sudden osmotic imbalances. New Biotechnol. https://doi.org/10.1016/j.nbt.2018.10.005

Slaninova E, Sedlacek P, Mravec F, Mullerova L, Samek O, Koller M, Hesko O, Kucera D, Marova I, Obruca S (2018) Light scattering on PHA granules protects bacterial cells against the harmful effects of UV. Appl Microbiol Biotechnol 102(4):1923–1931. https://doi.org/10.1007/s00253-018-8760-8

Soto G, Setten L, Lisi C, Maurelis C, Mozzicafreddo M, Cuccioloni M, Angeletti M, Ayub ND (2012) Hydroxybutyrate prevents protein aggregation in the halotolerant bacterium Pseudomonas sp. CT13 under abiotic stress. Exremophiles 16:455–462. https://doi.org/10.1007/s00792-012-0445-0

Sudesh K, Abe H, Doi Y (2000) Synthesis, structure and properties of polyhydroxyalkanoates: biological polyesters. Prog Polym Sci 25:1503–1555. https://doi.org/10.1016/S0079-6700(00)00035-6

Susi H, Byler DM (1986) Resolution-enhanced fourier transform infrared. Methods Enzymol 130:290–311. https://doi.org/10.1016/0076-6879(86)30015-6

Uchino K, Saito T, Jendrossek D (2008) Poly(3-hydroxybutyrate) (PHB) depolymerase PhaZa1 is involved in mobilization of accumulated PHB in Ralstonia eutropha H16. Appl Environ Microbiol 74(4):1057–1063. https://doi.org/10.1128/AEM.02342-07

Wang Q, Yu H, Xia Y, Kang Z, Qi Q (2009) Complete PHB mobilization in Escherichia coli enhances the stress tolerance: a potential biotechnological application. Microb Cell Factories 8:47. https://doi.org/10.1186/1475-2859-8-47

Wieczorek R, Pries A, Steinbuchel A, Mayer F (1995) Analysis of a 24-kilodalton protein associated with the polyhydroxyalkanoic acid granules in Alcaligenes eutrophus. J Bacteriol 177:2425–2435. https://doi.org/10.1128/jb.177.9.2425-2435.1995

Wittenborn EC, Jost M, Wei Y, Stubbe J, Drennan CL (2016) Structure of the catalytic domain of the class I polyhydroxybutyrate synthase from Cupriavidus necator. J Biol Chem 291:25264–25277. https://doi.org/10.1074/jbc.M116.756833

York GM, Lupberger J, Tian J, Lawrence AG, Stubbe JA, Sinskey AJ (2003) Ralstonia eutropha H16 encodes two and possibly three intracellular poly[D-(-)-3-hydroxybutyrate] depolymerase genes. J Bacteriol 185(13):3788–3794. https://doi.org/10.1128/JB.185.13.3788-3794.2003

Zhao YH, Li HM, Qin LF, Wang HH, Chen GQ (2007) Disruption of the polyhydroxyalkanoate synthase gene in Aeromonas hydrophila reduces its survival ability under stress conditions. FEMS Microbiol Lett 276:34–41. https://doi.org/10.1111/j.1574-6968.2007.00904.x

Appendix 12

Pernicova, I., Novackova, I., Sedlacek, P., Kourilova, X., Kalina, M., Kovalcik, A., Koller, M., Nebesarova, J., Krzyzanek, V., Hrubanova, K., Masilko, J., Slaninova, E., and Obruca, S. Introducing the Newly Isolated Bacterium Aneurinibacillus sp. H1 as an Auspicious Thermophilic Producer of Various Polyhydroxyalkanoates (PHA) Copolymers–1. Isolation and Characterization of the Bacterium. *Polymers* **2020**, 12, 1235.

Introducing the Newly Isolated Bacterium *Aneurinibacillus* sp. H1 as an Auspicious Thermophilic Producer of Various Polyhydroxyalkanoates (PHA) Copolymers–1. Isolation and Characterization of the Bacterium

Iva Pernicova [1], **Ivana Novackova** [1], **Petr Sedlacek** [1], **Xenie Kourilova** [1], **Michal Kalina** [1], **Adriana Kovalcik** [1], **Martin Koller** [2,3], **Jana Nebesarova** [4,5], **Vladislav Krzyzanek** [6], **Kamila Hrubanova** [6], **Jiri Masilko** [1], **Eva Slaninova** [1] and **Stanislav Obruca** [1,*]

[1] Faculty of Chemistry, Brno University of Technology, Purkynova 118, 612 00 Brno, Czech Republic; xcpernicovai@fch.vut.cz (I.P.); xcnovackova@fch.vut.cz (I.N.); sedkacek-p@fch.vut.cz (P.S.); xckourilovax@fch.vut.cz (X.K.); kalina-m@fch.vut.cz (M.K.); kovalcik@fch.vut.cz (A.K.); masilko@fch.vut.cz (J.M.); xcslaninovae@fch.vut.cz (E.S.)

[2] Office of Research and Management, c/o Institute of Chemistry, NAWI Graz, University of Graz, Heinrichstrasse 28/VI, 8010 Graz, Austria; martin.koller@uni-graz.at

[3] ARENA Arbeitsgemeinschaft für Ressourcenschonende & Nachhaltige Technologien, Inffeldgasse 21b, 8010 Graz, Austria

[4] Biology Centre, The Czech Academy of Sciences, v.v.i., Branisovska 31, 370 05 Ceske Budejovice, Czech Republic; nebe@paru.cas.cz

[5] Faculty of Science, University of South Bohemia, Branisovska 31, 370 05 Ceske Budejovice, Czech Republic

[6] Institute of Scientific Instruments of the Czech Academy of Sciences, v.v.i., Kralovopolska 147, 612 64 Brno, Czech Republic; krzyzanek@isibrno.cz (V.K.); hrubanova@isibrno.cz (K.H.)

* Correspondence: obruca@fch.vut.cz; Tel.: +420-541-149-354

Abstract: Extremophilic microorganisms are considered being very promising candidates for biotechnological production of various products including polyhydroxyalkanoates (PHA). The aim of this work was to evaluate the PHA production potential of a novel PHA-producing thermophilic Gram-positive isolate *Aneurinibacillus* sp. H1. This organism was capable of efficient conversion of glycerol into poly(3-hydroxybutyrate) (P3HB), the homopolyester of 3-hydroxybutyrate (3HB). In flasks experiment, under optimal cultivation temperature of 45 °C, the P3HB content in biomass and P3HB titers reached 55.31% of cell dry mass and 2.03 g/L, respectively. Further, the isolate was capable of biosynthesis of PHA copolymers and terpolymers containing high molar fractions of 3-hydroxyvalerate (3HV) and 4-hydroxybutyrate (4HB). Especially 4HB contents in PHA were very high (up to 91 mol %) when 1,4-butanediol was used as a substrate. Based on these results, it can be stated that *Aneurinibacillus* sp. H1 is a very promising candidate for production of PHA with tailored material properties.

Keywords: polyhydroxyalkanoates; thermophiles; *Aneurinibacillus* sp.; P(3HB-*co*-4HB); P(3HB-*co*-3HV-*co*-4HB)

1. Introduction

The term "thermophiles" is devoted to microorganisms revealing optimal growth temperature above 45 °C [1]. Actually, these microbes are ubiquitous since they can be isolated from a wide range of

habitats from freshly fallen snow to pasteurized milk to geothermal areas like hot springs [2]. Currently, thermophiles attract attention of industrial biotechnologists since bioprocesses operated at elevated temperatures have a number of advantages, including a reduced risk of microbial contamination, lowered jeopardy by phage infection, improved solubility of substrates such as polysaccharide-rich resources, continuous and direct recovery of volatile metabolites from fermentation broth such as alcohols or volatile fatty acids (VFAs) and decreased cooling costs and demands for cooling water due to the higher temperature difference between bioreactor and the ambient air. On the other side, it should be pointed out that final energy balance of the process must be precisely evaluated at large scale to estimate whether operation of the process at elevated temperature can be economically feasible. Moreover, another aspect which should be taken into account is reduced solubility of oxygen under higher temperatures, which might disadvantage aerobic processes [1]. Professor Chen has recently defined the concept of "Next Generation Industrial Biotechnology" (NGIB), which is based on utilization of extremophilic microorganisms as producing units. Since extremophiles are capable of thriving under conditions which exclude most common mesophilic contaminants, NGIB can be principally operated under semi-sterile or even non-sterile conditions, which reduces costs of the process. Moreover, since NGIB processes are naturally robust against contamination, they can be run in continuous mode for long periods. Continuous processes are positive in terms of productivity and efficiency of the process due to the elimination of permanent unproductive times of revamping, which is needed in non-continuous processes for emptying and preparation of the bioreactor between individual cultivation batches [3].

Polyhydroxyalkanoates (PHA) are microbial polyesters which are accumulated by numerous prokaryotes in form of intracellular granules primarily as storage compounds; nevertheless, they also enhance robustness of the microbes against various stressors [4]. In most microorganisms, PHA accumulation is favored when external carbon substrate is present in excess, but nitrogen, phosphorous or other elements are lacking in parallel, which inhibits multiplication of cells [5]. PHA are very promising materials because they can be used as fully biodegradable and bioresource-based alternatives to petrochemical polymers since mechanical and technological properties of PHA are similar to some polymers produced from petrochemical resources. In fact, properties of PHA strongly depend upon their monomer composition. The most common and the best-studied member of the PHA family, namely poly(3-hydroxybutyrate) (P(3HB)), the homopolymer of 3-hydroxybutyrate (3HB), has a rather high melting temperature (T_m) of about 180 °C, which is very close to the temperature of its degradation (T_d; about 200 °C). It is remarkable that the native PHA material, organized as intracellular granules ("carbonosomes") in the cytoplasm of bacterial cells, is completely amorphous, however, when the material is extracted from the cells, it quickly crystallizes; therefore, the material is rigid and brittle with only limited elongation at break (about 3%) [6]. Nevertheless, material properties can be tailored when other monomer subunits are incorporated into the polymer chain. For instance, when 3-hydroxyvalerate (3HV) is inserted into the polymer chain, the resulting copolymer poly(3-hydroxybuytyrate-*co*-3-hydroxyvalerate) (P(3HB-*co*-3HV)) possesses a lower melting temperature and also a less crystalline structure, which are very positive features considering the processing of the materials [7]. Alternatively, 4-hydroxybuytrate (4HB) can be also introduced into the polymer by some bacteria and haloarchaea; PHA containing 4HB subunits reveal only minor crystallinity, high flexibility and even improved biodegradability in numerous environments including the human body. Therefore, they are very suitable for applications in various fields including high-end medical applications such as implants or drug delivery systems [8].

To achieve biosynthesis of above mentioned copolymers, most microbes require supplementation of precursors structurally related to particular monomers. For instance, to induce synthesis of polymers containing 3HV subunits, odd carbon number precursors such as n-propanol, propionate, n-pentanol or valerate are applied. Similarly, for production of 4HB-containing polymers, precursor compounds structurally related to 4HB such as 1,4-butanediol, γ-butyrolactone (GBL) or 1,6-hexanediol are utilized [9].

PHA are very promising materials; however, they are disadvantaged in competition with petrochemical polymers by their high production costs [10]. There are several strategies which could facilitate sustainable and economically feasible production of PHA such as utilization of cheap carbon substrates, for instance waste or side products of food industry or agriculture [11], or the use of genetically engineered strains revealing high productivity and substrate-to-product conversion yields [12]. Furthermore, considering all the positive aspects of employing thermophiles in industrial biotechnology mentioned above, also the use of thermophilic PHA producers holds promise to gain sustainable and economically reasonable processes for PHA production. Nevertheless, despite the fact that PHA accumulation is a common feature among many prokaryotes, capability of PHA synthesis was described only for limited number of thermophiles such as *Chelatococcus thermostellatus* [13], *Thermus thermophilus* [14] or *Caldimonas taiwanensis* [15].

Therefore, we made an effort to isolate novel promising PHA-producing thermophiles. To reach this goal, we have recently developed a unique protocol for isolation of PHA-producing thermophiles described in [16]. We have isolated several interesting strains, and, among them, the isolate designated as H1 was identified to be the most promising one. Therefore, we have performed taxonomic classification, basic morphological and metabolic description and, what is the most important, we have also assessed the biotechnological potential of this novel thermophilic isolate for industrial production of PHA and various PHA copolymers with tailored material properties.

2. Materials and Methods

2.1. Isolation and Characterization of the Thermophilic PHA Producer

A compost sample was taken from the central urban composting plant of the city Brno, Czech Republic (Centrální kompostárna Brno operated by SUEZ CZ a.s.), the temperature of the compost was about 40 °C at time of sample collection. After homogenization of the compost collected, 1 g of the sample was mixed with 100 mL of mineral salt medium (MSM) of the following composition (g/L): $Na_2HPO_4 \cdot 12\ H_2O$, 9.0; KH_2PO_4, 1.5; $MgSO_4 \cdot 7\ H_2O$, 0.2; NH_4Cl 1.0; $CaCl_2 \cdot 2\ H_2O$, 0.02; $Fe^{III}NH_4citrate$, 0.0012; yeast extract, 0.5 with 20 g/L glycerol as sole carbon source. The MSM included 1 mL/L microelements solution (MES), which contains (g/L): EDTA, 50.0; $FeCl_3 \cdot 6\ H_2O$, 13.8; $ZnCl_2$, 0.84; $CuCl_2 \cdot 2\ H_2O$, 0.13; $CoCl_2 \cdot 6\ H_2O$, 0.1; $MnCl_2 \cdot 6\ H_2O$, 0.016; H_3BO_3, 0.1; all these compounds were dissolved in distilled water. The cultivation was carried out for 48 h at 50 °C with shaking at 180 rpm. After cultivation, the fresh culture was used to inoculate fresh MSM; this second cultivation was carried out for 48 h at 50 °C with shaking at 180 rpm. After the second cultivation, the original isolation protocol was used to isolate the PHA-producing bacteria. The isolation protocol is based on the protective role of PHA against osmotic challenge. During the isolation, the mixed bacterial consortium obtained after the second cultivation is exposed to hyperosmotic challenge induced by solution of NaCl at a concentration of 100 g/L; subsequently, the culture is exposed to sudden hypotonic shock introduced by transfer of the culture to distilled water. Such a rapid fluctuation of osmotic pressure favors survival of PHA-producing bacteria, which are plated on solidified media, and PHA positive colonies are identified by infrared spectroscopy. The principle of the isolation procedure is depicted at Figure 1 and it was described previously [16].
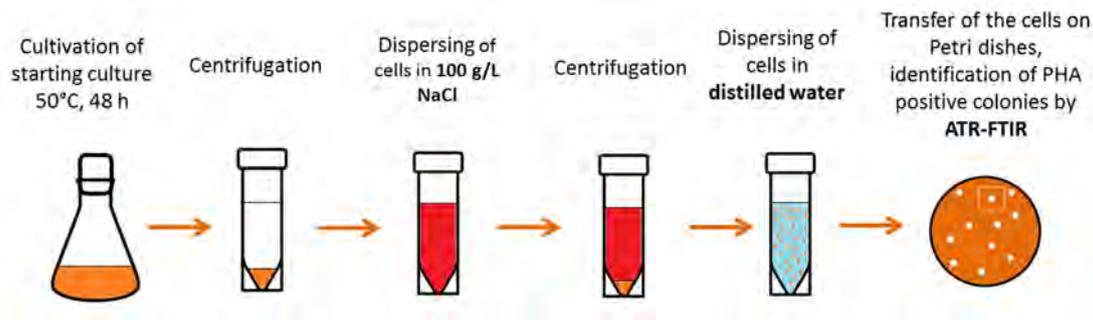
Figure 1. Principle of the "osmoselection"; procedure enabling isolation of PHA-producing thermophiles.

2.2. Identification and Metabolic and Morphological Characterization of the Isolate

The isolate was identified by sequencing the *16S* rRNA gene. Cells were lysed by heating to extract DNA. A small amount of culture from Petri dishes was added to the lyses buffer (5 mM TrisHCl, pH 8.5) and heated to 95 °C for 10 min. After heating, lysed cells were centrifuged, and the supernatant was used as a DNA template. Polymerase chain reaction (PCR) for detection of bacterial DNA and taxonomy (*16S* rRNA) was performed using the forward primer 16S-F (5'-AAGAGTTTGATCCTGGCTCAG-3') and the reverse primer 16S-R (5'-GGTTACCTTGTTACGACTT-3'). The PCR mixture consisted of 12.5 μL One TaqTM Hot Start 2X Master Mix with Standard Buffer, 2.6 μL MgCl₂, 2 μL DNA template, 0.2 μM of each primer; this solution was added to 25 μL H₂O, and the resulting PCR mixture was heated at 94 °C for 30 s. The PCR cycle consisted of three steps: denaturation for 30 s at 94 °C, annealing for 30 s at 55 °C and extension for 90 s at 68 °C. This cycle was repeated 30 times, the last extension step was extended for 5 min at 68 °C. The PCR amplicon was detected by 2% agarose gel electrophoresis with 1x TBE. PCR products of 16S rRNA gene were purified using the NucleoSpin Gel and PCR Clean-up kit and sent for commercial sequencing (SEQme, Dobris, Czech Republic). The taxonomic classification was evaluated using the blast NCBI database (https://blast.ncbi.nlm.nih.gov/Blast.cgi).

The standard set of physiological and biochemical tests such as shape and color of colonies, morphology of cells and spores, capability of hydrolysis of gelatin, urea, lecithin, starch, Tween 80, esculine, tyrosine and DNA, production catalase, arginine dehydrogenase and acid formation from various carbohydrates, spore formation, growth in presence of 10% and 70% NaCl, growth at various temperatures in range of 30–60 °C or hemolysis were performed at Czech Collection of Microorganisms according to procedures described in [17]. The isolate was also commercially identified using Biolog MicroStation system at Czech Collection of Microorganisms (CCM).

The morphology of cells was in more details investigated by Transmission Electron Microscopy (TEM) analysis using Microscope JEOL 1010 (JEOL, Pleasanton, USA) as described previously [18]. The high-pressure-freezing was performed using the instrument EM ICE (Leica Microsystems, Vienna, Austria) on the 3 mm aluminum carriers.

2.3. Production of PHA in Shaking Flasks by Aneurinibacillus sp. H1

To generate the inoculum, the culture was grown in complex media Nutrient Broth (10 g/L beef extract, 10 g/L peptone, 5 g/L NaCl) at 45 or 50 °C with shaking at 190 rpm. For production of PHA, mineral salt medium (MSM) was used consisting of: Na₂HPO₄·12 H₂O, 9.0 g/L; KH₂PO₄, 1.5 g/L; MgSO₄·7 H₂O, 0.2 g/L; NH₄NO₃ 1.0 g/L; CaCl₂·2 H₂O, 0.02 g/L; Feᴵᴵᴵ NH₄ citrate, 0.0012 g/L; Tryptone 0.5 g/L with 1 mL/L of MES (composition see 2.1). Various carbon sources (glycerol, glucose, sucrose, mannose, galactose, fructose, lactose, 1,4-butanediol, etc.) were usually applied at a concentration of 20 g/L if not stated otherwise. The inoculum ratio was 10 vol.%. Production cultivations were carried out for 72 h at selected temperature (usually 45 °C if not stated otherwise) under constant shaking of 180 rpm. All the cultivations were performed in duplicate. After cultivation, bacterial cells were harvested by centrifugation (6000× *g*, 5 min). Biomass was determined gravimetrically as

dry mass (CDM), and the amount and monomer composition of PHA in CDM was analyzed by Gas Chromatography as reported previously [19].

Among the tested substrates, we also included waste glycerol, which was obtained from the oil mill company Victoria Oil, Šid, Serbia. This side product of biodiesel production was previously analyzed on GC/FID as a part of regular control of biodiesel quality. It was found that the composition of waste glycerol mainly consisted of glycerol (83.72 *w/w* %), water (6.77 *w/w* %), ash/NaCl (6.5 *w/w* %) and other organic matter (1.58 *w/w* %). The pH value of waste glycerol was 6.77.

3. Results and Discussion

3.1. Taxonomic, Metabolic and Morphological Description the Isolate

Since we observed that among all isolates obtained from compost the strain designated as H1 reveals the most promising PHA production capacity, the isolate was phenotypically characterized by Czech Collection of Microorganisms. The cells are Gram-positive, and grow individually. **Positive tests**: spore formation; catalase; urease; anaerobic growth; hydrolysis of gelatin, ONPG and lecithin; acids produced from glucose, xylose and lactose; growth in presence of 7% NaCl; growth at 60 °C; hemolysis. **Negative tests**: starch hydrolysis, hydrolysis of: Tween 80, esculin, tyrosine and DNA, acetoin; reduction of nitrates; acids produced from mannitol, cellobiose, fructose and inositol; growth in presence of 10% NaCl, growth at 30 °C and 65 °C. Further, the isolate was also identified using the BIOLOG system, according to results of phenotype characterization and BIOLOG analysis, the strain was identified as *Aneurinibacillus* sp. H1 without possible reliable closer taxonomical classification. Further, the isolate was also identified by partial sequencing of *16S* rRNA gene, the sequence is available at MT112889; according to comparison of *16S* rRNA sequences available in BLAST database, the strain has high similarity to *Aneurinibacillus thermoaerophilus* strain DSM 10154 (99.91%), *Aneurinibacillus thermoaerophilus* strain L420-91 (99.83%), and *Aneurinibacillus sediminis* strain 1-10M-8-7-50 (96.47%).

The fact that the isolate is a Gram-positive bacterium can be considered being very beneficial. Most of the currently used PHA-producing strains are Gram-negative bacteria such as *Cupriavidus necator* [20,21], transgenic *Escherichia coli* [22] or members of the genus *Halomonas* [23,24]. Actually, one of the major obstacles preventing application of PHA in high-value applications such as health care, cosmetics or medicine is the fact that the polymers isolated from Gram-negative strains are heavily contaminated by lipopolysaccharides (LPS), a group of endotoxins produced by Gram-negative bacteria as important component of their outer cell membrane. LPS are co-isolated with PHA during down-stream processing and might cause severe immunological response making PHA biopolymers extremely unsuitable in medical uses [25].

Members of the genus *Aneurinibacillus* are mostly thermophilic or thermotolerant and, of course, they are taxonomically closely related to the genus *Bacillus*, which is well known for its capability of PHA biosynthesis [26–28]. Actually, the genus *Aneurinibacillus* was set aside from genus *Bacillus* in 1996 [29]. It should be pointed out that PHA production capacity was already described for thermophilic *Aneurinibacillus* sp. XH2 isolated from an oilfield in China [30]; hence, it seems that PHA biosynthesis is also ubiquitous among members of *Aneurinibacillus*.

The morphology of the cells of *Aneurinibacillus* sp. H1 grown for 72 h in mineral medium with glycerol was investigated by TEM, the results are shown in Figure 2. The cells contain 8–15 PHA granules, which are not localized in particular parts of the cells but are rather randomly distributed in the cellular space. Actually, size of the cells, localization and diameters of the granules are very similar to those reported for typical well-studied PHA producers such as *C. necator* H16 [31] or *Halomonas halophila* [32]. Apart from PHA granules, in some cells presence of spores in the central part of the cells can be observed as well (marked by red arrows). Generally, sporulation is not considered being a positive feature of the strains used in industrial biotechnology, since sporulation is associated with loss of desirable metabolic activity, and it was also reported that sporulation in *Bacillus* species is associated with mobilization of PHA storage [33]. From the economic point of view, spore formation depletes

view, spore formation depletes carbon sources dedicated to PHA biosynthesis. Nevertheless, despite the fact that cultivation was performed for a relatively long time (72 h), the number of sporulating cells is very low (below 10%), and PHA granules can be clearly seen also in spore forming cells, which indicates that sporulation should not be a major drawback preventing utilization of the isolate *Aneurinibacillus* sp. H1 in industrial production of PHA. However, gaining non-sporulating mutants of the strain would be very desirable. Further experiments could also clarify if shifting process parameters (e.g., pH-value) could be a tool to completely prevent spore formation, as it was previously demonstrated for PHA-accumulating *Bacillus cereus* SPV cultures, which at lower pH-value readily accumulated PHA, but completely stopped sporulation, thus drastically increasing the substrate-to-PHA yield [34].
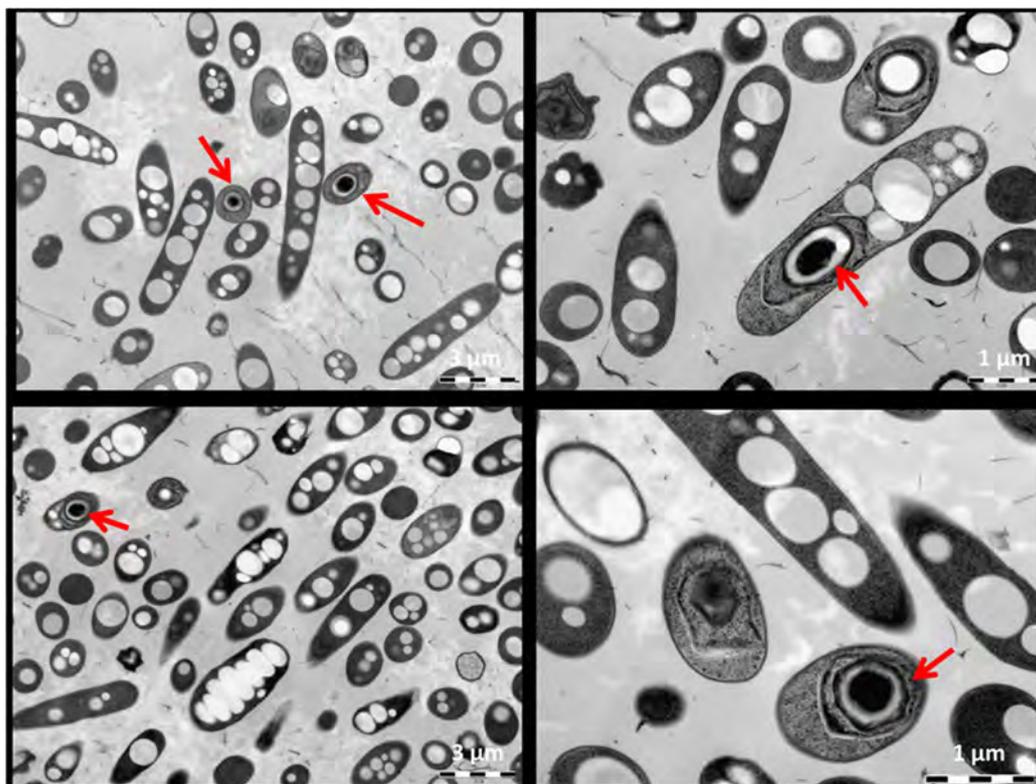
Figure 2. Morphology of the cells of *Aneurinibacillus* sp. H1 observed by TEM; the red arrows show endospores in bacterial cells.

3.2. Production of PHA on Various Carbon and Nitrogen Substrates

Further, the production capacity of the isolated strain *Aneurinibacillus* sp. H1 on various carbon substrates was evaluated; results are shown in Table 1. Obviously, the highest biomass growth and PHA titers were achieved on glycerol, since the bacterial strain was capable of reaching a CDM of 2.19 g/L, and the PHA content in CDM amounted to 45.95%. Since glycerol was used as the sole carbon substrate during isolation of the strain, it is not surprising that this strain gained high productivity on this substrate by adaptation. The second best results, namely a CDM of 2.00 g/L and PHA content in CDM of 27.74%, were obtained when glucose was used. In all the other tested carbohydrate substrates, CDM values as well as PHA contents were very low. It should be mentioned that, not surprisingly, on all the tested substrates the bacterial culture produced homopolymer P(3HB). Further, the culture is not capable of utilizing lipid substrates, since practically no biomass growth was observed on waste frying oil when used as a sole carbon source.

Table 1. Production of PHA on various carbon sources.

Substrate	CDM [g/L]	P(3HB) [% per CDM]	P(3HB) [g/L]
Sucrose	0.41 ± 0.10	16.52 ± 0.31	0.07 ± 0.02
Mannose	0.19 ± 0.08	14.85 ± 0.05	0.03 ± 0.01
Galactose	0.22 ± 0.04	8.94 ± 0.13	0.02 ± 0.00
Glucose	2.00 ± 0.36	27.74 ± 0.18	0.55 ± 0.10
Fructose	0.24 ± 0.01	14.32 ± 0.21	0.03 ± 0.00
Lactose	0.20 ± 0.01	9.06 ± 0.20	0.02 ± 0.00
Glycerol	2.19 ± 0.07	45.95 ± 0.10	1.00 ± 0.04
WFO [1]	0.01 ± 0.00	*n.d.*	*n.d.*

[1] WFO stands for Waste Frying Oils. n.d.: not detected.

The fact that glycerol is the most preferred substrate by *Aneurinibacillus* sp. H1 can be considered as positive since waste glycerol is currently produced at steadily increasing quantity as a waste stream of biodiesel production [35]. Glycerol stemming from biodiesel fabrication contains numerous microbial inhibitors such as free fatty acids, methanol and residues of metal catalyst, which complicates its utilization as a substrate in microbial biotechnology. Nevertheless, there are reports on PHA production from waste glycerol employing various mesophilic microbes such as *Bacillus cereus* [36], *Cupriavidus necator* [37], *Burholderia cepacia* [38] or the extremely halophilic archaeon *Haloferax mediterranei* [39]; moreover, there are also some reports on conversion of glycerol into PHA by thermophiles, in particular by *Chelatococcus* sp. isolated from an aerobic organic waste treatment plant in Germany [13], and also by *Caldimonas manganoxidans* [40]. To evaluate the potential of the isolate *Aneurinibacillus* sp. H1 for PHA production from waste glycerol and to estimate robustness of the strain against inhibitors contained in real waste glycerol, we performed an experiment in which PHA production on pure and waste glycerol was assessed at various initial concentrations of both carbon substrates; the results are shown in Table 2. In both waste and pure glycerol, the highest P(3HB) titers were gained at initial substrate concentration of 20 g/L, the better values were, in accordance with our expectations, obtained with pure glycerol. However, *Aneurinibacillus* sp. H1 demonstrated expedient robustness against inhibitors present in waste glycerol, since product titers obtained on waste glycerol were only about 20% lower than on pure glycerol (1.70 g/L in pure and 1.42 g/L in waste glycerol), and polymer contents in biomass were very similar (51.97 and 49.45% of CDM for pure and waste glycerol, respectively).

Table 2. Comparison of PHA biosynthesis on pure glycerol and waste glycerol from biodiesel production.

Substrate	Concentration [g/L]	Biomass [g/L]	P(3HB) [% per CDM]	P(3HB) [g/L]
Glycerol	10	1.60 ± 0.50	13.00 ± 1.20	0.21 ± 0.03
	20	3.27 ± 0.13	51.97 ± 2.28	1.70 ± 0.11
	30	2.72 ± 0.07	53.40 ± 4.82	1.45 ± 0.19
Waste/crude Glycerol	10	1.08 ± 0.08	10.78 ± 1.33	0.12 ± 0.02
	20	2.88 ± 0.13	49.45 ± 0.65	1.42 ± 0.03
	30	1.67 ± 0.32	46.10 ± 5.55	0.77 ± 0.13

3.3. Influence of Temperature on Production of PHA

We have also investigated the influence of the cultivation temperature on PHA production by *Aneurinibacillus* sp. H1. Cultivations were performed at temperatures in the range of 45–65 °C (Table 3.). The highest CDM concentration, PHA content and, therefore, also PHA titers were obtained at 45 °C; hence, this temperature can be considered being the optimal cultivation temperature. Further increase in cultivation temperature inhibited growth of the strain as well as PHA biosynthesis; nevertheless, the strain was capable of growing and synthesizing PHA even at 60 and 65 °C. Xiao et al. isolated *Aneurinibacillus* sp. designated as strain XH2 from the Gudao oilfield in China; optimal growth and PHA production temperature for this strain was reported as 55 °C, nevertheless, maximal PHA titers

were gained at optimal conditions were only 0.268 g/L [30], which is substantially less than achieved with our isolate *Aneurinibacillus* sp. H1, since the maximal P(3HB) titer gained by our strain in flasks experiment was 2.03 g/L, almost one order higher, indicating the auspicious biotechnological potential of our isolate.

Table 3. Effect of cultivation temperature on PHA yields obtained by *Aneurinibacillus* sp. H1.

Temperature [°C]	Biomass [g/L]	P(3HB) [% per CDM]	P(3HB) [g/L]
35	0.17 ± 0.01	30.20 ± 0.01	0.05 ± 0.01
40	2.66 ± 0.14	32.12 ± 4.49	0.92 ± 0.08
45	3.68 ± 0.63	55.31 ± 5.81	2.03 ± 0.41
50	3.23 ± 0.03	46.01 ± 3.55	1.49 ± 0.37
55	1.46 ± 0.05	50.18 ± 1.35	0.73 ± 0.03
60	0.80 ± 0.01	30.60 ± 1.35	0.24 ± 0.01
65	0.89 ± 0.06	32.66 ± 0.24	0.29 ± 0.02

The optimal cultivation temperature of 45 °C is most likely not high enough to eliminate the risk of contamination by ubiquitous thermotolerant microorganisms and, therefore, the biotechnological production process probably cannot be operated under economically and energetically attractive nonsterile open fermentation conditions. Nevertheless, despite this fact the industrial process could be energetically favorable since energy and water demands for cooling would be very low when cultivation would be performed at 45 °C as compared to standard mesophilic cultivation setups. Further, since 45 °C is not a very high temperature, energy demands on heating are not enormous and, moreover, it is likely that substantial amounts of heat needed to maintain the temperature at 45 °C would be generated by the metabolism of the microbes and also by the stirring system of the bioreactor, thus, the system could be partially operated as "self-heating system", as described before [41]. Last but not least, since oxygen solubility negatively correlates with temperature, rational aeration of the bioreactor would be feasible. Nevertheless, these technological presumptions must be evaluated during forthcoming scale-up experiments, which are, nevertheless, above scope of this work focused on characterization of the novel thermophilic PHA producer.

3.4. Biosynthesis of PHA Copolymers and Terpolymer

In a subsequent experiment, we looked into the capability of the *Aneurinibacillus* sp. H1 to incorporate 3HV and 4HB into the polymer structure by using structurally related precursor compounds; results are shown in Table 4. The 3HV precursors (levulinate, propionate, n-propanol, valerate) were applied at a concentration of 2 g/L along with glycerol (20 g/L), which was used as the main carbon substrate. Application of all the tested precursors partially inhibited growth of the bacterial culture, which is not surprising since all of them are well known microbial inhibitors. Among tested substrates, only application of levulinate did not result in production of P(3HB-*co*-3HV) copolymers, while using all the other 3HV precursors, the bacterial culture was able to incorporate 3HV into the polymer chain. Valerate seems to be the most suiTable 3HV precursor since its application resulted in very high 3HV content (66.62 mol %) in P(3HB-*co*-3HV) copolymer, and its inhibitory effect on the growth of microbial culture was the lowest among the tested precursors.

Based on our experience, we utilized a different cultivation approach to gain copolymers containing 4HB subunits. Selected 4HB precursors (1,6-hexanediol, γ-butyrolactone and 1,4-butanediol) were applied as the sole carbon sources at a concentration of 8 g/L. The bacterial culture was not capable of readily assimilating the precursor with 6 carbon atoms (1,6-hexanediol); hence, only a very low amount of PHA was obtained on this compound, and the polymer contained no 4HB subunits. Oppositely, precursors containing 4 carbon atoms were assimilated by the bacterial culture much more efficiently and their use resulted in very high PHA contents in cells (85.84 and 75.48% of CDM for GBL and 1,4-butanediol, respectively) and also in very high 4HB portion in copolymers (63.35 and 79.91 mol % for GBL and 1,4-butanediol, respectively).

Table 4. Production of PHA copolymers and terpolymer using various precursors of 3HV and 4HB.

Desired Monomer	Precursor	Biomass [g/L]	PHA [% per CDM]	PHA [g/L]	3HV [mol %]	4HB [mol %]	3HB [mol %]
3HV [1]	Levulinate	1.08 ± 0.06	36.70 ± 0.72	0.39 ± 0.02	*n.d.*	*n.d.*	100.00 ± 0.00
	Propionate	1.11 ± 0.04	28.15 ± 0.27	0.31 ± 0.01	32.10 ± 0.02	*n.d.*	67.90 ± 0.02
	Propanol	1.47 ± 0.04	45.11 ± 0.05	0.66 ± 0.02	3.66 ± 0.04	*n.d.*	96.34 ± 0.04
	Valerate	1.90 ± 0.02	36.29 ± 0.01	0.69 ± 0.01	66.62 ± 0.83	*n.d.*	33.38 ± 0.83
4HB [2]	1,6-hexandiol	0.37 ± 0.08	9.08 ± 0.31	0.03 ± 0.01	*n.d.*	*n.d.*	100 ± 0.00
	γ-butyrolactone	0.52 ± 0.00	85.84 ± 1.99	0.45 ± 0.01	*n.d.*	63.35 ± 3.27	36.65 ± 3.27
	1,4-butandiol	1.02 ± 0.04	75.48 ± 2.36	0.77 ± 0.04	*n.d.*	79.91 ± 1.84	20.09 ± 1.84
3HV + 4HB [3]	Valerate + 1,4-butanediol	1.44 ± 0.06	40.27 ± 2.08	0.58 ± 0.03	33.13 ± 1.03	54.18 ± 1.23	12.69 ± 2.26

[1] 3HV precursors were applied at the beginning of cultivation at concentration of 2 g/L. 20 g/L of glycerol was used as the main carbon source. [2] 4HB precursors were applied at the beginning of cultivations as the sole carbon sources at concentration of 20 g/L. [3] Terpolymer production was achieved by applying 1,4–butanediol (4 g/L) and valerate (2 g/L) at the beginning of cultivation, glycerol was not added. *n.d.*: not detected.

Further, we also attempted production of PHA terpolymer consisting of 3HB, 3HV and 4HB subunits. In this experiment, valerate (2 g/L) was used since it was identified as the most promising 3HV precursor, while 1,4-butanediol (4 g/L) was utilized as the most suiTable 4HB precursor. This cultivation strategy resulted in production of a very interesting terpolymer consisting of 33.13 mol % of 3HV, 54.18 mol % of 4HB and 12.69 mol % of 3HB.

These experiments proved the extraordinary capacity of *Aneurinibacillus* sp. H1 to biosynthesize polymers containing 3HV and/or 4HB subunits, which generally reveal superior mechanical properties compared to P(3HB) homopolymer. Especially the capacity of the strain to incorporate high portions of 4HB subunits into the polymer chain is very promising since the increased 4HB content in polymer is usually connected with improved flexibility as the crystallinity of the polymer is affected [42]. Capabilities to synthesize materials with so high 4HB fraction, reaching high intracellular PHA content and reasonable PHA titers are rare among PHA producers. Only few microorganisms are capable of production of PHA with 4HB fraction higher than 20–30 mol %. For instance, Huong et al. employed *Cupriavidus* sp. USMAA1020 for production of P(3HB-*co*-4HB) copolymer and 4HB fractions in polymer varying between 7 and 70 mol % depending on the applied cultivation conditions; nevertheless, increase of the 4HB fraction was accompanied by lowering of PHA content in bacterial cells, reduced biomass growth and lower product titers. When PHA with the highest 4HB portion of 70 mol % was produced, PHA content in CDM achieved only 13%, and the PHA concentration was only 0.3 g/L [43]. Similarly, *Comomonas acidovorans* was capable to synthesize P(3HB-*co*-4HB) copolymers with 4HB fractions up to 96 mol % when pure 4-hydroxybutyric acid was used as substrate; nevertheless, the PHA fraction in CDM reached only 25% [44]. Hence, it seems that isolate *Aneurinibacillus* sp. H1 is a very promising candidate for production of interesting PHA copolymers with tailored monomer composition and material properties. Apart from P(3HB-*co*-4HB) copolymers, it is also capable of production of P(3HB-*co*-3HV-*co*-4HB) terpolymers with high 3HV and 4HB fraction. Production of P(3HB-*co*-3HV-*co*-4HB) terpolymers was recently reported employing *Cupriavidus* sp. DSM 19379, nevertheless, to induce efficient terpolymer production, a sophisticated two-stage fermentation strategy was needed [45]. On the contrary, our isolate *Aneurinibacillus* sp. H1 produced desirable terpolymers in a simple single stage cultivation set up, which is a very positive feature. Further, it should be pointed out that, to our best knowledge, this is the first report on efficient production of PHA copolymers and terpolymers containing 4HB subunits by a thermophilic bacterium.

Since the ability to produce P(3HB-*co*-4HB) copolymer from 1,4-butanediol was extraordinary and it deserved further attention, we have tested a potential strategy how to further improve productivity and gain even higher product titers. At first, we optimized the initial concentration of 1,4-butanediol, the results are shown in Table 5. Decrease in initial concentration of the substrate from originally used concentration of 8 g/L increased biomass growth. According to our results, the optimal initial concentration of 1,4-butanediol is 4 g/L; at this concentration, biomass growth as well as PHA titer are

enhanced substantially compared to the previous experiment and, surprisingly, the portion of 4HB in copolymer reached even 90 mol %, which further confirmed the promising potential of the bacterium. Increase in substrate concentration above 4 g/L resulted in inhibited growth and reduced PHA yields.

Table 5. Effect of initial concentration of 1,4-butanediol and glycerol on production of P(3HB-*co*-4HB) by *Aneurinibacillus* sp. H1.

1,4-BD [g/L]	Glycerol [g/L]	Biomass [g/L]	PHA in CDM [%]	PHA [g/L]	4HB in PHA [mol %]
3	0	1.22 ± 0.11	50.14 ± 2.65	0.61 ± 0.07	90.56 ± 0.70
4	0	1.67 ± 0.02	54.78 ± 1.21	0.91 ± 0.02	90.89 ± 1.19
5	0	1.60 ± 0.23	45.73 ± 0.65	0.73 ± 0.11	88.31 ± 0.29
6	0	1.23 ± 0.15	56.32 ± 0.56	0.69 ± 0.08	92.81 ± 0.04
7	0	1.13 ± 0.01	51.80 ± 0.71	0.58 ± 0.01	88.02 ± 0.48
8	0	0.96 ± 0.00	44.00 ± 2.76	0.42 ± 0.03	86.87 ± 1.32
12	0	0.72 ± 0.06	43.90 ± 2.28	0.32 ± 0.03	83.61 ± 0.94
16	0	0.56 ± 0.05	43.38 ± 1.26	0.24 ± 0.02	85.99 ± 4.40
4	2	2.69 ± 0.15	68.25 ± 0.62	1.83 ± 0.10	83.56 ± 1.48
4	4	2.79 ± 0.03	65.23 ± 2.64	1.82 ± 0.08	74.43 ± 1.70
4	6	2.28 ± 0.26	50.37 ± 0.87	1.15 ± 0.13	42.45 ± 7.88
4	8	2.43 ± 0.01	40.74 ± 3.35	0.99 ± 0.08	36.42 ± 1.63
4	20	2.56 ± 0.11	44.69 ± 1.23	1.14 ± 0.06	4.59 ± 0.01

To further enhance productivity, we decided to apply also glycerol along with 1,4-butanediol. The purpose of this step was to use glycerol as a co-substrate, which is efficiently utilized by the culture to support growth of the strain and, therefore, also final product titers. Thus, 1,4-butanediol was applied at an optimal concentration of 4 g/L, and glycerol was added at various concentration levels from 2 to 20 g/L; results are shown in Table 5. According to our expectation, introduction of glycerol enhanced growth of the bacterium, CDM values obtained with a mixture of 1,4-butanediol and glycerol are substantially higher than with 1,4-butanediol only. Results indicate that the optimal concentration of additional glycerol is 2 or 4 g/L, since these conditions resulted in high biomass growth (about 2.7 g/L), high PHA content in biomass (more than 65% of CDM), and high portion of 4HB in copolymer (83.56 and 74.43 mol % for 2 and 4 g/L glycerol, respectively). Generally, manipulating the concentration ratios of 1,4-butanediol to glycerol seems to be a simple and rational strategy how to control 4HB content in the polymer.

4. Conclusions

A recently established isolation protocol was utilized to gain new thermophilic PHA producers. Among the isolates tested, isolate designated as H1 turned out to be the most promising strain in terms of PHA production capability. The isolate was further taxonomically classified as a member of the genus *Aneurinibacillus*. According to subsequent experiments, it seems that *Aneurinibacillus* sp. H1 is an interesting thermophilic Gram-positive PHA accumulating bacterium with extraordinary ability to synthesize PHA copolymers and terpolymers containing high molar fractions of 3HV and 4HB subunits when valerate and/or 1,4-butanediol are used as 3HV and 4HB precursors, respectively. In considering all of the positive aspects of PHA production employing thermophiles, our isolate seems to be a highly intriguing potential candidate for PHA production on an industrial scale; therefore, the organism was deposited in Czech Collection of Microorganisms as patent culture CCM 8960. It should be also pointed out that the PHA materials produced by *Aneurinibacillus* sp. H1 were in depth characterized and the results have been submitted in an accompanying paper. Further experiments will be focused on optimization of PHA production under controlled conditions and its scale-up to laboratory bioreactors. In addition, we plan to sequence the entire genome of the bacterium to identify potential targets for genetic improvement of the strain.

References

1. Zeldes, B.M.; Keller, M.W.; Loder, A.J.; Straub, C.T.; Adams, M.W.W.; Kelly, R.M. Extremely thermophilic microorganisms as metabolic engineering platforms for production of fuels and industrial chemicals. *Front. Microbiol.* **2015**, *6*, 1209. [CrossRef] [PubMed]

2. Ranawat, P.; Rawat, S. Stress response physiology of thermophiles. *Arch. Microbiol.* **2017**, *199*, 391–414. [PubMed]

3. Chen, G.-Q.; Jiang, X.-R. Next generation industrial biotechnology based on extremophilic bacteria. *Curr. Opin. Biotechnol.* **2018**, *50*, 94–100. [PubMed]

4. Obruca, S.; Sedlacek, P.; Koller, M.; Kucera, D.; Pernicova, I. Involvement of polyhydroxyalkanoates in stress resistance of microbial cells: Biotechnological consequences and applications. *Biotechnol. Adv.* **2018**, *36*, 856–870. [CrossRef] [PubMed]

5. Koller, M.; Maršálek, L.; Miranda de Sousa Dias, M.; Braunegg, G. Producing microbial polyhydroxyalkanoate (PHA) biopolyesters in a sustainable manner. *New Biotechnol.* **2017**, *37*, 24–38. [CrossRef] [PubMed]

6. Sudesh, K.; Abe, H.; Doi, Y. Synthesis, structure and properties of polyhydroxyalkanoates: Biological polyesters. *Prog. Polym. Sci.* **2000**, *25*, 1503–1555. [CrossRef]

7. Kunioka, M.; Tamaki, A.; Doi, Y. Crystalline and thermal properties of bacterial copolyesters: Poly(3-hydroxybutyrate-*co*-3-hydroxyvalerate) and poly(3-hydroxybutyrate-*co*-4-hydroxybutyrate). *Macromolecules* **1989**, *22*, 694–697. [CrossRef]

8. Koller, M. Biodegradable and biocompatible polyhydroxy-alkanoates (PHA): Auspicious microbial macromolecules for pharmaceutical and therapeutic applications. *Molecules* **2018**, *23*, 362. [CrossRef]

9. Koller, M. Chemical and biochemical engineering approaches in manufacturing Polyhydroxyalkanoate (PHA) biopolyesters of tailored structure with focus on the diversity of building blocks. *Chem. Biochem. Eng. Q.* **2019**, *32*, 413–438. [CrossRef]

10. Koller, M. Switching from petro-plastics to microbial polyhydroxyalkanoates (PHA): The biotechnological escape route of choice out of the plastic predicament? *Eur. Biotechnol. J.* **2019**, *3*, 32–44.

11. Dietrich, K.; Dumont, M.-J.; Del Rio, L.F.; Orsat, V. Sustainable PHA production in integrated lignocellulose biorefineries. *New Biotechnol.* **2019**, *49*, 161–168.

12. Favaro, L.; Basaglia, M.; Casella, S. Improving polyhydroxyalkanoate production from inexpensive carbon sources by genetic approaches: A review. *Biofuel Bioprod. Biorefin.* **2019**, *13*, 208–227. [CrossRef]

13. Ibrahim, M.H.; Willems, A.; Steinbüchel, A. Isolation and characterization of new poly (3HB)-accumulating star-shaped cell aggregates-forming thermophilic bacteria. *J. Appl. Microbiol.* **2010**, *109*, 1579–1590. [CrossRef] [PubMed]

14. Pantazaki, A.A.; Tambaka, M.G.; Langlois, V.; Guerin, P.; Kyriakidis, D.A. Polyhydroxyalkanoate (PHA) biosynthesis in *Thermus thermophilus*: Purification and biochemical properties of PHA synthase. *Mol. Cell. Biochem.* **2003**, *254*, 173–183. [CrossRef]

15. Sheu, D.S.; Chen, W.M.; Yang, J.Y.; Chang, R.C. Thermophilic bacterium *Caldimonas taiwanensis* produces poly (3-hydroxybutyrate-*co*-3-hydroxyvalerate) from starch and valerate as carbon sources. *Enzyme Microb. Technol.* **2009**, *44*, 289–294.

16.   Pernicova, I.; Novackova, I.; Sedlacek, P.; Kourilova, X.; Koller, M.; Obruca, S. Application of osmotic challenge for enrichment of microbial consortia in polyhydroxyalkanoates producing thermophilic and thermotolerant bacteria and their subsequent isolation. *Int. J. Biol. Macromol.* **2020**, *144*, 698–704.

17.   Nováková, D.; Švec, P.; Zeman, M.; Busse, H.-J.; Mašlaňová, I.; Pantůček, R.; Králová, S.; Krištofová, L.; Sedláček, I. *Pseudomonas leptonychotis* sp. nov., isolated from weddell seals in Antarctica. *Int. J. Syst. Evol. Microbiol.* **2020**, *70*, 302–308.

18.   Obruca, S.; Sedlacek, P.; Mravec, F.; Krzyzanek, V.; Nebesarova, J.; Samek, O.; Kucera, D.; Benesova, P.; Hrubanova, K.; Milerova, M.; et al. The presence of PHB granules in cytoplasm protects non-halophilic bacterial cells against the harmful impact of hypertonic environments. *New Biotechnol.* **2017**, *39*, 68–80. [CrossRef]

19.   Obruca, S.; Benesova, P.; Oborna, J.; Marova, I. Application of protease-hydrolyzed whey as a complex nitrogen source to increase poly(3-hydroxybutyrate) production from oils by *Cupriavidus necator*. *Biotechnol. Lett.* **2014**, *36*, 775–781.

20.   Novackova, I.; Kucera, D.; Porizka, J.; Pernicova, I.; Sedlacek, P.; Koller, M.; Kovalcik, A.; Obruca, S. Adaptation of *Cupriavidus necator* to levulinic acid for enhanced production of P(3HB-*co*-3HV) copolyesters. *Biochem. Eng. J.* **2019**, *151*, 107350.

21.   Johnston, B.; Radecka, I.; Hill, D.; Chiellini, E.; Ilieva, V.I.; Sikorska, W.; Musioł, M.; Zięba, M.; Marek, A.A.; Keddie, D.; et al. The microbial production of Polyhydroxyalkanoates from waste polystyrene fragments attained using oxidative degradation. *Polymers* **2018**, *10*, 957. [CrossRef] [PubMed]

22.   Fadzil, F.I.M.; Mizuno, S.; Hiroe, A.; Nomura, C.T.; Tsuge, T. Low Carbon concentration feeding improves medium-chain-length polyhydroxyalkanoate production in *Escherichia coli* strains with defective β-oxidation. *Front. Bioeng. Biotechnol.* **2018**, *6*, 178. [CrossRef] [PubMed]

23.   Pernicova, I.; Kucera, D.; Nebesarova, J.; Kalina, M.; Novackova, I.; Koller, M.; Obruca, S. Production of polyhydroxyalkanoates on waste frying oil employing selected *Halomonas* strains. *Bioresour. Technol.* **2019**, *292*, 122028. [PubMed]

24.   Ye, J.; Hu, D.; Yin, J.; Huang, W.; Xiang, R.; Zhang, L.; Wang, X.; Han, J.; Chen, G.-Q. Stimulus response-based fine-tuning of polyhydroxyalkanoate pathway in *Halomonas*. *Metab. Eng.* **2020**, *57*, 85–95. [CrossRef]

25.   Singh, A.K.; Srivastava, J.K.; Chandel, A.K.; Sharma, L.; Mallick, N.; Singh, S.P. Biomedical applications of microbially engineered polyhydroxyalkanoates: An insight into recent advances, bottlenecks, and solutions. *Appl. Microbiol. Biotechnol.* **2019**, *103*, 2007–2032.

26.   Kumar, P.; Patel, S.K.S.; Lee, J.-K.; Kalia, V.C. Extending the limits of *Bacillus* for novel biotechnological applications. *Biotechnol. Adv.* **2013**, *31*, 1543–1561. [CrossRef]

27.   Kumar, P.; Kim, B.S. Valorization of polyhydroxyalkanoates production process by co-synthesis of value-added products. *Bioresour. Technol.* **2018**, *269*, 544–556. [CrossRef]

28.   Kumar, P.; Ray, S.; Patel, S.K.S.; Lee, J.-K.; Kalia, V.C. Bioconversion of crude glycerol to polyhydroxyalkanoate by *Bacillus thuringiensis* under non-limiting nitrogen conditions. *Int. J. Biol. Macromol.* **2015**, *78*, 9–16. [CrossRef]

29.   Shida, O.; Takagi, H.; Kadowaki, K.; Komagata, K. Proposal for two new genera, *Brevibacillus* gen. nov. and *Aneurinibacillus* gen. nov. *Int. J. Syst. Bacteriol.* **1996**, *46*, 939–946. [CrossRef]

30.   Xiao, Z.; Zhang, Y.; Xi, L.; Huo, F.; Zhao, J.-Y.; Li, J. Thermophilic production of polyhydroxyalkanoates by a novel *Aneurinibacillus* strain isolated from Gudao oilfield, China. *J. Basic Microb.* **2015**, *55*, 1125–1133. [CrossRef]

31.   Mravec, F.; Obruca, S.; Krzyzanek, V.; Sedlacek, P.; Hrubanova, K.; Samek, O.; Kucera, D.; Benesova, P.; Nebesarova, J. Accumulation of PHA granules in *Cupriavidus necator* as seen by confocal fluorescence microscopy. *FEMS Microbiol. Lett.* **2016**, *363*, fnw094. [CrossRef] [PubMed]

32.   Kucera, D.; Pernicová, I.; Kovalcik, A.; Koller, M.; Mullerova, L.; Sedlacek, P.; Mravec, F.; Nebesarova, J.; Kalina, M.; Marova, I.; et al. Characterization of the promising poly(3-hydroxybutyrate) producing halophilic bacterium *Halomonas halophila*. *Bioresour. Technol.* **2018**, *256*, 552–556. [CrossRef] [PubMed]

33.   Sadykov, M.R.; Ahn, J.-S.; Widhelm, T.J.; Eckrich, V.M.; Endres, J.L.; Driks, A.; Rutkowski, G.E.; Wingerd, K.L.; Bayles, K.W. Poly(3-hydroxybutyrate) fuels the tricarboxylic acid cycle and de novo lipid biosynthesis during *Bacillus anthracis* sporulation. *Mol. Microbiol.* **2017**, *104*, 793–803.

34. Valappil, S.P.; Misra, S.K.; Boccaccini, A.R.; Keshavarz, T.; Bucke, C.; Roy, I. Large-scale production and efficient recovery of PHB with desirable material properties, from the newly characterised *Bacillus cereus* SPV. *J. Biotechnol.* **2007**, *132*, 251–258. [CrossRef] [PubMed]

35. Ciriminna, R.; Pina, C.D.; Rossi, M.; Pagliaro, M. Understanding the glycerol market. *Eur. J. Lipid Sci. Technol.* **2014**, *116*, 1432–1439.

36. Mohandas, S.P.; Balan, L.; Jayanath, G.; Anoop, B.S.; Philip, R.; Cubelio, S.S.; Bright Singh, I.S. Biosynthesis and characterization of polyhydroxyalkanoate from marine *Bacillus cereus* MCCB 281 utilizing glycerol as carbon source. *Int. J. Biol. Macromol.* **2018**, *119*, 380–392. [CrossRef] [PubMed]

37. Gahlawat, G.; Soni, S.K. Valorization of waste glycerol for the production of poly (3-hydroxybutyrate) and poly (3-hydroxybutyrate-*co*-3-hydroxyvalerate) copolymer by *Cupriavidus necator* and extraction in a sustainable manner. *Bioresour. Technol.* **2017**, *243*, 492–501. [CrossRef]

38. Zain, N.F.M.; Abdullah, W.N.W.; Shun, T.J.; Keong, L.C.; Samian, M.R. Optimization of polyhydroxyalkanoate (PHA) production by *Burkholderia cepacia* BPT1213 utilizing waste glycerol as the sole carbon source. *Malaysian J. Microbiol.* **2018**, *14*, 164–171.

39. Hermann-Krauss, C.; Koller, M.; Muhr, A.; Fasl, H.; Stelzer, F.; Braunegg, G. Archaeal production of polyhydroxyalkanoate (PHA) co- and terpolyesters from biodiesel industry-derived by-products. *Archaea* **2013**, *2013*, 129268. [CrossRef]

40. Hsiao, L.-J.; Lee, M.-C.; Chuang, P.-J.; Kuo, Y.-Y.; Lin, J.-H.; Wu, T.-M.; Li, S.-Y. The production of poly(3-hydroxybutyrate) by thermophilic *Caldimonas manganoxidans* from glycerol. *J. Polym. Res.* **2018**, *25*, 85. [CrossRef]

41. Ibrahim, M.H.; Steinbüchel, A. High-cell-density cyclic fed-batch fermentation of a poly (3-hydroxybutyrate)-accumulating thermophile, *Chelatococcus* sp. strain MW10. *Appl. Environ. Microbiol.* **2010**, *76*, 7890–7895. [CrossRef] [PubMed]

42. Vigneswari, S.; Vijaya, S.; Majid, M.I.A.; Sudesh, K.; Sipaut, C.S.; Azizan, M.N.M.; Amirul, A.A. Enhanced production of poly(3-hydroxybutyrate-*co*-4-hydroxybutyrate) copolymer with manipulated variables and its properties. *J. Ind. Microbiol. Biotechnol.* **2009**, *36*, 547–556. [CrossRef] [PubMed]

43. Huong, K.-H.; Mohd Yahya, A.R.; Amirul, A.A. Pronounced synergistic influence of mixed substrate cultivation on single step copolymer P(3HB-*co*-4HB) biosynthesis with a wide range of 4HB monomer composition. *J. Chem. Technol. Biotechnol.* **2014**, *89*, 1023–1029. [CrossRef]

44. Lee, W.-H.; Azizan, M.N.M.; Sudesh, K. Effects of culture conditions on the composition of poly(3-hydroxybutyrate-*co*-4-hydroxybutyrate) synthesized by *Comamonas acidovorans*. *Polym. Degrad. Stab.* **2004**, *84*, 129–134. [CrossRef]

45. Kucera, D.; Novackova, I.; Pernicova, I.; Sedlacek, P.; Obruca, S. Biotechnological Production of poly(3-hydroxybutyrate-*co*-4-hydroxybutyrate-*co*-3-hydroxyvalerate) terpolymer by *Cupriavidus* sp. DSM 19379. *Bioengineering* **2019**, *6*, 74. [CrossRef]
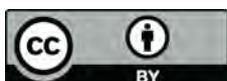
Appendix 13

Sedlacek, P., Pernicova, I., Novackova, I., Kourilova, X., Kalina, M., Kovalcik, A., Koller, M., Nebesarova, J., Krzyzanek, V., Hrubanova, K., Masilko, J., Slaninova, E., Trudicova, M., and Obruca, S. Introducing the Newly Isolated Bacterium Aneurinibacillus sp. H1 as an Auspicious Thermophilic Producer of Various Polyhydroxyalkanoates (PHA) Copolymers–2. Material Study on the Produced Copolymers. *Polymers* **2020**, 12, 1298.

Introducing the Newly Isolated Bacterium *Aneurinibacillus* sp. H1 as an Auspicious Thermophilic Producer of Various Polyhydroxyalkanoates (PHA) Copolymers–2. Material Study on the Produced Copolymers

Petr Sedlacek [1], **Iva Pernicova** [1], **Ivana Novackova** [1], **Xenie Kourilova** [1], **Michal Kalina** [1], **Adriana Kovalcik** [1], **Martin Koller** [2,3], **Jana Nebesarova** [4,5], **Vladislav Krzyzanek** [6], **Kamila Hrubanova** [6], **Jiri Masilko** [1], **Eva Slaninova** [1], **Monika Trudicova** [1] and **Stanislav Obruca** [1,*]

[1] Faculty of Chemistry, Brno University of Technology, Purkynova 118, 612 00 Brno, Czech Republic; sedlacek-p@fch.vut.cz (P.S.); xcpernicovai@fch.vut.cz (I.P.); xcnovackova@fch.vut.cz (I.N.); xckourilovax@fch.vut.cz (X.K.); kalina-m@fch.vut.cz (M.K.); kovalcik@fch.vut.cz (A.K.); masilko@fch.vut.cz (J.M.); xcslaninovae@fch.vut.cz (E.S.); xctrudicova@fch.vut.cz (M.T.)

[2] Institute of Chemistry, NAWI Graz, University of Graz, Heinrichstrasse 28/VI, 8010 Graz, Austria; martin.koller@uni-graz.at

[3] ARENA Arbeitsgemeinschaft für Ressourcenschonende & Nachhaltige Technologien, Inffeldgasse 21b, 8010 Graz, Austria

[4] Biology Centre, The Czech Academy of Sciences, v.v.i., Branisovska 31, 370 05 Ceske Budejovice, Czech Republic; nebe@paru.cas.cz

[5] Faculty of Science, University of South Bohemia, Branisovska 31, 370 05 Ceske Budejovice, Czech Republic

[6] Institute of Scientific Instruments of the Czech Academy of Sciences, v.v.i., Kralovopolska 147, 612 64 Brno, Czech Republic; krzyzanek@isibrno.cz (V.K.); hrubanova@isibrno.cz (K.H.)

* Correspondence: obruca@fch.vut.cz; Tel.: +420-541-149-354

Abstract: *Aneurinibacillus* sp. H1 is a promising, moderately thermophilic, novel Gram-positive bacterium capable of the biosynthesis of polyhydroxyalkanoates (PHA) with tunable monomer composition. In particular, the strain is able to synthesize copolymers of 3-hydroxybutyrate (3HB), 4-hydroxybutyrate (4HB) and 3-hydroxyvalerate (3HV) with remarkably high 4HB and 3HV fractions. In this study we performed an in-depth material analysis of PHA polymers produced by *Aneurinibacillus* sp. H1 in order to describe how the monomer composition affects fundamental structural and physicochemical parameters of the materials in the form of solvent-casted films. Results of infrared spectroscopy, X-ray diffractometry and thermal analysis clearly show that controlling the monomer composition enables optimization of PHA crystallinity both qualitatively (the type of the crystalline lattice) and quantitatively (the overall degree of crystallinity). Furthermore, resistance of the films against thermal and/or enzymatic degradation can also be manipulated by the monomer composition. Results of this study hence confirm *Aneurinibacillus* sp. H1 as an auspicious candidate for thermophilic production of PHA polymers with material properties that can be tuned together with their chemical composition by the corresponding adjustment of the cultivation process.

1. Introduction

Polyhydroxyalkanoates (PHA) represent the family of polyesters of hydroxyalkanoic acids under consideration, being renewable and biodegradable alternatives to petrochemical polymers [1]. These materials are accumulated by various bacteria and Archaea in the form of intracellular granules primarily serving as storage materials. Nevertheless, it was recently reported that these materials also enhance stress robustness and the resistance of microbes against a wide range of stress factors [2].

It is noteworthy that PHA in native intracellular granules are completely amorphous revealing the properties of super-cooled liquids. This unique, thermodynamically unfavorable state of the polymers is enabled by the synergy effects of (i) the presence of intergranular water which acts as a plasticizer and (ii) the small granular diameters, since crystallization is substantially inhibited in small volumes of native PHA granules [3]. It seems that the unique biophysical properties of amorphous PHA granules protect bacteria from a wide range of environmental stressors such as freezing-thawing events [4], osmotic pressure [5] or UV radiation [6]. However, when the native structure of the PHA granules is damaged, e.g., if the PHA are extracted from bacterial cells, the polymers quickly crystalize [3], which is accompanied by substantial changes in their material properties.

Material characteristics of PHA are strongly dependent upon monomer composition. PHA can be classified as short-chain-length (scl-PHA) if their monomer units consist of 3–5 carbon atoms, or medium-chain-length (mcl-PHA), which indicates that monomer units contain 6–14 carbons. Generally, scl-PHA are stiff thermoplastic polymers with a high degree of crystallinity and typically pronounced brittleness, while mcl-PHA reveals a much lower degree of crystallinity and ductility [7]. Nevertheless, even among scl-PHA there are great differences in properties. Poly(3-hydroxybutyrate) (P(3HB)), the homopolymer of 3-hydroxybutyrate (3HB), is the most common member of the PHA family; P(3HB) is highly crystalline and brittle with a melting temperature of about 180 °C, which is very close to its temperature of degradation (approx. 200 °C). However, when other monomer units such as 3-hydroxyvalerate (3HV) or 4-hydroxybutyrate (4HB) are introduced into the polymer chain, the melting temperature as well as the crystallinity of the material are substantially reduced, which is a very positive feature for the processing of the material and ultimately for numerous applications of these polymers [8]. In particular, copolymers containing high fractions of 4HB are considered as auspicious materials for various high-value applications, including but not limited to medicine and the health-care sector [9].

We have recently isolated the novel thermophilic bacterium *Aneurinibacillus* sp. H1 [10], which demonstrated extraordinary potential for PHA production. In general, biotechnological processes based on extremophilic bacteria are considered very promising since these bacteria are naturally resistant to microbial contamination which reduces operation costs and increases their efficiency as whole-cell biocatalysts [11]. *Aneurinibacillus* sp. H1 is a Gram-positive bacterium with optimal growth temperature between 45–50 °C, and capable of producing various scl-PHA polymers. When cultivated on glucose or glycerol, it accumulates the homopolymer P(3HB). However, when supplemented by suitable precursors such as 1,4-butanediol (1,4-BD) or valerate, it is capable of introducing 4HB or 3HV subunits into the polymer chain, respectively, resulting in production of copolymers poly(3-hydroxybutyrate-*co*-4-hydroxybutyrate) (P(3HB-*co*-4HB)) and poly(3-hydroxybutyrate-*co*-3-hydroxyvalerate) (P(3HB-*co*-3HV)) or even the terpolymer poly(3-hydroxybutyrate-*co*-3-hydroxyvalerate-*co*-4-hydroxybutyrate) (P(3HB-*co*-3HV-*co*-4HB)). The bacterium is able to synthesize PHA with very high portions of 4HB and 3HV units, and the monomer composition of PHA can be simply controlled by manipulating the composition of cultivation media.

Our previous work was dedicated to the evaluation of the biotechnological potential of *Aneurinibacillus* sp. H1 with respect to production of various PHA copolymers (submitted for publication). In this work we focused on the in-depth material characterization of PHA polymers produced by *Aneurinibacillus* sp. H1. To provide a general view on how the incorporation of 4HB monomer units changed the material properties of the polymer, we also included the homopolymer P(3HB) and P(3HB-*co*-4HB) copolymers with a low content of 4HB, produced by the routinely used PHA producing bacterium *Cupriavidus necator* H16, in the study.

2. Materials and Methods

2.1. Production of PHA in Shaking Flasks by Aneurinibacillus sp. H1

The inoculum was grown in complex media nutrient broth (10 g/L beef extract, 10 g/L peptone, 5 g/L NaCl) at 45 °C with shaking at 190 rpm. For production of PHA, mineral salt medium (MSM) was used consisting of: $Na_2HPO_4 \cdot 12H_2O$, 9.0 g/L; KH_2PO_4, 1.5 g/L; $MgSO_4 \cdot 7H_2O$, 0.2 g/L; NH_4NO_3, 1.0 g/L; $CaCl_2 \cdot 2H_2O$, 0.02 g/L; $Fe^{III}NH_4$citrate, 0.0012 g/L; Tryptone, 0.5 g/L with 1 mL/L of MES. Glycerol was used as the main carbon substrate, 1,4-BD was applied as precursor of 4HB. To gain various fractions of 4HB in polymers, glycerol and 1,4-BD were applied at various concentrations and ratios: glycerol 8 g/L + 4 g/L 1,4-BD resulted in a copolymer with 36 mol.% of 4HB, glycerol 6 g/L + 4 g/L 1,4-BD provided a copolymer with 42 mol.% of 4HB, glycerol 4 g/L + 4 g/L 1,4-BD gained a polymer with 74% of 4HB, glycerol 2 g/L + 4 g/L 1,4-BD yielded a polymer with 84% of 4HB, and by application of 4 g/L of 1,4-BD, the 4HB fraction achieved 90 mol.%. Valerate (2 g/L) was used as a precursor of 3HV for terpolymer production. The inoculum ratio was 10 vol.%. Production cultivations were carried out for 72 h at 45 °C under constant shaking of 180 rpm. All the cultivations were performed in duplicate. After cultivation, bacterial cells were harvested by centrifugation (6000× *g*, 5 min). Biomass was determined gravimetrically as the cell dry mass (CDM), and the amount and monomer composition of PHA were analyzed by Gas Chromatography as reported previously [12].

2.2. Production of P(3HB-co-4HB) Copolymers with Low 4HB Fraction Employing Cupriavidus necator H16

To gain P(3HB-*co*-4HB) copolymers with low fraction of 4HB we employed the well-described mesophilic PHA producer *Cupriavidus necator* H16 (CCM 3726). The production was carried out in Erlenmeyer flasks (volume 250 mL) containing 100 mL of mineral medium (composition: $(NH_4)_2SO_4$, 3 g/L; KH_2PO_4, 1 g/L; $Na_2HPO_4 \cdot 12H_2O$, 11.1 g/L; $MgSO_4$, 0.2 g/L; 1 mL of microelement solution and 1 L of distilled water. The microelement solution was composed of $FeCl_3$, 9.7 g/L; $CaCl_2 \cdot 2H_2O$, 7.8 g/L; $CuSO_4 \cdot 5H_2O$, 0.156 g/L; $CoCl_2 \cdot 6H_2O$, 0.119 g/L; $NiCl_2$, 0.118 g in 1 L of 0.1 M HCl. The cultivation setup was inoculated with 5 mL of overnight cultures grown in nutrient broth medium. To induce production of P(3HB) homopolymer, we used fructose (20 g/L) as a sole carbon source, production of P(3HB-*co*-4HB) copolymer was induced by application of fructose (8 g/L) and γ-butyrolactone (GBL) (2 and 6 g/L). After 72 h of cultivation, the cells were harvested (centrifugation, 8000× *g*, 5 min) and the biomass, PHA content and composition of PHA was determined as described above.

2.3. Preparation of PHA Films by Solvent Casting

PHA was extracted from approximately 100 mg of dried biomass by 5 mL of chloroform at 70 °C for 24 h. Afterwards, residual bacterial biomass was removed by filtration, and the chloroform phase containing dissolved PHA was poured onto glass Petri dishes (3 cm in diameter), and the solvent was allowed to evaporate at laboratory temperature overnight. Obtained films were stored in the dark to avoid light-induced polymer degradation, and subjected towards determination of material properties.

2.4. Characterization of PHA Films

2.4.1. Molecular Weight Determination by Size Exclusion Chromatography (SEC-MALS)

The molecular weight of the polymers was accessed as follows: 5 mg of the polymer was solubilized in 1 mL of HPLC-grade chloroform and the obtained samples were passed through syringe filters (nylon membrane, pore size 0.45 mm) and analyzed by gel size exclusion chromatography (Agilent, Santa Clara, CA, USA, Infinity 1260 system containing PLgel MIXED-C column) coupled with multiangle light scattering (Wyatt Technology, Dawn Heleos II, Santa Barbara, CA, USA) and differential refractive index (Wyatt Technology, Optilab T-rEX, Santa Barbara, CA, USA) detection. For the analysis, 100 mL of individual samples were injected into the chromatographic system containing HPLC-grade chloroform (pre-filtered through 0.02 mm membrane filter) as mobile phase.

The used flow rate was 0.6 mL/min. The weight-average molecular weight (Mw) and polydispersity index (PDI, ratio of weight-average and number-average molecular weight Mw/Mn) were determined using ASTRA software (Wyatt Technology, version 6.1, Santa Barbara, CA, USA) based on Zimm's equations. The used value of refractive index increment (dn/dc) for P(3HB) was 0.0336 mL/g. This value was determined from the differential refractometer response assuming a 100% sample mass recovery from the column.

2.4.2. Attenuated Total Reflectance Fourier-Transform Infrared (ATR-FTIR) Spectrometry

ATR FTIR spectra of the PHA films were collected with iS50 FTIR spectrometer (Thermo Scientific, Waltham, MA, USA). All measurements were taken from a sample surface at ambient temperature (in an air-conditioned room) on the built-in single-reflection diamond attenuated total reflectance (ATR) crystal. An individual absorption spectrum was collected as an average of 16 scans with a resolution of 1/cm. Every sample was measured at 10 different spots on its surface.

2.4.3. X-ray Diffractometry (XRD)

XRD diffraction patterns were collected using the X-ray diffraction analyzer EMPYREAN (PANalytical, Malvern, United Kingdom) in a central focusing arrangement with Bragg-Brentano parafocusing optics using CuKα radiation (range: 5–90°2th, step: 0.013°2th, voltage: 40 kV, current 30 mA), ADS: 10 mm, time per step: 96 s, without monochromator.

2.4.4. Methods of Thermal Analysis

Differential scanning calorimetry (DSC) was performed using a temperature-modulated calorimeter (DSC Q2000, TA Instruments, New Castle, DE, USA) equipped with an RCS90 cooling accessory. All experiments were performed in hermetically sealed TzeroTM (TA Instruments, Lukens, DE, USA) aluminum pans under a dynamic nitrogen atmosphere. Temperature-modulated DSC was applied in order to investigate the melting-crystallization behavior of the PHA films. Samples of a mass of approximately 5 μg were first equilibrated at 200 °C and then cooled down at a cooling rate of 2 °C/min and a temperature modulation of ±0.6 °C every 60 s. After another equilibration step (10 min at −80 °C), the sample was heated to 200 °C with an underlying heating rate of 2 °C/min and the same temperature modulation. Evaluation of the thermograms was performed by the TAUniversal Analysis 2000 software (TA Instruments, Lukens, DE, USA). In order to distinguish between individual reversible and irreversible processes (e.g., melting vs. cold crystallization), the total heat flow was divided into reversible and irreversible components, and the two respective thermograms were evaluated separately.

The thermogravimetry analyzer TGA Q5000 (TA Instruments, New Castle, DE, USA) was used to determine the mass loss in the temperature interval 25–600 °C under a dynamic dry air atmosphere with a heating rate of 10 °C/min.

2.4.5. Enzymatic Degradation Assay

The biodegradability of the tested materials was determined using two different enzymes: extracellular PHA depolymerase capable of hydrolysis of crystalline PHA. This enzyme was obtained as a supernatant after cultivation of *Schlegelella thermodepolymerans* DSM 15344 in medium consisting of 9 g/L $Na_2HPO_4 \cdot 12H_2O$; 1.5 g/L KH_2PO_4; 1 g/L NH_4Cl; 0.2 g/L $MgSO_4 \cdot 7H_2O$; 0.02 g/L $CaCl_2 \cdot 2H_2O$; 0.0012 g/L NH_4Fe^{III}citrate; 0.5 g/L yeast extract; 1 mL/L trace elements solution (TES). Composition of TES: 50 g/L EDTA; 8.3 g/L $FeCl_3$; 0.84 g/L $ZnCl_2$; 0.13 g/L $CuCl_2 \cdot 2H_2O$; 0.1 g/L $CoCl_2 \cdot 6H_2O$; 0.016 g/L $MnCl_2 \cdot 6H_2O$; 0.1 g/L H_3BO_3. Cultivations were performed for 72 h at 50 °C (180 rpm) using glycerol as the sole carbon source. In addition, also an intracellular depolymerase of *Bacillus subtilis* WB800 specific for amorphous PHA was expressed and purified as described by Hermawan and Jendrossek [13].

The biodegradation assay was performed using thin films of approximately 5 mg poured in 5 mL of 50 mM phosphate buffer (pH 7.4) with above described PHA depolymerases. Incubation was

performed for 3 h at 37 °C for *Bacillus subtilis* PHA depolymerase, or for 24 h at 50 °C for *Schlegelella thermodepolymerans* depolymerase.

Micrographs of the original and partially degraded films were recorded using Zeiss EVO LS-10 scanning electron microscope (SEM) (Carl Zeiss Ltd., Cambridge, UK). Before the analysis, a film cut-off was stuck on a carbon tape and sputter-coated with gold.

3. Results and Discussion

3.1. Monomer Composition and Molecular Weight

The isolated thermophilic strain *Aneurinibacillus* sp. H1 is capable of production of PHA copolymers with a great variety of accessible monomer compositions resulting from the proper adjustment of cultivation conditions. As no special cultivation protocol for block copolymer biosynthesis described in [8] was adopted in this study, we expected that in all the produced copolymers, monomer units would be randomly distributed in heteropolymer chains. In order to evaluate the relationship between the monomer composition and fundamental application-relevant properties of the resulting PHA materials, selected PHA copolymers produced by the strain were solvent-casted onto compact solid films and subjected to complex structural and physicochemical characterization. Furthermore, in order to cover the whole range of the accessible relative content of 3HB and 4HB monomers in P(3HB-*co*-4HB), in this material analysis we also included three reference materials with no or a very low content of 4HB in the polymer chains, produced by the routinely used mesophilic PHA producer *C. necator* H16. A complete list of materials included in this assay, together with their monomer compositions and molecular weights, is presented in Table 1, a visual illustration of the appearance of the films is provided in Supplementary Materials Figure S1.

Table 1. Solvent-casted films from polyhydroxyalkanoates (PHA) copolymers analyzed in the study.

Sample Identification	Bacterial Production Strain	Monomer Composition			Mw [kDa]	PDI
		3HB [mol. %]	4HB [mol. %]	3HV [mol. %]		
PHA1x	*C. necator* H16	100%	–	–	324 ± 4	1.18
PHA2x	*C. necator* H16	98.50%	1.50%	–	231 ± 2	1.18
PHA3x	*C. necator* H16	93.50%	6.50%	–	225 ± 4	1.14
PHA4	*Aneurinibacillus* sp. H1	64%	36%	–	66 ± 1	1.59
PHA5	*Aneurinibacillus* sp. H1	58%	42%	–	76 ± 1	1.78
PHA6	*Aneurinibacillus* sp. H1	26%	74%	–	86 ± 1	1.32
PHA7	*Aneurinibacillus* sp. H1	16%	84%	–	120 ± 1	1.27
PHA8	*Aneurinibacillus* sp. H1	10%	90%	–	128 ± 4	1.29
PHA9	*Aneurinibacillus* sp. H1	13%	54%	33%	109 ± 4	1.28

The molecular weight values of the PHA samples with low 4HB portions produced by *C. necator* were substantially higher than that of polymers produced by *Aneuribacillus* sp. H1 containing high 4HB fractions. This difference could be, of course, caused by biological dissimilarities between the producing strains; nevertheless, it was a common feature that incorporation of a high fraction of 4HB was associated with a decrease in Mw of PHA, such an effect was observed in *Cupriavidus* sp. USMAA1020 [14] and *Alcaligenes* sp. A-04 [15]. We can hypothesize that 4HB-CoA is a less suitable substrate for PHA synthase than 3HB-CoA and, therefore, its more frequent incorporation into PHA chains is associated with a presumable termination of polymerization needed for PHA chain growth, resulting in lower Mw of polymer. However, it could also be seen that in material produced by *Aneurinibacillus* the Mw of the polymer increased with the increase in 4HB content. The explanation could be that glycerol was used as the second substrate along with 1,4-BD. The higher the portion of glycerol applied, the lower the portion of 4HB obtained, with a decreased Mw. Generally, PHA produced on glycerol revealed lower Mw since glycerol terminated the synthesis of PHA chains by

the "endcapping effect" [16], and it was likely that the polymerization-terminating effect of glycerol was more pronounced than that of 4HB-CoA. In addition, there is another possible explanation why the Mw of polymer produced by *Aneurinibacillus* sp. H1 is substantially lower than that produced by *C. necator*: *C. necator* possesses a PHA synthase consisting of only one PhaC subunit. In contrast, PHA synthases of bacilli and related species, including members of the genus *Aneurinibacillus,* consist of two different subunits, PhaC and PhaR. It was recently reported that PhaR subunits catalyzed alcoholysis of the PHA chain when some alcohols were present in cultivation media [17]. Therefore, both substrates used for cultivation of *Aneurinibacillus* sp. H1–glycerol and 1,4-butanediol might be involved in this reaction, catalyzed by PhaR, which could substantially contribute to the fact that PHA produced by *Aneurinibacillus* sp. H1 reveals substantially lower Mw as compared to the polymer synthesized by *C. necator*.

3.2. Chemical and Physical Structure Determined by FTIR Spectra

The study of the variation in chemical structure of the PHA copolymer films was followed by ATR FTIR spectrometry. To deal with potential surface heterogeneity of the films, for an individual film 10 separate spectra were taken at different spots on the film surface and averaged. Figure 1 shows comparison of the normalized spectral cut-offs of the average spectra in analytically important spectral regions for all tested materials (complete spectra are provided as Supplementary Materials Figure S2).

As expected, FTIR spectra clearly illustrated differences in the chemical composition of the individual polymer materials. This was obvious mainly from the changes in characteristic absorption of alkyl groups (note, e.g., the varying intensity of methyl absorption at 1258 and 1378 cm^{-1}, and differences in relative intensity of methyl and methylene absorptions at around 2873 and 2852 cm^{-1}, respectively). Nevertheless, further analysis of the FTIR spectra could also provide additional information regarding the degree of structural order in the tested PHA materials. Utilization of FTIR spectroscopy for evaluating PHA crystallinity has been proposed by several authors [3,18–20].

All PHA materials tested in this study showed spectral signs of semi-crystalline solids combining the spectral attributes of crystalline and amorphous structural motifs. This was obvious for instance from the typical asymmetrical shape of the carbonyl C=O vibration band (see Figure 1b), which in fact represented a spectral envelope of the overlapping vibration bands of PHA ester carbonyls in ordered ($<1725\ cm^{-1}$) and disordered (about 1740 cm^{-1}) structures. Commonly, the FTIR-based crystallinity assay focuses on analysis of vibration modes specifically assigned to structural groups located either in crystalline or in amorphous polymer domains. In the case of PHA, absorption bands of ester groups are most often analyzed for this purpose. In the homopolymer P(3HB), the vibration band at 1180 cm^{-1} was attributed to amorphous PHA domains, while the characteristic conformational bands of the crystalline phase were those at 1276 and 1227 cm^{-1}, where the latter was specifically assigned to helical crystallites. It can be seen in Figure 1c that the intensity of both bands decreased with the decreasing relative content of 3HB in the polymer structure (note the significant shift in intensities of these two bands compared to the 1180 cm^{-1} band for the low 4HB content of 6.5% in PHA3x). Nevertheless, while the band at 1276 cm^{-1} was still present in the spectra of materials rich in 4HB, the 1227 cm^{-1} band was missing for a content of 3HB lower than about 20 wt.% (samples PHA7, PHA8 and PHA9). This confirmed a well-known fact that in 3HB-poor PHA chains, ordered structural motifs could still be found, but their structure was different than that of P(3HB) crystallites [21]. Disappearance of ordered structures specific for P(3HB) could also be tracked by changes in the C–H stretching region (lower relative intensity of blue-shifted antisymmetric stretching bands at about 3000 cm^{-1}) and in the C–C stretching region (e.g., disappearance of bands assigned to P(3HB) crystallites at 978 cm^{-1} and specific vibration mode of the helical structure at 826 cm^{-1}).
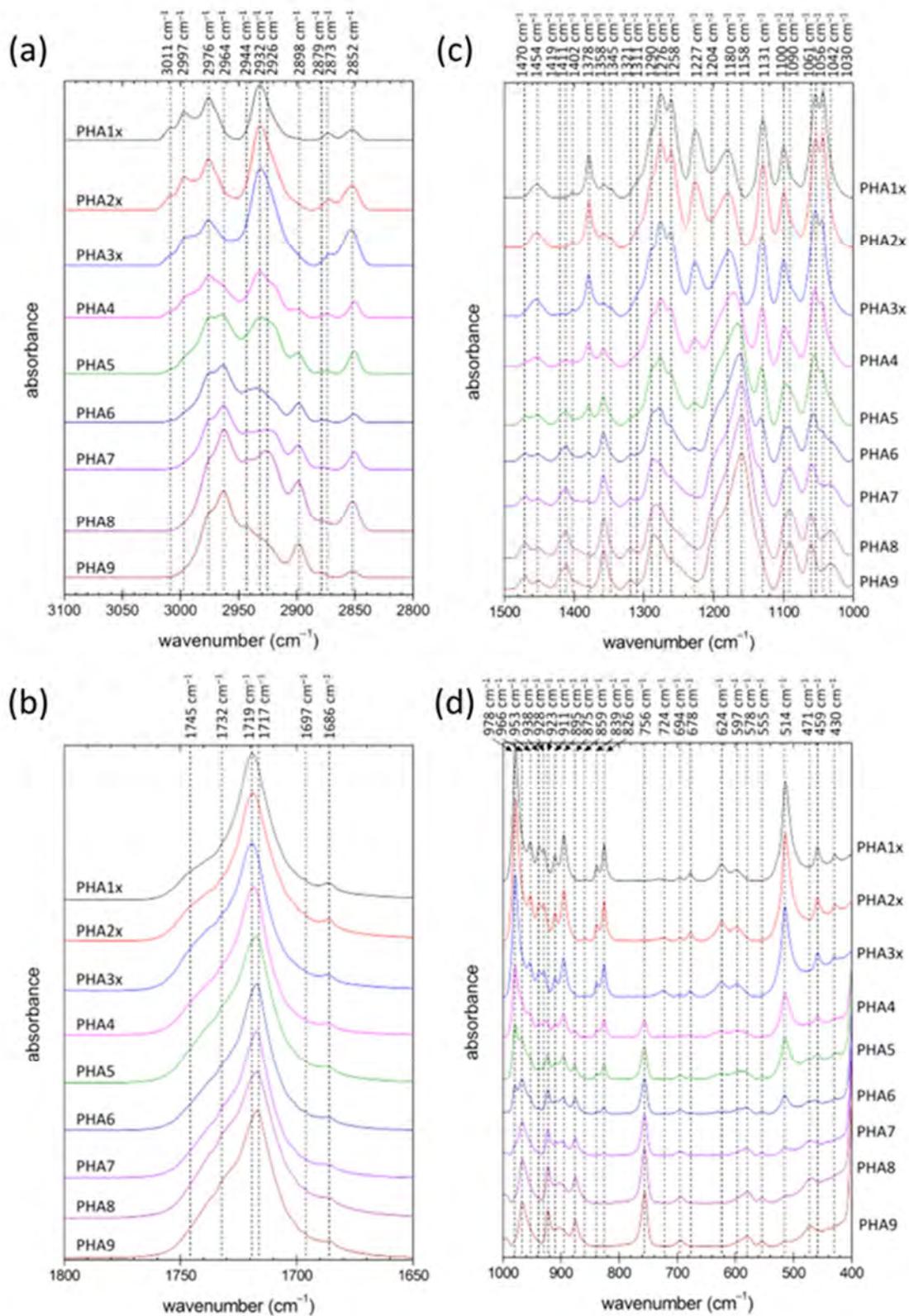
Figure 1. Normalized ATR-FTIR spectra (cut-offs for the analytically important spectral regions) of the solution-casted PHA films prepared from polymers with different monomer composition (each spectrum represents an arithmetic average of 10 individual spectra collected at different locations on the surface of the film). Frequencies of the absorption band maxima were determined from the second derivative of the spectra.

On the other hand, an increasing content of the monomer 4HB in the polymer chains gave rise to another ordered structure with its own signature in the FTIR spectra. The asymmetric C–H stretching band of methylene groups was blue-shifted from 2932 to 2964 cm^{-1} in crystalline structures (see Figure 1a). Similarly, the vibration band at 2898 cm^{-1} could be assigned to blue-shifted symmetric stretching of methylene groups in ordered domains. Similar spectral signs of crystallization were described for other PHA polymers such as poly(3-hydroxybutyrate-*co*-3-hydroxyhexanoate) [20] and their structural analogues of, e.g., poly(ε-caprolactone) (PCL) [22] or polyglycolic acid (PGA) [23]. Furthermore, methylene deformation bands were known to be sensitive to chain conformation as well. The main CH$_2$ deformation modes including methylene scissoring (1470 cm^{-1}), methylene wagging (1321 cm^{-1}) and the bending deformation that formed an absorption shoulder at 1204 cm^{-1} increased in intensity when associated with the trans isomer, which was more abundant in stretched polymer chains found in the crystalline structures. Similarly, the P(3HB) crystallites, and the ordered structure built up on the 4HB monomer, the vibration modes attributed to the ester bond might be taken as a crystallinity marker. Phillipson et al. noted that for PCL, stretching C–O bands at 1235 and 1275 cm^{-1} were blue-shifted on crystallization to 1245 and 1295 cm^{-1}, respectively. Apparently, a similar phenomenon could be observed for PHA copolymers rich in 4HB monomers, where shoulders at about 1250 and 1290 cm^{-1} were increasing in intensity with the relative content of 4HB. Similarly, the bending mode of C–O–C (966 cm^{-1}), which was intensive in copolymers rich in 4HB, was known to strengthen on crystallization of PCL [22].

To sum up the above discussed results of ATR FTIR analysis, it was shown that gradual substitution of 3HB monomer units by 4HB resulted firstly in a decrease in the degree of structural order in the material as the relative content of P(3HB) crystallites decreased, but, for higher content of 4HB, the crystallinity increased again as the P(4HB) crystallites started to predominate the structure; a switch from a P(3HB) to a P(4HB) lattice was observed. P(3HB) and P(4HB) crystallites are hence not structurally isomorphic, i.e., a crystallite cannot incorporate the other monomer into its structure without its significant deformation. This incompatibility of 3HB and 4HB monomers has already been described [21] and represents a promising tool for manipulating the overall crystallinity of PHA materials via controlling their monomer composition. Contrarily, the 3HV monomer could be incorporated into the P(3HB) lattice to some extent, thus showing some isomorphism of the P(3HB) and P(3HV) lattice [21]. Nevertheless, the terpolymer PHA9 (54% 4HB, 33% 3HV, 13% 3HB) manifested all the spectral features discussed above for 4HB-dominating copolymers. Apparently, the 3HB and 3HV content was so low that no crystallites of P(3HB) or the structurally similar P(3HV) lattice were formed together with the P(4HB) crystallites.

ATR FTIR analysis provided valuable but limited information on the crystallinity of the tested materials. The technique provided neither any detailed information on the morphology of the crystallites nor a direct quantification of the overall crystallinity of the material. For these purposes, the films were further subjected to X-ray diffractometry (XRD) and differential scanning calorimetry (DSC).

3.3. Detailed Crystallinity Assay Provided by XRD and DSC

The XRD patterns of all the tested films are shown in Figure 2. Again, all materials showed the characteristic features of semicrystalline solids as the XRD patterns combined the specific diffractions of ordered structural motifs with a broad background amorphous halo. The shape of the XRD patterns and position of diffraction maxima were in expedient correspondence with published XRD features of the P(3HB) and the P(4HB) lattice [21,24–27]. Individual diffraction maxima were assigned to the corresponding reflections of the two crystal lattices in Figure 2.
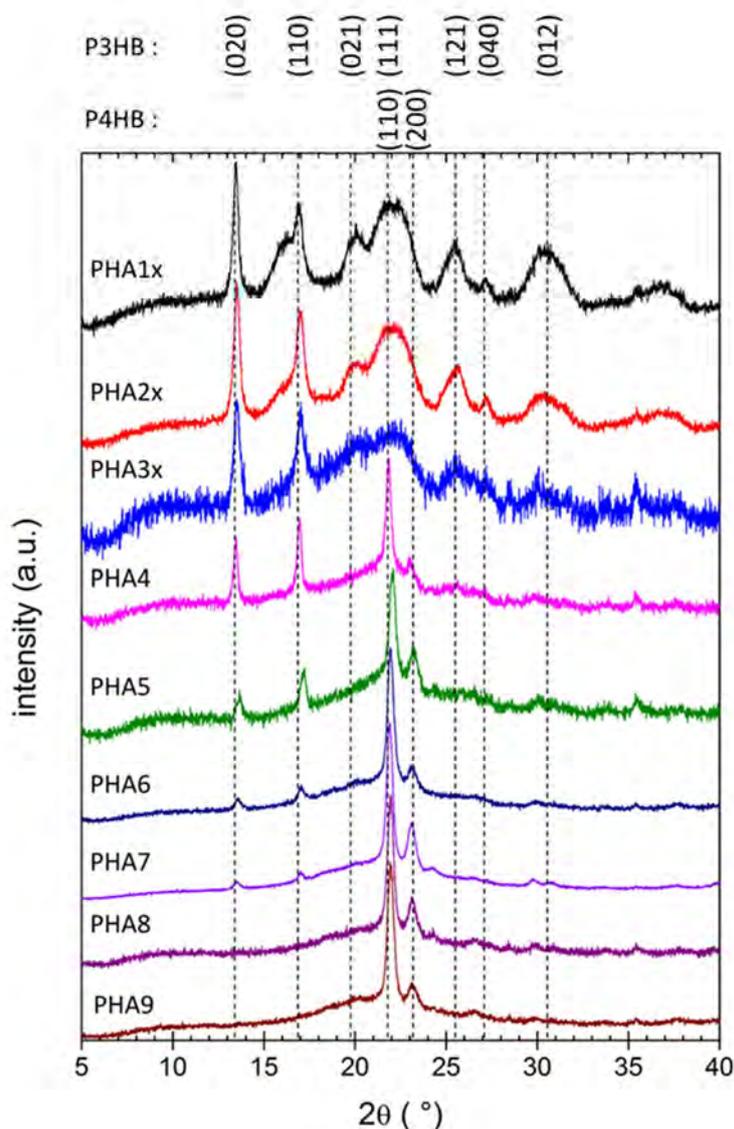
Figure 2. X-ray diffraction patterns of copolymer PHA films. Diffractograms were normalized for clarity. Reflections are assigned to P(3HB) and P(4HB) lattices, respectively, according to Gao et al. [25] and Keridou et al. [27].

The XRD patterns in Figure 2 were normalized for clarity of their comparison, and the overall crystallinity or amorphous content could therefore hardly be quantified from the figure. Nevertheless, from the qualitative viewpoint, it could clearly be seen that the relative content of P(3HB) and P(4HB) crystallites was gradually shifted with the corresponding change in monomer composition. The P(3HB) crystal lattice was the dominating structure for polymers with a low content of 4HB monomers (PHA1x, PHA2x, PHA3x). In this crystal lattice, the helical form of the polymer chain dominated (represented by sharp diffractions (020) and (110)), but stretched β-structures are present as well (diffraction (021)). For the copolymers with intermediate content of 4HB monomer (36% and 42% in this study), strong diffractions of both (P(3HB) and P(4HB)) crystal lattices could be found in the XRD pattern. This was in good agreement with results of FTIR analysis as far as the spectral signatures of both types of ordered structures were detected in ATR FTIR spectra of these copolymers. On the other hand, diffractions of the P(3HB) lattice were detected in the XRD pattern up to 4HB content as high as 84%. On the one side, this confirms that the XRD technique is more sensitive than FTIR for the qualitative description of PHA's crystallinity (no apparent spectral signs of P(3HB)'s

In general, the results of XRD analysis confirmed the qualitative conclusions of the FTIR-based crystallinity assay. It could be seen that, at a low content, the 4HB monomer acted as a structure-breaking component. This was in agreement with previous works reporting that even if both (P(3HB) and P(4HB)) lattices have orthorhombic unit cells with the space group P2$_1$2$_1$2$_1$ [21,26,27], differences in the spacings of the two-unit cells were so large that the 4HB unit could not crystallize in the sequence of 3HB monomers and formed a defect in the P(3HB) crystal lattice [21]. In the same perspective, when the 4HB monomer predominated the polymer composition, residual 3HB units reduced the overall P(4HB) crystal lattice content in a similar way. Different structural effects were described in literature for the presence of 3HV units in PHA copolymers [21]. In the P(3HB-*co*-3HV) copolymers, P(3HB) to P(3HV) crystal lattice transition occurred at 3HV content of approximately 40%. Furthermore, contrarily to 4HB, 3HV units could be incorporated into the P(3HB) lattice (and vice versa), and the negative effect of the monomer on the overall crystallinity was therefore smaller. Nevertheless, for the terpolymer tested in this study (PHA9), the content of 3HB and 3HV were too low to let the P(3HB) or P(3HV) crystallites form.

crystalline structures were found in the FTIR spectrum of the copolymer PHA7 with 84% 4HB). On the other hand, it contradicts the observations of Saito [24], who had not detected any diffractions of the P(3HB) lattice in XRD patterns of copolymers with a 4HB content higher than 64%. Similar to FTIR, the terpolymer PHA9 provided XRD features similar to P(3HB-*co*-4HB) copolymers with 4HB being the dominating component.

In general, the results of XRD analysis confirmed the qualitative conclusions of the FTIR-based crystallinity assay. It could be seen that, at a low content, the 4HB monomer acted as a structure-breaking component. This was in agreement with previous works reporting that even if both (P(3HB) and P(4HB)) lattices have orthorhombic unit cells with the space group $P2_12_12_1$ [21,26,27], differences in the spacings of the two-unit cells were so large that the 4HB unit could not crystallize in the sequence of 3HB monomers and formed a defect in the P(3HB) crystal lattice [21]. In the same perspective, when the 4HB monomer predominated the polymer composition, residual 3HB units reduced the overall P(4HB) crystal lattice content in a similar way. Different structural effects were described in literature for the presence of 3HV units in PHA copolymers [21]. In the P(3HB-*co*-3HV) copolymers, P(3HB) to P(3HV) crystal lattice transition occurred at 3HV content of approximately 40%. Furthermore, contrarily to 4HB, 3HV units could be incorporated into the P(3HB) lattice (and vice versa), and the negative effect of the monomer on the overall crystallinity was therefore smaller. Nevertheless, for the terpolymer tested in this study (PHA9), the content of 3HB and 3HV were too low to let the P(3HB) or P(3HV) crystallites form.

The melting behavior of the solvent-casted PHA films was studied using DSC. In order to evaluate the intrinsic tendency of the polymer to crystallize (unaffected by the potential artifacts of the film preparation procedure), all samples were first of all melted and cooled down with the same heating/cooling program to erase the polymers' thermal history. The second heating scan was then analyzed (corresponding thermograms are shown in Figure 3). It could be seen that while the homopolymer P(3HB) melted at about 170 °C, even a very low content of 4HB reduced the melting point dramatically. Furthermore, the initially sharp melting endotherm of P(3HB) broadened when a low content of 4HB was present. This further illustrated the above mentioned structure-breaking effect of 4HB monomers resulting in P(3HB) crystalline domains being reduced both in number and in size (decreasing size of P(3HB) crystallites could also be deduced from the widening diffraction peaks in XRD patterns; note, e.g., the different widths of diffraction peaks for PHA1x and PHA3x). Polymers of intermediate 4HB content (PHA4, PHA5) showed two melting endotherms, indicating again the presence of both types of crystallites (P(3HB), P(4HB)). For these samples, a higher content of the amorphous phase was manifested by the most pronounced glass transition at temperature about −20 °C (T_g; marked with blue arrow in Figure 3). The other prepared PHA samples also possessed a T_g, but DSC was not a sufficiently sensitive method to determine the T_g for semi-crystalline polymers with a high degree of crystallinity. Therefore, the appearance of T_g on the DSC thermogram might indicate a higher proportion of the amorphous phase in PHA compared to other samples. Copolymers with low and intermediate content of 4HB also showed an exothermic peak during the heating step, which represented the cold crystallization of the polymer chains (red arrow in Figure 3). P(3HB-*co*-4HB) copolymers with the highest content of 4HB melted at about 55 °C, where the increasing residual content of 3HB decreased the melting point again. Similar to the results of the other material analysis methods, the presence of 3HV in the terpolymer PHA9 virtually amplified the effects of 4HB (the material behaved like it had a higher 4HB content).

Figure 3. Differential scanning calorimetry (DSC) thermograms of PHAs copolymer films (thermograms show the second heating scan).

Total intrinsic crystallinity of the polymers was estimated from the second heating scan. For this purpose, specific heat of fusion was calculated separately for P(3HB) and P(4HB) crystallinity by integrating corresponding melting endotherms. Furthermore, the undesirable crystallinity overestimation caused by the cold crystallization was eliminated by integration of the cold crystallization exotherm and subtracting the corresponding integral from the total melting enthalpy. Values of the standard heat of fusion for 100% crystalline P(3HB) (146 J/g) and for 100% crystalline P(4HB) (110 J/g) were taken from literature [24,28]. For the copolymer (sample PHA9), heat of fusion for P(3HB) lattice was applied on the high-temperature endotherm even if it was not possible to attribute the lattice structure of this type of crystallites unambiguously. Nevertheless, this simplification could be justified taking into account the high structural similarity of P(3HB) and P(3HV) crystallites and low differences between heat of fusion values of P(3HB) and P(3HV) lattice [29] and melting points close to that of PHA homopolymer (< 10 °C melting point shift than expected for P(3HV) lattice [21] and also the minor contribution of the high-temperature endotherm to the total specific heat (approximately 1% of the total specific heat). Dependence of the total crystallinity on the 4HB content in the polymer composition is shown in Figure 4. Note that the results in the figure might be affected by some additional systematic errors (e.g. temperature dependency of the heat of fusion or dynamic effects linked to the non-zero heating effects were not taken into account). Nevertheless, they provide an intriguing illustration of the U-shaped crystallinity-composition function of PHA copolymers, which seems to be a general material feature of PHA copolymers [21].

they provide an intriguing illustration of the U-shaped crystallinity-composition function of PHA copolymers, which seems to be a general material feature of PHA copolymers [21].

Figure 4. Degree of crystallinity of PHA films estimated from DSC analysis.

3.4. Stability Against Thermal and Enzymatic Degradation

The above discussed results of material analyses confirm that controlling the monomer composition of PHA polymers enables the tailoring of the type and degree of ordering in the polymer structure. This represents a crucial material quality that influences the mechanical, thermal and chemical performance of the final products. To verify this connection, we performed preliminary stability tests dealing with resistance of the solvent-casted PHA films against thermal and enzymatic degradation.

Thermal degradation of tested PHA materials was followed by thermogravimetry. Figure 5 provides derivative thermograms (DTG) showing the rate of weight loss (derivative of residual weight with temperature) as a function of temperature during the heating of the sample at a constant heating rate (10 °C/min). It could be seen that the homopolymer P(3HB) was degraded in a single step process, while the P(3HB-*co*-4HB) copolymers were decomposed in two steps. However, these two steps did not represent separate decomposition of 3HB and 4HB units as it was sometimes incorrectly referred [30], because the two-step thermal degradation was reported also for the P(4HB) homopolymer [28]. In fact, the difference in thermal degradation dynamics illustrated different mechanisms of the decomposition processes. While P(3HB) was degraded primarily by *cis*-elimination reaction releasing crotonic acid as a volatile product [31], P(4HB) at first underwent an unzipping reaction from the ω-hydroxyl end, followed at higher temperatures by cyclic rupture via intramolecular transesterification [32]. In P(3HB-*co*-4HB) copolymers, all these mechanisms took place at the rates affected by the particular chemical composition. Nevertheless, it could be generalized from the DTG curves in Figure 5 that the incorporation of 4HB monomers in the polymer resulted in a gradual increase in thermal stability. This fact was even more obvious from the comparison of the temperatures of half-decomposition ($T_{50\%}$) presented in Figure 6. Moreover, it could be seen from the results shown in Figures 5 and 6 that the P(3HB-*co*-4HB-*co*-3HV) terpolymer PHA9 was decomposed in three stages and its $T_{50\%}$ was almost as high as that for a copolymer with 90% 4HB.
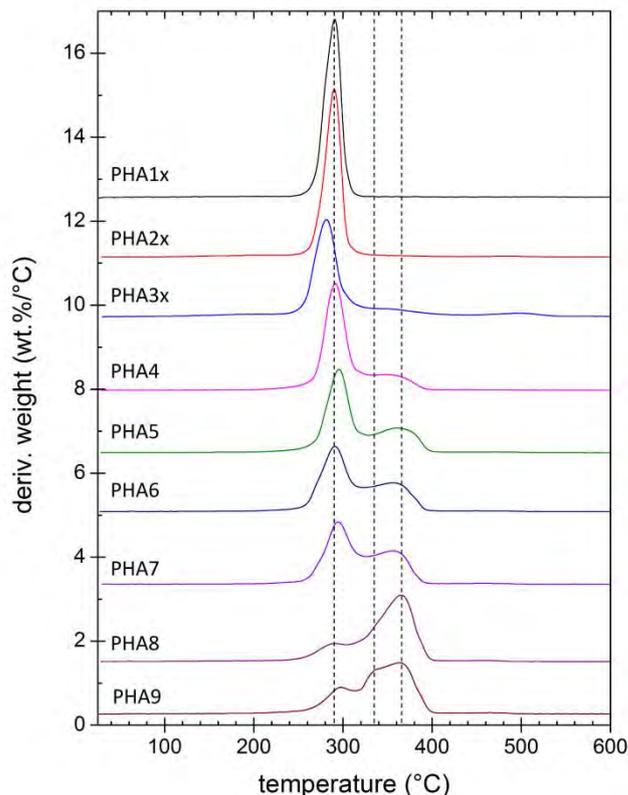
Figure 5. DTG curves of solvent-casted films from the tested PHA copolymers.
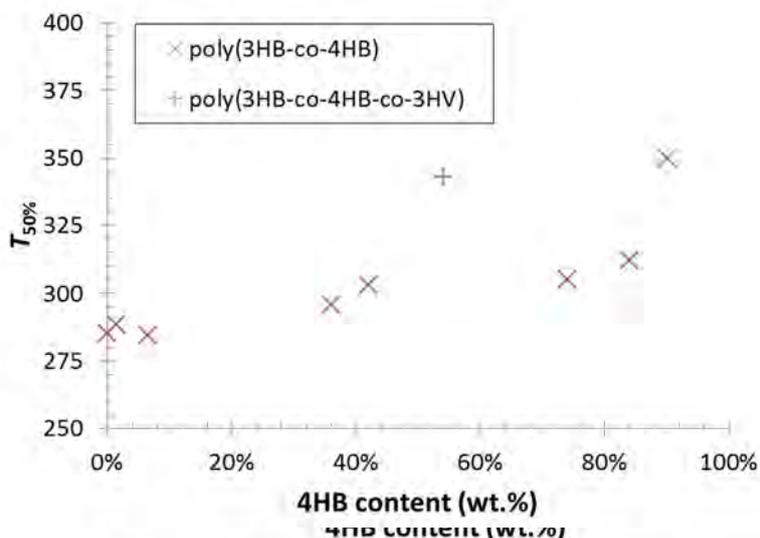
Figure 6. Half-decomposition temperatures ($T_{50\%}$; temperature corresponding to 50% residual weight) as a function of 4HB content in the polymer structure.

Another important advantage of the incorporation of 4HB monomers into the P(3HB) matrix arose from discussion of the results of DSC and TGA analyses. It could be seen that 4HB both lowered the melting point and increased the temperature of decomposition. Therefore, it widened the polymer processing temperature window, where the polymer in melt could be processed without serious thermal degradation. This is a key improvement from the perspective of polymer processing technology.

Finally, biodegradability as another essential application-relevant property of the PHA based material was checked by a preliminary enzymatic degradation assay. Both extracellular and

the two types of enzymes differ in their specificity to ordered and disordered PHA structures, respectively [33]. Because the film thickness was not controlled during solvent-casting, the degradation process was not followed by measurement of the weight losses over time. Instead, biodegradation was screened by directly visualizing changes in surface topography with scanning electron microscopy (SEM), which provided preliminary information about assessment of PHA films to biodegradation by a particular depolymerase. As can be seen in Figure 7 (and in Figure S3 on a smaller scale), surface topography differed significantly even for the as-prepared polymer films. High crystallinity of homopolymer P(3HB) (PHA1x) resulted in porosity caused by the sample shrinkage during film preparation. Consequently, the large specific surface of the porous P(3HB) film resulted in increased contact area with the enzymatic solution and more significant degradation even for intracellular depolymerase, which specifically decomposes amorphous PHA domains. The porous character of the film was to some extent also preserved for other polymers with a dominant content of 3HB (PHA2x, PHA3x), where the pore surface obviously constituted the center of the enzymatic attack. For the copolymers with a lower 3HB content, original films had a smooth surface with no apparent effect of specific polymer composition.
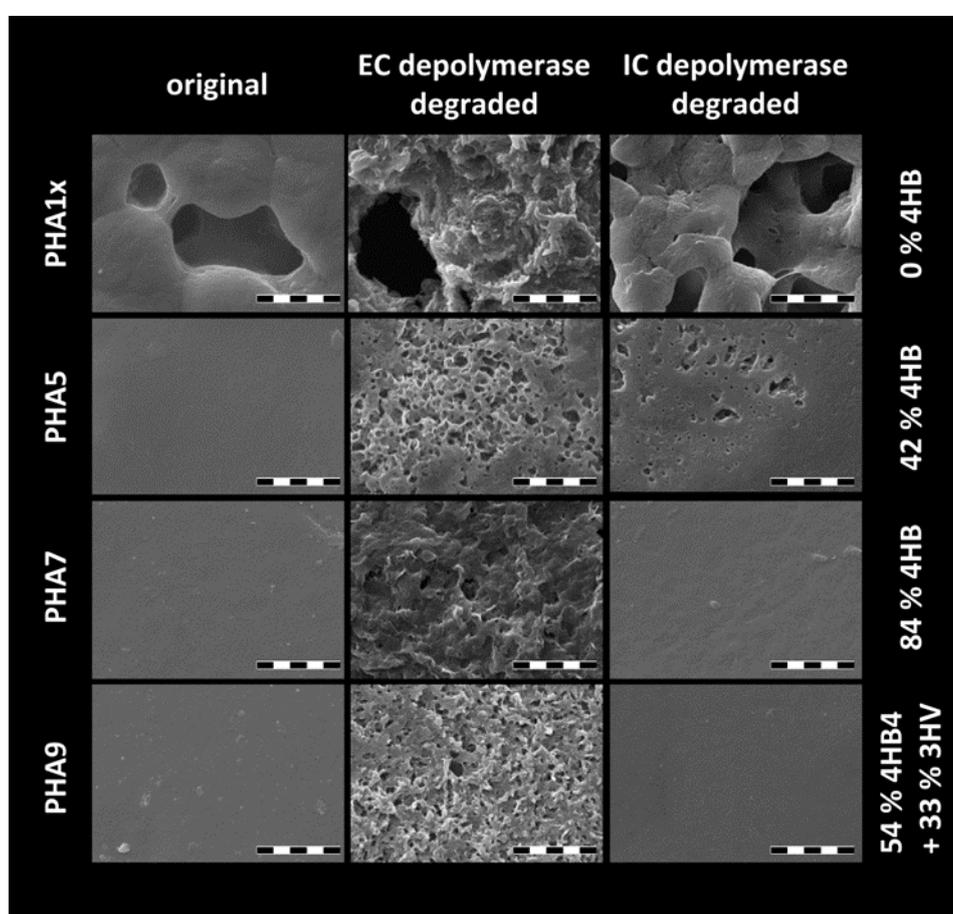
Figure 7. SEM micrographs of PHA copolymer films before and after the enzymatic degradation assay using extracellular (EC) PHA depolymerase and intracellular (IC) PHA depolymerase, respectively (magnification 10,000×; scalebar: 10 μm).

4. Conclusions

In this study, PHA polymers produced by the newly isolated, moderately thermophilic Gram-positive bacterium, *Aneurinibacillus* sp. H1, were subjected to an in-depth material analysis. With respect to the outstanding capability of the strain to change the monomer composition of accumulated PHA according to the cultivation conditions, we focused this initial study primarily on the way the relative content of 3HB and 4HB monomers affected the degree of structural order and basic physicochemical parameters of solvent-casted films prepared from the isolated PHA polymers. In order to cover the whole range of monomer compositions in this comparative study, reference P(3HB) homopolymer and P(3HB-*co*-4HB) copolymers with minor 4HB content were prepared by routinely used mesophilic PHA producer *C. necator* H16.

a higher rate of degradation by depolymerase from *Alcaligenes faecalis* at 37 °C for P(3HB-*co*-4HB) copolymers with low and intermediate content of 4HB compared to P(3HB), but higher resistance to the enzymatic degradation of P(4HB) homopolymer and copolymers with 4HB content higher than about 80%. Nevertheless, for a conclusive confirmation of this phenomenon, a more systematic follow-up investigation of the enzymatic degradation of materials tested in this study is needed. Concerning degradation of the copolymer films by intracellular depolymerase, films prepared from polymers with a higher content of 4HB (PHA6, PHA7 and PHA8) and from the terpolymer (PHA9) showed obviously higher stability than porous films with the highest content of 3HB (PHA1x, PHA2x, PHA3x) and also compared to the films with intermediate content of 4HB (PHA4, PHA5), where the degradation was evidently supported by lower crystallinity of the material.

As already noted, the degradation assay involved in this study was intended as a preliminary screening test, serving for a qualitative comparison of degradation behavior among the tested PHA materials. In a follow-up study, continuous monitoring of quantitative parameters accompanying the degradation process (weight loss, changes in film thickness, decrease in average molecular weight) will not only describe degradation kinetics on higher resolution, but it will also enable correlation of the material's stability with other quantitative chemical (monomer content, Mw) and physical parameters (degree of crystallinity) and thus help to understand the exact mechanism of the decomposition.

4. Conclusions

In this study, PHA polymers produced by the newly isolated, moderately thermophilic Gram-positive bacterium, *Aneurinibacillus* sp. H1, were subjected to an in-depth material analysis. With respect to the outstanding capability of the strain to change the monomer composition of accumulated PHA according to the cultivation conditions, we focused this initial study primarily on the way the relative content of 3HB and 4HB monomers affected the degree of structural order and basic physicochemical parameters of solvent-casted films prepared from the isolated PHA polymers. In order to cover the whole range of monomer compositions in this comparative study, reference P(3HB) homopolymer and P(3HB-*co*-4HB) copolymers with minor 4HB content were prepared by routinely used mesophilic PHA producer *C. necator* H16.

The results of molecular spectroscopy, XRD and DCS assays demonstrated clearly that in the 3HB prevailing polymers, the 4HB monomer acted as a structure-breaking component of P(3HB) crystalline lattice and, similarly, when the 4HB monomer predominated the polymer composition, residual 3HB units reduced the overall P(4HB) crystal lattice content. Consequently, polymers with a comparable content of 3HB and 4HB in the polymer chain showed the lowest crystallinity and the amorphous character of the material predominated. Presence of 3HV in terpolymer virtually amplified the effects of 4HB (the material behaved like it had a higher 4HB content). In this way, it was confirmed experimentally that adjusting of the monomer composition of the polymer enabled optimization of its crystallinity both qualitatively (the type of the crystalline lattice) and quantitatively (the overall degree of crystallinity).

Moreover, the results of the combination of thermoanalytical methods used (DSC and TGA) showed that while the incorporation of a 4HB monomer in the polymer composition lowered the melting temperature significantly, it also resulted in a gradual increase in stability against thermal decomposition. P(3HB-*co*-4HB) copolymers were thus less prone to thermal degradation during melt processing, which represented a key improvement from the perspective of polymer processing technology. Furthermore, qualitative results provided by the preliminary enzyme-degradation assay indicated that manipulating the monomer composition of the copolymers affected the rate of its biodegradation.

To sum up, our study confirms that the isolated bacterium *Aneurinibacillus* sp. H1 represents a highly promising candidate for the biotechnological production of PHA not only from the economical point of view (as discussed in detail in the preceding paper in this series), but also with respect to its capability to produce polymers with material properties that can be tuned together with their chemical

composition by the corresponding adjustment in the cultivation process. In order to evaluate the ability of PHA polymers produced by *Aneurinibacillus* sp. H1 to meet specific requirements of particular application areas, further material analysis focused on mechanical performance, transport properties (gas and solute permeabilities, etc.) and stability in various environments must be supplemented in a follow-up study.

Supplementary Materials: The following are available online at http://www.mdpi.com/2073-4360/12/6/1298/s1, Figure S1: Visual appearance of the PHA films investigated in this study. Figure S2: Complete FTIR spectra of the solution-casted PHA films prepared from polymers with different monomer composition (each spectrum represents an arithmetic average of 10 individual spectra collected at different locations on a surface of the film). Figure S3: SEM micrographs of PHA copolymer films before and after the enzymatic degradation assay (magnification 1000×, scalebar: 100 μm).

Author Contributions: Conceptualization, S.O. and P.S.; methodology, S.O. and P.S.; formal analysis, I.P.; investigation, I.P., I.N., X.K., M.K. (Michal Kalina), J.N., V.K., K.H., J.M., E.S., M.T.; resources, S.O.; writing—original draft preparation, S.O. and P.S.; writing—review and editing, A.K., M.K. (Martin Koller) All authors have read and agreed to the published version of the manuscript.

References

1. Nakajima, H.; Dijkstra, P.; Loos, K. The recent developments in biobased polymers toward general and engineering applications: Polymers that are upgraded from biodegradable polymers, analogous to petroleum-derived polymers, and newly developed. *Polymers* **2017**, *9*, 523. [CrossRef] [PubMed]
2. Obruca, S.; Sedlacek, P.; Slaninova, E.; Fritz, I.; Daffert, C.; Meixner, K.; Sedrlova, Z.; Koller, M. Novel unexpected functions of PHA granules. *Appl. Microbiol. Biotechnol.* **2020**. [CrossRef] [PubMed]
3. Sedlacek, P.; Slaninova, E.; Enev, V.; Koller, M.; Nebesarova, J.; Marova, I.; Hrubanova, K.; Krzyzanek, V.; Samek, O.; Obruca, S. What keeps polyhydroxyalkanoates in bacterial cells amorphous? A derivation from stress exposure experiments. *Appl. Microbiol. Biotechnol.* **2019**, *103*, 1905–1917. [CrossRef] [PubMed]
4. Obruca, S.; Sedlacek, P.; Krzyzanek, V.; Mravec, F.; Hrubanova, K.; Samek, O.; Kucera, D.; Benesova, P.; Marova, I. Accumulation of poly(3-hydroxybutyrate) helps bacterial cells to survive freezing. *PLoS ONE* **2016**, *11*, e0157778. [CrossRef]
5. Obruca, S.; Sedlacek, P.; Mravec, F.; Krzyzanek, V.; Nebesarova, J.; Samek, O.; Kucera, D.; Benesova, P.; Hrubanova, K.; Milerova, M.; et al. The presence of PHB granules in cytoplasm protects non-halophilic bacterial cells against the harmful impact of hypertonic environments. *New Biotechnol.* **2017**, *39*, 68–80. [CrossRef]
6. Slaninova, E.; Sedlacek, P.; Mravec, F.; Mullerova, L.; Samek, O.; Koller, M.; Hesko, O.; Kucera, D.; Marova, I.; Obruca, S. Light scattering on PHA granules protects bacterial cells against the harmful effects of UV radiation. *Appl. Microbiol. Biotechnol.* **2018**, *102*, 1923–1931. [CrossRef]
7. Wampfler, B.; Ramsauer, T.; Rezzonico, S.; Hischier, R.; Köhling, R.; Thöny-Meyer, L.; Zinn, M. Isolation and purification of medium chain length poly(3-hydroxyalkanoates) (mcl-PHA) for medical applications using nonchlorinated solvents. *Biomacromolecules* **2010**, *11*, 2716–2723. [CrossRef]
8. Koller, M. Chemical and biochemical engineering approaches in manufacturing Polyhydroxyalkanoate (PHA) biopolyesters of tailored structure with focus on the diversity of building blocks. *Chem. Biochem. Eng. Q.* **2019**, *32*, 413–438. [CrossRef]

9.　Singh, A.K.; Srivastava, J.K.; Chandel, A.K.; Sharma, L.; Mallick, N.; Singh, S.P. Biomedical applications of microbially engineered polyhydroxyalkanoates: An insight into recent advances, bottlenecks, and solutions. *Appl. Microbiol. Biotechnol.* **2019**, *103*, 2007–2032. [CrossRef]

10.　Pernicova, I.; Novackova, I.; Sedlacek, P.; Kourilova, X.; Koller, M.; Obruca, S. Application of osmotic challenge for enrichment of microbial consortia in polyhydroxyalkanoates producing thermophilic and thermotolerant bacteria and their subsequent isolation. *Int. J. Biol. Macromol.* **2020**, *144*, 698–704. [CrossRef]

11.　Chen, G.-Q.; Jiang, X.-R. Next generation industrial biotechnology based on extremophilic bacteria. *Curr. Opin. Biotechnol.* **2018**, *50*, 94–100. [CrossRef]

12.　Obruca, S.; Benesova, P.; Oborna, J.; Marova, I. Application of protease-hydrolyzed whey as a complex nitrogen source to increase poly(3-hydroxybutyrate) production from oils by *Cupriavidus necator*. *Biotechnol. Lett.* **2014**, *36*, 775–781. [CrossRef]

13.　Hermawan, S.; Jendrossek, D.J. Tyrosine 105 of *Paucimonas lemoignei* PHB depolymerase PhaZ7 is essential for polymer binding. *Polym. Degrad. Stabil.* **2010**, *95*, 1429–1435. [CrossRef]

14.　Amirul, A.A.; Yahya, A.R.M.; Sudesh, K.; Azizan, M.N.M.; Majid, M.I.A. Biosynthesis of poly(3-hydroxybutyrate-co-4-hydroxybutyrate) copolymer by *Cupriavidus* sp. USMAA1020 isolated from Lake Kulim, Malaysia. *Bioresour. Technol.* **2008**, *99*, 4903–4909. [CrossRef]

15.　Chanprateep, S.; Kulpreecha, S. Production and characterization of biodegradable terpolymer poly(3-hydroxybutyrate-co-3-hydroxyvalerate-co-4-hydroxybutyrate) by *Alcaligenes* sp. A-04. *J. Biosci. Bioeng.* **2006**, *101*, 51–56. [CrossRef]

16.　Tanadchangsaeng, N.; Yu, J. Microbial synthesis of polyhydroxybutyrate from glycerol: Gluconeogenesis, molecular weight and material properties of biopolyester. *Biotechnol. Bioeng.* **2012**, *109*, 2808–2818. [CrossRef]

17.　Tsuge, T.; Hyakutake, M.; Mizuno, K. Class IV polyhydroxyalkanoate (PHA) synthases and PHA-producing Bacillus. *Appl. Microbiol. Biotechnol.* **2015**, *99*, 6231–6624. [CrossRef]

18.　Porter, M.; Yu, J. Monitoring the in situ crystallization of native biopolyester granules in *Ralstonia eutropha via* infrared spectroscopy. *J. Microb. Meth.* **2011**, *87*, 49–55. [CrossRef]

19.　Kann, Y.; Shurgalin, M.; Krishnaswamy, R.K. FTIR spectroscopy for analysis of crystallinity of poly(3-hydroxybutyrate-co-4-hydroxybutyrate) polymers and its utilization in evaluation of aging, orientation and composition. *Polym. Test.* **2014**, *40*, 218–224. [CrossRef]

20.　Padermshoke, A.; Sato, H.; Katsumuto, Y.; Ekgasit, S.; Noda, I.; Ozaki, Y. Thermally induced phase transition of poly(3-hydroxybutyrate-co-3-hydroxyhexanoate) investigated by two-dimensional infrared correlation spectroscopy. *Vibrat. Spec.* **2004**, *36*, 241–249. [CrossRef]

21.　Kunioka, M.; Tamaki, A.; Doi, Y. Crystalline and thermal properties of bacterial copolyesters: Poly(3-hydroxybutyrate-co-3-hydroxyvalerate) and poly(3-hydroxybutyrate-co-4-hydroxybutyrate). *Macromolecules* **1989**, *22*, 694–697. [CrossRef]

22.　Phillipson, K.; Hay, J.N.; Jenkins, M.J. Thermal analysis FTIR spectroscopy of poly(ε-caprolactone). *Thermochim. Acta* **2014**, *595*, 74–82. [CrossRef]

23.　Yu, C.; Bao, J.; Xie, Q.; Shan, G.; Bao, Y.; Pan, P. Crystallization behavior and crystalline structural changes of poly(glycolic acid) investigated via temperature-variable WAXD and FTIR analysis. *Cryst. Eng. Comm.* **2016**, *18*, 7894–7902. [CrossRef]

24.　Saito, Y.; Doi, Y. Microbial synthesis and properties of poly(3-hydroxybutyrate-co-4-hydroxybutyrate) in *Comamonas acidovorans*. *Int. J. Biol. Macromol.* **1994**, *16*, 99–104. [CrossRef]

25.　Gao, Z.; Su, T.; Li, P.; Wang, Z. Biodegradation of P(3HB-co-4HB) powder by *Pseudomonas mendocina* for preparation low-molecular-mass P(3HB-co-4HB). *3 Biotech* **2017**, *7*, 281. [CrossRef] [PubMed]

26.　Su, F.; Iwata, T.; Sudesh, K.; Doi, Y. Electron and X-ray diffraction study on poly(4-hydroxybutyrate). *Polymer* **2001**, *42*, 8915–8918. [CrossRef]

27.　Keridou, I.; Valle, L.J.D.; Funk, L.; Turon, P.; Yousef, I.; Franco, L.; Puiggali, J. Isothermal crystallization kinetics of poly(4-hydroxybutyrate) biopolymer. *Materials* **2019**, *12*, 2488. [CrossRef]

28.　Barham, P.J.; Keller, A.; Otun, E.L.; Holmes, P.A. Crystallization and morphology of a bacterial thermoplastic: Poly-3-hydroxybutyrate. *J. Mater. Sci.* **1984**, *19*, 2781–2794. [CrossRef]

29.　Scandola, M.; Ceccorulli, G.; Pizzoli, M.; Gazzano, M. Study of the crystal phase and crystallization rate of bacterial poly(3-hydroxybutyrate-co-3-hydroxyvalerate). *Macromolecules* **1992**, *25*, 1405–1410. [CrossRef]

30.　Wang, X.; Zhang, H.; Liu, M.; Jia, D. Thermal stability of poly(3-hydroxybutyrate-co-4-hydroxybutyrate)/modified montmorillonite bio-nanocomposites. *Polym. Compos.* **2017**, *38*, 673–681. [CrossRef]

31. Kim, K.J.; Doi, Y.; Abe, H. Effects of residual metal compounds and chain-end structure on thermal degradation of poly(3-hydroxybutyric acid). *Polym. Degrad. Stabil.* **2006**, *91*, 769–777. [CrossRef]

32. Kim, K.J.; Doi, Y.; Abe, H.; Martin, D.P. Thermal degradation behavior of poly(4-hydroxybutyric acid). *Polym. Degrad. Stabil.* **2006**, *91*, 2333–2341. [CrossRef]

33. Merrick, J.M.; Steger, R.; Dombroski, D. Hydrolysis of native poly(hydroxybutyrate) granules (PHB), crystalline PHB, and artificial amorphous PHB granules by intracellular and extracellular depolymerases. *Int. J. Biol. Macromol.* **1999**, *25*, 129–134. [CrossRef]

34. Saito, Y.; Nakamura, S.; Hiramitsu, M.; Doi, Y. Microbial synthesis and properties of poly(3-hydroxybutyrate-co-4-hydroxybutyrate). *Polym. Int.* **1996**, *39*, 169–174. [CrossRef]
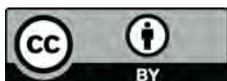
Appendix 14

Obruca, S., Sedlacek, P., Mravec, F., Krzyzanek, V., Nebesarova, J., Samek, O., Kucera, D., Benesova, P., Hrubanova, K., Milerova, M., and Marova, I. The presence of PHB granules in cytoplasm protects non-halophilic bacterial cells against the harmful impact of hypertonic environments. *New Biotechnology* **2017**, 39, 68–80.

Full length Article

The presence of PHB granules in cytoplasm protects non-halophilic bacterial cells against the harmful impact of hypertonic environments

Stanislav Obruca[a,*], Petr Sedlacek[a], Filip Mravec[a], Vladislav Krzyzanek[b], Jana Nebesarova[c], Ota Samek[b], Dan Kucera[a], Pavla Benesova[a], Kamila Hrubanova[b], Miluse Milerova[a], Ivana Marova[a]

[a] Faculty of Chemistry, Brno University of Technology, Purkynova 112, 612 00 Brno, Czech Republic
[b] Institute of Scientific Instruments, Academy of Sciences of The Czech Republic, Vvi, Kralovopolska 147, 612 64 Brno, Czech Republic
[c] Biology Centre, The Czech Academy of Sciences, v.v.i., Branisovska 31, 37005 Ceske Budejovice, Czech Republic

ARTICLE INFO

ABSTRACT

Numerous prokaryotes accumulate polyhydroxybutyrate (PHB) intracellularly as a storage material. It has also been proposed that PHB accumulation improves bacterial stress resistance. *Cupriavidus necator* and its PHB non-accumulating mutant were employed to investigate the protective role of PHB under hypertonic conditions. The presence of PHB granules enhanced survival of the bacteria after exposure to hypertonic conditions. Surprisingly, when coping with such conditions, the bacteria did not utilize PHB to harvest carbon or energy, suggesting that, in the osmotic upshock of *C. necator*, the protective mechanism of PHB granules is not associated with their hydrolysis. The presence of PHB granules influenced the overall properties of the cells, since challenged PHB-free cells underwent massive plasmolysis accompanied by damage to the cell membrane and the leakage of cytoplasm content, while no such effects were observed in PHB containing bacteria. Moreover, PHB granules demonstrated "liquid-like" properties indicating that they can partially repair and stabilize cell membranes by plugging small gaps formed during plasmolysis. In addition, the level of dehydration and changes in intracellular pH in osmotically challenged cells were less pronounced for PHB-containing cultures, demonstrating the important role of PHB for bacterial survival under hyperosmotic conditions.

Introduction

The fluctuation of external osmolarity is one of the most frequently encountered types of environmental stress factor for numerous microorganisms. For example, soil bacteria are often exposed to rapid alterations in external osmolarity as the water activity of soil is dependent on quickly changing weather conditions [1]. Therefore, the ability to adapt to fluctuations in external osmolarity is fundamental to survival and bacteria (regardless of their salinity preference) have developed different strategies to cope with osmotic pressure and changes in extracellular osmolarity [2].

Driven by the difference of osmotic pressure inside and outside the cell, a rapid increase in external salt concentration is inevitably accompanied by water efflux, resulting in dehydration of the cytoplasm [1]. The cell envelope of Gram-negative bacteria consists of an outer membrane, murein wall and cytoplasmic membrane, which contract together forming a kind of composite material. When cells dehydrate as a consequence of exposure to osmotic upshock, the cytoplasmic membrane separates from the outer layers of the cell envelope in order to cover a smaller volume of cytoplasm. Such a process is called "plasmolysis" and is accompanied by the formation of a periplasmic space, which depending on the conditions can represent 5–70% of cell volume [3]. The ability to undergo plasmolysis indicates that a semipermeable membrane is functioning and able to maintain protoplast integrity [4]. However, plasmolysis may also be a problem because the cytoplasmic membrane is unable to shrink by more than 2–5%, so that massive plasmolysis might result in its damage and collapse [5].

Polyhydroxyalkanoates (PHAs) are storage polyesters accumulated in the form of intracellular granules by a wide range of prokaryotic microorganisms. Among PHAs, the polymer of 3-

(, sedlacek-p@fch.vut.cz (P. Sedlacek), mravec@fch.vut.cz (F. Mravec),
krzyzanek@isibrno.cz (V. Krzyzanek), nebe@paru.cas.cz (J. Nebesarova),
osamek@isibrno.cz (O. Samek), xckucerad@fch.vut.cz (D. Kucera),
xcbenesova2@fch.vut.cz (P. Benesova), hrubanova@isibrno.cz (K. Hrubanova),
xcmilerova@fch.vut.cz (M. Milerova), marova@fch.vut.cz (I. Marova).

hydroxybutyrate, poly(3-hydroxybutyrate) (PHB) is commonest and best studied [6–8]. PHB granules can represent a large fraction of cellular dry matter − under extreme conditions, up to 90% [9]. However, bacterial cells control their size to restrict the volume content of PHB granules to a maximum of 40% [10]; hence, geometric factors are assumed to determine the upper limit of intracellular PHB content [11]. The biosynthesis and hydrolysis of intracellular PHB granules occur simultaneously; thus, PHB metabolism exhibits a cyclic mechanism. Biosynthesis prevails when an external carbon source is present in excess and, on the contrary, hydrolysis and utilization of PHB granules is dominant when an external carbon source is lacking [12]. Therefore, it is generally proposed that PHAs are primarily utilized as carbon and energy storage materials when exogenous carbon sources are exhausted.

Nevertheless, there are several reports indicating that the presence of PHA granules in the cytoplasm enhances the survival of bacteria under various stress conditions, including osmotic pressure. Zhao et al. observed that the disruption of the PHA synthase gene in *Aeromonas hydrophila* reduced its resistance against numerous environmental stress factors, including high osmotic pressure [13]. Breedveld et al. reported that *Rhizobium leguminosarum* TA-1 and *Rhizobium meliloti* SU-47 cultures responded to osmotic stress exposure by degrading the intracellular storage of PHB and simultaneously increasing trehalose content [14]. Wang et al. tested the stress durability of recombinant *Escherichia coli* strains. The first of these harbored only PHA synthetic genes, whereas the second recombinant strain harbored both PHB synthetic genes and intracellular PHB depolymerase. It was observed that both strains were more resistant against several stresses, including osmotic pressure, than the wild type which was incapable of PHB synthesis. However, the recombinant strain capable of synthesizing and degrading PHB was more resistant than the strain incapable of PHB degradation [15]. Further, it was reported that the application of mild osmotic pressure (about 10 g/L NaCl) supports PHB biosynthesis in *Cupriavidus necator* [16,17]. Moreover, the capacity to accumulate PHA was observed in many halotolerant and halophilic prokaryotes, while several Gram-negative halophiles such as *Haloferax mediterranei* or *Halomonas* sp. are considered as potential candidates for the industrial production of PHAs [18,19]. Recently, Gram-positive halotolerant strains have also been described as potential PHA producers under fluctuating salinities [20].

Therefore, we proposed to shed light on the effects of the presence of PHB granules in bacterial cells on the viability, morphology and other properties of osmo-mesophilic cells when exposed to a hypertonic environment. We employed the most studied organism in the context of PHA metabolism, namely the Gram-negative soil bacterium *Cupriavidus necator* H16 [21] and its mutant strain *Cupriavidus necator* PHB^{-4} which, due to the mutation in the gene encoding PHB synthase, is incapable of accumulating PHB [22].

Methods

Microorganisms

The PHB-producing strain *Cupriavidus necator* H16 (CCM 3726) was obtained from the Czech Collection of Microorganisms, Brno, Czech Republic, and its PHA non-producing mutant strain *Cupriavidus necator* PHB-4 (DSM-541) was purchased from the Leibnitz Institute DSMZ-German Collection of Microorganism and Cell Cultures, Braunschweig, Germany.

Cultivations and hyperosmotic challenge

Cultivations were performed in Erlenmeyer flasks (volume 250 mL) containing 100 mL of Mineral Salt (MS) medium. Composition of MS medium was: 20 g fructose, 3 g $(NH_4)_2SO_4$, 1 g KH_2PO_4, 11.1 g $Na_2HPO_4 \cdot 12 H_2O$, 0.2 g $MgSO_4 \cdot 7 H_2O$, 1 mL of microelement solution, and 1 L of distilled water; the microelement solution was composed of 9.7 g $FeCl_3$, 7.8 g $CaCl_2$, 0.156 g $CuSO_4 \cdot 5 H_2O$, 0.119 g $CoCl_2$, and 0.118 g $NiCl_2$ in 1 L of 0.1 M HCl. The flasks were inoculated with 5 mL of the overnight culture of a particular strain of *C. necator* grown in Nutrient Broth medium consisting of 10 g peptone, 10 g beef extract, and 5 g NaCl in 1 L of distilled water. After 72 h of cultivation, the cells were harvested (centrifugation, $8000 \times g$, 5 min), washed with Na-phosphate buffer (pH 7.4; 50 mM), and exposed to various concentrations of NaCl (0, 50, 100 and 200 g per liter of Na-phosphate buffer) for 3 h at 30 °C. Afterwards, various analyses of the challenged bacterial cells were performed as described below.

Analysis of cell viability

First, cell viability was assayed by the analysis of colony forming units (CFU/mL). Cells of both *C. necator* strains (between 1×10^8 and 1×10^9 cells/mL) were exposed to various concentrations of NaCl for 3 h as described above. The numbers of viable cells (CFU/mL) were determined by dilution plating on Petri dishes with NB medium agar prior to and at the end of incubation (three replicates). NB medium agar consisted of 10 g peptone, 10 g beef extract, and 5 g NaCl and 20 g agar per 1 L of distilled water.

Secondly, the viability of challenged bacterial populations was assessed by flow cytometry, using a membrane integrity assay employing propidium iodide staining. The protocol described by Coder was employed [23]. From each sample, 100 μL aliquots were taken, washed with PBS buffer, and diluted to a cell count of approximately 1×10^6 cells/mL. Then, 1 mL of cell suspension was stained with 1 μL of 1 mg/mL propidium iodide in the dark for 5 min. Subsequently, cell viability was analysed by flow cytometry (Apogee A50, Apogee, GB) using a 488 nm laser for excitation and the red channel (FL3) for fluorescence detection.

Analysis of intracellular PHB content

To determine the biomass concentration and PHB content in cells after exposure to a hypertonic environment, samples (10 mL) were centrifuged and the cells washed twice with distilled water and dried at 80 °C until they achieved constant mass. The PHB content of the dried cells was analysed by gas chromatography (Trace GC Ultra, Thermo Scientific, USA), as reported previously [24].

Raman spectroscopy

Approximately 20 μL of cells from *C. necator* H16 cultures exposed for 3 h to various concentrations of NaCl were pipetted onto CaF_2 (Raman grade glass) and analysed using a Renishaw Invia system (Renishaw inVia Raman Spectrometer, Renishaw plc., Wotton-under-Edge, UK), with a 785 nm single-mode diode laser as excitation source. The laser beam was focused onto a sample by the microscope objective (Leica, Wetzlar, Germany, 50×, NA (Numerical aperture) 0.5), with a laser spot diameter of approximately 2 μm × 10 μm. Overview spectra were acquired in the range 700–1800 cm^{-1}. Spectra from different parts of the sample were measured for 15 s, to a total of 3 measurements per sample; the results were averaged.

Cryo-SEM

A thin layer of bacterial cultures of *C. necator* H16 and *C. necator* PHB-4 exposed to hypertonic environments induced by various NaCl concentrations on a TEM mesh grids were frozen quickly in liquid nitrogen and moved into a cryo-vacuum chamber (ACE600, Leica Microsystems), where they were sublimated at −95 °C for 5 min. Further, the samples were moved under high vacuum using a shuttle (VCT100, Leica Microsystems) into a Scanning Electron Microscope (Magellan 400/L, FEI) equipped with a cold stage, and the samples were observed in a 1 keV electron beam at 120 °C without metal coating.

Transmission electron microscopy analysis of bacterial cells

Bacterial cells of both *C. necator* strains exposed to osmotic upshock induced by various NaCl concentrations were analysed by Transmission Electron Microscopy (TEM). After exposure to stress conditions, 1 mL of the suspension was centrifuged (1000 rpm for 15 min) and the preparation protocol was initiated by the addition of a cryoprotectant (20% BSA (Fluka)) to cell suspensions. Then, each sample (approx. 0.2 μL) was placed in a special carrier, frozen in a high pressure freezer (Leica EM Pact), and transferred under liquid N₂ into a freeze substitution unit (Leica EM AFS). 2% osmium tetroxide in acetone was used as a substitution solution. The substitution protocol was initiated at a temperature of −90° C for 96 h, and subsequently the samples were warmed up at −20° C for 24 h (5 ° C per hour) and finally the temperature was increased at 4° C after 8 h (3° C per hour), at which the samples were kept for 18 h. The samples were washed at room temperature in anhydrous acetone (15 min, three times). Next, the samples were infiltrated and embedded with Polybed resin (SPI) using acetone:resin

mixtures (2:1, 1:1 and 1:2, each set-up embedded for 1 h and then overnight in pure embedding media under vacuum using a desiccator). Polymerization was perfomed by heat treatment (48 h at 62° C). Ultrathin sections were cut on an Ultracut UCT ultramicrotome (Leica) using a diamond knife (Diatome) with a cutting angle of 45°. Sections were transferred onto 300Mesh copper grids and stained with uranyl acetate and lead citrate solutions.

The ultrastructure of PHA-accumulating cells was examined using a JEOL 1010 transmission electron microscope operating at an accelerating voltage of 80 kV. Images were recorded digitally using a Megaview III CCD camera (Olympus).

The volumes of the periplasmatic spaces of upshocked cells (the measure of plasmolysis) were determined by image analysis of TEM microphotographs using Harfa software, as described in Supplementary materials and our previous publication [10].

Time-resolved fluorescence microspectroscopy

This section covers two different measurement techniques. The first, Fluorescence Lifetime Imaging (FLIM), was used to resolve lifetime changes in differently localized fluorophores. A fluorescent probe (carboxyfluorescein) is formed *in situ* by enzymatic hydrolysis from BCECF-AM (Molecular Probes). The lifetime of the fluorescence of this probe is dependent on the local pH value of a cytosol (see Supplementary material for calibration of this dependence). The second method. fluorescence anisotropy imaging, is directly related to the free rotational motion of the fluorophore and so to the local viscosity. Carboxyfluorescein was excited with a pulsed laser at 467 nm and 40 MHz repetition (PicoQuant). Samples were scanned with the objective using a piezoelectric scanner (PhysikInstrumente, GmbH). Excitation and
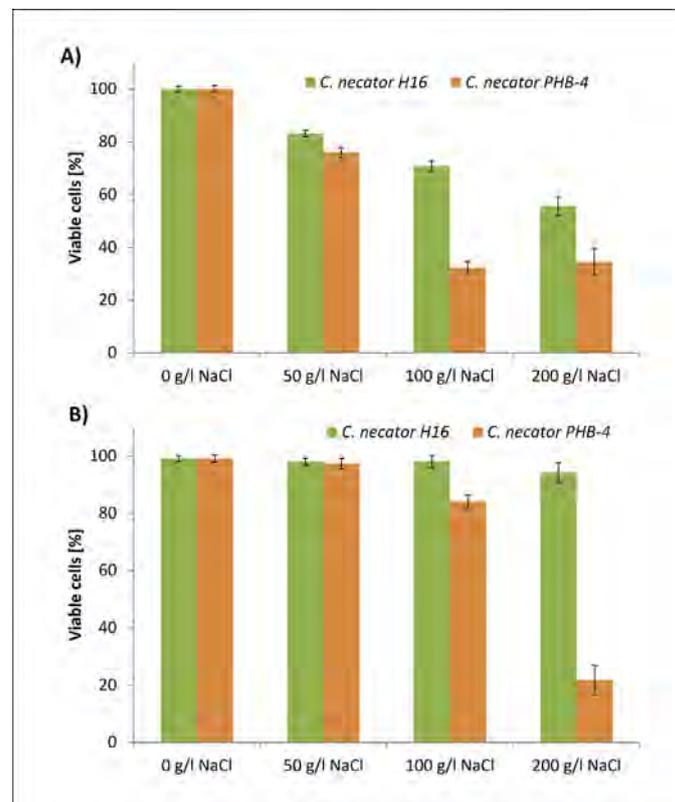
Fig 1. Viability of the PHB positive culture *C. necator* H16 and its PHB non-producing mutant *C. necator* PHB⁻⁴ exposed (3 h) to various NaCl concentrations assayed by (A) plating and (B) flow cytometry using propidium iodide staining.

emission light were collected via an UPlanSapo objective with $60\times$ magnification, water immersion, Numerical Aperture 1.2 (Olympus, Inc.). Fluorescence signal was collected through a $50\,\mu m$ pinhole, 520/35 emission filter (Semrock) and with a single photon avalanche-photodiode detector (MPD S.r.l.). Samples were fixed using a pre-heated 2% agarose solution in water and in a salt solution with a concentration of 200 g/L of NaCl. About $10\,\mu L$ of cell suspension was placed onto a microscopy cover slide and superimposed with 2% agarose at $\sim40\,°C$. In the case of pH measurement, the dependency of carboxyfluorescein lifetimes from hydrolysed BCECF-AM on different pH values was studied. It was found that the average lifetime of a fluorophore exhibits a non-linear dependency on the pH of the environment. The calibration is presented in Supplementary materials.

Thermogravimetry of bacterial cells

A thermogravimetric analyzer (TGA, TA Instruments, Q5000IR) was used to quantitatively analyze the dehydration of osmotically challenged bacterial cultures. Prior to TGA analysis, a corresponding cell sample, cultivated and osmotically challenged by the procedures described above, was centrifuged and the supernatant was carefully decanted. About 15 mg of the remaining cell suspension were weighed into the aluminium TGA pan. In the TGA analyzer, the sample was heated instantaneously to $60\,°C$ and subsequently kept at this temperature for 40 min. Then, the temperature was raised to $200\,°C$ and maintained for further 20 min in order to determine the dry mass of the sample. Both bacterial cultures (C. necator H16 and C. necator PHB^{-4}) were analysed in unchallenged form as well as after exposure to 50, 100 and 200 g/L NaCl, respectively. Every experiment was performed in four replicates; for each replicate, a fresh bacterial culture was prepared. All the thermograms were analysed according to Uribelarrea et al. [25] in order to determine critical water contents (i.e. the points in the drying curves corresponding to a sudden change in the drying rate) as a quantitative measure of the respective intracellular water content.

Results

Influence of PHB accumulation on survival of osmotic stress

In the first experiment, both bacterial cultures were exposed to osmotic shock induced by 50, 100, and 200 g/L of NaCl for 3 h; control exposure to buffer without the addition of NaCl was also performed. First, cell viability was assayed by comparing the numbers of cultivable cells (CFU/mL) in samples prior to and after incubation; data are shown in Fig. 1A. The results demonstrated that the application of NaCl decreased the number of cultivable cells in both cultures and this adverse effect increased with increasing concentration of NaCl. Importantly, the culture of C. necator H16 exhibited a higher survival rate than its PHB non-accumulating mutant.

Secondly, the viability of the cultures was further assessed by flow cytometry using propidium iodide as the viability probe. In principle, staining easily penetrates cells with damaged membranes, which consequently reveal high fluorescence and can be discriminated from intact cells. Therefore, propidium iodide is considered to be a membrane integrity probe [23]. The results are presented in Fig. 1B. Also in this case, the PHB accumulating culture demonstrated higher resistance to osmotic shock, its viability decreasing only slightly with increasing NaCl concentration, while the viability of the PHB non-accumulating mutant strain dropped dramatically when exposed to 100 and 200 g/L NaCl. These results suggest that the presence of PHB granules in bacterial cytoplasm provides protection for cell membranes against the effects of osmotic stress. Nevertheless, due to substantial differences in the results obtained by plating assay and flow cytometry (especially in C. necator H16), it appears that membrane damage caused by plasmolysis is not the only factor causing a reduction in the number of cultivable cells during osmotic challenge. The cultivability of PHB containing cells may be reduced by other mechanisms, despite the fact that they cells are able to maintain membrane integrity even at very high salt concentrations.

Change in PHB content and the state of the polymer in cells during hyperosmotic challenge

Since some authors have reported that the increased stress resistance of PHA accumulating bacteria against osmotic pressure is associated with the degradation of intracellular polymer granules [14,15], we determined the PHB content in bacterial cells before and after exposure of C. necator H16 to hyperosmotic challenge (Table 1). It was observed that a substantial decrease in polymer content occurred only in cells which were incubated in the absence of additional NaCl. In this case, prior to incubation, PHB content amounted to 85.0% of cell dry mass (CDM); after 3 h of incubation the polymer represented 80.7% of CDM. Thus, it seems that the absence of an external carbon source shifted the PHB metabolism from accumulation to degradation, which is in agreement with previous reports for this organism [21]. Conversely, when the cells were exposed to hyperosmotic shock, no PHB degradation occurred and, in contrast, a slight increase in PHB content was observed in the cell material with increasing NaCl concentration in the buffer. It is unlikely that the exposure of bacterial cells to such a high concentration of NaCl induced PHB biosynthesis in the absence of an external carbon substrate. The slight increase in PHB content was probably caused by the partial hypotonic lysis of upshocked cells, which were subsequently washed during the preparation of samples for GC analysis. Hence, the results suggest that the involvement of PHB granules in the response to suddenly induced high osmotic stress in C. necator is rather metabolically passive and most likely not connected with their degradation, in contrast to findings of Breedveld et al., who observed that osmotic upshock is associated with mobilization of PHA storage [14].

The state of PHB in upshocked cells was determined by Raman spectroscopy. Under normal conditions, intracellular PHB granules consist of amorphous polymer which is also the substrate for intracellular PHB depolymerases [26]. However, we observed that in some cases the amorphous state changed such that crystallization was clearly identifiable from Raman spectra. The process of crystallization is associated with enhancement of the intensity/shift of particular PHB Raman peaks. Thus, it was possible to estimate the state of the polymer in samples which were exposed to 100 and 200 g/L NaCl, and to enable the start of the crystallization process within the cells to be visualized. Here, qualitative differences between crystalline and amorphous

Table 1
The PHA content of intracellular polymer in cells of C. necator H16 exposed to hypertonic conditions induced by various NaCl concentrations.

	PHA content in biomass [w%]
Prior to exposition	85.0 ± 3.2
0 g/L NaCl	80.7 ± 2.1
50 g/L NaCl	87.2 ± 0.9
100 g/L NaCl	90.9 ± 2.0
200 g/L NaCl	90.7 ± 0.8
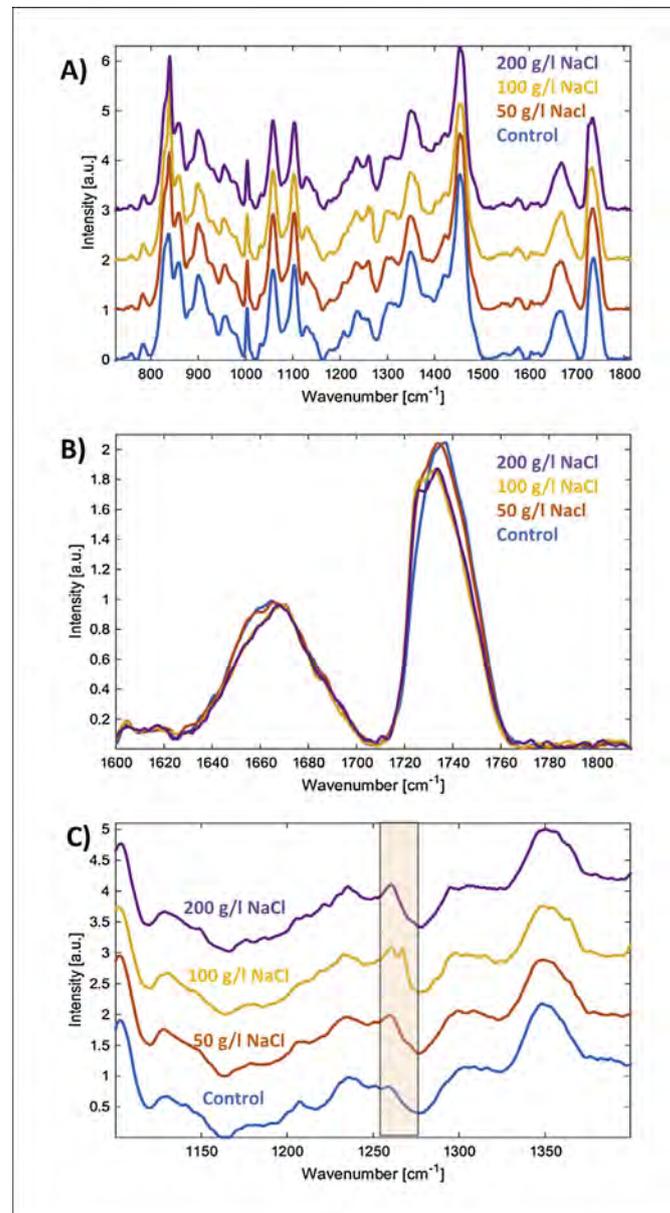
Fig. 2. Crystallization of PHB granules of upshocked cells of *C. necator* H16 recorded by Raman spectroscopy. (A) Whole Raman spectrum in the range 800–1800 cm^{-1}; (B) detail of crystallization indicating shift of PHB peak at 1736 cm^{-1} for samples exposed to 100 and 200 g/l NaCl; (C) formation of peak at 1260 cm^{-1} also indicating partial PHB granule crystallization.

polymer states can readily be evaluated by the naked eye using a set of 3 Raman emission lines which show quite significant changes (Fig. 2). The most significant changes in the line intensities of PHB during the process of crystallization were at 1260 and 841 cm^{-1}. The line shift related to the process of crystallization can also be observed for the PHB band from 1736 cm^{-1} (the amorphous state) to about 1725 cm^{-1} (the crystalline state), as reported previously [27–29]. Hence, it seems that the exposure of PHB containing bacterial cells to hyperosmotic shock causes the partial crystallization of PHB granules, which in turn might complicate its further mobilization by PHB depolymerases.

Observation of the morphology of challenged cells by Cryo-SEM

Cryo-SEM was used to analyze the surface morphologies of bacterial cells of both bacterial cultures exposed to hyperosmotic

shock. This technique, in general, should reveal changes in the shapes or sizes of challenged cells. The results are shown in Fig. 3. In fact, no substantial differences in the shapes of PHB accumulating and non-accumulating cells were recorded during their exposure to osmotic stress, which indicates that the outer layers of the cell envelope are not drastically damaged by hyperosmotic treatment. Nevertheless, cryo-SEM analysis revealed another interesting phenomenon. Surprising "string-like" structures were observed in the areas where the cells were ripped during sample preparation (see the structures indicated by red arrows in Fig. 3). These structures were observed only in PHB accumulating culture, which indicates that they were formed by plastically deformed PHB granules. Plastic deformation of freeze-fractured PHB granules investigated by Cryo-SEM has also been observed by other authors [30,31]. It is interesting that "string-like" structures were absent in bacterial culture incubated in buffer
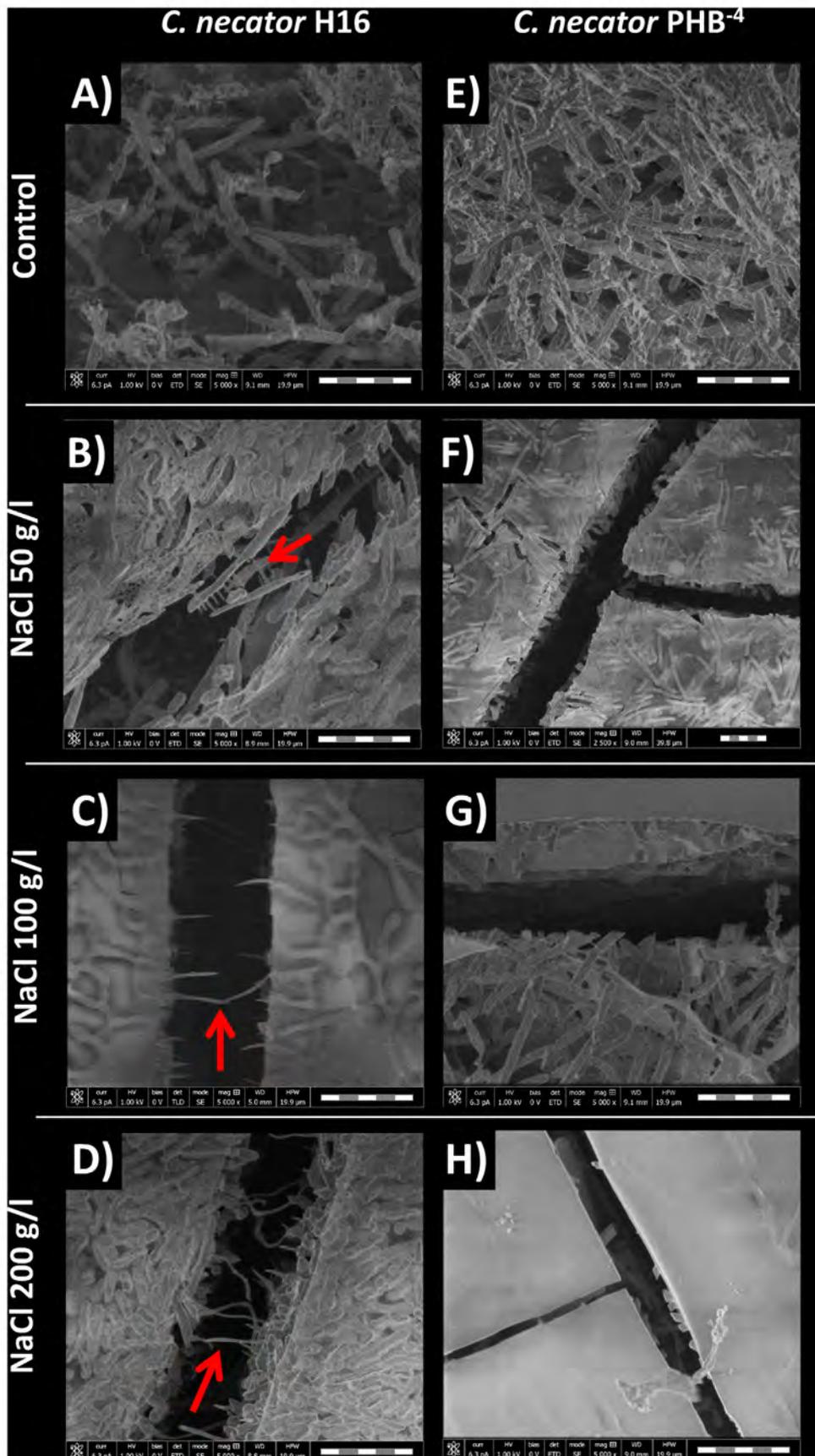
Fig. 3. Cryo-SEM analysis of PHB-accumulating *C. necator* H16 exposed to 0 (A), 50 g/L (B), 100 g/L (C), and 200 g/L NaCl (D); morphology of PHB non-accumulating strain *C. necator* PHB^{-4} exposed to 0 (E), 50 g/L (F), 100 g/L (G), and 200 g/L NaCl (H). Red arrows indicate "string-like" structures present in up-shocked PHB positive cells. Scale bar = 5 μm. (For interpretation of the references to colour in this figure legend, the reader is referred to the web version of this article.)
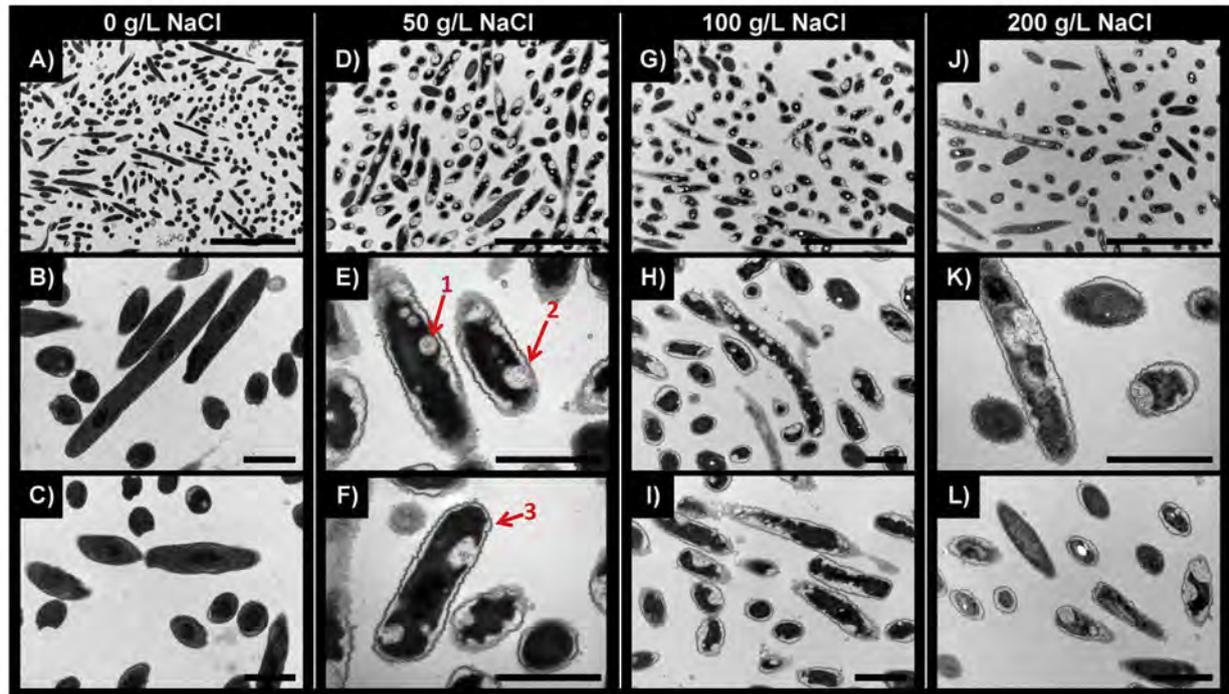
Fig. 4. TEM analysis of cells of the PHB non-accumulating strain *C. necator* PHB^{-4} exposed to 0 (A–C), 50 g/L (D–F), 100 g/L (G–I), and 200 g/L NaCl (J–L). Red arrows indicate the following observations: 1 – endocytotic vesicles; 2 – unsymmetrical plasmolysis of bacterial cells resulting in the formation of "hole-like" structures accompanied by the release of cytoplasm content into the periplasmatic space; 3–the wrinkling of the outer layers of the cell envelope – the outer membrane and murein layers. (A,D,G,J: scale bar = 5 μm, others: scale bar = 2 μm). (For interpretation of the references to colour in this figure legend, the reader is referred to the web version of this article.)

without NaCl and that their number as well as width seem to increase with increasing NaCl concentration. Evidently, the exposure of bacterial culture to osmotic upshock alters the properties of intracellular PHB granules, resulting in the more intensive formation of string-like structures. It is unlikely that the crystallization observed by Raman spectroscopy would support the formation of string-like structures requiring considerable plastic deformation of the polymer granules. Hence, it can be expected that hypertonic conditions induce further change(s) in the properties of PHB granules.

Transmission electron microscopy analysis of upshocked cells

Changes in the morphologies of the challenged cells of both bacterial cultures were also observed by TEM. Microphotographs of upshocked cells of the PHB non-accumulating mutant are shown in Fig. 4. Generally, the exposure of bacterial cells to hyperosmotic conditions induced massive plasmolysis in bacterial cells (the periplasmatic space represented about 44–49 vol% of the cells) and wrinkling of the outer layer of the cell envelope. The intensity of plasmolysis only changed slightly with increasing NaCl concentration and was accompanied by the formation of endocytotic vesicles in some bacterial cells and the formation of tubular structures and Scheie structures as described by Koch [3]. Surprisingly, the formation of the periplasmic space of upshocked PHB non-accumulating cells was not symmetrical or situated at the poles of the cells, as reported by others [3,5,32]; in numerous cases, "hole-like" structures (reminiscent of incompletely formed endocytotic vesicles) randomly distributed in the outer volume of bacterial cell cytoplasm were observed. It is very likely that such asymmetrical plasmolysis causes damage to the cytoplasmic

membrane. In these "holes" it is possible to observe darker areas, which may be attributed to the leakage of cytoplasmic content through the damaged membrane.

Fig. 5 shows the morphology of the PHB accumulating bacterial strain of *C. necator* exposed to various NaCl concentrations. In this case, osmotic challenge also resulted in wrinkling of the outer layer of the cell envelope and plasmolysis; however, the plasmolysis was considerably less intense since the periplasmatic space represented only about 20–24% of cell volume and no tubular or Scheie structures were observed. Furthermore, unlike in the PHB-non-accumulating mutant, plasmolysis in *C. necator* H16 did not result in the formation of hole-like structures accompanied by the leakage of cytoplasm content. On the contrary, when plasmolysis occurred in the close vicinity of PHB granules, the polymer granules exhibited unexpected "liquid-like" behavior associated with their influx into the periplasmic space. Thus, it seems that PHB granules are able to decrease the degree of plasmolysis and change its nature; it is also likely that, due to their liquid-like properties, they might partially protect membranes from damage and decrease the leakage of cytoplasm content.

In addition, when PHB-positive bacterial cells were exposed to 100 and 200 g/L of NaCl, the aggregation of PHB granules was clearly obsered, usually resulting in the formation of one or several non-spherical PHB granule(s) per cell.

Time-resolved fluorescence microscopy analysis of upshocked bacterial cells

The fluorescence properties of labelled cytosol determined by a BCECF-AM fluorogenic probe were studied using two different
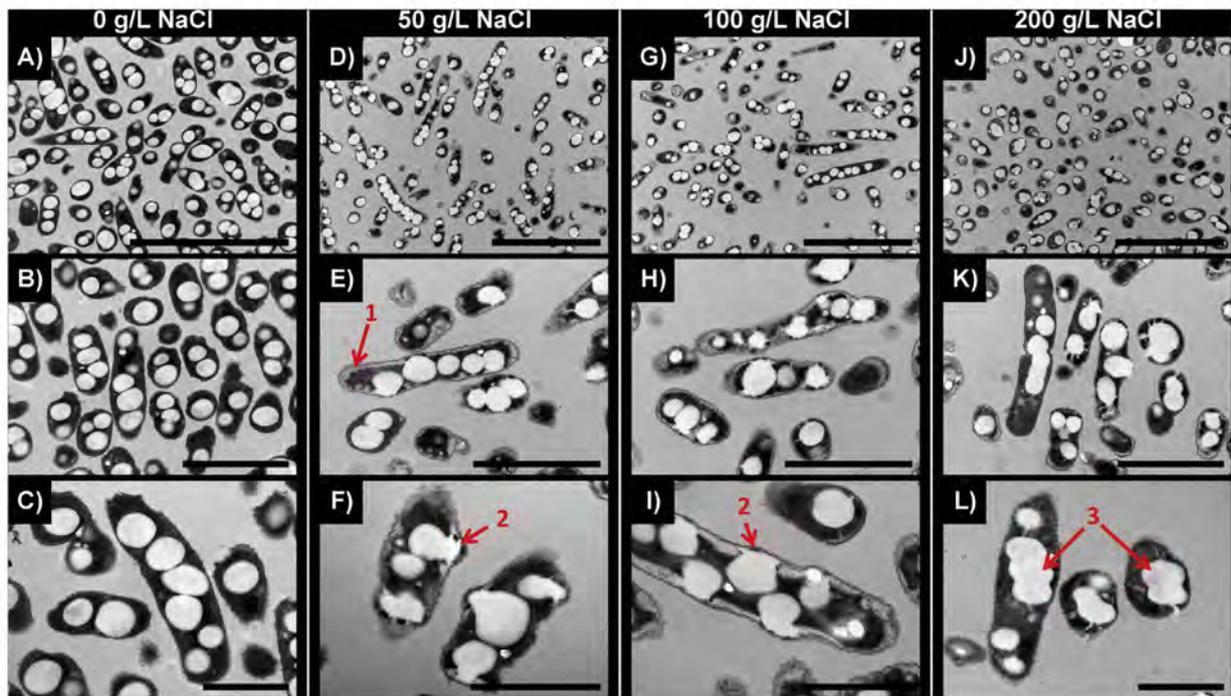
Fig. 5. TEM analysis of cells of the PHB-accumulating strain *C. necator* H16 exposed to 0 (A–C), 50 g/L (D–F), 100 g/L (G–I), and 200 g/L NaCl (J–L). Red arrows indicate the following observations: 1–the wrinkling of the outer layers of the cell envelope and symmetrical plasmolysis; 2–the influx of PHB granules into the periplasmic space; 3–the massive aggregation of PHB granules. (A,D,G,J: scale bar = 5 μm; B,E,H, K: scale bar = 2 μm; C,F,I,L: scale bar = 1 μm). (For interpretation of the references to colour in this figure legend, the reader is referred to the web version of this article.)

approaches. Fluorescence lifetimes, dependent on the pH of the environment (see Supplementary material), were comparable in the case of standard environments. In both cell types, intracellular pH was in the range 7.4–7.5, with a homogenous distribution inside the cells. However, osmotic upshock shifted the intracellular pH value differently in each tested bacterial culture. For *C. necator*, the pH decreased to a value of 7.0 ± 0.1. In contrast, as can be seen from the fluorescence probe lifetimes, intracellular pH in cells of the PHB non-containing mutant decreased more substantially to values around 6.5 ± 0.3 when exposed to hypertonic conditions. A further important effect of salt addition can be seen in Fig. 6a, which displays images with time-resolved information. Cells under standard conditions are very well defined; however, after exposure to osmotic stress, some cells, especially in PHB non-containing culture, reveal hazy edges, which can imply the partial leakage of the fluorescence probe into the external space.

Another fluorescence parameter which can uncover changes in properties of bacterial cells is steady-state fluorescence anisotropy. This describes the possibility of the free-rotation of the fluorescent probe and therefore is usually associated with the "viscosity" of the environment; its mapping can be used to study the rheology of bacterial cell cytoplasm [33]. Generally, anisotropy directly correlates with the viscosity of the environment – the higher the anisotropy, the higher the viscosity. In the PHB non-accumulating mutant, the fluorophore exhibited a relatively high value of anisotropy, 0.214 ± 0.005. The addition of salt caused a decrease in anisotropy (0.176 ± 0.008), which can be related to the decrease in viscosity of the intracellular matrix due to its partial leakage through the damaged membrane. Thus, the results of fluorescence anisotropy imaging confirm our observation of the

leakage of cytoplasm content in upshocked PHB non-containing cells obtained by TEM (see Fig. 5, arrow number 2). In contrast, anisotropy increased in *C. necator* H16 when the cells were exposed to osmotic upshock, indicating an increase in the viscosity of cytoplasm content associated with cell dehydration and plasmolysis. It seems that, unlike in the PHB negative strain, no substantial leakage of cytoplasm content occurred, implying that membranes were not heavily damaged by osmotic upshock (in agreement with the results of flow cytometry and TEM). Typical results are displayed as anisotropy-resolved images in Fig. 6b. The anisotropy values are scaled using a rainbow scale, with green dedicated to the free rotation of molecules and the low viscosity region. Red relates to the hindered rotation of fluorophores and high viscosity. Moreover, taking into account the homogeneity of the distribution of anisotropy values inside the cells, a further effect of salt addition can be seen. Both cell-types exhibit a homogenous distribution of anisotropy values before salt addition, whileafter exposure to the hypertonic environment, the anisotropy values are distributed more randomly inside the cells.

Quantitative analysis of the cell dehydration of up-shocked bacterial cells by TGA

Thermogravimetry (TGA) was employed to provide a quantitative estimate of the degree of osmotically-induced cell dehydration in PHB positive and negative bacterial cells. Centrifuged cell samples were continuously dried at 60 °C while corresponding changes in sample mass were recorded. Total water content in the sample was subsequently calculated from the residual mass content after further drying at 200 °C [34]. The results on both
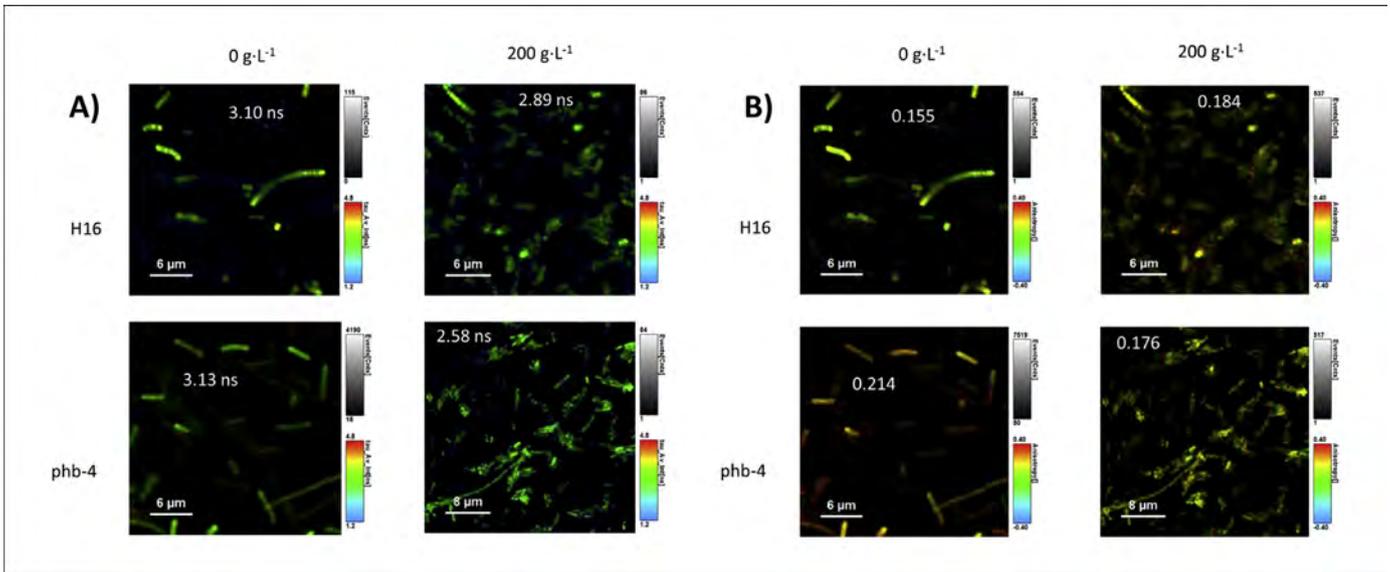
Fig. 6. The Influence of salt addition on cells stained with carboxyfluorescein. A) Fluorescence lifetimes, averaged by intensity, are displayed as rainbow scales. Inserted values are average values of lifetimes found for each sample. Corresponding pH values are for nonchallenged cells (7.4–7.5), which decrease with salt addition to 7.0 ± 0.1 in *C. necator* H16 and to 6.5 ± 0.3 in *C. necator* PHB^{-4}. B) Anisotropy of carboxy fluorescein inside the studied cells. Steady-state anisotropy values are displayed as rainbow scales in which green relates to low viscosity regions (an anisotropy value of approx. 0) and red to high viscosity regions (an anisotropy value close to 0.4). Inserted values are average values of anisotropy found for each sample. (For interpretation of the references to colour in this figure legend, the reader is referred to the web version of this article.)

tested bacterial cultures are shown in the form of drying curves in Fig. 7A, C.

It has been proposed that changes in the rate of water elimination from cell samples can be used as indicators of the quantitative content of various forms of water in cell samples [25,35,36]. For instance, Uribelarrea et al. interpret the critical point in the drying curve of a cell sample (i.e. the point where the evolution of sample mass versus time suddenly changes its course) simply as a boundary point where the drying of extracellular water ends and the elimination of intracellular water starts [25].

To obtain such critical points from the results of our TGA experiments, derivation of the water loss over time is given as a
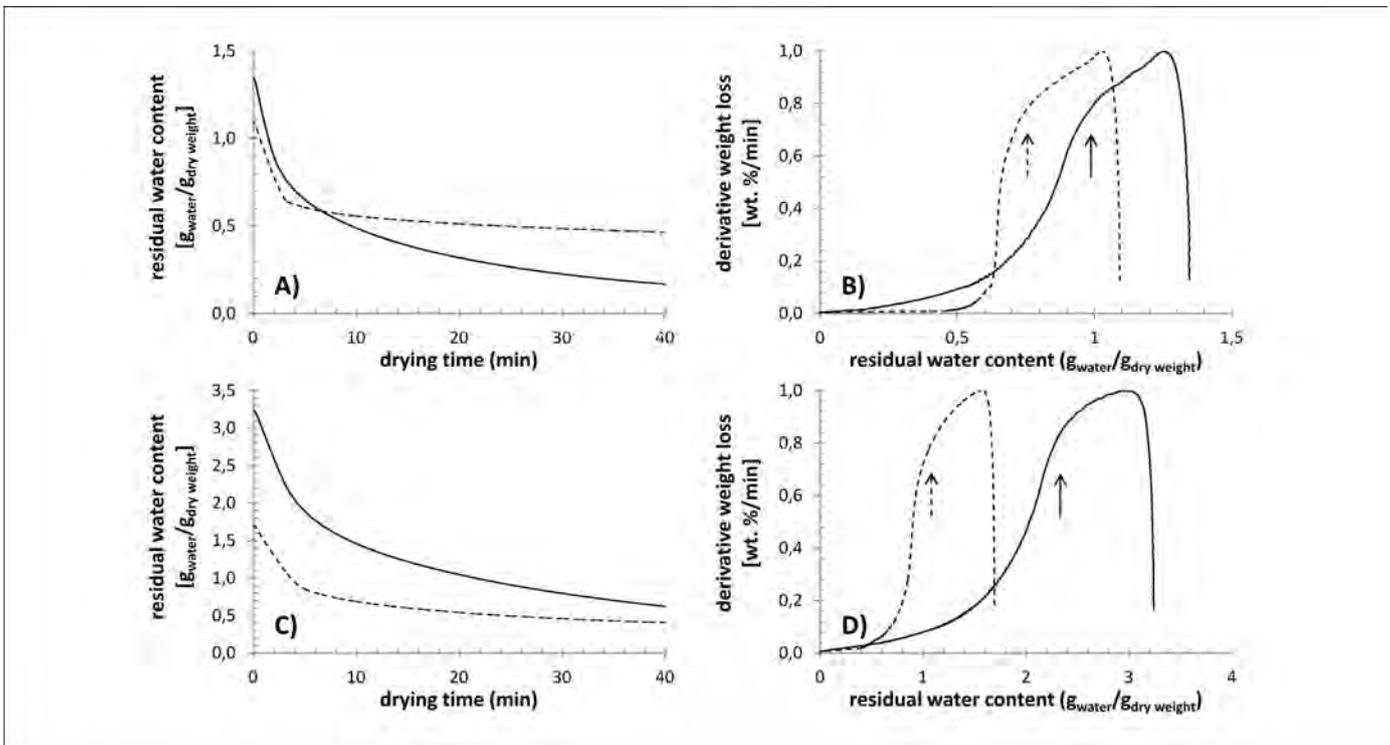
Fig. 7. The effect of osmotic challenge on drying curves determined by isothermal TGA experiments at 60 °C on *C. necator* H16 (A, B) and *C. necator* PHB-4 (C, D). Solid lines represent unchallenged bacterial samples, dashed lines represent samples exposed to 200 g/L NaCl. The heights of the derivative weight loss curves (B, D) were normalized for clarity. Arrows indicate respective critical water contents.
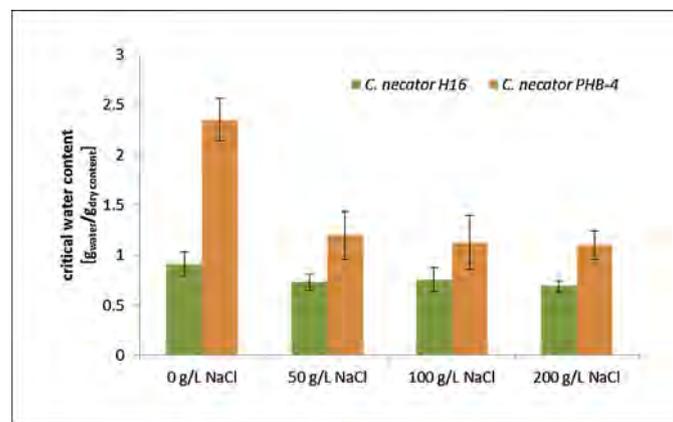
Fig. 8. Critical water content of the PHB-positive culture *C. necator* H16 and its PHB non-producing mutant *C. necator* PHB^{-4} exposed (3 h) to various NaCl concentrations determined by TGA (isothermal drying at 60 °C).

function of residual water content in the sample (see Fig. 7B, D). The drying rate curves of all the bacterial cells included in this study revealed a single critical point, corresponding to two distinguishable water contents in the samples. Because this critical point always represents the moment when the rate of sample drying begins to fall rapidly, a significant change in the drying process evidently occurs at this point. In Fig. 8, the relative water content at this critical point is shown for both tested bacterial cultures exposed to different concentrations of NaCl. It is evident from the comparison of unchallenged bacterial cultures that lower critical water content (i.e. water content at the critical point, given in $g_{water}/g_{dryweight}$) was found for *C. necator* H16 bacterial cultures, in which the dry mass of the cell samples was significantly increased by the presence of PHB granules.

A more interesting finding arises, however, from the comparison of unchallenged and osmotically upshocked cell samples. It was found that the critical water content was significantly decreased for osmotically challenged PHB negative cells. This decrease corresponds to about 50% of the original water content, determined for the unperturbed culture regardless of the concentration of NaCl in the medium. However, for PHB positive cells, the osmotically induced decrease in the critical water content, which can also be found in Fig. 8, was less pronounced at all NaCl concentrations (the average critical water content decreased by about 20% regardless of the concentration of NaCl).

Discussion

Since PHA is one of the most widespread storage materials in bacteria, it can be assumed that the ability to accumulate PHA represents a significant advantage in natural environments. The most obvious advantage is probably the possibility to utilize PHAs when external carbon sources are depleted. Nevertheless, PHAs play a much more complex role in stress survival and the adaptation of bacteria to various environments. There are reports that the capacity for PHA accumulation and degradation enhances the resistance of bacterial cells to stress conditions such as high temperature [37,38], low temperature and freezing [34,39], and oxidative stress [37,40]. However, the mechanisms by which PHA enables stress alleviation are not yet fully understood. It is likely that PHA granules offer physical protection under various stress conditions and it is also possible that their presence influences the overall properties of bacterial cells supporting their survival. Nonetheless, normally functioning PHA anabolic and catabolic pathways are considered to be essential in providing increased stress protection [12].

Although the ability to adapt to fluctuations in external osmolarity is fundamental to the survival of microorganisms and despite the fact that there are reports showing that the accumulation of PHA helps bacterial cells to survive osmotic challenge [13–15,41], we are not aware of any study investigating the possible protective mechanisms of PHA against hypertonic and/or hypotonic environments. To fill this gap, we have studied the possible protective mechanisms offered by the presence of PHB granules during hypertonic conditions by employing the common soil non-halophilic Gram-negative bacterium *Cupriavidus necator*, which is often in use as a model organism for PHB metabolism [21].

According to the results (Fig. 1), the presence of PHB in cell cytoplasm clearly supports the survival of *C. necator* cells exposed to osmotic challenge. Nevertheless, the mechanism of its protective action is unclear. Generally, the accumulation of a wide spectrum of so-called compatible solutes is the major strategy adopted by most bacteria under conditions of hyperosmotic stress. Along with balancing the external osmotic pressure, compatible solutes possess chemical chaperone activity providing protection for biomacromolecules, particularly proteins, against denaturation induced by various stressors [1,42]. It was recently reported that the monomer of PHB, 3HB, serves as a potent chemical chaperone protecting enzymes against various stress factors [43]. Alternatively, the hydrolysis of PHB can be used as a source of carbon and energy for the biosynthesis of other compatible solutes, as reported by Breedveld et al. [14]. Therefore, it was expected that upshocked PHB-containing cells hydrolyse PHB granules with the help of 3HB and/or other compatible solute(s) in order to cope with exposure to hypertonic environments. Nevertheless, no mobilization of PHB granules during the exposure of bacterial culture to hypertonic challenge was observed (Table 1).

Intracellular polymer in *C. necator* is hydrolysed by a battery of PHB depolymerases which are specific to the amorphous state of PHB [26]. Using Raman spectroscopy (Fig. 2), it was observed that the exposure of bacterial cells to hypertonic conditions initiated partial crystallization of the polymer, which, as a consequence, probably inhibited the mobilization of PHB granules by specific enzymes. According to Barnard and Sanders, a small amount of water is an integral component of PHB granules, acting as a plasticizer of the polymer [44]. Therefore, it seems likely that the partial dehydration of PHB granules during hypertonic challenge results in partial crystallization of the polymer and the inhibition of its hydrolysis. The results demonstrated that PHB hydrolysis yielding compatible solutes is not the mechanism by which PHB increases the survival of osmotically upshocked cells of *C. necator*.

The fact that the enhancement of stress tolerance in PHA producers can be achieved without mobilization of the previously accumulated granules was also reported by Goh et al., who observed that *E. coli* cells harboring PHA biosynthetic genes, but which were incapable of PHA mobilization, exhibited higher resistance to oxidative stress [40].

The results of viability analysis by means of flow cytometry using propidium iodide (Fig. 1B), TEM microphotographs (Figs. 4 and 5), and the results of the time-resolved fluorescence microscopy analysis (Fig. 6) indicated that the presence of PHB in bacterial cell cytoplasm stabilized cytoplasmic membranes against damage by hypertonic environments and the leakage of cytoplasm content. Generally, osmotic upshock leads to the dehydration and plasmolysis of bacterial cells. Due to the fact that the cell membrane is not able to shrink by more than 2–5%, intensive plasmolysis might be harmful, leading to cell membrane damage and even collapse [5]. The results of TEM analysis show that plasmolysis in PHB negative cells is much more intensive (Fig. 4) than in PHB-containing cells (Fig. 5). In addition, TEM demonstrated that while in PHB non-accumulating bacterial cells exposure to hypertonic environments resulted in the formation of "hole-like" structures and the leakage of cytoplasmic content into the periplasmatic space, no such fatal consequences were observed in PHB-containing cells. It seems that intracellular PHB granules serve as a scaffold protecting bacterial cells from adverse massive and unsymmetrical plasmolysis.

In addition, Bonthrone et al. reported that native intracellular PHB granules are formed by highly mobile amorphous elastomer, which is reminiscent of a supercooled liquid in terms of its properties [45]. When bacterial cells were exposed to hypertonic conditions, PHB granules revealed surprising liquid-like properties accompanying their efflux into the periplasmatic space when plasmolysis occurred in their close vicinity (see Fig. 5, red arrows number 2). Cryo-SEM observation also revealed PHB granules to have unusual plastic-like properties in challenged bacterial cells, as demonstrated by string-like structures in cells ripped during sample sublimation (Fig. 3). It should be pointed out that these deformations were formed at extremely low temperatures (-95 °C), demonstrating intracellular PHB granules to have very flexible liquid-like properties even at temperatures at which all the other components of bacterial cells are unambiguously crystalline and brittle. Taking into account their extraordinary liquid properties, it seems likely that PHB granules can partially repair and stabilize cell membranes by plugging small gaps in their structure which are formed during plasmolysis (see, for instance, Figs. 5F, I and L demonstrating a possible mechanism for this protective action).

Furthermore, when bacterial cells were exposed to higher NaCl concentrations (100 and 200 g/L), TEM microphotographs (Fig. 5, red arrow number 3) demonstrated another interesting phenomenon – the aggregation of PHB granules leading to the formation of one or several non-spherical granules per cell. Such behavior can explain the creation of the "string-like" structures observed by cryo-SEM (Fig. 3). As bacterial cells were exposed to increasing concentrations of NaCl, the PHB granules aggregated, and wider and more numerous string-like structures were formed when the cells were torn open during sample preparation for cryo-SEM analysis.

PHB granules, also designated "carbosomes" [46], are supra-molecular structures consisting of a hydrophobic PHB polymer core and a proteinaceous surface layer preventing polymer granules from aggregating and coming into direct contact with the aqueous environment of the cell's cytosol [47]. The aggregation of PHB granules in upshocked cells was, therefore, probably induced by the dehydration-mediated partial injury of the protein layer, which allowed hydrophobic polymer to aggregate into larger particles. Regardless of the mechanism of granule aggregation, it is likely that this process damages the cell's ability to divide, since in numerous cases granular aggregates were situated in the central parts of cells (see Fig. 5), where cell division is usually initiated and takes place [48]. This could explain the differences between the viabilities of the PHB-containing cultures determined by plating or by flow cytometry (Fig. 1A,B). Generally, plating underestimates the number of viable cells in cultures when the fraction of the original culture loses the capacity to grow [32]. Therefore, a considerable fraction of PHB-containing bacterial culture might retain non-damaged membranes and functional metabolism even when exposed to very high concentrations of NaCl but is not capable of division and growth.

Nonetheless, the numbers of viable cells determined by plating and flow cytometry in the PHB non-accumulating mutant strain of *C. necator* are also disproportionate (although to a much lesser degree). Therefore, membrane damage is obviously not the only mechanism reducing the cultivability of bacterial cells exposed to a hypertonic environment. Another harmful consequence of osmotic upshock is cell dehydration, which can cause denaturation of proteins and other macromolecules, leading to irreversible loss of their biological activity. Therefore, it was also investigated how the presence of PHB granules in bacterial cells influences the critical water content (the water content at the moment of a sudden change in the drying mechanism) in bacterial cells exposed to hyperosmotic conditions (Fig. 7). In agreement with previous reports [34], it was observed that the critical water content is considerably lower in PHB-containing bacterial strains of *C. necator* than in PHB non-containing cells prior to their exposure to osmotic challenge (Fig. 7A). Nevertheless, when cells were exposed to hyperosmotic conditions, the PHB-non containing culture underwent more pronounced elimination of this more strongly-bound water than the PHB-containing strain (Fig. 7B).

In general, it is difficult to interpret the exact origin of the critical water content without further empirical justification, because the bacteria studied represent a complex combination of diverse aqueous structures. This is especially true for osmotically challenged plasmolysed cultures with a growing periplasmatic volume. The simplified interpretation by Uribelarrea et al. [25] and others that the critical water content equals the total content of water in the cell seems inappropriate in the case of plasmolysed cell samples, because such a massive decrease in total intracellular (i.e. cytoplasmic plus periplasmatic) water would inevitably be accompanied by a significant decrease in the total cell volume. In fact, no such decrease in the volume delimited by the outer membrane of the cell was found in the TEM microphotographs of the PHB negative cells.

On the other hand, the value of the observed decrease in the critical water content for both PHB positive and negative cells is in striking accord with the relative volume of the periplasmatic space, estimated from the image analysis of TEM microphotographs. This indicates that the critical volume content could be closely linked to the water content in the cell cytoplasm. In fact, the quantity of cytoplasmic water, calculated from the TGA experiment, may be underestimated for PHB negative cells as a result of leakage from the damaged cytoplasmic membrane, indicated by the results of electron and fluorescence microscopy analyses. Nevertheless, it seems that the presence of PHB granules protects cells against the intensive loss of water from the cytoplasm. Our results are in agreement with those of Kadouri et al., who observed that the mutant strain of *Azospirillum brasilense* incapable of intracellular PHB hydrolysis is more resistant to desiccation than its parental strain, suggesting that the presence of intracellular polyester itself may be needed to protect the cell against the harmful effects of desiccation and dehydration [41].

Conclusions

Using *Cupriavidus necator* H16 and its PHB non-accumulating mutant strain it was demonstrated that presence of PHB granules in cytoplasm of bacterial cells substantially improves stress resistance of the bacterial culture against osmotic up-shock. Surprisingly, bacterial cells did not utilize PHB to harvest carbon or energy in order to cope with osmotic stress, which can be attributed to partial crystallization of PHB granules in challenged cells. The results show that the effect of PHB is rather indirect since the presence of PHB granules influences overall properties of the bacterial cells reducing membrane damage caused by plasmolysis and, moreover, it seems that PHB granules themselves are able to partially repair and stabilize membranes of challenged cells. Nevertheless, PHB granules in bacterial cells exposed to osmotic upshock aggregate, which probably complicates further division and reproduction of the bacterial cells.

Since *C. necator* PHB-4 is a chemically induced mutant, it would be useful to include a complementation control (reintroduction of a wild type PHB synthase gene copy into PHB^{-4}) or to perform the study with a chromosomal PHB synthase and/or PHB depolymerase gene deletion mutant of the wild type. A follow-up study focused on the osmotic down-shock would be welcome in order to complete the overall concept of the role of PHB granules in the response of bacteria to osmotic stress.

Conflict of interest

The authors declare no conflicts of interest.

Funding

Acknowledgment

Appendix A. Supplementary data

Supplementary data associated with this article can be found, in the online version, at http://dx.doi.org/10.1016/j.nbt.2017.07.008.

References

[1] Morbach S, Kramer R. Body shaping under water stress: osmosensing and osmoregulation of solute transport in bacteria. Chembiochem 2002;3:384–97.
[2] Wood JM. Bacterial responses to osmotic challenges. J Gen Physiol 2015;145:381–8.
[3] Koch AL. The geometry and osmotic relations of plasmolysis spaces in bacteria and the role of endocytosis, tubular structures and Scheie structures in their formation. J Theor Biol 1995;176:471–92.
[4] Korber DR, Choi A, Wolfaardt GM, Caldwell DE. Bacterial plasmolysis as a physical indicator of viability. Appl Environ Microbiol 1996;62:3939–47.
[5] Schwarz H, Koch AL. Phase and electron microscopic observation of osmotically induced wrinkling and the role of endocytotic vesicles in the plasmolysis of the gram-negative bacteria. Microbiology 1995;141:3161–70.
[6] Khosravi-Darani K, Mokhtari ZB, Amai T, Tanaka K. Microbial production of poly(hydroxybutyrate) from C1 carbon sources. Appl Microbiol Biotechnol 2013;97:1407–24.
[7] Tan GYA, Chen CL, Li L, Ge L, Wang L, et al. Start a research on biopolymer polyhydroxyalkanoate (PHA): a review. Polymers 2014;6:706–54.
[8] Chen GQ, Hajnal I. The'PHAome'. Trends Biotechnol 2015;33:559–64.
[9] Johnson K, Jiang Y, Kleerebezem R, Muyzer G, van Loosdrecht MCM. Enrichment of a mixed bacterial culture with a high polyhydroxyalkanoate storage capacity. Biomacromolecules 2009;10:670–6.
[10] Mravec F, Obruca S, Krzyzanek V, Sedlacek P, Hrubanova K, et al. Accumulation of PHA granules in *Cupriavidus necator* as seen by confocal fluorescence microscopy. FEMS Microbiol Lett 2016363: 0.1093/femsle/fnw094.
[11] Vadlja D, Koller M, Novak M, Braunegg G, Horvat P. Footprint area analysis of binary imaged *Cupriavidus necator* cells to study PHB production at balanced, transient, and limited growth conditions in a cascade process. Appl Microbiol Biotechnol 2016;100:10065–80.
[12] Kadouri D, Jurkevitch E, Okon Y. Ecological and agricultural significance of bacterial polyhydroxyalkanoates. Crit Rev Microbiol 2005;31:55–67.
[13] Zhao YH, Li HM, Qin LF, Wang HH, Chen GQ. Disruption of the polyhydroxyalkanoate synthase gene in *Aeromonas hydrophila* reduces its survival ability under stress conditions. FEMS Microbiol Lett 2007;276:34–41.
[14] Breedveld MW, Dijkema C, Zevenhuizen LPTM, Zehner AJB. Response of intracellular carbohydrates to NaCl shock in *Rhizobium leguminosarum* biovar triforii TA-1 and *Rhizobium meliloti* SU-47. J Gen Microbiol 1993;139:3157–63.
[15] Wang Q, Yu H, Xia Y, Kang Z, Qi Q. Complete PHB mobilization in *Escherichia coli* enhances the stress tolerance: a potential biotechnological application. Microb Cell Fact 20098(47), doi:http://dx.doi.org/10.1186/1475-2859-8-47.
[16] Obruca S, Marova I, Svoboda Z, Mikulikova R. Use of controlled exogenous stress for improvement of poly(3-hydroxybutyrate) production in *Cupriavidus necator*. Folia Microbiol 2010;55:17–22.
[17] Passanha P, Kedia G, Dinsdale RM, Guwy AJ, Esteves SR. The use of NaCl addition for the improvement of polyhydroxyalkanoate production by *Cupriavidus necator*. Bioresource Technol 2014;163:287–94.
[18] Hermann-Krauss C, Koller M, Muhr A, Fasl H, Stelzer F, Braunegg G. Archaeal production of polyhydroxyalkanoate (PHA) co- and terpolyesters from biodiesel industry-derived by-products. Archaea 2013 art. no. 129268.
[19] Yin J, Chen JC, Wu Q, Chen GQ. Halophiles, coming stars for industrial biotechnology. Biotechnol Adv 2015;33:1433–42.
[20] Rodríguez-Contreras A, Koller M, Braunegg G, Marqués-Calvo MS. Poly [(R)-3-hydroxybutyrate] production under different salinity conditions by a novel *Bacillus megaterium* strain. New Biotechnol 2016;33:73–7.
[21] Reinecke F, Steinbuchel A. *Ralstonia eutropha* Strain H16 as model organism for PHA metabolism and for biotechnological production of technically interesting biopolymers. J Mol Microbiol Biotechnol 2009;16:91–108.
[22] Raberg M, Voigt B, Hecker M, Steinbuchel A. A closer look on the polyhydroxybutyrate- (PHB-) negative phenotype of *Ralstonia eutropha* PHB-4. PLoS One 2014;9:e95907, doi:http://dx.doi.org/10.1371/journal.pone.0095907.
[23] Coder DM. Assessment of cell viability. Curr Protocols Cytometry 1997 9.2. 1-9.2.14.
[24] Obruca S, Benesova P, Oborna J, Marova I. Application of protease-hydrolyzed whey as a complex nitrogen source to increase poly(3-hydroxybutyrate) production from oils by *Cupriavidus necator*. Biotech Lett 2014;36:775–81.
[25] Uribelarrea JL, Pacaud S, Goma G. New method for measuring the cell water-content by thermogravimetry. Biotechnol Lett 1985;7:75–80.
[26] Jendrossek D. Peculiarities of PHA granules preparation and PHA depolymerase activity determination. Appl Microbiol Biotechnol 2007;74:1186–96.
[27] Furukawa T, Sato H, Murakami R, Zhang J, Noda I, Ochiain S, et al. Raman microspectroscopy study of structure, dispersibility, and crystallinity of poly (hydroxybutyrate)/poly(L-lactic acid) blends. Polymer 2006;47:3132–40.
[28] Izumi CMS, Temperini MLA. FT-Raman investigation of biodegradable polymers: poly(3-hydroxybutyrate) and poly(3-hydroxybutyrate-co-3-hydroxyvalerate). Vibr Spectrosc 2010;54:127–32.
[29] Samek O, Obruča S, Šiler M, Sedláček P, Benešová P, et al. Quantitative Raman spectroscopy analysis of polyhydroxyalkanoates produced by *Cupriavidus necator* H16. Sensors 201616:, doi:http://dx.doi.org/10.3390/s16111808.
[30] Dunlop WF, Robards AW. Ultrastructural study of poly-β-hydroxybutyrate granules from *Bacillus cereus*. J Bacteriol 1973;114:1271–80.
[31] Sudesh K, Fukui T, Iwata T, Doi Y. Factors affecting the freeze-fracture morphology of in vivo polyhydroxyalkanoate granules. Can J Microbiol 2000;45:304–11.
[32] Dvorak P, Chrast L, Nikel PI, Fedr R, Soucek K, et al. Exacerbation of substrate toxicity by IPTG in *Escherichia coli* BL21(DE3) carrying a synthetic metabolic pathway. Microb Cell Fact 201514(201), doi:http://dx.doi.org/10.1186/s12934-015-0393-3.
[33] Swaminathan R, Hoang CP, Verkman AS. Photobleaching recovery and anisotropy decay of green fluorescent protein GFP-S65T in solution and cells: cytoplasmic viscosity probed by green fluorescent protein translational and rotational diffusion. Biophys J 1997;72:1900–7.
[34] Obruca S, Sedlacek P, Krzyzanek V, Mravec F, Hrubanova K, et al. Accumulation of poly(3-hydroxybutyrate) helps bacterial cells to survive freezing. PLoS One 2016;11:e0157778, doi:http://dx.doi.org/10.1371/journal.pone.0157778.
[35] Alcazar EB, Rocha-Leao MHM, Dweck J. Yeast intracellular water determination by thermogravimetry. J Therm Anal Calorim 2000;59:643–8.
[36] Ilmer P, Erlebach C, Schinner F. A practicable and accurate method to differentiate between intra- and extracellular water of microbial cells. FEMS Microbiol Lett 1999;178:135–9.
[37] Wu D, He J, Gong Y, Chen D, Zhu X, et al. Proteomic analysis reveals the strategies of *Bacillus thuringiensis* YBT-1520 for survival under long-term heat stress. Proteomics 2011;11:2580–91.
[38] Iustman LJR, Tribelli PM, Ibarra JG, Catone MV, Venero ECS, Lopez NI. Genome sequence analysis of *Pseudomonas extremaustralis* provides new insights into environmental adaptability and extreme conditions resistance. Extremophiles 2015;19:207–20.

[39] Pavez P, Castillo JL, Gonzales C, Martinez M. Poly-β-hydroxyalkanoate exert protective effect against carbon starvation and frozen conditions in *Sphingopyxis chilensis*. Curr Microbiol 2009;59:636–40.

[40] Goh L-K, Purama RK, Sudesh K. Enhancement of stress tolerance in polyhydroxyalkanoate producers without mobilization of the accumulated granules. Appl Biochem Biotechnol 2014;172:1585–98.

[41] Kadouri D, Jurkevitch E, Okon Y. Poly-β-hydroxybutyrate depolymerase (PhaZ) in *Azospirillum brasilense* and characterization of a *phaZ* mutant. Arch Microbiol 2005;180:309–18.

[42] Roberts MF. Organic compatible solutes of halotolerant and halophilic microorganisms. Saline Systems 20051(5), doi:http://dx.doi.org/10.1186/1746-1448-1-5.

[43] Obruca S, Sedlacek P, Mravec F, Samek O, Marova I. Evaluation of 3-hydroxybutyrate as an enzyme-protective agent against heating and oxidative damage and its potential role in stress response of poly(3-hydroxybutyrate) accumulating cells. Appl Microbiol Biotechnol 2016;100:1365–76.

[44] Barnard GN, Sanders JKM. The poly-β-hydroxybutyrate granule in vivo: a new insight based on NMR spectroscopy of whole cells. J Biol Chem 1989;264:3286–91.

[45] Bonthrone KM, Clauss J, Horowitz DM, Hunter BK, Sanders JKM. The biological and physical chemistry of polyhydroxyalkanoates as seen by NMR spectroscopy. FEMS Microbiol Lett 1992;103:269–77.

[46] Jendrossek D, Pfeiffer D. New insights in the formation of polyhydroxyalkanoate granules (carbonosomes) and novel functions of poly (3-hydroxybutyrate). Environ Microbiol 2014;16:2357–73.

[47] Bresan S, Sznajder A, Hauf W, Forchhammer K, Pfeiffer D, Jendossek D. Polyhydroxyalkanoate (PHA) granules have no phospholipids. Sci Rep 2016;6:26612, doi:http://dx.doi.org/10.1038/srep26612.

[48] Harry E, Monahan L, Thompson L. Bacterial cell division: the mechanism and its precison. Int Rev Cytol 2006;253:27–94.

Appendix 15

Slaninova, E., Sedlacek, P., Mravec, F., Mullerova, L., Samek, O., Koller, M., Hesko, O., Kucera, D., Marova, I., and Obruca, S. Light scattering on PHA granules protects bacterial cells against the harmful effects of UV radiation. *Applied Microbiology and Biotechnology* **2018**, 102, 1923–1931.

CrossMark

Light scattering on PHA granules protects bacterial cells against the harmful effects of UV radiation

Eva Slaninova[1] · Petr Sedlacek[1] · Filip Mravec[1] · Lucie Mullerova[1] · Ota Samek[2] · Martin Koller[3,4] · Ondrej Hesko[1] · Dan Kucera[1] · Ivana Marova[1] · Stanislav Obruca[1]

Abstract
Numerous prokaryotes accumulate polyhydroxyalkanoates (PHA) in the form of intracellular granules. The primary function of PHA is the storage of carbon and energy. Nevertheless, there are numerous reports that the presence of PHA granules in microbial cells enhances their stress resistance and fitness when exposed to various stress factors. In this work, we studied the protective mechanism of PHA granules against UV irradiation employing *Cupriavidus necator* as a model bacterial strain. The PHA-accumulating wild type strain showed substantially higher UV radiation resistance than the PHA non-accumulating mutant. Furthermore, the differences in UV-Vis radiation interactions with both cell types were studied using various spectroscopic approaches (turbidimetry, absorption spectroscopy, and nephelometry). Our results clearly demonstrate that intracellular PHA granules efficiently scatter UV radiation, which provides a substantial UV-protective effect for bacterial cells and, moreover, decreases the intracellular level of reactive oxygen species in UV-challenged cells. The protective properties of the PHA granules are enhanced by the fact that granules specifically bind to DNA, which in turn provides shield-like protection of DNA as the most UV-sensitive molecule. To conclude, the UV-protective action of PHA granules adds considerable value to their primary storage function, which can be beneficial in numerous environments.

Keywords Polyhydroxyalkanoates · *Cupriavidus necator* · UV radiation · Turbidity · Integrating sphere · Nephelometry

Introduction

Bacteria are fascinating organisms due to their capability to cope with widely fluctuating environmental conditions such as changes in nutrient availability, temperature, pH value, or osmolarity. In addition, also radiation, which can be defined as energy manifested in the form of electromagnetic waves, can be considered an important stress factor and occurs in numerous ecological niches. UV radiation in sunlight is among the most common stressors and has many harmful impacts on living cells such as induction of oxidative pressure or the inducing of fatal changes to the molecular structure mainly of DNA, but also of RNA, lipids, and proteins (Gabani and Singh 2013). Generally, UV radiation is considered to be one of the most detrimental abiotic factors influencing microorganisms at both the community and single-cell level, thus severely affecting the diversity and dynamics of microbial communities. Moreover, it is expected that by the end of the twenty-first century, the intensity of UV radiation at the Earth's surface will increase by approximately 5–10% in temperate latitudes and by about 20% in high latitudes (Pérez et al. 2017). It can therefore be expected that the evolutionary significance of UV radiation and ability to face this stressor may even increase.

To cope with UV radiation, bacteria—and among them especially extremophiles inhabiting harsh environments exposed to harmful solar radiation—have evolved various strategies mainly based on efficient DNA repair mechanisms and active defense against UV-induced oxidative stress. Moreover,

✉ Stanislav Obruca
  Stana.O@seznam.cz

1 Faculty of Chemistry, Brno University of Technology, Purkynova 118, 612 00 Brno, Czech Republic

2 Institute of Scientific Instruments, Academy of Sciences of The Czech Republic, Vvi, Kralovopolska 147, 612 64 Brno, Czech Republic

3 Institute of Chemistry, NAWI Graz, University of Graz, Heinrichstrasse 28/III, 8010 Graz, Austria

4 ARENA Arbeitsgemeinschaft für Ressourcenschonende und Nachhaltige Technologien, Inffeldgasse 21b, 8010 Graz, Austria

many pro- and eukaryotic microorganisms also rely on production of UV-protective metabolites such as pigments, mycosporine-like amino acids, scytonemin, ectoines, bacterioruberin, sphaerophorin, pannarin, or melanin (Koller et al. 2014; Singh and Gabani 2011).

Polyhydroxyalkanoates (PHAs) are polyesters accumulated by numerous prokaryotes in the form of intracellular granules (Tan et al. 2014). The number of granules can reach up to 10–15 granules per cell and their average diameter is about 200–400 nm, though individual values particularly depend upon the specific microorganism and the physiological state of the bacterial culture (Vadlja et al. 2016). The weight content of PHA in bacterial cells can reach up to 90% of cell dry weight, though bacteria regulate their diameters to confine the volumetric content of PHA granules at a level below 40 vol% (Mravec et al. 2016). The PHA polymer itself represents the hydrophobic core of the granules which is covered by numerous specific proteins with various functions. These proteins include PHA synthase, PHA depolymerases, regulatory proteins, and various PHA granule structural proteins which create a functional interface between the hydrophobic polymer and water-containing cytoplasm. These proteins are also responsible for intracellular localization of granules within bacterial cells. To emphasize their complexity and multifunctionality as de facto organelles, these granules are also referred to as "carbonosomes" (Jendrossek 2009).

The primary function of PHAs is the storage of carbon and energy. However, recent research has shown that the biological function of PHAs is much more complex and that the capability to accumulate PHA has many biochemical and biophysical consequences, enhancing the survival and fitness of bacterial cells when exposed to numerous stress factors including but not limited to high temperature (Pham 2004; Wu et al. 2011), low temperature (Tribelli and Lopez 2011), freezing (Obruca et al. 2016a; Pavez et al. 2009), or osmotic upshock (Obruca et al. 2017).

Moreover, there are reports stating that the presence of PHA granules in microbial cells also protects bacteria against UV radiation. For instance, a protective effect of PHA granules in bacterial cells against UV irradiation was observed in *Azospirillum brasilense* when PHA-rich (about 40 wt.% of PHA in cell dry weight) and PHA-poor cells (about 5 wt.% of PHA in cell dry weight) were compared (Tal and Okon 1985). The importance of PHA for the UV-radiation survival of *A. brasilence* was confirmed in following studies by Kadouri et al., who observed that the wild type was more resistant to numerous stressors, including UV radiation, than the PHA synthase deletion mutant incapable of accumulating PHA (Kadouri et al. 2003a). It was also more resistant than the PHA depolymerase deletion mutant, which was not capable of PHA hydrolysis (Kadouri et al. 2003b). Similarly, Zhao

et al. (2007) compared the stress resistance of the wild type of *Aeromonas hydrophila* and its PHA synthase negative mutant incapable of PHA synthesis. As the major outcome, the wild type was substantially more resistant to several stress factors, including UV irradiation. Furthermore, the UV-radiation protective capacity of PHA granules was also confirmed with genetically modified *Escherichia coli* which harbored genes enabling either PHA biosynthesis or both PHA biosynthesis and hydrolysis. Both transgenic strains were more resistant to UV radiation and other stress factors than the PHA non-producing wild type (Wang et al. 2009).

Nevertheless, despite the fact that numerous studies have reported that the presence of PHA granules in microbial cells provides protection against UV radiation; to our best knowledge, there are no studies exploring the potential mechanism of the protective action. Therefore, we experimentally confirmed the UV-protecting effect of PHA granules for *Cupriavidus necator*, a soil bacterium which is considered the most important model strain for PHA metabolism. Subsequently, various spectroscopic approaches were employed to shed light on the interaction of PHA granules in bacterial cells with UV radiation and to provide an explanation for their UV-protective mechanism.

Materials and methods

Microorganisms and cultivation

The PHA-producing strain *Cupriavidus necator* H16 (CCM 3726) was obtained from the Czech Collection of Microorganisms, Brno, Czech Republic, and its PHA non-producing mutant strain *Cupriavidus necator* PHB^{-4} (DSM-541) was purchased from the Leibnitz Institute DSMZ-German Collection of Microorganism and Cell Cultures, Braunschweig, Germany.

Cultivations were performed in Erlenmeyer flasks (volume 250 mL) containing 100 mL of mineral salt (MS) medium. The composition of the MS medium was 20 g fructose, 1 g $(NH_4)_2SO_4$, 1 g KH_2PO_4, 11.1 g $Na_2HPO_4 \cdot 12 H_2O$, 0.2 g $MgSO_4 \cdot 7 H_2O$, 1 mL of microelement solution, and 1 L of distilled water; the microelement solution in turn was composed of 9.7 g $FeCl_3$, 7.8 g $CaCl_2$, 0.156 g $CuSO_4 \cdot 5 H_2O$, 0.119 g $CoCl_2$, and 0.118 g $NiCl_2$ in 1 L of 0.1 M HCl. The flasks were inoculated with 5 mL of an overnight culture of a particular strain of *C. necator* grown in Nutrient Broth medium consisting of 10 g peptone, 10 g beef extract, and 5 g NaCl in 1 L of distilled water. The cells were cultivated for 72 h. The PHA content in microbial cells was determined by gas chromatography as described previously (Obruca et al. 2014).

UV challenge of bacterial strains C. necator H16 and C. necator PHB^{-4}

The suspension of bacterial cells cultivated for 72 h as described above was first diluted 30 times. Thereafter, the suspension of bacterial cells of *Cupriavidus necator* H16 was diluted to reach the cell density of the suspension of its mutant strain *Cupriavidus necator* PHB^{-4}. The solutions thus prepared were further diluted into approx. 10^8 CFU and 3 mL of the cell suspension was placed on a sterile Petri dish to form a thin layer (approx. 1 mm). After this, cells were exposed to UV radiation emitted by an UVA lamp (400–320 nm, height 25 cm) and samples were taken at regular intervals (15, 30, 45 min). From these samples, the number of viable cells was determined as CFU by plating of appropriately diluted cell suspensions on NB agars.

UV-Vis spectroscopy and nephelometry of bacterial cells

For UV-Vis spectroscopy characterization, the same cultivation suspension as described above was used. Firstly, both the suspension of bacterial cells of *C. necator* H16 and the suspension of its mutant bacterial strain were diluted step by step five times. The dilution process was repeated until the final solutions were diluted by a factor of 100. All solutions prepared this way were analyzed by UV-Vis absorption spectrophotometry (in a U-3900H, Hitachi) both in a regular transmission measurement mode and also in a spatially integrating mode (integration sphere attachment 60mmDIA for Hitachi U-3900H spectrophotometer). Simultaneously with the preparation of samples for UV-Vis spectroscopy, the number of viable cells was determined as described above.

Similarly, diluted bacterial suspensions of defined cell concentration were also investigated by means of nephelometry. As a simple nephelometer, we used a fluorometer (AMINCO-Bowman Series 2 luminescence spectrometer, Thermo Inc.) which was employed to detect scattered light at a fixed scattering angle of 90° to the incidental beam. Furthermore, this device offers the advantageous possibility of using different wavelengths ranging from 250 nm (ozone-free xenon lamps lowest wavelength) to approximately 850 nm (highest range of PMT detectors). To suppress detection of fluorescence or phosphorescence, which is common for biological samples at different excitation wavelengths (~ 340 nm for NADH, ~ 470 nm for flavonoids, etc.) a synchronous scan method was applied, where excitation and emission monochromators were set to the zero wavelength difference during scanning. In order to obtain more accurate results and also to protect the detector, slits were set to the minimum (1 nm bandpass). To compensate for the non-flat intensity profile of the excitation source (a 150-W xenon lamp), intensity was detected relative to the diode. The scan rate was set to 5 nm·s^{-1} and spectra were collected with a 1-nm resolution in the range 250–700 nm.

Analysis of intracellular ROS by flow cytometry

Determination of the intracellular level of reactive oxygen species (ROS) in bacterial cells of *C. necator* H16 and *C. necator* PHB^{-4} before and after 15 min exposition to UV irradiation (in details described above) was performed by flow cytometry employing CM-H2CFDA (Thermo Fisher Scientific), a fluorescent stain used as general oxidative stress indicator. Suspensions of cells with cell density of approx. 10^6 cells per mL were washed twice with PBS buffer; after that, 5 μL of CM-H2CFDA dissolved in HPLC-grade DMSO (the final concentration of the stain in 1 mL of the sample was 5 μM) was added to the suspensions, and the cells were then left to incubate in the dark at laboratory temperature for 10 min. After that, the fluorescence of stained as well as non-stained cells was immediately measured at single-cell level using the green fluorescence collecting channel (535 ± 35 nm) of the used flow cytometer (Apogee A50, ApogeeFlow Systems).

Results

UV exposure of C. necator cells

In the first experiment, cells of the PHA-accumulating strain *C. necator* H16 (the PHA content in microbial cells was 74% of cell dry weight as determined by gas chromatography) and its mutant strain which is not capable of accumulating PHA due to a mutation of the PHA synthase (Raberg et al. 2014) were exposed to a UV challenge. The viability of both bacterial strains was assessed during their exposition to UV irradiation in regular intervals; the results, expressed as the percentage of viable cells, are shown in Fig. 1. Generally, the PHA-containing culture demonstrated substantially higher resistance to UV radiation during the entire period of UV exposure, thus confirming the UV-protective effect of PHA granules which has been reported also for other microbial strains (Kadouri et al. 2003a, b; Tal and Okon 1985; Wang et al. 2009; Zhao et al. 2007). The decrease in viability of reference samples of both cultures, which were exposed to the same conditions but without being UV irradiated, was negligible (< 5%). Therefore, it can be stated that accumulation of PHA granules in cytoplasm represents a potent and generally observed strategy which protects bacterial cells from the harmful effects of UV irradiation.
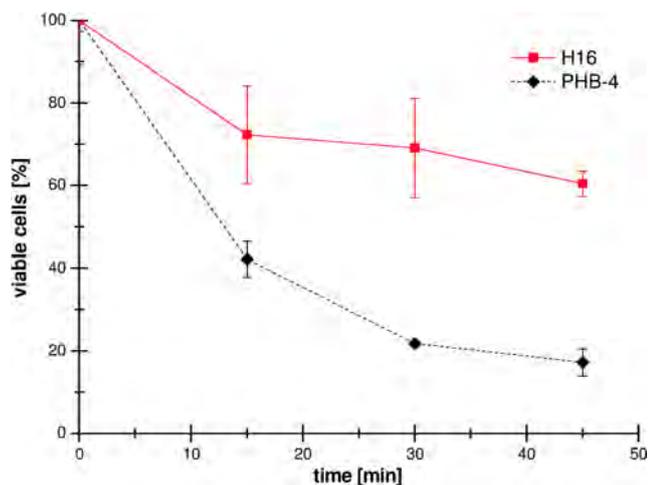
Fig. 1 Survival of both strains of *C. necator* during their exposition to UV irradiation

UV-Vis spectroscopy of bacterial cells

In order to understand how intracellular PHA granules interact with light, complex spectroscopic characterizations of the cell dispersions in the ultraviolet and the visible region were performed both for the PHA-accumulating strain (*C. necator* H16) and the non-accumulating mutant (*C. necator* PHB^{-4}). Three different optical arrangements were used for this purpose.

Firstly, turbidity measurements were performed using a standard UV-Vis spectrometer, where the intensity of the transmitted light is measured and optical density is calculated for the particular wavelength of the incident light. As the wavelengths are altered to cover the whole UV-Vis region, spectra such as those shown in Fig. 2a are collected. It is evident that except for the shortest measured wavelengths (close to 200 nm), the PHA-accumulating strain shows a significantly higher optical density of the cell dispersion with comparable cell density compared to the non-accumulating strain. It should be emphasized that the optical density measured this way comprises two individual contributions. On the one hand, the intensity of the transmitted light is decreased via absorption of the specific wavelengths by the photoactive cell components. Absorption of the radiant energy then initiates diverse photophysical (e.g., light emission in the form of fluorescence) or photochemical processes, where the latter ones may often (mainly in the case of light in the UV spectral region) have harmful or even fatal effects on the cell fitness. The other contribution to the optical density is represented by the light scattered away from the direction of the incident beam. Unlike the light absorption, light scattering is rarely damaging. On the contrary, it can even have a protective "shielding" effect on the photo-labile cell components caused by attenuation of the local intensity of the incident light in the cell, which might reduce the level of cell damage (Paunescu
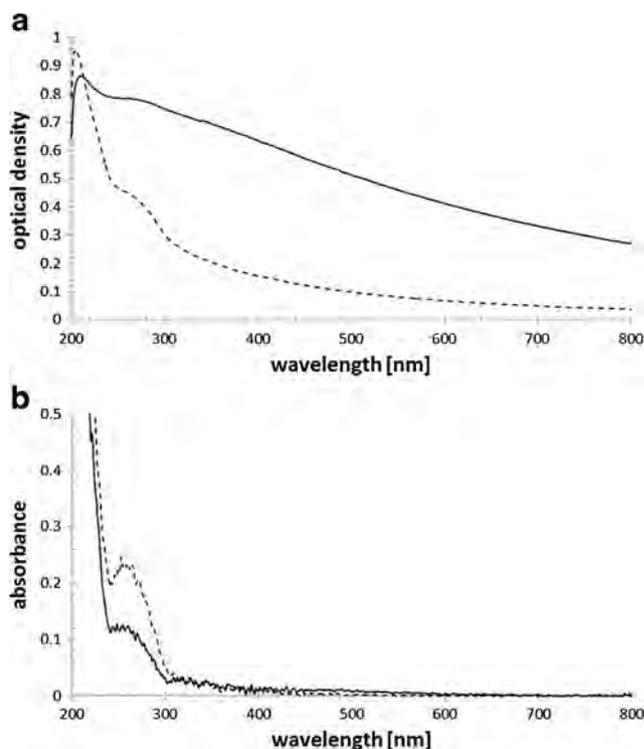
Fig. 2 Example of typical UV-Vis spectra of *C. necator* H16 (full line) and *C. necator* PHB^{-4} (dashed line). **a** Turbidity measurement of dispersions with cell density 1×10^6 CFU. **b** Absorbance measurement of dispersions with cell density 1×10^6 CFU

et al. 2014). Therefore, turbidity measurements such as those described above do not provide a relevant explanation of a harmful effect of light on the cells with light because they provide no direct information about the relative involvement of the light absorption and light scattering, respectively, in the interaction of the cells and their constituent with light.

With respect to this, we further measured the spectra of cell dispersions using the same UV-Vis spectrometer equipped with an integrating sphere accessory, specially designed for the absorbance measurement of turbid samples. Examples of the collected spectra are shown in Fig. 2b. In these spectra, effective suppression of the light-scattering artifacts can be clearly seen. No significant light absorption was found in the Vis region, which confirms the assumption that in this wavelength region, the optical density of the sample can be interpreted solely as a consequence of light scattering. With respect to this finding, additional interesting outcomes can further be deduced from the previously described differences in the turbidity spectra of dispersions of PHA-accumulating and non-accumulating strains with the same cell density. Generally, a significant increase in light scattering in the case of the PHA-accumulating cells of the *C. necator* H16 strain is evidently caused by light scattering on the cell ultrastructure, namely on the PHA granules present in the cell cytoplasm.

Figure 3 presents results from both types of spectroscopic assays in a more quantitative way. Fig. 3a shows very good

Fig. 3 Summarized results from UV-Vis turbidimetry and absorbance assays of cell suspensions of PHA-accumulating *C. necator* H16 strain (×) and PHA non-accumulating *C. necator* PHB^{-4} strain (+), respectively. **a**, **b** Dependency of optical density at 630 and 254 nm on cell density. **c**, **d** Dependency of absorbance at 630 and 254 nm on cell density
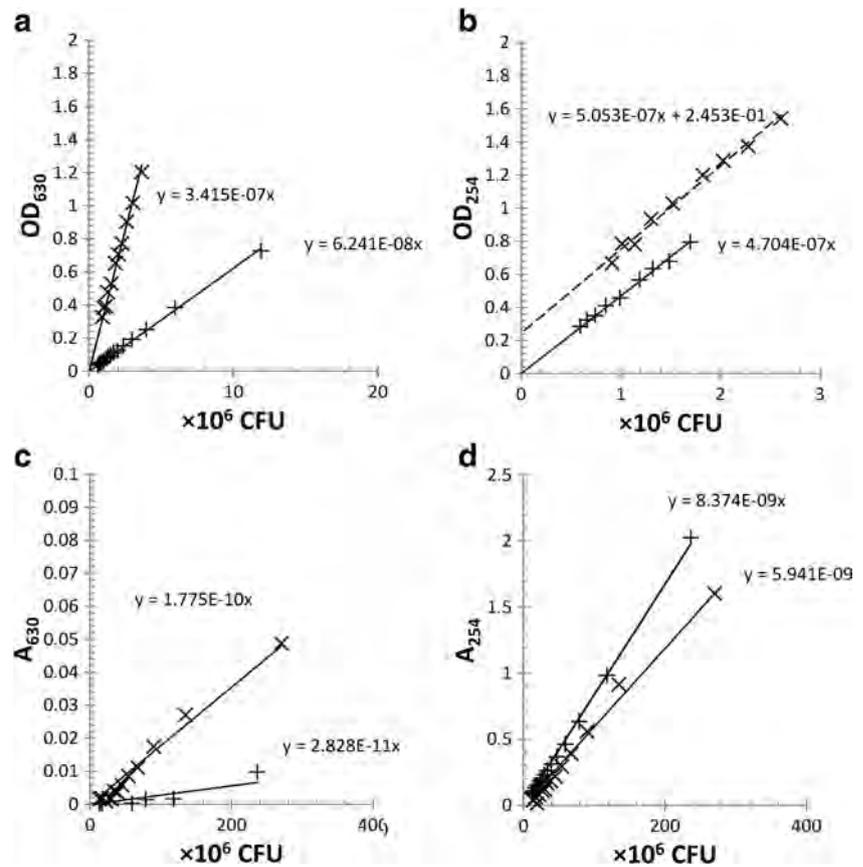
linearity of the dependency of optical density at 630 nm on the cell density for both strains. Evidently, light-scattering effects are cumulative regardless of a contribution of the light scattered by PHA granules. OD_{630} appears to represent a robust parameter suitable for quantification of cell density. Nevertheless, careful calibration is needed wherever intracellular light scatters occur, as is the case when PHA granules or other cell inclusions occur. However, it is evident from Fig. 3b that in the case of *C. necator* H16 strain, contributions of light scattering and light absorption in UV wavelength region are no longer cumulative (the dashed fitting line does not cross the origin of coordinates). Nevertheless, in this region, the crucial results are shown in Fig. 3d where a relative decrease of around 30% in the single cell absorption coefficient at 254 nm can be deduced. Finally, Fig. 3c is shown in order to illustrate the negligible residual apparent absorbance of the cell suspensions in the VIS region. This apparent absorbance represents an experimental artifact coming from the scattered light which does not reach the aperture of the integrating sphere.

In order to provide an experimental verification of the assumption that the difference between the optical density and absorbance of the cell suspensions is correctly assigned to the intensity of scattered light, we performed also a basic nephelometry assay of the same samples. Measurement was done with the synchronous scan method as was described above. We focused on monitoring the changes in scattered light intensity between the PHA-accumulating and non-accumulating strain suspension of the same cell density, where a high sensitivity of the fluorimeter photomultiplier and its strong light source provide an undisputed instrumental advantage. Figure 4 shows the ratio of the intensities of scattered light normalized per unit CFU for *C. necator* H16 and *C. necator* PHB^{-4}, respectively, vs. the wavelength. We use this means of data demonstration in order to suppress experimental artifacts coming from uneven light intensity emitted from the xenon lamp of the fluorimeter at different wavelengths (we assume that the results for both strains will be affected equally).

From the spectrum, it is evident that the nephelometry experiments confirmed the higher intensity of scattered light for the PHA-accumulating strain in the whole tested optical region. Furthermore, the relative efficiency of light scattering by the PHA producer as compared to the mutant strain increases significantly in the UV-region, where the light absorbance measurement revealed the most profound differences in intensity in the light absorption of the two strains. This finding was reproducible as far as similar results were found regardless of the particular suspension cell density. Therefore, it can be summarized that nephelometry confirmed the conclusions of the previous two spectroscopic assays.

Fig. 4 Ratio of the intensities of single-cell scattered light for *C. necator* H16 strain and PHA non-accumulating *C. necator* PHB^{-4} strain at 90° as determined by nephelometry
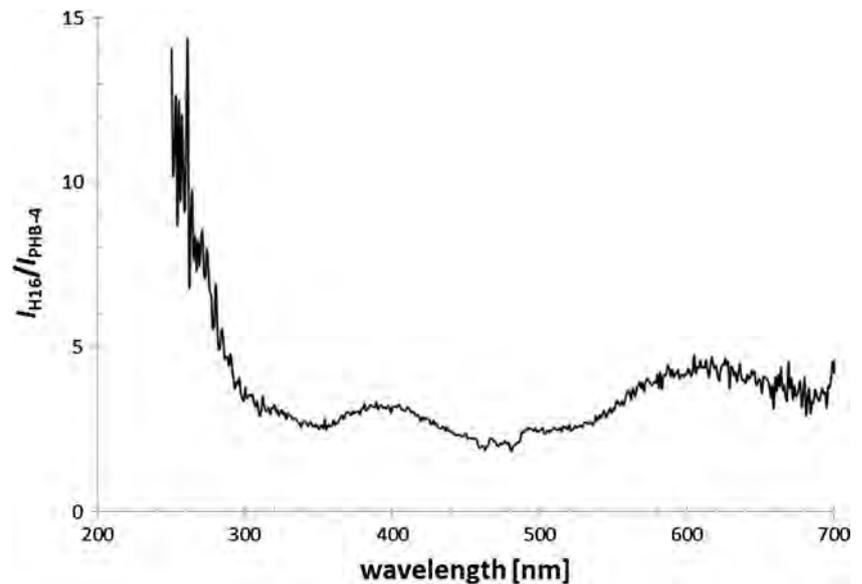
ROS analysis by flow cytometry

To investigate whether scattering of UV irradiation on PHA granules influences the intracellular level of ROS in UV-challenged cells, the amount of ROS before and after UV exposition was analyzed by flow cytometry employing fluorescent stress indicator CM-H2CFDA. Green fluorescence of this stain is activated by its reaction with ROS (Dong et al. 2015). Hence, at single-cell level, we analyzed intensity of green fluorescence of both bacterial cultures prior and after their exposition to UV irradiation in stained as well as non-stained bacterial cells; the results are demonstrated in Fig. 5. The mean value of intensity of green fluorescence of PHA granules containing bacterial was only slightly (approx. 10%) increased after exposition of the cells to UV irradiation. On the contrary, when the culture of cells not containing PHA granules was exposed to UV irradiation, green autofluorescence of

non-stained cells increased about 1.8-fold and, moreover, green fluorescence of CM-H2CFDA stained cells raised 3.6-fold. This clearly indicates that UV irradiation induces formation of substantially higher amount of ROS in PHA negative cells than in PHA-rich cells.

Discussion

Solar UV radiation on Earth can be considered an important stress factor which influences numerous living systems. Therefore, the influence of UV radiation on whole ecosystems has been studied for various aquatic environments (Häder et al. 2007), or high-altitude regions (Farías et al. 2009; Pérez et al. 2017). Moreover, UV-radiation resistance is also an important topic for astrobiology (Khodadad et al. 2017). The harmful effect of UV radiation is complex and it includes

Fig. 5 Mean intensity of green fluorescence of stained and non-stained cells of *C. necator* H16 and *C. necator* PHB^{-4} prior and after UV exposition as determined by flow cytometry
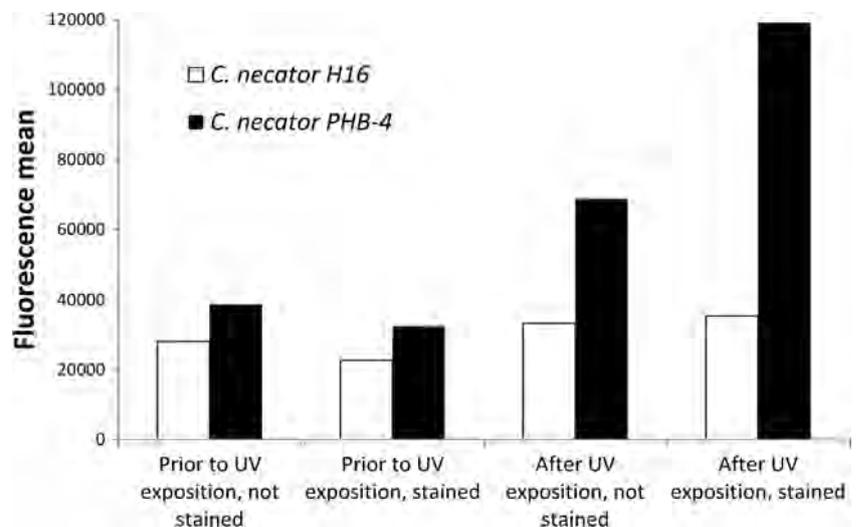
numerous cell-damaging mechanisms. First and foremost, UV radiation is known for its mutagenic potential because DNA directly absorbs UVB radiation and this radiation induces numerous grave changes in DNA structure, among which the formation of dimeric pyrimidines, photo-adducts, and DNA–protein cross-links are considered the most important (Ravanat et al. 2001). Furthermore, despite the fact that DNA does not absorb UVA radiation, UVA can be absorbed by endogenous photosensitizers which may damage DNA throughout subsequent reactions (Ravanat et al. 2001). Apart from DNA, also other photosensitive biomolecules such as RNA, proteins, or lipids can be damaged by direct or indirect absorption of UV radiation, though changes in these molecules' structure do not have such fatal consequences as is the case for DNA due to their quick turnover. In addition, UV radiation induces the formation of reactive oxygen species (ROS) which may further damage crucial cell components such as DNA, RNA, proteins, and lipids (Kim et al. 2015).

There are numerous reports that the capability to accumulate PHA enhances the stress resistance of bacteria against various stressors (Ayub et al. 2009; Kadouri et al. 2003a, b; Obruca et al. 2016a, b, 2017; Tal and Okon 1985; Wang et al. 2009; Zhao et al. 2007). This can be considered an important "added value" to their primary biological function—storage of carbon, energy, and also reduction power. Generally, it has been observed that the presence of PHA granules influences the overall biophysical properties of bacterial cells, which further increases stress survival when they are exposed to various stress factors. For instance, the presence of PHA granules enhanced the rate of water transport out of the cells during freezing, which subsequently protected bacterial cells from formation of intracellular ice; this substantially contributes to PHA's cryo-protective effect (Obruca et al. 2016a). Moreover, PHA polymers in native intracellular granules represent a unique amorphous form of matter which resembles "supercooled" liquid in its properties (Bonthrone et al. 1992). The liquid-like properties of PHA granules seem to play a crucial role in the protective mechanism of PHA against osmotic up-shock, since the presence of PHA granules turned out to reduce the level of plasmolysis in challenged cells and, moreover, according to the results of transmission electron microscopy analysis, PHA granules were even capable of stabilizing membranes of bacterial cells by closing the holes in the cytoplasmic membrane (Obruca et al. 2017). Therefore, even the simple presence of PHA granules in cytoplasm can be beneficial for bacterial cells when exposed to stress conditions.

Moreover, the enhancement of the UV resistance of PHA-accumulating bacteria which was reported in this work (Fig. 1), as well as by other authors (Kadouri et al. 2003a; Tal and Okon 1985; Wang et al. 2009; Zhao et al. 2007), is most likely primarily based on the biophysical consequence of the presence of PHA granules in cells. According to our results, PHA granules do not considerably absorb UV radiation but they are capable of efficient scattering of UV radiation as was indicated in the present study by the comparison of turbidity (Fig. 2a) and absorbance measurement (Fig. 2b) of the cells of PHA-accumulating C. necator and its PHA negative mutant. Furthermore, the fact that PHA granules efficiently scatter UV radiation was also confirmed by nephelometry measurement (Fig. 4). Because no considerable changes in cell dimensions were found for both strains in our previous work (Mravec et al. 2016), the significant increase in the light scattering of the C. necator H16 strain can be ascribed to the fraction of light scattered on the cell ultrastructure, namely on the PHA granules in the cell cytoplasm. This finding is in fact not surprising; a similar observation of an increase of the single cell light turbidity as a result of light scattering on inclusion bodies has previously been reported, e.g., for E. coli W3110 (Hwang and Feldberg 1990). Nevertheless, to the best of our knowledge, our results represent the first convincing experimental confirmation that intracellular PHA granules serve as effective in situ light-scatterers. Furthermore, according to the results presented in Fig. 2b, it is evident that UV radiation is absorbed by the bacterial cells quite effectively. The absorption band centered around 254 nm can be assigned to nucleic acid, especially to DNA. Nevertheless, from the comparison of the absorption spectra of cell suspensions with the same cell density, it can be seen that UV-radiation absorption in this wavelength region is considerably suppressed in the case of the PHA-accumulating strain. Bearing in mind that there is no significant difference in the cellular content of DNA for the two strains, this result supports the assumption of "shielding" effects of PHA granules resulting from their great light-scattering ability. Moreover, it can be stated that, apart from protecting DNA as the most sensitive molecule, scattering of UV irradiation on PHA granules also reduces level of intracellular ROS (see Fig. 5) generated by UV radiation. This new finding very likely substantially contributes to complex UV-protective function of PHA granules.

It should be pointed out that in natural producers, PHA granules are not randomly distributed in bacterial cells, but they are specifically attached to DNA. In C. necator, the attachment is performed via the protein PhaM which simultaneously binds to DNA and the PHA associated-protein PhaP5 (Wahl et al. 2012). Similarly, in Pseudomonas putida, the binding of PHA granules to DNA is enabled by the protein PhaF. This protein serves as a transcriptional regulator of PHA metabolism but it is also responsible for proper segregation of granules during cell division and ensures, under balanced conditions, equal distribution of granules between daughter cells. PhaF directs the PHA granules to the center of the cells, forming a characteristic needle array in the close vicinity of DNA (Galan et al. 2011). This might substantially contribute to a UV-protective effect since PHA granules represent a "shield" attached to the nucleoid which scatters UVB radiation away from the most sensitive molecule–DNA. Here, it

has to be emphasized that very recent findings by Karmann et al. (2017) show that, under carbon-limited conditions, the distribution of granules to daughter cells in statu nascendi occurs in an asymmetric way; the culture segregates into a PHA-rich and a PHA-poor subculture, thus displaying a "bistable behavior." Future investigations might provide insights if the PHA-rich subculture is definitely better protected when challenged by UV irradiation.

PHA metabolism reveals a cyclic nature, the so called PHA cycle, since in microbial cells the polymer is simultaneously synthesized and degraded (Kadouri et al. 2005). According to the results of Kadouri et al. (2003b), also the capability of intracellular PHA degradation is an important factor enhancing the UV-protective effect of PHA, since a PHA depolymerase deletion mutant strain of *Azospirillum brasilense* incapable of PHA degradation was shown to be more sensitive to UV irradiation than the wild type strain. The explanation can be that, due to the cyclic nature of PHA metabolism and activity of PHA depolymerase, a substantial amount of PHA monomers is present in bacterial cells. For instance, the intracellular concentration of 3-hydroxybutyrate (3HB) in the wild type strain of *C. necator* is 16.5-fold higher than in its PHA non-accumulating mutant. This is important since 3HB constitutes a potent chemical chaperone capable of preventing a model enzyme, lipase, against denaturation caused by high temperature or oxidative damage (Obruca et al. 2016b). Therefore, it is likely that the complete PHA cycle might in this way also prevent bacterial cells against oxidative pressure generated by UV radiation. Moreover, Ayub et al. (2009) suggested that PHA metabolism is essential for the maintenance of the redox state in *Pseudomonas* sp. 14-3 during oxidative pressure induced by exposure of bacterial cells to low temperatures.

In summary, the presence of PHA granules in bacterial cells has numerous biophysical and metabolic consequences, which alter the stress survival capacity of bacterial cells during their exposition to various stress factors. Their UV-protective action might be explained by their efficient UV-radiation scattering properties with high scattering efficiency in the wavelengths close to the DNA absorption maxima. Furthermore, presence of PHA granules in bacterial cells also protects them from ROS generated by UV irradiation since scattering of UV radiation on granules decreases levels of generated ROS and, moreover, PHA metabolism also provides efficient protection against oxidative stress induced by UV irradiation.

Compliance with ethical standards

Conflict of interest The authors declare that they have no conflict of interest.

Ethical approval This article does not contain any studies with human participants or animals performed by any of the authors.

References

Ayub ND, Tribelli PM, López NI (2009) Polyhydroxyalkanoates are essential for maintenance of redox state in the Antarctic bacterium *Pseudomonas* sp. 14-3 during low temperature adaptation. Extremophiles 13(1):59–66. https://doi.org/10.1007/s00792-008-0197-z

Bonthrone KM, Clauss J, Horowitz DM, Hunter BK, Sanders JKM (1992) The biological and physical chemistry of polyhydroxyalkanoates as seen by NMR spectroscopy. FEMS Microbiol Lett 103(2–4):269–277. https://doi.org/10.1111/j.1574-6968.1992.tb05848.x

Dong TG, Dong S, Catalano C, Moore R, Liang X, Mekalanos JJ (2015) Generation of reactive oxygen species by lethal attacks from competing microbes. Proc Natl Acad Sci USA 112(7):2181–2186. https://doi.org/10.1073/pnas.1425007112

Farías ME, Fernández-Zenoff V, Flores R, Ordóñez O, Estévez C (2009) Impact of solar radiation on bacterioplankton in Laguna Vilama, a hypersaline Andean lake (4650 m). J Geophys Res Biogeosci 114: G00D04

Gabani P, Singh OV (2013) Radiation-resistant extremophiles and their potential in biotechnology and therapeutics. Appl Microbiol Biotechnol 97(3):993–1004. https://doi.org/10.1007/s00253-012-4642-7

Galan B, Dinjaski N, Maestro B, de Eugenio LI, Escapa IF, Sanz JM, Garcia JL and Prieto MA (2011) Nucleoid-associated PhaF phasin drives intracellular location and segregation of polyhydroxyalkanoate granules in *Pseudomonas putida* KT2442. Mol Microbiol 79:402–418. https://doi.org/10.1111/j.1365-2958.2010.07450.x

Häder DP, Kumar HD, Smith RC, Worrest RC (2007) Effects of solar UV radiation on aquatic ecosystems and interactions with climate change. Photochem Photobiol Sci 6(3):267–285. https://doi.org/10.1039/B700020K

Hwang SO, Feldberg R (1990) Effect of inclusion body production on culture turbidity and cell dry-weight in growing bacterial cultures. Biotechnol Prog 6(1):48–50. https://doi.org/10.1021/bp00001a007

Jendrossek D (2009) Polyhydroxyalkanoate granules are complex subcellular organelles (Carbonosomes). J Bacteriol 191(10):3195–3202. https://doi.org/10.1128/JB.01723-08

Kadouri D, Jurkevitch E, Okon Y (2003a) Involvement of the reserve material poly-beta-hydroxybutyrate in *Azospirillum brasilense* stress endurance and root colonization. Appl Environ Microbiol 69(6):3244–3250. https://doi.org/10.1128/AEM.69.6.3244-3250.2003

Kadouri D, Jurkevitch E, Okon Y (2003b) Poly beta-hydroxybutyrate depolymerase (PhaZ) in *Azospirillum brasilense* and characterization of a *phaZ* mutant. Arch Microbiol 180(5):309–318. https://doi.org/10.1007/s00203-003-0590-z

Kadouri D, Jurkevitch E, Okon Y, Castro-Sowinski S (2005) Ecological and agricultural significance of bacterial polyhydroxyalkanoates. Crit Rev Microbiol 31(2):55–67. https://doi.org/10.1080/10408410590899228

Karmann S, Panke S, Zinn M (2017) The bistable behaviour of *Pseudomonas putida* KT2440 during PHA depolymerization under carbon limitation. Bioengineering 4(2):58. https://doi.org/10.3390/bioengineering4020058

Khodadad CL, Wong GM, James LM, Thakrar PJ, Lane MA, Catechis JA, Smith DJ (2017) Stratosphere conditions inactivate bacterial endospores from a Mars spacecraft assembly facility. Astrobiology 17(4):337–350. https://doi.org/10.1089/ast.2016.1549

Kim BM, Rhee JS, Lee KW, Kim MJ, Shin KH, Lee SJ, Lee YM, Lee JS (2015) UV-B radiation-induced oxidative stress and p38 signaling pathway involvement in the benthic copepod *Tigriopus japonicus*. Comp Biochem Physiol C 167:15–23

Koller M, Muhr A, Braunegg G (2014) Microalgae as versatile cellular factories for valued products. Algal Res 6:52–63. https://doi.org/10.1016/j.algal.2014.09.002

Mravec F, Obruca S, Krzyzanek V, Sedlacek P, Hrubanova K, Samek O, Kucera D, Benesova P, Nebesarova J (2016) Accumulation of PHA granules in *Cupriavidus necator* as seen by confocal fluorescence microscopy. FEMS Microbiol Lett 363:fnw094

Obruca S, Benesova P, Oborna J, Marova I (2014) Application of protease-hydrolyzed whey as a complex nitrogen source to increase poly(3-hydroxybutyrate) production from oils by *Cupriavidus necator*. Biotechnol Lett 36(4):775–781. https://doi.org/10.1007/s10529-013-1407-z

Obruca S, Sedlacek P, Krzyzanek V, Mravec F, Hrubanova K, Samek O, Kucera D, Benesova P, Marova I (2016a) Accumulation of poly(3-hydroxybutyrate) helps bacterial cells to survive freezing. PLoS One 11(6):e0157778. https://doi.org/10.1371/journal.pone.0157778

Obruca S, Sedlacek P, Mravec F, Samek O, Marova I (2016b) Evaluation of 3-hydroxybutyrate as an enzyme-protective agent against heating and oxidative damage and its potential role in stress response of poly(3-hydroxybutyrate) accumulating cells. Appl Microbiol Biotechnol 100(3):1365–1376. https://doi.org/10.1007/s00253-015-7162-4

Obruca S, Sedlacek P, Mravec F, Krzyzanek V, Nebesarova J, Samek O, Kucera D, Benesova P, Hrubanova K, Milerova M, Marova I (2017) The presence of PHB granules in cytoplasm protects non-halophilic bacterial cells against the harmful impact of hypertonic environments. New Biotechnol 39(Pt A):68–80. https://doi.org/10.1016/j.nbt.2017.07.008

Paunescu D, Mora CA, Puddu M, Krumeich F, Grass RN (2014) DNA protection against ultraviolet irradiation by encapsulation in a multilayered SiO2/TiO2 assembly. J Mater Chem B 2(48):8504–8509. https://doi.org/10.1039/C4TB01552E

Pavez P, Castillo JL, González C, Martínez M (2009) Poly-β-hydroxyalkanoate exert a protective effect against carbon starvation and frozen conditions in *Sphingopyxis chilensis*. Curr Microbiol 59(6):636–640. https://doi.org/10.1007/s00284-009-9485-9

Pérez V, Hengst M, Kurte L, Dorador C, Jeffrey WH, Wattiez R, Molina V, Matallana-Surget S (2017) Bacterial survival under extreme UV radiation: a comparative proteomics study of *Rhodobacter* sp., isolated from high altitude wetlands in Chile. Front Microbiol 8:1173. https://doi.org/10.3389/fmicb.2017.01173

Pham TH (2004) The role of polyhydroxyalkanoate biosynthesis by *Pseudomonas aeruginosa* in rhamnolipid and alginate production as well as stress tolerance and biofilm formation. Microbiology 150(10):3405–3413. https://doi.org/10.1099/mic.0.27357-0

Raberg M, Voigt B, Hecker M, Steinbuchel A (2014) A closer look on the polyhydroxybutyrate- (PHB-) negative phenotype of *Ralstonia eutropha* PHB-4. PLoS One 9(5):e95907. https://doi.org/10.1371/journal.pone.0095907

Ravanat JL, Douki T, Cadet J (2001) Direct and indirect effects of UV radiation on DNA and its component. J Photochem Photobiol B 63(1-3):88–102. https://doi.org/10.1016/S1011-1344(01)00206-8

Singh OV, Gabani P (2011) Extremophiles: radiation resistance microbial reserves and therapeutic implications. J Appl Microbiol 110(4):851–861. https://doi.org/10.1111/j.1365-2672.2011.04971.x

Tal S, Okon Y (1985) Production of the reserve material poly-β-hydroxybutyrate and its function in *Azospirillum brasilense* cd. Can J Microbiol 31(7):608–613. https://doi.org/10.1139/m85-115

Tan GYA, Chen CL, Li L, Ge L, Wang L, Razaad IMN, Li Y, Zhao L, Wang JY (2014) Start a research on biopolymer polyhydroxyalkanoate (PHA): a review. Polymers 6(3):706–754. https://doi.org/10.3390/polym6030706

Tribelli PM, López NI (2011) Poly(3-hydroxybutyrate) influences biofilm formation and motility in the novel Antarctic species *Pseudomonas extremaustralis* under cold conditions. Extremophiles 15(5):541–547. https://doi.org/10.1007/s00792-011-0384-1

Vadlja D, Koller M, Novak M, Braunegg G, Horvat P (2016) Footprint area analysis of binary imaged *Cupriavidus necator* cells to study PHB production at balanced, transient, and limited growth conditions in a cascade process. Appl Microbiol Biotechnol 100(23):10065–10080. https://doi.org/10.1007/s00253-016-7844-6

Wahl A, Schuth N, Pfeiffer D, Nussberger S, Jendrossek D (2012) PHB granules are attached to the nucleoid via PhaM in *Ralstonia eutropha*. BMC Microbiol 12(1):262. https://doi.org/10.1186/1471-2180-12-262

Wang Q, Yu H, Xia Y, Kang Z, Qi Q (2009) Complete PHB mobilization in *Escherichia coli* enhances the stress tolerance: a potential biotechnological application. Microb Cell Factories 8(1):47. https://doi.org/10.1186/1475-2859-8-47

Wu D, He J, Gong Y, Chen D, Zhu X, Qiu N, Sun M, Li M, Yu Z (2011) Proteomic analysis reveals the strategies of *Bacillus thuringiensis* YBT-1520 for survival under long-term heat stress. Proteomics 11(13):2580–2591. https://doi.org/10.1002/pmic.201000392

Zhao YH, Li HM, Qin LF, Wang HH, Chen GQ (2007) Disruption of the polyhydroxyalkanoate synthase gene in *Aeromonas hydrophila* reduces its survival ability under stress conditions. FEMS Microbiol Lett 276(1):34–41. https://doi.org/10.1111/j.1574-6968.2007.00904.x

Appendix 16

Obruca, S., Sedlacek, P., Krzyzanek, V., Mravec, F., Hrubanova, K., Samek, O., Kucera, D., Benesova, P., and Marova, I. Accumulation of Poly(3-hydroxybutyrate) Helps Bacterial Cells to Survive Freezing. *PLOS ONE* **2016**, 11, e0157778.

Accumulation of Poly(3-hydroxybutyrate) Helps Bacterial Cells to Survive Freezing

Stanislav Obruca[1]☯*, Petr Sedlacek[1]☯, Vladislav Krzyzanek[2], Filip Mravec[1], Kamila Hrubanova[2], Ota Samek[2], Dan Kucera[1], Pavla Benesova[1], Ivana Marova[1]

1 Materials Research Centre, Faculty of Chemistry, Brno University of Technology, Purkynova 118, 612 00, Brno, Czech Republic, **2** Institute of Scientific Instruments, Academy of Sciences of The Czech Republic, Vvi, Kralovopolska 147, 612 64, Brno, Czech Republic

☯ These authors contributed equally to this work.
* Stana.O@seznam.cz

Abstract

Accumulation of polyhydroxybutyrate (PHB) seems to be a common metabolic strategy adopted by many bacteria to cope with cold environments. This work aimed at evaluating and understanding the cryoprotective effect of PHB. At first a monomer of PHB, 3-hydroxy-butyrate, was identified as a potent cryoprotectant capable of protecting model enzyme (lipase), yeast (*Saccharomyces cerevisiae*) and bacterial cells (*Cupriavidus necator*) against the adverse effects of freezing-thawing cycles. Further, the viability of the frozen–thawed PHB accumulating strain of *C. necator* was compared to that of the PHB non-accumulating mutant. The presence of PHB granules in cells was revealed to be a significant advantage during freezing. This might be attributed to the higher intracellular level of 3-hydroxybutyrate in PHB accumulating cells (due to the action of parallel PHB synthesis and degradation, the so-called PHB cycle), but the cryoprotective effect of PHB granules seems to be more complex. Since intracellular PHB granules retain highly flexible properties even at extremely low temperatures (observed by cryo-SEM), it can be expected that PHB granules protect cells against injury from extracellular ice. Finally, thermal analysis indicates that PHB-containing cells exhibit a higher rate of transmembrane water transport, which protects cells against the formation of intracellular ice which usually has fatal consequences.

Introduction

Microorganisms are exposed to a series of various stress factors in the environment, among which great temperature oscillations are very frequent. It should be noted that approximately 80% of our planet's biosphere is permanently cold with average temperatures below 5°C and that even in the remaining regions the temperature fluctuates wildly, occasionally falling close to, or even below 0°C [1]. Therefore, many microorganisms have developed sophisticated strategies to help them endure low temperatures. These include the capacity to produce and accumulate cryoprotectants, substances which are able to protect cells from the adverse effects of freezing and low temperature [2]. There are numerous low molecular weight solutes (e.g. amino acids and their derivatives, sugars, ectoines and their derivatives, etc.) as well as high

molecular weight substances (e.g. proteins and polysaccharides) which are produced by bacteria and exhibit cryoprotective properties [2, 3].

Low temperatures induce distinct responses among bacterial cells depending on the actual temperature. Exposure to cold conditions above 0°C is usually accompanied by an active response from bacterial cells. On the contrary, the response of most prokaryotes is passive at subzero temperatures, which is connected with the formation of ice [4]. As ice crystals grow, a process which occurs initially in the extracellular medium, the concentration of the solutes in the medium is excluded into an ever-decreasing solvent volume which results in effective osmotic stress. This induces so-called "freeze-dehydration" which is an important harmful consequence of cell freezing. Another important damaging mechanism identified during freezing of the cells is formation and propagation of intracellular ice. It is proposed that crystals of intracellular ice cause the physical destruction of membranes, formation of gas bubbles, and might also result in organelle disruption [3]. More generally, the survival of bacterial cells during freezing depends on the cooling rate. Cell survival is maximal when cooling occurs slowly enough to avoid formation of intracellular ice but fast enough to prevent causing injury to the cells by substantial dehydration [5]. Apart from dehydration and intracellular ice formation, cells can also be harmed by reactive oxygen species (ROS) formed in cells during freezing [6]. In addition, a decrease in the size of the unfrozen channels in ice during freezing can cause shrinkage of the cells, resulting in mechanical injury [7].

Polyhydroxyalkanoates (PHAs) are storage polymers accumulated in the form of intracellular granules by a wide range of taxonomically different groups of microorganisms. Among the wide variety of PHAs, the polyester of 3-hydroxybutyrate, poly(3-hydroxybutyrate) (PHB), is the most common and the best studied [8]. The biosynthesis and degradation of intracellular PHB occur in cells simultaneously, and therefore the metabolism of PHB exhibits a cyclic mechanism [9]. It is generally proposed that PHAs serve primarily as a carbon and energy storage material when exogenous carbon sources are depleted. However, there are reports that the capacity for intracellular PHA accumulation and degradation also enhances the resistance of bacterial cells to various stress conditions including low temperatures and freezing.

PHAs have been observed to be essential for maintenance of the redox state in the Antarctic bacterium *Pseudomonas* sp. 14–3 during low-temperature adaptation [10]. Iustman et al. isolated and studied the Antarctic strain *Pseudomonas extremaustralis*, whose high resistance to a wide range of stress conditions including cold was attributed to its capacity to produce PHB [11]. The PHB biosynthetic genes of the bacterium are located within an adaptive genomic island and were probably acquired by horizontal gene transfer, which suggests the importance of PHA accumulation in adaptation to stress conditions, such as those found in the extreme Antarctic environment [12]. Further, Pavez et al. reported that PHAs exert a protective effect against freezing in *Sphingopyxis chilensis* [13]. Numerous PHA-producing bacterial strains have also been isolated from Antarctic freshwater [14] and Antarctic soil [15], which indicates that PHA accumulation is a common metabolic strategy adopted by many bacteria to cope with cold environments.

Hence, in this work we investigated and assessed the potential protective mechanisms of PHB when bacterial cells are exposed to freezing and thawing. We have recently revealed the monomer of PHB– 3-hydroxybutyrate (3HB)–to be a very potent chemical chaperone capable of protecting model enzymes against heat-mediated denaturation and oxidative damage. Due to continuous PHB synthesis and degradation in bacterial cells (the so-called PHB cycle), the 3HB concentration in the PHB accumulating strain *Cupriavidus necator* was more than 16.5-fold higher than in the strain unable to accumulate PHA [16]. In this work, we tested the cryoprotective effect of 3HB for lipase as a model enzyme as well as for selected eukaryotic (*Saccharomyces cerevisiae*) and prokaryotic (*Cupriavids necator*) microorganisms. In addition,

using flow cytometry, thermal analysis, and Cryo-Scanning Electron Microscopy (Cryo-SEM), we tried to shed light on the complex role of intracellular PHB granules with respect to the survival of bacterial cells during freezing and thawing.

Materials and Methods

Materials and microorganisms

Trehalose, 3-hydroxybutyrate, p-nitrophenylpalmitate and lipase from *Rhizopusoryzea* were purchased from Sigma Aldrich, Germany. *Cupriavidus necator* H16 (CCM 3726) was obtained from the Czech Collection of Microorganisms, Brno, Czech Republic. The PHB non-producing strain *Cupriavidus necator* PHB^{-4} (DSM-541) was purchased from the Leibnitz Institute DSMZ-German Collection of Microorganism and Cell Cultures, Braunschweig, Germany. *Saccharomyces cerevisiae* CCY 21-4-47 was purchased from the Culture Collection of Yeast, Bratislava, Slovakia.

Screening of cryoprotective effect of 3HB for lipase against freezing-thawing treatment

Samples of lipase (0.4 mg/ml) in 100 mM of phosphate buffer (pH 7.4) were prepared in the presence (50 and 100 mM) or absence of 3HB and in presence of 100 mM trehalose. The freezing-thawing stabilizing effect of 3HB on lipase was studied by incubating the samples (initial volume 1 ml) at -30°C for 2 h and thawing them at 30°C. After each cycle, aliquots (100 μl) for the determination of residual activity were taken.

The enzyme activity of lipase samples was determined spectrophotometrically according to the established procedure described by Pinsirodom and Parkin with a slight modification [17]. The assays were performed in standard 96-well microplates; the reaction mixture consisted of 230 μL of 100 mM phosphate buffer pH 7.4, 25 μL of 420 μM p-nitrophenylpalmitate substrate solution and 25 μL of suitable diluted enzyme solution. The reaction was started by the addition of substrate and the formation of the product (p-nitrophenol) at 40°C was followed at 405 nm using a Biotek ELx808 microplate reader. Under the specified conditions, 1 unit of enzyme activity was defined as the amount of enzyme releasing 1 μmol of the product per minute. All the analyses were performed in triplicates.

Evaluation of the cryoprotective effect of 3HB for yeast and bacterial cells

The yeast culture *Saccharomyces cerevisiae* was cultivated (25°C, 140 rpm) in 250 mL Erlenmeyer flasks containing 100 mL of YPD medium (20 g/L glucose, 20 g/L peptone, 10 g/L yeast extract) for 24 hours. Then, 2 mL aliquots were taken, washed with PBS buffer, and re-suspended in PBS buffer in the absence or presence of 3HB (50 mM and 100 mM). The cell suspensions were frozen at -30°C for 2 h, then thawed at laboratory temperature and the viability of the yeast culture was analyzed immediately. We performed 5 subsequent freezing-thawing cycles, each sample prepared in triplicate. In a further experiment, we compared the cryoprotective effect of 100 mM of 3HB with trehalose and glycerol applied at the same concentration level. In this experiment, the yeast culture was adapted to the presence of cryoprotectants at 4°C for 1 h, after which freezing-thawing cycles were performed as described above.

Similar experiments were also performed with the PHB-producing bacterial strain *C. necator* H16 and its PHB non-accumulating mutant *C. necator* PHB^{-4}. Erlenmeyer flasks (volume 250 mL) containing 100 mL of Mineral Salt (MS) medium (the MS medium was composed of 20 g fructose, 3 g $(NH_4)_2SO_4$, 1 g KH_2PO_4, 11.1 g $Na_2HPO_4 \cdot 12 H_2O$, 0.2 g $MgSO_4$, 1 mL of

microelement solution and 1 L of distilled water; the microelement solution was composed of 9.7 g $FeCl_3$, 7.8 g $CaCl_2$, 0.156 g $CuSO_4 \cdot 5 H_2O$, 0.119 g $CoCl_2$, 0.118 g $NiCl_2$ in 1 L of 0.1 M HCl) were inoculated with 5 mL of the overnight culture of the particular strain of *C. necator* grown in Nutrient Broth medium (NB medium: 10 g peptone, 10 g beef extract, 5 g NaCl in 1 L of distilled water). After 72 h of cultivation, 2 mL aliquots were taken, washed with PBS buffer, and re-suspended in PBS buffer in the absence or presence of 100 mM of 3HB. The cell suspensions were frozen at 30°C for 2 h, then thawed at laboratory temperature, and the viability of the bacterial culture was analyzed immediately. The freezing-thawing cycling was repeated 4 times, each sample prepared in triplicate. In addition, PHB content in the bacterial cultures was determined as described previously [18].

The capacity of *C. necator* H16 and *C. necator* PHB^{-4} to endure different freezing temperatures was also tested. Both bacterial strains were cultured as described above for 72 h, washed and re-suspended in PBS buffer, incubated at -5, -10, -15, and -20°C for 60 minutes, and thawed at laboratory temperature. After that, the viability of each bacterial culture was determined immediately.

The viability of yeast and bacterial cell populations was assessed by means of membrane integrity assay. Flow cytometry analysis using propidium iodide according to Coder was employed [19]. After each freezing-thawing cycle, 100 μl aliquots were taken, washed with PBS buffer, and diluted to a cell count of approx. 5·10^6 per ml. Then, 1 ml of cell suspension was stained by 1 μl of 1 mg/ml propidium iodide in the dark for 5 min. After that, the viability of the cells was analyzed by flow cytometry (Apogee A50, Apogee, GB) using a 488 nm laser for the excitation and the red channel (FL3) for the fluorescence detection.

Thermal analysis of bacterial cells

Basic calorimetric and thermogravimetric assays of bacterial samples were used in order to estimate whether the presence of PHB granules in cells can somehow affect the activity of the cellular water. For this purpose, we used bacterial cultures of *C. necator* H16 cultivated for 72 h in MS and NB medium, respectively. The fact that the strain does not accumulate PHB in NB medium is well documented [20] and was experimentally confirmed by the determination of the total PHB content in the cell by GC-FID as described previously [18]. Samples for the thermal analyses were always washed carefully with deionized water and centrifuged and the excess water was removed.

Differential scanning calorimetry was performed using a temperature-modulated calorimeter (DSC Q2000, TA Instruments, DE) equipped with an RCS90 cooling accessory and assessed by TA Universal Analysis 2000 software. All experiments were performed in hermetically sealed Tzero aluminum pans under a dynamic nitrogen atmosphere. Temperature-modulated DSC in the standard and quasi-isothermal modes, respectively, were applied in order to investigate the thermal effects of the freezing-thawing behavior of the bacterial cultures. In the former technique (MTDSC), the sample is cooled substantially from 20°C to -50°C and then heated back up with an underlying cooling/heating rate of 5°C/min and a temperature modulation of ± 1°C every 60 s. Quasi-isothermal temperature-modulated DSC (QiMTDSC; for details, see e.g. Otun et al. [21]) is a variant of traditional temperature-modulated DSC which involves the holding and modulation of a sample at a specific temperature for extended periods of time. This temperature can be increased or decreased incrementally in the course of the experiment. In the performed QiMTDSC experiment, samples were cooled down from 5°C to -30°C and heated back up in 1°C increments with an isotherm of 10 min at each increment. A temperature modulation of ±1°C every 60 s was applied.

Thermogravimetry (TGA, TA Instruments, Q5000IR) was used to determine the weight loss in the temperature interval 25–700°C under a dynamic dry air atmosphere with a heating

rate of 10°C/min. Weight loss in the interval 25–200°C was used to calculate the total water content in the samples. In addition, an isothermal TGA experiment at 60°C was performed in order to provide further comparison of the dynamics of the drying process for the samples under investigation.

Cryo-SEM

Bacterial cultures of *C. necator* H16 or *C. necator* PHB^{-4} grown on Petri dishes with the mineral medium described above were collected from agar plates, quickly frozen in liquid nitrogen and moved into a cryo-vacuum chamber (ACE600, Leica Microsystems), where they were freeze-fractured and briefly sublimated at -95°C. Further, the samples were moved at high vacuum using a shuttle (VCT100, Leica Microsystems) into a Scanning Electron Microscope (Magellan 400/L, FEI) equipped with a cold stage and the fractured structures were observed in a 1 keV electron beam at -135°C without any metal coating.

Results

Cryoprotective effect of 3HB for lipase

In our previous work, we observed that 3HB serves as a very effective protectant of enzymes (in particular, lipase from *Rhizopus oryzea* and lysozyme) against denaturation caused by high temperature and oxidative damage [16]. Hence, we also tested its cryoprotective efficiency using lipase–the same model enzyme. The enzyme was solubilized in phosphate buffer in the absence and presence of 3HB, which was tested at two concentration levels: 50 and 100 mM. Further, the enzyme was also tested in presence of well-established cryoprotectant trehalose, which was applied at 100 mM. The samples were subjected to repeated freezing-thawing cycles and the activity of the enzyme was determined after each cycle (Fig 1). The freezing-thawing treatment significantly reduced the activity of the enzyme in the control sample (without 3HB) which, after the 7th cycle, exhibited only 45.23% of its initial activity. In contrast, 3HB exhibited a significant concentration-dependent protective effect, since the relative enzyme activity was always higher when 3HB was present in the sample. The higher the dose of 3HB, the higher the enzyme activity that was observed. Surprisingly, when 100 mM of 3HB was applied, the relative enzyme activity of the enzyme in the sample actually increased during the initial 5 freezing-thawing cycles and a significant decrease in the activity was not observed until the 6th cycle; even after the 7th cycle the enzyme still possessed 87% of its relative activity. Protective effect of 100 mM 3HB is comparable to that of 100 mM trehalose, application of which also surprisingly increased enzyme activity during initial freezing-thawing cycles and after the 7th cycle 90% of its initial activity was recorded.

An increase in enzyme activity after freezing in presence of cryoprotectants was observed also by other authors and is ascribed to favorable conformation changes (partial unfolding) of enzyme at the level of active site and/or its neighborhood which leads to a higher affinity between enzyme and substrate [22, 23].

3HB as a protectant of *Saccharomyces cerevisiae*

In the first experiment, we demonstrated the cryoprotective activity of 3HB for enzymes. Therefore, we decided to test its ability also to protect whole cells against damage induced by freezing-thawing cycles. First, we utilized the yeast *Saccharomyces cerevisiae* as a model eukaryotic microorganism. Yeast cells suspended in PBS buffer with and without 3HB (50 and 100 mM) were repeatedly frozen at -30°C and thawed and the viability of the yeast culture was assayed after each cycle. Also in this case, 3HB exhibited a significant cryoprotective effect: the
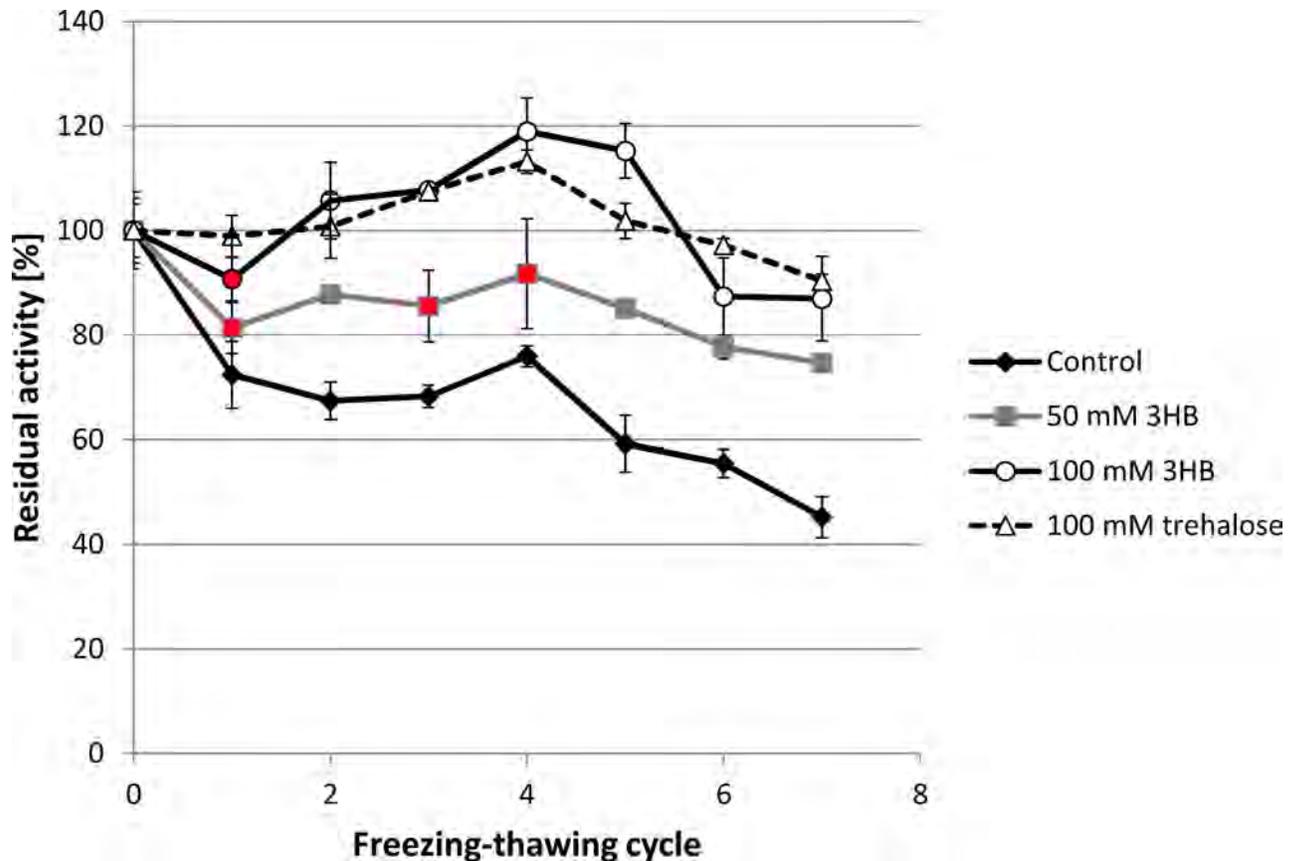
Fig 1. Effect of freezing-thawing treatment on the residual activity of lipase in the absence and presence of 50 mM and 100 mM 3HB. *note: Statistical significance was tested using 2 sample t-test (Minitab), each sample was compared with control, statistically insignificant results are labeled by red.

doi:10.1371/journal.pone.0157778.g001

viability of the yeast culture was always higher in the presence of 3HB than in the control culture (Fig 2A). After 5 freezing-thawing cycles, only 6% of cells in the control culture were viable, whereas the viabilities of the cultures with 50 and 100 mM 3HB were 48.7 and 57.1%, respectively.

In a further experiment, the cryoprotective effect of 3HB was compared with that of two other well-established cryoprotectants–trehalose and glycerol [3]. All the tested solutes were applied at a concentration of 100 mM. Unlike in the previous experiment, before exposure to the freezing-thawing cycles, the yeast culture was left to adapt to the cryoprotectants at 4°C for 1 h (the control culture was treated in the same manner). Such adaptation was reported to increase the effectiveness of most cryoprotectants [2]. A comparison of the protective effects of the tested solutes is presented in Fig 2B. All the tested solutes significantly enhanced the viability of the yeast culture in comparison with the control culture. After the 8th cycle, only 7.9% of cells in the control sample were viable, whereas the viability of yeast culture challenged in the presence of cryoprotectants did not fall below 60%. Among the tested cryoprotectants, 3HB exhibited the greatest protective effect, which was slightly greater than that of trehalose (the proportion of viable cells in the yeast culture after the 8th cycle was 79.3 and 76.0% in 3HB and trehalose, respectively). The protective effect of glycerol was less pronounced, with 61.7% of cells remaining viable after 8 freezing-thawing cycles. Hence, 3HB seems to be a very effective cryoprotectant, even in comparison with trehalose and glycerol, which are considered to be
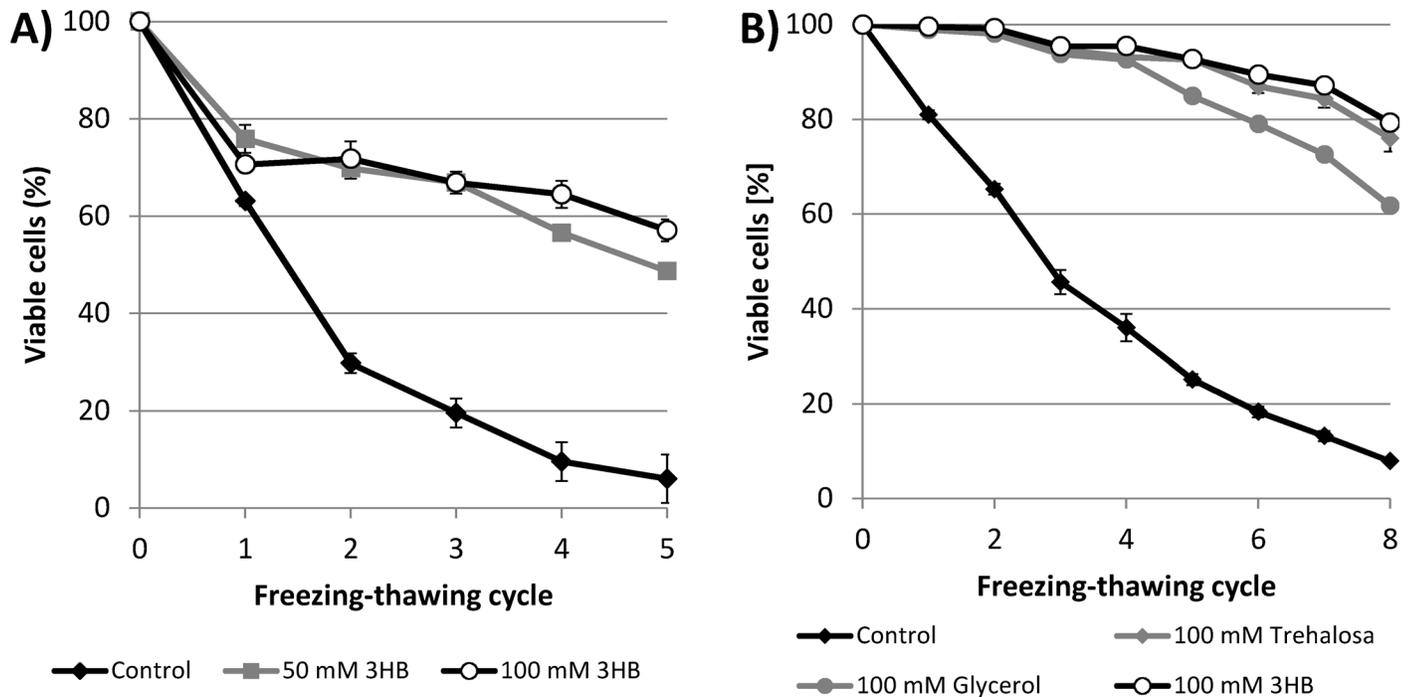
Fig 2. A) Viability of *S. cerevisiae* culture during freezing-thawing challenge in the presence of 3HB applied at 50 mM and 100 mM and in its absence B) Viability of the yeast culture exposed to repeated freezing-thawing in the presence of 3HB, trehalose and glycerol (all protectants were applied at 100 mM concentration) and in absence of a cryoprotectant. *note: Statistical significance was tested using 2 sample t-test (Minitab), each sample was compared with control, all the differences were found statistically significant.

doi:10.1371/journal.pone.0157778.g002

natural cryoprotectants used by various microbes and are also routinely applied in the cryo-preservation of microorganisms [2; 24].

Cryoprotective effect of 3HB and PHB for *Cupriavidus necator*

The protective effect of 3HB during freezing-thawing cycles was also tested with two bacterial cultures: PHB-producing *Cupriavidus necator* H16 and its mutant strain *Cupriavidus necator* PHB^{-4}, which, due to a mutation of the gene encoding for PHB synthase, is not capable of accumulating PHB [25]. The bacterial cultures were cultivated for 72 h, at which point both cultures had reached the stationary phase of their growth. The PHB content in *C. necator* H16, determined by GC-FID, reached 76% of cell dry weight; the PHB content in the culture of *C. necator* PHB^{-4} was negligible (about 0.4% of cell dry weight). Both cultures were exposed to freezing-thawing cycles (the temperature of freezing was -30°C) suspended in PBS buffer in the presence or absence of 100 mM of 3HB. The results are shown in Fig 3A.

Similarly to the previous experiments with *S. cerevisiae*, the application of 3HB significantly improved the survival of both bacterial cultures, as compared to samples without 3HB. Moreover, we observed a significantly higher proportion of viable cells in the bacterial culture capable of accumulating PHB than in the PHB non-accumulating mutant in both experimental settings–with and without 3HB. In addition, bacterial cultures in the absence of 3HB revealed a different profile to their viability curves during the freezing-thawing challenge compared to yeast cultures or bacterial cultures with 3HB. In the yeast cultures and also in the bacterial cultures with 3HB, viability decreased more or less constantly during the whole freezing-thawing test. In contrast, without exogenous 3HB, most bacterial cells lost their viability during the first freezing-thawing cycle (the proportions of viable cells after the 1st cycle were 40.1 and 26.3% in

C. necator H16 and *C. necator* PHB^{-4}, respectively). After that the viability of the cultures remained constant or decreased only slowly.

Therefore, we decided to compare the resistance of both bacterial strains without the addition of 3HB during a single freezing-thawing cycle challenge in which different temperatures of freezing (-5, -10, -15, and -20°C) were applied. The bacterial strain capable of PHB accumulation revealed a significantly higher ability to endure freezing than its PHB non-producing mutant strain. With decreasing temperature the differences between the viabilities of the bacterial strains increased (see Fig 3B). When the bacterial strains were exposed to -5°C, the proportions of viable cells in *C. necator* H16 and *C. necator* PHB^{-4} were 94.0 and 94.9%, respectively. However, at -20°C, in the culture of *C. necator* H16 84.1% of cells retained viability, while only 34.5% of cells were identified as viable in *C. necator* PHB^{-4}. Hence, it seems that the presence of PHB granules in cell cytoplasm represents a significant advantage when the cells are exposed to subzero temperatures: the lower the temperature, the more pronounced the protective effect that was observed.

In addition, to investigate whether PHB granules are actively metabolized by bacterial culture *C. necator* H16 during repeated freezing-thawing, we performed experiment in which we determined PHB content in the bacterial culture after the each cycle; data are provided in S1 Fig. Since none decrease in the PHB content was observed, it can be stated that the bacterial culture did not utilize PHB granules to increase intracellular level of 3HB and it seems that in perspective of PHB metabolism response of the bacterial culture to repeated freezing is rather passive than active.

Observation of PHB granules by Cryo-SEM

Cryo-SEM is a very interesting technique providing an ultrastructural insight into various biological samples in a deeply-frozen state. Therefore, we used this method to investigate the morphology of frozen intracellular PHB granules. Fig 4 shows Cryo-SEM microphotographs of PHB non-containing (*C. necator* PHB^{-4}) and containing (*C. necator* H16) bacterial cells. In PHB-containing cells, needle-like plastic deformations were observed, while these structures
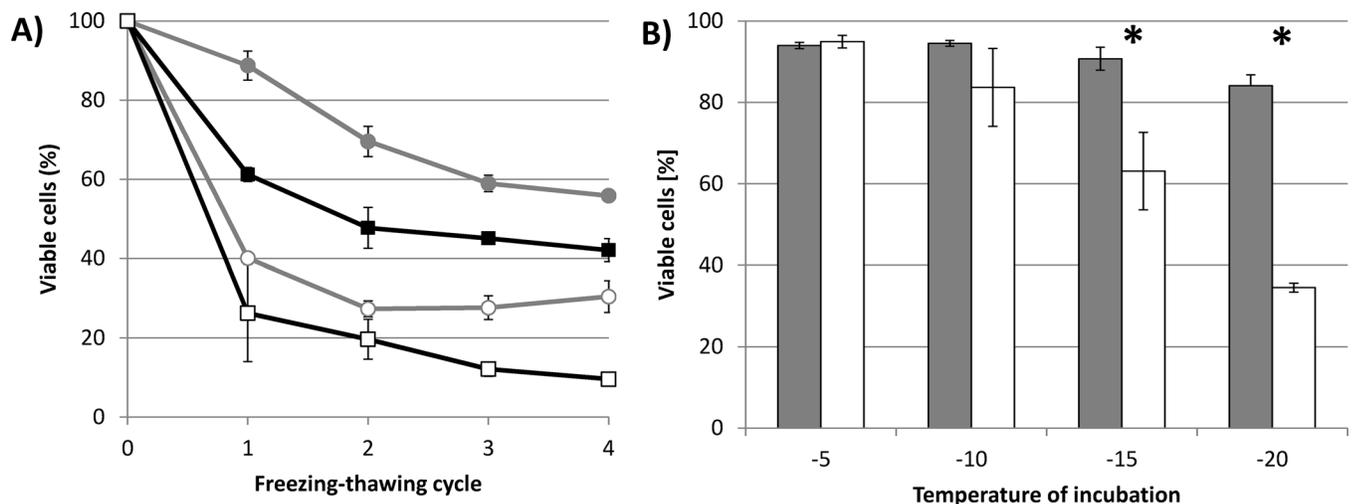
Fig 3. A) Viability of PHB-accumulating *C. necator* H16 and PHB non-accumulating *C. necator* PHB^{-4} exposed to repeated freezing-thawing challenge in the presence and absence of 100 mM 3HB. B) Viability of *C. necator* H16 and *C. necator* PHB^{-4} exposed to various sub-zero temperatures without addition of 3HB. *note: Statistical significance was tested using 2 sample t-test (Minitab). Presence of 3HB resulted in statistically significant increase in viability for both tested cultures and for all freezing-thawing cycles. Difference between viability of *C. necator* H16 and *C. necator* PHB–4 was statistically significant for all experimental conditions except for the initial 2 freezing-thawing cycles in absence of 3HB. In Fig 3B viability of *C. necator* H16 was compared with viability of *C. necator* PHB^{-4} for each temperature of incubation; statistically significant differences are labeled by asterisks.

doi:10.1371/journal.pone.0157778.g003
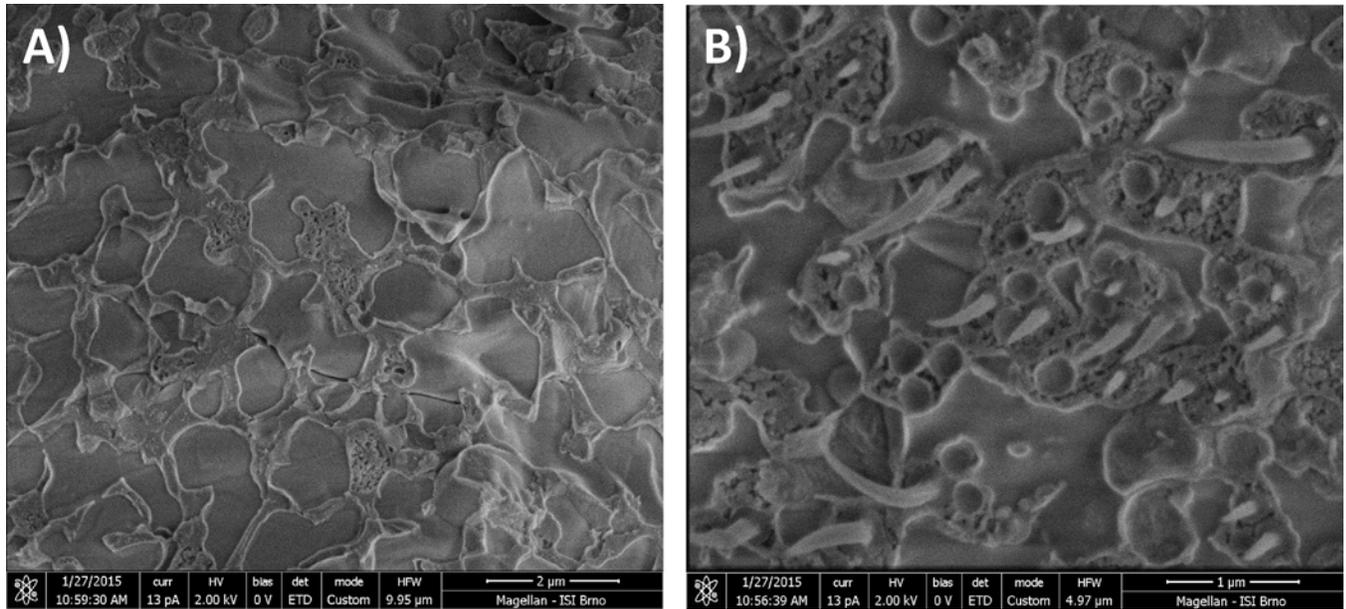
Fig 4. Cryo-SEM microphotographs of A) PHB non-producing *C. necator* PHB[-4], B) PHB-accumulating cells of *C. necator* H16.

were absent in cells without polymer, which indicates that these deformations can be clearly attributed to PHB granules. Employing the same experimental approach, similar structures were also observed by [26] in the PHA-producing bacteria *Comamonas acidovorans*. Despite the fact that the mechanism of the genesis of these deformations during freeze-fraction has not yet been explained, we can state that frozen PHB granules exhibit completely different mechanical and physico-chemical properties than any other components of bacterial cytoplasm and that their flexibility, even in deeply-frozen states, is significantly higher than that of PHB isolated from bacterial cells. When PHB polymer is extracted from cells, its elongation-to-break is about 4% [8], while in Cryo-SEM microphotographs we observed elongation corresponding to a value of more than 100%.

Effect of PHB on the freezing/melting of cellular water studied by DSC

A comparison of standard MTDSC thermograms recorded for *C. necator* H16 samples cultivated in the two different media is shown in Fig 5A. The freezing and thawing of water in the
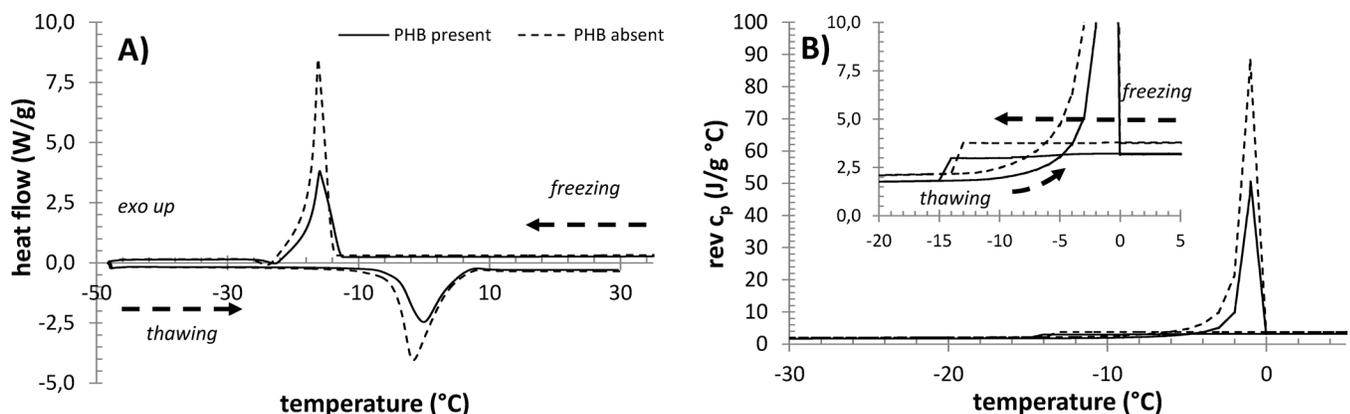
Fig 5. Results of DSC analysis of centrifuged PHB-containing and PHB non-containing cultures of *C. necator*. A) MTDSC thermograms, B) QiMTDSC thermograms.

samples are represented by corresponding exotherms and endotherms, respectively. The shape and position of the freezing exotherm provide little information about the state of water in the system, because the freezing phenomenon is greatly affected by the inevitable and hardly reproducible effect of water supercooling. On the other hand, the endothermic signal, which corresponds to the melting of the frozen water, gives an interesting overview of the activity of water in the sample [27].

Two interesting observations can be derived from the thermograms shown in Fig 5A. First, the melting endotherm which corresponds to the culture sample containing PHB granules is shifted to higher temperatures. Second, the total area of the endotherm (which represents the weight-specific heat consumed during the water melting) is significantly lower. The latter feature is easily explainable by the fact that the relative water content in PHB-containing cells is naturally lower, which correspondingly decreases the area of the ice-melting endotherm. The specific heats of fusion of water in the samples, which were calculated from the total area of the melting endotherm and from the total water content in the sample determined by TGA analysis (see below), did not show any significant differences either between the two analyzed samples or in comparison with the heat of fusion of pure water. This indicates that neither of the samples contains any significant amount of water which does not freeze (often referred to as non-freezing water).

On the other hand, the shift of the ice-melting endotherm towards higher temperatures for the MS medium-cultivated culture represents a significant experimental finding. It was demonstrated that the shift is reproducible–it was found repeatedly, no matter which particular DSC protocol was applied. In all these experiments, not only the peak but also the onset point of the endotherm was always shifted. The particular magnitude of the shift depended on the experimental conditions, e.g. the heating rate. For the results shown in Fig 5A, the peak of the endotherm was shifted by approx. 1.5°C.

An invaluable feature of MTDSC analysis is that it allows separation of the heat-flow signals related to reversible and non-reversible processes, respectively. The deconvolution of the total heat-flow signal, presented in Fig 5A, is shown in S2 Fig. The results of this deconvolution confirm that the freezing of water in the samples is an almost completely non-reversible process that is caused by the above-mentioned supercooling of liquid water. On the other hand, a further difference in the water-melting process between the PHB-containing and non-containing cultures was revealed: the non-reversible component of the melting signal in the absence of PHB was significantly more pronounced.

Effect of PHB on the drying of cells studied by TGA

TGA analysis was utilized in this study to provide further information on the activity of water in the studied bacterial cultures. Fig 6A shows the complete thermograms of PHB-containing and non-containing cells. The presence of PHB in the culture is evident from the significant weight loss at about 300°C, where the labile organic components of the cells (including PHB) are degraded. Additionally, it can be seen that the weight loss step associated with the drying of the sample is completed below 200°C. The total relative content of water, determined from the weight loss in this temperature interval, naturally differed for the two compared bacterial cultures. Nevertheless, when the content of PHB is excluded and the water content is given relative to the residual dry content of the cell, no important difference between the two samples is found. This shows that the presence of PHB granules does not significantly affect the total content of intracellular water.

Nevertheless, it has been proposed by several authors (e.g. by Uribelarrea et al. [28]) that TGA can be used also for the determination of different forms of water in cell samples. For this purpose, the derivation of water loss with temperature or time (i.e. the rate of drying of the
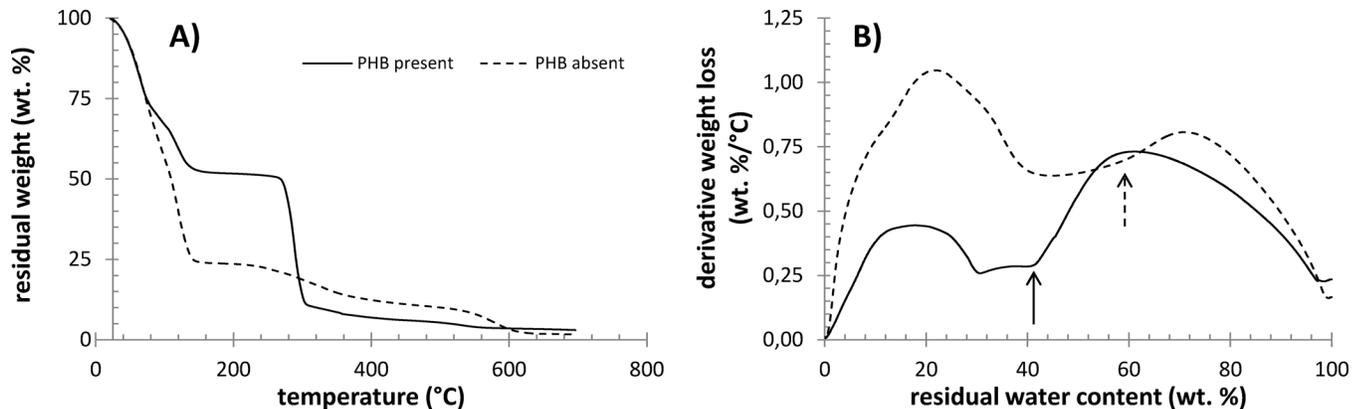
Fig 6. Results of dynamic TGA analysis of centrifuged PHB-containing and PHB non-containing cultures of *C. necator*. A) Weight loss at a heating rate of 10°C/min in the interval 25–700°C, B) derivative weight loss as a function of residual water content (arrows indicate critical water content).

sample) is given as a function of residual water content in the sample, and the critical points of this dependence are taken to be the indicators of moments at which a change in the mechanism of the drying process occurs. It can be seen in Fig 6B that these points can also be found for the tested samples. The arrows in the figure indicate the first critical point of the respective drying curve, when the release of the least strongly bound water is completed.

Discussion

In our previous study we identified 3HB as a very potent chemical chaperone capable of protecting lipase and lysozyme against adverse effects of heat and oxidative damage [16]. Hence, we decided also to test its cryoprotective efficiency for enzymes as well as whole microbial cells. Cryoprotective ability has been observed for a wide spectrum of compatible solutes which are produced and accumulated by various microorganisms to cope with ubiquitous environmental stresses such as high osmolality or temperature fluctuations [29, 30]. The cryoprotective ability of these molecules is not only scientifically interesting from a general stress-response point of view, it also has potential practical applications since proteins and other biological molecules as well as whole cells are routinely preserved in a frozen state. Hence, the application of appropriate cryoprotectants can help to maintain the activity and/or viability of preserved biological samples [2, 31].

Freezing-thawing represents a complex combination of several stress factors which reduce the activity of enzymes. Apart from low temperature and the formation of ice crystals, proteins can also be damaged by increasing concentrations of buffer salts and co-solutes which is accompanied by pH changes and increase of ionic strength [32]. Compatible solutes are usually classified as kosmotropes, which means that interactions of a compatible solute and water are stronger than water-water interaction. This effect on the water network and the ordering of water molecules by compatible solutes, therefore, affect the process of ice formation, thus providing their cryoprotective effect [24, 30]. Furthermore, compatible solutes are capable of stabilizing enzymes by affecting their hydration shell, which might provide protection not only against the adverse effects of low temperature, but also the effects of high osmolality and pH changes, as was reported for ectoines and trehalose by Van Thouc et al. [33].

Although 3HB is usually not ascribed as a typical compatible solute, it seems to be a very efficient cryoprotectant of our model enzyme–lipase from *Rhizopus oryzea* (Fig 1). When 3HB was added at a 100 mM concentration, it was capable of completely protecting lipase against

freezing-thawing mediated damage during the initial 5 freezing-thawing cycles, while in non-protected lipase we observed a decrease in relative activity to 59% of its initial value. Soto et al., reported that 3HB exhibited chemical chaperone activity preventing the aggregation of proteins of *Pseudomonas* sp. CT13 under combined salt and thermal stress [34]. However, to our knowledge, despite the fact that its cryoprotective efficiency is obvious, there are no reports regarding the cryoprotective activity of 3HB.

In comparison with enzymes, the spectrum of potential stresses associated with freezing of the whole cells becomes even wider. During freezing, cells experience either cellular dehydration (as a result of extracellular ice formation and consequent water transport driven by the resulting osmolality difference) or intracellular ice formation (IIF). These factors are oppositely dependent on the cooling rate during freezing (slow cooling leads to dehydration and fast cooling to IIF). While IIF is practically always lethal (cells have a finite volume; the expansion of water during freezing leads to rupture of the cell membrane), dehydration induces different cellular responses according to the particular freezing conditions–above all, the cooling rate [35]. Consequently, extensive cell dehydration causes freezing injury due to exposure to high concentrations of solute, while, on the other hand, partial cell dehydration protects the cell from IIF and is therefore used as a crucial step in cryopreservation protocols [5]. Obviously, the dynamics of the freezing process and of the cell response are crucial for cell survival.

Because of the complex nature of cell freezing, effective cryoprotectants should undertake multiple protective actions [2]. Our results show that 3HB served as a very potent cryoprotectant for *S. cerevisiae* cells (Fig 2); its protective efficiency was comparable with that of glycerol and trehalose, which are routinely used for the cryopreservation of microorganisms. Furthermore, 3HB exhibited even slightly higher cryoprotective activity than trehalose, itself suggested by Jain and Roy to be one of the best cryoprotectants known [24].

Apart from the mechanisms mentioned above, reactive oxygen species (ROS), generated as a consequence of an impaired aerobic respiration chain, also significantly contribute to the injury of cells during the freezing-thawing process [6]. In our previous study we observed that 3HB is, similarly to other compatible solutes such as ectoines [36], capable of protecting model enzymes from oxidative damage cause by hydrogen peroxide or heavy metals [16]. Hence, this important feature can also contribute to the cryoprotective activity of 3HB in yeast cells.

In a further experiment, we tested the cryoprotective potential of 3HB using two bacterial strains, PHB-producing *C. necator* H16 and its PHB non-accumulating mutant strain *C. necator* PHB^{-4}. Similarly as in the yeast culture, and also in both bacterial cultures, the addition of 100 mM 3HB increased the proportion of non-damaged cells in freezing-thawing tests compared with cultures challenged in the absence of 3HB. This observation demonstrates the effectiveness of 3HB as a cryoprotectant of whole microbial cells and shows that 3HB also works in bacterial cells.

However, we also observed a significant difference in the viability of the tested bacterial cultures in the absence of exogenous 3HB. The PHB-producing strain *C. necator* H16 exhibited superior viability to its PHB non-accumulating strain during the entire freezing-thawing test. Thus, it seems that intracellular reserves of PHB also play an important role in the freezing survival of bacteria, which is in agreement with the observations of other authors. Pavez et al. identified PHA accumulation in the bacterium *Sphingopyxis chilensis* (isolated from an oligotrophic aquatic environment where the temperature oscillates around 0°C) as the most important feature protecting cells from freezing conditions [13]. Moreover, PHA-producing bacteria were isolated from Antarctic freshwater [14] and Antarctic soil [15] confirming PHA accumulation as an efficient adaptation strategy for avoiding damage produced by intracellular ice crystals, oxygen-reactive species, and severe dehydration. When exposed to low temperatures, PHAs were observed to be essential for maintenance of the redox state in the Antarctic bacterium *Pseudomonas* sp. 14–3 [10]. In addition, there are several reports describing the

connection between PHA metabolism and cellular alternative sigma factor RpoS stimulating the expression of general stress response-associated genes [11, 37, 38]. Recently, Mezzina et al. reported that phasin, PHA granules associated protein of *Azotobacter* sp. FA-8, revealed chaperone-like activity in-vivo as well as in vitro [39]. However, in our opinion, the cryoprotective mechanism of PHAs is even more complex and is not yet completely understood.

Previously we reported that PHB-accumulating bacterial strain *C. necator* H16 contains a 16.5-fold higher intracellular level of 3HB than its PHB non-accumulating mutant. We estimated the intracellular concentration of 3HB in PHB-accumulating strains to exceed 100 mM [16]. Considering the cryoprotective capacity of 3HB, a complete and functional PHB cycle might be a very important factor providing a naturally higher level of cryoprotectant in cytoplasm. This might substantially contribute to the greater freezing survival of PHB-producing bacterial strains. Nonetheless, it seems that *C. necator* H16 does not actively hydrolyze PHB granules (S1 Fig) to enhance intracellular concentration of 3HB when exposed to repeated freezing, which is in agreement with general expectation that the response of microbial cells to subzero temperatures is usually passive [4].

It is likely that the involvement of PHB in subzero temperature survival is much more complex still. Goh et al. observed that *E. coli* cells harboring PHA biosynthetic genes of *C. necator* but unable to mobilize PHAs exhibited higher stress resistance to oxidative stress [40]. This indicates that only the presence of intracellular PHA granules significantly changes the properties of bacterial cells and influences their stress survival.

Bonthrone et al. reported that intracellular native PHA granules do not comprise rigid, non-flexible, highly crystalized polymer, but are rather formed by highly mobile amorphous elastomer, which is reminiscent of supercooled liquid in terms of its properties [41]. This is in agreement with the extremely flexible behavior of PHB observed by Cryo-SEM (Fig 5). Despite the fact that cells of *C. necator* H16 were fractured at very low temperature (-140°C), we observed pull-out structures corresponding to the elongation of PHB granules of more than 100%. It should be noted that PHB isolated from bacterial cells rapidly crystallizes and its elongation-to-break is about 4% [8]. Hence, intracellular native PHB granules exhibit unique properties which might also provide physical protection of cells against the formation of ice crystals and shearing-stress associated with the freezing of extracellular water. Mazur et al. stated that expanding ice fields during extracellular water freezing results in a decrease in the sizes of unfrozen channels, which may cause shrinkage, deformation, and injury of the cells. PHB granules might represent a highly flexible scaffold protecting bacterial cells from such harm [7].

Our thermal analytical study of bacterial cells also provides some indications of the influence of PHB granules on the state of intracellular water. The shift in the melting endotherm in the MTDSC thermogram to higher temperature, which was observed for the culture containing PHB granules, cannot be revealed solely on the basis of the results of thermal analysis. Nevertheless, several suggestions can be made. One possible explanation is that this effect is related to an alteration of the adhesive forces between water and cellular components in the presence and absence of PHB. The stronger the adhesive force, the more the water molecules are "pulled out" from the ice crystals and the lower the temperature at which the ice melts. Therefore, it can be hypothesized that the "dilution" of the strongly hydrophilic species in the intracellular space by the less hydrophilic surfaces of PHB granules can partially lower the strength of the hydration of the remaining solutes. Deconvolution of the MTDSC signal leads to the similar conclusion. Stronger non-reversible component of the melting signal in the absence of PHB supports the assumption that the released water is more strongly attracted to the cellular components in these cultures than in PHB-containing bacteria.

Also the thermogravimetric analysis of the cell drying experiments revealed similar differences in the state of water between the PHB accumulating and non-accumulation cultures. It is evident from the critical points shown in Fig 6B that the relative content of the least strongly
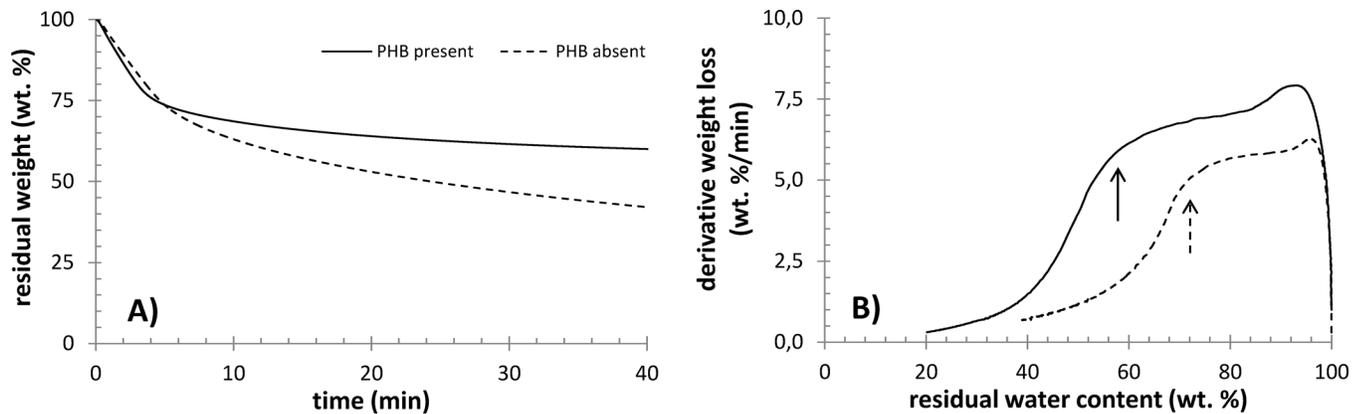
Fig 7. Results of isothermal TGA analysis of centrifuged PHB containing and PHB non-containing cultures of *C. necator*. A) Weight loss at 60°C, B) derivative weight loss as a function of residual water content (arrows indicate critical water content).

doi:10.1371/journal.pone.0157778.g007

bound form of water is higher in PHB-containing bacteria. The same conclusion can be drawn from the results of the isothermal drying experiment, which are presented in Fig 7. Comparison of Figs 6B and 7B indicates that the content of this form of water in the sample depends on the experimental conditions under which the drying occurred. This idea supports the assumption that this drying step is related to water which undergoes a kind of dynamic process such as transport through the cell membrane, desorption from the cell surface, etc.

In sum, the results of calorimetric and thermogravimetric analyses indicate that PHB-containing cells include water which can be more freely released from the cell either during drying or freezing. As discussed above, cell dehydration has diverse effects on cell survival according to the particular freezing conditions. When the cell faces severe dehydration, harmful solute effects cause the cell injury. On the other hand, when water release from the cell is completely suppressed, intracellular ice formation is not prevented and cell damage results from the rupture of the cell membrane. It is well documented that when the influence of the cooling rate is studied, the typical "inverted U" survival curve is obtained for a cell culture [7]. Obviously, a complex balance between the dynamics of external freezing stimuli (represented, for instance, by the rate of cooling) and cell response (the rate of dehydration) is needed in order to minimize the resulting cell mortality. Consequently, the effect of the presence of PHB granules on the state of water inside the cell and on the rate of its transmembrane transport may represent an important contribution to the overall cryoprotective strategy of PHB-producing bacteria.

Supporting Information

S1 Fig. Determination of PHB content (expressed as % of cell dry weight (CDW)) in *C. necator* H16 during freezing-thawing treatment (-30°C).
(DOCX)

S2 Fig. Results of the deconvolution of total MTDSC signals from Fig 5A into reversible (A) and non-reversible (B) components.
(DOCX)

Acknowledgments

Author Contributions

Conceived and designed the experiments: SO PS OS. Performed the experiments: SO PS VK FM KH DK PB. Analyzed the data: SO PS IM. Contributed reagents/materials/analysis tools: VK FM DK PB. Wrote the paper: SO PS VK OS IM.

References

1. De Maayer P, Anderson D, Cary C, Cowan DA. Some like it cold: understanding the survival strategies of psychrophiles. EMBO reports. 2014; 15: 508–517. doi: 10.1002/embr.201338170 PMID: 24671034

2. Hubalek Z. Protectants used in the cryopreservation of microorganisms. Cryobiology. 2003; 46: 205–229. PMID: 12818211

3. Fuller BJ. Cryoprotectants: The essential antifreezes to protect life in the frozen state. CryoLetters. 2004; 25: 375–388. PMID: 15660165

4. Panoff JM, Thammavongs B, Gueguen M, Boutibonnes P. Cold stress responses in mesophilicbacteria. Cryobiology. 1998; 36: 75–83. PMID: 9527869

5. Mori S, Choi J, Devireddy RV, Bischof JC. Calorimetric measurement of water transport and intracellular ice formation during freezing in cell suspension. Cryobiology. 2012; 65: 242–255. doi: 10.1016/j.cryobiol.2012.06.010 PMID: 22863747

6. Baek KH, Skinner DZ. Production of reactive oxygen species by freezing stress and the protective roles of antioxidant enzymes in plants. J Agric Chem Environ. 2012; 1: 34–40.

7. Mazur P. Freezing of living cells: mechanisms and implications. Am J Physiol. 1984; 247: C125–C142. PMID: 6383068

8. Sudesh K, Abe H, Do Y. Synthesis, structure and properties of polyhydroxyalkanoates: biological polyesters. Prog Polym Sci. 2000; 25: 1503–1555.

9. Kadouri D, Jurkevitch E, Okon Y. Ecological and agricultural significance of bacterial polyhydroxyalkanoates. Crit Rev Microbiol. 2005; 31: 55–67. PMID: 15986831

10. Ayub ND, Tribelli PM, Lopez NI. Polyhydroxyalkanoates are essential for maintenance of redox state in the Antarctic bacterium Pseudomonas sp. 14–3 during low temperature adaptation. Extremophiles. 2009; 13: 59–66. doi: 10.1007/s00792-008-0197-z PMID: 18931822

11. Iustman LJR, Ruiz JA. The alternative sigma factor σ^s, affects polyhydroxyalkanoate metabolism in *Pseudomonas putida*. FEMS Microbiol Lett. 2008; 284: 218–224. doi: 10.1111/j.1574-6968.2008.01203.x PMID: 18498401

12. Ayub ND, Pettinari MJ, Mendez BS, Lopez NI. The polyhydroxyalkanoate genes of a stress resistant Antarctic *Pseudomonas* are situated within a genomic island. Plasmid. 2007; 58: 240–248. PMID: 17629557

13. Pavez P, Castillo JL, Gonzales C, Martinez M. Poly-β-hydroxyalkanoate exert protective effect against carbon starvation and frozen coditions in *Sphingopyxischilensis*. Curr Microbiol. 2009; 59: 636–640. doi: 10.1007/s00284-009-9485-9 PMID: 19727947

14. Ciesielski S, Gorniak D, Mozejko J, Swiatecky A, Grzesiak J, Zdanowski M. The diversity of bacteria isolated from Antarctic freshwater reservoirs possessing the ability to produce polyhydroxyalkanoates. Curr Microbiol. 2014; 69: 594–603. doi: 10.1007/s00284-014-0629-1 PMID: 24939384

15. Goh YS, Tan IKP. Polyhydroxyalkanoate production by antarctic soil bacteria isolated from Casey Station and Signy Island. Microbial Res. 2012; 167: 211–219.

16. Obruca S, Sedlacek P, Mravec F, Samek O, Marova I. Evaluation of 3-hydroxybutyrate as an enzyme-protective agent against heating and oxidative damage and its potential role in stress response of poly (3-hydroxybutyrate) accumulating cells. Appl Microbiol Biotechnol. 2016; 100: 1365–1376. doi: 10.1007/s00253-015-7162-4 PMID: 26590589

17. Pinsirodom P, Parkin KL. Lipase assays. Current Protocols in Food Analytical Chemistry. 2001; C3.1.1–C3.1.13.

18. Obruca S, Petrik S, Benesova P, Svoboda Z, Eremka L, Marova I. Utilization of oil extracted from spent coffee grounds for sustainable production of polyhydroxyalkanoates. Appl Microbiol Biotechnol. 2014; 98: 5883–8590. doi: 10.1007/s00253-014-5653-3 PMID: 24652066

19. Coder DM. Assessment of Cell Viability. Current Protocols in Cytometry. 1997;9.2.1–9.2.14

20. Jendrossek D, Pfeiffer D. New insights in the formation of polyhydroxyalkanoate granules (carbonosomes) and novel functions of poly(3-hydroxybutyrate). Environ Microbiol. 2014; 16: 2357–2373. doi: 10.1111/1462-2920.12356 PMID: 24329995

21. Otun SO, Meehan E, Sheng Q, Craig DQM. The Use of quasi-isothermal modulated temperature differential scanning calorimetry for the characterization of slow crystallization processes in lipid-based solid self-emulsifying systems. Pharm Res. 2015; 32: 1316–1324. doi: 10.1007/s11095-014-1535-8 PMID: 25330742

22. Tamiya T, Okahashi N, Sakuma R, Aoyama T, Akahane T, Matsumoto JJ. Freeze denaturation of enzymes and its prevention with additives. Cryobiology. 1985; 22: 446–456. PMID: 2932302

23. Breda M, Vitolo M, Duranti MA, Pitombo RNM. Effect of freezing-thawing on invertase activity. Cryobiology. 1992; 29: 281–290.

24. Jain NK, Roy I. Effect of trehalose on protein structure. Protein Science. 2009; 18:24–36. doi: 10.1002/pro.3 PMID: 19177348

25. Raberg M, Voigt B, Hecker M, Steinbuchel A. A closer look on the polyhydroxybutyrate- (PHB-) negative phenotype of *Ralstonia eutropha* PHB-4. PLOS One. 2014; 9: e95907. doi: 10.1371/journal.pone.0095907 PMID: 24787649

26. Sudesh K, Fukui T, Iwata T, Doi Y. Factors affecting the freeze-fracture morphology of in vivo polyhydroxyalknoate granules. Can J Microbiol. 2000; 46: 304–311. PMID: 10779866

27. Seki S, Kleinhans FW, Mazur P. Intracellular ice formation in yeast cells vs. cooling rate: Predictions from modeling vs. experimental observations by differential scanning calorimetry. Cryobiology. 2009; 58: 157–165. doi: 10.1016/j.cryobiol.2008.11.011 PMID: 19118541

28. Uribelarrea JL, Pacaud S, Goma G. New Method for Measuring the Cell Water-Content by Thermogravimetry. Biotechnol Lett. 1985; 7: 75–80.

29. Roberts MF. Organic compatible solutes of halotolerant and halophilic microorganisms. Saline Systems. 2005; 1: 5. PMID: 16176595

30. Pastor JM, Salvador M, Argandona M, Bernal V, Reina-Bueno M, Csonka LN, et al. Ectoines in cell stress protection: uses and biotechnological production. Biotechnol Adv. 2010; 28: 782–801. doi: 10.1016/j.biotechadv.2010.06.005 PMID: 20600783

31. Sorokulova I, Olesen E, Vodyanoy V. Biopolymers for sample collection, protection, and preservation. Appl Microbiol Biotechnol. 2015; 99: 5397–5406. doi: 10.1007/s00253-015-6681-3 PMID: 25982001

32. Goller K, Galinski EA. Protection of a model enzyme (lactate dehydrogenase) against heat, urea and freeze-thaw treatment by compatible solutes additives. J MolCatal B: Enzym. 1999; 7: 37–45.

33. Van-Thuoc D, Hashim SO, Hatti-Kaul R, Mamo G. Ectoine-mediated protection of enzyme from the effect of pH and temperature stress: a study using *Bacillus halodurans* xylanase as a model. Appl Microbiol Biotechnol. 2013; 97: 6271–6278. doi: 10.1007/s00253-012-4528-8 PMID: 23132342

34. Soto G, Setten L, Lisi C, Maurelis C, Mozzicafreddo M, et al. Hydroxybutyrate prevents protein aggregation in the halotolerant bacterium *Pseudomonas* sp. CT13 under abiotic stress. Exremophiles. 2012; 16: 455–462.

35. Mazur P. Cryobiology–Freezing of biological systems. Science. 1970; 168:939–949. PMID: 5462399

36. Andersson MM, Breccia JD, Hatti-Kaul R. Stabilizing effect of chemical additives against oxidation of lactate dehydrogenase. Biotechnol Appl Biochem. 2000; 32: 145–153. PMID: 11115385

37. Ruiz JA, Lopez NI, Fernandez RO, Mendez BS. Polyhydroxyalkanoate degradation is associated with nucleotide accumulation and enhances stress resistance and survival of *Pseudomonas oleovorans* in natural water microcosm. Appl Environ Microbiol. 2001; 67: 225–230. PMID: 11133449

38. Brigham CJ, Speth DR, Rha CK, Sinskey AJ. Whole-genome microarray and gene deletion studies reveal regulation of the polyhydroxyalkanoate production cycle by the stringent response in *Ralstonia eutropha* H16. Appl Environ Microbiol. 2012; 78: 8033–8044. doi: 10.1128/AEM.01693-12 PMID: 22961894

39. Mezzina MP, Wetzler DE, de Almeida A, Dinjaski N, Prieto MA, Pettinari MJ. A phasin with extra talents: a polyhydroxyalkanoates granule-associated protein has chaperone activity. Environmental Microbiology. 2015; 17: 1765–1776. doi: 10.1111/1462-2920.12636 PMID: 25297625

40. Goh L-K, Purama RK, Sudesh K, Hunter BK, Sanders JKM. Enhancement of Stress Tolerance in the Polyhydroxyalkanoate Producers without Mobilization of the Accumulated Granules. Applied Biochemistry and Biotechnology. 2014; 172(3): 1585–1598. doi: 10.1007/s12010-013-0634-z PMID: 24233544

41. Bonthrone KM, Clauss J, Horowitz DM, Hunter BK, Sanders JKM. The biological and physical chemistry of polyhydroxyalkanoates as seen by NMR spectroscopy. FEMS Microbiology Letters. 1992; 103(2–4): 269–277.

Appendix 17

Sedlacek, P., Slaninova, E., Koller, M., Nebesarova, J., Marova, I., Krzyzanek, V., and Obruca, S. PHA granules help bacterial cells to preserve cell integrity when exposed to sudden osmotic imbalances. *New Biotechnology* **2019**, 49, 129–136..
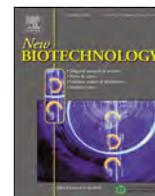
Full length article

PHA granules help bacterial cells to preserve cell integrity when exposed to sudden osmotic imbalances

Petr Sedlacek[a], Eva Slaninova[a], Martin Koller[b,c], Jana Nebesarova[d,e], Ivana Marova[a],
Vladislav Krzyzanek[f], Stanislav Obruca[a,*]

[a] Faculty of Chemistry, Brno University of Technology, Purkynova 118, 612 00, Brno, Czech Republic
[b] Institute of Chemistry, NAWI Graz, University of Graz, Heinrichstrasse 28/III, 8010, Graz, Austria
[c] ARENA Arbeitsgemeinschaft für Ressourcenschonende & Nachhaltige Technologien, Inffeldgasse 21b, 8010, Graz, Austria
[d] The Czech Academy of Sciences, Biology Centre, v.v.i., Branisovska 31, 370 05, Ceske Budejovice, Czech Republic
[e] University of South Bohemia, Faculty of Science, Branisovska 31, 370 05, Ceske Budejovice, Czech Republic
[f] The Czech Academy of Sciences, Institute of Scientific Instruments, v.v.i., Kralovopolska 147, 612 64, Brno, Czech Republic

ARTICLE INFO

ABSTRACT

Polyhydroxyalkanoates (PHA) are microbial polyesters which accumulate as intracellular granules in numerous prokaryotes and mainly serve as storage materials; beyond this primary function, PHA also enhance the robustness of bacteria against various stress factors. We have observed that the presence of PHA in bacterial cells substantially enhances their ability to maintain cell integrity when suddenly exposed to osmotic imbalances. In the case of the non-halophilic bacterium *Cupriavidus necator*, the presence of PHA decreased plasmolysis-induced cytoplasmic membrane damage during osmotic up-shock, which subsequently enabled the cells to withstand subsequent osmotic downshock. In contrast, sudden induction of osmotic up- and subsequent down-shock resulted in massive hypotonic lysis of non-PHA containing cells as determined by Transmission Electron Microscopy and Thermogravimetrical Analysis. Furthermore, a protective effect of PHA against hypotonic lysis was also observed in the case of the halophilic bacterium *Halomonas halophila*; here, challenged PHA-rich cells were capable of retaining cell integrity more effectively than their PHA-poor counterparts. Hence, it appears that the fact that PHA granules, as an added value to their primary storage function, protect halophiles from the harmful effect of osmotic down-shock might explain why PHA accumulation is such a common feature among halophilic prokaryotes. The results of this study, apart from their fundamental importance, are also of practical biotechnological significance: because PHA-rich bacterial cells are resistant to osmotic imbalances, they could be utilized in *in-situ* bioremediation technologies or during enrichment of mixed microbial consortia in PHA producers under conditions of fluctuating salinity.

Introduction

The osmotic strength of the environment is one of the crucial physical parameters which determine the capability of bacteria to survive and grow in a given habitat. Increase in extracellular osmolarity induces transport of water from the bacterial cells, which results in dehydration of cytoplasm and damage to the plasma membrane when massive plasmolysis occurs [1]. Sudden subsequent exposure of osmotically challenged cells to a hypotonic environment induces rapid transport of water into the cells, accompanied by an increase in their volume. Since the plasma membrane of the bacterial cells is at least partially damaged by plasmolysis, sudden hypotonic shock usually results in so called hypotonic lysis, which is accompanied by destruction of the structure of the challenged microbial cell [1,2]. Rapid fluctuations in extracellular osmolarity is a common feature of numerous environments, and bacteria have developed various strategies how to cope with hypertonic and hypotonic conditions [3]. The most common strategy is biosynthesis or accumulation of osmolytes under hypertonic conditions and their subsequent release under hypotonic conditions [4,5]. Under the latter, osmolytes as well as other intracellular solutes and water are released by so called "mechanosensitive channels", which are, to some extent, able to protect bacterial cells from losing their

---

integrity under osmotic down-shock [6,7].

Polyhydroxyalkanoates (PHA) are microbial polyesters, which accumulate as intracellular granules in numerous prokaryotes [8]. These materials serve primarily for internal storage of carbon and energy, but their biological function is far more comprehensive; it has been recently summarized that PHA enhance cell robustness and resistance of bacteria against various stress factors [9]. For example, the presence of PHA in bacterial cells influences water efflux from bacterial cells, which protects them against damage caused by intracellular ice formation during freezing [10]. Moreover, PHA monomers generated by the PHA metabolism are potent chemical chaperones, which protect enzymes and other biological molecules from the harmful effects of oxidative pressure and high temperature [5]. In addition, PHA also scatters UV irradiation, thus providing UV-protective function [11]. Finally, we have recently reported that PHA protect non-halophilic bacteria against adverse effects of osmotic up-shock by reducing the level of plasmolysis and membrane damage in challenged cells [12]. Moreover, a potential complex osmo-protective effect of PHA is indirectly evidenced by the fact that numerous halophiles including extremely halophilic Archea such as *Haloferax mediterranei* [13], *Halogeometricum borinquense* [14], or *Natrinema ajinwuensis* [15], which are capable of accumulation of substantial amounts of PHA [16]. Here we aimed at evaluating a potential protective effect of PHA for both non-halophilic and halophilic bacterial cells when exposed to sudden osmotic down-shock.

Materials and methods

Microorganisms

The PHA-producing bacterial strains *Cupriavidus necator* H16 (CCM 3726) and *Halomonas halophila* CCM 3662 were obtained from the Czech Collection of Microorganisms, Brno, Czech Republic. The PHA non-producing mutant strain *Cupriavidus necator* PHB-4 (DMS-541) was obtained from the Leibnitz Institute DSMZ-German Collection of Microorganism and Cell Cultures, Braunschweig, Germany.

Cultivations, hyperosmotic and hypo osmotic challenges

The cultivations were performed in Erlenmeyer flasks (volume 250 mL) containing 100 mL of particular cultivation media. To obtain PHA-rich phenotypes of the tested PHA accumulating strains, nitrogen-limited Mineral Salt (MS) cultivation medium supporting PHA accumulation was used [17]. Composition of MS medium for *C. necator* is described elsewhere [12]. For *H. halophila*, fructose was replaced by glucose in the MS medium, and 66 g NaCl per 1 L was added to induce hyperosmotic conditions required by this strain. When low intracellular PHA content was required, complex nitrogen-rich media were used. In this case, *C. necator* was cultivated in complex Nutrient Broth medium (10 g peptone, 10 g beef extract, 5 g NaCl per 1 L of distilled water). The composition of complex medium used for *Halomonas halophila* was: 15 g peptone, 3 g yeast extract, 66 g NaCl, and 1 g glucose in 1 L of distilled water.

The flasks were inoculated with 5 mL of the overnight culture of the individual strain grown in particular complex media. The cultivations were performed for 72 h at 30 °C under constant shaking (180 rpm) in a rotary incubator. When the cultivation was completed, the biomass concentration was measured gravimetrically and the PHA content in cell biomass was analyzed by GC-FID as reported previously [18]; subsequently, the cells were exposed to osmotic challenges.

Cells of *C. necator* H16 and *C. necator* PHB-4 were harvested by centrifugation (5000 × g, 5 min), washed with phosphate buffer saline (PBS; pH 7.4, 50 mM), centrifuged again and exposed to various concentrations of NaCl - 0, 50, 100 and 200 g/L of phosphate buffer. After exposure to hyperosmotic conditions (2 h at 30 °C), the cells were separated by centrifugation and exposed to subsequent osmotic down-shock induced by re-suspension in deionized water, and incubation

under permanent shaking for 1 h at 30 °C. Osmotic down-shock challenge exerted on *H. halophila* cells consisted of separation of the cells from cultivation media by centrifugation (5000 × g, 5 min) and subsequent replacement of cultivation media by deionized water. Thereafter, the prepared cells were subjected to analysis as described below.

Determination of cell viability

Cell viability of *C. necator* cultures after osmotic challenge was assessed by flow cytometry (Apogee A50, Apogee, GB) using a membrane integrity assay employing propidium iodide staining. The protocol described in [19] was employed.

The number of viable cells (CFU per mL) for *H. halophila* before and after osmotic down-shock challenge was determined by standard dilution plating assay on Petri dishes with complex medium agar, where the colonies were counted after 48 h of incubation in thermostat at 30 °C (three replicates).

Thermogravimetric and Transmission electron microscopy (TEM) analysis of bacterial cells

For qualitative and quantitative analysis of the dehydration of bacterial cells after cultivation and/or osmotic challenge, a thermogravimetric (TGA) analyzer Q5000 (TA Instruments) was used. Prior to the TGA analysis, the dispersion of the bacterial culture was centrifuged (5 min, 14,800 rpm) and the supernatant was discarded. Approximately 15 mg of the remaining cell suspension was weighed on the aluminium TGA pan. In the TGA analyzer, the pan with sample was heated instantantly to 70 °C and the weight of the sample was continuously recorded at this temperature for 40 min. After that, the temperature was further raised to 200 °C and the sample was held at this temperature for another 10 min to determine its dry mass. Every sample was measured in at least three replicates; for each measurement, a fresh bacterial culture was prepared. In order to determine critical water contents, analyses of thermograms were performed according to [20]. In this experimental aproach, the loss of water is attributed to the specific intracellular or extracellular region. More details on the data analysis approach are presented in the Results section.

Samples of the challenged and non-challenged bacterial cultures were visualized using Transmission Electron Microscope JEOL 1010 following the protocol described in our previous reports [12,17].

Results

Viability assay of osmotically challenged cells of C. necator

Various cultures of *C. necator* with different PHA content were exposed to osmotic up-shock induced by 200 g/L NaCl followed by sudden subsequent osmotic down-shock by replacement of NaCl-rich buffer by deionized water. After this substantial osmotic imbalance challenge, the total number of bacterial cells as well as the ratio of viable/dead cells was determined by flow cytometry and compared with non-challenged cultures. The results are demonstrated in Fig. 1.

The highest overall mortality, accompanied by considerable decrease of cell numbers caused by massive hypotonic lysis of the cells, was observed for the PHA-free culture of *C. necator* PHB-4. In this case, only 2% of the cells of the original population were capable of maintaining cell integrity when exposed to subsequent osmotic up- and down-shock. Among these non-disrupted cells, 20% were evaluated as non-viable. A very similar effect of osmotic challenge was observed in *C. necator* H16 cultivated in nitrogen-rich medium, which resulted in a PHA content of 1.6% of cell dry mass. In this case, the total number of cells after complete osmotic challenge (up- and down-shock) fell to 7.5% of its original value, and the proportion of non-viable cells in the challenged culture was about 43%. In contrast, when PHA-rich cells of
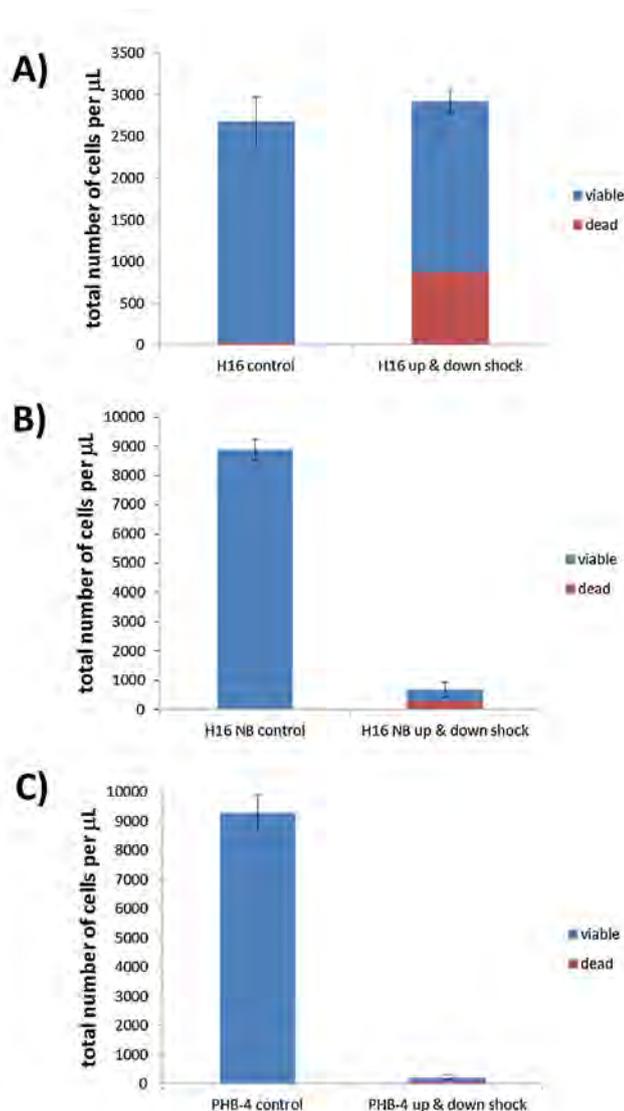
Fig. 1. Results of viability assay performed by flow cytometry. Comparison of number of detected cells (viable vs. dead) in 1 μL for the control and osmotically challenged (up & down shocked) cells of *C. necator* H16 cultivated in mineral medium (A), *C. necator H16* cultivated in nutrient broth medium (B) and for *C. necator* PHB-4 cultivated in mineral medium (C).

C. necator H16 cultivated in nitrogen limited medium (PHA content of 74% of cell dry mass) were exposed to rapid and massive changes in external osmolarity, no decrease in cell counts caused by hypotonic cell disruption was observed, and the proportion of dead cells was about 30%. These data indicate that the presence of intracellular PHA granules protected bacterial cells from adverse effect of rapid fluctuations in external osmolarity.

Thermal analysis of challenged bacterial cells of C. necator

Isothermal thermogravimetry was used primarily to monitor osmotically induced changes in intracellular water content and to reveal possible effects of altered cell integrity of the osmotically challenged cells on the rate of transmembrane movement of intracellular water during the drying process. The method of determination of intracellular water content based on the isothermal TGA was originally designed by Uribelarrea et al. [20], who proposed that in the drying rate curve, when plotted as a function of the residual mass of the cells (or residual

water content), individual stages of the drying process (i.e., drying of extracellular and intracellular water, respectively) can be distinguished as they are represented by respective curve sections with different curve trends. Thus, the critical water content, i.e., the water content at which the drying rate curve suddenly changes its course, represents the moment when a change in the mechanism of the drying process occurs.

The results of isothermal drying TGA analysis performed for all tested *C. necator* species at 70 °C are shown in Fig. 2. In Fig. 2a, an example of a raw thermogram (residual mass of the sample as a function of time) is shown for *C. necator* H16 cultivated in mineral (i.e., nitrogen limited) medium. In all drying rate curves (shown in Fig. 2b-d), residual water content is represented as g of water per g of cell dry mass (determined as residual mass reached during the post-drying step at 200 °C). Fig. 2b shows the drying kinetics of *C. necator* H16 cultivated in nitrogen limited medium (black curve) at different stages of the osmotic challenge. The drying rate curve shown for the osmotically non-challenged cells (black) displays the typical three-stage dependency described and explained in [20,21]. The first stage (I.– II.) is characterized by a sudden increase in the drying rate as the sample equilibrates at the drying temperature in TGA analyzer. The next stage (II. – III.) represents evaporation of extracellular water. The drying rate (water loss per time) during this stage is almost constant as the process reflects loss of free (i.e., unbound) water from surface. At the critical water content, represented by point III. in the drying rate curve, the drying rate begins to decrease rapidly as the more tightly bound surface water and the intracellular water begins to evaporate. This critical water content represents the main quantitative outcome of the isothermal TGA drying analysis.

From the comparison of drying rate curves of reference *C. necator* H16 strain with the osmotically up-shocked sample, it is evident that the cell dehydration, induced by the hyperosmotic conditions, manifests itself in significant decrease of the critical water content in the drying rate curve. Similar shifts in the critical water content at hyperosmotic conditions were found also in the case of *C. necator* strains with minor content of PHA, i.e., for *C. necator* H16 strain cultivated in nitrogen-rich medium and also for the PHA-free mutant strain *C. necator* PHB-4 (see Fig. 2c, d). It is evident that for both strains the absolute value of critical water content is significantly higher compared to PHA accumulating strain H16. This applies for the unchallenged as well as for the osmotically up-shocked cells, and is clearly attributed to great increase in cell dry mass caused by accumulated PHA in *C. necator* H16 cultivated in nitrogen-poor medium.

The most interesting differences between the three tested *C. necator* cultivation setups were found when the bacteria were first subjected to osmotic up-shock in NaCl-rich medium and then transferred to deionized water. This sudden hypoosmotic shock resulted in strongly different behavior of PHA containing cells compared to cells with minor or no PHA content. *C. necator* H16 strain with a high content of PHA in the cells hydrated to some extent as it is represented by a shift of critical water content to a higher value. The critical water content of the osmotically challenged PHA containing cells was always lower compared to the reference (unchallenged cells). This could indicate a change in barrier properties of the cell membranes or in cell ultrastructure, but the actual reason of this irreversibility of hyper/hypo osmotic challenge in the behavior of PHA accumulating cells cannot be revealed without further experimental study. Completely different drying rate curves were measured for PHA-free cells. It is evident that the drying rate curve of *C. necator* PHB-4 after the osmotic up- and down-shock lost the typical three-stage shape. There was no critical water content where a sudden change in the drying kinetics could be observed. This indicates that there is no barrier effect remaining which would make a difference between the rate of loss of water from inside and outside the cells. However, it is very likely that this change in the shape of the drying rate curve is a consequence of osmotically induced membrane damage and loss of cell integrity. A similar, though less profound, trend was found also for low PHA content in *C. necator* H16 cells (see Fig. 2c). In contrast
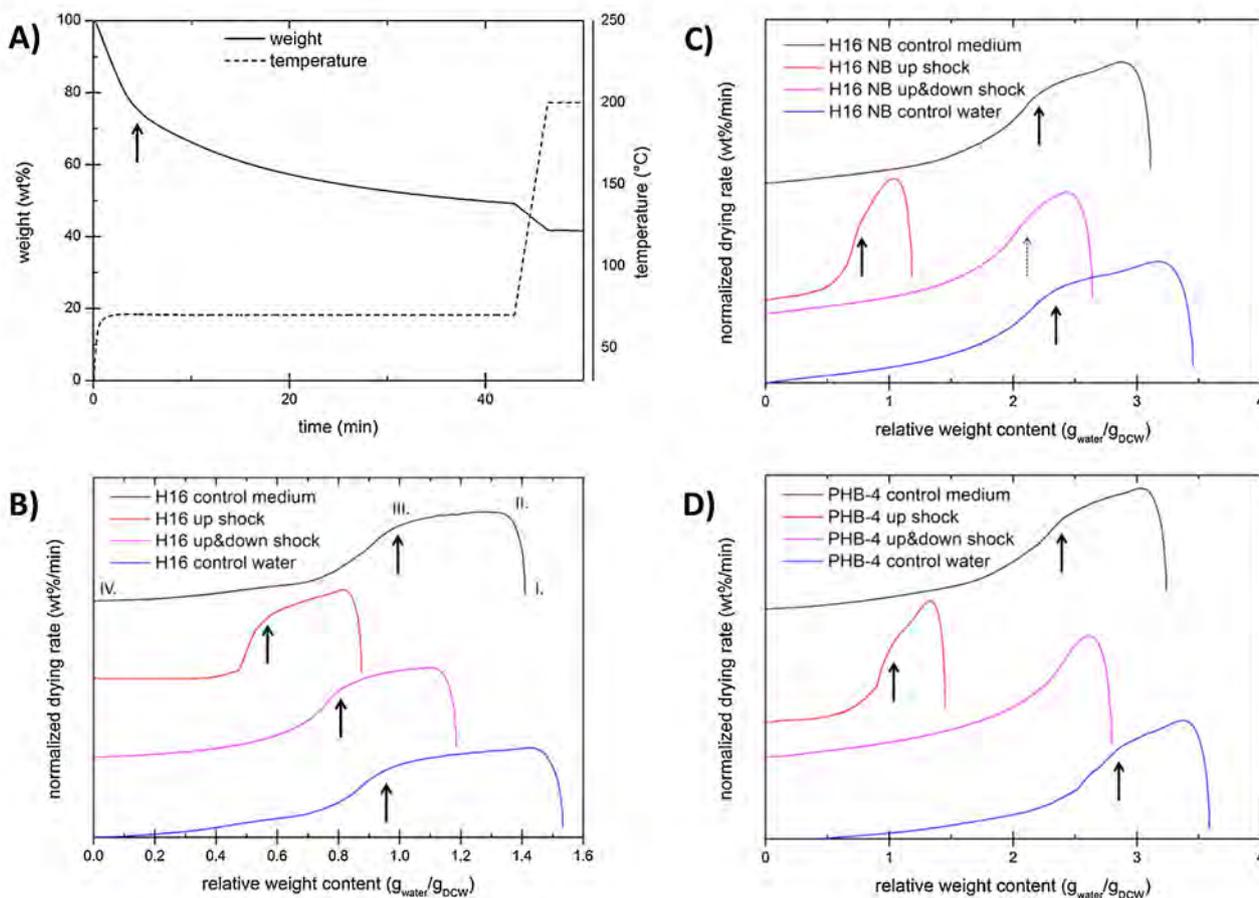
Fig. 2. Results of isothermal thermogravimetry presented as an example of raw thermogram for *C. necator* H16 after cultivation in mineral medium (A) and as individual series of drying rate curves for *C. necator* H16 cultivated in mineral medium (B), *C. necator* H16 cultivated in nutrient broth medium (C) and *C. necator* PHB-4 cultivated in mineral medium (D), respectively. In graphs (B) – (D), drying rate curves are shown for fresh cells after cultivation (black), for cells after hyperosmotic treatment in 200 g/L NaCl (red) and after additional hypoosmotic treatment in deionized water (violet). For comparison, drying rate curve for hypoosmotically challenged cells without previous hyperosmotic step are also shown (blue). Drying rate curves are offset for clarity.

to the PHA-free *C. necator PHB-4* strain, the drying rate curve of this low PHA content strain maintained the concave shape. Nevertheless, it can be seen that the critical water content disappeared as the initially rather detached drying of intracellular and extracellular water are overlapping. For greater clarity of the changes in the drying curve induced by the osmotic up- and down-shocks, the results are shown also in the normalized form in supplementary material (see Figure S1a-c). Beyond the results shown in Fig. 2, an influence of the extent of hyperosmotic challenge was also tested. For this purpose, the osmotic up-shock of the *C. necator* cultures was performed with differently concentrated NaCl solutions (50, 100 and 200 g/L NaCl, respectively). The results show that the higher the NaCl concentration during the hyperosmotic treatment, the more pronounced were the negative impacts on the drying rate curves of *C. necator* cultures with low or no PHA content after their subsequent hypoosmotic treatment in deionized water (see Figure S1 d–f).

Transmission electron microscopy (TEM) of osmotically challenged cells of C. necator

In order to explain the changes in water transport (drying) behavior of osmotically challenged cells revealed by thermogravimetry, morphological changes induced by individual steps of the osmotic challenge were observed by TEM for all tested *C. necator* cultures (see Figs. 3 and 4 and Fig. S2 in supplementary material). As can be seen in Fig. 3, no

lethal changes in cell morphology were found for PHA accumulating cells; osmotic up-shock caused only mild plasmolysis in these cells. Furthermore, significant coalescence of PHA granules resulting from the high osmolality was also confirmed, which may indicate a negative effect of the osmotic up-shock on the physiological state of the granule bound proteins. As demonstrated for the first time by the present study, no additional negative impacts on cell morphology of previously up-shocked PHA containing cells were revealed after the subsequent hypoosmotic challenge. On the contrary, severe harmful effects caused by the osmotic imbalances were observed in cells of non-PHA accumulating *C. necator* cultures. As can be seen in Fig. 4, osmotic up-shock of *C. necator* PHB-4 resulted in massive plasmolysis. Furthermore, as previously discussed [12], not only the total extent but also some interesting qualitative differences were found for the plasmolysis of up-shocked PHA accumulating and non-accumulating cells, respectively. Contrary to the symmetrical plasmolysis observed for PHA containing cells, both cultures cultivated with no or low content of PHA showed highly asymmetric formation of periplasmatic space accompanied by the formation of endocytotic vesicles in some bacterial cells and the formation of tubular structures and Scheie structures as described by [22]. In some cells, "hole-like" structures (reminiscent of incompletely formed endocytotic vesicles) randomly distributed in the outer volume of bacterial cell cytoplasm were observed. This asymmetric plasmolysis caused severe damage to the cytoplasmic membrane, as it was further confirmed by the subsequent osmotic down-shock of the cells. It can be
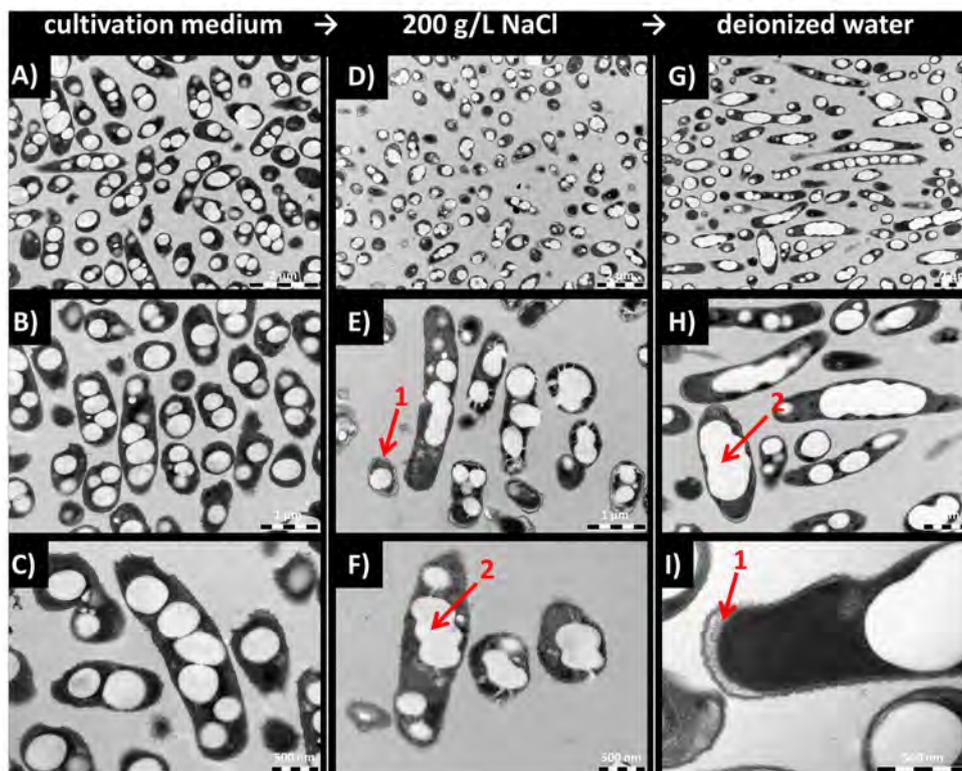
Fig. 3. TEM micrographs of *C. necator* H16 observed under different magnifications after cultivation in mineral medium (A – C), after hyperosmotic treatment in 200 g/L NaCl (D–F) and after additional hypoosmotic treatment in deionized water (G–I). Mild plasmolysis (1) and coalescence of PHB granules (2) is labeled in the pictures.

seen in Fig. 4 and S2 that PHA non-accumulating cells, after combined subsequent osmotic up- and down-shock, showed numerous aspects of cell damage. First, massive leakage of the cytoplasm was confirmed for PHA non-containing cells after their exposure to osmotic down-shock. Numerous cells were observed only as depletive cell envelopes. In the other cells, massive plasmolysis was maintained and the compact, but seriously deformed cytoplasmatic space was observed. In case of *C. necator* H16 culture cultivated in nitrogen-rich medium (see Figure S2), even in this medium some of the cells accumulated a significant amount of PHA. In agreement with general comparison of PHA accumulating and non-accumulating cultures exposed to suddenly induced hypotonic conditions, these individual PHA containing cells revealed much less intense negative impacts of fluctuation of osmolality on the cell morphology. The results of TEM confirmed conclusively that the different drying behavior of PHA accumulating and non-accumulating cells is a result of damage of the cell membrane caused by the fluctuation in osmolality. When the osmolality is suddenly increased and decreased, PHA containing cells are able to maintain cell integrity to a much greater extent compared to cells without PHA.

The effect of osmotic down-shock on the halophilic bacterium Halomonas halophila

In previous experiments, it was confirmed that for the non-halophilic bacterium *C. necator*, presence of PHA in the cells provides a protective effect against the harmful impacts of sudden osmotic imbalances. To test whether this protective effect can be observed also for halophilic bacteria, the above introduced methodology was used in the study of hypoosmotic challenge of *Halomonas halophila*. Previously, this halophile was proposed as a promising candidate for biotechnological production of PHA [17]. To be able to reveal an influence of the PHA

presence, *H. halophila* was cultivated in parallel in mineral and in complex cultivation media. In mineral medium, a high intracellular content of PHA was accumulated (up to 82%, see [17]), while in complex medium, only a low amount of PHA was detected (approx. 4%).

The hypoosmotic challenge of the PHA accumulating and non-accumulating cells was introduced by transferring them from their optimal osmolality (provided by 66 g/L NaCl to deionized water. The initial focus was on viability of the cells after the down-shock. Flow cytometry was found to be inappropriate for the determination of cell viability/mortality, because it was experimentally confirmed that the staining of the cells with propidium iodide is not efficient under the conditions of high salinity necessary for the tested bacteria. As an alternative experimental approach, analysis of colony forming units (CFU/mL) was employed. By this technique, a far higher mortality was revealed for osmotically down-shocked culture with low PHA content than for the PHA accumulating organisms. While for the PHA accumulating culture CFU decreased by one order of magnitude (from 10^9 in control to 10^8 in down-shocked sample), the decrease in CFU was several times higher for the non-accumulating culture (from 10^9 in control to 10^4).

Again, the results of thermal analysis confirmed the differences in drying behavior of *H. halophila* cultures with high and low PHA content, respectively. In Fig. 5 it can be seen that the cultures from mineral medium (high PHA content) maintained the typical profile even after osmotic down-shock. On the other hand, it can be seen that the drying rate curve for the down-shocked bacteria cultivated in complex medium (low PHA content) appears different. First, even if the sampling was similar to other cultures, it can be seen that the drying rate curves started at much higher relative weight content of water (see the inset in Fig. 5). This is because the sediment obtained by centrifugation of the
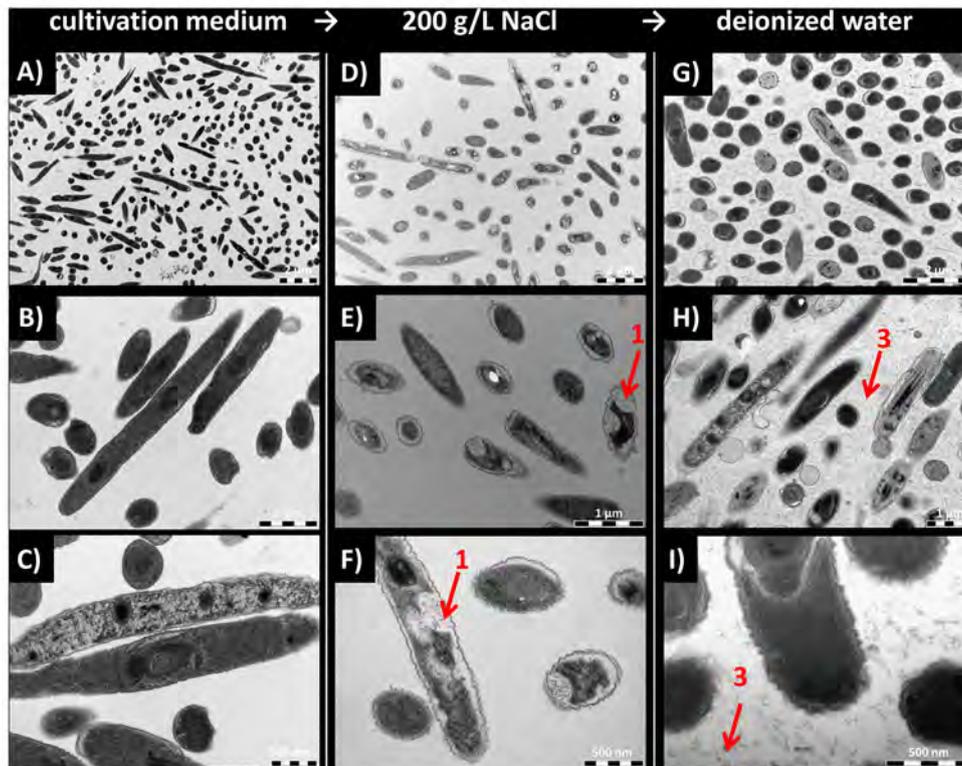
Fig. 4. TEM micrographs of *C. necator* PHB-4 observed under different magnifications after cultivation in mineral medium (A – C), after hyperosmotic treatment in 200 g/L NaCl (D–F) and after additional hypoosmotic treatment in deionized water (G–I). Severe plasmolysis (1) and leakage of the cytoplasmatic content (3) is labeled in the pictures.
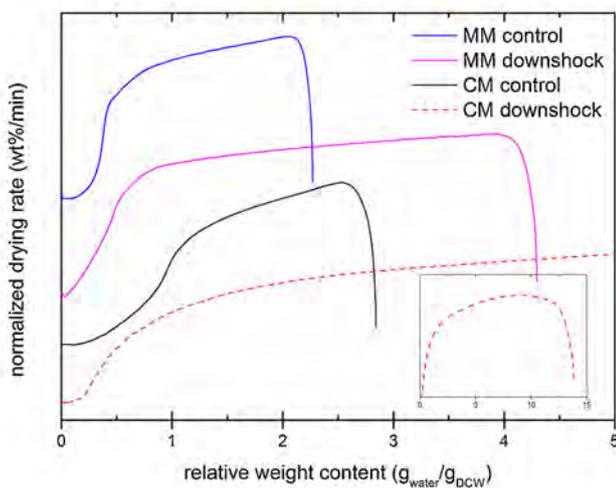
Fig. 5. Isothermal drying curves for *H. halophila* cultivated in mineral medium (blue: control, violet: osmotic down shock provided by treatment in deionized water) and in complex medium (black: control, dashed red: osmotic down shock provided by treatment in deionized water).

down-shocked culture with low PHA content contained significantly lower dry mass compared to all other tested samples (about 5 wt. % compared to at least 20 wt. % for all other *C. necator* and *H. halophila* samples). Furthermore, the drying rate remained similar and incomparably high (5–10 times, not seen in the normalized curves shown in Fig. 5) almost all along the drying process. This indicates that *H.*

halophila cells with low PHA content may be substantially damaged by the hypoosmotic challenge and that the drying process therefore occurs without any observable effect of the cell residues on the rate of the water loss. This assumption was further confirmed by TEM results, where the severe damage of the *H. halophila* cells cultivated in complex medium can be clearly observed (see Fig. 6). Similar to down-shocked PHA-free *C. necator* cells, a high number of hypoosmotically challenged *H. halophila* cells are observed as empty cell envelopes, which indicates fatal damage of the plasma membrane. Again, a higher presence of PHA granules in the cells provided significant protection against this morphological harm.

Discussion

Prokaryotes are known to have extreme adaptability to various stress conditions. Fluctuations in external osmolarity belong among very common environmental stress factors associated with numerous habitats. For instance, during dry or rainy periods, soil bacteria are repeatedly exposed to osmotic up- and down-shocks [1]. Further, some microorganisms are also capable of adapting to constant high salt concentrations. So called "halophiles" inhabit naturally salty environments, extremely halotolerant microorganisms are even able to survive and prosper at NaCl concentrations reaching values of saturated salt solution [23].

Apart from well described protective strategies to cope with osmotic imbalances (such as an accumulation or excretion of compatible solutes), which are exhaustively reviewed for instance by [1,23], there are reports that accumulation of intracellular PHA granules also substantially increases survival rate of bacteria when exposed to osmotic up-shock challenges [24–26]. We have recently investigated the protective effect of PHA granules for the non-halophilic bacterium *C.*
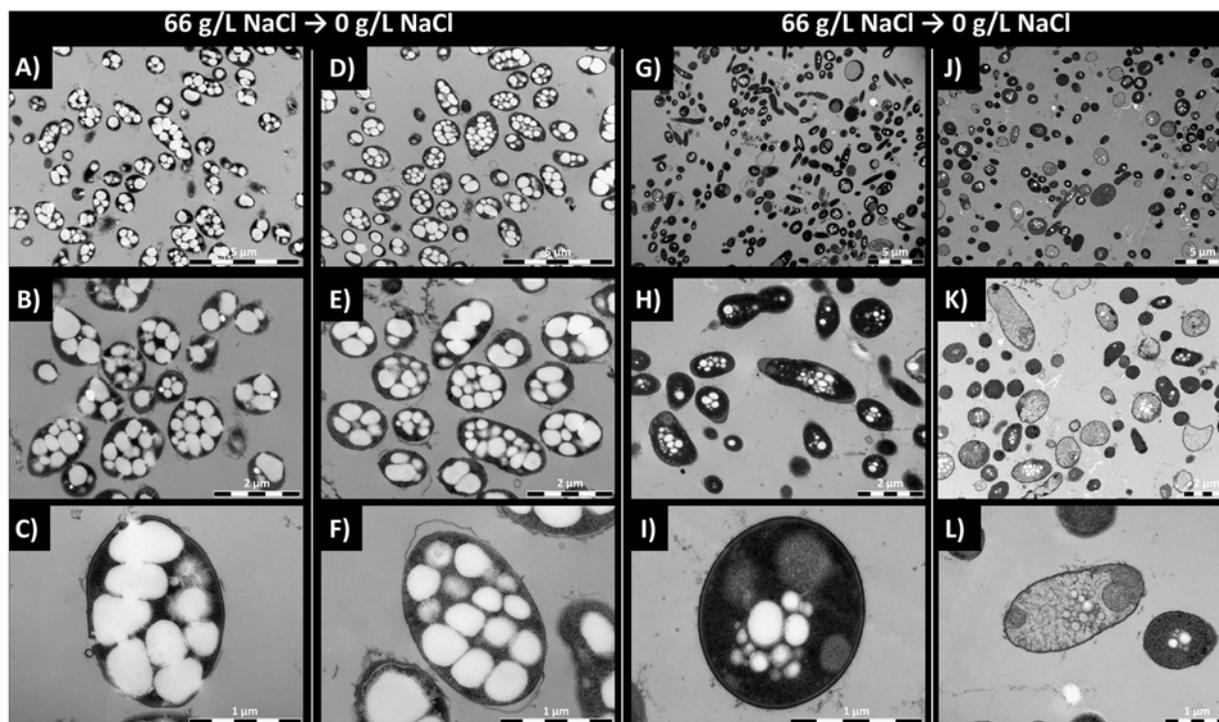
Fig. 6. TEM micrographs of the halophilic bacterial strain *H. halophila* cells after cultivation in mineral medium (A–C) and complex medium (G–I), respectively. Both cultures were kept at optimal osmolality provided by 66 g/L NaCl solution. Same cultures after hypoosmotic shock provided by treatment with deionized water (G–I and J–L for H. halophila cultivated in mineral and complex media, respectively).

necator when exposed to osmotic up-shock. Surprisingly, osmotic up-shock induced by NaCl did not initiate PHA hydrolysis to provide carbon and energy covering expenses of stress response [12]. Nevertheless, since PHA represent about 30 vol. % of bacterial cells cytoplasm [27], almost water-free PHA granules act as hydrophobic scaffolds which substantially reduce level of cytoplasm shrinkage as a consequence of cell dehydration, which caused substantially lower degree of plasmolysis. Moreover, PHA granules as a result of their "liquid-like" properties probably partially repair and stabilize cell membranes by plugging small gaps formed by plasmolysis. Therefore, PHA rich cells demonstrated a considerably lower level of cytoplasmic membrane damage than PHA non-accumulating mutant cells when exposed to hyperosmotic conditions [12]. Hence, it seems that PHA represents an important metabolite, which significantly contributes to robustness of bacterial cells against osmotic up-shock.

To complete knowledge on PHA´s role in protective effect against osmotic fluctuations, this work aimed at evaluating their protective function under subsequently applied hypotonic conditions. The results clearly indicate that a capability of PHA accumulation and intracellular PHA content are important parameters protecting non-halophilic bacteria exposed to hypotonic shock. Survival rate of PHA-rich *C. necator* H16 (PHA content of 74% of CDM) exposed to osmotic challenge was much higher than that of PHA non-accumulating mutant *C. necator* PHB-4 or PHA-poor *C. necator* H16 cells cultivated in complex medium (PHA content about 1.6 wt. % of CDM) (see Fig. 1). Moreover, results obtained by TGA (Fig. 2) and TEM analysis (Figs. 3,4,5) demonstrated that the presence of PHA granules in bacteria is essential for them to maintain cell integrity when suddenly confronted with hypotonic conditions. In other words, presence of PHA granules in non-halophilic bacterial cells considerably decreases their susceptibility to hypotonic lysis. The main reason could be a much lower level of cytoplasm membrane damage in PHA-rich cells caused during the first step of complex osmotic challenge - osmotic up-shock. When cells are

subsequently suddenly exposed to hypotonic conditions, PHA-rich cells with less or even non-damaged cytoplasmic membranes are capable of maintaining cell integrity *via* the action of appropriate pumps and mechanosensitive channels. In contrast, PHA–free cells or cells with low PHA content are unable, due to plasmolysis induced membrane damage, to compensate/control water influx and inevitably lose their cell integrity. As far as we are aware, this is the first report describing and explaining the protective role of PHA in non-halophilic bacterial cells facing hypotonic shock, since all previous works focused on exposure of mesophilic bacterial cells to hypertonic conditions [12,24–26]

Furthemore, using *H. halophila* as model halophilic strain, it was also demonstrated that the presence of PHA granules has beneficial consequences for the tested halophilic strain when exposed to sudden and massive osmotic down-shock. Generally, halophiles are microorganisms adapted to high salt concentration, therefore, in case of halophiles, hyperosmotic conditions do not induce plasmolysis, hence, they do not cause any harm to the cells. In particular, *H. halophila* belongs to the moderate halophiles, which are known to accumulate organic osmolytes to compensate osmotic imbalance in extracellular and intracellular space under hyperosmotic conditions. Intracellular concentration of these solutes can reach up to several moles per liter [28]. As a consequence of high intracellular concentration of osmolytes, halophiles are much more prone to a hypo-osmotic damage as compared with non-halophilic microorganisms. Since hydrophobic PHA granules represent a substantial portion of the intracellular volume, the total amount of osmolytes per cell will be considerably lower in PHA-rich cells. Furthermore, it is very likely that presence of PHA granules, due to their capability to protect bacterial cells from massive plasmolysis, reduces intracellular concentration of osmolytes. Therefore, we hypothesize that the protective effect of PHA for halophilic bacteria is a result of decreased amount of osmolytes in PHA-rich bacteria; nevertheless, we are aware of the fact that this hypothesis needs further experimental verification.

Regardless of the actual protective mechanisms, the results clearly indicate that presence of PHA granules helps cells when suddenly exposed to hypoosmotic conditions. It should be noted that the experiment in which halophiles were quickly transferred from high salinity conditions to deionized water does not correspond to the real environmental situation, since the sudden and massive changes in osmolarity are uncommon for most habitats. Nevertheless, less dramatic but still very important and frequent changes in osmolarity are common features of many ecological niches [23]. Therefore, it seems that the fact that PHA granules, as an added value to their primary storage function, protects halophiles from harm effect of osmotic down-shock might be the reason why PHA accumulation capability is such a common feature among halophilic prokaryotes.

The fact that PHA-rich cells are more resistant to osmotic fluctuations than their PHA-poor or non-accumulating counterparts is not only of scientific interest, but may also have practical biotechnological significance. Naturally PHA accumulating bacteria such as members of the genera *Pseudomonas* or *Cupriavidus* are frequently used in *in-situ* bioremediation technologies [29–32]. The fact that presence of PHA in bacteria enhances their robustness not only against osmotic imbalances but also other common stress factors could be considered during inoculum preparation, which could be operated to reach desired high amounts of PHA in bacterial biomass. Moreover, consideration of the fact that PHA-rich cells are more resistant to osmotic imbalances could be used when enriching microbial consortia in PHA accumulating strains. Thus, when PHA are produced by mixed microbial consortia, enrichment processes based on application of "feast-famine" cycles are usually employed. This strategy is based on the asumption that PHA accumulating cells are capable to survive famine periods better than bacteria unable of PHA accumulation [33,34]. Therefore, based on our experimental experience and observation, we suggest that application of subsequent series of osmotic up- and down-shock could be used as alternative or additional strategy to enrich mixed consortia in PHA accumulating strains.

Acknowledgments

Appendix A. Supplementary data

Supplementary material related to this article can be found, in the online version, at doi:https://doi.org/10.1016/j.nbt.2018.10.005.

References

[1] Wood JM. Bacterial responses to osmotic challenges. J Gen Physiol 2015;145:381–8.

[2] Morbach S, Kramer R. Body shaping under water stress: osmosensing and osmoregulation of solute transport in bacteria. ChemBioChem 2002;3:384–97.

[3] Guan N, Li J, Shin HD, Du G, Chen J, Liu L. Microbial response to environmental stresses: from fundamental mechanisms to practical applications. Appl Microbiol Biotechnol 2017;101:3991–4008.

[4] Krüger BA, Schäfers C, Schröder C, Antranikian G. Towards a sustainable biobased industry – highlighting the impact of extremophiles. New Biotechnol 2018;40:144–53.

[5] Obruca S, Sedlacek P, Mravec F, Samek O, Marova I. Evaluation of 3-hydroxybutyrate as an enzyme-protective agent against heating and oxidative damage and its potential role in stress response of poly(3-hydroxybutyrate) accumulating cells. Appl Microbiol Biotechnol 2016;100(3):1365–76.

[6] Kouwen TR, Antelmann H, van der Ploeg R, Denham EL, Hecker M, et al. MscL of *Bacillus subtilis* prevents selective release of cytoplasmic proteins in a hypotonic environment. Proteomics 2009;9(4):1033–43.

[7] Bialecka-Fornal M, Lee HJ, Phillips R. The rate of osmotic downshock determines the survival probability of bacteria mechanosensitive channel mutants. J Bacteriol 2015;197(1):231–7.

[8] Koller M, Maršálek L, Miranda de Sousa Dias M, Braunegg G. Producing microbial polyhydroxyalkanoate (PHA) biopolyesters in a sustainable manner. New Biotechnol 2017;37(A):24–38.

[9] Obruca S, Sedlacek P, Koller M, Kucera D, Pernicova I. Involvement of polyhydroxyalkanoates in stress resistance of microbial cells: biotechnological consequences and applications. Biotechnol Adv 2018;36:856–70.

[10] Obruca S, Sedlacek P, Kryzyanek V, Mravec F, Hrubanova K, Samek O, et al. Accumulation of poly(3-hydroxybutyrate) helps bacterial cells to survive freezing. PLoS ONE 2016;11(6):e0157778.

[11] Slaninova E, Sedlacek P, Mravec F, Mullerova L, Samek O, Koller M, et al. Light scattering on PHA granules protects bacterial cells against the harmful effects of UV radiation. Appl Microbiol Biotechnol 2018;102(4):1923–31.

[12] Obruca S, Sedlacek P, Mravec F, Krzyzanek V, Nebesarova J, Samek O, et al. The presence of PHB granules in cytoplasm protects non-halophilic bacterial cells against the harmful impact of hypertonic environments. New Biotechnol 2017;39:68–80.

[13] Mahler N, Tschirren S, Pflügl S, Herwig C. Optimized bioreactor setup for scale-up studies of extreme halophilic cultures. Biochem Eng J 2018;130:39–46.

[14] Salgaonkar BB, Bragança JM. Utilization of sugarcane bagasse by *Halogeometricum borinquense* strain E3 for biosynthesis of poly(3-hydroxybutyrate-co-3-hydroxyvalerate). Bioengineering 2017;4(2):50.

[15] Mahansaria R, Dhara A, Saha A, Haldar S, Mukherjee J. Production enhancement and characterization of the polyhydroxyalkanoate produced by *Natrinema ajinwuensis* (as synonym) ≡ *Natrinema altunense* strain RM-G10. Int J Biol Macromol 2018;107:1480–90.

[16] Koller M. Production of polyhydroxyalkanoate (PHA) biopolyesters by extremophiles. MOJ Poly Sci 2017;1(2):00011.

[17] Kucera D, Pernicová I, Kovalcik A, Koller M, Mullerova L, Sedlacek P, et al. Characterization of the promising poly(3-hydroxybutyrate) producing halophilic bacterium *Halomonas halophila*. Bioresour Technol 2018;256:552–6.

[18] Obruca S, Snajdar O, Svoboda Z, Marova I. Application of random mutagenesis to enhance the production of polyhydroxyalkanoates by *Cupriavidus necator* H16 on waste frying oil. World J Microbiol Biotechnol 2013;29(12):2417–28.

[19] Coder DM. Assessment of cell viability. In: Robinson JP, editor. Current protocols in cytometry. New York: John Wiley & Sons Inc.; 1997. p. 9.2.1–9.2.14.

[20] Uribelarrea JL, Pacaud S, Goma G. New method for measuring the cell water content by thermogravimetry. Biotechnol Lett 1985;7(2):75–80.

[21] Alcázar E, Rocha-Leão M, Dweck J. Yeast intracellular water determination by thermogravimetry. J Therm Anal Calorim 2000;59(3):643–8.

[22] Koch AL. The geometry and osmotic relations of plasmolysis spaces in bacteria and the role of endocytosis, tubular structures and Scheie structures in their formation. J Theor Biol 1995;176:471–92.

[23] Oren A. Microbial life at high salt concentrations: phylogenetic and metabolic diversity. Saline Systems 2008;4(1):2.

[24] Zhao YH, Li HM, Qin LF, Wang HH, Chen GQ. Disruption of the polyhydroxyalkanoate synthase gene in *Aeromonas hydrophila* reduces its survival ability under stress conditions. FEMS Microbiol Lett 2007;276:34–41.

[25] Breedveld MW, Dijkema C, LPTM Zevenhuizen, Zehner AJB. Response of intracellular carbohydrates to NaCl shock in *Rhizobium leguminosarum* biovar triforii TA-1 and *Rhizobium meliloti* SU-47. J Gen Microbiol 1993;139:3157–63.

[26] Wang Q, Yu H, Xia Y, Kang Z, Qi Q. Complete PHB mobilization in *Escherichia coli* enhances the stress tolerance: a potential biotechnological application. Microb Cell Fact 2009;8:47.

[27] Mravec F, Obruca S, Krzyzanek V, Sedlacek P, Hrubranova K, Samek O, et al. Accumulation of PHA granules in *Cupriavidus necator* as seen by confocal fluorescence microscopy. FEMS Microbiol Lett 2016;363(10). fnw094.

[28] Roberts MF. Organic compatible solutes of halotolerant and halophilic microorganisms. Saline Systems 2005;1:5.

[29] Berezina N, Yada B, Lefebvre R. From organic pollutants to bioplastics: insights into the bioremediation of aromatic compounds by *Cupriavidus necator*. New Biotechnol 2015;32:47–53.

[30] Teng Y, Wang X, Zhu Y, Chen W, Christie P, Li Z, et al. Biodegradation of pentachloronitrobenzene by *Cupriavidus* sp. YNS-85 and its potential for remediation of contaminated soils. Environ Sci Pollut Res 2017;24:9538–47.

[31] Arora PK, Srivastava A, Singh VP. Bacterial degradation of nitrophenols and their derivatives. J Hazard Mater 2014;266:42–59.

[32] Safiyanu I, Abdulwahid Isah A, Abubakar US, Rita Singh M. Review on comparative study on bioremediation for oil spills using microbes. Res J Pharm Biol Chem Sci 2015;6:783.

[33] Oliveira CSS, Silva CE, Carvalho G, Reis MAM. Strategies for efficiently selecting PHA producing mixed microbial cultures using complex feedstocks: feast and famine regime and uncoupled carbon and nitrogen availabilities. New Biotechnology 2017;37:69–79.

[34] Valentino F, Morgan-Sagastume F, Campanari S, Villano M, Werker A, et al. Carbon recovery from wastewater through bioconversion into biodegradable polymers. New Biotechnol 2017;37(A):9–23.

Appendix 18

Obruca, S., Sedlacek, P., Koller, M., Kucera, D., and Pernicova, I. Involvement of polyhydroxyalkanoates in stress resistance of microbial cells: Biotechnological consequences and applications. *Biotechnology Advances* **2018**, 36, 856–870.

Research review paper

Involvement of polyhydroxyalkanoates in stress resistance of microbial cells: Biotechnological consequences and applications

Stanislav Obruca[a,*], Petr Sedlacek[a], Martin Koller[b,c], Dan Kucera[a], Iva Pernicova[a]

[a] Faculty of Chemistry, Brno University of Technology, Purkynova 118, 612 00 Brno, Czech Republic
[b] Institute of Chemistry, NAWI Graz, University of Graz, Heinrichstrasse 28/III, 8010 Graz, Austria
[c] ARENA Arbeitsgemeinschaft für Ressourcenschonende & Nachhaltige Technologien, Inffeldgasse 21b, 8010 Graz, Austria

ARTICLE INFO

ABSTRACT

Polyhydroxyalkanoates (PHA) are polyesters accumulated by numerous prokaryotes as storage materials; they attract attention as "green" alternatives to petrochemical plastics. Recent research has demonstrated that their biological role goes beyong their storage function, since they presence in cytoplasm enhances stress resistance of microorganisms. To address these complex functions, this review summarizes the protective effects of PHA for microorganisms; the involvement of PHA in stress resistance is discussed also from a praxis-oriented perspective. The review discourses the controlled application of stress to improve PHA productivity. Also the manifold advantages of using stress adapted microbes - extremophiles as PHA producers are discussed.

1. Introduction

In 1926, Lemoigne demonstrated that *Bacillus megaterium* accumulates granules of poly(3-hydroxybutyrate) (P(3HB)), the homopolyester of 3-hydroxybuyric acid (3HB). Since this first report, the production and accumulation of polyesters of various hydroxy acids, so-called polyhydroxyalkanoates (PHA), has been reported for numerous prokaryots (Steinbüchel and Hein, 2001). Despite the fact that P(3HB) constitutes the most common and best-studied member of the PHA family, various microorganisms can produce differently composed PHA co- and terpolymers, characterized by different lengths of the monomer's side chains and/or backbones. The general chemical structure of PHA polyesters is provided in Fig. 1. Polymers containing monomer units with 3–5 carbon atoms are referred to as short-chain-length PHA (scl-PHA), whereas medium-chain-length PHA (mcl-PHA) consist of monomer units with 6–14 carbon atoms. Microorganisms accumulate PHA in the form of intracellular granules, which primarily serve as storage of carbon and energy. PHA granules are typically biosynthesized when a carbon substrate is present in excess in parallel to depletion of other nutrients essential for biomass formation, and are remobilized again when external carbon sources are depleted. Beyond this well-known storage function, recent studies revealed that microbial capability to accumulate PHA also enhances the stress resistance and fitness of microorganisms under various non-optimal environmental conditions. Since among PHA-producing microorganisms Gram-positive and Gram-negative bacteria as well as some *Archaea* are found, which, from a metabolic perspective, can be classified into aerobes, anaerobes, autotrophs, heterotrophs and even phototrophs (Koller et al., 2017), it can be assumed that the ability to biosynthesize PHA is among the most common and best-established microbial strategies to cope with adverse conditions. Aside from their complex biological function, PHA are attracting considerable attention as biodegradable, biocompatible and renewable-resource-based alternatives to petrochemical polymers. Due to their biocompatibility, they are increasingly implemented in numerous high-value applications in medicine and health care (Francis et al., 2016; Mota et al., 2017; Rai et al., 2016).

2. Involvement of PHA in the stress survival of bacteria

Prokaryotic microorganisms store PHA in the form of cytoplasmic spherical inclusion, so-called PHA granules consisting of an amorphous PHA fraction representing the hydrophobic core, which is sourrounded by attached PHA granule-associated proteins. These proteins include PHA synthase, PHA depolymerases, regulatory proteins and PHA granule structural proteins (Bresan et al., 2016). These complex multicomponent structures were assigned as "carbonosomes" to stress their

---

* Corresponding author.
  E-mail address: obruca@fch.vut.cz (S. Obruca).
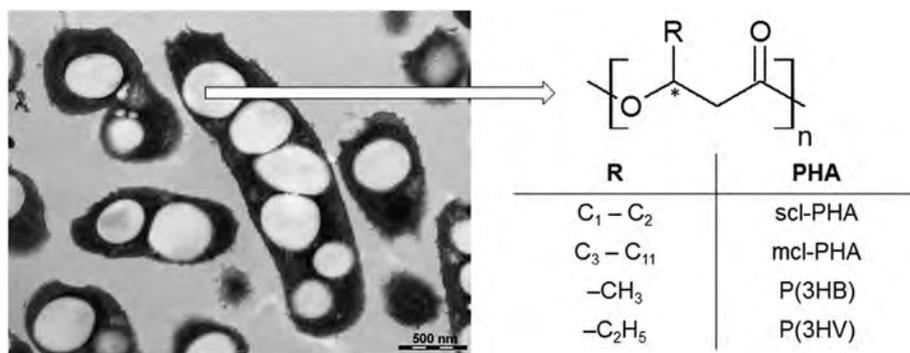
unique properties and multifunctionality (Jendrossek, 2009). Generally, under conditions favoring PHA biosynthesis, PHA granules may represent a dominant fraction of cellular dry matter (CDM) exceeding 90 wt% (Johnson et al., 2009; Tan et al., 2014). Nonetheless, it was recently reported that bacteria regulate their cellular dimensions to control the relative volume of PHA granules so that they do not exceed a value of approx. 40% of the total cell volume (Mravec et al., 2016). In other words, geometric factors most likely determine the upper limit of intracellular PHA contents (Vadlja et al., 2016).

The ability of microorganisms to accumulate storage compounds, such as glycogen, polyphosphates, or PHA, enables their occurrence and survival in environments of fluctuating availability of nutrients (Kadouri et al., 2005). In the particular case of PHA, apart from their primary storage function, PHA plays more sophisticated physiological roles such as maintaining anoxic photosynthesis and the sulfur cycle in microbial mats dependent on photosynthetic carbon fixation (Rothermich et al., 2000; Urmeneta et al., 1995), triggering sporulation in *Bacilli* (Slepecky and Law, 1961), supporting the prolongation of nitrogen fixation by diazotrophs in the dark (Bergersen et al., 1991), or maintaining energy production and NADH oxidation of nitrogen-fixing bacteria (Encarnacion et al., 2002).

Among these biological functions, the capability for PHA biosynthesis and degradation also substantially enhances the survival of bacteria when exposed to various stress conditions as demonstrated in numerous cases. Tal and Okon (1985) reported that bacterial cells of *Azospirilum brasilense* haboring PHA up to about 40% of CDM were substantially more resistant to UV irradiation, desiccation and osmotic pressure than cells containing a very low amount of PHA (about 5% of CDM). These results were further confirmed by a comparison of the stress survival of the PHA-accumulating wild type of *Azospirilum brasilense* with its PHA synthase- and PHA depolymerase deletion mutants incapable of PHA synthesis and hydrolysis, respectively. Investigated stress conditions encompassed UV radiation, high temperature, osmotic shock and supply of H_2O_2 (Kadouri et al., 2002, 2003a, 2003b). Similarly, when the stress survival capabilities of the wild type of *Aeromonas hydrophila* and its PHA synthase negative mutant incapable of PHA biosynthesis were compared, it was found that the wild type strain survived better when exposed to high and low temperatures, H_2O_2, UV radiation, ethanol and hyperosmotic shock (Zhao et al., 2007). The protective role of PHA was also observed in recombinant *Escherichia coli*. The first of two constructed recombinant *E. coli* strains harbored only the PHA synthetis genes, while the second recombinant strain harbored the PHA synthetis genes as well as the genes encoding intracellular PHA depolymerase. It was observed that both recombinant strains were more resistant to heat shock, UV radiation, acidic pH-value and osmotic pressure than the wild type of *E. coli* incapable of PHA synthesis (Wang et al., 2009). Hence, the fact that the presence of PHA in bacterial cells supports the stress resistance of bacteria was demonstrated for various bacteria. In addition, it was observed that PHA supports cell survival under various stress conditions such as extreme temperatures, freezing, osmotic and oxidative pressure, UV irradiation,

ethanol, desiccation or heavy metals. Furthermore, some bacteria are even capable of direct conversion of toxic substances such as methanol (Khosravi-Darani et al., 2013; Mokhtari-Hosseini et al., 2009) or styrene (Goff et al., 2007) into PHA.

From the above-summarized reports, it can be concluded that the protective role of PHA represents a general phenomenon regardless of the individual microorganism or the specific stressor. Nevertheless, the particular protective mechanisms of PHA are not yet completely understood. It is very likely that not just one single mechanism is responsible for PHA's protective effects. Rather, it seems that the presence of PHA granules has numerous biological and biophysical consequences, which in a synergistic way enhance the overall stress resistance of PHA-containing cells. For instance, it was reported that intracellular PHA hydrolysis induces the expression of the stationary phase regulator RpoS, which subsequently activates the expression of genes providing cross-protection against multiple stress factors (Ruiz et al., 2001). Further, Mezzina et al. (2015) investigated phasin, a PHA granule-associated protein, from *Azotobacter* sp. FA-8. It had previously been assumed that the primary and only function of phasins is to cover PHA granules, thus generating an amphiphilic interface between the aqueous cytoplasm and the hydrophobic core of PHA granules. Surprisingly, it was later found that phasins also evince considerable chaperone-like activity, which might contribute to the protective mechanism of PHA in their natural producers. An additional protective mechanism of PHA may originate even from its fundamental anabolism and catabolism depicted in Fig. 2. Actually, despite the fact that either the anabolic or the catabolic pathway prevails at the physiological state at a given moment, PHA are simultaneously biosynthesized and hydrolysed in microbial cells; therefore, the PHA metabolism is referred to as the so-called "PHA cycle" (Kadouri et al., 2005). As a consequence of this metabolic strategy, PHA-producing cells always contain a substantial amount of PHA monomers. For instance, it was reported that the intracellular concentration of P(3HB)´s monomer, 3HB, in a PHA accumulating strain of *Cupriavidus necator* is 16.5 times higher than in its mutant incapable of PHA biosynthesis. This is a significant finding since it was proven that 3HB serves as a potent chemical chaperone with the capability to protect proteins and other biomolecules from denaturation induced by high temperature, heavy metals or oxidative pressure (Obruca et al., 2016b), and constitutes also a highly efficient cryo-protectant (Obruca et al., 2016c).

2.1. Protective effect of PHA under cold conditions

These above-mentioned general protective features of PHA can shield bacteria from a wide range of stress factors, thus enhancing their general fitness, robustness and durability. This may also explain why PHA-accumulating microbes represent an important part of mixed microbial consortia (MMC) under non-optimal or even extreme conditions (*vide supra*). In this context, cold resistance represents an illustrative example: PHA producers are abundantly present in such consortia, which are exposed to low temperatures or even long periods of freezing.
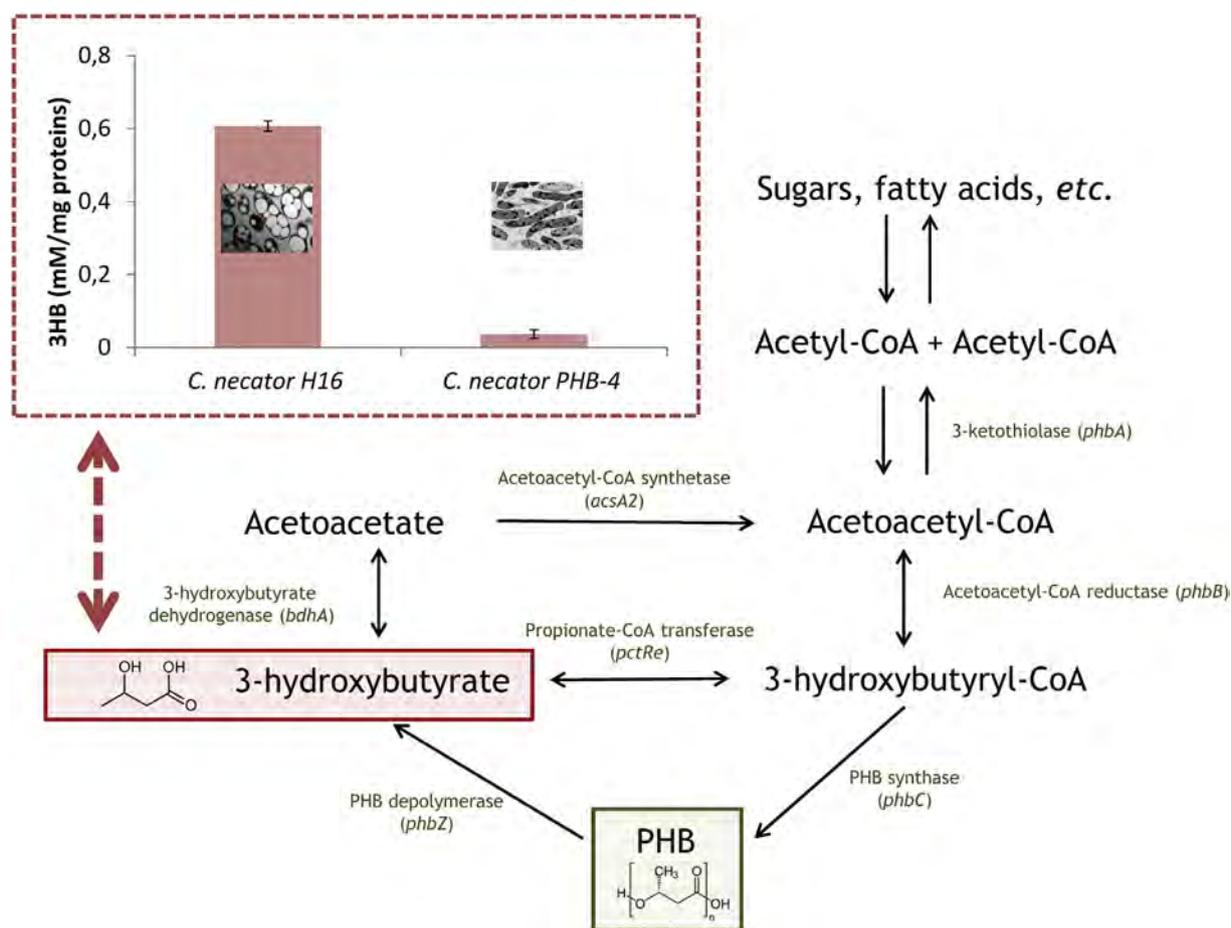
Fig. 2. Difference in 3HB content in PHB accumulating *C. necator* H16 and its PHB non-accumulating mutant *C. necator* PHB⁻4 as a consequence of fully functional PHB metabolic metabolism called PHB cycle. The mutant strain is not capable of PHB biosynthesis due to mutation of *phbC* gene encoding for PHB synthase; hence, the PHB cycle is interrupted and dysfunctional (Obruca et al., 2016c).

For instance, numerous PHA-accumulating bacteria have been identified in Antarctic freshwater (Ciesielski et al., 2014), Antarctic soil (Goh and Tan, 2012), subarctic sea ice in Greenland (Kaartokallio et al., 2013), or the Baltic Sea (Pärnänen et al., 2015). Moreover, an ability to survive freezing was directly associated with PHA accumulation in *Sphingopyxis chilensis* (Pavez et al., 2009) and *Pseudomonas* sp. 14-3 (Ayub et al., 2007). To better understand the involvement of PHA in the cold resistance of bacteria, Ayub et al. (2009) investigated the Antarctic bacterium *Pseudomonas* sp. 14-3 during adaptation to low temperatures. They discovered that the PHA metabolism was essential for the regulation and maintenance of the intracellular redox state of the bacterial culture. This PHA producer was further characterized in detail by 16S rRNA gene sequence analysis and various physiological and biochemical tests (López et al., 2009). The strain grew well in a temperature range between 4 and 37 °C, but not at a slightly elevated temperature of 42 °C. Cultivation on sodium octanoate resulted in the accumulation of P(3HB) homopolyester. The authors classified the isolate as the first representative of the new species *Pseudomonas extremaustralis* sp. nov. Tribelli and López (2011) investigated this strain and its PHA-negative mutant to study the correlation between its PHA- and extracellular polysaccharide (EPS) biosynthesis at low temperature. These studies showed that, at low temperature, PHA biosynthesis occurs in parallel with higher motility, and supports endurance especially of the mobile planktonic cells. Therefore, it was assumed that the ability to accumulate P(3HB) might be an adaptive benefit for microbes settling in new, environmentally stressful ecological niches. Furthermore, it was demonstrated that genes involved in PHA metabolism are situated together on a "genomic island" and, most probably, were acquired by

horizontal transfer, which implies that acquisition of PHA biosynthetic capability might be an important mechanism of adaptation to stress conditions related to cold environments (Ayub et al., 2007). Later, the entire genome of the strain was sequenced to identify all the genes involved in PHA synthesis and degradation, flexibility in adapting to extreme environments, and degradation of toxic substances; this was the first completely sequenced genome of a psychrophilic organism (Tribelli and López, 2011). To explain how accumulation of PHA helps bacteria confronted with freezing, Obruca et al. (2016b) recently investigated the cryo-protective mechanisms of PHA in *Cupriavius necator*. Apart from the already mentioned cryo-protective function of 3HB, it was observed in this work that P(3HB) retains highly flexible properties even under extremely low temperatures, which suggests that PHA granules might protect bacterial cells against injury from extracellular ice. Further, PHA-containing cells exhibited a substantially higher rate of water transport compared with PHA free cells, which might protect PHA-rich cells against the fatal consequences of intracellular ice formation. Hence, it can be stated that the cryo- and cold protective action of PHA granules and related metabolism involves numerous mechanisms that, as a whole, result in very complex and efficient protection of bacterial cells.

2.2. Protective effect of PHA under osmotic pressure

In addition, fluctuations in external osmolarity are a very common feature of numerous environments. Many authors (Breedveld et al., 1993; Kadouri et al., 2003a, 2003b; Tal and Okon, 1985; Wang et al., 2009; Zhao et al., 2007) have reported the fact that the ability to

PHA **negative** strain of *C. necator* PHA **positive** strain of *C. necator*
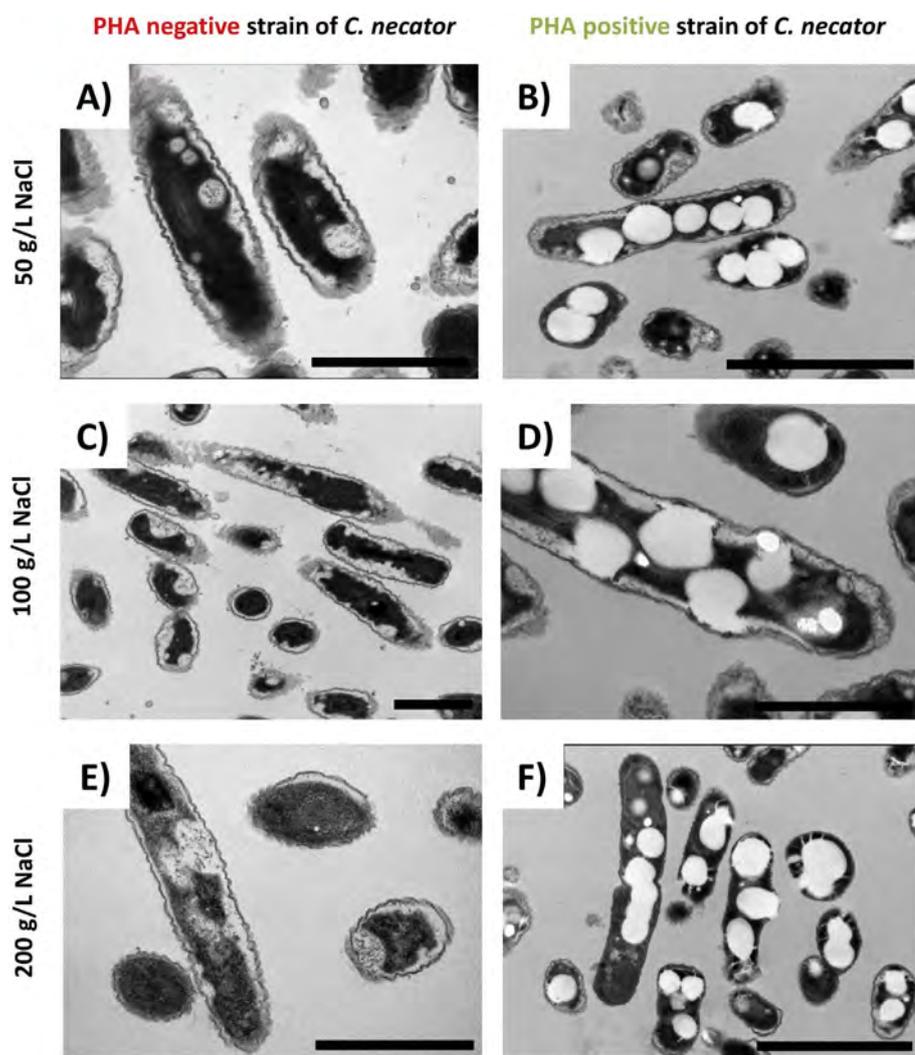
Fig. 3. Morphology of cells of *C. necator* H16 (B, D, F) and its PHB negative mutant strain (A, C, E) when exposed to various NaCl concentrations. In the mutant strain, osmotic up-shock induces massive plasmolysis which results in damage of cytoplasmatic membrane and release of cytoplasmatic content. On the contrary, the level of plasmolysis is substantially reduced in PHB containg cells without damage of cell membrane and subsequent leakage of cytoplasm. When plasmolysis occurrs in close vicinity of PHB granules, granules were able to influx into the periplasmic space. Therefore, due to their extraoridinary liquid-like properties, it seems that PHB granules might partially protect membranes from damage by osmotic up-shock. Moreover, PHA granules revealed substantial aggregation at high salt concentrations, as evidence by the formation of one or several non-spehrical granules per cell (Obruca et al., 2017, with permission).

accumulate PHA enhances the stress resistance of non-halophilic bacteria against osmotic pressure. Moreover, the vast number of halophiles displaying considerable PHA biosynthesis capability also evidences PHA's contribution to bacterial cells' resistance against osmotic pressure (Yin et al., 2015). The extraordinary potential of halophiles for biotechnological production of PHA is described in detail below. Similarly to the cryo-protective effect of PHA, also the protective role of PHA against osmotic pressure is complex and includes several modes of action which can differ depending upon the microorganism under investigation. Breedveld et al. (1993) observed that exposure of *Rhizobium leguminosarum* TA-1 and *Rhizobium meliloti* SU-47 to osmotic pressure resulted in hydrolysis of PHA storage, which was accompanied by accumulation of compatible solutes. In addition, other studies report that the product of P(3HB) hydrolysis – 3HB – *per se* represents a potent compatible solute with chaperoning activity protecting biomolecules from losing their activity under a wide spectrum of stressful conditions (Obruca et al., 2016c; Soto et al., 2012). On the contrary, *Cupriavidus necator* H16 did not respond to osmotic up-shock by mobilization of intracellular P(3HB), but, as shown in Fig. 3, the presence of PHA granules prevented massive plasmolysis of the up-shocked cells which was accompanied by membrane damage and leakage of the cytoplasm content in the PHA non-accumulating mutant strain. In the PHA-accumulating strain, transmission electron microscopy analysis revealed unique "liquid-like" properties of PHA granules and indicated that they can partially repair and stabilize cell membranes by plugging small gaps formed during plasmolysis. Moreover, also the level of dehydration and

fluctuations in intracellular pH-value were substantially lower for P(3HB)-containing cultures (Obruca et al., 2017).

2.3. Unique properties of native intracellular PHA granules

Therefore, it seems that, besides all the biological consequences of PHA metabolism, the chaperoning efficiency of phasins (*e.g.*, PhaP) and monomer units of PHA, as well as the mere presence of PHA granules in bacterial cells substantially affects the fundamental biophysical properties of these cells; this subsequently enhances their ability to cope with numerous stress factors. This statement is supported for instance by the results of Goh et al. (2014), who observed that no mobilization, but just the presence of PHA granules is needed to provide protection for cells of *Delftia acidovorans* against oxidative stress induced by photoactivated TiO$_2$. In addition, a protective effect of PHA granules was observed also in genetically modified bacteria, where neither a metabolic interconnection of the PHA metabolism with other metabolic pathways or regulatory strategies, nor PHA granules associated proteins such as phasins and PHA depolymerase are present (Goh et al., 2014; Wang et al., 2009).

It should be mentioned that when PHA is stored intracellularly in the form of native granules, this represents PHA in a unique form; native PHA dispplays properties considerably differing from those of isolated PHA. This is especially true for P(3HB) as the most common member of the PHA family. P(3HB) extracted from bacteria constitutes a highly crystalline material with an elongation at break of about 4%
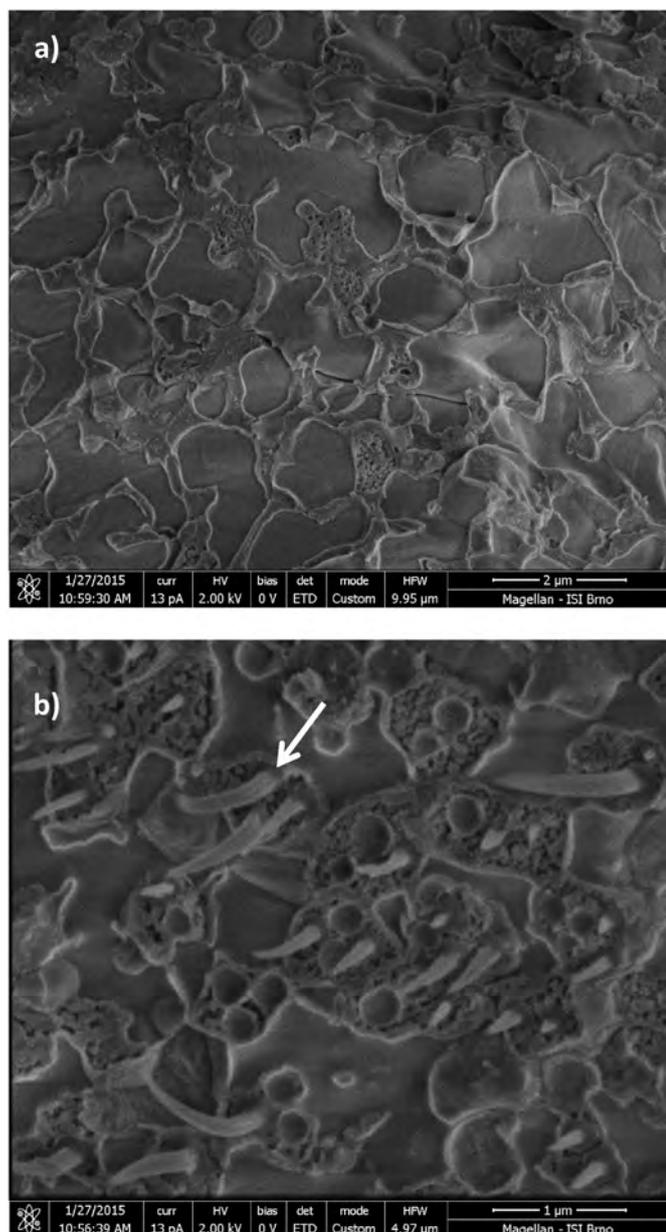
Fig. 4. A) Cryo-SEM microphotographs of freeze-fractured PHB non-containing (*C. necator* PHB-4) and B) PHB containing (*C. necator* H16) bacterial cells. In PHB containg cells, needle-like plastic deformation can be observed, which indicates extraordinary flexibility of intracellular PHB. It should be pointed out that bacterial cells were fractured at very low temperature (−140 °C) at which all the other components of bacterial cells are crystalline and very brittle. This unusual behavior demonstrates the extraordinary liquid-like properties of amorhous intracellular PHB granules (Obruca et al., 2016c, with permission).

(Sudesh et al., 2000a). On the contrary, native P(3HB) granules are formed by a highly mobile amorphous polymer with basic properties similar to supercooled liquids (Bonthrone et al., 1992). Unique features of amorphous P(3HB) can be demonstrated when freeze-fractured bacterial cells are observed by Cryo-SEM, see Fig. 4. Despite the fact that bacterial cells and, thus, even P(3HB) granules are fractured at very low temperatures (below −80 °C), P(3HB) granules still exhibit substantial flexibility by forming so-called needle-type plastic deformations with an elongation at break higher than 100% (Sudesh et al., 2000b; Obruca et al., 2016a). This demonstrates that P(3HB) granules possess mechanical properties completely different to any other component present in microbial cells. For instance, this exceptional flexibility might help bacterial cells to endure shearing stress caused by ice crystals during freezing (Obruca et al., 2016a, 2016b). Furthermore, a remarkably higher mobility of the PHA chains in intact living cells in comparison with isolated polymer has been repeatedly proven by means of ^{13}C NMR spectroscopy (Barnard and Sanders, 1989; Bonthrone et al., 1992; Harrison et al., 1992; Horowitz and Sanders, 1994). It seems that due to their liquid-like properties, PHA granules are able to partially repair cytoplasmic membranes, as it was demonstrated in osmotically up-shocked cells of *C. necator* H16 (Obruca et al., 2017).

Although the origin of the retained amorphous character of native PHA granules has been debated extensively in the literature (Calvert, 1992), the exact mechanism for how the polymer is protected from spontaneous crystallization *in vivo* is not yet completely understood. Nevertheless, several theories have been proposed. The involvement of intra-granular plasticizers is among the most frequently proposed explanations. The positive effect of various low-molecular (Ceccorulli et al., 1992; Choi and Park, 2004) or macromolecular (Avella and Martuscelli, 1988) substances on the mobility of PHA chains, reflected by a decrease of the polymer's glass transition temperature, is well described. Although the individual tested compounds have no direct relevance for plasticizing PHA *in vivo*, these experimental results reflect the general polymer behavior, which can be expected also in the case of native PHA. Among the intracellular plasticizers in question, water is the most commonly proposed. On the one hand, it has been proven that the native granules have a residual water content up to 10% by mass (Lauzier et al., 1992b; Mas et al., 1985), while on the other hand, the plasticizing effect of water on polymers, even those structurally similar such as poly(vinyl acetate) (Bair et al., 1981), is well known. According to the hypothesis proposed by Lauzier (Lauzier et al., 1992a, 1992b), chains of the newly biosynthesized PHA are in the granule's interior are stabilized in the extended β - conformation by hydrogen-bonded water, resulting in a mobile amorphous form of PHA incapable of crystallization. Nevertheless, the hypothesis has not found any experimental support yet as no model amorphous form of PHA stabilized only by complexation with water has been published so far. Probably the most widely accepted explanation of the maintenance of PHA in the stable amorphous form is provided by a simple chemical-kinetic mechanism, presented by de Koning and Lemstra (1992) and Bonthrone et al. (1992). This model takes into account a decrease in the bulk crystallization rate in small droplets of a mobile polymer, caused by the exceptionally low frequency of spontaneous nucleation in such a limited volume. The validity of this physicochemical argumentation, which has long been applied in describing the super-cooling of synthetic polymers such as polyethylene (Cormia et al., 1962), was experimentally supported in the case of PHA by successfully reconstructing crystalline PHA to sub-micron sized amorphous granules (Horowitz and Sanders, 1994, 1995; Martino et al., 2014). Nevertheless, this theory, based only on the restricted crystallization rate in the lack of nucleation sites, is not fully consistent with the observation of stable crystalline-shell/amorphous-core PHA granules described by Lauzier et al. (1992b). Furthermore, the role of intra-granular water, which is inevitably present in the artificial granules, is not taken into account. It is evident that the stability of the amorphous PHA *in vivo* still needs further experimental clarification, not only in the context of the stress response of PHA-accumulating bacteria.

3. Use of PHA accumulating bacteria in bioremediation, agriculture, and wastewater treatment

As reported above, accumulation of PHA enhances the fitness, robustness and stress survival capacity of bacteria, which can be highly beneficial for numerous biotechnological processes in which employed microorganisms are exposed to adverse conditions. Some of these applications will be described and discussed in this section.

3.1. Use of PHA producers as agriculture inoculants

Knowledge of the benefits of PHA accumulation has a far-reaching impact on agriculture applications. Inoculants based on PHA-producing bacteria can be used for plant protection and plant growth promotion.

Nitrogen-fixing bacteria, also called diazotrophs, are capable of converting atmospheric nitrogen into inorganic substances utilizable by plants. Their role is crucial in Nature's nitrogen cycle, since they are responsible for fixation of about 90% of organically bounded nitrogen (Rogers, 2011). Numerous diazotrophs in the soil form symbiotic complexes with some plant species, most often with legumes. Therefore, knowledge from this field of science is essential in agriculture and fertilizer production. In the context of global climate change, there is increasing interest in manufacturing agricultural products and inoculants containing bacteria that are capable of resisting unfavorable conditions associated with soil, such as carbon substrate starvation, desiccation and rapid changes in osmolarity or temperature. Therefore, in agricultural applications it would be reasonable to employ PHA-accumulating bacteria, which are naturally resistant to the above-mentioned stress factors.

Rhizobium and *Azospirillum* are well-studied examples of plant growth-promoting bacteria. Individual strains within these genera are distinguished by, among other properties, their ability to accumulate PHA. The fact that the stress resistance of these bacteria is a consequence of their PHA-accumulating capability was confirmed in numerous cases (Kadouri et al., 2002, 2003a, 2003b; Zhao et al., 2007). Therefore, PHA-producing diazotrophs are very promising plant growth promoters. For instance, Fallik and Okon (1996) compared two essential parameters for the preparation of agricultural inoculants: the type of inoculant carrier and the physiological state of bacteria. *Azospirillum brasilense* containing a higher amount of PHA demonstrated substantially more consistent plant growth promotion effects. These observations were confirmed by the increase in crop yields achieved on corn and wheat fields in Mexico, where PHA-rich cells of *A. brasilense* were used as peat inoculant (Dobbelaere et al., 2001).

Moreover, it was reported that different species of rhizobia require P(3HB) for a successful nodulation process. In this context, Aneja et al. (2005) reported that disruption of PHA biosynthesis in *Sinorhizobium meliloti* resulted in severe defects in competition for growth and nodule occupancy. Furthermore, biological nitrogen fixation is an energy-demanding process, the energy requirements of which can be partially covered by utilization of PHA. Moreover, nitrogen fixation also consumes a huge amount of reducing equivalents. In *Rhizobium* spp., PHA formation requires reducing equivalents as well, but reducing power can be further released during mobilization of the intracellular polymer. Cevallos et al. (1996) compared the nitrogenase activity of *Rhizobium etli* with its PHA synthase deletion mutant strain and observed that the PHA-negative mutant strain exhibited prolonged and higher nitrogenase activity. On the contrary, the oxidative capacity of the mutant was reduced, which indicates that PHA biosynthesis provides oxidative power under oxygen-limiting conditions. Inversely, PHA biosynthesis was impaired also in *Azorhizobium caulinodans*; in this case, the PHA-negative mutant completely lost its nitrogenase activity (Mandon et al., 1998).

Free-living ("planktonic") diazotrophs do not have the ability to attach to plant roots, or to form bacterial flocs and aggregates. Although generally relatively low, the amount of nitrogen fixed by these free-living diazotrophs is still considerable with a value of 2–25 kg per hectare per year (Herridge et al., 2008). Members of the genus *Azotobacter* belong to this group of diazotrophs. For instance, the *Azotobacter* strain Azo-8 assists the use of urea (60 kg N ha^{-1}) and farmyard manure (40 kg N ha^{-1}) by plants. This increased utilization of nitrogen led to higher crop productivity (Singh et al., 2013). The members of this genus, together with *Bacillus* spp., *Burkholderia* spp. and *Pseudomonas* spp., are significant PHA producers widely used as a supplement to conventional inoculants for their growth-promoting properties. For

instance, the PHA-producing bacterium *Bacillus megaterium* attracts attention due to its capability to solubilize phosphates (Patel et al., 2016). Moreover, numerous members of the genus *Azotobacter* are such efficient PHA producers that some of them, *e.g.*, *Azotobacter vinelandii*, are considered auspicious candidates for industrial PHA production (Segura et al., 2003).

3.2. Application of PHA-producing bacteria for in situ bioremediation

Naturally occuring PHA-producing microorganisms are also widely used in technologies aimed at removal of organic and even inorganic pollutants from the environment. For instance, due to their extraordinary broad metabolic activity, members of the species *Cupriavidus necator* (formerly *Ralstonia eutropha*, *Wautersia eutropha* and *Alcaligenes eutrophus*; Vandamme and Coenye, 2004), such as *C. necator* H16, the model microorganism for *scl*-PHA metabolism, can be used for removal of aromatic compounds such toluene, xylene, benzoic acid (Berezina et al., 2015), ethanethiol (Sedighi et al., 2013), chloro-aromatic compounds and chemically-related pollutants (Lykidis et al., 2010), or p-nitrophenol (Salehi et al., 2010). Moreover, the spectrum of degraded pollutants can be further extended using tools of genetic engineering as reported by Saavedra et al. (2010), who genetically modified *Cupriavidus necator* JMP134 to yield a strain capable of complete mineralization of polychlorinated biphenyls. Also further members of the genus *Cupriavidus* are capable of degradation of numerous organic pollutants such as pentachloronitrobenzene (Teng et al., 2017), or indole (Qu et al., 2015). Nevertheless, application of members of the genus *Cupriavidus* for detoxification of contaminated sites is advantageous not only because of these direct metabolic activities, but also for the strains´ outstanding resistance to stress conditions associated with such environments. For instance, Kuppusamy et al. (2016) isolated *Cupriavidus* sp. MTS-7 capable of biodegradation of both low molecular weight as well as high molecular weight polyaromatic hydrocarbons; this strain was also resistant to extreme pH-conditions or heavy metals. Generally, extraordinary heavy metal resistance is typical for the members of the genus *Cupriavidus*, as it is also reflected in the genus name, since *Cupriavidus* is the Latin expression for "enduring high copper concentrations" (Vandamme and Coenye, 2004). Therefore, mainly *Cupriavidus metallidurans*, but also other *Cupriavidus* strains are widely applied in metal decontamination efforts (Slaveykova et al., 2013). The ability of the *Cupriavidus* strains to cope with stress conditions including their tolerance to heavy metals can be attributed to their PHA accumulation capacity. For example, Chien et al. (2014) reported that the heavy metal resistance of *Cupriavidus taiwanensis* EJ02 might be associated with its PHA metabolism. When grown in complex media, the strain tolerated up to 5 mM Cd^{2+}, which is approximately five times the concentration tolerated by its PHA-negative mutant strains. Supplementing defined carbon sources in minimal media firstly boosted PHA biosynthesis in this strain, and, secondly, it further increased its heavy metal resistance up to 7 mM Cd^{2+} ions.

Furthermore, also other PHA-producing microorganisms are widely used in bioremediations. Members of the genus *Pseudomonas* typically capable of mcl-PHA accumulation are employed for removal of numerous pollutants including – but not limited to – nitrophenols (Arora et al., 2014), polyaromatic hydrocarbons (Bisht et al., 2015), phenol and its derivatives (Krastanov et al., 2013), and petroleum hydrocarbons (Safiyanu et al., 2015; Salleh et al., 2003). The biodegradation capacity of *Pseudomonas* spp. for organic pollutants is enhanced by their capability to produce biosurfactants, which make these hardly water soluble or even insoluble substrates accessible for bacterial cells (Li, 2017). It was reported that the products of intracellular degradation of mcl-PHA can be used by bacteria for bio-surfactant biosynthesis (Soberón-Chávez et al., 2005). Moreover, similarly to *Cupriavidus* spp., also members of the genus *Pseudomonas* reveal extraordinary resistance against various stress factors such as low and high temperature, organic compounds or heavy metals (Moreno and Rojo, 2013; Wasi et al.,

2013). Also in this case, the stress resistance of *Pseudomonas* spp. is partially associated with their PHA-accumulating abilities. For instance, the psychrophilic bacterium *P. extremaustralis*, the stress resistance of which was attributed to PHA production in numerous studies (Ayub et al., 2004, 2009; Tribelli and López, 2011), was investigated in the context of its potential use for bioremediation of petroleum hydrocarbons. The strain was cultivated in biofilms (benthic cultivation) and in agitated shaking flask setups (planktonic cultivation). Benthic cultivation in biofilms displayed better growth, higher bio-surfactant production and superior diesel degradation than using planktonic cultivation. Alkanes of both long- and branched chain were degraded by benthic cultures, while only medium-chain length alkanes were degraded by planktonic cultures. Based on these outcomes, *P. extremaustralis* was suggested as an auspicious candidate for bioremediation in extreme environments (Tribelli et al., 2012).

As demonstrated above, numerous PHA-producing bacteria can be advantageously applied as pure cultures or even as members of mixed microbial consortia for *in situ* bioremediation technologies. Generally, an essential advantage of PHA-producing microorganisms is their increased stress endurance and robustness. In this context, it would be beneficial to consider high PHA content in microbial cells as an important positive factor during inoculum preparation. Furthermore, despite the fact that there are some general doubts about the use of genetically engineered bacteria for *in situ* bioremediation technologies, genetic modification of bacteria is generally considered a promising strategy substantially improving the efficiency of the bioremediation process (Singh et al., 2011; Srivastava et al., 2014). Since PHA accumulation and related metabolic pathways has a great potential for improving the biodegradation process, it would be interesting to either genetically modify natural PHA producers to increase their biodegradation potential, or to use tools of genetic engineering to enable PHA biosynthesis in promising degraders incapable of PHA accumulation. In addition, PHA may not only serve as protective factor for employed microorganisms; beyond that, Pierro et al. (2017) recently reported that pure P(3HB) material can be efficiently used also as a slow-release carbon source and electron donor for *in-situ* bioremediation of chlorinated hydrocarbons by a naturally present MMC-microflora. Application of pure P(3HB) is economically questionable, but using PHA-rich biomass without the need for PHA isolation and purification might have a similarly positive effect. In this case, applied bacterial cells do not necessarily have to be directly capable of contaminant degradation, and the microbial biomass does not even have to be active.

3.3. Wastewater treatment by PHA-enriching mixed microbial consortia (MMC)

Activated sludge consists of mixed MMC, which are typically confronted with diverse exogenous stress consitions prevailing in their habitats, which, *inter alia*, encompass biological treatment systems for industrial, municipal, and process wastewater. In the MMC-microflora of such anthropogenic engineered ecosystems, a vast biodiversity of robust PHA-accumulating species is present (reviewed by Koller et al., 2011). An increasing number of research studies currently investigate the performance of such MMC in using carbon-rich industrial effluent streams for PHA production with at the same time mitigating their carbon, nitrogen, and phosphate contents (reviewed by Serafim et al., 2016). Only recently, the high performance of MMC for removal of (bio)chemical oxygen demand and nitrogen from municipal waste water, coupled with high-throughput PHA production, was demonstrated by pilot scale experiments described by Bengtsson et al. (2017). Already in the 1970's, Wallen and Rohwedder (1974) discovered the production of PHA copolyesters -as the first reported PHAs different from PHB- by MMC in an activated sludge community. Years later, the key role of PHA in the symbiotic competition between polyphosphate-accumulating organisms (PAOs) and glycogen-accumulating organisms (GAOs) for exogenous carbon source in enhanced biological phosphorus

removal systems (EBPRSs) was elucidated. In such EBPRSs, PHA are accumulated when external carbon source is supplied in the absence of an external electron sink; this prevents microbial growth, but boosts PHA production by those bacteria in the community capable of this metabolic feature (Pereira et al., 1996).

Generally, PHA production by MMC is based on enriching PHA-storing consortia by exerting a selective environmental pressure, mainly by applying a dynamic feeding regime. Such dynamic "feast-and-famine" regimes subject the MMC towards alternating carbon-rich (feast) and carbon-poor (famine) conditions. Typically, the applied carbon source constitutes a mixture of volatile fatty acids (VFAs), which are easily converted by PHA-accumulating microbes to PHA. The overall process can be separated in four phases: i) acidogenic formation of VFAs from cheap carbon compounds present in the effluent stream, ii) enrichment of a PHA-accumulating culture in sequencing batch bioreactors; iii) PHA accumulation by the enrichment culture in a batch cultivation regime; iv) recovery of PHA from biomass.

Such PHA production processes using MMC offer the possibility to upgrade organic compounds from liquid waste streams and industrial effluents. Several studies demonstrate the technical feasibility of such processes either by directly using VFA mixtures (Dionisi et al., 2004), or by using fermented waste streams. Examples of such waste streams are, *inter alia*: food waste (Rhu et al., 2003), effluents from pulp and paper industry (Bengtsson et al., 2008; Queirós et al., 2014; Queirós et al., 2016); sugarcane molasses (Albuquerque et al., 2007), fermented whey permeate (Valentino et al., 2015a), waste water from olive oil production (Campanari et al., 2017), starch industry wastewater (de Grazia et al., 2017), municipal wastewater (Pittmann and Steinmetz, 2017; Valentino et al., 2015b), and others. Recently, it was demonstrated that for robust long-term operation of such systems at high PHA-productivity, a fine-tuned ratio of carbon, nitrogen, and phosphate in the feed stream is needed (Valentino et al., 2015a; Silva et al., 2017).

Valentino et al. (2015c), who used cheese whey contaminated with β-hexachlorocyclohexane (β-HCH) for a MMC-based PHA-production process, demonstrated the high robustness of PHA-accumulating species in MMC to noxious compounds. In this study, β-HCH neither affected the acidogenic nor the PHA-accumulation step of the process. Another prime example is the conversion of hardwood spent sulfite liquor from pulp industry by MMC towards PHA in an aerobic dynamic feeding process. This substrate cocktail contains toxic compounds such as lignosulfonates and phenolic derivatives. Presence of these compounds did not inhibit the PHA-production process; in contrast, they were even partly metabolized for PHA biosynthesis (Queirós et al., 2014).

MMC-based PHA production definitely constitutes a paradigm shift in well-established techniques for wastewater treatment and management of organic residues (reviewed by Valentino et al., 2017). Although being challenging, this strategy is considered an auspicious approach for upgrading waste to biotechnological feedstocks. In addition, because PHA production displays a competitive advantage for microorganims, the enrichment in PHA-storing bacteria depends more on the operational conditions imposed to the process rather than on sterility precautions. MMC-based PHA producing processes using waste as substrates and at the same time using existing wastewater treatment facilities contributes to the reduction of PHA production costs and could contribute to the overall economic profit of waste-generating factories and wastewater treatment plants (reviewed by Serafim et al., 2016).

4. Application of stress factors as a strategy to improve PHA production

The fact that PHA are involved in the stress response of bacteria displays another potential technological significance. Application of certain amounts of stress factor(s) induces or supports PHA accumulation in bacterial cells. Therefore, it can be used as an innovative and efficient strategy to improve biotechnological PHA production processes. For instance, it was observed that application of an appropriate

amount of osmotic pressure, heavy metals, H_2O_2 and ethanol enhances PHA yields in *Cupriavidus necator* H16 by about 30% compared to the control cultivation of PHA-negative mutants (Obruca et al., 2010a). The metabolic consequences of enhancing PHA accumulation by H_2O_2 and ethanol were further investigated and it was observed that application of H_2O_2 induced an oxidative pressure response which is associated with enhanced activity of NAPDH-generating pathways, such as the pentose phosphate cycle; this consequently increases the intracellular ratio of $NADPH/NADP^+$. This increase further stimulated the flow of acetyl-CoA towards PHA biosynthesis rather than into the TCA cycle. Also during ethanol metabolisation by dehydrogenases, reduced coenzymes were formed which resulted in a similar PHA biosynthesis-supporting effect on acetyl-CoA flux as observed in the case of H_2O_2. Thus, application of ethanol or H_2O_2 can be considered an auspicious strategy to increase PHA productivity by well-dosed application of an inexpensive substance (Obruca et al., 2010b). The fact that the oxidative stress adaptation of bacteria supports PHA accumulation was also observed during metabolic analysis of a PHA over-producing mutant of *C. necator* prepared by random mutagenesis. The mutant strain exhibited considerably increased activities of NADPH-generating enzymes involved in the oxidative stress response of bacteria, such as NADP-dependent isocitrate dehydrogenase, glutamate dehydrogenase, glucose-6-phospahte dehydrogenase or malic enzymes. Furthermore, the mutant strain not only reached higher yields of PHA on waste frying oils, it was also capable of more efficient incorporation of 3-hydroxyvalerate (3HV) precursors into the P(3HB-*co*-3HV) copolymer structure than observed for the wild type (Obruca et al., 2013). Application of increased oxidative pressure to boost PHA production was also investigated by Follonier et al. (2012), who substantially enhanced the oxygen transfer rate in bioreactor by application of elevated pressure. Such a strategy tripled mcl-PHA yields by *Pseudomonas putida*. Therefore, simply "putting cells under pressure" might be a very simple and promising strategy to improve biotechnological processes of PHA production by controlled application of oxidative stress.

Apart from oxidative pressure, also the application of controlled osmotic pressure was reported as a potential strategy to improve PHA production. Passanha et al. (2014) enhanced PHA productivity employing *Cupriavidus necator* by controlled application of osmotic pressure induced by NaCl. Nevertheless, the dose of NaCl needs to be precisely optimized since NaCl applied at a concentration of 9 g/L enhanced PHA yields by about 30%, whereas the application of 12 and 15 g/L of NaCl inhibited PHA accumulation in bacterial cells. Further, employing *Zobellella denitrificans*, osmotic pressure induced by 20 g/L NaCl boosted PHA production on waste glycerol by about 5.9 times (Ibrahim and Steinbuchel, 2009). Similarly, enhancement of osmotic pressure induced by introduction of NaCl or poly(ethylene glycol) supported mcl-PHA accumulation in *Pseudomonas fluorescens* by 5.7 and 3.2 times, respectively (Khare et al., 2014). Enhanced osmotic pressure in cultivation media also improved PHA production in the cyanobacterium *Spirulina subsalsa* (Shrivastav et al., 2010) and the diazotroph bacterium *Rhizobium* DDSS-69 (Kamnev et al., 2005). Thus, it seems that application of cheap and environmentally friendly osmotic pressure-inducing compounds such as NaCl can be used as a viable strategy to improve PHA productivity. In this context it is noteworthy that inexpensive sea water can be used for cultivation media formulation, which would substantially reduce the overall cost of the PHA production process (Takahashi et al., 2017; Yue et al., 2014). Nevertheless, the osmolarity of cultivation media must be precisely optimized and controlled, since only mild osmotic pressure conditions induces PHA accumulation, while at osmotic pressure exceeding a critical value, growth of the bacterial culture is inhibited, and PHA production is impaired (Mozumder et al., 2015; Passanha et al., 2014). In some bacterial cultures, osmotic up-shock even induces degradation of intracellular PHA to help the cells coping with stress conditions (Breedveld et al., 1993).

Also the application of heavy metals was identified as a strategy to enhance PHA production. Pal and Paul (2012) isolated two bacterial strains capable of PHA accumulation, which were resistant to nickel. These bacteria were identified as *Cupriavidus pauculus* KPS 201 and *Bacillus firmus* AND 408. PHA accumulation was pronounced by the presence of heavy metals in the cultivation media. Moreover, in the presence of 4 mM Ni^{2+}, *C. pauculus* KPS 201 was capable of accumulating 81 wt% P(3HB-*co*-3HV) in CDM without the need for 3 HV precursors. Further, Chien et al. (2014) reported that specific P(3HB) productivity in *Cupriavidus taiwanensis* is enhanced by the presence of cadmium ions, although overall PHA yields were not improved since cadmium substantially reduced the growth of the bacterial culture. Similarly, reports exist that diverse heavy metals (Co^{2+}, Cu^{2+} and Zn^{2+}) enhance PHA accumulation in *A. brasilense*, but, unfortunately, data regarding the improvement of P(3HB) yields were not provided (Kamnev et al., 2005). In any event, despite the fact that PHA accumulation can obviously be enhanced by application of heavy metals, this strategy does not seem to be viable *in praxi*, since the presence of heavy metals in wastewater from the fermentation process could represent a serious environmental problem. Further, the enhancement of the system's productivity reported in the literature can hardly compensate for this serious economic and especially environmental concern provoked by heavy metal-contaminated wastewater.

5. PHA production employing extremophiles

Extremophiles are microorganisms capable of surviving and prospering at conditions, which are stressful or even lethal for "normal" (mesophilic) microorganisms. Although PHA production by extremophiles is not yet realized at industrial scale, significant PHA accumulation under high salinity, extremely acidic or alkaline pH-values, or very high or low temperature conditions are described in the current literature. Prokaryotic species from the domains Archaea and Bacteria are found among such physiological specialists. In many cases, adaptation to extremophile conditions is closely linked to the strain's potential for PHA accumulation. In this context, diverse mechanisms were proposed to explain the mechanistic role of PHA and its monomeric building blocks as cell- and enzyme protecting chaperons, and the factors fostering PHA biosynthesis under extreme environmental conditions.

During PHA production but also in many other biotechnological processes, microbial contamination poses a major risk to running fermentation batches and thus endangers the economic feasibility of new processes in development (Pirttijärvi et al., 1998). In this context, the application of extremophile production strains enables the cultivation under drastically reduced or even without any sterility precautions. Hence, applying such extremophiles in White Biotechnology, *e.g.*, for PHA production processes, can significantly reduce energy costs. Further, such strains can be subjected towards stable long-term cultivation in continuous, chemostat cultivation processes. This was demonstrated in the case of the halophile PHA-producing Archaeon *Haloferax mediterranei* (Hermann-Krauss et al., 2013) or the thermophile bacterium *Chelatococcus* sp. (Ibrahim and Steinbuchel, 2010). With these organisms, fermentation batches were operated without sterilizing the bioreactor equipment for extended periods. Therefore, application of extremophiles, especially halophiles and thermophiles, might pave the way towards cost-efficient PHA production by eliminating the need for axenic operation. This is combined with safe disposal of carbon-rich industrial waste streams, which can be applied as substrates for the bioprocesses. Currently, several challenges have to be tackled regarding strain improvement on the genetic level (Romanelli et al., 2014), as well as process engineering aspects.

5.1. Halophilic PHA producers

Halophiles constitute a phylogenetically versatile family of microbial strains, which require hypersaline milieus with NaCl acting as the

typical salt component. Nature has come up with various tactics by which cells adapt to high salinity. The main strategy involves the accumulation of compatible organic osmotic solutes without requiring in parallel exceptional adaptation of the proteome to the high salt concentrations (Wood et al., 2001). The multifarious approaches of halophiles to handle high salinity, together with the fact that halophile organisms are found throughout the tree of life, suggests that adaptation to high salinity is a metabolically rather common task. For example, the change of pigment patterns in microalgae as a response to changing salinity is a well-known example of the adaptive response to fluctuating environments (Borowitzka et al., 1990).

Using halophiles in biotechnology paves the way for several opportunities: First, high salinity in the cultivation media drastically reduces the risk of microbial contamination. Second, cultivating halophiles in saline media with high cell concentration results in the concentration of salt inside the cells, and thus in the reduction of salinity in the cultivation medium; highly diluted salt gets concentrated in the microbial biomass. This becomes important in the case of cultivating cells on highly saline waste streams, *e.g.*, whey permeate, which contains about 200 g/L NaCl. When whey permeate is applied as a carbon source for halophile PHA producers such as *Hfx. mediterranei*, both carbohydrate (lactose) and salt fraction are utilized by the cells. Third, mineral acid-catalyzed hydrolysis of inexpensive raw materials to generate feedstocks for PHA production, as demonstrated in the past for bagasse (Kulkarni et al., 2015), whey (Koller et al., 2016), straw (Ahn et al., 2016; Cesário et al., 2014), spent coffee grounds (Obruca et al., 2014), or "liquefied wood" (Koller et al., 2015) requires the subsequent neutralization of the cocktail of hydrolysis products. This neutralization, typically accomplished by addition of NaOH, generates considerable amounts of salts, which contribute to the salinity of the fermentation medium when added as substrate. Fourth, inexpensive seawater can be used for preparation of cultivation media (Takahashi et al., 2017; Yue et al., 2014). Fifth, compatible solutes, which are accumulated by bacteria to cope with high external salinity, such as ectoines, can represent valuable co-products (Guzmán et al., 2009). Last, but not least, the high inner osmotic pressure of halophile cells makes it easy to disintegrate them by exposure to hypotonic media such as deionized water; this approach releases intact PHA granules, which can be separated from residual cell debris by means of dissolved air floatation or centrifugation (Koller et al., 2013).

Due to its high robustness, fast growth, high PHA-accumulation capacity, and genetic stability, the Archaeon *Hfx. mediterranei* is currently regarded the most auspicious candidate for industrial-scale PHA production based on the surplus material whey, which accrues in vast quantities at dairies in different global regions (Koller et al., 2007; Pais et al., 2016). In a highly saline (200 g/L NaCl) cultivation medium based on hydrolyzed whey permeate as a carbon source, *Hfx. mediterranei* grows at a maximum specific growth rate (μmax.) of 0.11·1/h, which displays an excellent value for haloarchaea. The copolyester P(3HB-*co*-3HV) was accumulated at a maximum specific production rate (q_P) of 0.08 g/(g·h), and contained about 10 mol% 3HV. As a remarkable particularity, copolyester synthesis by this organism occurs without being supplied with precursor compounds structurally related to 3HV, which are typically needed for P(3HB-*co*-3HV) copolyester production by most described production strains (Koller et al., 2007). Only recently, it was demonstrated that P(3HB-*co*-3HV) production by *Hfx. mediterranei* is highly temperature-dependent (Cui et al., 2017). After optimization of the cultivation medium, volumetric and specific productivity amounted to 0.09 g/(L·h) and 0.15 g/(g·h), respectively. Highest biomass concentration achieved on hydrolyzed whey permeate was 16.8 g/L, containing 73 wt% P(3HB-*co*-3HV) (Koller et al., 2008). On a medium containing hydrolyzed whey permeate as the main carbon source and valeric acid and γ-butyrolactone (GBL) as precursors for 3HV and 4-hydroxybutyrate (4HB), respectively, the organisms produced a poly(3HB-*co*-21.8%-3HV-*co*-5.1%-4HB) terpolyester. This material displays low crystallinity and reduced melting temperature,

which enhances its plasticity and processibility (Koller et al., 2007). Based on the high salinity needed to farm *Hfx. mediterranei* efficiently, the risk of microbial contamination is indeed negligible. Even without any sterilization precautions, no microbial contamination was observed in cultivation setups running over extended periods of several weeks (Hermann-Krauss et al., 2013). An economic assessment of *Hfx. mediterranei* mediated PHA production on hydrolyzed whey and solvent-free downstream processing (decomposition of cells in hypotonic medium), estimated the production price to be below 3 euro/kg PHA based on experimental data from a 200 L pilot scale (Koller et al., 2007). More recently, further cultivation of *Hfx. mediterranei* for PHA production in a highly saline medium was carried out using other carbon-rich industrial surplus streams. In this context, crude glycerol phase from biodiesel production (Hermann-Krauss et al., 2013), vinasse (Bhattacharyya et al., 2012), ethanol stillage (Bhattacharyya et al., 2014), molasses (Cui et al., 2017), or olive mill wastewater (Alsafadi et al., 2017) as the main carbon source.

At the moment, other haloarchaea, such as the *Halogeometricum borinquense* strain E3, are being investigated for PHA biosynthesis on inexpensive carbon sources such as hydrolyzed bagasse from the sugar industry (Salgaonkar and Bragança, 2017). In addition to haloarchaea, also halophile eubacterial strains display a high potential for PHA biosynthesis. For example, Tan et al. (2014) cultivated the halophile bacterial strain *Halomonas* TD01, an organism originally isolated from a salt lake, in non-sterile processes. In fed-batch fermentations on glucose, the strain reached 80 g/L CDM with 80 wt% PHA after 56 h. In an open, non-sterile, continuous two-stage process, CDM reached about 40 g/L with around 60 wt% P(3HB) in CDM in the first stage, which contained a saline medium rich in glucose and nitrogen; this process was operated for two weeks. The fermentation broth was continuously transferred from the first to the second stage, which was supplied with glucose, but nitrogen-free. In this second stage, a P(3HB) fraction in CDM up to 70 wt% was reached. Whereas in the first stage only 0.2–0.3 g P(3HB) were formed per gram of glucose, more than 0.50 g per gram of glucose were surprisingly obtained in the second stage. *Halomonas* TD01 was later subjected to genetic engineering to increase its propionate-to-3HV conversion efficiency by knocking out the 2-methylcitrate synthase encoding gene. Using a medium containing glucose and 0.5 g/L propionate, engineered cells produced 70 wt% P(3HB-*co*-3HV) in CDM with 12 mol% 3HV. On a 500 L pilot-scale with glucose as the sole carbon source, genetically engineered *Halomonas* TD01 reached a CDM of 112 g/L, with 70 wt% P(3HB) in CDM. Supplementation of propionate resulted in a CDM of 80 g/L with 70 wt% P(3HB-*co*-3HV) and 8 mol% 3HV in the copolyester. From small shaking flask setups, P(3HB) mass fractions of even more than 90 wt% and increased glucose-to-PHA conversion yields were reported using this organism (Tan et al., 2014).

The high salinity of the cultivation media used for halophiles, which amounts to up to 200–250 g/L NaCl in the case of *Hfx. mediterranei*, necessitates special materials for the bioreactor and the measuring sensors. Steel of the highest quality or polymers like poly(ether ether ketone) (PEEK) were suggested in the literature (Hezayen et al., 2000). Salt disposal from spent fermentation broth constitutes another crucial aspect in using halophiles, because current environmental standards do not allow discharging wastewater with total dissolved solids exceeding 2000 mg/L. For economic and environmental reasons, recycling of the highly saline side streams of whey-based *Hfx. mediterranei* cultivation processes was studied. As a result, it was demonstrated that the spent fermentation broth could replace a considerable share of fresh saline cultivation medium in subsequent cultivation batches. Further, about 29% of the expensive growth additive yeast extract, acting as a nitrogen- and phosphate source for efficiently thriving *Hfx. mediterranei*, can be substituted by cell debris from previous cultivation setups (Koller, 2015). Additional recycling experiments were carried out by Bhattacharyya et al. (2014), who used stillage from rice-based ethanol distillation for P(3HB) production with *Hfx. mediterranei*. In shaking

Table 1
PHA production by halophiles.

Microorganism	Extreme conditions applied	Substrates used	Description of the process	PHA type and parameters of the process	Reference
Halomonas campaniensis (G-, Bacteria) engineered strain	2.7 wt% NaCl pH 10	Artificial carbonaceous kitchen waste	Open cultivation for 65 days	P(3HB) content 70 wt%	Yue et al., 2014
Halomonas boliviensis (G-, Bacteria)	4.5–15 wt% NaCl	Glucose + glutamate	Two subsequent fed-batch cultivations, first at 4.5 wt% NaCl to produce biomass, after that 7.5 wt% NaCl and limitation by N and P	P(3HB) content 68.5 wt%; 1 g/(L·h); coproduction of ectoines	Guzmán et al., 2009
Halomonas boliviensis (G-, Bacteria)	4.5 wt% NaCl	Starch hydrolysate	Air-lift bioreactor	P(3HB) content 41 wt%	Rivera-Terceros et al., 2015
Halomonas TD01 (G-, Bacteria) Engineered strain	6 wt% NaCl	Glucose + yeast extract	Engineered strain capable of P(3HB-*co*-3HV) production without use of precursors, shake flasks	P(3HB-*co*-3HV) content 82 wt%	Tan et al., 2014
Bacillus megaterium uyuni S29 (G +, Bacteria)	4.5 wt% NaCl	Glucose	Shaken flasks	P(3HB) 2.2 g/L, 0.1 g/(L·h)	Rodríguez-Contreras et al., 2013
Yangia sp. ND199 (G-, Bacteria)	3.0 wt% NaCl	Fructose + precursors	Shaking flasks, testing of various precursors of 3HV and 4HB	P(3HB) 2.6 g/L; P(3HB-*co*-4HB) 1.36 g/L; P (3HB-*co*-3HV) 1.44 g/L	Huu Phong et al., 2016
Yangia sp. ND199 (G-, Bacteria)	4.5 wt% NaCl	Crude glycerol + high fructose corn syrup + yeast extract	Bioreactor, Fed-batch cultivation	P(3HB-*co*-3HV) content 56 wt%, 0.61 g/(L·h)	Van-Thuoc et al., 2015
Bacillus megaterium H16 (G +, bacteria]	5 wt% NaCl	Glucose	Shaken flasks	P(3HB) content 39 wt%	Salgaonkar et al., 2013
Natrinema pallidum (Archaea)	25 wt% NaCl	Starch	Shaken flasks	P(3HB-*co*-3HV) content 54 wt%	Danis et al., 2015
Halogeometricum borinquense (Archaea)	25 wt% NaCl	Glucose + yeast extract	Shaken flasks	P(3HB-*co*-3HV) content 73.51 wt%	Salgaonkar and Bragança, 2015
Haloferax mediterranei (Archaea)	25 wt% marine salts	Starch and glucose	Continuous cultivation lasting over 3 months, bioreactor 1.5 L	P(3HB-*co*-3HV) 6.5 g/L for starch 3.5 g/L for glucose	Lillo and Rodriguez-Valera, 1990
Haloferax mediterranei (Archaea)	15 wt% NaCl	Glucose + yeast extract	Fed-batch in 10 L bioreactor	P(3HB-*co*-3HV) 0.21 g/(L·h)	Koller et al., 2015
Haloferax mediterranei (Archaea)	20 wt% NaCl	Hydrolyzed whey permeate + GBL	Bioreactor 42 L	P(3HB-*co*-3HV-*co*-4HB); 14.7 g/L, g/(L·h)	Koller, 2015
Haloferax mediterranei (Archaea)	15 wt% NaCl	Crude glycerol + GBL	Bioreactor 42 L	P(3HB-*co*-3HV-*co*-4HB); 11.1 g/L, 0.10 g/(L·h)	Hermann-Krauss et al., 2013
Haloferax mediterranei (Archaea)	23.4 wt% NaCl	Extruded rice bran and extruded corn starch	pH-stat, 5 L bioreactor	P(3HB-*co*-3HV) 24.2 g/L	Huang et al., 2006

flask cultivations, about 70 wt% PHA in CDM, a P(3HB) concentration of about 16.4 g/L, a volumetric PHA productivity of 0.17 g/(L·h), and a PHA yield of 0.35 g/g were obtained. Similar to setups using whey-derived substrates, a P(3HB-*co*-3HV) copolyester with a 3HV fraction of 15.3 mol% was produced by the strain. The (bio)chemical oxygen demand of stillage was reduced by about 85% due to the conversion of organic compounds by the cells. The final concentration of total dissolved solids in the discharge water amounted to only 670 mg/L, which is about 30% of the permitted level. Also in this study, PHA granules were released from the haloarchaeal cells by hypotonic cell decomposition. The overview of PHA production by halophiles is provided in Table 1.

5.2. Thermophile PHA production

Bioreactor cultivations of thermophilic microbes require only minor cooling efforts, which can make them more energy-efficient than cultivations of microbes in the thermo-mesophilic range. Further, thermophilic cultivations are "self-heating" systems due to the heat generation by the microbes' exothermic metabolism; this is especially important at high cell density. Moreover, the stirring system of the bioreactor generates heat energy to be used for the cultivation process. The synergism of these manifold effects enables the reduction of both heating and cooling expenses. As an additional benefit of cultivation at temperatures, which are already harmful for mesophilic organisms, sterility provisions can be drastically saved, analogous to the

advantages of cultivations of halophile organisms (Ibrahim and Steinbuchel, 2010).

Mechanistic consideration of the context between high temperature and PHA metabolism has been recently carried out by Obruca et al. (2016c), who revealed the protective role of the P(3HB) building block 3HB, which acts as a chemical chaperone for various enzymes like lipase and lysozyme, preventing the enzymes from denaturation by heat and oxidation. Lipase denaturation caused by high temperature with and without 3HB was studied. As a result, it was shown that P(3HB) displays a substantial shielding effect, which was even superior to the protective effect exerted by well-described chemical chaperones such as trehalose or hydroxyectoine. 3HB turned out to protect lipase not only against denaturation by heat, but also against oxidative impairment caused by Cu^{2+}-ions or H_2O_2. Also, the protective performance against oxidative stress was superior to that of trehalose, and in the same range as reported for hydroxyectoine. These results strengthen the outcomes of previous studies accomplished by Soto et al. (2012), who for the first time proposed a protective role of PHA in avoiding enzyme denaturation at high salinity and temperature.

Synechococcus sp. MA19, a thermophilic cyanobacterium highly capable of photoautotrophic P(3HB) production, was originally isolated from a volcanic rock by Miyake et al. (1996). This organism thrives best at 50 °C, and can accumulate up to 21 wt% P(3HB) in CDM in photoautotrophic cultivations in simple bottles aerated by an air stream enriched with 2% CO_2. Fine-tuning the CO_2-supply and illumination regime determines the PHA productivity of this strain, which makes

Table 2
PHA production by thermophiles.

Organism	Temp.	Substrate	Cultivation	Product	Reference
Thermus thermophilus (G-, Bacteria)	75 °C	Gluconate and octanoate	Shaken flasks	scl-*co*-mcl PHA content up to 40 wt%	Pantazaki et al. (2003)
Thermus thermophilus (G-, Bacteria)	70 °C	Enzymatically hydrolyzed whey	Shaken flasks	scl-*co*-mcl PHA, content up to 35 wt%	Pantazaki et al. (2009)
Chelatococcus sp. strain MW10 (G-, Bacteria)	55 °C	Glucose	42 L bioreactor, cyclic fed-batch cultivation	P(3HB) 16.8 g/L	Ibrahim and Steinbuchel (2010)
Chelatococcus daeguensis TAD1 (G-, Bacteria)	50 °C	Glucose and glycerol	Shaken flasks	P(3HB) content 80 wt%, 3.44 g/L	Xu et al. (2014)
Chelatococcus daeguensis TAD1 (G-, Bacteria)	50 °C	Glycerol + various nitrogen sources	Two-stage fed batch	P(3HB) 17.4 g/L, 0.434 g/(L·h)	Cui et al. (2015)
Bacillus shackletonii K5 (G +, Bacteria]	45 °C	Glucose	Batch cultivation	P(3HB) content 72.6 wt%, 9.76 g/L	Liu et al. (2014)
Aneurinibacillus sp. XH2 (Bacteria, G$^+$)	55 °C	Glucose + peptone + yeast extract	Shaken flasks	P(3HB-*co*-3 HV) 0.11 g/L	Xiao et al. (2015)
Caldimonas taiwanensis (Bacteria, G-)	55 °C	Starch + valerate	Shaken flasks	P(3HB-*co*-3 HV) content 67 wt%, 0.536 g/L for cassava starch	Sheu et al. (2009)
Cupriavidus sp. S-6 (Bacteria, G-)	50 °C	Gluconate	Shaken flasks, in-depth molecular characterization of PHA synthase	P(3HB) content 49 wt%	Sheu et al. (2012)
Pseudomonas sp. SG4502 (Bacteria, G-)	55 °C	Acetate, octanoate and dodecanoate	Shaken flasks, comparison of various substrates	mcl-PHA content up to 40.6 wt%	Satoh et al. (2011)

optimization of the engineering necessary for large-scale processing. In nitrogen-limited dark cultivations, the P(3HB) content in CDM increased to 27 wt% because of degradation of glycogen, the second storage product accumulated by this strain under similar conditions like PHA, in the dark, which reduces the overall CDM. In contrast to glycogen, intracellular P(3HB) was only degraded in nitrogen-rich conditions under illumination.

Pantazaki et al. (2003) reported the outcomes of the cultivation of the highly thermophilic bacterium *Thermus thermophilus* to study PHA biosynthesis at high temperature. *T. thermophilus* cells were grown on gluconate, and activities of the PHA biosynthesis key enzymes 3-ketothiolase, NADPH-dependent reductase, and PHA synthase were measured in the cytosol of harvested cells. PHA synthase revealed temperature and pH-optima of about 70 °C and an optimum pH value of 7.3, respectively (Papi et al., 2008). At exceptionally high temperatures up to 75 °C, sodium gluconate or sodium octanoate were applied as sole substrates, which resulted in PHA contents in CDM of up to 40 wt%. The two applied substrates were converted by the strain to PHA of varying monomeric composition. Utilization of gluconate resulted in the accumulation of a copolyester predominantly consisting of 3-hydroxydecanoate (3HD) and smaller fractions of 3-hydroxyoctanoate (3HO), 3 HV, and 3HB, the copolyester produced by the strain by using octanoate was predominantly composed of 3-hydroxyundecanoate (3HUD) (35.4 mol%), 3HB (24.5 mol%), and smaller fractions of 3HO, 3-hydroxynonanoate (3HN), 3HD, and 3-hydroxydodecanoate (3HDD). The copolyester produced from gluconate had a weight average molecular mass of Mw = 480 kDa, while the Mw of the product from octanoate amounted to 391 kDa (Pantazaki et al., 2003).

Advanced cultivation techniques were used by Ibrahim et al. to increase PHA productivity by the thermophile organism *Chelatococcus* sp. strain MW10. First, a fed-batch cultivation in a 2 L bioreactor was carried out by permanently providing glucose at a concentration above 20 g/L; glucose was provided *via* substrate pulses to increase biomass and P(3HB) productivity, and to avoid intracellular P(3HB) degradation due to substrate limitation. The highest P(3HB) (2.9 ± 0.7 g/L) and CDM (5.2 ± 0.6 g/L) concentration was achieved after 53 h. Despite the permanent availability of glucose, the P(3HB) content drastically declined in the later phase of the process. To overcome this shortcoming, a cyclic batch fermentation (CBF) was carried out in a 42 L bioreactor at 50 °C and a permanent glucose concentration of 50 g/L. 50 h cultivation batches were carried out per cycle based on the outcomes of the above-described 2 L fed-batch cultivations. The cultivation

was started with a volume of 25 L, the partial tension of oxygen (p$_{O2}$) was kept constant at 20% of saturation. During the first cycle, a high specific growth rate of μ$_{max.}$ = 0.125·1/h and a drastically improved CDM of 12.7 ± 0.9 g/L was obtained, however, the P(3HB) concentration (5–6 g/L) was similar to the fed-batch results. After this first cycle, the greater part (23 L) of the fermentation broth was withdrawn, and 23 L of fresh, non-sterilized medium were added to start the second cycle. After this second cycle, a similar CDM (about 11 g/L) was obtained, but reduced P(3HB) fractions in biomass of less than 40 wt% were reached in spite of the fact that glucose was permanently present. Therefore, a further process improvement strategy was tested, the so-called cyclic fed-batch fermentation (CFBF). CFBF describes a modified semi-continuous cultivation approach, where varying volumes of the fermentation broth are replaced by fresh medium in such a way to partly recycle 20 to 40% of the fermentation broth. This culture cycling was carried out at different intervals, taking into account the volume increase and the reduced p$_{O2}$ level occurring at high cell concentration. The CFBF was started as a batch process with 30 g/L glucose. Feeding of fresh medium started after 21 h of cultivation. After 44 h, the first cycling was accomplished in a period of fast biomass growth (μ of 0.070·1/h), significantly before P(3HB) degradation had to be anticipated. Five liters of fermentation broth were withdrawn and replaced by 5 L of fresh medium. After that, continuous glucose feeding was started, followed by subsequent medium replacement cycles according to the volume increase. To prevent extreme dilution of the culture, 10 L were withdrawn at the second cycle and replaced by only 5 L of fresh medium. A final refilling of 5 L of fresh medium was accomplished after 14 h in cycle 3. Highest P(3HB) fractions in biomass of more than 50 wt % occurred in cycle 2 between 82 h and 143 h. After the end of cycle 2 after 181 h, 43.0 ± 1.4 g/L CDM, 39.0 ± 8.5 wt% P(3HB) in CDM, and the highest P(3HB) productivity (16.8 ± 4.2 g/L) were obtained. Biomass growth increased considerably at the end of cycle 3, when a CDM of 115.0 ± 4.3 g/L was reached. Although a P(3HB) fraction in CDM of 11.8 ± 3.8 wt% was noticed at the end of this process, which is lower than those obtained by the fed-batch and the CBF process, an auspicious volumetric P(3HB) productivity of 13.7 ± 4.9 g/(L·h) was achieved (Ibrahim and Steinbuchel, 2010). Processes of PHA production employing thermophiles are summarized in Table 2.

6. Conclusions

The fact that PHA accumulation enhances the stress resistance of

bacteria has been proved in numerous studies with various microorganisms. It seems that the protective mechanisms exterted by PHA are complex and involve numerous biochemical as well as biophysical modes of action. The interconnection of the presence of PHA granules in bacterial cells and the cells´ improved stress resistance has numerous practical outcomes. Generally, the ability to accumulate PHA enhances the robustness and fitness of microbes under non-optimal conditions, which can be highly advantageous when microorganisms are employed as agricultural inoculants or as pollutant removers in *in-situ* bioremediation technologies. During these applications, microorganisms are exposed to numerous stress factors and starvation, and therefore PHA accumulating microorganisms could be preferentially selected and high PHA content in bacterial cells could be considered as important parameter for preparation of microbial cultures prior to their application. Especially robust PHA-producing species present in mixed cultures, typically exposed to environmentally harsh conditions, display a powerful option to convert various carbonaceous industrial and municipal waste streams into valued PHA. Furthermore, it was also observed that appropriately selected stress conditions support PHA accumulation, and therefore controlled extertion of stress conditions during fermentation could be considered a promising strategy to improve the PHA production process. Finally, probably as the consequence of adaptation to stressful conditions, numerous extremophiles demonstrate a PHA production ability. Utilization of extremophiles such as halophiles or thermophiles for PHA production provides numerous advantages such as reduction of sterility requirements and the possibility of operating fermentation batches in continuous mode without risk of contamination, which can considerably improve the economic aspect of PHA production.

Funding

References

Ahn, J., Jho, E.H., Kim, M., Nam, K., 2016. Increased 3HV concentration in the bacterial production of 3-hydroxybutyrate (3HB) and 3-hydroxyvalerate (3HV) copolymer with acid-digested rice straw waste. J. Polym. Environ. 24, 98–103.

Albuquerque, M.G.E., Eiroa, M., Torres, C., Nunes, B.R., Reis, M.A.M., 2007. Strategies for the development of a side stream process for polyhydroxyalkanoate (PHA) production from sugar cane molasses. J. Biotechnol. 130, 411–421.

Alsafadi, D., Al-Mashaqbeh, O., Kim, M., Nam, K., 2017. A one-stage cultivation process for the production of poly-3-(hydroxybutyrate-co-hydroxyvalerate) from olive mill wastewater by Haloferax mediterranei. New Biotechnol. 34, 47–53.

Aneja, P., Zachertowska, A., Charles, T.C., Nam, K., 2005. Comparison of the symbiotic and competition phenotypes of Sinorhizobium meliloti PHB synthesis and degradation pathway mutants. Can. J. Microbiol. 51, 599–604.

Arora, P.K., Srivastava, A., Singh, V.P., 2014. Bacterial degradation of nitrophenols and their derivatives. J. Hazard. Mater. 266, 42–59.

Avella, M., Martuscelli, E., 1988. Poly-d-(−)(3-hydroxybutyrate)/poly(ethylene oxide) blends: phase diagram, thermal and crystallization behaviour. Polymer 29, 1731–1737.

Ayub, N.D., Pettinari, M.J., Ruiz, J.A., López, N.I., 2004. A polyhydroxybutyrate-producing Pseudomonas sp. isolated from antarctic environments with high stress resistance. Curr. Microbiol. 49, 170–174.

Ayub, N.D., Pettinari, M.J., Méndez, B.S., López, N.I., 2007. The polyhydroxyalkanoate genes of a stress resistant Antarctic Pseudomonas are situated within a genomic island. Plasmid 58, 240–248.

Ayub, N.D., Tribelli, P.M., López, N.I., 2009. Polyhydroxyalkanoates are essential for maintenance of redox state in the Antarctic bacterium Pseudomonas sp. 14-3 during low temperature adaptation. Extremophiles 13, 59–66.

Bair, H.E., Johnson, G.E., Anderson, E.W., Matsuoka, S., 1981. Non equilibrium annealing behavior of poly(vinyl acetate): phase diagram, thermal and crystallization behaviour. Polym. Eng. Sci. 21, 930–935.

Barnard, G.N., Sanders, J.K.M., 1989. The poly-beta-hydroxybutyrate granule In vivo - a new insight based on nmr-spectroscopy of whole cells. J. Biol. Chem. 264, 3286–3291.

Bengtsson, S., Werker, A., Christensson, M., Welander, T., 2008. Production of polyhydroxyalkanoates by activated sludge treating a paper mill wastewater. Bioresour. Technol. 99, 509–516.

Bengtsson, S., Karlsson, A., Alexandersson, T., Quadri, L., Hjort, M., Johansson, P., Moragn-Sagastume, F., Anterrieu, S., Arcos-Hernandez, M., Karabegovic, L., Magnusson, P., Werker, A., 2017. A process for polyhydroxyalkanoate (PHA) production from municipal wastewater treatment with biological carbon and nitrogen removal demonstrated at pilot-scale. New Biotechnol. 35, 42–53.

Berezina, N., Yada, B., Lefebvre, R., 2015. From organic pollutants to bioplastics: insights into the bioremediation of aromatic compounds by Cupriavidus necator. New Biotechnol. 32, 47–53.

Bergersen, F.J., Peoples, M.B., Turner, G.L., 1991. A role for poly-beta-hydroxybutyrate in bacteroids of soybean root nodules. Proc. R. Soc. London, Ser. B 245, 59–64.

Bhattacharyya, A., Pramanik, A., Maji, S., Haldar, S., Mukhopadhyay, U., Mukherjee, J., 2012. Utilization of vinasse for production of poly-3-(hydroxybutyrate-co-hydroxyvalerate) by Haloferax mediterranei. AMB Express 2, 34.

Bhattacharyya, A., Saha, J., Haldar, S., Bhowmic, A., Mukhopadhyay, U.K., Mukherjee, J., 2014. Production of poly-3-(hydroxybutyrate-co-hydroxyvalerate) by Haloferax mediterranei using rice-based ethanol stillage with simultaneous recovery and re-use of medium salts. Extremophiles 18, 463–470.

Bisht, S., Pandey, P., Bhargava, B., Sharma, S., Kumar, V., Sharma, K.D., 2015. Bioremediation of polyaromatic hydrocarbons (PAHs) using rhizosphere technology. Braz. J. Microbiol. 46, 7–21.

Bonthrone, K.M., Clauss, J., Horowitz, D.M., Hunter, B.K., Sanders, J.K.M., 1992. The biological and physical chemistry of polyhydroxyalkanoates as seen by NMR spectroscopy. FEMS Microbiol. Lett. 103, 269–277.

Borowitzka, M.A., Borowitzka, L.J., Kessly, D., 1990. Effects of salinity increase on carotenoid accumulation in the green alga Dunaliella salina. J. Appl. Phycol. 2, 111–119.

Breedveld, M.W., Dijkema, C., Zevenhuizen, L.P.T.M., Zehnder, A.J.B., 1993. Response of intracellular carbohydrates to a NaCl shock in Rhizobium leguminosarum biovar trifolii TA-1 and Rhizobium meliloti SU-47. J. Gen. Microbiol. 139, 3157–3163.

Bresan, S., Sznajder, A., Hauf, W., Forchhammer, K., Pfeiffer, D., Jendrossek, D., 2016. Polyhydroxyalkanoate (PHA) granules have no phospholipids. Sci. Rep. 6, 26612.

Calvert, P., 1992. Tender Morsels for Microbes. Nature 360, 535.

Campanari, S., Augelletti, F., Rossetti, S., Sciubba, F., Villano, M., Majone, M., 2017. Enhancing a multi-stage process for olive oil mill wastewater valorization towards polyhydroxyalkanoates and biogas production. Chem. Eng. J. 317, 280–289.

Ceccorulli, G., Pizzoli, M., Scandola, M., 1992. Plasticization of bacterial poly(3-Hydroxybutyrate). Macromolecules 25, 3304–3306.

Cesário, M.T., Raposo, R.S., de Almeida, M.C.M.D., van Keulen, F., Ferreira, B.S., da Fonseca, M.M.R., 2014. Enhanced bioproduction of poly-3-hydroxybutyrate from wheat straw lignocellulosic hydrolysates. New Biotechnol. 31, 104–113.

Cevallos, M.A., Encarnación, S., Leija, A., Mora, Y., Mora, J., 1996. Genetic and physiological characterization of a Rhizobium etli mutant strain unable to synthesize poly-beta-hydroxybutyrate. J. Bacteriol. 178, 1646–1654.

Chien, C.-C., Wang, L.-J., Lin, W.-R., 2014. Polyhydroxybutyrate accumulation by a cadmium-resistant strain of Cupriavidus taiwanensis. J. Taiwan Inst. Chem. Eng. 45, 1164–1169.

Choi, J.S., Park, W.H., 2004. Effect of biodegradable plasticizers on thermal and mechanical properties of poly(3-hydroxybutyrate). Polym. Test. 23, 455–460.

Ciesielski, S., Górniak, D., Możejko, J., Świątecki, A., Grzesiak, J., Zdanowski, M., 2014. The diversity of bacteria isolated from Antarctic freshwater reservoirs possessing the ability to produce Polyhydroxyalkanoates. Curr. Microbiol. 69, 594–603.

Cormia, R.L., Price, F.P., Turnbull, D., 1962. Kinetics of crystal nucleation in polyethylene. J. Chem. Phys. 37, 1333–1340.

Cui, B., Huang, S., Xu, F., Zhang, R., Zhang, Y., 2015. Improved productivity of poly (3-hydroxybutyrate) (PHB) in thermophilic Chelatococcus daeguensis TAD1 using glycerol as the growth substrate in a fed-batch culture. Appl. Microbiol. Biotechnol. 99, 6009–6019.

Cui, Y.-W., Zhang, H.-Y., Ji, S.-Y., Wang, Z.-W., 2017. Kinetic analysis of the temperature effect on Polyhydroxyalkanoate production by Haloferax mediterranei in synthetic molasses wastewater. J. Polym. Environ. 25, 277–285.

Danis, O., Ogan, A., Tatlican, P., Attar, A., Cakmakci, E., Mertoglu, B., Birbir, M., 2015. Preparation of poly(3-hydroxybutyrate-co-hydroxyvalerate) films from halophilic archaea and their potential use in drug delivery. Extremophiles 19, 515–524.

De Grazia, G., Quadri, L., Majone, M., Morgan-Sagastume, F., Werker, A., 2017. Influence of temperature on mixed microbial culture polyhydroxyalkanoate production while treating a starch industry wastewater. J. Environ. Chem. Eng. 5, 5067–5075.

Dionisi, D., Majone, M., Papa, V., Beccari, M., 2004. Biodegradable polymers from organic acids by using activated sludge enriched by aerobic periodic feeding. Biotechnol. Bioeng. 85, 569–579.

Dobbelaere, S., Croonenborghs, A., Thys, A., Ptacek, D., Vanderleyden, J., Dutto, P., et al., 2001. Responses of agronomically important crops to inoculation with Azospirillum. Funct. Plant Biol. 28, 871–879.

Encarnacion, S., del Carmen Vargas, M., Dunn, M.F., Davalos, A., Mendoza, G., Mora, Y., Mora, J., 2002. AniA regulates reserve polymer accumulation and global protein expression in Rhizobium etli. J. Bacteriol. 184, 2287–2295.

Fallik, E., Okon, Y., 1996. The response of maize (Zea mays) to Azospirillum inoculation in various types of soils in the field. World J. Microbiol. Biotechnol. 12, 511–515.

Follonier, S., Henes, B., Panke, S., Zinn, M., 2012. Putting cells under pressure: a simple and efficient way to enhance the productivity of medium-chain-length polyhydroxyalkanoate in processes with Pseudomonas putida KT2440. Biotechnol. Bioeng. 109, 451–461.

Francis, L., Meng, D., Locke, I.C., Knowles, J.C., Mordan, N., Salih, V., et al., 2016. Novel poly(3-hydroxybutyrate) composite films containing bioactive glass nanoparticles for wound healing applications. Polym. Int. 65, 661–674.

Goff, M., Ward, P., Oconnor, K., 2007. Improvement of the conversion of polystyrene to polyhydroxyalkanoate through the manipulation of the microbial aspect of the process: a nitrogen feeding strategy for bacterial cells in a stirred tank reactor. J.

Biotechnol. 132, 283–286.

Goh, Y.S., Tan, I.K.P., 2012. Polyhydroxyalkanoate production by antarctic soil bacteria isolated from Casey Station and Signy Island. Microbiol. Res. 167, 211–219.

Goh, L.-K., Purama, R.K., Sudesh, K., 2014. Enhancement of stress tolerance in the Polyhydroxyalkanoate producers without mobilization of the accumulated granules. Appl. Biochem. Biotechnol. 172, 1585–1598.

Guzmán, H., Van-Thuoc, D., Martín, J., Hatti-Kaul, R., Quillaguamán, J., 2009. A process for the production of ectoine and poly(3-hydroxybutyrate) by *Halomonas boliviensis*. Appl. Microbiol. Biotechnol. 84, 1069–1077.

Harrison, S.T.L., Chase, H.A., Amor, S.R., Bonthrone, K.M., Sanders, J.K., 1992. Plasticization of poly(hydroxybutyrate) *in vivo*. Int. J. Biol. Macromol. 14, 50–56.

Hermann-Krauss, C., Koller, M., Muhr, A., Fasl, H., Stelzer, F., Braunegg, G., 2013. Archaeal production of Polyhydroxyalkanoate (PHA) co- and terpolyesters from biodiesel industry-derived by-products. Archaea 2013, 1–10.

Herridge, D.F., Peoples, M.B., Boddey, R.M., 2008. Global inputs of biological nitrogen fixation in agricultural systems. Plant Soil 311, 1–18.

Hezayen, F.F., Rehm, B.H.A., Eberhardt, R., Steinbüchel, A., 2000. Polymer production by two newly isolated extremely halophilic archaea: application of a novel corrosion-resistant bioreactor. Appl. Microbiol. Biotechnol. 54, 319–325.

Horowitz, D.M., Sanders, J.K.M., 1994. Amorphous, biomimetic granules of poly-hydroxybutyrate: preparation, characterization, and biological implications. J. Am. Chem. Soc. 116, 2695–2702.

Horowitz, D.M., Sanders, J.K.M., 1995. Biomimetic, amorphous granules of poly-hydroxyalkanoates: composition, mobility, and stabilization *in vitro* by proteins. Can. J. Microbiol. 41, 115–123.

Huang, T.-Y., Duan, K.-J., Huang, S.-Y., Chen, C.W., 2006. Production of poly-hydroxyalkanoates from inexpensive extruded rice bran and starch by *Haloferax mediterranei*. J. Ind. Microbiol. Biotechnol. 33, 701–706.

Huu Phong, T., Van Thuoc, D., Sudesh, K., 2016. Biosynthesis of poly(3-hydroxybutyrate) and its copolymers by *Yangia* sp. ND199 from different carbon sources. Int. J. Biol. Macromol. 84, 361–366.

Ibrahim, M.H.A., Steinbuchel, A., 2009. Poly(3-hydroxybutyrate) production from gly-cerol by *Zobellella denitrificans* MW1 via high-cell-density fed-batch fermentation and simplified solvent extraction. Appl. Environ. Microbiol. 75, 6222–6231.

Ibrahim, M.H.A., Steinbuchel, A., 2010. High-cell-density cyclic fed-batch fermentation of a poly(3-hydroxybutyrate)-accumulating thermophile, *Chelatococcus* sp. strain MW10. Appl. Environ. Microbiol. 76, 7890–7895.

Jendrossek, D., 2009. Polyhydroxyalkanoate granules are complex subcellular organelles (carbonosomes). J. Bacteriol. 191, 3195–3202.

Johnson, K., Jiang, Y., Kleerebezem, R., Muyzer, G., van Loosdrecht, M.C.M., 2009. Enrichment of a mixed bacterial culture with a high Polyhydroxyalkanoate storage capacity. Biomacromolecules 10, 670–676.

Kaartokallio, H., Søgaard, D.H., Norman, L., Rysgaard, S., Tison J, L., Delille, B., Thomas, D.N., 2013. Short-term variability in bacterial abundance, cell properties, and in-corporation of leucine and thymidine in subarctic sea ice. Aquat. Microb. Ecol. 71, 57–73.

Kadouri, D., Burdman, S., Jurkevitch, E., Okon, Y., 2002. Identification and isolation of genes involved in poly(β-hydroxybutyrate) biosynthesis in *Azospirillum brasilense* and characterization of a *phb*C mutant. Appl. Environ. Microbiol. 68, 2943–2949.

Kadouri, D., Jurkevitch, E., Okon, Y., 2003a. Involvement of the reserve material poly-beta-hydroxybutyrate in *Azospirillum brasilense* stress endurance and root coloniza-tion. Appl. Environ. Microbiol. 69, 3244–3250.

Kadouri, D., Jurkevitch, E., Okon, Y., 2003b. Poly beta-hydroxybutyrate depolymerase (PhaZ) in *Azospirillum brasilense* and characterization of a *pha*Z mutant. Arch. Microbiol. 180, 309–318.

Kadouri, D., Jurkevitch, E., Okon, Y., Castro-Sowinski, S., 2005. Ecological and agri-cultural significance of bacterial Polyhydroxyalkanoates. Crit. Rev. Microbiol. 31, 55–67.

Kamnev, A.A., Tugarova, A.V., Antonyuk, L.P., Tarantilis, P.A., Polissiou, M.G., Gardiner, P.H.E., 2005. Effects of heavy metals on plant-associated rhizobacteria: comparison of endophytic and non-endophytic strains of *Azospirillum brasilense*. J. Trace Elem. Med. Biol. 19, 91–95.

Khare, E., Chopra, J., Arora, N.K., 2014. Screening for mcl-PHA-producing fluorescent pseudomonads and comparison of mcl-PHA production under iso-osmotic conditions induced by PEG and NaCl. Curr. Microbiol. 68, 457–462.

Khosravi-Darani, K., Mokhtari, Z.-B., Amai, T., Tanaka, K., 2013. Microbial production of poly(hydroxybutyrate) from C1 carbon sources. Appl. Microbiol. Biotechnol. 97, 1407–1424.

Koller, M., 2015. Recycling of waste streams of the biotechnological poly(hydroxyalk-anoate) production by *Haloferax mediterranei* on whey. Int. J. Polym. Sci. 2015, 1–8.

Koller, M., Hesse, P., Bona, R., Kutschera, C., Atlić, A., Braunegg, G., 2007. Potential of various archae- and eubacterial strains as industrial Polyhydroxyalkanoate producers from whey. Macromol. Biosci. 7, 218–226.

Koller, M., Atlić, A., Gonzalez-Garcia, Y., Kutschera, C., Braunegg, G., 2008. Polyhydroxyalkanoate (PHA) biosynthesis from whey lactose. Macromol. Symp. 272, 87–92.

Koller, M., Gasser, I., Schmid, F., Berg, G., 2011. Linking ecology with economy: insights into polyhydroxyalkanoate-producing microorganisms. Eng. Life Sci. 11, 222–237.

Koller, M., Niebelschütz, H., Braunegg, G., 2013. Strategies for recovery and purification of poly[(*R*)-3-hydroxyalkanoates] (PHA) biopolyesters from surrounding biomass. Eng. Life Sci. 13, 549–562.

Koller, M., Chiellini, E., Braunegg, G., 2015. Study on the production and re-use of poly(3-hydroxybutyrate-*co*-3-hydroxyvalerate) and extracellular polysaccharide by the ar-chaeon *Haloferax mediterranei* strain DSM 1411. Chem. Biochem. Eng. Q. 29, 87–98.

Koller, M., Puppi, D., Chiellini, F., Braunegg, G., 2016. Comparing chemical and enzy-matic hydrolysis of whey lactose to generate feedstocks for haloarchaeal poly(3-

hydroxybutyrate-*co*-3-hydroxyvalerate) biosynthesis. Int. J. Pharm. Sci. Res. 3, IJPSR-112.

Koller, M., Maršálek, L., de Sousa Dias, M.M., Braunegg, G., 2017. Producing microbial polyhydroxyalkanoate (PHA) biopolyesters in a sustainable manner. New Biotechnol. 37, 24–38.

de Koning, G.J.M., Lemstra, P.J., 1992. The amorphous state of bacterial poly[(R)-3-hy-droxyalkanoate] *in vivo*. Polymer 33, 3292–3294.

Krastanov, A., Alexieva, Z., Yemendzhiev, H., 2013. Microbial degradation of phenol and phenolic derivatives. Eng. Life Sci. 13, 76–87.

Kulkarni, S.O., Kanekar, P.P., Jog, J.P., Sarnaik, S.S., Nilegaonkar, S.S., 2015. Production of copolymer, poly (hydroxybutyrate-*co*-hydroxyvalerate) by *Halomonas campisalis* MCM B-1027 using agro-wastes. Int. J. Biol. Macromol. 72, 784–789.

Kuppusamy, S., Thavamani, P., Megharaj, M., Lee, Y.B., Naidu, R., 2016. Polyaromatic hydrocarbon (PAH) degradation potential of a new acid tolerant, diazotrophic P-solubilizing and heavy metal resistant bacterium *Cupriavidus* sp. MTS-7 isolated from long-term mixed contaminated soil. Chemosphere 162, 31–39.

Lauzier, C., Marchessault, R.H., Smith, P., Chanzy, H., 1992a. Structural study of isolated poly(β-hydroxybutyrate) granules. Polymer 33, 823–827.

Lauzier, C., Revol, J.-F., Marchessault, R.H., 1992b. Topotactic crystallization of isolated poly(beta-hydroxybutyrate) granules from *Alcaligenes eutrophus*. FEMS Microbiol. Lett. 103, 299–310.

Li, Q., 2017. Rhamnolipid synthesis and production with diverse resources. Front. Chem. Sci. Eng. 11, 27–36.

Lillo, J.G., Rodriguez-Valera, F., 1990. Effects of culture conditions on poly (β-hydro-xybutyric acid) production by *Haloferax mediterranei*. Appl. Environ. Microbiol. 56, 2517–2521.

Liu, Y., Huang, S., Zhang, Y., Xu, F., 2014. Isolation and characterization of a thermo-philic *Bacillus shackletonii* K5 from a biotrickling filter for the production of poly-hydroxybutyrate. J. Environ. Sci. 26, 1453–1462.

López, N.I., Pettinari, M.J., Stackebrandt, E., Tribelli, P.M., Põtter, M., Steinbüchel, A., et al., 2009. *Pseudomonas extremaustralis* sp. nov., a poly(3-hydroxybutyrate) pro-ducer isolated from an Antarctic environment. Curr. Microbiol. 59, 514–519.

Lykidis, A., Pérez-Pantoja, D., Ledger, T., Mavromatis, K., Anderson, I.J., Ivanova, N.N., et al., 2010. The complete multipartite genome sequence of *Cupriavidus necator* JMP134, a versatile pollutant degrader. PLoS One 5, e9729.

Mandon, K., Michel-Reydellet, N., Encarnación, S., Kaminski, P.A., Leija, A., Cevallos, M.A., et al., 1998. Poly-beta-hydroxybutyrate turnover in *Azorhizobium caulinodans* is required for growth and affects *nifA* expression. J. Bacteriol. 180, 5070–5076.

Martino, L., Cruz, M.V., Scoma, A., Freitas, F., Bertin, L., Scandola, M., Reis, M.A.M., 2014. Recovery of amorphous polyhydroxybutyrate granules from *Cupriavidus ne-cator* cells grown on used cooking oil. Int. J. Biol. Macromol. 71, 117–123.

Mas, J., Pedros-Alio, C., Guerrero, R., 1985. Mathematical-model for determining the effects of intracytoplasmic inclusions on volume and density of microorganisms. J. Bacteriol. 164, 749–756.

Mezzina, M.P., Wetzler, D.E., de Almeida, A., Dinjaski, N., Prieto, M.A., Pettinari, M.J., 2015. A phasin with extra talents: a polyhydroxyalkanoate granule-associated protein has chaperone activity. Environ. Microbiol. 17, 1765–1776.

Miyake, M., Erata, M., Asada, Y., 1996. A thermophilic cyanobacterium, *Synechococcus* sp. MA19, capable of accumulating poly-β-hydroxybutyrate. J. Ferment. Bioeng. 82, 512–514.

Mokhtari-Hosseini, Z.B., Vasheghani-Farahani, E., Heidarzadeh-Vazifekhoran, A., Shojaosadati, S.A., Karimzadeh, R., Darani, K.K., 2009. Statistical media optimization for growth and PHB production from methanol by a methylotrophic bacterium. Bioresour. Technol. 100, 2436–2443.

Moreno, R., Rojo, F., 2013. The contribution of proteomics to the unveiling of the survival strategies used by *Pseudomonas putida* in changing and hostile environments. Proteomics 13, 2822–2830.

Mota, C., Wang, S.-Y., Puppi, D., Gazzarri, M., Migone, C., Chiellini, F., Chen, G.-Q., Chiellini, E., 2017. Additive manufacturing of poly[(*R*)-3-hydroxybutyrate-*co*-(*R*)-3-hydroxyhexanoate] scaffolds for engineered bone development. J. Tissue Eng. Regen. Med. 11, 175–186.

Mozumder, M.S.I., Garcia-Gonzalez, L., De Wever, H., Volcke, E.I.P., 2015. Effect of so-dium accumulation on heterotrophic growth and polyhydroxybutyrate (PHB) pro-duction by *Cupriavidus necator*. Bioresour. Technol. 191, 213–218.

Mravec, F., Obruca, S., Krzyzanek, V., Sedlacek, P., Hrubanova, K., Samek, O., et al., 2016. Accumulation of PHA granules in *Cupriavidus necator* as seen by confocal fluorescence microscopy. FEMS Microbiol. Lett. 363 fnw094.

Obruca, S., Marova, I., Stankova, M., Mravcova, L., Svoboda, Z., 2010a. Effect of ethanol and hydrogen peroxide on poly(3-hydroxybutyrate) biosynthetic pathway in *Cupriavidus necator* H16. World J. Microbiol. Biotechnol. 26, 1261–1267.

Obruca, S., Marova, I., Svoboda, Z., Mikulikova, R., 2010b. Use of controlled exogenous stress for improvement of poly(3-hydroxybutyrate) production in *Cupriavidus necator*. Folia Microbiol. 55, 17–22.

Obruca, S., Snajdar, O., Svoboda, Z., Marova, I., 2013. Application of random mutagen-esis to enhance the production of polyhydroxyalkanoates by *Cupriavidus necator* H16 on waste frying oil. World J. Microbiol. Biotechnol. 29, 2417–2428.

Obruca, S., Benesova, P., Petrik, S., Oborna, J., Prikryl, R., Marova, I., 2014. Production of polyhydroxyalkanoates using hydrolysate of spent coffee grounds. Process Biochem. 49, 1409–1414.

Obruca, S., Doskocil, L., Krzyzanek, V., Hrubanova, K., Sedlacek, P., Mravec, F., et al., 2016a. Polyhydroxyalkanoates in bacterial cells - more than just storage materials. Mater. Sci. Forum 851, 20–25.

Obruca, S., Sedlacek, P., Krzyzanek, V., Mravec, F., Hrubanova, K., Samek, O., et al., 2016b. Accumulation of poly(3-hydroxybutyrate) helps bacterial cells to survive freezing. PLoS One 11.

Obruca, S., Sedlacek, P., Mravec, F., Samek, O., Marova, I., 2016c. Evaluation of 3-

hydroxybutyrate as an enzyme-protective agent against heating and oxidative damage and its potential role in stress response of poly(3-hydroxybutyrate) accumulating cells. Appl. Microbiol. Biotechnol. 100, 1365–1376.

Obruca, S., Sedlacek, P., Mravec, F., Krzyzanek, V., Nebesarova, J., Samek, O., Kucera, D., Benesova, P., Hrubanova, K., Milerova, M., Marova, I., 2017. The presence of PHB granules in cytoplasm protects non-halophilic bacterial cells against the harmful impact of hypertonic environments. New Biotechnol. 39, 68–80.

Pais, J., Serafim, L.S., Freitas, F., Reis, M.A.M., 2016. Conversion of cheese whey into poly (3-hydroxybutyrate-*co*-3-hydroxyvalerate) by *Haloferax mediterranei*. New Biotechnol. 33, 224–230.

Pal, A., Paul, A.K., 2012. Accumulation of Polyhydroxyalkanoates by *Rhizobacteria* underneath nickel-hyperaccumulators from serpentine ecosystem. J. Polym. Environ. 20, 10–16.

Pantazaki, A.A., Tambaka, M.G., Langlois, V., Guerin, P., Kyriakidis, D.A., 2003. Polyhydroxyalkanoate (PHA) biosynthesis in *Thermus thermophilus*: purification and biochemical properties of PHA synthase. Mol. Cell. Biochem. 254, 173–183.

Pantazaki, A.A., Papaneophytou, C.P., Pritsa, A.G., Liakopoulou-Kyriakides, M., Kyriakidis, D.A., 2009. Production of polyhydroxyalkanoates from whey by *Thermus thermophilus* HB8. Process Biochem. 44, 847–853.

Papi, R.M., Mimikakou, G.E., Pantazaki, A.A., Kyriakidis, D.A., 2008. Identification of PHA loci in *Thermus thermophilus* HB8 genome. FEBS J. 275, 422.

Pärnänen, K., Karkman, A., Virta, M., Eronen-Rasimus, E., Kaartokallio, H., 2015. Discovery of bacterial polyhydroxyalkanoate synthase (PhaC)-encoding genes from seasonal Baltic Sea ice and cold estuarine waters. Extremophiles 19, 197–206.

Passanha, P., Kedia, G., Dinsdale, R.M., Guwy, A.J., Esteves, S.R., 2014. The use of NaCl addition for the improvement of polyhydroxyalkanoate production by *Cupriavidus necator*. Bioresour. Technol. 163, 287–294.

Patel, G., Singh, S., Saxena, D.S.K., Kaur, D.K.J., 2016. Isolation, biochemical characterization and production of biofertilizer from *Bacillus megaterium*. Int. J. Life. Sci. Sci. Res. 2, 749–752.

Pavez, P., Castillo, J.L., González, C., Martínez, M., 2009. Poly-β-hydroxyalkanoate exert a protective effect against carbon starvation and frozen conditions in *Sphingopyxis chilensis*. Curr. Microbiol. 59, 636–640.

Pereira, H., Lemos, P.C.P.C., Reis, M.A.M.A.M., Crespo, J.P.S.G., Carrondo, M.J.T., Santos, H., Cresp, J.P.S.G., Carrond, M.J.T., Santos, H., 1996. Model for carbon metabolism in biological phosphorus removal processes based on *in vivo* ^{13}C-NMR labelling experiments. Water Res. 30, 2128–2138.

Pierro, L., Matturro, B., Rossetti, S., Sagliaschi, M., Sucato, S., Alesi, E., et al., 2017. Polyhydroxyalkanoate as a slow-release carbon source for in situ bioremediation of contaminated aquifers: from laboratory investigation to pilot-scale testing in the field. New Biotechnol. 37, 60–68.

Pirttijärvi, T.S., Ahonen, L.M., Maunuksela, L.M., Salkinoja-Salonen, M.S., 1998. *Bacillus cereus* in a whey process. Int. J. Food Microbiol. 44, 31–41.

Pittmann, T., Steinmetz, H., 2017. Polyhydroxyalkanoate production on waste water treatment plants: process scheme, operating conditions and potential analysis for German and European municipal waste water treatment plants. Bioengineering 4, 54.

Qu, Y., Shen, E., Ma, Q., Zhang, Z., Liu, Z., Shen, W., et al., 2015. Biodegradation of indole by a newly isolated *Cupriavidus* sp. SHE. J. Environ. Sci. 34, 126–132.

Queirós, D., Rossetti, S., Serafim, L.S., 2014. PHA production by mixed cultures: a way to valorize wastes from pulp industry. Bioresour. Technol. 157, 197–205.

Queirós, D., Fonseca, A., Lemos, P.C., Serafim, L.S., 2016. Long-term operation of a two-stage polyhydroxyalkanoates production process from hardwood sulphite spent liquor. J. Chem. Technol. Biotechnol. 91, 2480–2487.

Rai, R., Roether, J.A., Knowles, J.C., Mordan, N., Salih, V., Locke, I.C., et al., 2016. Highly elastomeric poly(3-hydroxyoctanoate) based natural polymer composite for enhanced keratinocyte regeneration. Int. J. Polym. Mater. 66, 326–335.

Rhu, D.H., Lee, W.H., Kim, J.Y., Choi, E., 2003. Polyhydroxyalkanoate (PHA) production from waste. Water Sci. Technol. 48, 221–228.

Rivera-Terceros, P., Tito-Claros, E., Torrico, S., Carballo, S., Van-Thuoc, D., Quillaguamán, J., 2015. Production of poly(3-hydroxybutyrate) by *Halomonas boliviensis* in an air-lift reactor. J. Biol. Res. (Thessaloniki) 22.

Rodríguez-Contreras, A., Koller, M., Miranda-de Sousa Dias, M., Calafell-Monfort, M., Braunegg, G., Marqués-Calvo, M.S., 2013. High production of poly(3-hydroxybutyrate) from a wild *Bacillus megaterium* Bolivian strain. J. Appl. Microbiol. 114, 1378–1387.

Rogers, K., 2011. Bacteria and Viruses. Britannica Educational Pub. in association with Rosen Educational Services, New York, NY.

Romanelli, M.G., Povolo, S., Favaro, L., Fontana, F., Basaglia, M., Casella, S., 2014. Engineering *Delftia acidovorans* DSM39 to produce polyhydroxyalkanoates from slaughterhouse waste. Int. J. Biol. Macromol. 71, 21–27.

Rothermich, M.M., Guerrero, R., Lenz, R.W., Goodwin, S., 2000. Characterization, seasonal occurrence, and diel fluctuation of poly(hydroxyalkanoate) in photosynthetic microbial mats. Appl. Environ. Microbiol. 66, 4279–4291.

Ruiz, J.A., Lopez, N.I., Fernandez, R.O., Mendez, B.S., 2001. Polyhydroxyalkanoate degradation is associated with nucleotide accumulation and enhances stress resistance and survival of *Pseudomonas oleovorans* in natural water microcosms. Appl. Environ. Microbiol. 67, 225–230.

Saavedra, J.M., Acevedo, F., González, M., Seeger, M., 2010. Mineralization of PCBs by the genetically modified strain *Cupriavidus necator* JMS34 and its application for bioremediation of PCBs in soil. Appl. Microbiol. Biotechnol. 87, 1543–1554.

Safiyanu, I., Abdulwahid Isah, A., Abubakar, U.S., Rita Singh, M., 2015. Review on comparative study on bioremediation for oil spills using microbes. Res. J. Pharm. Biol. Chem. Sci. 6, 783.

Salehi, Z., Vahabzadeh, F., Sohrabi, M., Fatemi, S., Znad, H.T., 2010. Statistical medium optimization and biodegradative capacity of *Ralstonia eutropha* toward p-nitrophenol. Biodegradation 21, 645–657.

Salgaonkar, B.B., Bragança, J.M., 2015. Biosynthesis of poly(3-hydroxybutyrate- *co* -3-hydroxyvalerate) by *Halogeometricum borinquense* strain E3. Int. J. Biological. Macromolecules 78, 339–346.

Salgaonkar, B.B., Bragança, J.M., 2017. Utilization ofsSugarcane bagasse by *Halogeometricum borinquense* strain E3 for biosynthesis of poly(3-hydroxybutyrate-*co*-3-hydroxyvalerate). Bioengineering 4, 50.

Salgaonkar, B.B., Mani, K., Braganca, J.M., 2013. Characterization of polyhydroxyalkanoates accumulated by a moderately halophilic salt pan isolate *Bacillus megaterium* strain H16. J. Appl. Microbiol. 114, 1347–1356.

Salleh, A.B., Ghazali, F.M., Abd Rahman, R.N.Z., Basri, M., 2003. Bioremediation of petroleum hydrocarbon pollution. Indian J. Biotechnol. 2, 411–425.

Satoh, Y., Tajima, K., Nakamoto, S., Xuerong, H., Matsushima, T., Ohshima, T., et al., 2011. Isolation of a thermotolerant bacterium producing medium-chain-length polyhydroxyalkanoate. J. Appl. Microbiol. 111, 811–817.

Sedighi, M., Vahabzadeh, F., Zamir, S.M., Naderifar, A., 2013. Ethanethiol degradation by *Ralstonia eutropha*. Biotechnol. Bioprocess Eng. 18, 827–833.

Segura, D., Guzmán, J., Espín, G., 2003. *Azotobacter vinelandii* mutants that overproduce poly-beta-hydroxybutyrate or alginate. Appl. Microbiol. Biotechnol. 63, 159–163.

Serafim, L.S., Queirós, D., Rossetti, S., Costa Lemos, P., 2016. Biopolymer production by mixed microbial cultures: integrating remediation with valorization. In: Koller, M. (Ed.), Microbial Biopolyester Production, Performance and Processing. Vol. 1 (*Microbiology, feedstocks, and metabolism*). Book Series: Recent Advances in Biotechnology Bentham Science Publishers, pp. 26–264.

Sheu, D.-S., Chen, W.-M., Yang, J.-Y., Chang, R.-C., 2009. Thermophilic bacterium *Caldimonas taiwanensis* produces poly(3-hydroxybutyrate-co-3-hydroxyvalerate) from starch and valerate as carbon sources. Enzym. Microb. Technol. 44, 289–294.

Sheu, D.-S., Chen, W.-M., Lai, Y.-W., Chang, R.-C., 2012. Mutations derived from the thermophilic Polyhydroxyalkanoate synthase *PhaC* enhance the thermostability and activity of *PhaC* from *Cupriavidus necator* H16. J. Bacteriol. 194, 2620–2629.

Shrivastav, A., Mishra, S.K., Mishra, S., 2010. Polyhydroxyalkanoate (PHA) synthesis by *Spirulina subsalsa* from Gujarat coast of India. Int. J. Biol. Macromol. 46, 255–260.

Silva, F., Campanari, S., Matteo, S., Valentino, F., Majone, M., Villano, M., 2017. Impact of nitrogen feeding regulation on polyhydroxyalkanoates production by mixed microbial cultures. New Biotechnol. 37, 90–98.

Singh, J.S., Abhilash, P.C., Singh, H.B., Singh, R.P., Singh, D.P., 2011. Genetically engineered bacteria: an emerging tool for environmental remediation and future research perspectives. Gene 480, 1–9.

Singh, N.K., Chaudhary, F.K., Patel, D.B., 2013. Effectiveness of *Azotobacter* bio-inoculant for wheat grown under dryland condition. J. Environ. Biol. 34, 927–932.

Slaveykova, V.I., Pinheiro, J.P., Floriani, M., Garcia, M., 2013. Interactions of core–shell quantum dots with metal resistant bacterium *Cupriavidus metallidurans*: consequences for Cu and Pb removal. J. Hazard. Mater. 261, 123–129.

Slepecky, R.A., Law, J.H., 1961. Synthesis and degradation of poly-beta-hydroxybutyric acid in connection with sporulation of *Bacillus megaterium*. J. Bacteriol. 82, 37–42.

Soberón-Chávez, G., Aguirre-Ramírez, M., Sánchez, R., 2005. The *Pseudomonas aeruginosa* RhlA enzyme is involved in rhamnolipid and polyhydroxyalkanoate production. J. Ind. Microbiol. Biotechnol. 32, 675–677.

Soto, G., Setten, L., Lisi, C., Maurelis, C., Mozzicafreddo, M., Cuccioloni, M., et al., 2012. Hydroxybutyrate prevents protein aggregation in the halotolerant bacterium *Pseudomonas* sp. CT13 under abiotic stress. Extremophiles 16, 455–462.

Srivastava, J., Naraian, R., Kalra, S.J.S., Chandra, H., 2014. Advances in microbial bioremediation and the factors influencing the process. Int. J. Environ. Sci. Technol. 11, 1787–1800.

Steinbüchel, A., Hein, S., 2001. Biochemical and molecular basis of microbial synthesis of Polyhydroxyalkanoates in microorganisms. Adv. Biochem. Eng. Biotechnol. 71, 81–123.

Sudesh, K., Abe, H., Doi, Y., 2000a. Synthesis, structure and properties of poly-hydroxyalkanoates: biological polyesters. Prog. Polym. Sci. 25, 1503–1555.

Sudesh, K., Fukui, T., Iwata, T., Doi, Y., 2000b. Factors affecting the freeze-fracture morphology of *in vivo* polyhydroxyalkanoate granules. Can. J. Microbiol. 46, 304–311.

Takahashi, R.Y.U., Castilho, N.A.S., Silva, M.A.C.D., Miotto, M.C., Lima, A.O.D.S., 2017. Prospecting for marine bacteria for polyhydroxyalkanoate production on low-cost substrates. Bioengineering 4, 60.

Tal, S., Okon, Y., 1985. Production of the reserve material poly-β-hydroxybutyrate and its function in *Azospirillum brasilense* Cd. Can. J. Microbiol. 31, 608–613.

Tan, D., Wu, Q., Chen, J.-C., Chen, G.-Q., 2014. Engineering *Halomonas* TD01 for the low-cost production of polyhydroxyalkanoates. Metab. Eng. 26, 34–47.

Teng, Y., Wang, X., Zhu, Y., Chen, W., Christie, P., Li, Z., et al., 2017. Biodegradation of pentachloronitrobenzene by *Cupriavidus* sp. YNS-85 and its potential for remediation of contaminated soils. Environ. Sci. Pollut. Res. 24, 9538–9547.

Tribelli, P.M., López, N.I., 2011. Poly(3-hydroxybutyrate) influences biofilm formation and motility in the novel Antarctic species *Pseudomonas extremaustralis* under cold conditions. Extremophiles 15, 541–547.

Tribelli, P.M., Di Martino, C., López, N.I., Raiger Iustman, L.J., 2012. Biofilm lifestyle enhances diesel bioremediation and biosurfactant production in the Antarctic polyhydroxyalkanoate producer *Pseudomonas extremaustralis*. Biodegradation 23, 645–651.

Urmeneta, J., Mas-Castella, J., Guerrero, R., 1995. Biodegradation of poly-(beta)-hydroxyalkanoates in a lake sediment sample increases bacterial sulfate reduction. Appl. Environ. Microbiol. 61, 2046–2048.

Vadlja, D., Koller, M., Novak, M., Braunegg, G., Horvat, P., 2016. Footprint area analysis of binary imaged *Cupriavidus necator* cells to study PHB production at balanced, transient, and limited growth conditions in a cascade process. Appl. Microbiol. Biotechnol. 100, 10065–10080.

Valentino, F., Karabegovic, L., Majone, M., Morgan-Sagastume, F., Werker, A., 2015a.

Polyhydroxyalkanoate (PHA) storage within a mixed-culture biomass with simultaneous growth as a function of accumulation substrate nitrogen and phosphorus levels. Water Res. 77, 49–63.

Valentino, F., Morgan-Sagastume, F., Fraraccio, S., Corsi, G., Zanaroli, G., Werker, A., Majone, M., 2015b. Sludge minimization in municipal wastewater treatment by polyhydroxyalkanoate (PHA) production. Environ. Sci. Pollut. Res. 22, 7281–7294.

Valentino, F., Riccardi, C., Campanari, S., Pomata, D., Majone, M., 2015c. Fate of β-hexachlorocyclohexane in the mixed microbial cultures (MMCs) three-stage polyhydroxyalkanoates (PHA) production process from cheese whey. Bioresour. Technol. 192, 304–311.

Valentino, F., Morgan-Sagastume, F., Campanari, S., Villano, M., Werker, A., Majone, M., 2017. Carbon recovery from wastewater through bioconversion into biodegradable polymers. New Biotechnol. 37, 9–23.

Vandamme, P., Coenye, T., 2004. Taxonomy of the genus *Cupriavidus*: a tale of lost and found. Int. J. Syst. Evol. Microbiol. 54, 2285–2289.

Van-Thuoc, D., Huu-Phong, T., Minh-Khuong, D., Hatti-Kaul, R., 2015. Poly(3-hydroxybutyrate-co-3-Hydroxyvalerate) production by a moderate halophile *Yangia* sp. ND199 using glycerol as a carbon source. Appl. Biochem. Biotechnol. 175, 3120–3132.

Wallen, L.L., Rohwedder, W.K., 1974. Poly-β-hydroxyalkanoate from activated sludge. Environ. Sci. Technol. 8, 576–579.

Wang, Q., Yu, H., Xia, Y., Kang, Z., Qi, Q., 2009. Complete PHB mobilization in *Escherichia coli* enhances the stress tolerance: a potential biotechnological application. Microb. Cell Factories 8, 47.

Wasi, S., Tabrez, S., Ahmad, M., 2013. Use of *Pseudomonas* spp. for the bioremediation of environmental pollutants: a review. Environ. Monit. Assess. 185, 8147–8155.

Wood, J.M., Bremer, E., Csonka, L.N., Kraemer, R., Poolman, B., van der Heide, T., et al., 2001. Osmosensing and osmoregulatory compatible solute accumulation by bacteria. Comp. Biochem. Phys. A 130, 437–460.

Xiao, Z., Zhang, Y., Xi, L., Huo, F., Zhao, J. -yi, Li, J., 2015. Thermophilic production of polyhydroxyalkanoates by a novel *Aneurinibacillus* strain isolated from Gudao oilfield. China. J. Basic Microbiol. 55, 1125–1133.

Xu, F., Huang, S., Liu, Y., Zhang, Y., Chen, S., 2014. Comparative study on the production of poly(3-hydroxybutyrate) by thermophilic *Chelatococcus daeguensis* TAD1: a good candidate for large-scale production. Appl. Microbiol. Biotechnol. 98, 3965–3974.

Yin, J., Chen, J.-C., Wu, Q., Chen, G.-Q., 2015. Halophiles, coming stars for industrial biotechnology. Biotechnol. Adv. 33, 1433–1442.

Yue, H., Ling, C., Yang, T., Chen, X., Chen, Y., Deng, H., et al., 2014. A seawater-based open and continuous process for polyhydroxyalkanoates production by recombinant *Halomonas campaniensis* LS21 grown in mixed substrates. Biotechnol. Biofuels 7.

Zhao, Y.H., Li, H.M., Qin, L.F., Wang, H.H., Chen, G.-Q., 2007. Disruption of the polyhydroxyalkanoate synthase gene in *Aeromonas hydrophila* reduces its survival ability under stress conditions. FEMS Microbiol. Lett. 276, 34–41.

Appendix 19

Obruca, S., Sedlacek, P., and Koller, M. The underexplored role of diverse stress factors in microbial biopolymer synthesis. *Bioresource Technology* **2021**, 326, 124767.

Review

The underexplored role of diverse stress factors in microbial biopolymer synthesis

Stanislav Obruca [a,*], Petr Sedlacek [a], Martin Koller [b,c]

[a] Faculty of Chemistry, Brno University of Technology, Purkynova 118, 612 00 Brno, Czech Republic
[b] Institute of Chemistry, NAWI Graz, University of Graz, Heinrichstrasse 28/VI, 8010 Graz, Austria
[c] ARENA Arbeitsgemeinschaft für Ressourcenschonende & Nachhaltige Technologien, Inffeldgasse 21b, 11 8010 Graz, Austria

HIGHLIGHTS

- During biotechnological processes microorganisms are exposed to various stress factors.
- Polyhydroxyalkanoates enhance the stress robustness of microorganisms.
- Controlled application of stress can be used as a tool to improve PHA productivity.

ARTICLE INFO

ABSTRACT

Polyhydroxyalkanoates (PHA) are microbial polyesters which, apart from their primary storage role, enhance the stress robustness of PHA accumulating cells against various stressors. PHA also represent interesting alternatives to petrochemical polymers, which can be produced from renewable resources employing approaches of microbial biotechnology. During biotechnological processes, bacterial cells are exposed to various stressor factors such as fluctuations in temperature, osmolarity, pH-value, elevated pressure or the presence of microbial inhibitors. This review summarizes how PHA helps microbial cells to cope with biotechnological process-relevant stressors and, *vice versa*, how various stress conditions can affect PHA production processes. The review suggests a fundamentally new strategy for PHA production: the fine-tuned exposure to selected stressors, which might be used to boost PHA production and even to tailor their structure.

1. Introduction

Polyhydroxyalkanoates (PHA) are common microbial storage compounds accumulated by numerous prokaryotes in form of intracellular granules. PHA are important bacterial metabolites; the content of PHA in cells can exceed 50% of cell dry mass and reach up to 90% under certain circumstances (Sabapathy et al., 2020), while the maximal volumetric fraction of PHA granules in cells reaches about 40 vol% (Mravec et al., 2016). Numerous recent studies demonstrated that, apart from their primary carbon and energy storage function, PHA are also important metabolites in numerous biological processes. It was described that PHA play an important role in endospore formation in *Bacilli* and related species (Sadykov et al., 2017), the establishment of symbiosis between prokaryotes and plants (Alves et al., 2019; Sun et al., 2019) or even in insect-prokaryotes symbiosis (Kim et al., 2013),

maintenance of anoxic photosynthesis and sulfur cycle in microbial mats dependent on photosynthetic carbon fixation (Rothermich et al., 2000), or maintaining energy production and NADH oxidation of nitrogen-fixing bacteria (Encarnación et al., 2002). Furthermore, the presence of PHA granules in various bacterial strains provides a shielding effect against numerous common environmental stress factors as shown in Table 1 and summarized in several recent reviews (Obruca et al., 2018, Obruca et al., 2020, Müller-Santos et al., 2020).

Apart from their biological function, PHA are also considered to be very interesting polymeric materials. Since they are produced from renewable resources by approaches of microbial biotechnology and very positive features revealed by them such as biodegradability and biocompatibility, PHA can serve as a "green" sustainable alternative to petrochemical plastics (Sabapathy et al., 2020).

It is important to note that during biotechnological production of

---

Table 1
Involvement of PHA in stress response of microorganisms.

Stress factor	Microorganisms	Reference
Osmotic pressure	*Aeromonas hydrophila*	Zhao et al., 2007
	Azospirillum brasilense	Kadouri et al., 2003a
		Kadouri et al., 2003b
	Escherichia coli	Wang et al., 2009
	Cupriavidus necator	Obruca et al., 2017
		Sedlacek et al., 2019b
	Halomonas halophila	Sedlacek et al., 2019b
	Rhizobium spp.	Breedveld et al., 1993
Low temperature and freezing/ thawing	*Aeromonas hydrophila*	Zhao et al., 2007
	Pseudomonas extremaustralis	Tribelli and López, 2011
	Sphingopyrix chilensis	Pavez et al., 2009
	Cupriavidus necator	Obruca, et al., 2016b
		Nowroth et al., 2016
Heating	*Aeromonas hydrophila*	Zhao et al., 2007
	Azospirillum brasilense	Kadouri et al., 2003a
		Kadouri et al., 2003b
	Escherichia coli	Wang et al., 2009
Oxidative pressure	*Aeromonas hydrophila*	Zhao et al., 2007
	Azospirillum brasilense	Kadouri et al., 2003a
		Kadouri et al., 2003b
	Pseudomonas extremaustralis	Ayub et al., 2009
	Herbaspirillum seropedicae	Batista et al., 2018
	Delfia acidovorans	Goh and Tan, 2012
UV radiation	*Cupriavidus necator*	Slaninova et al., 2018
	Escherichia coli	Wang et al., 2009
	Pseudomonas extremaustralis	Tribelli et al., 2020

PHA, like during any other biotechnological process, bacterial cells are exposed to numerous stress factors such as fluctuations in pH-value, increase in osmolarity or presence of microbial inhibitors. Due to their complex biological functions, PHA accumulation can enhance the stress resistance of bacteria. Moreover, there are reports that the controlled introduction of stress conditions supports PHA accumulation (Obruca et al., 2018). However, when the stress dose exceeds a particular level, the biotechnological process of PHA production is harmed and, in many cases, bacterial cells are damaged and at least utilize PHA storage to cope with stress and to cover energy and carbon expenses of the stress response as survival strategy. Therefore, this review will focus on the importance of PHA concerning stress robustness against bio-technologically relevant stress factors and *vice versa* on the impact of microbial stress on the production of PHA by bacteria.

2. Physical stress factors

2.1. The osmotic pressure of cultivation media

During fermentation, microbial cells are usually exposed to the high salinity of cultivation media. In numerous cases, an increased concentration of inorganic salts is present in the carbon substrate. For instance, molasses, a waste product of the sugar production industry (Honmane et al., 2020), whey from the dairy industry (Koller et al., 2016), or waste glycerol stemming from biodiesel production facilities (Kumar et al., 2019) are very promising inexpensive substrates for PHA production; these substrate streams contain a high fraction of inorganic matter

inducing osmotic pressure to bacterial cells. Similarly, when lignocellulose materials are utilized as substrates for PHA production, diluted acids or, less frequently, bases are used to tap the wealth of fermentable sugars from the lignocellulose complex. Of course, inevitable subsequent neutralization results in the high salinity of the hydrolysate (Obruca et al., 2015). In addition to initial salt concentration from cultivation media, also during the fermentation process itself, the concentration of salts in the bioreactor is further increased as a consequence of the addition of pH control agents (usually mineral acids and/or bases) and carbon substrate feeding, especially in fed-batch processes. An increase in salinity can also be caused by the evaporation of water from cultivation media as a consequence of intensive aeration. Therefore, the exposition of microbial cells to osmotic pressure is a very common phenomenon in microbial biotechnologies including PHA production.

There are numerous reports that the presence of PHA granules in bacterial cells enhances their robustness and resistance against hypertonic conditions. Zhao et al., observed that a PHA synthase lacking mutant of *Aeromonas hydrophila* (unable to synthesize PHA) is much more prone to osmotic pressure than its wild-type strain (Zhao et al., 2007). A similar observation was also reported for *Azospirilum brasilense* (Kadouri et al., 2002, Kadouri et al., 2003a), *Cupriavidus necator* (Obruca et al., 2017), or recombinant *Escherichia coli* harboring the PHA operon from *C. necator* (Wang et al., 2009). It was observed that under osmotic pressure PHA granules serve as an intracellular scaffold in bacterial cells, preventing cells against massive plasmolysis which might damage the cell membrane. The presence of PHA granules also protects osmotically challenged cells against dehydration and changes in intracellular pH-value (Obruca et al., 2017). As mentioned before, the volume fraction of PHA granules in bacterial cells reaches up to 40% (Mravec et al., 2016). The fact that PHA granules occupy a substantial part of intracellular space reduces the total molar amount of osmolytes that need to be synthesized by cells to balance hyperonic conditions (Sedlacek et al., 2019a). This might be one of the reasons why PHA accumulation is so common among halophilic prokaryotes adapted to high salinity environments. PHA biosynthesis was for instance reported for numerous moderate halophiles such as members of the genus *Halomonas* (Kucera et al., 2018, Pernicova et al., 2019), but also for the extremely halotolerant archaeon *Haloferax mediterranei* and other haloarchaea (Ghosh et al., 2019).

It should be noted that halophiles are very interesting candidates for industrial production of PHA, because the presence of high salt concentration prevents the system from contamination by common microflora, which subsequently reduces sterility requirements and cost of the process (Chen and Jiang 2018). Moreover, halophiles can utilize substrates with high salt content such as lignocellulose hydrolysates (Dietrich et al., 2019), cheap seawater can be used for their cultivation (Takahashi et al., 2017), and simple and cheap hypotonic lysis can be utilized for efficient PHA isolation from biomass (Fernandez-Castillo et al., 1986); moreover, osmolytes (ectoines, trehalose, etc.) accumulated by halophilic bacterial cells can be considered being high-value co-products in addition to PHA (Kumar and Kim, 2018).

Considering the protective effect of PHA granules against hypertonic conditions, it is not surprising that the introduction of mild osmotic pressure supports PHA biosynthesis even in non-halophilic bacterial strains, which can be used as a simple biotechnological tool to improve the PHA production process. It was reported that the application of a well-tuned dose of NaCl supports PHA accumulation in *C. necator*, with the optimal dose of NaCl for this strain being about 10 g/L (Obruca et al., 2010a, Passanha et al., 2014). Likewise, the introduction of osmotic pressure (50 g/L) enhanced PHA synthesis also in the cyanobacterium *Spirulina subsalsa* (Shrivastav et al., 2010) or the Gram-positive PHA producer *Bacillus meagaterium* uyuni (Rodríguez-Contreras et al., 2016). Similarly, de Paula et al., isolated the novel PHA producer *Pandoraea* sp. MA03, which was capable of efficient PHA production from crude glycerol. It was observed that NaCl present in crude glycerol stimulated PHA synthesis in microbial cells (de Paula et al., 2017). Apart from

monoseptic cultivations, Wen et al., studied the effect of osmolarity on PHA production by a mixed microbial culture and they also observed that the addition of a low NaCl dose (2.5 g/L) substantially improved PHA accumulation by the mixed culture (Wen et al., 2018). In their subsequent study, the authors focused on the effect of NaCl addition on the settleability of the mixed culture. They observed that the addition of 10 g/L of NaCl significantly improved sludge sedimentation since the NaCl addition strategy suppressed the growth of undesired filamentous bacteria belonging to the genus *Meganema*. Oppositely, NaCl application enriched the microbial consortium in PHA producers belonging to the genera *Paracoccus* and *Thauera* (Wen et al., 2020).

Therefore, the application of osmotic pressure is not only a promising tool to enhance PHA biosynthesis but, due to the substantial osmoprotective function of PHA, it might be also utilized as an approach for the isolation of PHA producers from mixed microbial consortia. Pernicova et al. (2020a) recently introduced a technique called "osmoselection", which was used for the isolation of PHA producing thermophiles from activated sludge. The technique is based on the application of an osmotic challenge consisting of hypertonic (100 g/L NaCl) and subsequent hypotonic (distilled water) shock. The bacterial cells capable to survive such challenging treatment are plated on agar plates, and growing PHA-positive colonies can quickly be identified by ATR-FTIR.

Further, it seems that, in particular cases, the exposure of bacterial cells to hypertonic conditions does not support PHA biosynthesis but, oppositely, stimulates their degradation by a battery of intracellular PHA depolymerases. PHA monomers such as 3-hydroxybutyrate, the final products of PHA hydrolysis, are considered being effective osmolytes involved in compensation of osmotic pressure. Moreover, PHA monomers also serve as potent chemical chaperones protecting proteins and other biomolecules from denaturation by various stressors (Soto et al., 2012, Obruca et al., 2016a). The fact that degradation of intracellular PHA storage is an important strategy to cope with hypertonic conditions was demonstrated in several studies with PHA depolymerase deletion mutants unable of PHA granule mobilization; these mutants were much more prone to osmotic challenge than wild-type strains with complete PHA metabolism (Kadouri et al., 2003b, Soto et al., 2012, Wang et al., 2009). The fact that both PHA synthesis, as well as PHA degradation, are important metabolic processes under hypertonic conditions (30 g/L NaCl) was also confirmed in a recent proteomic study with *Pseudomonas protegens* (Wang et al., 2020). Breedveld et al. (1993) observed that the exposition of *Rhizobium* sp. to a highly saline medium (approx. 23 g/L of NaCl) induced mobilization of PHA granules. In this case, generated PHA monomers were most likely not utilized as primary compatible solutes, rather, carbon and energy stored in PHA were utilized for biosynthesis of mannitol and trehalose as preferred compatible solutes.

Therefore, it can be concluded that PHA metabolism is substantially impacted by the salinity of cultivation media. PHA biosynthesis is positively stimulated by mild hypertonic conditions. Of course, sensitivity and the particular response of the bacterial culture are strongly strain-specific; nevertheless, for most non-halophilic PHA producers, it seems that the optimal NaCl concentration is about 10–15 g/L. However, when osmotic pressure exceeds a certain level (in most non-halophiles, this is typically about 20 g/L), microbial growth, as well as PHA biosynthesis, are dramatically impaired, thus resulting in a substantial reduction of PHA yields. Moreover, a bacterial culture might start to hydrolyze PHA granules as a reservoir of compatible solutes, carbon, and energy to cope with increased stress levels. Hence, the response of bacterial cells concerning PHA metabolism to stress conditions induced by hypertonic conditions or by any other stress factor can be described by the well-known "stress curve". From a biotechnological point of view, one should be aware of the sensitivity of a PHA producing culture to osmotic pressure; it is important to define the maximum tolerable salinity, which just does not hamper PHA biosynthesis, and consider this fact during PHA production process development and optimization. The effect of various biotechnologically relevant stress factors on biotechnological production of PHA is shown in Fig. 1.

2.2. Temperature fluctuations

During the biotechnological process, bacterial cells can be also exposed to fluctuations in cultivation temperature. Of course, the vast majority of contemporarily used bioreactors enables control of temperature; both triggered heating and cooling are usually possible through the shell of the reactor. Nevertheless, especially during cultivation on large scale, temperature control is complicated by high volume/surface ratio, non-homogeneity of cultivation media, and heat transfer characteristics in fermentation broth (a suspension!) being dependent on cell density. Hence, cells can be exposed to a temperature lower than optimal when heating is not sufficient. The opposite scenario – exposure to high temperatures is also possible since especially fast-growing metabolically highly active cells release a substantial amount of metabolic heat, which might be difficult to compensate especially in large-scale volumes. Of course, any shift from the optimal cultivation temperature dramatically affects yields and productivity of the biotechnological process.

It seems that PHA are also very important microbial metabolites in context with adaptation to a cold environment. PHA accumulation was recently described for numerous psychrophiles inhabiting cold environments (Goh and Tan 2012, Ciesielski et al., 2014, Pärnänen et al., 2015, Kumar et al., 2018, Rogala et al., 2020). A typical example of an Antarctic bacterium that relies on the cold-protective function of PHA is *Pseudomonas extremaustralis* (Tribelli and López, 2011, Tribelli et al., 2020). PHA genes of this bacterium are situated within a genomic island, which suggests that they were acquired *via* horizontal gene transfer, thus indicating the importance of PHA for adaptation to the Antarctic environment (Ayub et al., 2007). Further, it was also reported that PHA biosynthesis protects cells of the mesophilic bacterium *Cupriavidus necator*, widely used as industrial PHA producer, from transient to non-cultivable physiological state induced by low temperature (4 °C) in contrast to its PHA non-accumulating mutant (Nowroth et al., 2016). It was also reported that PHA protects *C. necator* from the harmful effect of repeated freezing and thawing (Obruca et al., 2016b). Of course, very low temperatures close to or even below 0 °C are not relevant stress factors in a real biotechnological process. Nevertheless, the awareness of the fact that the presence of PHA enhance viability and maintains desirable physiological state during low and freezing temperatures could be utilized in culture storage and maintenance, which is frequently performed at such low temperatures.

It seems that PHA are involved also in response to heat stress. Heat protective function of PHA granules was reported for various microorganisms such as *Aeromonas hydrophila* (Zhao et al., 2007), *Azospirillum brasilense* (Kadouri et al., 2002, Kadouri et al., 2003a) or *Pseudomonas* spp. (Ruiz et al., 2004, Ayub et al., 2004). In particular, PHA monomers were identified as potent chemical chaperons protecting proteins from losing their activity and denaturation at high temperatures (Soto et al., 2012, Obruca et al., 2016a). Obruca et al. (2016a) reported that 3-hydroxybutyrate (3HB) protects model enzymes, namely microbial lipase and lysozyme, from denaturation by heating. For instance, in the case of lipase, the temperature of denaturation was increased by about 5 °C at physiologic concentration 3HB concentration (in PHA accumulating bacteria it is about 100 mM). Therefore, it is no surprise that bacterial cells initiate mobilization of PHA to increase the intracellular concentration of monomers and utilize their shielding effect when exposed to cultivation temperature higher than optimal. Such a stress response strategy was observed in *Herbaspirillum seropedicae*: when cells were exposed to heat shock (45 °C), mobilization of PHA storage increased the intracellular 3HB pool, which alleviated protein aggregation and denaturation (Alves et al., 2020). Of course, PHA monomers can be also used to cover energy and carbon demands of the other heat-stress response mechanisms such as the production of heat-shock proteins. In addition, there are reports that hydrolysis of PHA storage is

How biotech-relevant stress factors affect PHA production

ELEVATED PRESSURE

PHA protect cells from elevated pressure.

Elevated pressure can be used to improve PHA accumulation in cells..

pH FLUCTUATIONS

Informations on PHA ivolvement in pH-induced stress are lacking.

Manipulation in pH can be used to control Mw and monomer composition of polymers.

TEMPERATURE

PHA protects cells from high and low temperature.

Temperature should be kept at optimum to reach maximal productivity.

MICROBIAL INHIBITORS

PHA can protect cells from stress induced by some microbial inhibitors.

To ensure maximal productivity, cultivation media should be detoxified or microbil culture should be engineered towards their tolerance.

OXYGEN AVAILABILITY

PHA protect cells from adverse effect of oxygen limitation as well as oxidative pressure.

Controlled oxygen limitation or apllication of oxidative pressure boost PHA accumulation.

OSMOTIC PRESSURE

PHA protects cells from high osmotic pressure of cultivation media.

Induction of mild osmotic pressure is a promising strategy to improve PHA accumulation in cells.

Fig. 1. Summary of effects of various biotechnologically relevant stress factors on PHA production.

associated with an increased level of ppGpp, a cellular alarmone inducing alternative sigma factor modulating gene expression concerning stress response against multiple stressors (Ruiz et al., 2004). Besides, also phasins (PhaP), structural proteins attached to PHA granules providing the interface between the hydrophobic polymer and cytoplasm, reveal heat protecting effect, most likely acting as chaperones (Almeida et al., 2011; Alves et al., 2020).

Therefore, PHA seem to be important metabolites concerning high-temperature stress. Although PHA accumulation among thermophiles is not so common a feature as observed among halophiles, there are several PHA producing thermophiles that might be considered being interesting candidates for industrial production of PHA following principles of Next-Generation Industrial Biotechnology (NGIB) (Chen and Jiang, 2018). In this context, the thermophilic bacterium *Caldimonas taiwanensis* possesses amylolytic activity and, therefore, can be employed for direct PHA production from starch (Sheu et al., 2009). *Chelatococcus thermostellatus* was used for PHA production using a semi-continuous cultivation scenario, with a cultivation temperature of 50 °C being sufficient to keep the process monoseptic even during long-term cultivation (Ibrahim and Steinbüchel, 2010). Also, the thermophile *Schlegelella thermodepolymerans* seems to be a promising PHA producer; interestingly, this bacterium prefers xylose over other sugars including glucose and, therefore, can be advantageously utilized for PHA production from lignocellulose-based resources rich in xylose (Kourilova et al., 2020). The Gram-positive thermophilic bacterium *Aneurinibacillus* sp. H1 is capable of the production of PHA copolymers containing a high portion of 4-hydroxybutyrate (4HB) and 3-hydroxyvalerate (3HV) which reveal auspicious material properties (Pernicova et al., 2020b, Sedlacek et al., 2020).

PHA metabolism is substantially influenced by the cultivation

temperature. When cultivation temperature is sub-optimal, the metabolic activity of cultures is reduced, resulting in decreased productivity and yields of PHA production processes. PHA can provide a protective effect against an increase in cultivation temperature, which might occur when metabolic activity of the employed microbial culture releases a high amount of metabolic heat, which can not be compensated by the cooling system of the bioreactor. Nevertheless, it seems that the protective function of PHA is predominantly based on the hydrolysis of PHA storage, hence, even an increase in cultivation temperature reduces the productivity of the PHA production process. It should be pointed out that even in thermophiles maximal PHA production is obtained at the optimal cultivation temperature, and a further increase in cultivation temperature decrease PHA content in biomass (Kourilova et al., 2020, Pernicova et al., 2020b).

2.3. Elevated pressure

The application of elevated atmospheric pressure is a very common strategy used during the cultivation of microorganisms. Enhanced pressure supports the solubilization of oxygen and, therefore, it enhances the oxygen transfer rate. Of course, there are also other effects of pressurized cultivations. One positive aspect is that foaming is partially reduced but, what can be considered being a problem, elevated pressure also increases the solubility of CO_2, which might negatively affect the culture. Follonier et al., studied the effect of moderately elevated atmospheric pressure on medium-chain-length PHA (mcl-PHA) production by *Pseudomonas putida*. It was observed that a pressure of 7 bar rather supported PHA biosynthesis but decreased the growth rate of bacterial culture. The study revealed that "putting cells under pressure" is an adequate and efficient way to enhance oxygen transfer rate and

mcl-PHA productivity (Follonier et al., 2012). In their subsequent study, the authors studied the reorganization of gene expression under elevated pressure. It was observed that when cells were cultivated at 7 bar, the stress response, similar to heat shock and oxidative stress, was activated and indicators of cell envelope perturbations were identified as well. Nevertheless, neither expression of genes involved in PHA synthesis nor in degradation was directly affected by elevated pressure (Follonier et al., 2013). Mota et al., studied the application of very high pressure (35 and 50 MPa) on PHA biosynthesis by *Paracoccus denitrificans*. Such high-pressure conditions decreased final product titers (by inhibition of cell growth), but supported PHA accumulation in cells since PHA content in biomass was enhanced by the application of very high pressure (Mota et al., 2019, 2020).

Microbial cells can be also exposed to hydrodynamic pressure when PHA production is performed in large scale-bioreactors. There are numerous reports that PHA might be involved in stress response to high hydrodynamic pressure as indicated by the fact that PHA polymers and also PHA oligomers of various monomers were synthesized by numerous deep-sea bacteria growing exclusively or preferentially at very high hydrodynamic pressure conditions (Numata et al., 2013). It seems that in deep-sea bacteria low molecular weight PHA oligomers or even monomers serve as piezolytes protecting proteins and other molecules against high hydrostatic pressure. Such function of PHA and its monomers or oligomers was described for numerous deep-sea bacteria such as *Photobacterium profundum* (Martin et al., 2002), *Salinimonas sediminis* (Xue et al., 2020) or *Halomonas profundus* (Simon-Colin et al., 2008).

3. Chemical stressors

3.1. Oxygen availability and oxidative pressure

Oxygen availability is a very important parameter affecting the metabolism of the employed microbial culture. It should be stated that due to high growth rates and volumetric productivity, aerobes are predominantly employed for PHA production. During cultivation, a bacterial culture utilizes oxygen solubilized in the cultivation medium primarily as a final electron acceptor in the oxidative respiration chain (Xiao and Yu, 2020). Considering generally low values of oxygen transfer rate and high oxygen demands of quickly growing and metabolizing microbial cells, it can easily happen that supplementation of oxygen by the aeration system of the bioreactor is not sufficient, and the bacterial culture is exposed to oxygen limitation. Such a situation usually decreases the growth rate of the culture. Moreover, when nitrate is used as a nitrogen source, oxygen limitation might induce the partial biological reduction of nitrate to nitrite, the latter inhibiting the microbial culture. From a productivity point of view, such a situation has dramatic consequences since PHA is an intracellular product, and decreased final biomass concentration indeed results in lowered PHA titers and volumetric productivity. Nevertheless, on the metabolic level, oxygen limitation might support PHA biosynthesis since lack of oxygen inhibits the TCA cycle and drives the flux of acetyl-CoA to the PHA biosynthetic pathway (Kessler and Wiltholt, 2001). It is not very likely that increased PHA biosynthesis compensates for decreased biomass growth; nevertheless, the awareness that partial limitation of the bacterial culture by oxygen might support PHA production could be used as a tool to boost the PHA production process. For instance, partial oxygen limitation can be induced at a stationary phase when no more growth of the culture is desired, and PHA biosynthesis rate is at its highest level. It was found that the application of microaerophilic conditions supported mcl-PHA accumulation by *Pseudomonas putida*. Here, it turned out that maintaining dissolved oxygen (DO) at 1–5% of air saturation at 30 °C initiated significant mcl-PHA synthesis. Further reduction in dissolved oxygen level improved mcl-PHA accumulation. When the volumetric oxygen mass transfer coefficient ($k_L a$) was reduced to 38 h^{-1}, the concentration of dissolved oxygen in cultivation media was below the detection limit, and both the mcl-PHA content and yields reached the

maximum (Blunt et al., 2019a). In their subsequent work, the same group of authors proved that the inherent O$_2$-limitation induced to high cell density culture in the stationary phase can be used as a simple and effective control strategy for the improvement of mcl-PHA synthesis from fatty acids (Blunt et al., 2019b). Alternatively, partial oxygen limitation can be also applied during the entire time-course of cultivation. Such a strategy was adopted by Faccin et al., to improve short-chain-length PHA (scl-PHA) production by *Bacillus megaterium*. The highest product titer was observed for a relatively low $k_L a$ value of 0.006 s^{-1}, while further increase in $k_L a$ resulted in lower PHA amount in biomass and decreased final product titer (Faccin et al., 2013). Interestingly, oxygen limitation can also be used to tailor the composition of scl-PHA on the monomeric level. This was demonstrated by Lefebvre et al., for poly(3-hydroxybutyrate-*co*-3-hydroxyvalerate) copolyester biosynthesis by the strain *C. necator* DSM 545 (strain name used in original literature: *Alcaligenes eutrophus* DSM 545) using glucose as the main carbon source, and propionate as a precursor for 3HV. Keeping the DO level low (between 1 and 4 % of air saturation), the conversion yield of glucose to 3HB was not affected, while the conversion yield of propionate to 3HV was almost triplicated from 0.25 mol/mol (in control experiments with a DO of 50–70% of air concentration) to 0.73 mol/mol. The authors explained this outcome with the reduced activity of the oxidative decarboxylation of pyruvate, which typically converts propionyl-CoA at sufficient oxygen supply to acetyl-CoA and CO$_2$; hence, this decarboxylation converts the 3HV precursor propionyl-CoA into the 3HB precursor acetyl-CoA. In fed-batch cultivation setups, reduced DO levels resulted in slightly lower overall volumetric PHA productivity (0.36 vs. 0.44 g/(L·h)) due to slower substrate uptake and somewhat reduced PHA concentration (9.1 vs. 11.7 g/L), but in copolyesters with increased 3HV fraction (31.5 vs. 21.5 mol.-%), which is beneficial for PHÁs material properties (Lefebvre et al., 1997).

Further, PHA most likely helps bacterial cells to cope with oxygen limitation. It was recently demonstrated that high contents of PHA in *H. seropedicae* cells help this strain to maintain its normal metabolism under extremely low oxygen levels. The strain is exposed to micro-aerobic conditions when it colonizes plant roots, which, however, is beneficial to increase the root area and formation of lateral roots. By generating PHA-negative mutants, it was shown by Alves et al. (2019) that only the wild-type (PHA producing) strain was able to keep normal growth under oxygen-deficient conditions and to stimulate plant growth. Hence, PHA biosynthesis favors the symbiotic interaction between *H. seropedicae* and the plant.

To overcome the oxygen limitation of the bacterial culture and to reach the highest possible concentration of biomass, air enriched in oxygen or even pure oxygen can be supplemented to cultivation media. If such an aeration strategy is adopted, the cells are locally exposed to a very high concentration of oxygen, which might induce oxidative stress. A general bacterial strategy to face oxidative stress is the accumulation of NADPH, which is subsequently used as a reduction equivalent to eliminating harmful reactive oxygen species (ROS) (Shimizu and Matsuoka, 2019). It should be noted that such a metabolic situation has a very similar impact on PHA biosynthesis as a limitation by oxygen. The increased concentration of reduced coenzymes inhibits the TCA cycle and enhances the flux of acetyl-CoA towards PHA biosynthesis. Therefore, it seems that the exposition of the bacterial cells to oxidative pressure might be an exciting strategy to improve the productivity of PHA production processes (Obruca et al., 2010b). Obruca et al., utilized random chemical mutagenesis to improve PHA production in *C. necator*; the obtained PHA-overproducing mutant demonstrated all the features of the adaptation to oxidative pressure such as increased activities of NADPH generating enzymes, higher NADPH/NADP$^+$ ratio and also higher survival rate at hydrogen peroxide challenge (Obruca et al., 2013). Of course, there are also reports on the utilization of targeted gene engineering to enhance intracellular NADPH levels. A possible strategy for increasing NADPH level is the overexpression of the NADP-dependent glyceraldehyde 3-phosphate dehydrogenase gene (*gapC*)

from *Clostridium acetobutyricum* (Martinez et al., 2008) or NADP-dependent glyceraldehyde 3-phosphate dehydrogenase gene (*gapN*) from *Streptococcus* sp. (Centeno-Leija et al., 2014).

However, it seems that the interconnection of PHA and oxidative stress response is even more complex, and PHA are actively involved in stress resistance against ROS. Almeida at al. reported that phasins, PHA granules associated proteins, protect microbial cells not only from the adverse effect of heating as mentioned above but also against the harmful impact of ROS (Almeida et al., 2011). Furthermore, functional PHA metabolism is very important to maintain the correct redox state of the bacterial cells. Narancic et al., reported substantially reduced activity of ribulose 1,5-bisphosphate carboxylase (RuBisCO) in wild-type *Rhodospirillum rubrum* cells accumulating PHA. On the contrary, the PHA-negative mutant maintained the same level of RuBisCO activity over the entire growth period. Since RuBisCO controls the redox potential in cells of *R. rubrum*, the presence of PHA most likely substituted RuBisCO in this role (Narancic et al., 2016). Similarly, in *H. seropedicae*, inactivation of PHA synthesis perturbed redox balance and increased oxidative stress (Batista et al., 2018). PHA biosynthesis was also reported to be crucial for maintaining the redox state in *Pseudomonas* sp. 14–3 during low-temperature adaptation (Ayub et al., 2009). A very interesting oxidative stress response was observed in *Methylobacterium extorquens*. This bacterium degrades PHA storage to obtain methyl-esterified dimers and trimers of 3HB, which possess great hydroxyl radical–scavenging activity, even higher than that of glutathione or than vitamin C (Koskimäki et al., 2016).

Hence, PHA production is strongly affected by oxygen availability during fermentation. Oxygen limitation, as well as the application of mild oxidative pressure, might be implemented as tools to improve the productivity of PHA production processes. Nevertheless, it is wise to precisely optimize the level of the introduced stress factor to avoid serious harm to the cells, but rather to stimulate a positive metabolic effect associated with a particular stress response. It also should be taken into account that the application of stress reduces or even completely inhibits the growth of the microbial culture and, since high biomass concentration is the first prerequisite for obtaining high PHA titers and productivity, it is reasonable to introduce the stress at the beginning of the stationary phase, when no further growth of biomass is expected and PHA biosynthesis is provoked.

3.2. pH fluctuations

The pH-value in a cultivation setup is a decisive factor for the volumetric PHA productivity, the intracellular PHA fraction, and the substrate-to-PHA conversion yield (Mohanrasu et al., 2020). In this context, Khosravi-Darani et al. (2019) recently screened new microorganisms to produce PHA from methane in a bubble column bioreactor. The most promising isolated methanotroph for PHB production from natural gas, labeled as "strain 784" and identified as *Microbacterium* sp. via 16S rRNA analysis, was cultivated in different media. After medium selection, the impact of concentration of nitrogen source and Na_2HPO_4, the methane-to-air ratio in the gas stream, the inoculum age, and the pH-value on PHA production was evaluated via Taguchi design; importantly, the pH-value turned out to be the most decisive parameter impacting PHA productivity. Apart from pure microbial cultures, the impact of the pH-value on PHA production was also studied for mixed microbial culture setups; as shown by Chua et al. (2003), activated sludge consortia showed stimulated PHA biosynthesis at pH-values of 8 or 9 in comparison to processed operated at lower pH-values (6 or 7). In general, the pH-value of cultivation media has multiple effects on the outcome of cultivation setups dedicated to PHA biosynthesis:

First, it impacts growth kinetics of the microbial production strain; cultivations not matching the growth pH-optimum typically are characterized by low cell density, meaning a lower number of bioactive cells to be filled with PHA in the second phase of cultivation; lower volumetric productivity for PHA is the logical consequence. Second, pH-

value impacts the activity of the PHA synthesis enzymes; especially the impact of pH-value on PHA synthase activity is already well described for several PHA production strains. Here, one should keep in mind that running a process at the pH-optimum of a given PHA synthase generally results in high synthase activity, hence, in high specific PHA productivity. However, it was demonstrated that lower synthase activity (lower number of enzyme molecules expressed per cell) typically results in the formation of PHA of higher molecular mass, as already reviewed by Rehm and Steinbüchel (1999), or summarized by Tsuge (2016). Third, the pH-value impacts the composition of PHA on the monomeric level (*vide infra*).

Remarkably, the pH-optima for microbial growth and the enzymatic PHA formation machinery for one and the same organism are not necessarily identical. This was demonstrated by Suzuki et al. (1995), who already 25 years ago noticed increased intracellular PHA fraction in *Rhodobacter sphaeroides* RV, a phototrophic non-sulfur bacterium when running the cultivation process at pH-conditions suboptimal for biomass growth. While pH 7.5 was described as optimal for cell multiplication, higher pH-values between 8.0 and 8.5 increased the mass fraction of PHA in cells. Based on these results, the authors concluded that for achieving maximum volumetric productivity, it is of importance to evaluate pH-optima for both cultivation phases for a given production strain and to run the process at different pH-values during the two different phases. Moreover, the authors assumed that the higher PHA fraction at elevated pH-value supports the organism to withstand these challenging conditions. Similar results were reported by Sharma and Mallick (2005), who found out maximum PHA productivity for the diazotrophic cyanobacterium *Nostoc muscorum* at pH-values higher than the pH-optimum for growth. Other evidence on the role of PHA biosynthesis on microbial resilience against stress provoked by pH-shifts was found for *Sinorhizobium meliloti* (formerly known as *Rhizobium meliloti*), a PHA-accumulating *Rhizobium* strain involved in the microbial invasion of alfalfa nitrogen-fixing root nodules (Tombolini et al., 1995). Such organisms have also PHA synthases with optima in the neutral range (Kumbhakar et al., 2012). Mutants of *S. meliloti*, which lack the gene region containing genes encoding for PHA synthesis enzymes were reported to be unable to adapt to alkaline pH-values in presence of potassium ions, conditions prevailing in the nitrogen-fixing root nodules. The authors concluded that the presence of these PHA synthesis genes was involved in pH-adaptation of this strain, which is crucial for the adaptation to the changed environment conditions inside the plant noodles, characterized by increased alkalinity and potassium ion levels (Putnoky et al., 1998). This study can be considered further evidence for the role of PHA biosynthesis in symbiotic life forms.

As mentioned above, adapting the pH-value can also be a tool to trigger the molecular mass of obtained PHA biopolyesters based on impact of pH on PHA synthase activity. In analogy to lower substrate concentration (Tsuge, 2016) or insufficient oxygen transfer (Gómez-Hernández et al., 2020) typically leading to higher molecular masses as a consequence of lower PHA synthase activity, this effect can also be observed when shifting the pH-value away from the optimum. pH-optima of most PHA synthases from different bacteria and archaea are typically in the neutral range, as shown for *R. eutropha* class I synthase (Zhang et al., 2000), class III PHA synthase of *Chromatium vinosum* (Liebergesell et al., 1994), or the synthase isolated from the halophilic strain 56 (Hezayen et al., 2002). In this context, Kusaka et al. (1998) used the recombinant strain *Escherichia coli* XL-1 Blue (pSYL105) harboring *C. necator phaCAB* PHA biosynthesis genes, but no PHA depolymerase *phaZ* genes. Using glucose as a substrate, this strain produced, in dependence on the pH-value, PHA with M_w between 1.1×10^6 and 1.1×10^7. In this study, pH-values only 0.5 units lower than the pH optimum already resulted in strongly increased molecular mass.

Interestingly, suboptimal pH-values were also shown to trigger the composition of PHA copolyesters. As demonstrated by Villano et al. (2010), PHA biosynthesis by a mixed microbial culture enriched in PHA-producing species and co-supplied with acetate and propionate can be

triggered by increasing alkalinity. While at pH 7.5 higher PHA-in-biomass fractions were observed than at pH-value 9.5, the 3HV fraction in copolyesters was doubled at high pH-value. Authors explained this behavior with different energy requirements for biomass synthesis from acetyl-CoA and propionyl-CoA at different pH-values; at higher pH-values (8.5 and 9.5 were tested), acetyl-CoA is predominantly consumed for energy generation, and to a lower extent for the generation of 3HB via the condensation reaction of two acetyl-CoA molecules, and condensation of acetyl-CoA with propionyl-CoA becomes more likely. This increased acetyl-CoA utilization for energy generation is a consequence of adaptation to increased ATP synthase activity provoked by high pH-values. In the context of mixed microbial cultures, it was also shown that pH-shifts can positively impact the microbial composition of such consortia, increasing the fraction of PHA-accumulating species, which results in increased volumetric productivity for PHA, as shown by Oehmen et al. (2014) for a three-stage process for PHA production by a mixed culture starting from molasses as carbon source.

Spore formation typically hampers the utilization of Gram-positive strains for PHA production, because it results in an often considerable substrate loss, hence, lower substrate-to-PHA conversion yields. This is the main reason why the use of Gram-positives as PHA-production strains is still neglectable compared to Gram-negatives, especially on a larger scale (Kaur and Roy, 2015). However, PHA produced by Bacilli, Streptomycetes, etc., have favorable properties such as low levels of inflammatory endotoxins stemming from the outer cell membrane, which are typically co-extracted with PHA during downstream processing of Gram-negative Bacteria and Archaea, and impede the use of these materials for in vivo applications (Valappil et al., 2007). Typically, maximal PHA accumulation in Bacilli occurs prior to the formation of spores, and PHA degradation (favored by slightly alkaline conditions) provides the substrates for spore formation (Kominek and Halvorson, 1965). In the case of Bacillus cereus SPV, a strain isolated and described by Valappil et al. (2007), sporulation was suppressed by the acidic pH-value of the not buffered medium at pH-values between 4.5 and 5.8; this acidification was achieved simply by not keeping the pH-value constant; this prevented degradation of PHA during the late stationary phase, which in turn impeded sporulation, thus it increased the yield of PHA biosynthesis. Interestingly, this strain was also reported to produce building blocks others than 3HB from structurally unrelated carbon sources, namely 3HV (from gluconate) and 4HB (from fructose, sucrose, and gluconate).

3.3. Microbial inhibitors

Utilization of various cheap waste substrates of the food industry and agriculture improves the economic feasibility of PHA production; nevertheless, it also represents another challenge for PHA producing microorganisms. These waste substrates usually contain substances acting as microbial inhibitors potentially harming productivity and yields of the PHA production process (Palmqvist and Hahn-Hägerdal, 2000, Bhatia et al., 2020).

Crude waste glycerol stemming from biodiesel production represents an abundant and promising resource for PHA production; nevertheless, it contains various impurities such as water, methanol, hydroxide residues, salts, fatty acids, and esters (Hájek and Skopal, 2010; Wen et al., 2020). Since methanol represents a severe inhibitor for many microbial strains, the selection of a suitable PHA production strain capable of toleration or even metabolization of a certain concentration of this alcohol is desired. An example of such an organism is Methylomonas extorquens, which converts methanol before utilizing glycerol as a carbon substrate (Braunegg et al., 1999).

Substrates based on lignocellulose materials contain, apart from desirable fermentable sugars, also numerous microbial inhibitors that are released from lignocellulose biomass during the process of pretreatment and hydrolysis. These inhibitors include phenolic compounds released from the lignocellulose matrix, furfurals and organic acids

(formic acid, levulinic acid, acetic acid), which are usually formed as products of sugars degradation when the material is exposed to high temperature in the presence of diluted mineral acids, which is a commonly used pretreatment/hydrolysis approach (Sirohi et al., 2020).

The toxic effects of phenolic compounds, which inhibit both microbial growth and PHA yield, are very variable and can be related to specific functional groups. One possible mechanism is that phenolics interfere with the cell membrane by influencing its function and changing its protein-to-lipid ratio. Phenolic compounds are also suspected to harm microbial metabolism by inducing protein denaturation and precipitation (Palmqvist and Hahn-Hägerdal, 2000; Jönsson et al., 2013; Bouarab-Chibane et al., 2019). Inhibitory mechanisms of organic acids are mainly consequences of the fact that undissociated acids enter the cell through passive diffusion throughout the cell membrane and then dissociate in the cells due to the neutral cytosolic pH-value. The dissociation of the acid leads to a substantial drop in the intracellular pH, which seriously harms the microbial cells (Jönsson et al., 2013). Moreover, furfurals reveal very strong microbial inhibitory effects since they seriously affect metabolic fluxes and efficiency of energy metabolism (Horváth et al., 2003), and they may also act as specific inhibitors of particular enzymes (Chai et al., 2013). The toxic effects of lignocellulose-derived inhibitors for microbial cells are demonstrated in Fig. 2.

The inhibitors may negatively influence the PHA production process when their concentration reaches a critical value; nevertheless, it should be mentioned that when multiple inhibitors are present in the hydrolysate, their inhibitory potential reveals synergic behavior, e.g., inhibitory concentration is decreased by the presence of other inhibitors. Pan et al., used a response surface methodology to study the effect of selected lignocellulose-related inhibitors on PHA production employing Burkholderia cepacia. The authors confirmed the strong negative impact of inhibitors on the PHA production process; syringic acid was the most inhibitory among phenolics tested and synergistic inhibition was observed for the combinations of vanillin with syringic acid and vanillic acid with syringic acid. Further, strong synergistic inhibitory effects were observed for the combinations of acetate/phenolics and levulinic acid/furfural (Pan et al., 2012a).

Hence, the presence of multiple or even single microbial inhibitors represents a serious problem that can be solved by more or less selective removal of microbial inhibitors from lignocellulose hydrolysate in a separate process termed detoxification. Pan et al., utilized over-liming, a process in which inhibitors are destabilized and precipitated by lime, to detoxify hemicellulose hydrolysate for PHA production (Pan et al., 2012b). Various inexpensive sorbents such as active carbon or lignite can be also utilized for the removal of inhibitory compounds from lignocellulose hydrolysates (Kucera et al., 2017). Another approach is the removal of a major inhibitory compound from the lignocellulose material prior to its hydrolysis. For instance, extraction of phenolics from spent coffee grounds before hydrolysis enhanced fermentability of the hydrolysate and also PHA yields. Moreover, extracted phenolic compounds composed predominantly of chlorogenic acid and its derivatives are valuable side-product, which might be due to their positive biological activity for the human body, used in the food industry, cosmetics, or pharmacy (Obruca et al., 2014).

An alternative strategy to cope with the presence of microbial inhibitors in lignocellulose hydrolysates is the selection of a microbial strain robust to the negative effects of inhibitors. Dietrich et al. (2013) examined the sensitivity of seven PHA producing bacteria to several microbial inhibitors occurring in lignocellulose hydrolysates; among them, B. cepacia demonstrated the greatest inhibitor tolerance among the bacteria tested. Bhatia et al., recently introduced the novel PHA producer Ralstonia eutropha 5119, which demonstrated extraordinary robustness against microbial inhibitors present in lignocellulose-based hydrolysates; moreover, the strain was capable of utilizing various hydrolysates without the need of detoxification (Bhatia et al., 2019).

Besides, the sensitivity of the microbial culture to microbial

Fig. 2. Mechanisms of harmful effects of microbial inhibitors present in lignocellulose hydrolysates.

inhibitors can be reduced by adaptation or evolutionary engineering of the microbial culture. Yu and Stahl attempted to produce PHA on bagasse hydrolysate employing *Cupriavidus necator*. They reported that the adaptation of the microbial culture to inhibitors present in the hydrolysate is a potent strategy to increase PHA yields (Yu and Stahl, 2008). Novackova et al. (2019) utilized approaches of evolutionary engineering to gain strains of *C. necator* adapted to levulinic acid. Levulinic acid (4-oxopentanoic acid) is commonly present in lignocellulose hydrolysates since it is a product of chemical decomposition of hexoses and pentoses under high temperature and low pH-value. The adaptation experiments revealed that all the adapted strains showed better growth in the presence of levulinic acid than the wild-type strain. On the metabolic level, the adaptation was associated with enhanced metabolism of propionyl-CoA, enhanced activity of PHA biosynthetic pathways, respiratory activity, and also enhanced activities of NADPH generating enzymes. Further, although even the wild-type strain is capable of the utilization of levulinic acid as a precursor of 3HV for the synthesis of copolymer poly(3-hydroxybutyrate-*co*-3-hydroxyvalerate), adaptation to levulinic acid in most adapted cultures enhanced 3HV fraction in the copolymer.

Apart from adaptation, also advanced genetic engineering can be used to enhance tolerance to microbial inhibitors. Utilization of approaches of synthetic biology to improve the robustness of microbial cells against the action of microbial inhibitors was described mainly for *Saccharomyces cerevisiae* and *E. coli* as biotechnological "working-horses" utilized for the production of ethanol and other valuable products (Nieves et al., 2015). These strategies include mainly overexpression of

natural metabolic pathways enabling detoxification of the inhibitors (Petersson et al., 2006; Liu et al., 2008), the introduction of new metabolic pathways for elimination of inhibitors (Rodriguez et al., 2019; Song et al., 2017), or general improvement of stress robustness of the microorganisms (Glebes et al., 2014; Suo et al., 2019). In the field of PHA production, Cha et al., utilized approaches of synthetic biology to improve the metabolism of levulinic acid in *Pseudomonas putida*. The constructed strain was capable of the utilization of levulinic acid as a precursor of various PHA monomers such as 3HV or 4-hydroxyvalerate (Cha et al., 2020). Xu et al. (2021) constructed a strain of *Pseudomonas putida* capable of conversion of lignin-based aromatics and even lignin itself into PHA. Nduko et al. (2012) constructed a transgenic PHA producing strain of *E. coli* demonstrating extraordinary resistance to 5-hydroxymethylfurfural; this strain was successfully employed for PHA production on cellulose hydrolysate.

Vice versa, there is also a report that PHA biosynthesis improves the robustness of microbial cultures against microbial inhibitors. Jung et al. (2019) constructed a strain of *E. coli* harboring PHA synthetic genes of *C. necator*. Introduction of PHA synthetic genes improved cell growth in the presence of lignocellulose-associated inhibitors such as furfural, 4-hydroxybenzaldehyde, or vanillin, indicating that PHA synthetic capability provides resistance to these inhibitors. To gain a protective effect, a complete PHA biosynthetic pathway must be present and active in bacterial cells, thus demonstrating the importance and complex role of PHA metabolism. The authors suggested that a protective mechanism can be attributed to the fact that PHA accumulation in this non-natural PHA producer activated general stress response mechanisms such as

synthesis of heat-shock proteins and other chaperons which subsequently enhanced stress robustness of the bacterium also against microbial inhibitors. Further, increased PHA production was observed in the presence of furfural, suggesting that furfural could be used to improve biosynthesis of PHA in this particular strain of *E. coli*.

4. Interconnection of PHA with hormesis and its biotechnological utilization

Wherever an organism is exposed to adverse conditions, its fate is governed primarily by the actual dose of the chemical or physical stressor that it is facing, as already Paracelsus noted (Gantenbein, 2017). Therefore, an understanding of dose–response behavior represents a crucial step to predict and control the performance of the organism under any stress-involving environmental or technological circumstances. However, the basic features of dose–response performance seem to be surprisingly similar for diverse organisms, covering a wide range of their biological complexity independently of the type of harmful factor which they are facing. From this perspective, such biologically independent phenomena like the toxicity effect of an antibiotic on bacterial cells on the one side and performance of a human under physiological or mental arousal on the other, show conceptually similar dose–response relationships. This universality of the dose–response forms the foundation of the general concept of stress biology called hormesis (Calabrese, 2014).

Hormesis (from Greek "to set in motion" or "to excite") thus describes an evolutionarily conserved ability of organisms to be preconditioned, meaning that exposure to mild levels of harmful factors stimulates activation of diverse stress resistance mechanisms, which enhance the organism's capacity to cope with such adverse circumstances. From the quantitative point of view, this enhancement is invariantly modest (analysis of more than ten thousands of dose responses indicated that the preconditioned organisms show usually 30–60% higher stress response than the control group (Calabrese and Blain, 2011). Nevertheless, conceptual importance and potential benefits coming from even such modest enhancement of organism robustness have been already addressed in the field of toxicology, pharmacology and therapeutics (Calabrese, 2008). Nevertheless, to our best knowledge, none systematic effort has been ever made to exploiting the concept of hormesis in biotechnology. From this perspective, the abovementioned fact that exposure to mild stress doses seems to enhance the accumulation of PHA in bacteria together with the protective effect of PHA under higher stress doses indicates that production and accumulation of PHA in bacterial cells indeed represents another, not yet recognized, example of hormetic stress response.

Following the principle of hormesis, the application of mild stress conditions to enhance the performance of the system can be used as a very efficient, simple and cheap tool that might both increase PHA yields, simplify downstream processing or even tailor monomer composition and, therefore, even material properties of PHA polymers. The most interesting examples of utilization of stress conditions for boosting PHA production are summarized in Table 2. Utilization of controlled stress application in hand with principles of NGIB suggested by Chen and Jiang (2018) can represent very important steps towards sustainable industrial production of PHA. However, before introducing a suggested strategy to the industrial scale, we need to gain deeper knowledge on the interconnection of PHA biosynthesis and response of a given microbial PHA production strain to particular stressors and, furthermore, stress doses must be precisely defined and controlled which might be a difficult task especially on industrial scale. Hence, the well-grounded understanding of stress response of a new PHA production strain under investigation needs to become an integral part of development of enhanced PHA production processes, deserving the same attention as established media optimization procedures. Challenges ahead are the holistic comprehension of stress responses in terms of the impact of stress factors on co-formation of products others than

Table 2
Examples of utilization of stress conditions to improve PHA production process.

Microorganism	Stressor	Improvement of the PHA production process	Reference
Cupriavidus necator	Enhanced salinity (10 g/L NaCl)	scl-PHA yield enhanced about 30%	Obruca et al., 2010a Passanha et al., 2014
Mixed microbial consortium	Enhanced salinity (10 g/L NaCl)	Improved sludge settleability, enrichment of the consortium in scl-PHA producers	Wen et al., 2020
Pseudomonas putida	Elevated pressure (7 bar)	Elevated pressure triplicated mcl-PHA yields	Follonier et al., 2012
Bacillus megaterium	Oxygen limitation (kLa 0.006)	Oxygen limitation maximized scl-PHA yields	Faccin et al., 2013
Cupriavidus necator	Oxidative pressure (5 mM H2O2)	Enhancement of scl-PHA yields about 30%	Obruca et al., 2010b
Bacillus cereus	Non-optimal cultivation pH (acidic, pH 4.5–5.8)	Prevented sporulation, enhanced scl-PHA yields	Valappil et al., 2007
Mixed microbial consortium	Non-optimal cultivation pH (alkaline, pH 8.5–9.5)	Enhancement of 3HV fraction in scl-PHA copolymers	Villano et al., 2010
Trangenic *E. coli*	High furfural doses in cultivation media (10–15 mmol)	scl-PHA yields were enhanced 4-fold	Jung et al., 2019

PHA and residual biomass. This becomes particularly of importance when PHA producing organisms serve as real "cellular factories", able to produce a range of marketable products in one and the same cultivation process. Examples are found, e.g., among haloarchaea, where co-production of PHA, pigments, exopolysaccharides, and halocins is described for the strain *Hfx. mediterranei* (Koller et al., 2015). Applying a stress dose beneficial for formation of one desired product might drastically impede formation of by-productts of interest. Finally, the list of stressors to date described in literature to impact PHA biosynthesis in one or the other direction, summarized in this review, is not complete; it will be a challenging R&D avenue to elucidate the role of fine-tuned dose of antibiotics, heavy metals, toxic solvents, etc. in PHA biosynthesis by diverse production strains.

5. Conclusion

Currently, we only start comprehending multifaceted role of PHA in protecting microbes against diverse stress factors. Providing carbon and energy to fuel the microbial SOS-response machinery, enhancing the adaptability of PHA-rich cells to changing environments, acting as osmolytes, or repairing cell damage by PHA granules illustrate the manifold role of these versatile biopolyesters in protecting host cells against harmful environments. This will ultimately lead to a paradigm shift in how PHA production should be performed: instead of maintaining optimum conditions all through the cultivation, fine-tuned exposure to stressors might be a viable tool to boost PHA productivity and even to tailor its structure.

Funding

CRediT authorship contribution statement

Stanislav Obruca: Writing - original draft, Conceptualization, Visualization. **Petr Sedlacek:** Writing - original draft, Visualization. **Martin Koller:** Writing - original draft, Writing - review & editing.

Declaration of Competing Interest

The authors declare that they have no known competing financial interests or personal relationships that could have appeared to influence the work reported in this paper.

References

Almeida, A., Catone, M.V., Rhodius, V.A., Gross, C.A., Pettinari, M.J., 2011. Unexpected stress-Reducing effect of PhaP, a poly(3-hydroxybutyrate) granule-associated protein, in *Escherichia coli*. Appl. Environ. Microbiol. 77, 6622–6629.

Alves, L.P.S., do Amaral, F.P., Kim, D., Bom, M.T., Gavídia, M.P., Teixeira, C.S., Holthman, F., Pedrosa, F.O., de Souza, E.M., Chubatsu, L.S., Müller-Santos, M., Stacey, G., 2019. Importance of poly-3-hydroxybutyrate metabolism to the ability of *Herbaspirillum seropedicae* to promote plant growth. Appl. Environ. Microbiol. 85, art. no. e02586–18.

Alves, L.P.S., Santana-Filho, A.P., Sassaki, G.L., Pedrosa, F.O., de Souza, E.M., Chubatsu, L.S., Müller-Santos, M., 2020. 3-Hydroxybutyrate derived from poly-3-hydroxybutyrate mobilization alleviates protein aggregation in heat-stressed *Herbaspirillum seropedicae* SmR. Appl. Environ. Microbiol. 86, art. no. e01265.

Ayub, N.D., Pettinari, M.J., Ruiz, J.A., López, N.I., 2004. A polyhydroxybutyrate-producing *Pseudomonas* sp. isolated from antarctic environments with high stress resistence. Curr. Microbiol 49, 170–174.

Ayub, N.D., Pettinari, M.J., Méndez, B.S., López, N.I., 2007. The polyhydroxyalkanoate genes of a stress resistant Antarctic *Pseudomonas* are situated within a genomic island. Plasmid 58, 240–248.

Ayub, N.D., Tribelli, P.M., López, N.I., 2009. Polyhydroxyalkanoates are essential for maintenance of redox state in the Antarctic bacterium *Pseudomonas* sp. 14–3 during low temperature adaptation. Extremophiles 13, 59–66.

Batista, M.B., Teixeira, C.S., Sfeir, M.Z.T., Alves, L.P.S., Valdameri, G., Pedrosa, F.O., Sassaki, G.L., Steffens, M.B.R., de Souza, E.M., Dixon, R., Müller-Santos, M., 2018. PHB biosynthesis counteracts redox stress in *Herbaspirillum seropedicae*. Front. Microbiol. 9, art. no. 472.

Bhatia, S.K., Gurav, R., Choi, T.-R., Jung, H.-R., Yang, S.-Y., Moon, Y.-M., Song, H.-S., Jeon, J.-M., Choi, K.-Y., Yang, Y.-H., 2019. Bioconversion of plant biomass hydrolysate into bioplastic (polyhydroxyalkanoates) using *Ralstonia eutropha* 5119. Bioresource Technol 271, 306–315.

Bhatia, S.K., Jagtap, S.S., Bedekar, A.A., Bhatia, R.K., Patel, A.K., Pant, D., Rajesh Banu, J., Rao, C.V., Kim, Y.-G., Yang, Y.-H., 2020. Recent developments in pretreatment technologies on lignocellulosic biomass: Effect of key parameters, technological improvements, and challenges. Bioresource Technol. 300, art. no. 122724.

Blunt, W., Lagassé, A., Jin, Z., Dartiailh, C., Sparling, R., Gapes, D.J., Levin, D.B., Cicek, N., 2019. Efficacy of medium-chain-length polyhydroxyalkanoate biosynthesis from different biochemical pathways under oxygen-limited conditions using *Pseudomonas putida* LS46. Process Biochem. 82, 19–31.

Blunt, W., Dartiailh, C., Sparling, R., Gapes, D.J., Levin, D.B., Cicek, N., 2019b. Development of high cell density cultivation strategies for improved medium chain length polyhydroxyalkanoate productivity using Pseudomonas putida LS46. Bioengineering 6, art. no. 89.

Bouarab-Chibane, L., Forquet, V., Lantéri, P., Clément, Y., Léonard-Akkari, L., Oulahal, N., Degraeve, P., Bordes, C., 2019. Antibacterial properties of polyphenols: Characterization and QSAR (Quantitative structure-activity relationship) models. Front. Microbiol. 10, art. no. 829.

Braunegg, G., Genser, K., Bona, R., Haage, G., Schellauf, F., Winkler, E., 1999. Production of PHAs from agricultural waste material. Macromol. Symp. 144, 375–383.

Breedveld, M.W., Dijkema, C., Zevenhuizen, L.P.T.M., Zehnder, A.J.B., 1993. Response of intracellular carbohydrates to a NaCl shock in *Rhizobium leguminosarum* biovar trifolii TA-1 and *Rhizobium meliloti* SU-47. J. Gen. Microbiol. 139, 3157–3163.

Calabrese, E.J., 2008. Hormesis: why it is important to toxicology and toxicologists. Environ. Toxicol. Chem. 27, 1451–1474.

Calabrese, E.J., 2014. Hormesis: a fundamental concept in biology. Microbial Cell 1, 145.

Calabrese, E.J., Blain, R.B., 2011. The hormesis database: The occurrence of hormetic dose responses in the toxicological literature. Reg. Toxicol. Pharm. 61, 73–81.

Centeno-Leija, S., Huerta-Beristain, G., Giles-Gómez, M., Bolivar, F., Gosset, G., Martinez, A., 2014. Improving poly-3-hydroxybutyrate production in *Escherichia coli* by combining the increase in the NADPH pool and acetyl-CoA availability. Antonie Van Leeuwenhoek 105, 687–696.

Cha, D., Ha, H.S., Lee, S.K., 2020. Metabolic engineering of *Pseudomonas putida* for the production of various types of short-chain-length polyhydroxyalkanoates from levulinic acid. Bioresour. Technol. 309, art. no. 123332.

Chai, W.-M., Liu, X., Hu, Y.-H., Feng, H.-L., Jia, Y.-L., Guo, Y.-J., Zhou, H.-T., Chen, Q.-X., 2013. Antityrosinase and antimicrobial activities of furfuryl alcohol, furfural and furoic acid. Int. J. Biol. Macromol. 57, 151–155.

Chen, G.Q., Jiang, X.R., 2018. Next generation industrial biotechnology based on extremophilic bacteria. Curr. Opin. Biotechnol. 50, 94–100.

Chua, A.S., Takabatake, H., Satoh, H., Mino, T., 2003. Production of polyhydroxyalkanoates (PHA) by activated sludge treating municipal wastewater: effect of pH, sludge retention time (SRT), and acetate concentration in influent. Water Res. 37, 3602–3611.

Ciesielski, S., Górniak, D., Możejko, J., Świątecki, A., Grzesiak, J., Zdanowski, M., 2014. The diversity of bacteria isolated from Antarctic freshwater reservoirs possessing the ability to produce Polyhydroxyalkanoates. Curr. Microbiol. 69, 594–603.

de Paula, F.C., Kakazu, S., de Paula, C.B.C., Gomez, J.G.C., Contiero, J., 2017. Polyhydroxyalkanoate production from crude glycerol by newly isolated *Pandoraea* sp. Polyhydroxyalkanoate production from crude glycerol. J. King Saud Univ. Sci. 29, 166–173.

Dietrich, D., Illman, B., Crooks, C., 2013. Differential sensitivity of polyhydroxyalkanoate producing bacteria to fermentation inhibitors and comparison of polyhydroxybutyrate production from *Burkholderia cepacia* and *Pseudomonas pseudoflava*. BMC Res. Notes 6, art. no. 219.

Dietrich, K., Dumont, M.J., Del Rio, L.F., Orsat, V., 2019. Sustainable PHA production in integrated lignocellulose biorefineries. N. Biotechnol. 49, 161–168.

Encarnación, S., del Carmen Vargas, M., Dunn, M.F., Dávalos, A., Mendoza, G., Mora, Y., Mora, J., 2002. AniA regulates reserve polymer accumulation and global protein expression in *Rhizobium etli*. J Bacteriol 184, 2287–2295.

Faccin, D.J.L., Rech, R., Secchi, A.R., Cardozo, N.S.M., Ayub, M.A.Z., 2013. Influence of oxygen transfer rate on the accumulation of poly(3-hydroxybutyrate) by *Bacillus megaterium*. Process Biochem. 48, 420–425.

Fernandez-Castillo, R., Rodriguez-Valera, F., Gonzalez-Ramos, J., Ruiz-Berraquero, F., 1986. Accumulation of poly(β-hydroxybutyrate) by halobacteria. Appl. Environ. Microbiol. 51, 214–216.

Follonier, S., Henes, B., Panke, S., Zinn, M., 2012. Putting cells under pressure: A simple and efficient way to enhance the productivity of medium-chain-length polyhydroxyalkanoate in processes with *Pseudomonas putida* KT2440. Biotechnol. Bioeng. 109, 451–461.

Follonier, S., Escapa, I.F., Fonseca, P.M., Henes, B., Panke, S., Zinn, M., Prieto, M.A. 2013. New insights on the reorganization of gene transcription in Pseudomonas putida KT2440 at elevated pressure. Microb. Cell Fact. 12, art. no. 30.

Gantenbein, U.L., 2017. Poison and its dose: Paracelsus on toxicology. Toxicology in the Middle Ages and Renaissance. Academic Press.

Glebes, T.Y., Sandoval, N.R., Reeder, P.J., Schilling, K.D., Zhang, M., Gill, R.T., 2014. Genome-wide mapping of furfural tolerance genes in *Escherichia coli*. PLoS ONE 9, art. no. e87540.

Ghosh, S., Gnaim, R., Greiserman, S., Fadeev, L., Gozin, M., Golberg, A., 2019. Macroalgal biomass subcritical hydrolysates for the production of polyhydroxyalkanoate (PHA) by *Haloferax mediterranei*. Bioresource Technol. 271, 166–173.

Goh, Y.S., Tan, I.K.P., 2012. Polyhydroxyalkanoate production by antarctic soil bacteria isolated from Casey Station and Signy Island. Microbiol. Res. 167, 211–219.

Gómez-Hernández, E., Salgado-Lugo, H., Segura, D., García, A., Díaz-Barrera, A., Peña, C., 2020. Production of poly-3-Hydroxybutyrate (P3HB) with ultra-high molecular weight (UHMW) by mutant strains of *Azotobacter vinelandii* under microaerophilic conditions. Appl. Biochem. Biotechnol. 1–17 https://doi.org/10.1007/s12010-020-03384-w.

Hájek, M., Skopal, F., 2010. Treatment of glycerol phase formed by biodiesel production. Bioresource Technol. 101, 3242–3245.

Hezayen, F.F., Steinbüchel, A., Rehm, B.H., 2002. Biochemical and enzymological properties of the polyhydroxybutyrate synthase from the extremely halophilic archaeon strain 56. Arch. Biochem. Biophys. 403 (2), 284–291.

Honmane, B., Bhansali, R., Deshpande, T., Dhand, A., Mogha, S., Mukherjee, J., Ghosh, D., Sarode, G., Srivastava, S., Dive, A., Deshmukh, D., Ghosh, P.K., 2020. Harnessing the osmotic energy of cane molasses by forward osmosis: process studies and implications for a sugar mill (2020) Int. J. Environ. Stud. https://doi.org/10.1080/00207233.2020.1787036.

Horváth, I.S., Franzén, C.J., Taherzadeh, M.J., Niklasson, C., Lidén, G., 2003. Effects of furfural on the respiratory metabolism of *Saccharomyces cerevisiae* in glucose-limited chemostats. Appl. Environ. Microbiol. 69, 4076–4086.

Ibrahim, M.H., Steinbüchel, A., 2010. High-cell-density cyclic fed-batch fermentation of poly(3-hydroxybutyrate)-accumulating thermophile, *Chelatococcus* sp. strain MW10. Appl. Environ. Microbiol. 76, 7890–7895.

Jönsson, L.J., Alriksson, B., Nilvebrant, N.-O., 2013. Bioconversion of lignocellulose: Inhibitors and detoxification. Biotechnol. Biofuels, 6, art. no. 16.

Jung, H.-R., Lee, J.-H., Moon, Y.-M., Choi, T.-R., Yang, S.-Y., Song, H.-S., Park, J.Y., Park, Y.L., Bhatia, S.K., Gurav, R., Ko, B.J., Yang, Y.-H., 2019. Increased tolerance to furfural by introduction of polyhydroxybutyrate synthetic genes to *Escherichia coli*. J. Microbiol. Biotechnol. 29, 776–784.

Kadouri, D., Burdman, S., Jurkevitch, E., Okon, Y., 2002. Identification and isolation of genes involved in poly(β-hydroxybutyrate) biosynthesis in *Azospirillum brasilense* and characterization of a phbC mutant. Appl. Environ. Microbiol. 68, 2943–2949.

Kadouri, D., Jurkevitch, E., Okon, Y., 2003a. Involvement of the reserve material poly-β-hydroxybutyrate in *Azospirillum brasilense* stress endurance and root colonization. Appl. Environ. Microbiol. 69, 3244–3250.

Kadouri, D., Jurkevitch, E., Okon, Y., 2003b. Poly β-hydroxybutyrate depolymerase (PhaZ) in *Azospirillum brasilense* and characterization of a *phaZ* mutant. Arch. Microbiol. 180, 309–318.

Kim, J.K., Won, Y.J., Nikoh, N., Nakayama, H., Han, S.H., Kikuchi, Y., Rhee, Y.H., Park, H.Y., Kwon, J.Y., Kurokawa, K., Dohmae, N., Fukatsu, T., Lee, B.L., 2013. Polyester synthesis genes associated with stress resistance are involved in an insect-bacterium symbiosis. PNAS USA 110, E2381–E2389.

Kaur, G., Roy, I., 2015. Strategies for large-scale production of polyhydroxyalkanoates. Chem. Biochem. Eng. Q. 29, 157–172.

Kessler, B., Wiltholt, B., 2001. Factors involved in the regulatory network of polyhydroxyalkanoate metabolism. J Biotechnol. 86, 97–104.

Khosravi-Darani, K., Yazdian, F., Babapour, F., Amirsadeghi, A.R., 2019. Poly(3-hydroxybutyrate) production from natural gas by a methanotroph native bacterium in a bubble column bioreactor. Chem. Biochem. Eng. Q. 33, 69–77.

Koller, M., Chiellini, E., Braunegg, G., 2015. Study on the Production and Re-use of Poly (3-hydroxybutyrate-co-3-hydroxyvalerate) and Extracellular Polysaccharide by the Archaeon *Haloferax mediterranei* Strain DSM 1411. Chem. Biochem. Eng. Q. 29, 87–98.

Koller, M., Marsalek, L., Braunegg, G. (2016). PHA Biopolyester production from surplus whey: microbiological and engineering aspects. In: M. Koller, Ed.: Recent Advances in Biotechnology, 1, 100-172.) Bentham Science publishers.

Kominek, L.A., Halvorson, H.O., 1965. Metabolism of poly-β-hydroxybutyrate and acetoin in *Bacillus cereus*. J. Bacteriol. 90, 1251–1259.

Koskimäki, J.J., Kajula, M., Hokkanen, J., Ihantola, E.-L., Kim, J.H., Hautajärvi, H., Hankala, E., Suokas, M., Pohjanen, J., Podolich, O., Kozyrovska, N., Turpeinen, A., Pääkkönen, M., Mattila, S., Campbell, B.C., Pirttilä, A.M., 2016. Methyl-esterified 3-hydroxybutyrate oligomers protect bacteria from hydroxyl radicals. Nat. Chem.l Biol. 12, 332–338.

Kourilova, X., Pernicova, I., Sedlar, K., Musilova, J., Sedlacek, P., Kalina, M., Koller, M., Obruca, S., 2020. Production of polyhydroxyalkanoates (PHA) by a thermophilic strain of *Schlegelella thermodepolymerans* from xylose rich substrates. Bioresour. Technol. 315, art. no. 123885.

Kucera, D., Benesova, P., Ladicky, P., Pekar, M., Sedlacek, P., Obruca, S., 2017. Production of polyhydroxyalkanoates using hydrolyzates of spruce sawdust: Comparison of hydrolyzates detoxification by application of overliming, active carbon, and lignite. Bioengineering 4, art. no. 53.

Kucera, D., Pernicová, I., Kovalcik, A., Koller, M., Mullerova, L., Sedlacek, P., Mravec, F., Nebesarova, J., Kalina, M., Marova, I., Krzyzanek, V., Obruca, S., 2018. Characterization of the promising poly(3-hydroxybutyrate) producing halophilic bacterium *Halomonas halophila*. Bioresource Technol. 256, 552–556.

Kumar, P., Kim, B.S., 2018. Valorization of polyhydroxyalkanoates production process by co-synthesis of value-added products. Bioresource Technol. 269, 544–556.

Kumar V, Thakur VA, Kumar S, Singh D., 2018. Bioplastic reservoir of diverse bacterial communities revealed along altitude gradient of Pangi-Chamba trans-Himalayan region. FEMS Microbiol. Lett 365, art. no. fny144.

Kumar, L.R., Yellapu, S.K., Tyagi, R.D., Zhang, X., 2019. A review on variation in crude glycerol composition, bio-valorization of crude and purified glycerol as carbon source for lipid production. Bioresource Technol 293, art. no. 122155.

Kumbhakar, J., Singh, P.K., Vidyarthi, A.S., 2012. Screening of root nodule bacteria for the production of polyhydroxyalkanoate (PHA) and the study of parameters influencing the PHA accumulation. Afr. J. Biotechnol. 11, 7934–7946.

Kusaka, S., Iwata, T., Doi, Y., 1998. Microbial synthesis and physical properties of ultra-high-molecular-weight poly[(R)-3-hydroxybutyrate]. J. Macromol. Sci A. 35, 319–335.

Lefebvre, G., Rocher, M., Braunegg, G., 1997. Effects of low dissolved-oxygen concentrations on poly-(3-hydroxybutyrate-co-3-hydroxyvalerate) production by *Alcaligenes eutrophus*. Appl. Environ. Microbiol. 63 (3), 827–833. PubMed: 16535549.

Liebergesell, M., Sonomoto, K., Madkour, M., Mayer, F., Steinbüchel, A., 1994. Purification and characterization of the poly (hydroxyalkanoic acid) synthase from *Chromatium vinosum* and localization of the enzyme at the surface of poly (hydroxyalkanoic acid) granules. Eur. J. Biochem. 226 (1), 71–80.

Liu, Z.L., Moon, J., Andersh, B.J., Slininger, P.J., Weber, S., 2008. Multiple gene-mediated NAD(P)H-dependent aldehyde reduction is a mechanism of in situ detoxification of furfural and 5-hydroxymethylfurfural by *Saccharomyces cerevisiae*. Appl. Microbiol. Biotechnol. 81, 743–753.

Martin, D.D., Bartlett, D.H., Roberts, M.F., 2002. Solute accumulation in the deep-sea bacterium *Photobacterium profundum*. Extremophiles 6, 507–514.

Martinez, I., Zhu, J., Lin, H., Bennett, G.N., San, K.-Y., 2008. Replacing *Escherichia coli* NAD-dependent glyceraldehyde 3-phosphate dehydrogenase (GAPDH) with a NADPdependent enzyme fom *Clostridium acetobutyricum* facilitates NADPH dependent pathways. Metab. Eng. 10, 352–359.

Mohanrasu, K., Rao, R.G.R., Dinesh, G.H., Zhang, K., Prakash, G.S., Song, D.-P., Muniyasamy, S., Pugazhendhi, A., Jeyakanthan, J., Arun, A., 2020. Optimization of media components and culture conditions for polyhydroxyalkanoates production by *Bacillus megaterium*. Fuel 271, art. no. 117522.

Mota, M.J., Lopes, R.P., Simões, M.M.Q., Delgadillo, I., Saraiva, J.A., 2019. Effect of high pressure on *Paracoccus denitrificans* growth and polyhydroxyalkanoates production from glycerol. Appl. Biochem. Biotechnol. 188, 810–823.

Mota, M.J., Lopes, R.P., Pinto, C.A., Sousa, S., Gomes, A.M., Delgadillo, I., Saraiva, J.A., 2020. The use of different fermentative approaches on Paracoccus denitrificans: Effect of high pressure and air availability on growth and metabolism. Biocat. Agric. Biotechnol. 26, art. no. 101646.

Mravec, F., Obruca, S., Krzyzanek, V., Sedlacek, P., Hrubanova, K., Samek, O., Kucera, D., Benesova, P., Nebesarova, J., 2016. Accumulation of PHA granules in *Cupriavidus necator* as seen by confocal fluorescence microscopy. FEMS Microbiol. Lett. 363, art. no. fnw094.

Müller-Santos, M., Koskimäki, J.J., Alves, L.P.S., de Souza, E.M., Jendrossek, D., Pirttilä, A.M., 2020. The protective role of PHB and its degradation products against stress situations in bacteria, FEMS Microbiology Reviews, art. no. fuaa058. DOI: 10.1093/femsre/fuaa058.

Narancic, T., Scollica, E., Kenny, S.T., Gibbons, H., Carr, E., Brennan, L., Cagney, G., Wynne, K., Murphy, C., Raberg, M., Heinrich, D., Steinbüchel, A., O`Connor, K.E., 2016. Understanding the physiological roles of polyhydroxybutyrate (PHB) in

Rhodospirillum rubrum S1 under aerobic chemoheterotrophic conditions. Appl. Microbiol. Biotechnol. 100, 8901–8912.

Nduko, J.M., Suzuki, W., Matsumoto, K., Kobayashi, H., Ooi, T., Fukuoka, A., Taguchi, S., 2012. Polyhydroxyalkanoates production from cellulose hydrolysate in *Escherichia coli* LS5218 with superior resistance to 5-hydroxymethylfurfural. J. Biosci. Bioeng. 113, 70–72.

Nieves, L.M., Panyon, L.A., Wang, X. 2015. Engineering sugar utilization and microbial tolerance toward lignocellulose conversion. Front. Bioeng. Biotechnol. 3, art. no. 00017.

Novackova, I., Kucera, D., Porizka, J., Pernicova, I., Sedlacek, P., Koller, M., Kovalcik, A., Obruca, S., 2019. Adaptation of *Cupriavidus necator* to levulinic acid for enhanced production of P(3HB-co-3HV) copolyesters. Biochem. Eng. J. 151, art. no. 107350.

Nowroth, V., Marquart, L., Jendrossek, D., 2016. Low temperature-induced viable but not culturable state of *Ralstonia eutropha* and its relationship to accumulated polyhydroxybutyrate. FEMS Microbiol. Lett. 363, art. no. fnw249.

Numata, K., Morisaki, K., Tomizawa, S., Ohtani, M., Demura, T., Miyazaki, M., Nogi, Y., Deguchi, S., Doi, Y., 2013. Synthesis of poly- and oligo(hydroxyalkanoate)s by deep-sea bacteria, *Colwellia* spp., *Moritella* spp., and *Shewanella* spp. Polymer J. 45, 1094–1100.

Obruca, S., Marova, I., Svoboda, Z., Mikulikova, R., 2010a. Use of controlled exogenous stress for improvement of poly(3-hydroxybutyrate) production in *Cupriavidus necator*. Folia Microbiol. 55, 17–22.

Obruca, S., Marova, I., Stankova, M., Mravcova, L., Svoboda, Z., 2010b. Effect of ethanol and hydrogen peroxide on poly(3-hydroxybutyrate) biosynthetic pathway in *Cupriavidus necator* H16. World J. Microbiol. Biotechnol. 26, 1261–1267.

Obruca, S., Snajdar, O., Svoboda, Z., Marova, I., 2013. Application of random mutagenesis to enhance the production of polyhydroxyalkanoates by *Cupriavidus necator* H16 on waste frying oil. World J. Microbiol. Biotechnol. 29, 2417–2428.

Obruca, S., Benesova, P., Petrik, S., Oborna, J., Prikryl, R., Marova, I., 2014. Production of polyhydroxyalkanoates using hydrolysate of spent coffee grounds. Process Biochem. 49, 1409–1414.

Obruca, S., Benesova, P., Marsalek, L., Marova, I., 2015. Use of lignocellulosic materials for PHA production. Chem. Biochem. Eng. Q. 29, 135–144.

Obruca, S., Sedlacek, P., Mravec, F., Samek, O., Marova, I., 2016. Evaluation of 3-hydroxybutyrate as an enzyme-protective agent against heating and oxidative damage and its potential role in stress response of poly(3-hydroxybutyrate) accumulating cells. Appl. Microbiol. Biotechnol. 100, 1365–1376.

Obruca, S., Sedlacek, P., Krzyzanek, V., Mravec, F., Hrubanova, K., Samek, O., Kucera, D., Benesova, P., Marova, I. 2016b. Accumulation of poly(3-hydroxybutyrate) helps bacterial cells to survive freezing. PLoS ONE 11, art. no. e0157778.

Obruca, S., Sedlacek, P., Koller, M., Kucera, D., Pernicova, I., 2018. Involvement of polyhydroxyalkanoates in stress resistance of microbial cells: Biotechnological consequences and applications. Biotechnol. Adv. 36, 856–870.

Obruca, S., Sedlacek, P., Mravec, F., Krzyzanek, V., Nebesarova, J., Samek, O., Kucera, D., Benesova, P., Hrubanova, K., Milerova, M., Marova, I., 2017. The presence of PHB granules in cytoplasm protects non-halophilic bacterial cells against the harmful impact of hypertonic environments. N. Biotechnol. 39, 68–80.

Obruca, S., Sedlacek, P., Slaninova, E., Fritz, I., Daffert, C., Meixner, K., Sedrlova, Z., Koller, M., 2020. Novel unexpected functions of PHA granules. Appl. Microbiol. Biotechnol. 104, 4795–4810.

Oehmen, A., Pinto, F.V., Silva, V., Albuquerque, M.G., Reis, M.A., 2014. The impact of pH control on the volumetric productivity of mixed culture PHA production from fermented molasses. Eng. Life Sci. 14, 143–152.

Palmqvist, E., Hahn-Hägerdal, B., 2000. Fermentation of lignocellulosic hydrolysates. II: Inhibitors and mechanisms of inhibition. Bioresource Technol. 74, 25–33.

Pan, W., Nomura, C.T., Nakas, J.P., 2012a. Estimation of inhibitory effects of hemicellulosic wood hydrolysate inhibitors on PHA production by *Burkholderia cepacia* ATCC 17759 using response surface methodology. Bioresource Technol. 125, 275–282.

Pan, W., Perrotta, J.A., Stipanovic, A.J., Nomura, C.T., Nakas, J.P., 2012b. Production of polyhydroxyalkanoates by *Burkholderia cepacia* ATCC 17759 using a detoxified sugar maple hemicellulosic hydrolysate. J. Ind. Microbiol. Biotechnol. 39, 459–469.

Pärnänen, K., Karkman, A., Virta, M., Eronen-Rasimus, E., Kaartokallio, H., 2015. Discovery of bacterial polyhydroxyalkanoate synthase (PhaC)-encoding genes from seasonal Baltic Sea ice and cold estuarine waters. Extremophiles 19, 197–206.

Passanha, P., Kedia, G., Dinsdale, R.M., Guwy, A.J., Esteves, S.R., 2014. The use of NaCl addition for the improvement of polyhydroxyalkanoate production by *Cupriavidus necator*. Bioresource Technol. 163, 287–294.

Pernicova, I., Kucera, D., Nebesarova, J., Kalina, M., Novackova, I., Koller, M., Obruca, S., 2019. Production of polyhydroxyalkanoates on waste frying oil employing selected Halomonas strains. Bioresource Technol. 292, art. no. 122028.

Pernicova, I., Novackova, I., Sedlacek, P., Kourilova, X., Koller, M., Obruca, S., 2020. Application of osmotic challenge for enrichment of microbial consortia in polyhydroxyalkanoates producing thermophilic and thermotolerant bacteria and their subsequent isolation. Int. J. Biol. Macromol. 144, 698–704.

Pernicova, I., Novackova, I., Sedlacek, P., Kourilova, X., Kalina, M., Kovalcik, A., Koller, M., Nebesarova, J., Krzyzanek, V., Hrubanova, K., Masilko, J., Slaninova, E., Obruca, S., 2020b. Introducing the newly isolated bacterium Aneurinibacillus sp. H1 as an auspicious thermophilic producer of various polyhydroxyalkanoates (PHA) copolymers-1. isolation and characterization of the bacterium. Polymers 12, art. no. 1235.

Petersson, A., Almeida, J.R.M., Modig, T., Karhumaa, K., Hahn-Hagerdal, B., Gorwa-Grauslund, M.F., Liden, G., 2006. A 5-hydroxymethyl furfural reducing enzyme encoded by the *Saccharomyces cerevisiae* ADH6 gene conveys HMF tolerance. Yeast 23, 455–464.

Putnoky, P., Kereszt, A., Nakamura, T., Endre, G., Grosskopf, E., Kiss, P., Kondorosi, A., 1998. The pha gene cluster of *Rhizobium meliloti* involved in pH adaptation and symbiosis encodes a novel type of K⁺ efflux system. Mol. Microbiol. 28, 1091–1101.

Rehm, B.H., Steinbüchel, A., 1999. Biochemical and genetic analysis of PHA synthases and other proteins required for PHA synthesis. I. J. Biol. Macromol. 25, 3–19.

Rodriguez, A., Ersig, N., Geiselman, G.M., Seibel, K., Simmons, B.A., Magnuson, J.K., Eudes, A., Gladden, J.M., 2019. Conversion of depolymerized sugars and aromatics from engineered feedstocks by two oleaginous red yeasts. Bioresource Technol. 286, art. no. 121365.

Rodríguez-Contreras, A., Koller, M., Braunegg, G., Marqués-Calvo, M.S., 2016. Poly [(R)-3-hydroxybutyrate] production under different salinity conditions by a novel *Bacillus megaterium* strain. N. Biotechnol. 33, 73–77.

Rogala, M.M., Gawor, J., Gromadka, R., Kowalczyk, M., Grzesiak, J., 2020. Biodiversity and habitats of polar region polyhydroxyalkanoic acid-producing bacteria: Bioprospection by popular screening methods. Genes 11, art. no. 873.

Rothermich, M.M., Guerrero, R., Lenz, R.W., Goodwin, S., 2000. Characterization, seasonal occurrence, and diel fluctuation of poly(hydroxyalkanoate) in photosynthetic microbial mats. Appl. Environ. Microbiol. 66, 4279–4291.

Ruiz, J.A., López, N.I., Méndez, B.S., 2004. rpoS gene expression in carbon-starved cultures of the polyhydroxyalkanoate-accumulating species *Pseudomonas oleovorans*. Curr. Microbiol. 48, 396–400.

Sabapathy, P.C., Devaraj P., Meixner, K., Anburajan, P., Kathirvel, P., Ravikumar, Y., Zabed, H.M., Qi, X. Recent developments in polyhydroxyalkanoates (PHAs) production – A review, Bioresource Technol. 306, art. no. 123132.

Sadykov, M.R., Ahn, J.-S., Widhelm, T.J., Eckrich, V.M., Endres, J.L., Driks, A., Rutkowski, G.E., Wingerd, K.L., Bayles, K.W., 2017. Poly(3-hydroxybutyrate) fuels the tricarboxylic acid cycle and *de novo* lipid biosynthesis during *Bacillus anthracis* sporulation. Mol. Microbiol. 104, 793–803.

Sedlacek, P., Slaninova, E., Koller, M., Nebesarova, J., Marova, I., Krzyzanek, V., Obruca, S., 2019a. PHA granules help bacterial cells to preserve cell integrity when exposed to sudden osmotic imbalances. N. Biotechnol. 49, 129–136.

Sedlacek, P., Slaninova, E., Enev, V., Koller, M., Nebesarova, J., Marova, I., Hrubanova, K., Krzyzanek, V., Samek, O., Obruca, S., 2019b. What keeps polyhydroxyalkanoates in bacterial cells amorphous? A derivation from stress exposure experiments. Appl. Microbiol. Biotechnol. 103, 1905–1917.

Sedlacek, P., Pernicova, I., Novackova, I., Kourilova, X., Kalina, M., Kovalcik, A., Koller, M., Nebesarova, J., Krzyzanek, V., Hrubanova, K., Masilko, J., Slaninova, E., Trudicova, M., Obruca, S., 2020. Introducing the newly isolated bacterium *Aneurinibacillus* sp. H1 as an auspicious thermophilic producer of various polyhydroxyalkanoates (PHA) copolymers-2. Material study on the produced copolymers. Polymers 12, art. no. 1298.

Sharma, L., Mallick, N., 2005. Accumulation of poly-β-hydroxybutyrate in *Nostoc muscorum*: regulation by pH, light–dark cycles, N and P status and carbon sources. Bioresource Technol. 96, 1304–1310.

Sheu, D.-S., Chen, W.-M., Yang, J.-Y., Chang, R.-C., 2009. Thermophilic bacterium *Caldimonas taiwanensis* produces poly(3-hydroxybutyrate-co-3-hydroxyvalerate) from starch and valerate as carbon sources. Enzyme Microb. Technol. 44, 289–294.

Shimizu, K., Matsuoka, Y., 2019. Redox rebalance against genetic perturbations and modulation of central carbon metabolism by the oxidative stress regulation. Biotechnol. Adv. 37, art. no. 107441.

Shrivastav, A., Mishra, S.K., Mishra, S., 2010. Polyhydroxyalkanoate (PHA) synthesis by *Spirulina subsalsa* from Gujarat coast of India. Int. J. Biol. Macromol. 46, 255–260.

Simon-Colin, C., Raguénès, G., Cozien, J., Guezennec, J.G., 2008. *Halomonas profundus* sp. nov., a new PHA-producing bacterium isolated from a deep-sea hydrothermal vent shrimp. J. Appl. Microbiol. 104, 1425–1432.

Sirohi, R., Prakash Pandey, J., Kumar Gaur, V., Gnansounou, E., Sindhu, R., 2020. Critical overview of biomass feedstocks as sustainable substrates for the production of polyhydroxybutyrate (PHB). Bioresource Technol. 311, art. no. 123536.

Slaninova, E., Sedlacek, P., Mravec, F., Mullerova, L., Samek, O., Koller, M., Hesko, O., Kucera, D., Marova, I., Obruca, S., 2018. Light scattering on PHA granules protects bacterial cells against the harmful effects of UV radiation. Appl. Microbiol. Biotechnol. 102, 1923–1931.

Song, H.-S., Jeon, J.-M., Kim, H.-J., Bhatia, S.K., Sathiyanarayanan, G., Kim, J., Won Hong, J., Gi Hong, Y., Young Choi, K., Kim, Y.-G., Kim, W., Yang, Y.-H., 2017. Increase in furfural tolerance by combinatorial overexpression of NAD salvage

pathway enzymes in engineered isobutanol-producing *E. coli*. Bioresource Technol. 245, 1430–1435.

Soto, G., Setten, L., Lisi, C., Maurelis, C., Mozzicafreddo, M., Cuccioloni, M., Angeletti, M., Ayub, N.D., 2012. Hydroxybutyrate prevents protein aggregation in the halotolerant bacterium *Pseudomonas* sp. CT13 under abiotic stress. Extremophiles 16, 455–462.

Sun, Y.-W., Li, Y., Hu, Y., Chen, W.-X., Tian, C.-F., 2019. Coordinated regulation of the size and number of polyhydroxybutyrate granules by core and accessory phasins in the facultative microsymbiont *Sinorhizobium fredii* NGR234. Appl. Environ. Microbiol. 85, e00717–19.

Suo, Y., Liao, Z., Qu, C., Fu, H., Wang, J., 2019. Metabolic engineering of *Clostridium tyrobutyricum* for enhanced butyric acid production from undetoxified corncob acid hydrolysate. Bioresource Technol. 271, 266–273.

Suzuki, T., Tsygankov, A.A., Miyake, J., Tokiwa, Y., Asada, Y., 1995. Accumulation of poly-(hydroxybutyrate) by a non-sulfur photosynthetic bacterium *Rhodobacter sphaeroides* RV at different pH. Biotechnol. Lett. 17, 395–400.

Takahashi, R.Y.U., Castilho, N.A.S., Silva, M.A.C.D., Miotto, M.C., Lima, A.O.D.S., 2017. Prospecting for marine bacteria for polyhydroxyalkanoate production on low-cost substrates. Bioengineering 4, art. no. 60.

Tombolini, R., Povolo, S., Buson, A., Squartini, A., Nuti, M.P., 1995. Poly-β-hydroxybutyrate (PHB) biosynthetic genes in *Rhizobium meliloti* 41. Microbiol. 141, 2553–2559.

Tribelli, P.M., López, N.I., 2011. Poly(3-hydroxybutyrate) influences biofilm formation and motility in the novel Antarctic species *Pseudomonas extremaustralis* under cold conditions. Extremophiles 15, 541–547.

Tribelli, P.M., Pezzoni, M., Brito, M.G., Montesinos, N.V., Costa, C.S., López, N.I., 2020. Response to lethal UVA radiation in the Antarctic bacterium *Pseudomonas extremaustralis*: polyhydroxybutyrate and cold adaptation as protective factors. Extremophiles 24, 265–275.

Tsuge, T., 2016. Fundamental factors determining the molecular weight of polyhydroxyalkanoate during biosynthesis. Polym. J. 48, 1051–1057.

Valappil, S.P., Boccaccini, A.R., Bucke, C., Roy, I., 2007. Polyhydroxyalkanoates in Gram-positive bacteria: insights from the genera *Bacillus* and *Streptomyces*. Antonie van Leeuwenhoek 91, 1–17.

Villano, M., Beccari, M., Dionisi, D., Lampis, S., Miccheli, A., Vallini, G., Majone, M., 2010. Effect of pH on the production of bacterial polyhydroxyalkanoates by mixed cultures enriched under periodic feeding. Process Biochem. 45, 714–723.

Wang, Q., Yu, H., Xia, Y., Kang, Z., Qi, Q., 2009. Complete PHB mobilization in *Escherichia coli* enhances the stress tolerance: a potential biotechnological application. Microb. Cell Fact. 8, 47.

Wang, X., Tang, D., Wang, W., 2020. Adaptation strategies of *Pseudomonas protegens* SN15-2 to hyperosmotic growth environment. J. Appl. Microbiol. 128, 1720–1734.

Wen, Q., Ji, Y., Hao, Y., Huang, L., Chen, Z., Sposob, M., 2018. Effect of sodium chloride on polyhydroxyalkanoate production from food waste fermentation leachate under different organic loading rate. Bioresource Technol. 267, 133–140.

Wen, Q., Ji, Y., Chen, Z., Lee, D.-J., 2020. Use of sodium chloride to rapidly restore polyhydroxyalkanoates production from filamentous bulking without polyhydroxyalkanoates productivity impairment. Bioresource Technol. 313, art. no. 123663.

Xiao, X., Yu, H.-Q., 2020. Molecular mechanisms of microbial transmembrane electron transfer of electrochemically active bacteria. Curr. Opin. Chem. Biol. 59, 104–110.

Xu, Z., Xu, M., Cai, C., Chen, S., Jin, M., 2021. Microbial polyhydroxyalkanoate production from lignin by Pseudomonas putida NX-1. Bioresource Technol. 319, art. no. 124210.

Xue, J., Fang, J., Zhang, H., Wei, Y., Wang, L., Liu, R., Cao, J., 2020. Complete genome sequence of a piezophilic bacterium *Salinimonas sediminis* N102T, isolated from deep-sea sediment of the New Britain Trench. Marine Genomics, art. no. 100807.

Yu, J., Stahl, H., 2008. Microbial utilization and biopolyester synthesis of bagasse hydrolysates. Bioresource Technol. 99, 8042–8048.

Zhang, S., Yasuo, T., Lenz, R.W., Goodwin, S., 2000. Kinetic and mechanistic characterization of the polyhydroxybutyrate synthase from *Ralstonia eutropha*. Biomacromolecules 1, 244–251.

Zhao, Y.H., Li, H.M., Qin, L.F., Wang, H.H., Chen, G.Q., 2007. Disruption of the polyhydroxyalkanoate synthase gene in *Aeromonas hydrophila* reduces its survival ability under stress conditions. FEMS Microbiol Lett. 276, 34–41.

Appendix 20

Obruča, S., Dvořák, P., Sedláček, P., Koller, M., Sedlář, K., Pernicová, I., and Šafránek, D. Polyhydroxyalkanoates synthesis by halophiles and thermophiles: towards sustainable production of microbial bioplastics. *Biotechnology Advances* **2022**, 107906.

Research review paper

Polyhydroxyalkanoates synthesis by halophiles and thermophiles: towards sustainable production of microbial bioplastics

Stanislav Obruča [a,*], Pavel Dvořák [b], Petr Sedláček [a], Martin Koller [c,d], Karel Sedlář [e], Iva Pernicová [a], David Šafránek [f]

[a] Faculty of Chemistry, Brno University of Technology, Purkynova 118, 612 00 Brno, Czech Republic
[b] Department of Experimental Biology, Section of Microbiology, Faculty of Science, Masaryk University, Kamenice 753/5, Brno 62500, Czech Republic
[c] Institute of Chemistry, NAWI Graz, University of Graz, Heinrichstrasse 28/III, 8010 Graz, Austria
[d] ARENA Arbeitsgemeinschaft für Ressourcenschonende & Nachhaltige Technologien, Inffeldgasse 21b, 8010 Graz, Austria
[e] Department of Biomedical Engineering, Faculty of Electrical Engineering and Communication, Brno University of Technology, Technicka 12, Brno, 616 00, Czech Republic
[f] Faculty of Informatics, Masaryk University, Botanicka 68a, Brno 60200, Czech Republic

A R T I C L E   I N F O

A B S T R A C T

Polyhydroxyalkanoates (PHA) are microbial polyesters produced by numerous prokaryotes. These materials are generally considered to be renewable and biodegradable alternatives to petrochemical polymers in numerous applications. PHA are accumulated by microbial cells in form of intracellular granules primarily as storage compounds; nevertheless, numerous recent reports also highlight the importance of PHA for the stress robustness of bacteria. Therefore, in this review, we focus on summarizing current knowledge on PHA accumulation in halophiles and thermophiles – prokaryotic microorganisms adapted to high salinity and high temperature, respectively. Utilization of extremophiles for PHA production brings numerous benefits stemming especially from the enhanced robustness of the process against contamination by common mesophilic microflora as a basement of the Next-Generation Industrial Biotechnology concept. Further, recent advances and future perspectives in metabolic engineering and synthetic biology of halophiles and thermophiles for PHA production improvement are also summarized and suggested. Facts and ideas gathered in this review hold a promise that biotechnological production of PHA by extremophiles can be sustainable and economically feasible enabling PHA to enter the market massively and compete with non-biodegradable petrochemical polymers in suitable applications.

1. Introduction

During the long history of our planet, life has managed to penetrate all, even the least hospitable environmental niches. Nature has developed plenty of diverse mechanisms how to push the boundaries of life, some of which certainly remain hidden from our knowledge still. Prokaryotes from the domains Bacteria and Archaea, witnessing the history of evolution since its very beginning, represent the most suitable study subjects in our quest for understanding of how life at the extremes has evolved. Prospering in the harshest habitats imaginable, from extremely hot hydrothermal vents to deep-cold Antarctic soils, from the Dead sea ultra-salty water to acidic mine drainages, they display impressive examples of how the terrestrial life is constrained, providing crucial

implications not only for considering the origin of life on our planet, but also for the search for extraterrestrial life. Furthermore, as we humans have been employing microbes for centuries to improve our lives, research of these extreme-thriving microorganisms also opens up new horizons in various fields of science and technology.

Numerous prokaryotes – including the extremophilic ones – accumulate intracellular granules composed of polyesters of hydroxyalkanoic acids – polyhydroxyalkanoates (PHA). These granules are also termed „carbosonomes" to stress out their complex structure and multiple biological functions. The PHA polymer represents the core of the carbosonomes, while the surface is covered by numerous PHA granules-associated proteins representing an interface between the hydrophobic polymer and hydrophilic cytoplasm. Moreover, these proteins are also

ARTICLE IN PRESS

S. Obruča et al.   Biotechnology Advances xxx (xxxx) xxx

involved in PHA synthesis, degradation and regulation of these processes (Jendrossek, 2009). PHA may represent a substantial portion of a prokaryotic cell, with PHA contents reaching up to 90% of cell dry mass (CDM); nevertheless, PHA accumulating cells regulate their diameters to control the volumetric fraction of the PHA up to 40 vol% (Mravec et al., 2016). The primary biological function of PHA is the storage of carbon and energy; nevertheless, PHA are also involved in other biological processes such as fuelling sporulation in *Bacilli* and related species (Sadykov et al., 2017), or establishment of symbiosis between prokaryotes and plants (Alves et al., 2019) or between insects and prokaryotes (Kim et al., 2013). Moreover, numerous recent publications emphasize that the accumulation of PHA enhances the robustness of bacteria against various stressors such as osmotic pressure fluctuations (Obruca et al., 2017; Sedlacek et al., 2019), oxidative pressure (Batista et al., 2018; Koskimäki et al., 2016), UV irradiation (Slaninova et al., 2018; Tribelli et al., 2020) or high (Alves et al., 2020; Gonçalves et al., 2019) and low temperature (Nowroth et al., 2016) or even repeated freezing and subsequent thawing cycles (Obruca et al., 2016a). The current knowledge regarding the interconnection of PHA and stress survival and robustness of bacteria was also recently summarized by several reviews (Obruca et al., 2018, 2020, 2021; Müller-Santos et al., 2020). Apart from their biological importance, PHA attract the attention of the scientific community and industry due to their properties.

1.1. Characterization of polyhydroxyalkanoates

Generally, PHA are versatile polymers that are considered to be biodegradable, biocompatible, renewable and sustainable alternatives to petrochemical polymers (Koller et al., 2017). The mechanical and technological properties of PHA are generally dependant upon monomer composition of the polymer. Since prokaryotes are capable of introducing more than 150 various hydroxyalkanoic acids into the polymer chain (Park et al., 2012), PHA materials reveal a great variety of properties and functionalities. Generally, PHA are classified according to the number of carbon atoms per monomer unit: short-chain-length (scl-) PHA contain 3–5 carbon atoms per monomer unit and reveal thermoplastic properties, most of them are crystalline, rigid and fragile polymeric materials with high melting temperature and low glass transition temperature. Scl-PHA are the most abundant type of PHA among prokaryotes. Medium-chain-length (mcl-) PHA consist of monomers with 6–14 carbon atoms per monomer unit; these materials are elastic, possess low crystallinity and tensile strength and substantially lower melting and glass transition temperature as compared to scl-PHA. Predominantly *Pseudomonas* species are capable of mcl-PHA biosynthesis. Some bacteria, e.g., *Aeromonas caviae* or *Aeromonas hydrophila* are reported to synthesize hybride-type copolymers consisting of scl- and mcl-PHA building blocks. Generally, PHA monomers are usually chiral 3-hydroxyalkanoic acids; nevertheless, even chiral and achiral 2-, 4- and 5-hydroxy acids can be incorporated into the polymer chain. Importantly, due to the strict stereospecificity of PHA synthase (PhaC), the key enzyme responsible for the biosynthesis of the PHA polymer chain, all the monomer units are in *R* configuration (Mozejko-Ciesielska et al., 2019).

PHA synthases are, based on their substrate preference and subunit composition, divided into four classes. Class I accommodates enzymes consisting of a single subunit (PhaC) with molecular weight between 60 and 70 kDa and preferring scl-PHA monomers, the PHA synthase of *Cuprividus necator* (formerly *Alcaligenes eutrophus*, *Wautersia eutropha* and *Ralstonia eutropha*) represents the model enzyme of Class I synthases. Moreover, enzymes belonging to Class II synthases also contain only one subunit (PhaC1 or PhaC2); however, these enzymes catalyze the polymerization of mcl-PHA monomers, therefore, they are very common among *Pseudomonads*. Unlike Class I and Clas II synthases, Class III synthases are heterodimers requiring two subunits – PhaC and and PhaE (Mw of about 40 kDa) for full activity. The PHA synthase from *Allochromatium vinosum* (originally named *Chromatium vinosum*) is a

representative of the bacterial Class III PHA synthases, but also numerous *Haloarchaea* possess special types of Class III PHA synthases. Class IV of PHA synthases includes enzymes containing two subunits – PhaC and PhaR (Mw of PhaR is about 20 kDa) and are typical for *Bacilli* and related species; these enzymes are specific for scl-PHA polymerization. Such synthases of Class IV reveal a unique characteristic – in presence of alcohol, the PhaR subunit catalyzes alcohol cleavage of the PHA chain. The major purpose of this activity is probably the regulation of Mw of produced polymer. This phenomenon can be used to modify the carboxy terminus of PHA chain and incorporate active groups such as benzyl-, thiol- or hydroxy- group which might be beneficial for further modification and functionalization of the polymer (Zou et al., 2017). However, this long-established classification of PHA synthases in four Classes is currently in status of getting adapted; new synthases not fitting in one pof the four described Classes were recently isolated, such as a potentially new class of PHA synthase, which was recently identified from Antarctic bacterial isolates (Tan et al., 2020).

The substrates for PHA synthases are generated in three major pathways. The first pathway, which leads to scl-PHA synthesis, is based on the condensation of two acetyl-CoA molecules, which is catalyzed by 3-ketothiolase (PhaA; formerly known as β-ketothiolase) and results in the formation of acetoacetyl-CoA. The second step is a stereospecific reduction of acetoacetyl-CoA by NAD(P)H-dependant acetoacetyl-CoA reductases (PhaB); this "pseudofermentation" regenerates the oxidized form of NAD(P)H$^+$, and generates *R*-3-hydroxybutyryl-CoA, which is finally converted by the action of PHA synthase to the polymer chain of poly(3-hydroxybutyrate) (PHB). When mcl-PHA are synthesized, particular 3-hydroxyacyl-CoA acids can be obtained either from fatty acids *de-novo* synthesis or from β-oxidation of fatty acids. Further, it should be stated that PHA metabolism is of cyclic nature since PHA are intracellularly simultaneously synthesized and also hydrolyzed. Therefore, the PHA metabolism is also termed the "PHA cycle" (Prieto et al., 2016). The main metabolic pathways of PHA synthesis as well as the morphology of PHA granules, their properties and localization in bacterial cells are shown in Fig. 1.

1.2. PHA - polymers for numerous purposes

Apart from their complex biological and evolutionary role, PHA have continuously been researched also as highly promising polymers with a wide range of potential applications. As the (micro)plastic pollution became one of the major environmental concerns, the production of eco-friendly bio-based and biodegradable alternatives to conventional petroleum plastics has emerged among the most intensively addressed technological issues. Current global production of bioplastics (2.11 million tons in 2020) is expected to increase by more than 35% by 2025, still representing less than 1% of the total annual production of plastics (368 million tons in 2020 according to Bioplastics market data, 2020). Among the currently identified bioplastics, PHA still represents a minor contributor to the market (1.7% of the total amount of bioplastics produced in 2020); nevertheless, the market share is expected to increase significantly to 11.5% by 2025. The foreseen growth is promoted mainly by the outstanding versatility of material properties that can be provided by various members of PHA family. Depending on their monomer composition (at least 150 monomers are known currently (Steinbüchel, 1995)) and polymerization degree, PHA can be produced with a large variety of mechanical (from brittle to flexible, highly elastic), thermal (wide range of glass and melting temperatures as summarized in (Muhammadi et al., 2015)), chemical and physical properties. In combination with their high biodegradability, industrial- and home compostability, and non-toxicity, this makes PHA a promising candidate for replacing (or being blended with) the most important conventional petroleum-based plastics, such as polyethylene or polypropylene (Chen, 2010).

Over the past years, the range of end uses that PHA has been proposed or tested for, as well as the list of PHA producing and/or

ARTICLE IN PRESS

S. Obruča et al.   Biotechnology Advances xxx (xxxx) xxx
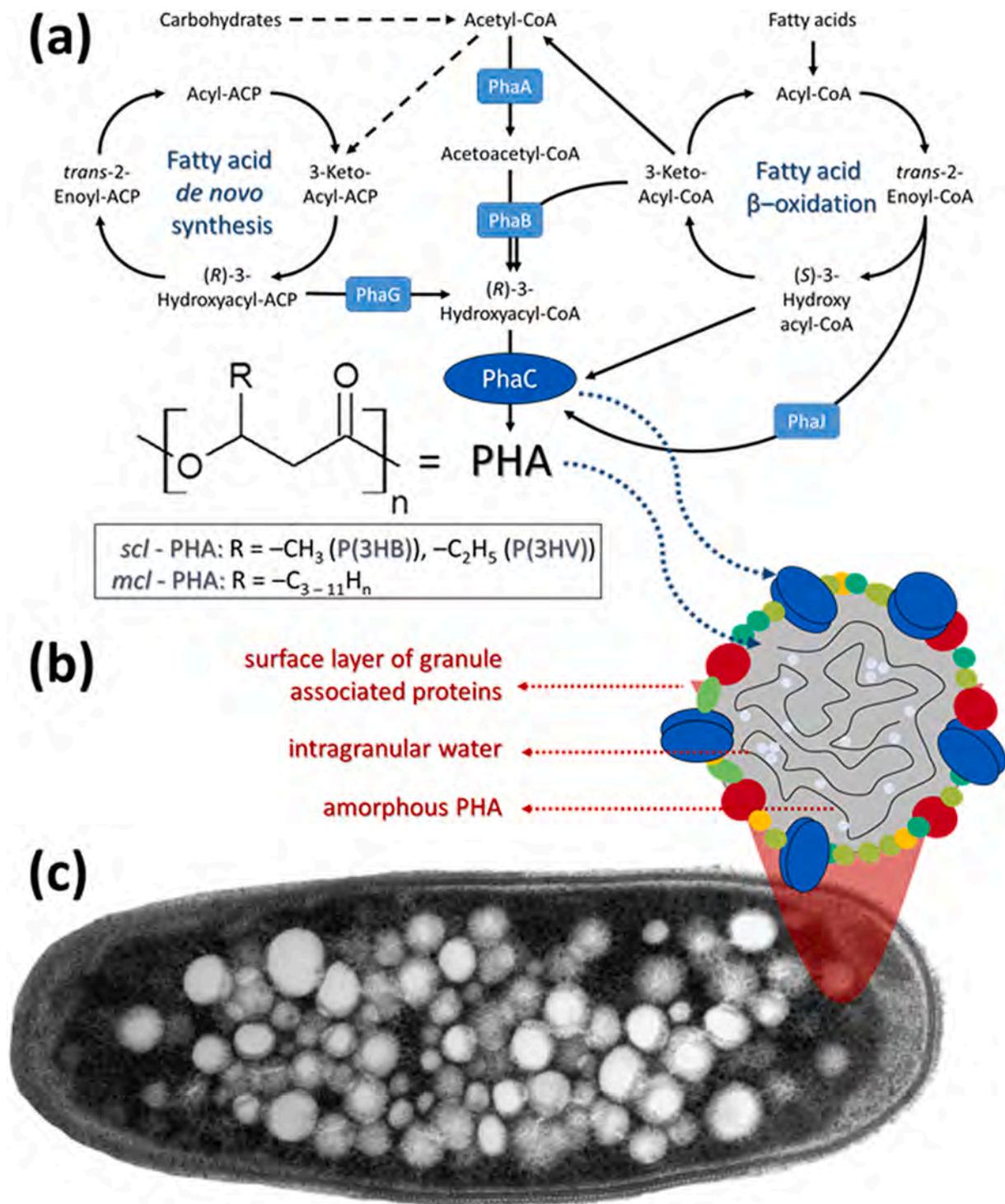
Fig. 1. The main metabolic pathways of PHA synthesis, morphology of PHA granules and their localization in cells of halophilic bacterium *Halomonas hydrothermalis*.

researching companies has steadily grown. A detailed overview of the currently operating PHA manufacturers together with their production scales and application specialization is listed elsewhere (Chen, 2009; Kourmentza et al., 2020). Probably the most often proposed use of PHA-based plastics is in the packaging industry, in particular in the production of packaging materials with a short lifespan, including food utensils and daily consumables, where the biodegradability and good gas barrier properties represent the main benefit of PHA. As the inherent brittleness and rigidity of PHB limits the usability of the PHB films, the efforts in packaging application have been targeted mainly to copolymers (e.g.,

the copolyester poly(3-hydroxybutyrate-co—3-hydroxyvalerate) (poly (3HB-*co*-3HV)) and mcl-PHAs and PHA-containing polymer blends or resins (Israni and Shivakumar, 2019; Vandewijngaarden et al., 2016; Zhang and Thomas, 2011)). Among the other low-end uses utilizing primarily fast and complete decomposition of PHA, agricultural applications (including production of biodegradable mulch films, growth bags or pesticide controlled-release systems (Grillo et al., 2011)), and production of single-use disposable items (such as bottles, cups, shopping bags, cosmetic containers) should be emphasized.

Nevertheless, specific biological and material properties of PHA

make them beneficial also for various high-end applications. PHA are biocompatible, i.e., non-harmful to human blood and tissues, rendering them attractive for a wide range of biomedical uses, targeted mainly to tissue engineering (production of medical implant materials from PHA) and drug delivery systems development (Ali and Jamil, 2016). Furthermore, PHA have also been concerned as the bulk materials for the synthesis of fine chemicals. Due to the chiral purity (all monomers are in (R)-configuration) and to the content of easily modifiable hydroxyl and carboxyl groups, monomers of PHA represent attractive precursors or intermediates for the synthesis of various fine chemicals such as antibiotics, vitamins, drugs, or pheromones (Ruth et al., 2007) and also for the production of novel tailor-made polyesters (Lakshmanan et al., 2019). Last but not least, also the versatile application potential of PHA granule-associated proteins biosynthesized together with PHA *in vivo*, was proposed by several authors (Chen, 2009; Mezzina et al., 2015, 2016).

Nevertheless, mainly in the field of low-cost applications, relatively high production costs compared to other (bio)plastics still represent the main limitation hindering the further expansion of PHA in the market. Therefore, strong efforts are currently targeted on searching for novel trends in the biotechnological production of PHA that would increase the economical feasibility and competitiveness of PHA uses.

1.3. Current trends in PHA production

There are numerous approaches to PHA production. The most traditional scenario includes the employment of an axenic microbial culture cultivated aseptically in submerged culture using defined media with pure carbon substrates, such as glucose or saccharose. However, the most important factor which prevents PHA from entering the market in the low-end application (e.g., packaging, single-use items, etc.) is the high price of PHA as compared to petrochemical polymers. The cost of carbon source in the above-mentioned scenario represents about 40% of the final cost of PHA (Kourmentza et al., 2017), therefore, there are attempts to omit expensive carbon substrates and utilize cheap, abundant, and human-food-chain non-competing resources such as waste streams of agriculture or food industry, which can be used as the carbon source for heterotrophic axenic culture (Koller, 2019a; Medeiros Garcia Alcântara et al., 2020). Apart from organic substrates, it is also possible to use CO_2 as a carbon source when photoautotrophic microbial cultures, for instance, cyanobacteria are used (Panuschka et al., 2019). More recent endeavors to save substrate costs involve the use of syngas, which can be produced as a homogenously composed carbon source from various organic waste streams by microbial specialists like *Rhodospirillum rubrum* (Amstutz and Zinn, 2020). In addition, several methanotrophs are reported to readily use methane, present, e.g., in biogas or natural gas, as C1 feedstock for PHA biosynthesis (Rodríguez et al., 2020).

Further, also the operation of the fermentation is expensive, especially the maintenance of aseptic conditions is energetically demanding. In this perspective, utilization of mixed microbial consortia which are cultivated without any sterility precautions seems to be a very promising approach. The cultivation is operated in a special open cultivation scenario which enables enrichment of mixed microbial culture in PHA producers. The most frequently used strategy - feast/famine cycling - is based on the periodic alternation of intervals of carbon substrate excess (feast phase) and relatively long periods of carbon substrate deprivation (famine phase). The microbes which are not capable of storing PHA are seriously disadvantaged during the famine period and are, therefore, eliminated from the system (Di Caprio, 2021; Oliveira et al., 2017). The bottleneck of PHA production by mixed microbial cultures are low volumetric productivity and inconstancy of properties of produced materials (monomer composition, molecular weight and polydispersity index), which might be limiting for some applications.

An alternative route towards sustainable production of PHA but also other microbial metabolites was recently proposed by Prof. Chen as a

concept of "Next-Generation Industrial Biotechnology" (NGIB). This concept is based on the employment of extremophiles as chassis instead of traditionally used mesophiles. Due to the application of extreme conditions which are required by extremophilic culture, the process is protected from contamination by commonly omnipresent mesophilic microflora which enables reduction or even complete omission of sterility precautions, and the process can be operated in highly productive continuous or semi-continuous scenarios in cheaper ceramic, cement or plastic bioreactors. NGIB should enable sustainable and economically feasible production of PHA competitive with cost-effective chemical production of petrochemical polymers (Chen and Jiang, 2018; Tan et al., 2021; Yu et al., 2019).

PHA production has already been described for numerous prokaryotic microbes including various extremophiles (Koller, 2017; Kumar et al., 2020; Obulisamy and Mehariya, 2021), nevertheless, due to high PHA yields, range of utilizable substrates and other advantages (discussed further in the text) the most promising extremophiles concerning PHA production seem to be found among halophiles and thermophiles. Therefore, this review focuses on the description and discussion of the current status of PHA synthesis by these microorganisms and provides also potential outcomes and perspectives.

2. Salt above gold – PHA production by halophiles

'Salt above gold' is not only the title of a famous Czech folkstory, but also a leitmotif surprisingly widespread in nature. Halophilicity, hence, the adaptability of life forms to high salinity, is described for all domains of life, such as for eukaryotes (e.g., halophytes or marine microalgae) or for halophilic prokaryotes (bacteria and archaea) (Oren, 2002). Hence, the group of halophilic species is phylogenetically highly diversified, and have one feature in common: they prefer or even require hypersaline environments for optimal growth, where NaCl usually acts as the main salt constituent. In this context, a steadily growing number of halophilic archaea and bacteria, identified in diverse saline habitats, are currently investigated as potential PHA-producing cell factories (reviewed by Koller et al., 2020; Stanley et al., 2021).

2.1. Adaptation of microbes to high salinity environments

To cope with extremely saline (hypertonic) conditions indeed is a challenging task for organisms, and requires specific adaptation strategies. Therefore, nature developed several fundamentally different approaches to support halophiles to manage high salt loads. The existence of these manifold approaches in turn substantiates the broad occurrence of halophilicity in nature (reviewed by Fathima et al., 2017).

The presumably most frequently occurring strategy involves the intracellular accumulation of soluble compatible osmotic compounds, such as the organic kosmotropics ectoine (first described as an osmoprotectant in the purple sulfur bacterium *Ectothiorhodospira halochloris* (Lippert et al., 1993), nowadays known to occur in both Gram-positive and Gram-negative bacteria), the glycine-derivative betaine (prevents loss of intracellular water) (Deole and Hoff, 2020), the osmoprotectant trehalose (described to be pivotal for yeast fermentations (Majara et al., 2018) and adaptation of bacteria (Dinnbier et al., 1988), or diverse amino acids.

Generally, the accumulation of these compatible organic solutes serves to stabilize the intracellular osmotic pressure; importantly, this strategy does not necessarily imply that involved organisms also need to adapt their proteome (enzymatic machinery) to the high salt loads. The intracellular accumulation of these compounds is based either on *de novo* osmolyte biosynthesis by the accumulating cells, or cells are supplied by them from the environment and transport them into the cell's interior. After the decline of the environmental salinity, these compatible solutes are excreted by the cells in order to balance osmotic pressure inside and outside the cells, which in turn allows for convenient isolation and purification of these often technologically relevant products (Wood

et al., 2001): because of their wide-ranging protective function and chaperons-like role, they are used in biotechnology, cosmetics (products for skin care), food industry, or the medicinal and pharmaceutical field (Sauer and Galinski, 1998). Regarding PHA-accumulating microbes, this formation of osmolytes is a typical feature of adaption among halotolerant and halophilic eubacteria, such as *Halomonas* spp. (Cummings and Gilmour, 1995; Shivanand and Mugeraya, 2011).

Such accumulation of compatible solutes considerably differs from the alternative "salt-in" strategy, which is based on intracellular salt accumulation, often potassium chloride, as a tool to balance the inner and outer osmotic pressure of cells. This "salt-in" strategy is the preferred approach followed by extremely halophilic haloarchaea, such as well-known PHA producers like *Hfx. mediterranei*. This strategy was first described in 1970 by Ginzburg et al. for a "*Halobacterium* sp.", a Dead Sea isolate; in this organism, changes of the intracellular ions composition during different growth conditions were observed (Ginzburg et al., 1970). As reported later, this strain, at the same time a halophile and thermophile, belongs to the genus *Haloarcula*, and was finally classified as strain *Haloarcula marismortui* Volcani (Oren et al., 1990). In contrast to the above-described accumulation of organic solutes, the "salt-in" strategy indispensably goes in parallel with an adaptation of enzymes and other universally conserved macromolecules (nucleic acids) by harnessing them with salt-resistance features; generated enzyme variants are termed "extremozymes" or "halozymes" (Danson and Hough, 1998). Mechanistically, this enzyme adaptation is mainly characterized by the formation of a surplus of acidic amino acids on the enzyme's surface, which allows the enzyme to work even under conditions near saturating salinity (Kennedy et al., 2001). For instance, *Hfx. mediterranei* glucose dehydrogenase (EC 1.1.1.47), an enzyme catalyzing the reaction of glucose to β-D-glucono-1,5-lactone, is reported to possess no flexible side chains on its surface, thus, it occurs as a highly ordered, multilayered solvation shell well adapted to avoid attachment of ions and thus to prevent damage (formation of inactive enzyme inclusion bodies) by salt (Bonete et al., 1996; Britton et al., 2006).

Besides the proteome, also the genome of extremely halophiles differs significantly from that of osmo-mesophiles and often requires specific editing. This is manifested, for example, by the high number of salt-resistant genes found in such halophiles (Das et al., 2015). As an example, Bolhuis et al. described that the genome of the square-shaped PHA-producing haloarchaeon *Haloquadratum walsbyi*, which is found in NaCl-saturated and MgCl$_2$-rich aquatic environments, features several exceptional adaptive particularities, enabling this strain to thrive well in highly saline environments. The probably most remarkable of these genomic particularities is the presence of a gene encoding a high molecular mass halomucin, similar to halomucins protecting animal tissue from desiccation and harsh chemical conditions. These halomucins with a negative overall charge reach from the inside to the outside of cells, thus forming a "water shield" sheltering the cell (Bolhuis et al., 2006). The genome of *Halobacterium* sp. NRC-1 also reveals several remarkable physical adaptations to high salinity, such as the encoding of predominately acidic enzymes, which is recognized as a crucial strategy to prevent salting-out of proteins in the hypersaline cytoplasm (Kennedy et al., 2001; Ng et al., 2000); such pronounced negative surface charge of folded proteins to overcome salting-out of hypersaline cytoplasm was also described for the haloarchaeon *Haloarcula marismortui* (Baliga et al., 2004).

In addition, the change of pigment patterns also constitutes a tool for organisms to adapt to changing salinity. As amply described in the literature, many eukaryotic microalgae adapt their pigment pattern under conditions of fluctuating salinity. This was reported by Masojídek et al. for the green microalga (chlorophyta) *Chlorococcum* spp., which drastically increased the intracellular carotenoids-to-chlorophylls ratio during exposure of the culture to nitrogen deficiency, high salinity and illumination stress (Masojídek et al., 2000). In addition to eukaryotes, this pigment pattern change was also reported for extremely halophilic prokaryotes like the haloarchaeal PHA producer *Hfx. mediterranei*. The

hyperproduction of the C50-carotenoid bacterioruberin, which is typically produced as a reaction to extreme UV-irradiation and excessive oxidative stress, for instance, provoked by H$_2$O$_2$ addition (Giani and Martínez-Espinosa, 2020), is also produced at suboptimal salt concentrations (D'Souza et al., 1997; Fang et al., 2010; Montero-Lobato et al., 2018). In this case, bacterioruberin is suspected to adapt the flexibility of the cell membrane and thus to maintain cells′ viability (D'Souza et al., 1997). Indeed, it was demonstrated by Chen et al. that for *Hfx. mediterranei*, when cultivated on extruded rice bran and starch under optimal salinity of brined medium, there exists an indirect relationship between the level of salinity and pigment formation, and a direct correlation of salinity and PHA biosynthesis; these authors demonstrated that the pigment bacterioruberin, a compound of potential technological application, for instance, as colorant on cosmetic products, can be produced by *Hfx. mediterranei* at high throughput (more than 0.5 g/L pigment) by adapting the salt concentration of the cultivation medium. Importantly, mentioned inexpensive carbon sources were successfully used as feedstocks for product formation, both for PHA and pigments (Chen et al., 2015).

2.2. Role of PHA in the adaptation of halophiles to hypertonic conditions

In the context of halophilic PHA production strains, it is of interest to reveal how biosynthesis of PHA and above-described compatible solutes is interlinked, and how these anabolic processes relate to the organisms′ strategy to cope with high external salinity. In 2006, Quillaguamán and colleagues noticed the sudden change of the morphology of PHA-accumulating cultures of the halophilic eubacterium *Halomonas boliviensis* LC1, a salt lake isolate, at suddenly increasing salinity; the authors proposed that the switch towards the accumulation of organic solutes serves to withstand the osmotic pressure before the onset of increased PHA biosynthesis (Quillaguamán et al., 2005). Mothes et al. reported the parallel production of PHA and ectoines by the halophilic bacterium *Halomonas elongata*. At a salinity of 10 wt% NaCl, the strain accumulated 0.5 g PHA per g biomass plus up to 14 wt% of ectoines, which substantiates the theory of the parallel formation of PHA and compatible organic solutes (Mothes et al., 2008). Guzmán et al. studied the parallel PHA and ectoines biosynthesis by the halophilic bacterium *Halomonas boliviensis* in two fed-batch cultivation experiments. While the first cultivation was performed at 45 g/L of NaCl without nitrogen or phosphate limitation to obtain a high concentration of active biomass, the salinity in the second cultivation setup was increased to 75 g/L NaCl in order to increase ectoine accumulation; moreover, in this second cultivation, nitrogen- and phosphate sources were supplied exclusively during the initial growth phase and were later depleted to boost PHB formation. Intracellular PHB fraction and volumetric PHB productivity amounted to about 0.96 g/g and 1 g/(L·h), respectively, while the ectoine concentration and content were reported with 4.3 g/L and 0.072 g/g, respectively (Guzmán et al., 2009).

Importantly, it was shown that the presence of PHA granules in cells protects them against damage caused by hyperosmotic shock (a sudden increase of salinity). This was for the first time demonstrated by Soto et al., who exposed the halotolerant Gram-negative PHA production strain *Pseudomonas* sp. CT13 and its PHA-negative mutant to hyperosmotic up-shock. It turned out that the presence of PHA granules boosts the intracellular level of 3-hydroxybutyrate (3HB), the monomer of the homopolyester PHB. 3HB, in turn, acts as a kind of "chaperone" by inhibiting protein agglomeration, which is a typical lethal consequence for PHA-negative cells when exposed to high salt concentration and/or elevated temperature. As demonstrated by increased PHA productivity at increased salinity, PHA and 3HB constitute compatible solutes, supporting the bacteria to counterattack hyperosmotic stress (Soto et al., 2012). More recently, Obruca et al. substantiated these outcomes by illuminating the indeed expedient chaperoning efficiency of 3HB. These authors showed that 3HB's protective effect was competitive with the effect described for well-known compatible solutes such as ectoines or

trehalose. From the mechanistic point of view, this effect can be understood by the fact that the presence of PHA granules, which are water-insoluble and of a high degree of polymerization, does not increase the intracellular osmotic pressure; however, they act as a storage of water-soluble compatible osmolytes (3HB), which are mobilized by the cells under conditions of sudden hyperosmotic pressure and other environmental stress factors (Obruca et al., 2016b). Later, it was detected by the same research team that the presence of PHA granules in bacterial cells prevents massive damage of the cytoplasmic membrane ("plasmolysis"), thereby supporting cells to maintain integrity under hyperosmotic conditions (Obruca et al., 2017). These studies evidence that significant amounts of PHA are commonly found among halophilic species due to their proficiency to overcome the negative effects of osmotic up-shock.

This adaptive role of PHA in halophilic microbes is fundamentally different from the effect of salinity on PHA biosynthesis for microbes industrially used for PHA production, such as the best described PHA producer *Cupriavidus necator* (used for PHA production at, e.g., PHB Industrial S.A. Brazil, Biomer, Germany, or Bio-On, Italy), turned out to be highly sensitive against increased salinity; as reported by Mozumder *et al.*, cell propagation and PHA biosynthesis by *C. necator* were completely stopped at sodium concentrations in the nutrient broth of 8.9 g/L and 10.5 g/L, respectively. In fed-batch cultivation setups carried out on a bioreactor scale, these studies showed that longer biomass growth phases under nutritionally balanced conditions, characterized by the permanent supply of NaOH for maintaining a neutral pH-value, causes sodium accumulation in cells, which results in decreased PHA production rates in the subsequent product formation phase (Mozumder et al., 2015).

2.3. Pros and cons of PHA production by halophiles

Occurring both among eubacteria and haloarchaea, such halophilic organisms are expected to render PHA production more cost-efficient in a not too distant future. This expectation is mainly based on the fact that halophilic PHA production strains can be cultivated at restricted sterility precautions, or even without any sterilization of the bioreactor equipment or the nutrient broth, which in turn saves energy and time during the upstream processing.

Also PHA recovery, hence, the downstream processing step, can be facilitated when using extreme halophilic PHA production strains. Due to their high intracellular osmotic pressure, cells of extremely halophilic species can conveniently be disintegrated by exposing them to hypotonic media (deionized water), which offers a convenient approach to recover intact PHA granules of remarkable purity by centrifugation. For mesophilic PHA production strains, recovery of PHA as an intracellular product requires cumbersome cell disintegration by chemical (use of strong oxidants), enzymatic (hydrolases) or mechanical methods, or solvent-intensive extraction of the product from biomass (reviewed by Koller, 2020).

A particular aspect of many PHA-producing extreme halophiles is the presence of certain metabolic pathways to produce PHA-building blocks different from 3HB, predominantly 3-hydroxyvalerate (3HV). Starting from different simple raw materials like carbohydrates, the intracellular carbon flux in such metabolic specialists gets shifted towards production of PHA copolyesters of improved processability (decreased crystallinity, broader temperature window between melting and decomposition temperature) when compared to PHB homopolyesters; for technically used, mesophilic PHA production strains like *C. necator*, PHA copolyester biosynthesis requires feeding the cells with precursor compounds chemically related to 3HV, such as propionic, levulinic or valeric acid. These precursor co-substrates are typically expensive and/or toxic, and are not needed in the case of copolyester biosynthesis by extreme halophiles like the haloarchaea *Hfx. mediterranei, Haloarcula hispanica, Halobacterium noricense, Halogeometricum borinquense* strain E3, *Halogranum amylolyticum,* or *Natrinema ajinwuensis* (reviewed by Koller, 2019b), or, as shown only recently, also for some moderately halophilic

eubacteria like *Halomonas pacifica* or *Halomonas salifodiane* (El-malek et al., 2020). For *Hfx. mediterranei*, this 3HV formation from unrelated substrates was well elucidated by Han *et al.*, who discovered multiple active pathways in this strain, which supply propionyl-CoA, which in turn acts as 3HV-precursor; propionyl-CoA couples with acetyl-CoA, forming of 3HV, which gets incorporated into growing poly(3HB-*co*-3HV) copolyester chains (Han et al., 2013).

Moreover, a range of technologically relevant by-products are produced in parallel to PHA biosynthesis by various both moderate or extreme halophiles; important examples are, besides above discussed organic osmolytes (Mothes et al., 2008; rational flux tuning for fine-tuned co-production of PHA and ectoines was only recently reported by Ma *et al.* for *Halomonas bluephagenensis* (Ma et al., 2020)), pigments like bacterioruberin (Giani et al., 2019; Giani and Martínez-Espinosa, 2020), antibacterial halocins (Kaur and Tiwari, 2021), or special exopolysaccharides (EPS) with xanthan-like properties, which might be of potential medical and food-industrial use (Cui et al., 2017a; Pacholak et al., 2021).

Hence, application of such halophiles for biotechnological product formation offers several beneficial options: firstly, the high salinity of the culture media minimizes the risk of microbial contamination ("infection") by foreign organisms, which makes the cultivation batches stable and less energy-demanding (Yin et al., 2015). Secondly, the cultivation of halophiles in saline media leads to the intracellular accumulation of salt, hence, the excessive salt load gets partially removed from the medium (Rodríguez-Contreras et al., 2016). This is advantageous in the case of salt-rich waste streams to be used as a culture medium (e.g., acidically hydrolyzed lignocellulose materials, whey, etc.); halophilic production strains used in such production processes need the salt generated by the acidic hydrolysis and the subsequent neutralization as an indispensable media component, and are therefore the ideal candidates for such bioprocesses. After the process, a considerable fraction of salts, which was highly diluted in the cultivation medium, is now stored in a limited volume of generated microbial biomass, which can easily be handled; hence, less salt remains in the spent fermentation broth, which is an environmental advantage regarding its disposal (Obruca et al., 2015; Obruca et al., 2014).

Despite all these positive aspects of PHA production by halophiles, we need to consider that this still is kind of a "double-edged sword"; as the downside of the medal, highly saline cultivation media are aggressive towards bioreactor equipment and electrodes used for bioprocess control. Therefore efforts are described in the literature to generate robust bioreactor facilities to farm such strains, such as reported by Hezayen *et al.*, who constructed a corrosion-resistant 8 L composite-type bioreactor made of poly(ether ether ketone) (PEEK), silicium nitrite ceramics and tech glass, stirred by corrosion-resistant magnetic coupling, to cultivate the PHA producing haloarchaeon *Halopiger aswanensis* at a salinity of 25 wt% NaCl (Hezayen et al., 2000). Alternatively, high-quality nickel-molybdenum-based Hastelloy alloy can be used to produce salt-corrosion resistant bioreactors to farm extremely halophilic strains, as shown by Mahler *et al.*, who developed a corrosion-resistant bubble column made of this material for this purpose (Mahler et al., 2018). Of course, such high-quality materials make the bioreactor equipment more expensive; alternatives, namely open, non-sterile cultivation process, as described in the previous paragraphs, might economically outperform processes requiring such expensive equipment, especially on a large scale. Moreover, in most cases, volumetric productivities for PHA and specific growth rates are still lower for haloarchael processes when compared to established processes using *C. necator*; promising exceptions are provided by genetically engineered *Halomonas bluephagenensis* strains, which are described in the subsequent section and summarized in Table 1.

2.4. Overview of PHA producing halophiles

A comprehensive literature review on diverse PHA homo- and

Table 1
Selected PHA production processes by halophiles.

Strain	Type of organisms; Classification according to halophilicity	NaCl concentration [g/L]; Cultivation scale	Carbon source	Type of PHA accumulated	Intracellular PHA fraction [g/g]; Volumetric productivity [g/(L·h)]	Strain origin (location of isolation)	Reference
Bacillus megaterium uyuni S29	Gram-positive eubacterium Halotolerant	45; Shaking flasks	Glucose	PHB	0.41; 0.1	Uyuni salt lake (Bolivia)	Rodríguez-Contreras et al., 2016
		10; Shaking flasks	Desugarized sugar beet molasses	PHB	0.6; 0.42		Schmid et al., 2019
		5; Pilot scale cultivation on 500 L (working volume) bioreactor scale	Desugarized sugar beet Molasses	PHB	0.65; 0.2		Schmid et al., 2021b
Salinivibrio sp. M318	Gram-negative eubacterium; Moderate halophile	30; Fed-batch bioreactor cultivation	Mixture of waste fish oil and glycerol (Nitrogen source: waste fish sauce)	PHB; PHBHV and PHB4HB after precursor addition in batch cultivations	0.52; 0.46	Isolated in Vietnam from fermented shrimp paste	Van Thuoc et al., 2019
Salinivibrio sp. TGB10	Gram-negative eubacterium; Moderate halophile	27.5; Fed-batch bioreactor cultivation		PHB; PHBHV with precursor addition	0.82; 0.25	Salt field in Binhai District, Tianjin (PR China)	Tao et al., 2021

Strain	Type of organisms; Classification according to halophilicity	NaCl concentration [g/L]; Cultivation scale	Carbon source	Type of PHA accumulated	Intracellular PHA fraction [g/g]; Volumetric productivity [g/(L·h)]	Strain origin (location of isolation)	Reference
Yangia sp. ND199	Gram-negative eubacterium; Moderate halophile	45; Fed-batch cultivations on shaking flask scale	(crude) glycerol (other inexpensive substrates, e.g., fructose corn syrup, converted to PHBHV)	PHBHV (PHB on glutamate)	0.53 (glycerol); 0.41 (crude glycerol); 0.56 (crude glycerol + fructose corn syrup); 0.44 (glycerol); 0.25 (crude glycerol); 1.10 (crude glycerol + fructose corn syrup)	Mangrove forest soil	Van-Thuoc et al., 2015
Halomonas venusta KT832796	Gram-negative eubacterium; Moderate halophile	15; 2 L bioreactor fed-batch cultivation	Glucose	PHB	0.88; 0.25	Indian coast samples	Stanley et al., 2018
Halomonas profundus	Gram-negative eubacterium; Moderate halophile	27; 2-stage batch 5 L bioreactor setup	Glucose	PHB (PHBHV after precursor feeding)	0.8–0.9; 0.004	Isolated from a shrimp	Simon-Colin et al., 2008
Halomonas pacifica ASL10	Gram-negative eubacterium; Moderate halophile, extremely halotolerant	tolerates up to 170 g/L NaCl; Shaking flasks	Sucrose	PHBHV	0.84; 0.04	Mariout salt lake (Egypt)	El-malek et al., 2020
Halomonas salifodiane ASL11	Gram-negative eubacterium; Moderate halophile, extremely halotolerant	tolerates up to 170 g/L NaCl; Shaking flasks	Sucrose	PHBHV	0.82; 0.04	Mariout salt lake (Egypt)	El-malek et al., 2020
Halomonas sp. YLGW01	Gram-negative eubacterium Moderate halophile; extremely halotolerant	20; high PHA productiovity even at 100 g/L NaCl Shaking flasks	Fructose syrup	PHB	0.95; 0.11	Gwangalli beach in Busan, South Korea.	Park et al., 2020

Strain	Type of organisms; Classification according to halophilicity	NaCl concentration [g/L]; Cultivation scale	Carbon source	Type of PHA accumulated	Intracellular PHA fraction [g/g]; Volumetric productivity [g/(L·h)]	Strain origin (location of isolation)	Reference
Halomonas halophila	Gram-negative eubacterium; Moderate halophile	66; Shaking flasks	Glucose (other saccharides from inexpensive sources converted)	PHB	0.72; 0.05	Salt pond located at the Costa Blanca near Alicante (Spain)	Kucera et al., 2018
Halomonas hydrothermalis	Gram-negative eubacterium; Moderate halophile	40; Shaking flasks	Waste frying oil	PHB (PHBHV after precursor addition)	0.62; 0.03	Deep-sea hydrothermal-vent environments; sea at West Coast of India	Pernicova et al., 2019

Table 1 (*continued*)

Strain	Type of organisms; Classification according to halophilicity	NaCl concentration [g/L]; Cultivation scale	Carbon source	Type of PHA accumulated	Intracellular PHA fraction [g/g]; Volumetric productivity [g/(L·h)]	Strain origin (location of isolation)	Reference
Halomonas neptunia	Gram-negative eubacterium; Moderate halophile	60; Shaking flasks	Waste frying oil	PHB (PHBHV after precursor addition)	0.56; 0.02	Deep-sea hydrothermal-vent environments	Pernicova et al., 2019
Halomonas organivorans	Gram-negative eubacterium; Moderate halophile	81; Shaking flasks	Waste frying oil	PHB	0.12; 0.02		Pernicova et al., 2019
Halomonas elongata 2FF	Gram-negative eubacterium; Moderate halophile, extremely halotolerant	100; Shaking flasks	Glucose	PHB	0.4; 0.02	Hypersaline meromictic Fără fund lake (Romania)	Cristea et al., 2017

Strain	Type of organisms; Classification according to halophilicity	NaCl concentration [g/L]; Cultivation scale	Carbon source	Type of PHA accumulated	Intracellular PHA fraction [g/g]; Volumetric productivity [g/(L·h)]	Strain origin (location of isolation)	Reference
Halomonas bluephagenensis	Gram-negative eubacterium (genetically engineered; wild type: *H. bluephagenensis* TD01); Moderate halophile	60; 500 L pilot scale open continous cultivation for 56 h	Glucose	PHB (PHBHV after precursor addition)	0.7 (0.92 in shaling flask setups); 1.12	Aydingkol salt lake (PR China)	Fu et al., 2014
		60; 5 m^3 pilot scale cultivation for 36 h	Glucose, γ-butyrolactone, and waste corn steep liquor; waste gluconate	PHB4HB	0.604 (max.: 0.74); 1.67		Ye et al., 2018
Haloferax mediterranei	Haloarchaeon (family: Haloferacaceae); Extreme halophile	150; 10 L bioreactor fed-batch cultivation	Glucose (plus yeast extract)	PHBHV (no precursor addition!)	0.7; 0.21	Salt pond located at the Costa Blanca near Alicante Spain)	Koller et al., 2015
		20; 42 L bioreactor fed-batch cultivation	Hydrolyzed whey permeate	PHBHV (no precursor addition!) PHBHV4HB (plus precursor)	0.73; 0.10		Koller et al., 2007a

Strain	Type of organisms; Classification according to halophilicity	NaCl concentration [g/L]; Cultivation scale	Carbon source	Type of PHA accumulated	Intracellular PHA fraction [g/g]; Volumetric productivity [g/(L·h)]	Strain origin (location of isolation)	Reference
Haloferax mediterranei (*cont.*)	Haloarchaeon (family: Haloferacaceae); Extreme halophile	200; 10 L bioreactor fed-batch cultivation	Hydrolyzed whey permeate, spent fermentation broth of previous whey-based processes	PHBHV	70; 0.04	Salt pond located at the Costa Blanca near Alicante Spain	Koller, 2015
		200; Shaking flasks	Waste stillage from rice-based ethanol production; recovery and re-use of medium salts	PHBHV	0.7; 0.17		Bhattacharyya et al., 2014
		234; 6 L bioreactor pH-stat fed-batch cultivation	Native cornstarch treated via enzymatic reactive extrusion plus yeast extract	PHBHV	0.5; 0.28		Chen et al., 2006b

Strain	Type of organisms; Classification according to halophilicity	NaCl concentration [g/L]; Cultivation scale	Carbon source	Type of PHA accumulated	Intracellular PHA fraction [g/g]; Volumetric productivity [g/(L·h)]	Strain origin (location of isolation)	Reference
Haloferax mediterranei (*cont.*)	Haloarchaeon (family: Haloferacaceae); Extreme halophile	220; Shaking flask	Native and dephenolized olive oil waste water	PHBHV	0.43; n.r.	Salt pond located at the Costa Blanca near Alicante Spain)	Alsafadi and Al-Mashaqbeh, 2017
		150; 10 L bioreactor fed-batch cultivation	Crude glycerol phase	PHBHV (no precursor addition!) PHBHV4HB (plus precursor)	0.75; 0.12		Hermann-Krauss et al., 2013

Table 1 (*continued*)

Strain	Type of organisms; Classification according to halophilicity	NaCl concentration [g/L]; Cultivation scale	Carbon source	Type of PHA accumulated	Intracellular PHA fraction [g/g]; Volumetric productivity [g/(L•h)]	Strain origin (location of isolation)	Reference
Haloteringena hispanica	Haloarchaeon (family: Natrialbaceae); Extreme halophile	200; 1 L Bioreactor batch cultivation	Complex carrot-waste medium	PHB	0.0013; n.r.	Saltern crystallizer pond at Fuente de Piedra saline lake, province Malaga (Spain)	Di Donato et al., 2011
Halopiger aswanensis	Haloarchaeon (family: Natrialbaceae); Extreme halophile	250; Batch cultivation in corrosion-resistant 8 L bioreactor	Sodium acetate and butyric acid	PHB	0.53; 0.0045	Samples collected from surface of hypersaline soil collected in Aswan (Egypt)	Hezayen et al., 2000
Halogranum amylolyticum	Haloarchaeon (family: Haloferacaceae); Extreme halophile	200; 7.5 L bioreactor fed-batch cultivation	Glucose	PHBHV	0.266; 0.013	Tainan marine solar salterns (PR China)	Zhao et al., 2015

Strain	Type of organisms; Classification according to halophilicity	NaCl concentration [g/L]; Cultivation scale	Carbon source	Type of PHA accumulated	Intracellular PHA fraction [g/g]; Volumetric productivity [g/(L•h)]	Strain origin (location of isolation)	Reference
Halogeometricum borinquense strain E3	Haloarchaeon; (family: Haloferacaceae); Extreme halophile	200; Shaking flask	Glucose	PHBHV	0.74; 0.21	Marakkanam solar salterns (India)	Salgaonkar and Bragança, 2015
		20; Shaking flask	Sugarcane bagasse hydrolysates	PHBHV	0.4–0.5; 0.0113		Salgaonkar and Bragança, 2017
		200; Shaking flask	Starch and carbon-rich fibrous cassava bagasse waste	PHBHV	0.74 (starch); 0.45 (cassava waste) 0.02 (starch); 0.006 (cassava waste)		Salgaonkar et al., 2019
Natrinema ajinwuensis (=*altunense*)	Haloarchaeon (family: Natrialbaceae); Extreme halophile	200; Repeated batch cultivations in shaking flaks	Glucose	PHBHV	0.61; 0.21	Indian salt production pans	Mahansaria et al., 2018

copolyester production processes by to date described eubacterial and haloarchaeal biopolyester accumulating organisms of different halophilicity, using different carbonaceous feedstocks, was only recently provided (Koller, 2019b). For classification of halophiles based on their salt tolerance/requirement, literature distinguishes at least three different clusters of halophilic microorganisms; this classification is based on the minimum salt required for growth and the maximum salt level these organisms are able to tolerate (reviewed by (Rodríguez-Contreras et al., 2016)).

The first cluster of "halotolerant" microbes are insensitive towards up to 2.5 M NaCl (upper salinity limit strongly fluctuating between different species), but are not dependent on such excessive salt concentration salinity. Halotolerant *Bacilli*, such as the expedient molasses converter *Bacillus megaterium* uyuni S29 isolated from a Bolivian salt lake (Rodríguez-Contreras et al., 2016; Schmid et al., 2021a, 2021b), are the prototype PHA-producing strains among this cluster, in addition to species like *Vibrio proteolyticus* (Hong et al., 2019).

Members of the cluster of "moderately halophiles" not only tolerate, but indispensably require 1–15 wt% (0.15–2.5 M) NaCl to thrive well; regarding PHA producers among them, *Halomonas* spp., such as *H. boliviensis*, *H. campaniensis*, *H. elongata*, *H. salina*, *H. profundus*, *H. venusta*, *H. neptunia*, *H. hydrothermalis*, *H. marina*, *H. smyrnensis*, *H. pacifica*, *H. salifodiane*, or *H. bluephagenensis* (genetically engineered organism originating from the wild type ancestor strain *Halomonas* sp. TD01) are prototype organisms of this cluster, besides other representatives like *Spriulina* sp. (Jau et al., 2005), *Salinivibrio* sp. (Tao et al., 2021; Van Thuoc et al., 2019) or *Yangia* sp., an expedient converter of crude glycerol from biodiesel production (Van-Thuoc et al., 2015) (reviewed by Koller, 2019b). Technologically, genetically engineered

H. bluephagenensis currently attracts attention as the only commercially implemented halophilic PHA production strain in several new biotech companies such as PhaBuilder© or MedPha©; these recombinants are constructed to accumulate PHA copolyesters poly(3HB-*co*-3HV); PHBHV) and poly(3-hydroxybutyrate-*co*-4-hydroxybutyrate) (poly (3HB-*co*-4HB); PHB4HB)) at high productivity at minor sterility conditions, and can be cultivated on inexpensive raw materials like corn steep liquor (Tan et al., 2021). It was shown before in pilot-scale experiments that genetically modified *H. bluephagenesis* can be readily cultivated in pilot-scale (500 L) open fermentation setups to PHA concentrations of more than 70 g/L, corresponding to volumetric productivities exceeding 1 g/(L•h), which is already approaching reported data for pilot-scale PHA production by mesophilic strains (Nonato et al., 2001). Later, the same group of authors reported the production of more than 60 g/L poly (3HB-*co*-15%-4HB) by *H. bluephagenensis* on a 5 m³ scale using glucose and corn step liquor as substrates plus γ-butyrolactone as 4HB-related precursor substrate. The productivity of this process amounted to an impressive value of 1.67 g/(L•h). Authors calculated the production costs of poly(3HB-*co*-15%-4HB) by this process with 2.57 € per kg; according to calculations performed based on data obtained by 7.5 L scale optimization experiments, this cost could further be reduced by 0.64 €/kg (Ye et al., 2018). These setups are described by the authors to be especially energy- and freshwater saving, which opened the door for mentioned industrial endeavors for PHA production by differently modified *H. bluephagenensis* strains (Fu et al., 2014).

Importantly, also for PHA production by *Halomonas* spp., there is a strong trend towards utilization of inexpensive raw materials, as recently shown by Liu *et al.*, who cultivated both a wild type *H. elongata* A1, isolated from a Chinese salt lake and its recombinants on glucose,

reaching intracellular PHB fractions of 22.81 wt% and 90.76 wt%, respectively. Recombinant strain *H. elongata* P2, subjected to further genetic modification, was able to readily accumulate PHB even from waste straw hydrolysate at a salinity of 50 g/L (Liu et al., 2021). In this context, *Salinivibrio* sp. M318, isolated from fermented shrimp paste in Vietnam was recently cultivated by Van Thuoc *et al.* on a mixture of fish oil and glycerol as a carbon source, while the fish waste sauce was used as a nitrogen source. In this process, a volumetric PHA productivity of 0.46 g/(L•h) was obtained (Van Thuoc et al., 2019). Other inexpensive raw materials for PHA production by moderately halophiles were used, for example by Pernicova *et al.*, who described the successful conversion of waste frying oil by *H. hydrothermalis* and *H. neptunia*, isolates from Deep-sea hydrothermal-vent environments, to PHB homopolyester (Pernicova et al., 2019). Moreover, Kucera *et al.* described the conversion of a variety of inexpensive hydrolysates, such as from cheese whey, spent coffee grounds, sawdust and corn stover, as well as sugar beet molasses, to PHB by *H. halophila*, a strain featuring a salinity optimum of 60 g/L. The salinity of cultivation media was conveniently adapted by neutralizing the acidic hydrolysis cocktails of applied inexpensive raw materials (Kucera et al., 2018).

The third and phylogenetically most ancient cluster encompasses the so-called "extreme halophilic" microbes; these microbial specialists require excessive salinity of 15–30 wt% (2.5–5 M) and even more for optimum growth. Within this cluster, some literature also classifies the so-called "borderline extreme halophiles", which thrive best in media containing 1.5–4.0 M NaCl (Park et al., 2006). Prototype organisms of extreme halophiles producing PHA are haloarchaea; exclusively scl-PHA production is reported for haloarchaea, while for eubacteria, both scl- and mcl-PHA production is reported (reviewed by Koller et al., 2020). Extremely challenging habitats are those environments, where such highly adaptive survivalists are typically isolated are, e.g., the Great Salt Lake, the Dead Sea, hypersaline anoxic deep-sea basins, solar saltern crystallizers, hypersaline soil samples, salt mine boreholes, salt production pans, or even alpine dry salt rocks (reviewed by Koller, 2019b).

Extremely halophilic haloarchaeal species reported to accumulate PHA belong to the families Halobacteriaceae (example of PHA producers: *Halobacterium noricense*), Haloarculaceae (PHA producers found among the genera *Haloarcula* and *Halorhabdus*), Halococcaceae (PHA producers occurring among the genus *Halococcus*), and Halorubraceae (PHA producers among the genus *Halorubrum*), Haloferacaceae (members of the genera *Haloferax*, *Haloquadratum*, *Halogranum*, and *Halogeometricum* are reported to accumulate PHA), and Natrialbaceae (members of the genera *Halopiger*, *Haloterringena*, *Natronobacterium*, *Halobiforma*, *Natronococcus*, and *Natrinema* reported to produce PHA) (reviewed by Koller, 2019b, Koller et al., 2020). Remarkably, most of the PHA production processes by these extreme halophiles are reported only for small shaking flask setups; exceptions are the steadily growing number of described bioreactor fermentation setups for *Hfx. mediterranei* on glucose, starch, hydrolyzed whey permeate from the dairy industry, extruded rice bran, rice-based stillage, mixtures of fatty acids, olive oil by-products, or crude glycerol phase as side-product of biodiesel production. In this context, *Hfx. mediterranei* was also cultivated on a pilot scale (200 L fed-batch setups in stirred tank reactor) on hydrolyzed whey permeate; this process was described and evaluated by a techno-economic assessment, which concluded that PHA production from surplus whey by extreme halophiles is at least competitive from an economic and life cycle perspective in comparison to competing technologies for whey utilization (Koller et al., 2013). Among the scarce assessments of potential processes for PHA production from inexpensive waste- and surplus materials, the *Hfx. mediterrei* process on hydrolyzed whey permeate was estimated with a production price per kg PHA of about 3 €, based on results from 200 L pilot scale, and including a polymer recovery by hypotonic cell disruption and recycling of the fermentation side streams (spent fermentation broth, saline cell debris) (Koller et al., 2007b). Similarly, Bhattacharyya *et al.* emphasized the need to close material cycles in *Hfx. mediterranei*-based PHA production

processes based on waste stillage originating from rice-based ethanol production to improve the process economically and environmentally (Bhattacharyya et al., 2014). Notably, in all these set-ups using *Hfx. mediterranei*, the strain accumulated PHBHV copolyester, even without the addition of 3HV-related precursor compounds. When adding 4HB-related precursors (GBL), poly(3HB-*co*-3HV-*co*-4HB) terpolyester was produced (Hermann-Krauss et al., 2013). In addition to *Hfx. mediterranei*, there is a small number of literature reports available for PHA-production process with other extreme halophiles under controlled conditions on bioreactor scale, such as for *Halogranum amylolyticum* on glucose (Zhao et al., 2015), *Halopinger aswanensis* on acetate and butyrate (Hezayen et al., 2000), or the thermohalophilic organism *Haloterringena hispanica* on a complex carrot-waste medium (Di Donato et al., 2011); these processes are summarized in Table 1. However, the industrial-scale application of extreme halophiles is still waiting for its realization.

Table 1 provides an overview of selected PHA production processes using different halotolerant, moderately halophilic and extremely halophilic PHA production strains on different carbon sources; the selection of examples is focused on most recent reports and, for haloarchaea, on processes performed under controlled conditions in bioreactors. Cultivation scale, type of PHA produced, PHA productivity and intracellular PHA fraction, as well as the location of isolation of strains, are compared.

3. Some like it hot - PHA biosynthesis by thermophiles

Thermophiles are microorganisms that are naturally adapted to the high temperature of the environment; literally, they are defined as microorganisms with optimal cultivation temperature above 45 °C. They have usually been classified into the three main categories: *i.* moderate thermophiles with optimal growth temperature in the range 45–65 °C, *ii.* extreme thermophiles with optimal growth temperature between 65 and 79 °C and *iii.* Hyperthermophiles, which reveal the best growth at temperatures above 80 °C (Zeldes et al., 2015). Actually, from our human perspectives, thermophiles can be regarded as exotic microbes colonizing rare niches with conditions close to the edge of life, nevertheless, habitats with high temperatures are surprisingly not uncommon. They are usually associated with volcanic activity, e.g., geothermally heated lakes or deep-sea vents. Also, solar activity can substantially enhance the temperature of some niches and other constantly hot habitats might be associated with human activity, such as household or agricultural compost piles (reaching up to 70 °C) or thermal effluents from various industrial processes (Urbieta et al., 2015). Thermophiles play also an important ecological role, for instance, they were likely the first microorganisms capable of thriving on Earth (Lusk, 2019) and they are also in the focus of astrobiologists as microbes that could survive and prosper at surfaces of planets that are hotter than the Earth (Hickey and Singer, 2004).

The adaptation to a high-temperature environment is a complex process that usually includes several strategies such as accumulation of compatible solutes (serving as molecular chaperones preventing biomolecules from heat-induced denaturation), changes in phospholipids structures (ensuring membrane integrity at high temperatures), and alternation in nucleic acids (prevalence of GC pairs) and proteins structure, which enhances their stability at elevated temperatures (Urbieta et al., 2015).

Also, PHA production by thermophiles provides numerous advantages as compared to mesophiles. Similar to increased media osmolarity in halophiles, also high cultivation temperature represents a hurdle that prevents the most common microflora from contamination of the biotechnological process. Therefore, also thermophilic processes can be considered being contamination-resistant. This assumption was confirmed by Ibrahim and Steinbüchel (2010) who performed long-term cyclic cultivations of the PHA producing thermophilic microorganism *Chelatoccus* sp. MW10 using a non-sterilized medium and the cultivation

ARTICLE IN PRESS

S. Obruča et al.   Biotechnology Advances xxx (xxxx) xxx

temperature of even 50 °C prevented the process from contamination (Ibrahim and Steinbüchel, 2010). Further, increased cultivation temperature provides also other advantages, for instance, it enhances the solubility of substrates (apart from oxygen), reduces the viscosity of the cultivation medium, and improves its homogeneity. Moreover, according to Arrhenius, high temperature enhances reaction rates (Peleg et al., 2012), hence, it accelerates desired metabolic processes (Krüger et al., 2018). It might seem that cultivations operated at elevated temperatures are energetically demanding since intensive heating is required, but the opposite is true. When the process is operated as high-cell density cultivation (which is the desired scenario in PHA production), the reactor is at least partially self-heated by metabolic heat of the employed microbial culture, and, importantly, no energetically challenging cooling is required. It should be pointed out that cooling is usually problematic (high energy and cooling water consumption, additional cooling systems might be needed which raises the cost of the equipment) in mesophilic processes operated in high-cell densities at large scales. Therefore, both heating and cooling demands are lowered when thermophiles are employed. Since also energy demands for sterilization are decreased, the thermophilic processes might be of beneficial energy balance (Ibrahim and Steinbüchel, 2010). In halophiles, the high salt concentration in cultivation media represents a serious problem for wastewater treatment management. An important advantage of thermophilic processes is the fact that the application of high temperature does not bring such consequences and complications.

However, unlike in halophiles, PHA production by thermophiles is not a deeply investigated field and was reported only in a very limited number of cases. Therefore, we performed a detailed literature search for reports on PHA production in thermophiles as well as in-depth bioinformatics analysis of available genomes of thermophilic microorganisms. In this case, we were looking for genes encoding for PHA synthases as the presence of *phaC* is a necessary prerequisite for the capability of PHA synthesis. The results are demonstrated in Table 2 and deeply discussed in the following text. We primarily searched through the database of non-redundant sequences standing for particular species, thus, where possible, accession numbers of PhaC synthases in NCBI RefSeq database (O'Leary et al., 2016) were used. Since not all genomes were stored in RefSeq database, in several cases accession numbers leading to GenBank database (Sayers et al., 2019) to sequences of particular strains of selected species were used. Moreover, we took all amino acid sequences from Table 2 and reconstructed a phylogenetic tree of all available PhaC synthases in thermophilic species (see Fig. 2). Two major clusters were formed in the phylogram. The smaller cluster contains three different *Aneurinibacillus* species and additional seven bacteria carrying putative Class III PhaC synthases. The larger cluster is formed by putative Class I PhaC synthases. However, there are five species (*Rubellimicrobium thermophillum*, *Pseudomonas* sp. SG4502, *Inmirania thermothiophila*, *Pseudonocardia thermophila*, and *Thermomonas hydrothermalis*) that each form a distinguished branch. These might be different, even unknown, classes of PHA synthases. Their classification is problematic, which is further supported by the low bootstrap support of these branches. Also, the inability to find PHA synthases in the genome of *Geobacilli*, *T. thermophilus*, and *T. elongatus* indicate that there might be some yet undiscovered classes of PhaC synthases. Even identification between known classes based on sequence similarity is impossible and has to be supplemented by the prediction of molecular weight (Kourilova et al., 2021b).

3.1. PHA production by Gram-negative thermophiles

PHA accumulation is likely a common feature typical for the members of the genus *Chelatococcus* which includes several thermophilic and thermotolerant strains. Ibrahim *et al.* isolated PHA producing thermophiles and obtained six gram-negative thermophilic isolates capable of PHA accumulation. Five isolates formed stable star-shaped cell aggregates, only the strain MW10 grew as free-living rod-shaped cells. By 16S

rRNA sequencing, the isolates were taxonomically classified as members of the *Chelatoccous* genus with an optimal growth temperature of 50 °C and strain-dependent preference for glucose or glycerol (Ibrahim et al., 2010). The strain MW9 was further systematically classified as a type strain of a novel species - *Chelatococcus thermostellatus* and is currently available in public collections of microorganisms (DSM 28244) (Ibrahim et al., 2016). The strain MW10 was successfully employed for PHA production in the advanced high-cell-density cyclic fed-batch cultivations in a 42-L bioreactor under semi-sterile conditions which proved the viability of the thermophiles-based PHA production (Ibrahim and Steinbüchel, 2010). *Chelatococcus daeguensis* TAD1 represents another thermophilic member of the genus *Chelatococcus* which can be considered being a potential candidate for industrial production of PHA, since PHA synthesis in this bacterium does not require limitation by any nutrient and is growth-associated. Hence, this strain was capable of reaching high PHA content (about 84% of CDM) in a relatively short period (24 h) at 50 °C using glucose as the sole carbon substrate. Apart from glucose, the strain is also able to utilize cheap substrates such as glycerol or starch (Xu et al., 2014). PHA production from glycerol employing *Chelatococcus daeguensis* TAD1 was further in-depth studied and optimized; utilization of two-stage fed-batch cultivation strategy resulted in a very high volumetric productivity (0.434 g/(L·h)) which could be a basis for economically feasible PHA production (Cui et al., 2015).

Another thermophilic Gram-negative genus for which PHA production was reported on phenotype level and also confirmed on genotype level by the identification of *phaC* gene in available genome databases is the genus *Caldimonas*. This genus contains two validly published strains and both were successfully used for PHA production. *Caldimonas manganoxidans* was isolated from a hot spring, and, interestingly, the bacterium was capable not only of accumulating PHA granules but it also revealed the ability to degrade extracellular PHB (Takeda et al., 2002). Later, the PHA accumulation potential of *C. manganoxidans* was investigated in detail; it was observed that it can achieve high product titers in short periods (5.4 g/L PHB in shaken flasks within 24 h) (Hsiao et al., 2016). In a follow-up study, *C. manganoxidans* was employed for PHA production from biodiesel-derived glycerol with promising results (Hsiao et al., 2018). Also the second validly published member of the genus – *Caldimonas taiwanensis* - can be used for PHA biosynthesis. Thanks to its amylolytic activity, Sheu *et al.* used this bacterial strain for PHA production from starch. The elevated cultivation temperature provides, in this case, not only a hurdle for microbial competitors, thus preventing the process from contamination, but it also enhances solubilization of starch, decreases the viscosity of the medium and, therefore, enhances homogeneity of the batch. When valerate was used as a 3HV precursor, the bacterium accumulated a copolymer consisting of 3HB and 3HV. The concentration of valerate in media was used as a regulatory factor influencing the monomer composition of the copolymer, 3HV fraction could reach a value as high as 95 mol% (Sheu et al., 2009).

PHA synthesis is likely a common feature also in the closely related thermophilic genus *Tepidimonas* since the presence of *phaC* gene was determined in numerous genus members such as *Tepidimonas alkaliphilus*, *Tepidimonas aquatica*, *Tepidimonas fonticaldi*, *Tepidimonas charontis*, *Tepidimonas ignava*, *Tepidimonas sediminis*, *Tepidimonas taiwanensis* or *Tepidimonas thermarum* (see Table 2). Nevertheless, studies describing PHA accumulation in *Tepidimonas* spp. are still lacking. The exception is the work of Chen *et al.*, who isolated a thermophilic alkaline-protease-producing bacterium from hot spring in the Pingtung area in Southern Taiwan. The bacterium was systematically classified as novel species *T. taiwanensis* and strong PHA accumulation was observed as one of the important physiological characteristics (Chen et al., 2006b). Generally, from a biotechnological point of view, the potential of *Tepidimonas* spp. for PHA production is limited by a relatively low range of utilizable substrates since most *Tepidimonas* species utilize neither carbohydrates nor lipids; they are restricted to organic acids and amino acids (Moreira

Table 2
List of thermophilic bacteria in which PHA synthesis was identified on genotype and/or phenotype level.

	Gram staining	Optimal cultivation temperature [°C]	PHA biosynthesis identified on genotype level	PhaC accession number	PHA synthesis described on phenotype level	Reference
Amphiplicatus metriothermophilus	G+	37–65	Yes	WP_089411661.1	No	
Aneurinibacillus danicus	G+	35–55	Yes	WP_146808431.1	No	
Aneurinibacillus terranovensis	G+	20–55	Yes	WP_027415498.1	No	
Aneurinibacillus thermoaerophilus	G+	45–60	Yes	WP_057899523.1	Yes	Pernicova et al., 2020a; Xiao et al., 2015
Anoxybacillus calidus	G+	35–70	Yes	WP_181538453.1	No	
Anoxybacillus vitaminiphilus	G+	35–70	Yes	WP_111643468.1	No	
Aquabacterium tepidiphilum	G-	25–50	Yes	WP_119153972.1	Yes	Khan et al., 2019
Bacillus thermoamylovorans	G+	50	No	–	Yes	Choonut et al., 2020a, 2020b
Caldimonas manganoxidans	G-	50	Yes	WP_026330149.1	Yes	Takeda et al., 2002; Hsiao et al., 2016
Caldimonas taiwanensis	G-	35–60	Yes	WP_062192707.1	Yes	Sheu et al., 2009
Chelatococcus daeguensis	G-	50	Yes	WP_071923939.1	Yes	Cui et al., 2015; Xu et al., 2014
Chelatococcus thermostalatus	G-	50	No	–	Yes	Ibrahim et al., 2016
Cupriavidus sp. S-6	G-	45	Yes	CCE46061.1	Yes	Sheu et al., 2012
Dichotomicrobium thermohalophilum	G-	20–65	Yes	WP_119062396.1	No	
Elioraea tepidiphila	G-		Yes	WP_019014986.1	No	
Elioraea thermophila	G-	45–60	Yes	WP_114377842.1	No	
Geobacillus kaustophilus	G+	55	No	–	Yes	Gedikli et al., 2019
Geobacillus stearothermophilus	G+	60	No	–	Yes	Gedikli et al., 2019
Hydrogenophilus thermoluteolus	G-	50	Yes	WP_197713626.1	Yes	Nguyen et al., 2019

	Gram staining	Optimal cultivation temperature [°C]	PHA biosynthesis identified on genotype level	PhaC accession number	PHA synthesis described on phenotype level	Reference
Inmirania thermothiophila	G-	35–68	Yes	WP_123400972.1	No	
Pseudomonas sp. SG4502	G-	45	No	–	Yes	Satoh et al., 2011
Pseudonocardia thermophila	G-	50	Yes	SHJ98529.1	No	
Rubellimicrobium thermophilum	G-	28–56	Yes	WP_021097566.1	Yes	Denner et al., 2006
Rubrobacter spartanus	G+	45–55	No	–	Yes	Kourilova et al., 2021b
Rubrobacter xylanophilus	G+	40–70	Yes	WP_143527769.1	Yes	Kourilova et al., 2021b
Schlegelella aquatica	G-	30–60	No	–	Yes	Chou et al., 2006
Schlegelella thermodepolymerans	G-	37–60	Yes	WP_104356814.1	Yes	Kourilova et al., 2020, 2021a
Synechococcus sp. MA19	G-	50	Yes	AAK38139.1	Yes	Miyake et al., 1996; Nishioka et al., 2001
Tepidicella baoligensis	G-	20–60	Yes	WP_180683314.1	Yes	You et al., 2019
Tepidicella xavieri	G-	25–55	Yes	WP_133596978.1	No	
Tepidimonas alkaliphilus	G-	37–55	Yes	TSE20543.1	No	
Tepidimonas aquatica	G-	35–60	Yes	WP_144324707.1	No	
Tepidimonas fonticaldi	G-	35–60	Yes	WP_143968067.1	No	
Tepidimonas charontis	G-	25–60	Yes	WP_144327474.1	No	
Tepidimonas ignava	G-	50–55	Yes	WP_132961516.1	No	
Tepidimonas sediminis	G-	37–55	Yes	WP_143892980.1	No	

	Gram staining	Optimal cultivation temperature [°C]	PHA biosynthesis identified on genotype level	PhaC accession number	PHA synthesis described on phenotype level	Reference
Tepidimonas taiwanensis	G-	35–60	Yes	TSE30381.1	Yes	Chen et al., 2006b, Kourilova et al., 2021c
Tepidimonas thermarum	G-	25–60	Yes	WP_143902344.1	No	
Tepidiphilus margaritifer	G-	25–61	Yes	WP_051240655.1	Yes	Manaia et al., 2003
Tepidiphilus succinatimandens	G-	50–55	Yes	WP_206202189.1	No	
Tepidiphilus thermophilus	G-	30–60	Yes	WP_055423697.1	No	
Thauera hydrothermalis	G-	37–55	Yes	WP_114649837.1	No	
Thermomonas hydrothermalis	G-	50–55	Yes	WP_072756679.1	No	
Thermosyntropha lipolytica	G+	52–70	Yes	WP_073089411.1	No	
Thermus thermophilus	G-	70–75	No	–	Yes	Pantazaki et al., 2003, 2009
Ureibacillus terrenus	G+	42–65	Yes	WP_141600988.1	No	
Ureibacillus thermophilus	G+	30–65	Yes	WP_208649453.1	No	
Zhizhongheella caldifontis	G-	40–50	Yes	PPE66523.1	No	

et al., 2000). Again, *T. taiwanensis* represents an interesting exception because it is, according to literature, capable of assimilation of glucose and fructose (Chen et al., 2006a). Therefore, it was recently used for PHA production from the inexpensive resource grape pomace, which is rich in these abundant sugars. At the cultivation temperature of 50 °C, the bacterial culture was capable of accumulating PHA up to 65% of CDM in flasks experiments, the final PHA titer reached a very promising value of 3.55 g/L (Kourilova et al., 2021c).

Similarly to *Tepidimonas*, also in genus *Tepidiphilus,* we identified the presence of *phaC* genes in available genomes of *Tepidiphilus margaritifer*, *Tepidiphilus succinatimandens* and *Tepidiphilus thermophilus* (see Table 2).

However, reports confirming PHA accumulation on phenotype level are lacking. Only Manaia *et al.* mentioned that *Tepidiphilus margaritifer* accumulates PHA granules as physiological characteristic of the strain without any further details (Manaia et al., 2003). Similar to *Tepidimonas* spp., also by *Tepidiphilus* species organic acids and amino acids, but no sugars or lipids, are used as carbon sources, which limits their potential biotechnological applications as chassis for PHA production (Manaia et al., 2003).

Moreover, very similarly to *Tepidimonas* and *Tepidiphilus*, *phaC* genes were detected also in the only two members of the genus *Tepidicella* - *Tepidicella baoligensis* and *Tepidicella xavieri* (Table 2). Presence of PHA

granules was observed in *Tepidicella baoligensis*, but *Tepidicella* species are not capable of effective assimilation of carbohydrates or lipids (You et al., 2019), thus their biotechnological potential within the concept of NGIB is negligible.

Further, the presence of *phaC* genes was observed in several other species (*Dichotomicrobium thermohalophilum, Elioraea tepidiphila, Elioraea thermophila, Inmirania thermothiophila, Pseudonocardia thermophila, Thauera hydrothermalis, Thermomonas hydrothermalis, Thermosyntropha lipolytica, Thauera hydrothermalis, , Thermosyntropha lipolytica* or *Zhizhongheella caldifontis*), which indicates that also these bacteria could be considered as PHA accumulators, but no definitive reports on PHA accumulation are available. Investigation of their PHA production capability and biotechnological potential could be an interesting topic for further research.

In other bacteria, PHA accumulation was identified on the genotype level and also mentioned as physiological characteristics without any reports regarding the type of polymer accumulated, PHA content in biomass or gained PHA titers. For instance, *Aquabacterium tepidiphilum* contains *PhaC* (Table 2) and the presence of PHA granules was observed by Khan et al. (2019). Also *in Rubellimicrobium thermophilum*, PHA synthesis capability was observed on genotype level and further detected on phenotype level. This bacterium could be an interesting candidate for PHA production since it is capable of assimilation of a wide range of carbohydrates and it also produces carotenoids, which, analogous to PHA and pigment co-production by many halophiles, could be interesting side-products to PHA (Denner et al., 2006); nevertheless, no study on PHA production potential of the strain is available.

On the contrary, PHA production was already studied in *Hydrogenophilus thermoluteolus* TH-1, a thermophilic hydrogen-oxidizing bacterium revealing the highest growth rate among autotrophs. This bacterium contains the genetic machinery for PHA synthesis, the strain was capable of PHB production under nitrogen limitations both under both autotrophic (gas mixture consisting of $H_2:O_2:CO_2$ 75:10:15 was used) as well as heterotrophic (various organic acids were used as substrates) conditions at 50 °C. Especially the autotrophic production potential of this bacterium seems to be very interesting (Nguyen et al., 2019).

The top position among thermophiles holds *Thermus thermophilus* HB8, which was used for PHA production at as high a temperature as 75 °C. Pantazaki *et al.* cultivated this bacterium on octanoate or gluconate; PHA represented about 35–40% of CDM, the polymer consisted of a mixture of scl- and mcl- monomers with 3-hydroxydecanoate as the major monomer unit (Pantazaki et al., 2003). In the follow-up study, *Themus thermophilus* HB8 was used for scl- and mcl-PHA copolymers production from cheese whey under nitrogen limitation, the maximal PHA titer reached 0.57 g/L (Pantazaki et al., 2009). Nevertheless, even though the complete information on genomes of various strains of *Thermus thermophilus* are available, we were not able to discover a *phaC* gene in these genomes, hence, the only evidence for the PHA accumulating capability of *Thermus thermophilus* are publications by Pantazaki et al. (2003, 2009).

Schlegella thermodepolymerans is a Gram-negative bacterium that was isolated from activated sludge under aerobic and thermophilic conditions by the group of Professor Alexander Steinbüchel as a representative of a novel genus. This microorganism was capable of biodegradation of poly(3-hydroxybutyrate-*co*-3-mercaptopropionate), a biosynthesized polymer that had been considered being non-biodegradable. Therefore, the species name reflects its special polymer degradation capacity (Elbanna et al., 2003). In the subsequent studies, extracellular PHA depolymerase of *Schlegella thermodepolymerans* was characterized in more detail and it was observed that the bacterium is not capable of efficient hydrolysis of thioester bonds as was originally expected (Elbanna et al., 2004). The bacterium was, for a long time, studied only from the perspective of PHA biodegradation, but we have recently suggested that *S. thermodepolymerans* is also a very promising PHA producer. It possesses the complete genetic machinery for PHA

biosynthesis, and the PHA portion in biomass can reach up to 87% of CDM at 55 °C. Most thermophilic PHA producers described above reveal only limited catabolic flexibility – hence, the number of substrates that can be converted to PHA is restricted. On the contrary, *S. thermodepolymerans* seems to be very flexible in this perspective; it can utilize a wide range of carbohydrates, lipids and glycerol. Surprisingly, the most preferred substrate was the pentose xylose, a substrate rather rarely accepted by microbes for PHA biosynthesis. Actually, *S. thermodepolymerans* prefers xylose even over glucose, therefore, it can be considered to be an astonishing candidate for PHA production following the NGIB principle from cheap xylose-rich lignocellulose-based resources (Kourilova et al., 2020; Musilova et al., 2021). In the follow-up study, the PHA production potential of *S. thermodepolymerans* from lignocellulose-based media was compared with the halophilic PHA producer *H. halophila* (also listed in Table 1) and the prototype xylose-converting mesophilic bacterium *Burkholderia sacchari*. Among the tested bacteria, *S. thermodepolymerans* demonstrated the highest PHA yields on substrates rich in xylose, and, compared to *H. halophila*, *S. thermodepolymerans* was also robust against microbial inhibitors present in lignocellulose hydrolysates such as ferulic acid, gallic acid, furfural or levulinic acid. This confirms that *S. thermodepolymerans* is an auspicious PHA producer deserving further attention (Kourilova et al., 2021a). Aside from *S. thermodepolymerans*, PHA granules accumulation was reported also for another moderately thermophilic member of the *Schlegelella* genus – *Schlegelella aguatica* (Chou et al., 2006), indicating that PHA synthesis might be a common feature for *Schlegelella* spp.

3.2. PHA production by Gram-positive thermophiles

Besides Gram-negative bacteria, PHA are also accumulated by numerous Gram-positive prokaryotes. Actually, Maurice Lemoigne who is considered being a discoverer of PHA, isolated and chemically described PHA from cells of Gram-positive bacterium *Bacillus megaterium* in 1926 (Lemoigne, 1926). Although mostly Gram-negative bacteria are currently considered as candidates for PHA production, Gram-positive PHA producers provide an important advantage. One of the major obstacles preventing the use of PHA in health care, cosmetics or medicine is the contamination of the polymer produced by Gram-negative bacteria by pyrogenic lipopolysaccharides - endotoxins. These contaminants are co-isolated along with PHA and induce a severe immunological response in the human body, which is extremely unsuitable in numerous uses of PHA (Singh et al., 2019). Of course, if a Gram-positive bacterium unable of endotoxin synthesis is used for PHA production, this contamination can not occur and does not represent a problem.

Very recently, Sangkharak *et al.* employed an isolate classified as *Bacillus thermoamylovorans* strain PHA005 for production of PHA from waste cooking oil; the cultivation was operated at 45 °C and the bacterium showed high PHA accumulating potential since within 48 h of cultivation in shaken flasks, the polymer content in biomass reached 87% of CDM. The accumulated polymer was composed of 85 mol% of 3HB and 15 mol% of 3HV (Sangkharak et al., 2020). In another work, the same collective of authors reported that *B. thermoamylovorans* strain PHA005 produces mcl-PHA when cultivated at 45 °C on sodium octanoate; polymer content in biomass reached up to 63% of CDM and the polymer consisted of C8-C18 monomers, 3-hydroxydecanoic acid (3HD) being the major monomer unit (Choonut et al., 2020b). As mentioned before in this article, mcl-PHA production is usually observed in *Psedomonads*; however, mcl-PHA synthesis in *Bacilli* was also already reported before (Shahid et al., 2013), but it is a very rare feature; hence, *B. thermoamylovorans* strain PHA005 seems to be a very interesting bacterium. To our best knowledge, the genome of the strain was not published so far and PhaC encoding genes were not identified in available genomes of *B. thermoamylovorans*. Thus, the unique PHA synthetic potential of *B. thermoamylovorans* sp. PHA005 might be a strain-dependant property not observed in other members of the genus.
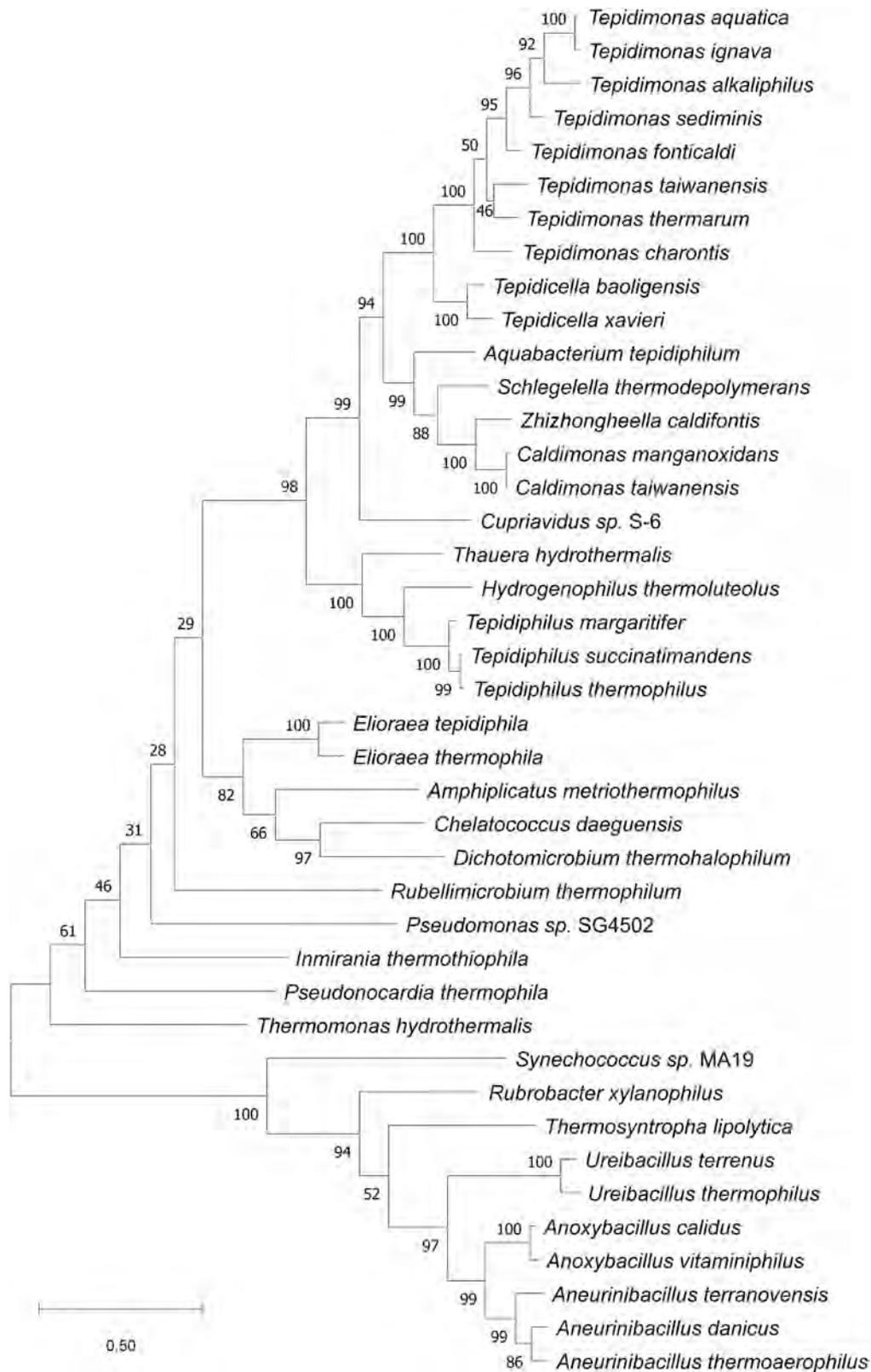
Fig. 2. The phylogeny was inferred by using the Maximum Likelihood method and Whelan And Goldman model (Whelan and Goldman, 2001). The tree with the highest log likelihood (−27,119,16) is shown. The boostrap support calculated from 500 replicates is shown next to the branches. Initial tree(s) for the heuristic search were obtained automatically by applying Neighbor-Join and BioNJ algorithms to a matrix of pairwise distances estimated using the JTT model, and then selecting the topology with superior log likelihood value. The tree is drawn to scale, with branch lengths measured in the number of substitutions per site. This analysis involved 41 amino acid sequences. There were a total of 780 positions in the final dataset. Evolutionary analyses were conducted in MEGA X (Kumar et al., 2018).

ARTICLE IN PRESS

S. Obruča et al.   Biotechnology Advances xxx (xxxx) xxx

As was already implied, PHA production is a very common feature among the genus *Bacillus* and related species. Historically, during the last decades, several genera were set aside from the parental genus *Bacillus*, including thermophilic or thermotolerant genera such as *Geobacillus*, *Anoxybacillus*, *Aneurinibacillus*, *Ureibacillus* or *Thermobacillus*. Therefore, it can be expected that members of at least some of these thermophilic genera could also accumulate PHA.

The genus *Geobacillus* comprises a group of Gram-positive endospore-formic thermophilic bacteria that can grow over a range of 45–75 °C. Due to their catabolic versatility and rapid growth, *Geobacillus* spp. have raised attention as microorganisms with great potential for biofuel or chemical production following the NGIB concept (Hussein et al., 2015); nevertheless, it seems that PHA synthesis capacity is not widespread among members of *Geobacillus*. Even though genomes of numerous *Geobacillus* species are available in public databases, we were not able to identify genes encoding PHA synthases in *Geobacilli*. Also, particular reports on PHA synthesis by members of the *Geobacillus* genus are scarce; PHA synthesis was observed only in one isolate, which was identified as *Geobacillus kaustophilus* (Gedikli et al., 2019). Hence, it seems that PHA accumulation is not a common feature among *Geobacillus* spp. but it is a rather rare and strain-dependent characteristic.

On the contrary, we have identified that two members of the *Ureibacillus* genus - *Ureibacillus terrenus* and *Ureibacillus thermophilus* (see Table 2) and also in two members of genus *Anoxybacillus* - *Anoxybacillus calidus* and *Anoxybacillus vitaminiphilus*, contain genes encoding for PHA synthase. Nevertheless, to our best knowledge, there are no literature reports on PHA accumulation on phenotype level by these bacteria.

In contrast, PHA synthesis in the genus *Aneurinibacillus* is very well documented. Xiao *et al.* isolated PHA accumulating Gram-positive bacterium from Gudao oilfield in China. The isolate was taxonomically classified as *Aneurinibacillus thermoaerophilus* XH2, its optimal temperature for growth as well as PHA synthesis is 55 °C. Interestingly, the accumulated PHA polymer consisted of 3HB and 3HV with a minor fraction of 3-hydroxyoctanoate and 3-hydroxy-4-phenylbutanoate, so the bacterium accumulated a very interesting PHA copolymer, nevertheless, product titers were rather low - about 0.25 g/L of PHA (Xiao et al., 2015). The authors subsequently published a complete genome sequence, therefore, PHA production capability was confirmed also on the genotype level. As expected, the isolate harbors PHA synthase belonging to class IV which is typical for *Bacillus* and related genera (Xi et al., 2016). Further, Pernicova *et al.* also focused on the isolation of PHA producing thermophiles and obtained several isolates classified as *Aneurinibacillus* sp. (Pernicova et al., 2020b). The most promising isolate – *Aneurinibacillus thermoaerophilus* H1 was capable of accumulation of PHA up to 50% of CDM, maximal PHA titers in shaking flasks were obtained with glycerol as a substrate (about 2 g/L) at 45 °C; nevertheless, the bacterium was capable of growth and PHA synthesis up to 65 °C even though enhancement cultivations at a temperature above 50 °C decreased biomass growth and PHA accumulation. The most interesting property of this bacterium was its capability of incorporating various 4HB (1,4-butanediol, gama-butyrolactone) and 3HV (propionate, valerate) precursors into the PHA structure, resulting in production of poly(3HB-*co*-4HB) copolymer and poly(3HB-*co*-4HB-*co*-3HV) terpolymers with very high 4HB (up to 93 mol%) and 3HV fractions. The monomer composition of poly(3HB-*co*-4HB) copolymer can be simply and precisely controlled by the ratio of 1,4-butanediol (4HB precursor) and glycerol (carbon substrate and 3HB precursor) in the cultivation media (Pernicova et al., 2020a). The material properties of produced copolymers were further studied in detail and it was proved that manipulation of the monomer composition enables regulation of the crucial material properties of PHA such as degree of crystallinity or melting temperature (Sedlacek et al., 2020). Since the presence of *phaC* gene was detected also in other *Aneurinibacilli* such as *Aneurinibacillus danicus* and *Aneurinibacillus terranovensis*, it is suggested that PHA accumulation is rather a common capability among the members of this genus.

The genus *Rubrobacter* accommodates non-motile, obligatory aerobic, asporogenic and Gram-positive actinobacteria. The genus members are considered to be "polyextremophiles" because they can survive under various adverse conditions. For instance, they are highly resistant to harmful effects of various radiations including UV and even ionogenic radiation, moreover, some members are also halotolerant and reveal thermophilic attributes (Castro et al., 2019). Recently, PHA production was confirmed both on genotype as well as phenotype level in two thermophilic members of the genus – *Rubrobacter spartanus* and *Rubrobacter xylanophilus*. Interestingly, the bioinformatic analysis indicated that *Rubrobacter* spp. contain two genes encoding for different PHA synthases – one gene encodes for Class I and the second for Class III PhaC, the second subunit of Class III synthase – PhaE - was identified as well. PHA content in both tested strains reached up to 50% of CDM, PHA polymer consisted of 3HB monomer, 3HV units were incorporated when the proper structural precursors (valerate, propionate, n-amyl alcohol) were supplemented. Especially *R. xylanophilus* demonstrated high robustness concerning cultivation temperature since cultivation temperature had only a very minor effect on both biomass growth and PHA accumulation in the temperature range 45–60 °C. This strain also revealed high catabolic flexibility, therefore, it might be an interesting candidate for PHA production. Importantly, *Rubrobacter* species are Gram-positive thus endotoxin none-forming bacteria but, unlike other Gram-positive PHA producers, *Rubrobacter* species are also not capable of sporulation, which is a very important attribute (Kourilova et al., 2021b). Sporulation is considered being an unfavorable characteristic of the strain to be employed in industrial PHA production because it is accompanied by mobilization of PHA storage and also a sudden loss of desired metabolic activity; moreover, sporulation shifts carbon flux from the formation of desired products (PHA) to unwanted by-products (endospores), which results in an economic loss (Sadykov et al., 2017). Thus, thanks to its thermophilic feature, catabolic flexibility, Gram-positivity and also an absence of sporulation capability, *Rubrobacter* species are also interesting chassis for industrial PHA production within the NGIB concept (Kourilova et al., 2021b).

3.3. PHA synthesis as an adaptation strategy to high temperature

In halophiles, the interconnection between adaptation to hypertonic conditions and PHA biosynthesis is well documented. Direct experimental observations are confirming the osmoprotective role of PHA granules (see the previous section) and there are also indirect hints such as the fact that the list of PHA producing halophiles is long (Table 1) and includes not only moderately halophilic bacteria but also extremely halophilic *Archaea* such as *Hfx. mediterranei* or *Hgm. borinquense* (Koller, 2019b; Pfeifer et al., 2021). On the contrary, it seems that the role of PHA in adaptation to high temperatures is not so evident. There are reports that PHA accumulation protects against heat. For instance, Zhao *et al.* observed that PHA biosynthesis capable wild-type strain of *Aeromonas hydrophila* was more resistant to heat than PHA synthase negative-mutant unable of PHA synthesis (Zhao et al., 2007). Nevertheless, potential protective mechanisms of PHA against high temperature are not clear. It is likely that PHA monomer units possessing strong chemical chaperone activity might protect bacteria from the adverse effects of high temperature (Obruca et al., 2016b; Soto et al., 2012). Furthermore, also phasins, PHA granules associated proteins, reveal chaperoning activity and might prevent cellular proteins from denaturation at high temperatures (de Almeida et al., 2011). Nevertheless, apart from *Thermus thermophilus* – the only extremely thermophilic bacterium on the list of PHA producers, PHA synthesis was reported only for thermotolerant and moderately thermophilic bacteria (see Table 2) with optimal growth temperature between 50 and 60 °C. To the best of our knowledge, PHA synthesis was observed neither in hyperthermophilic bacteria nor archaea. Hence, despite their proven protective function against slightly elevated temperatures (Alves et al., 2020; Gonçalves et al., 2019), it is likely that PHA are not the most suitable

metabolites for adaptation to extremely high temperatures. From the biotechnological point of view, this fact is not a limitation. At very high cultivation temperatures, considerably decreased oxygen solubility represents a serious obstacle practically thwarting to reach high cell density of aerobic microbial cultures. Since PHA are intracellular metabolites of the secondary metabolism, high cell density is a necessary prerequisite for gaining high product titers. Therefore, the fact that only moderately thermophilic prokaryotes produces PHA is not a drawback.

3.4. Thermophilic PHA producers as sources of genes encoding potent PHA-related enzymes

Besides direct utilization for biotechnological production of PHA, thermophilic bacteria capable of PHA production are also very interesting as sources of thermostable and highly active PHA synthases and other enzymes for PHA synthesis *in-vivo* or even *in-vitro*. Tajima *et al.* investigated *in-vitro* synthesis of PHA. These authors emphasized the importance of the utilization of thermostable enzymes for the rapid and sustainable process of *in-vitro* PHA production. In their study, they utilized thermostable acetyl-CoA synthase from the thermophilic bacterium *Pelotomaculum thermopropionicum* JCM10971, CoA transferase from *Thermus thermophilus* JCM10941 and PHA synthase from the thermotolerant bacterium *Pseudomonas* sp. SG4502. The system was capable of synthesis of PHB and a copolymer consisting of 3HB and lactic acid. Due to the thermostability of employed enzymes, the system was operated at 45 °C. Even at 37 °C, the yields obtained by thermophilic enzymes were 1.4-fold higher than those obtained by mesophilic enzymes (Tajima et al., 2016). In this context, all the bacteria listed in Table 2, even those which are no promising candidates for PHA synthesis, for instance because they can not be cultivated on biotechnologically relevant substrates or are not capable of reaching high cell densities or high PHA amounts in biomass, might be considered being interesting resources for thermostable and highly active PHA synthases and other enzymes which to be employed for PHA synthesis.

Further, discovery and in-depth characterization and understanding of thermostable and highly active PHA synthases from thermophilic prokaryotes might be used for the rational design of highly active and stable PHA synthases. Sheu *et al.* constructed a chimeric PHA synthase of the thermophilic strain *Cupriavidus* sp. S-6 and the mesophile *C. necator* H16. In details, this constructed chimeric enzyme was a PHA synthase from mesophilic *C. necator* H16 bearing 30 point mutations derived from the middle region of PHA synthase of the thermophilic strain; it demonstrated 3.45-fold higher specific activity than the parental enzyme at 30 °C and substantially higher stability since at 45 °C its half-life was 127-fold higher than that of the parental enzyme. Transgenic *Escherichia coli* harboring chimeric PHA synthase cultivated at 37 °C accumulated at 59% PHB per CDM, which was substantially more than in a strain harboring PHA synthase of mesophilic *C. necator* H16 strain (38% of CDM) (Tajima et al., 2016).

4. Making a good thing better- metabolic engineering and synthetic biology of extremophilic bacteria for tailored PHA production

Metabolic engineering (ME) and synthetic biology (SB) have generated numerous useful tools and engineering approaches of which some have revolutionized microbial biotechnology and the use of microorganisms, their metabolic pathways, and enzymes for biosynthesis of valuable chemicals (including PHA) or biodegradation of environmental pollutants (Choi et al., 2019; Dvořák et al., 2017). Initially, these powerful tools were restricted for modifications of microbial models *E. coli, Bacillus subtilis,* or *Saccharomyces cerevisiae*. The advent of ME in the 1990s enabled interspecies transplantation of whole metabolic pathways and gave rise, beside others, to recombinant PHA-producing *E. coli* strains with exogenous *phaCAB* operon (Choi et al., 1998). Some of the derivatives of these strains are now used for PHA

manufacturing on an industrial scale (Tan et al., 2021). Research communities that work with non-canonical microbial hosts including paradigmatic PHA producers *C. necator* or *Pseudomonas putida* also understood the potential of ME and SB and quickly adopted these disciplines in their work. This step enabled the construction of upgraded bacterial factories capable of enhanced accumulation of PHA with altered properties from a variety of low-cost substrates (Budde et al., 2011; Dvořák et al., 2020b; Park et al., 2013; Salvachúa et al., 2020). Extremophilic PHA producers - especially halophiles and thermophiles - have drawn the attention of biotechnologists more recently, which means that a less colorful palette of ME and SB methods and gadgets is available for them. The unsatisfactory situation is nonetheless rapidly changing for PHA-forming halophiles, namely for certain strains from genus *Halomonas* or the haloarchaeal genus *Haloferax* (Haque et al., 2020; Zhang et al., 2020). In the last couple of years, *Halomonas bluephagenesis* TD01 became a testbed for ME and SB tools in halophiles and, as mentioned previously in this article, its engineered derivatives are being used in several Chinese companies that develop NGIB based on this bacterium (Tan et al., 2021). To the best of our knowledge, no study reporting the use of genetically enhanced thermophilic microorganisms for PHA production has been published to date. But the wealth of inspiration for such an endeavor can be taken from the increasing number of publications that unveil the potential of moderately and extremely thermophilic bacteria and archaea for the biosynthesis of biofuels from lignocellulosic residues (Crosby et al., 2019; Jiang et al., 2017b).

In this chapter, we will discuss selected examples of studies from the last decade in which ME and SB played a key role in improving the yield, properties, and downstream processing of PHA in halophilic bacteria, or in broadening the substrate scope of these organisms. We will also map the history of adoption and development of genetic engineering, ME and SB tools and techniques for PHA-forming halophiles (Fig. 3). The prerequisites for successful engineering interventions in thermophilic PHA producers will be highlighted in the last part of the chapter.

4.1. Engineering halophiles for high-yield production of PHA with tailored properties

High production cost and limited biopolymer diversity are the two major issues that hinder wider commercialization of PHA produced by conventional microbial strains of *E. coli* or *C. necator* as well as by the next generation bacterial platforms derived from genus *Halomonas* (Tan et al., 2021; Zheng et al., 2020). Metabolic engineering of suitable natural PHA producers can lead to substantially increased PHA content in the cell, higher PHA yield, titer, and substrate-to-product conversion, or diversified arrangements of polymer structures with new functionalities and properties that fit market needs. Professor Chen's group work on *H. bluephagenesis* TD01 is an outstanding showcase to demonstrate the step-by-step adoption and development of ME and SB tools for a non-canonical extremophilic host and pushing the limits of the cell factory towards economically feasible bioprocess (Chen et al., 2017).

In 2011, Tan and co-workers (Tan et al., 2011) reported unsterile continuous cultivation of the wild-type strain TD01 in seawater with glucose as a sole carbon source during which PHB content in CDM reached up to 80 wt% and substrate-to-biopolymer conversion ranged from 20 to 50%. This engaging study drew attention to *H. bluephagenesis* as a potential candidate for the NGIB but also pointed to the lack of reliable ME tools for this organism. Basic molecular biology toolkit including a restricted number of cloning and expression shuttle plasmid vectors (such as pHS15, pEE5), selection markers (e.g., kanamycin, gentamycin, trimethoprim) and reporters (GFP), conjugation and electroporation protocols, some regulatory sequences for gene expression, or transposon Tn*1732* and suicide plasmid pKS18*mobsac* for random gene knockouts in halomonads was already available by that time (Argandoña et al., 2012). However, a true ME Swiss knife was urgently needed for advancing *H. bluephagenesis* from microbial Cinderella to a

biotech star.

4.1.1. Development of fundamental tools for genetic manipulations of Halomonas

Following studies of Chen's group therefore initially focused on the design of genetic tools for TD01 and their utilization for increasing content, productivity, and applicability of PHB, the biopolyester typically synthesized by *H. bluephagenesis*. Fu and co-workers (Fu et al., 2014) developed a scarless gene knockout and integration system based on the I-*Sce*I endonuclease-mediated homologous recombination technique established for *E. coli* (Posfai et al., 1999). Constructed suicide vector pRE112-6I-*Sce*I with R6kγ replicon and mobilizable broad-host-range plasmid pBBR1MCS1-I-*Sce*I with constitutively expressed I-*Sce*I gene were transferred to TD01 via conjugation with *E. coli* S17-1 (electroporation and chemical transformation did not work for *H. bluephagenesis*). The system was used to delete *prpC* gene encoding 2-methylcitrate synthase and to improve the otherwise poor production of PHBHV in mineral medium with glucose and propionate. The deletion prevented degradation of 3HV precursor propionyl-CoA in methylcitric cycle. As a result, 3HV fraction in PHBHV increased substantially and PHBHV content in CDM reached 70 wt% both in shake flask and 500 L fermentor experiments.

In another study from the same year, the conjugation efficiency and stability of exogenous plasmid DNA in *H. bluephagenesis* was improved by partial inactivation of the restriction-modification system via deletion of 8.4-kb *hsdRMS* gene cluster and *re1* and *re2* genes (Tan et al., 2014). The authors also looked for the optimal plasmid backbone that would secure the stable expression of heterologous genes in *Halomonas*. High-copy broad-host-range plasmid pSEVA341 (with chloramphenicol resistance) from Standard European Vector Architecture collection (Silva-Rocha et al., 2013) surpassed previously prepared plasmids (e.g., pRE112-pMB1) in its stability and conjugation efficiency. The expression vector was prepared by cloning the strong hybrid LacI^q-P$_{trc}$ promoter inducible with IPTG together with *Halomonas* porin gene RBS (ribosome binding site) into pSEVA341 polylinker. The new vector was used for the overexpression of the threonine synthesis pathway (*thrACB*) and threonine dehydrogenase gene (*ilvA*) which enabled PHBHV copolymer production solely from glucose or other unrelated carbon sources (glycerol, sucrose, maltose, fructose) without the need for co-feeding with costly and toxic propionic acid.

Subsequently, also the chromosomal expression of exogenous genes was tested and *Halomonas* operon outer membrane porin gene expressed from strong constitutive P$_{porin}$ promoter was used as a hot spot. Yin *et al.* employed the I-*Sce*I-based system for the insertion of *phaC* gene from *C. necator* downstream the porin gene in the *H. bluephagenesis* Δ*phaC* mutant (Yin et al., 2014). They demonstrated that *phaC$_{Cn}$* expression
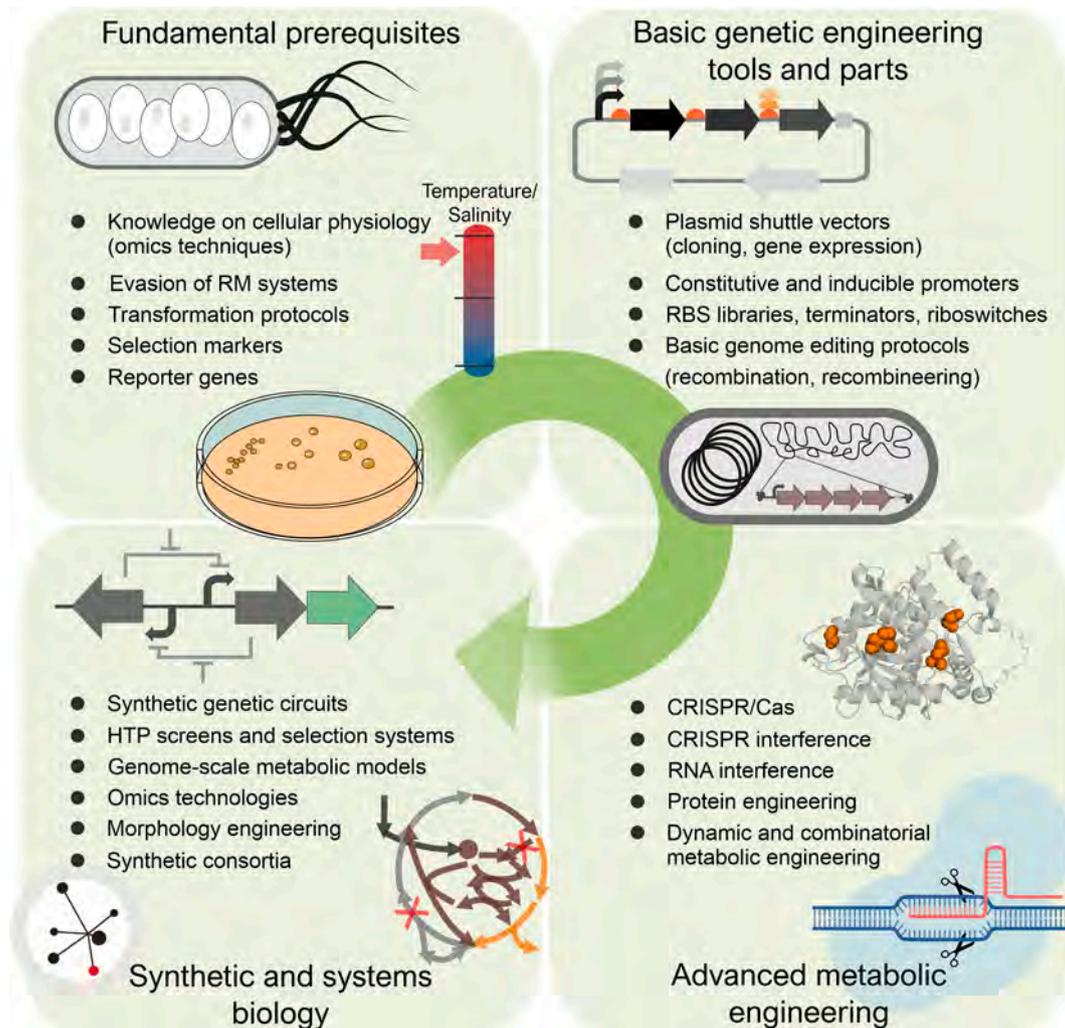
Fig. 3. Tools and approaches of modern microbial bioengineering disciplines that can be adopted to domesticate and upgrade environmental halophilic and thermophilic PHA producers. The figure outlines the roadmap towards the preparation of next-generation bacterial catalysts for biotechnological manufacturing of PHA. Abbreviations: RM systems, restriction-modification systems; RBS, ribosome binding site; CRISPR, clustered regularly interspaced short palindromic repeats; Cas, CRISPR-associated protein; HTP screens, high-throughput screens.

from this spot, in contrast to expression from several different chromosomal loci, fully compensated deletion of native *phaC* and enabled levels of PHB in *H. bluephagenesis* mutant very similar to the wild-type strain. The verified P*porin* was later characterized and randomized using degenerate oligos to give rise to the promoter library with over 300-fold variation in transcriptional activity (Li et al., 2016b). In general, constitutive promoters can be instrumental for stable robust expression of target genes especially in long-term large-scale cultivations under non-sterile conditions in which the addition of costly, sometimes even harmful chemical inducers is not practical (Dvorak et al., 2015). This was demonstrated by adopting broad-host-range hybrid promoter P*tac* for chromosomal expression of the *orfZ* gene of 4-hydroxybutyrate-CoA transferase from *Clostridium kluyveri* in TD01 strain. The mutant strain could for the first time synthesize the attractive elastic poly(3-hydroxybutyrate-*co*-4-hydroxybutyrate) [poly(3HB-*co*-4HB)] copolymer with a 4HB content of up to 16 mol.-% from glucose and γ-butyrolactone in a 48 h-lasting fed-batch cultivation in a 1000-L pilot fermentor under non-sterile conditions (Chen et al., 2017). The suboptimal productivity of the mutant (1.04 g/(L•h)) was surpassed by 53% in the follow-up work in which the authors placed the *orfZ* gene downstream the mutant variant of P*porin* promoter integrated into the genome of recombinant *H. bluephagenesis*; here a volumetric productivity for poly(3HB-*co*-11%-4HB) of 1.59 g/(L•h) was obtained (Shen et al., 2018).

Tightly regulated inducible promoters, on the other hand, are required especially for advanced ME and SB applications in the design of synthetic genetic circuits or for the precise control of expression of key enzymes in a metabolic network. Li *et al.* adopted the *E. coli lac* repressor operator system to construct an inducible expression machinery suitable for *H. bluephagenesis* (Li et al., 2016b). The *lacI* repressor gene was inserted downstream the porin ORF, while the *lacO* operator sequence was placed downstream the −10 element of P*porin* cloned into pBBR1-MCS1 or pSEVA341 bearing *phaCAB*$_{Cn}$ operon or only *phaC*$_{Cn}$ gene from *C. necator*, respectively (Yin et al., 2014; Li et al., 2016b). The controllability of the expression from the resulting plasmids was demonstrated by the PHB content in *Halomonas* cells, which could be tuned by the varying concentration of synthetic IPTG inducer in the culture medium.

The spectrum of inducible expression systems available for *Halomonas* spp. was substantially expanded by Zhao *et al.* in 2017. As the attempts to adopt the paradigmatic T7 system in *H. bluephagenesis* failed, the authors decided to mine novel T7-like expression machineries using BLAST searches in NCBI genome database and PHIRE (PHage In silico REgulatory elements) software package (Lavigne et al., 2004). Three new T7-like RNA polymerase-promoter pairs named MmP1, VP4, and K1F were described and studied in more detail. RNA polymerase modules were integrated into the chromosome, while the respective promoters were cloned into the pSEVA321 plasmid backbone bearing the GFP reporter gene. All three systems displayed broad-host-range functionality (proven in *E. coli*, *Halomonas* TD01, and *Pseudomonas entomophila*), orthogonality, and tight regulation (>3000-fold induction range depending on IPTG concentration). *Halomonas* TD01 with *phaCAB* operon expressed from MmP1 system embedded in chromosome produced by 38% more PHB than the wild-type control (69 g/L vs. 50 g/L) and broke the actual record of PHB content in dry *Halomonas* cells (92 wt.-%).

Besides transcription, the translation level is vital for balancing gene expression in native and synthetic operons encoding the key metabolic pathways for PHA formation. In combinatorial ME, these two levels are often varied simultaneously by combining pathway modules expressed from two or more plasmids, promoters, and RBS sites with different characteristics and searching for the optimum in the possible solution space (Ajikumar et al., 2010; Jeschek et al., 2017; Kurumbang et al., 2014). Ren et al. (2018) optimized the expression of *phaCAB*$_{Cn}$ operon in *H. bluephagenesis* by combining two mutated variants of P*porin* promoter with two synthetic RBS sites from the previously prepared library (Li

et al., 2016a). Synthetic RBS sites were used for *phaA* and *phaB* genes, while *phaC* retained the native RBS. The combination of individual elements gave rise to four *phaCAB* operon variants that were expressed from pSEVA331 plasmid backbone. The PHB content determined in the cells with the best operon variant was 12.3% higher than in the parental strain without the optimized *phaCAB* cassette.

4.1.2. Adoption of CRISPR/Cas technology in ME of halophiles

The new era of extremophile engineering started with the onset of CRISPR/Cas genome editing technology, which was readily adopted by the *Halomonas* community. Qin et al. (2018) designed and tested for the first time an editing system based on (i) the *Streptococcus pyogenes cas9* gene placed on low-copy plasmid pSEVA321 and (ii) sgRNA (single-guide RNA) cloned together with donor DNA for homology-directed repair into the high-copy pSEVA241 with CAS constitutive promoter of *cas9* gene. This setup enabled up to 80% efficiency of *phaC* gene disruption in the genome of TD01 strain. The slightly modified system was adopted also for genomic insertions of more than 4 kb-long ORFs. The authors used the new technology for the study of glucose metabolism in *Halomonas* and identified the Entner-Doudoroff pathway as a major route for glucose catabolism in strain TD01. The efficiency of the prepared deletions of glycolysis genes ranged from 12.5 to 100%. Importantly, developed CRISPR/Cas9 system with minor modifications was shown functional also for *H. campaniensis* LS21. As a real quantum leap, this work reduced the time needed for genome editing of *Halomonas* from months to weeks. Ling and others (2018) took the advantage of the new rapid genome-editing technique and intended to enhance PHB production in *H. bluephagenesis* by engineering its redox metabolism (Ling et al., 2018a). They identified that *H. bluephagenesis* naturally generates more biomass and PHA under oxygen-limiting conditions and revealed that acetoacetyl-CoA reductase PhaB is NADH-dependent. Extraordinary high NADH/NAD$^+$ ratio (1.5) and surplus NADH generated in metabolism of glucose-grown TD01 strain was beneficial for PhaB function but could inhibit pyruvate dehydrogenase in parallel. The authors used acetate in cell culture as a redox regulator to remove the inhibition and provide more acetyl-CoA for PHB synthesis under oxygen limitation. Additional disruption of the NADH utilization pathway – the NADH-dependent respiratory chain – by deleting the b subunit of electron transfer flavoprotein ETF using CRISPR/Cas9 system enabled a remarkable accumulation of PHB in mutant cells (94 wt.-%) on 30 g/L glucose and 3 g/L acetate without affecting growth. In another study, Chen and colleagues (Chen et al., 2019) achieved to obtain 65% PHBHV in CDM of glucose and gluconate-grown *H. bluephagenesis*. The PHBHV contained 25 mol.-% 3HV, which was the highest reported 3HV content in *Halomonas* cells with chromosomally encoded PHBHV pathway. Complex changes in the best production strain were conducted using CRISPR/Cas9. The genetic modifications together with added gluconate co-substrate enhanced the activity of TCA cycle and enabled a high 3 HV ratio in PHBHV copolyester. Moreover, the previously prepared P*porin* promoter library (Shen et al., 2018) found its use in this study for finetuning the expression of an exogenous operon from *E. coli*. A new genome-editing technique was also utilized for the construction of a *H. bluephagenesis* strain capable of producing functional scl- and mcl-PHA *co*-polymers containing unsaturated bonds (Yu et al., 2020). A heterologous biosynthetic pathway from *Aeromonas hydrophila* consisting of PHA synthase PhaC and enoyl-CoA-hydratase PhaJ for polymerization of 3HB and the mcl-PHA monomers 3-hydroxyhexanoate (3HHx; saturated monomer) or 3-hydroxy-5-hexenoate (3HHxE; unsaturated) into repsective co-polymers was introduced into *H. bluephagenesis* Δ*phaC* with overexpressed endogenous acyl-CoA synthetase (FadD). Optimization of promoter and RBS in introduced expression cassette, together with the finetuning of cell redox state and fed-batch cultivation strategy, resulted in the synthesis of functional PHA with unprecedented attractive properties that have never been produced by *Halomonas* before.

In contrast to null mutations, CRISPR interference (CRISPRi) enables

tunable downregulation of target genes on the translation level. The CRISPRi plasmid for halophilic PHA-producing bacteria was constructed by Tao and co-workers (Tao et al., 2017). The pli-dCas9-sgRNA bearing the dead Cas9 gene and the sgRNAs cassette expressed from IPTG-inducible Ptrc promoter was prepared using the previously published CRISPRi plasmid plv-dCas9-sgRNA for *E. coli* (Lv et al., 2015) and pSEVA321 backbone. The sgRNA cassette was designed using the recognition sites for isocaudomers and Biobricks standards, thus, several sgRNAs could be integrated into a single plasmid and target multiple genes in parallel. The system functioning in *H. bluephagenesis* was demonstrated on the partial repression of *prpC* and *gltA* (citrate synthase) genes which allowed flexible regulation of 3HV fraction in PHBHV copolymer and re-routing acetyl-CoA from TCA cycle to PHB synthesis, respectively.

4.1.3. Advanced metabolic flux fine-tuning in halophiles for higher product yields

Modern ME is based on much more than just knockouts and knockins of genes in a target host organism. Development of high-performance strains for NGIB requires knowledge-driven tuning of intracellular carbon fluxes, which should prevent system perturbations and suboptimal product yields caused by disorganized expression of exogenous operons and possible accumulation of toxic pathway intermediates. At this point, synthetic and systems biology come to the scene. Synthetic genetic circuits for tightly regulated gene expression, multi-omics analyses, high-throughput screens, and mathematical modeling of metabolic networks form an inseparable part of state-of-the-art ME approaches (Choi et al., 2019; Dvořák et al., 2017). This trend must be, of course, reflected also in the engineering of extremophilic PHA producers and although there is some debt in adopting synthetic and systems biology, first attempts have indeed emerged in the last couple of years.

In this context, Ma *et al.* aimed to manipulate *H. bluephagenesis* to become a suitable chassis for the co-production of PHA with another valuable chemical ectoine – above-mentioned compatible solute for hypersalinity resistance which has potential applications in cosmetics and medicine (Ma et al., 2020).

They combined three metabolic modules comprised of *de novo* ectoine pathway (endogenous *etcABC* gene cluster) with endogenous L-aspartate-semialdehyde-dehydrogenase (Asd) and aspartokinase (LysC) from *Corynebacterium glutamicum* that were overexpressed from the chromosome of *H. bluephagenesis* lacking competing pathways to channel more flux to ectoine synthesis. Importantly, two orthogonal inducible types of machinery based on LuxR/AHL (N-acyl homoserine lactone) and T7-like MmP1 systems, embedded in *Halomonas* chromosome and in low-copy pSEVA321 plasmid, were designed and used for GFP reporter-mediated transcriptional fine-tuning (Ye et al., 2020) of the three ectoine synthesis modules. Once the optimal transcriptional level for each of the three modules was identified with the help of the plasmid-based system, the P*porin* promoter library was searched to provide similar optimal ectoine titer with the expression of *etcABC*, *asd*, and *lysC* from the chromosome. The resulting *H. bluephagenesis* strain produced 32 g/L CDM with 75 wt.-% PHB and 8 g/L ectoine after 44 h cultivation on glucose and urea (low-cost nitrogen source for ectoine synthesis) under open unsterile conditions in a 7 L fermentor. The recent work of Jiang and colleagues (Jiang et al., 2021) is a notable example of a study in which omics techniques play an important role. The authors focused on the production of industrially valuable platform chemical 3-hydroxypropionic acid (3HP) and its copolymer with 3HB, poly(3-hydroxybutyrate-*co*-3-hydroxypropionate), in *H. bluephagenesis* from glucose and 1,3-propanediol. Extraordinary high titer of 3HP in final fed-batch culture (154 g/L) would not be possible without utilizing transcriptomics for the identification of a competitive 3HP-degradation pathway and endogenous 1,3-propanediol dehydrogenase, which enabled the efficient conversion of 1,3-propanediol to 3HP. The complete 3HP biosynthesis route comprising three metabolic modules with genes from four microorganisms was optimized using combinatorial ME

and promoter, RBS, and gene order adjustments.

The development of mathematical modeling towards optimization of PHA production, in general, has been reviewed by Novak *et al.* in 2015. They suggest that a compromise solution can be achieved with hybrid modeling approaches that combine existing high-level (low-structured) kinetic models with fluid dynamics and neural networks. To understand and synthesize optimal PHA pathways dynamics, low-level (highly structured) models have to be developed (Novak et al., 2015). In the context of halophiles, Cui *et al.* have proposed a high-level differential model targeting PHA production in *H. mediterranei* under different temperatures suggesting that high temperatures may provide a good strategy for improving the PHA productivity (Cui et al., 2017b). To bring the utility of such models to fine-tuning of PHA production in halophiles, a complete genome-scale reconstruction of the organism's metabolic network yet needs to be built to form a fundamental base for kinetic optimizations.

4.2. Expanding the substrate scope of halophiles for cost-effective PHA production

A significant portion (dozens of %) of the PHA production cost in both conventional and non-conventional hosts can be attributed to the substrate price (Braunegg et al., 2004; Dietrich et al., 2019; Lettner et al., 2017). PHA-related carbon sources (pure fatty acids, oils) or pure glucose have been frequently used in research studies coping with microbial PHA production. However, sustainable NGIB require cheap and abundant next-generation substrates. Glycerol from biodiesel production, waste organic polymers (lignocellulosic residues, kitchen waste, waste petroplastics), and C1 substrates (syngas, CO_2, CH_4) represent extremely attractive carbon sources for future biotechnological production of bulk chemicals including PHA and other biopolymers (Dietrich et al., 2019; Tiso et al., 2021; Weiss et al., 2017). Xylose and arabinose-rich hemicellulose fraction and lignin aromatics from lignocellulose waste processing have become the targets of intense research in the last years (Dietrich et al., 2019; Salvachúa et al., 2020). Some extremophilic bacteria including *H. halophila* or *S. thermodepolymerans* have the natural ability to grow and produce PHA on xylose or arabinose, but especially the former species is quite sensitive to the inhibitory effects of aromatic chemicals in lignocellulosic hydrolysates (Kucera et al., 2018; Kourilova et al., 2020). Metabolic engineers should therefore aim at improving the robustness of these organisms and at enhancing PHA yields and productivities on pentoses, but, to the best of our knowledge, such studies are not yet available.

The first attempt to convert organic polymeric feedstock directly to PHA using an engineered extremophilic bacterium has just recently been reported. Lin et al. (2021) modified *H. bluephagenesis* for growth and PHB production on starch. Codon-optimized α-amylase gene from *Bacillus licheniformis* and endogenous amyloglucosidase gene with a pre-selected Sec-secretion signal sequence were inserted into the chromosome of *Halomonas* and in a plasmid, respectively, and expressed from optimal constitutive P*porin* and inducible P*Mmp1* promoter variants. Well secreted enzymes hydrolyzed commercial insoluble corn starch to monomeric glucose. The thus designed recombinant *Halomonas* grew on 30 g/L starch in shake flasks to 9.5 g/L CDM containing 51.5 wt.-% PHB. These values are lower than those achieved on pure glucose, but future advances in engineering recombinant protein secretion in halophiles can push these limits and maybe even direct the authors towards second-generation polymeric feedstocks such as lignocellulosic residues.

All previously discussed halophilic and thermophilic heterotrophs cannot naturally utilize C1 substrates such as CO_2 or CH_4 for PHA synthesis. The engineering of efficient CO_2 fixation in heterotrophs is very challenging and is currently restricted to mesophilic model microorganisms (Gassler et al., 2020; Gleizer et al., 2019). This barrier can be nonetheless bypassed by a smart combination of PHA-producing extremophile with a suitable autotroph in a rationally designed synthetic consortium. An interesting example of such an approach is the work of

Weiss and co-workers (2017) in which an engineered cyanobacterium *Synechococcus elongatus* with implanted sucrose permease was co-cultured with PHB-forming *H. boliviensis*. The cyanobacterium autotrophically fixed CO_2 and generated sucrose, the major portion of it (up to 85%) was secreted into the bulk medium where it served as a heterotrophic carbon source for *Halomonas*. *H. boliviensis* was selected as a partner for *Synechococcus* in synthetic co-culture because it has low nutritional demands and grows well in the cyanobacterial minimal medium. *Synechococcus* cells were physically separated from *Halomonas* by encapsulation into alginate beads. This step improved co-culture stability, facilitated the selective recovery of PHB-producing *Halomonas* cells, and, quite unexpectedly, doubled sucrose secretion by the cyanobacterium. The co-culture was maintained stable and productive without any selection agents for remarkable five months. The PHB content in *Halomonas* biomass reached 37 wt.-%. It is not very surprising that the PHB productivity was low (peaked at 28.3 mg/(L•d)). However, it should be stressed that this value is equal or even higher than productivities achieved in monocultures of cyanobacteria engineered for autotrophic PHA production from CO_2 (Wang et al., 2013). This consortium approach thus represents an interesting alternative to single strain engineering in future research.

4.3. Engineering Halomonas for facilitated downstream processing of PHA

Another costly part of industrial PHA production includes downstream processes such as separation and disruption of cells and product purification (Wang et al., 2019). Conventional physical, physicochemical, or biological techniques used for this purpose are often expensive (centrifugation), time-consuming (gravity sedimentation of cells, enzymatic treatments), or harsh to the environment (acidic or alkaline treatments, application of solvents for product recovery) and their efficiency in terms of recovery yield and product purity can be limited. Genetic engineering and SB provide complementary or entirely alternative solutions for downstream processing of intracellular products including PHA. Some of them have already been tried in *Halomonas*. For instance, morphology engineering has the potential to kill two birds with one stone and produce more PHA in enlarged bacteria that settle faster in the medium than standard-shaped cells. The size of the *H. bluephagenesis* cells was expanded by blocking the cell division through inhibition of Z ring formation. This was achieved by inhibiting the polymerization of tubulin-like protein FtsZ (Tan et al., 2014; Zhao et al., 2017), which is necessary for binary fission of bacteria, or by the direct deletion of *ftsZ* gene (Jiang et al., 2017a). Proteins MinC and MinD belong among inhibitors of FtsZ polymerization. IPTG-induced expression of *minCD* from pSEVA341 plasmid resulted in 1.4-fold longer *H. bluephagenesis* cells (1.84 μm on average) when compared with uninduced control, and 19% higher PHB content in cells (Tan et al., 2014). Interestingly, expression of *minCD* genes from novel T7-like expression systems MmP1 in *H. bluephagenesis* chromosome gave rise to cells with a much higher average length of 102 μm (Zhao et al., 2017). Unfortunately, the effect of morphology engineering on PHB content and yield was not quantified in the latter study.

The drawback of the interventions in bacterial morphology is reduced cell growth and consequently lower PHA titer. Jiang and co-workers (2017a) developed a plasmid-based system for temperature-inducible morphology changes in *H. campaniensis* LS21. The strain with *ftsZ* deletion and temperature-sensitive plasmid pTKmf bearing constitutively expressed *ftsZ* gene was initially grown as usual at 30 °C for 12 h and then the morphology change was induced by removing the plasmid with the temperature raised to 37 °C for the rest of the culture. Both biomass and PHB content in cells was increased more than 1.3-fold when compared with the wild-type strain to 16 g/L CDM and 78 wt.-% PHB, respectively. The inhibition of FtsZ described previously (Zhao et al., 2017) also improved cell biomass separation by gravity sedimentation, but the reported 12 h time interval required to fully separate

the cells would probably not meet the needs of the industrial process. Therefore, it might be beneficial to promote self-flocculation of engineered PHA-producing cells which would accelerate their sedimentation. This was achieved for *H. campaniensis* LS21 (not yet for *H. bluephagenesis*) by increasing the hydrophobicity of cells through the deletion of electron transferring flavoprotein (*etf* operon) (Ling et al., 2018b). The mutant cells prepared by homologous recombination-based technique had reduced surface charge and could sediment rapidly within less than 1 min after stopping the agitation in the bioreactor.

Genetic engineering-based solutions are being developed also for facilitated PHA recovery from collected biomass of halophilic bacteria. The size of PHA granules in bacterial cells is typically around hundreds of nm in diameter (Anderson and Dawes, 1990). PHA recovery processes can benefit from bigger granules that would enable faster separation from aqueous suspensions obtained after chemical or biological treatment of collected cells. Shen and co-workers engineered a *H. bluephagenesis* strain which generated PHB granules of the unique and unprecedented size of up to 10 μm (Shen et al., 2019). The enlarged granules were observed only in filamentous recombinants that combined the deletion of phasin gene *phaP1* with overexpressed *minCD*. Deletion of *phaP1* alone did not result in enlarged PHB particles. The study thus identified that the size of PHB granules in *H. bluephagenesis* is primarily controlled by the cell size. Larger PHB granules were observed also in outer membrane-defective *H. bluephagenesis* mutants (Wang et al., 2021) prepared by deleting the genes *waaC* and *lpxL* whose products take part in lipopolysaccharide synthesis. The *lpxL* gene lacking mutant also showed improved secretion of the low molecular compound ectoine. Secretion of bigger molecules such as recombinant proteins was regrettably not tested. Recently, improved secretion and surface attachment of recombinant proteins including artificial adhesins or cellulosomal binding domains was reported for surface-shaved *P. putida* KT2440 mutant with removed lipopolysaccharide layer (Dvořák et al., 2020a; Fraile et al., 2021). One can envision that enhanced secretion of proteins in more permeable engineered PHA producers, including *Halomonas* spp. and other extremophilic candidates for NGIB, will further support the attempts to develop cost-effective downstream processes via facilitated self-flocculation or selective adhesion of cells (Fraile et al., 2021; Ling et al., 2018b), controlled cellular autolysis for intracellular product release (Borrero-de Acuña et al., 2017), or direct secretion of PHA granules out of the bacterium (Rahman et al., 2013).

4.4. The perspective of the development of genetic engineering tools for thermophilic PHA producers

In contrast to the world of halophiles, the bioengineering of PHA-producing thermophilic microorganisms is practically a non-existent field at the moment. Nevertheless, considering the great potential of this group of extremophiles, the emergence of ME and SB tools for it is just a matter of time. Researchers can find inspiration in the *Halomonas* story described above as well as in the toolkit already available for numerous biotechnologically relevant thermophilic microorganisms that do not form PHA granules but can synthesize other attractive chemicals at elevated temperatures. These include extreme thermophiles from the genera *Thermus*, *Thermococcus*, *Pyrococcus*, or *Caldicellulosiruptor* and moderate thermophiles such as *Geobacillus* spp., certain species from the *Bacillaceae* family, or *Clostridium thermocellum* (Drejer et al., 2018; Kananavičiūtė and Čitavičius, 2015; Lee et al., 2020; Mazzoli and Olson, 2020; Zeldes et al., 2015). The latter Gram-positive cellulolytic bacterium with a temperature optimum of around 60 °C is attracting lots of attention of bioengineers for its use in consolidated bioprocessing and its example could be instrumental for future engineering of thermophilic PHA producers (Mazzoli and Olson, 2020). It is, however, necessary to realize the specifics of individual species as well as the specifics of thermophilic bacteria in general. However, the devil is in the details, and these can make the engineering of particular species extremely challenging. Fortunately, massive advancements in omics

technologies and data analysis achieved during the last two decades substantially reduced the time needed to understand the fundamental physiology of newly isolated strains and made the selection of the best candidates for the process of microbial domestication the matter of rational knowledge-based choice rather than a fully empirical exercise (Fig. 3). Genomic sequences (available for most bacteria listed in Table 2), single-molecule real-time sequencing, and methylome analyses can help to reveal the host's restriction-modification (RM) systems. RM systems digest foreign DNA with a methylation pattern that differs from the host's one. Hence, their removal or evasion is a key prerequisite for genetic engineering attempts (Riley and Guss, 2021; Riley et al., 2019). They were identified in almost 90% of all known prokaryotic genomes including genomes of thermophiles (Vasu and Nagaraja, 2013). The RM systems of the target host can be either deleted (if functional genome editing machinery for a given host is already available) or evaded by the use of plasmid propagated in engineered E. coli strain with implanted restriction-associated methyltransferases that secure a methylation pattern acceptable for the target host (Riley et al., 2019).

Mitigation of unwanted restriction enables the next step - recombinant DNA transfer into the host cell. Both native and exogenous plasmids can be employed for genetic engineering purposes. Unfortunately, very little is known about endogenous plasmids in thermophilic PHA producers and, to the best of our knowledge, no molecules utilizable in ME have been identified yet. There is plenty of space for further research in this area. Meanwhile, popular broad-host-range plasmids such as pBC1 (medium-to-high copy replicon for G+ hosts), pBBR1 (medium-to-high copy replicon G- hosts) and pRK2 (low-copy replicon G- hosts), or SEVA vectors bearing pBBR1, RK2, or pBC1 origins of replication and suitable selection markers can be tested as backbones for heterologous gene expression in PHA-forming thermophiles (De Rossi et al., 1991; Drejer et al., 2018; Silva-Rocha et al., 2013). Available plasmids for thermophilic Bacilli and Geobacilli have been recently summarized in reviews of Drejer et al. (2018) and Kananavičiūtė and Čitavičius (2015) respectively. These shuttle vectors that are convenient for work in E. coli and target thermophiles often contain two replicons and two markers because equal functionality of the same component in two hosts with different temperature optima is rare. Thermophiles certainly have specific demands for selection markers. Only a few antibiotics (e.g., kanamycin, bleomycin, hygromycin, chloramphenicol, or simvastatin) are applicable for longer time intervals at temperatures above 50 °C (Zeldes et al., 2015). Also, the stability of products of resistance-conferring genes must be considered. Mutant variants of kanamycin resistance marker with improved thermal stability at temperatures as high as 70 °C were prepared by directed evolution (Hoseki et al., 1999). Nutritional selection (such as uracil or tryptophan prototrophy) is a possible alternative to the use of antibiotics in thermophile cultures, but this approach requires construction or selection of auxotrophic strain deficient in an essential nutrient gene (Tripathi et al., 2010; Tripathi et al., 2010). Concerning DNA transfer techniques, electroporation of circular plasmids or simple mixing of naturally competent cells with target linear or circular DNA are favorable for thermophilic bacteria (Olson and Lynd, 2012). Protoplast transformation and conjugation with E. coli were reported for thermophilic Geobacilli (Kananavičiūtė and Čitavičius, 2015).

Advanced genetic modifications in thermophilic PHA producers will require the establishment of a reliable gene expression toolbox including standardized constitutive and inducible promoters, terminators, libraries of RBS, and thermostable reporters. RBS sites, terminators, and constitutive promoters of essential genes can be relatively easily mined from thermophile genomes with the help of diverse available software packages or using RNAseq of cells grown under specific conditions (Drejer et al., 2018; Olson et al., 2015). Adopting well-characterized constitutive and inducible promoters from models in non-model microorganisms can be a challenge (Zeldes et al., 2015; Zhao et al., 2017). Instead, researchers may develop inducible expression types of machinery that would respond to the drop of temperature or to (non)native substrate molecules (Mearls et al., 2015; Williams-Rhaesa et al., 2018;

Zheng et al., 2019). Attractive alternatives for tunable gene expression in thermophiles are ligand-dependent mRNA leader sequences known as „riboswitches". Some natural and synthetic thermostable riboswitches have been recently proven well functional for gene up- and down-regulation in Geobacillus thermoglucosidasius and C. thermocellum at 55 °C (Marcano-Velazquez et al., 2019). Reliable molecular reporters for thermophiles are rare but they can be prepared by stabilization of mesophilic molecules via mutagenesis. New superfolder GFP variants with almost 900-fold enhanced fluorescence at temperatures as high as 60 °C were recently prepared by random mutagenesis coupled to fluorescence-activated cell sorting (Frenzel et al., 2018).

Reported genome editing techniques for thermophiles are mostly based on homologous recombination (Drejer et al., 2018; Zeldes et al., 2015). One of the first gene deletion protocols for C. thermocellum took advantage of (i) prepared ΔpyrF (orotidine 5′-phosphate decarboxylase) auxotrophic strain, (ii) a replicating plasmid with a sequence homologous to upstream and downstream regions (usually 500–1000 bp long) of the target gene in the chromosome, and (iii) pyrF gene used as a dual selection marker (Tripathi et al., 2010). Recombination-mediated genetic engineering methods („recombineering") can increase the efficiency of homologous recombination even with homologous sequences as short as 30 bp (Muyrers, 1999). However, the popular Red complex from bacteriophage l (including Exo, Beta, and Gam recombination proteins) which is used for recombineering in E. coli often does not function in non-model bacteria. Thermostable homologs to l Red proteins Exo/Beta were recently isolated from Acidithiobacillus caldus (Walker et al., 2020). These new recombinases helped to improve the performance of CRISPR/Cas genome editing systems for C. thermocellum firstly described in the same study. Endogenous Type I–B CRISPR system from C. thermocellum and exogenous Type II CRISPR system from Geobacillus stearothermophilus combined with thermophilic Cas9 variant from G. stearothermophilus and stable recombinases enabled 70% and 94% genome editing efficiency, respectively. The two-step CRISPR/Cas-recombineering method reduced the time needed for genome editing in C. thermocellum from four to two weeks. Geobacillus thermodenitrificans T12 became a source of another thermophilic Cas9 nuclease whose engineered inactive variant was employed for CRISPRi (CRISPR interference) gene silencing in Bacillus smithii and C. thermocellum (Ganguly et al., 2019; Mougiakos et al., 2017). These and other successful examples of efficient genome editing in thermophilic bacteria hold promise for accelerated development of new advanced ME and SB tools for thermophiles in near future. The vast experience collected during the last two decades for organisms such as C. thermocellum will help to reduce the time needed for genetic domestication of thermophilic PHA producers in the following years.

5. Conclusions/outlook

The development of sustainable and feasible biotechnological production of PHA is a holy grail of industrial biotechnology. Reaching this goal would decrease our dependency on non-renewable resources and reduce the amount of polymer-based resistant solid waste, which is currently generated in colossal amounts by modern civilization. The extremophile-based concept of Next-Generation Industrial Biotechnology holds a promise to provide the foundation for such processes since it principally enhances robustness and reduces costs of the biotechnological process. This work demonstrated that there are numerous promising PHA producers among halophiles and thermophiles. The biotechnological production of PHA employing H. bluephagenesis has already reached initial industrial scale, other microorganisms such as Haloferax mediterranei, H. halophila or S. thermodepolymerans can be also considered being strong candidates for industrial production of PHA; nevertheless, processes that utilize these microorganisms have not reached high technology readiness levels so far. Therefore, further research and development are needed in this field. Table 3 summarizes the most important advantages associated

Table 3
Comparison of the most important features associated with PHA production employing halophiles and thermophiles as compared to mesophiles.

	Mesophiles	Halophiles	Thermophiles
Range of utilizable substrates	High	High	Moderate
Robustness of the process against contamination	Low	High	High
Influence of cultivation conditions on the solubility of substrates	None	None	Positive
Influence of cultivation conditions on the solubility of oxygen	None	Negative	Negative
Rate of the metabolic processes	Normal - depending upon the employed culture	Normal - depending upon the employed culture	High
Energy demands related to the sterility of the process	High	Low	Low
Energy demands related to cultivation	Standard	Standard	Questionable
Down-stream processing	Standard	Hypotonic lysis of the cells can be employed	Standard
Availability of the tools for synthetic biology and metabolic engineering for improved PHA production	High	Medium	Low

with the employment of halophiles and thermophiles for PHA production as compared to mesophilic bacteria.

Furthermore, extremophiles can be considered not only as biotechnological chassis for direct PHA production but also very interesting sources of genes and enzymes for both *in-vivo* and *in-vitro* PHA synthesis as was demonstrated for PHA synthases from thermophilic bacteria revealing superior stability and activity (Tajima et al., 2016). Further, PHA synthases present especially in thermophilic bacteria reveal extraordinary substrate specificity resulting in the formation of co-polymers with unique monomer compositions and, therefore, also interesting mechanical and technological properties (Choonut et al., 2020b; Pantazaki et al., 2003; Sedlacek et al., 2020; Xi et al., 2016).

The biotechnological potential of extremophiles for commercial PHA production can be further enhanced by employing approaches of metabolic engineering. Despite substantial progress during the last decade, metabolic engineering and synthetic biology of halophilic PHA producers is still in its adolescence, or childhood when other species than *H. bluephagenesis* are considered. Bioengineering of PHA-forming thermophiles was not yet born, but this review clearly demonstrates that the new baby is awaited with great expectations. We summarized here the milestones that the genetic engineering-driven domestication of attractive thermophilic PHA producers must pass to get at least on the level achieved with halophiles: starting from the identification and evasion of restriction-modification systems, through the development or collection of basic genetic engineering tools and components, to the adoption of advanced metabolic engineering techniques and protocols (Fig. 3). The most recent trends in the engineering of industrially relevant microorganisms highlight interdisciplinary approaches that combine protein engineering and metabolic engineering with synthetic and systems biology for the knowledge-driven design and construction of high-performance strains (Choi et al., 2019; Dvořák et al., 2017). If the field of the bioengineering of extremophilic PHA producers aims to reach its full maturity, it should soon go in the same direction. Mutant variants of halophilic and thermophilic PhaC and other key enzymes in

PHA biosynthesis machinery should be prepared and tested for altered activity, specificity, stability, or selectivity that can have an immense effect on the quantity and quality of the product (Zheng et al., 2020). Available genomic sequences and other omics data should be applied for the preparation of high-resolution genome-scale metabolic models that will enable theoretical and experimental flux analyses and targeted re-direction of carbon fluxes in the cells. The obtained strains can be further finetuned by adaptive laboratory evolution combined with high-throughput screening or selection protocols based on the synthetic genetic circuits implanted in the evolved cells.

One more prerequisite and challenge for the bloom of bioengineering of extremophilic PHA producers is the popularization of bioplastics made in genetically modified organisms (GMOs). Some companies, especially in Europe, still refuse to release on the market biopolymers made in genetically modified organisms due to the alleged negative public perception of GMOs. It is quite a paradoxical position in the world in which, for instance, hundreds of millions of people with *diabetes mellitus* are cured with recombinant insulin produced in *E. coli* and *Saccharomyces cerevisiae* cell factories (Baeshen et al., 2014). We believe that the pros of the above-mentioned genetic engineering-based technologies for the biomanufacturing of PHA by far outweigh the potential risks linked to the use of GMOs in closed fermentation systems. It is thus important that the interested researchers dedicate part of their time to the activities that improve public awareness of GMOs and their benefits for NGIB.

Funding

Declaration of Competing Interest

The authors declare that they have no known competing financial interests or personal relationships that could have appeared to influence the work reported in this paper.

References

Ajikumar, P., Xiao, W., Tyo, K., Wang, Y., Simeon, F., Leonard, E., Mucha, O., Phon, T., Pfeifer, B., Stephanopoulos, G., 2010. Isoprenoid pathway optimization for taxol precursor overproduction in Escherichia coli. Science 330, 70–74. https://doi.org/10.1126/science.1191652.

Ali, I., Jamil, N., 2016. Polyhydroxyalkanoates: current applications in the medical field. Front. Biol. 11, 19–27. https://doi.org/10.1007/s11515-016-1389-z.

Alsafadi, D., Al-Mashaqbeh, O., 2017. A one-stage cultivation process for the production of poly-3-(hydroxybutyrate-co-hydroxyvalerate) from olive mill wastewater by Haloferax mediterranei. New Biotechnol. 34, 47–53. https://doi.org/10.1016/j.nbt.2016.05.003.

Alves, L., Plucani do Amaral, F., Kim, D., Todo Bom, M., Piñero Gavídia, M., Silvano Teixeira, C., Holthman, F., de Oliveira Pedrosa, F., Maltempi de Souza, E., Chubatsu, L., Müller-Santos, M., Stacey, G., Müller, V., 2019. Importance of poly-3-hydroxybutyrate metabolism to the ability of Herbaspirillum seropedicae to promote plant growth. Appl. Environ. Microbiol. 85 https://doi.org/10.1128/AEM.02586-18.

Alves, L., Santana-Filho, A., Sassaki, G., de Oliveira Pedrosa, F., Maltempi de Souza, E., Chubatsu, L., Müller-Santos, M., Stabb, E., 2020. 3-hydroxybutyrate derived from poly-3-hydroxybutyrate mobilization alleviates protein aggregation in heat-stressed Herbaspirillum seropedicae SmR1. Appl. Environ. Microbiol. 86 https://doi.org/10.1128/AEM.01265-20.

Amstutz, V., Zinn, M., 2020. Syngas as a sustainable carbon source for PHA production. In: The Handbook of Polyhydroxyalkanoates. CRC Press, Boca Raton, pp. 377–416.

Anderson, A., Dawes, E., 1990. Occurrence, metabolism, metabolic role, and industrial uses of bacterial polyhydroxyalkanoates. Microbiol. Rev. 54, 450–472. https://doi.org/10.1128/mr.54.4.450-472.1990.

Argandoña, M., Vargas, C., Reina-Bueno, M., Rodríguez-Moya, J., Salvador, M., Nieto, J., 2012. An extended suite of genetic tools for use in bacteria of the halomonadaceae: an overview. In: Lorence, A. (Ed.), Recombinant Gene Expression, Methods in Molecular Biology. Humana Press, Totowa, NJ, pp. 167–201. https://doi.org/10.1007/978-1-61779-433-9_9.

Baeshen, N., Baeshen, M., Sheikh, A., Bora, R., Ahmed, M., Ramadan, H., Saini, K., Redwan, E., 2014. Cell factories for insulin production. Microbial Cell Factor. 13 https://doi.org/10.1186/s12934-014-0141-0.

Baliga, N.S., Bonneau, R., Facciotti, M.T., Pan, M., Glusman, G., Deutsch, E.W., Shannon, P., Chiu, Y., Weng, R.S., Gan, R.R., Hung, P., Date, S.V., Marcotte, E.,

Ng, W.V., 2004. Genome sequence of Haloarcula marismortui: a halophilic archaeon from the Dead Sea. [published correction appears in Genome Res. 2004 Dec;14(12): 2510]. Genome Res. 14, 2221–2234. https://doi.org/10.1101/gr.2700304.

Batista, M., Teixeira, C., Sfeir, M., Alves, L., Valdameri, G., Pedrosa, F., Sassaki, G., Steffens, M., de Souza, E., Dixon, R., Müller-Santos, M., 2018. PHB Biosynthesis Counteracts Redox Stress in Herbaspirillum seropedicae. Front. Microbiol. 9 https://doi.org/10.3389/fmicb.2018.00472.

Bhattacharyya, A., Saha, J., Haldar, S., Bhowmic, A., Mukhopadhyay, U., Mukherjee, J., 2014. Production of poly-3-(hydroxybutyrate-co-hydroxyvalerate) by Haloferax mediterranei using rice-based ethanol stillage with simultaneous recovery and re-use of medium salts. Extremophiles 18, 463–470. https://doi.org/10.1007/s00792-013-0622-9.

Bioplastics market data, 2020. EuropeanBioplastics. https://www.european-bioplastics.org/market/ (accessed 8.20.2021).

Bolhuis, H., Palm, P., Wende, A., Falb, M., Rampp, M., Rodriguez-Valera, F., Pfeiffer, F., Oesterhelt, D., 2006. The genome of the square archaeon Haloquadratum walsbyi: life at the limits of water activity. BMC Genomics 7, 1–12. https://doi.org/10.1186/1471-2164-7-169.

Bonete, M., Pire, C., Llorca, F., Camacho, M., 1996. Glucose dehydrogenase from the halophilic Archaeon Haloferax mediterranei: enzyme purification, characterisation and N-terminal sequence. FEBS Lett. 383, 227–229. https://doi.org/10.1016/0014-5793(96)00235-9.

Borrero-de Acuña, J., Hidalgo-Dumont, C., Pacheco, N., Cabrera, A., Poblete-Castro, I., 2017. A novel programmable lysozyme-based lysis system in Pseudomonas putida for biopolymer production. Sci. Rep. 7, 4373. https://doi.org/10.1038/s41598-017-04741-2.

Braunegg, G., Bona, R., Koller, M., 2004. Sustainable polymer production. Polym.-Plast. Technol. Eng. 43, 1779–1793. https://doi.org/10.1081/PPT-200040130.

Britton, K., Baker, P., Fisher, M., Ruzheinikov, S., Gilmour, D., Bonete, M., Ferrer, J., Pire, C., Esclapez, J., Rice, D., 2006. Analysis of protein solvent interactions in glucose dehydrogenase from the extreme halophile Haloferax mediterranei. Proc. Natl. Acad. Sci. 103, 4846–4851. https://doi.org/10.1073/pnas.0508854103.

Budde, C., Riedel, S., Willis, L., Rha, C., Sinskey, A., 2011. Production of poly(3-hydroxybutyrate- co −3-hydroxyhexanoate) from plant oil by engineered ralstonia eutropha strains. Appl. Environ. Microbiol. 77, 2847–2854. https://doi.org/10.1128/AEM.02429-10.

Castro, J., Nouioui, I., Asenjo, J., Andrews, B., Bull, A., Goodfellow, M., 2019. New genus-specific primers for PCR identification of Rubrobacter strains. Antonie Van Leeuwenhoek 112, 1863–1874. https://doi.org/10.1007/s10482-019-01314-3.

Chen, G.-Q., 2009. A microbial polyhydroxyalkanoates (PHA) based bio- and materials industry. Chem. Soc. Rev. 38, 2434–2446. https://doi.org/10.1039/b812677c.

Chen, G.-Q., 2010. Introduction of bacterial plastics PHA, PLA, PBS, PE, PTT, and PPP. In: Plastics From Bacteria: Natural Functions And Applications. Springer, Berlin, Heidelberg, pp. 1–16.

Chen, G., Jiang, X., 2018. Next generation industrial biotechnology based on extremophilic bacteria. Curr. Opin. Biotechnol. 50, 94–100. https://doi.org/10.1016/j.copbio.2017.11.016.

Chen, C., Don, T., Yen, H., 2006a. Enzymatic extruded starch as a carbon source for the production of poly(3-hydroxybutyrate-co-3-hydroxyvalerate) by Haloferax mediterranei. Process Biochem. 41, 2289–2296. https://doi.org/10.1016/j.procbio.2006.05.026.

Chen, C., Chou, Y., Chen, W., Arun, B., Young, C., 2006b. Tepidimonas taiwanensis sp. nov., a novel alkaline-protease-producing bacterium isolated from a hot spring. Extremophiles 10, 35–40. https://doi.org/10.1007/s00792-005-0469-9.

Chen, C., Hsu, S., Lin, M., Hsu, Y., 2015. Mass production of C50 carotenoids by Haloferax mediterranei in using extruded rice bran and starch under optimal conductivity of brined medium. Bioprocess Biosyst. Eng. 38, 2361–2367. https://doi.org/10.1007/s00449-015-1471-y.

Chen, X., Yin, J., Ye, J., Zhang, H., Che, X., Ma, Y., Li, M., Wu, L., Chen, G., 2017. Engineering Halomonas bluephagenesis TD01 for non-sterile production of poly(3-hydroxybutyrate-co-4-hydroxybutyrate). Bioresour. Technol. 244, 534–541. https://doi.org/10.1016/j.biortech.2017.07.149.

Chen, Y., Chen, X., Du, H., Zhang, X., Ma, Y., Chen, J., Ye, J., Jiang, X., Chen, G., 2019. Chromosome engineering of the TCA cycle in Halomonas bluephagenesis for production of copolymers of 3-hydroxybutyrate and 3-hydroxyvalerate (PHBHV). Metab. Eng. 54, 69–82. https://doi.org/10.1016/j.ymben.2019.03.006.

Choi, J., Lee, S., Han, K., 1998. Cloning of the Alcaligenes latus polyhydroxyalkanoate biosynthesis genes and use of these genes for enhanced production of poly(3-hydroxybutyrate) in Escherichia coli. Appl. Environ. Microbiol. 64, 4897–4903. https://doi.org/10.1128/AEM.64.12.4897-4903.1998.

Choi, K., Jang, W., Yang, D., Cho, J., Park, D., Lee, S., 2019. Systems metabolic engineering strategies: integrating systems and synthetic biology with metabolic engineering. Trends Biotechnol. 37, 817–837. https://doi.org/10.1016/j.tibtech.2019.01.003.

Choonut, A., Prasertsan, P., Klomklao, S., Sangkharak, K., 2020a. Bacillus thermoamylovorans-related strain isolated from high temperature sites as potential producers of medium-chain-length polyhydroxyalkanoate (mcl-PHA). Curr. Microbiol. 77, 3044–3056. https://doi.org/10.1007/s00284-020-02118-9.

Choonut, A., Prasertsan, P., Klomklao, S., Sangkharak, K., 2020b. Study on mcl-PHA production by novel thermotolerant gram-positive isolate. J. Polym. Environ. 28, 2410–2421. https://doi.org/10.1007/s10924-020-01779-8.

Chou, Y., Sheu, S., Sheu, D., Wang, J., Chen, W., 2006. Schlegelella aquatica sp. nov., a novel thermophilic bacterium isolated from a hot spring. Int. J. Syst. Evol. Microbiol. 56, 2793–2797. https://doi.org/10.1099/ijs.0.64446-0.

Cristea, A., Floare, C., Borodi, G., Leopold, N., Kasco, I., Cadar, O., Banciu, H., 2017. Physical and chemical detection of polyhydroxybutyrate from Halomonas Elongata strain 2FFF. New front. Chem 26. S4_OP3.

Crosby, J., Laemthong, T., Lewis, A., Straub, C., Adams, M., Kelly, R., 2019. Extreme thermophiles as emerging metabolic engineering platforms. Curr. Opin. Biotechnol. 59, 55–64. https://doi.org/10.1016/j.copbio.2019.02.006.

Cui, B., Huang, S., Xu, F., Zhang, R., Zhang, Y., 2015. Improved productivity of poly (3-hydroxybutyrate) (PHB) in thermophilic Chelatococcus daeguensis TAD1 using glycerol as the growth substrate in a fed-batch culture. Appl. Microbiol. Biotechnol. 99, 6009–6019. https://doi.org/10.1007/s00253-015-6489-1.

Cui, Y.W., Gong, X., Shi, Y., Wang, Z., 2017a. Salinity effect on production of PHA and EPS by Haloferax mediterranei. RSC Adv. 7, 53587–53595. https://doi.org/10.1039/C7RA09652F.

Cui, Y.-W., Zhang, H.-Y., Ji, J., S.-Y., Wang, Z.-W., 2017b. Kinetic analysis of the temperature effect on polyhydroxyalkanoate production by haloferax mediterranei in synthetic molasses wastewater. J. Polym. Environ. 25, 277–285. https://doi.org/10.1007/s10924-016-0807-2.

Cummings, S., Gilmour, D., 1995. The effect of NaCl on the growth of a Halomonas species: accumulation and utilization of compatible solutes. Microbiology 141, 1413–1418. https://doi.org/10.1099/13500872-141-6-1413.

Danson, M., Hough, D., 1998. Structure, function and stability of enzymes from the Archaea. Trends Microbiol. 6, 307–314. https://doi.org/10.1016/S0966-842X(98)01316-X.

Das, P., Behera, B., Meena, D., Azmi, S., Chatterjee, S., Meena, K., Sharma, A., 2015. Salt stress tolerant genes in halophilic and halotolerant bacteria: paradigm for salt stress adaptation and osmoprotection. Int. J. Curr. Microbiol. App. Sci. 4, 642–658.

de Almeida, A., Catone, M., Rhodius, V., Gross, C., Pettinari, M., 2011. Unexpected stress-reducing effect of PhaP, a Poly(3-Hydroxybutyrate) granule-associated protein, in Escherichia coli. Appl. Environ. Microbiol. 77, 6622–6629. https://doi.org/10.1128/AEM.05469-11.

De Rossi, E., Brigidi, P., Rossi, M., Matteuzzi, D., Riccardi, G., 1991. Characterization of Gram-positive broad host-range plasmids carrying a thermophilic replicon. Res. Microbiol. 142, 389–396. https://doi.org/10.1016/0923-2508(91)90108-M.

Denner, E., Kolari, M., Hoornstra, D., Tsitko, I., Kämpfer, P., Busse, H., Salkinoja-Salonen, M., 2006. Rubellimicrobium thermophilum gen. nov., sp. nov., a red-pigmented, moderately thermophilic bacterium isolated from coloured slime deposits in paper machines. Int. J. Syst. Evol. Microbiol. 56, 1355–1362. https://doi.org/10.1099/ijs.0.63751-0.

Deole, R., Hoff, W., 2020. A potassium chloride to glycine betaine osmoprotectant switch in the extreme halophile Halorhodospira halophila. Sci. Rep. 10, 1–10. https://doi.org/10.1038/s41598-020-59231-9.

Di Caprio, F., 2021. Cultivation processes to select microorganisms with high accumulation ability. Biotechnol. Adv. 49 https://doi.org/10.1016/j.biotechadv.2021.107740.

Di Donato, P., Fiorentino, G., Anzelmo, G., Tommonaro, G., Nicolaus, B., Poli, A., 2011. Re-use of vegetable wastes as cheap substrates for extremophile biomass production. Waste Biomass Valorization 2, 103–111. https://doi.org/10.1007/s12649-011-9062-x.

Dietrich, K., Dumont, M., Del Rio, L., Orsat, V., 2019. Sustainable PHA production in integrated lignocellulose biorefineries. New Biotechnol. 49, 161–168. https://doi.org/10.1016/j.nbt.2018.11.004.

Dinnbier, U., Limpinsel, E., Schmid, R., Bakker, E., 1988. Transient accumulation of potassium glutamate and its replacement by trehalose during adaptation of growing cells of Escherichia coli K-12 to elevated sodium chloride concentrations. Arch. Microbiol. 150, 348–357. https://doi.org/10.1007/BF00408306.

Drejer, E., Hakvåg, S., Irla, M., Brautaset, T., 2018. Genetic tools and techniques for recombinant expression in Thermophilic Bacillaceae. Microorganisms 6, 42. https://doi.org/10.3390/microorganisms6020042.

D'Souza, S., Altekar, W., D'Souza, S., 1997. Adaptive response of *Haloferax mediterranei* to low concentrations of NaCl (20%) in the growth medium. Arch. Microbiol. 168, 68–71. https://doi.org/10.1007/s002030050471.

Dvorak, P., Chrast, L., Nikel, P., Fedr, R., Soucek, K., Sedlackova, M., Chaloupkova, R., de Lorenzo, V., Prokop, Z., Damborsky, J., 2015. Exacerbation of substrate toxicity by IPTG in Escherichia coli BL21(DE3) carrying a synthetic metabolic pathway. Microb. Cell Factories 14. https://doi.org/10.1186/s12934-015-0393-3.

Dvořák, P., Nikel, P., Damborský, J., de Lorenzo, V., 2017. Bioremediation 3. 0: Engineering pollutant-removing bacteria in the times of systemic biology. Biotechnol. Adv. 35, 845–866. https://doi.org/10.1016/j.biotechadv.2017.08.001.

Dvořák, P., Bayer, E., de Lorenzo, V., 2020a. Surface display of designer protein scaffolds on genome-reduced strains of Pseudomonas putida. ACS Synth. Biol. 9, 2749–2764. https://doi.org/10.1021/acssynbio.0c00276.

Dvořák, P., Kováč, J., Lorenzo, V., 2020b. Biotransformation of d -xylose to d -xylonate coupled to medium-chain-length polyhydroxyalkanoate production in cellobiose-grown Pseudomonas putida EM42. Microb. Biotechnol. 13, 1273–1283. https://doi.org/10.1111/1751-7915.13574.

Elbanna, K., Lütke-Eversloh, T., Van Trappen, S., Mergaert, J., Swings, J., Steinbüchel, A., 2003. Schlegelella thermodepolymerans gen. nov., sp. nov., a novel thermophilic bacterium that degrades poly(3-hydroxybutyrate-co-3-mercaptopropionate). Int. J. Syst. Evol. Microbiol. 53, 1165–1168. https://doi.org/10.1099/ijs.0.02562-0.

Elbanna, K., Lütke-Eversloh, T., Jendrossek, D., Luftmann, H., Steinbüchel, A., 2004. Studies on the biodegradability of polythioester copolymers and homopolymers by polyhydroxyalkanoate (PHA)-degrading bacteria and PHA depolymerases. Arch. Microbiol. 182, 212–225. https://doi.org/10.1007/s00203-004-0715-z.

El-malek, F., Farag, A., Omar, S., Khairy, H., 2020. Polyhydroxyalkanoates (PHA) from Halomonas pacifica ASL10 and Halomonas salifodiane ASL11 isolated from Mariout

salt lakes. Int. J. Biol. Macromol. 161, 1318–1328. https://doi.org/10.1016/j.ijbiomac.2020.07.258.

Fang, C., Ku, K., Lee, M., Su, N., 2010. Influence of nutritive factors on C50 carotenoids production by Haloferax mediterranei ATCC 33500 with two-stage cultivation. Bioresour. Technol. 101, 6487–6493. https://doi.org/10.1016/j.biortech.2010.03.044.

Fathima, S.N., Krishnaswamy, V., Shen, N., 2017. Isolation and screening of phb producing halotolerant bacterial strains from a saline environment. J. Biotechnol. Biomed. Sci. 1, 34–45. https://doi.org/10.14302/issn.2576-6694.jbbs-17-1783.

Fraile, S., Briones, M., Revenga-Parra, M., de Lorenzo, V., Lorenzo, E., Martínez-García, J., 2021. Engineering tropism of pseudomonas putida toward target surfaces through ectopic display of recombinant nanobodies. ACS Synth. Biol. 10, 2049–2059. https://doi.org/10.1021/acssynbio.1c00227.

Frenzel, E., Legebeke, J., van Stralen, A., van Kranenburg, R., Kuipers, O., 2018. In vivo selection of sfGFP variants with improved and reliable functionality in industrially important thermophilic bacteria. Biotechnol. Biofuels 11. https://doi.org/10.1186/s13068-017-1008-5.

Fu, X., Tan, D., Aibaidula, G., Wu, Q., Chen, J., Chen, G., 2014. Development of Halomonas TD01 as a host for open production of chemicals. Metab. Eng. 23, 78–91. https://doi.org/10.1016/j.ymben.2014.02.006.

Ganguly, J., Martin-Pascual, M., Kranenburg, R., 2019. CRISPR interference (CRISPRi) as transcriptional repression tool for Hungateiclostridium thermocellum DSM 1313. Microb. Biotechnol. 13, 339–349. https://doi.org/10.1111/1751-7915.13516.

Gassler, T., Sauer, M., Gasser, B., Egermeier, M., Troyer, C., Causon, T., Hann, S., Mattanovich, D., Steiger, M., 2020. The industrial yeast Pichia pastoris is converted from a heterotroph into an autotroph capable of growth on CO2. Nat. Biotechnol. 38, 210–216. https://doi.org/10.1038/s41587-019-0363-0.

Gedikli, S., Çelik, P., Demirbilek, M., Mutlu, M., Denkbaş, E., Çabuk, A., 2019. Experimental exploration of thermostable poly (β-Hydroxybutyrates) by Geobacillus kaustophilus using Box-Behnken design. J. Polym. Environ. 27, 245–255. https://doi.org/10.1007/s10924-018-1335-z.

Giani, M., Martínez-Espinosa, R., 2020. Carotenoids as a protection mechanism against oxidative stress in haloferax mediterranei. Antioxidants 9, 1060. https://doi.org/10.3390/antiox9111060.

Giani, M., Garbayo, I., Vílchez, C., Martínez-Espinosa, R., 2019. Haloarchaeal carotenoids: healthy novel compounds from extreme environments. Marine Drugs 17, 524. https://doi.org/10.3390/md17090524.

Ginzburg, M., Sachs, L., Ginzburg, B., 1970. Ion metabolism in a Halobacterium. J. Gen. Physiol. 55, 187–207. https://doi.org/10.1085/jgp.55.2.187.

Gleizer, S., Ben-Nissan, R., Bar-On, Y., Antonovsky, N., Noor, E., Zohar, Y., Jona, G., Krieger, E., Shamshoum, M., Bar-Even, A., Milo, A., 2019. Conversion of Escherichia coli to generate all biomass carbon from CO2. Cell 179. https://doi.org/10.1016/j.cell.2019.11.009, 1255-1263.e12.

Gonçalves, P., Hume, C., Ferreira, A., Tsui, S., Brocchi, M., Wren, B., Araujo, W., 2019. Environmental interactions are regulated by temperature in Burkholderia seminalis TC3.4.2R3. Sci. Rep. 9 https://doi.org/10.1038/s41598-019-41778-x.

Grillo, R., do Pereira, A.E.S., de Melo, N.F.S., Porto, R.M., Feitosa, L.O., Tonello, P.S., Filho, N.L.D., Rosa, A.H., Lima, R., Fraceto, L.F., 2011. Controlled release system for ametryn using polymer microspheres: preparation, characterization and release kinetics in water. J. Hazard. Mater. 186, 1645–1651. https://doi.org/10.1016/j.jhazmat.2010.12.044.

Guzmán, H., Van-Thuoc, D., Martín, J., Hatti-Kaul, R., Quillaguamán, J., 2009. A process for the production of ectoine and poly(3-hydroxybutyrate) by Halomonas boliviensis. Appl. Microbiol. Biotechnol. 84, 1069–1077. https://doi.org/10.1007/s00253-009-2036-2.

Han, J., Hou, J., Zhang, F., Ai, G., Li, M., Cai, S., Liu, H., Wang, L., Wang, Z., Zhang, S., Cai, L., Zhao, D., Zhou, J., Xiang, H., 2013. Multiple propionyl coenzyme A-supplying pathways for production of the bioplastic poly(3-hydroxybutyrate- co −3-hydroxyvalerate) in Haloferax mediterranei. Appl. Environ. Microbiol. 79, 2922–2931. https://doi.org/10.1128/AEM.03915-12.

Haque, R., Paradisi, F., Allers, T., 2020. Haloferax volcanii for biotechnology applications: challenges, current state and perspectives. Appl. Microbiol. Biotechnol. 104, 1371–1382. https://doi.org/10.1007/s00253-019-10314-2.

Hermann-Krauss, C., Koller, M., Muhr, A., Fasl, H., Stelzer, F., Braunegg, G., 2013. Archaeal production of polyhydroxyalkanoate (PHA) co- and terpolyesters from biodiesel industry-derived by-products. Archaea 2013, 1–10. https://doi.org/10.1155/2013/129268.

Hezayen, F., Rehm, B., Eberhardt, R., Steinbüchel, A., 2000. Polymer production by two newly isolated extremely halophilic archaea: application of a novel corrosion-resistant bioreactor. Appl. Microbiol. Biotechnol. 54, 319–325. https://doi.org/10.1007/s002530000394.

Hickey, D., Singer, G., 2004. Genomic and proteomic adaptations to growth at high temperature. Genome Biol. 5, 117. https://doi.org/10.1186/gb-2004-5-10-117.

Hong, J., Song, H., Moon, Y., Hong, Y., Bhatia, S., Jung, H., Choi, T., Yang, S., Park, H., Choi, Y., Yang, Y., 2019. Polyhydroxybutyrate production in halophilic marine bacteria Vibrio proteolyticus isolated from the Korean peninsula. Bioprocess Biosyst. Eng. 42, 603–610. https://doi.org/10.1007/s00449-018-02066-6.

Hoseki, J., Yano, T., Koyama, Y., Kuramitsu, S., Kagamiyama, H., 1999. Directed evolution of thermostable kanamycin-resistance gene: a convenient selection marker for Thermus thermophilus. J. Biochem. 126, 951–956. https://doi.org/10.1093/oxfordjournals.jbchem.a022539.

Hsiao, L., Lin, J., Sankatumvong, P., Wu, T., Li, S., 2016. The feasibility of thermophilic caldimonas manganoxidans as a platform for efficient PHB production. Appl. Biochem. Biotechnol. 180, 852–871. https://doi.org/10.1007/s12010-016-2138-0.

Hsiao, L., Lee, M., Chuang, P., Kuo, Y., Lin, J., Wu, T., Li, S., 2018. The production of poly (3-hydroxybutyrate) by thermophilic Caldimonas manganoxidans from glycerol. J. Polym. Res. 25, 85. https://doi.org/10.1007/s10965-018-1486-6.

Hussein, A., Lisowska, B., Leak, D., 2015. The genus geobacillus and their biotechnological potential. Adv. Appl. Microbiol. 94, 1–48. https://doi.org/10.1016/bs.aambs.2015.03.001.

Ibrahim, M., Steinbüchel, A., 2010. High-cell-density cyclic fed-batch fermentation of a poly(3-hydroxybutyrate)-accumulating thermophile, Chelatococcus sp. Strain MW10. Appl. Environ. Microbiol. 76, 7890–7895. https://doi.org/10.1128/AEM.01488-10.

Ibrahim, M., Willems, A., Steinbüchel, A., 2010. Isolation and characterization of new poly(3HB)-accumulating star-shaped cell-aggregates-forming thermophilic bacteria. J. Appl. Microbiol. 5 https://doi.org/10.1111/j.1365-2672.2010.04786.x no-no.

Ibrahim, M., Lebbe, L., Willems, A., Steinbüchel, A., 2016. Chelatococcus thermostellatus sp. nov., a new thermophile for bioplastic synthesis: comparative phylogenetic and physiological study. AMB Express 6, 39. https://doi.org/10.1186/s13568-016-0209-9.

Israni, N., Shivakumar, S., 2019. Polyhydroxyalkanoates in Packaging, in: Biotechnological Applications Of Polyhydroxyalkanoates. Springer Singapore, Singapore, pp. 363–388. https://doi.org/10.1007/978-981-13-3759-8_14.

Jau, M., Yew, S., Toh, P., Chong, A., Chu, W., Phang, S., Najimudin, N., Sudesh, K., 2005. Biosynthesis and mobilization of poly(3-hydroxybutyrate) [P(3HB)] by Spirulina platensis. Int. J. Biol. Macromol. 36, 144–151. https://doi.org/10.1016/j.ijbiomac.2005.05.002.

Jendrossek, D., 2009. Polyhydroxyalkanoate granules are complex subcellular organelles (carbonosomes). J. Bacteriol. 191, 3195–3202. https://doi.org/10.1128/JB.01723-08.

Jeschek, M., Gerngross, D., Panke, S., 2017. Combinatorial pathway optimization for streamlined metabolic engineering. Curr. Opin. Biotechnol. 47, 142–151. https://doi.org/10.1016/j.copbio.2017.06.014.

Jiang, X., Yao, Z., Chen, G., 2017a. Controlling cell volume for efficient PHB production by Halomonas. Metab. Eng. 44, 30–37. https://doi.org/10.1016/j.ymben.2017.09.004.

Jiang, Y., Xin, F., Lu, J., Dong, W., Zhang, W., Zhang, M., Wu, H., Ma, J., Jiang, M., 2017b. State of the art review of biofuels production from lignocellulose by thermophilic bacteria. Bioresour. Technol. 245, 1498–1506. https://doi.org/10.1016/j.biortech.2017.05.142.

Jiang, X., Yan, X., Yu, L., Liu, X., Chen, G., 2021. Hyperproduction of 3-hydroxypropionate by Halomonas bluephagenesis. Nat. Commun. 12 https://doi.org/10.1038/s41467-021-21632-3.

Kananavičiūtė, R., Čitavičius, D., 2015. Genetic engineering of Geobacillus spp. J. Microbiol. Methods 111, 31–39. https://doi.org/10.1016/j.mimet.2015.02.002.

Kaur, R., Tiwari, S., 2021. Purification and characterization of a new halocin HA4 from Haloferax larsenii HA4 isolated from a Salt Lake. Probiot. Antimicrob. Proteins 1-9. https://doi.org/10.1007/s12602-021-09823-2.

Kennedy, S., Ng, W., Salzberg, S., Hood, L., DasSarma, S., 2001. Understanding the adaptation of halobacterium species NRC-1 to its extreme environment through computational analysis of its genome sequence. Genome Res. 11, 1641–1650. https://doi.org/10.1101/gr.190201.

Khan, I., Habib, N., Asem, M., Salam, N., Xiao, M., Zhou, E., Zhi, X., Li, W., 2019. Aquabacterium tepidiphilum sp. nov., a moderately thermophilic bacterium isolated from a hot spring. Int. J. Syst. Evol. Microbiol. 69, 337–342. https://doi.org/10.1099/ijsem.0.003103.

Kim, J., Won, Y., Nikoh, N., Nakayama, H., Han, S., Kikuchi, Y., Rhee, Y., Park, H., Kwon, J., Kurokawa, K., Dohmae, N., Fukatsu, T., Lee, B., 2013. Polyester synthesis genes associated with stress resistance are involved in an insect-bacterium symbiosis. Proc. Natl. Acad. Sci. 110, E2381–E2389. https://doi.org/10.1073/pnas.1303228110.

Koller, M., 2015. Recycling of waste streams of the biotechnological poly (hydroxyalkanoate) production by Haloferax mediterranei on Whey. Int. J. Polym. Sci. 2015, 1–8. https://doi.org/10.1155/2015/370164.

Koller, M., 2017. Production of polyhydroxyalkanoate (PHA) biopolyesters by extremophiles. MOJ Polym. Sci. 1 https://doi.org/10.15406/mojps.2017.01.00011.

Koller, M., 2019a. Linking food industry to "green plastics" – polyhydroxyalkanoate (PHA) biopolyesters from agro-industrial by-products for securing food safety. Appl. Food Biotechnol. 6, 1–6. https://doi.org/10.22037/afb.v6i1.17979.

Koller, M., 2019b. Polyhydroxyalkanoate biosynthesis at the edge of water activity-haloarchaea as biopolyester factories. Bioengineering 6, 34. https://doi.org/10.3390/bioengineering6020034.

Koller, M., 2020. Established and advanced approaches for recovery of microbial polyhydroxyalkanoate (PHA) biopolyesters from surrounding microbial biomass. EuroBiotech J. 4, 113–126. https://doi.org/10.2478/ebtj-2020-0013.

Koller, M., Hesse, P., Bona, R., Kutschera, C., Atlić, A., Braunegg, G., 2007a. Biosynthesis of high quality polyhydroxyalkanoate co- and terpolyesters for potential medical application by the ArchaeonHaloferax mediterranei. Macromol. Symp. 253, 33–39. https://doi.org/10.1002/masy.200750704.

Koller, M., Hesse, P., Bona, R., Kutschera, C., Atlić, A., Braunegg, G., 2007b. Potential of various archae- and eubacterial strains as industrial polyhydroxyalkanoate producers from whey. Macromol. Biosci. 7, 218–226. https://doi.org/10.1002/mabi.200600211.

Koller, M., Sandholzer, D., Salerno, A., Braunegg, G., Narodoslawsky, M., 2013. Biopolymer from industrial residues: Life cycle assessment of poly (hydroxyalkanoates) from whey. Resour. Conserv. Recycl 73, 64–71. https://doi.org/10.1016/j.resconrec.2013.01.017.

Koller, M., Chiellini, E., Braunegg, G., 2015. Study on the production and re-use of poly (3-hydroxybutyrate-co-3- hydroxyvalerate) and extracellular polysaccharide by the

archaeon haloferax mediterranei strain DSM 1411. Chem. Biochem. Eng. Q. 29, 87–98. https://doi.org/10.15255/CABEQ.2014.2058.

Koller, M., Maršálek, L., de Sousa Dias, M., Braunegg, G., 2017. Producing microbial polyhydroxyalkanoate (PHA) biopolyesters in a sustainable manner. New Biotechnol. 37, 24–38. https://doi.org/10.1016/j.nbt.2016.05.001.

Koller, M., Braunegg, Obruca, S., 2020. Linking salinity to microbial biopolyesters biosynthesis: polyhydroxyalkanoate production by Haloarchaea and Halophilic Eubacteria. In: Koller, M. (Ed.), The Handbook of Polyhydroxyalkanoates. Vol. 2: Kinetics, Bioengineering, and Industrial Aspects. CRC Press, Boca Raton, pp. 185–212.

Koskimäki, J., Kajula, M., Hokkanen, J., Ihantola, E., Kim, J., Hautajärvi, H., Hankala, E., Suokas, M., Pohjanen, J., Podolich, O., Kozyrovska, N., Turpeinen, A., Pääkkönen, M., Mattila, S., Campbell, B., Pirttilä, A., 2016. Methyl-esterified 3-hydroxybutyrate oligomers protect bacteria from hydroxyl radicals. Nat. Chem. Biol. 12, 332–338. https://doi.org/10.1038/nchembio.2043.

Kourilova, X., Pernicova, I., Sedlar, K., Musilova, J., Sedlacek, P., Kalina, M., Koller, M., Obruca, S., 2020. Production of polyhydroxyalkanoates (PHA) by a thermophilic strain of Schlegelella thermodepolymerans from xylose rich substrates. Bioresour. Technol. 315, 123885. https://doi.org/10.1016/j.biortech.2020.123885.

Kourilova, X., Novackova, I., Koller, M., Obruca, S., 2021a. Evaluation of mesophilic Burkholderia sacchari, thermophilic Schlegelella thermodepolymerans and halophilic Halomonas halophila for polyhydroxyalkanoates production on model media mimicking lignocellulose hydrolysates. Bioresour. Technol. 325, 124704. https://doi.org/10.1016/j.biortech.2021.124704.

Kourilova, X., Schwarzerova, J., Pernicova, I., Sedlar, K., Mrazova, K., Krzyzanek, V., Nebesarova, J., Obruca, S., 2021b. The first insight into polyhydroxyalkanoates accumulation in multi-extremophilic Rubrobacter xylanophilus and Rubrobacter spartanus. Microorganisms 9, 909. https://doi.org/10.3390/microorganisms9050909.

Kourilova, X., Pernicova, I., Vidlakova, M., Krejcirik, R., Mrazova, K., Hrubanova, K., Krzyzanek, V., Nebesarova, J., Obruca, S., 2021c. Biotechnological conversion of grape pomace to poly(3-hydroxybutyrate) by moderately thermophilic bacterium Tepidimonas taiwanensis. Bioengineering 8, 141. https://doi.org/10.3390/bioengineering8100141.

Kourmentza, C., Plácido, J., Venetsaneas, N., Burniol-Figols, A., Varrone, C., Gavala, H., Reis, M., 2017. Recent advances and challenges towards sustainable polyhydroxyalkanoate (PHA) production. Bioengineering 4. https://doi.org/10.3390/bioengineering4020055.

Kourmentza, K., Kachrimanidou, V., Psaki, O., Pateraki, C., Ladakis, D., Koutinas, A., 2020. Competitive advantage and market introduction of PHA polymers and potential use of PHA monomers. In: The Handbook Of Polyhydroxyalkanoates. CRC Press, Boca Raton, pp. 167–202.

Krüger, A., Schäfers, C., Schröder, C., Antranikian, G., 2018. Towards a sustainable biobased industry – highlighting the impact of extremophiles. New Biotechnol. 40, 144–153. https://doi.org/10.1016/j.nbt.2017.05.002.

Kucera, D., Pernicová, I., Kovalcik, A., Koller, M., Mullerova, L., Sedlacek, P., Mravec, F., Nebesarova, J., Kalina, M., Marova, I., Krzyzanek, V., Obruca, S., 2018. Characterization of the promising poly(3-hydroxybutyrate) producing halophilic bacterium Halomonas halophila. Bioresour. Technol. 256, 552–556. https://doi.org/10.1016/j.biortech.2018.02.062.

Kumar, S., Stecher, G., Li, M., Knyaz, C., Tamura, K., Battistuzzi, F., 2018. MEGA X: molecular evolutionary genetics analysis across computing platforms. Mol. Biol. Evol. 35, 1547–1549. https://doi.org/10.1093/molbev/msy096.

Kumar, V., Kumar, S., Singh, D., 2020. Microbial polyhydroxyalkanoates from extreme niches: Bioprospection status, opportunities and challenges. Int. J. Biol. Macromol. 147, 1255–1267. https://doi.org/10.1016/j.ijbiomac.2019.09.253.

Kurumbang, N., Dvorak, P., Bendl, J., Brezovsky, J., Prokop, Z., Damborsky, J., 2014. Computer-assisted engineering of the synthetic pathway for biodegradation of a toxic persistent pollutant. ACS Synth. Biol. 3, 172–181. https://doi.org/10.1021/sb400147n.

Lakshmanan, M., Foong, C.P., Abe, H., Sudesh, K., 2019. Biosynthesis and characterization of co and ter-polyesters of polyhydroxyalkanoates containing high monomeric fractions of 4-hydroxybutyrate and 5-hydroxyvalerate via a novel PHA synthase. Polym. Degrad. Stab. 163, 122–135. https://doi.org/10.1016/j.polymdegradstab. 2019.03.005.

Lavigne, R., Sun, W., Volckaert, G., 2004. PHIRE, a deterministic approach to reveal regulatory elements in bacteriophage genomes. Bioinformatics 20, 629–635. https://doi.org/10.1093/bioinformatics/btg456.

Lee, L., Crosby, J., Rubinstein, G., Laemthong, T., Bing, R., Straub, C., Adams, M., Kelly, R., 2020. The biology and biotechnology of the genus Caldicellulosiruptor: recent developments in 'Caldi World'. Extremophiles 24, 1–15. https://doi.org/10.1007/s00792-019-01116-5.

Lemoigne, M., 1926. Produits de déshydration et de polymérisation de l'acide β-oxobutyrique. BULLETIN DE LA SOCIETÉ DE CHIMIE BIOLOGIQUE 8, 770–782.

Lettner, M., Schöggl, J., Stern, T., 2017. Factors influencing the market diffusion of bio-based plastics: Results of four comparative scenario analyses. J. Clean. Prod. 157, 289–298. https://doi.org/10.1016/j.jclepro.2017.04.077.

Li, T., Ye, J., Shen, R., Zong, Y., Zhao, X., Lou, C., Chen, G., 2016a. Semirational approach for ultrahigh poly(3-hydroxybutyrate) accumulation in Escherichia coli by combining one-step library construction and high-throughput screening. ACS Synth. Biol. 5, 1308–1317. https://doi.org/10.1021/acssynbio.6b00083.

Li, T., Li, T., Ji, W., Wang, Q., Zhang, H., Chen, G., Lou, C., Ouyang, Q., 2016b. Engineering of core promoter regions enables the construction of constitutive and inducible promoters in Halomonas sp. Biotechnol. J. 11, 219–227. https://doi.org/10.1002/biot.201400828.

Lin, Y., Guan, Y., Dong, X., Ma, Y., Wang, X., Leng, Y., Wu, F., Ye, J., Chen, G., 2021. Engineering Halomonas bluephagenesis as a chassis for bioproduction from starch. Metab. Eng. 64, 134–145. https://doi.org/10.1016/j.ymben.2021.01.014.

Ling, C., Qiao, G., Shuai, B., Olavarria, K., Yin, J., Xiang, R., Song, K., Shen, Y., Guo, Y., Chen, G., 2018a. Engineering NADH/NAD+ ratio in Halomonas bluephagenesis for enhanced production of polyhydroxyalkanoates (PHA). Metab. Eng. 49, 275–286. https://doi.org/10.1016/j.ymben.2018.09.007.

Ling, C., Qiao, G., Shuai, B., Song, K., Yao, W., Jiang, X., Chen, G., 2018b. Engineering self-flocculating halomonas campaniensis for wastewaterless open and continuous fermentation. Biotechnol. Bioeng. https://doi.org/10.1002/bit.26897.

Lippert, K., Galinski, E., Trüper, H., 1993. Biosynthesis and function of trehalose inEctothiorhodospira halochloris. Antonie Van Leeuwenhoek 63, 85–91. https://doi.org/10.1007/BF00871735.

Liu, C., Wang, X., Yang, H., Liu, C., Zhang, Z., Chen, G., 2021. Biodegradable polyhydroxyalkanoates production from wheat straw by recombinant Halomonas elongata A1. Int. J. Biol. Macromol. 187, 675–682. https://doi.org/10.1016/j.ijbiomac.2021.07.137.

Lusk, B., 2019. Thermophiles; or, the modern prometheus: the importance of extreme microorganisms for understanding and applying extracellular electron transfer. Front. Microbiol. 10, 818. https://doi.org/10.3389/fmicb.2019.00818.

Lv, L., Ren, Y., Chen, J., Wu, Q., Chen, G., 2015. Application of CRISPRi for prokaryotic metabolic engineering involving multiple genes, a case study: Controllable P(3HB-co-4HB) biosynthesis. Metab. Eng. 29, 160–168. https://doi.org/10.1016/j.ymben.2015.03.013.

Ma, H., Zhao, Y., Huang, W., Zhang, L., Wu, F., Ye, J., Chen, G., 2020. Rational flux-tuning of Halomonas bluephagenesis for co-production of bioplastic PHB and ectoine. Nat. Commun. 11, 1–12. https://doi.org/10.1038/s41467-020-17223-3.

Mahansaria, R., Dhara, A., Saha, A., Haldar, S., Mukherjee, J., 2018. Production enhancement and characterization of the polyhydroxyalkanoate produced by Natrinema ajinwuensis (as synonym) ≡ Natrinema altunense strain RM-G10. Int. J. Biol. Macromol. 107, 1480–1490. https://doi.org/10.1016/j.ijbiomac.2017.10.009.

Mahler, N., Tschirren, S., Pflügl, S., Herwig, C., 2018. Optimized bioreactor setup for scale-up studies of extreme halophilic cultures. Biochem. Eng. J. 130, 39–46. https://doi.org/10.1016/j.bej.2017.11.006.

Majara, M., O'Connor-Cox, E., Axcell, B., 2018. Trehalose—a stress protectant and stress indicator compound for yeast exposed to adverse conditions. J. Am. Soc. Brew. Chem. 54, 221–227. https://doi.org/10.1094/ASBCJ-54-0221.

Manaia, C., Nogales, B., Nunes, O., 2003. Tepidiphilus margaritifer gen. nov., sp. nov., isolated from a thermophilic aerobic digester. Int. J. Syst. Evol. Microbiol. 53, 1405–1410. https://doi.org/10.1099/ijs.0.02538-0.

Marcano-Velazquez, J., Lo, J., Nag, A., Maness, P., Chou, K., 2019. Developing riboswitch-mediated gene regulatory controls in thermophilic bacteria. ACS Synth. Biol. 8, 633–640. https://doi.org/10.1021/acssynbio.8b00487.

Masojídek, J., Torzillo, G., Kopecký, J., Koblížek, M., Nidiaci, L., Komenda, J., Lukavská, A., Sacchi, A., 2000. Changes in chlorophyll fluorescence quenching and pigment composition in the green alga Chlorococcum sp. grown under nitrogen deficiency and salinity stress. J. Appl. Phycol. 12, 417–426. https://doi.org/10.1023/A:1008165900780.

Mazzoli, R., Olson, D., 2020. Clostridium thermocellum: A microbial platform for high-value chemical production from lignocellulose. Adv. Appl. Microbiol., Adv. Appl. Microbiol. 113, 111–161. https://doi.org/10.1016/bs.aambs.2020.07.004.

Mearls, E., Olson, D., Herring, C., Lynd, L., 2015. Development of a regulatable plasmid-based gene expression system for Clostridium thermocellum. Appl. Microbiol. Biotechnol. 99, 7589–7599. https://doi.org/10.1007/s00253-015-6610-5.

Medeiros Garcia Alcântara, J., Distante, F., Storti, G., Moscatelli, D., Morbidelli, M., Sponchioni, M., 2020. Current trends in the production of biodegradable bioplastics: the case of polyhydroxyalkanoates. Biotechnol. Adv. 42 https://doi.org/10.1016/j.biotechadv.2020.107582.

Mezzina, M.P., Wetzler, D.E., de Almeida, A., Dinjaski, N., Prieto, M.A., Pettinari, M.J., 2015. A phasin with extra talents: a polyhydroxyalkanoate granule-associated protein has chaperone activity. Environ. Microbiol. 17, 1765–1776. https://doi.org/10.1111/1462-2920.12636.

Mezzina, M.P., Pettinari, M.J., Müller, V., 2016. Phasins, multifaceted polyhydroxyalkanoate granule-associated proteins. Appl. Environ. Microbiol. 82, 5060–5067. https://doi.org/10.1128/AEM.01161-16.

Miyake, M., Erata, M., Asada, Y., 1996. A thermophilic cyanobacterium, Synechococcus sp. MA19, capable of accumulating poly-β-hydroxybutyrate. J. Ferment. Bioeng. 82, 512–514. https://doi.org/10.1016/S0922-338X(97)86995-4.

Montero-Lobato, Z., Ramos-Merchante, A., Fuentes, J., Sayago, A., Fernández-Recamales, Á., Martínez-Espinosa, R., Vega, J., Vílchez, C., Garbayo, I., 2018. Optimization of growth and carotenoid production by Haloferax mediterranei using response surface methodology. Marine Drugs 16, 372. https://doi.org/10.3390/md16100372.

Moreira, C., Rainey, F., Nobre, M., da Silva, M., da Costa, M., 2000. Tepidimonas ignava gen. nov., sp. nov., a new chemolithoheterotrophic and slightly thermophilic member of the beta-Proteobacteria. Int. J. Syst. Evol. Microbiol. 50, 735–742. https://doi.org/10.1099/00207713-50-2-735.

Mothes, G., Schubert, T., Harms, H., Maskow, T., 2008. biotechnological coproduction of compatible solutes and polyhydroxyalkanoates using the genus Halomonas. Eng. Life Sci. 8, 658–662. https://doi.org/10.1002/elsc.200800097.

Mougiakos, I., Mohanraju, P., Bosma, E., Vrouwe, V., Finger Bou, M., Naduthodi, M., Gussak, A., Brinkman, R., van Kranenburg, R., van der Oost, J., 2017. Characterizing a thermostable Cas9 for bacterial genome editing and silencing. Nat. Commun. 8, 1647. https://doi.org/10.1038/s41467-017-01591-4.

ARTICLE IN PRESS

S. Obruča et al.   Biotechnology Advances xxx (xxxx) xxx

Mozejko-Ciesielska, J., Szacherska, K., Marciniak, P., 2019. Pseudomonas species as producers of eco-friendly polyhydroxyalkanoates. J. Polym. Environ. 27, 1151–1166. https://doi.org/10.1007/s10924-019-01422-1.

Mozumder, M., Garcia-Gonzalez, L., De Wever, H., Volcke, E., 2015. Effect of sodium accumulation on heterotrophic growth and polyhydroxybutyrate (PHB) production by Cupriavidus necator. Bioresour. Technol. 191, 213–218. https://doi.org/10.1016/j.biortech.2015.04.110.

Mravec, F., Obruca, S., Krzyzanek, V., Sedlacek, P., Hrubanova, K., Samek, O., Kucera, D., Benesova, P., Nebesarova, J., Steinbüchel, A., 2016. Accumulation of PHA granules in Cupriavidus necator as seen by confocal fluorescence microscopy. FEMS Microbiol. Lett. 363 https://doi.org/10.1093/femsle/fnw094.

Muhammadi, Shabina, Afzal, M., Hameed, S., 2015. Bacterial polyhydroxyalkanoates-eco-friendly next generation plastic: production, biocompatibility, biodegradation, physical properties and applications. Green Chem. Lett. Rev. 8, 56–77. https://doi.org/10.1080/17518253.2015.1109715.

Müller-Santos, M., Koskimäki, J., Alves, L., de Souza, E., Jendrossek, D., Pirttilä, A., 2020. The protective role of PHB and its degradation products against stress situations in bacteria. FEMS Microbiol. Rev. 45 https://doi.org/10.1093/femsre/fuaa058.

Musilova, J., Kourilova, X., Bezdicek, M., Lengerova, M., Obruca, S., Skutkova, H., Sedlar, K., Ochman, H., 2021. First complete genome of the thermophilic polyhydroxyalkanoates-producing bacterium schlegelella thermodepolymerans DSM 15344. Genome Biol. Evolut. 13 https://doi.org/10.1093/gbe/evab007 evab007.

Muyrers, J., 1999. Rapid modification of bacterial artificial chromosomes by ET-recombination. Nucleic Acids Res. 27, 1555–1557. https://doi.org/10.1093/nar/27.6.1555.

Ng, W., Kennedy, S., Mahairas, G., Berquist, B., Pan, M., Shukla, H., Lasky, S., Baliga, N., Thorsson, V., Sbrogna, J., Swartzell, S., Weir, D., Hall, J., Dahl, T., Welti, R., Goo, Y., Leithauser, B., Keller, K., Cruz, R., Danson, M., Hough, D., Maddocks, D., Jablonski, P., Krebs, M., Angevine, C., Dale, H., Isenbarger, T., Peck, R., Pohlschroder, M., Spudich, J., Jung, K., Alam, M., Freitas, T., Hou, S., Daniels, C., Dennis, P., Omer, A., Ebhardt, H., Lowe, T., Liang, P., Riley, M., Hood, L., DasSarma, S., 2000. Genome sequence of Halobacterium species NRC-1. Proc. Natl. Acad. Sci. 97, 12176–12181. https://doi.org/10.1073/pnas.190337797.

Nguyen, T., Ishizuna, F., Sato, Y., Arai, H., Ishii, M., 2019. Physiological characterization of poly-β-hydroxybutyrate accumulation in the moderately thermophilic hydrogen-oxidizing bacterium Hydrogenophilus thermoluteolus TH-1. J. Biosci. Bioeng. 127, 686–689. https://doi.org/10.1016/j.jbiosc.2018.11.011.

Nishioka, M., Nakai, K., Miyake, M., Asada, Y., Taya, M., 2001. Production of poly-β-hydroxybutyrate by thermophilic cyanobacterium, Synechococcus sp. MA19, under phosphate-limited conditions. Biotechnol. Lett. 23, 1095–1099. https://doi.org/10.1023/A:1010551614648.

Nonato, R., Mantelatto, P., Rossel, C., 2001. Integrated production of biodegradable plastic, sugar and ethanol. Appl. Microbiol. Biotechnol. 57, 1–5. https://doi.org/10.1007/s002530100732.

Novak, M., Koller, M., Braunegg, G., Horvat, P., 2015. Mathematical modelling as a tool for optimized PHA production. Chem. Biochem. Eng. Q. 29, 183–220. https://doi.org/10.15255/CABEQ.2014.2101.

Nowroth, V., Marquart, L., Jendrossek, D., Imperial, J., 2016. Low temperature-induced viable but not culturable state of Ralstonia eutropha and its relationship to accumulated polyhydroxybutyrate. FEMS Microbiology Letters vol. 363. https://doi.org/10.1093/femsle/fnw249.

Obruca, S., Benesova, P., Petrik, S., Oborna, J., Prikryl, R., Marova, I., 2014. Production of polyhydroxyalkanoates using hydrolysate of spent coffee grounds. Process Biochem. 49, 1409–1414. https://doi.org/10.1016/j.procbio.2014.05.013.

Obruca, S., Benesova, P., Marsalek, L., Marova, I., 2015. Use of lignocellulosic materials for PHA production. Chem. Biochem. Eng. Quart. 29, 135–144. https://doi.org/10.15255/CABEQ.2014.2253.

Obruca, S., Sedlacek, P., Krzyzanek, V., Mravec, F., Hrubanova, K., Samek, O., Kucera, D., Benesova, P., Marova, I., Chen, G., 2016a. Accumulation of poly(3-hydroxybutyrate) helps bacterial cells to survive freezing. PLOS ONE 11. https://doi.org/10.1371/journal.pone.0157778.

Obruca, S., Sedlacek, P., Mravec, F., Samek, O., Marova, I., 2016b. Evaluation of 3-hydroxybutyrate as an enzyme-protective agent against heating and oxidative damage and its potential role in stress response of poly(3-hydroxybutyrate) accumulating cells. Appl. Microbiol. Biotechnol. 100, 1365–1376. https://doi.org/10.1007/s00253-015-7162-4.

Obruca, S., Sedlacek, P., Mravec, F., Krzyzanek, V., Nebesarova, J., Samek, O., Kucera, D., Benesova, P., Hrubanova, K., Milerova, M., Marova, I., 2017. The presence of PHB granules in cytoplasm protects non-halophilic bacterial cells against the harmful impact of hypertonic environments. New Biotechnol. 39, 68–80. https://doi.org/10.1016/j.nbt.2017.07.008.

Obruca, S., Sedlacek, P., Koller, M., Kucera, D., Pernicova, I., 2018. Involvement of polyhydroxyalkanoates in stress resistance of microbial cells: Biotechnological consequences and applications. Biotechnol. Adv. 36, 856–870. https://doi.org/10.1016/j.biotechadv.2017.12.006.

Obruca, S., Sedlacek, P., Slaninova, E., Fritz, I., Daffert, C., Meixner, K., Sedrlova, Z., Koller, M., 2020. Novel unexpected functions of PHA granules. Appl. Microbiol. Biotechnol. 104, 4795–4810. https://doi.org/10.1007/s00253-020-10568-1.

Obruca, S., Sedlacek, P., Koller, M., 2021. The underexplored role of diverse stress factors in microbial biopolymer synthesis. Bioresource Technol. 326. https://doi.org/10.1016/j.biortech.2021.124767.

Obulisamy, P., Mehariya, S., 2021. Polyhydroxyalkanoates from extremophiles: a review. Bioresour. Technol. 325 https://doi.org/10.1016/j.biortech.2020.124653.

O'Leary, N., Wright, M., Brister, J., Ciufo, S., Haddad, D., McVeigh, R., Rajput, B., Robbertse, B., Smith-White, B., Ako-Adjei, D., Astashyn, A., Badretdin, A., Bao, Y.,

Blinkova, O., Brover, V., Chetvernin, V., Choi, J., Cox, E., Ermolaeva, O., Farrell, C., Goldfarb, T., Gupta, T., Haft, D., Hatcher, E., Hlavina, W., Joardar, V., Kodali, V., Li, W., Maglott, D., Masterson, P., McGarvey, K., Murphy, M., O'Neill, K., Pujar, S., Rangwala, S., Rausch, D., Riddick, L., Schoch, C., Shkeda, A., Storz, S., Sun, H., Thibaud-Nissen, F., Tolstoy, I., Tully, R., Vatsan, A., Wallin, C., Webb, D., Wu, W., Landrum, M., Kimchi, A., Tatusova, T., DiCuccio, M., Kitts, P., Murphy, T., Pruitt, K., 2016. Reference sequence (RefSeq) database at NCBI: current status, taxonomic expansion, and functional annotation. Nucleic Acids Res. 44, D733–D745. https://doi.org/10.1093/nar/gkv1189.

Oliveira, C., Silva, C., Carvalho, G., Reis, M., 2017. Strategies for efficiently selecting PHA producing mixed microbial cultures using complex feedstocks: Feast and famine regime and uncoupled carbon and nitrogen availabilities. New Biotechnol. 37, 69–79. https://doi.org/10.1016/j.nbt.2016.10.008.

Olson, D., Lynd, L., 2012. Transformation of clostridium thermocellum by electroporation. In: Cellulases, Methods in Enzymology. Elsevier, pp. 317–330. https://doi.org/10.1016/B978-0-12-415931-0.00017-3.

Olson, D., Maloney, M., Lanahan, A., Hon, S., Hauser, L., Lynd, L., 2015. Identifying promoters for gene expression in Clostridium thermocellum. Metabol. Eng. Commun. 2, 23–29. https://doi.org/10.1016/j.meteno.2015.03.002.

Oren, A., 2002. Diversity of halophilic microorganisms: environments, phylogeny, physiology, and applications. J. Ind. Microbiol. Biotechnol. 28, 56–63. https://doi.org/10.1038/sj/jim/7000176.

Oren, A., Ginzburg, M., Ginzburg, B., Hochstein, L., Volcani, B., 1990. Haloarcula marismortui (Volcani) sp. nov., nom. rev., an extremely halophilic bacterium from the dead sea. Int. J. Syst. Bacteriol. 40, 209–210. https://doi.org/10.1099/00207713-40-2-209.

Pacholak, A., Gao, Z., Gong, X., Kaczorek, E., Cui, Y., 2021. The metabolic pathways of polyhydroxyalkanoates and exopolysaccharides synthesized by Haloferax mediterranei in response to elevated salinity. J. Proteome 232, 104065. https://doi.org/10.1016/j.jprot.2020.104065.

Pantazaki, A., Tambaka, M., Langlois, V., Guerin, P., Kyriakidis, D., 2003. Polyhydroxyalkanoate (PHA) biosynthesis in Thermus thermophilus: purification and biochemical properties of PHA synthase. Mol. Cell. Biochem. 254, 173–183. https://doi.org/10.1023/A:1027373100955.

Pantazaki, A., Papaneophytou, C., Pritsa, A., Liakopoulou-Kyriakides, M., Kyriakidis, D., 2009. Production of polyhydroxyalkanoates from whey by Thermus thermophilus HB8. Process Biochem. 44, 847–853. https://doi.org/10.1016/j.procbio.2009.04.002.

Panuschka, S., Drosg, B., Ellersdorfer, M., Meixner, K., Fritz, I., 2019. Photoautotrophic production of poly-hydroxybutyrate – First detailed cost estimations. Algal Res. 41 https://doi.org/10.1016/j.algal.2019.101558.

Park, J., Cho, B., Simpson, A., 2006. Halocafeteria seosinensis gen. et sp. nov. (Bicosoecida), a halophilic bacterivorous nanoflagellate isolated from a solar saltern. Extremophiles 10, 493–504. https://doi.org/10.1007/s00792-006-0001-x.

Park, S., Kim, T., Kim, M., Lee, S., Lim, S., 2012. Advanced bacterial polyhydroxyalkanoates: towards a versatile and sustainable platform for unnatural tailor-made polyesters. Biotechnol. Adv. 30, 1196–1206. https://doi.org/10.1016/j.biotechadv.2011.11.007.

Park, S., Jang, Y., Lee, H., Park, A., Yang, J., Shin, J., Oh, Y., Song, B., Jegal, J., Lee, S., Lee, S., 2013. Metabolic engineering of Ralstonia eutropha for the biosynthesis of 2-hydroxyacid-containing polyhydroxyalkanoates. Metab. Eng. 20, 20–28. https://doi.org/10.1016/j.ymben.2013.08.002.

Park, Y., Bhatia, S., Gurav, R., Choi, T., Kim, H., Song, H., Park, J., Han, Y., Lee, S., Park, S., Lee, H., Kim, Y., Yang, Y., 2020. Fructose based hyper production of poly-3-hydroxybutyrate from Halomonas sp. YLGW01 and impact of carbon sources on bacteria morphologies. Int. J. Biol. Macromol. 154, 929–936. https://doi.org/10.1016/j.ijbiomac.2020.03.129.

Peleg, M., Normand, M., Corradini, M., 2012. The arrhenius equation revisited. Crit. Rev. Food Sci. Nutr. 52, 830–851. https://doi.org/10.1080/10408398.2012.667460.

Pernicova, I., Kucera, D., Nebesarova, J., Kalina, M., Novackova, I., Koller, M., Obruca, S., 2019. Production of polyhydroxyalkanoates on waste frying oil employing selected Halomonas strains. Bioresour. Technol. 292, 122028. https://doi.org/10.1016/j.biortech.2019.122028.

Pernicova, I., Novackova, I., Sedlacek, P., Kourilova, X., Kalina, M., Kovalcik, A., Koller, M., Nebesarova, J., Krzyzanek, V., Hrubanova, K., Masilko, J., Slaninova, E., Obruca, S., 2020a. Introducing the newly isolated bacterium aneurinibacillus sp. H1 as an auspicious thermophilic producer of various polyhydroxyalkanoates (PHA) copolymers–1. Isolation and characterization of the bacterium. Polymers 12, 1235. https://doi.org/10.3390/polym12061235.

Pernicova, I., Novackova, I., Sedlacek, P., Kourilova, X., Koller, M., Obruca, S., 2020b. Application of osmotic challenge for enrichment of microbial consortia in polyhydroxyalkanoates producing thermophilic and thermotolerant bacteria and their subsequent isolation. Int. J. Biol. Macromol. 144, 698–704. https://doi.org/10.1016/j.ijbiomac.2019.12.128.

Pfeifer, K., Ergal, İ., Koller, M., Basen, M., Schuster, B., Rittmann, S.K.-M.R., 2021. Archaea biotechnology. Biotechnol. Adv. 47, 107668. https://doi.org/10.1016/j.biotechadv.2020.107668.

Posfai, G., Kolisnychenko, V., Bereczki, Z., Blattner, F., 1999. Markerless gene replacement in Escherichia coli stimulated by a double-strand break in the chromosome. Nucleic Acids Res. 27, 4409–4415. https://doi.org/10.1093/nar/27.22.4409.

Prieto, A., Escapa, I., Martínez, V., Dinjaski, N., Herencias, C., de la Peña, F., Tarazona, N., Revelles, O., 2016. A holistic view of polyhydroxyalkanoate metabolism in Pseudomonas putida. Environ. Microbiol. 18, 341–357. https://doi.org/10.1111/1462-2920.12760.

Qin, Q., Ling, C., Zhao, Y., Yang, T., Yin, J., Guo, Y., Chen, G., 2018. CRISPR/Cas9 editing genome of extremophile Halomonas spp. Metab. Eng. 47, 219–229. https://doi.org/10.1016/j.ymben.2018.03.018.

Quillaguamán, J., Hashim, S., Bento, F., Mattiasson, B., Hatti-Kaul, R., 2005. Poly (β-hydroxybutyrate) production by a moderate halophile, Halomonas boliviensis LC1 using starch hydrolysate as substrate. J. Appl. Microbiol. 99, 151–157. https://doi.org/10.1111/j.1365-2672.2005.02589.x.

Rahman, A., Linton, E., Hatch, A., Sims, R., Miller, C., 2013. Secretion of polyhydroxybutyrate in Escherichia coli using a synthetic biological engineering approach. J. Biolog. Eng. 7 https://doi.org/10.1186/1754-1611-7-24.

Ren, Y., Ling, C., Hajnal, I., Wu, Q., Chen, G., 2018. Construction of Halomonas bluephagenesis capable of high cell density growth for efficient PHA production. Appl. Microbiol. Biotechnol. 102, 4499–4510. https://doi.org/10.1007/s00253-018-8931-7.

Riley, L., Guss, A., 2021. Approaches to genetic tool development for rapid domestication of non-model microorganisms. Biotechnol. Biofuels 14. https://doi.org/10.1186/s13068-020-01872-z.

Riley, L., Ji, L., Schmitz, R., Westpheling, J., Guss, A., 2019. Rational development of transformation in Clostridium thermocellum ATCC 27405 via complete methylome analysis and evasion of native restriction–modification systems. J. Ind. Microbiol. Biotechnol. 46, 1435–1443. https://doi.org/10.1007/s10295-019-02218-x.

Rodríguez, Y., Pérez, V., López, J., Bordel, S., Firmino, P., Lebrero, R., Muñoz, R., 2020. Coupling biogas with PHA biosynthesis. In: The Handbook of Polyhydroxyalkanoates. CRC Press, Boca Raton, pp. 357–376.

Rodríguez-Contreras, A., Koller, M., Braunegg, G., Marqués-Calvo, M., 2016. Poly[(R)-3-hydroxybutyrate] production under different salinity conditions by a novel Bacillus megaterium strain. New Biotechnol. 33, 73–77. https://doi.org/10.1016/j.nbt.2015.08.006.

Ruth, K., Grubelnik, A., Hartmann, R., Egli, T., Zinn, M., Ren, Q., 2007. Efficient production of (R)-3-hydroxycarboxylic acids by biotechnological conversion of polyhydroxyalkanoates and their purification. Biomacromolecules 8, 279–286. https://doi.org/10.1021/bm060585a.

Sadykov, M., Ahn, J., Widhelm, T., Eckrich, V., Endres, J., Driks, A., Rutkowski, G., Wingerd, K., Bayles, K., 2017. Poly(3-hydroxybutyrate) fuels the tricarboxylic acid cycle and de novo lipid biosynthesis during Bacillus anthracis sporulation. Mol. Microbiol. 104, 793–803. https://doi.org/10.1111/mmi.13665.

Salgaonkar, B., Bragança, J., 2015. Biosynthesis of poly(3-hydroxybutyrate- co −3-hydroxyvalerate) by Halogeometricum borinquense strain E3. Int. J. Biol. Macromol. 78, 339–346. https://doi.org/10.1016/j.ijbiomac.2015.04.016.

Salgaonkar, B., Bragança, J., 2017. Utilization of Sugarcane Bagasse by Halogeometricum borinquense Strain E3 for Biosynthesis of Poly(3-hydroxybutyrate-co-3-hydroxyvalerate). Bioengineering 4, 50. https://doi.org/10.3390/bioengineering4020050.

Salgaonkar, B., Mani, K., Bragança, J., 2019. Sustainable bioconversion of cassava waste to poly(3-hydroxybutyrate-co-3-hydroxyvalerate) by Halogeometricum borinquense strain E3. J. Polym. Environ. 27, 299–308. https://doi.org/10.1007/s10924-018-1346-9.

Salvachúa, D., Rydzak, T., Auwae, R., De Capite, A., Black, B., Bouvier, J., Cleveland, N., Elmore, J., Furches, A., Huenemann, J., Katahira, R., Michener, W., Peterson, D., Rohrer, H., Vardon, D., Beckham, G., Guss, A., 2020. Metabolic engineering of Pseudomonas putida for increased polyhydroxyalkanoate production from lignin. Microb. Biotechnol. 13, 290–298. https://doi.org/10.1111/1751-7915.13481.

Sangkharak, K., Khaithongkaeo, P., Chuaikhunupakarn, T., Choonut, A., Prasertsan, P., 2020. The production of polyhydroxyalkanoate from waste cooking oil and its application in biofuel production. Biomass Conversion Biorefinery. https://doi.org/10.1007/s13399-020-00657-6.

Satoh, Y., Tajima, K., Nakamoto, S., Xuerong, H., Matsushima, T., Ohshima, T., Kawano, S., Erata, T., Dairi, T., Munekata, M., 2011. Isolation of a thermotolerant bacterium producing medium-chain-length polyhydroxyalkanoate. J. Appl. Microbiol. 111, 811–817. https://doi.org/10.1111/j.1365-2672.2011.05093.x.

Sauer, T., Galinski, E., 1998. Bacterial milking: a novel bioprocess for production of compatible solutes. Biotechnol. Bioeng. 59, 128. https://doi.org/10.1002/(SICI)1097-0290(19980705)59:1128::AID-BIT173.0.CO;2-E.

Sayers, E., Cavanaugh, M., Clark, K., Ostell, J., Pruitt, K., Karsch-Mizrachi, I., 2019. GenBank. Nucleic Acids Res. D1, D84–D86. https://doi.org/10.1093/nar/gkz956.

Schmid, M., Song, H., Raschbauer, M., Emerstorfer, F., Omann, M., Stelzer, F., Neureiter, M., 2019. Utilization of desugarized sugar beet molasses for the production of poly(3-hydroxybutyrate) by halophilic Bacillus megaterium uyuni S29. Process Biochem. 86, 9–15. https://doi.org/10.1016/j.procbio.2019.08.001.

Schmid, M., Raschbauer, M., Song, H., Bauer, C., Neureiter, M., 2021a. Effects of nutrient and oxygen limitation, salinity and type of salt on the accumulation of poly(3-hydroxybutyrate) in Bacillus megaterium uyuni S29 with sucrose as a carbon source. New Biotechnol. 61, 137–144. https://doi.org/10.1016/j.nbt.2020.11.012.

Schmid, M., Sykacek, E., O'Connor, K., Omann, M., Mundigler, N., Neureiter, M., 2021b. Pilot scale production and evaluation of mechanical and thermal properties of P (3HB) from *Bacillus megaterium* cultivated on desugarized sugar beet molasses. J. Appl. Polym. Sci. 51503 https://doi.org/10.1002/app.51503.

Sedlacek, P., Slaninova, E., Koller, M., Nebesarova, J., Marova, I., Krzyzanek, V., Obruca, S., 2019. PHA granules help bacterial cells to preserve cell integrity when exposed to sudden osmotic imbalances. New Biotechnol. 49, 129–136. https://doi.org/10.1016/j.nbt.2018.10.005.

Sedlacek, P., Pernicova, I., Novackova, I., Kourilova, X., Kalina, M., Kovalcik, A., Koller, M., Nebesarova, J., Krzyzanek, V., Hrubanova, K., Masilko, J., Slaninova, E., Trudicova, M., Obruca, S., 2020. Introducing the newly isolated bacterium aneurinibacillus sp. H1 as an auspicious thermophilic producer of various

polyhydroxyalkanoates (PHA) copolymers–2. material study on the produced copolymers. Polymers 12, 1298. https://doi.org/10.3390/polym12061298.

Shahid, S., Mosrati, R., Ledauphin, J., Amiel, C., Fontaine, P., Gaillard, J., Corroler, D., 2013. Impact of carbon source and variable nitrogen conditions on bacterial biosynthesis of polyhydroxyalkanoates: evidence of an atypical metabolism in Bacillus megaterium DSM 509. J. Biosci. Bioeng. 116, 302–308. https://doi.org/10.1016/j.jbiosc.2013.02.017.

Shen, R., Yin, J., Ye, J., Xiang, R., Ning, Z., Huang, W., Chen, G., 2018. Promoter engineering for enhanced P(3HB-co-4HB) production by Halomonas bluephagenesis. ACS Synth. Biol. 7, 1897–1906. https://doi.org/10.1021/acssynbio.8b00102.

Shen, R., Ning, Z., Lan, Y., Chen, J., Chen, G., 2019. Manipulation of polyhydroxyalkanoate granular sizes in Halomonas bluephagenesis. Metab. Eng. 54, 117–126. https://doi.org/10.1016/j.ymben.2019.03.011.

Sheu, D., Chen, W., Yang, J., Chang, R., 2009. Thermophilic bacterium Caldimonas taiwanensis produces poly(3-hydroxybutyrate-co-3-hydroxyvalerate) from starch and valerate as carbon sources. Enzym. Microb. Technol. 44, 289–294. https://doi.org/10.1016/j.enzmictec.2009.01.004.

Sheu, D., Chen, W., Lai, Y., Chang, R., 2012. Mutations derived from the thermophilic polyhydroxyalkanoate synthase PhaC enhance the thermostability and activity of PhaC from cupriavidus necator H16. J. Bacteriol. 194, 2620–2629. https://doi.org/10.1128/JB.06543-11.

Shivanand, P., Mugeraya, G., 2011. Halophilic bacteria and their compatible solutes – osmoregulation and potential applications. Curr. Sci. 100, 1516–1521.

Silva-Rocha, R., Martínez-García, E., Calles, B., Chavarría, M., Arce-Rodríguez, A., de las Heras, A., Páez-Espino, A., Durante-Rodríguez, G., Kim, J., Nikel, P., Platero, R., de Lorenzo, V., 2013. The Standard European Vector Architecture (SEVA): a coherent platform for the analysis and deployment of complex prokaryotic phenotypes. Nucleic Acids Res. 41, D666–D675. https://doi.org/10.1093/nar/gks1119.

Simon-Colin, C., Raguénès, G., Cozien, J., Guezennec, J., 2008. Halomonas profundus sp. nov., a new PHA-producing bacterium isolated from a deep-sea hydrothermal vent shrimp. J. Appl. Microbiol. 104, 1425–1432. https://doi.org/10.1111/j.1365-2672.2007.03667.x.

Singh, A., Srivastava, J., Chandel, A., Sharma, L., Mallick, N., Singh, S., 2019. Biomedical applications of microbially engineered polyhydroxyalkanoates: an insight into recent advances, bottlenecks, and solutions. Appl. Microbiol. Biotechnol. 103, 2007–2032. https://doi.org/10.1007/s00253-018-09604-y.

Slaninova, E., Sedlacek, P., Mravec, F., Mullerova, L., Samek, O., Koller, M., Hesko, O., Kucera, D., Marova, I., Obruca, S., 2018. Light scattering on PHA granules protects bacterial cells against the harmful effects of UV radiation. Appl. Microbiol. Biotechnol. 102, 1923–1931. https://doi.org/10.1007/s00253-018-8760-8.

Soto, G., Setten, L., Lisi, C., Maurelis, C., Mozzicafreddo, M., Cuccioloni, M., Angeletti, M., Ayub, N., 2012. Hydroxybutyrate prevents protein aggregation in the halotolerant bacterium Pseudomonas sp. CT13 under abiotic stress. Extremophiles 16, 455–462. https://doi.org/10.1007/s00792-012-0445-0.

Stanley, A., Punil Kumar, H., Mutturi, S., Vijayendra, S., 2018. Fed-batch strategies for production of PHA using a native isolate of halomonas venusta KT832796 Strain. Appl. Biochem. Biotechnol. 184, 935–952. https://doi.org/10.1007/s12010-017-2601-6.

Stanley, A., Mutturi, S., Vijayendra, S., 2021. Halophilic microorganisms as potential producers of polyhydroxyalkanoates. In: Kuddus, M., Roohi (Eds.), Bioplastics for Sustainable Development. Springer Singapore, Singapore, pp. 277–294. https://doi.org/10.1007/978-981-16-1823-9_10.

Steinbüchel, A., 1995. Diversity of bacterial polyhydroxyalkanoic acids. FEMS Microbiol. Lett. 128, 219–228. https://doi.org/10.1016/0378-1097(95)00125-O.

Tajima, K., Han, X., Hashimoto, Y., Satoh, Y., Satoh, T., Taguchi, S., 2016. In vitro synthesis of polyhydroxyalkanoates using thermostable acetyl-CoA synthetase, CoA transferase, and PHA synthase from thermotorelant bacteria. J. Biosci. Bioeng. 122, 660–665. https://doi.org/10.1016/j.jbiosc.2016.06.001.

Takeda, M., Kamagata, Y., Ghiorse, W., Hanada, S., Koizumi, J., 2002. Caldimonas manganoxidans gen. nov., sp. nov., a poly(3-hydroxybutyrate)-degrading, manganese-oxidizing thermophile. Int. J. Syst. Evol. Microbiol. 52, 895–900. https://doi.org/10.1099/00207713-52-3-895.

Tan, D., Xue, Y., Aibaidula, G., Chen, G., 2011. Unsterile and continuous production of polyhydroxybutyrate by Halomonas TD01. Bioresour. Technol. 102, 8130–8136. https://doi.org/10.1016/j.biortech.2011.05.068.

Tan, D., Wu, Q., Chen, J., Chen, G., 2014. Engineering Halomonas TD01 for the low-cost production of polyhydroxyalkanoates. Metab. Eng. 26, 34–47. https://doi.org/10.1016/j.ymben.2014.09.001.

Tan, I.K.P., Foong, C.P., Tan, H.T., Lim, H., Zain, N.A.A., Tan, Y.C., Hoh, C.C., Sudesh, K., 2020. Polyhydroxyalkanoate (PHA) synthase genes and PHA-associated gene clusters in Pseudomonas spp. and Janthinobacterium spp. isolated from Antarctica. J. Biotechnol. 313, 18–28. https://doi.org/10.1016/j.jbiotec.2020.03.006.

Tan, D., Wang, Y., Tong, Y., Chen, G., 2021. Grand challenges for industrializing polyhydroxyalkanoates (PHAs). Trends Biotechnol. 39, 953–963. https://doi.org/10.1016/j.tibtech.2020.11.010.

Tao, W., Lv, L., Chen, G., 2017. Engineering halomonas species TD01 for enhanced polyhydroxyalkanoates synthesis via CRISPRi. Microb. Cell Factories 16. https://doi.org/10.1186/s12934-017-0655-3.

Tao, G., Tan, B., Li, Z., 2021. Production of polyhydroxyalkanoates by a moderately halophilic bacterium of Salinivibrio sp. TGB10. Int. J. Biol. Macromol. 186, 574–579. https://doi.org/10.1016/j.ijbiomac.2021.07.038.

Tiso, T., Narancic, T., Wei, R., Pollet, E., Beagan, N., Schröder, K., Honak, A., Jiang, M., Kenny, S., Wierckx, N., Perrin, R., Avérous, L., Zimmermann, W., O'Connor, K., Blank, L., 2021. Towards bio-upcycling of polyethylene terephthalate. Metab. Eng. 66, 167–178. https://doi.org/10.1016/j.ymben.2021.03.011.

Tribelli, P., Pezzoni, M., Brito, M., Montesinos, N., Costa, C., López, N., 2020. Response to lethal UVA radiation in the Antarctic bacterium Pseudomonas extremaustralis: polyhydroxybutyrate and cold adaptation as protective factors. Extremophiles 24, 265–275. https://doi.org/10.1007/s00792-019-01152-1.

Tripathi, S., Olson, D., Argyros, D., Miller, B., Barrett, T., Murphy, D., McCool, J., Warner, A., Rajgarhia, V., Lynd, L., Hogsett, D., Caiazza, N., 2010. Development of pyrF- based genetic system for targeted gene deletion in clostridium thermocellum and creation of a pta mutant. Appl. Environ. Microbiol. 76, 6591–6599. https://doi.org/10.1128/AEM.01484-10.

Urbieta, M.S., Donati, E.R., Chan, K.-G., Shahar, S., Sin, L.L., Goh, K.M., 2015. Thermophiles in the genomic era: biodiversity, science, and applications. Biotechnol. Adv. 33, 633–647. https://doi.org/10.1016/j.biotechadv.2015.04.007.

Van Thuoc, D., My, D., Loan, T., Sudesh, K., 2019. Utilization of waste fish oil and glycerol as carbon sources for polyhydroxyalkanoate production by Salinivibrio sp. M318. Int. J. Biol. Macromol. 141, 885–892. https://doi.org/10.1016/j.ijbiomac.2019.09.063.

Vandewijngaarden, J., Wauters, R., Murariu, M., Dubois, P., Carleer, R., Yperman, J., D'Haen, J., Ruttens, B., Schreurs, S., Lepot, N., Peeters, R., Buntinx, M., 2016. Poly (3-hydroxybutyrate-co-3-hydroxyhexanoate)/organomodified montmorillonite nanocomposites for potential food packaging applications. J. Polym. Environ. 24, 104–118. https://doi.org/10.1007/s10924-016-0751-1.

Van-Thuoc, D., Huu-Phong, T., Minh-Khuong, D., Hatti-Kaul, R., 2015. Poly(3-hydroxybutyrate-co-3-Hydroxyvalerate) production by a moderate Halophile Yangia sp. ND199 using glycerol as a carbon source. Appl. Biochem. Biotechnol. 175, 3120–3132. https://doi.org/10.1007/s12010-015-1479-4.

Vasu, K., Nagaraja, V., 2013. Diverse functions of restriction-modification systems in addition to cellular defense. Microbiol. Mol. Biol. Rev. 77, 53–72. https://doi.org/10.1128/MMBR.00044-12.

Walker, J., Lanahan, A., Zheng, T., Toruno, C., Lynd, L., Cameron, J., Olson, D., Eckert, C., 2020. Development of both type I–B and type II CRISPR/Cas genome editing systems in the cellulolytic bacterium Clostridium thermocellum. Metabol. Eng. Commun. 10, e00116 https://doi.org/10.1016/j.mec.2019.e00116.

Wang, B., Pugh, S., Nielsen, D., Zhang, W., Meldrum, D., 2013. Engineering cyanobacteria for photosynthetic production of 3-hydroxybutyrate directly from CO2. Metab. Eng. 16, 68–77. https://doi.org/10.1016/j.ymben.2013.01.001.

Wang, Y., Ling, C., Chen, Y., Jiang, X., Chen, G., 2019. Microbial engineering for easy downstream processing. Biotechnol. Adv. 37, 107365. https://doi.org/10.1016/j.biotechadv.2019.03.004.

Wang, Z., Qin, Q., Zheng, Y., Li, F., Zhao, Y., Chen, G., 2021. Engineering the permeability of Halomonas bluephagenesis enhanced its chassis properties. Metab. Eng. 67, 53–66. https://doi.org/10.1016/j.ymben.2021.05.010.

Weiss, T., Young, E., Ducat, D., 2017. A synthetic, light-driven consortium of cyanobacteria and heterotrophic bacteria enables stable polyhydroxybutyrate production. Metab. Eng. 44, 236–245. https://doi.org/10.1016/j.ymben.2017.10.009.

Whelan, S., Goldman, N., 2001. A general empirical model of protein evolution derived from multiple protein families using a maximum-likelihood approach. Mol. Biol. Evol. 18, 691–699. https://doi.org/10.1093/oxfordjournals.molbev.a003851.

Williams-Rhaesa, A., Awuku, N., Lipscomb, G., Poole, F., Rubinstein, G., Conway, J., Kelly, R., Adams, M., 2018. Native xylose-inducible promoter expands the genetic tools for the biomass-degrading, extremely thermophilic bacterium Caldicellulosiruptor bescii. Extremophiles 22, 629–638. https://doi.org/10.1007/s00792-018-1023-x.

Wood, J., Bremer, E., Csonka, L., Kraemer, R., Poolman, B., van der Heide, T., Smith, L., 2001. Osmosensing and osmoregulatory compatible solute accumulation by bacteria. Comp. Biochem. Physiol. A Mol. Integr. Physiol. 130, 437–460. https://doi.org/10.1016/S1095-6433(01)00442-1.

Xi, L., Zhang, Z., Qiao, N., Zhang, Y., Li, J., Zhao, J., Xiao, Z., 2016. Complete genome sequence of the novel thermophilic polyhydroxyalkanoates producer Aneurinibacillus sp. XH2 isolated from Gudao oilfield in China. J. Biotechnol. 227, 54–55. https://doi.org/10.1016/j.jbiotec.2016.03.056.

Xiao, Z., Zhang, Y., Xi, L., Huo, F., Zhao, J., Li, J., 2015. Thermophilic production of polyhydroxyalkanoates by a novel Aneurinibacillus strain isolated from Gudao

oilfield, China. J. Basic Microbiol. 55, 1125–1133. https://doi.org/10.1002/jobm.201400843.

Xu, F., Huang, S., Liu, Y., Zhang, Y., Chen, S., 2014. Comparative study on the production of poly(3-hydroxybutyrate) by thermophilic Chelatococcus daeguensis TAD1: a good candidate for large-scale production. Appl. Microbiol. Biotechnol. 98, 3965–3974. https://doi.org/10.1007/s00253-014-5524-y.

Ye, J., Huang, W., Wang, D., Chen, F., Yin, J., Li, T., Zhang, H., Chen, G., 2018. Pilot Scale-up of Poly(3-hydroxybutyrate- co −4-hydroxybutyrate) Production by Halomonas bluephagenesis via Cell Growth Adapted Optimization Process. Biotechnol. J. 13, 1800074. https://doi.org/10.1002/biot.201800074.

Ye, J., Hu, D., Yin, J., Huang, W., Xiang, R., Zhang, L., Wang, X., Han, J., Chen, G., 2020. Stimulus response-based fine-tuning of polyhydroxyalkanoate pathway in Halomonas. Metab. Eng. 57, 85–95. https://doi.org/10.1016/j.ymben.2019.10.007.

Yin, J., Fu, X., Wu, Q., Chen, J., Chen, G., 2014. Development of an enhanced chromosomal expression system based on porin synthesis operon for halophile Halomonas sp. Appl. Microbiol. Biotechnol. 98, 8987–8997. https://doi.org/10.1007/s00253-014-5959-1.

Yin, J., Chen, J., Wu, Q., Chen, G., 2015. Halophiles, coming stars for industrial biotechnology. Biotechnol. Adv. 33, 1433–1442. https://doi.org/10.1016/j.biotechadv.2014.10.008.

You, J., Li, Y., Hong, S., Wang, J., Yu, J., Mu, B., Ma, X., Xue, Y., 2019. Tepidicella baoligensis sp. nov., a novel member of betaproteobacterium isolated from an oil reservoir. Curr. Microbiol. 76, 410–414. https://doi.org/10.1007/s00284-018-1604-z.

Yu, L., Wu, F., Chen, G., 2019. Next-generation industrial biotechnology-transforming the current industrial biotechnology into competitive processes. Biotechnol. J. 14 https://doi.org/10.1002/biot.201800437.

Yu, L., Yan, X., Zhang, X., Chen, X., Wu, Q., Jiang, X., Chen, G., 2020. Biosynthesis of functional polyhydroxyalkanoates by engineered Halomonas bluephagenesis. Metab. Eng. 59, 119–130. https://doi.org/10.1016/j.ymben.2020.02.005.

Zeldes, B., Keller, M., Loder, A., Straub, C., Adams, M., Kelly, R., 2015. Extremely thermophilic microorganisms as metabolic engineering platforms for production of fuels and industrial chemicals. Front. Microbiol. 6, 1209. https://doi.org/10.3389/fmicb.2015.01209.

Zhang, M., Thomas, N.L., 2011. Blending polylactic acid with polyhydroxybutyrate: the effect on thermal, mechanical, and biodegradation properties. Adv. Polym. Technol. 30, 67–79. https://doi.org/10.1002/adv.20235.

Zhang, X., Lin, Y., Wu, Q., Wang, Y., Chen, G., 2020. Synthetic biology and genome-editing tools for improving PHA metabolic engineering. Trends Biotechnol. 38, 689–700. https://doi.org/10.1016/j.tibtech.2019.10.006.

Zhao, Y., Li, H., Qin, L., Wang, H., Chen, G., 2007. Disruption of the polyhydroxyalkanoate synthase gene in Aeromonas hydrophila reduces its survival ability under stress conditions. FEMS Microbiol. Lett. 276, 34–41. https://doi.org/10.1111/j.1574-6968.2007.00904.x.

Zhao, Y., Rao, Z., Xue, Y., Gong, P., Ji, Y., Ma, Y., 2015. Poly(3-hydroxybutyrate-co-3-hydroxyvalerate) production by Haloarchaeon Halogranum amylolyticum. Appl. Microbiol. Biotechnol. 99, 7639–7649. https://doi.org/10.1007/s00253-015-6609-y.

Zhao, H., Zhang, H., Chen, X., Li, T., Wu, Q., Ouyang, Q., Chen, G., 2017. Novel T7-like expression systems used for Halomonas. Metab. Eng. 39, 128–140. https://doi.org/10.1016/j.ymben.2016.11.007.

Zheng, Y., Meng, F., Zhu, Z., Wei, W., Sun, Z., Chen, J., Yu, B., Lou, C., Chen, G., 2019. A tight cold-inducible switch built by coupling thermosensitive transcriptional and proteolytic regulatory parts. Nucleic Acids Res. 47, e137. https://doi.org/10.1093/nar/gkz785.

Zheng, Y., Chen, J., Ma, Y., Chen, G., 2020. Engineering biosynthesis of polyhydroxyalkanoates (PHA) for diversity and cost reduction. Metab. Eng. 58, 82–93. https://doi.org/10.1016/j.ymben.2019.07.004.

Zou, H., Shi, M., Zhang, T., Li, L., Li, L., Xian, M., 2017. Natural and engineered polyhydroxyalkanoate (PHA) synthase: key enzyme in biopolyester production. Appl. Microbiol. Biotechnol. 101, 7417–7426. https://doi.org/10.1007/s00253-017-8485-0.

Appendix 21

Obruca, S., Sedlacek, P., Mravec, F., Samek, O., and Marova, I. Evaluation of 3-hydroxybutyrate as an enzyme-protective agent against heating and oxidative damage and its potential role in stress response of poly(3-hydroxybutyrate) accumulating cells. *Applied Microbiology and Biotechnology* **2016**, 100, 1365–1376.

CrossMark

APPLIED MICROBIAL AND CELL PHYSIOLOGY

Evaluation of 3-hydroxybutyrate as an enzyme-protective agent against heating and oxidative damage and its potential role in stress response of poly(3-hydroxybutyrate) accumulating cells

Stanislav Obruca[1] · Petr Sedlacek[1] · Filip Mravec[1] · Ota Samek[2] · Ivana Marova[1]

Abstract Poly(3-hydroxybutyrate) (PHB) is a common carbon- and energy-storage compound simultaneously produced and degraded into its monomer 3-hydroxybutyrate (3HB) by numerous bacteria and *Archae* in a metabolic pathway called the PHB cycle. We investigated 3HB as a chemical chaperone capable of protecting model enzymes, namely lipase and lysozyme, from adverse effects of high temperature and oxidation. Heat-mediated denaturation of lipase in the presence or absence of 3HB was monitored by dynamic light scattering (DLS) revealing a significant protective effect of 3HB which increased as its concentration rose. Furthermore, when compared at the same molar concentration, 3HB showed a greater protective effect than the well-known chemical chaperones trehalose and hydroxyectoine. The higher protective effect of 3HB was also confirmed when employing differential scanning calorimetry (DSC) and lysozyme as a model enzyme. Furthermore, 3HB was capable of protecting lipase not only against thermal-mediated denaturation but also against oxidative damage by Cu^{2+} and H_2O_2; its protection was higher than that of trehalose and comparable to that of hydroxyectoine. Taking into account that the PHB-producing strain *Cupriavidus necator* H16 reveals a 16.5-fold higher intracellular concentration than the PHB non-producing mutant *C. necator* PHB^{-4}, it might be expected that the functional PHB cycle might be responsible for maintaining a higher intracellular level of 3HB which, aside from other positive aspects of functional PHB metabolism, enhances stress resistance of bacterial strains capable of simultaneous PHB synthesis and mobilization. In addition, 3HB can be used in various applications and formulations as an efficient enzyme-stabilizing and enzyme-protecting additive.

Stanislav Obruca and Petr Sedlacek contributed equally to this work.

✉ Stanislav Obruca
Stana.O@seznam.cz

1 Materials Research Centre, Faculty of Chemistry, Brno University of Technology, Purkynova 118, 612 00 Brno, Czech Republic

2 Institute of Scientific Instruments, v.v.i., Czech Academy of Sciences, Kralovopolska 147, 612 64 Brno, Czech Republic

Introduction

Bacteria have successfully colonized every niche on the planet. In this vast range of different environments, bacterial cells are exposed to wildly fluctuating environmental conditions such as changes in temperature, pH, redox potential, and osmolality. To ensure survival in the face of such adversity, bacteria have developed sophisticated systems combining various strategies (Marles-Wright and Lewis 2007). One of the most common stress-response strategies widely distributed among halophiles as well as thermophiles and hyperthermophilles is accumulation of compatible solutes. These low molecular weight compounds are zwitterionic, non-charged, or anionic and are represented by various classes of organic compounds including polyols, sugars, amino acids and their derivatives, betaines, and ectoines and their derivatives (Van-Thuoc et al. 2013). Apart from their osmotic function, these molecules are also capable of protecting proteins, other labile biomolecules, and cells as well from the

Springer

deleterious effects of a wide range of environmental stresses such as heat, chemical agents (Goller and Galinski 1999), freezing and thawing (Barth et al. 2000), oxidative damage (Andersson et al. 2000), proteolysis (Kolp et al. 2006), or the effect of extreme pH (Van-Thuoc et al. 2013); hence, they are also termed chemical chaperones. The mechanism of their protective action is not clearly understood, but it is generally believed that they influence the hydration shell around proteins and other biomolecules. In fact, it is likely that there is no universal mode of action for all compatible solutes (Jain and Roy 2009). Nevertheless, due to their capability to protect cells as well as biomolecules from a wide array of stress conditions, compatible solutes have found many applications in industrial biotechnology, molecular biology, and biomedicine (Pastor et al. 2010).

Poly(3-hydroxybutyrate) (PHB) is a polyester accumulated in the form of intracellular granules by a wide variety of taxonomically different groups of microorganisms. The biosynthesis and degradation of intracellular PHB occur in cells simultaneously. Therefore, metabolism of PHB reveals a cyclic mechanism (Kadouri et al. 2005). It is generally proposed that PHB serves primarily as a carbon- and energy-storage material when extracellular substrates are exhausted. However, there are reports that the capability of PHB accumulation and degradation also enhances the resistance of bacterial cells to high temperatures (Wu et al. 2011; Iustman et al. 2015), low temperatures and freezing (Pavez et al. 2009; Iustman et al. 2015), or oxidative stress (Goh et al. 2014; Iustman et al. 2015). The mechanisms by which the PHB cycle favors stress alleviation are not yet fully understood. The granules may offer physical protection under various stress conditions, but normally functioning PHB anabolic and catabolic pathways seem to be essential in providing increased stress protection (Kadouri et al. 2005). It was found that intensive intracellular degradation of PHB raises intracellular levels of both ATP and guanosine tetraphosphate. The former is known to be an inducer of the expression of the stationary phase regulator RpoS which further activates the expression of genes providing cross-protection against various stresses (Ruiz et al. 2001).

Furthermore, it seems that also, the main product of intracellular degradation of PHB—3-hydroxybutyrate (3HB)—might play an additional role in the stress response of bacteria. The function of 3HB as a compatible solute of the deep-sea bacterium *Photobacterium produndum* was demonstrated by Martin et al. (2002), and more recently, Soto et al. (2012) reported that 3HB serves as a compatible solute also in *Pseudomonas* sp. CT13, protecting the cells from protein aggregation under combined salt and thermal stress.

In this study, the protective effect of 3HB against high temperature as well as oxidative damage was investigated using lipase and lysozyme as model enzymes. Furthermore, trehalose and hydroxyectoine—well-established protein-stabilizing agents produced intracellularly by many microorganisms (Van-Thuoc et al. 2013)—were also included in the study. The denaturation of model enzymes and the protective effects of tested solutes were studied using dynamic light scattering (DLS), differential scanning calorimetry (DSC), and activity assays. Furthermore, intracellular levels of 3HB in PHB accumulating and non-accumulating strains of *Cupriavidus necator* were determined, taking into account the potential role of PHB granules and the PHB cycle as a source of very potent chemical chaperones.

Materials and methods

Materials and microorganisms

Hydroxyectoine, trehalose, 3-hydroxybutyrate, 1,3-butanediol, sodium butyrate lipase from *Rhizopus oryzea*, lysozyme from chicken egg white, and hydrogen peroxide were purchased from Sigma-Aldrich, Germany. Sodium succinate was obtained from LachNer, Czech Republic. *C. necator* H16 (CCM 3726) was obtained from the Czech Collection of Microorganisms, Brno, Czech Republic. The PHB non-producing strain *C. necator* PHB^{-4} (DSM-541) was purchased from Leibnitz Institute DSMZ-German Collection of Microorganism and Cell Cultures, Braunschweig, Germany.

Dynamic light scattering

Dynamic light scattering analyses of the solutions of lipase (3 mg/mL) in a 100-mM phosphate buffer of pH 7.4 were performed on a ZetaSizer Nano ZS (Malvern Instruments Ltd., UK) using a 4-mW He-Ne laser with an incident beam of wavelength 633 nm. Samples were carefully degassed by means of a firm vacuum generated manually in a glass syringe, filtered through a 0.45-μm millipore filter, and measured in glass cuvettes. Each measurement was repeated three times—the results are presented as an average value and error bars represent the corresponding standard deviations. Temperature trends were collected automatically by the analyzer; a sample was always left to equilibrate at the intended temperature for 90 s prior to data collection.

To investigate the protective effect of 3HB against oxidative damage, solutions of lipase (3 mg/mL) in aqueous solutions of $CuSO_4$ (1 mM) were prepared in the presence (1000 mM) or absence of 3HB. Samples of the solutions were further treated in a similar way. Manual DLS measurement of the particle size was performed at desired time intervals.

Differential scanning calorimetry

Thermal analysis was performed using a modulated differential scanning calorimeter (DSC Q2000, TA Instruments, DE). Phase transitions of mercury and indium were used for the

calibration in the applied temperature range. Solutions of lyso-zyme in the presence or absence of the respective co-solute (trehalose, hydroxyectoine, sodium 3-hydroxybutyrate, 1,3-butanediol, sodium butyrate, sodium succinate) were prepared by dissolving a specific amount of the corresponding solid substance in a phosphate buffer of pH 7.4. The solution was carefully degassed by means of a firm vacuum generated manually in a glass syringe, filtered through a 0.45-μm millipore filter, placed in aluminum pans, and sealed hermetically. The temperature protocol proposed by Badkar et al. (2006) for characterization of model protein formulations was applied in the calorimetric analyses. DSC analysis was carried out in the modulated heat-only mode; samples were scanned in a temperature interval of 30–100 °C at an underlying heating rate of 2 °C/min and modulation amplitude of 0.5 °C every 100 s. The data was analyzed using the TA Universal Analysis 2000 software, and onset and peak temperatures of the unfolding endotherm were determined automatically using the peak sigmoidal horizontal extrapolation method. Mean uncertainty of the resulting temperatures was estimated on the basis of repetitive (5×) measurement of lysozyme solution without addition of any protectant. The relative uncertainty is 0.5 %.

Screening of heat treatment and oxidation on residual lipase activity in the presence of 3HB

Samples of lipase (0.4 mg/mL) in a 100*mM phosphate buffer of pH 7.4 were prepared in the presence (50 and 100 mM) or absence of 3HB. The heat-stabilizing effect of 3HB on lipase was studied by incubating the samples at 50, 55, and 60 °C. The samples were taken at 10, 20, and 30 min of incubation for determination of residual enzyme activity.

The stabilizing effect of 3HB on oxidative damage to lipase was investigated as described by Andersson et al. (2000). The samples of lipase in the presence or absence of 100 mM 3HB were exposed to either 100 μM $CuSO_4$ or 10 mM H_2O_2. The samples were kept at 30 °C and aliquots were taken at different time intervals to determine residual activity. Similarly, protective effect of 3HB, trehalose, and hydroxyectoine was compared by exposing lipase to 100 μM $CuSO_4$ or 10 mM H_2O_2 in the presence (100 mM) or absence of these solutes. Residual activity was recorded after 24 h of incubation at 30 °C.

The enzyme activity of lipase samples was determined spectrophotometrically according to the established procedure described by Pinsirodom and Parkin (2001) with a slight modification. The assays were performed in standard 96-well microplates, and the reaction mixture consisted of 230 μL of a 100-mM phosphate buffer of pH 7.4, 25 μL of 420 μM p-nitrophenyl palmitate substrate solution and 25 μL of suitable diluted enzyme solution. The reaction was started by addition of substrate. The formation of the product (p-nitrophenol) at 40 °C was followed at 405 nm using a microplate reader ELx808, Biotek. Under the specified conditions, 1 unit of enzyme activity was defined as the amount of enzyme releasing 1 μmol of the product per minute. All the analyses were performed in triplicates.

Cultivations and determination of intracellular PHB and 3HB

Erlenmeyer flasks (volume 250 mL) containing 100 mL of mineral salt (MS) medium (composition of MS medium: 20 g fructose, 3 g $(NH_4)_2SO_4$, 1 g KH_2PO_4, 11.1 g $Na_2HPO_4·12$ H_2O, 0.2 g $MgSO_4$, 1 mL of microelement solution, and 1 L of distilled water; the microelement solution was composed of 9.7 g $FeCl_3$, 7.8 g $CaCl_2$, 0.156 g $CuSO_4·5$ H_2O, 0.119 g $CoCl_2$, 0.118 g $NiCl_2$ in 1 L of 0.1 M HCl) were inoculated by 5 mL of the overnight culture of a particular strain of *C. necator* grown in nutrient broth medium (NB medium, 10 g peptone, 10 g beef extract, 5 g NaCl in 1 L of distilled water). After 72 h of cultivation, the cells were harvested (centrifugation, 8000×g, 5 min) and the biomass, PHB content, and intracellular concentration of 3HB were determined.

The biomass concentration was measured gravimetrically and the PHB content of cell biomass was analyzed by GC-FID as reported previously (Obruca et al. 2014). To determine the intracellular level of 3HB, the cells were suspended in a 100-mM Tris-HCl buffer (pH 8.5) and disrupted by sonication (Sonopuls HD 3200, Bandeline, Germany) at 4 °C, cytosol was separated from the cell debris by centrifugation (10,000×g, 20 min., 4 °C), and 3HB concentration in the supernatant was determined using a β-Hydroxybutyrate Colorimetric Assay Kit purchased from Cayman Chemical following the manufacturer protocol. Quantification of protein in supernatants was performed by Hartree-Lowry assay. The cultivations were performed in duplicates and the analyses in triplicates.

Results

Protective effect of 3HB against thermal unfolding of lipase studied by DLS

Heat-induced denaturation of proteins is commonly probed by techniques which monitor changes in the molecular size resulting from the unfolding of the protein tertiary structure (Mitra et al. 2007). Therefore; we performed a dynamic light scattering analysis of the thermal denaturation of the lipase and of how it is influenced by the presence of 3HB. In order to determine the melting point of a corresponding solution of lipase, DLS analysis was repeated at increasing temperature ranging from 45 to 70 °C. It was confirmed that thermal denaturation of lipase is easily detected by this technique because an unfolding of its molecules is associated with a significant shift of particle size distribution toward higher values (a comparison of volume-weighted particle size distributions

at 45 and 65 °C is provided as Fig. S1 in the supplementary information). In particular, heating of a lipase solution resulted in an increase of the particle sizes by more than two orders of magnitude.

Figures 1 and 2 show the dependences of lipase solution size parameters on temperature. Two different size parameters were derived from the DLS correlation functions: Z-average and volume-based mean particle diameter (often referred to as the "volume mean diameter"), respectively. These parameters provide a complementary perspective on the system. The Z-average is the primary and most stable parameter which considers all the particle sizes in the system and is defined in quality control setting (ISO 13321, ISO 22412). On the other hand, weighting the relative proportion of multiple components in the system on their volume simplifies monitoring of processes associated with a significant increase in the hydrodynamic size of the particles present. It can be seen in Figs. 1 and 2 that the heat-induced increase in a volume mean diameter is steeper as compared to the corresponding Z-average value and allows more precise estimation of the specific melting point of the protein.

Significant enhancement of the thermal stability of lipase (3 mg/mL) in the presence of 3HB is evident from the results shown in Fig. 1. This stability enhancement increases with increasing concentration of 3HB in the system. Surprisingly, as it is evident from the results shown in Fig. 2, the protective effect of 3HB is even higher than the similar effect of trehalose and hydroxyectoine (applied at 1000 mM) (Fig. S4 shows the experiment with protectants applied at 200 mM) as the model compatible solutes. In particular, while the unfolding of lipase in the absence of 3HB occurs at about 49 °C (see Fig. 2), 1000 mM of 3HB in the solution shifts the unfolding point by more than 5 °C. Similar results were obtained also for higher concentration of lipase in the solution (30 mg/mL, data not shown). Nevertheless, for lipase solutions at the higher concentration, characteristic Z-shaped trends like those presented in Figs. 1 and 2 were deformed by a significant sedimentation of heavy aggregates of denatured lipase at temperatures above the corresponding unfolding point.

In the similar way, an effect on the thermal stability of lipase was determined by means of DLS also for three other substitutes of four-carbon-based water-soluble compounds, i.e., for 1,3-butanediol, sodium butyrate, and sodium succinate. Figure 2c, d shows the comparison of these results at 1000 mM concentration of the respective solute. It is evident that the significant enhancement of the thermal stability of lipase was confirmed only for 3HB and succinate, i.e., for the compounds which contain carboxylate group in combination with another hydrophilic group in their molecular structure. Contrarily, the presence of 1,3-butanediol in the solution led to a significant destabilization of lipase. The temperature dependences of volume mean diameters, presented in Fig. 2d, also show that the presence of butanediol and butyrate

enhances an aggregation of unfolded lipase followed by sedimentation of the formed aggregates (see the reverse U shape of the corresponding dependences).

Screening of heat treatment residual lipase activity in the presence of 3HB

In a further experiment, residual enzymatic activity of lipase was recorded in the presence or absence of 3HB during incubation at 50, 55, and 60 °C (Fig. 3). The stabilizing effect of 3HB was tested at two concentration levels: 50 and 100 mM. In agreement with the data obtained by DLS, the lipase started to lose activity when incubated at a temperature above 50 °C. Furthermore, 3HB revealed significant protective effects; residual lipase activity was higher in the presence of 3HB than in a sample without 3HB at 50 and 55 °C and in the case of 100 mM 3HB also at 60 °C. When comparing both concentration levels of 3HB, surprisingly, higher residual activity was at 50 and 55 °C observed in a lower concentration of 3HB, only at 60 °C 100 mM 3HB showed a higher protective effect than 50 mM 3HB.

3HB as a protectant of lysozyme as seen by DSC

For the calorimetric study, chicken-egg lysozyme was proposed as a model enzyme. The heat-induced denaturation of this protein is well examined (Badkar et al. 2006) and shows a corresponding heat flow high enough to be recorded by DSC instruments. In other words, the use of a special microcalorimetry technique is not necessary, unlike other common proteins. A typical MDSC record for a buffer solution of lysozyme (20 mg/mL, see Fig. S2 in the supplementary information) shows an obvious endothermic event with a peak value at 71 °C. This event can be attributed to the lysozyme unfolding; absorption of the energy is associated with breaking non-covalent interactions during disruption of the coiled protein structure. This finding is in agreement with the experiment published by Badkar et al. (2006). A great advantage of the applied MDSC technique in comparison with conventional DSC is that it allows separation of the total heat flow signal into a reversing and non-reversing component. This separation confirmed that the observed endothermic transition is completely of a reversible nature. No significant irreversible event (e.g., an aggregation of the unfolded proteins) was detected in contrast to the previously published experiment (Badkar et al. 2006).

Analogically to the lipase unfolding study, an obvious increase in the thermal stability of the lysozyme was found in the presence of 3HB. Figure 4 shows temperature trends of the reversing heat capacity of various aqueous mixtures of lysozyme (20 mg/mL) and 3HB (0–2000 mM). It is evident that the excess heat capacity peak, which corresponds to the lysozyme unfolding, is gradually shifted to the higher

Fig. 1 Effect of thermal unfolding of lipase on size parameters determined by DLS. Comparison of data for lipase solution in buffer with various concentrations of 3HB. Data was evaluated in terms of Z-average (**a**) and volume mean diameter (**b**)
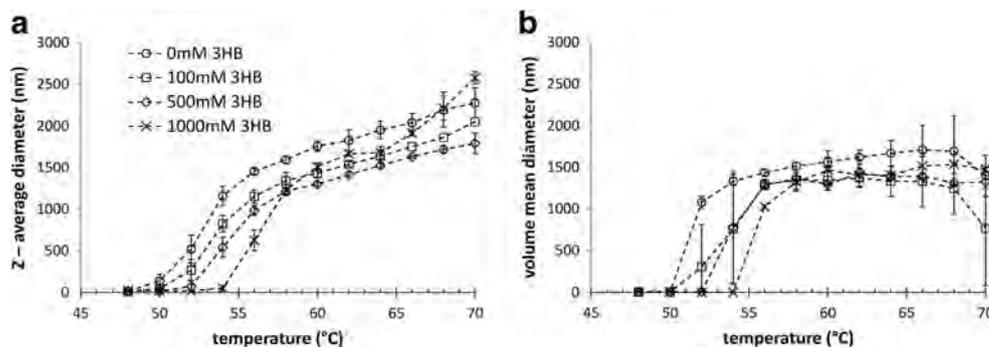
temperatures with increasing concentration of 3HB. In the concentration range studied here, the onset temperature of the unfolding transition increased almost linearly with the concentration from 65 °C to above 72 °C (corresponding onset and peak temperatures are shown in 4). With respect to the estimated mean uncertainty of the DSC experiment (see above), the determined increases in denaturation temperatures are significant for all the tested concentrations of 3HB.

Once again, in comparison with experimentally tested representatives of well-known compatible solutes (trehalose and hydroxyectoine), 3HB was proved to provide at least a comparable or even better protective effect (see Fig. 5 and Fig. S5). Except for 200 mM solution of hydroxyectoine (Fig. S5), the increase of the onset and peak temperatures of the denaturation endotherm was significant for all the tested solutes at both concentrations. Furthermore, the observed shift of the unfolding temperature is of a similar value as reported by Santoro et al. (1992) for naturally occurring glycine-based osmolytes of the same concentration. Furthermore, in order to verify the effect of molecular
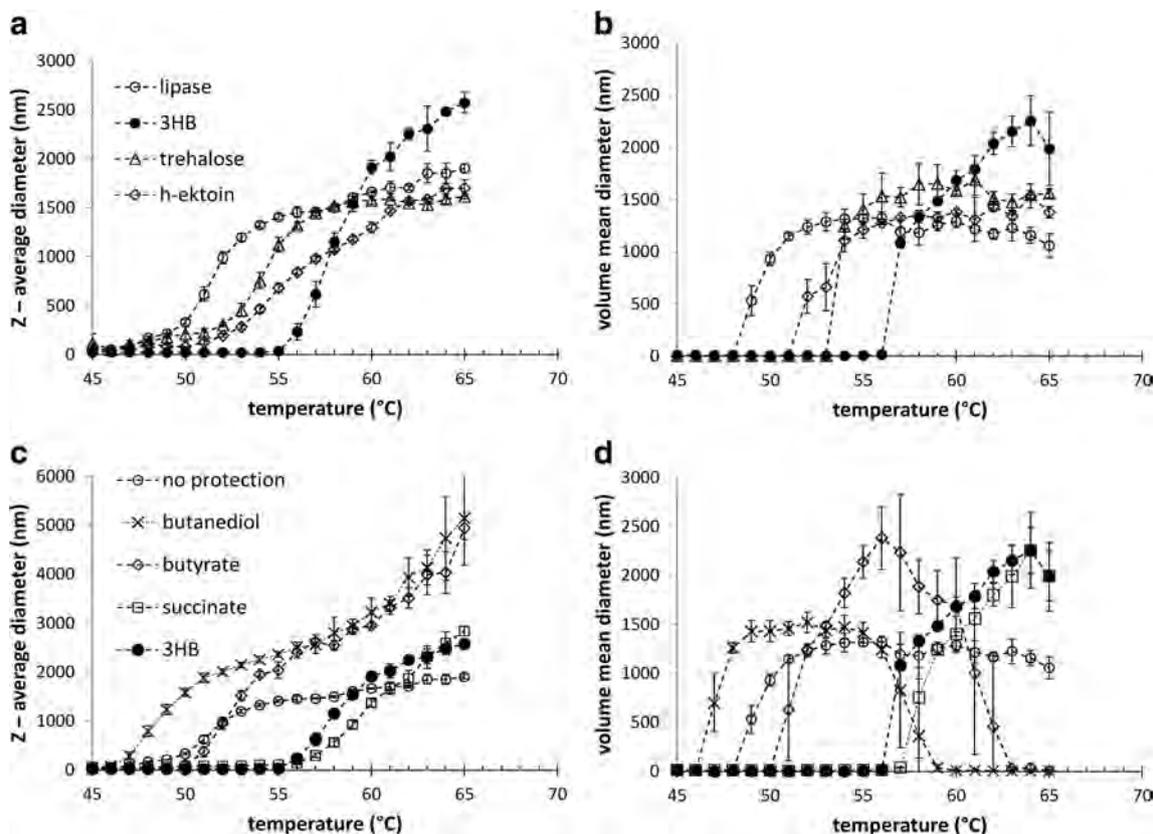
Fig. 2 Effect of 3HB, trehalose and hydroxyectoine (**a, b**) and 3HB, 1,3-butanediol and butyrate (**c, d**) on thermal-induced increase in the particle size of lipase solutions. Studied solutes were applied at 1000 mM concentration. Data was evaluated in terms of Z-average (**a, c**) and volume mean diameter (**b, d**)

Fig. 3 **a** Residual activity of lipase exposed for 10 min to 50, 55, and 60 °C and **b** time development of residual activity of the lipase exposed to 55 °C
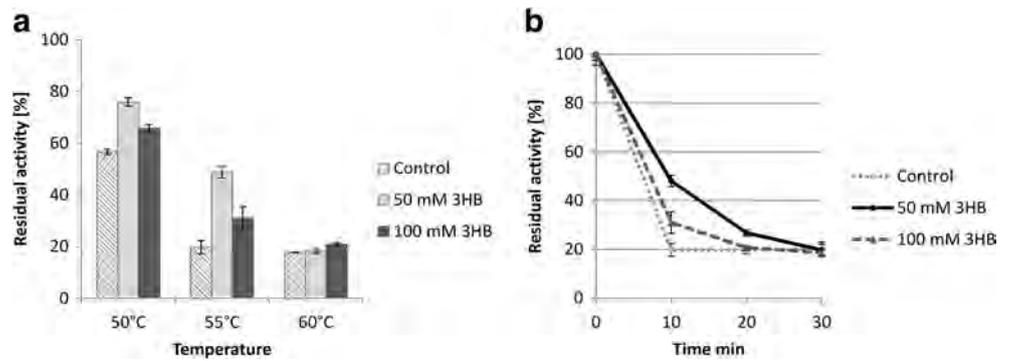
structure of the additive on the thermal stability of proteins, indicated by the foregoing DLS experiments, the DSC analysis was performed also for the structural analogues of the 3HB, i.e., for 1,3-butanediol, sodium butyrate, and sodium succinate at concentration of 1000 mM. Comparison of the unfolding temperatures of lysozyme, determined for the presence of these four-carbon-based additives, is shown in Fig. 5c, d. Again, it is evident that only 3HB and succinate provided a protective effect while the presence of 1,3-butanediol and butyrate caused a significant thermal destabilization of lysozyme. Hence, the unique role of carboxylate group in combination with another hydrophilic functionality was confirmed both by the DLS and DSC experiments.

Protective effect of 3HB of lipase against oxidative damage

To investigate the protective potential of 3HB against oxidative damage of proteins, lipase was exposed to the selected model oxidative agents Cu^{2+} and H_2O_2 for 24 h in the presence or absence of 3HB, and residual lipase activity was assayed during the incubation (Fig. 6). The enzyme lost its

activity in the presence of 10 μM Cu^{2+} more rapidly than in the presence of 10 mM H_2O_2. The residual activity of lipase was always higher in the presence of 3HB regardless of the oxidizing agent used, which indicates that 3HB can not only serve as a protective agent against heat denaturation, but it can also protect enzymes from oxidative damage.

The protective effect of 3HB was demonstrated also by the corresponding DLS study, where the long-term monitoring of the particle size distributions in lipase solutions with an addition of Cu^{2+} alone and the mixture of Cu^{2+} and 3HB, respectively, was performed. The corresponding volume-weighted particle size distributions in the solutions after 90 h are shown in Fig. S3 in the supplementary information. Again, oxidative damage caused by Cu^{2+} was associated with an obvious lipase unfolding; the peak size in the volume-weighted distribution was shifted to almost the same extent as in the case of heat-induced denaturation. Nevertheless, compared to lipase solution at the temperature above the melting point, the particle size distribution of the lipase solution with the addition of Cu^{2+} is obviously wider, which signalizes the higher polydispersity of the
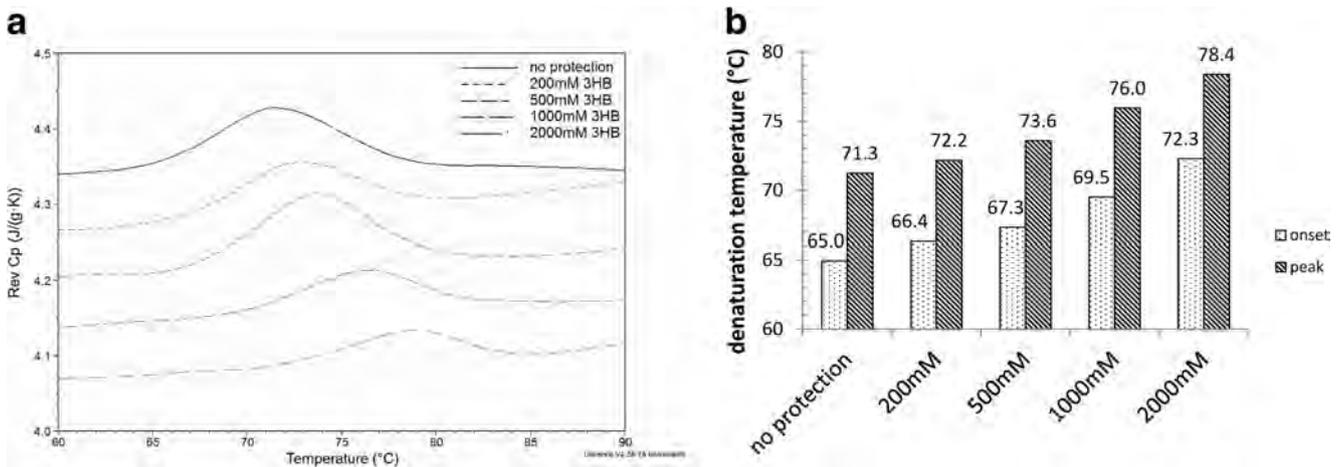
Fig. 4 **a** DSC signals showing thermal denaturation of lysozyme at different concentrations of 3HB (*curves* are offset for clarity). Thermoprotective effect is illustrated by the shift of the denaturation

peak to higher temperatures. **b** Comparison of onset and peak points of the denaturation peak for lysozyme protected with different concentrations of 3HB
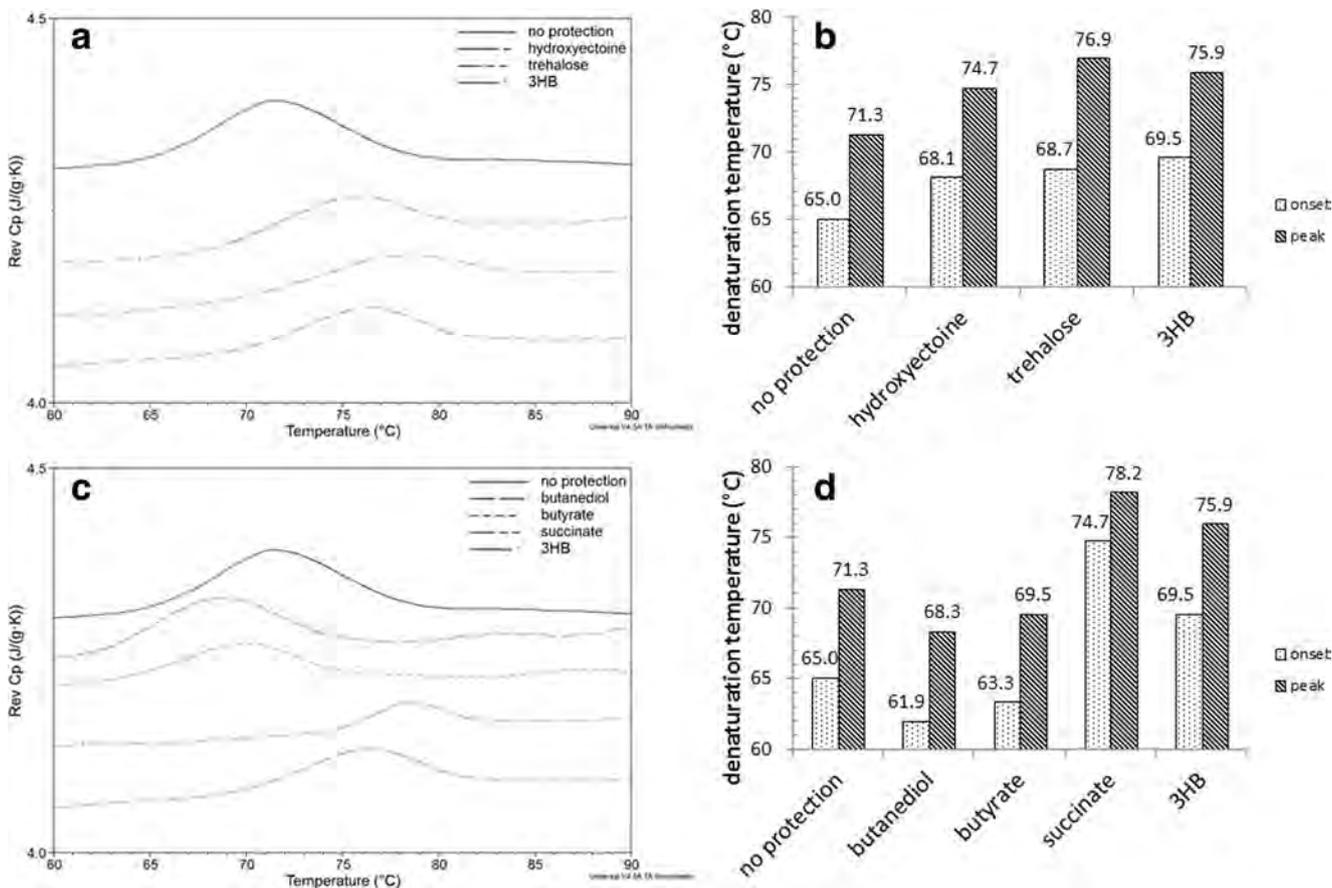
Fig. 5 DSC signals showing thermal denaturation of lysozyme comparing thermoprotective effect of 3HB, trehalose and hydroxyectoine at 1000 mM (**a**) and 3HB, 1,3-butanediol, butyrate, and succinate at 1000 mM, respectively (**c**); *curves* are offset for clarity.

Comparison of onset and peak points of the denaturation peak for lysozyme protected by 3HB, trehalose, and hydroxyectoine at 1000 mM (**b**) and 3HB, 1,3-butanediol, butyrate, and succinate at 1000 mM, respectively (**d**)

system where completely unfolded lipase molecules may coexist with the folded and partially unfolded ones.

The abovementioned difference points to the different course of the two denaturation processes; while the heat-

Fig. 6 Protective effect of 3HB against oxidative damage of lipase. Residual enzyme activity of lipase was recorded during incubation with 10 mM or 100 μM H_2O_2 Cu^{2+} in the presence or absence of 100 mM 3HB
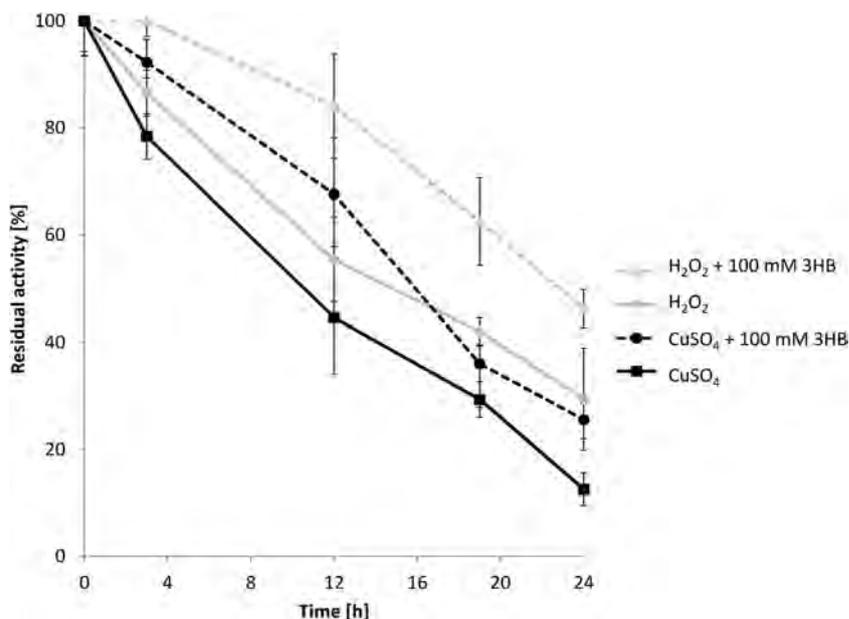
induced unfolding represents a fast, thermodynamically driven process which proceeds in an *all-or-nothing* manner, unfolding induced by Cu^{2+} is significantly slower and different lipase molecules are exposed to this conversion to a different extent. Different kinetics of the two processes are implied also from the comparison of Figs. 3b and 6, where a significant residual activity of lipase after the oxidative attack is evident even after 24 h, while the activity falls after the heat-induced denaturation in a matter of minutes. Furthermore, Fig. 7 shows the time dependence of the Z-average particle size in the lipase solutions with the addition of Cu^{2+}. In the absence of 3HB, after the initial step-increase in the average particle size, attributed to the emergence of the first unfolded lipase molecules in the system, the Z-average particle size continues to increase gradually for the next several hours. On the other hand, when the 3HB is present in the solution, an increase in the particle size is significantly slower and the initial step-increase is missing.

In further experiment, the protective effect of trehalose, hydroxyectoine, and 3HB for proteins against oxidative damage was assayed using determination of residual activity of lipase after 24-h incubation with 10 μM $CuSO_4$ and 10 mM H_2O_2 in the presence (100 mM) and absence of these solutes (Fig. 8). Generally, all the tested compounds provided protection against both oxidizing agents; however, effect of trehalose was the less pronounced than that of 3HB or hydroxyectoine. On the other side, efficiency of 3HB and hydroxyectoine was comparable.

Determination of intracellular concentration of 3HB in PHB-producing and non-producing bacterial cells

To clarify the influence of a completed PHB cycle on intracellular concentration of 3HB in bacterial cells, we analyzed bacterial cells capable of PHB accumulation—*C. necator* H16 and *C. necator* PHB^{-4} which, due to mutation of the gene encoding for PHB synthase, is not capable of PHB accumulation (Raberg et al. 2014). After 72 h of cultivation, the PHB content in *C. necator* H16 culture reached 76 % of the cell dry weight, while the amount of PHB in *C. necator* PHB^{-4} cells was negligible (about 0.6 %). When comparing the intracellular level of 3HB, it seems that a functional PHB cycle helps to maintain a significantly higher intracellular pool of 3HB, because in the PHB-producing bacterial strain, the intracellular concentration of 3HB (0.607 μmol per mg proteins) was more than 16 times higher than in the PHB non-accumulating strain (0.037 μmol per mg proteins). Since intracellular concentration of proteins in cells is 200 mg/mL or even higher (Ellis 2001), we can roughly estimate intracellular concentration of 3HB in PHB-producing bacteria to be higher than 100 mM and lower than 10 mM in PHB non-producing bacterial strain.

Discussion

The question of how organisms adapt to life in a stressful environment is an area of current research interest. Biosynthesis and intracellular accumulation of compatible solutes is a common strategy widely adopted by many extremophiles to cope with adverse conditions. Along with balancing external osmotic pressure, compatible solutes stabilize biomacromolecules, especially proteins against denaturation induced by various stress factors such as heat, oxidative damage, and freezing. Although it is generally accepted that compatible solutes influence primarily the hydration shell of the proteins (Roberts 2005; Jain and Roy 2009; Pastor et al. 2010), the exact mechanism of the stabilizing effect has not yet been clearly explained. Bolen and Baskakov (2001) have proposed that the protective effect of osmolytes originates from their unfavorable interaction with the peptide backbone. Since more of the protein backbone surface is exposed to these interactions in the unfolded state, the native state of the protein is protected by the presence of osmolytes. Although this approach—often called *preferential exclusion theory*—is by far the most commonly employed in the explanation of the bioprotective role of osmolytes, alternative rationales such as the *vitrification* or *water-replacement theories* have been discussed in the recent literature as well (Jain and Roy 2009).

In this work, we investigated the protective effect of 3HB against two common stress factors, namely high temperature and oxidative damage, by employing the three different experimental approaches DLS, DSC, and enzyme activity assay. We have shown that 3HB is capable of protecting both lipase and lysozyme against heat denaturation. According to the DLS and DSC results, the protective effect of 3HB increases with its concentration. On the other hand, the highest residual lipase activity was observed when the enzyme was exposed to high temperature in the presence of a lower 3HB concentration. This observation implies that the increase in enzyme stability might be partially inversely proportional to enzyme activity. Van-Thuoc et al. (2013) reported that higher concentrations of hydroxyectoine partially decreased xylanase activity, suggesting that high concentration of compatible solutes may reduce enzymes' conformational flexibility and, in turn, their catalytic efficiency while increasing the stability.

Furthermore, we have compared the protective effect of 3HB with the protection provided by trehalose and hydroxyectoine, compatible solutes which are accumulated in the cytoplasm of numerous (micro)organisms including bacteria and are considered to be very potent and efficient protectants of biomolecules (Jain and Roy 2009; Pastor et al. 2010). Note that their protective effect is higher than that of other disaccharides, polyols, proline, or betaine (Borges et al. 2002). A comparison of the fundamental physico-chemical parameters of 3HB, trehalose, and hydroxyectoine is provided in Table S1 (supplementary information). Based on our results

Fig. 7 Time development of the particle size in lipase solution with the addition of CuSO₄ in the presence and absence of 100 mM 3HB
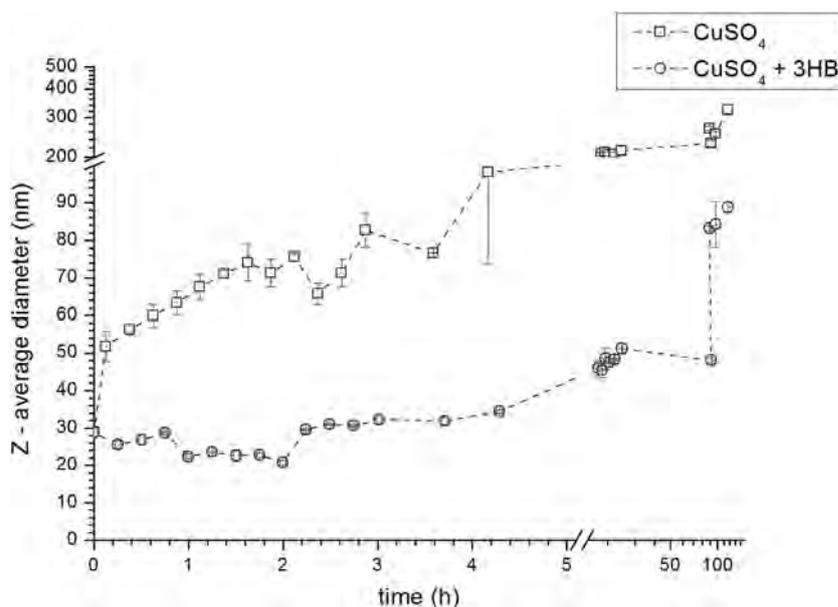
testing 3HB at the same concentration as trehalose and hydroxyectoine, we have found that 3HB showed the highest protective effect against heat denaturation of lipase and lysozyme (Figs. 2 and 5). Generally, it was observed that efficiency of protectant increases with presence of carboxylic acid group (Busby and Ingham 1984; Kaushik and Bhat 1999; Faria et al. 2008) which might explain superior protective efficiency of 3HB possessing carboxylic group to trehalose or hydroxyectoine which lacks this functional group. Hence, the protective effect of 3HB can be attributed to its chemical structure. To look more deeply into mechanism of protective effect

of 3HB, we have also tested protective activity of 1,3-butanediol, butyrate, and succinate. All these compounds consist of four-carbon atoms and contain various combination of the hydroxyl and carboxyl group. Neither butyrate (possessing only carboxyl group) nor 1,3-butanediol (possessing two hydroxyl group but no carboxyl group) revealed protecting effect for any of the tested model enzymes. Significant enhancement of the thermal stability of lipase as well as lysozyme was observed only for 3HB and succinate, i.e., for the compounds which contain carboxylate group in the combination with another hydrophilic group in their molecular structure. The fact

Fig. 8 Comparison of protective effect of 3HB, trehalose and hydroxyectoine against oxidative damage of lipase induced by 10 μM Cu²⁺ or 10 mM H₂O₂. Protectants were applied at concentration of 100 mM, and residual lipase activity was recorded after 24-h incubation of enzyme with particular oxidizing agent at 30 °C
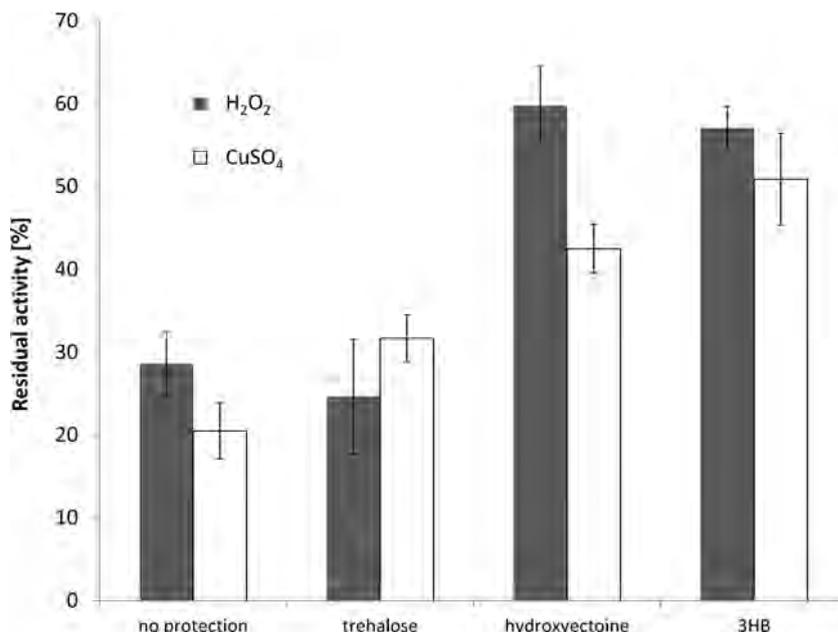
that succinate provided slightly higher protection of lipase (see Fig. 2) and significantly higher protection of lysozyme (see Fig. 5) is in good agreement with the abovementioned well-recognized protective efficiency of carboxylic acid group.

Oxidative damage of enzymes is one of the major protein degradation pathways in in vivo as well as in vitro. Oxidation can proceed spontaneously in air at ambient temperatures. However, it can be dramatically accelerated by trace amounts of metals or various oxidants such as reactive oxygen species and hydrogen peroxide. The metal-catalyzed oxidation is a site-specific process in which the amino acid residues located at the metal-binding sites are primary targets. On the contrary, hydrogen peroxide and other oxidative agents react with the polypeptide chain in a non-site-specific manner (Nguyen and Sok 2003). According to our results, 3HB is capable of protecting lipase against oxidative damage by metals as well as by hydrogen peroxide. It is to be expected that proteins will be shielded from oxidative damage by antioxidants or chelating agents. Nevertheless, there was evidence that also compatible solutes with no special antioxidant or chelating effects, such as hydroxyectoine, can partially protect enzymes from oxidative damage in vitro (Andersson et al. 2000), although the mechanism of this protection is not clear. According to our experimental results, 3HB provides significant oxidative protection as well and its protective efficiency is higher than that of trehalose and comparable to that of hydroxyectoine (Fig. 8). It is unlikely that hydroxyectoine or 3HB can undergo oxidation by H_2O_2 or Cu^{2+}, providing additional antioxidant effects (Witzemann 1926), and their chelating properties are also doubtful. Therefore, it is possible that the abovementioned changes in water structure in close vicinity to proteins caused by 3HB, hydroxyectoine, or other compatible solutes provide protective effects not only against heat but may also be capable of partial exclusion of the oxidative agents from the protein surface and of the corresponding protection of the amino acid residues against specific and non-specific oxidation.

Since enzymes are, due to their unique catalytic properties, widely used in various fields such as the chemical industry, food industry, medicine, or cosmetics, improvement of their shelf-life stability or regeneration/protection during biocatalytic process is of high concern (Jain and Roy 2009; Van-Thuoc et al. 2013). In order to increase enzymes' stability, several approaches including protein engineering or immobilization have been adopted. Nevertheless, the use of stabilizing additives is technically simple, fast, and cheap (Miyawaki et al. 2008; Van-Thuoc et al. 2013). For instance, Wang and Zhang (2010) report that supplementation of ectoine greatly improved the production of biodiesel by enzymatic conversion of triglycerides from cottonseed oil by using immobilized lipases. In our experiments, we confirmed that the lipase-protecting efficiency of 3HB is higher than that of hydroxyectoine, which is considered to be an even more prominent protectant than ectoine (Van-Thuoc et al. 2013),

suggesting that 3HB may serve as an additive improving enzyme stability in biodiesel production or other biotechnological processes. It is, however, a well-known fact that the stabilizing properties of solutes strongly depend on the enzyme under investigation (Goller and Galinski 1999).

Apart from the technological interest, the bioprotective effects of 3HB, demonstrated in the present work, raise significant questions about its possible involvement in natural cytoprotective mechanisms. An ability to accumulate poly(3-hydroxybutyrate) (PHB) is widely distributed among bacteria and Archae. PHB accumulation in the cells is a dynamic process of simultaneous synthesis and degradation, which is called the PHB cycle (Kadouri et al. 2005). Despite the fact that PHB is primarily considered as carbon- and energy-storage material, numerous studies have suggested its involvement in bacterial stress response, because mutant strains unable of either PHB synthesis (Kadouri et al. 2002; Ayub et al. 2007, 2009; Zhao et al. 2007) or PHB degradation (Ruiz et al. 2001; Kadouri et al. 2003) revealed significantly lower resistance against various stress factors. Therefore, it seems that a disruption of PHB cycle reduces the stress resistance of bacteria. The mechanisms for how the bacterial capability of intracellular PHB accumulation and degradation influence the stress resistance of bacterial cells are not clear. Ayub et al. (2007) have reported that PHB is essential for maintenance of redox state in the Antarctic bacterium Pseudomonas sp. 14-3 at low temperature. The presence of PHB granules might represent physical protection against mechanical damage of bacterial cells (Kadouri et al. 2005), and it has been suggested that PHB granules may also serve as a specific site for binding of the stress-resistant protein, which enhances bacterial stress tolerance (Goh et al. 2014). Furthermore, there are several articles dealing with connection of polyhydroxyalkanoates (PHA, family of bacterial polyesters which includes PHB), production and/or degradation with enhanced levels of cellular alarmone ppGpp and alternative sigma factor RpoS which increases the expression of general stress response-associated genes (Ruiz et al. 2001; Iustman and Ruiz 2008; Brigham et al. 2012).

Our experimental data show that 3HB works as a chemical chaperone and with a protecting and stabilizing efficiency more than comparable to that of hydroxyectoine or trehalose. Therefore, our results could represent an additional piece in the puzzle of the complex role of PHB contribution to the stress resistance of bacteria. According to our results, a bacterial strain with a functional PHB cycle (C. necator H16) has a significantly higher intracellular level of 3HB than a mutant that is not capable of PHB synthesis (and therefore also degradation) (Table 1). We roughly estimated intracellular concentration of 3HB in PHB-producing bacteria to be higher than 100 mM and lower than 10 mM in PHB non-producing bacterial strain. Taking into account the protective ability of 3HB, this might significantly contribute to the higher stress

Table 1 Comparison of CDW, PHB content, and intracellular concentration of 3HB in PHB accumulating strain *C. necator* H16 and PHB non-accumulating strain *C. necator* PHB^{-4}

	CDW (g/L)	PHB content (wt% of CDW)	3HB (μmol/mg proteins)
Cupravidus necator H16	9.201±0.344	75.957±0.282	0.607±0.014
Cupravidus necator PHB^{-4}	2.005±0.093	0.599±0.050	0.037±0.012

Each value is an average of two independent cultivations and analysis of each sample was performed in triplicate. Results are represented as mean±standard deviation

CDW cell dry weight

resistance of bacterial cells capable of simultaneous PHB synthesis and degradation, which has been reported by numerous authors (Ruiz et al. 2001; Kadouri et al. 2002, 2003; Ayub et al. 2007, 2009; Zhao et al. 2007). The intracellular concentration of 3HB in PHB-producing cells is about two orders higher than is expected for succinate, citrate, and other similar organic acids harboring more than one carboxyl groups (Bennett et al. 2009) which might also provide significant protective effect.

Therefore, PHB can be considered not only as a carbon- and energy-storage material but also as a unique reserve of chemical chaperone. It should be noted that 3HB and its storage form PHB reveals completely different physico-chemical properties. 3HB is a well-soluble substance with interesting protective effects, but its presence in cell cytoplasm at high concentration might increase intracellular osmotic pressure as well as influence intracellular pH, and therefore partially inhibit cells' metabolism in a similar way as was suggested for ectoines by Van-Thuoc et al. (2013). On the contrary, PHB is completely insoluble, so it influences neither intracellular osmotic pressure nor pH.

We have previously observed that application of mild stress conditions stimulates PHB synthesis, but higher doses of stress factors resulted in PHB degradation (Obruca et al. 2010a, b). Hence, it can be expected that flux of substrates in PHB cycle is not dependent only on the availability of extracellular carbon substrate but also on other stress conditions which might stimulate PHB-containing cells to partially hydrolyse PHB granules in order to increase the 3HB level in cell cytoplasm. Furthermore, in most cases, compatible solutes are rather excreted than metabolized by the accumulating cells when stress conditions vanish (Roberts 2005). This might be another important advantage of 3HB, which can be simply reincorporated into PHB, providing a more efficient carbon and energy metabolic balance.

To sum up, the role of the PHB cycle as a source of potent chemical chaperone should be taken into account when considering the complex role of PHB in the stress response of bacteria. PHB is accumulated by a wide variety of bacteria and *Archae* including halophiles (Quillaguaman et al. 2010), where 3HB might serve as one component in a complex cocktail of compatible solutes. Nevertheless, we suppose that 3HB serves as a chemical chaperone also in non-extremophiles where it helps to face short-term exposure to various stress conditions including, but not limited to, heating and oxidative stress. Furthermore, thanks to its protective efficiency, 3HB can be used in various enzyme applications and formulations as an efficient stabilizing and protecting additive.

Compliance with ethical standards

Conflict of interest All authors declare that they have no competing interests.

Ethical approval This article does not contain any studies with human participants or animals performed by any of the authors.

References

Andersson MM, Breccia JD, Hatti-Kaul R (2000) Stabilizing effect of chemical additives against oxidation of lactate dehydrogenase. Biotechnol Appl Biochem 32:145–153

Ayub ND, Pettinari MJ, Mendez BS, Lopez NI (2007) The polyhydroxyalkanoate genes of a stress resistant Antarctic *Pseudomonas* are situated within a genomic island. Plasmid 58: 240–248

Ayub ND, Tribelli PM, Lopez NI (2009) Polyhydroxyalkanoates are essential for maintenance of redox state in the Antarctic bacterium *Pseudomonas* sp. 14–3 during low temperature adaptation. Extremophiles 13:59–66

Badkar A, Yohannes P, Banga A (2006) Application of T_{ZERO} calibrated modulated temperature differential scanning calorimetry to characterize model protein formulations. Int J Pharm 309:146–156

Barth S, Huhn M, Matthey B, Klimka A, Galinski EA, Engert A (2000) Compatible-solutes-supported periplasmic expression of functional recombinant proteins under stress conditions. Appl Microbiol Biotechnol 66:1572–1579

Bennett BD, Kimball EH, Gao M, Osterhout R, Van Dien SJ, Rabinowitz JD (2009) Absolute metabolite concentrations and implied enzyme active site occupancy in *Escherichia coli*. Nat Chem Biol 5:593–599

Bolen DW, Baskakov IV (2001) The osmophobic effect: natural selection of a thermodynamic force in protein folding. J Mol Biol 310:955–963

Borges N, Ramos A, Raven NDH, Sharp RJ, Santos H (2002) Comparative study of the thermostabilizing properties of

mannosylglycerate and other compatible solutes on model enzymes. Extremophiles 6:209–216

Brigham CJ, Speth DR, Rha CK, Sinskey AJ (2012) Whole-genome microarray and gene deletion studies reveal regulation of the polyhydroxyalkanoate production cycle by the stringent response in *Ralstonia eutropha* H16. Appl Environ Microbiol 78:8033–8044

Busby TF, Ingham KC (1984) Thermal stabilization of antithrombin III by sugars and sugar derivatives and the effects of nonenzymatic glycosylation. Biochim Biophys Acta 799:80–89

Ellis RJ (2001) Macromolecular crowding: obvious but underappreciated. Trends Biochem Sci 10:597–604

Faria TQ, Mingote A, Siopa F, Ventura R, Maycock C, Santos H (2008) Design of new enzyme stabilizers inspired by glycosides of hyperthermophilic microorganisms. Carbohydr Res 343:3025–3033

Goh L-K, Purama RK, Sudesh K (2014) Enhancement of stress tolerance in polyhydroxyalkanoate producers without mobilization of the accumulated granules. Appl Biochem Biotechnol 172:1585–1598

Goller K, Galinski EA (1999) Protection of a model enzyme (lactate dehydrogenase) against heat, urea and freeze-thaw treatment by compatible solutes additives. J Mol Catal B: Enzym 7:37–45

Iustman LJR, Ruiz JA (2008) The alternative sigma factor σ^s, affects polyhydroxyalkanoate metabolism in *Pseudomonas putida*. FEMS Microbiol Lett 284:218–224

Iustman LJR, Tribelli PM, Ibarra JG, Catone MV, Venero ECS, Lopez NI (2015) Genome sequence analysis of *Pseudomonas extremaustralis* provides new insights into environmental adaptability and extreme conditions resistance. Extremophiles 19:207–220

Jain NK, Roy I (2009) Effect of trehalose on protein structure. Protein Sci 18:24–36

Kadouri D, Burdman S, Jurkevitch E, Okon Y (2002) Identification and isolation of genes involved in poly(beta-hydroxybutyrate) biosynthesis in *Azospirillum brasilense* and characterization of a phbC mutant. Appl Environ Microbiol 68:2943–2949

Kadouri D, Jurkevitch E, Okon Y (2003) Poly beta-hydroxybutyrate depolymerase (PhaZ) in *Azospirillum brasilense* and characterization of a phaZ mutant. Arch Microbiol 180:309–318

Kadouri D, Jurkevitch E, Okon Y (2005) Ecological and agricultural significance of bacterial polyhydroxyalkanoates. Crit Rev Microbiol 31:55–67

Kaushik JK, Bhat R (1999) A mechanistic analysis of the increase in the thermal stability of proteins in aqueous carboxylic acid salt solutions. Protein Sci 8:222–233

Kolp S, Pietsch M, Galinski EA, Gutschow M (2006) Compatible solutes as protectants for zymogenes against proteolysis. Biochim Biophys Acta 1764:1234–1242

Marles-Wright J, Lewis RJ (2007) Stress responses of bacteria. Curr Opin Struct Biol 17:755–760

Martin DD, Bartlett DH, Roberts MF (2002) Solute accumulation in the deep-sea bacterium *Photobacterium profundum*. Extremophiles 6:507–514

Mitra RK, Sinha SS, Pal SK (2007) Hydration in protein folding: thermal unfolding/refolding of human serum albumin. Langmuir 23:10224–10229

Miyawaki O, Ma GL, Horie T, Hibi A, Ishikawa T, Kimura S (2008) Thermodynamic, kinetic, and operational stabilities of yeast alcohol dehydrogenase in sugar and compatible osmolyte solutions. Enzyme Microb Technol 43:495–499

Nguyen SD, Sok DE (2003) Oxidative inactivation of paraoxonase1, an antioxidant protein and its effect on antioxidant action. Free Radic Res 37:1319–1330

Obruca S, Marova I, Stankova M, Mravcova L, Svoboda Z (2010a) Effect of ethanol and hydrogen peroxide on poly(3-hydroxybutyrate) biosynthetic pathway in *Cupriavidus necator* H16. World J Microbiol Biotechnol 26:1261–1267

Obruca S, Marova I, Svoboda Z, Mikulikova R (2010b) Use of controlled exogenous stress for improvement of poly(3-hydroxybutyrate) production in *Wautersia eutropha*: a preliminary study. Folia Microbiol 55:17–22

Obruca S, Petrik S, Benesova P, Svoboda Z, Eremka L, Marova I (2014) Utilization of oil extracted from spent coffee grounds for sustainable production of polyhydroxyalkanoates. Appl Microbiol Biotechnol 98:5883–8590

Pastor JM, Salvador M, Argandona M, Bernal V, Reina-Bueno M, Csonka LN, Iborra JL, Vargas C, Nieto JJ, Canovas M (2010) Ectoines in cell stress protection: uses and biotechnological production. Biotechnol Adv 28:782–801

Pavez P, Castillo JL, Gonzales C, Martinez M (2009) Poly-β-hydroxyalkanoate exert protective effect against carbon starvation and frozen conditions in *Sphingopyxis chilensis*. Curr Microbiol 59:636–640

Pinsirodom P, Parkin KL (2001) Lipase assays. Curr Protocols Food Anal Chem C3.1.1-C3.1.13

Quillaguaman J, Guzman H, Van-Thouc D, Hatti-Kaul R (2010) Synthesis and production of polyhydroxyalkanoates by halophiles: current potential and future prospects. Appl Microbiol Biotechnol 85:1687–1696

Raberg M, Voigt B, Hecker M, Steinbuchel A (2014) A closer look on the polyhydroxybutyrate- (PHB-) negative phenotype of *Ralstonia eutropha* PHB-4. PLoS One 9, e95907

Roberts MF (2005) Organic compatible solutes of halotolerant and halophilic microorganisms. Saline Syst 1:5. doi:10.1186/1746-1448-1-5

Ruiz JA, Lopez NI, Fernandez RO, Mendez BS (2001) Polyhydroxyalkanoate degradation is associated with nucleotide accumulation and enhances stress resistance and survival of *Pseudomonas oleovorans* in natural water microcosm. Appl Environ Microbiol 67:225–230

Santoro MM, Liu YF, Khan SMA, Hou LX, Bolen DW (1992) Increased thermal-stability of proteins in the presence of naturally occurring osmolytes. Biochemistry 31:5278–5283

Soto G, Setten L, Lisi C, Maurelis C, Mozzicafreddo M, Cuccioloni M, Angeletti M, Ayub ND (2012) Hydroxybutyrate prevents protein aggregation in the halotolerant bacterium *Pseudomonas* sp. CT13 under abiotic stress. Exremophiles 16:455–462

Van-Thuoc D, Hashim SO, Hatti-Kaul R, Mamo G (2013) Ectoine-mediated protection of enzyme from the effect of pH and temperature stress: a study using *Bacillus halodurans* xylanase as a model. Appl Microbiol Biotechnol 97:6271–6278

Wang Y, Zhang L (2010) Ectoine improves yield of biodiesel catalyzed by immobilized lipase. J Mol Catal B: Enzym 62:90–95

Witzemann EJ (1926) The oxidation of alpha- and beta-hydroxybutyric acids with hydrogen peroxide. J Am Chem Soc 48:211–222

Wu D, He J, Gong Y, Chen D, Zhu X, Qiu N, Sun M, Li M, Yu Z (2011) Proteomic analysis reveals the strategies of *Bacillus thuringiensis* YBT-1520 for survival under long-term heat stress. Proteomics 11:2580–2591

Zhao YH, Li HM, Qin LF, Wang HH, Chen GQ (2007) Disruption of the polyhydroxyalkanoate synthase gene in *Aeromonas hydrophila* reduces its survival ability under stress conditions. FEMS Microbiol Lett 276:34–41

Appendix 22

S Slaninova, E., Obruca, S., Kocherbitov, V., and Sedlacek, P. On the bioprotective effects of sodium 3-hydroxybutyrate: thermodynamic study of binary Na3HB-water systems. *Submitted for publication*.

1 **On the bioprotective effects of sodium 3-hydroxybutyrate: thermodynamic**
2 **study of binary Na3HB-water systems.**

3 Eva Slaninova[1], Stanislav Obruca[1], Vitaly Kocherbitov[2,*] and Petr Sedlacek[1,*]

4 [1] Faculty of Chemistry, Brno University of Technology, Purkynova 118, 612 00 Brno, Czech
5 Republic.
6 [2] Biomedical Science, Faculty of Health & Society, Malmö University, SE-20506 Malmö,
7 Sweden
8 *   Correspondence: sedlacek-p@fch.vut.cz;   Tel.:   +420 541 149 486   [PS];
9 vitaly.kocherbitov@mau.se, Tel.: +46 70 7457220 [VK].

10 Abstract

11 Microorganisms must face various inconvenient conditions; therefore, they
12 developed several approaches how to protect themselves such as the accumulation of
13 compatible solutes, osmolytes etc. It was already proved that monomer units 3-
14 hydroxybutyrate (3HB) which are present in sufficient concentration in poly(3-
15 hydroxybutyrate) (PHB) accumulating cells, serve as a chemical chaperone protecting
16 enzymes against heat and oxidative stress and as cryoprotectant for enzymes,
17 bacterial cells, and yeast. However, the ability of cells to protect themselves is also
18 strongly dependent on the behavior and state of intracellular water, especially during
19 stress exposure. For a better understanding of the protective mechanism and effect of
20 strongly hydrophilic 3HB in solutions at a wide range of temperatures, a binary phase
21 diagram of system Na3HB-water in equilibrium and non-equilibrium was constructed.
22 To investigate the activity of water in various compositions of Na3HB-water system,
23 three experimental techniques have been used (dynamic water sorption analysis,
24 water activity measurements and sorption calorimetry). Firstly, Na3HB proved its great
25 hydrophilic nature even better than known compatible solutes (trehalose). In
26 combination with data from differential scanning calorimetry, phase diagrams
27 demonstrated Na3HB as highly effective to depress freezing point making a large
28 amount of non-frozen water (1.35 g water per g of Na3HB). Therefore, Na3HB
29 represents a very effective cryoprotectant that can be widely used for numerous
30 applications.

31 **Statement of Significance**
32 This study is focused on phase behavior of sodium hydroxybutyrate to explain its
33 unique cryoprotectivity. High hydrophilic affinity of Na3HB for water was proved in
34 comparison with common compatible solutes such as trehalose. Simultaneously,
35 based on obtained data, a phase diagrams of sodium 3-hydroxybutyrate-water
36 systems were constructed which showed that hydrophilic Sodium 3-hydroxybutyrate is
37 highly effective to depress freezing point of water solutions. That means, lower freezing
38 point of water solutions providing large amount of non-frozen water. These new results
39 of this study open various potential applications of utilization Na3HB.
40

41   **Keywords:** cryoprotectant; 3-hydroxybutyrate; sorption isotherm; phase diagram;
42   compatible solutes; differential scanning calorimetry

43   **Abbreviation**

44   CPA   Cryoprotectants

45   PHB   Poly(3-hydroxybutyrate)

46   3HB   3-hydroxybutyrate

47   Na3HB   Sodium 3-hydroxybutyrate

48   DSC   Differential scanning calorimetry

49   DVS   Differential Vapor sorption

50   **Nomenclature**

51   T_g glass transition temperature

52   T_m melting temperature

53   ΔH enthalpy of melting of Na3HB dihydrate

54   Δc_p heat capacity of glass transitions

55   MW_2 crystalline dihydrates of Na3HB

56    $M_{(anh)}$ anhydrous Na3HB

57

1. Introduction

Natural cryoprotectants (or cryo-protective agents, CPA) have been known since the 19th century when the earliest concepts of cryoprotection were established. Nowadays, cryobiology belongs to the essential field with high application in biotechnology and modern medicine where macromolecules, cell components and cells are protected against freezing and/or desiccation by cryoprotective additives. The presence of CPA stabilizes the activity of enzymes and promotes glassy state during freezing which is crucial for the viability of cells. CPA are generally classified as i. penetrating CPA (capable of diffusing through the plasma membrane) revealing common properties such as low molecular weight, high solubility, nontoxicity, etc., and ii. non-penetrating CPA which are generally long-chain polymers, also soluble in water with high osmotic coefficients [1, 2]. This division of CPA is closely related to the course of freezing, the penetrating CPA which are known as compatible solutes (e.g. glucose, sucrose, trehalose, glycerol etc.) are efficient for protection against slow freezing because of their great ability to mitigate damage considering osmotic changes. On the contrary, non-penetrating CPA (poly(vinyl alcohol), polyethylene glycol etc.) are suitable for protection against rapid freezing, they act as dehydration agents for reduction of an amount of intracellular water before cooling. Thus, the extent of the freeze-induced damage is dependent both on the rate of cooling and on concentrations of the intracellular and the extracellular solution, respectively. Generally, the dependence between the cooling rate and the cell survival is often expressed as an inverse-U function where the maximum cell survival at optimal cooling rate sharply falls down on both directions (Figure 1) [1-5]. Furthermore, many of the penetrating CPA (e.g. trehalose, ectoin, betaine) often combine the cryoprotection with shielding of labile cellular components against other environmental stress factors, including high temperature [6], oxidative damage [7] and/or extreme pH [8]. The mechanism of the universal protective performance of these compounds – often referred to as compatible solutes or chemical chaperones – is not clearly understood, nevertheless, it is believed that they are able to stabilize labile biopolymers (e.g. proteins) by affecting their hydration in the cell [1, 9]. Therefore, revealing how a biomolecule affects the activity of water in aqueous solutions seems to represent an essential step to evaluate or understand its bioprotective potential.

Microorganisms employ several approaches on how to protect themselves against various factors in the environment such as freezing and thawing, starvation, fluctuations in temperatures, UV exposure etc. One of the protective mechanisms which numerous strains of bacteria and such as *Cupriavidus necator* or *Rhodospirillum rubrum* and even some *Archaea* can use is the capability of production and accumulation of poly(3-hydroxybutyrate) (PHB) in a form of intracellular granules [10]. These PHB granules had been considered primarily as storage of energy and carbon (from 25 up to 91 % of cell dry weight), however, nowadays it was revealed that PHB plays a much more important metabolic role. For instance, in *R. rubrum* PHB metabolism helps to maintain intracellular redox potential [11]. Moreover, PHB granules belong to the highly investigated protectants against various stressors such as high temperature, osmotic shock, UV exposure or oxidative pressure etc. [12-14].

Nevertheless, the principle of such a wide range of protectivity of these compounds is based both on PHB metabolism and unique structural and physicochemical properties. In numerous cases, PHB monomer 3-hydroxybutyrate (3HB) plays its role. PHB granules are simultaneously biosynthesized and degraded, therefore, the metabolism of PHB is called PHB cycle. As a consequence of the PHB cycle, PHB accumulating microorganisms possess a high intracellular pool of 3HB monomers [15]. It was found that 3HB serves as a compatible solute protecting bacteria against the high salinity of the environment [16]. Moreover, it was also observed that 3HB serves as a chemical chaperone protecting lysozyme and lipase (representing model enzymes) against heat and oxidative stress [17]. In another report, 3HB was identified as a potential cryoprotectant for enzymes (lipase), yeast (*Saccharomyces cerevisiae*) and bacterial cells (*Cupriavidus necator*) [18]. The fact that PHB and 3HB might be involved in adaptation of prokaryotes is also indirectly suggested by the fact that numerous PHB producers were isolated from cold environments such as Antarctic freshwater [19], Antarctic soil [20], the Baltic Sea [21], Pangi-Chamba trans-Himalayan region [22] or other polar regions [23].

It is very unlikely that the recently revealed stabilizing effect of 3HB for biological samples under such fundamentally distinct stress conditions as cryo- and high temperatures, or in an oxidative environment, respectively, could be attributed to a single physical or chemical mechanism of protection. On the other hand, it is indisputable that the state of intracellular water plays an essential role under all of these circumstances. Protein stabilization by compatible solutes has most often been ascribed to the so-called preferential hydration phenomenon [1], which combines a general colligative decrease of water activity in a solution with a solute-specific preferential binding or exclusion of the solute molecules from the immediate surface of the protein. Thermodynamic model of the preferential exclusion of stabilizing solutes from the protein hydration layer was elaborated [24] and, furthermore, a structural concept was proposed which explains the phenomenon based on the structural distinction and different solvent properties of the hydration ("high-density") and the bulk ("low-density") water, respectively [25]. The role of water activity is even more obvious wherever the exposure to harmful conditions results in cell desiccation. This is provided not only by a high osmolality of the environment, but it also represents a severe harmful consequence of cell freezing under a slow cooling rate, where the formation of extracellular ice concentrates the solutes outside the cells which result in so-called "freeze-dehydration". On the other hand, cell freezing under higher cooling rates most often results in a cell injury *via* intracellular ice formation, once again strongly dependent on the thermodynamic state of the cellular water. Finally, a decrease in water availability is known to be accompanied by disruption of electron transfer systems and with an increased generation of reactive oxygen species resulting in oxidative stress manifestations such as metabolic enzyme inactivation and damage to membrane lipids and/or nucleic acids [26]. Bearing this essential role of water in mind, we decided to perform a complex study on the thermodynamics of 3HB/water system as an inevitable first step to a better understanding of stabilizing effects provided by 3HB. Two distinct experimental strategies were used for this purpose: first, hydration

of 3HB was studied using a combination of three different methods of sorption analysis, second, phase transitions in aqueous solutions of 3HB were studied *via* DSC under equilibrium and non-equilibrium conditions, respectively.

Hence, in the present work, we aim at investigating the interactions of sodium 3-hydroxybutyrate (Na3HB), PHB monomer, with water, especially at low and subzero temperatures. Understanding of behavior of Na3HB in water solutions is essential not only for revealing its cryoprotective potential, it might also contribute to understanding of its general protective action for various biomolecules and cells. Apart from its fundamental biological importance, this highly hydrophilic compound offers wide application potential in cryobiology, freeze-preservation of food and other biological materials etc. For the purpose of in-depth analysis of the protective mechanism of Na3HB, we decided to construct equilibrium and non-equilibrium phase diagrams of Na3HB-water system. Data were obtained by several techniques such as isothermal sorption calorimetry, differential calorimetry scanning (DSC), dynamic vapor sorption analysis, and water activity measurements.

2. Materials and Methods

2.1. Preparation of samples

Sodium 3-hydroxybutyrate (Na3HB) was obtained by Sigma-Aldrich with purity $\geq$ 99.0 % (NT), CAS Number 150-83-4. Before all hydration experiments, Na3HB was dried in vacuum in contact with 3 Å molecular sieves at least 24 hours at room temperature. Samples of various ratios of Na3HB and water were obtained either by direct pipetting of water to dried Na3HB or hydrated at a controlled relative humidity (RH) in desiccators with saturated salt solutions from several minutes to hours at 25 °C; The following salts were used: K_2SO_4 (97.3% RH), KCl (84.34% RH), NaCl (75.29% RH), $Mg(NO_3)_2$ (52.89% RH), $MgCl_2$ (32.78% RH) [27].

2.2. Determination of water activity

2.2.1. Dynamic vapor sorption

For vapor sorption analysis was used dynamic vapor sorption Q5000 SA (TA Instruments, the United States). Initially, the dried Na3HB sample was conditioned for 60 min at 60 °C at 0 %RH and then the %RH value was increased in the stepwise manner covering the range from 40 %RH to 70 %RH with 5 %RH step. At each %RH level, the sample was kept for 5 hours and its weight was recorded continuously. Only the data from %RH steps where the sample weight was equilibrated at the constant value were used for further evaluation. The DVS experiment was repeated for various temperatures (10; 15; 25; 40 °C). To determine the critical level of %RH, where the dry Na3HB begins to absorb the hydration water, the stepwise %RH tests described above increase was supplemented by the ramp test where the %RH level was increased linearly with the 0.1 %RH/min rate.

2.2.2. Static activity measurements with commercial water activity analyzer

The activity of water in the hydrated Na3HB samples with various water/Na3HB contents (prepared according to 2.1) was determined at 25 °C by commercial resistive electrolytic analyzer LabMaster-a_w (Novasina, Switzerland). Firstly, the analyzer was calibrated by commercial reusable SAL-T calibration standards.

2.2.3. Sorption calorimetry

Sorption calorimetry experiments were performed at 25 °C in the double twin calorimeter according to [28] where the dried samples of Na3HB were loaded into the upper chamber (called sorption chamber) and the lower chamber was filled with pure water. This method provides the values of water activity and the corresponding equilibrium water content in the sorbent (Na3HB) as calculated according to [29] from the thermal powers determined separately in both chambers of the twin calorimeter.

2.3. Differential Scanning Calorimetry (DSC)

Experiments with Na3HB containing different amounts of water were performed by differential scanning calorimeter (DSC 1 Mettler Toledo, Switzerland). For calibration of heat flow and temperature, indium in a hermetically sealed aluminum pan (mp 156.6 °C; ΔH = 28.45 J/g) and an empty sealed aluminum pan as a reference were used. As purge gas dry nitrogen with a gas flow 80 mL/min was used.

Firstly, samples were loaded into an aluminum pan, hermetically sealed and cooled down (10 °C/min) to a low temperature depending on the phase transitions we wanted to investigate. In the case of measurements related to phase diagram in equilibrium, we set the lowest temperature (-70 °C) in the method to avoid glass transition due to the previous optimization in contrast with setting up for phase diagram in no-equilibrium, where the lowest temperature was equal to -90 °C. For instance, the method proceeded as follows from 25 °C to -90°C and held for an equilibration time of 5 min, then heated up to 100 °C and cooled down back to low temperature and once more held at this temperature for 5 min. The whole method ran with a scan rate of 10 °C/min, however other scan rates (1, 2 and 5 °C/min) were used for samples to extrapolate the endset of melting of ice and melting of anhydrous Na3HB to zero scan rate. To get phase transitions from 42 to 65 wt% of Na3HB for phase diagram in equilibrium, scan rate was decreased into the limit of the device to 0.2 °C/min and equilibration time was 30 min when temperatures were chosen above the glass transition temperature. For evaluation, we used only second scans except for measurements with a scan rate of 0.2 °C/min.

3. Results and Discussion

3.1. Water sorption on 3-hydroxybutyrate

Sorption analysis was performed to evaluate the hygroscopicity of Na3HB at different hydration levels. Sorption isotherms (water activity as a function of water content in binary Na3HB/water systems), determined by three independent analytical techniques at 25°C, are shown in Fig. 2.a. Dynamic water sorption analysis (DVS) is a gravimetry technique based on determining the sample weight after its equilibration at a specific level of relative humidity (RH) of the controlled measuring atmosphere. Hereby, the corresponding equilibrium water contents in the sample are determined for different values of water activity (numerically equals to the relative humidity in % RH divided by 100). Furthermore, water activity was measured in step mode and continual increasing of relative humidity mode (Figure S1). The second applied experimental technique uses an opposite principle, i.e., the values of water activity were determined using commercial electric hygrometer LabMaster-aw (Novasina) for samples prepared with controlled water contents. And finally, the sorption microcalorimetry technique, whose instrumentation and methodology are described in detail elsewhere [29], enables simultaneous measurement of both the water activity (relative humidity) and the sample moisture content. Furthermore, as a modified calorimetric method, it also provides differential sorption enthalpy as an additional valuable parameter characterizing the water sorption process.

240
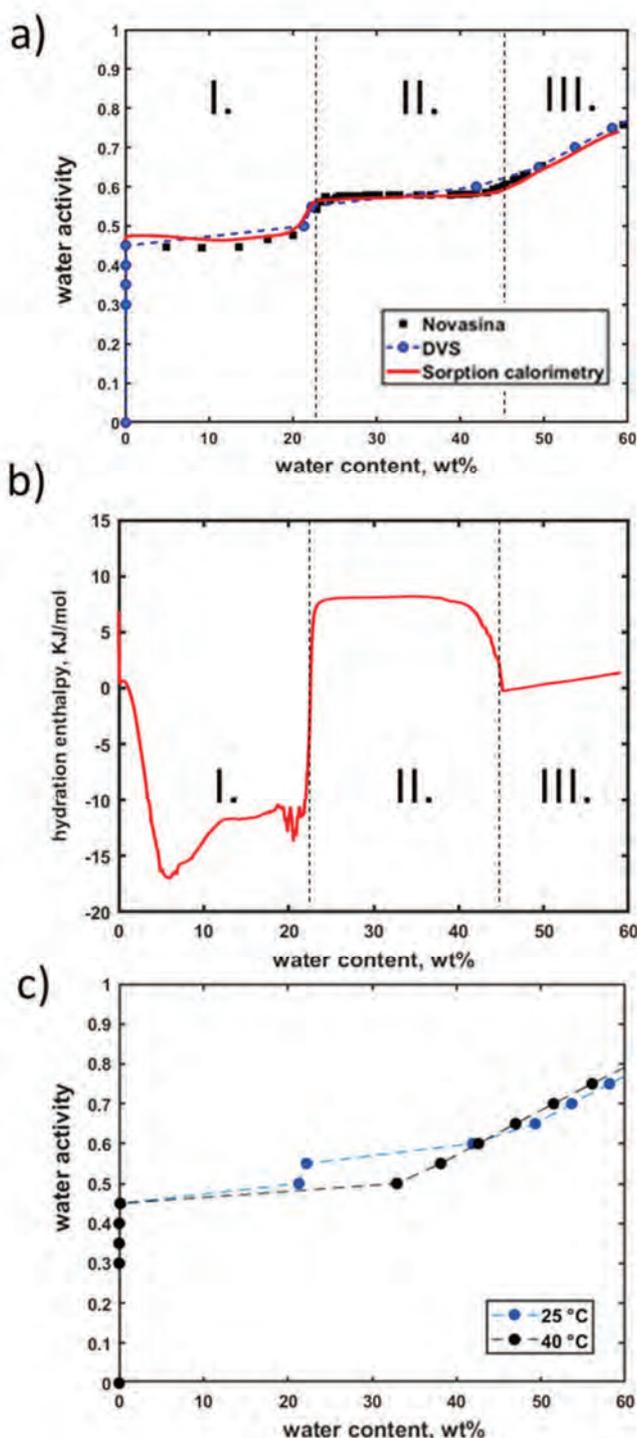
Figure 2. (**a**) Sorption isotherms for water vapor sorption on Na3HB at 25°C determined by Novasina LabMaster, DVS, and Sorption calorimetry respectively. (**b**) Enthalpy of hydration of Na3HB as a function of water content as measured by sorption calorimetry at 25 °C. (**c**) Comparison of water vapor sorption isotherms measured by DVS at 25 °C and 40°C, respectively.

The results of all three methods are in great agreement indicating good reproducibility of the water sorption process and they also provide several interesting findings regarding phase behavior in the Na3HB/water system. Primarily, the stepwise shape

of the isotherm indicates a complex phase behavior with several phase transitions occurring at specific levels of Na3HB hydration. The example of the determination of sorption isotherm at 25°C was achieved by evaluation data from DVS in stepwise mode (Fig. S1a,b) where the weight of the sample was monitored in increasing relative humidity. Starting from the lowest water content, dry crystalline Na3HB does not uptake any water until the relative humidity exceeds a critical level (about 48.5% RH). To establish the value of relative humidity, which is necessary for hydration of crystalline Na3HB, we used DVS technique in scanning mode to define the exact threshold of relative humidity when crystalline Na3HB started hydrated (Fig S1c,d). The low water absorbency of the crystalline forms of cryoprotectants is neither unexpected nor unique. For instance, while the amount of water absorbed by the amorphous form of trehalose (routinely used cryoprotective agent) increases almost linearly with RH of the atmosphere [30], crystalline form of the same sugar starts to absorb a significant amount of water only at RH above 95%. [31]. When exceeding the required limit of water activity, the amount of absorbed water increases to 22.5 wt.%. (region I. in Fig. 2a), whereby this hydration of the solid Na3HB is exothermic as revealed by the results of sorption calorimetry (Fig. 2.b). This threshold amount of water (22.5 wt.%) corresponds to two water molecules per one Na3HB. Therefore, the plateau region below this amount of water (depicted as I. in Fig. 2a) represents the equilibrium mixtures of anhydrous crystals and Na3HB dihydrates.

The next region of constant water activity (region II. in Fig. 2a) represents the coexistence of solid Na3HB dihydrate and its saturated solution. From the border concentration of this area (about 45,2 wt.% of water), the solubility of Na3HB dihydrate can be determined (54.8 wt.% of Na3HB, equivalent to ca 120 g Na3HB per 100 g water). The solubility is well comparable with those of α, α-trehalose (109.6 g per 100 g water at 30°C, [31]. The final step of the sorption isotherm (region III., above 60% RH) represents water uptake by Na3HB solution. In this region, water activity increases with the water content in solution, whereby the activity coefficient (calculated as a ratio of water activity and molar fraction of water in solution) increases from 0.7 to 0.9. The value of the activity coefficient lower than 1 confirms the hydrophilic nature of Na3HB in its aqueous solution. Moreover, the determined water activities are significantly lower than those published for aqueous solutions of other compatible solutes, e.g., trehalose or sucrose [32].

To check the effect of temperature on the vapor sorption on Na3HB, DVS analysis was repeated also at 40°C. It can be seen in Fig. 2c that the sorption isotherm shows some similar features, but also significant differences as compared to that determined at 25°C. Again, a negligible water uptake on dry crystalline Na3HB was observed below 50 %RH (this phenomenon proved to be general as far as we observed it also at temperatures below 25°C, data not shown). Furthermore, also the vapor sorption by Na3HB solution does not significantly differ, showing only slightly lower hydrophilicity of Na3HB (represented by moderately higher activity coefficient of water). On the other hand, only one step change is found in the isotherm suggesting that no transition between different crystal modifications occurs at the higher temperature. Finally, the solubility of crystalline Na3HB at 40°C increases to 67.1 wt.% of 3NaHB (204 g Na3HB

per 100 g water) which is again higher as compared to trehalose (148 g per 100 g water, [31]).

To sum up the results of this experimental part, results of the vapor sorption analyses proved the hydrophilic nature of Na3HB in the aqueous solution which is at least comparable to, but in some perspectives (solubility, water activity decrease in solution) even better than some well recognized compatible solutes such as trehalose. This represents an original and important finding which may motivate further research of Na3HB as a chemical chaperon and bioprotective molecule, not only with respect to its possible stabilizing role in various biological systems (e.g., in PHB accumulating microorganisms) but also from the view of its potential application in the fields in which stabilization of biological molecules is required e.g., cryopreservation of biological samples, food preservation, cosmetics, etc. Apart from this, the study also revealed that Na3HB can form, depending on the conditions (temperature, relative humidity), at least two different crystalline forms – anhydrous crystal and crystalline dihydrates.

3.2. Phase diagram of Na3HB/water at equilibrium

The vapor sorption analysis describes the thermodynamics of Na3HB – water systems at temperatures close to physiological optima. Nevertheless, when discussing the actual bioprotective effects (in particular the cryoprotective ones) it is necessary to analyze the thermodynamics of Na3HB - water binary systems over a much wider range of temperatures. For this purpose, we performed a DSC analysis of the phase transitions occurring during controlled freezing and thawing of various Na3HB-water mixtures. Examples of recorded DSC thermograms and the illustration of their evaluation are shown in Supplementary materials. As the result of this evaluation, onset, peak and endset temperatures were obtained as well as the integral heat of the transition (see the example of ice melting peak evaluation in Figure S2a). For samples with a concentration of Na3HB ranging from 6.3 to 37.8 wt%, two separate endotherm peaks were observed in the thermograms below 0 °C upon heating (Figure S2b). In this case, the first endothermic peaks belong to the eutectic line where the crystalline hydrates of Na3HB melt, while the second peaks correspond to the melting of ice. On the other hand, thermograms of the samples with a high content of Na3HB (from 72.4 to 81.6 wt%, Figure S2c) are featureless until about 30°C where they show a dominant peak corresponding to melting of solid Na3HB hydrates and a minor peak shifted to a higher temperature attributed to melting of anhydrous Na3HB (marked with the red arrow in Figure S2d).

To provide a complete overview of the equilibrium phase behavior of binary Na3HB-water systems, the results of DSC and the vapor sorption analysis were combined to construct the phase diagram, shown in Figure 3. To construct the eutectic and peritectic lines, respectively, onset temperatures of the corresponding endothermic peaks were used, while for the solubility and the ice melting curves, endset temperatures were utilized. To minimalize the effects of the scan rate on the determined values of the ice melting point and solubility, respectively, DSC measurements were performed at three scan rates (1, 2 and 5 °C/min, see Figure S3) and the endset temperatures were extrapolated to zero scan rate. From the

methodological point of view, it was also quite tricky to get any results for samples with the content of Na3HB ranging from 42 to 65 wt%. because the peak corresponding to the eutectic line was hardly detectable for these samples. The reason is that as far as the second melting scans were analyzed for all the samples (see Materials and Methods), which means that the liquid sample coming from the first scan was cooled down to crystallize, samples of this compositions showed a high tendency to adopt the glassy state preventing the sample from crystallization. Actually, the ability to keep the amorphous glassy state at the temperature as low as in this case represents a highly required property of cryoprotectants. Eventually, these experimental difficulties have been overcome by equilibrating the sample for half an hour to be above the glass transition point (supporting sample crystallization) and by decreasing the scan rate to the limit of the device (0.2 °C/min).
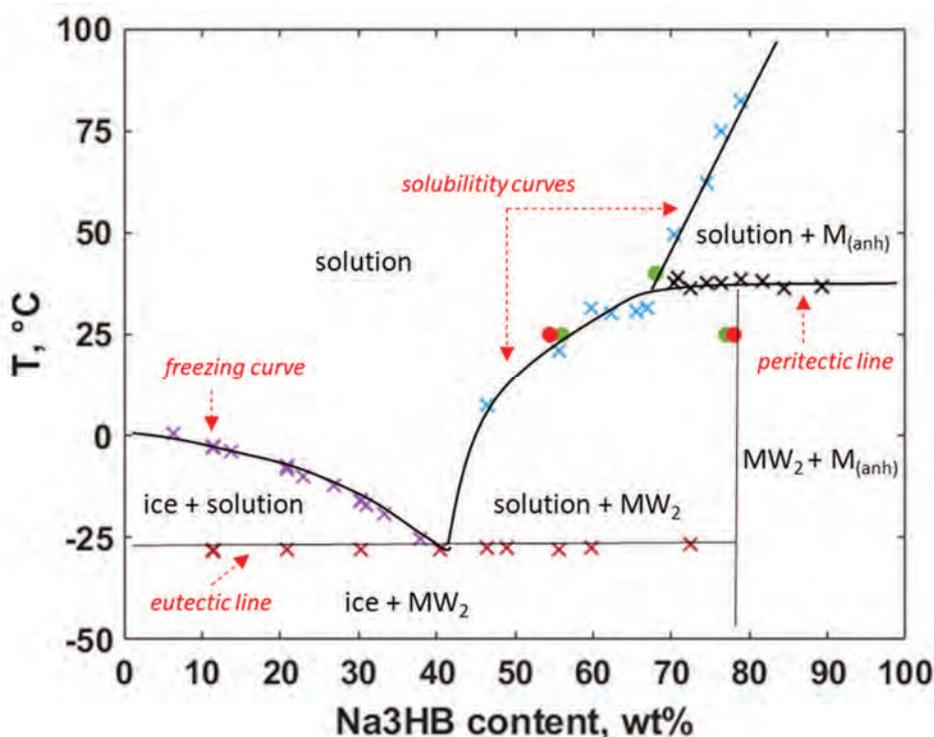
Figure 3. The phase diagram in the equilibrium of Na3HB-water complex using DSC (×); sorption calorimetry (●) and DVS (●). All lines are drawn as a guide for the eye to follow the respective phase boundaries.

In the equilibrium phase diagram, the water freezing curve represents the most important phase boundary as far as a cryoprotective effect of Na3HB is concerned. The curve ends in the eutectic point that occurs at Na3HB content of 40.5 wt.% and temperature -28.1 °C. This means that no ice is formed in solutions above this Na3HB content and temperature higher than -28.1 °C. Furthermore, it also indicates the lowest temperature to which the water freezing point can be depressed by the presence of Na3HB. Similar complete or partial phase diagrams have already been published for some compatible solutes and routinely used cryoprotectants such as trehalose [33, 34], sucrose [35] or glycerol [36]. Compared to these compounds, the effect of Na3HB

on the freezing point depression is again either comparable or even more pronounced. For instance, published values of eutectic points of trehalose range from -2.5 °C to -18.8 °C [37 – 39] and for sucrose from -8.5 °C to -13.95 °C [40]. Glycerol can decrease the water freezing point down to -45 °C (eutectic point), nevertheless, significantly higher glycerol content is needed (about 65 wt.%, [37]), while the similar weight content of glycerol (40 wt.%) decrease water freezing less than Na3HB (only to -15.4 °C, [37]). Similarly, to the results of vapor sorption analysis, Na3HB thus proved to affect water activity in the binary systems at least comparably to the well-recognized compatible solutes.

Based on the DSC data, it was also further confirmed that Na3HB in the solid-state does form the crystalline dihydrates. For this purpose, the enthalpies of the melting endothermic peak that corresponds to the peritectic line in the phase diagram in Figure 3 (the thermograms are shown in Figure S2c) were plotted as a function of Na3HB content. As can be seen in Figure 4, the melting enthalpy increases as the relative content of this hydrated crystalline form in the sample increases at the expense of the solution (lower Na3HB contents) and anhydrous Na3HB (higher contents), respectively. The intersection point of the two linear parts of this dependency occurs at the content of Na3HB equal to 77.5 wt%. Once again, this relative weight content corresponds to the presence of two water molecules per one molecule of Na3HB in the crystalline hydrate. (Figure 2b). The stoichiometry of this crystalline form was hence confirmed by two independent experimental approaches.
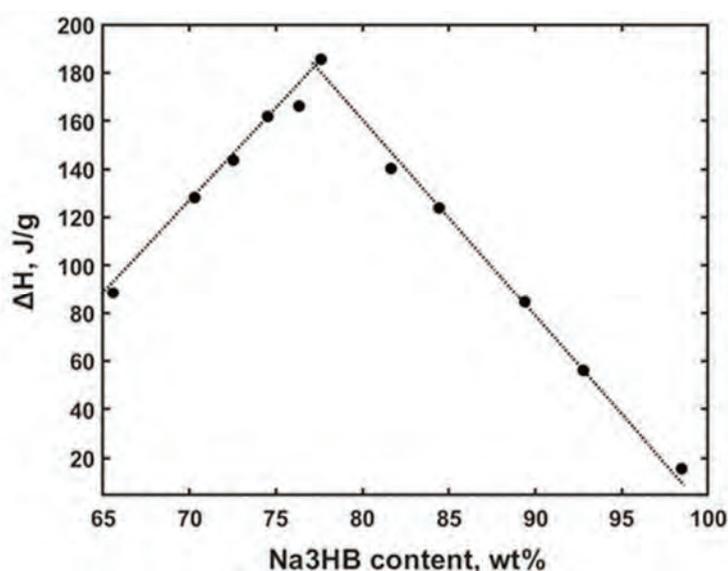

Figure 4. The dependence of the enthalpy of melting of Na3HB dihydrate on concentration.

3.3.   A non-equilibrium phase diagram

The previous section describes the effect of Na3HB from the viewpoint of equilibrium freezing. On the other hand, freezing of the living organisms is usually occurring far from equilibrium, with a great influence on the freezing dynamics. As already noted, when determining the equilibrium phase diagram, the most crucial experimental

390   condition was represented by preventing the sample to turn into a glassy state. In
391   contrast, the bioprotective effects of compatible solutes during freezing or desiccation
392   of an organism are often attributed exactly to this tendency to maintain an amorphous
393   form with water molecules kinetically trapped inside [41,42]. Therefore, we have
394   complemented the study with the DSC analysis focused on the phase transition in
395   Na3HB-water systems out of equilibrium.
396   From the experimental point of view, the main difference lies in cooling the sample
397   to a temperature well below the glass point prior to the evaluated heating DSC scan.
398   Hereby, efficient conversion of the sample to the glassy state is assured. The obtained
399   DSC thermograms including an example of the evaluation of the glass transition are
400   shown in Supplementary material (Figure S4). The composition of the samples
401   significantly influenced their ability to form a glass. For example, samples with Na3HB
402   concentrations from 6.3 to 37.9 wt% showed both the glass transition step and the ice
403   melting peak (Figure S4b). In the zoomed glass transition steps of these thermograms
404   (Figure S4c-e), it can better be seen that the glass transition varies in temperature and
405   the heat capacity change. Both parameters of the glass transition are plotted against
406   Na3HB content in Figure 5.
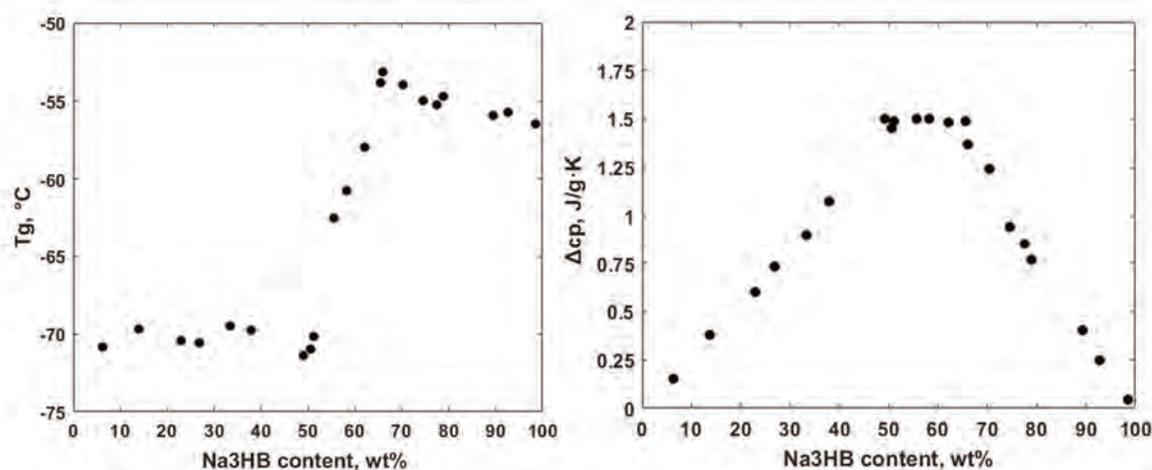
407

408   **Figure 5**. Glass transitions obtained by DSC data: (left) temperature dependence and
409   independence of glass transition on water content; (right) heat capacity of glass
410   transitions.

411   Evidently, three distinct concentration regions can be distinguished in both plots shown
412   in Figure 5. First, samples with Na3HB content below 50 wt.% show the coexistence
413   of the glassy state and ice. The ratio of water and Na3HB in the glassy phase does not
414   change over this region as indicated by the constant glass transition temperature, while
415   the relative content of the glassy state increases with total Na3HB content in the
416   sample as confirmed by increasing heat capacity change. Similarly, in the samples rich
417   in Na3HB (above 68 wt.%) there is an equilibrium between crystals and glass, in this
418   case, represented by the coexistence of glassy Na3HB-water and crystalline Na3HB
419   phases. Interestingly, it can be seen that the composition of the glassy phases of the
420   two regions differs as can be derived from the border concentration of the two regions

421 (50 wt% and 68 wt.%, respectively). While the glassy state in the low-Na3HB region
422 contains 7 water molecules per one molecule of Na3HB, in the high-Na3HB region this
423 drops to about 3 water molecules per one Na3HB molecule. This again confirms the
424 extraordinary hydrophilicity of Na3HB, for instance, glassy trehalose at ambient
425 temperature is known to contain about one water molecule per glucose ring (i.e. two
426 per one molecule) [41].

427   In contrast, the region of medium concentrations (50 – 68 wt.% Na3HB) differs from
428 the neighboring ones in that the glass temperature increases with Na3HB content while
429 the heat capacity change remains constant. This indicates that these samples are fully
430 in a glassy state. This was confirmed also by the fact that no ice melting was detected
431 in this concentration region. All the water in the sample is restricted in its motion by
432 locking up in the amorphous Na3HB matrix. The disordered state of the Na3HB-water
433 system is prevented from any ordering by too high energetic barriers of molecular
434 motion which are hence slowed down below the timescale of the experiment. The
435 range of glass transition temperatures (from about -70 to -55 °C) covered in this
436 concentration region is comparable to the Tg values reported for carbohydrate-based
437 compatible solutes. For instance, a meta-analysis of Tg values of trehalose-water
438 mixtures presented in [34] gives the value of -80 °C for mixture with 40 wt.% of water
439 (compare with Tg -60.7 °C determined in our study for Na3HB/water mixture with the
440 same water content). Similarly, glass temperatures at equilibrium with ice close to -
441 50°C were reported for sucrose and fructose, whereas it is about -70 °C for 3HB as
442 determined in our study [43].

443   The results for DSC analysis were again used to construct a phase diagram of the
444 Na3HB-water binary systems, in this case out of the equilibrium conditions. The
445 diagram is shown in Fig. 6. Similarly, to the equilibrium phase diagram, the
446 cryoprotective effect of Na3HB can be seen in several features of the diagram. Water
447 freezing is reduced partially (below Na3HB content of 40-50 wt.%) or completely
448 (above this Na3HB content). Furthermore, in the region where the water freezes a
449 significant freezing temperature depression is found again.

450
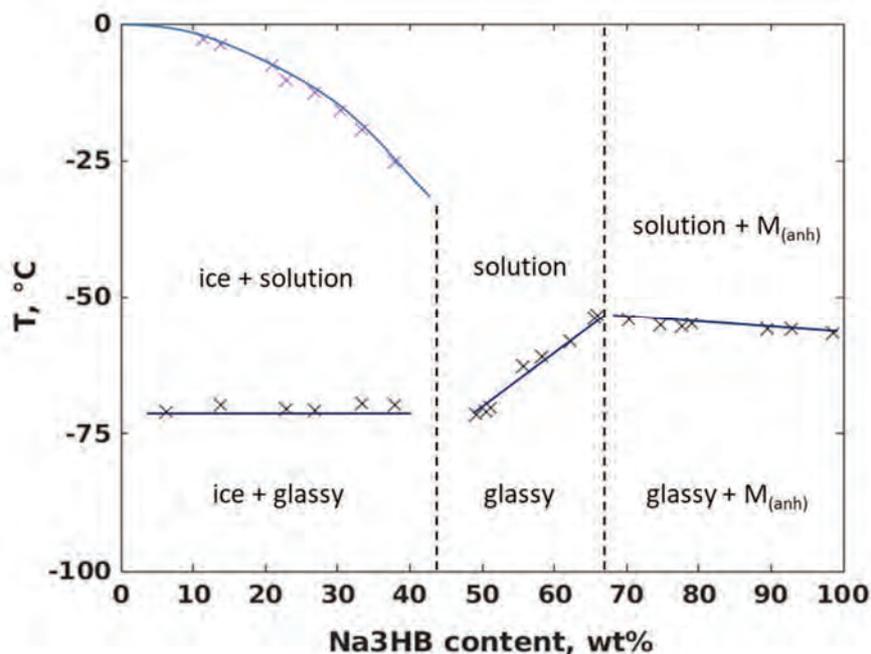
Figure 6. Phase diagram in non-equilibrium of Na3HB-water complex using DSC data from second scans represented by stars (×). All lines are drawn as a guide for eye to follow the respective phase boundaries.

From the non-equilibrium phase diagram shown in Figure 6, it is hardly possible to determine more precisely the limiting composition of Na3HB-water mixtures at which the water in the sample stops freezing. For that purpose, the total enthalpies, determined from the corresponding ice melting endotherms (shown in Figure S4b), were plotted against the water content in the sample (Figure 7). From the linear regression and extrapolation to zero enthalpy, the amount of nonfrozen water was determined to be approximately 1.35 g water per g of Na3HB (or 0.57 g water per g of sample). Once again, this illustrates the outstanding position of Na3HB among the recognized compatible solutes. For instance, published values of non-freezing water for sugars range from 0.21 g water per g of fructose, through 0.26 g water per g sucrose, to 0.31 g water per g trehalose [44].
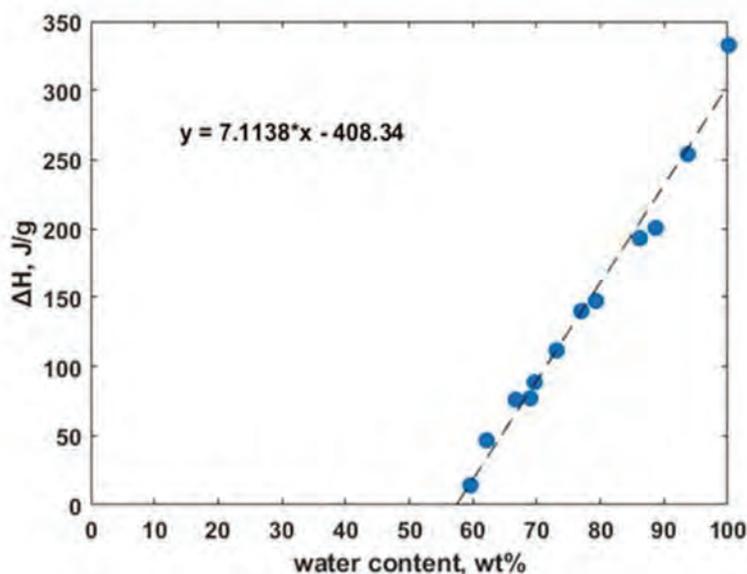
Figure 7. Amount of nonfreezing water per gram of Na3HB obtained by DSC data as a function of water content on enthalpy of melting of water.

3.4.   Biological implications

Generally, 3HB is a very important biomolecule that can be found in numerous biological systems fulfilling various functions. 3HB is an intermediate precursor of various metabolite pathways such as the metabolism of leucine in humans. More importantly, in humans and other higher organisms, 3HB is synthesized in the liver, circulates in the blood, and along with glucose and other ketone bodies it serves as an energy fuel for cells. The concentration of 3HB in the blood of adults varies between 5-335 µmol/l notably higher concentrations (1–2 mmol/l) occur in individuals experiencing ketosis [45]. A substantially higher concentration of 3HB can be found in prokaryotes capable of PHB accumulation. Since the PHB metabolism constitutes of simultaneous synthesis and hydrolysis of PHB granules by the action of PHB granules associated enzymes PHB synthase and PHB depolymerase, the intracellular concentration of 3HB reaches about 100 mmol/l [16, 17], which is about 16.5 fold higher than 3HB concentration in PHB non-accumulating mutant bacterial strain [17]. Therefore, based on its relatively high intracellular concentration 3HB represent a very important low-molecular solute which can be, in terms of concentration, compared to compatible solutes such as glycerol, trehalose or ectoines which are under stress conditions accumulated in a comparable amounts. Therefore, even 3HB is sometimes classified among compatible solutes [46].

Similar to other compatible solutes, also 3HB reveals a general protective function, it is capable of shielding biomolecules from denaturation induced by high temperature or oxidation [17]. Based on our results, Na3HB is very efficient to bind molecules of water, which supposes an important role in the stabilization of the structure of biomolecules or provides the desired environment for chemical and enzymatic reactions. Moreover, it was also observed that Na3HB acts as a potent cryoprotectant that could protect various biological systems when exposed to repeated freezing and

16

thawing. When Na3HB was applied at the concentration of 100 mmol/l it protected the model enzyme from losing activity during 7 subsequent freezing/thawing cycles, its protective effect was even slightly higher than that observed in trehalose. Similarly, when Na3HB was added to a final concentration of 100 mmol/l to the suspension of yeast *Saccharomyces cerevisiae,* it also protected the cells against repeated freezing and thawing even more efficiently than trehalose, ectoine, or a glycerol – well-known cryoprotectants [18]. Also, the results obtained in this study confirmed the high cryoprotective potential of Na3HB, where the already position of the eutectic point which corresponds to the lowest possible melting temperature shows the high potential of Na3HB. Even ice melting temperatures indicate a presumable cryoprotective effect of low concentrations of Na3HB in comparison with conventional cryoprotectants such as sucrose [30] and trehalose [34, 43]. Nevertheless, the unique and unexpected results of glass transitions of Na3HB-water system and then the determined amount of nonfrozen water prove that Na3HB corresponds to a strong cryoprotective function.

The fact that Na3HB represents a very potent cryoprotectant is not only of fundamental interest with respect to its biological importance especially in PHB accumulating prokaryotes, but it might have also numerous applications. For instance, trehalose or glycerol are frequently used as protectants for cryopreservation of various biological samples e.g. viable microbial or cellular cultures, proteins, nucleic acids, antibodies and other biologically active substances [5]. Our results suggest that Na3HB could be advantageously used in the same manner. Moreover, since numerous cryoprotectants are also used to maintain the activity of various biological samples during and after freeze-drying, it would be also interesting to test the protective potential of Na3HB with this respect. Considering all the fundamental physicochemical properties of Na3HB determined in this work, it seems that Na3HB possesses all the prerequisites to be used also as lyoprotectant in freeze-drying. Further, various cryoprotectants are widely used in food preservation to protect food from undesirable changes in texture, taste and overall acceptability upon freezing, frozen storage and subsequent thawing [47, 48]. Considering all the qualities of Na3HB described in this work and also the facts that Na3HB is a safe substance naturally present in the human body in high concentrations and that it is sensorially neutral substance (e.g. not influencing natural flavor and taste of foods), it could be used as a food additive to improve the quality and stability of frozen foodstuffs. Last but not least, Na3HB can be relatively simply produced biotechnologically or by chemical or enzymatical hydrolysis of PHB [49, 50]; therefore, it could be easily available and relatively cheap substance able to compete with well-established cryopreservatives.

4. Conclusions

The study emphasizes the fundamental properties of Na3HB, ubiquitous biological molecules which provide numerous biological functions. This work was focused on the characterization of Na3HB with respect to its important cryoprotective function. Na3HB demonstrates an extraordinary affinity for water which is even higher than in other known compatible solutes such as trehalose. Furthermore, the data demonstrated that Na3HB effectively decreases the freezing point of water solutions providing a large amount of non-frozen water. These results are not only of fundamental importance for instance concerning the explanation of the widely spread capability of PHB synthesis among psychrophilic bacteria, but this study might also open a gate for application of Na3HB in the food industry or biotechnology as a potent cryoprotectant or lyoprotectant. These potential applications are of focus of the follow-up studies.

Credit author statement

Eva Slaninova: Investigation, Data curation, Writing – original draft preparation
Stanislav Obruca: Writing - review and editing, Supervision, Funding acquisition.
Vitaly Kocherbitov: Conceptualization, Investigation, Validation, Methodology, Supervision, Writing - review and editing, Project administration. **Petr Sedlacek**: Conceptualization, Methodology, Writing – original draft, Writing-review and editing, Supervision, Project administration.

Declaration of competing interest

The authors declare that they have no known competing financial interests or personal relationships that could have appeared to influence the work reported in this paper.

Supplementary Materials:

Figure S1: Measurements of water vapor sorption on Na3HB at 25°C: (**a**) example of measurement in stepwise mode; (**b**) sorption isotherm for water vapor sorption on Na3HB determined by stepwise mode; (**c**) example of continual mode; (**d**) detail of sorption isotherm measured in continual mode to determine the beginning of water hydration of dry Na3HB. **Figure S2:** DSC thermograms of mixtures of Na3HB and water in different proportions: (**a**) example of evaluation of ice melting, Na3HB concentration 30.3 wt%; (**b**) endotherms at -27.5 °C corresponding eutectic points and second endotherms corresponding of ice melting, low Na3HB concentrations from 11.3 to 40.5 wt%; (**c**) endotherms, melting of dihydrates and melting of crystalline Na3HB, high Na3HB concentrations from 72.4 to 81.6 °wt%; (**d**) magnified endotherms of crystalline Na3HB highlighted by red arrow. Scanning rates were 10 °C·min^{-1}. **Figure S3**: DSC thermograms measured by different scan rates for extrapolations to zero scan rate. **Figure S4**: DSC thermograms of Na3HB and water in different proportions: (**a**) example of glass transition, Na3HB concentration 67.0 wt%; (**b**) observed scans with glass transitions and melting of ice, Na3HB concentrations from 6.3 to 37.9 wt%; (**c**)

glass transitions with low concentrations of Na3HB; (**d**) glass transitions, Na3HB concentrations from 48 to 68 wt%; (**e**) glass transitions, Na3HB concentrations from 68 to 98 wt%. Scanning rates were 10 °C min^{-1}.

References

[1]   Da Costa, M. S., H. Santos, and E. A. Galinski. 1998. An overview of the role and diversity of compatible solutes in Bacteria and Archaea. In Biotechnology of extremophiles. G. Antranikian, editor. Springer/Berlin, Heidelberg, pp. 117-153.

[2]   Fuller, B. J. 2004. Cryoprotectants: the essential antifreezes to protect life in the frozen state. *CryoLetters.* 25:375-388.

[3]   Cleland, D., P. Krader, C. McCree, J. Tang, and D. Emerson. 2004. Glycine betaine as a cryoprotectant for prokaryotes, *J. Microbiol. Methods.* 58:31-38, doi: 10.1016/j.mimet.2004.02.015.

[4]   Muldrew, K., J. P. Acker, J. A. W. Elliott, and L. E. McGann. 2004. The water to ice transition: Implications for living cells. In Life in the frozen state, vol 1. B. J. Fuller, N. Lane and E. E. Benson, editors. CRC Press/Boca Raton, Florida, pp. 67-108.

[5]   Hubalek, Z. 2003. Protectants used in the cryopreservation of microorganisms. *Cryobiol.* 46:205-229, doi: 10.1016/S0011-2240(03)00046-4.

[6]   Goller, K., and E. A. Galinski. 1999. Protection of a model enzyme (lactate dehydrogenase) against heat, urea and freeze-thaw treatment by compatible solute additives." *J. Mol. Catal. B. Enzym.* 7:37-45, doi: 10.1016/S1381-1177(99)00043-0.

[7]   Andersson, M. M., J. D. Breccia, and R. Hatti-Kaul. 2000. Stabilizing effect of chemical additives against oxidation of lactate dehydrogenase. *Biotechnol. Appl. Biochem.* 32:145-153, doi: 10.1042/BA20000014.

[8]   Van-Thuoc, D., S. O. Hashim, R. Hatti-Kaul, and G. Mamo. 2013. Ectoine-mediated protection of enzyme from the effect of pH and temperature stress: a study using *Bacillus halodurans xylanase* as a model. *Appl. Microbiol Biotechnol.* 97:6271-6278, doi: 10.1007/s00253-012-4528-8.

[9]   Jain, N. K., and I. Roy. 2009. Effect of trehalose on protein structure. *Protein Sci.* 18:24-36, doi: 10.1002/pro.3.

[10]   Obruca, S., P. Sedlacek, E. Slaninova, I. Fritz, C. Daffert, K. Meixner, Z. Sedrlova, and M. Koller. 2020. Novel unexpected functions of PHA granules. *Appl. Microbiol. Biotechnol.* 104:4795-4810, doi: 10.1007/s00253-020-10568-1.

608 [11] Narancic, T., E. Scollica, S.T. Kenny, H. Gibbons, E. Carr, L. Brennan, G.
609   Cagney, K. Wynne, C. Murphy, M. Raberg, D. Heinrich, A. Steinbüchel, and K.
610   E. O'Connor. 2016. Understanding the physiological roles of
611   polyhydroxybutyrate (PHB) in *Rhodospirillum rubrum* S1 under aerobic
612   chemoheterotrophic conditions. *Appl. Microbiol. Biotechnol.* 100:8901-8912,
613   doi: 10.1007/s00253-016-7711-5.

614 [12] Wu, D., J. He, Y. Gong, D. Chen, X. Zhu, N. Qiu, M. Sun, M. Li, and Y. Ziniu.
615   2011. Proteomic analysis reveals the strategies of *Bacillus thuringiensis* YBT –
616   for survival under long-term heat stress. *Proteomics.* 11:2580-2591, doi:
617   10.1002/pmic.201000392.

618 [13] Sedlacek, P., E. Slaninova, M. Koller, J. Nebesarova, I. Marova, V. Krzyzanek,
619   and S. Obruca. 2019. PHA granules help bacterial cells to preserve cell integrity
620   when exposed to sudden osmotic imbalances. *New Biotechnol.* 49:129-136,
621   doi: 10.1016/j.nbt.2018.10.005.

622 [14] Slaninova, E., P. Sedlacek, F. Mravec, L. Mullerova, O. Samek, M. Koller, O.
623   Hesko, D. Kucera, I. Marova, and S. Obruca. 2018. Light Scattering on PHA
624   granules protects bacterial cells against the harmful effects of UV
625   radiation. *Appl. Microbiol. Biotechnol.* 102:1923-1931, doi: 10.1007/s00253-
626   018-8760-8.

627 [15] Kadouri, D., E. Jurkevitch, Y. Okon, and S. Castro-Sowinsk. 2005. Ecological
628   and agricultural significance of bacterial polyhydroxyalkanoates. *Crit. Rev.*
629   *Microbiol.* 31:55-67, doi: 10.1080/10408410590899228.

630 [16] Soto, G., L. Setten, C. Lisi, C. Maurelis, M. Mozzincafreddo, M Cuccioloni, M.
631   Angeletti, and N. D. Ayub. 2012. Hydroxybutyrate prevents protein aggregation
632   in the halotolerant bacterium *Pseudomonas sp.* CT13 under abiotic
633   stress. *Extremophiles.* 16:455-462, doi: 10.1007/s00792-012-0445-0.

634 [17] Obruca, S., P. Sedlacek, F. Mravec, O. Samek, and I. Marova. 2016. Evaluation
635   of 3-hydroxybutyrate as an enzyme-protective agent against heating and
636   oxidative damage and its potential role in stress response of poly (3-
637   hydroxybutyrate) accumulating cells. *Appl. Microbiol. Biotechnol.* 100:1365-
638   1376, doi: 10.1007/s00253-015-7162-4.

639 [18] Obruca, S., P. Sedlacek, V. Krzyzanek, F. Mravec, K. Hrubanova, O. Samek,
640   D. Kucera, P. Benesova, and I. Marova. 2016. Accumulation of poly (3-
641   hydroxybutyrate) helps bacterial cells to survive freezing. *PloS one.* 11:
642   e0157778, doi: 10.1371/journal.pone.0157778.

643 [19] Cielsielski, S., D. Gorniak, J. Mozejko, A. Swiatecky, J. Grzesiak, and M.
644   Zdanowski. 2014. The diversity of bacteria isolated from Antarctic freshwater
645   reservoirs possessing the ability to produce polyhydroxyalkanoates. *Curr.*
646   *Microbiol.* 69:594-603, doi: 10.1007/s00284-014-0629-1.

647   [20]   Goh, Y. S., and I. L. P. Tan. 2012. Polyhydroxyalkanoate production by Antarctic
648   soil bacteria isolated from Casey Station and Signy Island. *Microbial. Res.*
649   167:211-219, doi: 10.1016/j.micres.2011.08.002.

650   [21]   Pämänen, K., A. Karkman, M. Virta, E. Eronen-Rasimus, and H. Kaartokallio.
651   2015. Discovery of bacterial polyhydroxyalkanoate synthase (PhaC) encoding
652   genes from seasonal Baltic Sea ice and cold estuarine waters. *Extremophiles.*
653   19:197-206, doi: 10.1007/s00792-014-0699-9.

654   [22]   Kumar, V., V. A. Thakur, S. Kumar, and D. Singh. 2018. Bioplastic reservoir of
655   diverse bacterial communities revealed along altitude gradient of Pangi-
656   Chamba trans-Himalayan region. *FEMS Microbiol. Lett.* 365, doi:
657   10.1093/femsle/fny144.

658   [23]   Rogala, M. M., J. Gawor, R. Gromadka, M. Kowalczyk, and J. Grzesiak. 2020.
659   Biodiversity and habitats of polar region polyhydroxyalkanoic acid producing
660   bacteria: Biopropection by popular screening methods. *Genes.* 11, doi:
661   org/10.3390/genes11080873.

662   [24]   Timasheff, S. N. 2002. Protein-solvent preferential interactions, protein
663   hydration, and the modulation of biochemical reactions by solvent components.
664   *Proc. Natl. Acad. Sci.* 99:9721-9726, doi: 10.1073/pnas.122225399.

665   [25]   Wiggins, P. M. 1990. Role of water in some biological processes. *Microbiol. Mol.*
666   *Biol. Rev.* 54:432-449, doi: 10.1128/mr.54.4.432-449.1990.

667   [26]   Mittler, R. 2002. Oxidative stress, antioxidants and stress tolerance. *Trends*
668   *Plant Sci.* 7:405-410, doi: 10.1016/S1360-1385(02)02312-9.

669   [27]   Greenspan, L. 1977. Humidity Fixed-Points of Binary Saturated Aqueous
670   Solutions. *J. Res. Natl. Bur. Stand.*, Sect. A 81:89–96.

671   [28]   Wadso, L., and N. Markova. 2002. A Method to Simultaneously Determine
672   Sorption Isotherms and Sorption Enthalpies with a Double Twin
673   Microcalorimeter. *Rev. Sci. Instrum.* 73:2743–2754, doi: 10.1063/1.1484159.

674   [29]   Kocherbitov, V. 2004. A New Formula for Accurate Calculation of Water Activity
675   in Sorption Calorimetric Experiments. *Thermochim. Acta.* 414:43–45, doi:
676   10.1016/j.tca.2003.11.011.

677   [30]   Roe, K. D., and T. P. Labuza. 2005. Glass transition and crystallization of
678   amorphous trehalose-sucrose mixtures. *Int. J. Food Prop.* 8:559-574, doi:
679   10.1080/10942910500269824.

680   [31]   Lammert, A. M., S. J. Schmidt, and G. A. Day. 1998. Water activity and solubility
681   of trehalose. *Food Chem.* 61:139-144, doi: org/10.1016/S0308-8146(97)00132-
682   5.

683   [32]   Galmarini, M. V., J. Chirife, M.C. Zamora, and A. Pérez. 2008. Determination
684   and correlation of the water activity of unsaturated, supersaturated and

685   saturated trehalose solutions. *LWT-Food Sci. Technol.* 41:628-631, doi:
686   org/10.1016/j.lwt.2007.04.007.

687   [33]   Roberts, C. J., and F. Franks. 1996. Crystalline and amorphous phases in the
688   binary system water–β, β-trehalose. *J. Chem. Soc. Faraday Trans.* 92:1337-
689   1343, doi: 10.1039/FT9969201337.

690   [34]   Chen, T., A. Fowler, and M. Toner. 2000. Literature review: supplemented
691   phase diagram of the trehalose–water binary mixture. *Cryobiol.* 40:277-282, doi:
692   10.1006/cryo.2000.2244.

693   [35]   Mathlouthi, M., and P. Reiser. 1995. Sucrose: properties and application, first
694   edition. Springer Science & Business Media, Glasgow.

695   [36]   Nakagawa, H., and T. Oyama. 2019. Molecular Basis of Water Activity in
696   Glycerol–Water Mixtures. *Front. Chem.* 7:731, doi: 10.3389/fchem.2019.00731.

697   [37]   Green, J. L., and C. A. Angel. 1989. Phase relation and vitrification of
698   saccharide-water solution and the trehalose anomaly. *J. Phy. Chem.* 93:2880-
699   2882.

700   [38]   Miller, D. P., J. J. de Pablo, and H. Corti. 1997. Thermophysical properties of
701   trehalose and its concentrated aqueous solutions. *Pharm. Res.* 14:578-590, doi:
702   10.1023/A:1012192725996.

703   [39]   Nicolajsen, H., and A. Hvidt. 1994. Phase behaviour of the system trehalose-
704   NaCl-water. *Cryobiol.* 31:199-205, doi:10.1006/cryo.1994.1024.

705   [40]   Young, F. E., and F. T. Jones. 1949. Sucrose Hydrates. The Sucrose–Water
706   Phase Diagram. *J. Phys. Chem.* 53:1334-1350.

707   [41]   Lane, L. B. 1925. Freezing Points of Glycerol and Its Aqueous Solutions. *Ind.*
708   *Eng. Chem.* 17:924-924.

709   [42]   Elbein, A. D., Y. T. Pan, and I. Pastuszak, D. Carroll. 2003. New insights on
710   trehalose: a multifunctional molecule. *Glycobiol.* 13:17-27, doi:
711   10.1093/glycob/cwg047.

712   [43]   Goff, H. D., and M. E. Sahagian. 1996. Glass transitions in aqueous
713   carbohydrate solutions and their relevance to frozen food stability.
714   *Thermochimica Acta.* 280:449-464, doi: 10.1016/0040-6031(95)02656-8.

715   [44]   Xu, M., G. Chen, C. Zhang, and S. Zhang. 2017. Study on the Unfrozen Water
716   Quantity of Maximally Freeze-Concentrated Solutions for Multicomponent
717   Lyoprotectants. *J. Pharm. Sci.* 106:83-91, doi: 10.1016/j.xphs.2016.05.007.

718   [45]   McNeil, C. A., C. Pramfalk, S. M. Humphreys, and L. Hodson. 2014. The storage
719   stability and concentration of acetoacetate differs between blood fractions. *Clin.*
720   *Chim. Acta.* 433:278-283, doi: 10.1016/j.cca.2014.03.033.

721 [46] Roberts, M. F. 2005. Organic compatible solutes of halotolerant and halophilic
722 microorganisms. *Saline Syst.* 1, doi: 10.1186/1746-1448-1-5.

723 [47] MacDonald, G. A., and T. C. Lanier. 1997. Cryoprotectants for Improving
724 Frozen-Food Quality. In Quality in Frozen Food. M. C. Erickson and Y. C. Hung,
725 editors. Springer/Boston, MA, pp. 197-232.

726 [48] Maity, T., A. Saxena, and P. S. Raju. 2018. Use of hydrocolloids as
727 cryoprotectant for frozen foods. *Crit. Rev. Food Sci. Nutr.* 58:420-435, doi:
728 10.1080/10408398.2016.1182892.

729 [49] Tokiwa, Y., and C. U. Ugwu. 2007. Biotechnological production of (R)-3-
730 hydroxybutyric acid monomer. *J. Biotechnol.* 132:264-272, doi:
731 10.1016/j.jbiotec.2007.03.015.

732 [50] Uefuji, M., K. I. Kasuya, and Y. Doi. 1997. Enzymatic degradation of poly[(*R*)-3-
733 hydroxybutyrate]: Secretion and properties of PHB depolymerase from
734 *Pseudomonas stutzeri. Polym. Degr. Stab.* 58: 275-281, doi: 10.1016/S0141-
735 3910(97)00058-X.

Appendix 23

Trudicova, M., Smilek, J., Kalina, M., Smilkova, M., Adamkova, K., Hrubanova, K., ... & Sedlacek, P. (2020). Multiscale experimental evaluation of agarose-based semi-interpenetrating polymer network hydrogels as materials with tunable rheological and transport performance. Polymers, 12(11), 2561.

Multiscale Experimental Evaluation of Agarose-Based Semi-Interpenetrating Polymer Network Hydrogels as Materials with Tunable Rheological and Transport Performance

Monika Trudicova [1] , **Jiri Smilek** [1] , **Michal Kalina** [1] , **Marcela Smilkova** [1] ,
Katerina Adamkova [2] , **Kamila Hrubanova** [2] , **Vladislav Krzyzanek** [2] **and Petr Sedlacek** [1,*]

[1] Faculty of Chemistry, Brno University of Technology, Purkynova 118, 61200 Brno, Czech Republic; xctrudicova@fch.vut.cz (M.T.); smilek@fch.vut.cz (J.S.); kalina-m@fch.vut.cz (M.K.); smilkova@fch.vut.cz (M.S.)
[2] Institute of Scientific Instruments of the Czech Academy of Sciences, Kralovopolska 147, 61264 Brno, Czech Republic; katka@isibrno.cz (K.A.); hrubanova@isibrno.cz (K.H.); krzyzanek@isibrno.cz (V.K.)
*   Correspondence: sedlacek-p@fch.vut.cz; Tel.: +420-541-149-486

Abstract: This study introduces an original concept in the development of hydrogel materials for controlled release of charged organic compounds based on semi-interpenetrating polymer networks composed by an inert gel-forming polymer component and interpenetrating linear polyelectrolyte with specific binding affinity towards the carried active compound. As it is experimentally illustrated on the prototype hydrogels prepared from agarose interpenetrated by poly(styrene sulfonate) (PSS) and alginate (ALG), respectively, the main benefit brought by this concept is represented by the ability to tune the mechanical and transport performance of the material independently via manipulating the relative content of the two structural components. A unique analytical methodology is proposed to provide complex insight into composition–structure–performance relationships in the hydrogel material combining methods of analysis on the macroscopic scale, but also in the specific microcosms of the gel network. Rheological analysis has confirmed that the complex modulus of the gels can be adjusted in a wide range by the gelling component (agarose) with negligible effect of the interpenetrating component (PSS or ALG). On the other hand, the content of PSS as low as 0.01 wt.% of the gel resulted in a more than 10-fold decrease of diffusivity of model-charged organic solute (Rhodamine 6G).

1. Introduction

Hydrogel represents a three-dimensional, water-swollen network assembled from cross-linked chains of either polymer molecules or partially coagulated colloidal particles. Because a macromolecular gel network can be formed from virtually any water-soluble polymer, hydrogel materials generally encompass a wide range of chemical compositions possessing a great variety of miscellaneous physicochemical functionalities that can be exploited in numerous applications [1]. Among them, the biomedical use of hydrogels has attracted particular interest since their first appearance. In a fact, hydrogels were the first biomaterials designed intentionally for the use in the human body [2,3]. The main benefits regarding their biomedical application include a combination of high water content and physicochemical similarity to the native extracellular matrix [4] which together results in their high

biocompatibility. Furthermore, their internal structure, as well as the rate of degradation or dissolution in vivo, can be tuned by controlling their chemical composition, type and density of the cross-links, etc. Since the first pioneer works on covalently cross-linked poly(2-hydroxyethyl methacrylate) gels published by Wichterle and Lim in 1960 [3], significant progress has been made in the field of hydrogel design for biomaterial use, in particular in improving the physical form of the hydrogel delivery (including micro- or nanoparticulate gels [5,6], gel films [7,8], etc.), in providing a specific response to a change in the external conditions (such as temperature [9,10], pH [11,12] or concentration of a particular biomolecule [13,14]), or in obtaining materials with precisely designed internal architecture such as the superporous gels [15,16], hydrogels self-assembled from biopolymers produced by genetically engineered microorganisms [17,18], dual network gels [19,20] and many others. Hence, until now, hydrogel materials have not only gained a prominent position in the field of medical research but have also been put into common practice in tissue engineering [21,22], regenerative medicine [23,24], diagnostic [25,26] or separation techniques [27,28], cell immobilization and cultivation and, perhaps most exclusively, in drug-delivery applications [29].

Despite many beneficial properties, hydrogels have also some specific limitations and risks regarding their uses in the development of drug-delivery systems [29]. For example, poor mechanical properties (i.e., low tensile strength) of the gels compared to 'hard' drug-delivery systems such as nanoparticles may lead to a premature disintegration of the gel carrier and instantaneous release of the active substance under a mechanical strain [30]. Perhaps even more important are the specific limitations connected to the transport properties of the gels. Drug loading capacity, as a complex product of multiple influences (drug solubility in water, its partition between gel and solution, or its effect on the stability of the gel network junctions) is usually limited even in the case of hydrophilic active substances [31,32]. Moreover, high water content and large pore size indispensably result in rapid drug release on a time scale of hours to days which again barely competes with the long-term release profiles of other delivery systems such as microspheres [33]. Until now, a range of strategies has been proposed to improve the partition of the active substance in the gel and to retard its release from the hydrogel carrier. These strategies usually aim at supporting the binding (either chemical or physical) between the drug and the polymer network. Hence, numerous procedures have been explored to incorporate monomers with a specific ionic or non-ionic affinity to the drug into the preparation of synthetic polymer networks [34], to exploit the presence of native functional groups of biopolymers (e.g., carbohydrates) in their physically cross-linked gels [35,36] or to conjugate the drug to the gel network via covalent bonds prone to enzymatic or chemical cleavage in situ [37].

In the present work, we put forward an alternative strategy, which aims to address both the aforementioned issues of the hydrogel drug carriers independently to each other. Our hydrogel system is based on semi-interpenetrating polymer networks (semiIPNs) which, together with interpenetrating polymer networks (IPNs), belong to the class of polymer blends. IPNs are defined by International Union of Pure and Applied Chemistry (IUPAC) as "A polymer comprising two or more networks which are at least partially interlaced on a molecular scale but not covalently bonded to each other and cannot be separated unless chemical bonds are broken." [38] SemiIPNs differ from the IPNs in the fact that the chains of the second polymer are dispersed in the network formed by the first polymer without forming a separate network and, consequently, the linear polymer component can in principle be separated from the constituent polymer network without breaking chemical bonds [38]. In recent years, both IPNs and semiIPNs have attracted special attention in novel material applications mainly due to the possibility of combining favorable properties of each polymer component to the final properties superior to those provided by the two polymer constituents alone. Hence, several IPN- and semiIPN-based hydrogel compositions have recently been proposed for application in tissue engineering [39] and in controlled-release (CR) systems [40], where the synergistic effect brought by the combination of the two polymer component is primarily focused on the specific improvement of mechanical properties, biocompatibility, thermal stability or chemical resistance of the gel.

In our study, we introduce a different approach to the utilization of semiIPN hydrogels in drug-delivery systems. Rather than focusing on a specific polymer composition developing carriers of hydrophilic (in particular ionic) active compounds based on semiIPN hydrogels which comprise a 'structure–ruling' gel-forming component, with a low affinity to the drug substance, interpenetrated by a 'binding' component that does not interfere with the internal morphology and the mechanical properties of the gel but significantly improves hydrogel reactivity. We hypothesize that such a system would allow an independent dual-tuning of mechanical and transport performance via manipulating the relative content of the two structural components. As a prototype material, we here introduce hydrogels based on an agarose network interpenetrated by a linear polyelectrolyte component. Agarose is involved in the study as a model representative of thermomelting polysaccharides which form physical hydrogels via thermally induced phase separation. Among versatile applications of agarose [41], its use in tissue engineering [42] and drug delivery [43] has recently attracted special attention mainly for its great biocompatibility, temperature-dependent behavior [43,44], and multiple options of manipulating its internal architecture [45,46]. As an interpenetrating component, two structurally distinct linear polyanions, alginate and poly(styrenesulfonate), are used in this study to provide an attractive binding affinity towards model low-molecular solute—Rhodamine 6G. This compound was used mainly for its complex molecular structure combining highly hydrophilic positively charged nitrogen atom with neighboring aromatic structural moieties, which represents a common structural motif widespread in different groups in pharmaceuticals [47,48].

The main aim of the study is to test the ability of the system to tailor the chemical structure and internal morphology of the proposed semiIPN hydrogels separately and, consequently, to manipulate its mechanical (rheological) and transport properties independently. To evaluate the relation between internal structure (both physical and chemical), mechanical properties, and transport performance of the resulting gels, we present a unique analytical approach, where the three fundamental material qualities (structure, rheological properties, and transport performance) are studied both on the macroscopic (i.e., the sample-averaged) and the microscopic scale.

2. Materials and Methods

2.1. Preparation of the Gels

All hydrogels, utilized in this study were prepared via the thermoreversible gelation of the aqueous solution of agarose (Type I, low electroendoosmosis; Sigma-Aldrich, Prague, Czech Republic). Agarose hydrogels (without any addition of a polyelectrolyte component) were prepared from the aqueous solution of agarose (concentration of agarose in solution/gel: 0.5%, 1%, 2%, and 4% by weight), while agarose-based semiIPN gels from the aqueous solution of agarose (1 wt.%) with a corresponding addition of a dissolved polyelectrolyte (0.002, 0.005 and 0.010% by weight). As a polyelectrolyte component, alginic acid sodium salt (ALG; Sigma-Aldrich, Prague, Czech Republic, 180947, average MW 120–160 kDa, M/G ratio 1.33 [49]) and poly(sodium 4-styrenesulfonate) (PSS; Sigma-Aldrich, Prague, Czech Republic, average MW 70 kDa), respectively, were used.

The gelation proceeded as follows: the accurately weighed amount of agarose powder was dispersed in deionized water (preparation of agarose gels) or in the aqueous solution of the respective polyelectrolyte of the required concentration (semiIPN gels), respectively. The mixture was at first slowly heated with continuous stirring to 85 °C and then maintained at the constant temperature until the solution turned transparent. Subsequently, the solution was degassed in an ultrasonic bath (1 min. at 85 °C) and slowly poured into the corresponding container (according to the needs of subsequent analysis) which was then stored in a closed bottle above the water-level (i.e., at 100% relative humidity to prevent unwanted surface evaporation of water). Upon the gradual cooling to room temperature (approximately 45 min), the mixture gradually gelled.

2.2. Turbidimetry

For the turbidimetric experiment, the respective heated and degassed agarose solution (with or without the respective polyelectrolyte component) was poured and let to cross-link in the poly(methyl methacrylate) cuvettes for spectrophotometry ($10 \times 10 \times 45$ mm^3). Subsequently, the ultraviolet–visible (UV-VIS) transmittance spectrum of the gel was collected in the wavelength range 300–800 nm on Hitachi U3900 spectrophotometer (Tokyo, Japan), whereby deionized water was used as a reference sample. From the transmittance spectrum, optical densities (OD) in the spectral range of 700 to 800 nm (where no specific light absorption by the gel components is expected) were calculated according to OD $(\lambda) = -\log T(\lambda)$. From the optical density, turbidity was calculated (considering optical path length = 10 mm) from $\tau(\lambda) = 2.3$ OD (λ). Calculated turbidities in the spectral range 700–800 nm were plotted as $\log \tau(\lambda) = f(\log \lambda)$ and the linear fit of the plot was performed using MS Excel. The wavelength exponent then was determined as the slope of the linear fit and further transformed into the correlation length (in μm) using data published by Aymard [50]. Finally, the correlation length value is presented as an effective value of mesh size determined from turbidimetry.

2.3. Oscillatory Rheometry

For the analysis of macroscopic viscoelastic behavior of a hydrogel sample, the circular cut of the gel (40 mm in diameter, 1.1 mm in height), gelled in a Petri dish before the analysis, was placed on the bottom Peltier plate of the Rheometer AR-G2 (TA Instruments, New Castle, DE, USA) pre-tempered to 25 °C. The oscillatory analysis was performed using plate-plate geometry (titanium plate sensor, 40 mm in diameter) at a constant temperature of 25 °C. The upper rheometer shaft with geometry was moved into the trim gap (1020 μm) and excess of hydrogel outside of both plates was cut away by a spatula. The geometry gap (1000 μm) was reached (normal force during compressing did not exceed 5 N). Due to the high content of water in hydrogels, the solvent trap was used to prevent the potential change in viscoelastic properties due to the evaporation of the dispersion medium. Frequency sweep measurements were performed on the whole set of hydrogel samples in duplicate. The conditioning step (25 °C, 5 min) preceded before each measurement. Thanks to the conditioning step, each hydrogel was relaxed and tempered to the required temperature before measurement. Firstly, the linear viscoelastic region (LVR) was determined by strain sweep test at a constant frequency of oscillation (1 Hz) in the range 0.01–1000%, 6 points per decade (Figure S2 in Supplementary Materials). The constant amplitude of deformation chosen from the LVR (0.5%) was used for all frequency sweep measurements. Frequency sweep measurements were performed on the whole set of hydrogel samples in duplicate (at least) with parameters as follows: 0.01–20 Hz, 6 points per decade, decimal logarithmic mode. The relative deviation of the duplicate measurements never exceeded 10% (in terms of elastic (storage) modulus G' and viscous (loss) modulus G'', respectively). From the recorded values of G' and G'', the corresponding values of complex modulus $|G^*|$ and phase angle δ were calculated according to:

$$|G^*| = \sqrt{(G')^2 + (G'')^2} \tag{1}$$

$$\delta = \text{arctg} \frac{G''}{G'} \tag{2}$$

To calculate the effective mesh size from frequency sweep data, frequency dependencies of elastic and viscous moduli were fitted (using least square regression algorithm) with a generalized Maxwell model [51] using the procedure described by Pescolido et al. [52]. Fitting functions were as follows:

$$G' = \sum_{i=1}^{n} G_i \frac{(2\pi f \lambda_i)^2}{1 + (2\pi f \lambda_i)^2} \tag{3}$$

$$G'' = \sum_{i=1}^{n} G_i \frac{2\pi f \lambda_i}{1 + (2\pi f \lambda_i)^2} \tag{4}$$

where f is the frequency of oscillations (in Hz), $n = 4$ is the number of considered Maxwell elements (determined via the statistical procedure described in [53]), G_i and λ_i represents the corresponding spring constant and relaxation time, respectively, of the i-th Maxwell element. Data fitting was performed using the Solver tool in MS Excel. Based on the results of the data fitting, hydrogel shear modulus was calculated as the sum of the spring constants of Maxwell elements $G = \sum_{i=1}^{n} G_i$ and transformed into the density of crosslinking ρ_x and into the average network mesh size ξ, according to:

$$\rho_x = \frac{G}{RT} \tag{5}$$

and,

$$\xi = \sqrt[3]{\frac{6}{\pi \rho_x N_A}} \tag{6}$$

where T is the thermodynamic temperature, while R and N_A the universal gas constant and Avogadro constant, respectively.

2.4. Microrheometry

A colloidal analyzer Zetasizer Nano ZS (Malvern Panalytical Ltd., Great Malvern, UK) was used to collect dynamic light scattering (DLS) microrheological data. This method is based on observing the movement of tracer particles with defined particle size (polystyrene monodisperse with nominal particle size 100 nm, Sigma-Aldrich, Prague, Czech Republic) in the sample via monitoring the time development of intensity of the light scattered by these particles. The tracer particles were homogeneously incorporated inside the analyzed hydrogels during the initial preparation step (they were added to the mixture before heating up to dissolve agarose powder). The experimental parameters of DLS microrheological measurements were set as follows: temperature: 25 °C, equilibration time: 60 s, duration of one run: 10 s, number of runs: 12, number of measurements of each sample: 5. Each sample was prepared and analyzed in three replicates. The main experimental outcomes from DLS microrheology was the dependence of mean square displacement (MSD) of tracer particles in the studied hydrogels on the observation time. From the respective MSD, viscoelastic parameters (primarily the storage and loss moduli) were calculated in the Microrheology software tool in Zetasizer Software (Malvern Panalytical Ltd., Great Malvern, UK). Other viscoelastic parameters (complex modulus, phase angle) were calculated using equations shown above for the oscillatory rheology.

2.5. Macroscopic Diffusion Experiments

The whole set of prepared hydrogels was subjected to diffusion experiments proposed and optimized in our previous study [54,55]. For this purpose, hydrogel samples were prepared directly in PMMA cuvettes for spectrophotometry similarly to turbidimetry analysis. In this case, the cuvettes were overfilled with the solution to achieve the concave meniscus of the agarose solution at the cuvette edge. After the solidification (approximately 30 min, room temperature), the excess hydrogel was cut away to obtain a flat hydrogel surface at the open orifice of the cuvette.

The hydrogel-filled cuvettes were then immersed in a solution of model solute to study its diffusion in the gels qualitatively and quantitatively. As the model solute, positively charged organic dye Rhodamine 6G (R6G, dye content > 95 wt.%, Sigma-Aldrich, Prague, Czech Republic) was used. The concentration of the source solution of R6G in the diffusion experiment was 0.01 g.dm^{-3}, the solution was continuously stirred via a magnetic stirrer (250 RPM) during the whole diffusion experiment. At selected times (24, 48, and 72 h), the cuvettes were taken out of the solution and the UV-VIS absorption spectra were measured in the 300 to 800 nm spectral range at various distances from the orifice on Varian Cary 50 UV–VIS spectrophotometer (Varian, Inc., Paolo Alto, California, USA) equipped with the custom-made accessory providing controlled fine vertical movement of the cuvette in the spectrophotometer (for details on the accessory, see [56]). For a determination of R6G

concentration in the gel from the recorded spectra, a set of reference hydrogel samples was prepared for every tested agarose-polyelectrolyte composition. In the reference hydrogel samples, a known concentration of homogeneously dispersed R6G was provided by the addition of the corresponding amount of R6G to the agarose solution before its gelation. Further data processing of the spectra (suppression of the light scattering background signal) was described in detail previously [54,56]. Diffusion experiments were performed in duplicates for each of the analyzed hydrogel compositions.

Each concentration profile (dependence of R6G concentration on the position in the gel, i.e., on distance from the solution/gel interface) determined for a particular hydrogel at the time of diffusion *t* were fitted by following diffusion equation (for the derivation, see [57]) using the Solver tool in MS Excel:

$$c(x) = c_0 \cdot erfc \frac{x}{\sqrt{4D_{eff}t}} \tag{7}$$

where *c(x)* and c_0 are concentrations of R6G in the gel (in $g \cdot m^{-3}$) at distance *x* from the interface or at the interface, respectively, and D_{eff} is the effective diffusion coefficient of R6G in the gel. From the fitting parameters (D_{eff}, c_0) the rate of R6G diffusion and its partition in the gel is described quantitatively. The partition coefficient is then calculated as the ratio of the interface concentrations of R6G in the gel and the solution (c_{sol}), respectively:

$$\varepsilon = c_0 / c_{sol} \tag{8}$$

Mean values and standard deviations of these parameters were calculated by averaging the results for three diffusion times and duplicated measurements.

2.6. Fluorescence Correlation Spectroscopy

Self-diffusion of the molecules of the model solute (R6G) was studied by fluorescence correlation spectroscopy (FCS). For this purpose, the homogeneous distribution of the R6G molecules (concentration in the order of nM) was achieved similarly to the preparation of reference hydrogel samples for the evaluation of macro-diffusion experiments.

The FCS measurements were performed on MicroTime 200 instrument (PicoQuant, Berlin, Germany) equipped with a fluorescence microscope Olympus IX71 (Olympus, Tokio, Japan) (setup of the system: laser wavelength 510 nm, dichroic mirror 514/640 nm, emission filter 550/49, laser intensity 6.6 µW). Moreover, during FCS measurements, two single photon avalanche diode detectors were used, which allowed us to use cross-correlation for data evaluation. To maintain uniform measurement conditions, at the beginning of the experiment the vertical (*xz*) scan was performed and the position of the glass-gel interface was identified. Afterward, a horizontal (*xy*) scan was performed 5 µm above the glass surface and three different positions were chosen for measurements for each sample. Subsequently, for FCS analysis each hydrogel sample was prepared in five replicates. The main outcome from FCS analysis is the coefficient of self-diffusion of R6G in each hydrogel sample.

2.7. Scanning Electron Microscopy Imaging

For the scanning electron microscopy (SEM) imaging of the internal structures of the gels, samples were first cryogenically fixed. Small copper-based thin-wall tubes with a diameter of approximately 1 mm were at first filled with the particular hydrogel sample—each tube was filled by performing a horizontal motion through the already gelled agarose or agarose/polyelectrolyte solution using tweezers so that the hydrogel protruded from the tube at both ends. The plunge-freezing technique of fixation was used, where a small amount of hydrogel is rapidly cooled by immersion in cryogen (liquid nitrogen in this case). After having been plunge-frozen, the tubes containing hydrogel samples were kept at cryogenic temperatures throughout the whole experiment including the imaging. Before the imaging, freeze-fracture was also applied by cutting off the protruding part and scratching the surface superficially with a sharp blade at high vacuum and low temperature in the EM ACE600 preparation chamber (Leica microsystems, Vienna, Austria). Three successive steps of freeze etching to reveal

the internal microstructure were applied. During each of the etching steps, the temperature was increased to −100 °C, and after it stabilized, decreased back to −120 °C. All the frozen samples were imaged in the SEM Magellan 400L (FEI-Thermo Fisher Scientific, Hillsboro, OR, USA) equipped by a temperature-controlled cryo-stage at the temperature of −120 °C; the imaging was performed before any freeze etching and after each freeze etching step.

Image processing and analysis of the cryo-SEM images was performed in ImageJ open-source image processing toolbox (National Institute of Health, Bethesda, Maryland, USA and Laboratory for Optical and Computational Instrumentation, University of Wisconsin, Madison, USA; version 1.51, [58,59]). For this purpose, square sections of the raw cryo-SEM images (512 × 512 pixels) were processed by the following procedures: contrast and brightness of the section were first adjusted according to the image histogram and the bandpass filter was used to suppress lightening inhomogeneities and horizontal stripes. Then the processed images need to be converted from grayscale to black and white projections in an effort to display only the uppermost layer of the 3D network structure. For this conversion, the image sections were thresholded using the MaxEntropy algorithm. Subsequently, the actual analysis of the internal structure proceeded using 'Analyze particles' and 'Analyze skeleton' commands (details are provided in the Results section).

3. Results

3.1. Mechanical Properties of the Gels

Overall viscoelastic properties of the semiIPN gel samples were examined by standard techniques of oscillatory rheometry. Results of the frequency sweeps are shown for agarose gels and selected semiIPN gels in Figure 1a,b (corresponding frequency dependencies of storage and loss moduli as the raw experimental data are provided in Figure S1 in Supplementary Materials). As can be seen, the value of complex modulus (calculated using Equation (1)) is almost frequency-independent for all analyzed hydrogels (see Figure 1a). This represents a characteristic rheological feature of densely cross-linked gel networks where the deformation response in the linear viscoelastic region is not significantly affected by the timescale of the deformation [60–62]. Perhaps more important, it can be seen in the same figure that the overall stiffness of semiIPN gels can be adjusted over a wide range of values by alternating the concentration of the network-making component. In the case of agarose gels, changing the concentration of agarose from 0.5% to 4% by weight shifts the complex modulus of the gels to the values higher by more than two orders of magnitude. On the other hand, the presence of the interpenetrating polyelectrolyte components (PSS and ALG) in the range of concentrations used in this work (max. 0.01% by weight of the gels) does not affect the stiffness of the gel severely (see Figure 1, for other concentrations of polyelectrolytes, see Figures S2 and S3 in Supplementary Materials). The frequency dependence of the phase-shift angle (calculated using Equation (2)) illustrates the relative contribution of the elastic and viscous type of deformation on different time scales (see Figure 1b). It can be seen that even at the lowest frequencies of the oscillatory shear deformation, the phase-shift angle is still lower than 45° for all prepared gels (including as well the semiIPN gels with lower content of polyelectrolyte component, data shown in Figure S3 Supplementary Materials). In other words, even for the slowest deformations that take place on the longest timescales, the gel is deformed predominantly elastically. At the deformation timescale of seconds, the value of phase angle is so low for all gels (<10°), that their deformation behavior resembles ideal solids. Finally, it should be also mentioned that all prepared hydrogels were subjected also to complementary oscillatory tests such as amplitude sweep (alternatively called strain sweep) and relaxation tests. Although all the particular results are not shown here (see results of the strain sweep test in Figure S4 in Supplementary Materials), they can be concluded similarly—differences in the deformation response of the gels caused by the presence of interpenetrating polyelectrolyte component was insignificant compared to the impact of the different content of the gel-forming component (agarose).

visual observations can easily be transformed into quantitative information by measuring UV-VIS spectra at different positions in the gels. Using the calibration method based on gels prepared with a known content of R6G, concentration profiles of R6G can be determined for different gel compositions and for various times of the diffusion experiment. A comparison of such concentration profiles corresponding to gels with different contents of PSS and ALG is shown in Figures 2b and 2d, respectively.
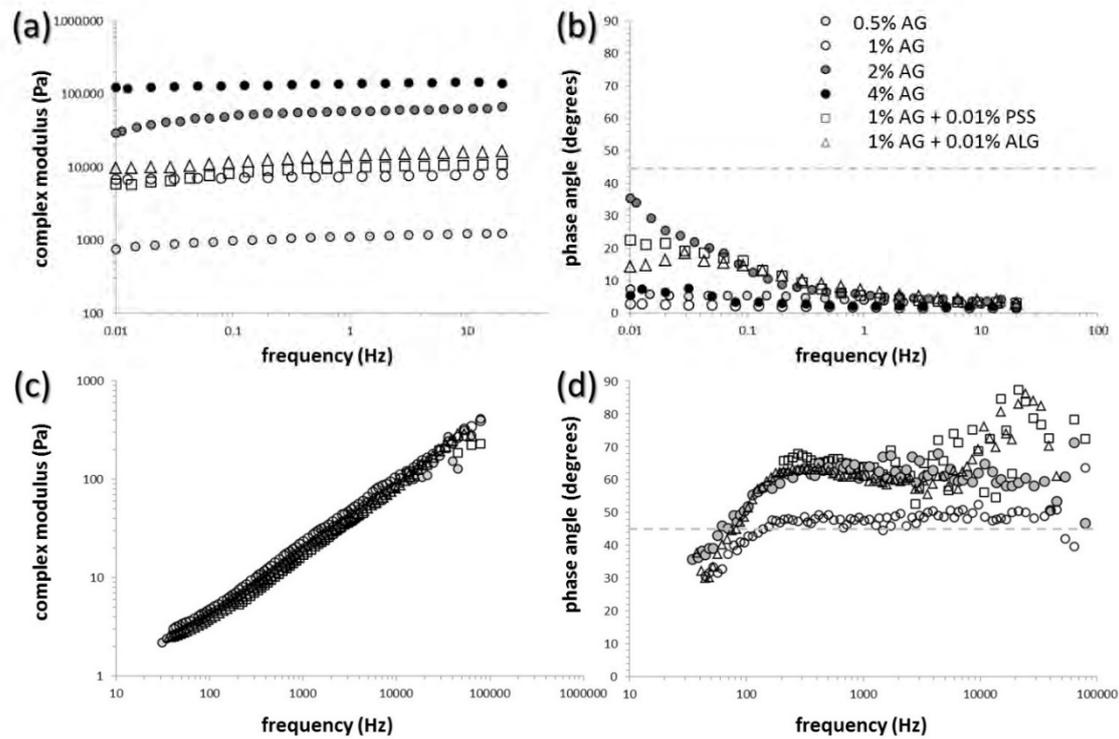
Figure 1. Parameters of viscoelasticity of the gels determined on macroscopic **(a,b)** and microscopic scale **(c,d)**. Frequency dependence of the complex modulus **(a,c)** and the phase angle **(b,d)**, respectively.

The microrheological assay describes the deformation behavior of the gels from a different perspective. The method based on DLS observation was used for monitoring the thermal motion of standard tracer microparticles incorporated into the internal structure of the gels. In this approach, from the scattering correlogram (a function which correlates the scattering intensity over time), the mean square displacement function of the tracer particles is derived and the basic viscoelastic parameters (storage and loss moduli and the others related with these two) are calculated for individual characteristic times or frequencies. This approach therefore provides the microrheometric analog to standard oscillatory frequency sweep tests—viscoelastic parameters which are obtained are the same in their essence for both methods; nevertheless, in the case of microrheology, they characterize viscoelasticity of that part of the internal space of the hydrogel where the thermal motion of the tracer particles takes place.

Basic results of the DLS microrheology are presented in Figure 1c,d and Figure S5 in Supplementary Materials. Figure 1c,d shows frequency dependencies of the complex moduli and phase angles, respectively, derived from the thermal motion of tracer microparticles in the internal pores of the particular hydrogel structure. As can be seen, the results of this experiment show (see also Table 2) differences as compared to the results of common oscillatory (macro)rheometry. Complex moduli of the gels determined by DLS microrheometry are significantly lower and considerably more dependent on the frequency of the deformation. Furthermore, as far as the frequency-dependent complex moduli (as well as the complex viscosity) an alternative quantitative parameter describing stiffness of the material) of all tested gels (taking into account also such as those describing our previous study [56] graphically in Figure S5 in Supplementary Materials) show virtually the same values, and it can be deduced that the local environments of the microparticle motion in particular gels provide similar deformation response. Contrarily to the classical oscillatory rheometry, the viscous character of the deformation behavior predominates (note the values of phase angle > 45° in Figure 1d). This is reasonable from the point of view that the thermal motion of the particles takes place in the liquid pores of the hydrogel matrix and that the microrheological approach, therefore, provides insight into the deformation behavior of

this local microenvironment. Furthermore, it can be seen from the frequency dependencies of phase angles that while the lowest applied frequencies induce the most viscous deformation response in the case of oscillatory macrorheometric analysis, the opposite is observed for the microrheology assay (most elastic response is measured for the lowest characteristic frequencies). Again, this apparent discrepancy of the viscoelastic properties arises from the essential difference between the two rheometric approaches. While for the oscillatory rheometry the lowest frequencies characterize the slowest applied oscillatory deformation where the liquid-like character of the material is most manifested, in the case of microrheology the lowest frequencies correspond to the longest correlation time where the trace particle motion reaches also more distant surroundings of the particle. Therefore, the presence of a polymer network that surrounds liquid pores filled with tracer particles affects the particle motion most strongly just for the lowest frequencies. It can be seen in Figure 1d that concerning both discussed aspects of the viscoelastic response of tested gels on the microscopic scale, no fundamental differences were found for the gels no matter what the content of gel-forming or interpenetrating component was.

3.2. Transport Properties of the Gels

Similarly to the investigation of mechanical properties of the gels, also the analysis of transport performance towards the model hydrophilic solute (Rhodamine 6G, R6G) was performed using both a macro- and a micro-scale approach. The results of the diffusion experiments are shown in Figure 2 and Tables 1 and 2. Firstly, macroscopic investigation of the diffusion of R6G from source solution into the gels was involved using the methodology developed in our previous work [37–39]. It can be seen in Figure 2a,c that, using this simple method, the effects of the interpenetrated components on the rate of transport in the gels can be evaluated even visually. In particular, the picture in Figure 2a shows that the presence of interpenetrating PSS chains severely affects (decelerates) the rate of R6G diffusion in the gel and that the effect correlates with the content of PSS in the gels. Furthermore, different color saturation in the gel near the interface with the source solution indicates that also the partition of the R6G between the solution and the gel is affected by the presence of PSS. On the other hand, no such effects can be observed in the case of ALG's presence in the gels (see Figure 2c). These visual observations can easily be transformed into quantitative information by measuring UV-VIS spectra at different positions in the gels. Using the calibration method based on gels prepared with a known content of R6G, concentration profiles of R6G can be determined for different gel compositions and for various times of the diffusion experiment. A comparison of such concentration profiles corresponding to gels with different contents of PSS and ALG is shown in Figure 2b,d, respectively.

By the regression of the concentration profiles (using fitting Equation (7)), effective diffusion coefficients (D_{eff}) and boundary concentrations of R6G in the gel (c_0) can be calculated (see Tables 1 and 2). It can be seen that the comparison of absolute values of the calculated diffusivities agrees well with the qualitative features discussed based on the visual investigation of the gels. The presence of PSS in the gel reduces the effective diffusivity of R6G significantly; the highest content of PSS reduced the diffusivity by more than 90% of the value corresponding to the agarose gel with no interpenetrating component. The effect of ALG was much less pronounced and rather inverse at first sight—the presence of ALG in the gels slightly increases the average diffusivity. Nevertheless, taking into account the confidence interval of the diffusivity values, no definite conclusions can be derived for an effect of ALG on the rate of R6G diffusion in the gels.

A similar difference in effects of the two interpenetrating polyelectrolytes was observed also for partition coefficients calculated using Equation (8). While the concentration of R6G in the gel at the boundary with the source solution was not significantly affected even by the highest concentration (0.01 wt.%) of ALG as compared to the reference agarose gel (see Table 2), the same content of PSS increased the partition drastically (to more than 10-fold higher average concentration compared to reference agarose gel). In a fact, partition coefficients determined in this study illustrate the dynamic partitioning of the solute during its diffusion into the gel. Equilibrium distribution of the solute between the solution and the gel could be described more accurately by the results of equilibrium

absorption experiments such as those described in our previous study [55]. On the other hand, the diffusion experiments proposed here benefits mainly from providing the simultaneous monitoring of partitioning and diffusion parameters in the single experiment.
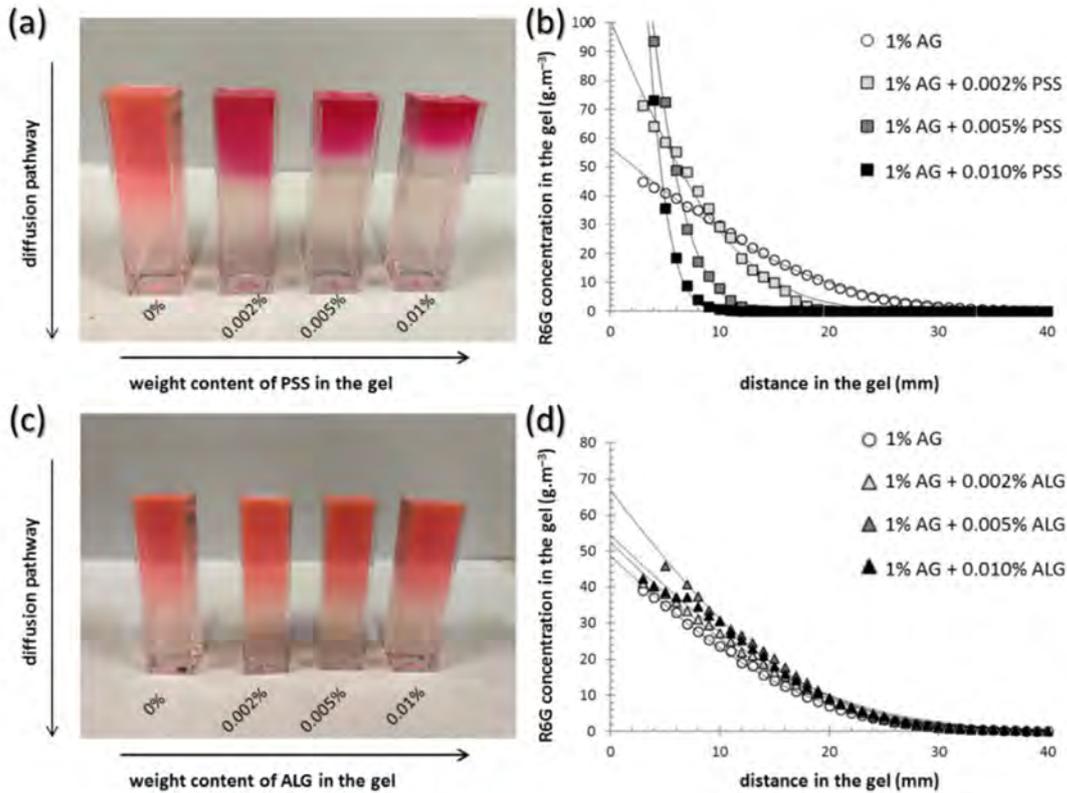
Figure 2. Diffusion of Rhodamine 6G (R6G) in the gels investigated on the macroscopic scale. (a,c) Visual comparison of agarose gels (1 wt% of ag.%) with different content of the interpenetrating component after 72 h of diffusion of R6G from solution (b,d) Experimentally determined concentration profiles of the same gels.

FCS analysis provides a complementary view on the transport properties of the gels as far as self-diffusion of individual, homogeneously distributed R6G molecules is monitored. Self-diffusion coefficient (Ds) of the R6G molecules in a respective gel is determined here from the time evolution of correlation function that characterizes the time scales of fluctuations in the intensity of the R6G fluorescence. Different diffusion models can be used in the mathematical evaluation of the correlation function. In our work, we have applied the simplest model involving a single characteristic decay-time to the autocorrelation function providing one global diffusion coefficient of the present chromophores. The diffusion coefficient values determined for the semi-IPN hydrogels are summarized in Tables 1 and 2. It can be seen that for both polyelectrolyte components interpenetrating the agarose matrix, the self-diffusivity of R6G decreases with the concentration of the binding component in the gel, only the exact extent of the suppression of R6G diffusivity is different for PSS and ALG. In the case of PSS, the FCS diffusivity is slightly less suppressed than in the case of effective diffusivities determined by the macroscopic diffusion assay. On the other hand, a modest reduction of the rate of thermal motion of R6G is here found out also for ALG, unlike the macroscopic assay. The apparent discrepancy between the results of macroscopic and FCS diffusivity assays may be attributed to the different experimental conditions as well as to the distinct physical phenomena behind the two methods. First, the macroscopic diffusion assay uses the concentration of tracked diffusion probe (R6G) orders of magnitude higher than FCS. The relative content of freely moving RG6 molecules not affected by the interpenetrated polyelectrolyte must be significantly different in the two methods. Therefore, macroscopic diffusion assay may not be sufficiently sensitive to detect an effect of weakly binding components (such as ALG). On the other side, when the binding is strong enough to entirely immobilize the fluorescent molecule, this molecule becomes "invisible"

Table 1. Summarized results of investigation of R6G diffusion on the macroscopic and molecular scale in hydrogels with/without poly(styrene sulfonate) (PSS).

Weight Content of PSS in the Gel	Macroscopic Diffusivity D_{eff} (µm²·s⁻¹)	FCS Diffusivity * D_s (µm²·s⁻¹)	Partition Coefficient ε (-)	Fluorescence Lifetime τ (ns)
0%	389 ± 7	343 ± 7	5.3 ± 2.0	4.21 ± 0.06
0.002%	158 ± 27	196 ± 27	10.2 ± 2.6	4.21 ± 0.09
0.005%	32 ± 25	128 ± 23	91.0 ± 51.0	4.27 ± 0.07
0.010%	27 ± 22	96 ± 22	118 ± 37	4.30 ± 0.06

Table 2. Summarized results of investigation of R6G diffusion on the macroscopic and molecular scale in hydrogels with/without alginate (ALG).

Weight Content of ALG in the Gel	Macroscopic Diffusivity D_{eff} (µm²·s⁻¹)	FCS Diffusivity D_s (µm²·s⁻¹)	Partition Coefficient ε (-)	Fluorescence Lifetime τ (ns)
0%	333 ± 38	385 ± 15	7.0 ± 1.6	4.17 ± 0.02
0.002%	379 ± 27	309 ± 21	6.4 ± 1.2	3.73 ± 0.03
0.005%	379 ± 46	304 ± 48	6.4 ± 1.0	3.69 ± 0.01
0.010%	341 ± 22	261 ± 41	6.1 ± 1.0	3.64 ± 0.1

coefficient (D_s) of the R6G molecules in a respective gel is determined here from the time evolution of correlation function that characterizes the time scales of fluctuations in the intensity of the R6G fluorescence. Different diffusion models can be used in the mathematical evaluation of the correlation function. In our work, we have applied the simplest model involving a single characteristic decay-time to the autocorrelation function providing one global diffusion coefficient of the present chromophores. The diffusion coefficient values determined for the semiIPN hydrogels are summarized in Tables 1 and 2. It can be seen that for both polyelectrolyte components interpenetrating the agarose matrix, the self-diffusivity of R6G decreases with the concentration of the binding component in the gel, only the exact extent of the suppression of P6G diffusivity is different for PSS and ALG, respectively. In the case of PSS, the effect is slightly less pronounced than in the case of effective diffusivities determined by the macroscopic diffusion assay. On the other hand, a modest reduction of the rate of thermal motion of R6G is here found out also for ALG, unlike the macroscopic assay. The apparent discrepancy between the results of macroscopic and FCS diffusivity assays may be attributed to the different experimental conditions as well as to the distinct physical phenomena behind the two methods. First, the macroscopic diffusion assay uses the concentration of tracked diffusion probe (R6G) orders of magnitude higher than FCS. The relative content of freely moving RG6 molecules, not affected by the interpenetrated polyelectrolyte, must be significantly different in the two methods. Therefore, macroscopic diffusion assay may not be sufficiently sensitive to detect an effect of weakly binding components (such as ALG). On the other side, when the binding is strong enough to entirely immobilize the fluorescent molecule, this molecule becomes "invisible" for the FCS methods and the average self-diffusivity determined by FCS may be overvalued. Actually, in contrast to the macro-scale experiments with the UV-VIS absorption detection of diffusing R6G, the FCS technique can analyze only the motion of fluorescence-emitting molecules. Therefore, the strongly physically bound R6G molecules that lose the light-emitting ability via static fluorescence quenching are not monitored and do not contribute to the calculated diffusion coefficient any more. In general, results of the FCS diffusivity assay confirm that R6G molecules are subjected to an attractive interaction with both the polyelectrolyte components, whereby the interaction is significantly stronger in the case of PSS.

Aside from the determination of the self-diffusion coefficient of a solute, the FCS method can also provide some additional parameters which might be interpreted concerning the mode of binding of the solute by the polymer network. For instance, in the case of time-resolved FCS technique, the average diffusion coefficients of R6G in the analyzed volume are complemented with corresponding average fluorescence lifetimes. Tables 1 and 2 show the values of the average fluorescence lifetime of R6G determined by TCSPC (time-correlated single photon counting) analysis of the time-resolved FCS experiment. Once again, a dissimilar effect has risen from the presence of ALG and PSS, respectively. The presence of PSS in the gel matrix leads to a slightly increased value of fluorescence lifetime, while higher content of ALG rather decreases the value. As far as the fluorescence lifetime is inversely proportional to rates of non-radiative de-excitation processes, its value is sensitive to a local environment in which a motion of the molecule occurs. In particular, the increase in fluorescence lifetime can be explained in terms of loss of the rotational freedom of the fluorophore caused by the R6G binding by PSS.

On the other hand, the R6G fluorescence lifetime, the value of which usually varies around 4 ns [63], is known to be highly concentration-dependent, as Förster energy transfer between monomers and weakly fluorescent stable dimers at higher R6G concentrations decreases the quantum yield and causes the fluorescence lifetime shortening [64]. Therefore, a decrease of fluorescence lifetimes in the gel with the highest ALG content may be assigned to a change in the spatial distribution of R6G molecules in the gel, which does not alter the rotational freedom significantly but causes colocalization of R6G molecules and the formation of R6G dimers. Similarly, concentration effects may explain also a difference in the average fluorescence lifetimes determined for agarose gels without polyelectrolyte components in the two independent experimental batches (compare the values for 0% ALG and PSS, in Tables 1 and 2, respectively). As far as all the analyzed gels in the respective experimental batch

were prepared simultaneously using the same R6G source solution and gelation conditions, it can be expected that the total R6G concentration in the gels is well comparable. On the other hand, in the case of a very low concentration of the R6G in the gel (order of nM), this is difficult to reproduce among the different experimental batches.

The qualitative difference in the effects of PSS and ALG on the fluorescence lifetime can be attributed to the dissimilar types of solute binding by the two polyelectrolytes. Electrostatic binding between opposite charges on the functional moieties of ALG and R6G molecules is less orientation-specific and, therefore, does not limit the rotation of the electrostatically bound R6G molecules significantly. On the other hand, this binding concentrates the fluorophore in the vicinity of oppositely charged polyelectrolyte which may enhance its aggregation. Unlike that, the presence of benzene moieties in the molecular structure of PSS complements the electrostatic attraction of R6G molecules with the planar stacking of the π electron-rich aromatic systems which results in significant loss of the rotational freedom of R6G and the corresponding increase in fluorescence lifetime.

3.3. Characterization of the Internal Structure of the Gels

Because both mechanical and transport properties of hydrogels are inevitably coupled with their internal structure, for a reasonable interpretation of results provided by the diffusion and rheological analyses of the studied hydrogels it is essential to provide their qualitative and, at best, quantitative structural characterization. For this purpose, we have included in our study also a complex structural assay comprising methods of either direct visualization or an indirect physicochemical mapping of the hydrogel network morphology.

For an indirect structural investigation of the agarose-based semiIPN hydrogels, we have at first utilized a simple turbidimetric assay, where turbidity is calculated from the optical density of the gels (determined by a standard transmission UV-VIS spectrometer) and plotted in log-log coordinates versus wavelength of the incident light. The exact mathematical apparatus for extracting internal structure parameters from such turbidity spectra was first proposed by Doty and Steiner [65] and further utilized by numerous authors [50,66–69]. We have followed the data-processing procedure that has been successfully applied by Aymard on various aqueous dispersions including swelled agarose hydrogels [50]. In this approach, linear regression of the log-log turbidity spectrum is performed in the range of wavelengths from 700 to 800 nm, and from the slope of the fitting line, the mesh size of an average scattering unit is determined (the log-log plots used for the calculation of the effective mesh size are shown in Figure S6 in Supplementary Materials). Aymard interprets the mesh size as the average distance between entanglements in the hydrogel network and, therefore, a value of this parameter can be taken as a rough estimate of the dimensions of pores in the gels. Mesh size values, determined from the turbidity data, are summarized in Figure 3a. As expected, the effective mesh size decreases significantly with the concentration of agarose in the gel as an indicator of the increasing density of crosslinking in the gel network. The order of magnitude of the calculated mesh sizes is in good agreement with the published range of pore sizes in agarose gels between 80 and 500 nm [70,71]. It was expected that the minor addition of polyelectrolyte interpenetrating components (PSS or ALG) will not remarkably alter the internal structure of the gels. It can be seen in Figure 3a that the addition of 0.01 wt.% of PSS or ALG increased in mesh size. The result can seem surprising as far as any addition of other polymer components should result in presence of more scattering centers which would hereby rather decrease the calculated mesh size value. Nevertheless, it must be emphasized that the method only characterizes a mean isometric dimension of the average scattering unit in the gel, and provides limited information about the other qualitative and quantitative structural parameters such as the actual shape of the network pores, width of the pore size distribution, etc. Therefore, conclusions about the results shown in Figure 3a should, rather, be about how the presence of minor contents of interpenetrating components does not significantly (in terms of the orders of magnitude) affect the size of the representative scatterer in the gel.

Figure 3. Results of indirect structural mapping of the hydrogels with different concentrations of agarose (◎) and of the gels containing 1 wt.% of agarose-based interpenetrated by 0.01 wt.% PSS (⊡) and ALG (⊕), respectively. The analysis is specific effective sizes were calculated from the results of turbidimetry (a) and rheometry (b), respectively.

Not only the light scattering, but also the mechanical properties (mainly the elastic component of the deformation response) of the polymer networks are fundamentally connected with their crosslinking densities. Therefore, the results of rheometric assays may be used for the determination of effective mesh size, which in this case represents the mean size of the elastically active sections of polymer chains. Calculation of the mesh sizes from frequency sweep tests (using Equations (3) to (6)) is based on the rubber elasticity theory [72]. Although the validity provided by the plunging of the sample in liquid nitrogen. this theory for gels has continuously been questioned [73,74], it has been repeatedly utilized to calculate the mesh size of hydrogels based on rheometric parameters [52,75]. Previously, we have applied this approach in the determination of mesh size of polysaccharide-based phase-separated hydrogels [76]. The results of the calculations for the gels studied in the current study are shown in Figure 3b. As with the turbidimetry-derived values, also in this case the mesh sizes should be used for qualitative monitoring of changes in the internal structure rather than to provide absolute dimensions of the hydrogel pores. Again, it is evident that the increasing agarose content results in decreasing mesh sizes as a result of a more densely physically crosslinked agarose network. Compared to the turbidity-based mesh sizes, it can be seen that much lower values of the mesh size are calculated from the results of oscillatory rheometry. The elastically active chain sections differ naturally from those that participate in light scattering. Further comparing the results with published values of agarose gels pore sizes, it is also evident that the mesh size is significantly lower than the mean pore size. This is not a surprising fact when considering that also other than physical and chemical junction in the gel network (e.g., mechanical entanglements of the free polymer chains) can contribute to the elastic response to deformation. In this perspective, the most important outcome of this indirect structural mapping is that, in accordance with results from turbidimetry, no fundamental effect of the presence of interpenetrating polyelectrolyte component was observed (compare the effective mesh sizes for 1wt.% agarose gels with similar agarose gels containing also 0.01 wt.% ALG or PSS in Figure 3) as compared with the principal influence of the network-forming agarose component.

The gross picture of the morphology of the gels, provided by indirect structural mapping with rheometry and turbidimetry, was further refined by direct visualization of their internal porous structure by scanning electron microscopy (SEM). Cryogenic SEM (cryo-SEM) imaging was applied because aqueous samples cannot be directly observed in a high vacuum that needs to be maintained in the SEM chamber without any preceding stabilization. Therefore, the cryogenic fixation of the sample was performed via rapid cooling provided by the plunging of the sample in liquid nitrogen. To visualize the internal structure of a hydrogel sample, plunge freezing is followed by freeze-fracture (scratching the sample at high vacuum and cryogenic temperature) and freeze etching (letting the frozen water sublime to reveal the sample surface). Although plunging is not an optimal cryogenic

fixation method for preparation of such hydrated samples in electron microscopy because of the Leidenfrost effect during which a thermally insulating film of vaporized nitrogen forms around the sample, preventing fast cooling and allowing water ice crystals to form inside the specimen [77,78], it could be also beneficial in the case of hydrogel structural studies. We assume that the size and distribution of the ice crystals correspond to the chemical composition of the hydrogels and the amount of free water.

Results of the cryo-SEM imaging of the gels with different content of agarose (with the absence of an interpenetrating component) are shown in Figure 4, while the results for semiIPN hydrogels with the highest content of the respective interpenetrating component are provided in Figure 5. As expected, the principal role of agarose concentration in controlling the density of the crosslinking of the hydrogel network is obvious. On the other hand, as can be seen in Figure 5, even the highest applied concentration of an interpenetrating component (ALG or PSS) does not induce noticeable changes in the internal structure of the gels. Taking a closer look at the cryo-SEM images, it can be concluded that the plunge freezing of the gels in liquid nitrogen satisfactorily preserved the internal structure of the gels that is in correlation with the other applied methods. The network structure is largely isomorphic, with no apparent signs of anisotropic deformation during cooling. Nevertheless, some structural artifacts can be found in the images (such as those marked with arrows in Figure 4) indicating that the formation of ice crystals was not completely prevented.

The cryo-SEM images such as those shown in Figures 4 and 5 serve primarily as a visual illustration of the qualitative characteristics of the internal structure of the studied gel networks. From this point of view, the visual evaluation of the cryo-SEM images confirms the qualitative findings provided by indirect structure-mapping methods (turbidimetry, rheometry), i.e., the principle that the network-forming role of agarose is not particularly disturbed by a presence of the polyelectrolyte component. Nevertheless, cryo-SEM imaging can also be further processed to support these qualitative conclusions from some quantitative outcomes. For this purpose, we have applied two techniques of the image processing that are implemented in the open-source scientific image-processing toolbox ImageJ and that are suggested for the analysis of porous structures.

Firstly, the 'Analyze particles' tool (an automatic particle segmentation algorithm implemented in ImageJ) was used to identify individual pores in the image of the gel network. The outlines of the pores detected in the binary projection (Figure 6b) of an original image (Figure 6a) are shown in Figure 6c. As a numerical result of the Analyze particles tool, every outlined pore is described by its area and perimeter. Wherever it is necessary to take care of the pores which are displayed in the binary picture touching one another, the Watershed algorithm can be used before particle analysis. This algorithm uses a density profile to determine if one object with a peninsula should be two objects. If it determines that they should, it will draw a line to separate them. From the particle analysis, the distribution of pore areas and perimeters is obtained and processed into statistical parameters, e.g., average or mean values. The box plot projection of the pore areas and perimeters is shown in Figure 7a,b. These results again confirm that the size of pores, detected in the cryo-SEM images, decreases significantly with the increasing concentration of agarose in the gel. Once again, no such considerable pore size reduction is found for the semiIPN gels as a result of the presence of polyelectrolyte component.
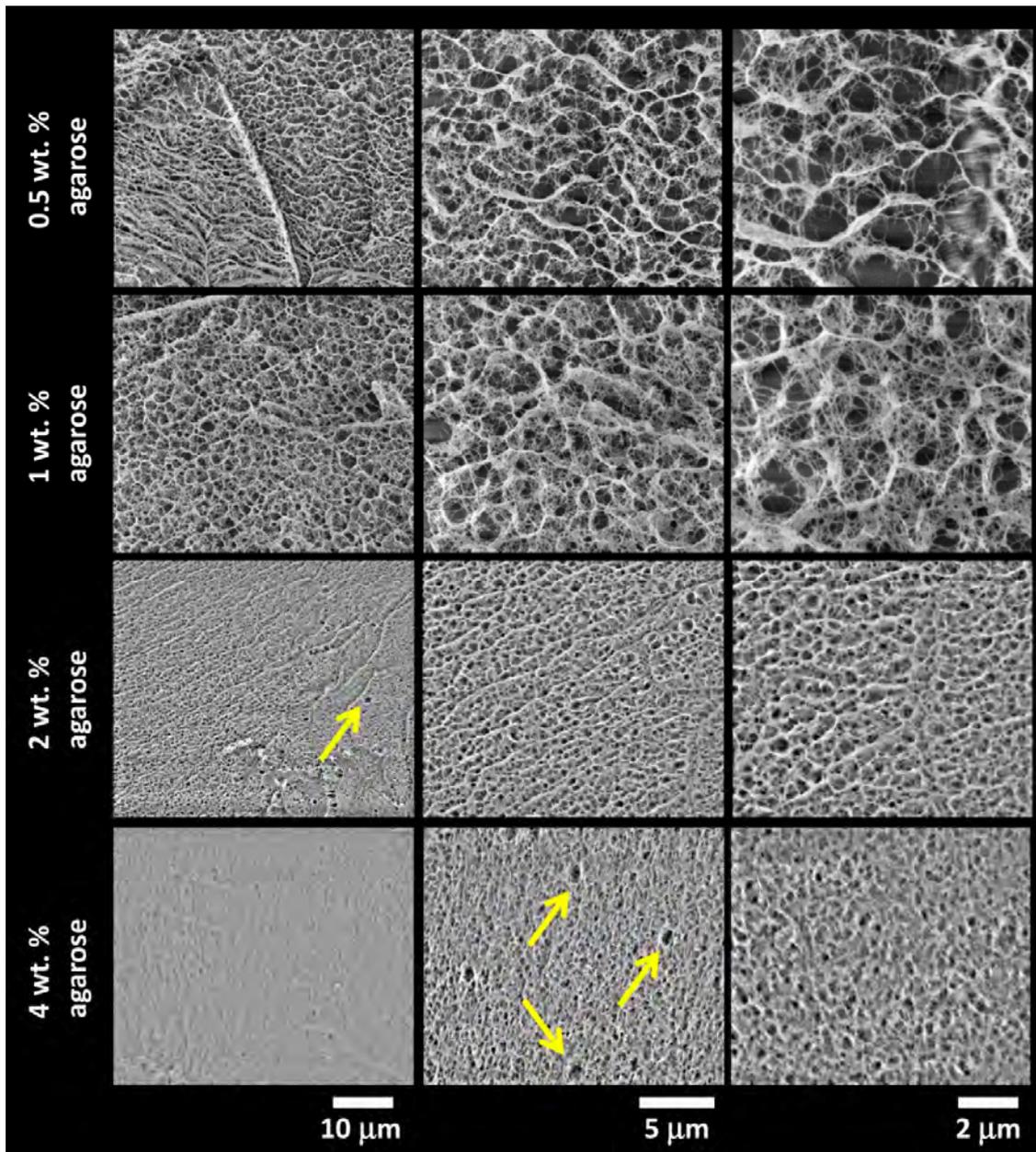
Figure 4. Results of cryogenic scanning electron microscopy (cryo-SEM) imaging of the internal structure of the plunge-frozen hydrogels with various content of agarose (with the absence of an interpenetrating polyelectrolyte component). Structure alterations caused by the formation of ice crystals are marked with arrows.
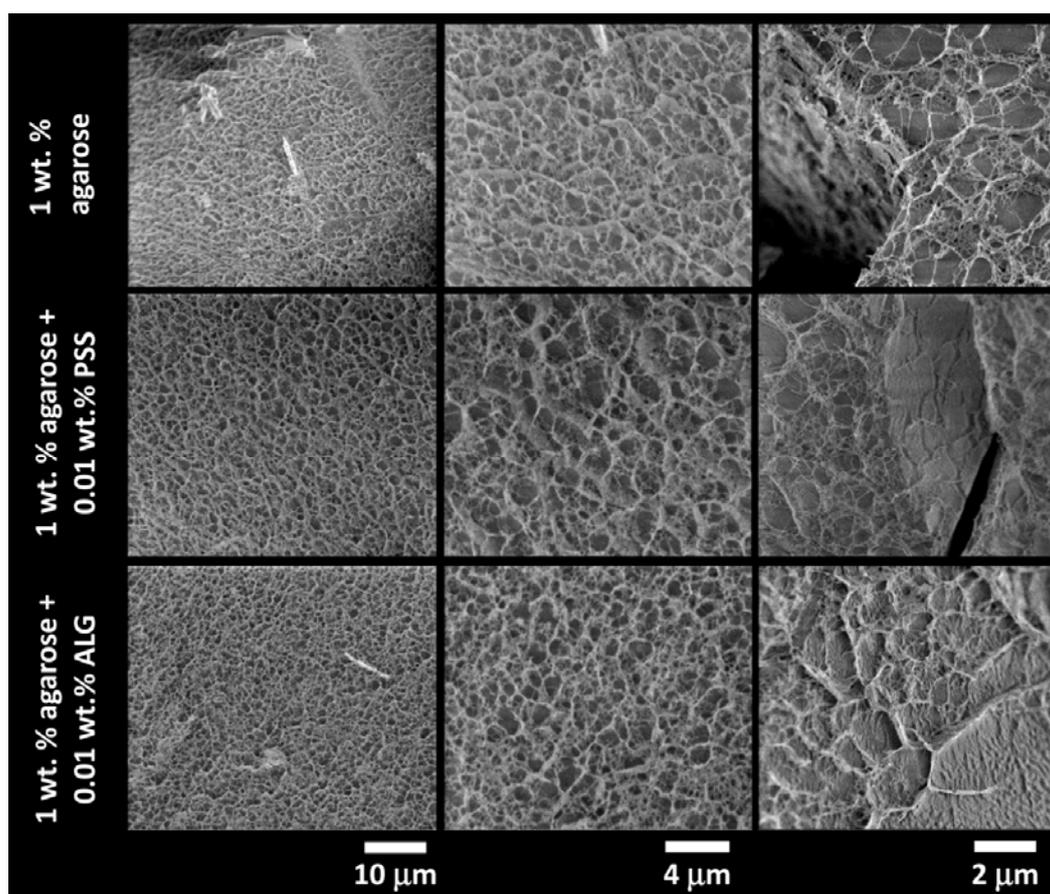
Figure 5. Results of cryo-SEM imaging of the internal structure of the plunge-frozen 1wt.% agarose hydrogels with and without the presence of an interpenetrating polyelectrolyte component (0.01 wt.% of PSS and ALG, respectively).

Pore areas/perimeters are not in their absolute values reasonably comparable with the results of indirect structural analyses summarized in Figure 3. Furthermore, as can be seen in Figure 6c, the pores detected in the cryo-SEM images have complex, rarely isometric shapes and, therefore, neither pore areas nor pore perimeters can be simply transformed into an isometric representation of the pore size, such as the diameters in the case of circular pore projections. Therefore, aside from the 'Analyse particles' approach, we used also another image analysis option implemented in the ImageJ toolbox—the 'Analyze skeleton' tool. In this procedure, the network structure displayed in the analyzed image is first skeletonized, i.e., replaced by the line skeleton using a topology-maintaining medial axis thinning algorithm (example of the skeletonized representation of the processed image is shown in Figure 6d). Using the subsequent analysis tool, branches and junctions of such a skeleton are classified, counted, and measured. The Box plot which represents the statistical treatment of branch sizes, detected in the skeleton of cryo-SEM images of analyzed hydrogels, is shown in Figure 7c. Unlike the areas or perimeters of the pores, the mesh size represents a linear size parameter and as such can be directly compared with the effective mesh sizes determined by turbidimetry or rheometry. As can be seen in Figure 7c, the effect of agarose content in the gels surpasses the influence of the interpenetrating component also in the distribution of branch sizes. Increasing concentration of agarose induces denser crosslinking, which results in shorter branches in the skeletonized image. The mean values of the branch sizes are in the order of hundreds of nm, which represents larger pore dimensions compared to the values determined by indirect structural techniques (Figure 3) as well as to the published pore sizes detected in agarose gels by other techniques [70,71]. This is probably caused by the partial expansion

Figure 6. Processing of cryo-SEM images using the tools implemented in ImageJ software (National Institute of Health, Bethesda, Maryland, USA and Laboratory for Optical and Computational Instrumentation, University of Wisconsin, Madison, USA). Scalebar = 10 µm. (**a**) Original image (1 wt.% agarose gel without any interpenetrating component). (**b**) Binary projection (grayscale

1 wt. % agarose
0.01 wt.%

10 µm   4 µm   2 µm
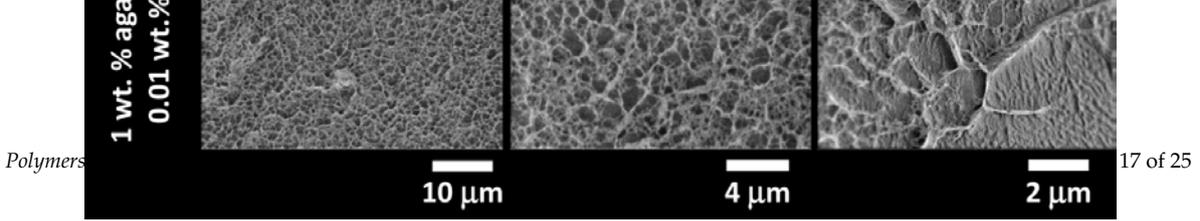
of dispersed water resulting from its imperfect vitrification and partial crystallization (see the signs of ice formation mentioned above).

Figure 5. Results of cryo-SEM imaging of the vitrification run of the thin crystalline 1 wt.% agarose hydrogels with and without the presence of an interpenetrating polyelectrolyte component (0.01 wt.% of PSS and ALG, respectively).
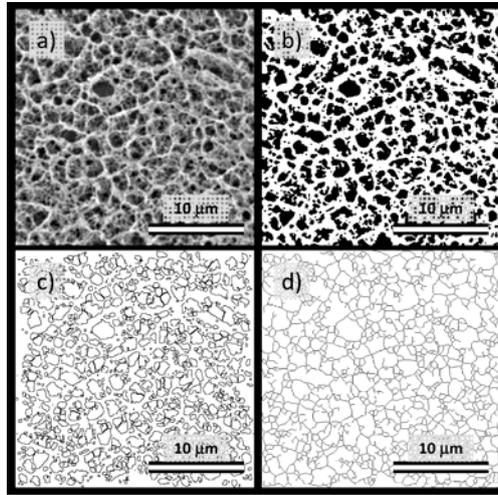
Figure 6. Processing of cryo-SEM images using the tools implemented in ImageJ software ((National Institute of Health, Bethesda, MD, USA and Laboratory for Optical and Computational Instrumentation, University of Wisconsin, Madison, WI, USA). Scalebar = 10 µm. (**a**) Original image (1 wt.% agarose gel without any interpenetrating component). (**b**) Binary projection (grayscale thresholding using MaxEntropy algorithm) of the original image. (**c**) An image mask is provided by the application of the 'Analyze particles' tool. (**d**) Image mask is provided by the application of the 'Analyze skeleton' tool.
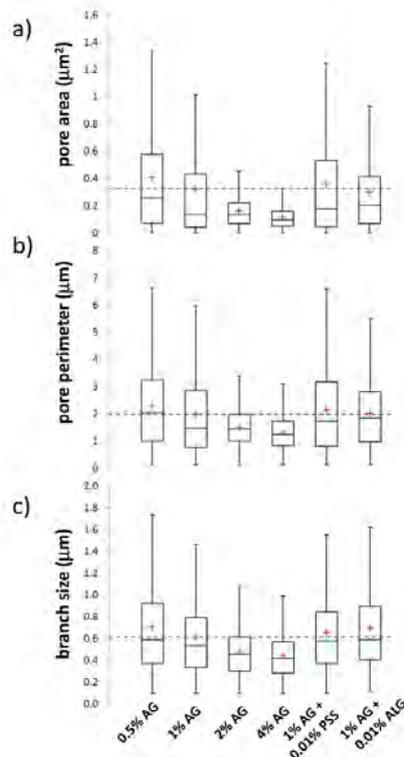
Figure 7. Box plots of pore size parameters determined from analysis of cryo-SEM images using ImageJ software. (**a,b**) Pore areas and perimeters determined using the 'Analyze Particles' tool. (**c**) Branch sizes using the 'Analyze skeleton' tool. Blue dashed lines in the box plots represent the mean values of the displayed parameters for 1 wt.% agarose gels without the presence of an interpenetrating polyelectrolyte component.

4. Discussion

The work presented here was set two major objectives. The first was to evaluate a simple material strategy proposed for the development of hydrogel-based controlled release systems that would allow independent tuning of their mechanical and transport features. The strategy is based on hybrid (dual component) hydrogels that consist of a network formed by a hydrophilic gelling

4. Discussion

The work presented here was set two major objectives. The first was to evaluate a simple material strategy proposed for the development of hydrogel-based controlled release systems that would allow independent tuning of their mechanical and transport features. The strategy is based on hybrid (dual component) hydrogels that consist of a network formed by a hydrophilic gelling component with reduced affinity to bind the carried active substance, interpenetrated by chains of a linear polymer that possess functional groups prone to a strong attractive interaction with the active substance. The second objective was to propose and test an appropriate analytical methodology that could provide a complex insight into composition–structure–performance relationships in the resulting hydrogel materials with the main concern on mechanical and transport properties investigated not only on the macroscopic scale but also in the specific microcosms of the aqueous gel pores. Combining these two central viewpoints, the presented study represents a fundamental contribution to the state of the art in controlled release systems with the potential to open up a new area of research and development of hydrogel-based CR materials.

The idea of semiIPN hydrogels with rheological and transport properties tunable independently via manipulating the relative composition of a network-making and a binding component is amazingly simple and it is surprising that, to our best knowledge, no systematic effort has been made to evaluate the potential of the use of such materials in the development of novel CR systems. The approach has a great advantage in its modularity—a broad portfolio of gel-making hydrophilic polymers with a limited capacity of physical binding by strong interactions such as coulomb forces or hydrogen bonds can be found, including the materials most routinely used in research and development of the first generation hydrogels for drug-delivery systems (e.g., poly(vinyl alcohol) [79], poly(2-hydroxyethyl methacrylate) [3,80], poly(ethylene glycols) [81] or thermomelting polysaccharides like gellan, dextran or agar [82,83]). During their gelation process, all these matrices allow easy incorporation of the interpenetrating component—a linear hydrophilic polymer with the chemical structure selected concerning specific binding preferences of intended carried substance. In our study, charged polymers were suggested as the interpenetrating component as they are generally applicable as a binding component in CR systems carrying ionic active compounds. A wide range of polyelectrolytes bearing various densities of positive or negative charges in combination with diverse accompanying chemical functionalities may be found among natural polymers (anionic and cationic polysaccharides such as alginate, hyaluronan, chitosan, polypeptides poly-γ-glutamate, poly-lysine), their chemically modified analogs (trimethyl chitosan, quaternized dextran, etc.) or among fully synthetic polymers (e.g., polymerized substituted acrylic monomers like polyacrylates, polyacrylamides, substituted polystyrenes, etc.). As a prototype material, agarose-based hydrogels interpenetrated by a minor content (less than or equal to 1:100 ratio by weight) of anionic polyelectrolytes (PSS and ALG) were prepared and analyzed in this work. The structure, mechanical properties, and transport of positively charged organic solute (Rhodamine 6G) in these gels were described thoroughly.

As expected, it was confirmed experimentally that the internal structure of the prepared gels in terms of their crosslinking density and corresponding internal porosity is principally governed by the concentration of agarose as the network-forming component (see the schematic representation of the effect in Figure 8a,b). As far as the morphology of the gel network predetermines its overall deformation response, also the mechanical performance of the gels is ruled by the content of agarose. By manipulating the concentration of the network-making component (agarose), the stiffness of the prepared gels may be altered over several orders of magnitude while the predominantly elastic (solid-like) rheological behavior typical for densely cross-linked hydrogels always prevails. Controlled stiffness of the hydrogel drug-delivery system is, on the one hand, a special concern mainly in load-bearing applications where the risk of premature mechanical destruction of a carrier is followed by a flow-away of the active compound which must be taken into account. On the other hand, a direct in vivo application of the highly elastic hydrogel materials may be problematic and limited to special physical forms such as gel micro- or nano-spheres [29]. Nevertheless, several strategies have

been proposed to overcome this hydrogel-delivery issue. One of the most common approaches is based on the injection of a viscous polymer solution followed by in situ crosslinking induced by an appropriate environmental trigger. One example which may be fully compatible with the proposed strategy of a semiIPN-based hydrogel-controlled release system is represented by block copolymers with hydrophobic domains which can crosslink at increased (physiological) temperatures via reverse thermal gelation caused by an entropically driven aggregation of the hydrophobic blocks (e.g., triblock ABA copolymers of A = poly(ethylene oxide) (PEO) and B = poly(propylene oxide) (PPO) [84]). The controlled interpenetration of the networks prepared from these temperature-sensitive sol-gel systems with a linear binding polymer component should be free of experimental difficulties as far as several PEO-based semiIPN systems have already been studied [85,86]. From this perspective, the proposed hybrid-network concept was proved to provide the expected ability to manipulate easily the material viscoelasticity with existing options on how to meet the specific requirements on flow properties of materials used in contemporary CR applications.
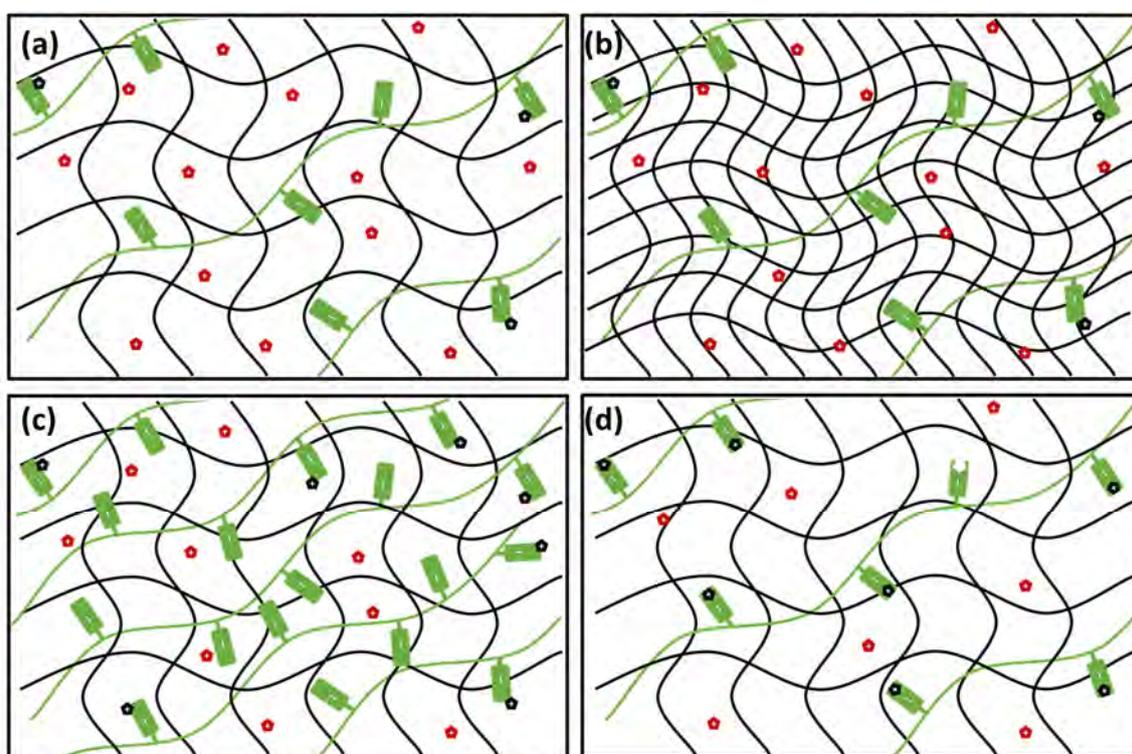
Figure 8. Schematic representation of the proposed concept of use of semiIPN hydrogels as controlled release (CR) systems with tunable rheological and transport properties. (**a**) Gelling component (black) with interpenetrating polyanion (green) possess universal binding affinity towards cations (red = free cations, black = bound cations). (**b**) With increasing content of the gelling component, gel stiffness and rigidity is increased with a negligible effect on the binding and diffusion of the cations. (**c**) With increasing content of the interpenetrating component, number of binding sites is increased affecting the transport properties of the gel with no effect on the mechanical properties. (**d**) Higher affinity of the binding sites (such as those provided for organic ions by PSS as compared with ALG) enhance the binding effectivity and shows more pronounced influence on the transport properties of the gel.

Furthermore, it was confirmed by the systematic diffusion-mapping assay that transport of the carried compounds in the dual-component gels may be significantly influenced even by a trace content of a suitable interpenetrating component (again, the schematic representation of the effect is provided in Figure 8a,c). In the present work, we focused our attention on the molecular transport of Rhodamine 6G. This model solute was used on the one side for its specific molecular structure combining the positive charge on nitrogen atom with aromatic structural residues. This specific structural motif is common

for numerous pharmaceutically active substances, e.g., for local anesthetics [47] or antibiotics [48]. Furthermore, well-described light absorption and emission behavior of R6G allows for the combination of various spectrometric techniques in the investigation of its transport in the hydrogel matrix on a different scale (macroscopic vs. microscopic scale). Results of experiments monitoring the diffusion of R6G from a source solution into the gels containing PSS confirmed that increasing the content of the interpenetrating component gradually suppresses the rate of R6G transport. In terms of the relative decrease in diffusion coefficient compared to a respective agarose gel, for the gels with ratio 1:100 (PSS to agarose) by weight, more than 90% decrease in diffusion coefficient was found for interpenetrated poly(styrene sulfonate). No such great alteration of R6G mobility may be achieved by manipulating the content of agarose itself, as was experimentally proved in our previous study [87]. Furthermore, not only the diffusion rate but also the partitioning of the solute in the gel is influenced significantly (more than a 10-fold increase in the partition coefficient was found in the case of PSS). Enhanced partitioning of the active compound may significantly increase the loading capacity of the drug carrier and consequently improve its pharmacokinetic profile [29]. On the other hand, a comparison of diffusion-related behavior of the gels interpenetrated by ALG and PSS, respectively, confirms that the degree to which the transport performance of the gel can be influenced is significantly dependent on the type of interaction between the active substance and the binding component (schematically represented in Figure 8a,d). In the case of ALG the binding of R6G is provided by the Coulomb electrostatic attraction alone while in the presence of PSS, we assume the stacking of aromatic moieties contributes to the binding significantly. This results in the fact that the extent to which the diffusion of R6G is affected (or, more precisely, the levels of R6G concentration at which these effects are manifested) differs significantly for the two interpenetrated polyelectrolytes.

Overall, on the example of prototype semiIPN hydrogels (in particular those containing PSS), it is illustrated that the transport properties of this type of hybrid network system may be altered greatly without any significant influence on their internal morphology and, hence, independently on their mechanical behavior. Furthermore, this strategy is not necessarily limited to the transport of hydrophilic active substances. Recently, several approaches have been proposed for the modification of hydrogels to provide controlled transport of water-insoluble solutes [88]. In our previous work, we have developed and characterized hydrogel systems with hydrophobic domains formed by surfactant micelles [89,90]. Controlled incorporation of such mechanically trapped hydrophobic domains in a supporting structure-defining hydrogel network could open new horizons in an independent tuning of mechanical and release behavior also for non-polar drug-releasing systems.

As was already noted, an additional merit of the present study is represented by the unique methodology that was utilized in providing the morphological, rheological, and also transport characterization of the studied hydrogels not only on the macroscopic but also on a microscopic scale. It was confirmed that this original analytical approach is highly beneficial in explaining the causal link between chemical composition, internal morphology, and mechanical and transport properties of the gels. For instance, our results clearly illustrate how the oscillatory (macro-)rheometry is complemented with the information provided by microrheometry in the completion of the overview of specific contributions of the polymer network and the surrounding aqueous solution, respectively, to the elastic and viscous components of the deformation response. Similarly, the involvement of a self-diffusion assay on the scale of individual molecules in parallel to common macroscopic monitoring of the diffusion of the same substance in the concentration gradient helps to explain how the binding of individual molecules in their local environment affects the rate of their molecular transport. Of course, the particular techniques described here do not represent the only and irreplaceable analytical option. For example, alternative techniques suggested for microrheological characterization of hydrogels include video microscopy [91] or fluorescence correlation spectroscopy [92]. Similarly, macroscopic diffusion experiments with hydrogels are often performed in a diffusion cell apparatus [87] while the self-diffusion of the solutes in the gels is commonly monitored via nuclear magnetic resonance

(NMR) [93]. Nevertheless, a combination of the macroscopic and microscopic scale of the analysis in a single study is still rather scarce.

Finally, for a reasonable discussion of deformation or transport performance of hydrogel materials, it is always necessary to have at one's disposal an analytical tool for mapping changes in the internal structure of the gel. Here, we have shown that cryo-SEM imaging of the gels provides detailed qualitative (and in combination with appropriate image processing techniques also quantitative) structural information. As noted, some indicators of alteration of the internal structure by the freezing artifacts can be found in our results. Nevertheless, this could be overcome e.g., by the utilization of a more appropriate cryofixation technique such as high-pressure freezing [94]. Aside from the direct visualization of the internal structure, our study also shows that valuable approximate structural information can be achieved also from much more accessible techniques of indirect structural mapping such as turbidimetry, rheometry, and additionally, for example, also differential scanning calorimetry [95].

5. Conclusions

It this study, we have experimentally verified through the results of a complex multiscale analysis of structure, viscoelastic, and transport properties of model agarose-based hydrogels with interpenetrating polyelectrolyte components that the concept of semiIPN gels containing an inert polymer network interpenetrated by a linear polymer component with the properly selected binding functionality can be successfully applied in the development of hydrogel materials with the ability of independent manipulation of mechanical and transport properties. Such materials possess a great application potential in controlled release systems, where one of the fundamental selection criteria for a suitable material candidate is represented by agreeing the required viscoelasticity and release-kinetic properties. In so far as this concept in general necessitates minimal requirements in the gelation procedure, it may be easily implemented in diverse state-of-the-art approaches in hydrogel preparation. Therefore, we believe that the presented work may become a stepping stone for a brand-new direction in the research and development of hydrogel-based controlled release systems. Furthermore, the original analytical approach designed and applied in this study is proposed as the methodological framework for these follow-up studies providing complex insights into composition–structure–performance relationships in developed hydrogel material.

References

1. Ahmed, E.M. Hydrogel: Preparation, characterization, and applications: A review. *J. Adv. Res.* **2015**, *6*, 105–121. [CrossRef] [PubMed]
2. Kopeček, J. Hydrogel biomaterials: A smart future? *Biomaterials* **2007**, *28*, 5185–5192. [CrossRef] [PubMed]
3. Wichterle, O.; Lím, D. Hydrophilic Gels for Biological Use. *Nature* **1960**, *185*, 117–118. [CrossRef]
4. Geckil, H.; Xu, F.; Zhang, X.; Moon, S.; Demirci, U. Engineering hydrogels as extracellular matrix mimics. *Nanomedicine* **2010**, *5*, 469–484. [CrossRef] [PubMed]
5. Oh, J.K.; Drumright, R.; Siegwart, D.J.; Matyjaszewski, K. The development of microgels/nanogels for drug delivery applications. *Prog. Polym. Sci.* **2008**, *33*, 448–477. [CrossRef]
6. Vinogradov, S.V.; Bronich, T.K.; Kabanov, A.V. Nanosized cationic hydrogels for drug delivery: Preparation, properties and interactions with cells. *Adv. Drug Deliver. Rev.* **2002**, *54*, 135–147. [CrossRef]
7. Tokarev, I.; Minko, S. Stimuli-responsive hydrogel thin films. *Soft Matter* **2009**, *5*, 511–524. [CrossRef]
8. Ishihara, K.; Ueda, T.; Nakabayashi, N. Preparation of Phospholipid Polylners and Their Properties as Polymer Hydrogel Membranes. *Polym. J.* **1990**, *22*, 355–360. [CrossRef]
9. Klouda, L.; Mikos, A.G. Thermoresponsive hydrogels in biomedical applications. *Eur. J. Pharm. Biopharm.* **2008**, *68*, 34–45. [CrossRef]
10. Klouda, L. Thermoresponsive hydrogels in biomedical applications. *Eur. J. Pharm. Biopharm.* **2015**, *97*, 338–349. [CrossRef]
11. Qiu, Y.; Park, K. Environment-sensitive hydrogels for drug delivery. *Adv. Drug Deliver. Rev.* **2001**, *53*, 321–339. [CrossRef]
12. Gupta, P.; Vermani, K.; Garg, S. Hydrogels: From controlled release to pH-responsive drug delivery. *Drug Discov. Today* **2002**, *7*, 569–579. [CrossRef]
13. Miyata, T.; Asami, N.; Uragami, T. A reversibly antigen-responsive hydrogel. *Nature* **1999**, *399*, 766–769. [CrossRef] [PubMed]
14. Miyata, T.; Uragami, T.; Nakamae, K. Biomolecule-sensitive hydrogels. *Adv. Drug Deliver. Rev.* **2002**, *54*, 79–98. [CrossRef]
15. Spiller, K.L.; Laurencin, S.J.; Charlton, D.; Maher, S.A.; Lowman, A.M. Superporous hydrogels for cartilage repair: Evaluation of the morphological and mechanical properties. *Acta Biomater.* **2008**, *4*, 17–25. [CrossRef] [PubMed]
16. Chen, J.; Park, H.; Park, K. Synthesis of superporous hydrogels: Hydrogels with fast swelling and superabsorbent properties. *J. Biomed. Mater. Res.* **1999**, *44*, 53–62. [CrossRef]
17. Petka, W.A.; Harden, J.L.; McGrath, K.P.; Wirtz, D.; Tirrell, D.A. Reversible Hydrogels from Self-Assembling Artificial Proteins. *Science* **1998**, *281*, 389–392. [CrossRef]
18. Ehrick, J.D.; Deo, S.K.; Browning, T.W.; Bachas, L.G.; Madou, M.J.; Daunert, S. Genetically engineered protein in hydrogels tailors stimuli-responsive characteristics. *Nat. Mater.* **2005**, *4*, 298–302. [CrossRef]
19. Gong, J.P.; Katsuyama, Y.; Kurokawa, T.; Osada, Y. Double-Network Hydrogels with Extremely High Mechanical Strength. *Adv. Mater.* **2003**, *15*, 1155–1158. [CrossRef]
20. Yasuda, K.; Ping Gong, J.; Katsuyama, Y.; Nakayama, A.; Tanabe, Y.; Kondo, E.; Ueno, M.; Osada, Y. Biomechanical properties of high-toughness double network hydrogels. *Biomaterials* **2005**, *26*, 4468–4475. [CrossRef]
21. Lee, K.Y.; Mooney, D.J. Hydrogels for Tissue Engineering. *Chem. Rev.* **2001**, *101*, 1869–1880. [CrossRef] [PubMed]
22. Drury, J.L.; Mooney, D.J. Hydrogels for tissue engineering: Scaffold design variables and applications. *Biomaterials* **2003**, *24*, 4337–4351. [CrossRef]
23. Slaughter, B.V.; Khurshid, S.S.; Fisher, O.Z.; Khademhosseini, A.; Peppas, N.A. Hydrogels in Regenerative Medicine. *Adv. Mater.* **2009**, *21*, 3307–3329. [CrossRef]
24. Annabi, N.; Tamayol, A.; Uquillas, J.A.; Akbari, M.; Bertassoni, L.E.; Cha, C.; Camci-Unal, G.; Dokmeci, M.R.; Peppas, N.A.; Khademhosseini, A. 25th Anniversary Article: Rational Design and Applications of Hydrogels in Regenerative Medicine. *Adv. Mater.* **2014**, *26*, 85–124. [CrossRef] [PubMed]
25. van der Linden, H.J.; Herber, S.; Olthuis, W.; Bergveld, P. Stimulus-sensitive hydrogels and their applications in chemical (micro)analysis. *Analyst* **2003**, *128*, 325–331. [CrossRef]

26. Rubina, A.Y.; Pan'kov, S.V.; Dementieva, E.I.; Pen'kov, D.N.; Butygin, A.V.; Vasiliskov, V.A.; Chudinov, A.V.; Mikheikin, A.L.; Mikhailovich, V.M.; Mirzabekov, A.D. Hydrogel drop microchips with immobilized DNA: Properties and methods for large-scale production. *Anal. Biochem.* **2004**, *325*, 92–106. [CrossRef]

27. Wang, K.L.; Burban, J.H.; Cussler, E.L. Hydrogels as separation agents. In *Responsive Gels: Volume Transitions II.*; Springer: Berlin/Heidelberg, Germany, 1993; pp. 67–79.

28. Ozay, O.; Ekici, S.; Baran, Y.; Kubilay, S.; Aktas, N.; Sahiner, N. Utilization of magnetic hydrogels in the separation of toxic metal ions from aqueous environments. *Desalination* **2010**, *260*, 57–64. [CrossRef]

29. Hoare, T.R.; Kohane, D.S. Hydrogels in drug delivery: Progress and challenges. *Polymer* **2008**, *49*, 1993–2007. [CrossRef]

30. Narayanaswamy, R.; Torchilin, V.P. Hydrogels and Their Applications in Targeted Drug Delivery. *Molecules* **2019**, *24*, 603. [CrossRef] [PubMed]

31. Li, J.; Mooney, D.J. Designing hydrogels for controlled drug delivery. *Nat. Rev. Mater.* **2016**, *1*, 1–17. [CrossRef]

32. Trongsatitkul, T.; Budhlall, B.M. Microgels or microcapsules? Role of morphology on the release kinetics of thermoresponsive PNIPAm-co-PEGMa hydrogels. *Polym. Chem.* **2013**, *4*, 1502–1516. [CrossRef]

33. Perugini, P.; Genta, I.; Conti, B.; Modena, T.; Pavanetto, F. Long-term release of clodronate from biodegradable microspheres. *AAPS PharmSciTech* **2001**, *2*, 6–14. [CrossRef]

34. Lee, B.H.; Lee, Y.M.; Sohn, Y.S.; Song, S.-C. A Thermosensitive Poly(organophosphazene) Gel. *Macromolecules* **2002**, *35*, 3876–3879. [CrossRef]

35. Andrade-Vivero, P.; Fernandez-Gabriel, E.; Alvarez-Lorenzo, C.; Concheiro, A. Improving the Loading and Release of NSAIDs from pHEMA Hydrogels by Copolymerization with Functionalized Monomers. *J. Pharm. Sci.* **2007**, *96*, 802–813. [CrossRef] [PubMed]

36. Sato, T.; Uchida, R.; Tanigawa, H.; Uno, K.; Murakami, A. Application of polymer gels containing side-chain phosphate groups to drug-delivery contact lenses. *J. Appl. Polym. Sci.* **2005**, *98*, 731–735. [CrossRef]

37. Young, S.; Wong, M.; Tabata, Y.; Mikos, A.G. Gelatin as a delivery vehicle for the controlled release of bioactive molecules. *J. Control. Release* **2005**, *109*, 256–274. [CrossRef]

38. Jenkins, A.D.; Kratochvíl, P.; Stepto, R.F.T.; Suter, U.W. Glossary of basic terms in polymer science (IUPAC Recommendations 1996). *Pure Appl. Chem.* **1996**, *68*, 2287–2311. [CrossRef]

39. Zoratto, N.; Matricardi, P. Semi-IPNs and IPN-based hydrogels. In *Polymeric Gels*; Woodhead Publishing: Cambridge, UK, 2018; pp. 91–124.

40. Aminabhavi, T.M.; Nadagouda, M.N.; More, U.A.; Joshi, S.D.; Kulkarni, V.H.; Noolvi, M.N.; Kulkarni, P.V. Controlled release of therapeutics using interpenetrating polymeric networks. *Expert Opin. Drug Deliv.* **2015**, *12*, 669–688. [CrossRef] [PubMed]

41. Rinaudo, M. Main properties and current applications of some polysaccharides as biomaterials. *Polym. Int.* **2008**, *57*, 397–430. [CrossRef]

42. Zarrintaj, P.; Manouchehri, S.; Ahmadi, Z.; Saeb, M.R.; Urbanska, A.M.; Kaplan, D.L.; Mozafari, M. Agarose-based biomaterials for tissue engineering. *Carbohydr. Polym.* **2018**, *187*, 66–84. [CrossRef]

43. Wang, N.; Wu, X.S. Preparation and Characterization of Agarose Hydrogel Nanoparticles for Protein and Peptide Drug Delivery. *Pharm. Dev. Technol.* **1997**, *2*, 135–142. [CrossRef] [PubMed]

44. Liang, S.; Xu, J.; Weng, L.; Dai, H.; Zhang, X.; Zhang, L. Protein diffusion in agarose hydrogel in situ measured by improved refractive index method. *J. Control. Release* **2006**, *115*, 189–196. [CrossRef] [PubMed]

45. Marras-Marquez, T.; Peña, J.; Veiga-Ochoa, M.D. Agarose drug delivery systems upgraded by surfactants inclusion: Critical role of the pore architecture. *Carbohydr. Polym.* **2014**, *103*, 359–368. [CrossRef]

46. Meilander, N.J.; Yu, X.; Ziats, N.P.; Bellamkonda, R.V. Lipid-based microtubular drug delivery vehicles. *J. Control. Release* **2001**, *71*, 141–152. [CrossRef]

47. Narahashi, T.; Yamada, M.; Frazier, D.T. Cationic Forms of Local Anaesthetics block Action Potentials from Inside the Nerve Membrane. *Nature* **1969**, *223*, 748–749. [CrossRef]

48. Gunasekaran, P.; Rajasekaran, G.; Han, E.H.; Chung, Y.-H.; Choi, Y.-J.; Yang, Y.J.; Lee, J.E.; Kim, H.N.; Lee, K.; Kim, J.-S.; et al. Cationic Amphipathic Triazines with Potent Anti-bacterial, Anti-inflammatory and Anti-atopic Dermatitis Properties. *Sci. Rep.* **2019**, *9*, 1292. [CrossRef]

49. Broderick, E.; Lyons, H.; Pembroke, T.; Byrne, H.; Murray, B.; Hall, M. The characterisation of a novel, covalently modified, amphiphilic alginate derivative, which retains gelling and non-toxic properties. *J. Colloid Interface Sci.* **2006**, *298*, 154–161. [CrossRef] [PubMed]

50. Aymard, P.; Martin, D.R.; Plucknett, K.; Foster, T.J.; Clark, A.H.; Norton, I.T. Influence of thermal history on the structural and mechanical properties of agarose gels. *Biopolymers* **2001**, *59*, 131–144. [CrossRef]

51. Lapasin, R.; Pricl, S. *Rheology of Industrial Polysaccharides: Theory and Applications*; Springer: Boston, MA, USA, 1995; ISBN 978-1-4613-5915-9.

52. Pescosolido, L.; Feruglio, L.; Farra, R.; Fiorentino, S.; Colombo, I.; Coviello, T.; Matricardi, P.; Hennink, W.E.; Vermonden, T.; Grassi, M. Mesh size distribution determination of interpenetrating polymer network hydrogels. *Soft Matter* **2012**, *8*, 7708–7715. [CrossRef]

53. Draper, N.R.; Smith, H. *Applied Regression Analysis*; John Wiley & Sons, Inc: New York, NY, USA, 1996.

54. Sedláček, P.; Smilek, J.; Klučáková, M. How the interactions with humic acids affect the mobility of ionic dyes in hydrogels—2. Non-stationary diffusion experiments. *React. Funct. Polym.* **2014**, *75*, 41–50. [CrossRef]

55. Smilek, J.; Sedláček, P.; Kalina, M.; Klučáková, M. On the role of humic acids' carboxyl groups in the binding of charged organic compounds. *Chemosphere* **2015**, *138*, 503–510. [CrossRef] [PubMed]

56. Sedláček, P.; Smilek, J.; Laštůvková, M.; Kalina, M.; Klučáková, M. Hydrogels: Invaluable experimental tool for demonstrating diffusion phenomena in physical chemistry laboratory courses. *J. Mater. Educ.* **2017**, *39*, 59–90.

57. Crank, J. *The Mathematics of Diffusion*; Oxford University Press Inc: New York, NY, USA, 1979.

58. ImageJ Website. Available online: https://imagej.nih.gov/ij/ (accessed on 20 August 2020).

59. Schneider, C.A.; Rasband, W.S.; Eliceiri, K.W. NIH Image to ImageJ: 25 years of image analysis. *Nat. Methods* **2012**, *9*, 671–675. [CrossRef] [PubMed]

60. Normand, V.; Lootens, D.L.; Amici, E.; Plucknett, K.P.; Aymard, P. New Insight into Agarose Gel Mechanical Properties. *Biomacromolecules* **2000**, *1*, 730–738. [CrossRef]

61. Grillet, A.M.; Wyatt, N.B.; Gloe, L.M. Polymer Gel Rheology and Adhesion. In *Rheology*; InTech: Rijeka, Croatia, 2012; pp. 59–80.

62. Weng, L.; Chen, X.; Chen, W. Rheological Characterization of in Situ Crosslinkable Hydrogels Formulated from Oxidized Dextran and *N*-Carboxyethyl Chitosan. *Biomacromolecules* **2007**, *8*, 1109–1115. [CrossRef] [PubMed]

63. Trenkmann, I.; Bok, S.; Korampally, V.R.; Gangopadhyay, S.; Graaf, H.; von Borczyskowski, C. Counting single Rhodamine 6G dye molecules in organosilicate nanoparticles. *Chem. Phys.* **2012**, *406*, 41–46. [CrossRef]

64. Penzkofer, A.; Leupacher, W. Fluorescence behaviour of highly concentrated rhodamine 6G solutions. *J. Lumin.* **1987**, *37*, 61–72. [CrossRef]

65. Doty, P.; Steiner, R.F. Light Scattering and Spectrophotometry of Colloidal Solutions. *J. Chem. Phys.* **1950**, *18*, 1211–1220. [CrossRef]

66. Horne, D.S. Determination of the fractal dimension using turbidimetric techniques. Application to aggregating protein systems. *Faraday Discuss. Chem. Soc.* **1987**, *83*, 259–280. [CrossRef]

67. Camerini-Otero, R.D.; Day, L.A. The wavelength dependence of the turbidity of solutions of macromolecules. *Biopolymers* **1978**, *17*, 2241–2249. [CrossRef]

68. Leone, M.; Sciortino, F.; Migliore, M.; Fornili, S.L.; Vittorelli, M.B.P. Order parameters of gels and gelation kinetics of aqueous agarose systems: Relation to the spinodal decomposition of the sol. *Biopolymers* **1987**, *26*, 743–761. [CrossRef]

69. Aymard, P.; Williams, M.A.K.; Clark, A.H.; Norton, I.T. A Turbidimetric Study of Phase Separating Biopolymer Mixtures during Thermal Ramping. *Langmuir* **2000**, *16*, 7383–7391. [CrossRef]

70. Singh, T.R.R. *Hydrogels*; CRC Press: Boca Raton, FL, USA, 2018; ISBN 9781315152226.

71. Stellwagen, N.C. Effect of the electric field on the apparent mobility of large DNA fragments in agarose gels. *Biopolymers* **1985**, *24*, 2243–2255. [CrossRef]

72. Flory, P.J. *Principles of Polymer Chemistry*; Cornell University Press: Ithaca, New York, NY, USA, 1953.

73. Larson, R.G. *The Structure and Rheology of Complex Fluids*; Oxford University Press Inc.: New York, NY, USA, 1999.

74. Chai, Q.; Jiao, Y.; Yu, X. Hydrogels for Biomedical Applications: Their Characteristics and the Mechanisms behind Them. *Gels* **2017**, *3*, 6. [CrossRef]

75. Calhoun, M.A.; Bentil, S.A.; Elliott, E.; Otero, J.J.; Winter, J.O.; Dupaix, R.B. Beyond linear elastic modulus: Viscoelastic models for brain and brain mimetic hydrogels. *ACS Biomater. Sci. Eng.* **2019**, *5*, 3964–3973. [CrossRef]

76. Smilek, J.; Jarábková, S.; Velcer, T.; Pekař, M. Compositional and Temperature Effects on the Rheological Properties of Polyelectrolyte–Surfactant Hydrogels. *Polymers* **2019**, *11*, 927. [CrossRef]

77. Galway, M.E.; Heckman, J.W., Jr.; Hyde, G.J.; Fowke, L.C. Advances in high-pressure and plunge-freeze fixation. In *Methods in Cell Biology*; Academic Press: Cambridge, MA, USA, 1995; Volume 49, pp. 3–19. [CrossRef]

78. Hrubanova, K.; Nebesarova, J.; Ruzicka, F.; Krzyzanek, V. The innovation of cryo-SEM freeze-fracturing methodology demonstrated on high pressure frozen biofilm. *Micron* **2018**, *110*, 28–35. [CrossRef]

79. Paradossi, G.; Cavalieri, F.; Chiessi, E.; Spagnoli, C.; Cowman, M.K. Poly (vinyl alcohol) as versatile biomaterial for potential biomedical applications. *J. Mater. Sci. Mater.* **2003**, *14*, 687–691. [CrossRef]

80. Holly, F.J.; Refojo, M.F. Wettability of hydrogels I. Poly(2-hydroxyethyl methacrylate). *J. Biomed. Mater. Res.* **1975**, *9*, 315–326. [CrossRef]

81. Zhu, J. Bioactive modification of poly(ethylene glycol) hydrogels for tissue engineering. *Biomaterials* **2010**, *31*, 4639–4656. [CrossRef]

82. Osmałek, T.; Froelich, A.; Tasarek, S. Application of gellan gum in pharmacy and medicine. *Int. J. Pharm.* **2014**, *466*, 328–340. [CrossRef] [PubMed]

83. Park, H.; Park, K.; Shalaby, W.S.W. *Biodegradable Hydrogels for Drug Delivery*; CRC Press: Boca Raton, FL, USA, 2011.

84. Xiong, X.Y.; Tam, K.C.; Gan, L.H. Polymeric Nanostructures for Drug Delivery Applications Based on Pluronic Copolymer Systems. *J. Nanosci. Nanotechno.* **2006**, *6*, 2638–2650. [CrossRef] [PubMed]

85. Amiji, M.; Tailor, R.; Ly, M.-K.; Goreham, J. Gelatin-Poly(Ethylene Oxide) Semi-interpenetrating Polymer Network with pH-Sensitive Swelling and Enzyme-Degradable Properties for Oral Drug Delivery. *Drug Dev. Ind. Pharm.* **1997**, *23*, 575–582. [CrossRef]

86. Elisseeff, J.; McIntosh, W.; Anseth, K.; Riley, S.; Ragan, P.; Langer, R. Photoencapsulation of chondrocytes in poly(ethylene oxide)-based semi-interpenetrating networks. *J. Biomed. Mater. Res.* **2000**, *51*, 164–171. [CrossRef]

87. Sedláček, P.; Smilek, J.; Klučáková, M. How the interactions with humic acids affect the mobility of ionic dyes in hydrogels—Results from diffusion cells. *React. Funct. Polym.* **2013**, *73*, 1500–1509. [CrossRef]

88. Larrañeta, E.; Stewart, S.; Ervine, M.; Al-Kasasbeh, R.; Donnelly, R. Hydrogels for Hydrophobic Drug Delivery. Classification, Synthesis and Applications. *J. Funct. Biomater.* **2018**, *9*, 13. [CrossRef]

89. Venerová, T.; Pekař, M. Rheological properties of gels formed by physical interactions between hyaluronan and cationic surfactants. *Carbohydr. Polym.* **2017**, *170*, 176–181. [CrossRef]

90. Enev, V.; Sedláček, P.; Jarábková, S.; Velcer, T.; Pekař, M. ATR-FTIR spectroscopy and thermogravimetry characterization of water in polyelectrolyte-surfactant hydrogels. *Colloids Surf. A* **2019**, *575*, 1–9. [CrossRef]

91. Moschakis, T. Microrheology and particle tracking in food gels and emulsions. *Curr. Opin. Colloid Interface Sci.* **2013**, *18*, 311–323. [CrossRef]

92. Rathgeber, S.; Beauvisage, H.-J.; Chevreau, H.; Willenbacher, N.; Oelschlaeger, C. Microrheology with Fluorescence Correlation Spectroscopy. *Langmuir* **2009**, *25*, 6368–6376. [CrossRef]

93. García-Aparicio, C.; Quijada-Garrido, I.; Garrido, L. Diffusion of small molecules in a chitosan/water gel determined by proton localized NMR spectroscopy. *J. Colloid Interface Sci.* **2012**, *368*, 14–20. [CrossRef] [PubMed]

94. Severs, N.; Shotton, D. Rapid Freezing of Biological Specimens for Freeze Fracture and Deep Etching. *Cell Biol.* **2006**, *3*, 249–255.

95. Landry, M.R. Thermoporometry by differential scanning calorimetry: Experimental considerations and applications. *Thermochim. Acta* **2005**, *433*, 27–50. [CrossRef]

Publisher's Note: MDPI stays neutral with regard to jurisdictional claims in published maps and institutional affiliations.
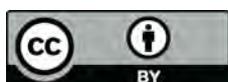
Appendix 24

Kratochvilova, R., Sedlacek, P., Porizka, J., and Klucakova, M. Composite materials for controlled release of mineral nutrients and humic substances for agricultural application. *Soil Use and Management* **2021**, 37, 460–467.

RESEARCH PAPER

Soil Use and Management   BRITISH SOCIETY OF SOIL SCIENCE   WILEY

Composite materials for controlled release of mineral nutrients and humic substances for agricultural application

Romana Kratochvilova | Petr Sedlacek | Jaromir Porizka | Martina Klucakova [iD]

Faculty of Chemistry, Brno University of Technology, Brno, Czech Republic

Correspondence
Martina Klucakova, Faculty of Chemistry, Brno University of Technology, Purkynova 464/118, Brno 612 00, Czech Republic.
Email: klucakova@fch.vutbr.cz

Funding information
Ministerstvo Školství, Mládeže a Tělovýchovy, Grant/Award Number: LO1211

Abstract

Controlled-release fertilizers based on superabsorbents containing lignohumate and conventional mineral fertilizer (NPK) were prepared. Their water absorption was supported by the presence of lignohumate (LH) and suppressed by the presence of NPK. The release of mineral nutrients was prolonged up to four weeks in the case of increased content of NPK. The addition of LH had negligible influence on the release of P and N. The release of LH was partially suppressed by the higher content of NPK. The release of nutrients from all used samples was connected with the strong increase in conductivity and weak increase in pH values. The application of superabsorbents supported growth of corn. The length of roots was probably more influenced by better water management, while the growth of above-ground plant was more affected by release of nutrients.

KEYWORDS
fertilizer, lignohumate, release, superabsorbent, swelling

1 | INTRODUCTION

Humic substances are the principal components of organic soil matter. They affect biological uptake and bioaccumulation of toxic chemicals in plants as well as the pollution of underground water supplies. They influence soil fertility and stabilize soil aggregates. Because of their colloidal and poly-functional character, these substances play important roles in the mobility and bioavailability of nutrients and contaminants in the environment (Bryan et al., 2007; Frimmel et al., 2002; Lee & Sung, 2014; Tan, 2014). Humic substances play irreplaceable role from agronomical point of view. Most agricultural soils have gradually lost much of this capacity as the use of heavy machinery and synthetic fertilizers has replaced careful soil utilization and natural fertilizer application (Klucakova, 2014; Lal, 2004; Novotny, Blum, Gerzabek, & Mangrich, 1999; Sedlacek & Klucakova, 2009; Shepherd,

Saggar, Newman, Ross, & Dando, 2001); therefore, it must now be supported artificially. This is the main reason why they are used as additives in fertilizing products (Garcia, Cegarra, Roig, & Abad, 1994; Piccolo & Mbagwu 1997; Albiach, Canet, Pomares, & Ingelmo, 2001; Madejon, Lopez, Murillo, & Cabrera, 2001; Shepherd et al., 2001). Although their water soluble complexes with toxic metals can be absorbed by plants more easily which has inhibiting effect on their growth (Chu, Zhu, Huang, & Li, 2008; Klucakova & Novackova, 2014; Klucakova & Pekar, 2003; Klucakova & Veznikova, 2016; Pacheco & Havel, 2001), humic substances have a beneficial effect on soil quality and plant growth (Bai, Zhang, Liu, Wu, & Song, 2010; Bharadwaj et al., 2007; Enev, Pospisilova, Klucakova, Liptaj, & Doskocil, 2014; Klucakova, 2010; Liu, Wang, & Wang, 2007; Zhang, Li, & Wang, 2005). However, humic substances are suitable for agricultural application only if care is taken to ensure limited dosing. This means that

humic substances should have a certain concentration, which should not be exceeded. This can be accomplished by using fertilizer systems that are capable of providing controlled release of nutrients (Bai et al., 2010; Davidson & Gu, 2012; Du, Zhou, & Shaviv, 2006; Klucakova, 2010; Mo, Shu-quan, Hua-Min, Zhan-bin, & Shu-qin, 2006).

Superabsorbent polymers have the unique ability to absorb and retain relatively large amounts of water or water solutions in their structure (Dadhaniya, Patel, & Patel, 2006; Li, Wang, & Chen, 2004; Nnadi & Brave, 2011; Raju & Raju, 2001; Raju, Raju, & Mohan, 2002). Therefore, they are able to regulate soil moisture. Swelling behaviour of superabsorbents studied in this work is described in detail in Appendix S1.

Humic substances as a source of organic carbon for composite fertilizer have been studied by several authors (Chu et al., 2008; Gao, Wang, & Zhao, 2013; Li, Zhang, & Wang, 2005; Liu et al., 2007; Mo et al., 2006; Zhang et al., 2005; Zhang, Li, & Wang, 2006). Zhang et al. (2005), Zhang et al. (2006) used sodium humate in combination with poly(acrylic acid-co-acrylamide) and later in combination with attapulgite. They investigated the release of humate into distilled water and reported that a material containing humate caused sturdier roots and stems. Gao et al. (2013) synthetized and characterized controllable agricultural superabsorbent based on poly(acrylic acid-co-acrylamide) and sodium humate. Li et al. (2005) and Mo et al. (2006) incorporated sodium humate into poly(acrylic acid) as a kind of functional filler and studied its influence on water absorption. Chu et al. (2008) dealt with the influence of potassium humate on the swelling properties of a poly(acrylic acid-co-acrylamide)/ potassium humate superabsorbent. Liu et al. (2007) combined poly(acrylic acid) with chitosan and sodium humate. A review of Mikula et al., 2020) presents current achievements in the field of fertilizers with controlled release of microelements, which, apart from the main fertilizer components, are also very significant for proper plant growth.

In the light of the above-mentioned works and their results, our study investigates the development of multifunctional superabsorbent composite materials containing commercial NPK fertilizer as a source of mineral constituents and lignohumate as organic functional materials in combination with poly(acrylic acid-co-acrylamide) as polymer providing high water retention. In comparison with composite materials combining humic substance with mineral fertilizers (Erro, Urrutia, Francisco, & Garcia-Mina, 2007) and fertilizers coated by polymers (Davidson & Gu, 2012), our systems should combine advantages of controlled release of nutrients (organic and mineral) with the ability of swell (water conservation).

The aim of this work was to investigate the release of active substances in the prepared superabsorbents in order to optimize their composition for further pot experiments. Superabsorbent materials enriched by mineral fertilizer and lignohumate are investigated. The novelty of our work lay in the combination of mineral and organic fertilizer and the connection with high ability to absorb water. This work is a complex study covering all aspects of this type of composite materials: swelling and water absorption, release of mineral and organic fertilizers, repeated leaching (washing) of nutrients and application of prepared composite materials in pot experiments.

2 | EXPERIMENTAL

2.1 | Materials

2.1.1 | Chemicals

Eight different samples of superabsorbent polymers were synthesized through the rapid solution polymerization of partially neutralized acrylic acid (AA; Sigma-Aldrich) under normal atmospheric conditions. Powders of potassium lignohumate (LH; Amagro s. r. o.) and NPK 20-8-8 (NPK, Lovochemie a.s.) were used as organic and mineral nutrients.

2.1.2 | Preparation of superabsorbents

Weight quantity of AA (57 g) was dissolved in distilled water (100 cm^3). AA solution (25 cm^3) was neutralized by 10 cm^3 of 8.5M potassium hydroxide solution (KOH, Penta). Powders of LH and NPK were dispersed in this mixture and cross-linked by MBA (0.016 g). Then, the initiator KPS was added (0.5 g). The mixture was continuously heated and stirred until reaching of temperature of approx 85°C; then, highly viscous mixture was removed from the beaker and replaced to an oven for 24 hr, which was settled up on 80°C. Dried product was crushed by hammer into small pieces (Mo et al., 2006). The compositions of prepared samples are described in detail in Tables 1 and 2.

2.2 | Methods

2.2.1 | Releasing experiments

Samples in form of xerogel were mixed with distilled water in the ratio 50 mg: 100 cm^3. Releasing of active substances was monitored in time by means of several methods. The time development of pH and conductivity was measured using a S47 SevenMulti pH and conductivity meter (Mettler Toledo). The amounts of released K and P were determined by the means of ICP-OES (an Ultima 2 ICP-OES spectrometer,

TABLE 1 Composition of superabsorbent hydrogels—starting materials

Sample	A	B	C	D	H
AA (g)	14.25	14.25	14.25	14.25	14.25
MBA (g)	0.016	0.016	0.016	0.016	0.016
KPS (g)	0.5	0.5	0.5	0.5	0.5
KOH (g)	4.75	4.75	4.75	4.75	4.75
NPK (g)	0.6602	6.602	0.6602	6.602	0
LH (g)	0	0	1	1	1
H_2O (g)	35	35	35	35	35

TABLE 2 Composition of superabsorbent xerogels—active components

Sample	A	B	C	D	H
K (% wt.)	17.34	14.91	17.57	15.17	17.92
N (% wt.)	0.67	5.07	0.82	5.02	0.20
P (% wt.)	0.11	0.88	0.11	0.85	0.00
LH (% wt.)	0.00	0.00	4.72	3.69	4.87

Horiba, Thermo Fisher Scientific). Concentrations of anions (NO_3^- and PO_4^{3-}) were monitored using a 850 Professional IC Anion-MCS ion chromatography system, Metrohm AG, Herisau, Switzerland.

The release of LH was measured by the means of an U-3900H UV/Vis spectrometer (Hitachi, Tokyo, Japan). In order to determine the amounts of N, P and K in LH and NPK, their solutions in distilled water (1 g/dm^3) were analysed by the means of ICP-OES (Horiba Ultima 2, Thermo Fisher Scientific, Waltham, MA USA) and ion chromatography (see above).

2.2.2 | Leaching experiments

This experiment was done in order to determine the release of nutrients in repeated leaching of superabsorbents. Samples in form of xerogel were mixed with distilled water in the ratio 400 mg: 100 cm^3. After one hour, the leachate was decanted and replaced by 100 cm^3 of fresh distilled water. Whole process was repeated fifteen times. Obtained leachates were analysed by the same way as in the case of releasing experiments.

2.3 | Pot experiments

The model soil was prepared by mixing of peat (200 g), kaolin (120 g), silica sand (1,660 g) and $CaCO_3$ (20 g). Corn seeds were extracted in 0.05M NaClO (5 min) in order to remove pickling agent and washed by distilled water. After 24 hr, the

seeds were placed separately into curled up paper towels and covered by distilled water (5 days at $28 \pm 2°C$). The germinated seeds were placed into the 250 g of model soil mixed with 1 g of xerogel and 40 cm^3 of water (3 seeds into 1 pot). The pots were placed in the growing box at $26 \pm 2°C$ with periodical watering. Shoot and root were separated and individually measured. All experiments were triplicated, and average values are presented in this study.

3 | RESULTS AND DISCUSSION

3.1 | Releasing experiments

Active components were released from hydrogel progressively (Figure 1). In beginning, the release was partially influenced by the swelling of hydrogel. The cumulative amount of the nutrient increased in time up to the achievement of stable concentration in the leachate. The content of potassium in samples was a combination of potassium coming from NPK and LH and added in samples as active components, and KOH and KPS used in the preparation of hydrogels. While the amounts of potassium coming from KOH and KPS were the same for all samples, they differed in the contents of NPK and LH. Sample A contained lower amount of NPK and no LH. The release of K from this sample corresponded with its content in the hydrogel. The majority of potassium was released in one week, and the following release rate was very low. The increased content of NPK in hydrogels B and D thus resulted in the increased cumulative release of potassium. In this case, the addition of LH had negligible influence (samples B and D). In contrast, the addition of LH supported the release of K from sample C. The release of K from samples B, C, D and H was retarded after two or three weeks (Figure 1a). The release of P (Figure 1b) and NO_3^- (Figure 1c) was strongly dependent on the contents of NPK. In the case of increased content of NPK (samples B and D), the release was prolonged up to four weeks. The addition of LH had negligible influence on the release of P and NO_3^- from samples B and D. In contrast, the release of P from sample C was prolonged in the comparison with the sample A containing the same initial amount of NPK. The release of LH, which was primarily added in hydrogels as a source of organic carbon, was partially suppressed by the higher content of NPK (sample D). In this case, the release was stopped after three days, while it continued for more than two months in samples C and H (Figure 2). The release of nutrients from all used samples was connected with a strong increase of conductivity and weak increase in pH values.

Erro et al. (2007) developed a fertilizer based on humic substances and NPK (without polymers). Their results showed that nutrients were released into water in about 30 min (K and N) or two hours (P), while the release of ammonia ions
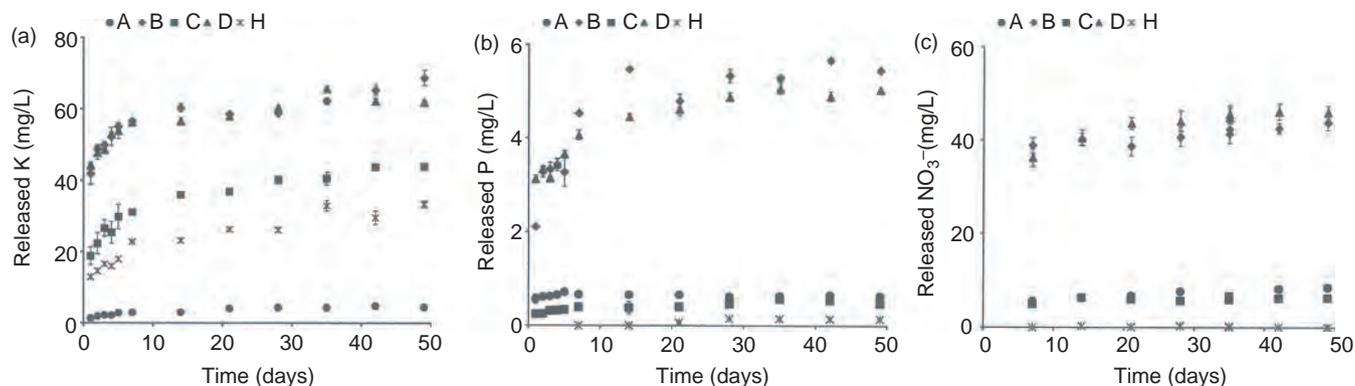
FIGURE 1 The release of K (left), P (middle), and NO_3^- (right) from studied materials in the dependence on time.

was slower with a maximum achieved in several days. The amount of nitrogen released was enhanced by the addition of straw. Du et al. (2006) studied the release of K, N and P from polymer-coated fertilizers, which could be released up to two months in the dependence on the temperature and thickness of surface polymer layer. Nutrients release was the fastest into water than into water saturated sand. Similarly, Davidson and GU (2012) studied the release of nutrients from fertilizers coated, for example by polylactic acids and wax. The release of urea was stopped in 20 days in both cases. Zhan, Liu, Guo, and Wu (2004) investigated the release of phosphate from superabsorbent polymer based on PVA, H_3PO_4 and Na_2CO_3 provided. The proportion of released phosphate increased during first day up to 26.5%. No release was detected during second day. After that, the release increased from 26,5 to 47% during third day of experiment. On the 28th day, the total proportion of released phosphate was 79%. The authors concluded that the results were because of the enrichment of the surface layer and the slow diffusion of phosphate encapsulated inside the material. In contrast, the release of sodium

humate from superabsorbents based on AA, acrylamide and attapulgite was stopped after several days in dependence on the content of humate (Zhang et al., 2005). However, the use of acrylamide is problematic because of its toxicity (Matoso, Bargi-Souza, Ivanski, Romano, & Romano, 2019; Spencer, Wahome, & Haasch, 2018; Spencer & Schaumburg 1974a, Spencer & Schaumburg 1974b). We performed some experiments with superabsorbents containing acrylamide, but the results did not show any improvement in their properties in comparison with samples used in this work.

3.2 | Leaching experiments

The gradual leaching of active components from hydrogels can be characterized by the measurement of conductivity. Obtained results are shown in Figure 3. In our study, the development of amounts of individual ions in leachates corresponded with conductivity values, which did not change after seven washing cycles. An exception was the leaching of LH, which can be extracted for ten washing cycles. This means that if the hydrogel is applied in soil with very good supply of water the active components can be repeatedly washed out from the surroundings of plant roots. The leaching of nutrients from fertilizer prepared and studied by Erro et al. (2007) was in most cases faster. The release of phosphate was completed after three cycles and that of potassium after for cycles. In contrast, no nitrogen was leached after seven cycles.

3.3 | Pot experiments

The influence of superabsorbent application on corn growth is shown in Figure 4. A positive effect on corn height was observed for all prepared samples. As can be seen in Figure 4, the growth of shoots was much slower in soil without superabsorbent and no changes in plant height were observed after two weeks. In contrast, higher content of
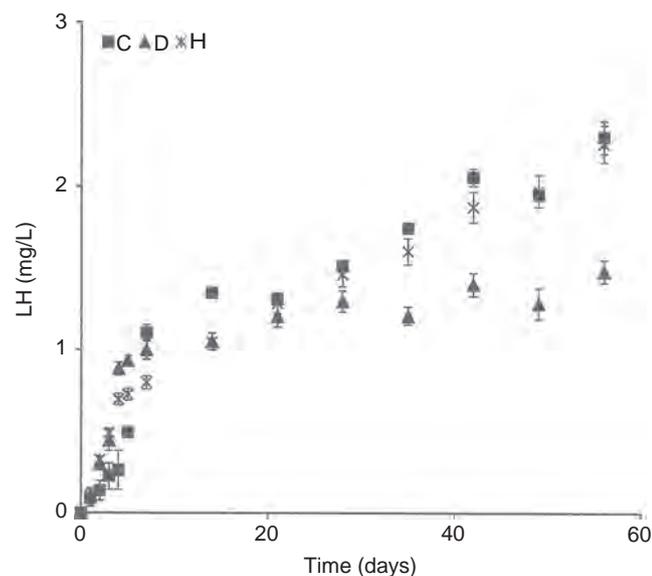

FIGURE 2 The release of LH from studied materials over time.

FIGURE 3 The conductivity of aqueous leachates for samples A and C in relation to washing cycle
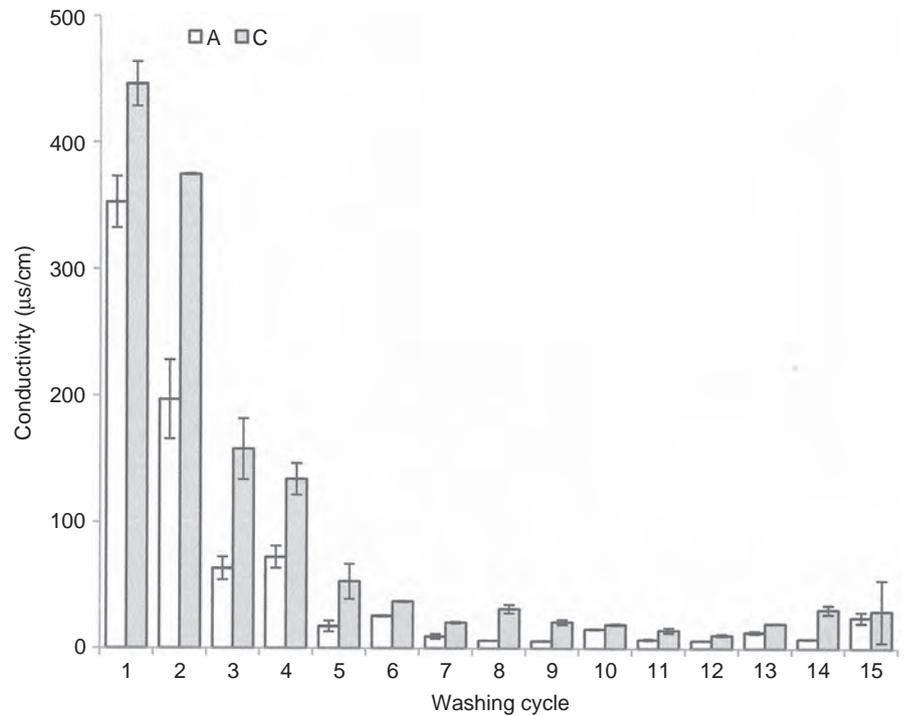
NPK in superabsorbent enriched by LH had the most positive effect on corn growth. It was confirmed that the presence of LH in superabsorbent supported corn growth, but it was lower in comparison with the application of superabsorbents containing NPK. This effect was partly the result of better water management and partly the result of the slow supply of nutrients from NPK and LH. The improvement of plant growth as a result of the more effective utilization of water was confirmed also by Raju and Raju (2001), Abedi-Koupai and Asadkazemi (2006), and Dorraji, Golchin, and

Ahmadi (2010) who applied superabsorbents without addition of nutrients. The application of fertilizer without superabsorbent polymer supported the growth of wheat (Erro et al., 2007), but the growth was small than that induced by composite materials in our study. Chatzistathis et al. (2020) compared effects between manure application and a controlled-release fertilizer on the growth and nutrient uptake of *Olea europaea* L. They concluded that the total plant biomass and total per plant macronutrient were significantly higher in the case of controlled-release fertilizer because of
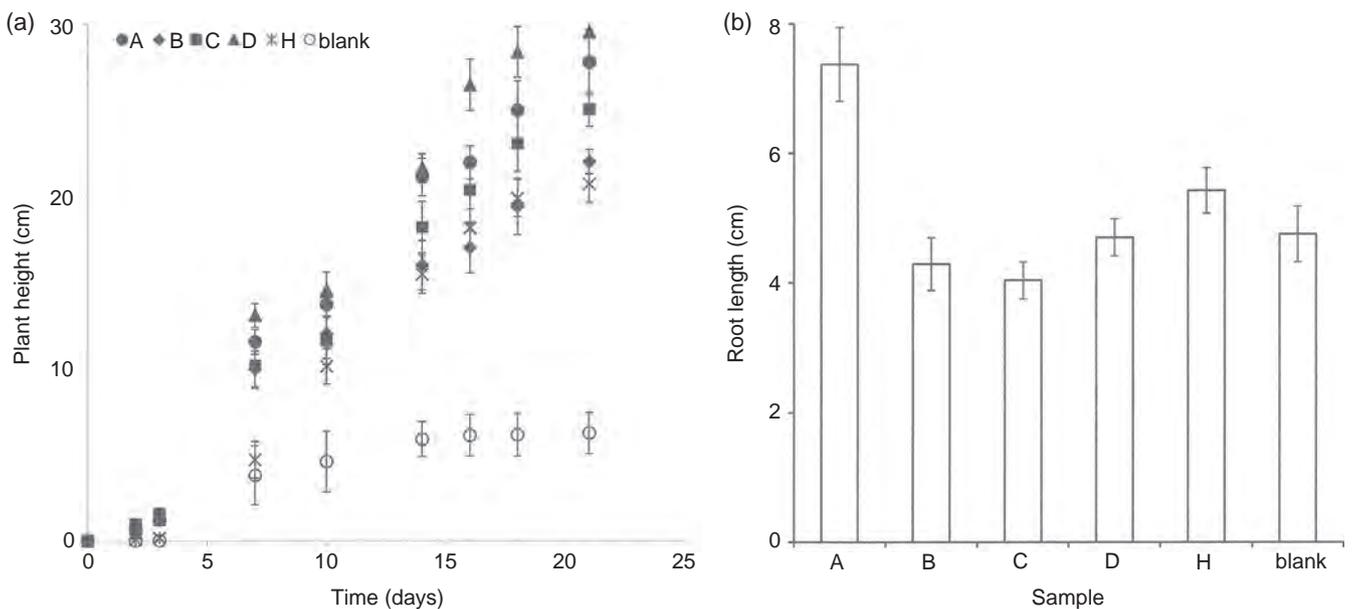
FIGURE 4 The time development of the height of corn (left) and the final lengths of roots for the used superabsorbents (right). The blank experiment is without application of superabsorbent

higher biomass production. Zhao, Song, Zhao, Xiang, and Liu (2019) demonstrated that the combination of fertilizers with superabsorbents improved soil fertility, increased soil nutrient supply capacity and yield of tomatoes. Four different types of controlled-release fertilizers were used in container-grown ornamental plants (Japanese spiraea) and arborvitae by Grable, Knight, and Ingram (2017). The most positive effect on the growth was observed for the prototype blends with experimental polymer coatings. They produced a deeper green foliage and higher shoot dry weight in comparison with others. Similarly, Girardi, Mourao Filho, Graf, and Olic (2005) observed positive effect of slow-release fertilizers on growth of containerized citrus nursery trees and Silva et al. (2017) concluded that associating organo-mineral fertilizer application with the organo-mineral fertilizer slow release of nutrients can ensure greater yield of lavender essential oil and had a noticeable impact on its chemical composition.

Our results showed that higher contents of NPK in superabsorbent without LH (sample B) had slightly inhibiting effect. This could be the result of a greater release of nutrients that cannot be effectively utilized in the first days of growth. A similar effect was observed by Nnadi and Brave (2011) who used polymers based on carboxymethyl cellulose sodium salt and several commercial starch powders. Higher amounts of this polymer in soil resulted in lower plant height as well as smaller plant weight.

In contrast, the combination of LH and higher amount of NPK had a synergic effect on corn growth. Material containing only LH (sample H) affected corn growth positively in comparison with plant grown without application of superabsorbent, but its effect was weaker.

Figge, Hetrick, and Wilson (1995) used expanded clay and porous ceramics (as materials to enhance water management) in combination with manure, KH_2PO_4, and KCl (as nutrients) in order to improve plant growth in minespoils. They observed that germination and growth of plants were improved if the materials were applied on the surface, but no benefit was observed in the case of mixing.

The influence of our composite materials on root growth was different. The best results were obtained with sample A containing only a small content of NPK without LH. It seems that water management is more important for root growth than the addition of nutrients. The addition of LH had negative effect in the case of low NPK content. Root growth was slightly improved if a higher content of NPK was combined with the addition of LH. In contrast, the results with sample H which contained LH without NPK were the best (with the exception of those with sample A). The negative effect of humic substances on the growth of plants and roots was described by Rastghalam, Hoodaji, and Javanmard (2011). The effect was more important in the case of plant growth (in comparison with roots). In contrast, Zhang et al. (2005) observed that the roots and stems of grass were sturdier if superabsorbent containing sodium humate was applied in soil (compared with grass grown without such application). This discrepancy can be explained by the existence of an optimal level of humic addition. If the addition of humic substances increases above, a certain threshold, negative effects on nutrient uptake and plant growth can be observed (Panuccio et al. 2001).

4 | CONCLUSIONS

In this work, several different superabsorbents containing lignohumate and conventional mineral fertilizer (NPK) were prepared. Their swelling behaviour, release of nutrients, periodic washing out and the influence on the growth of corn were studied. It was found that the swelling was relatively fast and it was completed in 24 hr. While the addition of NPK suppressed the water absorption, the swelling was supported by the presence of LH. Simultaneously, the swelling influenced the release of nutrients from superabsorbents during the first day. The release of mineral nutrients corresponded with their contents in different samples. The higher content of NPK resulted in the prolongation of the release of nutrients. The addition of LH had negligible influence on the release of P and N. In contrast, the amount of released K increased because of the potassium content in added LH. On the other hand, the release of LH was partially suppressed by the higher content of NPK. In leaching experiments, realized be repeated washing out of active substances from hydrogels, the mineral nutrients were washed out after seven cycles and LH after ten cycles. In general, the application of superabsorbents supported growth of corn. Better water management and a slow supplying by nutrients had positive effect on the height of plants. The length of roots is probably influenced more by better water management. The combination of superabsorbent polymers with NPK and LH in suitable amounts can improve soil properties, water management, nutrient uptake and growth of plants. Such materials can be utilized mainly in problematic areas with dry soils and low levels of organic matter and nutrient elements.

ORCID
Martina Klucakova 🆔 https://orcid.org/0000-0003-4969-6988

REFERENCES

Abedi-Koupai, J. & Asadkazemi, J. (2006). Effects of a hydrophilic polymer on the field performance of an ornamental plant (Cupressus arizonica) under reduced irrigation regimes. *Iranian Polymer Journal*, 15, 715–725.

Albiach, R., Canet, R., Pomares, F. & Ingelmo, F. (2001). Organic matter components, aggregate stability and biological activity in a horticultural soil fertilized with different rates of two sewage sludges during ten years. *Bioresource Technology*, 77, 109–114. https://doi.org/10.1016/S0960-8524(00)00166-8

Bai, W., Zhang, H., Liu, B., Wu, Y. & Song, J. (2010). Effects of super-absorbent polymers on the physical and chemical properties of soil following different wetting and drying cycles. *Soil Use Management*, 26, 253–260. https://doi.org/10.1111/j.1475-2743.2010.00271.x

Bharadwaj, A. K., Shainberg, I., Goldstein, D., Warrington, D., Levy, J. G. & Reisenauer, A. E. (2007). Water retention and hydraulic conductivity of cross-linked polyacrylamides in sandy soils. *Soil Science Society of America Journal*, 71, 406–412. https://doi.org/10.2136/sssaj2006.0138

Bryan, N. D., Jones, D. L. M., Keepax, R. E., Farrelly, D. H., Abrahamsen, L. G., Pitois, A., … Evans, N. (2007). The role of humic non-exchangeable binding in the promotion of metal ion transport in groundwaters in the environment. *Journal of Environmental Monitoring*, 9, 329–347. https://doi.org/10.1039/b701891f

Chatzistathis, T., Papadakis, I. E., Papaioannou, A., Chatzissavvidis, C. & Giannakoula, A. (2020). Comparative study effects between manure application and a controlled release fertilizer on the growth, nutrient uptake, photosystem II activity and photosynthetic rate of *Olea europaea* L. (cv. 'Koroneiki'). *Scientia Horticulturae*, 264, 109176. https://doi.org/10.1016/j.scienta.2020.109176

Chu, M., Zhu, S. Q., Huang, Z. B. & Li, H. M. (2008). Influence of potassium humate on the swelling properties of a poly(acrylic acid-co-acrylamide)/ potassium humate superabsorbent composite. *Journal of Applied Polymer Science*, 107, 3727–3733. https://doi.org/10.1002/app.27410

Dadhaniya, P. V., Patel, M. P. & Patel, R. G. (2006). Swelling and dye adsorption study of novel superswelling [Acrylamide/ N-vinylpyrrolidone/ 3(2-hydroxyethyl carbamoyl) acrylic acid] hydrogels. *Polymer Bulletin*, 57, 21–31. https://doi.org/10.1007/s00289-006-0531-5

Davidson, D. & Gu, F. X. (2012). Materials for sustained and controlled release of nutrients and molecules to support plant growth. *Journal of Agricultural and Food Chemistry*, 60, 870–876. https://doi.org/10.1021/jf204092h

Dorraji, S. S., Golchin, A. & Ahmadi, S. (2010). The effects of hydrophilic polymer and soil salinity on corn growth in sandy and loamy soils. *Clean*, 38, 584–591. https://doi.org/10.1002/clen.201000017

Du, C. W., Zhou, J. & Shaviv, A. (2006). Release characteristics of nutrients from polymer-coated compound controlled release fertilizers. *Journal of Polymers and the Environment*, 14, 223–230. https://doi.org/10.1007/s10924-006-0025-4

Enev, V., Pospisilova, L., Klucakova, M., Liptaj, T. & Doskocil, L. (2014). Spectral characterization of selected natural humic substances. *Soil and Water Research*, 9, 9–17. https://doi.org/10.17221/39/2013-SWR

Erro, J., Urrutia, O., Francisco, S. S. & Garcia-Mina, J. M. (2007). Development and agronomical validation of new fertilizer compositions of high bioavailability and reduced potential nutrient losses. *Journal of Agricultural and Food Chemistry*, 55, 7831–7839. https://doi.org/10.1021/jf0708490

Figge, D., Hetrick, B. A. D. & Wilson, G. W. T. (1995). Role of expanded clay and porous ceramic amendments on plant establishment in minespoils. *Environmental Pollution*, 88, 161–165. https://doi.org/10.1016/0269-7491(95)91440-V

Frimmel, F. H., Abbt-Braun, G., Heumann, K. G., Hock, B., Ludemann, H. D. & Spiteller, M. (2002). *Refractory organic substances in the environment*. Wiley-VCH, Weinheim, Germany.

Gao, L., Wang, S. & Zhao, X. (2013). Synthesis and characterization of agricultural controllable humic acid superabsorbent. *Journal of Environmental Sciences*, 25, S69–S76. https://doi.org/10.1016/S1001-0742(14)60629-X

Garcia, D., Cegarra, J., Roig, A. & Abad, M. (1994). Effects of the extraction temperature on the characteristics of a humic fertilizer obtained from lignite. *Bioresource Technology*, 47, 103–106. https://doi.org/10.1016/0960-8524(94)90106-6

Girardi, E. A., Mourao Filho, F. A. A., Graf, C. C. D. & Olic, F. B. (2005). Influence of soluble and slow-release fertilizers on vegetative growth of containerized citrus nursery trees. *Journal of Plant Nutrition*, 28, 1465–1480. https://doi.org/10.1080/01904160500201337

Grable, C., Knight, J. & Ingram, D. L. (2017). Plant growth and leachate electrical conductivity and pH as influenced by controlled-release fertilizer blends and coating technologies. *Horttechnology*, 27, 639–643. https://doi.org/10.21273/HORTTECH03767-17

Klucakova, M. (2010). Adsorption of nitrate on humic acids studied by flow-through coulometry. *Environmental Chemistry. Letters*, 8, 145–148. https://doi.org/10.1007/s10311-009-0201-6

Klucakova, M. (2014). Complexation of metal ions with solid humic acids, humic colloidal solutions, and humic hydrogel. *Environmental Engineering Science*, 31, 612–620. https://doi.org/10.1089/ees.2013.0487

Klucakova, M. & Novackova, K. (2014). Comparison of thermal and chemical stability of Cu-humic complexes. *Journal of Soils Sediments*, 14, 360–367. https://doi.org/10.1007/s11368-013-0699-x

Klucakova, M. & Pekar, M. (2003). Study of structure and properties of humic and fulvic acids. III. Study of complexation of Cu2+ ions with humic acid in sols. *Journal of Polymer Materials*, 20, 145–154.

Klucakova, M. & Veznikova, K. (2016). The role of concentration and solvent character in the molecular organization of humic acids. *Molecules*, 21, 1410–1418. https://doi.org/10.3390/molecules21111410

Lal, R. (2004). Soil carbon sequestration impacts on global climate change and food security. *Science*, 304, 1623–1627. https://doi.org/10.1126/science.1097396

Lee, J. & Sung, K. (2014). Effects of chelates on soil microbial properties, plant growth and heavy metal accumulation in plants. *Ecological Engineering*, 73, 386–394. https://doi.org/10.1016/j.ecoleng.2014.09.053

Li, A., Wang, A. & Chen, J. (2004). Studies on poly(acrylic acid)/attapulgite superabsorbent composites. II. Swelling behaviors of superabsorbent composites in saline solutions and hydrophilic solvent–water mixtures. *Journal of Applied Polymer Science*, 94, 1869–1876. https://doi.org/10.1002/app.20850

Li, A., Zhang, J. & Wang, A. (2005). Synthesis, characterization and water absorbency properties of poly(acrylic acid)/sodium humate superabsorbent composite. *Polymers for Advanced Technologies*, 16, 675–680. https://doi.org/10.1002/pat.641

Liu, J., Wang, Q. & Wang, A. (2007). Synthesis and characterization of chitosan-g-poly(acrylic acid)/sodium humate superabsorbent. *Carbohydrate Polymers*, *70*, 166–173. https://doi.org/10.1016/j.carbpol.2007.03.015

Madejon, E., Lopez, R., Murillo, J. M. & Cabrera, F. (2001). Agricultural use of three (sugar-beet) vinasse composts: Effect on crops and chemical properties of a Cambisol soil in the Guadalquivir river valley (SW Spain). *Agriculture, Ecosystems & Environment*, *84*, 55–65. https://doi.org/10.1016/S0167-8809(00)00191-2

Matoso, V., Bargi-Souza, P., Ivanski, F., Romano, M. A. & Romano, R. M. (2019). Acrylamide: A review about its toxic effects in the light of Developmental Origin of Health and Disease (DOHaD) concept. *Food Chemistry*, *283*, 422–430. https://doi.org/10.1016/j.foodchem.2019.01.054

Mikula, K., Izydorczyk, G., Skrzypczak, D., Mironiuk, M., Moustakas, K., Witek-Krowiak, A. & Chojnacka, K. (2020). Controlled release micronutrient fertilizers for precision agriculture – A review. *Science of the Total Environment*, *712*, 136365. https://doi.org/10.1016/j.scitotenv.2019.136365

Mo, C., Shu-quan, Z., Hua-Min, L., Zhan-bin, H. & Shu-qin, L. (2006). Synthesis of poly(acrylic acid)/sodium humate superabsorbent composite for agricultural use. *Journal of Applied Polymer Science*, *102*, 5137–5143. https://doi.org/10.1002/app.24661

Nnadi, F. & Brave, C. (2011). Environmentally friendly superabsorbent polymers for water conservation in agricultural lands. *Journal of Soil Science and Environmental Management*, *2*, 206–211.

Novotny, E. H., Blum, W. E. H., Gerzabek, M. H. & Mangrich, A. S. (1999). Soil management system effects on size fractionated humic substances. *Geoderma*, *92*, 87–109. https://doi.org/10.1016/S0016-7061(99)00022-1

Pacheco, M. L. & Havel, J. (2001). Capillary zone electrophoretic (CZE) study of uranium(VI) complexation with humic acids. *Journal of Radioanalytical and Nuclear Chemistry*, *248*, 565–570. https://doi.org/10.1023/A:1010618628705

Panuccio, M. R., Muscolo, A. & Nardi, S. (2001). Effect of humic substances on nitrogen uptake and assimilation in two species of pinus. *Journal of Plant Nutrition*, *24*, 693–704. https://doi.org/10.1081/PLN-100103663

Piccolo, A. & Mbagwu, H. S. C. (1997). Exogenous humic substances as conditioners for the rehabilitation of degraded soils. *Agro Food Industry Hi Tech*, *8*, 2–4.

Raju, M. P. & Raju, K. M. (2001). Design and synthesis of superabsorbent polymers. *Journal of Applied Polymer Science*, *80*, 2635–2639. https://doi.org/10.1002/app.1376

Raju, M. P., Raju, K. M. & Mohan, Y. M. (2002). Synthesis and water absorbency of crosslinked superabsorbent polymers. *Journal of Applied Polymer Science*, *85*, 1795–1801. https://doi.org/10.1002/app.10731

Rastghalam, Z. S., Hoodaji, M. & Javanmard, H. (2011). The influence of humic acid and nano-superabsorbent application on the growth of *Brassica Napus L*, in:lead-contaminated soil, in: *International Conference on Environmental and Agriculture Engineering IPCBEE 2011*. IACSIT Press, Chengdu, pp. 71-75.

Sedlacek, P. & Klucakova, M. (2009). Simple diffusion method applied in evaluation of metal transport in model humic matrices. *Geoderma*, *153*, 286–292. https://doi.org/10.1016/j.geoderma.2009.07.002

Shepherd, T. G., Saggar, S., Newman, R. H., Ross, C. W. & Dando, J. L. (2001). Tillage-induced changes to soil structure and organic carbon fractions in New Zealand soils. *Australian Journal of Soil Research*, *39*, 465–489. https://doi.org/10.1071/SR00018

Silva, S. M., Luz, J. M. Q., Nogueira, P. A. M., Blank, A. F., Sampaio, T. S., Pinto, J. A. O. & Junior, A. W. (2017). Organo-mineral fertilization effects on biomass and essential oil of lavender (*Lavandula dentata* L.). *Industrial Crops & Products*, *103*, 133–140. https://doi.org/10.1016/j.indcrop.2017.04.004

Spencer, H., Wahome, J. & Haasch, M. (2018). Toxicity evaluation of acrylamide on the early life stages of the zebrafish embryos (Danio rerio). *Journal of Environmental Protection*, *9*, 1082–1091. https://doi.org/10.4236/jep.2018.910067

Spencer, P. & Schaumburg, H. (1974a). A review of acrylamide neurotoxicity part I. Properties, uses and human exposure. *Canadian Journal of Neurological Sciences*, *1*, 143–150. https://doi.org/10.1017/S0317167100019739

Spencer, P. & Schaumburg, H. (1974b). A review of acrylamide neurotoxicity part II. Experimental animal neurotoxicity and pathologic mechanisms. *Canadian Journal of Neurological Sciences*, *1*, 152–169. https://doi.org/10.1017/S0317167100119201

Tan, K. H. (2014). *Humic matter in soil and the environment: Principles and controversies*, 2nd edn. Boca Raton, FL: CRC Press.

Zhan, F., Liu, M., Guo, M. & Wu, L. (2004). Preparation of superabsorbent polymer with slow-release phosphate fertilizer. *Journal of Applied Polymer Science*, *92*, 3417–3421. https://doi.org/10.1002/app.20361

Zhang, J. P., Li, A. & Wang, A. Q. (2005). Study on superabsorbent composite. V. Synthesis, swelling behaviors and application of poly(acrylic acid-co-acrylamide)/sodium humate/attapulgite superabsorbent composite. *Polymers for Advanced Technologies*, *16*, 813–820. https://doi.org/10.1002/pat.657

Zhang, J., Li, A. & Wang, A. (2006). Synthesis and characterization of multifunctional poly(acrylic acid-co-acrylamide)/sodium humate superabsorbent composite. *Reactive and Functional Polymers*, *66*, 747–756. https://doi.org/10.1016/j.reactfunctpolym.2005.11.002

Zhao, H., Song, J., Zhao, G., Xiang, Y. & Liu, Y. (2019). Novel semi-IPN nanocomposites with functions of both nutrient slow-release and water retention. 2. Effects on soil fertility and tomato quality. *Journal of Agricultural and Food Chemistry*, *67*, 7598–7608. https://doi.org/10.1021/acs.jafc.9b00889

SUPPORTING INFORMATION

Additional supporting information may be found online in the Supporting Information section.

Appendix 25

Enev, V., Sedláček, P., Jarábková, S., Velcer, T., and Pekař, M. ATR-FTIR spectroscopy and thermogravimetry characterization of water in polyelectrolyte-surfactant hydrogels. *Colloids and Surfaces A: Physicochemical and Engineering Aspects* **2019**, 575, 1–9.

ATR-FTIR spectroscopy and thermogravimetry characterization of water in polyelectrolyte-surfactant hydrogels

Vojtěch Enev[1], Petr Sedláček[1], Sabína Jarábková, Tomáš Velcer, Miloslav Pekař*

Faculty of Chemistry, Brno University of Technology, Purkyňova 118, Brno, 612 00, Czech Republic

GRAPHICAL ABSTRACT
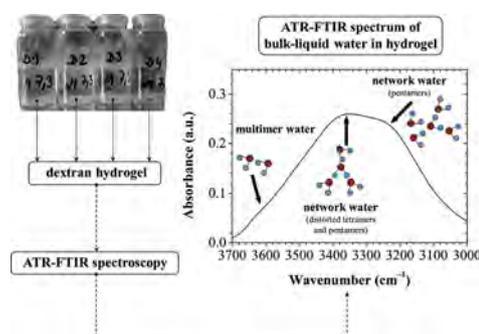
ARTICLE INFO

ABSTRACT

Attenuated total reflection Fourier transform infrared (ATR-FTIR) spectroscopy and thermogravimetric analysis (TGA) were evaluated as useful techniques to study bulk and hydration water in hydrogels. Hydrogels formed by cationized dextran (DEAE-dextran) and anionic surfactants were used as model materials. The IR technique was applied both on fresh samples and on dehydrating samples during the evaporation process. Not only overall IR spectra but especially the deconvoluted OH band was used in the analysis. IR spectroscopy was shown to provide especially structural information which is nicely complemented by the mainly quantitative data provided by TGA. Significant differences between the dehydration processes for the model gels with different surfactants were revealed. The DEAE-dextran-based hydrogels were characterized by a continuous step dehydration with different drying rates in the initial evaporation period. Three different water subpopulations were identified in all model hydrogel samples. Water molecules in these hydrogels containing a higher concentration of surfactants demonstrated a more ordered hydrogen network, which was formed by subpopulations of pentamers, tetramers and/or distorted pentamers.

1. Introduction

Hydrogels are well-known colloids in which the dispersion medium (phase) is formed by water (aqueous solution) and the dispersed phase is in a solid state formed usually by chains of hydrophilic polymers forming the hydrogel network. Hydrogels find applications in a broad range of products such as pharmaceutical, food, cosmetic, agricultural or horticultural products [1,2]. Biocompatible hydrogels are important materials for drug delivery or tissue engineering where they are applied as soft contact lenses, artificial implants, actuators, wound healing

---

dressings, etc. [3,4]. Hydrogel applications benefit from the high content of water which is embedded in their solid-like matrix. Due to the high water content, the transport of low molecular weight compounds in hydrogels is not greatly slower than in liquids but hydrogels retain shapes and can be easily deformed, cut, or even injected [5]. Hydrogels are viscoelastic and therefore moderate deformations of their structural network are reversible (recoverable).

Water content is among the principal characteristics of any hydrogel. This basic and gross parameter can be supplied by a more detailed insight into the water state and binding within the hydrogel meshwork. NMR spectroscopy is a fine tool to address this task [6,7] but even IR spectroscopy, which is much less expensive and in its ATR version easily applicable, can provide valuable information. The IR absorption bands of water (especially those in the range of 3800–3000 cm^{-1}) can provide a molecular-level information related to the involvement of water subpopulations in specific structural arrangements such as water multimers and the water network. Recently, two ways for determining these water subpopulations have been successfully utilized in describing the hydration of polymers: Fourier self-deconvolution and fitting the measured envelope band by the summation of usually three Gaussian components using non-linear fitting tools (i.e. data analysis software) [8–10].

In our previous work, we have focused on preparation and characterization of hydrogels prepared by mixing oppositely charged polyelectrolyte with surfactant in the micellar form [11]. Experimental data suggests that physical crosslinks in these materials are formed preferably by electrostatic interactions between surfactant micelles and charged groups on the polyelectrolyte. Furthermore, by means of a rheological analysis of the gels we have shown that their viscoelasticity can be controlled in a broad range by the molecular weight of the polyelectrolyte and the concentration of micelles. Obviously, water in these hydrogels is expected to form not only a dispersion medium but also to create a hydration shell around micelles and biopolymer chains. Therefore, the current study is aimed at IR-spectroscopic study of water in the polyelectrolyte/surfactant hydrogels. In particular, we focus on hydrogels formed via mixing cationic polyelectrolyte (amino-modified dextran) with anionic surfactants as model materials to evaluate the capability of the IR technique. IR spectroscopy was applied not only on the fresh (fully hydrated) samples but used also in order to follow water loss from hydrogels during evaporation over time in order to detect any changes in the amount of water in the hydrogel. From this perspective, thermogravimetry was also employed as a supporting technique routinely used in monitoring the drying process in highly hydrated materials.

2. Materials and methods

2.1. Preparation of polyelectrolyte-surfactant hydrogels

In this study diethylaminoethyl-dextran (in the hydrochloride form) was used as a model cationic polyelectrolyte. It was selected on the basis of preliminary tests as a representative of cationic polysaccharides which formed hydrogels with surfactants readily and without specific pH control. It belongs to the class of the low charge density polyelectrolytes [12], similarly as hyaluronan used in our previous work [11]. Dry polymer was purchased from Sigma-Aldrich (Czech Republic; product number D9885, batch number BCBQ8681) and used without any further treatment, The weight averaged molar weight (573 ± 9 kDa) and polydispersity index (2.2) of the DEAE-dextran were determined via gel Size Exclusion Chromatography (Agilent, Infinity 1260 system, PLgel MIXED-C column) with Multiangle Light Scattering (Wyatt Technology, Dawn Heleos II) and Differential Refractive Index (Wyatt Technology, Optilab T-rEX) detection. The nitrogen content reported by the producer was 3%. Two model anionic surfactants were used: sodium dodecyl sulfate (SDS) and sodium tetradecyl sulfate (STS). Both surfactants were purchased from Sigma-

Table 1
Concentration of initial stock solutions of DEAE-dextran, SDS and STS used to prepare hydrogels.

Sample of hydrogel	DEAE-dextran % (wt/vol)	SDS mM	STS
D1	4	400	
D2	4	100	
D3	4		200
D4	4		150

Aldrich (Czech Republic).

Hydrogels were prepared via mixing a stock solution of biopolymer and a stock solution of surfactant in the volume ratio 1:1. The exact compositions of the respective stock solutions were selected on the basis of preliminary tests (formation of sufficient amount of gel-like material) are summarized in Table 1. The resulting mixtures were left on a shaker overnight to complete the gelation process after which the system was centrifuged, the supernatant was discarded and the gel collected for further experiments. All the stock solutions were prepared in 0.15 mol/L NaCl using ultra-pure water (Purelab Flex, ELGA system, Lane End, United Kingdom). The composition of the formed hydrogels was estimated on the basis of the residual component contents in the supernatant and is given in Table S1 (Supplementary material).

2.2. Thermogravimetric analysis

Thermogravimetry of the polyelectrolyte-surfactant hydrogels was performed using a Q5000 TG analyzer (TA Instruments, New Castle, Delaware, USA). Approximately 15 mg of fresh hydrogel was weighted into a platinum pan. After inserting the pan into the TG analyser, the sample was either heated from room temperature at a defined heating rate in the air or under a nitrogen atmosphere (dynamic TGA) or the sample temperature was instantaneously equilibrated and maintained at 70 °C in a nitrogen atmosphere (isothermal TGA). In both types of TG analyses, the relative sample weight was recorded continuously with ± 0.1% mass accuracy.

2.3. Infrared spectroscopy

Steady-state and time-resolved FTIR spectra were obtained by means of an Attenuated Total Reflectance (ATR) technique using a Nicolet iS50 spectrometer (Thermo Fisher Scientific, Waltham, USA). All measurements were taken at room temperature (in an air-conditioned room) on the built-in diamond ATR crystal. Steady-state FTIR spectra were recorded over the range 4000–400 cm^{-1} at 4 cm^{-1} resolutions and represented an average of 128 scans. The spectrum of the clean dry diamond ATR crystal in ambient atmosphere (air) was used as the background for infrared measurement. For time-resolved measurement, a small amount (approximately 200 μL) of the polyelectrolyte-surfactant hydrogel was placed directly on the clean dry surface of the ATR crystal and the data collection using Omnic Series data collection software was started. The time-resolved FTIR spectra were collected at regular time intervals while water evaporated from the hydrogels. The individual FTIR spectrum was collected every 5 s as an average of 8 scans with a resolution of 4 cm^{-1} over the course of the drying experiment (total time 200 min at minimum). In order to monitor the water content of hydrogels over time, raw absorption spectra were evaluated with no artificial processing (e.g. baseline or ATR corrections, atmospheric suppression). In order to investigate the change in the water structure in polyelectrolyte-surfactant hydrogels, the absorption band that corresponds to O−H stretching in hydroxyls (3800–3000 cm^{-1}) was processed by deconvolution into individual overlapping components attributed to three states of the water molecule. The positions of the overlapping bands were acquired by the 2nd derivative method according to [13]. Subsequently, the deconvolution was made

by fitting the experimental band to three calculated Gaussian components using Origin 8.1 software. Interpretation of three calculated components was based on the literature [9].

3. Results and discussion

3.1. TGA analysis of the gel-drying process

Thermogravimetry (TGA) regularly represents the first experimental choice when a drying of highly hydrated materials (such as hydrogels) is to be analyzed. The method is based on monitoring the weight of the sample during a user-defined thermal program (i.e. heating/cooling of the sample) in a controlled ambient atmosphere. Therefore, TGA was included in this study to complement and to support the interpretation of the results of the method of that mainly interests us here, i.e. the FTIR spectroscopic drying assay.

Initially, the thermal stability of the gel-forming components was checked via the standard TGA procedure. The respective compound in its original (powder) state was heated to 600 °C with a heating rate of 10 °C/min and the decomposition temperature was determined from the onset of the drop in the sample weight that corresponds to the thermal decomposition. It was confirmed that all the individual gel components in their dry state are on the time scale of the performed experiments thermally stable up to 200 °C.

Subsequently, all the studied polyelectrolyte-surfactant hydrogels were subjected to a similar TGA assay. The respective thermograms are shown in Fig. 1. It can be clearly seen that the weight of all the hydrogel samples drops in a stepwise manner. The first two stages of the sample weight drop, which proceed from the very start of the experiment until the sample reaches a temperature around 120–150 °C, can be attributed to the removal of water from the hydrogel matrix, while at higher temperatures thermal decomposition of the dry content of the hydrogel proceeds. When focusing on the drying behavior of the tested gels, it is noticeable that the main character of the drying process is similar for all four considered hydrogel compositions. Removal of water from a sample proceeds in two steps, the first one arising immediately when the experiment starts, while the second drying step begins when the temperature is approaching the boiling point of water (100 °C). These results indicate that at least two distinguishable types of water are found in the sample, namely more freely bound water which evaporates faster and more strongly bound hydration water removed at higher temperatures. From the thermograms shown in Fig. 1, it is also evident that the latter step of water removal is continuously followed by thermal decomposition of the hydrogel matrix (note the partially overlapping peaks in derivative thermograms represented by dashed
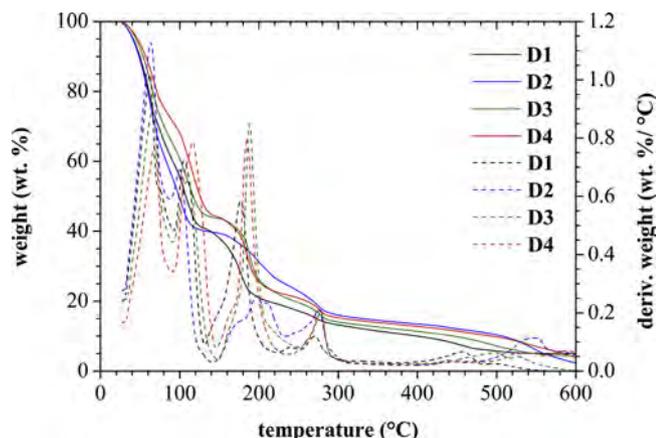
Fig. 1. TGA thermograms provided as time evolution of relative weight (solid curves) and the rate of the weight loss (dashed curves) during heating of tested hydrogels in air (heating rate 10 °C/min). Analyzed gels are labeled according to Table 1.

curves in the temperature region 100–200 °C). For this reason, it is not possible to determine the dry content weights of the tested hydrogels based solely on this basic TGA assay. Therefore, further TGA analyses were performed to provide a more comprehensive view of the drying of the studied gels.

At first, lower heating rates (5 °C/min and 2 °C/min, respectively) were applied. The results of these analyses are shown in the Supplementary material (see Fig. S1). Application of lower heating rates aimed primarily at separating the individual drying steps and also the drying and decomposition processes during the sample heating. Nevertheless, it was found that even at the lowest heating rate applied (2 °C/min), the drying of the sample passes continuously to the thermal decomposition (see Fig. S1). Furthermore, also the drying process maintains its character of more drying steps continuously following each other. The main difference in the drying behavior at the lower drying rates is represented by the shift of the drying steps to the lower temperatures. Similar information was provided also from TGA analysis performed in an inert (nitrogen) atmosphere. Fig. S2 (Supplementary material) shows a comparison of the thermograms of the tested hydrogels obtained under an air and a nitrogen atmosphere, respectively. It can be seen that the zero humidity of the inert atmosphere supports and accelerates drying. This is again represented by the shift of drying rate peaks to the lower temperature. Furthermore, it can be seen that more water is removed during the first drying step in nitrogen than in air (note the increased relative height of the first peak in the drying rate curve). Similarly to drying in air atmosphere, no significant difference in the drying behavior of the tested hydrogels was revealed in the inert ambient atmosphere either.

As far as monitoring of the drying process is concerned, a major limitation of the above-mentioned dynamic (heating) TGA experiments is represented by the fact that decomposition of the thermally labile polymer-surfactant network begins soon after or even during the water-removal process. Therefore, we complemented our study with an isothermal TGA experiment, where the weight of the measured sample and the rate of its change are monitored over time at a constant temperature (at 70 °C in our case). This method has previously been successfully utilized for instance in differentiation of intracellular and extracellular water in microbial cell cultures [14,15]. Fig. 2 shows the initial period (0–20 min) of the isothermal drying process for all tested hydrogels. It can be seen that for all samples the drying rate first increases while the temperature is raised, followed by a substantial decrease in the drying rate during the equilibration of the measurement temperature and isothermal drying. When comparing the particular thermograms of samples D1–D4, several tiny but noticeable differences can be found. Firstly, in agreement with the results of the dynamic TGA analysis presented above, it is evident that when comparing the gels prepared using the same surfactant (D1/D2 and D3/D4), the hydrogel prepared with a higher concentration of surfactant applied is always represented by a lower drying rate in the initial drying period (see the respective maxima in the drying rate curves), but at later times its drying rate curve crosses and exceeds the curve of its counterpart prepared with a lower concentration of surfactant. This can be interpreted as a manifestation of the more densely cross-linked hydrogel network with more strongly-bound hydration water where the higher concentration of the cross-linking agent (surfactant) is used. A more pronounced difference is found for DEAE-dextran gels cross-linked by SDS (D1 and D2) than for those prepared with STS, which is probably caused by the greater difference in the applied surfactant concentrations and, correspondingly, in the density of cross-links in gels with SDS. Furthermore, in these gels (D1 and D2) a sudden change in the drying-rate curve can be found in the initial period (indicated with arrows in Fig. 2). These sudden changes in the drying rate curves are often assigned to a change in the drying mechanism [16]. This indicates that the initial mechanism of the drying process is changed during this initial period for SDS-containing hydrogels but is maintained for the STS-based gels where no such feature is found in the drying curves.
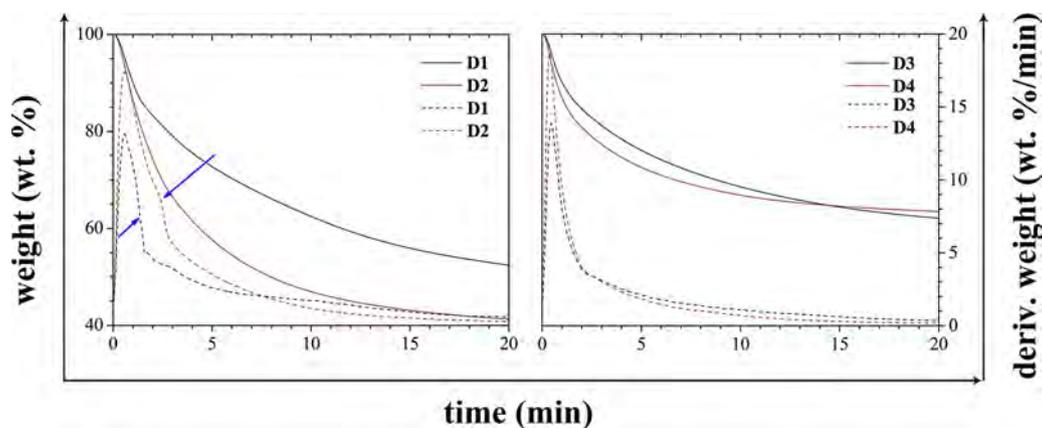
Fig. 2. Initial part (0–210 min) of TGA thermograms recorded during isothermal drying of all tested gels. Evolution over time of the sample weight (solid), drying rate (dashed) and temperature (dash dotted) is shown.

3.2. Steady-state FTIR spectrometry

As a first part of the spectroscopic study of the tested DEAE-dextran hydrogels, the FTIR spectra of the gels were measured immediately after their preparation to see their basic IR features and to characterize their molecular structure in the fully hydrated state. The steady-state ATR-FTIR spectra of polyelectrolyte-surfactant hydrogels are presented in Fig. 3. Interpretation of their absorption bands has been carried out according to the literature data [17–19]. The spectra are mainly characterized by bands of aliphatic, alcohol and polysaccharide groups. All the spectra of polyelectrolyte-surfactant hydrogels contain a broad band at 3400–3300 cm^{-1} corresponding to the O−H stretching of bulk liquid water. The water molecules are also indicated by the broad deformation band centered at about 1645 cm^{-1} resulting from bending vibration.

The presence of aliphatic chains is demonstrated in the spectral
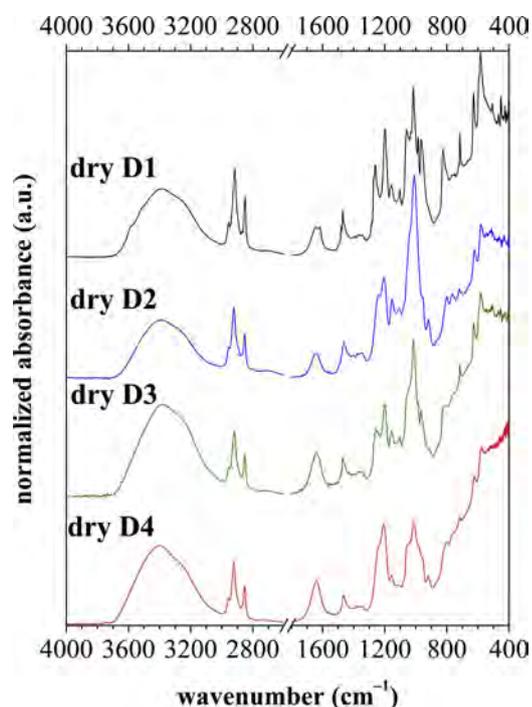

Fig. 3. ATR-FTIR spectra of all tested dry polyelectrolyte-surfactant hydrogels. DEAE-dextran gels with SDS (black and blue solid curve) and DEAE-dextran gels with linear STS (green and red solid curve) (For interpretation of the references to colour in this figure legend, the reader is referred to the web version of this article).

range of 2960–2840 cm^{-1}. Sharp and intensive bands at 2919 cm^{-1} and 2850 cm^{-1} were ascribed to asymmetric and symmetric C−H stretching in methylene groups, respectively. An absorption band of asymmetric stretching in methyl groups (2956 cm^{-1}) was only observed for sample D1; it occurred as less pronounced shoulders in the rest of the polyelectrolyte-surfactant hydrogels. The deformation vibrations of −CH_2− and −CH_3 groups occur in the spectra at 1470 cm^{-1}. The relative intensity of this band was higher for hydrogels prepared from SDS surfactant. Deformation vibrations of methyl groups are only present in ATR spectra of D1 and D2 hydrogels at 1382 cm^{-1}.

The presence of long carbon chains with more than four atoms (e.g. surfactants), was revealed by the band at 719 cm^{-1}, which is ascribed to C−H in-plane bending of methylene groups. Another significant band occurring at 1300 cm^{-1} can be assigned to out-of-plane C−H bending (methylene twisting) in aliphatic chains. The out-of-plane C−H vibration (methylene wagging) of methylene groups occurs in the spectra at 1315 cm^{-1}. This band was found as a weak band and/or shoulder.

All the spectra of DEAE-dextran hydrogels contain a sharp and intensive band at 1200 cm^{-1} corresponding to tertiary amine groups. All the spectra also contain a less intensive band and/or shoulder at 1260 cm^{-1} corresponding to primary and/or secondary alcohol. Many authors consider the band at 1260 cm^{-1} to be an indicator of C−O stretching in cyclic ethers [18]. In all ATR spectra bands are apparent at 1159 cm^{-1} and 1100 cm^{-1} due to the glycoside C−O−C stretching of polysaccharides.

The main difference among the spectra of polyelectrolyte-surfactant hydrogels appear in the fingerprint region 1100–900 cm^{-1}. A band at about 1018 cm^{-1}, preferentially ascribed to S═O stretching of sulfate groups (salt form), or possibly C−O stretching of primary and secondary alcohols, is apparent in all samples. The sulfate sodium salt groups are also indicated by the sharp band centered at about 1195 cm^{-1} resulting from the S═O symmetric stretching vibrations of the R−O−SO_2−O^-. Bands and shoulders at wavenumbers less than 850 cm^{-1} are attributed to asymmetric C−H bending of the methylene groups from which bands at 815 cm^{-1} and 580 cm^{-1} are more evident in hydrogels with SDS.

3.3. Time-resolved FTIR analysis of polyelectrolyte-surfactant hydrogels

In Fig. 4 we show the temporal course of the FTIR spectra of the polyelectrolyte-surfactant hydrogels, i.e., of the D1–D4 samples, during drying. Naturally, drying of the samples is accompanied by decreasing intensity of the O−H vibration bands, which are observed in the regions 3700–3100 cm^{-1} (stretching vibrations) and 1680–1620 cm^{-1} (bending vibration) (see the decrease of the vibration modes depicted in Fig. 2), whereas the relative intensity of the aliphatic, polysaccharide and alcohol bands increase with drying time. These bands were
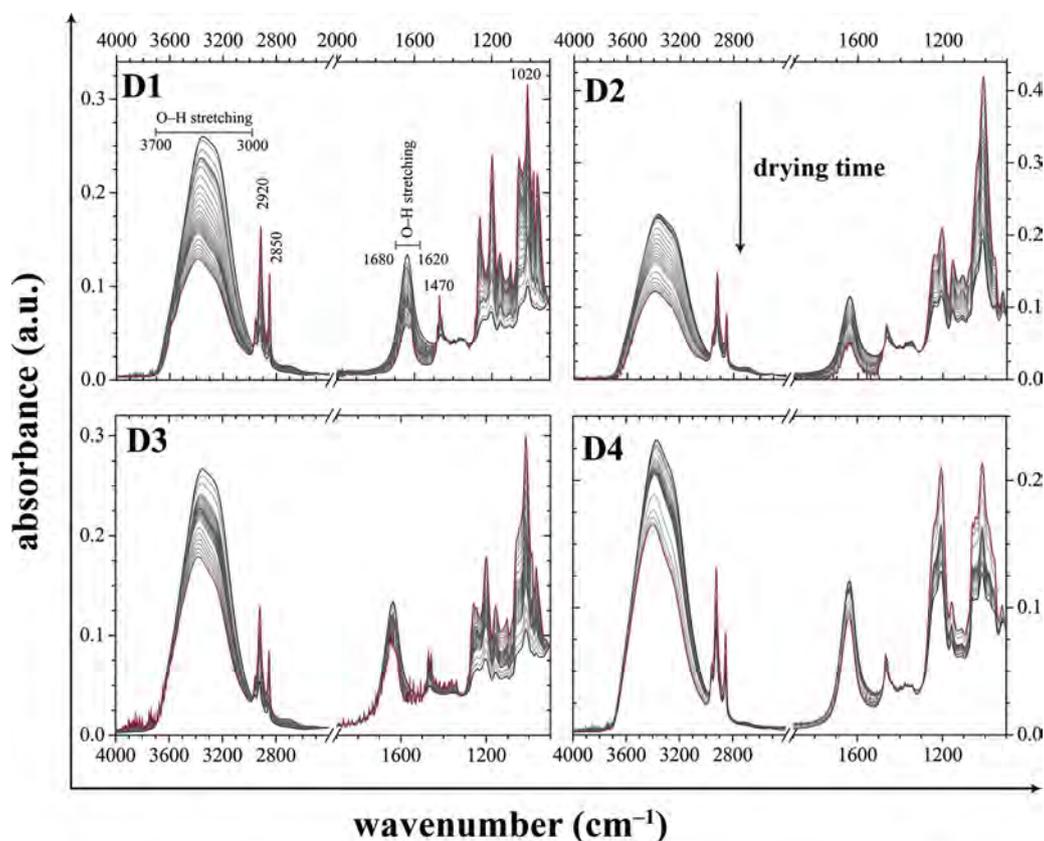
Fig. 4. Development over time of the ATR-FTIR spectra of tested polyelectrolyte-surfactant hydrogels.

observed at around $2956\,cm^{-1}$, $2920\,cm^{-1}$, $2850\,cm^{-1}$, $1470\,cm^{-1}$, $1260\,cm^{-1}$, $1160\,cm^{-1}$, $1100\,cm^{-1}$ and $1020\,cm^{-1}$.

The broad $-OH$ stretching band within the $3700–3100\,cm^{-1}$ range represents in fact a convolution envelope which comprises as well FTIR bands arising from different subpopulations of water molecules as the bands that correspond to the hydroxyl groups in DEAE-dextran. In the FTIR spectra of all samples, the position of this broad envelope band was shifted to higher frequencies during the dehydration process. Generally, an increase in the frequency of the O−H vibrations mode is an indicative of a decrease in the degree of hydrogen bonding. The positions of $\nu(OH)$ bonds and $\Delta\nu$ values which correspond to the middle frequency of the O−H stretching vibrations before and after drying are listed in Table 2. Interestingly, the value of the red shift of the middle frequency of the O−H stretching band seems to correlate with cross-linking density – hydrogel D1, prepared with a higher concentration of SDS, shows a more pronounced red shift in comparison with the less densely cross-linked gel D2. For the two gels cross-linked by STS micelles (D3 and D4), the mutual difference in the red shifting caused by sample dehydration was much less pronounced, nevertheless also the concentration of the surfactant in the gelling mixture used differed

much less for these two gels when compared to their SDS-based analogues.

The results of the time-resolved FTIR-assisted drying assay can be provided in several different ways. Aside from the overlap of the individual FTIR spectra recorded at different times (shown in Fig. 4), it can be also presented as a time-frequency 2D absorbance map (Fig. 5) or temporal evolution of absorbance at a selected frequency (Fig. 6). In Figs. 5 and 6, it can be seen that the dehydration of the samples can be clearly monitored and the completion of the dehydration can be easily identified by means of these types of data projection.

The smooth character of the 2D time-resolved FTIR spectra without any abrupt changes points to the continuous character of the dehydration process of the analyzed gels. Nevertheless, under a closer look, it can be revealed that the drying process can be divided into several drying steps. These separate drying steps are even more clearly seen in Fig. 6 where temporal evolutions of absorbances at $3350\,cm^{-1}$ ($-OH$ groups) and $1158\,cm^{-1}$ (glycosides) are shown.

For all samples, the initial dehydration step is accompanied by a rapid decrease in the intensity of water-related bands (see the decrease in absorbance at $3350\,cm^{-1}$ in Fig. 6) while the relative intensity of the vibration bands of the dry matter components increases (note an increase in absorbance at $1158\,cm^{-1}$ in Fig. 6) as the dry matter concentrates at the ATR crystal. This initial time period is probably connected with an equilibration in the contact between the ATR crystal and the gel matrix.

In the second stage of the sample drying, the temporal change in the absorbances at the selected frequencies is much slower. In fact, for samples D1 and D3 the absorbances are almost constant and, surprisingly, for D2 the absorbance at $3350\,cm^{-1}$ even slightly increases during this period. The steady FTIR signal in this stage indicates that drying of the gel proceeds at the meniscus of the gel drop and that the respective change in the water content at this air/gel boundary does not manifest in the FTIR spectra collected at the ATR/gel interface.

Table 2
The positions of $\nu(OH)$ bonds and $\Delta\nu$ values.

Sample of hydrogel	frequency of $\nu(OH)$ band (cm^{-1})[a]		$\Delta\nu$ (cm^{-1})[b]
	before drying	after drying	
D1	3350	3384	34
D2	3366	3389	23
D3	3351	3382	31
D4	3370	3400	30

[a] Frequency was determined as the centre of gravity of absorption band.
[b] $\Delta\nu$ value calculated as difference of centre of gravity of absorption band before and after drying process.
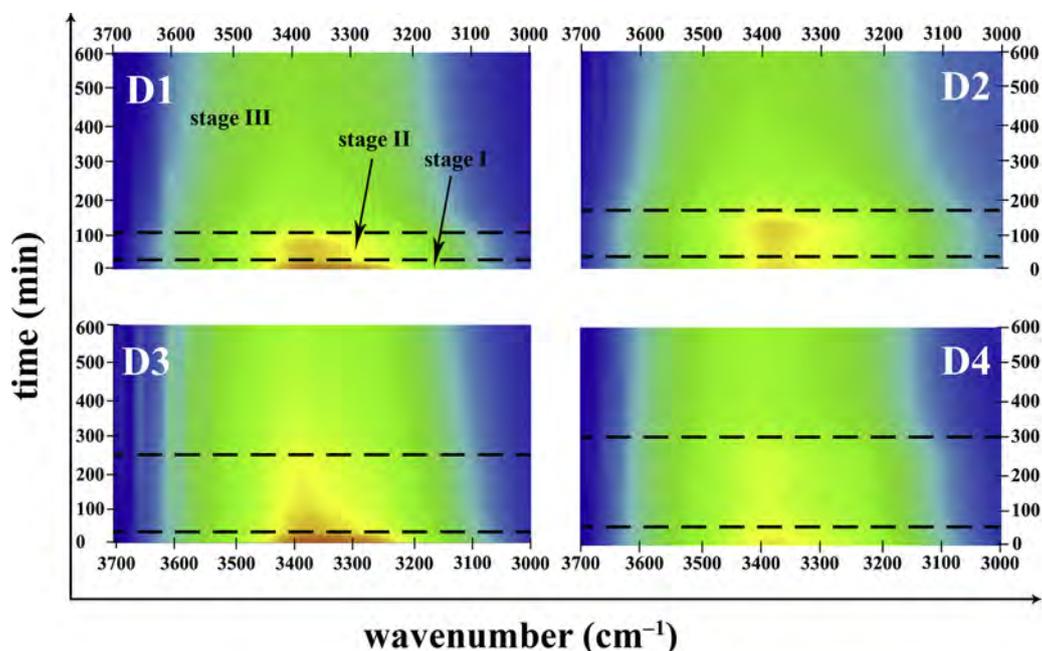
Fig. 5. 2D time-resolved FTIR spectra of the drying of tested polyelectrolyte-surfactant hydrogels. Detail on spectral region with characteristic water molecules vibration band (3700–3000 cm^{-1}). Individual stages of the samples drying are separated by black dashed curves.

The final stage of the sample drying then follows. This stage is characterized by a continuous removal of water from the sample, as illustrated by the gradual decrease in the intensity of the −OH related band and the corresponding increase in the intensity of vibration of the dry matter content (represented by glycosides in Fig. 6).

In general, the main qualitative features found in the results of the time-resolved FTIR analysis stand in good agreement with the TG analysis of the gel drying process. Consistently with the TG results, the FTIR results indicate that the drying proceeds in several steps. Furthermore, the differences between the individual drying steps are less pronounced in the STS-based gels than in the SDS-based ones (note the similar conclusion of the isothermal TG analysis). Nevertheless, there are also several contradictory features found when the results of the two analyses are compared. For instance, the FTIR results indicate a
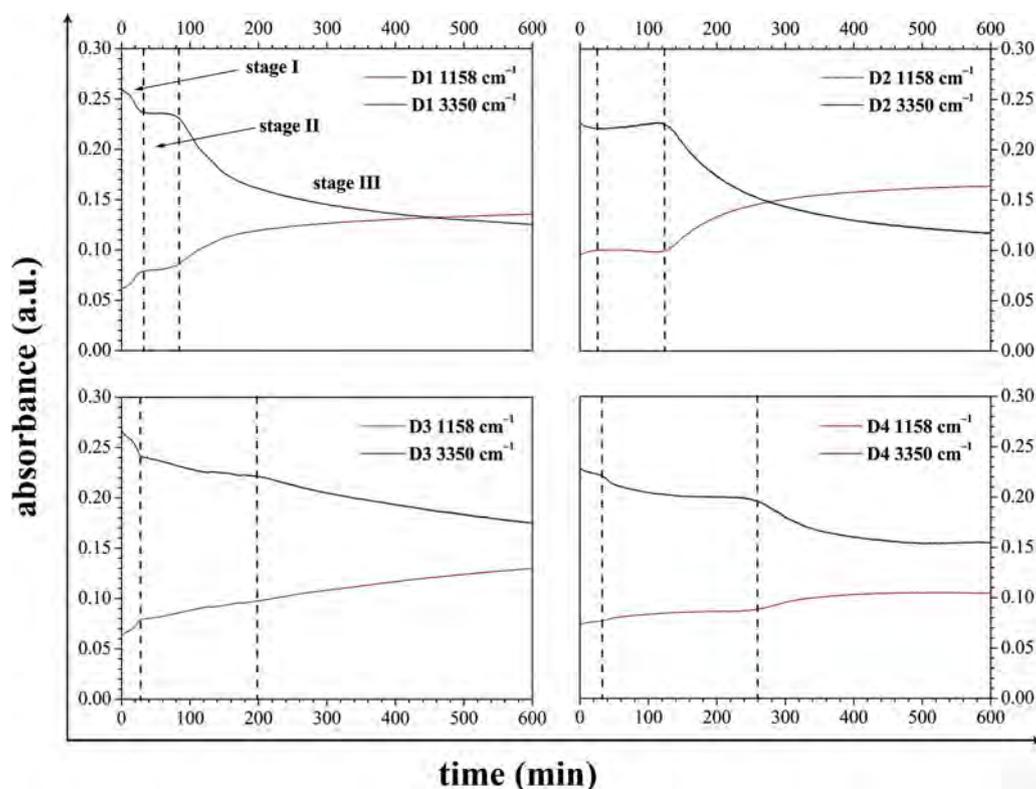

Fig. 6. Time dependences of absorbances at frequencies characteristic for water (−OH at 3350 cm^{-1}) and for dry matter content (glycosidic bond at 1158 cm^{-1}), respectively, during the FTIR-assisted drying of the gels.
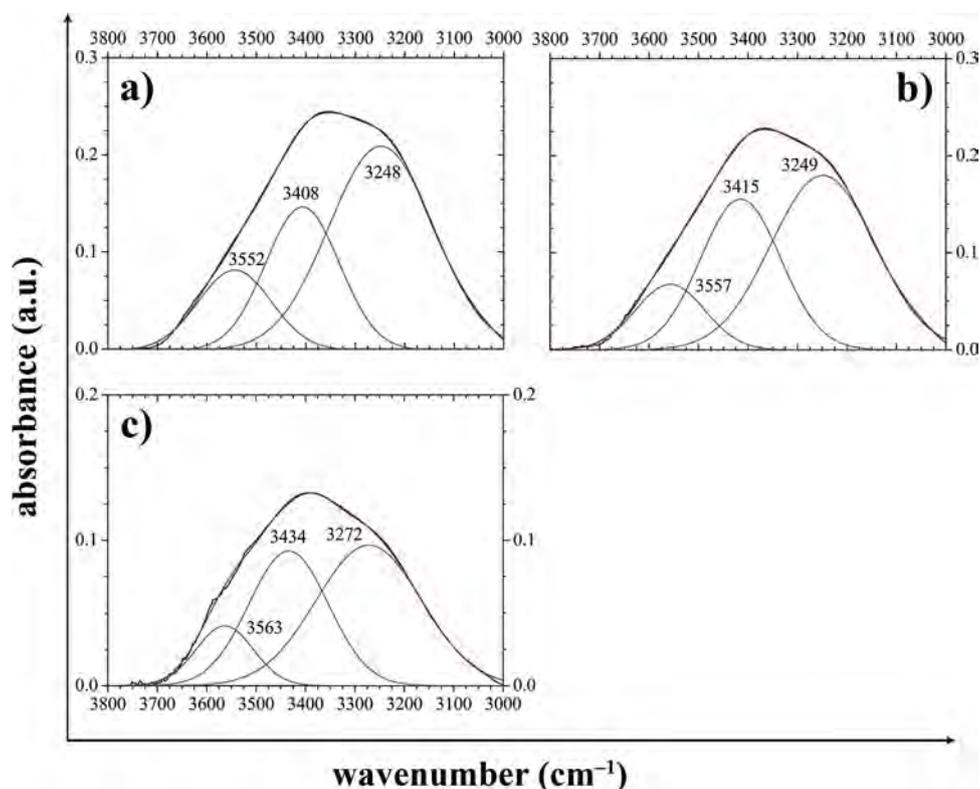
Fig. 7. Example of deconvolution of O−H stretching band for D1 hydrogel at time 0 (a), 60 (b) and 360 min (c), respectively.

slower drying process for the D2 sample as compared to D1 (compare the second stages for the two gels in Fig. 6). It conflicts with the conclusion of the TG analysis that the more densely cross-linked gels have a higher content of bound water. Nevertheless, it is necessary to take into account fundamental differences in the experimental arrangement of the two drying assays. Firstly, the FTIR results may be seriously influenced by the fact that the composition of the gel may affect the wetting of the surface of the ATR crystal and, therefore, the shape of the measured drop. Consequently, different ratios of air/gel to gel/crystal surface areas will necessarily lead to different drying rates detected in the FTIR results. Furthermore, we must bear in mind that contrary to TG analysis performed under a defined atmosphere (dry air or nitrogen), FTIR assisted drying proceeds under ambient laboratory conditions. Therefore, it is almost impossible to maintain the same conditions during different drying experiments. Even slight changes in temperature or relative humidity in close vicinity to the hydrogel drop may result in severe alteration of the drying kinetics (for instance, the above-mentioned temporal increase in absorbance at 3350 cm^{-1} for sample D2 in the drying stage II or a similar feature found in the spectra of D4 at the end of the drying experiments could in fact be an indicator of reverse absorption of the air humidity). Therefore, without adjusting and controlling for the drying atmosphere, the results of the time-resolved ATR FTIR drying assay should be interpreted rather in qualitative and structural terms than for determination of any quantitative parameters describing particular drying kinetics.

3.4. Water structure assay by deconvolution of O−H stretching band

Therefore, we focused our further interpretation of the time-resolved FTIR analysis on a more detailed evaluation of structural changes in gels that take place during their dehydration. It has already been discussed that the drying is accompanied by a red shift of the O−H stretching band (in particular its middle frequency). From this observation it was concluded that drying of the gels is accompanied by weakening of the hydrogen bonding in the system, but no structural

interpretation of this information can be provided without further analysis of the shape of this complex vibration band.

Generally, bulk liquid water molecules in hydrogels can form up to four hydrogen bonds, which results in formation of various structural motifs such as multimer and network water clusters. Several spectrometric techniques such as X-ray spectrometry, IR and Raman spectrometry were used to determine different local structures in bulk water that arise from variations in the arrangement of hydrogen bonds [20,21]. The FTIR approach is based on a detailed analysis of the broad vibration band centered at about 3350 cm^{-1} which corresponds to the O−H stretching of water molecules and is sensitive to the proportional representation of the local structures of liquid water.

Three principal water subpopulations with specific component vibration bands are usually distinguished in the OH stretching envelope. An intensive component peak centered at about 3250 cm^{-1} is ascribed to water molecules strongly bonded via linear hydrogen bonds into tetrahedrally coordinated water pentamers (often called quasi-crystalline water). Another significant peak occurs near 3400 cm^{-1} and is assigned to out-of-phase O−H stretching in less perfectly organized structures such as distorted pentamers and tetramers (solid-like water). These structures are usually characterized by non-linear and/or partially disrupted hydrogen bonds. The two above-mentioned subpopulations are often collectively referred to as network water. The less intensive band centered at about 3560 cm^{-1} corresponds to the water molecules with a highly disturbed hydrogen bond network (liquid-like water).

In our work, a time-resolved variant of such a structural analysis was performed on the OH stretching band in order to reveal any observable effects of the dehydration process on the local structures of water molecules in the tested hydrogel samples. For this purpose, deconvolution of the broad envelope band was performed in the region 3800–3000 cm^{-1} at three sample-specific times. These times were chosen in order to cover the three main stages of the drying process as described in the previous text (see Fig. 6). For example, Fig. 7 shows the results of this deconvolution for the sample D1. The specific times for

Table 3
Position and proportional representation of subpopulation water molecules in DEAE-dextran hydrogels (and in reference dry DEAE-dextran for comparison).

	t (min)	frequency of the component peak (cm^{-1})			relative peak area (% of total peak area)		
		liquid-like	solid-like	quasi-crystalline	liquid-like	solid-like	quasi-crystalline
D1	st. I (0 min)	3552	3408	3248	18%	28%	54%
	st. II (60 min)	3557	3415	3249	13%	35%	52%
	st. III (360 min)	3563	3434	3272	12%	37%	51%
D2	st. I (0 min)	3551	3415	3253	20%	28%	52%
	st. II (60 min)	3550	3416	3255	15%	32%	53%
	st. III (400 min)	3550	3437	3292	12%	26%	62%
D3	st. I (0 min)	3564	3409	3236	19%	35%	46%
	st. II (120 min)	3561	3417	3248	11%	40%	49%
	st. III (500 min)	3560	3435	3276	10%	33%	57%
D4	st. I (0 min)	3553	3416	3254	20%	29%	51%
	st. II (170 min)	3559	3423	3261	14%	38%	48%
	st. III (510 min)	3557	3431	3278	11%	37%	52%
DEAE-dextran		3510	3367	3222	7%	63%	30%

sample D1 were chosen as follows: the start of the drying process (representing stage I of the drying process, Fig. 7a), at 60 min of the drying process (stage II of the drying process, Fig. 7b) and at 360 min of the drying process (stage III of the drying process, Fig. 7c), respectively.

The results of the deconvolution of the OH stretching band at the specific times are summarized for all tested samples in Table 3. For the three deconvolution components, both the frequency and the relative proportion of the total area of the envelope stretching band are provided in the Table 3. Apparently, the time evolution of the relative areas of the component bands could lead to the interpretation that no significant changes over time were revealed for the relative representation of the component bands, although it can be seen that the relative area of the more structured water subpopulations (quasi-crystalline and solid-like) slightly increase over time at the expense of a corresponding decrease in the area of the liquid-like water component. Nevertheless, at this point it should be emphasized that the relative area of the respective bands is not equal to the relative content, because hydrogen bonded structures always show a significantly increased intensity of the respective infrared band [17]. Therefore, the absolute content of the least-structured subpopulation will in fact be significantly higher compared to the percentage values provided in Table 3. The relative decrease in the representation of this component between the first evaluated time (the start of the experiment) and the last (stage III) is approaching 50% of its initial relative content, which is not negligible. Evidently, the highest losses of liquid-like water molecules occur at first step of drying process. This step took place in the time range from 0 min to 60 min for hydrogels with SDS, while this step was significantly longer for STS-based hydrogels. We also see that the relative content of the multimer (liquid-like) subpopulation at the beginning of the drying process is very similar for all DEAE-dextran hydrogels, which indicates that the relative representation of the network forming and liquid-like water subpopulations is controlled primarily by the polysaccharide component rather than by the density and nature of the cross-links in the gel matrix.

Moreover, it is evident from the results shown in Table 3 that for all hydrogel samples, the position of absorption bands which correspond to the network water molecules shifts to higher frequencies during the drying process (red shifts up to 40 cm^{-1} were found). On the contrary, the position of the liquid-like water components remains almost unaltered. In the first step of the evaporation process, a less-pronounced shift to higher frequencies was observed while the **red**-shift of network subpopulations such as pentamers, tetramers and/or distorted pentamers was more apparent in the subsequent drying step (stage III). These results suggest that during the excess dehydration stage, a progressive distortion of the hydrogen bonds takes place in the structure of network water molecules. Most likely, the gradual destruction of the hydrogen bonded structures during the drying process can be attributed to the

increasing relative content of water that is strongly bound in the hydration layer of the polysaccharide content where the water molecules are less accessible to network-forming water-water interactions. This finding is in good agreement with the generally-accepted strong hydration of hydrophilic polysaccharides, i.e. hyaluronic acid, chitosan and phytoglycogen [9], and of the high relative content of strongly-bound hydration water (referred to as "high-density" water [22],) in the hydrogels of these biopolymers [23]. Last but not least, it is necessary to take into account also the fact that as a result of excess drying of the gel, the intrinsic OH groups of the DEAE-dextran participate more in the overall shape of the OH stretching band. Nevertheless, as can be seen in Fig.S3 and Table 3, results of the deconvolution of dry DEAE-dextran are significantly shifted in frequencies as well as in relative peak areas which indicates that even in the final drying stage, the discussed results of −OH stretching band deconvolution do represent the residual water content rather than the dry mass of the gel.

4. Conclusion

ATR-IR spectroscopy is a relatively simple and effective technique to study the structure of water molecules in polyelectrolyte/surfactant hydrogels. Structural details can be obtained particularly from the deconvolution of the broad band located around 3350 cm^{-1} that corresponds to the O−H stretching of water molecules. The effect of the water content can be addressed by taking the spectra over time during the drying of the gel sample. IR spectroscopy provides limited quantitative information. It was shown that thermogravimetry is a suitable complementary technique providing the quantitative data, including kinetic data on the drying (dehydration) process, while being much less informative about the structural details. Thermogravimetry also enables simpler control of the measurement atmosphere. The usefulness of the combination of these two techniques was demonstrated using the example of polyelectrolyte/surfactant hydrogels, but we believe that it can be applied to other hydrogel systems as well.

Appendix A. Supplementary data

Supplementary data associated with this article can be found, in the online version, at https://doi.org/10.1016/j.colsurfa.2019.04.089.

References

[1] E.M. Ahmed, Hydrogel: preparation, characterization, and applications: a review, J. Adv. Res. 6 (2015) 105–121, https://doi.org/10.1016/j.jare.2013.07.006.

[2] K.J. De France, F. Xu, T. Hoare, Structured macroporous hydrogels: progress, challenges, and opportunities, Adv. Healthc. Mater. 7 (2018) 1700927, , https://doi.org/10.1002/adhm.201700927.

[3] S.K. Shukla, A.W. Shaikh, N. Gunari, A.K. Bajpai, R.A. Kulkarni, Self assembled hydrophobic nanoclusters of poly(methyl methacrylate) embedded into polyvinyl alcohol based hydrophilic matrix: preparation and water sorption study, J. Appl. Polym. Sci. 111 (2009) 1300–1310, https://doi.org/10.1002/app.29155.

[4] K.M. Park, D. Lewis, S. Gerecht, Bioinspired hydrogels to engineer cancer micro-environments, Annu. Rev. Biomed. Eng. 19 (2017) 109–133, https://doi.org/10.1146/annurev-bioeng-071516-044619.

[5] K.H. Bae, L.-S. Wang, M. Kurisawa, Injectable biodegradable hydrogels: progress and challenges, J. Mater. Chem. A. 40 (2013) 5371–5538, https://doi.org/10.1039/C3TB20940G.

[6] I.D. Kuntz, W. Kauzmann, Hydration of proteins and polypeptides, Adv. Protein Chem. 28 (1974) 239–345, https://doi.org/10.1016/S0065-3233(08)60232-6.

[7] E.V. Sillatta, M.I. Velasco, C.G. Gómez, R.H. Acosta, M.C. Strumia, G.A. Monti, Evaporation kinetics in swollen porous polymeric networks, Langmuir 30 (2014) 4129–4136, https://doi.org/10.1021/la500031t.

[8] P. Musto, M. Galizia, M. Pannico, G. Scherillo, G. Mensitieri, Time-resolved fourier transform infrared spectroscopy, gravimetry, and thermodynamic modeling for a molecular level description of water sorption in poly(ε-caprolactone), J. Phys. Chem. B 118 (2014) 7414–7429, https://doi.org/10.1021/jp502270h.

[9] M. Grossutti, J.R. Dutcher, Correlation between chain architecture and hydration water structure in polysaccharides, Biomacromolecules 17 (2016) 1198–1204, https://doi.org/10.1021/acs.biomac.6b00026.

[10] E.A. Disalvo, M.A. Frias, Water state and carbonyl distribution populations in confined regions of lipid bilayers observed by FTIR spectroscopy, Langmuir 29 (2013) 6969–6974, https://doi.org/10.1021/la304390r.

[11] T. Venerová, M. Pekař, Rheological properties of gels formed by physical interactions between hyaluronan and cationic surfactants, Carbohydr. Polym. 170 (2017) 176–181, https://doi.org/10.1016/j.carbpol.2017.04.087.

[12] D.E. Wingrove, P. Ander, Conductivity of aqueous solutions of ionic polysaccharides containing simple salts, Macromolecules. 12 (1979) 135–140, https://doi.org/10.1021/ma60067a028.

[13] A. De Ninno, A. Congiu Castellano, E. Del Giudice, The supramolecular structure of liquid water and quantum coherent processes in biology, J. Phys. Conf. Ser. 442 (2013) 1–9, https://doi.org/10.1088/1742-6596/442/1/012031.

[14] S. Obruca, P. Sedlacek, F. Mravec, V. Krzyzanek, J. Nebesarova, O. Samek, D. Kucera, P. Benesova, K. Hrubanova, M. Milerova, I. Marova, The presence of PHB granules in cytoplasm protects non-halophilic bacterial cells against the harmful impact of hypertonic environments, N. Biotechnol. 39 (2017) 68–80, https://doi.org/10.1016/j.nbt.2017.07.008.

[15] P. Sedlacek, E. Slaninova, V. Enev, M. Koller, J. Nebesarova, I. Marova, K. Hrubanova, V. Krzyzanek, O. Samek, S. Obruca, What keeps polyhydroxyalk-anoates in bacterial cells amorphous? A derivation from stress exposure experiments, Appl. Microbiol. Biotechnol. (2019), https://doi.org/10.1007/s00253-018-09584-z.

[16] P. Sedlacek, E. Slaninova, M. Koller, J. Nebesarova, I. Marova, V. Krzyzanek, S. Obruca, PHA granules help bacterial cells to preserve cell integrity when exposed to sudden osmotic imbalances, N. Biotechnol. 49 (2019) 129–136, https://doi.org/10.1016/j.nbt.2018.10.005.

[17] B.H. Stuart, Infrared Spectroscopy: Fundamentals and Applications, 1st ed., John Wiley & Sons, Chichester, West Sussex, England, Hoboken, 2004.

[18] K. Haxaire, Y. Maréchal, M. Milas, M. Rinaudo, Hydration of polysaccharide hya-luronan observed by IR spectrometry. I. Preliminary experiments and band assignments, Biopolymers 72 (2003) 10–20, https://doi.org/10.1002/bip.10245.

[19] K. Haxaire, Y. Maréchal, M. Milas, M. Rinaudo, Hydration of hyaluronan poly-saccharide observed by IR spectrometry. II. Definition and quantitative analysis of elementary hydration spectra and water uptake, Biopolymers 72 (2003) 149–161, https://doi.org/10.1002/bip.10342.

[20] M.W. Mahoney, W.L. Jorgensen, A five-site model for liquid water and the re-production of the density anomaly by rigid, nonpolarizable potential functions, J. Chem. Phys. 112 (2000) 8910–8922, https://doi.org/10.1063/1.481505.

[21] A. Nilsson, L.G.M. Pettersson, Perspective on the structure of liquid water, Chem. Phys. 389 (2011) 1–34, https://doi.org/10.1016/j.chemphys.2011.07.021.

[22] P.M. Wiggins, High and low density water in gels, Prog. Polym. Sci. 20 (1995) 1121–1163, https://doi.org/10.1016/0079-6700(95)00015-8.

[23] P.M. Wiggins, R.T. Vanryn, D.G.C. Ormrod, Donnan membrane equilibrium is not directly applicable to distributions of ions and water in gels or cells, Biophys. J. 60 (1991) 8–14, https://doi.org/10.1016/S0006-3495(91)82026-4.